Vol. 66 October, 1962 No. 10

THE JOURNAL OF PHYSICAL CHEMISTRY

(Registered in U. S. Patent Office)

CONTENTS

36th National Colloid Symposium, Stanford University, Stanford, California, June 25–27, 1962

Contents continued on page 1A

THE JOURNAL OF PHYSICAL CHEMISTRY

(Registered in U. S. Patent Office)

Published monthly by the American Chemical Society at 20th and Northampton Sts., Easton, Pa. Second-class postage paid at Easton, Pa.

The *Journal of Physical Chemistry* is devoted to the publication of selected symposia in the broad field of physical chemistry and to other contributed papers.

Manuscripts originating in the British Isles, Europe, and Africa should be sent to F. C. Tompkins, The Faraday Society, 6 Gray's Inn Square, London W. C. 1, England.

Manuscripts originating elsewhere should be sent to W. Albert Noyes, Jr., Department of Chemistry, University of Rochester, Rochester 20, N. Y.

Correspondence regarding accepted copy, proofs, and reprints should be directed to Senior Production Editor, Allen D. Bliss, ACS Office, Mack Printing Company, 20th and Northampton Sts., Easton, Pa.

Advertising Office: Reinhold Publishing Corporation, 430 Park Avenue, New York 22, N. Y.

Articles must be submitted in duplicate, typed, and double spaced. They should have at the beginning a brief Abstract, in no case exceeding 300 words. Original drawings should accompany the manuscript. Lettering at the sides of graphs (black on white or blue) may be pencilled in and will be typeset. Figures and tables should be held to a minimum consistent with adequate presentation of information. Photographs will not be printed on glossy paper except by special arrangement. All footnotes and references to the literature should be numbered consecutively and placed in the manuscript at the proper places. Initials of authors referred to in citations should be given. Nomenclature should conform to that used in *Chemical Abstracts*, mathematical characters be marked for italic, Greek letters carefully made or annotated, and subscripts and superscripts clearly shown. Articles should be written as briefly as possible consistent with clarity and should avoid historical background unnecessary for specialists.

Notes describe fragmentary or incomplete studies but do not otherwise differ fundamentally from articles and are subjected to the same editorial appraisal as are articles. In their preparation particular attention should be paid to brevity and conciseness. Material included in Notes must be definitive and may not be republished subsequently.

Communications to the Editor are designed to afford prompt preliminary publication of observations or discoveries whose value to science is so great that immediate publication is imperative. The appearance of related work from other laboratories is in itself not considered sufficient justification for the publication of a Communication, which must in addition meet special requirements of timeliness and significance. Their total length may in no case exceed 1000 words or their equivalent. They differ from Articles and Notes in that their subject matter may be republished.

Symposium papers should be sent in all cases to Secretaries of Divisions sponsoring the symposium, who will be responsible for their transmittal to the Editor. The Secretary of the Division by agreement with the Editor will specify a time after which symposium papers cannot be accepted. The Editor reserves the right to refuse to publish symposium articles, for valid scientific reasons. Each symposium paper may not exceed four printed pages (about sixteen double spaced typewritten pages) in length except by prior arrangement with the Editor.

Remittances and orders for subscriptions and for single copies, notices of changes of address and new professional connections, and claims for missing numbers should be sent to the Subscription Service Department, American Chemical Society, 1155 Sixteenth St., N. W., Washington 6, D. C. Changes of address for the *Journal of Physical Chemistry* must be received on or before the 30th of the preceding month. Please include an old address label with the notification.

Claims for missing numbers will not be allowed (1) if received more than sixty days from date of issue (because of delivery hazards, no claims can be honored from subscribers in Central Europe, Asia, or Pacific Islands other than Hawaii), (2) if loss was due to failure of notice of change of address to be received before the date specified in the preceding paragraph, or (3) if the reason for the claim is "missing from files."

Subscription rates (1962): members of American Chemical Society, $12.00 for 1 year; to non-members, $24.00 for 1 year. Postage to countries in the Pan-American Union $0.80; Canada, $0.40; all other countries, $1.20. Single copies, current volume, $2.50; foreign postage, $0.15; Canadian postage $0.10; Pan-American Union, $0.10. Back volumes (Vol. 56–65) $30.00 per volume; foreign postage, per volume $1.20, Canadian, $0.40; Pan-American Union, $0.80. Single copies: back issues, $3.00; for current year, $2.50; postage, single copies: foreign, $0.15; Canadian, $0.10; Pan-American Union, $0.10.

The American Chemical Society also publishes *Journal of the American Chemical Society, Chemical Abstracts, Industrial and Engineering Chemistry,* International Edition of *Industrial and Engineering Chemistry, Chemical and Engineering News, Analytical Chemistry, Journal of Agricultural and Food Chemistry, Journal of Organic Chemistry, Journal of Chemical and Engineering Data, Chemical Reviews, Chemical Titles, Journal of Chemical Documentation, Journal of Medicinal and Pharmaceutical Chemistry, Inorganic Chemistry, Biochemistry,* and *CA — Biochemical Sections.* Rates on request.

Contents continued

NOTES

COMMUNICATION TO THE EDITOR

AUTHOR INDEX

Special Notice to Authors

Beginning with the January issue, 1963, a page charge for publication will go into effect. The ACS position is described in detail *via* a series of questions and answers in "The Case for Page Charges," *Chem. Eng. News*, March 19, 1962, p. 92. The editors of the *Journal of Physical Chemistry* wish to emphasize the following points.

1. The page charge is a publication service charge designed to aid in covering the costs of publishing an article in a journal. The page charge covers only costs of setting the article in type and preparing it for the presses. As administered by the ACS, it will also include 100 reprints supplied to the author.

2. Manuscripts received after August 15, 1962, or accepted for publication after September 15, may be published in January, 1963, and subsequent issues, and therefore be subject to the page charge.

3. Payment is expected from sponsored funds supporting the research reported. Page charge payment is not a condition for publication.

4. The editor's decision to publish is made before assessment of page charges and the editor's office will not be advised on charges or payment.

5. With the institution of page charges, subscription rates to ACS journals should be stabilized at current levels for an indefinite period of time.

Do you sometimes want all the information you can find on a given subject in chemistry?

That's almost what you'll get if you use the BIBLIOGRAPHY OF CHEMICAL REVIEWS. Volume 4 is a collection of 6,799 abstracts of review articles from CHEMICAL ABSTRACTS, Volume 55 (1961). It includes a keyword title index and an author index, which make searching easier and more effective. The only information it doesn't find for you is that which has come to light since a review was published.

You can (1) turn to the keyword index and seek out the subject you are most interested in, (2) use the reference there to find the review abstract in the front of the book, (3) then locate the original paper through your library or by writing publisher or author.

The keyword index lists permuted title words in context, with the keyword of each title in the center of the column. Each title appears several times so that you can look under *different* headings and this way make virtually certain of finding sources in the areas you wish to cover.

What You Get With the BIBLIOGRAPHY

About 6% of all abstracts in CA are review abstracts, and 1961 was the biggest abstract year in history, making the BIBLIOGRAPHY OF CHEMICAL REVIEWS, Volume 4 the most comprehensive to date. All abstracted reviews and published bibliographies are included, arranged by regular CA sections. There is an average of at least 40 bibliographic references with each review.

If you do not have Volumes 1 and 2 (11,848 CA abstracts between common covers for 1958 and 1959) and Volume 3 (6,506 abstracts from the 1960 CA), why not send for them along with this latest one?

The four volumes together contain more than 25,000 abstracts of reviews and give between 1 million and 1.7 million references to the literature. The BIBLIOGRAPHY OF CHEMICAL REVIEWS series provides information to speed your searching in a form unobtainable any other way.

Volume 4

332 columns • 113 index pages
paper bound • $6.50

Volume 3

320 columns • 106 index pages
paper bound • $6.00

Volumes 1 and 2 (bound together without index)

293 pages • paper bound • $5.00

Order from:

Special Issues Sales/American Chemical Society/1155 Sixteenth St., N.W./Washington 6, D.C.

THE JOURNAL OF
PHYSICAL CHEMISTRY

(Registered in U. S. Patent Office) (© Copyright, 1962, by the American Chemical Society)

VOLUME 66 OCTOBER 18, 1962 NUMBER 10

THE INTERNAL STRUCTURE OF COLLOIDAL CRYSTALS OF β-FeOOH AND REMARKS ON THEIR ASSEMBLIES IN SCHILLER LAYERS

BY JOHN H. L. WATSON AND R. R. CARDELL, JR.,

Edsel B. Ford Institute for Medical Research, Detroit 2, Michigan

AND WILFRIED HELLER

Department of Chemistry, Wayne State University, Detroit, Michigan

Received March 5, 1962

It is shown how ultrathin sectioning of colloidal crystals can be applied to electron microscopical studies of their structure The technique is described and applied to tactoid-forming deposits of β-FeOOH crystals. Cross sections of the single crystals show that they are square and remarkably uniform with a side of about 550 Å. Their mutual orientation has been maintained during specimen preparation and the crystals are shown to exist in an orthogonal array. A structure is demonstrated *within* the crystals, which is shown to be most probably that of an oriented bundle of loosely packed rods, also in an orthogonal array, wherein the repeating distance is about 60 Å. The long rods are themselves crystals and are referred to as "subcrystals," regularly arranged within the conventional crystal. They are about 30 ± 5 Å. thick, separated by about the same distance. Electron micrographs illustrate evidence for the substructure from both longitudinally and cross sectioned crystals, as well as unsectioned crystals. An example of fringes 11 Å. apart (±10%) is shown, in good agreement with the *a* dimension (10.48 Å.) in the tetragonal unit cell. The observations suggest that the crystals grow by reason of tetragonal unit cells forming subcrystals in such a way as to promote a uniform rate of growth in the *a* and *b* directions and in this sample about 14× more rapid growth in the *c* direction. There is some evidence to support the view that the subcrystals might be hollow rods. Pertinent observations also are reported concerning the occurrence of twins and other irregularly shaped crystals (somatoids) among the β-FeOOH crystals.

Introduction

The purpose of this paper is twofold: (a) to show how a very old technique in the preparation and study of biological and petrographic specimens, thin sectioning, adapted more recently to electron microscopy and renamed "ultrathin sectioning," can be used to give useful information concerning the microstructure of certain non-biological materials, notably inorganic colloidal crystals, and (b) to demonstrate the use of the technique in studying tactoid-forming deposits in β-FeOOH suspensions.

The sectioning experiments were undertaken in the present work[1] to discover what information might be derived from them concerning (a) the packing of crystals of β-FeOOH[2] in the sediments formed by slowly hydrolyzing ferric chloride solutions at room temperature,[3] (b) the shape and the thickness of the cross sections of the single β-FeOOH crystals and their individual volumes, and (c) the fine structure, if any, of these crystals From such data one can hope to derive, in conjunction with optical data, the exact equilibrium distances between the β-FeOOH crystals in schiller layers. Until now only approximate values could be given for these[4] and they were not sufficiently accurate to be used as a basis for calculations of the interaction energy between these crystalline particles.

Conventional transmission electron micrographs (Fig. 1) demonstrate the highly monodisperse nature of the crystals, a fact which will be discussed in detail in a separate publication. They also show that these crystals deviate from usual crystals by reason of their rounded or irregularly shaped ends. They therefore may be related to the crystal habitus classified by Kohlschütter[5] as *somatoids*, which are defined as crystals of regular internal structure but of more or less irregular external shape. Similarly, the numerous twins observed in these specimens could be referred to as

(1) Presented before the 36th National Colloid Symposium, Palo Alto, California, June 25–27, 1962. The work is part of a larger, continuing project being conducted by Dr. Heller on the properties of schiller layers of β-FeOOH and other crystals.

(2) The common name for β-FeOOH is *β-ferric oxide monohydrate.*

(3) H. Zocher and W. Heller, *Z. anorg. allgem. Chem.*, **186**, 73 (1930).

(4) W. Heller, *Compt. rend.*, **201** 831 (1935).

(5) V. Kohlschütter, C. Egg, and M. Bobtelsky, *Helv. Chim. Acta.*, **8**, 457 (1925).

Fig. 1.—Unsectioned, whole crystals of β-FeOOH, ×50,000, 80 kv. electrons. (In each figure, unless indicated otherwise, the line represents 0.1 μ.) The insert shows the appearance of a true twin (clear arrow) compared with that of overlapping crystals (solid arrow), ×77,000.

somatoids. These micrographs give length and width of the single crystals easily, indicate when there is mere overlapping as compared with twinning, but are able to tell little or nothing accurately about the dimension or shape of the crystal in the direction of the electron beam. By the admittedly inaccurate method of "shadow casting," the crystals were surmised to be about square in cross section. Many examples of star-shaped crystals and *X*- and *Y*-shaped twins are observed in these β-FeOOH dispersions. Mere overlapping of two crystals (solid arrow in the Fig. 1 insert) is easily differentiated from true twinning (clear arrow). The crystals in Fig. 1 have not been sectioned. Both *X*- and *Y*-twins yield measured angles of about 60° in the micrographs, in good agreement with Mackay's more accurate X-ray data of 62° 52′ 10″. In Fig. 1 there is also a cross-shaped twin (clear arrow) with a 90° angle. The internal structure of such forms can be demonstrated more clearly by the application to them of thin sectioning.

β-FeOOH crystals are known to form tactoids of smectic symmetry[3] under proper conditions,[6] which manifest themselves as regularly layered sediments, "schiller layers."[7] These exhibit brilliant interference colors, which has led to the quoted designation. The individual crystals composing these schiller layers were recognized at an early stage to represent β-FeOOH.[8] More detailed examination[9] led to the following dimensions of the unit cell of β-FeOOH: $a = b = 10.5$ Å., $c = 3.03$ Å., in correction of the dimensions previously given by Milligan and Weiser, $a = 5.28$, $b = 10.24$, $c = 3.34$ Å. Milligan and Weiser were the first to identify the previously unknown crystalline compound β-FeOOH.[10] More recently, A. L. Mackay[11] and others[12,13] confirmed and improved the values given by Kratky and Nowotny. Mackay's values are a tetragonal unit cell of $a = b = 10.48$ and $c = 3.023$ Å. Observations and conclusions made in the present work are consistent with the earlier results but the sectioning experiments add considerably to the information available both on the ultrastructure of the crystals and their probable mode of packing within the schiller layers. We have recently published complete *d*-value data for β-FeOOH.[14]

Specimen Preparation

The experiments were carried out with colloidal dispersions of β-FeOOH which contained schiller layers. The particular specimen described in this paper was one which had an $FeCl_3$ concentration of 2.34 mmoles/l. and was embedded 326 days after its original preparation.[15] The specimen had a measured average length of 234 ± 23 mμ, an average width of 60 ± 10 mμ, and an average ratio of length to width of 4.0 ± 0.3. With minimal disturbance of the layers, the supernatant sol (actosol) was removed by pipet. With extreme care, absolute alcohol was added and after some time the supernatant liquid was removed again. Several such changes were effected over a period of 12 hr. in order to ensure maximum dehydration of the material. The alcohol of the final change was replaced by a 3:1 mixture of catalyzed *n*-butyl to methyl methacrylate and several changes of the methacrylate mixture made to ensure complete replacement of alcohol by methacrylate. Polymerization of the methacrylate about the crystals was accomplished at

(6) "Proper conditions" for the formation of β-FeOOH crystals in tactoids of smectic symmetry are that the concentration of the original iron chloride solution be between the limits of approximately 20 to 60 mmoles of $FeCl_3$. Schiller layers can be expected to form at the earliest in about two months after preparation of the solution, and later, the time required being longer the lower the original concentration within the range given. These conditions apply for room temperature.

A definition of the term "tactoid" is frequently requested and since a clear understanding of this word is required here, the following discussion is offered. Tactoids are highly visco-elastic droplets of a concentrated colloidal solution dispersed within a dilute colloidal solution which contains the same components. They exhibit optical anisotropy and generally assume a non-spherical shape. The internal structure of a tactoid is nematic or smectic, with some more complex structures being occasionally possible. A tactoid differs from a liquid crystal (mesophase) by the fact that it consists of two phases of which one is dispersed in the other, while a mesophase consists of a single phase. Thus a tactoid of tobacco mosaic virus represents a dispersion of mutually oriented virus particles in an aqueous medium, and a multitude of these tactoids, in turn, are dispersed in a dilute aqueous solution of randomly oriented virus particles.

(7) H. Zocher, *Z. anorg. allgem. Chem.*, **147**, 91 (1925). The term "schiller layer" originates from "schiller-schichten," a term introduced by H. Zocher, who discovered tactoids.

(8) W. Heller, O. Kratky, and H. Nowotny, *Compt. rend.*, **202**, 1171 (1936).

(9) O. Kratky and H. Nowotny, *Z. Krist.*, **A100**, 356 (1938).

(10) W. O. Milligan and H. B. Weiser, *J. Am. Chem. Soc.*, **57**, 238 (1935).

(11) A. L. Mackay, *Mineral. Mag.*, **32**, 545 (1960).

(12) D. R. Dasgupta and A. L. Mackay, *J. Phys. Soc. Japan*, **14**, 932 (1959).

(13) J. D. Bernal, D. R. Dasgupta, and A. L. Mackay, *Clay Minerals Bull.*, **4**, 15 (1959).

(14) J. H. L. Watson, W. Heller, and T. Schuster, *Proc. European Regional Conf. Electron Microscopy*, Delft, **1**, 229, 1960.

(15) The sample was one taken from the large series studied by L. E. Poplowski and reported on in "A Study of the Growth of Colloidal β-FeOOH Crystals." Master's Thesis, unpublished, Wayne State University, 1962.

80° over 24 hr. Small pieces of the methacrylate-embedded crystals were cut off, mounted in wax fused to 1/8 in. diam. blocks, and trimmed for the ultrathin sectioning procedure. Both a Porter-Blum and an L.K.B. ultramicrotome were used with both polished diamond and glass knives to cut ultrathin sections which were approximately 0.01 μ thick. The thin sections were mounted upon carbon-coated parlodian on Athene #100 specimen grids and viewed both with an R.C.A. modified EMU-2B electron microscope at magnification from ×8,000 to ×18,000 and ultimate resolutions of about 15 Å., and with a Siemens' Elmiskop I at from ×20,000 to ×160,000 and maximum resolution of about 7 Å.

Observations

Figure 2 shows a typical section of an array of β-FeOOH crystals cut at approximately 90° to the long axis of the single crystals. It immediately is apparent that each crystal is approximately square in cross section. Their mutual orientation has survived, in part, the handling of the specimen during preparation. The crystals are seen to be arranged in an orthogonal array, with any one of them situated immediately adjacent and opposite to its eight neighbors to present a striking *checker board* appearance in two dimensions. This orientation undoubtedly reflects the general type of orientation of the individual crystals prior to replacement of water by alcohol and finally by polymer.

It is most likely that in the original schiller layers the direction of the long range spacings (of the order of the wave length of light) is in a direction perpendicular to the arrow shown in Fig. 2 and parallel to the plane of the micrograph. It must be emphasized that electron micrographs are 2-dimensional while schiller layers are 3-dimensional.

The crystals are remarkably uniform with square sides of about 550, standard deviation 30 Å. This section (Fig. 2) has been cut at not quite 90° to the long axis so that there tends to be overlapping of the crystal sections in one direction (vertically, as shown by the arrow) with less, or no overlapping in the other. The maximum residual separation of the crystals is about 90 Å. This distance is obviously very much smaller (about 60 times) than that in the schiller layers of the original system. In Fig. 2 no recognizable nor reproducible structure was observed *within* the crystals. They were merely broken in some areas by the sectioning. In any case, each section represents crystal planes of β-FeOOH, either broken or cleaved along lattice planes.

In Fig. 3 and others, whether cut from more advantageous angles or better resolved in the electron micrographs, structure is seen *within* the cross sections of the crystals. Identical orientation of the crystals was not preserved everywhere and consequently, since the appearance of the structure depends, among other things, upon the angle of the knife relative to the orientation of the crystals themselves, all of the cross sections did not have the same appearance. The following discussion and conclusions are a result of observations made during a study of numerous micrographs.

Many of the crystals were seen to be composed of a series of what first were interpreted erroneously to be "layers,"[14] a maximum of 12 to 16 usually being recognizable in any one crystal (Fig. 3A). In any one group of crystals the layers were oriented similarly (usually parallel to one side of the square cross section) as long as the crystals themselves were oriented identically.

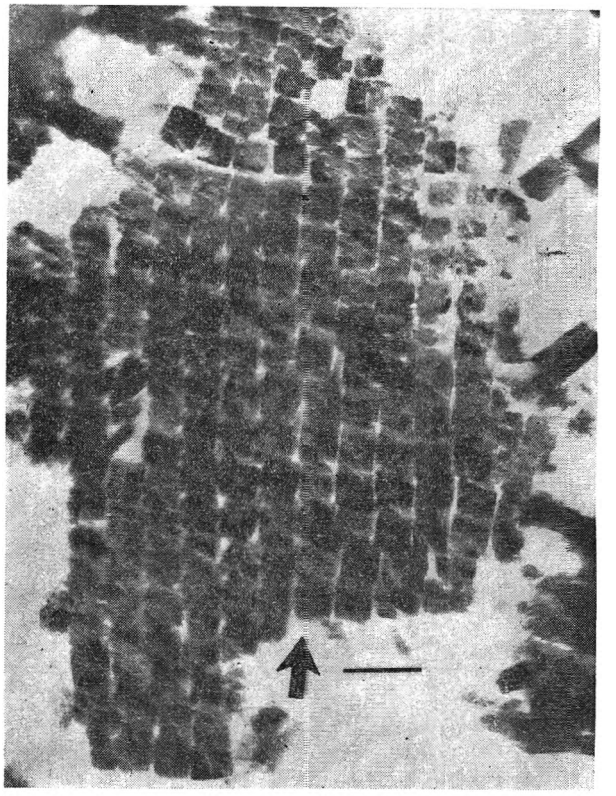

Fig. 2.—A cross section of an orthogonal array of crystals of β-FeOOH, ×90,000.

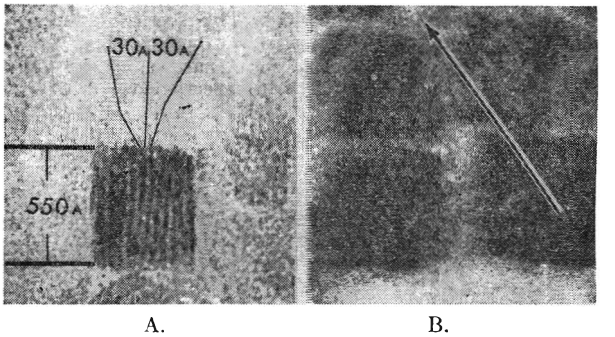

A. B.

Fig. 3.—Sections of β-FeOOH crystals at higher magnification to show their internal structure. A. A crystal sectioned at an angle significantly less than 90°, showing lines parallel to the sides, ×280,000. B. Four crystals sectioned at such an angle that lines along the *diagonals* predominate, ×250,000.

One was tempted to interpret these "layers" (alternating linear areas of light and shade) as indicative of a true laminated structure within the crystals. However, more extensive observations negated this and suggested instead that the structure was rather that of a bundle of laterally oriented rods and that the apparent laminated appearance was a function of the cutting angle through such a bundle. An appearance of lines (layers) in the cross sections, parallel to their sides, occurred due to the foreshortening effect of the non-perpendicular cutting angles. The repeating distance in these groups of lines measured as about 60, their thickness as about 30, and their separation as about 30 Å.

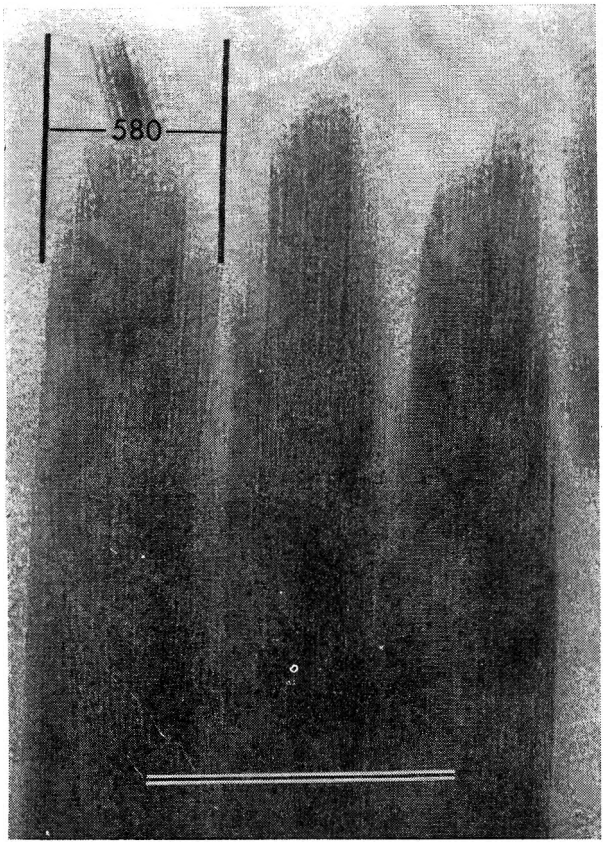

Fig. 4.—An approximately longitudinal section of a group of β-FeO(OH crystals, ×410,000. This section is inclined somewhat toward the diagonal of the orthogonal crystals, so that their apparent widths (580 Å.) are somewhat larger than they would be if they had been sectioned parallel to a side (550 A.).

to its sides. This is observed infrequently, but can be explained only if the structure of the single crystal is indeed the nature of a square, orderly bundle of separated rods in an orthogonal packing. For clarity in the exposition these individual rods, of which the crystal is composed, will be referred to as *subcrystals*.

In those fields where the layers had the symmetrical appearance of a true 90° section, the lines across the cross section did not appear and there was a mottled appearance instead, many of the rows of spots being arranged in straight lines. These spot patterns were interpreted as the electron microscope images of the cross sections of the subcrystals within a crystal. Their dimensions and separations were consistent with the dimensions given earlier for the "layers" or lines. Difficulties of resolution, and particularly of contrast in ultrathin sections of embedded specimens, hamper clear direct observation of such tiny structures, even by electron microscopy, and make it particularly difficult to illustrate them satisfactorily on the printed page.

In order to devise a model of the structure both to illustrate and to satisfy the observations, it was advisable to examine the crystals sectioned longitudinally and at intermediate angles longitudinally. This was done and completely consistent observations were made (Fig. 4). The long parallel sides, the tapered ends, and lines running the length of the crystals were seen. The sides were smooth and the widths uniform for long distances to agree with the observation of square cross sections. The widths were consistent, measuring about 550 Å. As far as the limit of resolution allowed, the subcrystals (rods) did not seem to taper, but appeared

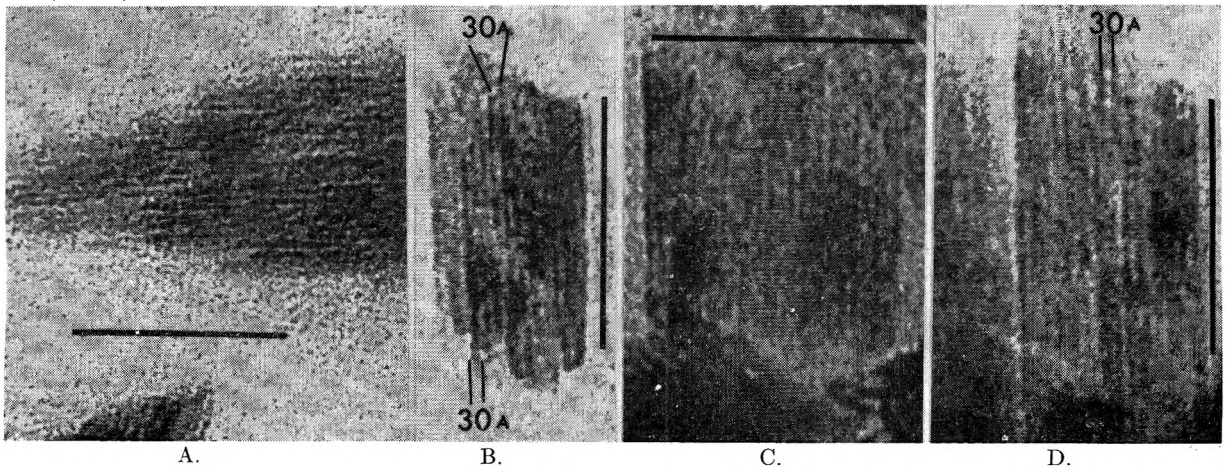

A. B. C. D.

Fig. 5.—A composite of crystals sectioned at intermediate angles. A. Sectioned obliquely through the tip of a crystal, ×280,000. B, C, D. Sectioned as thin fragments, B ×326,000, C ×344,000, D ×326,000.

Only when the sectioning angle was a perfect 90° (a very fortuitous circumstance) would discrete ends of such rods be visible and only then, if both resolution and contrast were particularly favorable.

Cut at some angles, an appearance of lines along the diagonals could be expected to occur in electron micrographs from such a structure as we have proposed (arrow, Fig. 3B). This usually is seen best in micrographs which have been taken slightly out of focus to enhance contrast. The lines are along one diagonal of the square rather than parallel to be of constant width. They were observed best toward the tips of the crystals (Fig. 4) but often were observed to run their full length. They are about 30 Å. across, separated from their neighbors by like distances. Their presence in longitudinal sections can only be reconciled with the observations already described from cross sections if the structure of the crystal is a bundle of oriented subcrystals as has been described.

Figure 5 shows a number of crystals sectioned at intermediate angles which give further information

to confirm the structure already described. In Fig. 5A is a section cut at an oblique angle through the tip of the main body of a crystal. It is seen that at the thinner ends of the section the rods are easily discerned, while further on into the crystal where it is thicker and where the cut has perhaps influenced its structure (more than at its peripheral areas), the electron intensity pattern is more complex and more difficult to interpret. These micrographs are overenlarged photographically in order to make the structure visible to the reader's eye. While sectioned tips are tapered, those crystals which have been cut off short have square ends, as would be expected from a body with square cross section. Extremely thin fragments of crystals show the structure very well (Fig. 5B, C, D). These observations all were confirmed repeatedly. Typical dimensions are marked upon the micrographs.

With 50-kv. electrons incident upon unsectioned crystals, the subcrystals were visible only in the feathered, tapered ends. The crystals had to be "thinned down" by the sectioning process in order to be penetrated adequately at 50 kv. Using higher voltage electrons (80 to 100 kv.), the whole crystals sometimes could be penetrated sufficiently to demonstrate the fine structure. However, in the thicker areas toward the centers of the whole unsectioned crystals, very complicated patterns of electron scattering were observed.

Figure 6 shows several examples of sections made at or near 90° to the long axis of the crystals. In Fig. 6A is an example sectioned at exactly 90°, in which it will be noticed that the sides at high magnification sometimes are slightly bowed. In Fig. 6B is a slightly thicker cross section, in which the crystal has corners which are "stepped," indicating an incomplete crystal growth. The smallest step is about 25 Å. and is consequently in the range of the subcrystals we have been discussing. The sides of this crystal section are not bowed. Figure 6C shows a crystal sectioned almost at 90° in which the lines are just beginning to appear in the peripheral areas, while in the central areas the mottled pattern is visible.

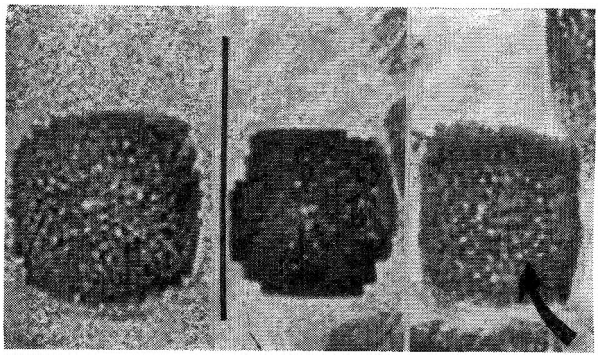

A. B. C.

Fig. 6.—Approximate cross sections of β-FeOOH crystals at high magnification to show mottled appearance, and arrangements of "holes" over the sections, ×364,000. A. The sides are slightly bowed. B. The corners are stepped. C. The central area contains curved lines of "holes," as well as holes in straight line arrangement.

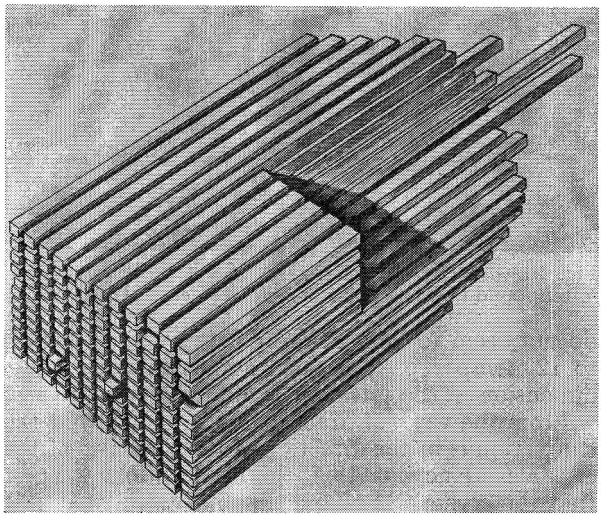

Fig. 7.—A drawing to illustrate a probable structure for the crystals.

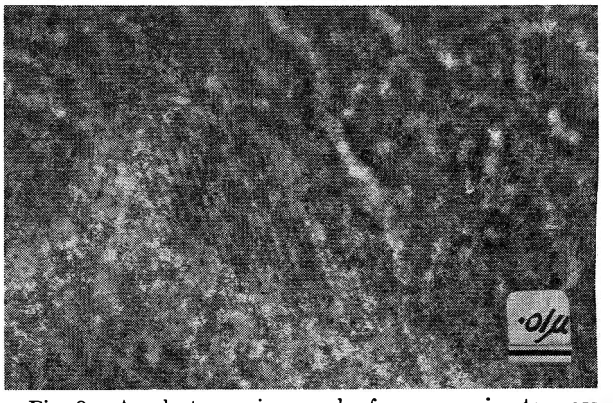

Fig. 8.—An electron micrograph of an approximate cross section of β-FeOOH crystals, to show fringes 10 to 12 Å. apart, ×800,000.

Discussion

The electron microscopic observations of thin sectioned crystals of β-FeOOH have demonstrated that their structure may be described as an oriented pile of separated subcrystals of square cross section somewhat like those shown in the schematic drawing of Fig. 7. In Fig. 2 the sides of the cross sections have a mean of 550, a standard deviation of 30, and a total range of from 460 to 620 Å. The mean width of the crystals when dried in air on a supporting film for electron microscopy (Fig. 1) is 600 ± 100 Å. Therefore, it is likely that some shrinkage (approximately 8%) has occurred. This shrinkage most probably is due to the dehydration of the crystals prior to embedding them in the methacrylate. It would suggest that water is held within them when they are in solution and that it is not entirely removed by mere drying in air but is removed more completely by the treatment with alcohol.

The repeating distance observed within the crystals is about 60 Å. in an over-all square side of about 550 Å., to give 9 or 10 subcrystals on a side of the crystal, or from 80 to 100 subcrystals to compose the crystal. On the square side of each orthogonal subcrystal there would be about 3 unit cells, or 9 unit cells over its square face. In Fig. 8 is a micrograph of fringes obtained from crystals of β-FeOOH sectioned at 90° to the c direction. These

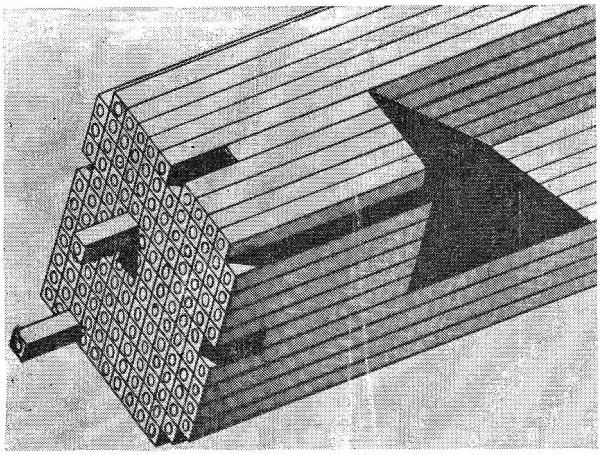

Fig. 9.—A drawing to illustrate a possible structure for the crystals wherein the subcrystals are *hollow* rods, more closely packed than in Fig. 7.

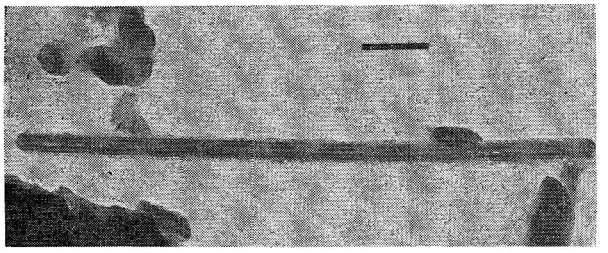

Fig. 10.—An electron micrograph of a typical hollow rod, often found in suspensions of β-FeOOH crystals, ×93,000.

do not seem to be a Moiré pattern. They are 10 to 12 Å. apart and in good agreement with the *a* dimension in the tetragonal unit cell.

From the work of Mackay[11] it is known that the *c* direction is in the direction of the long axis of the crystals. Knowing this, the observations suggest that the crystals grow by reason of tetragonal unit cells forming subcrystals in such a way as to promote a uniform rate of growth of the major crystal in the *a* and *b* directions (and consequently, a square cross section) and a 14-times[16] more rapid growth in the *c* direction to produce rectangular longitudinal sections. Toward the crystal center, the subcrystals tend to grow more rapidly so that the crystals taper toward their tips. Now that the square nature of the cross section is known, measurements made upon the crystals in statistical studies to determine the kinetics of their growth can be greatly simplified. Overlapping crystals can be recognized and touching crystals can be counted and measured. Volumes can be estimated accurately and corrections made for tapering if necessary. Sectioning, applied to other colloidal crystal systems, might work equal simplification upon them.

While the schematic drawing in Fig. 7 satisfies the observations, the lines of "holes" observed in some of the better cross sections, Fig. 6A, B, and C, could be explained by a model as in Fig. 9, where the subcrystals are more tightly packed but where each is a *tube* about 60 Å. wide with an internal diameter of 30 Å. Such a tubular structure would not as readily explain the striated images in unsectioned specimens, but the closer packing could account better for the stepped corners which sometimes are observed (Fig. 6B). This hypothesis is supported indirectly by the fact that long, tubular fibers, which have the appearance of hollow whiskers, are observed to occur fairly frequently in β-FeOOH preparations (Fig. 10). The mean *internal* diameter of these fibers is about 25 Å., their standard deviation 16 Å. The smallest measured internal diameter was 9 Å. The fibers have a very large range of *outside* diameters, from 110 to 2000 Å., with a mean of 440 Å. and a standard deviation of 280 Å. The single fiber shown in Fig. 10 has an outside diameter of 240 Å. and an internal diameter of 30 Å. While the smaller diameter fibers clearly appear to be single (Fig. 10), the larger ones are striated and could represent large bundles of parallel, smaller hollow fibers, arranged in a manner similar to that proposed for the subcrystals in Fig. 9. Many other examples of tubular growth of crystals are known—asbestos, crysotile, halloysite, and NaCl, to mention only a few.[17,18]

Probably the best model of β-FeOOH structure would be one in which the subcrystals are somewhat more closely packed than in Fig. 7 but where they still possess a loose structure, and where electron scattering phenomena explain part of the intensity pattern over the crystalline sections.

The results of the investigation indicate that the internal structure of β-FeOOH is strikingly similar to that of liquid crystals of the nematic type. The subcrystals associate in a nematic structure to form the crystals, which, in turn, associate in tactoids of a basically smectic type.[5] While the individual units, of which a liquid crystal is composed, are easily separated from each other, the cohesion of the solid components of a β-FeOOH crystal is apparently incomparably larger. The rounded outer edges of some of the crystals in cross section (Fig. 6A for example), as well as the occasional occurrence of subcrystals in curved lines (the arrow in Fig. 6C), may be evidence for high interfacial energy, which results in curvature of some of the individual crystals. Experiments are contemplated by means of which it is hoped to bring about a "peptization" of the subcrystals within a single β-FeOOH crystal.

Acknowledgment.—All experiments were carried out with systems kindly provided by Mr. Todd Schuster and by Miss Lillian Poplowski, graduate students at Wayne State University.

DISCUSSION

J. L. SHERESHEFSKY (Howard University).—From the microphotographs it seems that while there is considerable variation in the length of the crystals, the cross sections seem fairly uniform and almost constant. Have you considered this, and have you an explanation for the latter?

J. H. L. WATSON.—It appears that once the crystals have grown to a certain thickness (a side of about 550 Å.) they stop growing in these directions and grow only (or more

(16) In order to have the unit cells form a crystal where the mean ratio of their length to their width is 4.0 (the crystals of Fig. 1), the rate of build-up of unit cells in the *c* direction would have to be [10.5/3.03] × 4.0 times as fast as in the *a* or *b* directions.

(17) "Growth and Perfection of Crystals," R. H. Doremus, B. W. Roberts, and David Turnbull, Eds., John Wiley & Sons, Inc., New York, N. Y., 1958.

(18) T. F. Bates, F. A. Hildebrand, and A. Swineford, *Am. Mineralogist*, **35**, 463 (1950).

rapidly) lengthwise. Actually, as described in the text, they grow 14× faster in the c than in the *a* or *b* directions. In the *a* and *b* directions they grow at equal rates.

A. BAIDENS (du Pont Company).—Are X-ray diffraction patterns sharp or broad? If they are broadened, then what is the approximate diameter of the diffracting crystalline region?

J. H. L. WATSON.—The X-ray diffraction pattern lines are broadened but not extremely so. We have not calculated particle sizes from line broadening.

A. S. MICHAELS (Massachusetts Institute of Technology).—Is there, perhaps, a parallelism between the apparent "single crystal" character of β-FeOOH tactoids, and the same character of hydroxyapatite sub-crystals formed within collagen fibers, as reported by M. Glimscher and his Colleagues of Massachusetts General Hospital?

J. H. L. WATSON.—In principle there is no reason why any crystal might not form tactoids if the proper conditions for such formation are established. It is precisely these "proper conditions" for β-FeOOH which are under investigation in our work.

INVESTIGATION OF A FIRST-ORDER SLIP-FLOW CONTINUUM ANALYSIS: THE THERMAL FORCE[1]

BY JAMES R. BROCK

Department of Chemical Engineering, The University of Texas, Austin, Texas

Received March 12, 1962

Comparison of an equation for the thermal force on aerosol particles, derived by a first-order slip-flow continuum analysis, with experimental thermal force data reveals that the analysis breaks down for Knudsen numbers greater than 0.25. Evaluation of first-order slip-flow coefficients from thermal force data is discussed. Numerical values of the slip-flow coefficients are reported for several gas–surface systems.

In a previous note by the author,[2] the Navier–Stokes equations with first-order slip-flow boundary conditions were used to develop an equation for the thermal force acting on aerosol particles. The disagreement, pointed out by Schadt and Cadle,[3a] between a previous continuum theory[3b] of the thermal force and experiment was explained. It was suggested[2] that the analysis was valid for only the slip-flow regime, characterized by values of the Knudsen number,[4] l/a, less than one.

A purpose of this note is to fix the range of Knudsen number for which the first-order slip-flow description of the thermal force can be applied.

An unresolved problem of rarefied gas dynamics is the determination of the upper limit of the Knudsen number for which a description of a physical system using the Navier–Stokes equations and first-order slip-flow boundary conditions breaks down. Inasmuch as the thermal force on aerosol particles is a phenomenon existing only for $(l/a) > 0$, one has in the thermal force a sensitive test of a first-order slip-flow continuum analysis.

Here the developed thermal force equation[2] will be tested with appropriate existing experimental data for the thermal force on aerosol particles. The range of validity of a first-order slip-flow continuum analysis will be specified and methods for determining the slip-flow coefficients from thermal force experimental data will be investigated.

Thermal Force Theory in the Slip-Flow Regime.—From the solution of the steady-state Navier–Stokes equations with first-order slip-flow boundary conditions, the following expression for the force experienced by a spherical particle suspended in a gas in a temperature gradient is obtained.[2]

$$\vec{K} = -12\pi a^2 \mu \frac{c_{tm}\left(\frac{l}{a}\right)}{\left(1 + 3c_m\left(\frac{l}{a}\right)\right)} \times \frac{\left(\frac{k_f}{k_s} + c_t\left(\frac{l}{a}\right)\right)}{\left(1 + 2\frac{k_f}{k_s} + 2c_t\left(\frac{l}{a}\right)\right)} \nabla T_\infty \quad (1)$$

$\vec{K}$	=	thermal force
a	=	radius of aerosol particle
k_f	=	thermal conductivity of gas surrounding particle
k_s	=	thermal conductivity of particle
∇T_∞	=	uniform temp. gradient, large distance from particle
T	=	absolute temperature
ρ	=	mass density
μ	=	coefficient of shear viscosity
c_m	=	tangential momentum first-order slip coefficient
c_t	=	temp. jump first-order slip coefficient
c_{tm}	=	thermal creep first-order coefficient

In comparing eq. 1 with experimental data the major difficulty arises in the determination of the correct values of the slip-flow coefficients, c_t, c_m, and c_{tm}.

Expressions for c_t, c_m, and c_{tm} were first developed by Maxwell[5a] and Knudsen[5b] from simple kinetic theory arguments. Since then, more exact treatments of boundary conditions have led to slight alterations in the magnitudes of c_t, c_m, and c_{tm}. A discussion of these treatments may be found elsewhere.[6]

These more exact expressions for the slip-flow coefficients have all been for monatomic gases impinging on plane walls. Much of the appropriate data for the thermal force has been taken

(1) This work was supported by Grant G 19432 of the National Science Foundation.

(2) J. R. Brock, *J. Colloid Sci.*, to be published.

(3) (a) C. F. Schadt and R. D. Cadle, *J. Phys. Chem.*, **65**, 1689 (1961); (b) P. S. Epstein, *Z. Physik*, **54**, 537 (1929).

(4) l is the molecular mean free path and a is the radius of the aerosol particle.

(5) (a) J. C. Maxwell, "The Scientific Papers of James Clerk Maxwell," Dover Publications, Inc., New York, N. Y., 1952, pp. 681–712; (b) M. Knudsen, *Ann. Physik*, **34**, 593 (1911).

(6) R. E. Street, in "Rarified Gas Dynamics," Pergamon Press, New York, N. Y., 1960, pp. 276–292.

with air impinging on spherical aerosol particles of such size that curvature effects cannot be ignored.

Simple semi-macroscopic arguments have been used in deriving the slip-flow coefficients[7] which are supposed valid for monatomic and polyatomic gases impinging on plane walls. The correctness of applying these expressions to the *a priori* evaluation of the slip-flow coefficients remains to be determined.

Fortunately, in measuring the thermal force on aerosol particles it is necessary to obtain independently an isothermal value of c_m. The problem of comparing eq. 1 with experiment is reduced, therefore, to the determination of the two remaining coefficients, c_t and c_{tm}.

The semi-macroscopic derivations of the slip-flow coefficients mentioned above apply analogous arguments for the development of c_t and c_m. In the instance of c_m one considers the net tangential momentum transfer to a wall; for c_t one considers the net energy transfer to a wall. The same simple kinetic theory assumptions are involved in each instance and the effect of any deviation from plane wall geometry should be the same for both c_t and c_m. Consequently from a known experimental value of c_m a good estimate of c_t should be possible. This method will now be discussed briefly.

The expression given for the semi-macroscopic derivation[7] of c_m can be modified to remove the simple kinetic theory and plane wall assumptions. If this is done, c_m is given by

$$c_m = \frac{\lambda_1(1 - \lambda_2 a_m)}{\lambda_3 a_m} \qquad (2)$$

where λ_1, λ_2, and λ_3 indicate unknown constants whose values would be determined by a rigorous analysis of the physical system. a_m is the tangential momentum accommodation coefficient and has a value of one if a molecule striking the surface achieves complete equilibrium with the surface and a value of zero if specular reflection occurs. Discussion of a_m can be found in various sources.[7,8] It is sufficient to observe that at present it is not possible to make an *a priori* calculation of a_m.

By similar argument, the following expression can be found for c_t

$$c_t = 2\lambda_1 \frac{(1 - \lambda_2 a_t)}{\lambda_3 a_t} \frac{k_f}{(1 + \gamma)c_v \mu} \qquad (3)$$

where γ is the ratio of the heat capacity at constant pressure to that at constant volume, c_p/c_v. λ_1, λ_2, and λ_3 are taken as the same constants appearing in eq. 2. Here, a_t is the thermal accommodation coefficient. A value of a_t of one signifies that a molecule hitting the surface achieves complete thermodynamic equilibrium with the surface before leaving; an a_t of zero signifies specular reflection with no net energy interchange. As for a_m, a_t cannot be calculated by present methods with any certainty and must be regarded as subject to experimental determination.

In view of the fact that a_t and a_m are both measures of the extent to which impinging molecules achieve thermodynamic equilibrium with the surface, it seems appropriate to assume $a_t \approx a_m$, which is, however, probably not valid in general for polyatomic molecules where the relaxation time for transfer of energy between translational and internal degrees of freedom may be large. For air on various surfaces, it is usually observed[9] that a_t and a_m are both very near 1.0.

With the assumption noted above, the following expression can be used for estimation of c_t from an experimental value of c_m

$$c_t = \frac{2\left(\frac{k_f}{c_v \mu}\right)}{(\gamma + 1)} (c_{m,exptl.}) \qquad (4)$$

where $c_{m,exptl.}$ indicates an isothermal experimentally determined value in thermal force measurements.

c_{tm} remains as the only undetermined coefficient in eq. 1. According to a semi-macroscopic analysis,[7] c_{tm} is

$$c_{tm} = \frac{3}{4}\left(\frac{2R}{\pi T}\right)^{1/2} \qquad (5)$$

More rigorous calculations of c_{tm} were not found in the literature nor evidently have any experimental determinations of this coefficient been reported.

It will be shown that from eq. 1 and an experimental determination of c_m, c_t and c_{tm} can be evaluated from experimental thermal force measurements.

Evaluation of Slip-Flow Coefficients and Range of Validity of the Slip-Flow Continuum Analysis.—Equation 1 can be rearranged in the following manner

$$\frac{|\vec{K}|\left[\frac{a}{l} + 3c_m\right]}{|\nabla T_\infty| a^2 \delta} \equiv \frac{|\vec{K}|\left[\frac{a}{l} + 3c_m\right]}{9\pi\left(\frac{2R}{\pi T}\right)^{1/2} \mu a^2 |\nabla T_\infty|} = \epsilon\left(\frac{\frac{k_f}{k_s} + c_t\left(\frac{l}{a}\right)}{1 + 2\frac{k_f}{k_s} + 2c_t\left(\frac{l}{a}\right)}\right) \qquad (6)$$

where ϵ denotes the ratio of the true value of c_{tm} to that given by eq. 5. From eq. 6 it is evident that ϵ is given by the limit of eq. 6 as $l/a \to 0$. This value is independent of any estimated value for $c_t \cdot \epsilon$ and therefore c_{tm} can then be evaluated from experimental thermal force data at sufficiently low (l/a) and experimental values of c_m, k_f, and k_s.

Equation 1 can be rearranged further to give eq. 7

(7) E. H. Kennard, "Kinetic Theory of Gases," Chapt. 8, McGraw-Hill Book Co., New York, N. Y., 1938.

(8) I. Estermann, in "Rarified Gas Dynamics," Pergamon Press New York, N. Y., 1960, pp. 38–53.

(9) S. A. Schaaf and L. Talbot, "Mechanics of Rarified Gases," NAVORD Report 1488, Vol. 5, 1959.

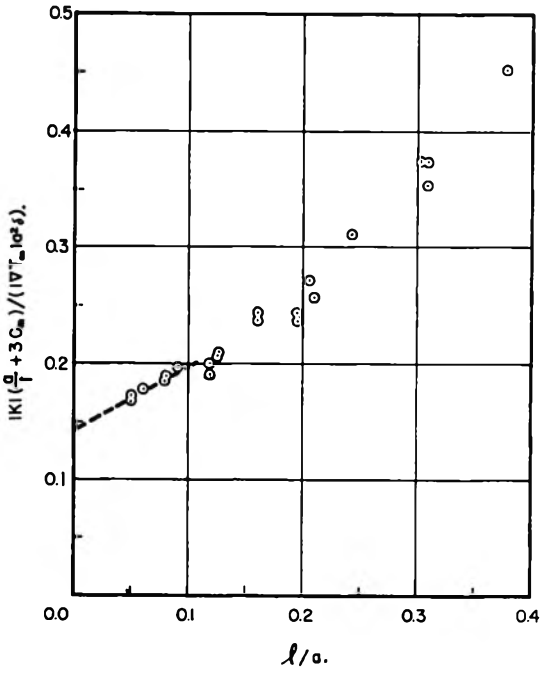

Fig. 1.—Intercept determination of ϵ for the data of Rosenblatt and LaMer.[11]

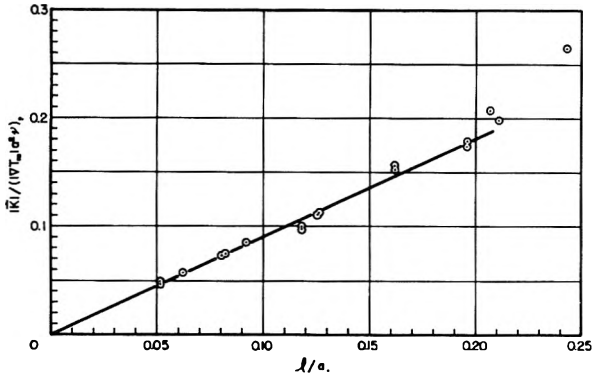

Fig. 2.—The predicted linear relation of eq. 7 for the data of Rosenblatt and LaMer.[11]

$$\frac{|\vec{K}|}{|\nabla T_\infty| a^2 \nu} \equiv \frac{|\vec{K}| \left[1 + 3c_m \left(\frac{l}{a}\right)\right]\left[1 + 2\frac{k_f}{k_s} + 2c_t \left(\frac{l}{a}\right)\right]}{9\pi \left(\frac{2R}{\pi T}\right)^{1/2} \mu a^2 |\nabla T_\infty| \left[\frac{k_f}{k_s} + c_t \left(\frac{l}{a}\right)\right]} = \epsilon \left(\frac{l}{a}\right) \quad (7)$$

where ϵ is now given by the slope of the indicated linear relation. The value of ϵ determined by this equation does depend on the estimated value of c_t. If values of ϵ determined by these methods, eq. 6 and 7, are in agreement, then the estimated value of c_t is the correct value.

Therefore, experimental thermal force measurements at sufficiently low l/a provide a useful technique for determination of the slip-flow coefficients c_t and c_{tm}.

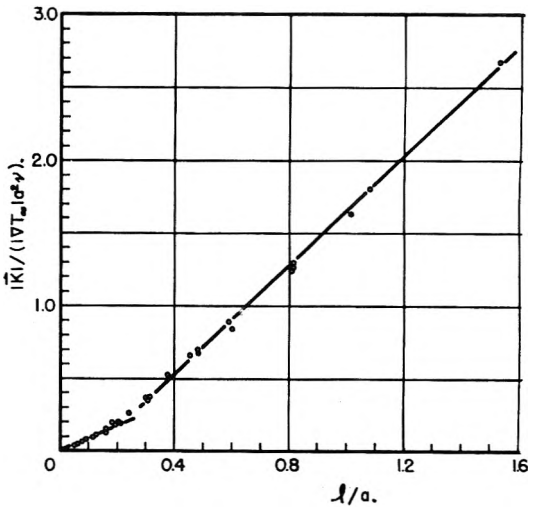

Fig. 3.—Departure of experimental data from first-order slip-flow continuum analysis for data of Rosenblatt and LaMer.[11]

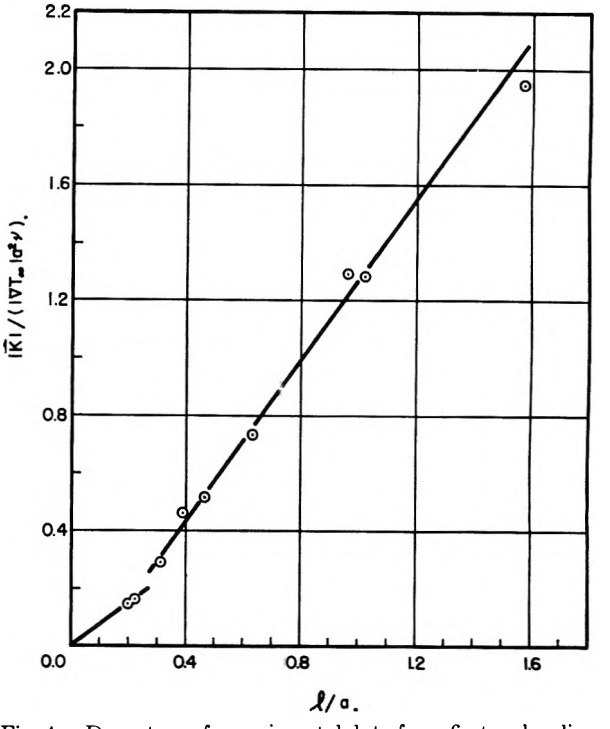

Fig. 4.—Departure of experimental data from first-order slip-flow continuum analysis for data of Schmitt.[12]

Various experimental thermal force measurements have been reported.[3a,10-12] Of these measurements, only the data of Rosenblatt and LaMer were taken at sufficiently low l/a and were sufficiently free of scatter to permit a test of the methods discussed above.

Figure 1 shows the intercept determination of ϵ for the data of Rosenblatt and LaMer for TCP droplets in air at 300°K. A recent experimental determination[13] of the thermal conductivity of TCP was used in the calculation by eq. 6 of the value of ϵ reported in Table I. It would be desir-

(10) R. L. Saxton and W. E. Ranz, *J. Appl. Phys.*, **23**, 917 (1952).
(11) P. Rosenblatt and V. K. LaMer, *Phys. Rev.*, **70**, 385 (1946).
(12) K. H. Schmitt, *Z. Naturforsch.*, **14a**, 589 (1959).
(13) O. B. Cecil and R. H. Munch, *Ind. Eng. Chem.*, **48**, 437 (1956).

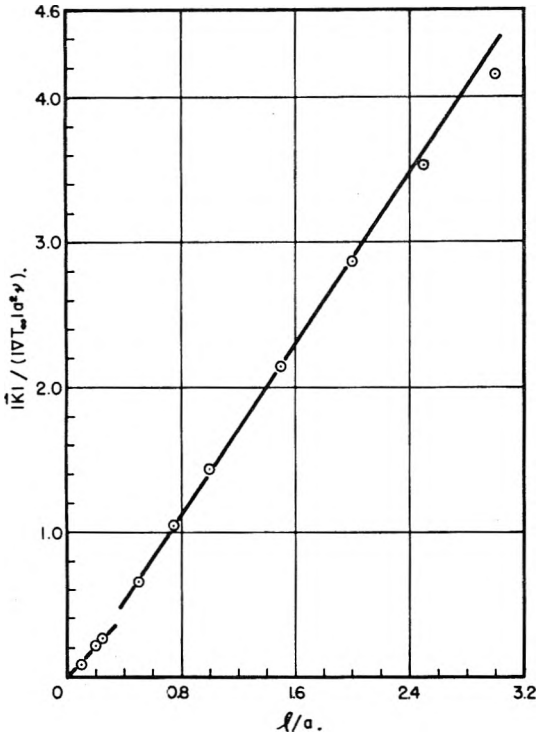

Fig. 5.—Departure of experimental data from first-order slip-flow continuum analysis for data of Schadt and Cadle,[3a] sodium chloride aerosols in air.

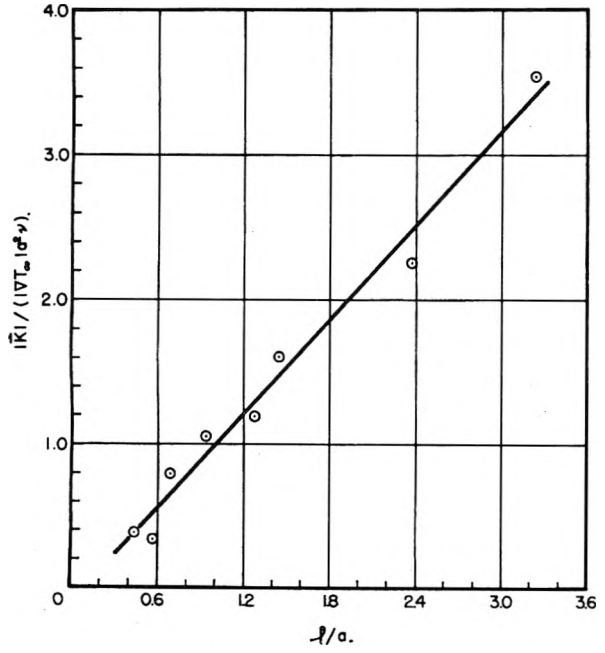

Fig. 6.—The empirical linear relation of eq. 8 for the data of Schadt and Cadle,[3a] mercury aerosols in air.

able to have thermal force measurements at lower l/a since the indicated extrapolation cannot be performed with great accuracy.

Figure 2 shows the predicted linear relation of eq. 7 for the same data of Rosenblatt and LaMer for $(l/a) < 0.30$. The value of c_t estimated from eq. 4 was used in the calculations. The isothermal experimental value of c_m reported by Rosenblatt and LaMer was 1.23. The data were fitted by a least-squares line to within an average deviation of $\pm 3.0\%$, giving the indicated value of ϵ shown in Table I.

As stated above, the intercept evaluation of ϵ is rather uncertain. Consequently, alteration of the value of c_t reported in Table I is not justified without additional thermal force data at lower values of l/a.

TABLE I

DETERMINED VALUES FOR THE SLIP COEFFICIENTS

Thermal force data source	c_m Exptl.	c_t Eq. 4	ϵ Eq. 7	ϵ Eq. 6
Rosenblatt and LaMer,[11] TCP aerosols in air	1.23	1.94	0.91	0.99
Schmitt,[12] PH300 silicon oil in argon	1.42	2.57	1.06	..
Schadt and Cadle,[3a] sodium chloride aerosols in air	..	..	(0.74)	..

Figure 3 presents all the reported data of Rosenblatt and LaMer. It can be seen that the first-order slip-flow analysis breaks down at $(l/a) \approx 0.25$. The data for $0.25 < (l/a) < 1.6$ can be represented by an empirical modification of eq. 7 to within $\pm 8\%$

$$\frac{|\bar{K}|}{|\nabla T_\infty| a^2 \nu} = \epsilon' \left(\frac{l}{a}\right) + r \qquad (8)$$

where for the reported data $\epsilon' = 1.860$ and $r = -0.212$.

The data of Schmitt for PH300 silicon oil droplets in argon at 299°K. are presented according to eq. 7 in Fig. 4. Schmitt reported a value of c_m of 1.42. c_t was estimated by eq. 4. The calculated value of ϵ according to eq. 7 is given in Table I. An intercept determination of ϵ was not possible.

For $0.25 < (l/a) < 2.2$ the data of Schmitt are represented to within approximately $\pm 1\%$ by the empirical relation, eq. 8, with $\epsilon' = 1.42$ and $r = -0.06$.

The data of Schadt and Cadle for sodium chloride aerosols in air at 307°K. are shown in Fig. 5 according to eq. 7 for $(l/a) < 0.25$. No value of c_m was reported, so the value of 1.23 was assumed. The determined value of ϵ, subject to correction, is given in Table I. It can be seen that the data for $0.25 < (l/a) < 1.6$ obey the apparent empirical linear relation of eq. 8. The data of Schadt and Cadle for mercury aerosols in air also show this empirical linear relation, as can be seen in Fig. 6.

Discussion

On the basis of the present limited comparison with existing appropriate thermal force data, it may be concluded that the first-order slip-flow continuum description of the thermal force breaks down rather abruptly at $(l/a) \approx 0.25$.

Where an approximate determination of ϵ and c_t was possible, it appears that the value of c_{tm} is not greatly different from the value predicted by eq. 5. Also on the basis of the limited comparison, the estimation method for c_t of eq. 4 appears applicable.

The linear relation observed for $0.25 < (l/a) < 2$ remains to be explained, as well as the rather abrupt departure from the first-order slip-flow analysis that has been noted.

From these preliminary results it may be inferred that experimental thermal force measurements may prove to be a useful method for gaining a better understanding of the rather complicated behavior of a non-uniform gas at a boundary.

DISCUSSION

V. K. LA MER (Columbia University).—It appears from recent work, particularly that of Schadt and Cadle, that proof of the Epstein equation, although well checked for aerosols like tricresyl phosphate, is not found for thermally conducting metallic aerosols. Does the author's treatment shed any light on this problem?

J. R. BROCK.—The agreement (within 20% at $(l/a) \sim 0.1$, 50% at $(l/a) \sim 0.2$) of the Epstein equation with experimental data for tricresyl phosphate and substances of similar thermal conductivity ($\sim 10^{-4}$ cal./cm.-sec.-deg.) is merely circumstantial and has been misleading. The apparent agreement is dependent on the relative magnitudes of the thermal conductivity of the aerosol particle and the thermal conductivity of the fluid surrounding the particle.

The experimental work of Schadt and Cadle with aerosols of thermal conductivity ($\sim 10^{-2}$ cal./cm.-sec.-deg.) much larger than that of tricresyl phosphate, gives results, by extrapolation in the first-order slip-flow regime, for the thermal force which are higher than those predicted by the Epstein equation by *factors* of 30 to 50. Thus the Epstein equation fails in this instance.

The data of Schadt and Cadle for these high thermal conductivity aerosols were not taken to $(l/a) < 0.25$. Hence a comparison of direct experimental data with the first-order slip-flow analysis presented here is not possible. However, extrapolation of the data of Schadt and Cadle to $(l/a) < 0.25$ for these aerosols indicates agreement with the present analysis within ~ 10–30%.

The agreement of the accurate thermal force data of Rosenblatt and La Mer for tricresyl phosphate aerosols with the present analysis must be regarded as very good. Additional accurate thermal force data for $(l/a) < 0.25$ for a variety of substances would be most valuable. In such data it should be remembered that the surface properties of the aerosol are of importance.

PARTICLE SIZE DISTRIBUTION IN RUBBER LATEX

BY M. WALES

Shell Development Company, Emeryville, California

Received March 12, 1962

Turbidity spectra were measured for various polyisoprene latex samples in the region 0.6–1.1 μ on a Cary Model 14 spectrophotometer. The validity of the measurements was checked by comparison with turbidity spectra of polystyrene latices of known diameter. Results were interpreted in terms of a weight median particle diameter and a breadth parameter for an equivalent log normal distribution. These results were compared with particle count *vs.* diameter from Coulter counter measurements. The actual particle size distributions are quite closely log normal, at least on the high diameter end.

Introduction

This paper is concerned with the general problem of rapid, routine particle size analyses in aqueous dispersions, particularly in latex produced artificially from synthetic *cis*-polyisoprenes. Data on comparison of turbidity spectra with Coulter counter[1–3] results on Hevea and synthetic *cis*-polyisoprene latices will be presented.

Experimental

Turbidity Spectra.—Recently, Wallach, Heller, and Stevenson[4] have prepared tables for use in interpreting turbidity spectra. These tables were not available at the time this work was done. The interpretation of our turbidity data was done in much the same way as suggested by these authors, except that the data were not normalized to a reference wave length and that a log normal distribution of diameter was employed as a standard distribution function instead of the function used by Wallach, *et al.* In our work, tables of τ/c (turbidity/concentration) were calculated on a Bendix G-15D computer at each of four standard wave lengths for a range of the two distribution parameters in the log normal function using the Mie theory.[5] A brief outline of these calculations is given in the Appendix. A simplified representative plot of these values is shown for $\lambda = 0.65$ μ in Fig. 1. Here β is the breadth parameter of the log normal and is equal to $\sigma\sqrt{2}$, where σ is the standard deviation and D_{wm} is the weight median diameter. (Diameter at the 50% by weight point.) Then, from the value of τ/c at each of the four wave lengths, a curve of β *vs.* D_{wm} is determined. The intersection of these four curves fixes the parameters D_{wm} and β for an equivalent log normal distribution, as in Fig. 2. It must be borne in mind in using these curves that for dispersions of very small particle size, the size distribution has no effect on the turbidity, which is determined solely by the diameter equivalent to the weight average particle weight, rather than the weight median diameter. (Rayleigh scattering, $D \leq 0.1\lambda$). A criterion for this condition is, of course, the constancy of the quantity $(\lambda^4\tau/c)/(n - n_0)^2$.

In the calculation of these families of τ/c curves, the effect of dispersion was taken into account, in the refractive indices of both phases. The refractive index of Hevea, as measured by Wood, *et al.*,[6] was used. The refractive index of water was calculated from a relation in the International Critical Tables.[7] The resulting values of m for the rubber-water system can be fitted by least squares to a function of the form

$$m = \frac{n}{n_0} = 1.134406 + \frac{0.00152547}{\lambda^2} + \frac{0.000149881}{\lambda^4} \quad (1)$$

where n is refractive index of particles, n_0 that of the medium, and λ is the wave length in microns, *in vacuo*. A small correction was made in calculating τ/c, for the fact that latices were diluted for measurement in 0.1% Triton X-100, rather than in pure water, but this was insignificant. The density of rubber was taken as 0.906 g./cc.

Measurement of Turbidity.—The turbidity of latex dilutions of 2–15 $\times 10^{-6}$ g./ml. solids was measured in 10-cm. cells in a Cary Model 14 spectrophotometer, in the range $\lambda = 0.6$ to 1.1 μ. No change of τ/c with concentration was observed in this range. (At very small pen displacements τ/c tended to be larger than at large displacements, but the same effect was found with the ratio of absorbance to concentration for aqueous $CuSO_4$.) This instrument was selected because in this wave length range its optical system has a very small angle of acceptance at the detector, minimizing reception of forward scattered radiation,[8,9] and the beam has to pass through a number of slits. Furthermore, the instrument has a wave length dispersion, $\Delta\lambda$, of 37 Å./mm. slit. The instrument is of the double beam type, with blackened cell chambers. A solution of 0.1% Triton X-100 in water served as the reference. In order to test the reliability of these measurements, the turbidity of a number of Dow standard polystyrene latices was measured over the wave length range 0.6 to 1.1 μ. Results are shown in Table I. Agreement with theory for the 0.814 μ latex is almost perfect; in the case of the 0.088 μ latex the material seems to behave more like a monodisperse material of 0.083 μ than 0.088 μ.[10]

The deviations between the theoretical and measured values of τ/c may also be connected in some cases with the value of $\Delta\lambda/\lambda$; *i.e.*, one cannot distinguish[11] in fact between a dispersion in diameter (D) and between a dispersion in α, where

$$\alpha = \frac{\pi n_0 D}{\lambda} \quad (2)$$

In the case of the 1.17 μ latex, some forward scattering radiation may have been received, because of its large particle size.[8] The deviations from theory in this case cannot be explained from the deviations from monodispersity found by Coulter counter measurements.[12] (Last row of Table I.) We are indebted to Dr. J. W. van der Hoff of Dow Chemical Company for these latices. This is Sample 1 of reference 12.

In order to compare theory with experiment it was necessary to estimate values of m for the polystyrene–water system. The refractive index of polystyrene *vs.* wave length was obtained from industrial research.[13] For polystyrene

$$m = 1.18392 + \frac{0.00261227}{\lambda^2} + \frac{0.000309505}{\lambda^4} \quad (3)$$

where λ is wave length *in vacuo*, microns. The density of polystyrene was taken as 1.057.

(1) R. H. Berg, ASTM Special Publication No. 234 (1958).

(2) H. E. Kubitschek, *Nature*, **182**, 234 (1958).

(3) C. F. T. Mattern, F. S. Brackett, and B. J. Olson, *J. Appl. Physiol.*, No. **10**, 1 (1957).

(4) M. L. Wallach, W. Heller, and A. F. Stevenson, *J. Chem. Phys.*, **34**, 1796 (1961).

(5) G. Mie, *Ann. Phys.*, **25**, 377 (1908); H. C. Van de Hulst, "Light Scattering by Small Particles," John Wiley and Sons, Inc., New York, N. Y., 1957.

(6) L. A. Wood and L. W. Tilton, *J. Research Natl. Bur. Standards*, **43**, 57 (1949).

(7) "International Critical Tables," McGraw-Hill Book Co., New York, N. Y., Vol. VII, p. 13.

(8) R. O. Gumprecht and C. M. Sliepcevich, *J. Phys. Chem.*, **59**, 849 (1955).

(9) W. Heller and R. M. Tabibian, *J. Colloid Sci.*, **12**, 25 (1957).

(10) In this connection see G. Dezelic and J. P. Kratohvil, *J. Colloid Sci.*, **16**, 561 (1961).

(11) M. L. Wallach, private communication.

(12) M. Wales and J. N. Wilson, *Rev. Sci. Instr.*, **32**, 1132 (1961).

(13) Polaroid Corporation, "Optical Plastic Material: Synthesis, Fabrication, and Instrument Design," OSRD Report No. 4417 (1945).

TABLE I

TURBIDITY MEASUREMENTS ON DOW MONODISPERSE POLYSTYRENE LATICES

A. $D = 0.088\ \mu$											
λ_1, μ	0.60	0.65	0.70	0.75	0.80	0.85	0.90	0.95	1.00	1.05	1.10
Av. τ/c, 4.5–13.5 $\times 10^{-4}$ g./ml. Four concn.	685	489	361	275	215	171	138	115	97	83	71
Theoretical τ/c. $D = 0.083\ \mu$	716	520	384	290	223	175	138	108	90	74	61
$D = 0.088\ \mu$	850	616	456	348	265	208	165	132	108	88	73
B. $D = 0.264\ \mu$; τ/c multiplied by 10^{-3}											
Av. τ/c, 2–6 $\times 10^{-6}$ g./ml. Four concn.	9.65	7.66	6.25	5.11	4.26	3.55	2.95	2.47	2.13	1.80	1.53
Theoretical τ/c	9.74	7.90	6.48	5.36	4.43	3.68	3.09	2.59	2.18	1.84	1.57
C. $D = 0.365\ \mu$; τ/c multiplied by 10^{-3}											
Av. τ/c, 8–20 $\times 10^{-6}$ g./ml. Four concn.	15.6	12.3	9.88	8.18	7.04	6.03	5.23	4.54	4.03	3.74	3.18
Theoretical τ/c	16.7	13.2	10.6	8.75	7.30	6.17	5.31	4.64	4.08	3.60	3.11
D. $D = 0.814\ \mu$; τ/c multiplied by 10^{-4}											
Av. τ/c, 7–11 $\times 10^{-6}$ g./ml. Two concn.	3.50	3.02	2.62	2.30	2.05	1.82	1.63	1.46	1.31	1.19	1.07
Theoretical τ/c	3.62	3.11	2.69	2.36	2.07	1.82	1.62	1.45	1.33	1.21	1.11
E. Sample 1; $D = 1.171\ \mu$; τ/c multiplied by 10^{-4}											
τ/c at 10^{-6} g./ml.	3.12	2.93	2.72	2.53	2.34	2.17	1.99	1.82	1.68	1.56	1.45
Theoretical τ/c	3.89	3.60	3.28	2.94	2.68	2.42	2.20	2.00	1.82	1.66	1.52
τ/c from Coulter counter distribution[12]		3.32			2.59			1.98			1.54

Coulter Counter Measurements.—The Coulter counter is an instrument in which colloidal particles flow through a small orifice in very dilute suspension. Simultaneously an electric current is flowing through the orifice and as each particle passes, a momentary change in voltage drop occurs, which is amplified and counted. By means of a discriminator circuit it is possible to count only those pulses greater than some adjustable arbitrary threshold, the size of the pulse being nearly proportional to particle volume. A known small volume of suspension is automatically metered through the orifice. The instrument is described more fully elsewhere.[1-3,14]

With a 30 μ orifice, the instrument can detect particles not smaller than 0.5 μ in diameter. This restricts its applicability to latices of small particle size.

Preparation of Latex for Measurements.—Suspensions first were diluted in 0.1% Triton X-100 (a non-ionic surfactant) and then a very small known quantity of this dilution was added with stirring *via* a gravimetrically calibrated Calab micro-syringe to 250 ml. of the electrolyte, 2% NaCl containing 0.1% Triton X-100 as a dispersant. It is believed that the very low final particle concentration (of the order of 1 p.p.m. latex solids or less) plus the presence of relatively large amounts of surfactant are effective in suppressing coagulation, at least for times an order of magnitude greater than the time of measurement. No evidence of instability, as shown by a systematic drift of count with time, has ever been noticed.

The electrolyte always was filtered through Millipore filters of 0.3 or 0.45 μ pore size. The 250 ml. graduated sample beaker of the apparatus was filled with filtered electrolyte, after washing with the same. Then a background count was made over the whole range of thresholds. The measured amount of latex dilution then was added, and the final count made over the range of thresholds, the background count being subtracted. If necessary, more latex dilution was added to the beaker to obtain counts at high thresholds and the resulting count scaled appropriately to tie in with the previous lower concentration count. Usually this scaling was done by repeating several counts at thresholds previously counted and employing the ratios of coincidence corrected counts.

Results and Discussion

A representative cumulative number distribution for a Hevea latex, obtained with the Coulter counter, is shown in Fig. 3. The general form of these curves for the polyisoprene latices is the same as in Fig. 3. The curves through the data were obtained by fitting the points to a cumulative log-normal distribution in threshold, where the threshold, t, is proportional to particle volume.

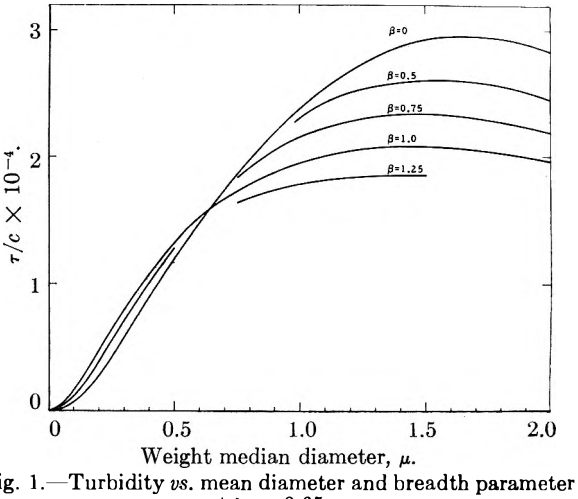

Fig. 1.—Turbidity *vs.* mean diameter and breadth parameter at $\lambda = 0.65\ \mu$.

$$1 - \frac{2N}{N_0} = P\left(\frac{1}{\beta_t} \ln \frac{t}{t_0}\right) \qquad (4)$$

where N is the true count at threshold t, N_0 is the total number of particles in the metered volume which passes through the orifice, t_0 is the number median threshold, and $\beta_t = 3\beta$. The P notation refers to the probability integral

$$P(x) = \frac{2}{\sqrt{\pi}} \int_0^x e^{-s^2}\, ds \qquad (5)$$

The fitting was done by a machine procedure for a number of assumed values of N_0, subject to the constraint that

$$V = \frac{\pi N_0 D_{wm}{}^3}{6} e^{-2.25\beta^2} \qquad (6)$$

(14) Operating Manual, Coulter Industrial Sales Corp., P. O. Box 22, Elmhurst, Ill.

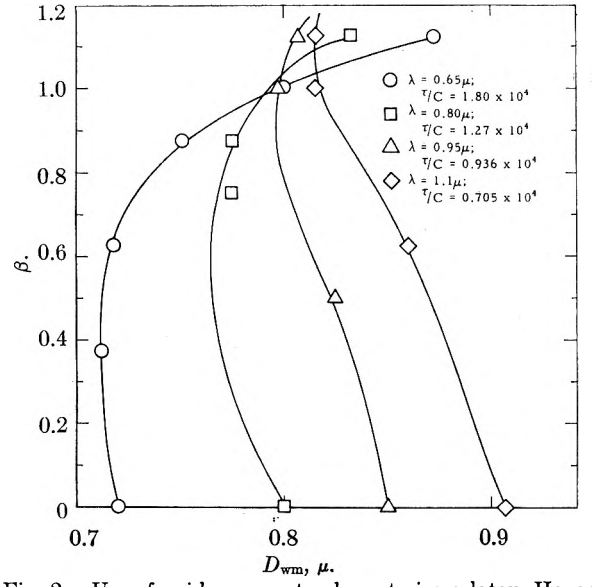

Fig. 2.—Use of guide curves to characterize a latex, Hevea NC400.

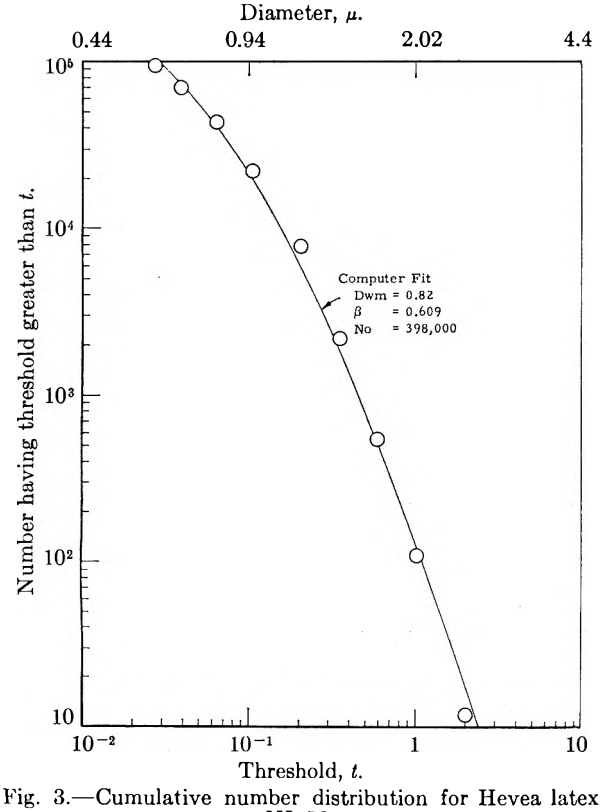

Fig. 3.—Cumulative number distribution for Hevea latex NL 76.

where V is a known quantity, the volume of particles in cubic microns per metered volume. The residual sum of squares also was obtained, but this was insensitive to the choice of N_0. Since the fit of eq. 4 to the data was uniformly good, the values of D_{wm} and β obtained from this type of curve fitting were taken as characteristic parameters for each latex sample.

Note that for the Hevea latices, about 30% *by number* of the sample is accessible to the counter. The weight percentage is, of course, much higher, since we are dealing with a lower counting limit of 0.5 μ and values of D_{wm} which usually are considerably higher than this.

In Table II is shown a comparison between values of D_{wm} and β obtained from the Coulter counter and from turbidity spectra, for a number of polyisoprene and Hevea latices.

TABLE II

DISTRIBUTION PARAMETERS FOR VARIOUS LATICES

Latex	Polymer	D_{wm}, wt. median diameter in μ — Counter	D_{wm} — Turbidity	β, distribution breadth — Counter	β — Turbidity	β from regression
1	Polyisoprene	0.92	0.84	0.94	1.34	0.97
2	Polyisoprene	1.02	1.05	.98	1.48	1.06
3	Polyisoprene	1.31	1.05	.81	1.25	0.90
4	Polyisoprene	1.23	1.18	.70	1.00	.72
5	Polyisoprene	1.82	2.0	.98	1.10	.79
6	Polyisoprene	..	0.51	..	1.1	.79
7	Polyisoprene	..	1.2	..	1.25	.90
NL 76	Hevea	0.82	0.78	.61	0.92	.66
NL 356	Hevea	0.83	0.72	.65	1.05	.76

Latices 6 and 7 were studied by electron microscopy, giving for latex 6, a number median diameter of 0.127 μ, D_{wm} of 0.53 μ, from which $\beta = 0.98$. Latex 7 had D_{wm} of 1.4 μ from electron microscope measurements.

Note that there is a slight tendency for turbidity spectra to give low weight median diameters compared to the counter, but that the parameter β obtained from turbidity measurements is uniformly high.

It is believed that the reasons for this finding are (a) the wave length dispersion $\Delta\lambda$ for the Cary spectrophotometer is not zero; (b) forward scattered radiation is being received by the detector to some extent.

Use of a wave length band of finite width would tend to have little effect on apparent diameter at a mean diameter where turbidity is not increasing very rapidly with diameter as is the case with these materials, but would produce an apparent widening of the distribution by a dispersion in α. The second effect would lower the apparent turbidity more at lower wave lengths than at higher ones and would tend to lower D_{wm} if the system lies below the maximum in τ/c *vs.* λ and to raise β. The second effect should lower the apparent turbidity increasingly severely as particle size increases.[8]

If anything, β values from the Coulter counter have been suspected as being too large.[12]

Finally, since the Coulter counter actually traces an appreciable part of the particle size distribution function, the β parameter derived from it is preferred. We find that if β from the counter is plotted *vs.* the turbidity β, the results can be represented quite well by a linear regression, using the method of least squares

$$\beta_{cc} = -0.008 + 0.728\beta_{turb} \approx 0.728\beta_{turb} \quad (7)$$

More data than are presented here were used in obtaining this relation, twelve comparisons in all. Values of β calculated from the turbidity values, by this relation, are shown in the last column of Table II.

Nearly all the polyisoprene samples in Table II were prepared as part of a polyisoprene latex research program by G. S. Ronay, W. M. Sawyer, K. E. Manchester, N. C. May, and W. C. Simpson of these Laboratories. Electron microscope data on two of these materials were made available through the courtesy of A. M. Cravath of these Laboratories.

Appendix

Turbidity Relationships in Polydisperse Suspensions.—For a monodisperse suspension

$$\tau = \frac{1}{l} \ln \frac{I_0}{I} = \frac{\pi K D^2 N}{4} \qquad (8)$$

where l = length of scattering path, I_0 and I are incident and emergent light intensities, D is particle diameter, N = number of particles/cc., and K is an involved function[15,16]

$$K = f(m,\alpha) \qquad (9)$$

where $m = n/n_0$ as previously defined and $\alpha = \pi n_0 D/\lambda$, λ measured *in vacuo*. For polydisperse suspensions

$$\tau = \frac{\pi}{4} \sum_i K_i D_i^2 N_i \qquad (10)$$

which becomes, in terms of concentration, c, in g./ml.

$$\tau/c = \frac{3}{2\rho} \sum_i \frac{K_i \gamma_i}{D_i} \qquad (11)$$

where ρ is particle density and γ_i is the weight fraction of species i in the disperse phase. For the case of a continuous distribution

$$\tau/c = \frac{3}{2\rho} \int_0^\infty \frac{K(\alpha,m)}{D} f(D)\mathrm{d}D \qquad (12)$$

where $f(D)$ is a differential *weight* distribution function in D normalized to unity.

A *number* distribution function

$$\mathrm{d}N = \frac{1}{\sqrt{\pi}} e^{-y^2} \mathrm{d}y \qquad (13)$$

was chosen, where

$$y = \frac{1}{\beta} \ln \frac{D}{D_0} \qquad (14)$$

and

$$D_{\mathrm{wm}} = D_0 e^{1.5\beta^2} \qquad (15)$$

With this choice, eq. 12 becomes

$$\tau/c = \frac{e^{-2.25\beta^2}}{\beta D_0^3 \sqrt{\pi}} \int_0^\infty \left(\frac{\tau}{c}\right)_i D^2 e^{-\frac{1}{\beta^2} \ln^2 \frac{D}{D_0}} \mathrm{d}D \qquad (16)$$

Here $(\tau/c)_i$ refers to τ/c for a monodisperse suspension of diameter D. The integration of eq. 16 for various values of D_{wm} and β at different wave lengths was carried out numerically by Weddle's Rule on the Bendix computer using the values of (τ/c_i) from Table III, which here have been rounded off to save space. A triangle approximation was used for the portion of the integral from $D = 5.4\ \mu$ to $D = \infty$.

The values in Table III had in turn been machine calculated from $K(\alpha,m)$ from the Mie relations. The reduction of these to an algebraic form suitable for computation is too long to reproduce here; Intercom 201 was used and the Bessel functions involved and their derivatives were obtained from $J_{\pm 3/2}(\alpha)$ and $J_{\pm 1/2}(\alpha)$ by repeatedly using the recursion relationships between successive cylinder functions. Values of $K(\alpha,m)$ for $m = 1.20$ and $\alpha = 0.2$, 3.0, and 10.0 were compared with the tables of Pangonis, Heller, and Jacobson[16] in checking out the program. Agreement to at least four significant figures was obtained.

TABLE III

CALCULATED TURBIDITIES OF MONODISPERSE POLYISOPRENE LATICES AT FOUR STANDARD WAVE LENGTHS

$10^{-4} \times \tau/c$, cm.²/g.

Diameter[a]	Wave length[a] 0.65	0.80	0.95	1.10
0.05	0.00745	0.00317	0.00157	0.000864
.10	.0548	.0240	.01209	.00672
.15	.1584	.0735	.0382	.0216
.20	.2980	.1505	.0819	.0476
.25	.4364	.2415	.1397	.0844
.30	.5688	.3307	.2037	.1288
.35	.7236	.4147	.2660	.1762
.40	.8981	.5055	.3248	.2223
.45	1.056	.6118	.3851	.2659
.50	1.195	.7235	.4353	.3093
.55	1.340	.8245	.5303	.3567
.60	1.484	.9148	.6077	.4101
.65	1.618	1.006	.6781	.4676
.70	1.745	1.100	.7418	.5243
.75	1.865	1.191	.8043	.5763
.80	1.981	1.276	.8691	.6237
.85	2.094	1.359	.9346	.6696
.90	2.197	1.438	.9974	.7167
.95	2.290	1.513	1.057	.7651
1.00	2.383	1.587	1.115	.8130
1.05	2.469	1.660	1.171	.8589
1.10	2.543	1.728	1.225	.9029
1.15	2.614	1.789	1.277	.9457
1.20	2.679	1.849	1.329	.9874
1.30	2.786	1.964	1.427	1.067
1.40	2.865	2.059	1.513	1.144
1.50	2.921	2.144	1.597	1.217
1.60	2.949	2.214	1.669	1.281
1.70	2.952	2.269	1.734	1.343
1.80	2.932	2.314	1.792	1.401
1.90	2.893	2.341	1.841	1.451
2.00	2.830	2.359	1.882	1.499
2.10	2.752	2.362	1.916	1.540
2.20	2.659	2.354	1.942	1.577
2.30	2.551	2.334	1.958	1.608
2.40	2.431	2.303	1.969	1.634
2.50	2.307	2.263	1.972	1.657
2.60	2.173	2.213	1.968	1.672
2.70	2.036	2.157	1.956	1.684
2.80	1.900	2.090	1.940	1.691
2.90	1.763	2.021	1.915	1.693
3.00	1.626	1.943	1.888	1.691
3.40	1.150	1.605	1.723	1.640
3.80	0.8232	1.259	1.503	1.534
4.20	.6600	0.9513	1.259	1.386
4.60	.6279	.7186	1.020	1.213
5.00	.6707	.5756	0.8080	1.033
5.40	.7250	.5125	0.6391	0.8572

[a] Both expressed in μ, λ *in vacuo*.

Acknowledgment.—The author is indebted to S. J. Rehfeld for experimental assistance.

(15) "Tables of Scattering Functions for Spherical Particles," National Bureau of Standards, Applied Math. Series 4, U. S. Govt. Printing Office, 1948.

(16) W. S. Pangonis, W. Heller, and A. Jacobson, "Tables of Light Scattering Functions for Spherical Particles," Wayne Univ. Press, 1957.

DISCUSSION

V. K. LA MER (Columbia University).—In a paper to appear shortly in *J. Colloid Sci.*, Wachtel and I find agreement with Dr. Wales that the Coulter counter is a very rapid and accurate method of getting size distribution curves of fine and, in some cases, electrically charged emulsion droplets in the range 0.4 to 1.0 μ. After working the last fifteen years to determine particle size distributions from light scattering data alone in the absence of knowledge of the distribution function, I have abandoned these attempts as too tedious and unrewarding for the effort spent in favor of direct counting methods which extend light microscopic methods to much lower values.

R. D. VOLD (University of Southern California).—Do you have definitive evidence that your system is free of aggregates? If there should be any aggregation it is necessary to know the refractive index of the aggregate, the density of the aggregate, and the internal structure of the aggregate in order to derive its scattering coefficient and, since this information is generally not derivable from the observed data, interpretation in terms of a physically real system becomes nearly impossible.

M. WALES.—I would like to emphasize that there is no attempt here to determine a detailed particle size distribution by light scattering, but merely to derive a parameter by which one can rank various preparations in their order of polydispersity. Furthermore, for the distribution of sizes to have an effect on the turbidity, it is necessary that the ratio of particle diameter to wave length be such that one be not too far from the maximum in τ/c (see Fig. 1).

In regard to aggregation, if this were such that "interpretation in terms of a physically real system were impossible," the data of Table I could not have been obtained. These results are in agreement with those of Heller, *et al.*, *J. Colloid Sci.*, **11**, 195 (1956); Bateman, *et al.*, *ibid.*, **14**, 308 (1959); and Deželić, *et al.*, *ibid*, **16**, 561 (1961). We also have found that mean diameters of two Dow latices by the Coulter counter, using suspensions of known solids content, agree quite well with optical and electron microscope values. Also from dilution data in the Coulter counter, we find that concentration-dependent aggregation is most certainly absent. Changing the mode of dilution and the electrolyte does not change Coulter counter results for polystyrene or rubber latices. Finally, all of these measurements were made in the p.p.m. range of solids content or less, and in the presence of a large amount of surfactant.

THE STRUCTURE OF WATER AND HYDROPHOBIC BONDING IN PROTEINS. III. THE THERMODYNAMIC PROPERTIES OF HYDROPHOBIC BONDS IN PROTEINS[1,2]

GEORGE NÉMETHY[3] AND HAROLD A. SCHERAGA

Department of Chemistry, Cornell University, Ithaca, New York

Received February 27, 1962

A quantitative treatment of the thermodynamic properties of hydrophobic bonds in proteins is presented; it is based on the behavior of aqueous hydrocarbon solutions as a model system. A hydrophobic bond is considered to be formed when two or more non-polar groups come into contact, thereby decreasing the extent of the interaction with the surrounding water. The thermodynamic parameters are derived from a statistical thermodynamic treatment of pure water and of aqueous hydrocarbon solutions, developed in earlier papers. The conditions determining the thermodynamic parameters are discussed in terms of changes in the water structure, of intermolecular forces, and of the restrictions on internal bond rotation. It is shown that the latter restriction is less serious than for side-chain hydrogen bonding. Numerical values and closed expressions for the temperature dependence of the free energy, enthalpy, entropy, and heat capacity of formation of hydrophobic bonds between isolated pairs of non-polar side chains are given for the following residues: alanine, valine, leucine, isoleucine, methionine, cysteine, proline, and phenylalanine. The contributions of cystine and tryptophan are estimated. The dependence of the thermodynamic parameters on the size of the side chains and on the extent of contact between them is discussed, and the limiting values of the possible ranges are given. For an interaction between two side chains, the parameters at 25° have the ranges: $\Delta F_{H\phi}^0 = -0.2$ to -1.5 kcal./mole, $\Delta H_{H\phi}^0 = +0.3$ to $+1.8$ kcal./mole, $\Delta S_{H\phi}^0 = +1.7$ to $+11$ e.u., $(\Delta c_p^0)_{H\phi} = -10$ to -50 cal./deg. mole. The error in $\Delta F_{H\phi}^0$ is estimated to be less than 0.1 kcal./mole. The existence of hydrophobic bonds is due mainly to the entropy change connected with changes in the water structure around the side chains. The endothermicity of the process of formation of the hydrophobic bonds makes them stronger with increasing temperature up to 50–60°. It is shown that the thermodynamic parameters characterizing *isolated* side chains are affected only slightly in structures where there are few water layers between side chains not in contact. The free energy of formation of the hydrophobic bond can be attributed almost entirely to the step in which the two side chains actually come into contact, reducing the number of contacts with water. Hydrophobic bonds can contribute to the stabilization of various protein structures. Such bonds can exist in the random coil. In an α-helix, a given side chain can form hydrophobic bonds of limited strength with the next residues along the sequence, and with the third and fourth groups along the sequence, *i.e.*, on the next turns of the helix, nearest to it in space. The possible side-chain interactions in an α-helix are listed. Strong hydrophobic bonds between side chains are possible in the two pleated sheet structures. This may cause the β-structures to be favored over the α-helix at higher temperatures in polypeptides containing many groups capable of forming hydrophobic bonds. In compactly folded protein structures, several side chains can interact simultaneously to form hydrophobic bonds or hydrophobic regions, of greater strength. Expressions are given for the calculation of the thermodynamic parameters of formation of such bonds and for the transfer of side chains into a non-polar environment, discussed earlier by Kauzmann. Non-polar side chains carrying polar end groups can participate in hydrophobic bonding to a limited extent. The parameters for such bonds are estimated. An estimate of the volume increase on forming a hydrophobic bond is given.

1. Introduction

Papers I[5] and II[6] of this series were preliminary to the present one; the earlier papers contain a statistical thermodynamic treatment of water[5] and of aqueous hydrocarbon solutions.[6] The physical model and mathematical treatment, on which the present paper is based, are given in those papers.[5-7]

The conformations of proteins, as well as many of their reactions, are determined to a large extent by covalent disulfide bonds and by the non-covalent interactions of the side-chain groups; the latter include hydrogen bonds, hydrophobic bonds, and ionic interactions. Although increasing attention has been paid in recent years[4,8-13] to the role of hydrophobic bonds, *i.e.*, the interactions involving non-polar side chains, very little quantitative work has been directed so far toward the elucidation of their thermodynamic properties.[10] In the present paper, a quantitative treatment of the thermodynamic behavior of hydrophobic bonds and of their role in protein structure is given.[7]

Since non-polar groups can interact with each other and with the solvent only by means of van der Waals forces, early discussions of hydrophobic bonding considered it only in terms of these interactions.[14,15] However, it soon became recognized that changes in the structure of water surrounding the non-polar groups must play an important role in the formation of hydrophobic bonds and in determining the free energy change for this process.[16,17]

The interaction of non-polar groups with water is unfavorable; thus, there is a thermodynamic

(1) This work was supported by the Office of Naval Research (Contract Nonr-401(36)), by a research grant (E-1473) from the National Institute of Allergy and Infectious Diseases of the National Institutes of Health, Public Health Service, and by a research grant (G-14792) from the National Science Foundation.

(2) Presented in part at the Brookhaven Symposium on Protein Structure and Function, June, 1960 (Discussion following paper by Klotz[4]), and in part before the Division of Biological Chemistry at the 138th National Meeting of the American Chemical Society, New York, N. Y., September, 1960.

(3) General Electric Educational Fund, Charles E. Coffin Fellow 1957–1959, Cornell Senior Graduate Fellow 1959–1960, duPont Summer Research Fellow, summer 1958 and 1959.

(4) I. M. Klotz, *Brookhaven Symp. Biol.*, **13**, 25 (1960).

(5) G. Némethy and H. A. Scheraga, *J. Chem. Phys.*, **36**, 3382 (1962); to be referred to hereafter as paper I, with (I-) denoting equations cited.

(6) G. Némethy and H. A. Scheraga, *ibid.*, **36**, 3401 (1962); to be referred to hereafter as paper II, with (II-) denoting equations cited.

(7) It will be necessary for the reader to consult paper II for a full understanding of the material presented in paper III.

(8) I. M. Klotz, *Science*, **128**, 815 (1958).

(9) S. J. Leach, *Rev. Pure Appl. Chem.*, **9**, 33 (1959).

(10) W. Kauzmann, *Advan. Protein Chem.*, **14**, 1 (1959).

(11) H. A. Scheraga, *J. Phys. Chem.*, **65**, 1071 (1961).

(12) H. A. Scheraga, "Protein Structure," Academic Press, New York, N. Y., 1961.

(13) C. Tanford, "Physical Chemistry of Macromolecules," John Wiley & Sons, Inc., New York, N. Y., 1961, p. 129.

(14) K. U. Linderstrøm-Lang, "Proteins and Enzymes," Lane Medical Lectures, Stanford Univ. Press, Stanford, Cal., 1952, p. 57.

(15) D. F. Waugh, *Advan. Protein Chem.*, **9**, 325 (1954).

(16) W. Kauzmann, in "A Symposium on the Mechanism of Enzyme Action," W. D. McElroy and B. Glass, eds., Johns Hopkins University Press, Baltimore, Md., 1954, p. 70.

(17) J. G. Kirkwood, ref. 16, p. 16.

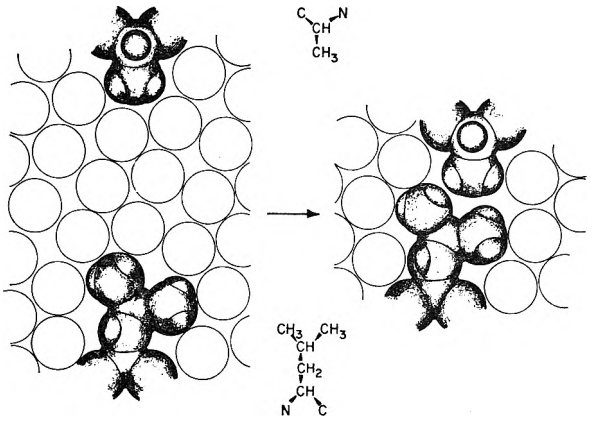

Fig. 1.—Schematic representation of the formation of a hydrophobic bond between two isolated side chains (alanine and leucine). The bond is formed through an approach of the two side chains until they touch, with a reduction of the number of nearest water neighbors. The extent of contact shown here is less than the maximum obtainable for the two side chains. Water molecules are shown only schematically, without indicating particular orientations or hydrogen-bonded networks.

tendency for non-polar groups to contact each other (with an accompanying decrease in their interactions with water), rather than remain apart from each other and surrounded by water. Solution data for hydrocarbons and related compounds (alcohols, quaternary ammonium salts, etc.) in water indicate that the large positive free energy of solution (corresponding to low solubility) arises because the excess entropy of solution (over the ideal mixing entropy) is negative, and not because of an unfavorable enthalpy of solution. In fact, many such solution processes are exothermic, but nevertheless endergonic because of the large decrease in entropy. The large entropy loss, together with the large observed partial molal heat capacity, indicates that a change in the structure of water is a crucial factor. The effect of non-polar solutes on water structure has been discussed by Frank and Evans,[18] who introduced the concept of "iceberg formation," *i.e.*, an increased ordering of water around the non-polar solute, accompanied by an increase in the degree of hydrogen bonding. This accounts for both the negative entropy change (increased ordering) and the negative enthalpy change (increase in degree of hydrogen bonding). The high heat capacity can be explained by the breakdown of the structure with increasing temperature. A quantitative discussion has been given in paper II.[6,7]

The most complete review so far of the important factors in hydrophobic bonding has been given by Kauzmann.[10] Though mostly qualitative in nature, it contains estimates of thermodynamic parameters derived from solution data for hydrocarbons. The basic concepts of his discussion, including the emphasis on aqueous solutions of hydrocarbons as model systems, as well as most of his conclusions, are similar to those presented here. There is only one important difference. Kauzmann gives estimates for the transfer of side chains from water into non-polar surroundings. On the other hand, an entire series of side chain interactions is possible in proteins, as will be discussed here. Kauzmann's treatment thus comprises a limiting case, as discussed in section 6c.

A different view of hydrophobic bonding is adopted by Klotz.[4,8,19] While assigning an important role to water in hydrophobic interactions, he considers the ordering of water in a lattice around non-polar groups as a *stabilizing* effect, in analogy with gas hydrates.[4] According to his picture, the presence of many nearby non-polar side chains in a protein should lead to a coöperative effect, stabilizing extended regions of ice-like water on the surfaces of proteins. As discussed more fully in section 5, the formation of such a structure is thermodynamically unfavorable, according to the evidence provided by the low solubility in water of hydrocarbons and other molecules containing non-polar parts.

2. Factors Affecting the Strength of the Hydrophobic Bond

a. General Concepts.—In agreement with the proposal by Kauzmann,[10] we consider the formation of a hydrophobic bond in a protein to consist of the approach of two or more amino acid side chains (previously surrounded by water) until they touch (within their van der Waals radii) and thereby decrease the total number of water molecules in contact with them (Fig. 1). This can be considered as a *partial* reversal of the solution process discussed in paper II, and the thermodynamic parameters accompanying it are related to those for solution.[7,20] The magnitudes of the changes in the thermodynamic parameters must be smaller than for the solution process because, in general, the side chains are not completely removed from aqueous environment on forming the hydrophobic bond. When two or three side chains establish contact, they still retain some water neighbors; hence it is correct to use the term *partial* reversal.

Although the non-polar side chains can be considered as analogs of the small hydrocarbon solutes, it would be incorrect to completely identify their behavior with the hydrocarbon of identical carbon skeleton, *e.g.*, valine with propane. The presence of the peptide backbone modifies the interactions with the solvent; (i) fewer water molecules can exist as nearest neighbors, and (ii) the extension of cage structures is sterically limited, even around small side-chains.

In analogy with eq. II-19,[7] the total standard free energy of formation of the hydrophobic bond can be written as

$$\Delta F_{H\phi}^{0} = \Delta F_{W}^{0} + \Delta F_{S}^{0} \qquad (1)$$

i.e., a sum of the contributions from the change

(18) H. S. Frank and M. W. Evans, *J. Chem. Phys.*, **13**, 507 (1945).

(19) I. M. Klotz and S. W. Luborsky, *J. Am. Chem. Soc.*, **81**, 5119 (1959).

(20) The formation of a hydrophobic bond might be considered to be similar to a dimerization reaction. No analogous "dimerization" can occur in aqueous solutions of low molecular weight hydrocarbons at the low concentrations achieved experimentally; dimerization would lead to a large loss of translational and rotational entropy for the freely movable hydrocarbon molecules, and this makes the equilibrium constant for the reaction very small. The corresponding degrees of freedom of side chains on proteins always are restricted because the side chains are attached to the bulky backbone; thus, side chains can associate more easily.

of the water structure and from the change in the states of the side chains themselves.

Throughout this paper, the peptide backbone to which the side chains are attached is considered to be rigid and not to make any contributions, due to changes in folding, to the thermodynamic parameters. In discussing protein reactions accompanied by chain unfolding, this has to be treated separately.

b. Changes of the Water Structure.—A side chain not engaged in hydrophobic bonding is surrounded by Y^s water molecules adjacent to it.[21] The states of these molecules are described by the partition function $Z_W{}^c$ of eq. II-20. On forming a hydrophobic bond involving two side chains, an equal number of water molecules are removed from the first shells around each of them, totalling ΔY^s. They become part of the bulk water to which the partition function $Z_W{}^0$ (eq. I-9) applies. The value taken by ΔY^s depends on the arrangement of the side chains in the bond, as discussed in later sections, and also, in the case of "multiple" bonds, on the number of side chains participating in the bond. Thus the total contribution of water to the hydrophobic bond is

$$\Delta F_W{}^0 = \Delta Y^s(F_W{}^0 - F_W{}^c) \qquad (2)$$

where $F_W{}^0$ and $F_W{}^c$ are obtained from the partition functions $Z_W{}^0$ and $Z_W{}^c$, given in papers I and II, respectively. The value of $\Delta F_W{}^0$ is different for aliphatic and for aromatic side chains because the corresponding $F_w{}^c$'s are different. The computed theoretical values of $F_W{}^0 - F_W{}^c$, the free energy change (per mole of water undergoing the change), can be expressed to within 1 cal./mole as a second degree function of temperature

$$\Delta F_W{}^0/\Delta Y^s = F_W{}^0 - F_W{}^c = 957 - 6.08T + 0.00824T^2 \qquad (3)$$

in cal./mole for aliphatic side chains and

$$\Delta F_W{}^0/\Delta Y^s = 703 - 4.35T + 0.00617T^2 \qquad (4)$$

in cal./mole for aromatic side chains. From eq. 3 and 4, closed functions for the enthalpy and entropy changes also can be derived by differentiation (see section 3a), good to 5 cal./mole. At 25°, they take the values: $\Delta F_W{}^0/\Delta Y^s = -0.123$ and -0.046 kcal./mole, $\Delta H_W{}^0/\Delta Y^s = +0.23$ and $+0.16$ kcal./mole, $\Delta S_W{}^0/\Delta Y^s = +1.17$ and $+0.67$ e.u., for aliphatic and aromatic side chains, respectively.[22]

c. Changes of State of the Side Chains.—When the hydrophobic bond is formed, ΔY^s water–hydrocarbon interactions are broken, accompanied by an energy loss of $\Delta Y^s E_{RW}$ (where E_{RW} is the energy of water–solute interaction[7]), and Z_R hydrocarbon pair (*i.e.*, $CH_3 \ldots CH_3$, $CH_2 \ldots CH_3$, or $CH_2 \ldots CH_2$) interactions are introduced, with a total energy gain of $Z_R E_R$.[24] One-half of the $\Delta Y^s E_{RW}$ term already has been included in the partition function for water by means of the energy level shifts discussed in paper II[7]; therefore, only half of it has to be included in the free energy contribution of the side chain. The total contribution of the side chain to the free energy of formation of the bond is then

$$\Delta F_S{}^0 = -(1/2)E_{RW}\Delta Y^s + Z_R E_R + \Sigma \Delta F_{rot} \qquad (5)$$

The last term represents an increase in free energy, arising because internal C–C bond rotations in the side chains are restricted more severely than in the absence of the bond, as discussed below.

Z_R depends on the extent of contact between the side chains and has to be determined from the arrangement of the side chains in the bond. For a bond between two side chains, it will be equal to or slightly smaller than $^1/_2\Delta Y^s$; a CH_3-group is slightly larger than a water molecule (in terms of van der Waals radii), a CH_2-group is approximately equal to it.

The values of the two constants E_{RW} and E_R in eq. 5 can be taken from paper II. There $^1/_2$ E_{RW} was found to be -0.031 kcal./mole for aliphatic, and -0.16 kcal./mole for aromatic groups. The latter value represents an average of the interactions with water molecules over various parts of the aromatic ring. For pair interactions between aliphatic groups, $E_R = -0.15$ kcal./mole was used. This value agrees with the increments of E_{RR} for homologous series in paper II and with theoretical calculations of Corner.[26] The value of E_R to be used for aromatic groups is somewhat uncertain. A larger value, $E_R = -0.50$ kcal./mole, was estimated. This reflects the assumption that aromatic side chains may prefer to lie flat against each other (*cf.* section 3c), resulting in a large surface of contact and an increase in the number of interacting C . . . C pairs.

The two first terms of eq. 5 represent van der Waals interactions. Because a considerable part of $\Delta F_{H\phi}{}^0$ arises from changes in the water structure, as given by $\Delta F_W{}^0$, the van der Waals interactions themselves contribute only *part* of the total energy of formation of the hydrophobic bond (*cf.* 10, 16, 17).

d. Restriction of Internal Bond Rotation.—The formation of a bond between side chains puts a limitation on their internal degrees of freedom. This question has been discussed earlier[27] in connection with the theoretical treatment of side-chain hydrogen bonding. There it was shown that

(21) The physical meaning of Y^s is identical to that of the symbol Y^c used in paper II, both referring to the number of water molecules nearest to the non-polar group or non-polar solute considered, respectively. The new symbol was introduced here to emphasize that there are differences, as discussed above, between side chains and freely moving solute molecules, surrounded on all sides by water.

(22) Complete numerical tables of these thermodynamic parameters (for the transfer of *one mole* of water from the first water layer next to a non-polar group into bulk water), as well as those of ΔF_{rot}, ΔH_{rot}, ΔS_{rot}, discussed below, are published elsewhere.[23]

(23) G. Némethy, Ph.D. Thesis, Cornell University, June, 1962.

(24) In paper II, the corresponding term for hydrocarbon–hydrocarbon interactions was denoted by F_{RR}, representing the *total* van der Waals interaction energy of a molecule with its neighbors in the pure liquid. Here, the van der Waals interaction is considered to be the sum of effective pairwise interactions, E_R, *i.e.*, it is given by a term $Z_R E_R$. The assumption of additivity is not rigorously correct.[25] In the present approximation, E_R is to be considered as an effective pairwise interaction, already incorporating corrections for the deviation from additivity.

(25) F. London, *J. Phys. Chem.*, **46**, 305 (1942).

(26) J. Corner, *Proc. Roy. Soc.* (London), **A192**, 275 (1948).

(27) M. Laskowski, Jr., and H. A. Scheraga, *J. Am. Chem. Soc.*, **76**, 6305 (1954).

only the internal rotations (active as torsional oscillations about single covalent bonds) are affected by side-chain bonding. It was stated that these rotations may be frozen in almost completely in the case of hydrogen bonding, resulting in an entropy loss of about 5 e.u. per covalent bond in the side chains involved.

The internal rotations of non-polar side chains are influenced by several factors which reduce the entropy loss to a value much smaller than 5 e.u. (i) Even in the absence of a hydrophobic bond, the torsional oscillations of the side chains must be considerably restricted, since the side chains tend to fold against the backbone in order to reduce the number of water contacts.[28] If the bond rotations were not so restricted, this would cause an increase in the number of contacts with water in some conformations. (ii) On forming a hydrophobic bond, the restriction of the internal rotation does not have to be quite as severe as for the hydrogen bond. The latter must be essentially linear due to its partial covalent character, and its bond length is fixed. Neither bond angle nor length are uniquely fixed for the hydrophobic bond. The relative orientation of the non-polar groups in contact is unimportant, and even the degree to which the side chains overlap can vary. As a result, a certain amount of motion, causing some sliding of the side chains past each other, is permissible. The amplitude of the vibrations is always small; therefore, the thermally permitted amount of torsional oscillations cannot cause much change in the extent of contact of the non-polar groups in the hydrophobic bond.

From a consideration of potential functions for various carbon–carbon single bonds in hydrocarbons, it has been found[27] that the torsional force constant τ is approximately 5 kcal./rad.^{2} Since RT = 0.6 kcal./mole at room temperature, only a low amplitude torsional oscillation about the carbon–carbon bonds is possible within the temperature range considered here, even in the absence of hydrophobic bonds. Treating these oscillations as harmonic vibrations, their frequency can be found as[27]

$$\nu = \frac{1}{2\pi}\sqrt{\frac{\tau}{I_r}} \qquad (6)$$

where I_r is the reduced moment of inertia around the single bond. The partition function for such an oscillation is given by an Einstein function

$$z_{rot} = (1 - e^{-h\nu/kT})^{-1} \qquad (7)$$

$$F_{rot} \approx A_{rot} = -RT \ln z_{rot} \qquad (8)$$

On formation of a hydrophobic bond, I_r remains essentially the same as before, except in some cases noted in section 2e. Therefore any change in the freedom of bond rotation must arise from a change in τ. Were a side chain, engaged in a hydrophobic bond, to rotate past the potential barrier into a new minimum, it would have to break the hydrophobic bond in addition to overcoming the usual barrier to rotation. Thus the effective rotational barrier is raised by the amount corresponding to the strength of the hydrophobic bond. That is, when the bond is formed

$$\tau = \tau_0 + \tau' \qquad (9)$$

where τ' corresponds to the steepening of the potential function due to the increase in the height of the potential barrier, and τ_0 is the force constant in the absence of the bond.

In calculating ΔF_{rot} of eq. 5, a term of the form of eq. 8 has to be included for each of the κ single bonds whose rotational freedom is affected by the hydrophobic bond

$$\Delta F_{rot} = \sum_{\kappa} [F_{rot}(H\phi\text{-bonded}) - F_{rot}(\text{unbonded})] \qquad (10)$$

The rotation of CH_3 groups, which are nearly spherical, is unaffected by hydrophobic bonding, so they do not have to be considered in determining κ.

Preliminary calculations have indicated that, for hydrophobic bonds of maximum strength between two side chains, $\Delta F_{H\phi}^0$ ranges from -0.5 to -1.8 kcal./mole (*cf.* section 3a). Based on these values, ΔF_{rot} was calculated for all side-chain pairs using a constant value for the change in the force constant, substituting $\tau = 1.2\tau_0$ in eq. 7 except where noted otherwise. This corresponds to a 9% change in ν. The values of I_r used and values of ΔF_{rot} at 25° are given in Table I.[22] A refinement by means of successive approximations for determining τ' is not warranted because ΔF_{rot} is not sensitive to small changes of τ', and hence the improvements in $\Delta F_{H\phi}^0$ would have been smaller than the limit of precision of the over-all calculation (see section 2f). Also, a larger error is introduced by the inherent uncertainty of τ_0 itself, because $V_0 >> \Delta F_{H\phi}^0$. V_0 is the height of the potential barrier, corresponding to τ_0.

ΔF_{rot} arises essentially from a decrease in entropy due to the restriction of rotation. The corresponding enthalpy decrease is very small, below 0.02 kcal./mole in all cases. The ΔF_{rot} values in Table I correspond to an entropy loss in the range of 0 to 1 e.u. per side chain, in contrast to 5 e.u. per single bond for hydrogen-bonded side chains.[27]

e. Amino Acids Considered and Structural Parameters.—Detailed calculations have been performed for eight amino acids, listed in Table I. Six of them possess hydrocarbon-like side chains, so the model applies to them directly. Methionine and cysteine also are sufficiently non-polar so that they interact in a similar way with water. This is indicated by the existence of crystalline hydrates[4,29] of H_2S, CH_3SH, and $(CH_3)_2S$. Differences in the interactions with water between the CH_2-group and the sulfur seem to be small and have been neglected in determining ΔF_S^0.[30]

(28) For this reason, it is permissible to neglect the distribution of conformations among the various potential minima: the deepest minimum will correspond to the folding of the side chain against the backbone. A small entropy contribution corresponding to the distribution in the various minima may be cancelled by a similar term for the hydrophobic bond which is not completely rigid.

(29) M. v. Stackelberg and H. R. Müller, *Z. Elektrochem.*, **58**, 25 (1954).

(30) Reference to the carbon atoms of the side chains in the subsequent discussion is intended to apply to the sulfur of methionine, cysteine, and cystine, too.

TABLE I

STRUCTURAL PARAMETERS FOR AMINO ACID SIDE CHAINS PARTICIPATING IN HYDROPHOBIC BONDING

Side chain	Abbrev.	Structure	$(Y^s)^a$	κ	$(I_r)^b$	ΔF_{rot} at 25° kcal./mole
Alanine	Ala	$-CH_3$	8	0	—	0
Valine	Val	$-CH(CH_3)_2$	12	1	74.4	0.05
Leucine	Leu	$-CH_2-CH(CH_3)_2$	13	2	74.4, 240[c]	0.15
Isoleucine	Ileu	$-CH(CH_2-CH_3)(CH_3)$	13	2	37.2, 140	0.10
Methionine	Met	$-CH_2-CH_2-S-CH_3$	15	3	53.1, 200, 400[d]	0.28, 0.15[e]
Cysteine	CySH	$-CH_2-SH$	10	1	101	0.05
Proline	Pro	$-(N)(CH_2)_3-CH-$ (α)	12	0	—	—
Phenylalanine	Phe	$-CH_2-C_6H_5$	15	2	89.0, 520	0.09

[a] Y^s includes the water molecules next to the α-carbon. [b] Units for I_r: length in Å., mass in terms of unit atomic weight. [c] Value for unbonded side chain. For groups in a hydrophobic bond, 200 was used instead of 240 (see discussion in text). [d] Value for unbonded side chain or in bonds with valine and leucine. For other bonds, 250 was used instead of 400. [e] For bonds with valine and leucine (see discussion in text).

Other amino acids to which the discussion is relevant are cystine and tryptophan. The side chain of cystine is similar to methionine in size and structure. Its ability to participate in hydrophobic bonds is limited by its lesser flexibility and by the steric restrictions imposed by the presence of two backbones to which it is attached.

Tryptophan, of less frequent occurrence in proteins[31] and hence of smaller importance, may participate in interactions similar to phenylalanine. Part of the tryptophan side chain has some polar nature due to the NH-group. The bulkiness of the side chain may make accommodation difficult to fit maximum bonding conditions. The net interaction with other groups (except possibly in the case of two suitably oriented tryptophans) will be of the same magnitude as for phenylalanine, so the bond strengths listed for the latter are applicable. These ten amino acids constitute 35 to 50% of the residues in many proteins.[31]

The number of water molecules in the first layer around each side chain, denoted by Y^s, is listed in Table I. It was derived from molecular models, by observing the packing of water around the side chains, including the α carbon. Its value may fluctuate somewhat.[32] The value chosen takes into account that side chains must prefer conformations in which they are folded against the backbone, if possible.

The reduced moments of inertia, I_r, can be calculated from molecular dimensions, assuming the moment of inertia of the whole protein molecule (for these rotational motions) to be infinite.[27] The calculation has to be approximate, because I_r for a given bond depends also on the orientation of the groups around bonds which are further removed from the backbone.[27] The values listed in Table I therefore in most cases are to be considered as averages for various conformations. In determining them, account was taken of the condition mentioned above, namely, that the side chain must prefer conformations bringing it close to the backbone. On forming a hydrophobic bond, the values of I_r do not seem to change significantly, as judged from consideration of molecular models, so the same numerical values were used in most cases for bonded and unbonded groups. Changes had to be introduced only in the case of leucine and methionine: except for methionine in the Val–Met and Leu–Met bonds, the formation of bonds of maximum strength requires a large change in the conformation of the leucine and methionine side chains. This was taken into account by changing the value of I_r for the rotation affected (Table I).

f. Precision of the Calculations.—Z_R, Y^s, and ΔY^s were estimated to the nearest integer. The numbers given are averages, with some fluctuation possible, so they may be in error by ± 0.5 unit. Such an error in ΔY^s causes an error of about 0.06 kcal./mole in $\Delta F_{H\phi}^0$ near room temperature. Uncertainties in E_{RW} and E_R can give rise to errors of a

(31) G. R. Tristram, in "The Proteins," H. Neurath and K. Bailey, ed., Academic Press, New York, N. Y., 1953, Vol. IA, p. 181.

(32) The fluctuations are caused by the melting and formation of the water clusters, since the densities of clusters and of unbonded water are different. Density changes with temperature cause Y^s to be temperature dependent, too. For the side chain sizes considered here, the change of Y^s with temperature is too small to be significant within the precision of the model.

similar magnitude. The free energy contribution from the change in water structure ($F_W^0 - F_W^c$) can be considered as accurate within 2–3% according to the results presented in paper II. The uncertainty in the values of ΔF_{rot} is within 0.03 kcal./mole.

Considering these limits on the accuracy of the results, the calculated free energies and enthalpies of formation of the hydrophobic bonds are significant only to within 0.1 kcal./mole. The calculated values have been rounded off correspondingly in the subsequent tables. 0.1 kcal./mole in $\Delta F_{H\phi}^0$ or $\Delta H_{H\phi}^0$ corresponds to a possible error of 0.3 e.u. in $\Delta S_{H\phi}^0$. The entropies in the tables therefore are given to the nearest tenth of an e.u., although this exceeds the true accuracy somewhat.

Due to the non-specific nature of hydrophobic interactions, a variety of different hydrophobic bonds can exist. The above general considerations apply to all cases. For further details, they have to be discussed separately.

3. Hydrophobic Bond between Two Isolated Side Chains

The hydrophobic bond between two isolated side chains is the simplest case of such bonding. It is formed by the interaction of two side chains, which are attached to rigid peptide backbones, and surrounded by water before the bond is formed. That is, there are no other side chains sufficiently close to interact with the two side chains forming the bond or to affect the water structure significantly, either before or after the formation of the bond. With this postulate, a basic assumption made in the treatment of hydrocarbon solutions in paper II is still rigorously valid: *viz.*, the solution is sufficiently dilute so that each water molecule can have at most one hydrocarbon neighbor. Consequently, the treatment of paper II can be used here without qualifications.

The formation of the hydrophobic bond takes place as pictured in Fig. 1. The two side chains approach each other and establish as many contacts as possible; at the same time the total number of water molecules in the first layer is diminished. The maximum amount of "overlap" is determined by the nature of the two side chains. If the chains are free to do so, they will form a bond in which ΔY^s and Z_R are made as high as the requirements of packing will permit. Structural conditions, such as the presence of other interactions or steric restrictions, may prevent the formation of a bond of maximal strength. Other interactions may keep two peptide chains at a fixed distance, larger than the optimum for the two side chains in question; therefore, these can form only a weaker hydrophobic bond. Side chains on adjacent turns of an α-helix may be cited as an example. As a result, an entire range of hydrophobic bonds of various strengths is possible for a given pair of side chains, from the maximum bond to a bond of minimum strength. The latter is formed when the two side chains are just able to touch each other. In the following sections, calculated maximum and minimum values are given for the bond strengths. The free energy of formation of the bond is obtained by substituting eq. 2 and 5 into eq. 1 to give

$$\Delta F_{II\phi}^0 = \Delta Y^s(F_W^0 - F_W^c) + Z_R E_R - (1/2)\Delta Y^s E_{RW} + \Sigma \Delta F_{rot} \quad (11)$$

where the sum is taken over the corresponding κ's of *both* side chains.

a. Bonds of Maximum Strength.—These can be formed by two side chains which are free to approach each other. Illustrative examples are given in Fig. 2 (B to D). ΔY^s and Z_R, listed for various pairs in Table II, are in this case determined by the nature of the two side chains only. The tabulated values were determined from molecular models. The thermodynamic parameters for the formation of the various bonds at 25° are shown in Tables III to V. Tables of the parameters at other temperatures have been published elsewhere[23] for various pairs of side chains.

TABLE II

PARAMETERS DESCRIBING HYDROPHOBIC BONDS OF MAXIMUM STRENGTH BETWEEN ISOLATED SIDE CHAINS

Bond	ΔY^s	Z_R	Coefficients for eq. 12 a	b	c
Ala–Ala	4	2	3650	−24.3	0.0330
–Val	4	2	3650	−24.1	.0330
–Leu	4	2	3650	−23.8	.0330
–Ileu	4	2	3650	−24.0	.0330
–Met	4	2	3650	−23.3	.0330
–CySH	4	2	3650	−24.1	.0330
–Pro	4	2	3650	−24.3	.0330
Val–Val	6	3	5480	−36.2	.0495
–Leu	6	3	5470	−35.8	.0495
–Ileu	8	4	7300	−48.2	.0660
–Met	8	4	7300	−48.0	.0660
–CySH	5	2	4640	−30.1	.0412
–Pro	6	3	5480	−36.3	.0495
Leu–Leu	6	3	5460	−35.4	.0495
–Ileu	8	4	7290	−47.8	.0660
–Met	8	4	7290	−47.6	.0660
–CySH	5	2	4650	−29.8	.0412
–Pro	6	3	5470	−36.0	.0495
Ileu–Ileu	10	5	9120	−60.1	.0824
–Met	10	5	9110	−59.5	.0824
–CySH	5	2	4630	−29.9	.0412
–Pro	8	4	7300	−48.3	.0660
Met–Met	10	5	9110	−58.9	.0824
–CySH	5	2	4630	−29.3	.0412
–Pro	8	4	7290	−47.7	.0660
CySH–CySH	4	2	3650	−24.0	.0330
–Pro	4	2	3650	−24.2	.0330
Pro–Pro	6	3	5500	−36.6	.0495
Phe–Phe	12	6	7350	−51.6	.0740
Phe–Ala[a]	2	1	1570	−10.2	.0144
–Val	6	3	4730	−30.8	.0432
–Leu	6	3	4720	−30.4	.0432
–Ileu	8	4	6300	−41.0	.0576
–Met	8	4	6290	−40.4	.0576
–CySH	4	2	3150	−20.3	.0288
–Pro	6	3	4740	−31.0	.0432

[a] The maximum and minimum bond strengths coincide for this case because there is only one way of establishing a contact between the two side chains.

$\Delta F_{H\phi}^0$ can be expressed in closed form as a func-

TABLE III

STANDARD FREE ENERGY OF FORMATION OF HYDROPHOBIC BONDS OF MAXIMUM STRENGTH BETWEEN ISOLATED SIDE CHAINS AT 25° (KCAL./MOLE)

	Ala	Val	Leu	Ileu	Met	CySH	Pro	Phe
Ala	−0.7	−0.6	−0.5	−0.6	−0.4	−0.6	−0.7	−0.2
Val	−0.6	−0.9	−0.8	−1.2	−1.1	−0.7	−1.0	−0.6
Leu	−0.5	−0.8	−0.7	−1.1	−1.0	−0.6	−0.9	−0.5
Ileu	−0.6	−1.2	−1.1	−1.5	−1.3	−0.6	−1.2	−0.8
Met	−0.4	−1.1	−1.0	−1.3	−1.1	−0.4	−1.1	−0.6
CySH	−0.6	−0.7	−0.6	−0.6	−0.4	−0.6	−0.6	−0.4
Pro	−0.7	−1.0	−0.9	−1.2	−1.1	−0.6	−1.0	−0.7
Phe	−0.2	−0.6	−0.5	−0.8	−0.6	−0.4	−0.7	−1.4

TABLE IV

STANDARD ENTHALPY OF FORMATION OF HYDROPHOBIC BONDS OF MAXIMUM STRENGTH BETWEEN ISOLATED SIDE CHAINS AT 25° (KCAL./MOLE)

	Ala	Val	Leu	Ileu	Met	CySH	Pro	Phe
Ala	0.7	0.7	0.7	0.7	0.7	0.7	0.7	0.3
Val	.7	1.1	1.1	1.5	1.5	1.0	1.1	.9
Leu	.7	1.1	1.1	1.4	1.4	1.0	1.1	.9
Ileu	.7	1.5	1.4	1.8	1.8	1.0	1.5	1.2
Met	.7	1.5	1.4	1.8	1.8	1.0	1.5	1.2
CySH	.7	1.0	1.0	1.0	1.0	0.7	0.7	0.6
Pro	.7	1.1	1.1	1.5	1.5	.7	1.1	.9
Phe	.3	0.9	0.9	1.2	1.2	.6	0.9	.8

TABLE V

STANDARD ENTROPY OF FORMATION OF HYDROPHOBIC BONDS OF MAXIMUM STRENGTH BETWEEN ISOLATED SIDE CHAINS AT 25° (E.U.)

	Ala	Val	Leu	Ileu	Met	CySH	Pro	Phe
Ala	4.7	4.5	4.2	4.4	3.7	4.5	4.7	1.7
Val	4.5	6.7	6.4	8.9	8.7	5.5	6.9	5.1
Leu	4.2	6.4	6.0	8.5	8.4	5.2	6.5	4.7
Ileu	4.4	8.9	8.5	11.1	10.4	5.4	9.1	6.8
Met	3.7	8.7	8.4	10.4	9.8	4.7	8.4	6.1
CySH	4.5	5.5	5.2	5.4	4.7	4.4	4.5	3.2
Pro	4.7	6.9	6.5	9.1	8.4	4.5	7.1	5.2
Phe	1.7	5.1	4.7	6.8	6.1	3.2	5.2	7.5

tion of the temperature as shown in equation 12

$$\Delta F_{H\phi}{}^0 = a + bT + cT^2 \qquad (12)$$

in cal./mole. The coefficients a, b, and c for all pairs are listed in Table II. They were obtained by fitting eq. 12 to the numerically computed values of $\Delta F_{H\phi}{}^0$ at 0, 25, and 50°. Equation 12 reproduces the computed values of $\Delta F_{H\phi}{}^0$ over the whole temperature range from 0 to 70° with a deviation of less than 5 cal./mole.

The other thermodynamic parameters can be derived from $\Delta F_{H\phi}{}^0$ as

$$\Delta H_{H\phi}{}^0 = a - cT^2 \qquad (13)$$

$$\Delta S_{H\phi}{}^0 = -b - 2cT \qquad (14)$$

$$(\Delta c_p)_{H\phi} = -2cT \qquad (15)$$

In determining ΔF_{rot}, $\tau/\tau_0 = 1.2$ was used for all bonds with the exception of the weak phenylalanine–alanine bond, for which $\tau/\tau_0 = 1.05$ was used.

b. Bonds of Minimum Strength.—Such bonds are formed when the two side chains can barely touch (Fig. 2A). The same parameters, $\Delta Y^s = 2$ and $Z_R = 1$, have to be used for all bonds. Since all bond strengths fall within the range of 0 to −0.5 kcal./mole for the entire temperature range, $\tau/\tau_0 = 1.05$ was used in determining ΔF_{rot}. For the small τ/τ_0, ΔF_{rot} does not depend significantly on the type of side chain, but only on the number, $\Sigma\kappa$, of bonds restricted. Hence, it can be expressed as

$$\Delta F_{rot} = -(1 - 0.05T)\,\Sigma\,\kappa \qquad (16)$$

for all side-chain pairs. The thermodynamic parameters are given in Table VI for 25°. For other temperatures, they can be determined from eq. 12 to 16, substituting for the coefficients $a = 1830 - \Sigma\kappa$, $b = -12.2 + 0.05\,\Sigma\kappa$, and $c = 0.0165$ for bonds between aliphatic side chains; $a = 1580 - \Sigma\kappa$, $b = -10.3 + 0.05\,\Sigma\kappa$, and $c = 0.0144$ for bonds involving phenylalanine.

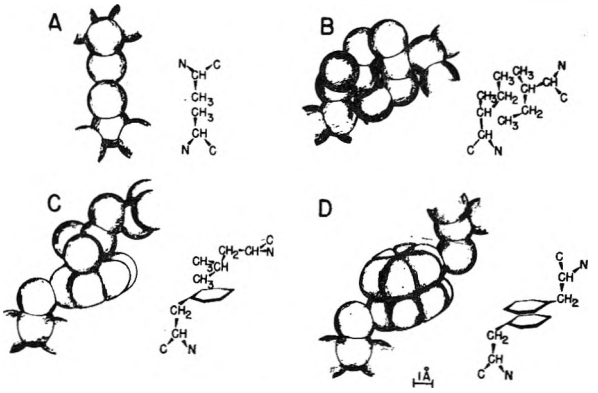

Fig. 2.—Illustrative examples of hydrophobic bonds between pairs of isolated side chains. The hydrogens are not indicated individually. Drawn to scale, but with the van der Waals radii reduced by 20% for the sake of clarity. The structural formulas to the right of each space-filling drawing indicate the arrangement of the atoms: A, alanine–alanine bond (minimum strength); B, isoleucine–isoleucine bond (maximum strength); C, phenylalanine–leucine bond (maximum strength); D, phenylalanine–phenylalanine bond (maximum strength).

TABLE VI

THERMODYNAMIC PARAMETERS FOR THE FORMATION OF HYDROPHOBIC BONDS OF MINIMUM STRENGTH BETWEEN ISOLATED SIDE CHAINS AT 25°

Bond type	$\Delta F_{H\phi}{}^0$, kcal./mole	$\Delta H_{H\phi}{}^0$, kcal./mole	$\Delta S_{H\phi}{}^0$, e.u.
Between aliphatic side chains	−0.3	0.4	2.1 to 2.4
Involving Phe	−0.2	.3	1.6 to 1.7

c. Bonds between Aromatic Side Chains.—In determining the number of water molecules in the first shell around the phenylalanine side chains, Y^s, it was assumed that the side chain takes

up a conformation approaching the backbone as much as possible, making Y^s a minimum. Thereby, one of the flat surfaces of the ring is only partly exposed to water. When forming a hydrophobic bond, this folding must be maintained approximately; otherwise ΔY^s might be reduced.

In the Phe–Phe bond of maximum strength, the two benzene rings were assumed to lie flat on top of each other to give a maximum of ΔY^s and Z_R (Fig. 2D). Such a maximum bond could be achieved only with a very favorable positioning of the two backbones.

The minimum interaction involves just one CH-group of each side chain.

d. Bonds between an Aliphatic and an Aromatic Side Chain.—In this case, half of the water molecules removed from a first layer next to a non-polar group originate next to an aliphatic side chain, one half next to an aromatic side chain. In computing the free energy of formation, eq. 11 has to be modified to take this into account, giving the new expression

$$\Delta F_{H\phi}^0 = \Delta Y^s\{F_W^0 - (1/2)[F_W^c(al) + F_W^c(ar)]\} + Z_R E_R - (1/2)\Delta Y^s\{(1/2)[E_{RW}(al) + E_{RW}(ar)]\} + \Sigma\Delta F_{rot} \quad (17)$$

The hydrocarbon–hydrocarbon interaction now is given by $E_R = \sqrt{E_R(al) \times E_R(ar)}$. The remarks concerning the orientation of the phenylalanine side chain, made above, hold for this case, too.

e. Effects of Temperature.—For the formation of the hydrophobic bond near room temperature, $\Delta F_{H\phi}^0 < 0$, $\Delta S_{H\phi}^0 > 0$, but $\Delta H_{H\phi}^0 > 0$. The unfavorable enthalpy of formation is more than counterbalanced by the positive entropy, resulting in a favorable free energy. Thus, it is seen that the entropy is the most important factor in stabilizing the hydrophobic bond, due to the changes in the water structure.

As an illustration, the thermodynamic parameters are given as a function of temperature in Table VII for the leucine–isoleucine bond. The temperature dependence for other bonds is similar. Numerical values for them can be obtained with the aid of eq. 12 to 15 and Table II.

The calculations have been limited to temperatures below 70°, because the model for water itself is no longer valid at higher temperatures, as shown in paper I.

TABLE VII

THERMODYNAMIC PARAMETERS FOR THE FORMATION OF A LEUCINE–ISOLEUCINE HYDROPHOBIC BOND OF MAXIMUM BOND STRENGTH

t, °C.	$\Delta F_{H\phi}^0$, kcal./mole	$\Delta H_{H\phi}^0$, kcal./mole	$\Delta S_{H\phi}^0$, e.u.
0	−0.84	2.3	11.6
10	−0.95	2.0	10.4
20	−1.05	1.6	9.2
25	*−1.09*	*1.45*	*8.5*
30	−1.13	1.2	7.8
40	−1.21	0.8	6.5
50	−1.26	0.4	5.1
60	−1.31	−0.1	3.6
70	−1.34	−0.6	2.1

At high temperatures, both $\Delta H_{H\phi}^0$ and $\Delta S_{H\phi}^0$ approach zero. The enthalpy of formation even becomes negative above 56–58° (42° for phenylalanine–phenylalanine). This occurs because the solubility relationships at high temperatures, where the water structure breaks down, will be determined mainly by the interaction energies. This causes the enthalpy term to predominate and, because water–water interactions are the strongest, will result in a large negative $\Delta F_{H\phi}^0$.

The endothermic nature of the formation of hydrophobic bonds causes them to become stronger with increasing temperature up to 58° (or 42° for Phe–Phe bonds). This has important implications for the thermal stability of proteins, which have been discussed elsewhere.[33]

The change in heat capacity for hydrophobic bond formation is negative, *i.e.*, of the opposite sign as Δc_p for hydrocarbon solutions. It becomes more negative with increasing temperature. Using eq. 15, it can be seen that it takes values from −10 to −50 cal./deg./mole at room temperature per side-chain pair.

For bonds involving aromatic side chains, both $\Delta H_{H\phi}^0$ and $\Delta S_{H\phi}^0$ are much more positive than for aliphatic bonds, resulting in a smaller value for $|\Delta F_{H\phi}^0|$. This parallels the solution process.

4. Hydrophobic Bonds in Typical Protein Structures

The possible contribution of hydrophobic bonds to the stabilization of various protein conformations can be determined by the application of the results of section 3.

a. The α-Helix.—A given side chain on the helix may interact with the side chains nearest to it in space. These are the next groups along the backbone chain, and the ones on the next turn of the helix, *i.e.*, the third and the fourth along the sequence. In the subsequent discussion, the atoms of the various side chains are identified in the following manner: the carbon atoms along any side chain are denoted by greek letters, the α-carbon being part of the backbone; the separation by residues along the sequence, counting the residue under consideration as zero, with the numbers increasing *toward* the N-terminus, is given by subscript numbers.

In each side-chain residue, the positions of the α- and β-carbons are fixed. The position of other atoms of the side chains is variable, depending on the orientation of the side chain, and is subject to the restrictions imposed by fixed bond lengths and angles. Additional restriction is placed on the bending of the side chains by steric hindrance of the backbone atoms. This restriction is quite severe, ruling out many conformations, and must not be disregarded when studying side chain interactions.[34] The minimum distances to which atoms on various side chains can approach are listed in Table VIII. The van der Waals radius[35] of the

(33) H. A. Scheraga, G. Némethy, and I. Z. Steinberg, *J. Biol. Chem.*, **237**, 2506 (1962).

(34) The interatomic distances of Table VIII and the possibilities of hydrophobic bonding in the α-helix were determined with the aid of Courtaulds–Ealing space-filling atomic models.

(35) L. Pauling, "The Nature of the Chemical Bond," Cornell University Press, Ithaca, N. Y., 1960, 3rd ed., p. 260.

CH_3 or CH_2 group is 2.0 Å. Therefore an approach of 4 Å. (center-to-center) is necessary for a strong non-polar interaction. The van der Waals radius of sulfur is 1.85 Å., so the following considerations apply to it, too, as a good approximation. It can form essentially the same bonds as a CH_2-group, and is able to approach even closer than 4 Å. in the cases marked *b* in Table VIII. If the center-to-center distance exceeds about 5.5 Å., water molecules can be packed sufficiently closely between the side-chain groups so as to form a complete intermediate layer. At distances of 4 to 5.5 Å. a small empty cavity remains. Although the number of water molecules in the first layers has been reduced even in this case, the van der Waals energy gain is smaller and therefore such an arrangement leads to a somewhat weaker hydrophobic bond.

TABLE VIII

DISTANCE OF CLOSEST APPROACH OF ATOMS ON VARIOUS SIDE CHAINS IN A RIGHT HANDED α-HELIX COMPOSED OF L-AMINO ACIDS

Atoms	*d* (Å.)	Remarks	Atoms	*d* (Å.)	Remarks
Aliphatic side chains					
γ_0–γ_1	4.0	*c*	β_0–α_4	5.6	*a*
γ_0–δ_1	<4.0	*b,c*	β_0–β_4	6.2	*a*
δ_0–γ_1	<4.0	*b,c*	γ_0–β_4	5.2	
δ_0–δ_1	<4.0	*b,c*	γ_0–γ_4	4.3	*c*
α_0–α_3	5.0	*a*	γ_0–δ_4	<4.0	*b,c*
β_0–α_3	3.8	*a,c*	δ_0–β_4	4.5	
β_0–β_3	5.0	*a*	δ_0–γ_4	<4.0	*b,c*
β_0–γ_3	5.5		δ_0–δ_4	<4.0	*b,c*
γ_0–α_3	4.5		Aliphatic–aromatic side chains		
γ_0–β_3	5.2		Bz_0–β_1	5.1	
γ_0–γ_3	5.2		Bz_0–γ_1	4.0	*c*
γ_0–δ_3	4.0	*c,e*	Bz_0–δ_1	4.0	*c*
δ_0–α_3	4.0	*c,d*	Bz_0–γ_3	5.4	
δ_0–β_3	5.0		Bz_0–δ_3	4.0	*c*
δ_0–γ_3	4.2	*c,d,e*	Bz_0–α_4	5.5	
δ_0–δ_3	<4.0	*b,c*	Bz_0–β_4	4.8	
α_0–α_4	6.0	*a*	Bz_0–γ_4	<4.0	*b,c*
			Bz_0–δ_4	<4.0	*b,c*

[a] Distance fixed by the structure of the α-helix. In all other cases, the distances given are the minima obtainable with suitable orientation. [b] The distance of minimum approach is determined by the sum of the van der Waals radii, not by the limitations due to the orientation of the side chains. [c] Distance corresponds to the formation of a strong hydrophobic bond. [d] The two interactions, δ_0–α_3 and δ_0–γ_3, must occur simultaneously. [e] The two interactions, γ_0–δ_3 and δ_0–γ_3, cannot occur simultaneously.

Hydrophobic bonds are possible involving the pairs of atoms marked *c* in Table VIII. A side chain can bond to only one of its neighbors, and usually only one of the interactions listed in the table can be realized, with the following exceptions: β_0–α_3 always has to occur; the pairs δ_0–α_3 and γ_0–γ_3, γ_0–γ_4 and δ_0–δ_4, γ_0–δ_4 and δ_0–γ_4, Bz_0–γ_4 and Bz_0–δ_4, Bz_0–γ_1 and Bz_0–δ_1 may occur simultaneously. Two phenylalanines can interact only by a weak Bz_0–β_1 bond without unfavorable rotation of the two side chains.[36] An example of a δ_0–γ_4 bond between a leucine and a valine side chain is given in Fig. 3.

(36) Interactions of the phenyl group, denoted by Bz in Table VIII, are possible only on the edge of the ring, where the van der Waals radius 2.0 Å. is applicable.

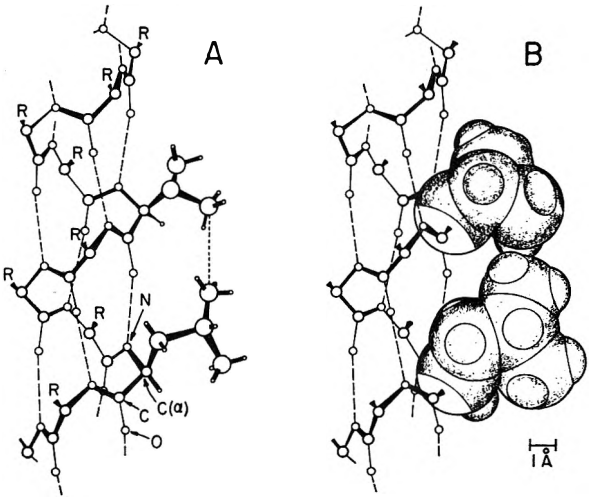

Fig. 3.—Hydrophobic bond between a leucine and a valine residue in the 0–4 relative positions on a right handed α-helix composed of L-amino acids. Other side chains are omitted for the sake of clarity. (A) Skeleton drawing showing the positions of the atoms in the helix[37] and in the side chains. Dashed lines represent backbone hydrogen bonds; the dotted line the leucine–valine hydrophobic bond. The position of other side chains is indicated by R, with all residues corresponding to L-amino acids. (B) Space-filling model, drawn to scale, using van der Waals radii as given by Pauling.[35] Only the atoms in the two side chains forming the hydrophobic bond and the α-carbons carrying them are drawn with van der Waals radii.

Thus it can be seen that valine is barely able to make minimum contact with other side chains by means of a γ–γ or γ–δ interaction, characterized by $\Delta Y^s = 4$ and $Z_R = 1$. Longer side chains can make more contacts, up to $\Delta Y^s = 5$ and $Z_R = 2$ for 0–3 interactions with suitably long side chains as their partners, and $\Delta Y^s = 6$ and $Z_R = 2$ for 0–4 or 0–1 interactions. These interactions are weaker than the maximum bond strengths discussed in section 3a for these side chains. $\Delta F_{H\phi}^0$ may be about −0.4 to −0.7 kcal./mole, depending on the side chains involved.

Methionine, having a fifth atom in its side chain, or lysine (see section 7), can in general make one more contact with its neighbor, contributing a further −0.3 kcal./mole to $\Delta F_{H\phi}^0$, approximately.

The bonds mentioned above can be formed only if both side chains can take up the most favorable orientation, and are not engaged in other interactions. When two side chains are not bonded to each other, they are in general separated by a single layer of water molecules. This case will be discussed in section 5.

In an α-helix consisting of D- and L-amino acid residues, the orientation of the side chains allows much stronger hydrophobic bonds to be formed than in the helix containing all L- or all D-amino acids. Such interactions on a poly-D,L-alanine α-helix have been discussed by Linderstrøm-Lang.[37] For this case, $\Delta Y^s = 4$ and $Z_R = 1$ have to be used, since the backbone itself contributes to the steric exclusion of water around the methyl groups. The free energy of the bond can be expressed as

$$\Delta F_{H\phi}^0 = 3800 - 24.3T + 0.0330T^2 \quad (18)$$

(37) K. Linderstrøm-Lang, *Acta Chem. Scand.*, **12**, 851 (1958).

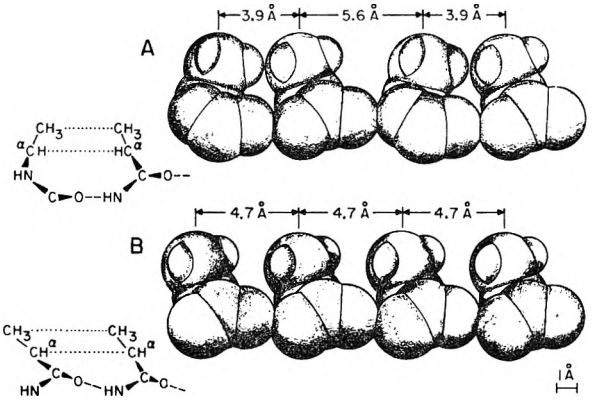

Fig. 4.—Hydrophobic bonds in β-structures, with van der Waals radii of the atoms drawn to scale. The primary backbone chains run perpendicularly to the plane of the drawing. The distances used in preparing the drawing are based on Table II and Fig. 6 and 7 of Pauling and Corey's paper[38] describing the β-structures. The residues drawn represent alanines; longer side chains could be able to form stronger hydrophobic bonds. The arrangements of the atoms is shown in the structural formulas on the left. (A) Antiparallel-chain pleated sheet structure, showing the alternation of two distances between adjacent residues. Only the shorter distance corresponds to a hydrophobic bond. (B) Parallel chain pleated sheet structure, with a weakened hydrophobic bond between each adjacent pair of residues.

A discussion of the thermal stability of this polypeptide has been presented elsewhere.[33]

b. Pleated Sheets (β-Configurations.)—The two pleated sheet structures proposed by Pauling and Corey[38] allow extensive hydrophobic bonding. In both, the side chains are alternately above and below the peptide sheet along each main chain.

In the antiparallel chain pleated sheet, the distance between similarly oriented groups *along* the chain axis is 6.68 Å. (Measured between the α- or β-carbons.) In the perpendicular direction, the nearest α-carbons are at 4.6 and 4.9 Å., with the corresponding β-carbons at 3.9 and 5.6 Å. The two lateral distances alternate. A diagrammatic representation is given in Fig. 4A. Each side chain can form a hydrophobic bond with one of its neighbors with at least α–α and β–β contacts, with parameters $\Delta Y^s = 4$, $Z_R = 2$. If the side chains are longer, the γ (and δ) carbons also can approach each other to within 4.0 Å., making the bond stronger. Some weakening occurs because $d_{\alpha-\alpha} >$ 4.0 Å. The pairs of lateral side chains and the chains along the chain axes are separated by one water layer. The hydrophobic bonding contributes a free energy of −0.6 kcal./mole per bond, or −0.3 kcal./mole per residue for bonds involving alanine at 25°, with a higher value for longer side chains. For these, the increment in $\Delta F_{H\phi}^0$ for each additional pair of CH_2-groups in contact is about −0.3 kcal./mole.

In the parallel chain pleated sheet, the distances between the α-carbons of two similarly oriented side chains are 6.68 Å. *along* the chain axis and 4.73 Å. laterally. The distances are the same for the corresponding β-carbons. Along the chain axis, the side chains are separated by one water layer, but a water molecule cannot fit between the β-carbons, perpendicularly to the chain. Laterally, each side chain forms a hydrophobic bond with *both* of its neighbors The bond is similar to that discussed in the case of the antiparallel chains, except that it is weakened due to the increased separation of the side chains. Its strength is between −0.5 and −0.6 kcal./mole per bond. Here this is also the value per residue for extended sheets (neglecting edge effects). With longer side chains, the bond strength is increased as in the previous case.

In both pleated sheets, additional bonds may be formed by leucine, isoleucine, or longer side chains, through bridging the gap to the β-carbon of the next residue along the *same* main chain, or between the γ-carbons of two valines next to each other along the *same* main chain.

Thus, the hydrophobic bond is of importance not only for the α-helix but for other structures as well. Due to the large number and greater strength of the hydrophobic bonds in the β-structures as compared with the α-helix, the former can receive more stabilization from them, and the temperature dependence of the strength of hydrophobic bonds[33] may assume a higher importance in their case.

This may provide an explanation[33] of the observation by Rosenheck and Doty[39] that α-helical poly-L-lysine at pH 10.8 is converted into the β-form, with accompanying association, as the temperature is increased. The ε-amino groups are uncharged at this pH, and so the side chains can participate in strong hydrophobic bonding (*cf.* section 7); in addition to the α- and β-carbons, there are three more CH_2 groups, of which at least two can form bonds, possibly even three if the NH_2 groups do not interfere strongly. ($\Delta Y^s =$ 8 to 10, $Z_R = 4$ to 5.) At 25° this may give at least $\Delta F_{H\phi}^0 = -1.4$ kcal./mole per bond, *i.e.*, −1.4 or −0.7 kcal./mole per residue, depending on which type of sheet is formed, not counting possible additional bonds between side chains along the same backbone. The corresponding enthalpy is $\Delta H_{H\phi}^0 = 1.8$ kcal./mole per bond at 25°, increasing the thermal stability of the β-structure. In the α-helical form, there can be only fewer and weaker hydrophobic bonds, which do not contribute as much to the thermal stability. The ε-NH_2-groups also are important; being on the surface of the pleated sheets, they can interact favorably with water, enhancing the solubility of the structure.

c. The Random Coil.—Hydrophobic bonds must occur even in the randomly coiled protein or polypeptide, because of the tendency of the non-polar side chains to associate.[33] An estimation of the number of bonds is difficult, but molecular models indicate that not many side chains can be brought into contact simultaneously in the random coil. Nevertheless, they may have a relatively high importance because hydrogen bonds no longer can exist in a significant number. Even though they may not contribute much to the free energy of the random coil, their temperature dependence is the

(38) L. Pauling and R. B. Corey, *Proc. Natl. Acad. Sci. U. S.*, **37**, 729 (1951).

(39) K. Rosenheck and P. Doty, *ibid.*, **47**, 1775 (1960).

predominant factor in the over-all thermal stability. They may be one of the factors making the random coil the favored conformation at higher temperatures. Consequently, when calculating the free energy of unfolding of any structure, a smaller value of $\Delta F_{H\phi}^0$ has to be used than would be calculated by considering the number of hydrophobic bonds in the folded structure alone, because of the possible existence of such bonds in the random coil.

5. Effects due to Side Chains Not in Contact

a. Side Chains Separated by a Single Layer of Water Molecules.—This structure occurs in the α-helix and in both pleated sheets discussed in section 4, and also may occur between adjacent helices or similar structures held rigidly by other interactions.

In the case of the formation of such a layer, one of the basic assumptions for solutions and for the isolated side chain no longer holds, *i.e.*, the existence of at most one solute neighbor per water molecule.[7] The molecules in the single layer between the two side chains have two solute neighbors. As a result, their energy levels will be different from those discussed earlier.[7] The unbonded and the mono- and di-bonded water molecules in this layer have two of their water neighbors replaced by hydrocarbon neighbors.[7] Therefore their energy is raised[7] by $2\Delta E_r$ with respect to the corresponding levels in pure water. A tetra-bonded molecule must be part of two partial cages, extending around both side chains (see Fig. 5). Its coordination is increased by two due to the hydrocarbon–water contacts.[40] Its energy level is lowered[7] by $2\Delta E_l$ with respect to the ground state in water. The tri-bonded molecule has a special position. It is on the edge of the partial cage extending around one of the side chains, but at a point where the cage does not extend around the other side chain (Fig. 5). This water molecule thus will have one hydrocarbon neighbor which replaced an unbonded water neighbor and one (in the partial cage) causing an increase of coördination number. Therefore its net energy level shift will be $\Delta E_r + \Delta E_l$.

In order to determine the thermodynamic parameters characterizing the structure, the same procedure is followed as for the aqueous hydrocarbon solution.[7] The water molecules within this region can be described by means of a partition function of the same form as that for the molecules in the first layer around isolated solutes (eq. II-20), but with the appropriate E_i values substituted. It can be evaluated numerically as in the other cases, giving the standard free energy for water in the intermediate layer, denoted by F_W^{cc}.

Comparison of the free energy of the intermediate water layer with *pure water* indicates a difference in the free energy, given as $\Delta F_W^{cc} = F_W^{cc} - F_W^0$, with similar expressions for ΔH_W^{cc} and ΔS_W^{cc}. The three quantities are listed in columns 2 to 4 of Table IX. As indicated by the changes, a transfer of water from the bulk to the intermediate layer would correspond to an increase in "ice-likeness," with an increase in the degree of hydrogen bonding

(40) The structure is similar to the gas hydrates, except that the coördination number increases by two instead of by four.

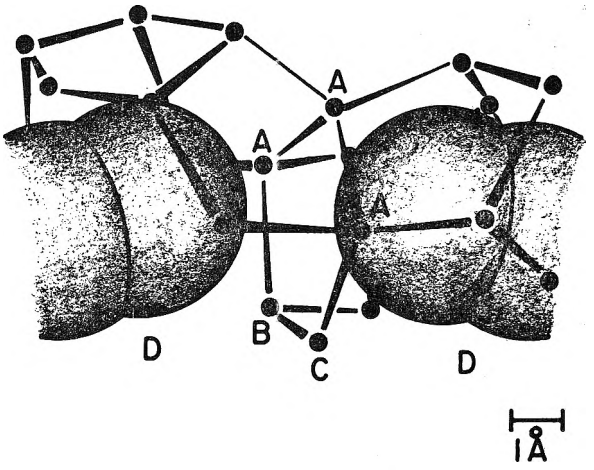

Fig. 5.—Schematic drawing of a structure with a single layer of water molecules (AAABC) between two nearby side chains. The two side chains are drawn with van der Waals radii to scale. Only the centers (oxygens) of the water molecules are shown. For the sake of clarity, hydrogen bonds are not shown extending from the structure to the rest of the cluster of which it is a part. The cluster is to be pictured as lying mainly behind the plane of the drawing, extending into the plane above the structure. A, B, and C represent tetra-, tri-, and di-hydrogen-bonded water molecules, respectively, in contact with *both* side chains. They are discussed more fully in the text. In the regions D, unbonded water molecules are next neighbors of the two side chains (corresponding to the partial character of the cages).

and with $\Delta F_W^{cc} > 0$. The changes per mole of water are about twice as large as for the formation of the first layer about isolated solute molecules so that this intermediate layer in itself is even less favorable thermodynamically. This is caused by the larger shifts in the energy levels.[7]

TABLE IX

THERMODYNAMIC PARAMETERS FOR THE FORMATION OF A SINGLE INTERMEDIATE WATER LAYER BETWEEN TWO NEARBY ALIPHATIC SIDE CHAINS

(ΔF and ΔH in kcal./mole, ΔS in e.u.)

	Difference between the intermediate layer and pure water			Formation of the structure starting from two isolated side chains[a]		
t, °C.	ΔF_W^{cc}	ΔH_W^{cc}	ΔS_W^{cc}	ΔF_{sl}^0	ΔH_{sl}^0	ΔS_{sl}^0
0	0.17	−0.69	−3.2	-1.7×10^{-3}	-11×10^{-3}	−0.03
25	.25	−0.56	−2.7	+1.1	−53	−0.18
50	.31	−0.36	−2.1	7.2	−87	−0.29
70	.34	−0.17	−1.5	13.7	−113	−0.37

[a] The values are given for $\Delta Y^s = 1$ and have to be multiplied by the appropriate ΔY^s for a particular structure.

When such a structure is formed, the actual starting state corresponds to two isolated side chains separated from each other by a large distance, each surrounded by water, as discussed in paper II. The free energy of formation therefore has to refer to this starting state rather than to pure water. When the two side chains approach each other to a distance where they are separated by a single water layer, only $^1/_2\Delta Y^s$ water molecules enter the bulk water out of the first layers. The other $^1/_2\Delta Y^s$ water molecules compose the single intermediate layer, described in the previous paragraphs, having more hydrogen bonds due to the increased energy level shifts. There is no net change in the number of hydrocarbon–water con-

tacts, and no hydrocarbon–hydrocarbon contacts are established. There is essentially no change in the restriction of bond rotation because the over-all free energy changes are small. Therefore the total free energy of formation of a structure, as depicted in Fig. 5, and starting with two isolated side chains, is given by

$$\Delta F_{sl}{}^{0} = \Delta Y^{s}[(1/2)(F_{W}{}^{cc} + F_{W}{}^{0}) - F_{W}{}^{c}] \quad (19)$$

$$= \Delta Y^{s}[(1/2)\Delta F_{W}{}^{cc} + (F_{W}{}^{0} - F_{W}{}^{c})]$$

Numerical values of the thermodynamic parameters are given in Table IX for $\Delta Y^{s} = 1$. The actual values for any particular structure can be obtained by multiplication with the appropriate ΔY^{s}. In most cases, $\Delta Y^{s} = 4$ is to be used; higher values may be needed for large side chains on adjacent turns of the α-helix. The free energy change reaches 0.1 kcal./mole only for high temperatures, with large ΔY^{s}. Below 40°, its contribution to the over-all free energies of structural changes is negligible within the precision of the model. This result justifies the application of the results for isolated hydrophobic bonds in section 4.

The hydrophobic bond is strongly favored over the structure involving the single water layer. Therefore, it will form whenever this is sterically possible.

b. Side Chains Separated by Several Water Layers.—According to the present model, only the energy levels of water molecules next to non-polar solutes are changed, because the van der Waals forces causing the changes fall off rapidly with distance. Retaining this picture, the energy levels will remain unchanged for water molecules between side chains which are separated by more than one water layer. Therefore, the intervening water molecules behave thermodynamically just as the bulk water far from the solute. Thus, within the accuracy of the model, hydrophobic side chains can be considered as non-interacting until they actually touch, with the elimination of some intervening water neighbors. Practically all of the free energy change during the approach of the two side chains arises in this last step.

c. High Side-Chain Concentration.—Locally, the concentration of side chains in proteins is very large; they are separated by only a few water molecules in folded protein structures. According to the above discussion, the free energy of formation of this structure (starting from isolated side chains) is very close to zero near room temperature, and is very small even at higher temperatures. Within the accuracy of the model, this effect is unimportant and contributes only small changes in the quantities determining protein stability.

d. The Analogy with the Crystalline Gas Hydrates.—The structure of water near a non-polar solute has been compared in paper II with that prevailing in gas hydrates. However, it would be misleading to push the analogy too far and to consider the structure of water around non-polar groups in proteins as fully comparable with that in gas hydrates.[4] The possibility of forming extended gas hydrate-like ice structures on a protein surface is limited because the side chains, fixed to the backbone, cannot always be located at distances and in conformations required for the establishment of a spatially extended gas hydrate lattice. This renders the "coupling of ice-like lattices"[4] around the side-chains improbable. Even if the position of the side chains is geometrically suited for the formation of such lattices, these would have a much lower thermodynamic stability than the gas hydrates; in the latter, each cavity (or a large number of them) is occupied by a solute molecule, thereby increasing the effective coördination[41] by 3 or 4. What is more important, every water molecule in the gas hydrates (except on the surfaces of the crystal) is able to form its full complement of four hydrogen bonds. The energy of these bonds compensates for the entropy loss due to immobilization of the water molecules. The corresponding enthalpy is much smaller for structures around side chains or for large solute molecules; not all the molecules can form four hydrogen bonds, this being prevented sterically by the backbone or part of the solute (or side chain). Many water molecules can have at most two or three hydrogen bonds, but they are largely immobilized, resulting in a large entropy loss. This results in a much more positive free energy of formation than in the case of the gas hydrates. As a consequence, the free energies of formation of the gas hydrates and of the structures around protein side chains are not comparable. Side chains and solute molecules, even when of the same size (*e.g.*, valine and propane), cannot be fitted in an identical way into the water structure.

e. Extended Ice Layers around Proteins.—Klotz discusses protein behavior in several papers[4,8,19,42,43] in terms of the formation of a stable extended ice layer around the protein, stabilized by the coöperative interaction of the non-polar groups with water.

Both Klotz's and our treatment of non-polar side chains start from the same basic observation: non-polar solutes must cause an increase in "ice-likeness" of the water structure around them.[18,44] However, in this paper and in paper II it has been shown that this increase is unfavorable thermodynamically (see also ref. 10). An increased exposure of non-polar side chains to water, causing an increase of "ice-likeness," must result in an increase of the free energy. This in itself already is unfavorable. In a corresponding manner, the formation of an extensive ice lattice over several molecular layers around protein side chains would result in an even larger positive free energy change. Thus, even if such a lattice would form, contrary to the previous discussion, it would be unstable.

When side chains form hydrophobic bonds, some of them must still be exposed to water partially or totally. Thus there will be some non-polar portions on the surface of the protein, causing some ice-likeness of the water near the protein, but they

(41) This must be the source of the added stabilization of the gas hydrates over ordinary ice, rendering some of them capable of existence at temperatures above 0°.

(42) I. M. Klotz and J. Ayers, *J. Am. Chem. Soc.*, **79**, 4078 (1957).

(43) I. M. Klotz and H. A. Fiess, *Biochim. Biophys. Acta*, **38**, 57 (1960).

(44) H. S. Frank and W.-Y. Wen, *Discussions Faraday Soc.*, **24**, 133 (1957).

cannot have a stabilizing effect. The existence of very many non-polar groups must result in a tendency toward aggregation and precipitation.[10]

The clusters in water are short-lived,[44] and the presence of the non-polar solute probably will not affect the life-time very much, even though it increases the equilibrium degree of hydrogen bonding. In view of this, an explanation of a decreased reactivity of various groups on proteins in terms of masking by an ice-like lattice of water[43] is improbable.

Klotz points out correctly that there are differences between freely moving small organic solutes and the side chains attached to the polypeptide framework.[4] While utilizing solution data for hydrocarbons for the calculation of strengths of hydrophobic bonds earlier in this paper, differences between the two kinds of solutes have been taken into account[20] (see also section 6c).

The observations to which Klotz applies the concept of extended ice formation in the papers cited can be explained just as well on the basis of hydrophobic bonding while, at the same time, meeting the thermodynamic requirements.

Masking of reactive groups in native proteins may occur if such groups are buried in hydrophobic regions (section 6b). This may even take place in randomly coiled structures, where hydrophobic bonding is possible, as indicated in section 4c. Klotz discusses[4] the pK changes of a conjugate of polyvinylpyrrolidone containing 5-dimethylamino-1-naphthalene sulfonyl groups. The polymer cannot form hydrogen-bonded folded structures due to the absence of hydrogen bonding groups. The masking of the $N(CH_3)_2$ group, observed in aqueous solution, may well be due to hydrophobic bonding in the random coil. This is the more likely since the naphthalene group next to the reactive group offers a large surface for hydrophobic bonding. The normalization of the pK by urea in this polymer[4] and in others mentioned by Klotz[4] can be explained if urea breaks hydrophobic bonds.[45,46]

The effect of masking ionizable groups by burying them in hydrophobic regions has been discusssed recently by Tanford.[47] A similar case may exist in the binding of small ions[19]; if placing a charge on the binding site has to result in a breaking of hydrophobic surroundings, binding will be enhanced. In detergent binding, stabilization must occur through the formation of hydrophobic bonds between side chains and detergent molecules. The sudden increase of detergent binding to serum albumin at a certain detergent concentration,[48,49] discussed by Klotz and Luborsky[19] in terms of a coöperative stabilization of the water lattice, may be caused either by unfolding, leading to exposure of non-polar side chains,[48,49] or by an increase of the effective binding surface, due to the bridging of the side chains by the detergent molecules.

(45) W. Bruning and A. Holtzer, *J. Am. Chem. Soc.*, **83**, 4865 (1961).
(46) I. Z. Steinberg and H. A. Scheraga, *ibid.*, **84**, 2890 (1962).
(47) C. Tanford, *ibid.*, **83**, 1628 (1961).
(48) J. T. Yang and J. F. Foster, *ibid.*, **75**, 5560 (1953).
(49) M. J. Pallansch and D. R. Briggs, *ibid.*, **76**, 1396 (1954).

6. Interactions of Several Side Chains

In large proteins, more than two side chains can interact simultaneously in some conformations. Except for special cases, such interactions are possible only when side chains belonging to more than one peptide backbone can be placed adjacent to each other. A great variety of hydrophobic bonds of various strengths, *i.e.*, extent of contact, is possible, ranging from the interaction of two side chains to the formation of entire hydrophobic regions. The free energy changes of formation of larger structures are related to those of the pair interaction (section 3), but they are not obtained from them as their simple multiples.

a. Interaction of More Than Two Side Chains.—If k side chains interact with each other simultaneously, an expression similar to eq. 11 can be used to calculate the free energy of formation for such a hydrophobic bond.

$$\Delta F_{H\phi}^{0} = \Delta Y_k^{s}[F_W^{0} - F_W^{c} - (1/2)E_{RW}] + Z_{R,k}E_R + \sum_{j=1}^{k} \Delta F_{rot,j} \quad (20)$$

Here, ΔY_k^{s} and $Z_{R,k}$ are the total number of water molecules removed from contact with side chains and the total number of C...C contacts established, respectively. Their value depends on the geometry of the interaction, and may differ from the sum of the values for pairwise contacts between the side chains involved. A ΔF_{rot} term has to be included only once for each side chain, rendering $\Delta F_{H\phi}^{0}$ more favorable than the sum of the free energies over the various pairwise contacts.

When estimating ΔY_k^{s}, it has to be kept in mind that portions of the peptide backbones may contribute to the prevention of water molecules from having contacts with parts of some side chains, thereby strengthening the hydrophobic bond. Examples of hydrophobic bonds between three side chains are given in Fig. 6; thermodynamic parameters for the formation of bonds of this type are given in Table X (see also ref. 23).

TABLE X

THERMODYNAMIC PARAMETERS FOR THE FORMATION OF A HYDROPHOBIC BOND BY THREE ISOLEUCINE SIDE CHAINS AT 25°

Type of bond	r/r_0	ΔY_k^{s}	$Z_{R,k}$	$\Delta F_{H\phi}^{0}$ kcal./mole	$\Delta H_{H\phi}^{0}$	$\Delta S_{H\phi}^{0}$ e.u.
(*i*) Two pairwise contacts (Fig. 6-I)						
maximum	1.5	32	13	−4.2	6.4	35
minimum	1.05	4	2	−0.6	0.7	4.4
(*ii*) Triple contact (Fig. 6-II)						
maximum	2.0	36	18	−4.9	6.7	38
minimum	1.2	8	3	−0.9	1.6	8

b. Hydrophobic Regions.—Several side chains, belonging to different backbone portions, may associate so as to form a "hydrophobic region." This is a conglomeration of several side chains, creating a region in space of several atomic diameters, from which water is completely excluded.

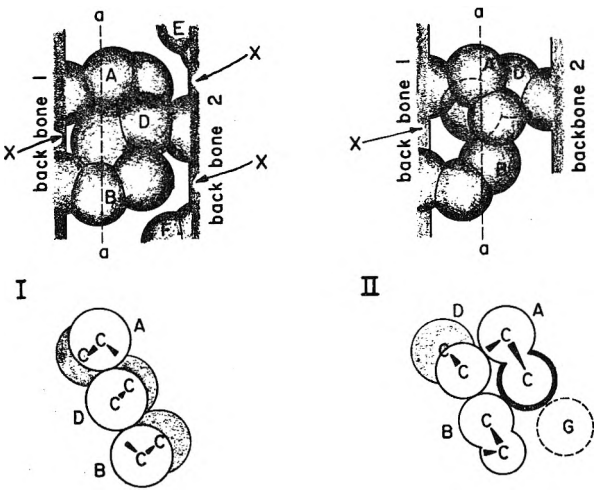

Fig. 6.—Schematic representation of typical hydrophobic bonds involving three side chains. (Covalent bond lengths and van der Waals radii not to the same scale.) The upper drawings represent a side view of the structure. The lower drawings are sections along a plane through a---a, perpendicular to the plane of the paper. (I) Two pairwise contacts between side chains A...D and B...D, respectively. Further interactions of A and B are possible with side chains in locations E and F, respectively. (II) One triple contact of the three side chains A, B, and D. An additional side chain (belonging to backbone 2) may be located in position G in the case of a bond of higher order. X marks the locations where contacts between side chains and the opposite backbone are possible.

The region may enclose some side chains completely. An important example would be the trapping of a polar group, *i.e.*, one capable of ionization or hydrogen bond formation (*cf.* section 7). These groups would exhibit anomalous reactivity as a result of being "buried" among the non-polar groups.[11,47,50]

The formation of a hydrophobic region of sufficient size to contain "buried" groups is possible only by means of interaction of side chains on three or more backbone portions. Observations with space-filling models indicate that two helices are not sufficient.

Equation 20 also applies to the free energy of formation of a hydrophobic region.

The presence of a buried polar group will affect the interactions and hence will change the free energy of formation of the hydrophobic region, but eq. 20 still can be used as a first approximation.

c. Transfer of a Non-polar Side Chain from Water into a Non-polar Environment.—Within a hydrophobic region, a non-polar side chain may be surrounded completely by other side chains, without being in contact with water molecules. It is possible to calculate the difference of the free energy between this state and that of the isolated side chain surrounded completely by water. This difference can be termed the free energy of transfer of a side chain from water into a non-polar region. It is given by

$$\Delta F_{tr}^0 = Y^s[F_w^0 - F_w^c - (1/2)E_{RW}] + Z_R E_R + \Delta F_{rot} \quad (21)$$

where Y^s is the total number of water neighbors around the side chain, given in Table I, and $Z_R = {}^1/_2 Y^s$ in this case. Numerical values for various side chains are given in Table XI. In determining ΔF_{rot}, $\tau/\tau_0 = 1.5$ was used.

TABLE XI

THERMODYNAMIC PARAMETERS FOR THE TRANSFER OF A NON-POLAR SIDE CHAIN FROM WATER INTO A NON-POLAR REGION AT 25°

Nature of region	Side chain	ΔF_{tr}^0	ΔH_{tr}^0	ΔS_{tr}^0
		kcal./mole		e.u.
Aliphatic	Ala	−1.3	+1.5	+ 9.4
	Val	−1.9	2.2	13.7
	Leu	−1.9	2.4	14.3
	Ileu	−1.9	2.4	14.5
	Met	−2.0	2.7	16.0
	CySH	−1.6	1.8	11.4
	Pro	−2.0	2.2	14.0
	Phe[a]	−0.3	2.7	10.1
Aromatic	Phe	−1.8	1.0	9.5

[a] In determing ΔF_{rot}, $\tau/\tau_0 = 1.1$ was used.

The thermodynamic parameters estimated by Kauzmann[10] correspond to an analog of *this* process, not to the formation of a pairwise hydrophobic bond as discussed above. Kauzmann's numbers must be compared with those of Table XI. The absolute values of the free energies in Table XI are still smaller than his numbers. This difference arises because in the present calculation the effect of the backbone has been taken into account. Y^s is smaller than Y^c, the number of water neighbors around the comparable hydrocarbon, because the side chain is attached to the polypeptide backbone. (*E.g.*, the hydrocarbon, whose size corresponds to the valine side chain, is propane, or else isobutane if the α-carbon also is counted.) There is an additional difference between the two sets of data. While the hydrocarbons considered by Kauzmann,[10] and also in paper II of this series,[6] are straight chain homologs, most of the amino acid side chains are branched and hence more compact in shape. For this reason, Z_R in the non-polar surroundings increases with size more slowly for the branched side chains than for these normal hydrocarbons. As a result, ΔH_{tr}^0 becomes more positive with increasing side-chain size instead of the reversed trend observed[6,10] for the hydrocarbons. The increments in ΔH_{tr}^0 with size are small numbers; hence small differences in the intermolecular interactions can cause considerable changes in the observed trends. These small differences arise from a balance between the first and second terms of eq. 21; in the case of the normal hydrocarbons the term $Z_R E_R$ predominates, whereas in the case of branched side chains the first term predominates. Since eq. 21 was derived from the considerations of paper II, its application to normal hydrocarbons yields theoretical values in agreement with experimental data.

A note of caution is in place here concerning the use of either Kauzmann's data or those of Table XI for the prediction of free energies involved in protein interactions. It would not be correct to use these numbers or a multiple of them (multiplying by the number of side chains) to predict the free energy of formation of the *entire* hydrophobic region. When the hydrophobic region is formed,

(50) J. Hermans, Jr., and H. A. Scheraga, *J. Am. Chem. Soc.*, **83**, 3293 (1961).

some of the side chains comprising it, located on the surface of the region, will retain some water neighbors. This has to be taken into account by using eq. 20 to determine the free energy of formation.

7. Participation of Polar Side Chains

Some amino acids can be classified as "polar." They have long hydrocarbon side chain portions carrying a group which can ionize or form hydrogen bonds. Tyrosine, arginine, lysine, glutamic acid, and glutamine fall into this group. Asparagine also may be included here, though the effects must be marginal.

The polar end of these side chains is hydrophilic, especially when ionized. It presumably seeks to be in aqueous surroundings when this is possible. On the other hand, the non-polar portion must seek to form hydrophobic bonds with neighboring side chains wherever these can be established. A detailed quantitative treatment of the changed reactivities of a hydrogen bond in the presence of hydrophobic bonds has been developed in this Laboratory, and will be reported elsewhere.[51]

An estimate of the strength of hydrophobic bonds involving non-polar portions of the side chains listed above can be approximative at most. The polar group interacts strongly with water and interferes with the establishment of the water structure characteristic for the neighborhood of non-polar solutes. This effect is most pronounced when the polar group acquires a charge; ions affect the structure of water around them locally over a distance of several molecular diameters by means of strong electrostatic interactions.[44,52] Even interactions of the un-ionized polar group with water may perturb the spacing of the energy levels of the water molecules at least as much as the non-polar groups. However, the model presented above can be applied to these side chains as an approximation, keeping in mind that the results are less reliable than those for entirely non-polar side chains. Representative values are given in Table XII.

TABLE XII

THERMODYNAMIC PARAMETERS FOR THE FORMATION OF HYDROPHOBIC BONDS INVOLVING SIDE CHAINS CARRYING POLAR END GROUPS (25°)

(Maximum bond strengths)

Amino acid	ΔY^s	Z_R	$\Delta F_{H\phi^0}$ kcal./mole	$\Delta H_{H\phi^0}$ kcal./mole	$\Delta S_{H\phi^0}$ e.u.
Glutamic acid[a] / Glutamine[a]	4	2	−0.5	0.7	4.0
Arginine[a]	6	3	−0.7	1.1	6.0
Lysine[a]	8	4	−1.0	1.4	8.1
Tyrosine[b]	10	5	−1.2	0.7	6.1

[a] Bonded to leucine. [b] Bonded to phenylalanine.

Some justification of such a calculation can be derived from heat capacity measurements of aqueous carboxylic acid solutions. Schreiner[53,54] has found an increment of about 20 cal./deg. mole in the partial molal heat capacities per CH_2-group for formic, acetic, and propionic acids and their respective Na-salts, and, for the acids, an increment of about 10 cal./deg. mole in the difference between the partial molal heat capacity in solution and in the pure liquid. The latter quantity is in good agreement with the observed and calculated increments for the solution of hydrocarbons (see Table VII of paper II). Apparently, the non-polar portions of the acids still can exert about the same influence on the energy states of water as in non-polar solutes, in spite of the presence of the polar or ionic head, although the exact local structure of water in their neighborhood might be different from that in solutions of pure hydrocarbons.

The non-polar parts of the side chains considered here are located near the backbone and hence are less accessible for hydrophobic bonding than the unobstructed ends of completely non-polar side chains. Consequently, they can form bonds only with large side chains, and the maximum values of all parameters must be smaller than those for isolated non-polar side chains.

8. Estimates of Volume Changes

It has been found experimentally that the partial molal volumes of non-polar solutes in aqueous solutions are much smaller than in the liquid or in a non-polar solvent.[55,56] A mechanism for the volume change was given in paper II. The formation of a hydrophobic bond, corresponding to a partial reversal of the solution process, should be accompanied by a volume increase, computed in paper II as

$$\Delta V_{H\phi}{}^0 = 1.79\,\Delta Y^s x_4{}^c \qquad (22)$$

The quantity $1.79x_4{}^c$ for aliphatic and aromatic hydrocarbons, derived from data presented in paper II, is given in Table XIII for various temperatures. For an aromatic–aliphatic hydrophobic bond, the arithmetic mean has to be taken. At 25°, $\Delta V_{H\phi}{}^0 = 3$ to 7.7 cm.³/mole, depending on the value of ΔY^s. This most probably is an underestimate, because the calculated ΔV^0 values in paper II also were too low for the aliphatic hydrocarbons. However, if part of the observed ΔV^0 for solution originates in the packing of the non-polar liquid, this contribution may be different for the interaction of a pair of side chains. In cases where the packing of the side chains is imperfect, leaving small cavities between them which cannot be occupied by a water molecule, $\Delta V_{H\phi}{}^0$ will be increased to an even higher value.

If hydrophobic bonds are broken during the denaturation or hydrolysis of proteins, exposing more non-polar side chains to water, the process will be accompanied by a volume decrease. This furnishes an explanation of the volume changes cited by Klotz.[8,57] The present theory also can

(51) G. Némethy, I. Z. Steinberg, and H. A. Scheraga, *J. Am. Chem. Soc.*, to be submitted.

(52) Ions contained in the solution may have another non-localized, more general influence on hydrophobic bonding, particularly at high concentrations, by changing the association equilibria for pure water, which is a result of the formation of hydration shells around the ions.

(53) F. Schreiner, Ph.D. Thesis, Universität Hamburg, 1959.

(54) Th. Ackermann and F. Schreiner, *Z. Elektrochem.*, **62**, 1143 (1958).

(55) D. D. Eley, *Trans. Faraday Soc.*, **35**, 1421 (1939).

(56) W. L. Masterton, *J. Chem. Phys.*, **22**, 1830 (1954).

account for the observation[8,57] that the volume decrease is larger at lower temperatures; the changes in the water structure near non-polar groups are more pronounced at low temperature.

9. The Role of Hydrophobic Bonds in Proteins

Hydrophobic bonds, taken individually, are perhaps weaker than some of the other side-chain interactions in proteins. They become important because of the large number and high frequency of occurrence in proteins of non-polar side chains (including the non-polar portions of the polar amino acids). Hydrophobic bonds exhibit less specificity than other interactions such as hydrogen bonds, both with respect to the steric requirements of side-chain orientation and the number and kind of side chains which can participate in their formation.

TABLE XIII

VOLUME CHANGES FOR THE FORMATION OF HYDROPHOBIC BONDS, EXPRESSED PER MOLE OF WATER REMOVED FROM CONTACT WITH THE SIDE CHAINS

t, °C.	$\Delta V_{H\phi}^0/\Delta Y^s = 1.79x_4^s$ (cm.³/mole) for aliphatic side chains	aromatic side chains
0	0.94	0.83
25	.74	.65
50	.57	.50
70	.46	.40

A second property unique to hydrophobic bonds is their dependence on the solvent medium for their existence. They can achieve a high degree of importance only in aqueous systems. Even in other strongly polar solvents, the interactions between non-polar side chains are due only to differences in van der Waals forces between various solution components, with no important contribution from changes in the solvent structure. In such solvents, it might be more appropriate to term the interactions "non-polar bonds." The changes in solvent structure are unique to water with its special structural features. However, since the behavior of proteins *in aqueous systems* is of greatest interest, hydrophobic bonds must be considered an important factor in discussing protein behavior.

In non-aqueous solvents whose molecules consist partly of non-polar, hydrocarbon-like groups, there is no need for the non-polar side chains to form strong bonds with each other. Interaction with the solvent is just as favorable as with other side chains. This effect may be important in the denaturation of proteins by alcohols and other organic solvents. Even in solvent mixtures containing water and an organic solvent, the latter may form hydrophobic bonds with the non-polar side chains, facilitating unfolding of the protein.

This effect is related to detergent binding, too. Although the binding of a detergent on a protein presumably is determined primarily by interactions involving its polar head, the binding will be enhanced if the non-polar tail of the detergent can form hydrophobic bonds with exposed side chains. If the non-polar tail of the bound molecule is sufficiently large, it can interact with more than one non-polar side chain on the protein. In this manner, low concentrations of detergents may stabilize the folded structure. However, at higher concentrations, the detergent may act as a denaturant by breaking the side-chain hydrophobic bonds and establishing detergent–side-chain hydrophobic bonds.

In general, hydrophobic bonds and other types of side-chain interactions are present simultaneously in proteins. The folding of the molecule and the stability of the various conformations is a resultant of all the interactions. The various interactions exist side by side and may act coöperatively in stabilizing certain structures.[11,58] In such cases, the individual contributions may not always be separable experimentally. A detailed discussion of the coöperative effects with other interactions and of the role of hydrophobic bonds in protein reactions[11] is beyond the scope of this paper. A detailed quantitative investigation, applying the results presented here, has been carried out and will be reported elsewhere.[51]

It has been pointed out to us by Eigen[59] that activation energies of enzyme–substrate complex formation are more sensitive to the influences of hydrophobic bonding than the equilibrium thermodynamic parameters which show only the difference of the amount of hydrophobic bonding in two structures. Observed high entropies of activation in dye complexing of serum albumin[59] may be due to this effect.

The activation energies of other protein reactions involving side-chain interactions may be affected in a similar manner by hydrophobic bonds if forming the activated state requires the breaking of hydrophobic bonds.[11]

Klotz and Franzen[60] report a $\Delta H = 0$ for the dimerization of N-methylacetamide in water (in contrast to a negative ΔH_{dim} in organic solvents) and conclude that the zero value represents the intrinsic strength of the N–H...O=C hydrogen bond in water. In the dimer formed by this compound, the methyl group on the nitrogen of the molecule acting as acceptor in the hydrogen bond, and the methyl group on the carbonyl carbon of the second molecule approach each other to within 4 Å. when a linear hydrogen bond is formed; thus a hydrophobic bond is formed between the two molecules. Such an interaction corresponds to that described as the bond of minimum strength in section 3b, with a $\Delta H_{H\phi}^0 = +0.4$ kcal./mole. The possible presence of a hydrophobic bond furnishes an alternative explanation of Klotz's observation, because the positive enthalpy of formation of the hydrophobic bond may cancel a negative enthalpy contribution made by the hydrogen bond. Higher homologs should show even stronger hydrophobic bonding and currently are being investigated in this Laboratory.

(57) K. U. Linderstrøm-Lang, *Cold Spring Harbor Symp. Quant. Biol.*, **14** 117 (1950).

(58) C. Tanford, in "Symposium on Protein Structure," A. Neuberger, ed., John Wiley & Sons, New York, N. Y., 1958, p. 35.

(59) M. Eigen, personal communication.

(60) I. M. Klotz and J. S. Franzen, *J. Am. Chem. Soc.*, 84, 3461 (1962). We are indebted to Dr. Klotz for permission to quote these results prior to publication.

10. Conclusions

The theoretical model and the calculations presented in this paper provide a sufficient basis for a quantitative estimation of the contribution of hydrophobic bonds to the stabilization and to the reactions of proteins. Their role in various protein reactions has been reviewed earlier qualitatively.[11]

It is recognized that the theory contains assumptions that may be oversimplifications, and that it may later become subject to revisions or improvements, based on a fuller understanding of the behavior of liquids than is available at present. One particular point where such refinement might be possible is the treatment of the effects of high side-chain concentrations. However, based on the present state of knowledge, the theory presents a unified treatment of the behavior of non-polar side chains, and it can be utilized to form part of quantitative treatments of proteins in terms of the various possible types of interactions.

It has to be noted that, while the methods used here or perhaps even some of the exact numerical values obtained with their aid may become modified as a result of improvements due to a better insight into the behavior of liquids, there are various aspects of the present discussion which do not depend on the details of the model and are of an even more general validity than the model itself. The conclusions about the sign and magnitude of the thermodynamic changes, and of their temperature dependence, are inherent in any model based on the analogy with aqueous solutions of small hydrocarbons and organic solutes. These results would not be affected by changes in the methods used to derive the thermodynamic parameters of formation of the hydrophobic bond. The changes might affect the exact values of the parameters at most, and this only to a limited extent. The discussion of the behavior of hydrophobic bonds in different protein structures, presented mainly in the second half of this paper, is independent of the particular model used for describing the solute–water interactions.

The concepts presented here suggest several kinds of possible experiments. Valuable data could result from detailed studies of polypeptides composed of a limited number of different amino acids, investigating their changes of conformation as a result of changes in temperature or solvent composition, or of the addition of small molecules such as detergents or hydrocarbons. A study of the possible solubilization of hydrocarbons by proteins may yield information concerning the nature of the surface of the protein molecule.

Further extensions of the theory presented here are possible, such as a treatment of the behavior of proteins in mixed solvents, considering both the effects of the changes in the water structure and of direct interactions of the solvent components with the groups on the proteins. Similarly, the binding of small molecules to proteins, or solvation in micelles, might be treated on the basis of the present theory.

Acknowledgment.—We wish to thank Dr. I. Z. Steinberg for helpful discussions and suggestions in connection with some of the questions treated in this paper. Also, we wish to acknowledge the opportunity for the use of the facilities of the Cornell Computing Center, under the direction of R. C. Lesser, for extensive numerical calculations involved in the present work.

DISCUSSION

H. E. RIES, JR. (American Oil Company).—Would you give the approximate size of the holes in the so-called "water clusters?" Are they large enough for normal hydrocarbon chains?

H. A. SCHERAGA.—The water cluster forms a *partial* cage around the hydrocarbon solute. The cage does not *completely* enclose the hydrocarbon chain. See Fig. 3 and 4 of paper II for an illustration of the relative size of the partial cage.

J. LYKLEMA (University of Southern California).—Is it possible to obtain inference on the hydration and iceberg-formation of actual systems from electrokinetic measurements?

H. A. SCHERAGA.—We cannot do so in the present stage of the theory. Our calculations pertain to the influence of *non*-polar groups on water structure. We have, as yet, made no calculations about the influence of polar groups on the solvent; the polar groups would play an important role in electrokinetic measurements. We are, however, considering the extension of our calculations to take account of the influence of polar groups (ions and dipoles) on the structure of water.

Also, we are carrying out several experimental studies (other than electrokinetic measurements) on model systems in order to assess the influence of non-polar groups on the water structure.

R. J. GOOD (General Dynamics).—Does your theory of water explain the change in slope of the surface tension of supercooled water that occurs around $-14°$?

H. A. SCHERAGA.—While our theory is applicable to a calculation of the surface tension of water, we have not computed this quantity. In the first paper of this series we have pointed out that our model does not give rise to any discontinuity of the calculated properties near 35°, a temperature at which discontinuities have been reported. Therefore, I doubt if calculations with our model would show any discontinuities in the surface tension of supercooled water. However, it may be possible to modify eq. 6-8 of paper I in order that the model lead to discontinuities in the thermodynamic properties.

CONTACT ANGLE RELATIONSHIPS ON SILICA AQUAGEL SURFACES

BY ALAN S. MICHAELS AND SHELDON W. DEAN, JR.

Department of Chemical Engineering, Massachusetts Institute of Technology, Cambridge, Massachusetts

Received March 12, 1962

Silica gels were prepared by acidification of purified sodium silicate solution containing 4% SiO_2. These gels were used as substrates for contact angle measurements with paraffin oil drops and methylene iodide drops in air. In the absence of capillary active contaminants, no significant hysteresis of the contact angle was observed, and the values of the contact angles checked closely with the Young's equation values predicted from the surface and interfacial tensions of the oils against pure water. Traces of such contaminants caused marked hysteresis. Contact angles made by solutions of hexadecanol in purified paraffin oil against pure silica gel were determined as a function of solute concentration. At hexadecanol concentrations below 0.25% by weight of oil, contact angle hysteresis was appreciable and concentration dependent, although advancing angles approximated those predicted from Young's equation. Above 0.25%, hysteresis disappeared, and Young's equation was obeyed. Oil containing *n*-decanol did not exhibit hysteresis at any concentration studied. A mechanism, based on local compression of the interfacial film, has been suggested to explain the contact angle behavior. This type of phenomenon may also occur on solid surfaces, and can constitute a cause of hysteresis.

I. Introduction

The equilibrium angle of contact of a liquid–gas interface with a plane solid surface is related to the boundary tensions of the system by Young's equation

$$\cos\theta = \frac{\gamma_S - \gamma_{SL}}{\gamma_L} \qquad (1)$$

where θ is the contact angle, γ_S, γ_L, and γ_{SL} are the solid surface, liquid surface, and interfacial tensions, respectively. This relation has been derived in a rigorous and general manner.[1] However, neither the solid surface nor the solid interfacial tensions are directly measurable so that it has not been possible to verify this relationship experimentally. Furthermore, hysteresis of the contact angle introduces further ambiguities into the experimental confirmation of eq. 1. Surface roughness, contamination, and heterogeneity have all been found to be contributory to hysteresis.

Since contact angle hysteresis has not been reported to exist at the intersection of three fluid phases, and since a properly prepared gel surface would approach an ideal solid surface, investigation of the contact angle of oils on dilute aquagel surfaces might give insight into the origin of hysteresis on solid surfaces. A further advantage of using a gel surface as a substrate for wetting measurements is that the boundary tensions of a dilute gel (provided the gelling agent is not capillary active) are probably quite close to those of the solution that exists before gelation occurs, so that the relationship between the observed advancing and receding angles to the predicted Young's equation angle can be established.

Silica gel was chosen as the gel phase because: (1) silica is a neutral material, *i.e.*, is not capillary active; (2) it forms strong gels at low concentrations; and (3) silica gel can be prepared with relative ease by acidification of a dilute sodium silicate solution, and the setting time (the time between mixing of the reagents and gelation) can be specified at almost any value[2] by carefully controlling the final pH of the system. Paraffin oil and methylene iodide were chosen as oil phases because of their high calculated contact angles based on their boundary tensions against water. The majority of the studies were conducted with paraffin oil, since methylene iodide was found to decompose spontaneously due to a reaction which was accelerated by light.

(1) R. E. Johnson, Jr., *J. Phys. Chem.*, **63**, 1655 (1959).

(2) R. C. Merrill and R. W. Spencer, *ibid.*, **54**, 806 (1950).

Nomenclature

c	concentration, % by weight
R	gas constant, ergs per g. mole, °K.
T	temperature, °K.

Greek letters

γ	boundary tension, dynes/cm.
Γ	boundary concn. (or excess), moles/Å.^{2}
π	boundary (spreading) pressure, dynes/cm.
θ	contact angle, degrees

Subscripts

L	liquid
S	solid
V	vapor
(c)	equilibrium value at concn. c

Superscripts

A	advancing
0	no solute present
R	receding
RA	readvancing
RR	rereceding

II. Experimental

A. Materials.—White, light, paraffin oil, obtained from Fischer Scientific Co., was purified by treatment with fuming sulfuric acid. The oil was then washed with water and dilute sodium hydroxide. The last traces of capillary active materials were removed by percolation of the oil through activated silica gel. The resulting oil was colorless, odorless, and its interfacial tension against a 2% aqueous sodium hydroxide solution was 53.5 dynes/cm. and showed no significant lowering for a 2-hr. period.

Methylene iodide, obtained from Eastman Distillation Products, Inc., Rochester, New York, was purified by fractional distillation in an all-glass apparatus at a total pressure of 5.0 mm. The center 50% was combined and fractionally crystallized twice from the melt. The final product had a clear, pale yellow color and melted at 6.06°, compared to Fox's value of 6.10°[3] and Carter and Jones, 6.05°.[4] The surface and distilled water interfacial tensions were found to be 50.2 and 41.4 dynes/cm., and the surface tension of water saturated with methylene iodide was found to be 71.9 dynes per cm. at 25°.

Sodium silicate solution, grade 33, obtained from the Diamond Alkali Co., with a SiO_2 to Na_2O weight ratio of 3.4 to 1 and density of 1.3916 g./cc., was used to prepare the silica gels by acidification of a dilute solution with sulfuric acid. The sodium silicate solution was purified by contact filtration with activated charcoal until the silicate caused no lowering of the interfacial tension of the purified

(3) W. Fox, *J. Chem. Phys.*, **10**, 623, 743 (1942).

(4) E. G. Carter and D. C. Jones, *Trans. Faraday Soc.*, **30**, 1025 (1934).

paraffin oil in a 6% solids content aqueous solution during a 2 hr. test.

Du Pont reagent grade sulfuric acid was purified by three fractional crystallizations of the monohydrate. The final product was clear, colorless, and a 2% solution showed no significant lowering of interfacial tension against the purified paraffin oil for a 2 hr. period.

Hexadecanol, obtained from Eastman Distillation Products Industries, was purified by crystallization from an ethanol–water mixed solvent. After purification the melting point range was 48.5 to 49.5°, compared to the literature value of 49.3°.[5]

Decanol, obtained from Eastman Distillation Products, Inc., was purified by fractional distillation in an all-glass unit at a pressure of 10 mm. The center 60% was combined and fractionally crystallized from the melt, discarding the least fusible third each time. The final product froze between 6.363 and 6.008°, compared to the cited value of 6.0°.[6]

Distilled water from a commercial block tin laboratory distillation apparatus was found to be sufficiently free of capillary active impurities ($\gamma_{23}° = 71.98 \pm 0.02$ dynes/cm.); therefore, no further purification was necessary.

B. Apparatus.—The surface tension measurements were made with a Wilhelmy slide apparatus constructed from a chainweight type analytical balance. A glass slide was used for measurements on aqueous solution; a platinum slide was used for organic materials. This apparatus was accurate to ±0.05 dyne/cm. Interfacial tensions were obtained from measurements of the Neumann "contact" angles, the angles associated with the three fluid phase intersection of an oil drop on the aqueous phase in air. This method was generally accurate to ±0.1 dyne/cm. Both the Wilhelmy slide and Neumann angle technique were reproducible and permitted the surface and interfacial tensions to be measured as a function of time. Drop weight, du Nouy ring, and pendant drop methods were also investigated, but they were not generally satisfactory; the former two because they were insensitive to traces of capillary active contaminants, and the latter, because of its physical limitations in handling gelling solutions.

Contact angles, including the Neumann angles, were photographed by means of a photomicrographic apparatus employing a Polaroid-Land camera. The angles formed by sessile drops were silhouetted by means of a collimated light source, and the resulting image was magnified about 60 diameters. The system under consideration was held in a closed, temperature controlled cell. The angles were measured directly from the photographs with an accuracy of about ±0.4°.

C. Procedure.—Silica gels were prepared from the purified reagents by acidifying a dilute sodium silicate solution so that a silicic acid sol, which gelled in about 3 hr. at 25°, resulted, containing 4.0% SiO_2 at pH 4.05. The gels were allowed to age and harden before measurements could be made without deformation of the gel surface. During this hardening period, exudation (syneresis) of aqueous liquid from the gels occurred, necessitating a careful drying process before contact angles could be measured. This was accomplished by placing the gels in a desiccator over an indicating silica gel dehydrating agent. As soon as the last trace of free liquid had evaporated, the gel was removed from the drying desiccator and stored in another desiccator over an aqueous 0.19 *M* sodium sulfate solution until the measurements were begun.

Solutions of hexadecanol in purified paraffin oil were prepared ranging from 0.0001 to 1.0% hexadecanol, and the surface tension, distilled water interfacial tension, and the distilled water surface tension in equilibrium with the oil were measured. Contact angles of these oils on gel surfaces were also measured. Solutions of decanol in purified paraffin oil were prepared, ranging from 0.001 to 1.0% decanol. Boundary tensions and contact angles were measured for these solutions as they were for hexadecanol.

With the hexadecanol–oil–water system, rate of attainment of boundary tension equilibrium was quite slow. Complete equilibration at the oil–water interface was attained in about 2 hr. at 0.001% hexadecanol concentration, the time increasing to about 4 hr. at the higher concentrations studied. Equilibration at the water surface was virtually instantaneous below 0.1% hexadecanol, but required extremely long periods of time (upwards of one week) at a concentration of 0.15%, corresponding to the condition where the alcohol first adsorbed in substantial concentration at the water surface. At still higher concentrations, the equilibration time for the water-surface decreased to about 8 hr. The greatest changes in both surface and interfacial tensions took place during the first half-hour of measurement; subsequent changes with time seldom exceeded 1.0 dyne/cm. These changes were reflected in a 5–10° change in the Neumann angle during the first 10 min. of observation, and an additional 5–10° change during the next 20 min.

With the decanol–oil–water system, wherein both phases were initially mutually saturated, the time for boundary equilibration was much shorter—seldom longer than 2 hr. The major changes invariably took place within the first 5 min. of observation.

With the alcohol–oil–gel systems, on the other hand, no time-dependent variations in contact-angles were observed (within experimental error) within the period of observation of approximately 30 min. The period of observation was necessarily limited by continued shrinkage of the gel, which eventually caused the gel surface to fall below the rim of the confining vessel.

III. Results

A. Pure System Contact Angles.—Contact angle measurements performed on gel surfaces before they harden completely were unsuccessful because the gel deformed in the region of the three phase intersection; the gel surface apparently was pulled upward into a ridge by the vertical component of the surface tension of the oil phase. This deformation was in many respects similar to that predicted by Lester[7] for the elastic deformation of a low-modulus solid in contact with a liquid droplet. The angle formed between the gel surface and the liquid surface in this case was close to the appropriate Neumann angle for the system. However, as the gel became more rigid, this deformation became smaller, and the angle increased from the Neumann angle typical of a three fluid phase system to the Young's angle value for a rigid solid, thus indicating the validity of Young's equation for a "hardened" gel surface.

The results of the pure system boundary tension measurements appear in Table I. The contact angle measurements with purified paraffin oil and methylene iodide on purified silica gel, together with the results of pure paraffin oil on an unpurified gel, appear in Table II. The Young's equation contact angles computed from the boundary tension data presented in Table I also appear in Table II. From these results it was deduced that: (1) in the absence of capillary active impurities, contact angle hysteresis is virtually absent; (2) in purified systems the observed angles are essentially equal to the values predicted from Young's equation; and (3) trace amounts of capillary active contaminants can cause major changes in the observed contact angles and can cause marked contact angle hysteresis. It was further concluded that these silica gel surfaces are satisfactory for studying the effect of capillary active agents on contact angle hysteresis.

B. Hexadecanol in Oil.—The results of the boundary tension measurements of the solutions of

(5) C. D. Hodgman, Ed., "Handbook of Chemistry and Physics," 34th Ed., Chemical Rubber Publishing Co., Cleveland, Ohio, 1952, p. 822.

(6) C. C. Addison and S. K. Hutchinson, *J. Chem. Soc.*, 3387 (1949).

(7) G. Lester, *J. Colloid Sci.*, 315 (1961).

TABLE I

SELECTED BOUNDARY TENSION VALUES AT 25.0°

Phase 1	Phase 2	γ_{12} accuracy, dynes/cm.	Method
Water	Air	71.98 ± 0.02	Wilhelmy slide
4% SiO_2 sol	Air	72.72 ± .03	Wilhelmy slide
Pure paraffin oil	Air	30.3 ± .1	Wilhelmy slide and ring
Pure paraffin oil	Air	30.2 ± .1	Drop weight
Par. oil + 1% cetyl alc.	Air	30.1 ± .2	Drop weight
Par. oil + 1% decyl alc.	Air	30.2 ± .2	Drop weight
Water	Pure para. oil	53.0 ± .1	Neumann angle
4% SiO_2 sol	Pure para. oil	53.5 ± .2	Neumann angle
Water sat. w. MeI_2	Air	71.9 ± .1	Wilhelmy slide
MeI_2	Air	50.2 ± .1	Wilhelmy slide
MeI_2	Air	50.2 ± .2	Neumann angle
MeI_2	Air	50.1 ± .5	Pendant drop
MeI_2	Water	41.4 ± .2	Neumann angle

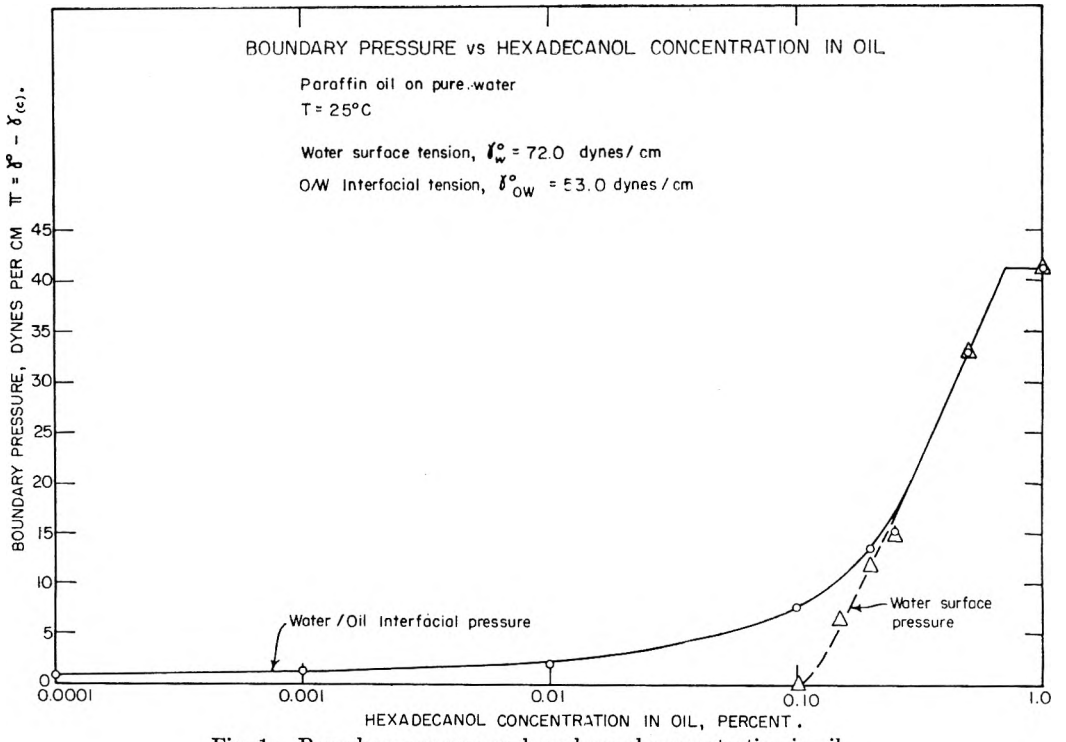

Fig. 1.—Boundary pressure *vs.* hexadecanol concentration in oil.

TABLE II

CONTACT ANGLES ON GEL SURFACES AT 25.0°

Gel 4.0% SiO_2, setting time, 3 hr.

Gel	Oil (pure)	θ_{adv} degrees	θ_{rec} degrees	θ_{cal} degrees	No. of meas.
Pure[a]	Paraffin	50.5 ± 0.5	49.5 ± 0.5	50.8 ± 0.5	12
Pure[b]	Paraffin	51.3 ± .5	51.3 ± .5	50.8 ± .5	4
Pure[a]	MeI_2	52.2 ± .4	52.0 ± .7	52.8 ± .4	12
Impure[a]	Paraffin	32.5 ± 2.5	0	.....	12

[a] By sessile drop. [b] By captive bubble.

hexadecanol in oil appear in Fig. 1. The boundary pressure, π, *i.e.*, the lowering of boundary tension

$$\pi_{(c)} = \gamma^0 - \gamma_{(c)} \qquad (2)$$

where γ^0 is the boundary tension in the absence of additive, and $\gamma_{(c)}$ is the boundary tension at additive concentration c, is plotted in Fig. 1 *vs.* the hexadecanol concentration on a logarithmic scale. The boundary pressure is employed because it allows a direct comparison of the effect of the additive on each of the tensions involved. The data in Fig. 1 can be analyzed in terms of the boundary concentration, Γ, by means of the appropriate Gibbs adsorption isotherm

$$\frac{-d\pi}{d \ln c} = RT\Gamma \qquad (3)$$

where R is the gas law constant, and T the absolute temperature. The boundary concentration, Γ, is in reality the surface excess and is equal to the boundary concentration only in the case of dilute solutions of capillary active materials. Equation 3 also assumes that the concentration is directly proportional to the activity over the concentration range that the relationship is applied.

The interfacial pressure of the hexadecanol solutions increased with concentration in a normal manner, the interfacial monolayer becoming compact in the concentration region above 0.25% as deduced from eq. 3. The surface tension of the water in equilibrium with the oil was not detectably

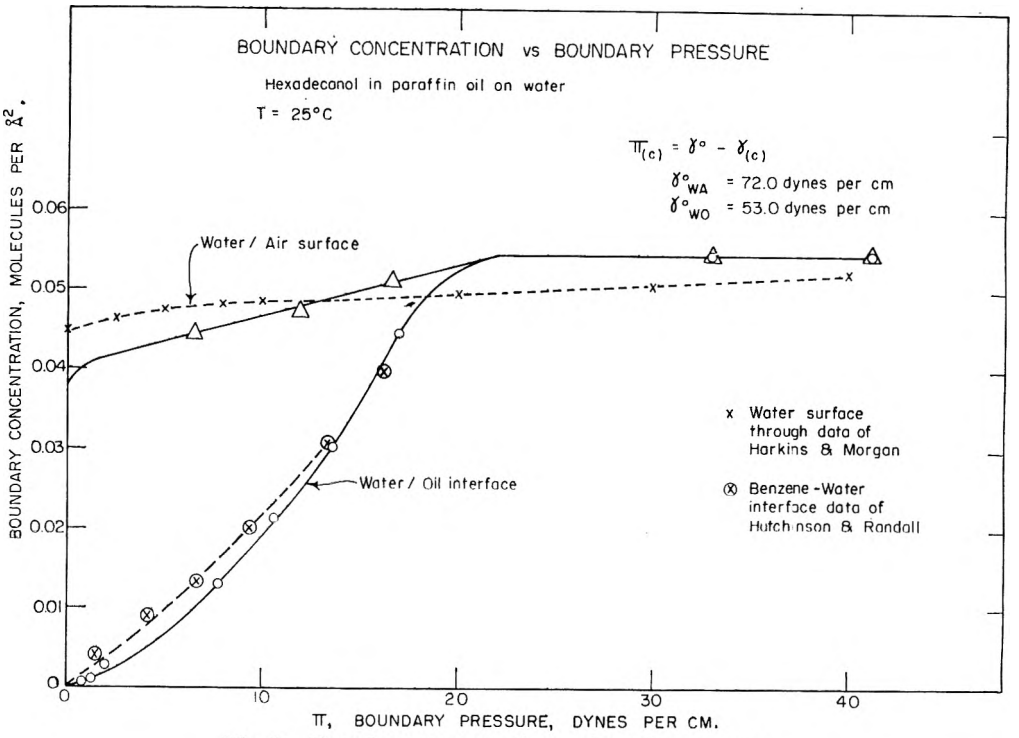

Fig. 2.—Boundary concentration *vs.* boundary pressure.

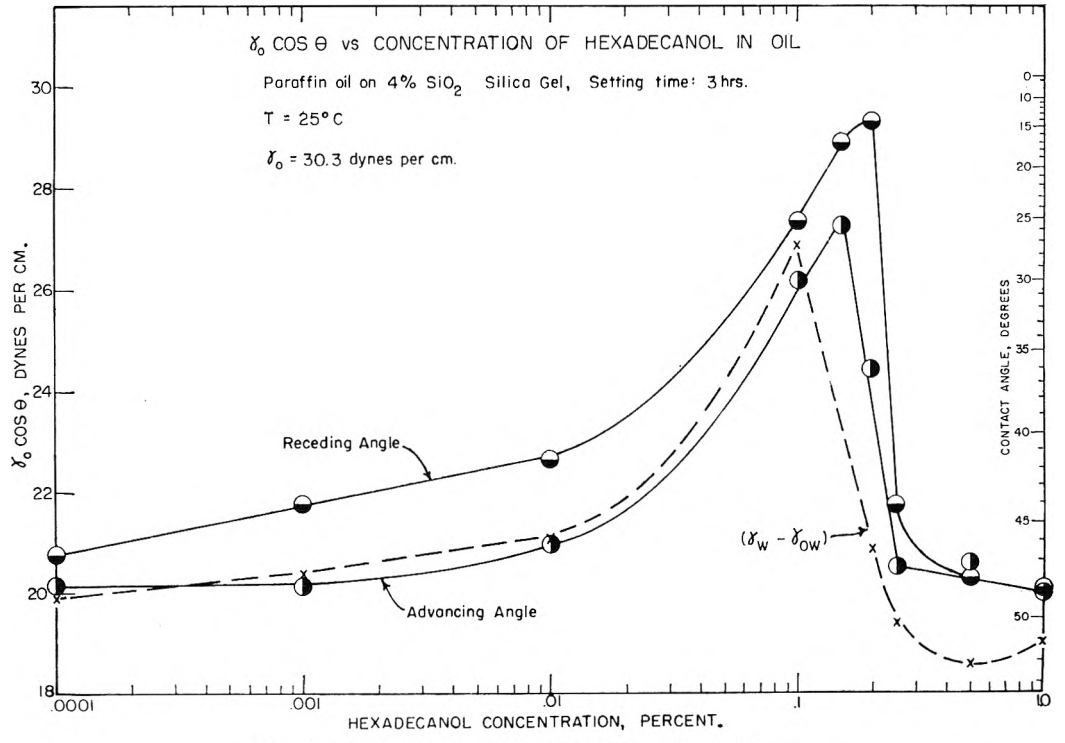

Fig. 3.—$\gamma_0 \cos \theta$ *vs.* concentration of hexadecanol in oil.

lowered until the hexadecanol concentration exceeded 0.10%, the "critical spreading concentration." Then an almost compact monolayer shed from the three phase intersection to the water surface. The surface and interfacial pressures were identical above 0.25% hexadecanol. The oil surface tension was unchanged by the presence of hexadecanol. A plot of the boundary concentrations *vs.* boundary pressure computed from eq. 3 is presented in Fig. 2. The Langmuir trough data of Harkins and Morgan[8] for the surface concentration of pure hexadecanol on water surfaces *vs.* surface pressure and the interfacial concentration–interfacial pressure data of Hutchinson and Ran-

(8) W. D. Harkins and J. W. Morgan, *Proc. Natl. Acad. Sci.*, **11**, 637 (1952).

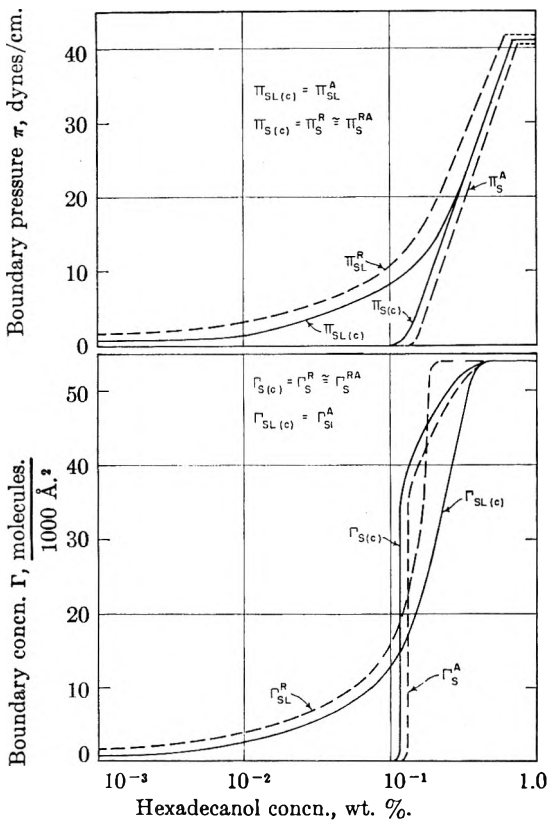

Fig. 4.—Interfacial pressures and concentrations during advancement and recession (hexadecanol–paraffin oil–silica gel).

dall[9] for the hexadecanol–benzene–water system, are presented for comparison. Agreement among these three independent studies is reasonably good.

Contact angles of these hexadecanol solutions were measured on gel surfaces, and the results of these measurements appear in Fig. 3. The dotted curve on Fig. 3 represents the Young's equation angle calculated from the measured boundary tensions for the oil–air–water system. The advancing and receding angles were almost equal at concentrations below 0.001% hexadecanol but between 0.001 and 0.10% hexadecanol, the hysteresis remained constant at about 6°. In this region the advancing angle was equal to the Young's equation angle computed from the surface and interfacial tension data for the oil on pure water. Between 0.10 and 0.25% hexadecanol concentrations, the hysteresis was very much greater, and both advancing and receding angles were significantly lower than the computed values. Above 0.25% the hysteresis again disappeared, and the angles approached the computed values.

The derivation of Young's equation is based on the tacit assumption that the phase boundaries and bulk phases are in thermodynamic equilibrium; in three-phase systems where such equilibrium exists, there can be but one value of the contact angle, and barring dynamic effects, hysteresis must be absent. This is clearly the situation which exists in the silica gel–oil–air systems in the absence of capillary active components. On the other hand, it seems reasonable to postulate that if phase boundaries and bulk phases are not in thermodynamic equilibrium, the observed contact angle will be determined through Young's equation by the *local* boundary tensions at the three phase intersection. In such systems the observed contact angle may be substantially different from that predicted for the equilibrium case, and if the local boundary tensions vary with position or motion of the three phase interline, contact angle hysteresis can be expected. The subsequent analysis of the contact angle data for systems containing hexadecanol is based on this postulate; *viz.*, any departure of the measured contact angles of oil on the gel surfaces from the equilibrium angle, calculated from the boundary tensions of the corresponding oil–air–water system, is presumed to arise from "non-equilibrium" tensions at the oil–gel or gel–air boundaries.

In analytical terms these postulates are as follows: If equilibrium exists between the bulk phases and boundaries, then

$$\gamma_L \cos\theta = \gamma_{S(c)} - \gamma_{SL(c)} \qquad (4)$$

where $\gamma_{S(c)}$ and $\gamma_{SL(c)}$ represent the equilibrium boundary tensions at concentration c, and θ is the equilibrium contact angle.

Since, in the absence of solute

$$\gamma_L \cos\theta^0 = \gamma_S{}^0 - \gamma_{SL}{}^0 \qquad (5)$$

then in the presence of an additive concentration, c

$$\gamma_L (\cos\theta^0 - \cos\theta) = \pi_{S(c)} - \pi_{SL(c)} \qquad (6)$$

If hysteresis is observed, or if the measured angle is different from that predicted from eq. 6, then

$$\gamma_L (\cos\theta^0 - \cos\theta^A) = \pi_S{}^A - \pi_{SL}{}^A \qquad (7)$$

and

$$\gamma_L (\cos\theta^0 - \cos\theta^R) = \pi_S{}^R - \pi_{SL}{}^R \qquad (8)$$

where the superscripts A and R refer to advancement and recession.

At hexadecanol concentrations in the oil phase below 0.1%, the receding angle is lower than the equilibrium angle. Inspection of Fig. 1 reveals that this can result only from a reduction in the oil–gel interfacial tension, since the maximum possible value for the gel surface tension is that for the pure gel. Assuming that each boundary tension is uniquely determined by the hexadecanol boundary concentration, recession of the drop must cause an increase in the interfacial concentration of hexadecanol, *i.e.*, a compression of the interfacial film.

To determine the extent of this compression it was assumed that

$$\pi_S{}^R = \pi_{S(c)} = 0 \qquad (9)$$

whence

$$\gamma_L (\cos\theta^0 - \cos\theta^R) = -\pi_{SL}{}^R \qquad (10)$$

Since π_{SL}, the interfacial pressure, is a unique function of Γ_{SL}, the interfacial concentration, the values of $\Gamma_{SL}{}^R$ corresponding to the compressed film with interfacial pressure $\pi_{SL}{}^R$ have been estimated from Fig. 2 and plotted in Fig. 4. The assumption that $\pi_S{}^R = 0$ is supported by the ex-

(9) E. Hutchinson and D. Randall, *J. Colloid Sci.*, **7**, 151 (1952).

perimental fact that the angle measured on readvancement of the drop over gel surface previously contacted with the oil was essentially equal to the initial advancing angle.

For such compression to take place, the oil–gel–air interline must act as a barrier to hexadecanol molecules in the interface. Compression of the interfacial film is evidently possible because the desorption rate of hexadecanol molecules from compressed interfacial films into the bulk oil phase is extremely low. (This property appears to be characteristic of many amphipathic compounds of extremely low water-solubility, and may be due to the existence of an energy barrier to detachment of the hydrophile from the aqueous phase.) It is also necessary to postulate the existence of barriers to lateral diffusion of hexadecanol molecules in the interface; otherwise, as recession proceeds, the contact angle will become smaller, showing a progressive variation of contact angle with interline position or a variation of the receding angle with drop size, effects which were never observed with this system. These barriers in the gel surface are probably polysilicate molecules in a net-like array. The existence of such barriers was confirmed by experiments in which hexadecanol–saturated oil was placed on one portion of an otherwise pristine gel surface. On free water surfaces a hexadecanol film will shed rapidly from such an oil drop and cover the entire surface in a short period of time; however, this does not occur on the gel surface since the contact angle made by pure oil on an adjacent portion of the gel surface was found to be identical to that observed in the absence of hexadecanol, and underwent no change over the lifetime of the gel.

At hexadecanol concentrations in oil exceeding 0.1%, both advancing and receding contact angles are less than those corresponding to equilibrium (see Fig. 3). Since it has been established that the shedding of a compact hexadecanol monolayer from the drop phase above the "critical spreading concentration" does take place on a free water surface but not on the gel surface, a low advancing angle, in this case, can be ascribed to a *deficiency* of hexadecanol at the gel–air boundary adjacent to the three-phase interline. If it be assumed that during advancement the interface is in equilibrium with the oil phase, the local surface pressure at the gel–air boundary can be estimated by means of the relation

$$\gamma_L (\cos \theta^A - \cos \theta) = \pi_S - \pi_S{}^A \quad (11)$$

The values of the local surface concentration present during advancement, based on these calculations, are also plotted in Fig. 4. The deficiency of hexadecanol at the gel surface during advancement need not be very great to account for a marked depression in the advancing angle, inasmuch as the surface pressure is extremely sensitive to the surface concentration in this region, as seen in Fig. 2.

The low receding angles observed in the concentration interval 0.10 to 0.25% can result from two effects: (1) incomplete saturation of the gel surface with hexadecanol following removal of the oil phase; and/or (2) compression of the interfacial film; there is no *a priori* reason for ascribing the observation to either possibility alone. A proper choice of alternative can, however, be made from the observation that (in the range of 0.1–0.25% hexadecanol) the contact angle measured on drop-*readvancement* over gel surface previously covered with the oil solution is significantly *greater* than the initial advancing angle, while the angle measured on drop-*re-recession* is little different from the initial receding angle. These results are shown in Table III. If, consistent with the preceding analysis, one assumes that the interfacial pressure and concentration during advancement are always equal to the equilibrium values, then a rise in contact angle on readvancement requires a rise in surface pressure (and concentration) during readvancement

$$\gamma_L (\cos \theta^{RA} - \cos \theta) = \pi_{S(e)} - \pi_S{}^{RA} \quad (12)$$

Whence, from eq. 11

$$\pi_S{}^{RA} > \pi_S{}^A$$

Since, during drop-readvancement, the gel surface external to the three-phase interline can hardly be expected to gain more hexadecanol molecules than were left on that surface during the previous recession, it seems reasonable to assume that the surface pressure and concentration during recession (or re-recession) are essentially equal to the values calculated for readvancement, based on eq. 12

$$\gamma_L (\cos \theta^0 - \cos \theta^R) = \pi_S{}^{RA} - \pi_{SL}{}^R \quad (13)$$

Whence, from eq. 13, the interfacial pressure and concentration on recession can be estimated.

The results of these calculations are summarized in Table III. It will be noted that the surface pressures on readvancement (above 0.10% hexadecanol) are greater than the surface pressures during initial advancement, and more importantly, are *almost identical with the equilibrium surface pressures.* Evidently, during recession, sufficient hexadecanol can pass through the three-phase boundary to permit the gel surface to reach substantial equilibrium with the bulk oil phase. During drop recession, interfacial film-compression is, as before, seen to take place; the maximum "excess interfacial pressure," $(\pi_{SL}{}^R - \pi_{SL(e)})$, is observed at 0.20% hexadecanol, and amounts to slightly less than 8 dynes/cm., and drops to less than 2 dynes/cm. at higher concentrations. It is of interest, and of possible significance, that the maximum "excess interfacial pressure" observed during recession never exceeds the interfacial pressure (8 dynes/cm.) at which hexadecanol first escapes from the oil–water interface and spreads onto a free water surface (*cf.* Fig. 1). The postulate that the drop-periphery may serve as a two-dimensional barrier to hexadecanol migration thus appears reasonable.

Above 0.50% hexadecanol, a close-packed hexadecanol monolayer exists at both oil–gel and gel–air boundaries during drop advancement or recession; under these conditions, hysteresis is virtually ab-

TABLE III

BOUNDARY PRESSURES AND BOUNDARY CONCENTRATIONS DURING ADVANCEMENT AND RECESSION
Hexadecanol–paraffin oil–air–silica gel, 25°

Hexadecanol concn., wt. %	$\gamma_a \cos\theta$, dynes/cm.			π_s, dynes/cm.				π_{SL}, dynes/cm.				Γ_S, molec's/1000 Å.^{2}		Γ_{SL}, molec's/1000 Å.^{2}	
	Adv.	Rec.	Readv.	Rerec.	Eq.	Adv.	Rec.	Readv.	Rerec.	Eq.	Adv.	Rec.	Readv.	Rerec.	Eq.	Adv.	Rec.	Adv.	Rec.
0.1	26.2	27.4	26.2	27.4	~0.1	0	0	0	0	7.9	7.9	8.4	7.9	8.4	~0?	0	~13	13	13	14
.15	27.3	28.9	26.6	29.1	6.6	2.4	3.1	3.1	3.1	10.7	10.7	13.1	10.7	13.1	44	41	43	20	20	31
.20	24.4	29.4	20.6	28.5	11.9	8.3	12.1	12.1	12.1	13.7	13.7	21.6	13.7	21.6	47	45	48	30	30	54
.25	20.6	21.8	18.9	22.7	14.8(?)	13.7	15.4	15.4	15.4	15.3(?)	15.3	19.1	15.3	19.1	51	50	51	45	45	54
.50	20.6	20.2	19.8	19.8	31.5	32.3	32.3	32.3	32.3	33.1	33.1	33.1	33.1	33.1	54	54	54	54	54	54
1.00	20.0	20.1	19.4	20.6	41.4	41.1	41.7	41.7	41.7	42.1	42.1	43.3	42.1	43.3	54	54	54	54	54	54

sent and the measured angles are, within the limits of experimental accuracy, equal to the equilibrium values. These observations suggest that, when a close-packed hexadecanol monolayer is formed at both gel–air and gel–oil boundaries, the three-phase interline is no longer capable of serving as a two-dimensional barrier to sorbate molecules. If it is argued that the passage of a sorbate molecule through the interline requires activated desorption of an oil molecule in the interline from the solid surface, and that such desorption gives rise to the barrier-properties of the interline, clearly the presence of a close-packed sorbate monolayer on both sides of the interline eliminates the barrier effect inasmuch as no direct contact between oil and solid then exists.

The changes in boundary pressures and concentrations with drop advancement and recession, as a function of hexadecanol concentration, can be graphically presented in the form of "hysteresis loops" bounding the equilibrium values of these parameters, as shown in Fig. 4. During initial drop advancement, the gel surface is invariably deficient in hexadecanol, while on recession, the interface always contains excess sorbate. These plots conveniently interrelate contact angle hysteresis with sorption–hysteresis, and thereby may help to put the former phenomenon in its proper physical perspective.

C. Decanol.—Decanol differs in boundary behavior from hexadecanol in that its monolayer at a water surface or oil–water interface cannot be subjected to compression because of its relatively high water solubility and its rapid rate of desorption into the aqueous phase.[5] If the observed hysteresis effects on silica gel in the presence of hexadecanol are indeed due to the interfacial film compressibility and show equilibration between the boundaries and bulk phases, then these effects should be absent in the presence of decanol.

Solutions of decanol in purified paraffin oil ranging from 0.001 to 1.0% by weight were prepared and the behavior of these solutions on decanol-free, *i.e.*, pure silica aquagels examined. The boundary tensions of the decanol–paraffin oil–water system at equilibrium were measured, and these results appear in Fig. 5. These data were used to calculate equilibrium contact angles for decanol-containing paraffin oil on the aquagel.

The contact angles were measured on pure, decanol-free gel surfaces, and the results of these measurements appear in Fig. 6. The decanol solutions showed no significant hysteresis at any concentration, and the observed angles were approximately equal to the predicted Young's equation angles up to a concentration of 0.10%. Above 0.10% the observed angles were smaller than the predicted values. Since the gel was initially decanol-free, and since the surface pressure of decanol becomes appreciable only at about 0.1% decanol in oil, deviations of the contact angles from the predicted values at the higher decanol concentrations are in all likelihood due to a deficiency of decanol at the gel–air interface.

The absence of contact angle hysteresis and the close correspondence of the experimental and pre-

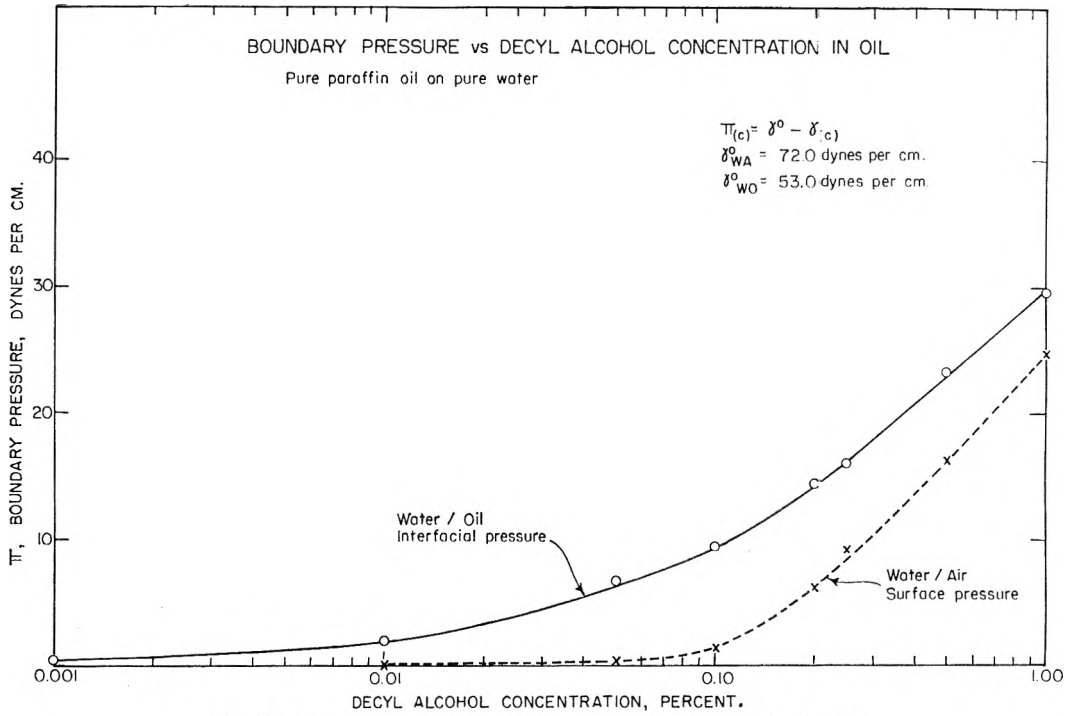

Fig. 5.—Boundary pressure *vs.* decyl alcohol concentration in oil.

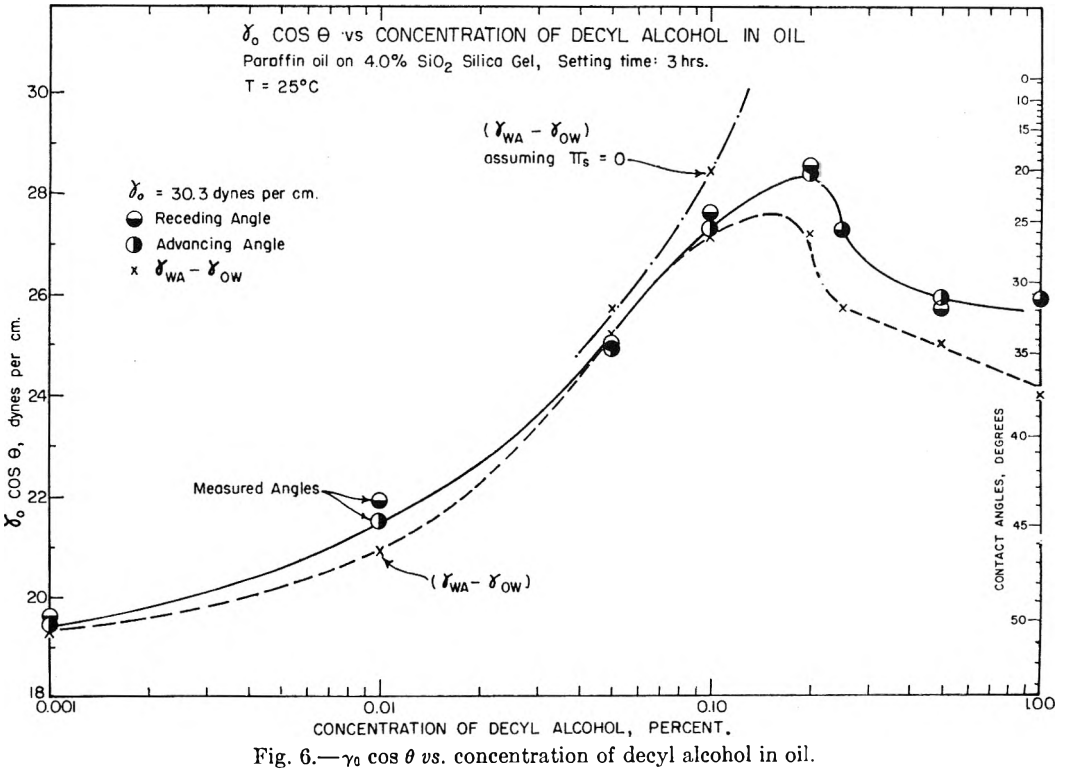

Fig. 6.—$\gamma_0 \cos \theta$ *vs.* concentration of decyl alcohol in oil.

dicted contact angles for this system provide support for the hypothesis that: (1) Young's equation is rigorously applicable to oil–silica gel–air systems when equilibrium exists between bulk phases and phase boundaries; and (2) deviations from Young's equation and contact angle hysteresis occur in oil–gel–air systems in the presence of a capillary active material whose rate of adsorption or desorption is sufficiently slow to permit abnormally high or low boundary concentrations to persist for long periods. Inasmuch as both decanol and hexadecanol are quite soluble in oil, while only decanol shows appreciable water solubility, one is prompted to generalize that only capillary active species which are virtually insoluble in the bulk solid (gel) phase are capable of causing hysteresis. Fragmentary

support for this postulate is provided by the observation that paraffin oil drops on silica aquagel containing low concentrations of sodium nonylbenzene sulfonate (which is essentially oil-insoluble) do not exhibit hysteresis. Additional investigation of a wider variety of gel systems is obviously required to resolve this question properly.

It is hardly to be inferred from the foregoing analysis that compressible boundary films provide the only source of contact angle hysteresis on solid surfaces. Surely macroscopic or microscopic roughness and/or energetic heterogeneity are features of most solid surfaces, and such features can give rise to contact angle hysteresis in the absence of adsorbed components. The success of this analysis in accounting for hysteresis effects on silica aquagel surfaces does, however, suggest that boundary film compression is real, and can constitute an important contributing factor in contact angle hysteresis.

IV. Conclusions

The major conclusions drawn from this investigation are the following.

(1) Contact angle hysteresis of pure paraffin oil and methylene iodide on silica aquagel surfaces is absent when the system is free of capillary active agents. Moreover, the observed contact angles are essentially equal to the predicted Young's equation angles, based on the boundary tensions of the solutions before gelation.

(2) The applicability of Young's equation to smooth, energetically homogeneous, solid surfaces in the absence of capillary active contaminants has been experimentally verified.

(3) Trace concentrations of hexadecanol dissolved in the oil phase cause marked contact angle hysteresis provided surface and interfacial concentrations are less than those corresponding to a compact monolayer. Hysteresis and disparity between observed and predicted contact angles are adequately accounted for in terms of compression of the interfacial hexadecanol monolayer during drop recession and/or incomplete equilibration of the gel surface with hexadecanol during drop advancement. Restricted lateral mobility of adsorbed molecules at the gel boundaries, due to the presence of barriers in the gel surface, must also exist to account for the observations.

(4) Low concentrations of decanol in an oil–silica gel–air system do not cause contact angle hysteresis and do produce contact angles essentially identical with those calculated with Young's equation from experimentally measured boundary tensions.

(5) Only capillary active substances which can withstand boundary compression without rapid desorption are capable of causing contact angle hysteresis in oil–silica gel–air systems.

(6) The concept of boundary film compression as a cause of contact angle hysteresis on normal solid surfaces may prove useful in the interpretation and analysis of solid wetting phenomena.

Acknowledgment.—The junior author was granted a National Science Foundation Fellowship for the summer and fall of 1959 and spring of 1960; the research was supported by a Grant-in-Aid from the American Chemical Society, Petroleum Research Fund, Grant No. PRF 438A. This financial assistance is gratefully acknowledged. The advice and guidance of Dr. M. J. Rzasa, Manager, Research Laboratories, Cities Service Research and Development Company, New York City, who served as PRF Liaison Representative for this program, and the helpful comments of Professor N. K. Adam, are warmly appreciated.

DISCUSSION

HARLEY Y. JENNINGS, JR. (California Research Corp.).—I am impressed with the accuracy claimed for the direct measurement of contact angle, *i.e.*, ±0.4°. How was the accuracy established and were any special mechanical devices employed?

A. S. MICHAELS.—No special or unusual techniques were employed to measure contact angles from drop-photomicrographs. The mean deviation of several independent measurements (by protractor) of a given drop-profile was of the order of 0.4°. As noted, however, the *reproducibility* of angle measurements (from drop to drop under identical conditions) was definitely poorer than the accuracy of measurement.

K. J. MYSELS (University of Southern California) and A. S. MICHAELS (communicated).—An alternative explanation for the failure of hexadecanol to spread rapidly over a silica aquagel surface from an oil droplet may be as follows: The spreading of monolayers from droplets onto a free water surface is accompanied by significant shear in the laminar sublayer of the substrate, since there is evidently no "slip" between monolayer and substrate. The commonly observed rapid spreading rates observed on water surfaces may, therefore, not be a consequence of high "lateral mobility" of molecules on the monolayer, but rather of the high fluidity of the substrate. In the present case, this mechanism of spreading must be almost completely inhibited by virtue of the rigidity of the gel substrate. If so, the only remaining spreading mechanism operative may be surface-diffusion which, for hexadecanol, whose "surface vapor pressure" at ordinary temperatures is extremely small, may be an exceedingly slow process. The indirect evidence that *n*-decanol monolayers do spread with reasonable rapidity on silica gel surfaces is consistent with this picture, since this alcohol forms expanded monolayers on water whose surface diffusion rates would be expected to be quite high. These observations suggest that the use of gelled substrates may provide a valuable approach for the study of surface diffusion kinetics on water and other liquid surfaces.

F. M. FOWKES (Shell Development Company).—Attention should be directed to similar studies [W. M. Sawyer and F. M. Fowkes, *J. Chem. Phys.*, **20**, 1650 (1952); *J. Phys. Chem.*, **60**, 1235 (1956)] which corroborate several of the important points of this paper. In the first of these the Young equation was tested with a series of distillation fractions of a perfluorinated lubricating oil. These ranged from fluid liquids to a glassy solid. All liquid fractions had the same surface tension or interfacial tension *vs.* water or hydrocarbons, and these measured tensions were used to predict (with considerable success) the contact angles on the glassy solid fraction. The second paper was concerned with the spreading of octadecanol from a lens of oil onto an aqueous substrate. Just as Prof. Michaels has demonstrated, a critical concentration was found below which no monolayer appears on the water surface, and above which monolayers are present at both the water surface and water/oil interface. These monolayers had identical film pressure and area per molecule in the case of octadecanol, but with shorter chain fatty acids the film at the oil/water interface had a greater film pressure than that on the surface. This difference was concentration-independent, in contrast to some of the data presented by Prof. Michaels.

The lack of spreading of a monolayer from the lens onto a silica gel surface is probably not an equilibrium situation, but a rate effect. The slow rate of spontaneous spreading on the very thin mobile layer of water on the surface of the gel can be estimated from the rate data of D. J. Crisp, *Trans. Faraday Soc.*, **42**, 619 (1946).

DETECTION OF METAL ION HYDROLYSIS BY COAGULATION. V.[1] ZIRCONIUM[2]

BY E. MATIJEVIĆ, K. G. MATHAI, AND M. KERKER

Department of Chemistry, Clarkson College, Potsdam, N. Y.

Received March 15, 1962

The charge of the cationic species in *dilute* zirconium nitrate and zirconium sulfate solutions has been determined by coagulation using negative silver bromide and silver iodide sols *in statu nascendi*. At pH <2.5 the prevailing species in dilute solutions of zirconium nitrate is Zr^{4+}. Over the pH range 5.5–7, a triply charged hydrolysis product is formed. Analysis of the coagulation data indicates the formation of either dimeric species, $Zr_2(OH)_8^{3+}$, or trimeric species, $Zr_3(OH)_9^{3+}$. At concentrations somewhat higher than those which cause coagulation, the zirconium solutions reverse the charge of the silver halides. This effect is also pH dependent. In solutions of zirconium sulfate, a slow hydrolysis from Zr^{4+} to triply charged species occurs which has been followed by coagulation. This aging eventually culminates in a precipitation.

Introduction

In the older literature, the "zirconyl" ion, ZrO^{2+}, was generally considered the prevailing species in aqueous solutions of zirconium salts.[3] However, as early as 1925, Britton[4] disputed its existence and this opinion is now shared by many other investigators.[5,6] There have been a great many studies which show that zirconium hydrolyzes and polymerizes and also that it complexes readily with many anionic species. These processes depend upon pH and concentration and in some cases they are time dependent. The actual zirconium ionic species in solution have been established with certainty in only a few cases, although a tremendous variety of different species has been suggested by a large number of investigators.

The classical method for investigation of metal ion hydrolysis, *i.e.*, potentiometric titration, has only limited use for zirconium because of the precipitation and flocculation that take place upon addition of strong bases to zirconium solutions even at low pH.[3,7,8] Larsen and Gammill[8] have shown that such data can be used only indirectly for the detection of hydrolyzed zirconium species in solution.

Accordingly, other methods have been sought among which the most successful appear to be (a) an extraction method developed by Connick and collaborators,[9-11] using thenoyltrifluoroacetone as a chelating agent for zirconium, (b) ultracentrifugation as employed by Johnson and Kraus,[6,12,13] and (c) ion exchange studies performed by Lister and McDonald[14] and Larsen and Wang.[15] These methods also give data from which the extent of hydrolysis and/or polymerization of zirconium may be estimated but like the potentiometric method do not lead directly to information about the ionic charge. It should be pointed out that these methods are usually carried out in the presence of high concentrations of perchlorate with the assumption that perchlorate does not complex with zirconium,[8,14] although such complexing has been proposed by Jander and Jahr.[16]

The exact formulation of a complex hydrolyzed species (in the absence of specific anionic complexing) can be deduced if any two of the following three quantities are known: (a) the metal–hydroxyl ratio in the complex ion, (b) the degree of polymerization, and (c) the ionic charge. We will apply the coagulation method to the direct determination of the charge of the prevailing ionic species at various pH's. Lister and McDonald have attempted to determine the ionic charge by ion-exchange measurements, but their method has been questioned.[17]

Coagulation has been applied successfully to detect the charge of the hydrolyzed species of thorium,[18] aluminum,[19,20] and zinc.[1] In connection with other data such as the metal–hydroxyl ratio, it has enabled complete characterization of such species. The method is based upon the determination of the concentration of salt necessary to coagulate a lyophobic sol. This concentration, the critical coagulation concentration (c.c.c.), depends upon the charge of the counterion of the coagulating electrolyte, decreasing very sharply with increasing ionic charge (the Schulze–Hardy rule). In our previous work silver halide sols have been used and the relationship between the c.c.c. and the charge of the counterion in solution has been quite precisely established.[21-23] This method has several significant advantages: (a) it gives the charge of the ionic species directly, (b) since the concentrations of solutions used in coagulation experiments, especially for counterions of higher charges, are extremely low, activity effects and complexing

(1) Part IV, E. Matijević, J. P. Couch, and M. Kerker, *J. Phys. Chem.*, **66**, 111 (1962).

(2) Supported by the U.S. Army Research Office Contract No. DA-ORD-10.

(3) See, *e.g.*, A. Rosenheim and P. Frank, *Ber.*, **40**, 803 (1907).

(4) H. T. S. Britton, *J. Chem. Soc.*, **127**, 2120 (1925).

(5) W. S. Castor, Jr., and F. Basolo, *J. Am. Chem. Soc.*, **75**, 4807 (1953).

(6) J. S. Johnson and K. A. Kraus, *ibid.*, **78**, 3937 (1956).

(7) J. H. Hildebrand, *ibid.*, **35**, 847 (1913).

(8) E. M. Larsen and A. M. Gammill, *ibid.*, **72**, 3615 (1950).

(9) R. E. Connick and W. H. McVey, *ibid.*, **71**, 3182 (1949).

(10) R. E. Connick and W. H. Reas, *ibid.*, **73**, 1171 (1951).

(11) A. J. Zielen and R. E. Connick, *ibid.*, **78**, 5785 (1956).

(12) K. A. Kraus and J. S. Johnson, *ibid.*, **75**, 5769 (1953).

(13) J. S. Johnson and K. A. Kraus, Reports ORNL-607 (1949); ORNL-1053 (1951).

(14) B. A. J. Lister and L. A. McDonald, *J. Chem. Soc.*, 4315 (1952).

(15) E. M. Larsen and P. Wang, *J. Am. Chem. Soc.*, **76**, 6223 (1954).

(16) G. Jander and K. F. Jahr, *Kolloid-Beih.*, **43**, 295 (1936).

(17) A. J. Zielen, Thesis, Report URCL-2268, 1953.

(18) E. Matijević, M. B. Abramson, K. F. Schulz, and M. Kerker, *J. Phys. Chem.*, **64**, 1157 (1960).

(19) E. Matijević, K. G. Mathai, R. H. Ottewill, and M. Kerker, *ibid.*, **65**, 826 (1961).

(20) E. Matijević and B. Težak, *ibid.*, **57**, 951 (1953).

(21) E. Matijević, D. Broadhurst, and M. Kerker, *ibid.*, **63**, 1552 (1959).

(22) E. Matijević, K. F. Schulz, and B. Težak, *Croat. Chem. Acta*, **28**, 81 (1956).

(23) B. Težak, E. Matijević, and K. Schulz, *J. Phys. Chem.*, **59**, 769 (1955).

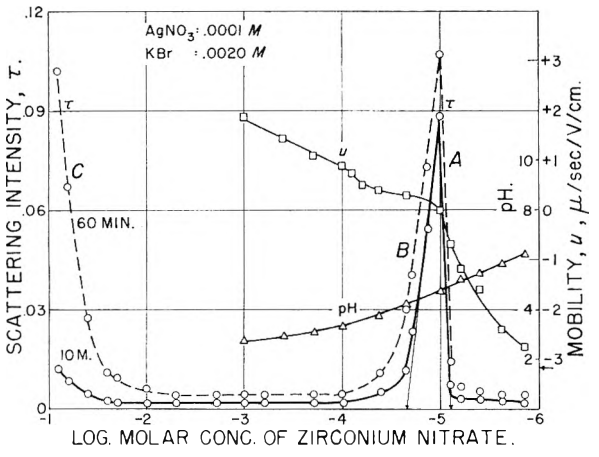

Fig. 1.—Coagulation (τ, O; full line, 10 min., dashed line, 60 min.), mobility (u, □), and pH (Δ) curves of a negative silver bromide sol *in statu nascendi* in the presence of various concentrations of zirconium nitrate. Concentrations: $AgNO_3$, 1×10^{-4} *M*; KBr, 2×10^{-3} *M*. *A*, the coagulation limit of zirconium species for negative AgBr sol; *B*, stability limit due to the reversal of charge effect; *C*, coagulation limit of nitrate ion for the AgBr sol of reversed (positive) charge.

with anions other than OH^- are usually negligible, and (c) the method does not require the presence of large quantities of neutral electrolytes (such as perchlorates). The shortcoming of the method is that the concentration range of solutions under investigation is limited to the c.c.c.

In this work we have determined the ionic charge of the cationic species in aqueous solutions of zirconium nitrate at various pH's using the coagulation method. Also, specific time dependent effects encountered with zirconium sulfate have been explored. All of these studies apply to dilute solutions ($<10^{-4}$ *M*). We have concluded that at pH <2.5 the predominant species both in zirconium nitrate and zirconium sulfate solutions is non-hydrolyzed, non-polymerized Zr^{4+} and that for zirconium nitrate solutions there is a triply charged species over the pH range 5.5 to 7.0, which is either a dimer $Zr_2(OH)_5^{3+}$ or a trimer $Zr_3(OH)_9^{3+}$. Aged zirconium sulfate solutions also contain a triply charged species which may include sulfate ligands.

All the zirconium solutions studied reverse the charge of the initially negative silver halide sols at sufficiently high salt concentrations.

Experimental

Materials.—All materials used were of highest purity grade, and the water was doubly distilled, the second distillation being carried out from an all-Pyrex still. The concentration of all stock solutions was determined by gravimetric analysis of zirconium.

Methods.—Coagulation experiments were performed with silver bromide and silver iodide sols *in statu nascendi* following the procedure described in detail previously.[19,20,24] The sol concentration was 1×10^{-4} *M* silver halide and the concentration of excess halide ion was 1.9×10^{-3} *M*. The pH of solutions was adjusted by addition of HNO_3 or NaOH. When NaOH was used, $AgNO_3$ and zirconium nitrate were in one solution prior to mixing and KBr (or KI) and NaOH in another. Parallel runs were prepared without KBr (or KI) in order to determine whether insoluble metal hydroxides were formed. Only systems where no precipitate appeared in these blanks were utilized in the coagulation experiments.

The electrophoretic mobility of the silver halide sol particles was determined using a microelectrophoresis equipment with a Mattson type cell,[25] as described previously.[19]

All pH measurements were made with a Beckman Model G pH meter with glass electrodes, calibrated with appropriate buffer solutions prior to each measurement.

Results

Experiments with Zirconium Nitrate.—An example of the coagulation curves of zirconium nitrate with a silver bromide sol, with accompanying pH and electrophoretic mobility data, is given in Fig. 1. In this case, where there is neither addition of free acid nor free base, the pH is determined primarily by the zirconium concentration. These coagulation curves are quite typical of counterions that reverse the charge of the colloidal particles. That such reversal of charge actually takes place in this particular case is shown by the electrophoresis experiments. The mobility of the originally negatively charged sol in the absence of added zirconium nitrate is indicated by the arrow on the mobility coördinate. The negative charge decreases with increasing Zr concentration, eventually becoming positive. This explains the shape of the coagulation curve. The extent of coagulation is detected by the intensity of light scattered by the sol particles.[26] At very low concentrations of added zirconium salt there is too little electrolyte to coagulate the sol, which is stabilized by the adsorbed excess halide ions. At limit *A* the negatively charged sol is coagulated as is indicated by the increase in light scattering. This coagulation is due to the cationic species present in the zirconium nitrate solution. At still higher concentrations, reversal of charge takes place and the sol again is stabilized. At limit *C* the now positively charged sol is coagulated by anions, mainly NO_3^- in this case. The *critical coagulation concentration* (c.c.c.) of zirconium species is obtained by extrapolating the steep part of limit *A* to zero light scattering. The *stability limit* is obtained by a similar extrapolation of *B*. Both *A* and *B* are quite sensitive to the charge of the counterion. Accordingly, as the counterion undergoes change of charge with pH due to either hydrolysis or polymerization, these limits will shift accordingly. It is the coagulation limit *A* to which the Schulze-Hardy rule applies and which is used in this work to determine the charge of the cationic species. The two curves represent the light scattering 10 and 60 minutes from the moment of mixing the reacting components. In this case, there is only a small difference between the results at these two times and either can be used to follow these effects.

The influence of pH upon the c.c.c. and the stability limit of reversal of charge (*B*) is demonstrated in Fig. 2. In the upper diagram, 2×10^{-3} *M* nitric acid was added to the system. At this lower pH the c.c.c. is about one order of magnitude lower than in the previous diagram. Limit (*B*) undergoes a much smaller shift. In the lower dia-

(24) B. Težak, E. Matijević, and K. Schulz, *J. Phys. Chem.*, **55**, 1557 (1951).

(25) S. Mattson, *ibid.*, **32**, 1532 (1928); **37**, 223 (1933).

(26) The intensity of scattered light plotted in Fig. 1 and 2 actually corresponds to turbidity when the particles are sufficiently small to act as Rayleigh scatterers and the sol sufficiently dilute.

gram, the pH has been increased by addition of a small amount of NaOH with a consequent shift in both limits A and B toward higher zirconium concentrations. Only the 10-minute diagrams are given.

Additional experiments were performed with a large number of systems systematically changing the pH and using both silver bromide and silver iodide sols. The c.c.c.'s and the stability limits obtained by extrapolation of limits A and B, respectively, are plotted against the corresponding pH in Fig. 3. Open circles and squares give the dependence of the c.c.c. on pH whereas the full circles and squares give the stability limits for silver bromide and silver iodide sols, respectively. The dependence of c.c.c. on pH shows a very characteristic trend. For pH <2.5 the c.c.c. remains constant. It then increases steadily until another plateau is reached over the range from pH 5.5 to 7. Above pH ~7, the c.c.c. rises again. The concentration of zirconium at the reversal of charge stability limit decreases with decreasing pH and also levels off below pH ~3.3.

Experiments with Zirconium Sulfate.—That there are differences in the properties of aqueous solutions of zirconium sulfate and those of other zirconium salts has been pointed out by many investigators.[8,9,14,27-30] Although zirconium sulfate, $Zr(SO_4)_2$, is extremely soluble,[31] a white colloidal precipitate will separate out from a solution of even moderate concentration after a short time. Apparently an insoluble basic sulfate is formed. We have studied the solubility relations of zirconium sulfate and these will be reported later. Here, we present coagulation studies of the zirconium sulfate solutions prior to the formation of a precipitate. These provide information about the ionic species in the homogeneous solution. The age of the solution at which the solid phase appears in zirconium sulfate solutions depends upon concentration and pH. Addition of nitric acid delays the formation of the precipitate, suggesting that hydroxyl ions are incorporated in the hydrolyzed cation which precipitates with sulfate. Thus, a precipitate will form in a 2×10^{-4} M solution of zirconium sulfate in the presence of 0.004, 0.002, and 0.001 M HNO_3 after 4 days, 2 days, and 10 hr., respectively. Precipitate forms sooner with increasing concentration of zirconium sulfate. At about 10^{-3} M, a solid separates out within minutes of dissolution of the salt. However, at still higher concentrations, the process is slowed down again and at about 10^{-2} M the precipitate appears only after several hours. This probably is due to the lower pH caused by the hydrolysis of zirconium at these high concentrations.

Coagulation experiments were carried out with solutions obtained by dilution of 2×10^{-4} M zirconium sulfate stock solutions which were either 0.004, 0.002, or 0.001 M HNO_3. The dependence of c.c.c. as a function of age of the stock solution was studied. Silver bromide sols *in statu nascendi* served as the colloidal system. The light scattering data were taken 10 minutes after preparation of the colloidal system in order to minimize the duration of the coagulation experiment with respect to the age of the zirconium sulfate solution.

The results are shown in Fig. 4 as c.c.c. against *age* of the stock solution. All experiments were

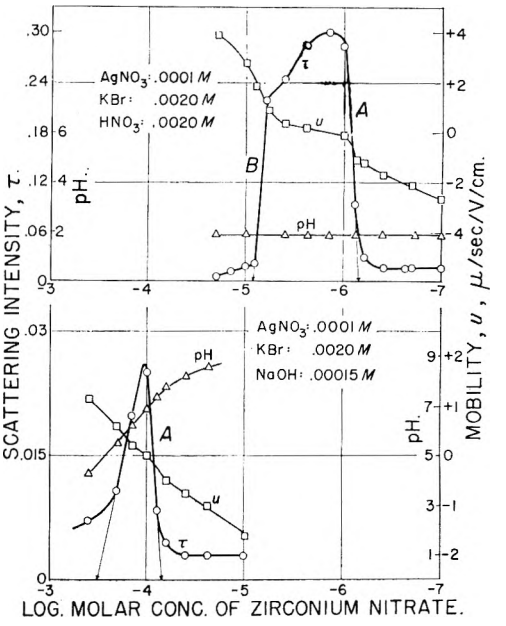

Fig. 2.—Coagulation (τ,○), mobility (u,□), and pH (△) curves of a silver bromide sol *in statu nascendi* in the presence of various amounts of zirconium nitrate. Concentrations: $AgNO_3$, 1×10^{-4} M; KBr, 2×10^{-3} M; HNO_3, 2×10^{-3} M (upper); NaOH, 1.5×10^{-4} M (lower curve).

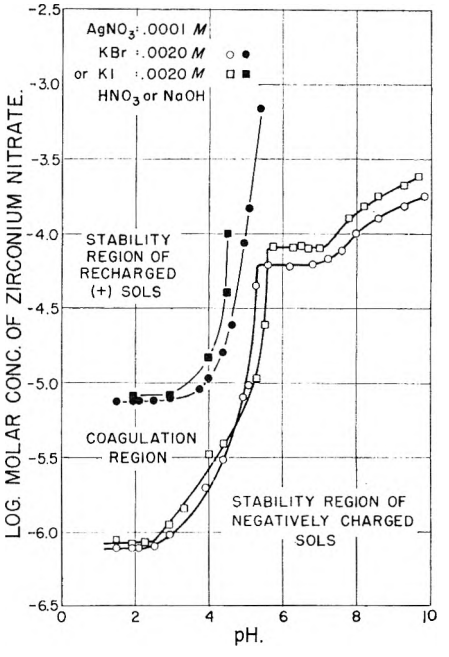

Fig. 3.—Plot of the critical coagulation concentration (lower curves, open signs) and stability limit due to the reversal of charge (upper curve, blackened signs) against pH for zirconium nitrate for a silver bromide sol (○,●) and a silver iodide sol (□,■) *in statu nascendi*. Concentrations: $AgNO_3$, 1×10^{-4} M; KBr or KI, 2×10^{-3} M; HNO_3 or NaOH, varied.

(27) E. Chauvenet, *Ann. chim.* (Paris), **13**, 59 (1920).
(28) W. B. Blumenthal, *J. Chem. Educ.*, **26**, 472 (1949).
(29) R. Ruer, *Z. anorg. Chem.*, **42**, 87 (1904).
(30) M. Adolf and W. Pauli, *Kolloid-Z.*, **29**, 173 (1921).
(31) O. Hauser, *Z. anorg. Chem.*, **54**, 196 (1907).

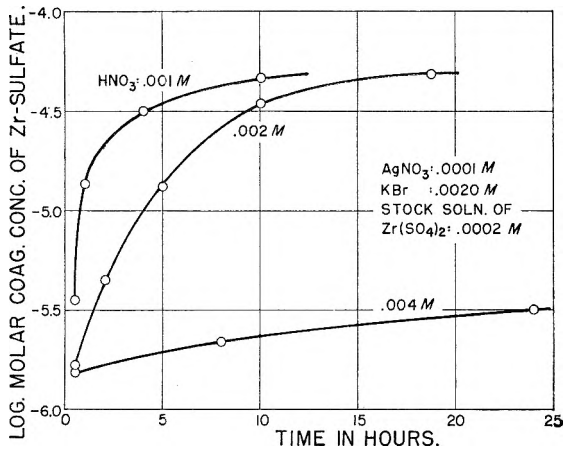

Fig. 4.—Plot of the critical coagulation concentration of zirconium sulfate for a negative silver bromide sol *in statu nascendi* against the *age* of the zirconium sulfate stock solution. Concentrations: $AgNO_3$ 1×10^{-4} *M*; KBr, 2×10^{-3} *M*; HNO_3, 1×10^{-3}, 2×10^{-3}, and 4×10^{-3} *M*, respectively. The concentration of the zirconium sulfate stock solution was 2×10^{-4} *M*.

performed before onset of precipitation. In the presence of 0.001 and 0.002 *M* HNO_3 the c.c.c. increases rapidly with age to a limiting value. The process is considerably slower in the presence of 0.004 *M* HNO_3.

Similar experiments were performed with zirconium sulfate stock solutions of both higher and lower concentrations and analogous effects were observed.

Discussion

The c.c.c. of the zirconium nitrate solutions at pH <2.5 is 8×10^{-7} *M*, which agrees quite precisely with the value for counter ions with a charge of +4.[18,21,22,32,33] There seems little doubt, then, that in these *extremely dilute* solutions and at pH <2.5 the zirconium species is hydrated Zr^{4+}. The existence of Zr^{4+} ion in acidic solutions also has been reported recently by several other investigators.[11,15,17,34] The only ones to oppose it were Lister and McDonald,[14] but Larsen and Wang[15] have indicated that their interpretation of the data was not entirely correct.

It should be pointed out that we find nonhydrolyzed zirconium species at pH's that are somewhat higher than those reported by others. However, the concentration of zirconium in our experiments is considerably lower than reported elsewhere. In view of the strong concentration dependence of hydrolysis and polymerization,[11,17,30] it is quite reasonable to assume that in very dilute solutions of zirconium the simple species are predominant at somewhat higher pH's than in concentrated solutions.

Still another problem should be mentioned, *viz.*, possible complexing with nitrate ions since it is known that nitrate may form complex species with zirconium.[27,34,35] However, these complexes were detected in concentrated nitrate solutions (HNO_3 solutions having ionic strength up to 4). Also, unless such a complex was polymeric, which is unlikely at such high dilutions, the ionic charge would be less than four and so under the conditions considered here the possibility of such complexing with nitrate may justifiably be eliminated.

As the pH increases above 2.5 the coagulation concentration also increases, indicating the formation of species of lower charge. Since the trend is continuous, there is a range of pH where there is a mixture of at least two species in variable ratios.

Over the pH range 5.5 to 7 another plateau is encountered where the existence of one predominant species may be assumed. The c.c.c. is 6×10^{-5} *M* and 8×10^{-5} *M* for AgBr and AgI sols, respectively. This c.c.c. is quite close to the values obtained with triply charged counterions, which is normally in the range of 3×10^{-5} *M*. Doubly charged counterions coagulate at much higher concentrations ($>10^{-3}$ *M*) and quadruply charged ions as seen above coagulate at much lower concentrations ($<10^{-6}$ *M*). Accordingly, the zirconium species under these conditions (pH 5.5–7.0) must be *triply* charged and can be represented by the formula $[Zr_n(OH)_{4n-3}]^{3+}$. It will be our next task to try to elucidate which of the possible species is most probable. This could be done directly if either the metal–hydroxyl ratio or the degree of polymerization was known.

We have been unable to obtain these data for the highly dilute solutions used in these experiments. However, a more careful analysis of the coagulation data as follows does lead to either the species $Zr_2(OH)_5^{3+}$ or $Zr_3(OH)_9^{3+}$.

The c.c.c. of 6×10^{-5} *M* reported here with the AgBr sols is somewhat higher than encountered for other triply charged counterions using the same AgBr sol. Thus the c.c.c. for Al^{3+} is 2.8×10^{-5} *M*,[19] for La^{3+} is 3×10^{-5} *M*,[22,36] and for $ThOH^{3+}$ is 2.5×10^{-5} *M*.[18] However, if the zirconium species were polymerized, the molarity of actual hydrolyzed zirconium ions in solution would be lower and the calculated c.c.c. would depend on degree of polymerization. Assuming a dimer or a trimer the c.c.c. would be 3×10^{-5} and 2×10^{-5}, respectively. Both values are within the range of c.c.c. for ionic species of +3. However, it is not possible to distinguish between $Zr_2(OH)_5^{3+}$ and $Zr_3(OH)_9^{3+}$ from coagulation measurements alone. Tetramers do not seem likely because the c.c.c. thus obtained is on the low side of the range normally expected for triply charged cations.

It was mentioned earlier that the Zr–OH ratio is very difficult to determine. Larsen and Gammill[8] proposed $[Zr(OH)_{3.4}^{0.6+}]_n$ based upon potentiometric titration. In order to have a species of charge of +3 a pentamer must be assumed. However, their method is rather difficult to apply because of precipitate formation during the titrations. Also, their lowest concentration was more than two orders of magnitude higher than the highest concentration used here. We have attempted to titrate solutions in the concentration range of the c.c.c.

(32) H. R. Kruyt and S. A. Troelstra, *Kolloid-Beih.*, **54**, 262 (1943).

(33) B. Težak, E. Matijević, and K. Schulz, *J. Am. Chem. Soc.*, **73**, 1602 (1951).

(34) W. H. McVey, unclassified U.S. Atomic Energy Commission Report, HW-21487, 1951.

(35) A. S. Solovkin, *Zhur. Neorg. Khim.*, 2, 611 (1957).

(36) B. Težak, E. Matijević, and K. Schulz, *J. Phys. Chem.*, **55**, 1567 (1951).

but because of the very low concentrations the results are inconclusive.

Also, there are very few conclusive data on the degree of polymerization. Several investigators assumed the existence of dimeric hydrolyzed species.[5,10,28,37,38] Recent experiments using an ultracentrifugation method indicate that zirconium does not show continuous polymerization and that only polymers of lower molecular weight are formed. This is in agreement with our findings. Furthermore, these ultracentrifugation data indicate trimers and tetramers as predominant species.[6,12] Similar results were obtained from extraction experiments. Connick and collaborators[11,17] have proposed that hydrolyzed zirconium ions are trimers and tetramers, but the number of OH ligands could not be definitely evaluated by their technique. It would follow from our charge determination that, if trimers are the predominant species, nine OH groups are coördinated in the complex ion.

We prefer, however, to leave the question, whether $Zr_2(OH)_5^{3+}$ or $Zr_3(OH)_9^{3+}$ is the predominant species, open until degree of polymerization or the Zr:OH ratio is determined beyond any doubt.

Finally, it is interesting to note, that the onset of polymerization was found by other investigators to be in the range of 10^{-4} *M* zirconium (varying to a certain extent with the amount of added acid), which is also in good agreement with our observations.

From Fig. 4 it is apparent that in the fresh solutions of zirconium sulfate the c.c.c. is about the same as in zirconium nitrate solutions at the corresponding pH. However, unlike zirconium nitrate, which does not change over a period of several months, the zirconium sulfate shows an aging effect resulting finally in the formation of a precipitate. Figure 4 reveals (a) that the formation of the precipitate is preceded, during the homogeneous stage, by a reaction which results in the formation of cationic species of lower charge and (b) that this reaction is progressively retarded with increasing concentration of hydrogen ions. Accordingly, this aging must involve the formation of basic zirconium sulfate ions. Since the c.c.c. in the presence of 0.001 *M* and 0.002 *M* HNO_3 levels off at values characteristic for triply charged counterions, such ions must be polymerized and can be represented by $[Zr_n(OH)_m(SO_4)_{2n-(m+3)/2}]^{3+}$. Although the precipitate has not yet been characterized completely, analysis shows that it contains both zirconium and sulfate and in view of the pH effect it most probably is a basic zirconium sulfate. If this precipitate can be characterized then an analysis of the general precipitation curves as carried out earlier with other systems[39] may lead to elucidation of this basic zirconium sulfate complex ion.

(37) W. B. Blumenthal, *Ind. Eng. Chem.*, **40**, 510 (1948).
(38) E. Chauvenet and L. Nicolle, *Compt. rend.*, **166**, 781 (1918).
(39) K. F. Schulz, E. Matijević, and M. Kerker, *J. Chem. Eng. Data*, **6**, 333 (1961).

DEVELOPMENT OF SURFACE IN THE HYDRATION OF CALCIUM SILICATES. II. EXTENSION OF INVESTIGATIONS TO EARLIER AND LATER STAGES OF HYDRATION

BY D. L. KANTRO, STEPHEN BRUNAUER, AND C. H. WEISE

Portland Cement Association Research and Development Laboratories, Skokie, Illinois

Received March 12, 1962

The investigation of the paste hydration of tricalcium silicate, Ca_3SiO_5, and β-dicalcium silicate, β-Ca_2SiO_4, published earlier has been extended to reaction times shorter than 1 day and longer than 200 days. As in the earlier work, the reactions were investigated at three temperatures, 5, 25, and 50°. On the basis of determinations of the compositions and the specific surface areas of the hydration products at various times, it has been found that there are three stages in the hydration reactions: (1) the formation of a lime-rich, low surface area primary product, (2) the conversion of this into a lime-poor, high surface area intermediate product, and (3) the conversion of the unstable intermediate into the final stable calcium silicate hydrate, called tobermorite gel or tobermorite (G). A mechanism is proposed for both reactions, which involves (1) the formation of a gel coating on the surfaces of the unhydrated substrate, (2) the splitting-off of thin sheets, one and two molecular layers in thickness, from the gel coating, and (3) the conversion of the thin sheets into stable tobermorite (G), which consists of sheets having thicknesses of two and three molecular layers. Some quantitative and qualitative consequences of the proposed mechanism are deduced, and they are shown to account for several important aspects of the hydration reactions.

Introduction

An understanding of the reactions of tricalcium silicate, Ca_3SiO_5, and β-dicalcium silicate, Ca_2SiO_4, with water is of fundamental importance in the investigation of the chemistry of portland cement. These silicates are the major constituents of portland cement, and the behavior of the cement–water system is similar to the behavior of the Ca_3SiO_5–H_2O and Ca_2SiO_4–H_2O systems.

Over a period of years, the stoichiometry and energetics of the Ca_3SiO_5–H_2O and Ca_2SiO_4–H_2O reactions have been investigated.[1-3] It was shown that the products of hydration are well crystallized calcium hydroxide and a poorly crystallized calcium silicate hydrate of variable composition.[4] There is a group of calcium silicate hydrates which has been called tobermorites, because of their similarity to the natural mineral tobermorite ($5CaO{\cdot}6SiO_2{\cdot}5H_2O$). The hydrates obtained in the hydration of the calcium silicates constitute a subgroup of this group. Because the hydrates are gels, the subgroup is called tobermorite gel or tobermorite (G).

The calcium silicates are low surface area substances, but tobermorite (G) has a high specific surface area. The development of surface area in the hydration of calcium silicates has been investigated earlier[5] for periods ranging from 1 to 200 days. The paper on this work will be referred to as Part I. It reported on the variation of the composition of tobermorite (G) with time and temperature as well as on the relationship between specific surface area and composition. Most of Part I was concerned with that part of the hydration process during which composition and specific surface area changed slowly and only slightly. The present paper deals primarily with the early stages of hydration, during which the changes in composition and surface were rapid and large.

The two papers together cover the hydration of Ca_3SiO_5 from 0.5 hr. to 400 days (5 to 100% hydration) and that of Ca_2SiO_4 from 1 hr. to 400 days (0 to 84% hydration). The temperatures employed were 5, 25, and 50°, as before. From the compositions and the specific surface areas of the hydration products, a mechanism of the hydration process is deduced which is consistent with the experimental findings.

Experimental

The Ca_3SiO_5 and β-Ca_2SiO_4 used were from the same supply as in Part I. The paste preparations were carried out by the vacuum mixing technique. Each paste was subjected to loss-on-ignition and carbon dioxide content determinations. Free calcium hydroxide contents were determined by the modified Franke method (time variation method)[6] and X-ray quantitative analyses were performed as described in Part I. The surface areas of all pastes were measured by water vapor adsorption, those of Ca_3SiO_5 and Ca_2SiO_4, prior to hydration, were measured by nitrogen adsorption.

Results

X-Ray analysis showed that the composition of Ca_2SiO_4 reported in Part I had to be revised. The composition used in the present paper is 99.37% Ca_2SiO_4 (with 2.47% CaO and 0.47% B_2O_3 dissolved in it), 0.32% $Ca_3Al_2O_6$, 0.05% MgO, 0.20% CaO, and 0.06% SiO_2. The composition of the Ca_3SiO_5 preparation is the same as in Part I, 98.18% Ca_3SiO_5, 0.53% $Ca_3Al_2O_6$, and 1.29% CaO. The compositions of the pastes were calculated as in Part I. The revised compositions of the older Ca_2SiO_4 pastes, based on the newly calculated composition of Ca_2SiO_4, are not significantly different from those reported in Part I.

The pastes included in this investigation which were not reported in Part I were those, both Ca_3SiO_5 and Ca_2SiO_4, hydrated for times less than 1 day; Ca_2SiO_4 pastes hydrated at 5° for 9, 120, and 400 days (the 9-day paste being a repeat of a previous one), at 25° for 120 days, and at 50° for 400

(1) S. Brunauer, L. E. Copeland, and R. H. Bragg, *J. Phys. Chem.*, **60**, 112, 116 (1956).

(2) S. Brunauer, D. L. Kantro, and L. E. Copeland, *J. Am. Chem. Soc.*, **80**, 761 (1958).

(3) S. Brunauer, D. L. Kantro, and C. H. Weise, *Can. J. Chem.*, **37**, 714 (1959).

(4) S. Brunauer, *Am. Scientist*, **50**, 210 (1962).

(5) D. L. Kantro, S. Brunauer, and C. H. Weise, "Development of Surface in the Hydration of Calcium Silicates," Advances in Chemistry Series, No. 33, American Chemical Society, Washington, D. C., 1962, p. 199.

(6) E. E. Pressler, S. Brunauer, D. L. Kantro, and C. H. Weise, *Anal. Chem.*, **33**, 877 (1961).

days; and Ca_3SiO_5 pastes hydrated at 5° for 400 days and at 50° for 400 days.

A separate group of Ca_2SiO_4 pastes was hydrated at 25° for 4, 5½, 7, 12, and 24 hr. These pastes, which had not yet set, were filtered, and the filtrates were analyzed for calcium ion concentration and pH. The calcium ion concentrations were 0.0295, 0.0275, 0.0262, 0.0216, and 0.0161 *M*, and the pH values were 12.48, 12.45, 12.45, 12.40, and 12.20, respectively.

The *degree of hydration* of a paste is, as previously, the ratio of the amount of calcium silicate which has disappeared in the hydration to the amount originally present. The correction for excess CaO in Ca_2SiO_4 will be discussed later. The degrees of hydration of Ca_2SiO_4 and Ca_3SiO_5 as functions of time at the three temperatures used are plotted in Fig. 1 and 3, respectively. The corresponding V_m values (which are proportional to the surface area) are plotted as functions of time in Fig. 2 and 4, respectively. The logarithmic time scales in Fig. 1 through 4 have been used only to facilitate graphical presentation of the data.

Discussion

A. Surface Area and the Degree of Hydration. —A comparison of Fig. 1 and 2 and of Fig. 3 and 4 shows that the similarities in V_m *vs.* time curves to degree of hydration *vs.* time curves found previously for hydration times from 1 to 200 days extend to the earlier and later times included in the present investigation.

It also can be seen in Fig. 1 that no measurable hydration of Ca_2SiO_4 at 5° occurs in pastes as old as 12 hr. Similarly, as shown in Fig. 2, there is no measurable surface area in these samples. In spite of these results, the free $Ca(OH)_2$ contents increase continuously from an initial value of 0.0020 g. CaO/g. ignited weight in the unhydrated material to 0.0113 g. CaO/g. ignited weight in the 12-hr. sample. This increase in free $Ca(OH)_2$ is attributed to hydration of the excess CaO dissolved in Ca_2SiO_4, even though no reaction of Ca_2SiO_4 itself has yet occurred, as determined by X-rays. On the basis of this result, it was assumed that this much CaO hydrated prior to Ca_2SiO_4 reaction at any temperature and that the remaining excess CaO hydrated in proportion to the degree of hydration of the Ca_2SiO_4.

The temperature dependence of the Ca_2SiO_4 hydration is normal up to 60 days. At equal times, the 50° specimens are more hydrated than the 25° specimens, which are in turn more hydrated than the 5° specimens. After 60 days, the normal temperature dependence breaks down. The hydration at 50° seems to stop, though incomplete, at about 100 days, and the 5 and 25° curves appear to cross each other at about 400 days. That the V_m curves are not exactly like the degree of hydration curves is illustrated by the slight increase in V_m values from 100 to 400 days for Ca_2SiO_4 hydrated at 50° while the degree of hydration remains unchanged.

The Ca_3SiO_5 hydration at early ages bears certain resemblances to that of Ca_2SiO_4. There is a normal temperature relationship for the degree of hydration up to about 20 hr. Although some Ca_3-

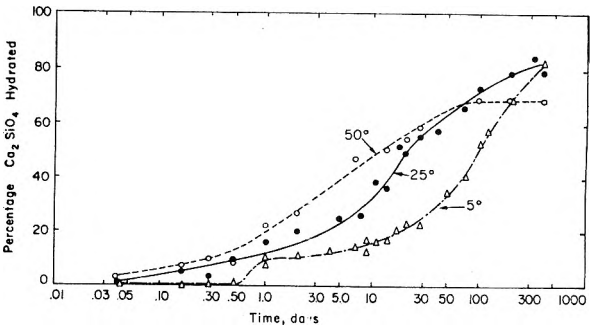

Fig. 1.—Percentage hydration of Ca_2SiO_4 *vs.* time.

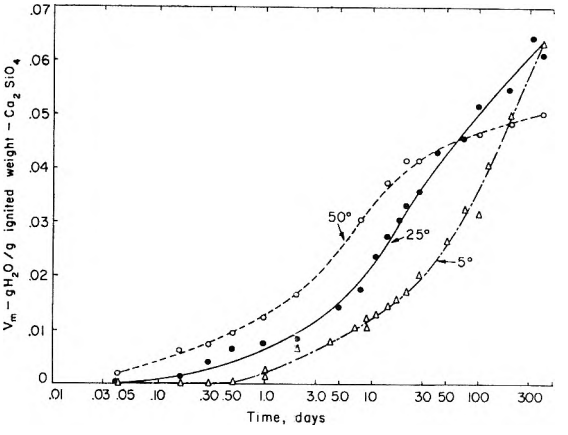

Fig. 2.—Surface development in the hydration of Ca_2SiO_4 *vs.* time.

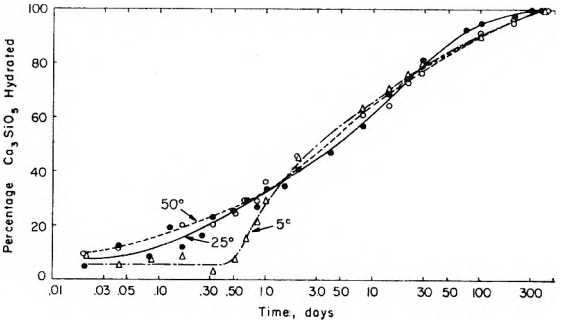

Fig. 3.—Percentage hydration of Ca_3SiO_5 *vs.* time.

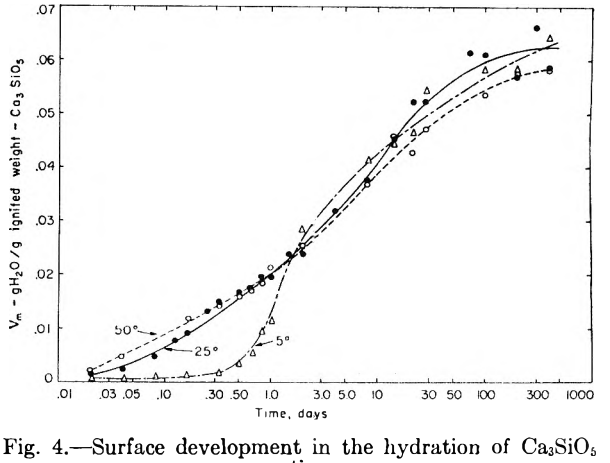

Fig. 4.—Surface development in the hydration of Ca_3SiO_5 *vs.* time.

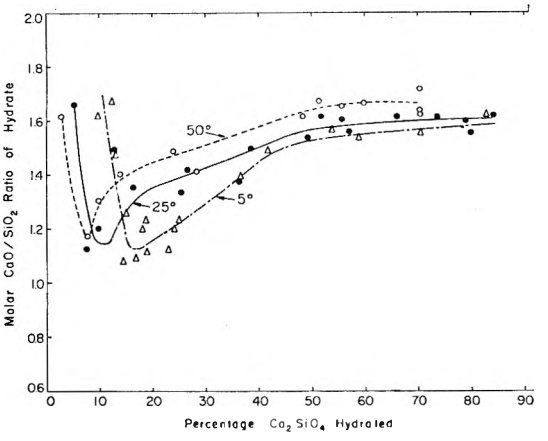

Fig. 5.—Molar CaO/SiO_2 ratio of tobermorite (G) *vs.* percentage hydration of Ca_2SiO_4.

SiO_5 is hydrated at 5° even at only 0.5 hr., there is no change in the degree of hydration within experimental error up to 12 hr. During this same period, the V_m values increase only slightly. After 12 hr., there is a sharp increase in hydration, and after 1.5 days, the 5° samples are more hydrated than those at higher temperatures. Hydration is complete at 400 days regardless of temperature.

Thus hydration of both Ca_2SiO_4 and Ca_3SiO_5 at 5° proceeds at a significant rate only after an induction period of about 12 hr. A similar result was found for portland cement. An induction period of about 1 hr. is indicated in the hydration of Ca_2SiO_4 at 25°. The induction periods in the hydration of Ca_2SiO_4 at 50° and Ca_3SiO_5 at 25 and 50°, if they exist at all, last for considerably shorter times than half an hour.

B. The Stoichiometry of the Hydration Reactions.—In the presentdiscussion, the stoichiometric considerations will berestricted to an examination of the molar CaO/SiO_2 ratios of the calcium silicate hydrate formed. These ratios for hydrates produced in the hydration of Ca_2SiO_4 are plotted in Fig. 5 against the degree of hydration for the three temperatures. The three curves are similar in that each passes through a minimum and continues to rise thereafter. The product formed at the inception of hydration has a high CaO/SiO_2 ratio, perhaps as high as 2, which is that of Ca_2SiO_4 itself. This intermediate product loses CaO and the CaO/SiO_2 ratio of the product falls off, then the resultant low CaO/SiO_2 ratio material takes up CaO, and the CaO/SiO_2 ratio increases. At the minimum, the CaO/SiO_2 ratio is between about 1.1 and 1.2. The minimum occurs at higher degrees of hydration the lower the temperature. Because the experimental points for the 25° data did not define the position of the minimum well, it was estimated from the positions of the better defined 5 and 50° minima.

The calcium ion concentration and the pH results at 25° indicate a gradually decreasing supersaturation with respect to $Ca(OH)_2$ from 4 to 12 hr. Shortly after 12 hr., the solution becomes unsaturated, and at about the same time the minimum CaO/SiO_2 ratio in the solid is reached. These results indicate that (1) the initial high-lime product is so unstable that it loses lime even in a supersaturated solution; and (2) the low-lime intermediate which results takes up lime from the solution because it is unstable with respect to the final tobermorite (G). The solution becomes unsaturated for a while because the rate of uptake is greater than the rate at which the solution can be replenished by the free solid $Ca(OH)_2$ also present.

The observed CaO/SiO_2 ratios are mean results for mixtures of intermediates and final products and only when hydration has proceeded to more than about 50% do the ratios provide a good estimate of the composition of the stable tobermorite (G).

The CaO/SiO_2 ratios of the calcium silicate hydrates formed in the hydration of Ca_3SiO_5 at the three temperatures investigated are plotted in Fig. 6. Here, too, the initial product has a high CaO/SiO_2 ratio, perhaps as high as 3, the ratio in Ca_3SiO_5. The ratio falls rapidly at first, then gradually to complete hydration. There is no indication that the CaO/SiO_2 ratio passes through a minimum. It seems likely that the first step in the reactions of both Ca_2SiO_4 and Ca_3SiO_5 with water is the formation of a product with a CaO/SiO_2 ratio the same as the material from which it formed. This initial product loses lime rapidly, but not instantaneously. In the case of Ca_2SiO_4, the calcium silicate hydrate is low in CaO with respect to the final product, whereas in the case of Ca_3SiO_5, it is still high in CaO; hence it continues to lose CaO.

C. Stoichiometry and Surface Development. A Hydration Mechanism.—1. The variation in the surface area of tobermorite (G) as a function of degree of hydration for pastes of Ca_2SiO_4 and Ca_3SiO_5 hydrated at 25° is represented in Fig. 7. Each curve passes through a maximum before attaining a practically constant value. These data indicate three different stages in the hydration process: (1) the formation of a low area hydration product, (2) the transformation of this to a high area intermediate, and (3) the conversion of this intermediate to the stable tobermorite (G) with somewhat lower specific area. The CaO/SiO_2 data also indicate three stages in the process, though the last two stages are not as distinct for Ca_3SiO_5 as for Ca_2SiO_4.

Taken together, these results can be interpreted in the following manner. The primary product of hydration is a gel coating on the original unhydrated substrate, which builds up to many layers in thickness. The CaO/SiO_2 ratio of this gel may be as high as that of the substrate itself. During the second stage, thin sheets split off the gel coating, and the CaO/SiO_2 ratio drops sharply. The specific surface area indicates that the split-off sheets are one and two molecular layers in thickness. During the third stage, the unstable intermediate converts into stable tobermorite (G), which consists of sheets that are two and three molecular layers in thickness, as has been shown in Part I. It also has been shown in Part I that thicker sheets have higher CaO/SiO_2 ratios, so during the third stage this ratio increases.

2. With certain assumptions, both the composition and the thickness of the gel coating can be estimated for the lowest and highest area samples,

the thickness in terms of number of layers. First of all, assumptions must be made regarding the compositions of the split-off sheets L_1 and L_2, which have thicknesses of one and two molecular layers, respectively. It was shown in Part I that the layers of tobermorite are cemented to each other by lime; it is reasonable to suppose, therefore, that L_1 contains no such cementing lime. The simplest assumption is that L_1 is the 2:1 tobermorite layer of Megaw and Kelsey,[7] which has a CaO/SiO_2 ratio of 0.67. There must be some cementing lime in L_2; it must have, therefore, a higher CaO/SiO_2 ratio than L_1. If it is assumed that one molecule of CaO is needed to cement two unit cells (more accurately, pseudocells) to each other, the CaO/SiO_2 ratio in L_2 is 0.92. One may arrive at the ratio in L_2 in a somewhat different way. In the third stage of the hydration, lime is taken up; consequently, L_2 must have a lower CaO/SiO_2 ratio than the stable two-layer tobermorite (G), which will be designated $T(G)_2$. The CaO/SiO_2 ratio of $T(G)_2$ is 1.39, as was shown in Part I. The CaO/SiO_2 ratio of L_2 must be between 0.67 and 1.39; and not knowing what it actually is, one may take the average, which is 1.03. On the basis of these considerations, it will be assumed that the CaO/SiO_2 ratio in L_2 is 1.00, which cannot be too far wrong.

The specific surface areas of L_1 and L_2 can be calculated from the equation

$$A_T = \frac{2N\sigma}{nM_T} \qquad (1)$$

where A_T is the specific surface area of a tobermorite sheet n layers thick, N is Avogadro's number, M_T is the weight of a pseudocell containing one molecule (or the molecular weight), and $\sigma = 20.35 \times 10^{-16}$ cm.^{2}, the area of the *ab* face of a pseudocell. Because the area contributed by the two sides of the sheet is orders of magnitude greater than the area along the edges, the latter is neglected. Equation 1 gives 1257 and 526 m.^{2}/g. for the specific surface areas of L_1 and L_2, respectively.

Besides the assumptions about the compositions of L_1 and L_2, two other assumptions enter into the calculation of the gel coating thickness. The first is

$$A_u = A_0(1 - \alpha) \qquad (2)$$

where A_u is the area of the remaining unhydrated material in the paste per gram of the original silicate, A_0 is the specific surface area of the original silicate (0.67 m.^{2}/g. for both silicates), and α is the fraction of the material hydrated. Equation 2 is strictly valid only for monodisperse systems. The second is

$$A_p = A_u + \beta_1 A_1 + \beta_2 A_2 \qquad (3)$$

where A_p is the area of the paste per gram of original silicate; β_1 and β_2 are weight fractions of L_1 and L_2, and A_1 and A_2 are the specific surface areas of L_1 and L_2, respectively. The assumption here is that at the early stages of hydration considered, the amounts of the stable two and three-layer tobermorites, $T(G)_2$ and $T(G)_3$, present in the system can be neglected.

(7) H. D. Megaw and C. H. Kelsey, *Nature*, **177**, 390 (1956).

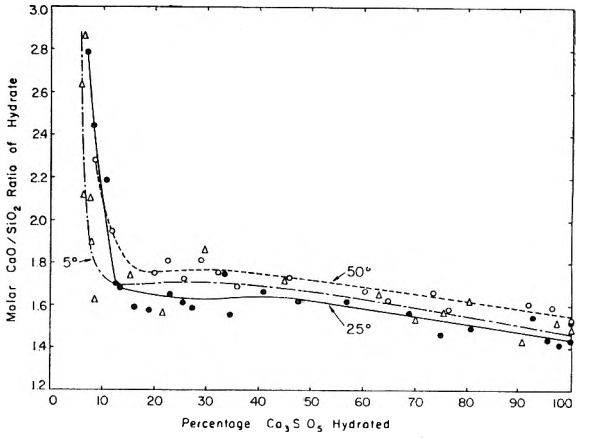

Fig. 6.—Molar CaO/SiO_2 ratio of tobermorite (G) *vs.* percentage hydration of Ca_3SiO_5.

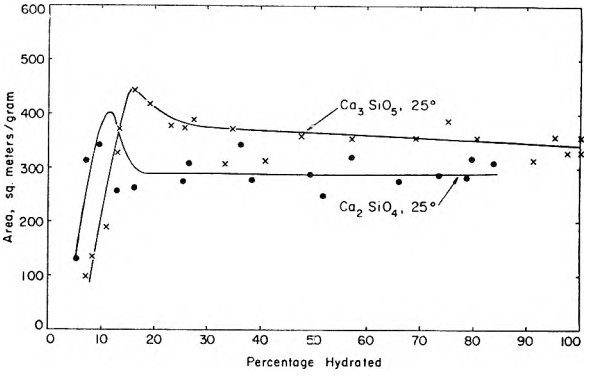

Fig. 7.—Surface area of tobermorite (G) as a function of percentage hydration.

3. The calculated CaO/SiO_2 ratios and thicknesses of the gel coating are given in Table I. For Ca_3SiO_5, the lowest specific surface area was observed for the paste hydrated at 5° for 0.5 hr. If all the split-off gel was L_1, the maximum thickness of gel coating is obtained, which is 25 layers. If all the split-off gel was L_2, the minimum thickness of 24 layers is obtained. The latter calculation leads to an absurd value for the CaO/SiO_2 ratio, 3.12. The ratio cannot be higher than 3.00, which is the ratio in Ca_3SiO_5. This indicates that all the split-off gel was L_1.

TABLE I

GEL COATING CaO/SiO_2 RATIOS AND THICKNESSES

Hydrated substance	Hydration conditions	$\beta_1/(\beta_1 + \beta_2)$	Gel coating CaO/SiO$_2$	Gel coating Thickness, layers
Ca_3SiO_5	0.5 hr. at 5°	1.00	3.01	25
Ca_3SiO_5	0.5 hr. at 5°	0.00	3.12	24
Ca_3SiO_5	6 hr. at 25°	1.00	2.87	33
Ca_3SiO_5	6 hr. at 25°	0.90	3.00	30
Ca_2SiO_4	4 hr. at 25°	1.00	1.83	28
Ca_2SiO_4	4 hr. at 25°	0.00	1.94	23
Ca_2SiO_4	14 days at 5°	1.00	1.43	72
Ca_2SiO_4	14 days at 5°	0.68	1.44	62

For the lowest area Ca_2SiO_4 paste, 4 hr. at 25°, the calculations of both extremes give reasonable values. The average of the extremes is a CaO/SiO_2 ratio of 1.9 and a coating thickness of 25 layers.

The minimum area for both silicates was obtained after about 5% hydration. At this stage of hydration, the thickness of the gel coating is about 25 layers for both silicates, and the CaO/SiO_2 ratio is close to that of the original silicate. It may be added that the thickness of one layer is about 10 Å., and the diameter of the unhydrated grain is of the order of 3 to 6 μ.

4. The calculation of the composition and thickness of the gel coating in the maximum surface area pastes involves an additional assumption. Because the stable tobermorites consist of two and three-layer sheets and the unstable tobermorites of one and two-layer sheets, the following reactions must take place

$$\left.\begin{array}{ll}(a) & L_1 + L_1 = T(G)_2 \\ (b) & L_1 + L_2 = T(G)_3\end{array}\right\} \qquad (4)$$

It is unlikely that two sheets can condense in the aqueous phase to form a thicker sheet; it is more likely that some of the sheets dissolve and precipitate on other undissolved sheets to form thicker sheets. Because the surface free energy of L_1 is twice as high as that of L_2, L_1 dissolves much more rapidly than L_2. It is reasonable to assume, therefore, that first L_2 reacts with L_1, then L_1 reacts with L_1. On this basis, one can calculate the proportions of L_1 and L_2 responsible for the final hydration products of Ca_2SiO_4 and Ca_3SiO_5.

As Fig. 7 shows, the specific surface area of the final tobermorite (G) is 290 m.²/g. for Ca_2SiO_4 and 355 m.²/g. for Ca_3SiO_5. The specific surface area of $T(G)_2$ is 387 m.²/g., that of $T(G)_3$ is 240 m.²/g., as was shown in Part I. Thus, the weight fractions of $T(G)_2$ and $T(G)_3$ in the final tobermorite of Ca_2SiO_4 are 0.34 and 0.66, respectively, and for Ca_3SiO_5, 0.78 and 0.22, respectively.

The CaO/SiO_2 ratio in $T(G)_2$, the two-layer tobermorite (G), is 1.39, and in $T(G)_3$, the three-layer tobermorite, 1.72, as was shown in Part I. From this it follows that the fractions of the $T(G)_2$ and $T(G)_3$ molecules in the final tobermorite of Ca_2SiO_4 are 0.37 and 0.63, respectively, and for Ca_3SiO_5, 0.80 and 0.20, respectively. The mole fractions of L_1 and L_2 which, on the basis of eq. 4, lead to these mole fractions of $T(G)_2$ and $T(G)_3$, are 0.68 and 0.32 for Ca_2SiO_4 and 0.90 and 0.10 for Ca_3SiO_5, respectively.

It was shown earlier for the Ca_3SiO_5 paste of minimum surface that up to 5% hydration only L_1 sheets split off the gel coating. The final product, at 100% hydration, contains 90% L_1 and 10% L_2. Thus, the proportion of L_2 to L_1 increases as the hydration progresses.

5. The maximum surface area for Ca_3SiO_5 was reached after 6 hr. of hydration at 25°, and for Ca_2SiO_4 after 14 days at 5°. Both pastes were about 16% hydrated. One extreme possibility is that the split-off gel still consisted only of L_1 sheets; the other is that the proportion of L_2 to L_1 already had reached its final value. The calculated values for these extremes are given in Table I. The average values are 32 layers with a CaO/SiO_2 ratio of about 2.9 for Ca_3SiO_5, and 67 layers with a CaO/SiO_2 ratio of 1.44 for Ca_2SiO_4.

Thus, between 5 and 16% hydration, the gel coating on the Ca_3SiO_5 grains increased only slightly in thickness, from 25 to 32 layers, and the CaO/SiO_2 ratio of the coating decreased only slightly, from 3.0 to 2.9. On the other hand, the thickness of the coating on the Ca_2SiO_4 grains increased strongly, from 25 to 67 layers, and the CaO/SiO_2 ratio dropped considerably, from 1.9 to 1.44.

6. A reasonable explanation for the differences between the behaviors of Ca_2SiO_4 and Ca_3SiO_5 can be given in terms of the compositions of the primary hydration products.

As water reaches the surfaces of the anhydrous grains, reaction takes place, and a gel coating is formed on the surface. The mechanism of the building up of the gel coating involves diffusion processes through the gel, but the nature of these processes is not known as yet. The diffusion may occur through holes in the crystals, through cracks in the gel coating, or, as Powers[8] proposes, through pores in the gel. In the calculation of the thickness of the gel coating it was assumed that the coating was continuous; if cracks or pores constitute a sizable fraction of the volume of the coating, the calculated thicknesses are too small.

The unstable primary products have a large excess of lime in their structures. This excess lime tends to come out of the structure to form the coarsely crystalline $Ca(OH)_2$ found in all pastes. The amount of excess lime may be considered a measure of the escaping tendency of this lime, and also a measure of the excess free energy—or the degree of instability—of the unstable hydrates. The gel coating of Ca_3SiO_5 has a greater excess of lime than that of Ca_2SiO_4, which implies a greater disruptive power and a faster rate of the splitting-off process.

While layers of tobermorite split off the coating, new layers form by the diffusion processes described before. For Ca_3SiO_5, the rate of splitting-off is almost as high as the rate of new layer formation, so the thickness of the gel coating increases only slowly. However, the rate of splitting-off, because of the much smaller amount excess of lime, is much lower for Ca_2SiO_4 than for Ca_3SiO_5, which results in a considerable increase in the thickness of the gel coating.

The gel coating may be visualized as consisting of alternate layers of calcium hydroxide and calcium silicate hydrate. The calcium hydroxide is not a separate substance—it is not free calcium hydroxide, and it cannot be extracted readily by organic solvents. At an early stage of the hydration reaction, the gel coatings are quite rich in excess lime, so single layers of calcium silicate hydrate alternate with layers of calcium hydroxide in the coating. Because the Ca_2SiO_4 coating is poorer in excess lime than the Ca_3SiO_5 coating, there may be an occasional double layer of calcium silicate hydrate sandwiched between calcium hydroxide even early in the hydration process. When the disruptive tendency of the excess lime manifests itself by the lime leaving the gel coating—probably by solution, possibly by splitting off—the sandwiched-in

(8) T. C. Powers, *J. Portland Cement Assoc. Res. Develop. Lab.*, **3**, 47 (1961).

single or double layer tobermorite sheets also split off the coating.

As the hydration progresses, the CaO/SiO_2 ratio of the gel coating decreases. Between 5 and 15% hydration, the decrease is slight for Ca_3SiO_5; it is much greater for Ca_2SiO_4. This is because the fast reaction of Ca_3SiO_5 with water can keep the composition of the coating close to its initial high value, whereas the slow reaction of Ca_2SiO_4 with water cannot. The decrease in CaO/SiO_2 ratio has two effects: the excess lime decreases, resulting in a decrease in the rate of splitting-off; and the proportion of double layer tobermorite sheets sandwiched between calcium hydroxide increases. Thus, the ratio of L_2 to L_1 increases as the hydration progresses.

The model described explains the long known but unexplained fact that tobermorite (G) in well hydrated Ca_3SiO_5 pastes has a higher specific surface area than in Ca_2SiO_4 pastes. The ultimate cause is that the CaO/SiO_2 ratio in Ca_3SiO_5 is 3, whereas in Ca_2SiO_4 only 2, leading to the conditions already described. The model also may explain the anomalous behavior of Ca_2SiO_4 at 50°, shown in Fig. 1. The hydration appears to stop after 100 days, even though the Ca_2SiO_4 is only about 70% hydrated. As Fig. 5 shows, the CaO/SiO_2 ratio of the stable tobermorite (G) obtained in the hydration of Ca_2SiO_4 increases with temperature. It is possible that the unstable primary product also can accommodate more lime in its structure at 50° than at lower temperatures. This would mean that there is less excess lime in the gel coating, resulting in less disruption of the coating. Thus, the gel coating may build up to such a thickness that the rate of diffusion through the gel becomes negligible and the reaction stops.

7. There has been a good deal of controversy among cement chemists about the mechanism of the hydration of portland cements, some advocating a surface reaction mechanism, others a mechanism of solution and precipitation. There is no reason why both mechanisms should not be operative in the hydration of calcium silicates and portland cements. When the anhydrous grains come in contact with water, it is reasonable to expect that immediate reaction should take place at the interface. The aqueous phase surrounding the calcium silicates and portland cements quickly becomes saturated with calcium and hydrosilicate ions[9]; it is reasonable to expect, therefore, that the calcium silicate hydrate should precipitate on the available surfaces. In the present paper both the surface reaction and the solution mechanism have been employed to account for different phases of the hydration reactions.

No attempt has been made in this paper to account for *all* of the features of the curves presented in the seven figures. The mechanism accounts for a number of important features, and further work is needed to account for the rest.

Acknowledgments.—The authors wish to express their great indebtedness to Mr. Donn Hathaway, Miss Elaine Anderson, and Mr. Tao-nan Chang for performing most of the experimental work reported in this paper.

(9) S. A. Greenberg and V. S. Mehra, "The Factors Controlling the Compositions of the Aqueous Phases in Contact with Portland Cement," *Proc. Fourth Intern. Sym. Chem. Cement*, in press.

MULTILAYERS OF ARGON AND NITROGEN ON HEXAGONAL BORON NITRIDE[1]

BY ROBERT A. PIEROTTI

School of Chemistry, Georgia Institute of Technology, Atlanta 13, Georgia

Received February 28, 1962

Multilayer adsorption isotherms of argon on boron nitride have been determined at 66.0, 68.9, and 75.9°K. In addition, multilayer isotherms of nitrogen on boron nitride have been determined at 63.30 and 65.79°K. Isosteric heats of adsorption have been obtained and are compared with the isosteric heats of adsorption of argon on graphite (P-33). The interaction energies of adsorption are determined for argon on P-33 and boron nitride by means of the Singleton–Halsey isotherm equation and are compared with the interaction energies calculated by dispersion energy summations. The calculated and observed interaction energies for argon–boron nitride are in good agreement. The observed interaction energy of argon with graphite is larger than that calculated. This discrepancy is discussed in terms of various interaction theories.

Introduction

The physical adsorption of argon on graphite has been of interest to investigators for many years. This interest stems from the energetic homogeneity of the graphite surface. Adsorption studies in the submonolayer region have been made recently by Ross and Pultz[2] and by Lopez-Gonzalez, Carpenter, and Deitz.[3] The multilayer region has been investigated experimentally and theoretically by a number of authors.[4,5] The most complete experimental study of multilayers of argon on graphite was that of Prenzlow and Halsey.[6] They determined the isotherms of argon on a highly graphitized carbon black designated P-33 and on xenon layers which had been preadsorbed on the P-33 surface. Isosteric heats and entropies of adsorption were calculated for their systems.

The hexagonal modification of boron nitride and the graphite form of carbon are structurally very similar and are isoelectronic; therefore, it seemed worthwhile to investigate the formation of multilayers of argon on boron nitride. Dispersion energy calculations[7] indicate that the two adsorbents are virtually identical in respect to the adsorption of argon except for about 200 cal./mole in the interaction energy of adsorption. Both adsorbents should be equally compatible for the growth of argon layers and therefore differences in the isotherms and in the isosteric heats should be a consequence of only the difference in the interaction energy of an argon atom with each adsorbent.

Experimental

Vacuum System.—A three-stage mercury diffusion pump with a liquid nitrogen trap capable of attaining pressures of 10^{-6} mm. was used. An ion gage was used to determine the limiting pressure.

Pressure Measurements.—A conventional constant volume adsorption system was used. Adsorption pressures were measured with a manometer constructed from 20 mm. Pyrex tubing and read with a cathetometer graduated to 0.01 mm. An electrical contact was used to produce the zero-setting of the manometer.

The pressure of the gas dose and the vapor pressures of argon and nitrogen were measured with standard U-tube manometers constructed of 18 mm. Pyrex tubing and read with a cathetometer.

All pressures were corrected for altitude and for the temperature of the mercury.

The Adsorption Cell.—The absorption cell was similar in design to that of Singleton and Halsey.[5] The adsorption cell, with a compartment for pure adsorbate, was suspended by its leads in a vacuum jacket in which a low pressure of helium could be maintained. This jacket was a thermal lag preventing the cell from responding to sudden changes in temperature of the refrigerant.

The Cryostat.—The cryostat was of the usual design.[8] The temperature was maintained by either an argon or nitrogen vapor pressure thermometer which actuated a relay-controlled valve. When this valve was open a mechanical oil pump pumped on the liquid nitrogen refrigerant causing the bath to cool.

Temperatures were measured with either an argon vapor pressure thermometer using the data of Clark, Din, and Robb[9] or with a nitrogen vapor pressure thermometer using the data of Armstrong.[10] Temperatures could be maintained to ±0.05°K. from 63.3°K. (the triple point of nitrogen) to 77°K. (a little below the boiling point of liquid nitrogen).

As a precaution to avoid errors caused by possible temperature fluctuations, measurements of p_0 were made simultaneously with measurements of p.

Dosage Measurement.—A thermostated gas buret was used in conjunction with the U-tube manometer mentioned above under the sub-heading "pressure measurements."

Outgassing Procedure.—The boron nitride sample was outgassed for five days at 200°, and then for 48 hr. at 450°. No measurable build-up of pressure was observed at the higher temperature when the cell with sample was isolated from the pumping system. The sample was heated to 400° for at least 4 hr. and evacuated to 10^{-5} mm. before each isotherm was determined.

Special Materials and Chemicals.—One-millimeter thin-walled capillary tubing was used in the adsorption portion of the system in order to keep the dead space at room temperature to a minimum. A small trap was placed between the cell and all stopcocks and mercury containers. This trap was kept at Dry Ice–acetone temperatures at all times.

Assayed-reagent, spectroscopically pure gases obtained from Air Reduction Sales, Inc., in Pyrex flasks were used without further purification.

Boron nitride powder, 325 mesh, was obtained from the Research and Development Division of the Carborundum Company. The sample was analyzed spectrographically and found to be greater than 99.92% pure. X-Ray diffraction of the sample showed it to be highly crystalline, having a pseudo-hexagonal crystal structure with crystal parameters a and c equal to 2.50 and 6.66 Å., respectively. This corresponds to a nearest neighbor distance of 1.44 Å. and an interlaminar spacing of 3.33 Å. Giardini reported these same values.[11]

(1) This work was supported by a grant from the Petroleum Research Fund of the American Chemical Society.

(2) S. Ross and W. W. Pultz, *J. Colloid Sci.*, **13**, 397 (1958).

(3) J. de D. Lopez-Gonzalez, F. G. Carpenter, and V. R. Deitz, *J. Phys. Chem.*, **65**, 112 (1961).

(4) (a) R. A. Beebe and D. M. Young, *ibid.*, **58**, 93 (1954); (b) E. L. Pace, *J. Chem. Phys.*, **27**, 134 (1957).

(5) J. H. Singleton and G. D. Halsey, Jr., *J. Phys. Chem.*, **58**, 330 (1954).

(6) C. F. Prenzlow and G. D. Halsey, Jr., *ibid.*, **61**, 1158 (1957).

(7) R. A. Pierotti and J. C. Petricciani, *ibid.*, **64**, 1596 (1960).

(8) W. J. C. Orr, *Proc. Roy. Soc.* (London), **A173**, 349 (1939).

(9) A. M. Clark, F. Din, and J. Robb, *Physica*, **17**, 876 (1951).

(10) G. T. Armstrong, *J. Res. Natl. Bur. Std.*, **53**, 263 (1954).

(11) A. A. Giardini, U. S. Bur. Mines Circ. 7664, 1953.

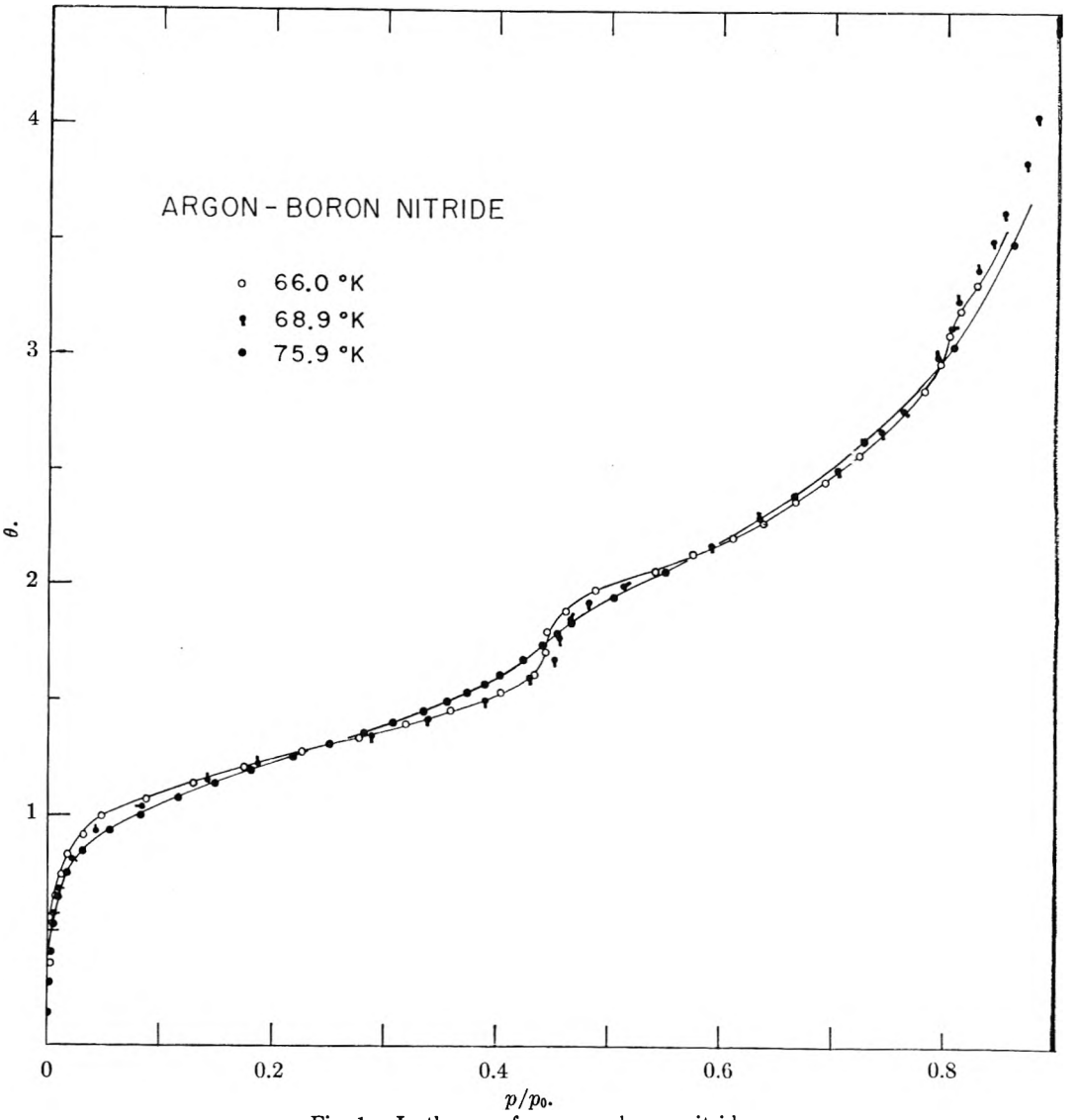

Fig. 1.—Isotherms of argon on boron nitride.

Results

Argon–Boron Nitride System.—The isotherms for argon adsorbed on boron nitride are shown in Fig. 1. The coördinate, θ, is the fraction of the surface covered and is equal to V/V_m, where V is the volume adsorbed and V_m is the volume of a monolayer. V_m was determined from a BET plot (argon on BN gives a linear BET plot, whereas argon on graphite does not) and was equal to 5.30 ml. (STP)/g. This corresponds to an area of 19.6 m.²/g. V_m estimated from point B would have been somewhat lower than that given above. Ross and Pultz[2] obtained V_m equal to 5.06 ml./g. for argon on their sample of BN presumably obtained from point B. This is in good agreement with the V_m of this sample.

The isosteric heats of adsorption of argon on BN as a function of coverage are shown in Fig. 2. They were calculated using

$$q_{st} = \left(\frac{\partial \ln (p/p_0)}{\partial (1/RT)}\right)_\theta \qquad (1)$$

The plots of $\ln (p/p_0)$ *vs.* $1/RT$ at constant θ for the three temperatures reported yielded good straight lines. It should be noted that the reference state chosen was bulk solid argon at the temperatures of the isotherms; therefore, the energy zero in Fig. 2 is equal to the heat of sublimation of argon.

Nitrogen–Boron Nitride System.—The isotherms for nitrogen adsorbed on boron nitride are shown in Fig. 3. V_m obtained from a BET plot is 5.41 ml./g. at 65.8°K., corresponding to an area of 22.6 m.²/g. Point B again would yield a lower V_m. The V_m for nitrogen determined by Ross and Pultz is smaller than that reported here, but their isotherm was determined at a temperature 12° higher than that used here.

The isosteric heats for this system are shown in Fig. 4. These heats were calculated in the same manner as for argon. Again it should be noted that the reference state is the bulk adsorbate, in this case liquid nitrogen; therefore, the energy zero in Fig. 4 is the heat of vaporization of nitrogen.

Interaction Energies.—Singleton and Halsey[12]

(12) J. H. Singleton and G. D. Halsey, Jr., *Can. J. Chem.*, **33**, 184 (1954).

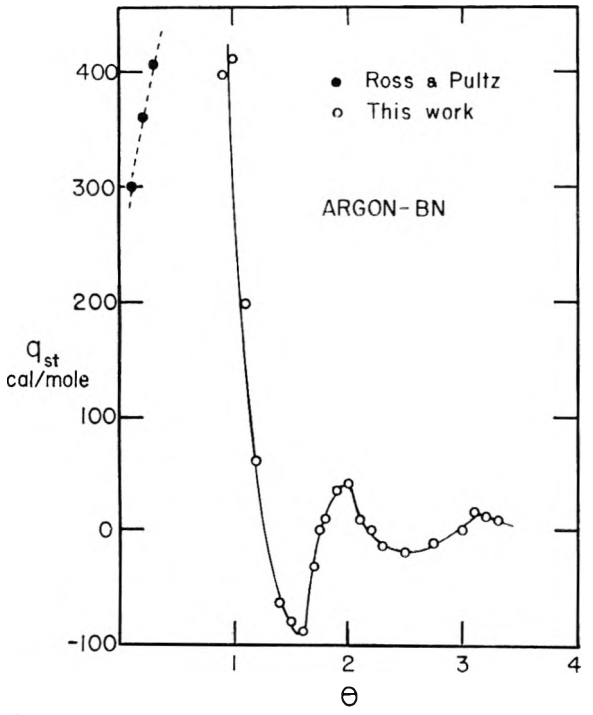

Fig. 2.—Isosteric heats of adsorption for argon on boron nitride.

have modified the Hill isotherm equation to read

$$\ln (p/p_0)_n = -\frac{E_1}{n^3kT} + \frac{w}{kT}(1 - g) \quad (2)$$

applicable to adsorption of a crystalline adsorbate on an homogeneous surface. In this equation p is the equilibrium pressure of the adsorbate over the solid, p_0 is the vapor pressure of pure adsorbate at the temperature of the isotherm(T), n is the number of adsorbed layers, k is the Boltzmann constant, E_1 is the interaction energy in the first layer exclusive of the short range forces, w is the lateral interaction energy, and g is a compatibility factor. This isotherm equation has been found to yield reliable interaction energies for physically adsorbed atoms on many surfaces.[13]

E_1/kT was calculated from equation 2 using the values of p/p_0 evaluated at θ equal to 1.5 and 2.5. E_1 is the difference between the interaction energy of the adsorbate–adsorbent (E_{int}) and the self-interaction energy of the adsorbate.[12] The self-interaction energy is equal to one-half the heat of sublimation of argon. Table I contains the results of these calculations for both argon and nitrogen on P-33 and on BN. The calculated interaction energy of argon with P-33 is in excellent agreement with that obtained from the high-temperature, low coverage measurements of Sams, Constabaris, and Halsey[14] (2200 cal./mole), considering the diverse approaches used.

Discussion

The isotherms of argon on BN are similar in shape to those of argon on P-33[6] with the clear-cut occurrence of steps and with the isotherms crossing one another at near integral and half-integral θ. The steps occur at slightly higher values of p/p_0 indicating a slightly smaller interaction energy. The steps are not as sharp nor are the risers as long as for the argon–graphite system. Although the BN sample is probably more heterogeneous than the sample of P-33 used by Prenzlow and Halsey,[6] it is believed that the major cause of the difference in the sharpness and length of the risers resides in the relative populations of the 1st, 2nd, and 3rd layers, an effect which is of some importance even in the argon–graphite system.[4b] The lower interaction energy of argon–BN favors an increased population in the higher layers at a given θ. This same effect should be noted in the heat curves.

Prenzlow and Halsey report a "pseudo" critical temperature of 68°K. for argon on graphite in the second layer; the same critical phenomenon and temperature is observed on BN. The isotherms reported here, together with the multilayer data of Prenzlow and Halsey and the submonolayer data of Ross and Pultz,[2] permit a model-independent verification of the inverse cube law in physical adsorption,[15] thereby giving added significance to the cube law assumption used in the derivation of equation 2.

The isosteric heat curve for argon–BN is of the same general shape as that for argon–P-33 having maxima in the vicinity of integral θ. The P-33 curves have higher and sharper maxima and lower and sharper minima. The higher maxima are in accord with the greater interaction energy for argon–graphite. The broadening of the curve, the less sharp peaks, and the lower minima can be accounted for by the greater population of higher layers on BN. For each system, as θ increases the isosteric heat approaches the heat of sublimation of argon, indicating that the adsorbed phase is "solid-like" in the measured temperature range. Note that the heats of adsorption on BN for all layers other than the first are nearly equal to the heat of sublimation of argon, partially accounting for this system yielding a linear BET plot.

The nitrogen isotherms are similar in shape to those of argon on P-33[6] having pronounced humps in the vicinity of integral θ. The isosteric heat curve has the characteristic maxima and minima of the heat curves for argon. It is clear from Fig. 4 that if superheated solid nitrogen were used as the reference state, the isotherms would have crossed one another at about θ equal to 1, 1.5, and 2, thereafter diverging from one another. There is, therefore, no particular significance to be assigned to crossover points as has been implied[3] other than that the isosteric heat of adsorption is equal to the heat of condensation in the reference state. The adsorbed nitrogen phase probably behaves as a compressed liquid being held more firmly in the direction normal to the surface than it is in the reference state. During the filling of the third layer, the adsorbent is less influential and the heats decrease, approaching the heat of vaporization of bulk liquid nitrogen.

Dispersion energy calculations for argon on

(13) R. A. Pierotti and G. D. Halsey, Jr., *J. Phys. Chem.*, **63**, 680 (1959).

(14) J. R. Sams, Jr., G. Constabaris, and G. D. Halsey, Jr., *ibid.*, **64**, 1689 (1960).

(15) R. A. Pierotti, *J. Chem. Phys.*, **36**, to be published.

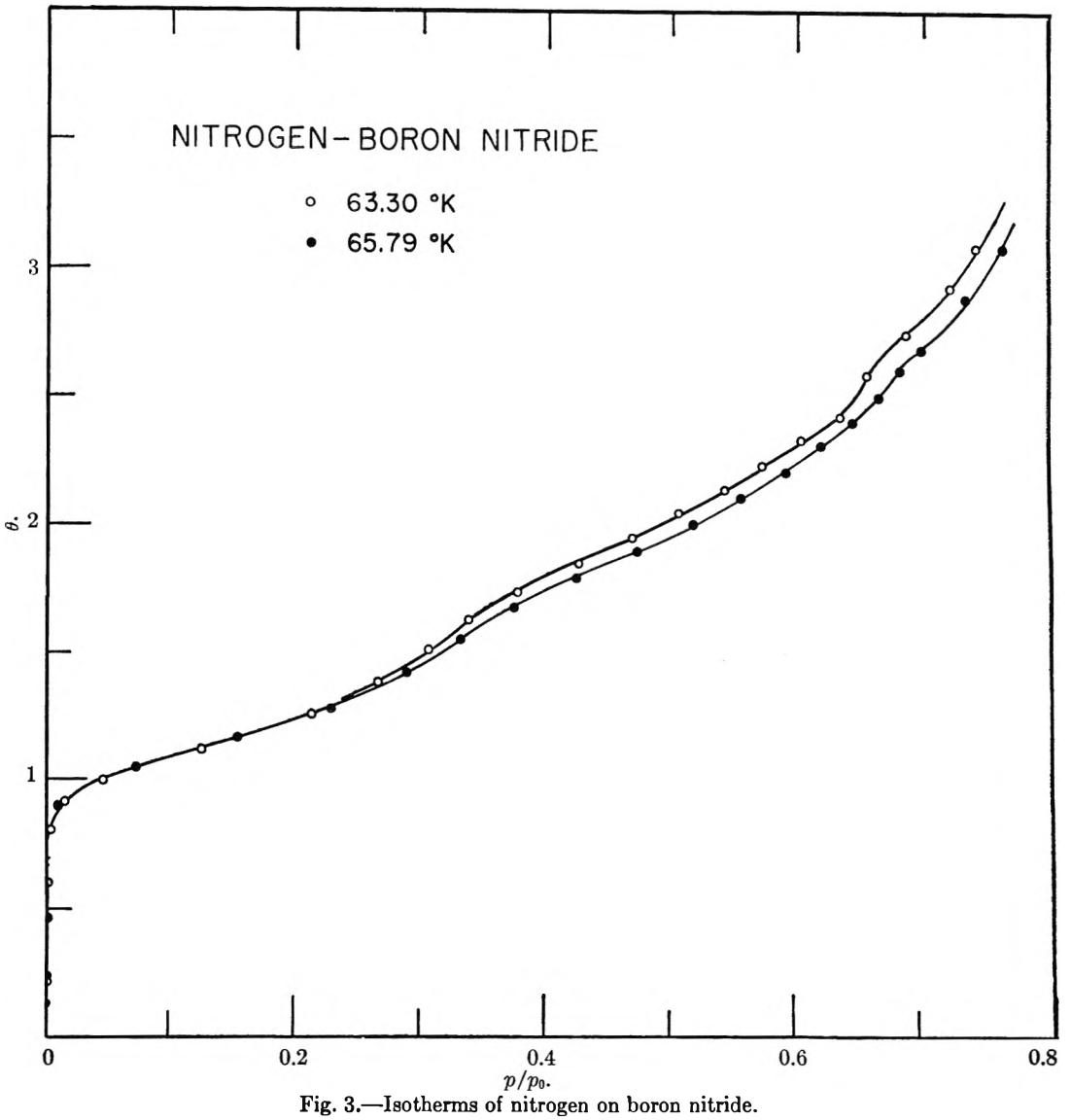

Fig. 3.—Isotherms of nitrogen on boron nitride.

graphite[16] and for argon on boron nitride[7] have been carried out by summing a Lennard-Jones (6–12) potential over all pairwise interactions of an argon atom with the atoms of the adsorbent. These energies appear in Table I along with the experimental values. Good agreement is obtained between the calculated and observed interaction energy for the argon–BN system. This agreement was to be expected because boron nitride meets the requirements of the Lennard-Jones summation quite well, being a covalent, non-polar, non-conducting solid. Graphite, of course, does not meet these requirements and disagreement between the calculated and observed interaction energies has been the subject of much discussion.[17] Attempts have been made to account for this discrepancy by changing the method of obtaining the attractive and repulsive constants used in the Lennard-Jones potential,[18] by assuming that the interaction of argon with the conduction electrons of graphite accounts for the entire interaction energy,[17] or by assuming that the interaction does not have its origin in dispersion forces at all but rather in some force such as the Mullikin charge transfer force.[19] The present work clearly displays the inadequacy of any of these positions and indicates that more than one effect is operable.

TABLE I

COMPARISON OF THE CALCULATED AND PREDICTED INTERACTION ENERGIES

System	Calcd.[a] r_0 (Å.)	Calcd.[a] r_e (Å.)	Expt. r_e (Å.)	Calcd. E_{int}, cal./mole	Expt.[b] E_{int}, cal./mole	Expt. g
Ar–C	4.05[c]	3.55[c]	(3.58)[e]	1750[c]	2150	0.997
Ar–BN	4.04[d]	3.54[d]	(3.58)[e]	1960[d]	1950	0.997
N_2–C	...	...	....		2070	1.02
N_2–BN	...	...	....		1800	1.02

[a] r_0 is the repulsive constant and r_e is the equilibrium distance of the first layer from the surface. [b] Obtained by using equation 2. [c] Crowell and Young.[16] [d] Pierotti and Petricciani.[7] [e] Pierotti[15] (the values are assumed equal).

(16) A. D. Crowell and D. M. Young, *Trans. Faraday Soc.*, **49**, 1080 (1953).

(17) J. H. de Boer, "Advances in Catalysis," Vol. VIII, Academic Press, New York, N. Y., 1956, p. 17.

(18) A. D. Crowell and R. B. Steele, *J. Chem. Phys.*, **34**, 1347 (1961).

(19) D. G. Tuck, *ibid.*, **29**, 724 (1958).

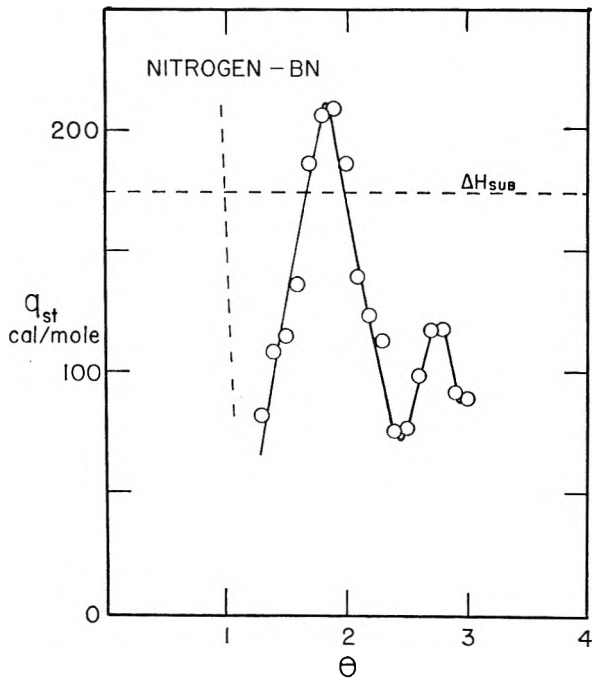

Fig. 4.—Isosteric heats of adsorption for nitrogen on boron nitride. The horizontal dashed line represents the heat of sublimation of nitrogen. The vertical dashed line is presumably how the heats would vary near θ equal one. The submonolayer data of Ross and Pultz fall in the region of 900 cal./mole.

The Lennard-Jones potential, when summed in the manner described in ref. 7, does yield good agreement with experiment for the interaction energy for argon with BN. The atomic cores in graphite must certainly behave in a manner similar to boron nitride insofar as the dispersion interaction with argon is concerned. This is evidenced by the calculation of Crowell and Young[16]; therefore, the energy in excess of that calculated appears to be the result of the π-electron system of graphite. Since the observed interaction energies in Table I were obtained at large distance from the surface (from the 2nd and 3rd layers), it is impossible to attribute the excess energy to charge transfer forces as suggested by Tuck[19] and Gundry and Tompkins.[20] The inverse-cube decay law for the argon on these solids has been verified[15] indicating that the interactions are the result of dispersion forces. It appears, therefore, that the interaction energy of argon with graphite is made up of two parts: (1) the dispersion interaction energy of argon with the carbon cores and (2) the dispersion interaction energy of argon with the π-electrons.

The interaction with the π-electrons is certainly related to the theories of Bardeen[21] and of Margenau and Pollard,[22] except that their theories are based upon the conduction electrons in metals being free electrons. It is interesting to equate the energy in excess of that calculated by Crowell and Young to the expression for the interaction energy derived by Margenau and Pollard

$$E_{excess} = \frac{e^2\alpha}{16}\left(\frac{2.5}{r_s} - \frac{nh}{\pi m\nu}\right) \times \frac{1}{R^3} \quad (3)$$

In this expression e and m are the charge and mass of an electron, α and ν are the polarizability and resonant frequency of the gas atom, n is the number of conduction electrons per cc. of solid, r_s is the radius of a sphere containing one conduction electron, and R is the distance of the gas atom from the solid. Solving this equation with E_{excess} equal to 400 cal./mole and R equal to 3.58 Å., one obtains r_s equal to 4.6 Å. and n equal to 4.3×10^{21} electrons/cc. This corresponds to only about 4% of the π-electrons in graphite being conduction electrons. Qualitatively, this is in accord with the small conductivity of graphite at low temperatures and with the high diamagnetic susceptibility of graphite. It is interesting to note that since the number of conduction electrons in graphite should increase with temperature,[23] the adsorption interaction energy also should be temperature dependent. It is not known to the author whether this has been observed.

Conclusion

Boron nitride and graphite behave similarly insofar as the formation of multilayers of argon and nitrogen is concerned. The slight differences in the isotherms and in the isosteric heat curves appear to be explainable on the basis of a small difference in the interaction energy. A statistical model similar to that used by Pace[4b] or one based upon the order–disorder approach of Hijmans and de Boer[24] should be capable of predicting the observed differences. This is being undertaken at present.

The interaction of argon with graphite seems to be made up of two parts (both with their origin in dispersion forces): the interaction with the carbon cores and the interaction with the π-electrons. Charge transfer forces are not appropriate here. Attempts to explain the argon–graphite interaction solely on the basis of a Lennard-Jones potential between atoms or solely on the basis of metallic-like interactions are unfounded.

DISCUSSION

E. V. BALLOU (Gulf Research & Development Co.).—You have shown curves of isosteric heat values at low surface coverages. Have you found it experimentally feasible to obtain valid data for isosteric heat values at coverages much below monolayer coverage?

R. A. PIEROTTI.—The isosteric heats at low surface coverage were determined by Ross and Pultz and are in accord with what might be expected. The experimental arrangement used in the work reported here could not be used to determine the low coverage portion of the isotherms precisely enough to warrant making calculations of the isosteric heat.

HERMAN E. RIES, JR. (American Oil Company).—I believe you did not show adsorption–desorption isotherms. Did you obtain such curves—and if so was hysteresis observed? I am particularly interested in the stepwise adsorption effects as related to hysteresis.

(20) P. M. Gundry and F. C. Tompkins, *Trans. Faraday Soc.*, **56**, 846 (1960).

(21) J. Bardeen, *Phys. Rev.*, **58**, 727 (1940).

(22) H. Margenau and W. G. Pollard, *ibid.*, **60**, 128 (1941).

(23) K. S. Pitzer, "Quantum Chemistry," Prentice-Hall, Inc., New York, N. Y., 1953, ch. 10.

(24) J. Hijmans and J. de Boer, *Physica*, **21**, 471 (1955); S. Bumble and J. M. Honig, *J. Chem. Phys.*, **33**, 424 (1960).

R. A. PIEROTTI.—The isotherms were a composite of adsorption and desorption points. Hysteresis was not observed anywhere along the isotherms.

W. H. WADE (University of Texas).—Why were the adsorption temperatures so close together?

R. A. PIEROTTI.—While the design of the cryostat would have permitted studies at temperatures up to the boiling point of liquid oxygen, the temperature range of greatest interest was where the steps are steepest and this is where the measurements were made.

W. D. SCHAEFFER (Lehigh University).—The argon adsorption isotherm and heats of adsorption on graphitized P-33 depend markedly on the thermal history of the sample and the extent of surface homogeneity. Before undertaking extensive calculations and comparisons of interaction energies, would it not be advisable to determine the influence of the thermal history on the argon adsorption? Increased homogeneity of the BN surface can be expected to have a significant influence on the relative population of the successively adsorbed layers.

R. A. PIEROTTI.—The thermal history and surface homogeneity are important considerations. The method of preparation of BN guarantees the uniform high temperature treatment associated with the graphitization of carbon blacks. Moreover, the stepwise argon adsorption isotherms and the shape of the heat curves are excellent indications of a high degree of homogeneity. In light of this and the method used to calculate the interaction energies, the comparison of the interaction energies seems well justified. A *detailed* comparison of the heats as a function of coverage is unwarranted unless further studies concerning surface homogeneity are made; however, a comparison of the general features of the heat curves certainly is justified and significant.

PHYSICAL ADSORPTION ON LOW ENERGY SOLIDS. I. ADSORPTION OF CARBON TETRAFLUORIDE, ARGON, AND NITROGEN ON POLYTETRAFLUOROETHYLENE

BY DONALD GRAHAM

Contribution No. 327, Jackson Laboratory, Organic Chemicals Department, E. I. du Pont de Nemours and Company, Wilmington, Delaware

Received February 28, 1962

Carbon tetrafluoride, argon, and nitrogen, at temperatures near their respective boiling points, are adsorbed on polytetrafluoroethylene with isosteric heats of adsorption only slightly greater than the corresponding latent heats of condensation. In all cases, the adsorbates are mobile, nitrogen retaining some "super mobility." Film pressures at a coverage representing one statistical monolayer are 9.5 to 10 ergs/sq. cm. Additional monolayers are adsorbed with abnormally low isosteric heats indicating multilayer films of low density.

Introduction

Polytetrafluoroethylene comprises an assembly of fluorinated carbon chains, bound to each other by relatively weak forces of essentially van der Waals type. The lattice energy of the intermolecular bonding has been estimated to be 2.0 kcal. per mole of recurrent $-CF_2-CF_2-$units.[1] Its total surface energy[2] has been estimated to lie between 56 and 69 ergs/cm.^{2}, and its critical surface tension,[3] approximately 18 dynes/cm. Its importance as an adsorbent is based not only on its small cohesive energy but also on its possible relation to recent developments in studies of highly fluorinated surfactants. The choice of carbon tetrafluoride as the first adsorbate studied was based on its chemical similarity to the adsorbent, its symmetry, and its boiling point. Argon and nitrogen were included as simple variants.

Experimental

Materials.—The polytetrafluoroethylene used as the adsorbent in this investigation was a powdered product available commercially as "Teflon" 6. The surface area of the sample, as determined by application of the BET equation to the nitrogen isotherm, was 11.67 m.^{2}/g. The sample was subjected to repeated adsorption and desorption of nitrogen before reproducible data were obtained.

Carbon tetrafluoride was obtained as a still fraction with the following analysis

CF_4	99.7% (mass spectrometer)
CF_3Cl	<0.02% (infrared)
CF_2Cl_2	<0.02% (infrared)
Air	0.13% (vapor phase chromatography) (remainder believed to be largely carbon monoxide)

The sample was redistilled several times to minimize noncondensable gases and, as used, melted at 89.5°K. at a vapor pressure of 0.819 mm.

Argon was obtained from the Matheson Company with a minimum purity specification of 99.998% argon.

The nitrogen used as adsorbate and in the gas thermometer was the Linde "high purity" grade, 99.995% N_2 minimum.

The oxygen used in the gas thermometer was the Linde spectroscopic grade.

The ethylene used in the gas thermometer was the Matheson research grade, minimum purity 99.9 mole % (remainder propane).

Equipment.—The adsorption measurements were carried out using equipment and methods previously described.[4] Liquid nitrogen and liquid oxygen baths were used for cooling the adsorbent sample to the temperatures desired for adsorption of argon and of nitrogen. A simple cryostat was employed for the adsorption of carbon tetrafluoride, which required temperatures of 145–155°K. This consisted of a stirred bath cooled by liquid nitrogen drawn through a copper coil immersed in the bath. The flow of liquid nitrogen was controlled by an ethylene gas thermometer with its bulb close to the sample. This thermometer actuated a "Thermocap" relay which in turn caused a Fisher Electro Hosecock to close a vacuum bleed in the suction line, drawing liquid nitrogen through the cooling coil when required. The bath liquid was Mallinckrodt petroleum ether (ligroin), boiling range 30–60°, Cat. No. 4980. There was some variation in the freezing point of this petroleum ether, and it was necessary to select material

(1) W. Brandt, *J. Chem. Phys.*, **26**, 262 (1957).

(2) R. J. Good, L. A. Girifalco, and G. Kraus, *J. Phys. Chem.*, **62**, 1418 (1958).

(3) H. W. Fox and W. A. Zisman, *J. Colloid Sci.*, **5**, 514 (1950).

(4) D. Graham, *J. Phys. Chem.*, **61**, 1310 (1957).

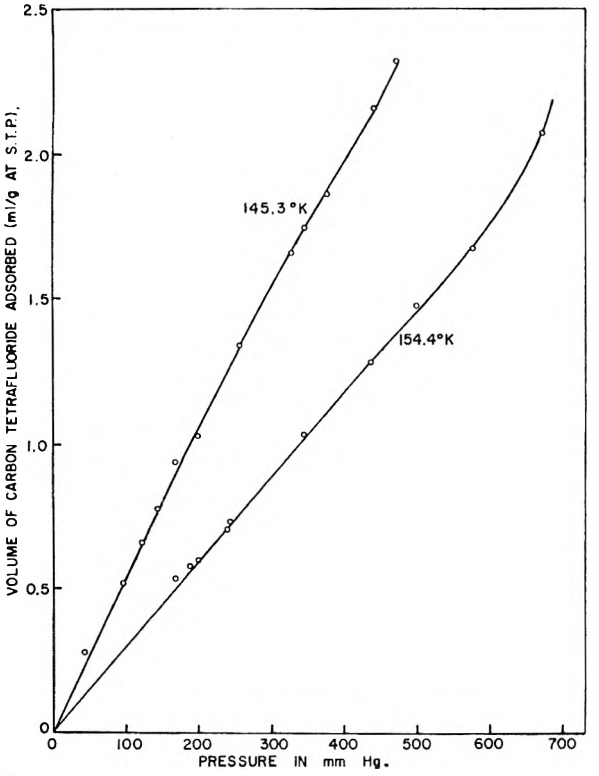

Fig. 1.—Adsorption of carbon tetrafluoride on polytetrafluoroethylene at 145.3 and 154.4°K.

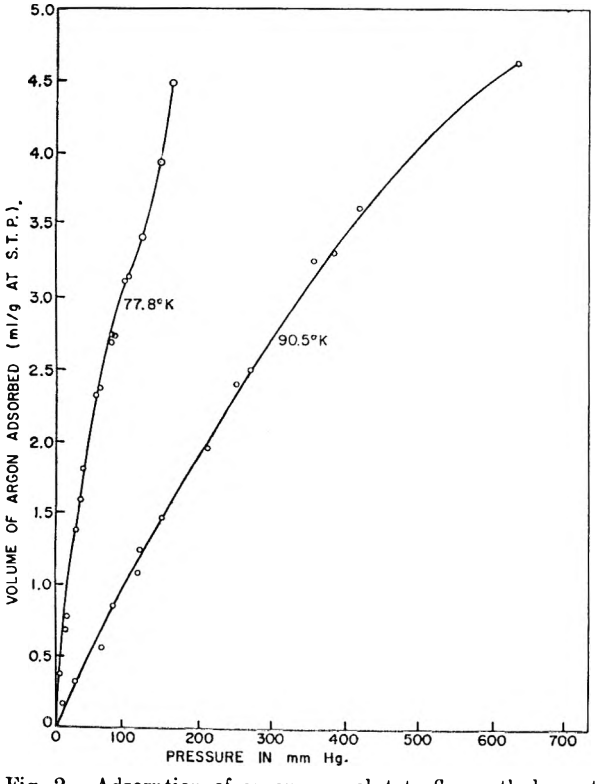

Fig. 2.—Adsorption of argon on polytetrafluoroethylene at 77.8 and 90.5°K.

freezing below 145°K. The bath volume was approximately 2 l. With this equipment, the maximum temperature fluctuation was approximately ±0.002°.

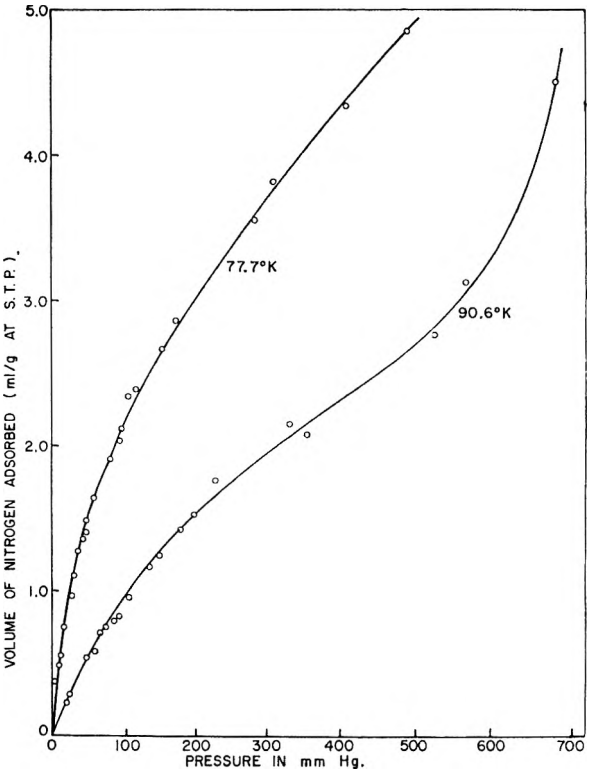

Fig. 3.—Adsorption of nitrogen on polytetrafluoroethylene at 77.7 and 90.6°K.

Results and Discussion

Adsorption Data.—To provide a basis for the calculation of isosteric heats of adsorption and related values, adsorption isotherms were obtained with each adsorbate at two temperatures. The temperatures selected were near the normal boiling points of the respective adsorptive materials and separated by about 10°. Since the calculations are based on constant adsorbate volume rather than constant coverage, it was convenient to use values of σ (cross-sectional area of an adsorptive molecule) and, in turn, of θ (fractional coverage of the adsorbent surface) representing an average temperature. The physical constants of these systems are given in Table I.

TABLE I

PHYSICAL CONSTANTS OF ADSORPTION SYSTEMS

Adsorbate	CF_4	Ar	N_2
Latent heat of vaporization at T_{Av}, cal./mole	2550	1580	1270
T_1, °K.	145.3	77.8	77.7
T_2	154.4	90.5	90.6
T_{Av}	149.8	84.2	84.2
Vapor pressures of adsorptive materials at the adsorption temp., mm.			
$P_0(1)$ (at T_1)	764.5	217.8	792
$P_0(2)$ (at T_2)	1395	1053	2812
Adsorbent surface area, m.²/g.	11.67	11.67	11.67
Cross-sectional area per molecule, Å.² (at T_{Av})	22.2	14.1	16.6
Capacity of monolayer (V_m) in ml. at STP/g. adsorbent	1.95	3.07	2.61

TABLE II

COMPARISON OF OBSERVED ENTROPY CHANGES WITH THOSE OF IDEALIZED MODELS REPRESENTING SITE ADSORPTION AND MOBILE ADSORPTION

θ	$-\Delta H$, kcal./mole	$-\Delta F$, kcal./mole	$-\Delta S$	Std. diff. molar entropy of adsorption: Site adsorption, Experiment $-\Delta S^0_i$	Site adsorption, Theory gS^0_{tr}	Mobile adsorption, Experiment $-\Delta S^0_m$	Mobile adsorption, Theory $gS^0_{tr} - aS^0_{tr}$
				Carbon tetrafluoride			
0.20	2.95	0.71	15.0	17.7	35.9	11.6	11.7
.50	2.90	.42	16.5	16.5	35.9	11.3	11.7
.70	2.83	.32	16.7	15.1	35.9	10.1	11.7
.85	2.70	.26	16.3	12.9	35.9	10.1	11.7
				Argon			
0.20	1.70	0.50	14.3	17.1	30.8	11.1	10.0
.50	1.68	.32	16.2	16.2	30.8	10.0	10.0
.70	1.63	.25	16.4	14.7	30.8	10.8	10.0
.85	1.56	.20	16.2	12.7	30.8	10.0	10.0
				Nitrogen			
0.20	1.50	0.68	8.6	11.4	29.7	5.7	10.0
.50	1.41	.48	10.3	10.3	29.7	5.6	10.0
.70	1.40	.39	11.0	9.3	29.7	5.5	10.0
.85	1.37	.34	11.3	8.1	29.7	5.9	10.0

The adsorption isotherms for carbon tetrafluoride, argon, and nitrogen are shown in Fig. 1, 2, and 3, respectively.

Film Pressures.—Film pressures (or changes in surface free energy with adsorption) were calculated at a coverage representing one statistical monolayer, by graphical integration of the Gibbs equation (using data from the experimental isotherms) as has been described.[5] In each case, the result was between 9.5 and 10.0 ergs/cm.^{2}, any differences being within the probable limits of the experimental precision. This agreement among the three systems is consistent with their corresponding states (at temperatures close to their respective normal boiling points and at the same surface coverage). The low values are an indication of weak adsorption bonding.

Isosteric Heats of Adsorption.—Isosteric heats of adsorption, calculated by application of the Clausius–Clapeyron equation to the adsorption data, are shown in Fig. 4, together with the corresponding values of the latent heats of condensation of the adsorptive materials. Each of these systems shows three important characteristics. First, the major part of the first statistical monolayer is adsorbed with an isosteric heat only slightly greater than the corresponding latent heat of condensation (small net isosteric heat). Second, the heat begins to fall off (indicating appreciable deposition of the second or higher monolayers) considerably short of completion of the first statistical monolayer. Finally, with build-up of the second and subsequent layers, the heat drops below the latent heat of condensation, indicating an adsorbed multilayer film of unusually low density.

Adsorbate Mobility.—The relative weakness of the adsorption, as indicated by the low film pressure and small net isosteric heats, is a strong indication of adsorbate mobility. A more unambiguous characterization is obtained from consideration of the entropy change accompanying the adsorption process, an approach employed in different ways by different investigators.[6-9]

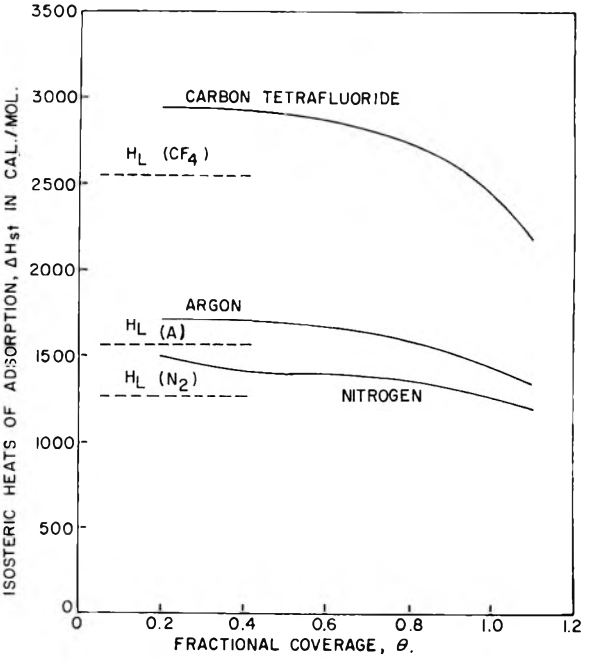

Fig. 4.—Isosteric heats of absorption of carbon tetrafluoride, argon, and nitrogen on polytetrafluoroethylene.

Using the methods and notation of ref. 8, the standard differential molar entropy changes calculated from the experimental isotherms were compared with those from theoretical entropically ideal processes representing adsorption on sites and adsorption as a mobile two-dimensional gas.

(5) W. D. Harkins, "The Physical Chemistry of Surface Films," Reinhold Publ. Corp., New York, N. Y., 1952, p. 211.

(6) D. H. Everett, *Trans. Faraday Soc.*, **46**, 453 (1950); **46**, 942 (1950); **46**, 957 (1950).

(7) C. Kemball, "Advances in Catalysis," Vol. II, Academic Press, Inc., New York, N. Y., 1950, p. 223.

(8) J. H. de Boer and S. Kruyer, *Proc. Koninkl. Ned. Akad. Wetenschap.*, **B55**, 451 (1952).

(9) J. W. Ross and R. J. Good, *J. Phys. Chem.*, **60**, 1167 (1956).

The results from all three systems, brought together in Table II, strongly support earlier indications of adsorbate mobility. $-\Delta S^0_1$ (a combination of the experimental entropy of adsorption with a configurational term) is in every case much smaller than ${}_gS^0_{tr}$ (the translational entropy of the adsorptive gas). The observed loss of entropy is thus much less than that which would occur in localized adsorption on fixed sites.

The picture with regard to mobile adsorption is different. The test is a comparison of $-\Delta S^0_m$ (a combination of the experimental entropy of adsorption with a measure of the area over which a mobile adsorbed molecule can move at a specified coverage) with ${}_gS^0_{tr} - {}_aS^0_{tr}$ (the difference between the translational entropy of the adsorptive gas and that of the adsorbate as an ideal, mobile, two-dimensional gas, or the entropy change resulting from loss of one degree of translational freedom). For both carbon tetrafluoride and argon, the experimental results agree very closely with the model for adsorption as a mobile, two-dimensional gas.

In the adsorption of nitrogen, the decrease in entropy was even less than that associated with the loss of one degree of translational freedom, indicating some "super mobility" in the adsorbed film. This may involve retention of part of the translational entropy as a vibration normal to the adsorbent surface.

The difference between the adsorbed films of argon and nitrogen is qualitatively evident from the isotherms and heat curves in that the heat of adsorption of argon is the greater while the reverse is true of the free energies. The greater heat of adsorption of argon is closely associated with its greater latent heat of condensation. The greater free energy of adsorption of nitrogen (evident from the lower relative pressure required for a specified coverage and temperature) also is observed in the adsorption of these gases on other solids but is not simply explained.

Conclusions.—Carbon tetrafluoride, argon, and nitrogen, at temperatures near their respective boiling points, were all weakly adsorbed on polytetrafluoroethylene as mobile, two-dimensional gases, nitrogen retaining some "super mobility." The densities of the multilayer adsorbed films are low.

DISCUSSION

R. J. GOOD (General Dynamics).—Have you applied the Polyanyi potential theory to this system? Also, the Frenkel–Halsey–Hill theory ($\ln (p/P_0) = -a/\theta^3$) seems appropriate to treat molecules at distances from the surface corresponding to second or third layers.

D. GRAHAM.—No attempt was made in this investigation to express the isotherms in equation form. However, the low density of the adsorbate films would lead me to expect that some form of a potential theory would represent the data better than any expression assuming a more fully populated first monolayer.

W. H. WADE (University of Texas).—Why do the heats fall with coverage? Lateral interactions would predict the opposite.

D. GRAHAM.—The low coverage part of the heat curves (not shown in the figure and not pertinent to the objectives of this study) drops sharply due to adsorbent heterogeneity. The continuing fall as coverage approaches completion of the first statistical monolayer results from the considerable contribution to higher monolayers before actual completion of the first. This is characteristic of weak adsorption.

ADSORPTION STUDIES ON METALS. XI. WATER ON n-TYPE GERMANIUM POWDERS

BY G. SRINIVASAN, J. J. CHESSICK, AND A. C. ZETTLEMOYER

Surface Chemistry Laboratory, Lehigh University, Bethlehem, Pennsylvania

Received March 12, 1962

Water adsorption measurements were carried out at 25° for three n-type germanium powders previously exposed to the atmosphere. These, as well as argon adsorption measurements for surface areas, were conducted on samples evacuated and temperature activated at 25, 100, 200, 300, 400, and 500°. The amount of water irreversibly adsorbed also was determined. The results revealed that the extent and energetics of chemisorbed water decreased with decreasing resistivity. In addition, the stability of the thin oxide film formed on the germanium powders during grinding of the single crystals to prepare the powders and during storage decreased in the same order. Evidently, water adsorbs donor-fashion on surface hydroxyl groups. Therefore, samples of low resistivity and high electron concentration chemisorb little or no water.

Introduction

Recently it was shown that the adsorption characteristics for propanol of the oxide surfaces of a series of four n-type germanium powders varied in an orderly manner with the resistivity.[1] The mechanism proposed to explain the results depends upon the trapping of electrons by the germanium ions in the oxide film. Thus, the donor electrons from the propanol oxygen are not as energetically attracted to surface hydroxyls on the oxide film, the lower is the resistivity.

The present work on water adsorption was initiated to compare its adsorption behavior on three of the same germanium samples. It was recognized that adsorbed water was present at least at the lower activation temperatures employed in the propanol work. In addition, water adsorption is known often to affect device performance adversely and "getters" are inserted into capsules to remove traces of water vapor. The water adsorption results are explained on the basis of a mechanism similar to that used to explain the propanol results. This work is being extended to a series of p-type samples and to a study of oxide-free germanium surfaces under ultra high vacuum.

Experimental

Single crystals of n-type germanium with resistivities of 5–10 and 0.14 ohm-cm. supplied by the General Electric Co. were ground to powder in an agate mortar under atmospheric conditions. The preparation and storage time of these samples was one day compared to the 15 days used in the previous propanol studies.[1] A 4 ohm-cm., n-type sample was prepared by reducing Eagle-Pitcher GeO_2 with dry hydrogen at 650°; this powdered sample was stored for about 6 months before use. Areas were determined by argon adsorption at −195° after the pre-treatments described below.

Water isotherms were followed at 25° using a modified Orr apparatus described previously.[2] Blank experiments showed the adsorption of the water vapor by the glass walls of the system and the manometer oil to be negligible. Isotherms were determined on 1 m.² of a given sample after various pre-treatments consisting of evacuation at 25, 100, 200, 300, 400, and 500° for 14 hr. to an ultimate pressure of *ca.* 10^{-6} mm. A liquid nitrogen trap was positioned between the sample and the pumps throughout the activation period. The first water isotherm after a given activation measured total adsorption. The second isotherm, a measure of physically adsorbed water, was determined after evacuation at 25° for an additional 14 hr. The B.E.T. equation was applied to calculate the V_m values for total and physical adsorption. The difference between the two V_m's gave the chemisorbed quantity. All these V_m values of water adsorption were converted into corresponding area values using a multiplication factor of 2.87, assuming a liquid-like, two-dimensional film of adsorbed water molecules.

Results

Water Adsorption on Activated Samples of Different Resistivities.—The ratios of total, physically adsorbed, and chemically adsorbed water in the monolayer, calculated from isotherm data in the manner described above, to argon areas were plotted as a function of activation temperature. These results for 0.14, 5–10, and 4 ohm-cm. resistivity samples are illustrated in Fig. 1, 2, and 3, respectively. This manner of representing the results was adopted to account for changes in external area with temperature. The surface area changes, however, were generally small except at 400 and 500°, where 10 to 20% increase was found. It had previously been pointed out[1] that the different germanium specimens, crushed and stored for some time before use, were covered with a thin oxide film. Even though adsorption of water occurred on the oxide-covered surfaces, significant differences were observed in the adsorption characteristics of these three different resistivity samples, as seen in the figures.

The results of Fig. 1 reveal that water was adsorbed physically to form a monolayer on the 0.14 ohm-cm. germanium after 25° outgassing. Close packing was indicated by the calculated C.S.A. of 11.8 A.² per water molecule. Ligenza[3] observed an uptake of 3.82×10^{-8} g. of oxygen/cm.² of germanium and showed that this value corresponded to two oxygen atoms per surface germanium atom in the 111 plane. Based on this observation, 13.6 A.² was calculated to be the C.S.A. of each site on the oxide-covered surface. This value is in reasonable agreement with the C.S.A. calculated for the adsorbed water molecule, despite surface heterogeneity and polycrystallinity of the surface.

The total water adsorption on the 0.14 ohm-cm. sample on a unit area basis decreased only slightly after evacuation at 100°, whereas the physical adsorption dropped considerably. The corresponding increase in the chemisorbed quantity, compared to that at 25°, amounted to about 0.2θ. A marked and parallel decrease was observed for the total and physical adsorption after activation at temperatures above 100°, but there was only a small change in the amount of chemisorbed water. This

(1) A. C. Zettlemoyer, C. H. Hassis, J. J. Chessick, and G. Srinivasan, *Advan. Chem. Ser.*, **33**, 229 (1962).

(2) A. C. Zettlemoyer and J. J. Chessick, *J. Phys. Chem.*, **58**, 242 (1954).

(3) J. R. Ligenza, *ibid.*, **64**, 1017 (1960).

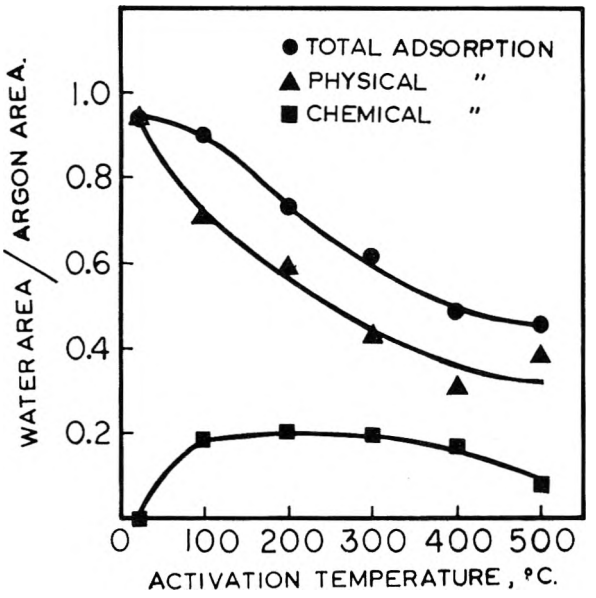

Fig. 1.—Adsorption of water on 0.14 ohm-cm., *n*-type germanium.

observation suggests that the mild outgassing between 25 and 100° is sufficient to drive off all the preadsorbed water from this sample. The decrease in total water adsorption with activation temperature was unexpected but was an important clue for deducing the mechanism of adsorption. It appears that evacuation at elevated temperatures produced hydrophobic surface sites increasing in number with increasing activation temperature.

The total and physical amounts of water adsorbed on the 5–10 ohm-cm. sample after 25° evacuation amounted to *ca.* 0.7θ and the total approached $\theta = 1$ as the activation temperature increased to *ca.* 300°. This increase was due predominantly to the desorption of strongly bound water in the oxide layer formed during crushing—the chemisorbed water of Fig. 2. Evidently, water molecules do not adsorb physically on strongly bound or chemisorbed water molecules initially present on the surface. Similar results have been previously reported,[4] but only rarely.

Above the 300° activation step, the amounts of total and chemically adsorbed water in the monolayer decreased. It is interesting that this decrease in water adsorption had its onset at an activation temperature just required to remove completely the monolayer of physically and chemically adsorbed water originally bound to the surface.

Water adsorption on the 4 ohm-cm. sample might well be expected to be intermediate between that found for the 0.14 and 5–10 ohm-cm. samples. While this was true in part, significant differences were found, particularly on adsorption of water on the 4 ohm-cm. sample activated in the lower temperature range. Area ratio values greater than 1.0 were found, due apparently to a somewhat thicker film of oxide or one of different surface stoichiometry formed during the six-months storage period in air. The 25° outgassed sample, for example, adsorbed the equivalent of 1.3 layers of water as calculated from BET V_m's. This total adsorption per unit area increased further to 1.7 layers after activation of the sample at 150°. After activation at temperatures greater than 150°,

(4) F. H. Healey, J. J. Chessick, and A. V. Fraioli, *J. Phys. Chem.*, **60**, 1001 (1956).

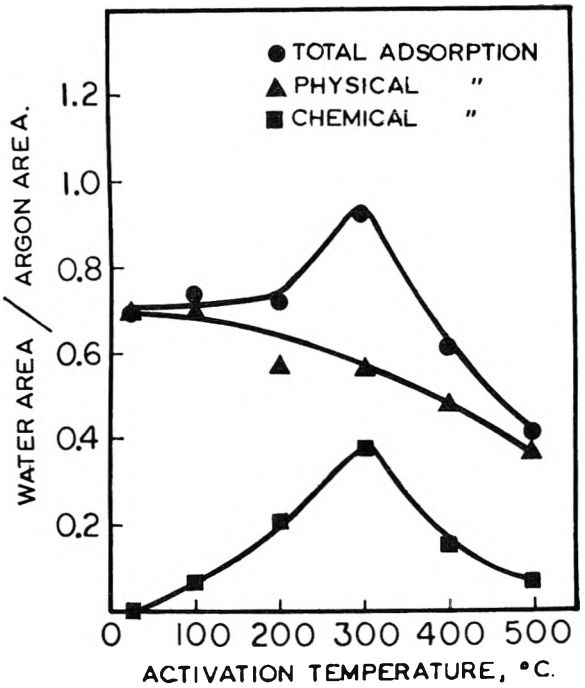

Fig. 2.—Adsorption of water on 5–10 ohm-cm., *n*-type germanium.

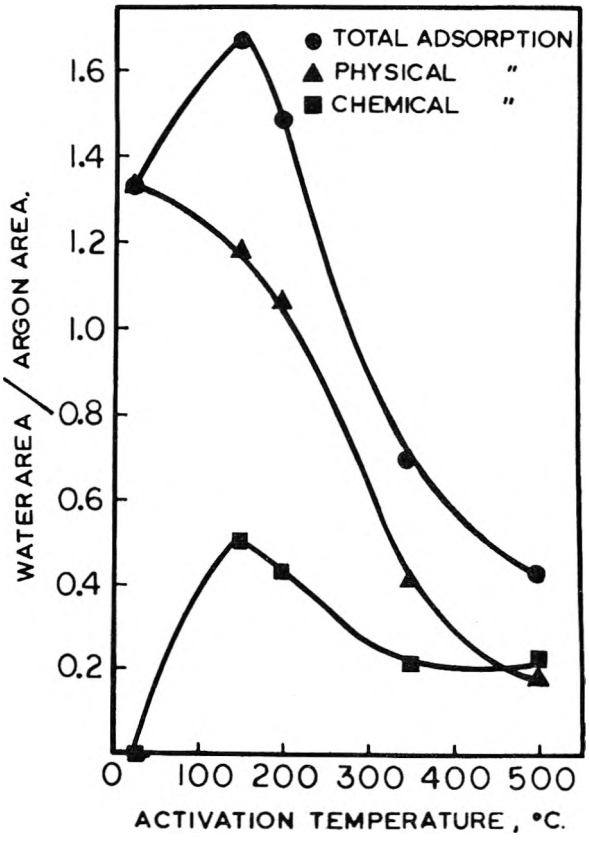

Fig. 3.—Adsorption of water on 4 ohm-cm., *n*-type germanium.

an abrupt decrease in amounts adsorbed occurred, as observed with the other samples to a lesser degree.

Table I records the results of water adsorption after activation at 300°. Activation at this temperature was chosen as the basis for comparison among germanium samples including the 4 ohm-cm. sample which had a different history and adsorbed more water per unit area than the other samples. In addition, at this outgassing temperature, all the pre-adsorbed water was finally lost by the 5–10 ohm-cm. sample. It can be seen from Table I that the amount of water chemisorbed in the monolayer decreases with decreasing resistivity of the germanium powders. This trend in adsorption was also exhibited by all the *n*-type specimens at higher temperatures. The results obtained after activations at 400 and 500° were not considered further because of the hydrophobing of the oxide surface which presumably occurs by dehydration of surface hydroxyls similar to that which occurs on silicas. The earlier studies of propanol adsorption[1] exhibited a similar adsorption pattern for *n*-type germanium powders after thermal activations above 200°.

TABLE I

TOTAL, PHYSICAL, AND CHEMICAL ADSORPTION OF WATER AT 25° ON *n*-TYPE Ge POWDERS AFTER ACTIVATION AT 300°

	ΣH_2O (water area (m.²/g.))			$\Sigma H_2O/\Sigma A$		
Sample	Total	Physical	Chemical	Total	Physical	Chemical
0.14 ohm-cm.	0.107	0.072	0.035	0.62	0.42	0.20
4 ohm-cm.	.135	.090	.045	.93	.63	.30
5–10 ohm-cm.	.161	.096	.065	.94	.56	.38

Discussion

The Influence of Thermal Activation on Water Adsorption per Unit Area of Ge Samples.—The finding that less than a monolayer of water adsorbs per unit area on the one-day stored samples as well as the decrease in water adsorption at activation temperatures above a specific temperature will be explained. It is more convenient to discuss the decreased adsorption at higher activation temperatures first to provide a foundation for explaining the other results observed.

Three possible explanations for the decrease in water adsorption above a specific temperature of activation can be advanced, *viz.*, (1) recrystallization of the oxide layer into discrete crystallites of oxide which cover only a portion of the surface; (2) loss of oxide due to volatilization; and (3) change in the chemical nature of the oxide film.

Recrystallization during high temperature evacuation of thin oxide films produced by oxidation at 25° on nickel and cobalt metal with the formation of discrete, bulk-like crystallites appears plausible.[5] The crystallites occupy only a small portion of the surface and are located at heterogeneous sites such as those produced by surface roughness, by the intersection of two planes on the surface, and by chemical impurities. Law[6] observed that bare germanium chemisorbed one layer of water and adsorbed a second layer of physically bound water on top. Furthermore, he reported that germanium dioxide adsorbed only about half as much. If recrystallization occurred in the samples used here, islands of fresh germanium surface would have been exposed and water adsorption would have increased with temperature of activation. Contrary behavior was exhibited by all three samples. Therefore, the recrystallization mechanism appears to be ruled out.

The decrease in water adsorption cannot be attributed to volatilization of the oxide from the surface, particularly at the low temperatures and at the pressure of 10^{-6} mm. employed. Law[6] used an outgassing temperature of 800° to produce oxide-free germanium surface. Ligenza had pointed out that temperatures above 530° and pressures below 10^{-8} mm., conditions not employed in our present study, were necessary to produce clean germanium surface.[3]

Change in the chemical nature of the oxide film as a result of thermal evacuation is the other possibility. This possibility is consistent with the mechanistic description of water adsorption discussed below. If the outermost surface layer formed during exposure to the atmosphere consists of hydroxyl groups, water can be lost according to the equation

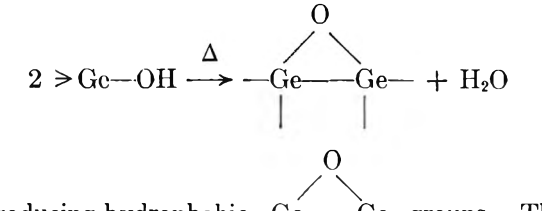

producing hydrophobic –Ge——Ge– groups. This process is similar to the dehydroxylation of silanol groups on silica which can begin between 100 and 200°[7]; the siloxane, Si Si, groups formed also do not adsorb water in the relative pressure region below saturation.

The germanium powders studied here resemble activated silica and alumina samples in exhibiting a decrease in the water uptake above a specific temperature of outgassing. The presence of hydroxyls on high area silica and alumina samples has been demonstrated. Some experimental confirmation has been obtained for the existence of surface hydroxyls on Ge. Such groups are known to react with chlorosilanes producing a hydrophobic surface film of –O–silane groups and HCl. A chemisorbed, hydrophobic layer was produced on the 4 ohm-cm. sample treated in this manner. Unfortunately, no direct method of detecting surface hydroxyls on large diameter Ge is known.

The presence of hydroxyl groups on crushed germanium powders and the adsorption of water molecules in donor fashion best explain the experimental results. Indeed, the adsorption of water on an oxide-type surface of Ge in donor fashion has been demonstrated by electrical measurements

(5) (a) R. M. Dell, *J. Phys. Chem.*, **62**, 1138 (1958); (b) A. C. Zettlemoyer, Yung-Fang Yu, and J. J. Chessick, *ibid.*, **64**, 1099 (1960).

(6) J. T. Law, *ibid.*, **59**, 67 (1955).

(7) G. J. Young, *J. Colloid Sci.*, **13**, 67 (1958).

conducted by solid state physicists.[8] A similar approach was very successful in interpreting the results of propanol adsorption. The thickness of the oxide or hydroxyl layer formed during exposure to the atmosphere is not known. Two experimental facts suggest that this layer is thin, perhaps monomolecular. First is the definite influence of the electronic properties of the metal on water adsorption (*vide infra*) and second the fact that exposure of the crushed powder for 6 months did not alter significantly the adsorption characteristics as demonstrated by comparing these results with those obtained for samples stored only one day.

Water Adsorption and the Electronic Properties of Germanium Powders.—Thermal activations at temperatures *ca.* 100, 150, and 300° were necessary to deplete the monomolecular films of water adsorbed at the oxide–vapor interface from the 0.14, 4, and 5–10 ohm-cm. samples, respectively. This important result indicates that the interaction of water with the oxide coating becomes stronger with increasing resistivity of the underlying germanium.

In addition, the decrease in the water adsorption per unit area had its onset at 300° activation for the 5–10 ohm-cm. sample, at 150° activation for the 4 ohm-cm. powder, and at 100° for the 0.14 ohm-cm. sample. These results reflect significantly the decreasing stability of the oxide film to temperature with the decreasing resistivity of the bulk germanium. If the results of Table I also are used, the proportion of the strongly bound water in the monolayer, the energetics of the water adsorption, and the stability of the oxide film to temperature all decrease in the order

5–10 ohm-cm. > 4 ohm-cm. > 0.14 ohm-cm.

The model used in the interpretation of propanol adsorption results[1] is likewise extended to water. Adsorption of water molecules with the oxygen directed toward the surface is illustrated below.

(8) See, for example, "The Surface Chemistry of Metals and Semiconductors," Harry C. Gatos, Ed., John Wiley and Sons, New York, N. Y., 1959, p. 60.

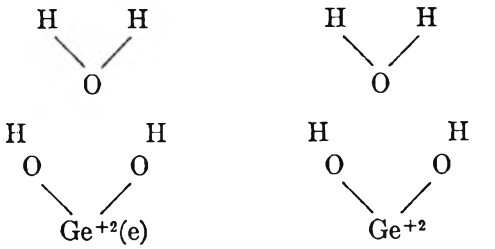

Low resistivity Ge High resistivity Ge

Here, Ge^{+2} entities are assumed to act as surface traps for conduction electrons. Whether the electron resides at a Ge ion trap or is "quasi-free" in the outermost hydroxyl layer cannot be determined from the results of experiments performed. Nevertheless, an increased electron concentration at the hydroxyl–water vapor interface is postulated which reduces the strength of binding of water molecules absorbed donor fashion in the monolayer. This model is consistent with the finding that the extent of chemisorbed water and the strength of the water–surface bond in the monolayer increase as the resistivity of the *n*-type Ge samples increases.

The instability of oxide films on *n*-type Ge, the differences in chemisorptive characteristics, the energetics of bound water on oxidized Ge powders, which have been shown to be directly related to the electronic properties of a variety of *n*-type specimens, illustrate dramatically the changes in semiconductor properties with temperature. Other environmental changes may also have a profound effect. The lack of stability of Ge semiconductors which are not maintained in an unchanging environment is therefore not surprising.

Acknowledgment.—The authors gratefully acknowledge the financial support for this work received from Semiconductor Products Department, General Electric Co., Electronics Park, Syracuse, New York.

HEATS OF IMMERSION. VII. THE IMMERSION OF SILICA, ALUMINA, AND TITANIA IN HEXANE—VARIATION WITH PARTICLE SIZE AND OUTGASSING TEMPERATURE

BY W. H. WADE AND NORMAN HACKERMAN

The University of Texas, Department of Chemistry, Austin 12, Texas

Received March 12, 1962

The heats of immersion of the three substrate materials in hexane have been measured as a function of particle size and outgassing temperature. The results are interpreted in terms of van der Waals and ion–induced dipole interactions.

In the past fifteen years there have been sporadic measurements of the heats of immersion (ΔH_i) of SiO_2, Al_2O_3, and TiO_2 in saturated hydrocarbons. Healey, *et al.*,[1] measured the heats of immersion of a 7.3 $m.^2/g.$ TiO_2 specimen in a number of organic liquids including hexane, heptane, and octane. The latter three adsorbates gave ΔH_i's of approximately 140 ergs/$cm.^2$. Stowe[2] obtained a ΔH_i of 73 ergs/$cm.^2$ for an alumina gel of 155 $m.^2/g.$ specific surface area in hexane. Aleksandrova and co-workers[3] measured ΔH_i's for SiO_2 gels with specific surface areas varying from 275–695 $m.^2/g.$ in heptane and obtained values of 50–75 ergs/$cm.^2$. Recently Whalen[4] has studied the immersion of SiO_2 gels in cyclohexane and obtained values of ΔH_i varying from 90 to 280 ergs/$cm.^2$.

No ΔH_i measurements have been made on a series of any of the above three adsorbents as a function of outgassing temperature and particle size and since similar measurements with a polar liquid (*e.g.*, H_2O) have shed some light on adsorbent surface structure,[5] it was believed that measurements with non-polar adsorbates would be a logical extension. Moreover, since there are a number of hexane adsorption isotherms on the contemplated SiO_2, Al_2O_3, and TiO_2 samples available from this Laboratory,[6,7] hexane appeared to be a logical choice for a non-polar liquid.

Experimental

Adsorbents.—The three adsorbents are those previously used for H_2O, and methanol, and hexane adsorption studies and have been described earlier.[6-8] The samples ranged in purity from 99.5 to 99.96%. Prior to immersion the samples were vacuum outgassed at 10^{-6} mm. torr. for 48 hr. at the temperatures noted in Table I. The outgassing temperatures carry an accuracy of ±3°.

Adsorbate.—Two grades of Phillips Petroleum Company *n*-hexane were employed: Research Grade and Pure Grade. The Research Grade is 99.6+ mole % *n*-hexane, whereas the Pure Grade is 99+ mole % *n*-hexane. The principal impurities of both grades are other hexane isomers. No differences in ΔH_i's were noted for identical samples with the different grades and consequently, the Pure Grade was used for the majority of the measurements.

The water content of the hexane was reduced to levels undetectable by Karl Fischer reagent (> 1 p.p.m.) by storing gallon quantities of hexane over kilogram quantities of Linde 4Å Molecular Sieve exhaustively dehydrated at 450°. The hexane was decanted into the calorimeter dewars just prior to sealing the calorimeter and simultaneously a small amount of "fresh" molecular sieve was added.

Calorimeter.—The calorimeter used in the present studies is a revised version of the type used previously.[9] It is an adiabatic differential calorimeter with thermistor temperature sensing elements. It differs from the old design in the following ways: (1) provision has been made for handling 12 samples during a single run, (2) the sample breakers are coupled through the calorimeter head with brass diaphragms, and (3) the stirring is accomplished through a magnetic coupling. The object of the new design is both to obtain a maximum amount of information for a given filling of immersion liquid and to ensure complete vacuum sealing for the calorimeter vessels. These factors were considered essential for measurements with high vapor pressure organic liquids which are both expensive and difficult to keep moisture free.

The performance of the new calorimeter is very similar to that of the older version. Relative temperature excursions in the calorimeters were less than $\pm 4 \times 10^{-6}$/°C. at the highest sensitivities used. The electrical calibrations at the beginning and end of each series of measurements agreed to ±2%. All ΔH_i measurements are in duplicate with a representative agreement of ±3%. All measurements were at 25 ± 0.05°.

Corrections to ΔH_i for the vaporization of hexane during the shattering of the sample bulbs became progressively larger for samples of lower specific surface and for samples of specific area 2.72 $m.^2/g.$ amounted to 100%.

Results and Discussions

The heats of immersion of the various SiO_2, Al_2O_3, and TiO_2 samples are presented in Table I. There are four trends evident in the data: (1) there is a slight but real increase of ΔH_i with outgassing temperature, (2) the heats of immersion of Al_2O_3 and TiO_2 are similar in magnitude whereas the SiO_2 heats are about 50–75% of these, (3) in general the heats are much smaller than those observed during H_2O absorption on these samples, and (4) there is a small but general increase of ΔH_i with increased particle size.

The low heats of immersion are to be expected since the only significant attractive forces involved in the absorptive process arise from van der Waals and ion–induced dipole sorbent–sorbate interactions and van der Waals attractive lateral interactions (somewhat perturbed by polarization of the adsorbate molecules). The heats are similar in magnitude to those obtained by calculation on the basis of simple Lennard-Jones potential energy functions for inert gases on KCl crystal faces.[10,11] For orientation purposes, 100 ergs/$cm.^2$, on the

(1) F. H. Healey, J. J. Chessick, A. C. Zettlemoyer, and G. J. Young, *J. Phys. Chem.*, **58**, 887 (1954).

(2) V. M. Stowe, *ibid.*, **56**, 487 (1952).

(3) G. I. Aleksandrova, V. F. Kiselev, K. G. Krasil'nikov, V. V. Murina, and E. A. Sysoev, *Doklady Akad. Nauk, S.S.S.R.*, **108**, 283 (1956).

(4) J. W. Whalen, *J. Phys. Chem.*, **66**, 511 (1962).

(5) W. H. Wade, H. D. Cole, D. E. Meyer, and N. Hackerman, *Advances in Chem.*, **33**, 35 (1961).

(6) R. L. Every, W. H. Wade, and N. Hackerman, *J. Phys. Chem.*, **65**, 25 (1961).

(7) R. L. Every, W. H. Wade, and N. Hackerman, *ibid.*, **65**, 937 (1961).

(8) W. H. Wade and N. Hackerman, *ibid.*, **65**, 1681 (1961).

(9) A. C. Makrides and N. Hackerman, *ibid.*, **63**, 594 (1959).

(10) J. M. Honig, *Ann. N. Y. Acad. Sci.*, **58**, 741 (1954).

(11) J. H. DeBoer, *Advan. Colloid Sci.*, **3**, 1 (1950).

TABLE I

HEATS OF IMMERSION (ΔH_i) OF VARIOUS SiO_2, Al_2O_3, AND TiO_2 SAMPLES FOR SPECIFIC SURFACE AREAS ($\bar{S}$) IN M.²/G. AND OUTGASSING TEMPERATURES [T(OG)] AS NOTED

	Sample													
	SiO_2		Al_2O_3						TiO_2 (Rutile)			TiO_2 (Anatase)		
$\bar{S}$	3.56	188	2.72	4.56	312	65.2	109	221	6.45	114	188	10.5	174	202
			100	100		100	100	100				100		100
			142	108		103	81	65				119		87
	200	200	170	170	200		170		200	200	200	170	200	170
	86	65	150	112	145		85		134	99	74	137	107	95
T(OG)			240	240		240		240				240		240
ΔH			152	120		111		68				142		93
			310	310			310	310						310
			151	117			82	69						95
	400	400	380	380		380	380	380	400	400	400		400	
	95	67	149	121		112	80	70	137	112	69		111	
			450	450			450	450						
			155	125			89	70						

basis of complete heat development in a monolayer (probably a good assumption for short range van der Waals interactions) of hexane molecules of area around 65 Å.²,[6,7] corresponds to approximately 1 kcal./mole.

The slight increase of ΔH_i with outgassing temperature is understandable from the nature of van der Waals forces and a more detailed consideration of the adsorbent surface structure. All these oxide surfaces have been shown to be populated by –OH groups. During the adsorption of H_2O and CH_3OH, these OH groups increase the total interaction energy *via* hydrogen bonding. With hexane, hydrogen bonding contributes nothing to the interaction and, in fact, these groups weaken the van der Waals interactions by prohibiting intimate contact between the hexane molecules and the SiO_2, Al_2O_3, and TiO_2 lattices. Thus, reducing the surface OH concentration by elevating the outgassing temperature increases the heats of immersion.

The low values for the heats of immersion of SiO_2 as compared to Al_2O_3 and TiO_2 can be semiquantitatively explained on the basis of a continuum model of the substrate.[10] In this model the particulate nature of the substrate is lost and the vertical interaction energies are simply related to the density *via*

$$W_v = \pi\rho r^3 U(q^3/3 - q^9/45) \qquad (1)$$

where W_v is the van der Waals interaction energy at zero coverage, ρ is the bulk density of the adsorbent, and the other terms are of no interest in the present discussion. This simple model says that at low coverage, the heat of adsorption is directly proportional to the substrate density. This is borne out in the present study for the three substrates SiO_2, Al_2O_3, and TiO_2 with their respective densities of 2.5, 4.0, and 4.0. The contribution of vertical van der Waals interaction energies to the total heat of absorption must be comparable in magnitude to all of the other contributions to the total adsorbent–adsorbate interaction energy before this effect becomes noticeable.

In considering the variation of ΔH_i with particle size a more refined model than that presented above must be used. Any argument considering only the van der Waals forces operative in the adsorption of a non-polar molecule such as hexane on a substrate (either ionic or covalent) would predict a heat of adsorption independent of the substrate particle size. This statement is true even including lateral interactions. This position might need to be modified when the particle diameter is dimensionally comparable to the hexane molecule (about 20 Å. in particle diameter) as is the case for surface areas exceeding 200 m.²/g. Further complications with the former model arise if the surfaces were contaminated or if change in bulk density in the surface region accompanied the variation in particle size. Surface contamination is not a likely explanation of the present set of data since the variation with particle size tends uniformly in a given direction and surface contamination would probably exhibit a random variation with particle size.

Furthermore, variations of surface density of the three substrate materials with particle size cannot be a complete explanation of the phenomenon. From a consideration of equation 1 and considering no additional exothermic contributions to the ΔH_i from lateral interactions, a 50% increase in ΔH_i would require at least a 50% increase in density of the substrate in the surface region. The changes in ΔH_i with particle size of the adsorbents (Table I) would require implausibly large changes in surface density with the possible exception of SiO_2. However, the experimental variation is in the right direction to be explained in this manner. There are strong indications that small particles are more amorphous than large crystalline ones and the "amorphous" densities are undoubtedly lower than the "crystalline" densities.

Probably the major contribution to the variation of ΔH_i with particle size for hexane adsorbed on any of the three substrates lies in the variation in contribution of ion–induced dipole interactions to the over-all heat of adsorption. This contribution to the total energy for an isolated molecule is

$$W_{I\text{-}ID} = {}^1/_2\alpha E^2 \qquad (2)$$

where α is the polarizability in cc., and E is the electrostatic field strength in e.s.u. units. W_{I-ID} is the energy per adsorbed molecule in ergs. Of

course the electrostatic field in the vicinity of an adsorbed particle (especially a long hydrocarbon chain) is too inhomogeneous to permit other than crude calculations on the basis of equation 2. Honig[10] has reviewed the status of ion–induced dipole calculations for somewhat simpler systems, *e.g.*, argon adsorbed on oriented crystal faces of KCl lattices. Calculations based on equation 2 gives W_{I-ID} values about 100% too low compared to more refined calculations where the interaction energy is integrated over the variation in electrostatic field for an argon atom in a fixed geometric position on the lattice.

Healey, *et al.*,[1] estimated the electrostatic field strength at 3.0 Å. distance from a TiO_2 surface by measuring the variations of ΔH_i with dipole moment of a number of polar adsorbates and used the relationship

$$W_{I-D} = \mu E \qquad (3)$$

where μ is the dipole moment, E has the same significance as before, and W_{I-D} is the ion–dipole interaction energy per adsorbed molecule. They obtained a value of 3.2×10^5 e.s.u. The polarizability of hexane calculated from the Clausius–Mosotti equation is 12×10^{-24} cc./molecule, and this with the estimated field strength dictates an ion–induced dipole interaction energy of approximately 9 kcal./mole. This is an order of magnitude higher than the presently observed interaction energies on the three surfaces where 100 ergs/cm.^{2} is equivalent to approximately 1 kcal./mole referred to the pure liquid. Apparently E^2 is too high by a factor of at least 10 for hexane–TiO_2. This restricts the argument to one which is qualitative in nature.

Previous measurements[5-9] have supported the hypothesis that small particles are amorphous, having a low electrostatic field strength compared to crystalline oxides having a uniform outer layer of oxide or hydroxide ions and a relatively high associated electrostatic field strength. Due to dependence on E^2, relatively small perturbations in the electrostatic field strength (*via* recrystallization or grinding) can have a large effect on W_{I-ID}. If W_{I-ID} contributes appreciably to ΔH_i, then ΔH_i will once again vary with particle size as found previously for H_2O on all these substrates.

With regard to the estimation of the $W_{I-ID} = 9$ kcal./mole it should be recognized that E is very sensitive to the "distance" of the hexane molecule from the surface. The field strength is exponentially related to this distance. Thus a 50% increase in distance from 3.0 to 4.5 Å. corresponds to a 4.5-fold decrease in field strength, a 20-fold decrease in E^2, and thus a change from 9 kcal./mole to a more reasonable 0.45 kcal./mole.

An examination of the immersional heat data for TiO_2 samples in Table I indicates some disagreement with respect to a uniform decrease of ΔH_i with decreasing particle size. Actually if the data for the two crystalline modifications (anatase and rutile) are considered separately, no disagreement exists. This has been noted previously for ΔH_i's observed during immersion of these samples in water.[8]

Some of the samples studied in the present investigations have had hexane adsorption isotherms measured on them. These samples are listed separately in Table II, which gives their integral heats of adsorption as calculated from ΔH_i's by

$$\Delta H_a = \Delta H_i - 17.9 \qquad (4)$$

Here 17.9 is the surface enthalpy of *n*-hexane in ergs/cm.^{2} as calculated from the surface tension and its temperature coefficient. Also listed are the previously reported[6,7] π values and the BET molecular areas, ω. The integral entropies of adsorption have been unfolded from these data. They show larger relative variations than do the heats of adsorption. The same explanation as offered before[6,7] can be used to explain the decrease in entropy of the adsorbed state compared to the liquid state. That is, as the particle size increases, the surfaces become more crystalline and there is a more ordered arrangement of the adsorbed hexane molecules.

TABLE II

MEASURED AND CALCULATED ADSORPTION PARAMETERS

	$\bar{S}$ (m.^{2}/g.)	ω (Å.^{2})	π (ergs/cm.^{2})	ΔH_a (ergs/cm.^{2})	ΔS_a (ergs/cm.^{2}-°C.)
SiO_2	188	76.2	19.0	47	0.094
	2.72	61.5	33.4	133	.335
Al_2O_3	65.2	64.7	29.9	89	.198
	109	60.7	44.2	67	.076
TiO_2	10.5	53.9	46.4	119	.244
	188	69.7	34.8	56	.071

Acknowledgment.—The authors wish to express their appreciation to the American Petroleum Institute for continued interest and support *via* A.P.I. Project 47D. Also, appreciation is expressed to Mr. Charles Allen and Mr. James Gardiner for assistance in the operation of the calorimeter.

DISCUSSION

E. V. BALLOU (Gulf Research & Development Co.).—I think a key to the anomalously low values of the heat of wetting of alumina gel samples equilibrated with water lies in the pore size distribution of the sample. If this is known, it should be feasible to calculate the area of pores blocked at a given vapor pressure of water. The remaining area may or may not agree with the value from the experimental heat of immersion. Disagreement would offer some measure of the degree of pore blockage in small necks or constrictions.

W. H. WADE.—We plan to measure the nitrogen area for these gel samples equilibrated to various water vapor pressures and apply this correction to see if the disagreement with theory can be eliminated.

A. BAIDINS (du Pont Company).—Have you considered the concentration of impurities with decreasing surface area as a reason for increasing heat of immersion? Thus, for a 100 m.^{2}/g. sample there may be only one NaOH molecule per 10,000 Å.^{2}, which can be neglected, but for 1 m.^{2}/g. sample of the same material there will be one NaOH per 100 Å.^{2}, which no longer can be neglected.

J. Brown, W. J. Jaap, and P. D. Ritchie [*J. Appl. Chem.* (London), **9**, 153 (1959)] investigated the rate of dissolution of quartz and rutile in dilute HF. They found that quartz did have a disturbed, easily soluble amorphous surface layer, but that rutile did not have it. Thus, your explanation in the case of rutile contradicts previous experimental data.

W. H. WADE.—We observe variations with particle size for samples where surface concentration of impurities is negligible; therefore, the variation for these high area samples must be due to another cause. Of course, with low area samples, this does become a serious consideration.

Our rutile studies do not necessarily contradict previous measurements since there is no fundamental reason why an amorphous layer should dissolve more rapidly than a crystalline layer.

R. J. GOOD (General Dynamics).—I wish to call your attention to Conway Pierce's recent papers on the effect of intergranular condensation on heat of adsorption.

W. H. WADE.—There are several Russian studies of a similar nature but none are applicable to gels in any sort of quantitative way.

ORIENTATION OF NEMATIC MESOPHASES*

BY ROGER S. PORTER AND JULIAN F. JOHNSON

California Research Corporation, Richmond, California

Received March 12, 1962

Orientation studies have been performed on pure, one-component mesophase systems. Both the mesophase, *i.e.*, liquid crystal state, and the isotropic liquid range have been studied for the two compounds, *p*-azoxyanisole and anisaldazine. These two compounds exhibit a nematic type mesophase between defined temperature limits. New results on viscosity and orientation are reported. Previous magnetic and shear orientation results for the nematic phases of these compounds have been placed on an absolute scale, reinterpreted, and compared with new data. The rigid rod approximation for the nematic phase is discussed. Flow activation energies for various orientations are calculated. The size of nematic aggregates and the thickness of adsorbed layers are discussed. The general characteristics of the nematic phase are compared with those for the other major types of mesophase.

Introduction

This study of liquid crystals gives results which substantiate and extend an understanding of the flow properties and order of the nematic and isotropic states of *p*-azoxyanisole and anisaldazine.

Experimental

The compounds were obtained from Eastman Kodak Company and the Matheson Company, Inc. The compounds were purified by dissolving them in either hot absolute alcohol or toluene, followed by filtration and recrystallization. Elemental analyses indicate excellent purity for the recrystallized compounds. This also is indicated by a comparison of transition temperatures for these compounds with values reported in the literature. Table I gives the nematic temperature ranges for the compounds studied.[1-4]

TABLE I

TRANSITION TEMPERATURES FOR COMPOUNDS STUDIED

Compound	Literature values, °C.[1,2,4] Solid–nematic	Literature values, °C.[1,2,4] Nematic–isotropic	This work, °C. Solid–nematic	This work, °C. Nematic–isotropic
p-Azoxyanisole	118	135	118.5	135
Anisaldazine	169	182	169	182

Cross-arm capillary viscometers were used to obtain low shear viscosity measurements.[5] Viscosity measurements, made in closely regulated oil baths, are accurate to ±0.2%. High shear viscosity measurements were made with a thin film, double-thermostated concentric cylinder rotational viscometer.[6,7] The accuracy of high shear viscosity and shear rate measurements is about ±2%. Within these limits, pure, linear hydrocarbons with molecular weights to above 500 show entirely Newtonian flow up to near 10^6 sec.$^{-1}$.[7] The concentric cylinder viscometer has the advantage of being a "working" viscometer and does not require a meniscus observation, which can be difficult with mesophases.[8]

Results

Orientation Viscosities: *p*-Azoxyanisole.—In the stable solid of *p*-azoxyanisole, the molecules are oriented with their axes parallel. The azoxy group of one molecule is adjacent to the ether group of another. These dipoles lead to threadlike molecular aggregates which are typical of the fluid nematic phase.[9] The viscosity measured by both conventional capillary flow and by the concentric cylinder viscometer corresponds to the lowest of magnetic orientation viscosities. This indicates that nematic aggregates readily attain maximum orientation in the direction of flow.[10-13] The consistent concentric cylinder results indicate that the nematic phase orients not only in a plane parallel to the shearing surfaces but also aligns totally in the direction of flow. Data in Fig. 1 show that nematic aggregates are at maximum orientation over a wide range of shear rates. Figure 1 also indicates that shear rates to above a half million reciprocal seconds do not orient individual molecules in the isotropic liquid. Viscosities for the nematic state do increase, however, if shear rate is decreased below a homogeneous value of about 2000 sec.$^{-1}$. This agrees with the general region of fractional orientation and non-Newtonian flow indicated by previous light transparency and low shear, capillary flow measurements.[13]

The energy conversion in the concentric cylinder viscometer causes small temperature gradients within the test fluid. These gradients represent a force for orienting the nematic phase.[14,15] This

* Part I of a series on Order and Flow of Liquid Crystals.

(1) G. H. Brown and W. G. Shaw, *Chem. Rev.*, **57**, 1049 (1957).

(2) V. Frederiks and V. Zolina, *Trans. Faraday Soc.*, **29**, 919 (1933).

(3) "International Critical Tables," Vol. 1, 1926, p. 314.

(4) D. Vorlander, "Chemische Kristallographie der Flussigkeiten," Leipzig, 1924.

(5) J. F. Johnson, R. L. LeTourneau, and R. Matteson, *Anal. Chem.*, **24**, 1505 (1952).

(6) E. M. Barber, J. R. Muenger, and F. J. Villforth, Jr., *ibid.*, **27**, 425 (1955).

(7) R. S. Porter and J. F. Johnson, *Wear*, **4**, 32 (1961).

(8) W. Ostwald and H. Malss, *Kolloid-Z.*, **63**, 192 (1933).

(9) J. D. Bernal and D. Crowfoot, *Trans. Faraday Soc.*, **29**, 1032 (1933).

(10) M. Miesowicz, *Nature*, **158**, 27 (1946).

(11) J. Falgueirettes, *Compt. Rend.*, **241**, 71 (1955).

(12) G. Becherer and W. Kast, *Ann. Physik.*, **41**, 355 (1942).

(13) S. Peters and H. Peters, *Z. Physik. Chem.* (Frankfurt), **3**, 103 (1955).

(14) G. W. Stewart, *Phys. Rev.*, **69**, 51 (1945).

thermal alignment is perpendicular and in opposition to orientation in the direction of flow.[14,15] The observation of maximum orientation nematic viscosity in the rotational viscometer thus indicates that neither random nor directional thermal effects in the nematic phase compete successfully with shear orientation at stresses above 500 dynes/cm.[2]

Miesowicz has shown the influence of an orienting magnetic field on the viscosity of *p*-azoxyanisole.[10,16] Limiting high and low viscosities were obtained as a function of temperature at 3800 gauss for orientation parallel to the direction of flow and parallel to the velocity gradient. These values of Miesowicz have been replotted in Fig. 2. The previously described capillary and rotational viscometer measurements also are plotted; they agree within precision with the Miesowicz values for magnetic orientation in the direction of flow. Viscosities for unoriented nematic structures of *p*-azoxyanisole have been measured by Becherer and Kast using the Helmholtz method.[12] The Becherer and Kast values have been replotted and reinterpreted by least squares analyses as given in Fig. 2.

It is of interest that neither oriented nor unoriented nematic viscosities form a continuous series with isotropic viscosities. For anisaldazine a continuous series of nematic and isotropic values has been proposed in terms of microwave dielectric loss.[18] Because of the change of state at the nematic–isotropic transition, a continuous series for viscosities or dielectric properties would seem not to be required. The dielectric loss for the randomly oriented nematic state also has been related to the corresponding quantities in a perpendicular magnetic field and in a parallel field.[18] Applying the approximation that the nematic liquid crystalline state consists of rigid rods leads to a simple integer relationship between the dielectric loss for the various orientations. Such simple expressions have been only moderately successful.[17,18]

An orientation relationship of the general dielectric type has been applied to viscosity data for the nematic state of *p*-azoxyanisole. The use of this form is rationalized by the fact that dielectric loss can be inversely proportional to relaxation times. Hence, by simple Debye theory, dielectric loss should be proportional to T/η, where T is absolute temperature and η is absolute viscosity.[18] By these considerations, a strikingly simple and accurate relationship has been developed for nematic orientation viscosities.

$$\frac{4}{\eta_0} = \frac{3}{\eta_1} + \frac{1}{\eta_2} \qquad (1)$$

Equation 1 describes within the precision of measurement the relation between viscosity for the random oriented nematic phase, η_0, and the limiting low and high viscosities, η_1 and η_2, for nematic orientation parallel to flow and parallel to the shear gradient, respectively. Equation 1 holds with notable constancy over the entire nematic range for *p*-azoxyanisole.

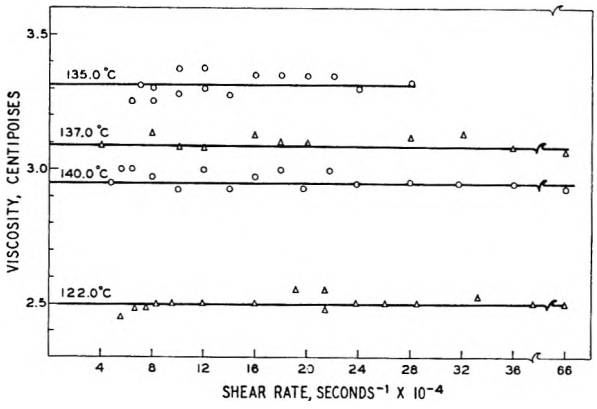

Fig. 1.—*p*-Azoxyanisole: viscosity *vs.* shear rate.

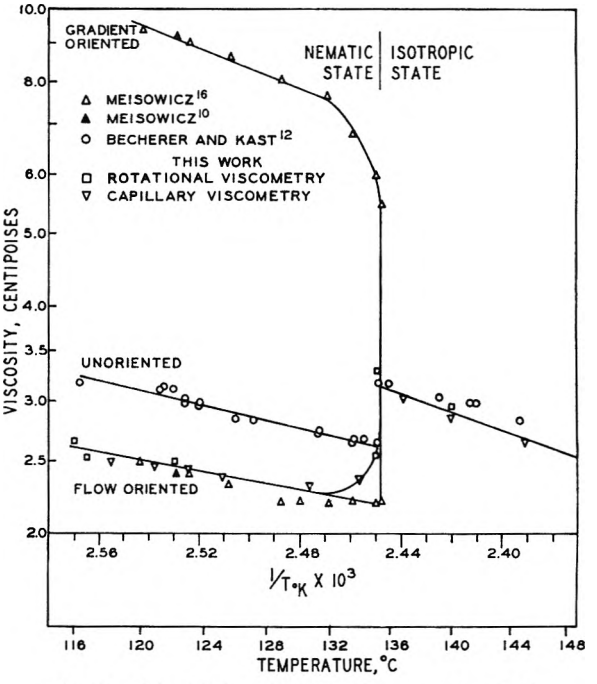

Fig. 2.—Orientation viscosities for *p*-azoxyanisole.

Flow Activation Energies.—The original presentations of random and magnetic orientation viscosities for *p*-azoxyanisole were in plots of linear viscosity *vs.* linear temperature.[12,16] The log viscosity *vs.* reciprocal of absolute temperature plot, used in Fig. 2, gives a generally more linear correlation. Apparent flow activation energies also may be calculated from slopes for the linear portions in Fig. 2. Flow activation energy is defined here as $R(\mathrm{d} \ln \eta/1/T°_{\mathrm{K}})$, where R is the gas constant and η is absolute viscosity. Flow activation energies calculated from least squares analyses are given in Table II. Values for flow oriented nematic viscosities and for the isotropic state of *p*-azoxyanisole have been derived from more complete data.[13]

Adsorption.—Adsorption represents a potential error in viscosity measurements. Viscosities measured in the concentric cylinder instrument generally were found to be independent of fluid thickness and to agree with limiting orientation values;

(15) R. C. Davis and G. W. Stewart, *Proc. Iowa Acad. Sci.*, **45**, 189 (1938).

(16) M. Miesowicz, *Bull. Acad. Pol.*, A, 228 (1936).

(17) E. F. Carr, *J. Chem. Phys.*, **26**, 420 (1957).

(18) E. F. Carr and R. D. Spence *ibid.*, **22**, 1481 (1954).

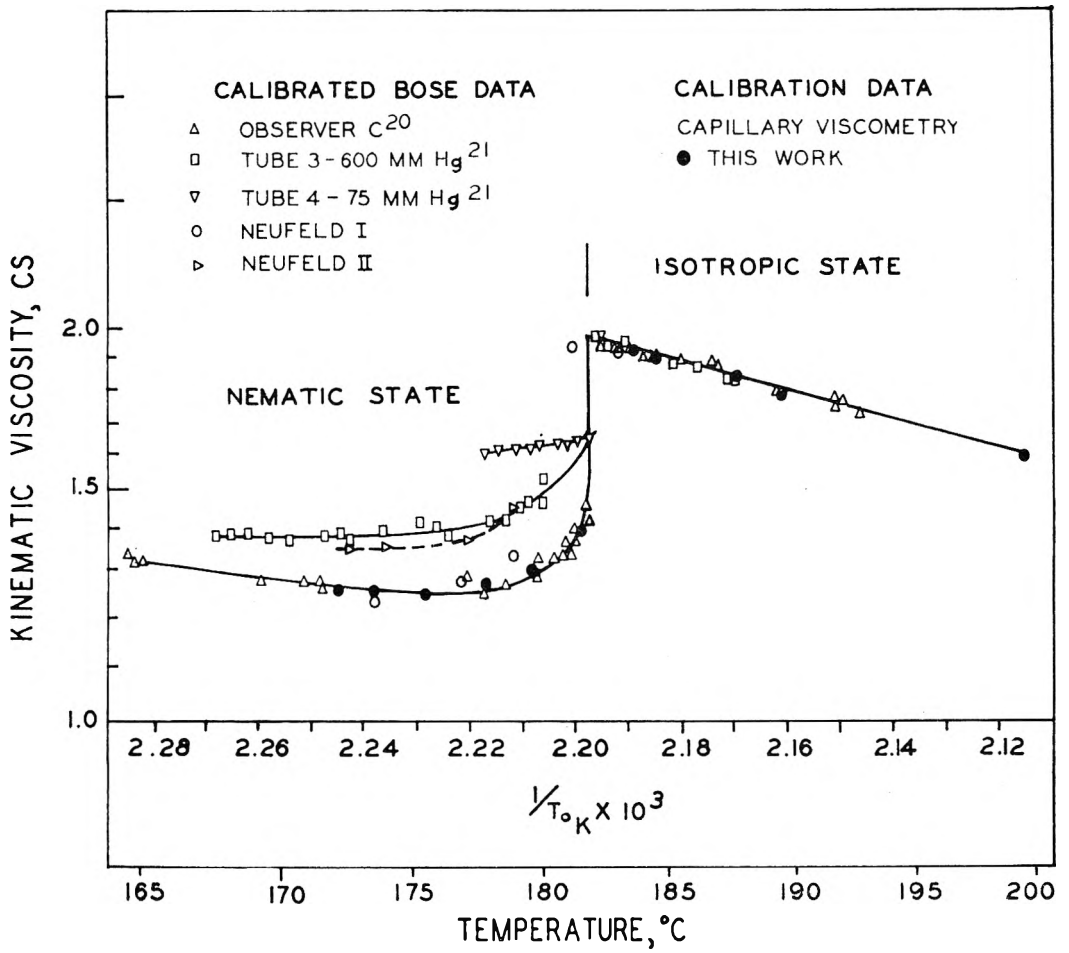

Fig. 3.—Mesophase transition viscosities for anisaldazine.

TABLE II

FLOW ACTIVATION ENERGIES FOR *p*-AZOXYANISOLE

Fluid state	Nematic liquid crystals, 119–132°			Isotropic
Molecular orientation	Flow oriented	Gradient oriented	Unoriented	>135° Unoriented
Flow activation energy	2.7	13.0	3.5	5.7

compare Fig. 1 and 2. In several nematic phase determinations, however, apparent viscosities were above precision limits. For example at 128°, high apparent viscosities near 2.8 and 2.9 cp. were obtained with fluid thicknesses of 3.35 and 2.79 $\times 10^{-4}$ cm., respectively. This corresponds to an effective decrease in fluid thickness of about 0.6 μ. This suggests an adsorbed film of *p*-azoxyanisole of 0.3–0.6 μ, depending on whether the film is adsorbed on one or both of the steel cylinders. In two cases, the probable adsorbed layer appeared to be slightly less thick, but not destroyed, at high shear. Apparent adsorption was observed at temperatures in the nematic range and up to 137°.

Previously reported dimensions for nematic aggregates are similar to thicknesses of adsorption layers measured here. From nematic viscosities in a rotating magnetic field, it appears that *p*-azoxyanisole is associated in groups with diameters of the order of 0.7 μ.[1] By studying light diffusion, it has been concluded that nematic structures of 0.2–0.3 μ in largest dimension are present.[1] The nematic aggregates decrease in size with increasing temperature. From the effect of orientation of the aggregates on the mobility of foreign ions, aggregate size has been calculated to vary from 10^6–10^5 molecules over the nematic range.[19]

Anisaldazine.—Figure 3 compares new viscosity results with the earlier values for anisaldazine. The data of Bose have been put on an absolute kinematic scale by using new anisaldazine nematic and isotropic viscosities obtained in this study.[20,21] The calibrated Bose data, Observer C, are in excellent accord with the new results over the full temperature range. Bose's data, Observer B, also show agreement but with less definition.[20] The earlier data are generally less accurate as temperature fluctuations of over 1° were reported during individual capillary flow measurements. Neufeld's capillary flow data on anisaldazine also have been calibrated with new data obtained here.[22] The lowest values for the nematic state, obtained in Poiseuille or laminar flow, likely correspond to maximum orientation in shear flow. This is because results with different viscometers give equivalent results. Bose was able to obtain flow measurements up to 5° below the nominal transition for his good quality anisaldazine. Similarly,

(19) L. S. Ornstein and W. Kast, *Trans. Faraday Soc.*, **29**, 931 (1933).
(20) E. Bose and F. Conrat, *Z. Physik.*, **9**, 169 (1908).
(21) E. Bose, *ibid.*, **10**, 32 (1909).
(22) F. Kruger, *ibid.*, **14**, 651 (1913).

in this study viscosity measurements were obtainable to several degrees below the observed solid transition of *p*-azoxyanisole; see Fig. 2 and Table I.

The higher nematic viscosities in Fig. 3 have been obtained by Bose and by Neufeld from measurements at higher shear induced by an overpressure on special capillary viscometers.[21,22] The increase in nematic viscosity has been attributed to Reynolds type turbulence.[21] The Reynolds numbers for turbulence, however, may not be sufficiently large, although they cannot be calculated exactly. It is possible that other causes are responsible for the viscosity increase, such as need for capillary corrections or capillary residence times approaching relaxation times for the nematic microstructure. Kruger, who quotes Neufeld's thesis data, says nematic anisaldazine at high pressure shoots through the capillary viscometer like a rigid body.[22] It is significant that such high shear anomalies were not observed here for nematic structures of *p*-azoxyanisole; see Fig. 1. The results in Fig. 1 also indicate that oriented nematic structures are not broken up at high shear. Such a speculation has been made to account for the higher nematic viscosities in Fig. 3 induced by higher pressures and shear rates in capillary viscometers.[22] Tests comparable to those in Fig. 1 were not made on anisaldazine, as its nematic state exists beyond the operational temperature limits of the concentric cylinder viscometer.

Acknowledgment.—The authors express appreciation to Mr. A. R. Bruzzone for help in the experimental work.

CRITICAL PHENOMENON IN AQUEOUS SOLUTIONS OF LONG CHAIN QUATERNARY AMMONIUM SALTS. IV. HYAMINE 1622–IODINE COMPLEX SYSTEMS

BY IRVING COHEN, PETER ECONOMOU, AND ANFIR LIBACKYJ

Department of Chemistry, Polytechnic Institute of Brooklyn, Brooklyn 1, New York

Received March 5, 1962

The coacervating quaternary ammonium salt, Hyamine 1622, forms a complex with molecular iodine. The micellar molecular weights and the charge properties of the homogeneous phase of this cationic soap system, as a function of NaCl concentration and I_2 concentration, were determined from light scattering measurements. An over-all two-stage growth process is indicated in these systems. At low NaCl concentration, the micelle grows to a limiting isotropic structure. At higher NaCl concentrations, the micellar growth is an exponential function of the NaCl concentration. The Hyamine–I_2 complex systems show the typical micellar ionization suppression with increasing NaCl concentration encountered in a number of coacervating cationic soap systems.[3] The infusion of small quantities of I_2 in an aqueous Hyamine 1622 solution produces changes in all of the characteristic properties of the system. Experimentally, detectable changes in the critical electrolyte concentration (c.e.c.) necessary for two-solution phase formation may be observed for an I_2/Hyamine 1622 molecular ratio as low as 10^{-3}. A number of simple empirical equations have been developed which show the functional relationships that exist among several characteristic properties of these solutions. Specifically, the c.e.c. may be predicted for these systems from the rate of micellar growth in the initial growth process as a function of NaCl concentration, and independently from the initial ionization properties of these aqueous polyelectrolyte systems.

Introduction

The separation of aqueous soaps into two solution phases (coacervation) occurs for a number of cationic[1] and anionic[2] soap species with the addition of simple electrolytes to their aqueous solutions. The homogeneous phase of several cationic soaps, which form coacervates, shows two pronounced effects prior to two-phase formation[3]: (a) at low electrolyte concentrations, the degree of micellar ionization is critically suppressed and (b) the soap micelles grow to a size which is of the order of 10^2- to 5×10^2-fold larger than the micelles in an electrolyte-free solution. An additional effect has been observed.[3] Intermediate between zero electrolyte and the critical electrolyte concentration (c.e.c.), a narrow electrolyte transition range (e.t.r.) may be identified, for each coacervating system at a fixed temperature, in which light scattering, viscosity, and diffusion studies indicate an apparent transformation of the micellar species from an essentially isotropic to an anisotropic entity.

The purpose of this study is a detailed examination of soap micellar growth as a function of electrolyte concentration in a typical cationic coacervating system. The system chosen for this study was the Hyamine 1622 (Hy)–NaCl–H_2O system. Although structurally the Hy soap monomer is a rather complicated molecule, this system has the advantage that gross changes in the system may be observed for small electrolyte increments. A further advantage of this system rests in the fact that Hy forms a complex with molecular I_2. The infusion of small quantities of I_2 into this micellar system produces changes in all of the characteristic properties (of the homogeneous phase) of the system. Specifically, in an over-all aqueous 1% Hy solution for a I_2/Hy molecular ratio of 1.25×10^{-3} the critical NaCl concentration is lowered by 0.01 *M* as compared to the non-iodinated system. A comparable shift in the e.t.r. for the system is observed. In addition to the non-iodinated system, this investigation encompasses Hy–I_2 complex systems in which I_2/Hy molecular ratios (R) range between 5×10^{-3} and 5×10^{-2}.

(1) I. Cohen, C. F. Hiskey, and G. Oster, *J. Colloid Sci.*, **9**, 243 (1954).

(2) A. C. Bungenberg de Jong, "H. R. Kruyt Colloid Sci.," Vol. II, Elsevier, Amsterdam, 1949, Chap. X.

(3) I. Cohen and T. Vassiliades, *J. Phys. Chem.*, **65**, 1781 (1961).

In a previous study of the electrolyte specificity observed in aqueous Hy systems with a number of monovalent anions[4] it was shown that the c.e.c. for each of the systems studied may be qualitatively correlated with the initial ionization properties of the system at low electrolyte concentrations. The primary observable effects of relatively small infusions of I_2 in aqueous Hy solutions are small changes in the initial ionization properties of the Hy micelles. A functional regularity is observed in the ionization changes with increasing I_2 concentration. Hence, an examination of Hy–I_2 complex systems provides a method for developing quantitative relationships between the various properties of the homogeneous phase of these systems. Of special interest are quantitative relationships between the c.e.c. and characteristic properties of the homogeneous phase.

Experimental

Materials.—The following materials were used in this investigation

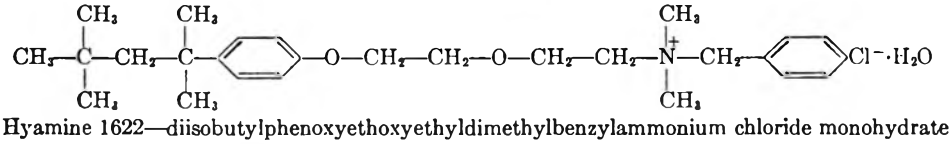

Hyamine 1622—diisobutylphenoxyethoxyethyldimethylbenzylammonium chloride monohydrate

(1) Hyamine 1622 (Hy) is a commercial bactericide produced by Rohm and Haas. This material was purified in the following manner. A quantity of Hy was dissolved in boiling acetone. The concentrated solution was filtered while hot and left to cool slowly. A crystalline product precipitated. The crystals were filtered, washed with diethyl ether, then dried in a vacuum desiccator for 24 hr.

(2) I_2 was C.P. grade which was freshly sublimed before use in these experiments.

(3) NaCl was C.P. grade.

Apparatus. Light Scattering.—Light scattering measurements were performed in a Brice-Phoenix photometer, using incident unpolarized monochromatic light of wave length 5460 Å. In this spectral region, I_2 absorption is minimal and does not interfere with light scattering measurements. The measurements were carried out in a cylindrical cell, with solutions which had been filtered through millipore filters of 0.45 μ pore size. Refractive index increments (dn/dc) were measured with a Zeiss dipping refractometer. For soap concentrations in excess of the critical micelle concentration (dn/dc) is independent of electrolyte concentration, iodine concentration, micellar size, and micellar shape. The refractive index increment for Hy–I_2–NaCl–H_2O systems is 0.1913 cm.^{3}/g.

Hyamine–I_2 Complex.—Molecular I_2 forms a complex with Hy. Figure 1 represents the optical absorption spectra for the titration of a $CHCl_3$–I_2 solution in which the I_2 concentration is 2.53×10^{-4} M, with a $CHCl_3$–Hy solution. These curves show typical two-component spectra for the solvated I_2 and the Hy–I_2 complex. A binding constant for the Hy–I_2 complex was calculated from these data.

The mode of preparation of the Hy–I_2 complex is the addition of solid freshly sublimed I_2 to an aqueous Hy solution. The heterogeneous mixture is then shaken for a prolonged period of time (5–6 days) until all of the I_2 goes into solution. In a 6% Hy solution at room temperature, when the I_2/Hy molecular ratio is an excess of 10^{-1}, two immiscible products are formed, a heavy opaque viscous material, and a supernatant aqueous solution of the Hy–I_2 complex. The heavy opaque material was not investigated beyond the extraction of I_2 with $CHCl_3$ from this material. I_2 could not be extracted with $CHCl_3$ from the aqueous Hy–I_2 complex phase. The complex is soluble in both the H_2O and $CHCl_3$ layers.

A carefully prepared stock solution of 6% Hy was made up in which the I_2/Hy molecular ratio was 5×10^{-3}. Experimental solutions were prepared by appropriate dilutions with H_2O and I_2-free Hy solutions. All experimental solutions were equilibrated in a thermostat for at least 3 hr. prior to making any measurements on these solutions.

(4) I. Cohen and T. Vassiliades, *J. Phys. Chem.*, **65**, 1774 (1961).

Results and Discussion

Micellar Molecular Weights.—Figure 2 represents the micellar molecular weights of a series of aqueous Hy–I_2 complex systems with I_2/Hy molecular ratios (R) ranging from 5×10^{-3} to 5×10^{-2}, in addition to the non-iodinated system. It is apparent from these curves that the micellar molecular weights are not a monotonic function of NaCl concentration. In fact, a complicated micellar growth pattern is indicated with the addition of NaCl in small increments to the system. Initially there occurs a relatively small micellar growth with the first small additions of NaCl. The initial small growth is followed by a relatively sharp rise in micellar molecular weight over a narrow range of NaCl concentration, to a near plateau. This transition resembles a disorder–order transition of higher order than one. Small infusions of I_2 in these systems make the transition sharper and shift the transition to lower NaCl concentrations. With further additions of NaCl beyond the plateau, a sharp discontinuity is observed in the micellar molecular weights corresponding to a 20% growth of the micelle. The remaining micellar growth to the c.e.c. falls on a smoooth curve. In the latter NaCl interval, the micellar growth is an exponential function of the NaCl concentration (Fig. 3) and, for the non-iodinated system at 30°, may be represented by

$$M = M_x e^{12.25(C-C_x)} \qquad (1)$$

where M is the micellar molecular weight at NaCl concentration, C; M_x is the micellar molecular weight at NaCl concentration, C_x, which was arbitrarily chosen as the first experimental point on the smooth curve which characterizes micellar growth at higher NaCl concentrations. This expression may be related to the I_2/Hy molecular ratio (R) by

$$M = M_x e^{12.25(C-C_x)e^{10R}} \qquad (2)$$

The differential equation describing the growth process at higher NaCl concentrations may be put in the form

$$dM/M = 12.25e^{10R}\, dc \qquad (2a)$$

It previously was observed[4] that the micellar molecular weights at the onset of two-phase formation for a number of coacervating cationic soap systems varied over a considerable range of approximately 10^6 to 5×10^6. This same variability in micellar molecular weights is observed in the Hy–I_2 complex system. The vertical lines in Fig. 3 represent the critical micelle molecular weights for the non-iodinated and for iodinated systems. The derived critical micelle molecular weight for

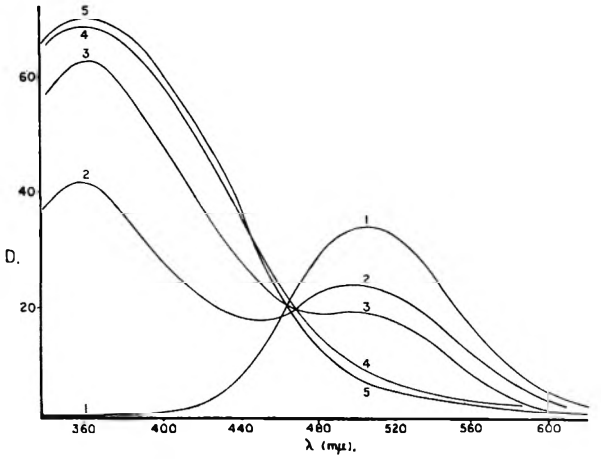

Fig. 1.—Absorption spectra of $CHCl_3$–Hy–I_2 solutions

I_2 concn., M	Hy concn., M	I_2/Hy (R)
(1) 2.53×10^{-4}	0	
(2) 2.53×10^{-4}	2.59×10^{-4}	0.94
(3) 2.53×10^{-4}	5.37×10^{-4}	.47
(4) 2.53×10^{-4}	1.17×10^{-3}	.21
(5) 2.53×10^{-4}	2.49×10^{-3}	.10

the non-iodinated Hy–NaCl system is 1.98×10^6; for the iodinated system in which the (I_2/Hy) molecular ratio is 5×10^{-2}, the derived critical micellar molecular weight is 1.10×10^6. This is a further indication of the fact, previously noted,[4] that micellar size is not the sole critical factor related to coacervation in soap systems and coacervation can occur in the same cationic systems of different critical micellar sizes.

Flory[5] has developed the theory for the limiting case of coacervation in uncharged rodlike macromolecular solute systems. The driving force for coacervation in anisotropic non-electrolyte systems is the geometry of the system. When the effective volume of a solute particle exceeds the total available volume per solute particle the systems separate into two phases, an ordered phase and a randomly oriented phase.

In aqueous macro-ion systems, the geometry of the solute particles is complicated by double layer charge effects. Oster[6] reported that in salt-free, highly purified aqueous tobacco mosaic virus solutions (TMV), the co-volume of a rodlike TMV particle is approximately ten times the co-volume calculated for non-interacting rods. The addition of NaCl to a TMV solution reduces the virus co-volume by virtue of shrinking the diffuse double layer of the charged TMV solute particle. Two macroscopic effects are observed with the addition of NaCl to a TMV solution. At low NaCl concentrations (less than 0.05 M), the critical virus concentration necessary for two-phase formation is increased as compared to salt-free TMV solutions. At higher NaCl concentrations, the two-phase TMV system is dispersed and the system becomes a homogeneous solution. In the latter region of NaCl concentration, the virus co-volume is twice the co-volume calculated for non-interacting rods.

In the Hy–I_2 systems, a further complication is observed with the addition of NaCl to the systems. In the NaCl concentration region, corresponding

(5) P. J. Flory, *Proc. Roy. Soc.* (London), **A234**, 73 (1956).
(6) G. Oster, *J. Gen. Physiol.*, **33**, 445 (1950).

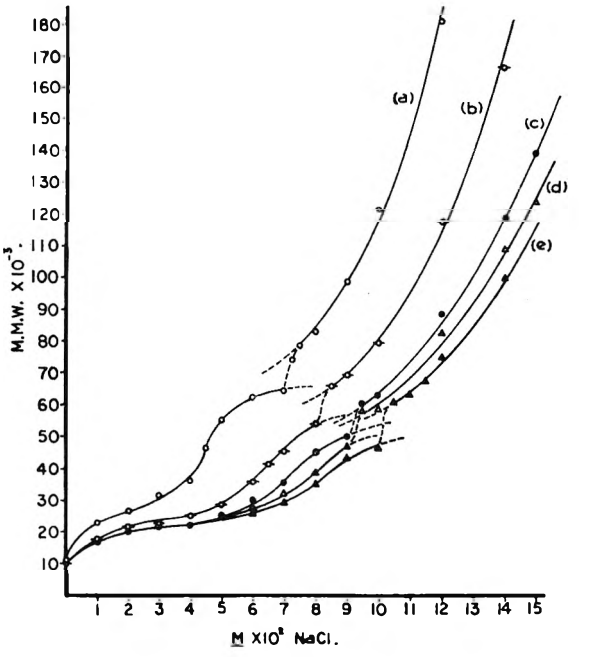

Fig. 2.—Micellar molecular weights (m.m.w.) of hyamine 1622–I_2–NaCl–H_2O systems as a function of NaCl concentration at 30°: (a) I_2/Hy = $R = 5 \times 10^{-2}$; (b) $R = 2 \times 10^{-2}$; (c) $R = 1 \times 10^{-2}$; (d) $R = 0.5 \times 10^{-2}$; (e) $R = 0$.

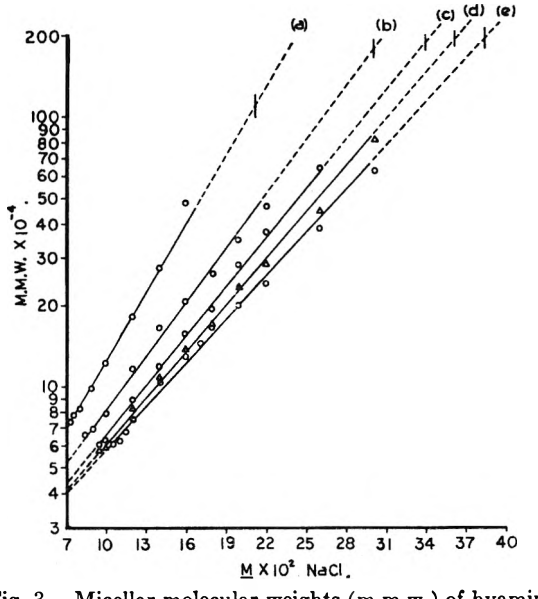

Fig. 3.—Micellar molecular weights (m.m.w.) of hyamine 1622–I_2–NaCl–H_2O systems as a function of NaCl concentration at 30°: (a) I_2/Hy = $R = 5 \times 10^{-2}$; (b) $R = 2 \times 10^{-2}$; (c) $R = 1 \times 10^{-2}$; (d) $R = 0.5 \times 10^{-2}$; (e) $R = 0$.

to the onset of two-phase formation, a tremendous growth of the soap micelles occurs as a function of NaCl concentration. It may be seen from the slope of the curves in Fig. 3 that in the iodinated systems, the rate of micellar growth increases with increasing I_2 concentration. The increased rate of micellar growth, as a function of NaCl concentration, may be associated with the micellar ionization suppression induced by the presence of I_2 in the system.

A qualitative model for coacervation in Hy–I_2 complex systems, consistent with the data developed

TABLE I

SUMMARY OF DATA FOR Hy–I_2–NaCl–H_2O SYSTEMS. 1% Hy AT 30° EXPERIMENTAL AND CALCULATED VALUES OF C_{max}, M_{max}, C.E.C., AND CRITICAL MICELLE MOLECULAR WEIGHTS

I_2/Hy = R	NaCl C_{max} exp. M	NaCl C_{max} calcd. [a](6) M	M_{max} exp.	M_{max} calcd. (8)	NaCl c.e.c. exp. M	C.e.c./ C_{max} exp.	NaCl c.e.c. calcd. (7) M	NaCl c.e.c. calcd. (11) M	M.m.w. at c.e.c. Fig. 3
0.0	0.0825	0.0825	38,000	38,000	0.383	4.64	0.383	0.356	1.98×10^6
0.5×10^{-2}	.0804	.0785	40,000	36,000	.363	4.52	.362	.353	1.97×10^6
1.0×10^{-2}	.0733	.0730	39,500	37,900	.339	4.62	.340	.338	1.95×10^6
2.0×10^{-2}	.0644	.0650	41,500	43,500	.302	4.69	.302	.297	1.80×10^6
5.0×10^{-2}	.0446	.0455	45,000	43,200	.213	4.77	.211	.211	1.10×10^6

[a] Numbers refer to empirical formulas: (6) $C_{max} = (C_{max})_{R=0}\, e^{-12R}$; (7) c.e.c. $= (\text{c.e.c.})_{R=0}\, e^{-12R}$; (8) $M_{max} = {}^1/_2(dm/dc)_{max} \times (C_{max})_{R=0}\, e^{-12R}$; (11) c.e.c. $= 0.72 \ln Q_{max}/18$.

in this study, is one in which coacervation occurs in soap systems when the micelles achieve a critical effective volume. The critical effective volume is related to both the micellar dimensions and the diffuse double layer.

The double layer thickness, $1/\kappa$, is a function of the ionic strength of the bulk solution. The critical NaCl concentrations for the iodinated systems are lower than the critical NaCl concentrations for the non-iodinated system. The lower critical NaCl concentrations combined with the lower micellar ionization results in a lower ionic strength, and consequently, a larger $1/\kappa$ for the iodinated systems. In addition, since the solutions described here are solutions of constant soap monomer concentration, the iodinated solutions contain a larger number of micellar particles than the non-iodinated system. The two effects, the larger $1/\kappa$ and the larger number of micellar particles, would account for the attainment of a critical effective volume necessary for two-phase formation of the smaller iodinated micelles.

Figure 4 represents a differential plot of the data, $(\Delta M/\Delta C)$ *versus* NaCl concentration. Each of these curves is characterized by a well defined maximum at low NaCl concentrations corresponding to the first molecular weight transition described above. The quantities, C_{max}, representing the electrolyte concentration at which the maximum in the differential curve occurs, $(\Delta M/\Delta C)_{max}$, and M_{max}, the micellar molecular weight at $(\Delta M/\Delta C)_{max}$, which are distinctive for each curve, are of considerable interest in this study. These parameters provide the basis for a number of simple empirical expressions which relate the c.e.c. to characteristic properties of Hy–I_2 solutions at low NaCl concentrations.

C_{max} may be determined with some accuracy analytically. However, there is some uncertainty in the experimental value of $(\Delta M/\Delta C)_{max}$. The first of these expressions relates the c.e.c. to C_{max}. For all of the systems observed, the c.e.c. is directly proportioned to C_{max}.

$$\text{c.e.c.} = 4.65 C_{max} \text{ (Table I)} \qquad (3)$$

Additionally, for each of these solutions

$$M_{max} = {}^1/_2(\Delta M/\Delta C)_{max} \times C_{max} \text{ (Table I)} \qquad (4)$$

and combining (2) and (3)

$$\text{c.e.c.} = \frac{9.8 M_{max}}{(\Delta M/\Delta C)_{max}} \qquad (5)$$

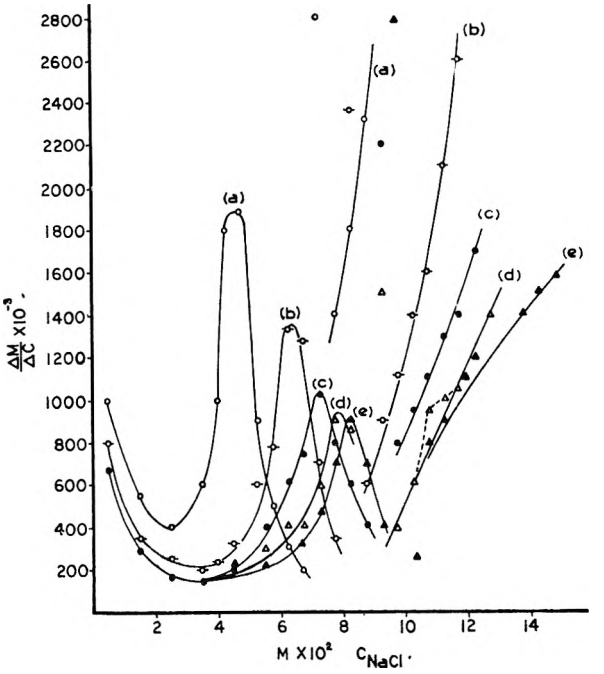

Fig. 4.—Differential plot of $\Delta M/\Delta C$ *versus* NaCl concentration for hyamine 1622–I_2–NaCl–H_2O systems at 30°: (a) $R = 5 \times 10^{-2}$; (b) $R = 2 \times 10^{-2}$; (c) $R = 1 \times 10^{-2}$; (d) $R = 5 \times 10^{-3}$; (e) $R = 0$.

The infusion of I_2 in the aqueous Hyamine 1622 solution has the effect of decreasing C_{max} and increasing $(\Delta M/\Delta C)_{max}$. C_{max} is related to the I_2/Hy molecular ratio (R) by the following exponential expression

$$C_{max} = (C_{max})_{R=0}\, e^{-12R} \text{ (Fig. 5c)} \qquad (6)$$

substituting for C_{max} in (3), the c.e.c. may be related to the I_2/Hy molecular ratios (R) in these systems by

$$\text{c.e.c.} = (\text{c.e.c.})_{R=0}\, e^{-12R} \qquad (7)$$

From (4) and (6), M_{max} may be related to R by

$$M_{max} = {}^1/_2(\Delta M/\Delta C)_{max} \times (C_{max})_{R=0}\, e^{-12R} \qquad (8)$$

M_{max} falls in a very narrow range of micellar molecular weights for all of the systems investigated in spite of the fact that C_{max} and $(\Delta M/\Delta C)_{max}$ vary considerably. This would indicate that M_{max} represents a particular state of the system.

Charge Properties.—Figure 6 represents the curves for p/m *vs.* NaCl concentration where p is

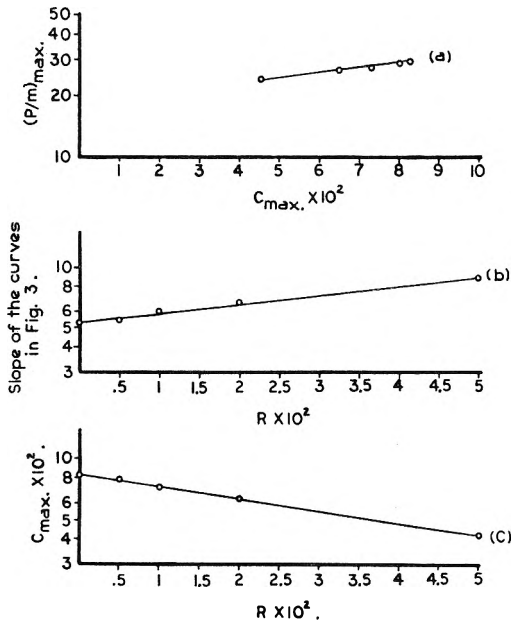

Fig. 5.—Functional relationships of the properties of the homogeneous phase of Hy–I_2–NaCl system: (a) $(p/m)_{max}$ as a function of C_{max}; (b) slope of curves in Fig. 3 as a function of R; (c) C_{max} as a function of R.

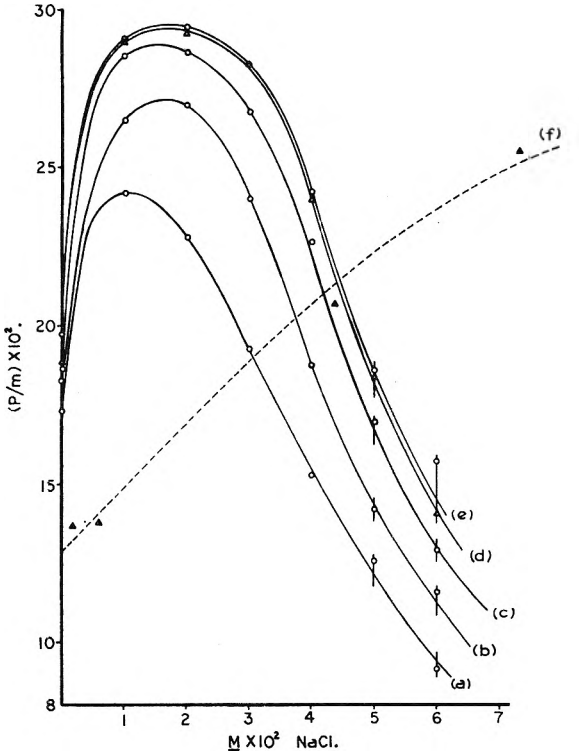

Fig. 6.—Micellar charge density (p/m) as a function of NaCl concn. for hyamine 1622–I_2–NaCl–H_2O systems at 30°: (a) $R = I_2/Hy = 5 \times 10^{-2}$; (b) $R = 2 \times 10^{-2}$; (c) $R = 1 \times 10^{-2}$; (d) $R = 0.5 \times 10^{-2}$; (e) $R = 0$; (f) non-coacervating cetylpyridinium chloride–NaCl–H_2O systems at 31°.

the number of monovalent charge sites on a micelle and m is the micellar aggregation number. The p/m values were derived from light scattering data by the methods developed by Hermans and Prins,[7] and Mysels and Princen[8] which were modified by Anacker.[9] This method was described in a previous paper in this series.[4] These curves show the distinctive ionization properties of coacervating cationic soap systems. An initial rise in ionization to a maximum is observed, followed by a critical suppression of the ionization with increasing NaCl concentration. The dotted curve represents the ionization pattern of a typical non-coacervating cationic micellar system, cetylpyridinium chloride–NaCl–H_2O,[9] where the ionization tends to rise to limiting p/m value of 0.26. The latter system is one in which, on the average, alternate polar heads on the micellar surface are charged. A similar ionization pattern is observed in the non-coacervating Hy–NaAc–H_2O system.[4]

The initial rise in ionization at low NaCl concentrations may be accounted for in terms of nearest neighbor charge site interactions typical of polyelectrolytes. Theories related to this phenomenon have been developed by Oosowa.[10] The effects of relatively small infusions of I_2 into Hy–NaCl solutions upon the ionization properties of these aqueous systems are twofold: the ionization maximum is depressed and the ionization corresponding to $(p/m)_{max}/2$ is shifted to lower NaCl concentrations. If a p/m curve is superimposed upon the corresponding differential curve $(p/m)_{max}/2$ occurs at an NaCl concentration which is very nearly coincident with C_{max} previously described. C_{max} may be related to $(p/m)_{max}$ by

$$C_{max} = 0.16 \ln Q_{max}/18 \text{ (Fig. 5a)} \qquad (9)$$

where $Q = p/m$, and from (6) Q_{max} is related to the (I_2/Hy) molecular ratio (R) by

$$Q_{max} = 18e^{6.2(C_{max})_{R=0}-12R} \qquad (10)$$

and from (3) and (9) the c.e.c. is related to Q_{max} by

$$\text{c.e.c.} = 0.72 \ln Q_{max}/18 \qquad (11)$$

Although two growth processes in these micellar systems as a function of NaCl concentrations may be clearly distinguished, the first, at low NaCl concentration, and the second at higher NaCl concentrations, these growth processes are not independent of each other. The ability to predict the c.e.c. from the rates of growth in the initial growth process and the initial charge properties would indicate that these are coupled consecutive processes. The second growth process occurs only after the first process has attained some state of completion.

Conclusions

A detailed investigation of micellar growth in the homogeneous phase of a series of Hy–I_2 complex–NaCl–H_2O cationic soap systems shows two distinct consecutive micellar growth processes. A micellar model which is consistent with these observations of this soap system is the following. Initially, at soap concentrations in excess of the critical micelle concentration, the micelle is a relatively loose isotropic structure. Debye[11] and Ooshika[12] have developed expressions for the energy per micelle

(7) J. J. Hermans and W. Prins, *Konikl. Ned. Akad. Wetenschap. Proc.*, **B59**, 162 (1956).
(8) K. J. Mysels and L. H. Princen, *J. Colloid Sci.*, **12**, 594 (1957).
(9) E. W. Anacker, *J. Phys. Chem.*, **62**, 41 (1958).
(10) F. Oosowa, *J. Polymer Sci.*, **23**, 421 (1957).

involving a coulombic term related to the repulsive interactions of the charged polar heads of the soap molecules in the micelle, and a van der Waals term related to attractive interactions of the hydrophobic tails of the soap molecules. The Ooshika expression contains a third term which takes into account the change in surface energy with micelle formation

$$W = N^{2/3}W_e + N^{1/3}W_s + NW_m$$

where N is the micelle aggregation number and W_e, W_s, and W_m are the coulombic, surface, and van der Waals energies per soap monomer.

The major effect of electrolyte addition to a soap system involves the coulombic term of this expression. The first small addition of NaCl to Hy soap systems results in two effects which operate in opposite directions, increased ionization and the screening of intra-micellar adjacent charge sites by the counterions added to the system. The latter effect would seem to be more pronounced since a small increase in micellar molecular weights occurs with the first additions of electrolyte. In the NaCl concentration range corresponding to ionization suppression, the counter-ion screening effects and the ionization suppression coöperatively decrease the coulombic term. The net result here is a relatively sharp micellar growth.

At the near plateau in the micelle molecular weight–NaCl function, although further ionization suppression is evident, micellar growth tapers off. This may be interpreted as the approach to a saturated isotropic structure. Light scattering, viscosity, and self-diffusion data[3] are consistent with a spherical micellar model in this region of NaCl concentration.

The effects of small infusions of I_2 in this system support the argument that the micellar transition discussed above is a disorder–order transition. The limiting micellar molecular weights at the micelle molecular weight plateau range from 4.8×10^4 for the non-iodinated systems to 6.2×10^4 for the system in which the Hy/I_2 molecular ratio (R) is 5×10^{-2}.

There are three possible sites on the Hy molecule for attachment of the acidic I_2 molecule, *i.e.*, the phenyl group, the ether linkage, and the nitrogen atom. Iodine renders the cationic micelle periphery slightly more positive. This, in turn, results in a small suppression of micellar ionization. At any given point in the system, the lower the micellar ionization, the more efficient will be the packing of polar heads at the micellar periphery and a larger number of polar heads may be accommodated in a given structure. As a result of the lowered ionization with a higher I_2 concentration in the system, a somewhat more highly ordered micelle may be expected. This is reflected in the higher micelle molecular weight and in the greater sharpness of the transition in the iodinated systems as compared to the non-iodinated system.

The transitory persistence of the limiting isotropic structure as a function of NaCl concentration may be related to the residual intra-micellar coulombic repulsive interactions in a narrow range of NaCl concentration.

The discontinuities observed in the micellar molecular weight curves resemble phase changes and may be considered to be due to internal micellar rearrangements to incipient non-spherical structures. The sharp transition may be associated with a critical suppression of the intra-micellar coulombic field to the point where this coulombic field no longer constrains the micelles to a sphere or spheroidal structure. For NaCl concentrations in excess of this second transition region the van der Waals association forces modified by stearic factors are the essential micellar shape-determining forces.

The e.t.r. previously described[4] represents the electrolyte concentration range at which this micellar transformation to a non-spherical structure becomes sufficiently pronounced to be detected by the conventional experimental techniques employed in these studies.

In a previous study of the Hyamine 1622–NaCl–H_2O system,[3] it was noted that the temperature properties of constant composition systems at 0.05 M NaCl concentrations are quite different from the temperature properties of constant composition systems at higher NaCl concentration. In a 2% Hy solution in which the NaCl concentration was 0.05 M, a decrease in the temperature from 30 to 5° resulted in an increase in the micellar molecular weight from 2.3×10^4 to 1.1×10^5. In a 2% Hy solution in which the NaCl concentration was 0.145 M, the system was extremely temperature sensitive in the same temperature interval; the micellar molecular weight increased from 1.08×10^5 to 9.05×10^5. This difference in temperature sensitivity of a 0.05 M NaCl solution as compared to a 0.145 M NaCl solution points up the differences in the systems at NaCl concentrations corresponding to the two stages of micellar growth.

Acknowledgment.—The authors wish to express their appreciation for support provided by the Department of Health, Education, and Welfare, Public Health Service Grant No. A-2300 (C2).

DISCUSSION

F. M. FOWKES (Shell Development Company).—What is the physical significance of the fraction of ions ionized (p/m ratio) with respect to the actual degree of charge separation? Could the uncharged molecules really be ion pairs? How much separation could occur and be indicated by this method as "uncharged?"

I. COHEN.—The p/m ratio is derived from the intermicellar coulombic interactions. No distinction is possible between bound ions and ion-pair formation. An indirect indication of considerable counter-ion binding is the charge neutralization of adjacent polar head charge sites on the micelle periphery at low p/m values. This is reflected in the large micellar growth and the change in micellar shape from a spheroidal to a rod-shaped cylindrical structure.

(11) P. Debye, *Ann. N. Y. Acad. Sci.*, **51**, 575 (1949); *J. Phys. Chem.*, **53**, 1 (1949).

(12) Y. Ooshika, *J. Colloid Sci.*, **9**, 254 (1954); Y. Ooshika and Y. Ikeda, *Kolloid-Z.*, **145**, 3 (1956).

THE ADSORPTION–FLOCCULATION REACTIONS OF A POLYMER WITH AN AQUEOUS COLLOIDAL DISPERSION

BY THOMAS W. HEALY AND VICTOR K. LA MER

Department of Chemistry, Columbia University, New York, N. Y.

Received March 5, 1962

The theoretical equations for the stability of suspensions in the presence of polymer flocculants have been extended to include two variables previously held constant, *viz.*, the number of segments per polymer molecule, τ, and the number of these which adsorb and cover surface sites, β. The "extended segment" model of polymer adsorption, together with the "bridging" model of polymer flocculation, is described in terms of an adsorption parameter and in terms of β and $(\tau - \beta)$, where $(\tau - \beta)$ is the number of extended segments per polymer molecule. The solid–polymer aqueous system studied was calcium phosphate–polyacrylamide and variables examined were polymer concentration, polymer molecular weight, and the time of agitation.

Introduction

The phenomenon of polymer flocculation can best be analyzed in terms of: 1, the adsorption process, and 2, the flocculation process.

The theoretical and experimental work on the adsorption process, *e.g.*[1,2] is at present of a preliminary nature, particularly for the case of aqueous systems. It seems probable that when a polymer molecule concentrates at a solid–liquid interface, only a fraction of the total segments per molecule adsorb and cover surface sites. The remainder of the molecule protrudes into the surrounding medium as an extended segment.[3,4] There is an obvious simplification involved in this description, since the polymer molecule is more or less coiled at the interface, and contact between the polymer molecule and the surface can be made at any number of points along the molecule. Nevertheless, the description in terms of extended segments does allow us to explain much of the second topic above, *viz.*, the flocculation process, *e.g.*[5,6].

Since the work of Smellie and La Mer on the filtration of slimes flocculated with polymers[7,8] was summarized,[9] little new work has been reported on the mechanism of the flocculation process. In the present paper we extend the work of Smellie and La Mer[8] to include certain important variables previously held constant, *viz.*, molecular weight of the polymer and the conditions of agitation of the suspension.

Theoretical

In their treatment of the adsorption process in the flocculation of suspensions, Smellie and La Mer proposed that the decrease in bulk concentration of polymer due to adsorption is equal to the number of solid surface sites covered, (eq. 2, ref. 8). This is true only if every segment per polymer molecule covers a surface site. As pointed out in the introduction, it is probable that only a fraction of the segments per molecule adsorb and cover surface sites. For later purposes, it is necessary to include the parameter β in deriving the filtration equations, where β is the number of segments that adsorb per molecule of polymer.

Suppose $(P_0 - P)$ moles of polymer concentrate at the interface, where P_0 is the initial or added concentration of polymer, and P is the residual polymer concentration in solution after adsorption. Then $(P_0 - P)N$ molecules concentrate at the interface, where N is Avogadro's number. Since each polymer has τ segments, then $(P_0 - P)N\tau$ segments concentrate at the interface. If a fraction β/τ absorb and cover surface sites, then

$$\frac{\beta(P_0 - P)N\tau}{\tau} = \text{number of surface sites covered}$$

i.e.,

$$\frac{\beta(P_0 - P)N}{sS_0} = \theta = \text{fraction of surface covered}$$

where s is the number of sites/unit area of surface, and S_0 is the surface area of solid.

Note that it has been assumed that a surface site is equal in area to a polymer segment (see *e.g.*, ref. 1).

Rearranging

$$P = P_0 - \frac{k\theta}{\beta} \qquad (1)$$

where

$$k = \frac{sS_0}{N}$$

Equation 1 above may be compared to eq. 2 of Smellie and La Mer.[8] The subsequent equations of ref. 8 may then be modified to include β.

For example, eq. 21, ref. 8 becomes

$$\frac{P_0^{1/2}}{(Q - Q_0)^{1/2}} = A_m + B_m P_0 \qquad (2)$$

where

$$A_M = C\,\frac{(1 + bk/\beta)^{1/2}}{b^{1/2}} \qquad (3)$$

$$B_M = C\,\frac{b^{1/2}}{(1 + bk/\beta)^{3/2}} \qquad (4)$$

(1) R. Simha, H. L. Frisch, and F. R. Eirich, *J. Phys. Chem.*, **57**, 584 (1953).
(2) R. Perkel and R. Ullman, *J. Polymer Sci.*, **54**, 127 (1961).
(3) S. Ellerstein and R. Ullman, *ibid.*, **55**, 123 (1961).
(4) B. J. Fontana and J. R. Thomas, *J. Phys. Chem.*, **65**, 480 (1961).
(5) W. F. Linke and R. B. Booth, *Trans. AIME*, **217**, 364 (1960).
(6) T. W. Healy, *J. Colloid Sci.*, **16**, 609 (1961).
(7) V. K. La Mer, R. H. Smellie, Jr., and P. K. Lee, *ibid.*, **12**, 230 (1957).
(8) R. H. Smellie, Jr., and V. K. La Mer, *ibid.*, **13**, 589 (1958).
(9) V. K. La Mer and R. H. Smellie, Jr., "Proc. 2nd. International Conference," Geneva, 1958, p. 178; see also *Clays Clay Minerals*, **9**, 295 (1962).

where C is a constant. Similarly by setting $dQ/dP_0 = 0$, at $P_0 = P_m$ as in ref. 8

$$P_m = \frac{A_M}{B_M} \quad (5)$$

$$= \frac{(1 + bk/\beta)^2}{b} \quad (6)$$

Experimental

An assembly similar to that previously described[10] was used to obtain filtration rates. A technique of mixing the polymer solution with the suspension, agitation of the suspension, and filtration, was developed, such that identical suspensions did not differ in filtration rate by more than 3%. Agitation of the suspension was carried out with a magnetic stirrer assembly set at a fixed degree of intensity for all the results reported.

Fresh calcium phosphate suspensions of 3% by weight of solids in distilled water were used to obtain each individual filtration rate. The calcium phosphate (tribasic) was Fisher A.R. grade reagent and the particles had an average radius of approximately 10 μ.

We are indebted to the Cyanamid Co. for furnishing samples of polyacrylamide having molecular weights, determined by viscosity measurements, of 0.5×10^6, 1.0×10^6, 3.0×10^6, and 5.3×10^6.

Results

The curves for filtration rate *vs.* concentration of polymer were of the same type previously observed,[7] a typical set being shown in Fig. 1. These curves may be characterized by Q_m, the maximum filtration rate for a given set of conditions, and P_m, the concentration of polymer to attain that maximum filtration rate. Both Q_m and P_m change with the following variables: molecular weight of the polymer (M), time of agitation (t), intensity of agitation (A), and the surface area of the solids (S_0).

In this discussion we restrict ourselves to a consideration of the effect of molecular weight and time of agitation. The effect of surface area has been well discussed.[11] Intensity of agitation is an important variable, but one that is difficult to specify precisely. It should be referred to the shear stress at the site or sites of polymer–solid contact. It has been suggested[6] that for a polymer molecule to remain attached at the surface, a critical number of polymer segments must be adsorbed, and the extent to which this is achieved depends on the shearing forces at the solid–liquid interface. In general, for a given initial or added concentration of polymer, the amount adsorbed after a given time decreases as the intensity of agitation increases.[6]

The variation of P_m, the optimum concentration of polymer, with molecular weight and time of agitation is shown in Table I. In Fig. 2 the value of Q_m is plotted as a function of the molecular weight for three times of agitation. It is obvious from these results that the variation of P_m and Q_m with M is a complex process. It is thought that a more meaningful analysis of the data can be obtained from eq. 2 and 3. The applicability of these equations is shown in Fig. 3 where the quantity $P_0^{1/2}/(Q - Q_0)^{1/3}$ is plotted as a function of

(10) V. K. La Mer and R. H. Smellie, Jr., *J. Colloid Sci.*, **11**, 710 (1956).

(11) V. K. La Mer, R. H. Smellie, Jr., and P. K. Lee, *ibid.*, **12**, 566 (1957).

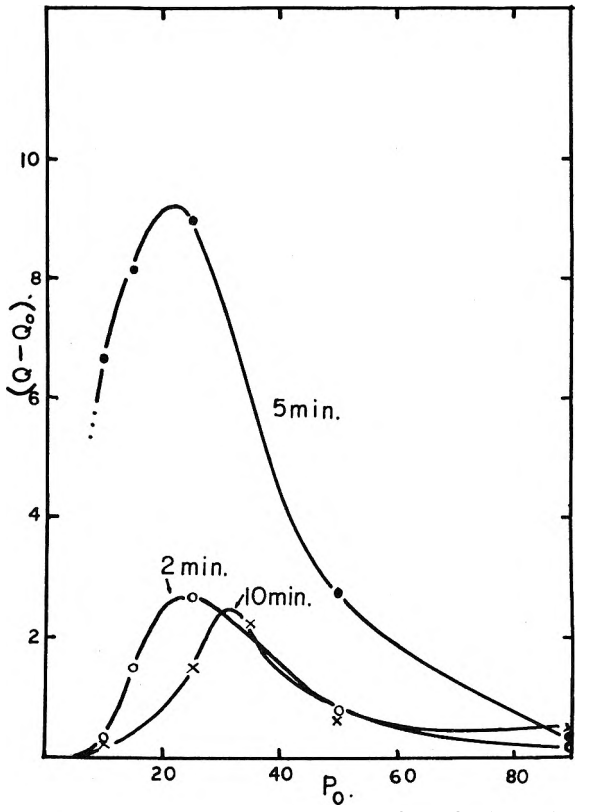

Fig. 1.—Variation of filtration rate ($Q - Q_0$) in cc./sec. as a function of polymer concentration (P_0), expressed as mole $\times 10^{-10}$/g. solid for 3% $Ca_3(PO_4)_2$ suspension in the presence of polyacrylamide (mol. wt. = 1×10^6).

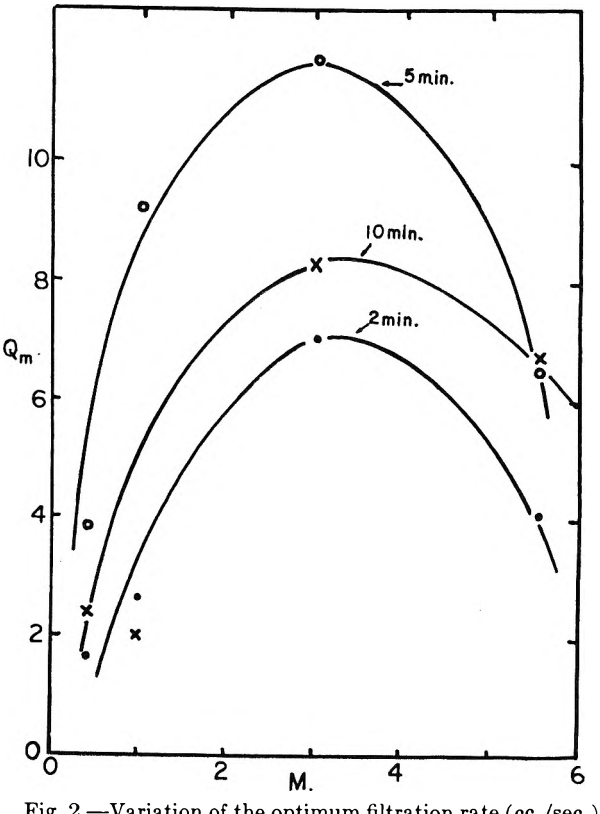

Fig. 2.—Variation of the optimum filtration rate (cc./sec.) as a function of molecular weight ($\times 10^{-6}$) at three times of agitation, 2 min., 5 min., and 10 min.

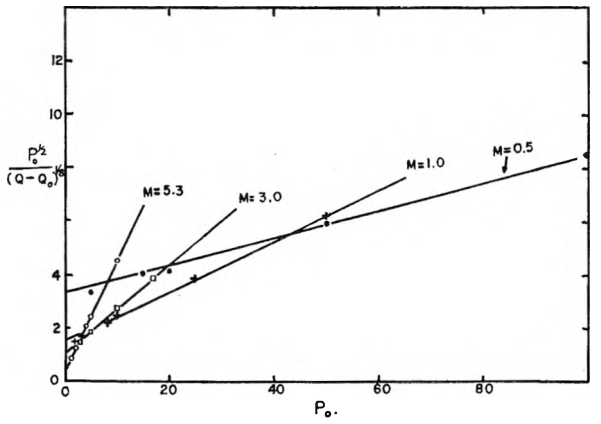

Fig. 3.—Linear plot of eq. 2 for a time of agitation of 5 min. for polyacrylamide samples of molecular weight 5.3, 3, 1, 0.5 million, respectively (P_0 = mole × 10^{-10}/g. of solid).

P_0, for four values of M and at a fixed time of agitation. Similar sets of curves are obtained at other times of agitation. The values of the intercept A_M of eq. 4 are listed in Table II.

TABLE I

VARIATION OF P_m WITH MOLECULAR WEIGHT AND TIME OF AGITATION

M (× 10^{-6})	t (min.) 2	5	10
0.5	100	66	160
1.0	25	22	31
3.0	4.7	6	8
5.3	1.0	1.1	3.3

TABLE II

VARIATION OF A_m WITH MOLECULAR WEIGHT AND TIME OF AGITATION

M × (10^{-6})	t (min.) 2	5	10
0.5	3.9	3.4	5.0
1.0	2.8	1.5	2.9
3.0	1.5	1.0	1.2
5.3	0.4	0.3	0.4

Preliminary adsorption measurements for this present system[12] have provided the following information. (1) Adsorption follows the Langmuir relationship. (2) The b value of the Langmuir equation decreases with increase in molecular weight (M) of the polymer and with increasing time of agitation (t). (3) The adsorption measurements were not sufficiently accurate to check the change in β with change in M and t. However, these changes in β were generally small compared to the change in b.

Discussion

Effect of Polymer Concentration.—The optimum effect shown in Fig. 1 has been considered by several workers and is best understood in terms of a model of polymer flocculation involving "bridging" between adjacent solid particles by extended polymer segments. As a first approximation the bridging hypothesis has proved useful. In brief, it is postulated that the degree of flocculation (as measured by the filtration rate in this paper) at any particular concentration of polymer depends on: (a) the length and number of extended segments, and (b) the available surface onto which extended segments can bridge.

As polymer adsorbs, the number of extended segments increases, but at the same time the free surface area is decreasing. In terms of the parameters τ, the total segments per polymer molecule, and β, the number that adsorb and cover surface sites, it is further proposed that as more and more polymer is adsorbed, each incoming molecule finds progressively less and less surface onto which it can attach; *i.e.*, as P_0 increases, for a given molecular weight, β will decrease to a constant value determined by the conditions of agitation. The constant value may be thought of as that critical number of segments per molecule that must be attached, under a given condition of shear, for the polymer molecule to stay adsorbed.[6]

Effect of Molecular Weight.—The $Q_m - M$ behavior of Fig. 2 may also be a result of two competing processes. From the data of Jankovics,[12] b decreases with increasing molecular weight. As a first approximation, and by analogy to the Langmuir treatment, b is proportional to the ratio of the forward to reverse reaction rate constants for adsorption. For the present system, high molecular weight polymer reacts less extensively with the surface than does low molecular weight polymer. On the other hand, since β is changing only slightly, $(\tau - \beta)$ must be increasing rapidly with increase in M. The situation described previously as "steric" stabilization may thus result.[13] The extended segments in the case of the high molecular weight polymers may reduce the distance of closest approach between adjacent particles to an extent where their thermal energy may be in excess of their negative potential energy.[14]

The maximum in Q_m with increasing M, Fig. 2, can be described in terms of an increase in $(\tau - \beta)$, which at first favors bridging (Q_m increases), but which at high M leads to "steric" stabilization and consequently a decrease in Q_m.

Effect of Time of Agitation.—Consider a floc linked together by polymer bridges. It has been suggested that with prolonged time of agitation extended segments can curl back, adsorb on solid sites, and cause a contraction of the floc (contraction). Due to the reduction in bridge lengths in this process, the floc is less resistant to shear and will begin to break up. At the break-up of flocs, new surface is exposed, allowing further adsorption of polymer (redispersion). A third effect of time may be termed a redistribution reaction. Upon addition of the initial polymer solution to the dispersion, there may be regions of local excess concentration. Improved flocculation will result from distributing these local excesses.

The redistribution, contraction, and redispersion reactions, as defined above, may be thought to have the following independent effects.

1. Redistribution: No change in b or β but an increase in $(Q - Q_0)$ due to more efficient floc formation.

(12) L. Jankovics, Ph.D. Dissertation, Columbia University, 1961.

(13) W. Heller and T. L. Pugh, *J. Chem. Phys.*, **24**, 1107 (1956).

(14) W. Heller and T. L. Pugh, *J. Polymer Sci.*, **47**, 203 (1960).

2. Contraction: Increase in b and β, decrease in $(\tau - \beta)$ and hence decrease in floc size and filtration rate. The increase in b also reduces bridging.

3. Redispersion: Increase in b, probably no change in β. As more surface is covered $(Q - Q_0)$ will decrease.

The appearance of an optimum time of agitation can be understood in terms of these reactions. With prolonged time of agitation, contraction follows redistribution, and redispersion then follows contraction, so that Q_m first increases, passes through a maximum determined by the molecular weight and the intensity of agitation, and then finally decreases.

The variation of filtration rate with P_0, M, and t is thus a three-dimensional surface with sections of the form of Fig. 2, the maximum filtration rate and hence the maximum flocculation for the system being determined by P_0, M, and t, or formally: maximum in $(Q - Q_0)$ for the system occurs at $P_0 = P_m$ for $M = M_{0p}$ and $t = t_{0p}$.

In view of the complex nature of polymer adsorption–flocculation phenomena, it is felt that a more meaningful approach can be found by the use of eq. 2 (see Fig. 3). Sets of data in the form of Fig. 3 have been reproduced and except for the low concentration region, the equation has been found to have wide applicability.

Variation of P_m with M and t.—The effect of change in molecular weight and time of agitation on the optimum concentration of polymer is considerable. In eq. 6

$$P_m = \frac{(1 + bk/\beta)^2}{b} \qquad (6)$$

since b decreases with increase in molecular weight,[12] the numerator of the equation must decrease to a greater extent than b decreases with increase in molecular weight. This may be controlled by both b and β in the numerator, and to explain the $P_m - M$ dependence $d\beta/dM$ must be positive. It is probable that the factors of redistribution, contraction, and redispersion affect P_m in much the same way as they affect $(Q - Q_0)$. Further analysis of P_m in terms of b, β, and $(\tau - \beta)$ is in progress.

Concluding Remarks

It has been inferred that b is related to the ratio of rate constants for adsorption of polymer. At present this is an oversimplification, for it is not certain which reaction of polymer at the interface is described by this ratio. This question has been examined recently by Peterson and Kwei,[15] who like several other groups of workers found agreement of experiment with the Langmuir equation for polymer adsorption. Nevertheless, b can be thought of in terms of an extent of adsorption of polymer at the solid–liquid interface.

We have endeavored to point out that the adsorption reaction parameter, b, the number of segments adsorbed per polymer molecule β, and the number of extended segments per adsorbed molecule $(\tau - \beta)$ are the controlling factors in determining the adsorption-flocculation behavior for polymer–solid systems when P_0, M, t, and A are varied. The problem is complicated by the fact that adsorption and flocculation techniques do not yet yield accurate data. This is particularly so for the adsorption determinations.

(15) C. Peterson and T. K. Kwei, *J. Phys. Chem.*, **65**, 1330 (1961).

DISCUSSION

F. M. FOWKES (Shell Development Company).—In considering relative rates of coagulation of particles and adsorption of the polymers promoting the coagulation, the rate of adsorption should be considered in two steps as proposed by Peterson and Kwei (ref. 15). For rapid coagulation the first step (attachment of part of polymer molecule to surface) must be fast, and the second step (unrolling of polymer onto surface as a thin film) must be slow.

V. K. LA MER.—I think this view is correct. We had reached similar views independently of Peterson and Kwei. As explained in reply to Dr. Van Olphen's question, special methods must be developed to isolate and measure the component consecutive rate processes. I know of no way to do this at present, so all answers must be made on the basis of physical intuition and experience borrowed from other systems and processes.

H. VAN OLPHEN (Shell Development Company).—Is it permissible to consider the rate of establishment of polymer adsorption equilibrium fast with respect to the rate of coagulation?

V. K. LA MER.—We believe that the rate of coagulation of particles produced by the "bridging" action of polymers is the slower process and consequently the rate determining step. We believe that the primary adsorption of a polymer is fairly rapid but that the slow attainment of adsorption equilibrium under agitation arises at least in part from the breakdown of flocs offering new surfaces for adsorption. The bridging process we believe is slow because a polymer adsorbed on one particle must find another particle having a free surface available to complete the bridge. All of these questions are pertinent and merit further investigation when methods and procedures have been developed to measure the rates of these individual steps.

A. BAIDINS (du Pont Company).—In your discussion of flocculation of inorganic colloids by polymers you have completely neglected any charge on the colloid, and any ionization of the functional groups of the polymer. Since neutralization of the colloid charge by the ionized polymer also could effect flocculation, what is your reason for neglecting these effects?

V. K. LA MER.—Electric charge interactions, of course, enter into all colloid interactions and are mainly but not entirely responsible for pH effects with polymers. However, we learned early (about 1951) in the flocculation studies that electric charge was a secondary factor compared to the chemical adsorption of polymers with subsequent bridging as the main factor in polymeric flocculation. The fact that negatively charged polymers when acting on negatively charged colloidal particles induced more rapid and complete flocculation than did many positively charged polymers on the same particles offers incontrovertible evidence that chemical attractions between polymer and particle, when acting at short distances, overbalance the smaller long range electrostatic effects. Electrostatic effects are not to be ignored but the subject of flocculation has suffered from overemphasis on electrostatics to the neglect of chemical forces.

W. E. WALLES (Dow Chemical Company).—You have used the filtration rate as a parameter of flocculation. I wonder if you have considered other ways of characterizing flocculation and if so, why you selected filtration rate.

V. K. LA MER.—Yes, we have used rate of subsidence and to a lesser extent light scattering in the early work (1950–1954) as a measure of flocculation. However, we found that rate of filtration, when properly controlled and executed, furnished a much more reproducible, precisely measurable parameter. Since previous workers had neglected filtration and this parameter is of the greatest importance in many chemical engineering applications we decided to place our emphasis on filtration, which culminated in a theory of filtration.

THE EFFECT OF PRESSURE ON MICELLE FORMATION IN SOAP SOLUTIONS

BY R. F. TUDDENHAM AND A. E. ALEXANDER

Department of Physical Chemistry, University of Sydney, Australia

Received March 5, 1962

The electrical conductances of solutions of octyl-, decyl-, and dodecyltrimethylammonium bromides at pressures up to 3000 atm. have been measured and used to determine the critical micellar concentrations (c.m.c.). The expression $\Delta \bar{V}^0 = RT\,(\partial/\partial P \ln \text{c.m.c.})_{T,n_1,n_2}$, derived on the assumption that micelle formation can be approximated to a phase change, shows that the volume change accompanying micelle formation ($\Delta \bar{V}^0$) is initially positive but decreases with pressure and changes sign. Of the factors which could bring about the observed decrease in the c.m.c. above *ca.* 750 atm., an increase in dielectric constant of water would seem the most likely. This factor would influence the c.m.c. through the electrical forces involved in bringing the charged heads together.

Introduction

It is now generally agreed that the properties of dilute soap solutions, at concentrations not too far removed from the critical micellar concentration (c.m.c.) may be interpreted in terms of the spherical micelle proposed by Hartley.[1] The interior of these micelles approximates to the random distribution state of a liquid paraffin, while at their surface the hydrophilic end groups are constrained to remain in contact with the surrounding water.

To date, no investigation of the effect of pressure on the micelle-forming properties of soap solutions has been published in the literature. This is unfortunate for, apart from the intrinsic value of knowing the effect of pressure on the behavior of soap solutions, information about the factors affecting micelle formation and the structure of the micelles themselves may be gained by the introduction of pressure as a variable. In the present work our aim has been to determine the pressure-dependence of the c.m.c., to deduce from this the partial molar volume change in micelle formation, and to discuss the results in terms of the structure of the micelles.

Owing to the ease and accuracy of measurement, electrical conductance has been one of the most widely investigated properties of soap solutions. It has proved particularly convenient in studying the effect of temperature on micelle formation[2] and its measurement under high pressure, using the apparatus described below, involves no real difficulties.

Experimental

(a) Materials.—The *n*-decyl- and *n*-dodecyltrimethylammonium bromides were prepared from carefully purified alcohols kindly donated by Unilever Ltd. The alcohols were converted to the corresponding bromides by reaction with PBr_3. After distillation the bromides were dissolved in acetone and shaken with an excess of trimethylamine for several days during which time the quaternary ammonium salts crystallized out. The products then were extracted with ether in a Soxhlet extraction apparatus for 16 hr. and finally recrystallized from acetone. The *n*-octyltrimethylammonium bromide was prepared from *n*-octyl alcohol which had been carefully fractionated under reduced pressure.

Phenol (May and Baker) was purified by fractional distillation under reduced pressure and kept *in vacuo* over P_2O_5 prior to use.

(b) Apparatus.—The high pressure conductivity cell consists of a Pyrex hypodermic syringe of capacity 20 cc. with a sliding plunger which transmits the pressure from the surrounding oil to the solution within. Electrical connection between the solution and the wires from the pressure bomb is made *via* mercury contained in two side arms. The electrodes are lightly platinized to minimize the effects of polarization.

The cell constant, determined by calibration against 0.01 demal KCl at 25° using the data of Jones and Bradshaw,[3] was checked after each pressure run. It was assumed that the cell constant did not vary with pressure. The pressure vessel is designed to withstand pressures up to 3000 atm. The body of the bomb is constructed of Vibrac 30 (Ni-Cr-Mo) steel hardened to 70 tons/sq. in. ultimate tensile strength. Insulation of the electrical connecting leads from the remainder of the pressure vessel, by the method used here, requires that the plug unit and the conical connectors be made of a 25/20 stainless steel. This particular material has the property of forming a pressure-tight bond between itself and Pyrex glass when heated to slightly below the softening temperature of the glass. The tapered glass sleeves in this way insulate at pressures up to 3000 atm., although the weakness of the Ni-Cr steel precludes its use at higher pressures.

In order to prevent leakage of oil from the pressure vessel, the plug is sealed by an unsupported area packing (*cf.* Bridgman[4]). This rubber packing is backed up by the mild steel washers and a brass washer. Over the top of the packing materials fits a ring made of dead hard P.R.N.2 steel and, when the head nut is locked in position, the ring is forced down until the plug unit rests on the shelf inside the bomb. When connection between the oil tube of the plug unit and that from the pumping system is made and a pressure within the bomb is developed, the pressure in the packing exceeds this value and the seal is made.

The pressures were generated by means of the 3000 atm. pressure bench of W.C.t' Hart and Zn., Rotterdam. Briefly, this consists of a priming hand pump which serves to fill the apparatus with oil to a pressure of about 800 atm., and a pressure intensifier. The latter consists of a hand pump which applies a primary pressure P_1 to a piston of area A_1, thereby activating a smaller piston of area A_2 on the high pressure side. The ratio of the secondary pressure P_2 to P_1 approximately equals A_1/A_2. This ratio in our apparatus was 10:1 so that a primary pressure of only 300 atm. could be used to generate a pressure of 3000 atm. in the pressure vessel.

Pressures were measured on direct-reading Budenberg gages (0–6000 atm.). The resistances of the soap solutions were measured by means of the Wayne Kerr Universal Bridge B221. The instrument is capable of an accuracy of 0.1% in the range 9 ohms to 10C megohms and has a source frequency of 1590 c.p.s. Corrections for lead resistances and solvent conductance were made when these terms had a significant effect.

Temperature control was effected by means of a large oil thermostat in which the pressure vessel was immersed. In practice it was found that the heat generated by the stirrer exceeded heat losses to the surroundings. For this

(1) G. S. Hartley, "Aqueous Solutions of Paraffin Chain Salts," Hermann et Cie, Paris, 1936.

(2) B. D. Flockhart and A. R. Ubbelohde, *J. Colloid Sci.*, **8**, 428 (1953).

(3) G. Jones and B. C. Bradshaw, *J. Am. Chem. Soc.*, **55**, 1780 (1933).

(4) P. W. Bridgman, *Proc. Am. Acad. Arts and Sci.*, **49**, 625 (1914).

TABLE I

Concn. (molal)	Specific conductances × 10^2 (ohm^{-1} cm.$^{-1}$) 1 atm.	500 atm.	1000 atm.	1500 atm.	3000 atm.
	(a) Octyltrimethylammonium bromide (25°)				
0.1052	0.780	0.796	0.805	0.808	0.784
.1234	0.886	0.904	0.915	0.917	0.885
.1473	1.011	1.034	1.041	1.043	1.009
.1754	1.154	1.174	1.184	1.184	1.143
.2048	1.294	1.314	1.326	1.325	1.275
.2443	1.481	1.502	1.512	1.508	1.447
.2754	1.597	1.616	1.626	1.621	1.552
.3072	1.685	1.708	1.716	1.697	1.628
.346	1.825	1.849	1.852	1.843	1.732
	(b) Decyltrimethylammonium bromide (25°)				
0.02048	0.1845	0.1892	0.1916	0.1925	0.1877
.03167	.2752	.2815	.2858	.2869	.2790
.04105	.347	.356	.3605	.362	.3515
.06402	.513	.525	....	.532	.484
.08151	.577	.601	.606	.600	.526
.09884	.620	.644	.651	.642	.565
.1227	.677	.701	.710	.700	.616
C.m.c. (molal)	0.0646	0.0670	0.0670	0.0650	0.0556

Concn. × 10^2 (molal)	Specific conductances × 10^2 (ohm^{-1} cm.$^{-1}$) 1 atm.	500 atm.	1000 atm.	1500 atm.	3000 atm.
	(c) Dodecyltrimethylammonium bromide (25°)				
0.901	0.861	0.881	0.897	0.901	0.880
0.998	0.946	0.969	0.984	0.991	0.966
1.205	1.127	1.156	1.174	1.179	1.150
1.793	1.492	1.572	1.595	1.568	1.335
1.902	1.518	1.601	1.627	1.599	1.361
2.105	1.572	1.659	1.683	1.654	1.411
C.m.c. (molal)	0.01564	0.0161	0.01616	0.0156	0.01272
	(d) Dodecyltrimethylammonium bromide + phenol (0.1 molal) (25°)				
0.3029	0.285	0.294	0.299	0.302	0.298
.3532	.329	.338	.344	.348	.340
.4030	.375	.386	.392	.395	.375
.5028	.443	.469	.477	.475	.419
.7007	.524	.556	.569	.564	.504
.9015	.599	.632	.647	.644	...
1.099	.671	.708	.724	.720	.659
1.297	.741	.778	.796	.794	.735
C.m.c. (molal)	0.462×10^{-2}	0.500×10^{-2}	0.503×10^{-2}	0.488×10^{-2}	0.388×10^{-2}

reason, cooling water from a thermostat was circulated through a copper coil in the oil-bath. By proper choice of the temperature of the cooling water and the heater current, adjustable by means of a double decade transformer, the temperature of the bath could be controlled to ±0.01°.

Results and Discussion

The conductivities of the following soaps have been determined at varying pressures and concentrations: (a) dodecyltrimethylammonium bromide, (b) decyltrimethylammonium bromide, (c) octyltrimethylammonium bromide, (d) dodecyltrimethylammonium bromide in the presence of 0.1 molal phenol.

The c.m.c.'s were determined by plotting specific conductance against soap concentration. Of several plots examined, this was found the most satisfactory since, in general, two nearly linear branches are obtained with slopes sufficiently different to afford an accurate estimate of the c.m.c. as the point of intersection. However, in the case of the octyl soap, the change in slope at the c.m.c. (0.224 M[5]) was too small to permit reliable estimation of the c.m.c.

The detailed results, which are given in Table I, show that the c.m.c. *vs.* pressure curve passes through a maximum at *ca.* 750 atm., and that this curve is similar in shape with all the systems studied. The c.m.c.'s were also calculated in molar units, by making the assumption that the compressibility of the dilute solutions used equaled that of pure water, and by using the data of Bridgman.[6] This somewhat increases the initial slope of the curve and the maximum is shifted to *ca.* 1000 atm. but the general shape is unchanged.

If we consider the equilibrium

soap molecule in solution $\rightleftharpoons$ soap molecule in micelle

we may write for the chemical potential of the non-micellar soap

(5) H. J. S. Trap and J. J. Hermans, *Konikl. Ned. Akad. Wetenschap.*, **B59**, 298 (1956).

(6) P. W. Bridgman, *Proc. Am. Acad. Arts and Sci.*, **48**, 338 (1912–1913).

$$\mu_s = \mu_s^0 + RT \ln a_s$$

and for the micellar soap

$$\mu_m = \mu_m^0 + RT \ln a_m$$

If true equilibrium exists between the two species

$$\mu_m = \mu_s$$

We have, therefore

$$\Delta\mu^0 = \mu_m^0 - \mu_s^0 = RT \ln m_s\gamma_s - RT \ln a_m$$

where m_s and γ_s are the molality and corresponding activity coefficient of the non-micellar soap.

Introducing the expression

$$\left(\frac{\partial\mu_i}{\partial p}\right)_{T,n_1,n_2..} = \bar{V}_i$$

$$\Delta\bar{V}^0 = RT\left(\frac{\partial}{\partial p}\ln m_s\right)_{T,n_1,n_2..} + RT\left(\frac{\partial}{\partial p}\ln \gamma_s\right)_{T,n_1,n_2..} - RT\left(\frac{\partial}{\partial p}\ln a_m\right)_{T,n_1,n_2}$$

If we make the assumption that the activity of the soap molecule in the micelle is constant and that the process of micelle formation can be approximated to a phase change, the last term disappears. Further, assuming that the change in the activity coefficient of the single soap molecules with pressure can be neglected, we arrive at the expression

$$\Delta\bar{V}^0 = RT\left(\frac{\partial}{\partial p}\ln m_s\right)_{T,n_1,n_2..} \qquad (1)$$

In equation 1 $\Delta\bar{V}^0$ is the partial molar volume change involved in the formation of micelles from single soap molecules in their standard state. Moreover, if we make the usual assumption that the concentration of single soap molecules becomes constant and equal to the c.m.c. once micelles start to form, m_s becomes identified with the c.m.c.

Equation 1 thus affords a method of determining the partial molar volume change in micelle formation from the pressure dependence of the c.m.c. Although the above relationships were derived for non-ionic soaps, similar results are obtained for uni-univalent colloidal electrolytes. For dodecyltrimethylammonium bromide $\Delta\bar{V}^0$ varies from +2.3 cc. at 1 atm. to −4.5 cc. at 3000 atm., the change of sign occurring at *ca.* 750 atm.

The positive $\Delta\bar{V}^0$ at atmospheric pressure has been explained[7] as follows: The paraffin chains of the single soap molecules possess a high hydrocarbon–water interfacial energy and as a result are under a high compressive force tending to reduce the surface area. Upon aggregation, when the hydrocarbon–water contact area is almost completely eliminated, the chains are more free to expand, so that $\Delta\bar{V}^0$ increases.

The micelles having necessarily a fairly "open" structure will no doubt have a high compressibility relative to the molecularly dispersed soap whose volume should decrease only slightly under pressure. Thus a decrease in $\Delta\bar{V}^0$ with increasing pressure could reasonably be expected.

No density data is available for the systems studied here, so that $\Delta\bar{V}^0$ at 1 atm. is not known. Such data is, however, available for *n*-dodecyl sodium sulfate, dodecyl sulfonic acid, potassium octoate, and potassium laurate, giving values for $\Delta\bar{V}^0$ of approximately 12, 12, 11, and 13.5 cc. per mole, respectively. These are seen to be substantially greater than the values of $\Delta\bar{V}^0$ found here at 1 atm. on the assumptions made in the derivation of equation 1.

However, in the derivation of $\Delta\bar{V}^0$ in equation 1 it was assumed that the micelles could be approximated to a separate phase and it is probably the inaccuracy of this assumption which leads to the surprising observation that at pressures above 750 atm., $\Delta\bar{V}^0$ becomes negative. Hutchinson and co-workers[8] have discussed the question of regarding the micelles as a pseudo-phase and point out that although a number of the properties of soap solutions may be treated in this way, certain results, *e.g.*, the depression of the c.m.c. by added salts, must be regarded as surface effects.

An alternative approach is to apply the law of mass action to the single soap ion–micelle equilibrium

$$NR^+ + (N - Z)Br^- \rightleftarrows M^{Z+}$$

The micelle (M) of net charge Z is formed from N long-chain quaternary ammonium ions and $(N-Z)$ bromide ions. The calculation of the equilibrium constant K_m, from which the standard free energy change ΔG^0 can be found, has been performed by Phillips,[9] who found

$$\Delta G^0 = RT\left(2 - q/N - \frac{1}{N}\right)\ln \text{c.m.c.} \qquad (2)$$

In equation 2, q, the effective charge on the micelle, may be calculated from light-scattering data.[10] Also since

$$(\partial G/\partial p)_{T,n_1,n_2\ldots} = V$$

$$\Delta V^0 = RT\frac{\partial}{\partial p}\left\{\left(2 - q/N - \frac{1}{N}\right)\ln \text{c.m.c.}\right\}_{T,n_1,n_2} \qquad (3)$$

Equation 3 shows that ΔV^0 depends not only on the pressure-dependence of the c.m.c. but also on the effect of pressure on the charge and size of the micelles. Unfortunately, no data on the latter effect is available at present. It should be noted that when the micelles become infinitely large $(1/N \rightarrow 0)$ and complete ionization occurs $(q \rightarrow N)$ at all pressures, the terms involving q and N vanish. Under these conditions the phase separation and mass action approaches yield the same result.

Of the factors affecting micelle formation the two probably influenced most by the application of pressure are: (a) the hydrocarbon–water inter-

(7) A. E. Alexander and P. Johnson, "Colloid Science," Oxford, 1949, p. 688.

(8) E. Hutchinson, A. Inaba, and L. G. Bailey, *Z. physik. Chem.* (Frankfurt), **5**, 344 (1955).

(9) J. Phillips, *Trans. Faraday Soc.*, **51**, 561 (1955).

(10) K. J. Mysels, *J. Phys. Chem.*, **58**, 303 (1954).

facial energy and (b) the electrical work required to bring the charged heads of the soap ions together.

With regard to the former, we would expect that an increase in interfacial tension would decrease (*i.e.*, make more negative) the free energy of micelle formation and lead to a decrease in the c.m.c. Of the limited data available, Michaels and Hauser[11] have measured the interfacial tension between *n*-decane and water at elevated temperatures and pressures up to 700 atm. At room temperature there is a slight increase in γ followed by a decrease at pressures over 500 atm. The effect of this alone would be the reverse of that actually observed—*i.e.*, a minimum in the c.m.c. *vs.* pressure curve would be obtained.

The electrical work performed in bringing the ionic heads together depends directly on the dielectric constant of the medium. Scaife[12] has found a steady increase in the dielectric constant of water at 20° up to 6000 atm. and at 3000 atm. it has increased by about 14%. Now, an increase in dielectric constant means that the coulombic repulsive forces between the ionic parts of the soap ions are reduced. Micelle formation occurs therefore with greater ease and the c.m.c. is depressed.

In conclusion, we may offer a tentative explanation of the changes in the c.m.c. with pressure as follows. Initially there is a rise in the c.m.c. owing to the positive sign of the volume change involved in the formation of micelles from single molecules. This may arise from the expansion of the soap ion in the micelle as a result of the loss of hydrocarbon–water interfacial energy as suggested above, or it may be due to decreased solvation in the micellar state as a result of the proximity of the ionic heads and the subsequent incomplete orientation of the surrounding water of solvation. Both explanations seem reasonable. The decrease in the slope of the c.m.c. *vs.* pressure curve with pressure is explained by two effects—the decrease in $\Delta\bar{V}^0$ as a result of the higher compressibility of the micelles and the increase in the dielectric constant of water, resulting in the micelles forming at lower concentrations. The negative slope of the curve above 750 atm. is ascribed to the predominance of the latter effect. On available data any change of the interfacial tension between the hydrocarbon part of the soap molecule and water would appear unlikely to affect the c.m.c. markedly.

(11) A. S. Michaels and E. A. Hauser, *J. Phys. Chem.*, **55**, 408 (1951).
(12) B. K. P. Scaife, *Proc. Phys. Soc.* (London), **B68**, 790 (1955).

Acknowledgment.—We would like to record our considerable debt to Dr. A. Ewald of the C.S.I.R.O. High Pressure Laboratory for the provision of facilities and assistance. The alcohols used were kindly donated by Unilever Ltd. This work was carried out during the tenure by R. F. T. of a General Motors–Holden Research Fellowship.

DISCUSSION

K. J. MYSELS (University of Southern California).—It may be worth pointing out some surprising peculiarities of the interesting data given in this paper, especially for the two pure compounds showing a c.m.c. First, pressure generally increases the conductance by a small amount below the c.m.c. and by somewhat more above the c.m.c., except that at the highest pressure the conductance is decreased substantially for concentrations above the c.m.c. Second, the conductance of a surfactant solution is generally ascribable as a first approximation to the conductivity of the unmicellized component plus that of the micellized one, and depending on the concentration can be represented as either

$$\kappa = aC \quad \text{or} \quad \kappa = a\ (\text{c.m.c.}) + b\ (\text{C-c.m.c.})$$

where a and b are the differential (or more exactly, partial) conductivities. Different factors, such as temperature, common ions, or changes in chain length, affect a, b, and the c.m.c. so that κ is affected proportionately below the c.m.c. but in a complicated way above the c.m.c.

According to the present results, the ratio of κ at any pressure to that at one atmosphere is almost constant below the c.m.c. as expected, but is also quite constant, though at a different value, above the c.m.c. For example, for the C_{12} compound at 3000 atm. the values are 1.021 ± 0.001 and 0.896 ± 0.002. As a direct consequence the differential conductivity above the c.m.c., b, is affected very differently at different concentrations. The effect involves small differences, but seems to be beyond the experimental error.

A. E. ALEXANDER.—The specific conductances of soap solutions both above and below the c.m.c. undergo an initial increase followed by a decrease at higher pressures. The maximum in the conductance *vs.* pressure curve is common to solutions of all strong electrolytes in water. The initial rise is due to two effects: (a) the concentration of electrolyte is increased upon the application of pressure owing to the compressibility of the solution, and (b) the viscosity of water passes through a minimum at about 1000 atm. The fall in conductance at pressures above 1500 atm. is attributable to the rapidly increasing viscosity of water (P. W. Bridgman, *Proc. Amer. Acad. Arts Sci.*, 61, 57 (1926). Owing to our lack of knowledge of the way in which pressure affects such factors as the charge and size of the micelles, no explanation of the pressure dependence of the conductance of micellar solutions can be offered at present.

THE MICELLE PHASE OF CALCIUM DINONYLNAPHTHALENE SULFONATE IN *n*-DECANE

BY FREDERICK M. FOWKES*

Shell Development Company, Emeryville, California

Received March 12, 1962

In *n*-decane at 25° calcium dinonylnaphthalene sulfonate (CaDNNS) forms a saturated molecular solution at concentrations less than 10^{-6} mole/liter. Solute in excess of this concentration is in the form of micelles with an axial ratio of 2 averaging 12 molecules each. Interfacial tension measurements at the decane/$Ca(NO_3)_2$ solution interface show the chemical potential of CaDNNS to be constant from 10^{-6} to 10^{-3} mole/liter. This means that the micelles are a separate, though soluble, phase of CaDNNS. This is in contrast to the previously accepted hypothesis that micelles equilibrate with dissolved molecules according to the mass law principle.

Introduction

Micellar equilibria have been studied primarily in aqueous solutions of ionized detergents such as the sodium alkyl sulfates, where the effect of concentration[1] or added salt[2] has been explained by use of the mass law equations. Hutchinson proposed that in these systems the micelles may be treated better as a separate phase in equilibrium with molecularly dispersed solute having a chemical potential independent of the amount of micelle phase present.[3]

Micelles in non-aqueous media are hardly representative of all micelles, but it is certainly of interest to see whether these equilibrate by mass law equations or as a separate phase. Several investigators have reported on the properties of these micelles[4-10] in which the polar "heads" form the center of the micelle and the hydrocarbon "tails" are in contact with the solvent.

Theory.— If micelles are a separate but soluble phase in equilibrium with a saturated molecular solution, the chemical potential of the latter must remain constant no matter how much solute is in the micellar phase. Any measure of the chemical potential of the solute could be used to determine whether it is changed by changing ratios of micellar to molecular dissolved phase. Interfacial tensions between the decane solutions of CaDNNS and 1 *M* aqueous $Ca(NO_3)_2$ have been used in this study.

If CaDNNS associates in *n*-decane to form *n*-mers according to the mass law principle

$$n\text{CaDNNS} \rightleftarrows (\text{CaDNNS})_n$$

$$K_m = \frac{[(\text{CaDNNS})_n]}{[\text{CaDNNS}]^n} \times \frac{f_m}{f^n} \qquad (1)$$

where f is the activity coefficient of the molecularly dispersed sulfonate and f_m is the activity coefficient of the micelles. When $[(\text{CaDNNS})_n] >> [\text{CaDNNS}]$, the total concentration C is negligibly different than $[(\text{CaDNNS})_n]$. Then

$$\text{d ln } [\text{CaDNNS}]f = \frac{1}{n} \text{d ln } Cf_m \qquad (2)$$

The interfacial tension between the decane solution and the 1 *M* $Ca(NO_3)_2$ is governed by the Gibbs absorption equation

$$\frac{d\gamma_{ow}}{\text{d log } [\text{CaDNNS}]f} = \frac{-2.3kT}{A} \qquad (3)$$

where γ_{ow} is the interfacial tension and A the area per molecule in this interfacial film. Combination of equations 2 and 3 gives

$$\frac{d\gamma_{ow}}{\text{d log } Cf_m} = \frac{-2.3kT}{nA} \qquad (4)$$

for the change of γ_{ow} with C well above the critical concentration for micelle formation *if* the mass law is valid.

Experimental Details

Materials.—Dinonylnaphthalene was prepared by aluminum chloride-catalyzed alkylation at 60° using fractionally distilled 1-α-nonenes derived from trimerization of propylene. A heart cut of the dinonylnaphthalene fraction was then sulfonated with Sulfan B at −8° and titrated to neutralization with sodium hydroxide. Isopropyl alcohol extraction was used to separate NaDNNS from the unsulfonated oil, and the calcium salt was prepared by contacting with concentrated $CaCl_2$ solutions. The molecular weight was found by sulfate ash determinations to be 930, as compared with the theoretical value of 958. Presumably a small amount of dealkylation occurred during sulfonation. CaDNNS is quite hygroscopic; consequently it was freeze-dried from benzene solutions, pumped out at room temperature at less than 1 mm. pressure, and the resulting fluffy powder dissolved in dry solvent, Phillips 99 mole % *n*-decane, which was dried with molecular sieves. Reagent grade $Ca(NO_3)_2$ was used in doubly distilled water.

Diffusion coefficients were measured at 25° in the Spinco Electrophoresis-Diffusion apparatus, using schlieren optics. Concentration differences of 2 g./l. were used and the coefficients were calculated from the time dependence of the second moments; the latter were calculated with a Bendix computer programmed for second moments by S. J. Rehfeld.

Sedimentation coefficients were determined at 25° with the Spinco Analytical ultracentrifuge using schlieren optics at the higher concentrations and ultraviolet absorption optics at 10^{-4} mole/liter.

Intrinsic viscosity [η] and partial specific volume $\bar{v}$ were measured at 25° by normal analytical methods.

Interfacial tensions were measured at 25° by the pendant drop method. At the higher concentrations equilibrium was attained rapidly but at concentrations of less than 10^{-4}

* Sprague Electric Co., North Adams, Mass.

(1) K. Durham, "Surface Activity and Detergency," The Macmillan Co., London, 1961, Chapter 2.

(2) M. L. Corrin and W. D. Harkins, *J. Am. Chem. Soc.*, **69**, 683 (1947).

(3) E. Hutchinson, A. Inaba, and L. G. Bailey, *Z. physik. Chem.*, **5**, 344 (1955); E. Hutchinson and K. Shinoda, *J. Phys. Chem.*, **66**, 577 (1962).

(4) S. M. Nelson and R. C. Pink, *J. Chem. Soc.*, 1744 (1952).

(5) M. B. Mathews and E. Hirschhorn, *J. Colloid Sci.*, **8**, 86 (1953).

(6) C. R. Singleterry, *J. Am. Oil Chemists' Soc.*, **32**, 446 (1955).

(7) M. van der Waarden, *J. Colloid Sci.*, **5**, 448 (1950).

(8) J. G. Honig and C. R. Singleterry, *J. Phys. Chem.*, **58**, 201 (1954).

(9) S. Kaufman and C. R. Singleterry, *J. Colloid Sci.*, **10**, 139 (1955).

(10) S. Kaufman and C. R. Singleterry, *ibid.*, **12**, 465 (1957).

mole/liter more than an hour was required. To speed this process drops were purposely made large originally and then partly retracted into the syringe to compress the adsorbed film. In these drops interfacial tensions lower than equilibrium were obtained but these rose rapidly to the equilibrium values. Apparently there is a lower energy barrier to desorption than adsorption in these monolayers.

Pressure—area relations of an insoluble monolayer on 1 M $CaCl_2$ were measured at 25° with an automatic recording film balance[11] by Dr. R. C. Nelson. This will be reported in more detail later. From this isotherm it is estimated that $A = 110$ Å.^{2}/molecule at 50 dynes/cm.

Experimental Results

Table I shows the sedimentation coefficients which extrapolate to $s_0 = 2.54 \pm 0.07 \times 10^{-13}$ sec. for dry systems; larger values were obtained in the presence of moisture. The partial specific volume of CaDNNS in n-decane at 25° was 0.882 ± 0.002 ml./g. The intrinsic viscosity $[\eta]$ is 0.0254 g./dl. or 0.0288 ml./dl. This corresponds to an axial ratio of 1.9 if rod-shaped and 2.1 if disk-shaped.[12] From these values the ratio of the frictional coefficient to the frictional coefficient of non-solvated spheres f/f_0 is found to be 1.038 for rods and 1.047 for disks.[13] These values of s_0 and f/f_0 give the gram-micellar weight M as 11,000 ± 300. This corresponds to an average of 11.8

TABLE I

SEDIMENTATION AND DIFFUSION COEFFICIENTS FOR CaDNNS IN n-DECANE AT 25°

Concn., g./l.	s, sec. ($\times 10^{13}$)	D, cm.^{2}/sec. ($\times 10^6$)
20	2.07	..
10	2.36, 2.26	..
9	.....	1.17
7	.....	1.15
5	2.35, 2.45	1.16
3	.....	1.21
1	.....	1.32
0.01	2.47	..

± 0.3 molecules/micelle. The diffusion coefficients shown in Table I extrapolate at infinite dilution to $D_0 = 1.43 \times 10^{-6}$, which together with the value of s_0 gives $M = 12{,}240 \pm 400$; this corresponds to 13.1 ± 0.4 molecules/micelle. A proposed structure for a 12-molecule micelle with axial ratio 1.8 is shown in Fig. 1. This aggregation number is definitely larger than the 5 reported previously in fluorescence depolarization measurements of Rhodamine B solubilized by CaDNNS in benzene.[8] It was suspected that this dye may have reduced the aggregation number because of interaction with the polar groups, so some leuco-Rhodamine B was added to a CaDNNS solution and centrifuged with schlieren optics. It was found that the schlieren peak sediments nearly twice as fast as the red color of the relatively few micelles with solubilized dye; the sedimentation coefficient for the latter was 1.6×10^{-13} sec. at a total concentration of 5 g./l. of CaDNNS.

The equilibrium interfacial tensions of n-decane solutions of CaDNNS *versus* 1 M $Ca(NO_3)_2$ at 25° are shown in Table II at concentrations from

(11) M. J. Schick, *J. Polymer Sci.*, **25**, 465 (1957).

(12) R. Simha, Proceedings International Congress Rheology, Amsterdam, 1948, Vol. II, p. 70.

(13) T. Svedberg and K. O. Pedersen, "The Ultracentrifuge," Oxford Press, New York, N. Y., 1940, p. 41.

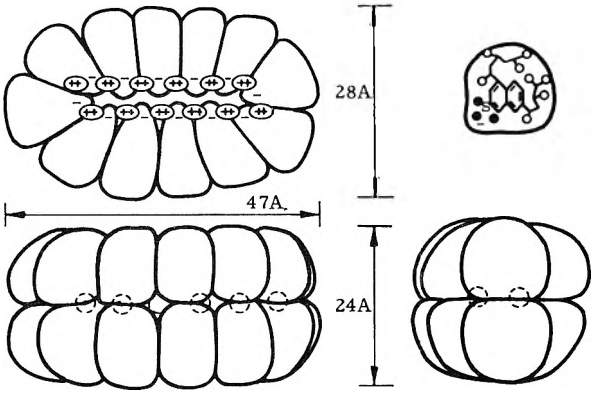

Fig. 1.—A model of the CaDNNS micelle in agreement with sedimentation and viscosity measurements. Methyl groups in upper right diagram are shown as open circles.

10^{-3} to 10^{-6} mole/l. The values at all concentrations are 0.93 ± 0.09 dyne/cm., with no significant concentration-dependence of interfacial tension.

TABLE II

EQUILIBRIUM INTERFACIAL TENSIONS OF CaDNNS SOLUTIONS IN n-DECANE AT 25°

Concn., moles/l.	Interfacial tension, dynes/cm.	Av. ± std. dev., dynes/cm.
10^{-6}	0.85, 0.97, 1.08, 1.10	1.00 ± 0.11
10^{-5}	.85, .92, .97, 0.99	0.93 ± .06
10^{-4}	.83, .85, .95, 1.00	.91 ± .08
10^{-3}	.89, .89	.89
		0.93 ± 0.09

Discussion

If the mass law were to govern the equilibrium between CaDNNS molecules and micelles the slope of interfacial tension *versus* log c would be as shown in equation 4

$$\frac{d\gamma_{ow}}{d \log cf_m} = \frac{-2.3kT}{nA} = \frac{-960 \times 10^{-16}}{12 \times 110 \times 10^{16}} =$$

$$-0.73 \text{ dyne/cm.}$$

The value of f_m is nearly constant at all concentrations as shown by the values in Table I of the diffusion coefficient. If the mass law applied, a 2.2 dynes/cm. fall of interfacial tension would be found from 10^{-6} to 10^{-3} mole/l., 25 times the standard deviation. Thus, the constancy of interfacial tension is strong evidence that these micelles act as a separate soluble phase in equilibrium with a saturated solution of CaDNNS molecules of very low concentration (below 10^{-6} mole/l.).

Similar results have been obtained with NaDNNS and NH_4DNNS solutions in n-decane.

Acknowledgment.—The interfacial tension measurements are the result of the patience and painstaking care of S. Beckley. The help of S. J. Rehfeld in measurements of sedimentation and diffusion coefficients is gratefully acknowledged.

DISCUSSION

C. R. SINGLETERRY (Naval Research Laboratory).—Experience in our Laboratory confirms Dr. Fowkes's observation that the activity of the monomeric CaDNNS is nearly constant in the experimentally accessible range of sulfonate concentrations. Monolayers of BaDNNS isolated on stainless steel surfaces by retraction of an aromatic

solvent have critical surface tensions which appear to be independent of solute concentration over a considerable range.

Our experience in comparing the dye method with the ultracentrifuge method for micelle size is somewhat different than that just reported. We find substantial agreement between the fluorescence depolarization technique, the ultracentrifuge, osmotic pressure, and cryoscopic methods when we study BaDNNS in benzene. It is reasonable to expect that the micelle size for a given sulfonate may be distinctly different in aliphatic and in aromatic solvents.

F. M. FOWKES.—Prof. Kitahara has directed my attention to his publication on micelle size of aerosol OT in cyclohexane, benzene, and other solvents [*J. Phys. Chem.*, **66**, 363 (1962)]. The much larger micellar weight in cyclohexane (25,000) as compared with benzene (10,500) is interesting in comparison with our 12,000 for CaDNNS in decane *vs.* the Naval Research Laboratory finding of 5,000 for CaDNNS in benzene.

J. LYKLEMA (University of Southern California).—In this work the micellar weight was considered to be constant, whereas in other cases of micelle formation in non-polar media n increases with concentration. Is there any justification for this? In connection with this, the diffusion and sedimentation constants decreased markedly with increasing concentration (Table I). What is the physical significance of these variations and of the extrapolations?

F. M. FOWKES.—The 10% decrease in sedimentation coefficient with a change of concentration of 10 g./l. is only slightly greater than the value expected for non-solvated spheres of concentration-independent mass. The concentration effect on diffusion coefficient is also small. The s values measured at 0.01 g./l. were nearly identical with those found at 5 g./l. Thus it has been experimentally demonstrated that the size of these micelles is concentration-independent.

K. J. MYSELS (University of Southern California).—There is mention that the presence of water changes the sedimentation behavior of this system. How can you compare interfacial measurements in which an effort has been made to equilibrate with an aqueous phase with centrifugation results in the anhydrous system?

F. M. FOWKES.—The sedimentation measurements were made in rather dry systems but not dry enough to remove the last water molecule from each calcium ion. The effect of adding excess water (without salt) is to double the micellar size, apparently by solubilization of water. The aggregation number may increase at the same time, but certainly not by very much (not to 20, for example). If n were as large as 20, the slope of interfacial tension *vs.* log concentration should be -0.4 as compared with experimental values of less than -0.04. The presence of 1 M salt should reduce the amount of water solubilized.

MONOLAYERS OF MYRISTYL AND CETYL ESTERS OF OXALIC, MALONIC, SUCCINIC, GLUTARIC, ADIPIC, AND PIMELIC ACIDS[1]

BY J. L. SHERESHEFSKY, H. T. CARTER,[2] E. NICHOLS,[3] AND P. L. ROBINSON[4]

Chemistry Department, Howard University, Washington, D. C.

Received March 2, 1962

Monolayers of dicetyl esters of the first six members of the homologous series of dicarboxylic acids were studied, including dimyristyl oxalate, monocetyl oxalate, and monocetyl malonate. The study included measurements of surface pressure *vs.* area and surface potentials *vs.* area. It was found that the monolayers were dependent upon the concentration of the spreading solution, and also on the maximum spreading area. These substances form condensed and liquid-expanded films, and vapor-expanded films tend to form when spread from very dilute solutions. The oxalates tend to form a condensed film of high stability that folds upon itself. Orientations of the head-groups are given, and the calculated vertical components of the dipole moments are in good agreement with the measured values.

This work is a continuation of previous studies[5,6] on the properties of monolayers of esters of dibasic acids. Alexander and Schulman[7] have studied the properties of monolayers of ethyl esters of fatty acids, and Adam and Jessop[8] of diethyl esters of long-chain dibasic acids, while in the present study an attempt has been made to elucidate the behavior of long-chain esters of dibasic acids with short CH_2– group bridges between the carboxylic groups. The orientation of the polar groups and the properties of the latter esters are different in many respects.

Experimental

Preparation of Materials.—The dimyristyl and dicetyl esters of the acids, except adipic, were prepared by digesting an excess of the myristyl or cetyl alcohol with a quantity of the acid at a temperature near 100° but lower than the m.p. of the acid, after the addition of 2 or 3 drops of sulfuric acid. The disappearance of the solid phase, which was not very soluble in the molten alcohol, served to indicate when the esterification was near completion. In the case of adipic acid dry hydrogen chloride gas was used instead of sulfuric acid in order to eliminate excessive charring of the reaction mixture.

The mixture was cooled, dissolved in benzene, and the sulfuric acid was removed with powdered barium hydroxide. The solution was dried by allowing it to stand over anhydrous sodium carbonate. After removing the solid material by filtration, the benzene was distilled off, and the product was crystallized from ethyl alcohol several times.

The monocetyl oxalate and malonate were prepared from the silver salt of the acid and cetyl chloride, and the purified product was obtained by crystallization.

The molecular weights of the products were determined by the Rast method, and the values obtained differed from the formula weights by 3.5–9.8%. The m.p.'s of the compounds are given in Table I.

The solvents, benzene and chloroform, were distilled several times and tested for surface impurities.

Film Balance.—The surface pressure–area relationships were determined by Wilhelmy and Langmuir balances. The former was equipped with an analytical chainomatic balance sensitive to 0.1 mg., from which was suspended a microscope cover glass 0.2 mm. thick and 5 cm. wide. The tray made of opaque quartz had the dimensions of 13 × 41 × 3 cm. The balance was enclosed and the enclosure was equipped with a mechanism that allowed compression and expansion of the film from the outside. The enclosure was also provided with a carriage that allowed the movement in *xy*-direction of an arm, carrying an air-electrode parallel to the surface of the substrate.

TABLE I

Compound	M.p., °C.
Dimyristyl oxalate	51.2–52.0
Dicetyl oxalate	55.2–55.9
Dicetyl malonate	50.4–51.1
Dicetyl succinate	58.4–58.8
Dicetyl glutarate	54.2–54.6
Dicetyl adipate	54.5–55.2
Dicetyl pimelate	56.8–56.9
Monocetyl oxalate	49.4–50.1
Monocetyl malonate	38.0–38.5

The surface pressure–area and potential–area measurements on the esters of glutaric, adipic, and pimelic acids were made with this balance. The pressure–area measurements of the other esters investigated in this study were made with a modified Langmuir type balance described elsewhere,[5] except that it was provided with an opaque quartz tray of dimensions 15.9 × 29 × 1.8 cm., and the mica float was attached to the tray with Teflon strips. The sensitivity of the balance varied, 0.14, 0.074, and 0.044 dyne per cm., depending on the gage of the tension wire used.

Electrometer.—The surface potentials were determined with a vacuum tube voltmeter or a Lindemann electrometer. In either case, the air electrode consisted of a silver or gold disk about 0.35 sq. cm. in area, coated with polonium or Ra 226 and emitting about 2000 alpha particles per second; it was held within 3 mm. of the surface.

The Lindemann electrometer with a precision Rubicon potentiometer was used in measuring the potentials of the monolayers of dicetyl and monocetyl malonate and dicetyl succinate. The General Radio Corp. Electrometer 1230A, with a maximum input resistance of 5×10^{14} ohms, was used in measuring the surface potentials of the monolayers of dimyristyl oxalate, monocetyl oxalate, dicetyl glutarate, dicetyl adipate, and dicetyl pimelate. The potentials of dicetyl oxalate were measured with both instruments.

Spreading of Monolayers.—The spreading solutions were of various concentrations: 1, 0.5, 0.25, 0.2, and 0.1 mg. per ml. of benzene or chloroform, as appropriately indicated in each case. The deposition of the spreading solution was made mainly with lambda pipets and occasionally with an "Agla" syringe. The substrates were either doubly distilled water, or 0.01 *N* aqueous hydrochloric acid, or both. From 10 to 15 min. was allowed for the evaporation of the solvent.

Experimental Results[9]

The Esters of Oxalic Acid.—The pressure–area diagram of dimyristyl oxalate, when the monolayer is spread from a 1 mg. per ml. benzene solution, is reproducible within a range of a fourfold amount of

(1) This work was supported under a project by the Naval Propellant Plant through the Office of Naval Research.

(2) A portion of this work is taken from the thesis of Herbert Thomas Carter, submitted in partial fulfillment of the requirements for the degree of Master of Science in Chemistry, Howard University, June, 1959.

(3) A portion of this work is taken from a thesis of Edgar Nichols which is being submitted in partial fulfillment of the requirements for the degree of Master of Science in Chemistry, Howard University.

(4) A portion of this work is taken from a thesis of Press Lee Robinson which is being submitted in partial fulfillment of the requirements for the degree of Master of Science in Chemistry, Howard University.

(5) J. L. Shereshefsky and A. A. Wall, *J. Am. Chem. Soc.*, **66**, 1072 (1944).

(6) J. L. Shereshefsky, *J. Phys. Chem.*, **61**, 1053 (1957).

(7) A. E. Alexander and J. H. Schulman, *Proc. Roy. Soc.* (London), **A161**, 115 (1937).

(8) N. K. Adam and G. Jessop, *ibid.*, **A112**, 376 (1926).

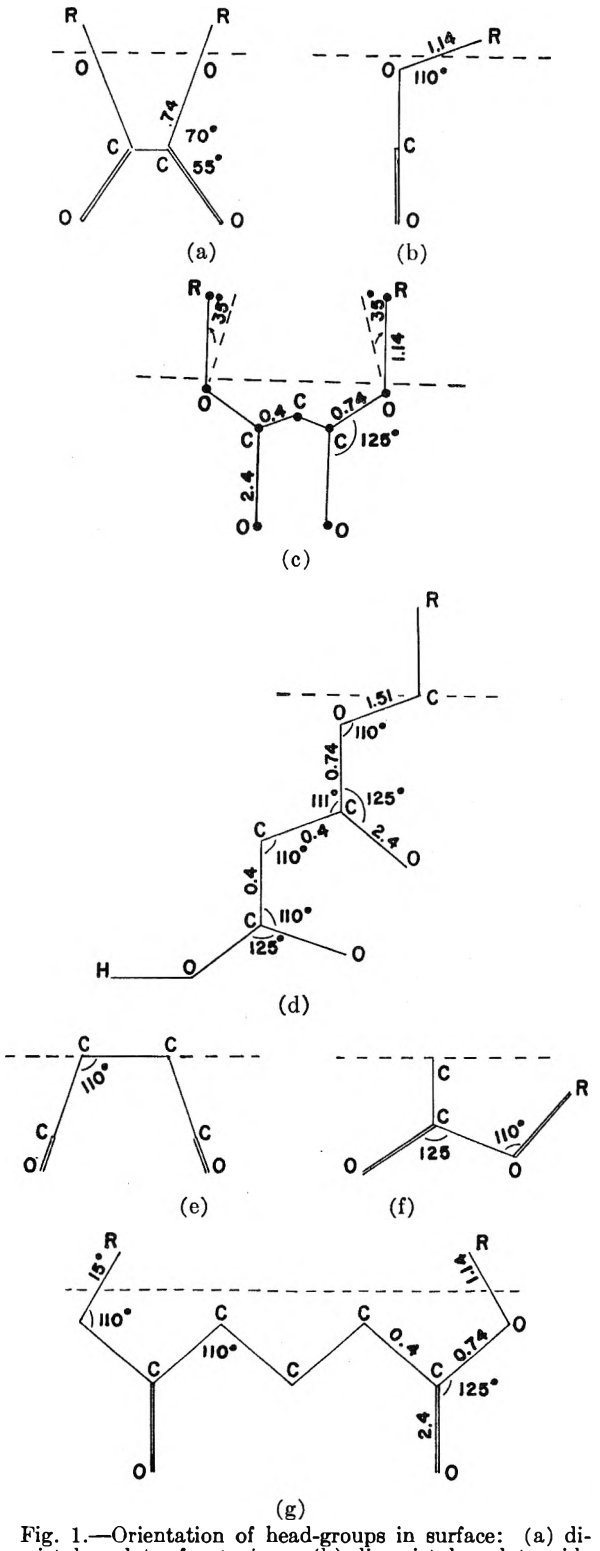

Fig. 1.—Orientation of head-groups in surface: (a) dimyristyl oxalate, front view; (b) dimyristyl oxalate, side view; (c) dicetyl malonate; (d) monocetyl malonate; (e) dicetyl succinate, front view; (f) dicetyl succinate, side view; (g) dicetyl glutarate.

material and a spreading area per molecule of about 140 sq. Å. Yet, this monolayer is abnormal in that its apparent limiting area is 19 sq. Å. per molecule, even though the molecule consists of two hydrocarbon chains with fourteen carbon atoms in each and no collapse or transition is evidenced up to 34 dynes per cm. of surface pressure.

The monolayer of this substance is concentration dependent, as its characteristics, such as state and limiting area, depend on the concentration of the spreading solution. Monolayers spread from a 0.2 mg. per ml. solution show the presence of a liquid-expanded state with a limiting area characteristic for a two-chain molecule, and a transition into the condensed state with a limiting area somewhat smaller than the characteristic value. In monolayers spread from benzene solutions 0.5 and 1.0 mg. per ml., the expanded state apparently is absent and the limiting areas decrease with increase in concentration of spreading solution.

The surface potentials of the expanded state increase on compression from about 175 to 275 mv. at 90 sq. Å. per molecule, where, at a pressure of 1.1 dynes per cm., transition to the condensed state sets in. The transition is accompanied by a continuous drop in potential to about 160 mv. at the highest compression of 19 sq. Å. per molecule. The vertical component of the dipole moment calculated from these potentials is the same for all compressions in the expanded state, indicating constancy of orientation of the polar group in the interface of the liquid-expanded state. The orientation giving a calculated value of 480 mD. for the vertical component, which is in good agreement with the experimental value of 495 mD., is shown in Fig. 1a, b. The moment was calculated from bond moments given in Smyth's[10] book, using the formula

$$\mu = \frac{n}{D}\,(m_1 \cos 35^\circ - m_2 \cos 21^\circ + m_3 \cos 70^\circ)$$

where n is the number of ester groups in the molecule, D is the dielectric constant of the medium assumed to be equal to 7, m_1, m_2, and m_3 are the bond moments for C=O, C–O, and O–R, taken as 2.4, 0.74, and 1.14 D., respectively.

The continuous fall from 495 to 70 mD. of the vertical moment in the condensed state shows that on compression to areas less than 90 sq. Å. per molecule, the head-groups are subject to continuous reorientation. X-Ray[11] analysis of the structure of dimethyl oxalate and Raman spectra[12] of oxalic acid in solution and crystalline state show a *trans* configuration in the crystal. This evidence, together with the above observations, leads us to believe that the reorientation in the condensed state consists of a gradual rotation of the ester groups with respect to each other, causing a greater and greater inclination to the vertical of the plane of the

C=O group, and tending to a planar *trans* configuration of least steric interference. The final

(9) Supplementary diagrams have been deposited as Document number 7154 with the ADI Auxiliary Publications Project, Photoduplication Service, Library of Congress, Washington 25, D. C. A copy may be secured by citing the document number and by remitting in advance $2.50 for photoprints or $1.75 for 35-mm. microfilm payable to: Chief, Photoduplication Service, Library of Congress.

(10) C. P. Smyth, "Dielectric Behavior and Structure," McGraw-Hill Book Co., New York, N. Y., 1955, p. 306.

(11) M. W. Dougill and G. A. Jeffrey, *Acta Cryst.*, **6**, 831 (1953).

(12) L. Bourdet, *J. Chem. Phys.*, **50**, 390 (1953).

vertical component of the dipole moment is, most likely, due to the moment of the O–R group which is inclined to the vertical with an angle of about 80°. This, of course, does not mean that the chain is not free to assume a more erect orientation, as only the first CH_2-group adjacent to the ether oxygen is involved.

The monolayers formed from the spreading solutions of 0.5 and 1 mg. per ml., except in the region larger than 90 sq. Å., where they start with lower values than for the expanded states, and where they continuously increase on compression, the potentials and vertical components of the dipole moments parallel the changes in the orientation of the headgroups in the condensed state. However, the values of these quantities are considerably higher. The potentials are about 75 mv. higher and the moments about 50 mD. higher.

The absence of an expanded state and the values of the moments in areas larger than 100 sq. Å., which are approximately equal to those in the condensed state at much smaller areas, lead us to the conclusion that dimyristyl oxalate tends to form dimers in the higher concentration spreading solutions because, perhaps, of dipole–dipole interaction, and the aggregates being in the *trans* configuration. This explains why the monolayers formed from concentrated spreading solutions show values for the limiting area which are about one-half or some other fraction of the normal value.

Surface pressure–area and potential–area diagrams of dicetyl oxalate monolayers on 0.1 *N* HCl and distilled water obtained from spreading solutions of 1 mg. per ml. of benzene are similar in all respects to the diagrams for dimyristyl oxalate obtained from concentrated spreading solutions. Monolayers obtained from dilute spreading solutions show larger limiting areas, such as 38 sq. Å. in the case of a spreading solution of 0.2 mg. per ml. These monolayers also depend on the quantity of material spread, as similar limiting areas were also obtained from a benzene solution 1 mg. per ml., when the maximum spreading area was about 250 sq. Å. per molecule. However, at high compression they tend to go over into monolayers with low limiting areas.

The surface potentials and vertical moments are similar to those for the dimyristyl ester in the condensed state and the molecular orientations in the film are very likely similar. From the value of the moment in the region larger than 45 sq. Å. per molecule, namely 125 mD., it follows that the orientation of the O–R group is inclined about 67° to the vertical.

The pressure–area diagrams for monocetyl oxalate indicate that monolayers of this substance on 0.01 *N* HCl are dependent on the quantity of material deposited and also on the concentration of the spreading solution. At a maximum spreading area of 51 sq. Å. per molecule, a monolayer on 0.01 *N* HCl gave a limiting area of 13 sq. Å. per molecule, while a monolayer with a maximum spreading area of 170 sq. Å. gave a value of 20 sq. Å. per molecule. Monolayers formed from dilute solutions, as for instance 0.2 mg. per ml., gave limiting areas of about 26–28 sq. Å. per molecule. The dipole moments were approximately equal to those for the dicetyl oxalate.

The Esters of Malonic and Succinic Acids.— The monolayers of dicetyl malonate on aqueous 0.01 *N* hydrochloric acid and on distilled water are condensed films with normal limiting areas between 45.7 and 46.7 sq. Å., and collapse pressures between 20 and 22 dynes per cm. The potentials rise on compression from about 650 to 950 mv. on 0.01 *N* hydrochloric acid, and from about 650 to 1050 mv. on distilled water. The vertical components of the dipole moments, on the other hand, drop from about 800 mD. to a constant value of 710 for the region of the condensed film extending from about 47 to 41 sq. Å. per molecule, on the acid substrate. On distilled water the vertical moment falls from about 875 to 790 mD. for the region extending from 49 to 41 sq. Å. per molecule. The calculated value of the vertical moment on the basis of the orientation shown in Fig. 1c is 900 mD. However, the steric interference due to the proximity of the two $C{\overset{O}{\diagup}}=O$ groups would cause the planes of each C=O group to rotate with respect to each other and around the carbon atom in the bridge, with the effect that the groups would incline toward the surface. Comparison of the measured values of the vertical moment with the calculated indicates that the angles of inclination of these groups toward the surface are about 63 and 55° in the low and high pressure regions, respectively, on the acid substrate, and 75 and 59° in the corresponding regions of the film on distilled water. The vertical component of the dipole moment was calculated by means of the formula

$$\mu = \frac{n}{D}(m_1 - m_2 \cos 124° + m_3 \cos 35° + m_4 \sin 35°) \cos\theta$$

where n, D, m_1, m_2, and m_3 have the same significance as defined earlier, and where m_4 is the C–C bond moment and θ is the angle of inclination of the C=O group toward the vertical.

The monolayers of monocetyl malonate have a limiting area per molecule of 28 sq. Å. on both the acid and the distilled water substrates, and their collapse pressure is about 24 dynes per cm. Their potentials rise steeply on compression, from about 350 to 1000 mv. on the acid substrate, and from about 550 to 950 mv. on distilled water. The vertical components of the moments rise only slightly from about 320 to 425 mD. on the acid substrate, and fall slightly from about 475 to 425 mD. on distilled water. The calculated value on the basis of the orientation represented in Fig. 1d is 432 mD. and the formula used for the calculations is

$$\mu = \frac{1}{D}(m_3 \cos 70° - m_2 + m_1 \cos 56° - m_4 \cos 69° + m_4 + m_1 \cos 55° + m_2 \cos 69°)$$

The monolayers of dicetyl succinate are in the condensed state, with limiting areas of 50.5 sq. Å. per molecule on the acid substrate and 48.8 sq. Å.

TABLE II

MONOLAYER PROPERTIES

Monolayer	No. molec. × 10^{-16}	Concn., mg./cc.	Area, sq. Å./molecule Max.	Lim.	Trans.	State	Pressure, dynes/cm. Max.	Collapse	Trans.
Dimyristyl oxalate	1.08–4.38	1.0	140	18		Condensed	34		
Dimyristyl oxalate	1.25	0.2	140	38		Condensed	17		
Dimyristyl oxalate	1.25	.2	140	100		Liq. expd.			1.1
Dimyristyl oxalate	1.25	.5	140	33		Condensed			
Dicetyl oxalate	3.76–9.33	0.5–1.0	55	21		Condensed	36		
Dicetyl oxalate	1.15	.2	90	34		Condensed	34		
Dicetyl oxalate	0.9 –1.12	.2	280	43		Condensed	14		
Monocetyl oxalate	1.70	1.0	170	20		Condensed	17		
Monocetyl oxalate	6.01	1.0	51	13		Condensed	10		
Monocetyl oxalate	0.77	0.2	350	26		Condensed	10		
Dicetyl malonate	3.46–5.28	1.0	~70	46		Condensed		21	
Monocetyl malonate	4.86–7.48	1.0	~45	28		Condensed		24	
Dicetyl succinate	2.63–4.16	1.0	~75	~50		Condensed		8	
Dicetyl glutarate	2.0	0.25	138	~43		Condensed	19		
Dicetyl glutarate	2.0	.25	138	~100	85	Liq. expd.			~4
Dicetyl glutarate	1.04	.10	269		135	Vap. expd.			~4
Dicetyl adipate	5.08	.5	92	31		Condensed	20		
Dicetyl adipate	2.54	0.25–0.20	159	43–48		Condensed	10		
Dicetyl adipate	2.72	.20	148	95	70	Liq. expd.			~3
Dicetyl pimelate	2.47	.25	156	~50		Condensed	9		
Dicetyl pimelate	2.47	.25	156	~120	90	Liq. expd.			~3

on distilled water. Their collapse pressure is very much lower than for the malonate esters, namely about 8 dynes per cm. Their potentials and vertical moments are approximately equal to those of the malonate esters; however, the orientation of the molecules in the monolayer must be different, as shown in Fig. 1e, f. At large areas per molecule, the potentials are higher than for the malonates and rise less steeply on compression until they reach values comparable to those of the malonate. The vertical moments remain nearly constant for the whole range of areas. The vertical components of the dipoles were calculated from the formula

$$\mu = \frac{n}{D}(m_1 \cos 55° + m_2 \cos 69° + m_3 \cos 40° + m_4 \cos 20°)$$

where the terms have the same significance as above. The value thus calculated is 785 mD. while the measured values are 765 mD. on the acid substrate and 850 mD. on distilled water. The difference can be accounted for by assuming different tilting of the O–R group.

Dicetyl Glutarate.—Monolayers of this substance obtained from spreading solutions of 0.5 and 1 mg. per ml. of solvent were not reproducible in the region of low pressure, and had limiting areas that varied with concentration of spreading solution. When spread from dilute solutions, the monolayers showed the presence of the condensed, liquid-expanded, and vapor-expanded states.

The limiting area of the condensed film is 43 sq. Å., and of the liquid-expanded about 100 sq. Å. The transition from liquid-expanded to vapor-expanded takes place at a pressure of 4 dynes per cm. and 135 sq. Å. per molecule. It was carefully explored and resembles a three-dimensional van der Waals isotherm below the critical temperature in that it goes through a point of maximum pressure in the transition region. A liquid-expanded film obtained from a spreading solution of 0.1 mg. per ml. of benzene is seemingly more stable than the one obtained from a spreading solution of 0.25 mg. per ml., as it withstands a higher pressure before changing into the condensed state.

The head-group of this molecule is highly flexible, insofar as the spacial arrangement of the various sub-groups, and its orientation is greatly influenced by pressure changes. The free orientation of the head-group is shown in Fig. 1g. The vertical component of its dipole moment calculated from the formula

$$\mu = \frac{n}{D}(m_3 \cos 15° - m_2 \sin 35° + m_1 + m_4 \sin 35°)$$

where the terms have the previously designated meaning, is 1.188 D., while the measured value at about 120 sq. Å. is 1.2 D. This moment falls only slightly on compression to about 70 sq. Å. per molecule, but falls steeply to 500 mD. at the limiting area of 43 sq. Å., and to 175 mD. at 27 sq. Å.

Dicetyl Adipate.—The monolayers of this substance resemble the preceding ones. When obtained from spreading solutions of benzene or chloroform of concentrations of 0.25 mg. per ml. and higher, the monolayers were not completely spread and had limiting areas that were concentration dependent. This is shown in Table II. Monolayers spread from more dilute solutions of either benzene or chloroform show the transition from the condensed to the liquid-expanded state, with a limiting area of the latter of about 95 sq. Å. It is to be noted that solutions of higher dilution are required to obtain the liquid-expanded state than in the case of dicetyl glutarate.

The head-groups of this molecule are bridged by four CH_2-groups and seem less flexible than in the glutarate ester for orientation in the surface with the maximum vertical moment. The representation

of its orientation is similar to that of the glutarate ester, as shown in Fig. 1g, and its vertical component of the moment is the same. The observed moments are low for monolayers obtained from the concentrated spreading solution; they are about 150 mD. from 90 to 31 sq. Å. per molecule, and from this limiting area to about 19 sq. Å. the vertical moment drops to 90 mD. The monolayers obtained from less concentrated spreading solutions possess higher moments, which continually decrease on compression until they reach a value of 275 mD. at the limiting area of 43 sq. Å., and 190 mD. at an area of 31 sq. Å. The monolayers formed from solutions 0.2 mg. per ml. possess the highest vertical component of the dipole, 1.1 D., which remains constant from 120 to about 70 sq. Å. per molecule. From the latter point, at which the expanded state begins to change to the condensed, the moment continually falls on compression, reaching values of 650 mD. at the limiting area of 48 sq. Å., and 350 mD. at 31 sq. Å.

Dicetyl Pimelate.—This substance formed condensed and liquid-expanded monolayers, the characteristic values of which, such as limiting area and transition pressure, varied with each monolayer. However, the potentials and the vertical components of the dipole moments were much more reproducible. The characteristic values of one of many surface pressure–area diagrams obtained are given in Table II. The correspondence between the pressure–area and potential–area measurements is good and the changes in the vertical moment in the transition region are characteristically similar to those of the two preceding members of the homologous series.

The head-groups of this molecule are even more flexible than in dicetyl glutarate; however, the orientation is the same. The maximum vertical moment measured, 1.210 D., is in good agreement with the calculated value of 1.188 D.

DISCUSSION

HERMAN E. RIES, JR. (American Oil Company).—What time intervals did you allow between pressure–area readings (points on curves)? Did you vary the rate of compression?

J. L. SHERESHEFSKY.—In general, from 3 to 5 min. were allowed to elapse from deposition to beginning of compression. However, in the case of the glutarates, adipates, and pimelates longer periods were used, particularly in transition regions.

J. N. WILSON (Shell Development Company).—How reversible are the force–area diagrams? Is the same force–area curve obtained during compression as during subsequent expansion? This question is relevant since the phenomena you have observed are complicated and the esters you have studied all melt above room temperature.

J. L. SHERESHEFSKY.—We have not studied the reversibility of the isotherms described. However, we have duplicated all isotherms, except those of the pimelate esters, under different experimental conditions.

V. K. LA MER (Columbia University).—It appears that by using benzene as solvent you have confirmed the findings of Robbins and La Mer that in this solvent the pressure–area isotherm is dependent upon the concentration of solute in that solvent, yielding different values for the area per molecule. Why did you not use a constant low-boiling petroleum ether fraction as solvent which obviates these difficulties in our hands?

HERMAN E. RIES, JR. (American Oil Company).—Prof. La Mer, is it not true that the higher pressure regions of the pressure–area isotherms are in good agreement whether the film be spread from *n*-hexane, benzene, or chloroform (as we have found)? [*n*-Hexane may be preferable to ligroin (petroleum ether).]

V. K. LA MER.—It is my recollectionthat this is true.

J. L. SHERESHEFSKY.—I do not think that in the present instances benzene is the sole cause of the concentration effect. No such effect was observed for the monolayers of the esters of malonic and succinic acids. There is ample evidence that in the oxalate monolayers the major and perhaps only factor is the steric interference and the resulting *trans*-configuration.

SPREADING AND COLLAPSE PHENOMENA IN THE FATTY ALCOHOL SERIES

BY J. H. BROOKS AND A. E. ALEXANDER

Department of Physical Chemistry, The University of Sydney, N.S.W., Australia

Received March 12, 1962

The formation of monolayers of pure fatty alcohols by spreading from the crystal and their behavior at the air–water interface shows many interesting phenomena and is relevant to the use of hexadecanol for reducing evaporation from water storages. These phenomena include spreading rates from crystals, losses of monolayer by evaporation and solution, equilibrium spreading pressures over a range of temperature, the effect of the crystalline phase of the alcohol and how this is influenced by the presence of water, and collapse phenomena when the film pressure exceeds the equilibrium spreading pressure. One particularly interesting conclusion is the existence of hydrates of the fatty alcohols.

Introduction

The last decade has witnessed a considerable resurgence of interest in the surface behavior of alcohols, both the lower-chain (soluble) members and the longer-chain homologs which form insoluble monolayers on water. The behavior of the latter is of considerable importance in relation to the effect of monolayers upon diffusion of gases across the air–water interface, particularly the evaporation of water.

The use of cetyl alcohol (commercial hexadecanol) as a practical means of reducing evaporation from water storages involves a variety of phenomena, such as spreading rates from crystals (and from different faces of the same crystal), losses by evaporation and solution, equilibrium spreading pressures, the effect of the crystalline phase of the alcohol and how this is influenced by the presence of water, and collapse phenomena when the film pressure (due to wind pressure or other causes) exceeds the equilibrium spreading pressure. All these phenomena are very sensitive to the purity of the alcohol, and a knowledge of pure compounds is essential for an understanding of the behavior of the mixtures present in commercial cetyl alcohols.

The present paper seeks to survey existing knowledge concerning the behavior of pure alcohols and to point out where further investigation is particularly needed. Full details of the experimental techniques and the composition of the alcohols (as indicated by vapor phase chromatography) will be found in earlier publications.[1,2] It might be pointed out here that the hexadecanol used by us appeared to be particularly pure (at least 99.8%) as judged by gas chromatography and surface behavior.

1. Crystalline Phases of Alcohols and the Influence of Water.—Fatty alcohols with an even number of carbon atoms exist in three crystalline forms termed α, sub-α, and β.[3] The first two have vertical chains thought to be rotating in the α and non-rotating in the sub-α form; in the β-form the chains are inclined to the planes formed by their ends. On cooling from the melt the α-form first appears; this then transforms into the sub-α and this in turn into the β-form. Transformations can be followed in various ways,[4] thermal curves being particularly convenient.

The presence of water has a marked effect on these phase transformations[5] and also on the melting point of the alcohol. The melting point is *raised* about 2° whereas the α–sub-α transition temperature is *lowered* by about 10°. With hexadecanol the full lowering of the transition temperature requires only about one water molecule to two alcohol molecules.[2]

These phenomena strongly point to the existence of hydrates of the long-chain alcohols,[6] although none has been reported in the literature.[7] This conclusion receives support from the measurements of equilibrium spreading pressures on water, as discussed in section 5 below.

2. Loss of Alcohols by Evaporation and Solution from Monolayers.—Many workers in the field of insoluble monolayers on water have reported slow losses with time,[8–10] this usually being ascribed to solution in the aqueous phase, although a later theoretical analysis had suggested evaporation as the cause.[11]

In order to determine the cause in the fatty alcohol series, the losses from monolayers of tetradecanol, hexadecanol, and octadecanol (all saturated) as well as oleyl alcohol (C_{18} unsaturated) have been quantitatively measured on water and 50% ammonium sulfate solution, over a range of temperature.[1] The results show that only in the case of oleyl alcohol is the loss appreciably reduced by the strong salt solution and that, on water, the temperature coefficient for oleyl is very much smaller than for the saturated alcohols.

These results suggested that evaporation is the chief cause of loss with the saturated alcohols, whereas with the unsaturated oleyl compound solution is mainly responsible. This conclusion was confirmed by a number of other experimental studies, particularly the influence of a metal plate placed in close proximity above the monolayer.

From the temperature coefficient of tetradecanol (the one most suitable for accurate measurement)

(1) J. H. Brooks and A. E. Alexander, "Proc. 3rd Intern. Congr. on Surface Activity," Cologne, 1960, Vol. II, p. 196.

(2) J. H. Brooks and A. E. Alexander in "Retardation of Evaporation by Monolayers," Ed., V. K. La Mer, Academic Press, New York, N. Y., 1962.

(3) D. G. Kolp and E. S. Lutton, *J. Am. Chem. Soc.*, **73**, 5593 (1951).

(4) R. G. Vines and R. J. Meakins, *Australian J. Appl. Sci.*, **10**, 190 (1959).

(5) F. H. C. Stewart, *ibid.*, **11**, 157 (1960).

(6) A. Trapeznikov, *Acta Physicochim. U.R.S.S.*, **20**, 589 (1945).

(7) H. H. Hatt, *Rev. Pure and Applied Chem.*, **6**, 153 (1956).

(8) N. K. Adam and J. W. Dyer, *Proc. Roy. Soc.* (London), **A106**, 694 (1924).

(9) G. C. Nutting and W. D. Harkins, *J. Am. Chem. Soc.*, **61**, 1180 (1939).

(10) F. Sebba and H. V. Briscoe, *J. Chem. Soc.*, 114 (1940).

(11) W. W. Mansfield, *Australian J. Appl. Sci.*, **10**, 73 (1959).

the heat of vaporization from the monolayer was estimated as 25 ± 2 kcal. mole^{-1}. This agrees reasonably with the values calculated as follows: (a) from the difference between the heat of vaporization of the solid and its heat of spreading on water, (b) from the energy to remove one OH group from water and 14 CH_2 groups from a hydrocarbon environment.

This study suggests that measurement of losses from monolayers may be a means of measuring heats of vaporization of high molecular weight compounds unstable at elevated temperatures.

3. Collapse Phenomena in Alcohol Monolayers.—At film pressures above the equilibrium spreading pressure (e.s.p.) of the most stable solid form (in contact with water—see section I above) the film is metastable and should tend to collapse. Early work had indicated that establishment of equilibrium from the film side was very slow,[12] which is not surprising since one-half of the molecules in the monolayer must undergo a reorientation of 180° before the polar groups can associate in the solid phase.

Collapse can be followed most conveniently under two conditions, namely, in the absence of, or in the presence of, the stable crystal. Quantitative measurements have been made with the C_{14}, C_{16}, and C_{18} saturated alcohols.[2]

In the absence of the stable bulk phase (*i.e.*, self-nucleated collapse) it is found that the spreading pressure of the collapsed material depends on the rate at which it has been formed, and that the collapsed material always spreads much faster than the stable crystal. Dust seems to play an important part in the nucleation process. The collapsed material ages at a moderate rate to the slow spreading (stable) form.

With stable crystals on the surface and a monolayer held at a pressure several dynes above the e.s.p., the alcohol does not deposit in the stable form, since on increasing the area, the alcohol respreads to a pressure *above* the e.s.p.

A great deal more remains to be done in this very interesting, although complex, field.

4. Kinetics of Spreading from the Crystal.—As would be expected, the rate depends upon the particular crystal face and upon the crystalline phase of the alcohol.[4,5,13] In the case of hexadecanol the spreading rate per unit area of the large parallel faces of the plate-like crystal is about 20 times that from the edge-faces. For the solidified melt the rate approximates that for the parallel faces.

For precise measurements over a range of temperature it is convenient to use as spreading source a glass rod or mica plate coated by immersion in molten alcohol. The spreading rate increases with temperature and a plot of log (spreading rate) against $1/T$ gave values for the activation energy of the alcohols of 36 to 42 kcal./mole. For the purest alcohol studied, hexadecanol, it was 42 ± 2 kcal./mole, a value close to that required to remove a single molecule from the crystal to the gaseous state.[2]

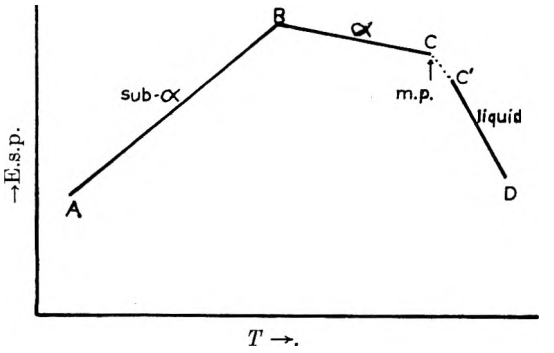

Fig. 1.—Variation of equilibrium spreading pressure (e.s.p.) with temperature (T) for a typical fatty alcohol.

With the C_{14} and C_{16} alcohols small but quite definite discontinuities in the rate–T curves were found. The temperatures of these discontinuities are close to the values for the α–sub-α phase change in the presence of water (see section 1, and Fig. 1) and probably reflect the same transformation.

5. Equilibrium Spreading Pressures (E.s.p.) and the Energetics of Spreading.—From the Clapeyron relation in the form

$$\frac{d\Pi_e}{dT} = \frac{Q_s}{T(A_2 - A_1)}$$

the molar heat of spreading (Q_s) may be found from the temperature coefficient of the e.s.p. ($d\Pi_e/dT$), the absolute temperature, T, and the molar areas of the monolayer (A_2) and crystal (A_1).[14] (A_1 is $<< A_2$ and can be neglected.)

The molar free energy of spreading $\Delta G_S = -\Pi_e(A_2 - A_1)$, and the molar enthalpy of spreading $\Delta H_S = Q_s + \Delta G_S$.[15]

In view of the knowledge acquired on such relevant factors as phase changes, losses by evaporation and solution, spreading rates, and collapse, as outlined in sections 1–4 above, it became possible to make accurate measurements of e.s.p. over a range of temperature, and hence of the thermodynamic quantities Q_S, ΔG_S, and ΔH_S.[2]

With the solid alcohols (C_{14}, C_{16}, and C_{18}) the general form of the e.s.p.–T curve is as shown in Fig. 1, consisting of three reasonably linear portions AB, BC, and C'D. Point B corresponds to the α–sub-α transition point and point C to the melting point in the presence of water (see section 1); the reason for the break at C' (about 1–2° above C) is considered later.

On measuring the e.s.p. of a single sample with first rising and then falling temperature, hysteresis effects frequently were observed. These appear to arise first from the time delay involved in the transition between the α and sub-α forms; second from slow changes in the composition of the spreading surface of monolayer when the alcohol is not completely pure. The addition of 1 mole % of the C_{14} or C_{18} homologs markedly affected the behavior of hexadecanol and such spreading experiments appear to provide a very sensitive indicator of purity. For example the octadecanol used in this

(12) N. K. Adam, "The Physics and Chemistry of Surfaces," Oxford, 1938.

(13) A. Roylance and T. G. Jones, *J. Appl. Chem.*, **9**, 621 (1959).

(14) A. Cary and E. K. Rideal, *Proc. Roy. Soc.* (London), **A109**, 301, 318, 331 (1925).

(15) G. E. Boyd and J. Schubert, *J. Phys. Chem.*, **61**, 1271 (1957).

work appeared from its spreading behavior to contain impurities, whereas according to gas chromatography it did not. Possibly the impurities were not resolved under the conditions used in the chromatograph. The marked discrepancies between our results for hexadecanol (the purest compound available) and those found by other workers,[6,15] also can be ascribed to impurities.

The liquid oleyl alcohol showed only the C'D region of Fig. 1, with no significant time effects. Although the sample used contained impurities (homologous alcohols) these do not have the same influence as in spreading from the solid owing to rapid diffusion within the lens.

The non-coincidence of the melting point of the solid alcohol with the main change in slope of the e.s.p. curve (*i.e.*, C'D in Fig. 1) is very interesting, and warrants further study. The existence of a liquid crystalline hydrate in the region CC', as has been suggested,[6] could explain the shape of the observed curves.

The molar heats, entropy, free energy, and enthalpy changes for monolayer formation have been calculated for tetradecanol, hexadecanol, and oleyl alcohol.[2]

From these data it is possible to calculate the heat change associated with the α–sub-α transition (*i.e.*, between AB and BC) and also that between the liquid and α phases (*i.e.*, between BC and C'D), the latter being the heat of fusion. For hexadecanol the molar heat change for the α–sub-α transition in the presence of water is thus 5.2 kcal.; the corresponding value for the anhydrous system does not appear to have been measured.

The heat of fusion of hexadecanol from the e.s.p. data is 6.08 kcal./mole, whereas direct calorimetric measurements at its melting point have given a value of 8.46 kcal./mole.[16] It seems reasonable to ascribe the difference to the formation of a hydrate of the α-phase of solid hexadecanol (as previously suggested in section 1). Assuming that the liquid above point C' in the e.s.p. experiment is the same as the liquid in the heat of fusion experiment (*i.e.*, no hydration, which seems very plausible), then the value for the heat of hydration of the solid α-phase is 8.46 − 6.08 = 2.38 kcal./mole. This value would seem quite reasonable for the reaction

$$\text{alcohol} + H_2O \longrightarrow \text{alcohol hydrate}$$

in the light of current information on hydrogen bond energies.

(16) G. S. Parks and R. D. Rowe, *J. Chem. Phys.*, **14**, 507 (1946).

General Conclusions.—Although the main features associated with spreading and collapse phenomena in the fatty alcohol series would seem to have been established, there clearly remain many gaps to be filled and certain tentative conclusions require further confirmation.

The proposed alcohol hydrates need examining by other techniques, such as X-ray diffraction or n.m.r. spectroscopy.

When really pure tetradecanol and octadecanol become available, accurate equilibrium spreading pressure studies would be warranted; with the inclusion of dodecanol, the pattern over the homologous series should then become apparent.

More attention should certainly be given to nucleation and collapse, a very intriguing field in relation to the formation of a three-dimensional from a two-dimensional phase.

The possibility of using evaporation from monolayers to estimate heats of sublimation of other high molecular weight compounds also warrants further study.

DISCUSSION

F. C. GOODRICH (California Research Corporation).—I wish to point out that the use of the Clapeyron equation in the form adopted by Dr. Alexander is not a matter which has been properly investigated thermodynamically. The question is whether it should be written in terms of $d\Pi_e/dT$ as Dr. Alexander has done in analogy with the three dimensional Clapeyron equation or whether the fundamental temperature coefficient is not $-dY/dT$. In the latter case, the quantity $d\Pi_e/dT$ in Dr. Alexander's equation should be replaced by $d\Pi_e/dT - dY_0/dT$ where Y_0 is the surface tension of the pure substrate. In more experimental language, should not the temperature coefficient of the surface pressure be corrected for the changing surface tension of the substrate?

A. E. ALEXANDER.—I have not yet had the opportunity to examine this question in detail, but a cursory check of the derivation of the two-dimensional Clapeyron equation suggests that the form as used is correct. In the case of the fatty acids heats of fusion calculated from the monolayer data agree very closely with those found calorimetrically, which could be regarded as supporting evidence.

A. A. BONDI (Shell Development Company).—While the heat of vaporization of tetradecanol which you deduce from monolayer loss data comes quite close to the experimental value [24 kcal./mole, Hoyer and Peperle, *Z. Elektrochem.*, **62**, 64 (1958)], I doubt the advisability of using that method indiscriminately. Don't you agree that an amine– (or amide–) water interaction might have given rather different results, and that the similarity of the ROH–H_2O and the ROH–HOR interaction was the reason for the tolerable agreement with the observed heat of vaporization?

A. E. ALEXANDER.—In my view the similarity in interaction between the groups in this system should not have been responsible for the agreement found. However, we hope to have a look at other systems with known heats of vaporization, in order to check this point experimentally.

HYDROGEN BONDING IN MONOMOLECULAR FILMS: THE STRENGTH OF THE KETO–IMINO HYDROGEN BOND IN AQUEOUS MEDIA

BY G. E. HIBBERD* AND A. E. ALEXANDER

Department of Physical Chemistry, University of Sydney, N.S.W., Australia

Received March 12, 1962

The association between the >C=O and H—N< groups in an aqueous environment, *i.e.*, $(>C{=}O)_{aq} + (H{-}N<)_{aq} \rightleftarrows (>C{=}O\ldots H{-}N<)_{aq}$ has been examined by monolayer studies of octadecyl acetamide. From the temperature coefficient of the above equilibrium, the energy of the hydrogen bond in the presence of water was found to be close to 2 kcal./mole. The effect on the equilibrium of added salts of different types, and of urea, has been measured quantitatively. These additives tend to inhibit hydrogen bond formation and when arranged in order of efficacy, both the cations and anions fall into the well known lyotropic series.

Introduction

In a recent review, Kauzmann[1] has pointed out that the interpretation of protein denaturation requires an examination of the interactions responsible for maintaining the native configurations of proteins and the effects of denaturing agents on these interactions. The effects of hydrogen bonds, salt linkages, disulfide bonds, and the aqueous environment in which they normally exist are but a few of the factors that determine the stability of a particular protein configuration.

Although hydrogen bonding between the >C=O and H—N< groups of the peptide linkage is assumed to play a major role in the stability of protein configuration, little is known about the interaction between these groups in aqueous media. This information cannot easily be obtained by the normal methods of studying hydrogen bonding. However, it does appear from earlier work[2-4] that an application of monolayer techniques to simple compounds containing the —CO·NH— link is helpful. Some related studies also have been reported on the surface chemistry of poly-α-amino acids[5-10] and of nylon-type polyamides of different but related molecular structure.[11,12]

In this investigation, the monolayer behavior of a long chain acetamide has been studied on solutions believed to affect hydrogen bonds, particularly salt solutions and urea.

Experimental

N-*n*-Octadecyl acetamide was prepared from octadecyl amine that had been fractionated on a spinning band column by treatment with acetic anhydride and subsequent recrystallization from ether.

A simple type of film balance with a hanging mica plate was used for the measurement of surface pressures (Π) and a polonium-210 ionizing air electrode with valve electrometer was used for the measurement of surface potentials (ΔV). Surface moments (μ) were calculated from the Helmholtz equation, $\Delta V = 4\pi\mu/A$, where A denotes the surface area per molecule. The surface viscosity (η_s) was determined by means of a surface torsion pendulum viscometer employing a perspex disk oscillating in the surface.

Temperatures were maintained to $\pm 0.1°$ by circulating water from a thermostat through glass coils. All salt solutions were shaken with activated charcoal and filtered immediately before use and, after 5-min. standing, produced no measurable surface pressure when the surface area was reduced by 90%.

Solutions of octadecyl acetamide for spreading contained about 0.7 mg./ml. in a 1:4 mixture of chloroform and petroleum ether (b.p. 60–70°). In order to obtain reproducible results, all condensed monolayers were spread to give an area of 30 Å.²/molecule and, after a period of 5 min., were compressed with the aid of a small synchronous motor at a constant rate of 2.0 Å.²/molecule/min.

Results and Discussion

It is convenient to subdivide the work into two sections.

1. Calculation of the Keto–Imino Bond Energy from the Behavior of Monolayers on 0.001 *N* H_2SO_4.—The condensed monolayers of octadecyl acetamide were found to exist in two forms with a definite transition pressure, provided the temperature was within a certain range. (See Fig. 1a and 1b.) Where comparable, the results are in good agreement with those of Adam and Dyer[13] and Alexander.[3] Above the transition point, the monolayers were liquid with negligible surface viscosity and a limiting area of 24.0 Å.²/molecule; below the transition point, they were rigid solids with a limiting area of 20.5 Å.²/molecule. The transition was indicated by the rapid increase in the surface viscosity and a pronounced discontinuity in the Π/A curve (see Fig. 1b). The influence of impurities on this discontinuity was analogous to their effect on the melting of pure solids.

In the configurations suggested by Alexander,[3] the low temperature form is stabilized by strong cross hydrogen bonds (configuration I), whereas in the high temperature form (configuration II) there is no possibility of intermolecular bonding between the >C=O and >N—H groups, thus accounting for the liquid state and negligible surface viscosity.

The influence of temperature on the transition pressure (Π_{tr}) is shown in Fig. 2 for sub-solutions

* Bread Research Institute of Australia, North Ryde, N.S.W., Australia.

(1) W. Kauzmann, *Advan. Protein Chem.*, **14**, 1 (1959).

(2) A. E. Alexander and E. K. Rideal, *Nature*, **147**, 541 (1941).

(3) A. E. Alexander, *Proc. Roy. Soc.*, **A179**, 470 (1941).

(4) J. Glazer and A. E. Alexander, *Trans. Faraday Soc.*, **47**, 401 (1951).

(5) T. Isemura and K. Hamaguchi, *Bull. Chem. Soc. Japan*, **25**, 40 (1952).

(6) T. Isemura and K. Hamaguchi, *ibid.*, **26**, 425 (1953).

(7) T. Isemura and K. Hamaguchi, *ibid.*, **27**, 125 (1954).

(8) T. Isemura and K. Hamaguchi, *ibid.*, **27**, 339 (1954).

(9) D. F. Cheesman and J. T. Davies, *Advan. Protein Chem.*, **9**, 439 (1954).

(10) E. Mishuck and F. R. Eirich, *J. Polymer Sci.*, **16**, 397 (1955).

(11) D. J. Crisp, *J. Colloid Sci.*, **1**, 49 (1954).

(12) G. E. Hibberd and A. E. Alexander, *Proc. 3rd Intern. Congr. Surface Activity*, **IV**, 144 (1960).

(13) N. K. Adam and J. W. Dyer, *Proc. Roy. Soc.*, **A106**, 694 (1924).

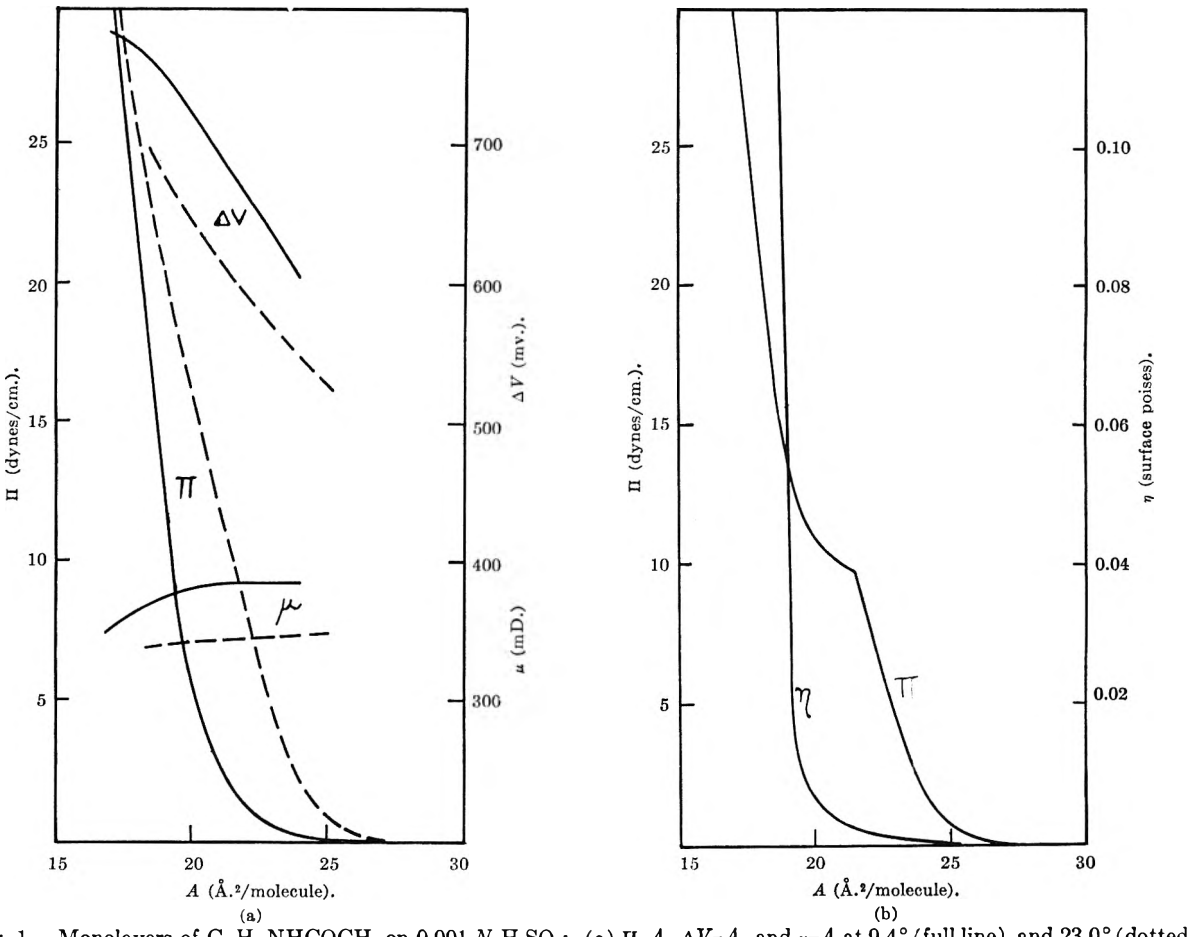

Fig. 1.—Monolayers of $C_{18}H_{37}NHCOCH_3$ on 0.001 N H_2SO_4: (a) Π–A, ΔV–A, and μ–A at 9.4° (full line), and 23.0° (dotted line); (b) Π–A and η_s–A at 20.3°.

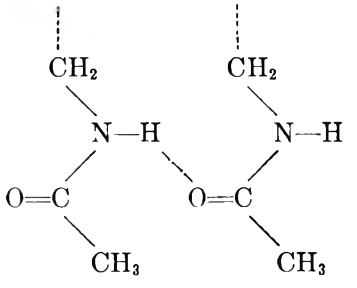

Configuration I (solid)

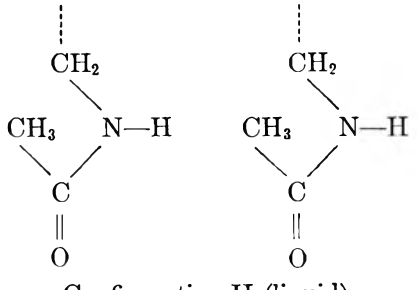

Configuration II (liquid)

containing various concentrations of H_2SO_4 and LiCl. From an application of the two-dimensional form of the Clapeyron relation

$$\left(\frac{\partial \Pi_{tr}}{\partial T}\right)_A = \frac{\Delta H}{T \times \Delta A}$$

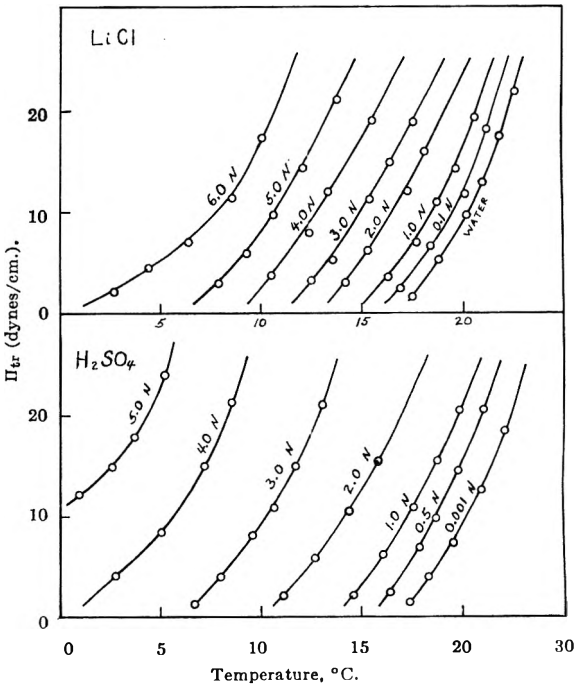

Fig. 2.—Monolayers of $C_{18}H_{37}NHCOCH_3$ on salt solutions. Effect of salt concentration on the transition pressure (Π_{tr}) *vs.* temperature curve: upper set—LiCl; lower set—H_2SO_4.

the value of ΔH for the solid to liquid transition can be found. Furthermore $\Delta H = \Delta E + \Pi\Delta A$,

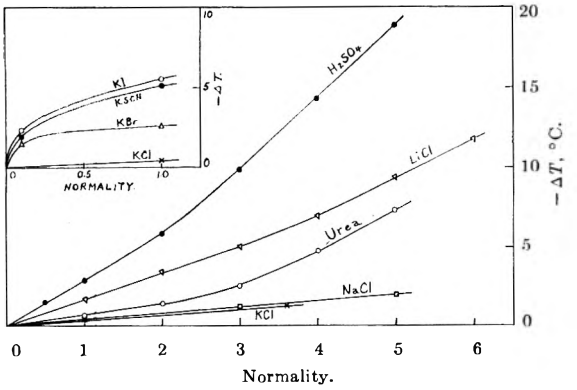

Fig. 3.—Monolayers of $C_{18}H_{37}NHCOCH_3$ on salt solutions. Change of transition temperature (ΔT) with salt concentration at a fixed surface pressure (π_{tr} = 15 dynes/em.). (Note different abscissa scale for inset.)

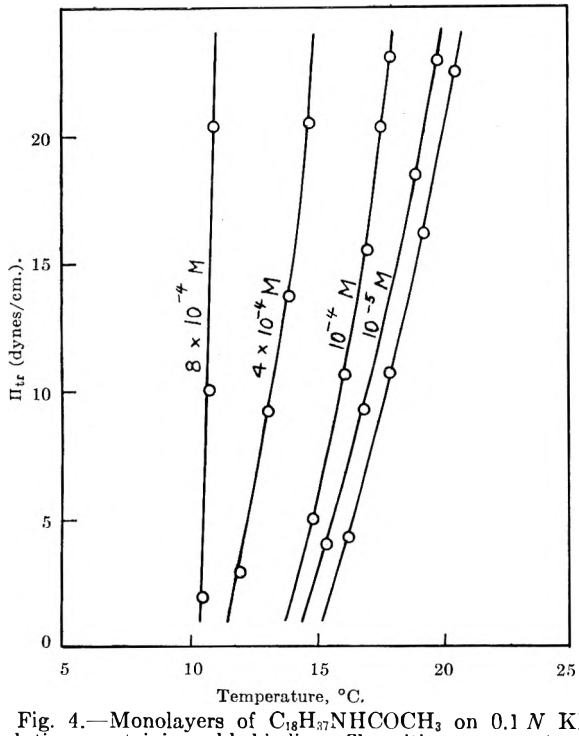

Fig. 4.—Monolayers of $C_{18}H_{37}NHCOCH_3$ on 0.1 *N* KI solutions containing added iodine. Transition pressure (π_{tr}) *vs.* temperature.

so that by plotting ΔH against Π_{tr} and extrapolating to zero pressure, the value of ΔE also can be found. (ΔA, ΔH, and ΔE are the net changes in molar area, molar heat content, and molar internal energy accompanying the transition.)

It was found that within the experimental error ΔH was independent of Π_{tr}, so that $\Delta E \simeq \Delta H = -3000 \pm 200$ cal./mole. This value is negative, denoting an energy evolution during the transformation from the liquid (large area) to the solid (low area) form. (*Cf.* ureas.[4])

The solid condensed form is also stabilized, relative to the liquid, by the stronger cohesion between the hydrocarbon chains owing to their slightly closer proximity. From a study of the long chain ureas, where the change in area is almost identical, Glazer and Alexander[4] have estimated this contribution to be 50 cal./mole for every methylene group. Applying this correction, ΔE for the head group transformation would be −2100 cal./mole.

The thermodynamic properties of the hydrogen bond in water have been discussed by Schellman,[14] who employed aqueous urea solutions as his model system. Interpreting deviations from ideality in terms of an equilibrium between monomer and dimer, he obtained for ΔH at 25° a value of −2090 cal./mole. Schellman[15] also has obtained a value of −1900 cal./mole for the heat of hydrogen bonding from studies of the denaturation of β-lactoglobulin by heat and urea.

As pointed out by Leach,[16] "the heat of hydrogen bonding for OH. . . .N or O. . . . .HN interactions has been quoted as 6 to 8 kcal./mole. However, in aqueous media, the presence of water at a concentration of about 55 *M* reduces this figure considerably. The breaking of a peptide hydrogen bond is in fact a hydrogen bond interchange in which the total number of bonds is unchanged."

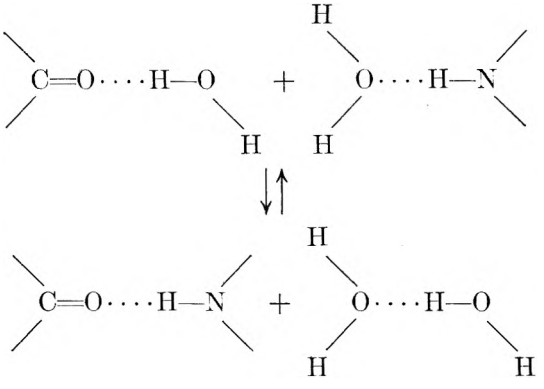

2. The Effect of Electrolytes and Urea on Hydrogen Bonding.—The transition between the two configurations (I and II) was found to be influenced markedly by the presence of salts or urea in the sub-solution. In addition to urea, the following electrolytes were examined—H_2SO_4, LiCl, NaCl, KCl, KBr, KI, KI_3, and KCNS, thus covering a range of cations and anions. Certain systems are shown graphically in Fig. 2 and 3; the full experimental data are given in Table I.

It can be seen that the cations, when placed in order of decreasing effectiveness (*i.e.*, $H^+ > Li^+ > Na^+ > K^+$), reproduce the well known lyotropic series. The relative effect can be explained in terms of the greater polarizing power of the smaller cations. It has been suggested[17] that in lithium halide solutions there may be lithium to carbonyl bonding as in (III) or bonding of carbonyl to water of the lithium hydration sphere as in (IV). Both interactions would tend to stabilize configuration II of the acetamide monolayers.

As is clear from Fig. 3, urea is not particularly effective at low concentrations, but its efficiency increases markedly above about 3 *M*. A similar effect was observed with monolayers of lysozyme,

(14) J. A. Schellman, *Compt. rend. trav. lab. Carlsberg, Sér. chim.* **29**, 223 (1955).
(15) J. A. Schellman, *ibid.*, **30**, 363 (1958).
(16) S. J. Leach, *Rev. Pure Appl. Chem.*, **9**, 33 (1959).
(17) J. Bello and H. R. Bello, *Nature*, **190**, 440 (1961).

TABLE I

TRANSITION PRESSURES (Π_{tr}) AT VARIOUS TEMPERATURES (T), ON WATER, UREA, AND VARIOUS SALT SOLUTIONS

(Π_{tr} in dynes/cm., T in °C.)

Water

T	17.5	18.8	20.1	21.0	21.8	22.6
Π_{tr}	1.5	5.3	9.8	12.8	17.4	21.9

Urea

1.0 M		2.0 M		3.0 M		4.0 M		5.0 M	
T	Π_{tr}	T	Π_{tr}	T	Π_{tr}	T	Π_{tr}	T	Π_{tr}
18.4	6.1	17.5	5.0	17.2	8.6	14.0	4.9	11.8	4.5
19.5	9.9	19.1	10.9	18.9	14.4	15.6	11.3	13.6	11.6
21.4	18.0	21.3	21.7	20.0	20.9	17.4	19.4	15.1	21.5

Sulfuric acid

0.001 N		0.5 N		1.0 N		2.0 N		3.0 N		4.0 N		5.0 N	
T	Π_{tr}	T	Π_{tr}	T	Π_{tr}	T	Π_{tr}	T	Π_{tr}	T	Π_{tr}	T	Π_{tr}
17.4	1.5	16.4	2.4	14.6	2.2	11.1	2.2	6.7	1.3	2.8	4.2	1.0	12.2
18.4	4.0	17.9	7.0	16.1	6.1	12.7	5.7	8.0	3.9	5.1	8.3	2.5	14.9
19.5	7.4	18.7	9.9	17.6	10.9	14.5	10.5	9.6	8.1	7.2	15.0	3.7	17.8
20.9	12.7	19.8	14.6	18.7	15.5	15.8	15.4	10.6	10.9	8.6	21.3	5.2	23.7
22.1	18.6	21.0	20.5	19.8	20.6			11.7	15.0				
								13.1	21.1				

Lithium chloride

0.1 M		1.0 M		2.0 M		3.0 M		4.0 M		5.0 M		6.0 M	
T	Π_{tr}	T	Π_{tr}	T	Π_{tr}	T	Π_{tr}	T	Π_{tr}	T	Π_{tr}	T	Π_{tr}
16.9	1.4	16.3	3.4	14.2	2.9	12.5	3.2	10.5	3.7	7.9	2.9	2.7	2.1
18.4	6.7	17.7	6.9	15.3	6.1	13.6	5.1	12.4	6.9	9.3	5.8	4.4	4.5
20.1	11.7	18.7	10.8	17.2	12.0	15.4	11.1	13.4	11.7	10.6	9.7	6.4	7.0
21.2	18.0	19.6	14.1	18.1	15.9	16.4	14.8	15.5	18.9	12.1	14.2	8.6	11.3
		20.6	19.1			17.5	18.8			13.8	21.0	10.1	17.3

Sodium chloride

3.0 M		5.0 M	
T	Π_{tr}	T	Π_{tr}
16.8	3.5	15.7	2.7
18.3	7.9	17.2	7.0
19.5	12.2	18.8	12.2
21.2	19.5	20.1	17.4

Potassium chloride

1.0 M		3.6 M	
T	Π_{tr}	T	Π_{tr}
16.8	1.9	16.5	3.2
19.6	9.9	18.0	7.5
21.1	16.0	19.9	13.3
22.2	22.1	20.8	17.3
		21.8	22.1

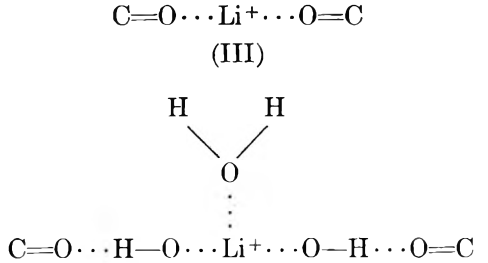

(III)

(IV)

ovalbumin, and poly-sc-leucine,[18] and it conceivably could be due to the formation of associated urea molecules as discussed earlier.

The halide ions, when placed in order of decreasing effectiveness (*i.e.*, I′ > Br′ > Cl′), reproduce the lyotropic series for anions. In this case the greater polarizability of the larger anions would afford a suitable explanation. However, the thiocyanate ion (see Fig. 3, inset) appeared to be anomalous in view of its size and position in the lyotropic series (CNS′ > I′). It was thought that traces of triiodide (I_3') ion (the iodine being formed by aerial oxidation) in the KI solutions could have been the cause, so the influence of added iodine was investigated.

Figure 4 shows the effect on the transition pressure produced by small additions of iodine to 0.1 N KI solution. Under these conditions all the added iodine would be effectively present as I_3', so this ion is clearly even more effective than the CNS′ ion. (The influence of iodine was not due to a chemical reaction with the amide, since on adding a little thiosulfate to the sub-solution, the film returned to its normal behavior.)

It would be extremely interesting to determine ΔH (and ΔE) for the films on salt solutions, as was done in the previous section for films on dilute acid. Unfortunately, the transition becomes less definite as the salt concentration increases, and because of the reduced accuracy no figures are reported here.

Acknowledgments.—Thanks are due to Dr. R. J. Meakins for assistance in the purification of *n*-octadecylamine, and to the Bread Research Institute of Australia for financial help to G. E. H.

(18) T. Isemura and K. Hamaguchi, *Ann. Rept. Sci. Works*, **5**, 65 (1957).

DISCUSSION

M. L. HUGGINS (Stanford Research Institute).—The computed energy of 2100 cal. is of course not the hydrogen bond energy for the N—H—O=C bond, but the difference between that energy and the sum of the energies of the hydrogen bonds between the individual molecules and the solvent which are broken during the process.

A. E. ALEXANDER.—Yes. This point is made clear in the published form of the paper.

J. L. SHERESHEFSKY (Howard University).—Areas per molecule of stearic acid obtained at very low surface pressures on urea substrates of various concentrations correspond to the area of the base of the urea–hydrocarbon clathrate structural cell, as determined by X-rays. This structure is broken up on compression. Will this phenomenon interfere with the postulated reaction in your study?

A. E. ALEXANDER.—We have never found any evidence that urea behaves in an anomalous manner, even at the highest concentrations studied.

H. A. SCHERAGA (Cornell University).—Klotz and Franzen obtained a value of $\Delta H = 0$ for the dimerization of N-methylacetamide. From a model, the dimer appears to contain a CH_3–CH_3 hydrophobic bond, as well as a linear hydrogen bond. Thus, the value $\Delta H = 0$ is a sum of a negative contribution from the hydrogen bond and a positive contribution from the hydrophobic bond. Is there any possibility that the methyl groups of the octadecyl acetamide (on the side pointing into the water) can form a hydrophobic bond (with an accompanying positive contribution to ΔH)?

A. E. ALEXANDER.—The case of octadecyl acetamide in the form of an oriented monolayer on water is rather different from the system quoted above since in going from configuration I to configuration II (see paper) the methyl group does not greatly change its local environment. For this reason we have assumed that this process makes no contribution to the over-all ΔH.

ON THE DAMPING OF WATER WAVES BY MONOMOLECULAR FILMS

BY F. C. GOODRICH

California Research Corporation, Richmond, California

Received March 2, 1962

Some features of a generalized theory of monolayer rheology are described, with particular reference to the problem of wave damping by surface active substances. Experiments on wave attenuation by fatty alcohols and acids are reported and discussed in terms of the theory.

1. Introduction

It is the objective of this article to provide a descriptive treatment of a rigorous hydrodynamic and rheological theory[1] which has been devised to account for the well known ability of thin films of oil to extinguish water waves and to report some experiments on wave damping by monomolecular films. The research was initiated to see what might be learned of the rheological properties of monolayers by studying the rate at which they accelerate the dissipation of wave energy in a gently undulating interface. These rates have been found to be surprisingly low, as will be seen in the sequel.

Throughout the work, effort has been directed toward an application of the formal mathematical apparatus of classical Newtonian rheology to problems in interfacial motion. A great deal of rheological material on interfaces has accumulated in the literature, but most of it is not sufficiently general to apply to systems undergoing wave motion, first because both theory and experiment usually restrict themselves to motion within the plane of the interface exclusive of motion vertical to it, and second because rarely is proper account taken of the inevitable coupling of the hydrodynamic motion of the substrate to the viscoelastic motion of the surface film. Only a theoretical apparatus which does both of these things can lead to the definition of rheological parameters which are truly characteristic of the surface.

The author also hopes to make more precise the term "dynamic surface tension" which is frequently seen in the literature. The implication of this terminology is that the interface under study is undergoing rate processes which cause an elastic parameter, the surface tension, to deviate from its static value. Now for an insoluble monolayer, *i.e.*, one whose chemical composition is not changing, a classical rheological description of a non-equilibrium elasticity is by a Voigt element with a pair of rheological constants, one elastic, one viscous, whose magnitudes measure the relative importance of a reversible and an irreversible response to stress within the monolayer. The "dynamic surface tension" from this point of view separates into a pair of constants, one the static surface tension, the other a viscosity coefficient.

This separation of static elasticity coefficients into pairs of rheological constants is a familiar procedure for bulk rheological systems, and our program here is to investigate its possibilities for interfaces. The reader will therefore find in the following that each of the various elastic moduli which can be defined for an interface carries with it a corresponding viscosity index.

2. The Characterization of Surface Rheology

The intrinsic elastic property of fluid interfaces known as surface tension has been recognized since the end of the eighteenth century. Less well recognized and certainly less experimentally investigated is the surface elasticity of Gibbs,[2] which plays a role for those fluid interfaces at which adsorbed films are present. The work of Boussinesq[3] led to the characterization of the viscous properties of an adsorbed surface film by a pair of viscosity coefficients. Only one of these has survived in the experimental literature,[4] where it is known simply

(1) F. C. Goodrich, *Proc. Roy. Soc.* (London), **A260**, 481, 490, 503 (1961).

(2) J. W. Gibbs, "Collected Works," Vol. I, Longmans, Green, and Co., New York, N. Y., 1928, p. 302.

(3) J. Boussinesq, *Ann. chim. et phys.*, **29**, 349, 357, 364 (1913).

(4) D. W. Criddle, in Eirich, "Rheology," Vol. 3, Academic Press, New York, N. Y., 1960.

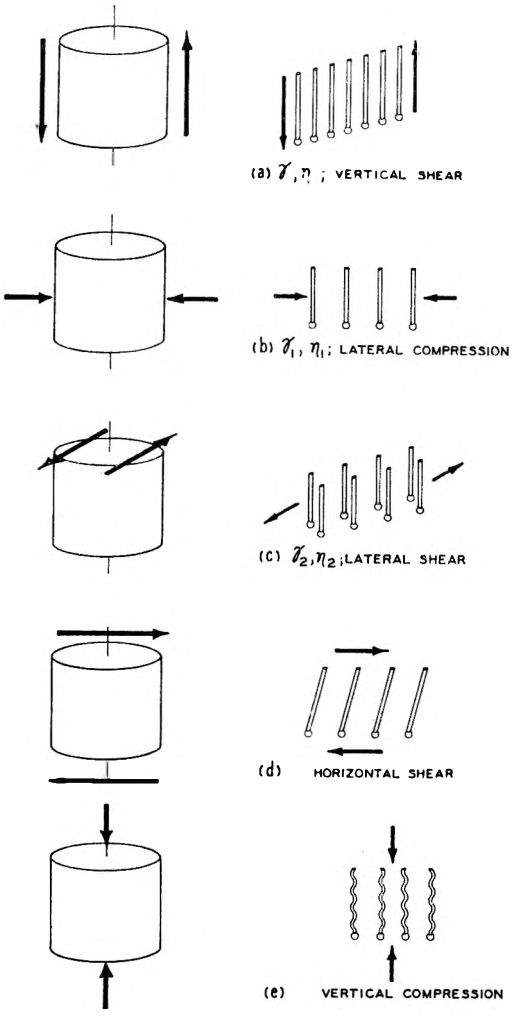

Fig. 1.—Possible types of motion in monolayers.

as the surface viscosity. Finally, Shuleykin and Ivanov[5] introduced into surface rheology still a third viscosity coefficient.

The number of independent viscoelastic constants introduced into surface rheology is thus already confusingly large. Mathematical schemes which incorporate many of them into quantitative predictions of the influence of interfacial phenomena upon macroscopic behavior have been devised,[1,6-10] and the author will give here a descriptive account of the role played by each of these viscoelastic constants in the theory of surface rheology.

Let us begin by remarking that an adsorbed monomolecular film, while it is exceedingly thin, nonetheless possesses a finite thickness and must hence in the most general case be treated as a non-isotropic rheological body. More specifically, the monolayer is axially symmetric, having properties in a direction perpendicular to the interface different from those which lie in the plane of the interface. It is known from classical elasticity theory[11] that the most general axially symmetric body requires fully five independent elastic constants γ and that an equivalent number of viscosity coefficients η must be appended to the theory if dissipative effects are to be included. By supposing that one is able to cut out a cylindrical specimen of the monolayer, the pairs of constants γ, η, and the motions with which they are associated are sketched in Fig. 1. Motions (a), (c), (d) are shear deformations of the specimen. Motions (b), (e) require volume changes.

The elastic constant γ for motion (a), vertical shear, is the surface tension. This identification may seem startling to those accustomed to the thermodynamic definition of this quantity, but it can be fully established mathematically.[1] The corresponding viscosity coefficient η which measures the degree to which mechanical energy can be degraded into heat by shearing the monolayer along the vertical axis is the viscosity coefficient of Shuleykin and Ivanov. The elastic reaction of the monolayer to deformation (b) involving a lateral compression of the film is the Gibbs elasticity. Gibbs[2] showed that

$$\gamma_1 = A\,(\partial\gamma/\partial A)$$

for A the area of the monolayer, a relationship which enables γ_1 to be calculated from the force–area curve. The viscosity coefficient η_1 is the first or dilational coefficient of Boussinesq,[3] while η_2, associated with a lateral shear of the film [motion (c)], is Boussinesq's second viscosity coefficient. It is η_2 which is almost universally reported in the experimental literature as "the surface viscosity." Comparatively little is known experimentally about the elastic constant γ_2 for lateral shear, and it would appear that in many cases the elastic limit for motion (c) is very small. Fortunately for the calculations on closely packed monolayers to be reported here, a knowledge of γ_2 is irrelevant.

To date, no quantitative theory has incorporated any of the complications arising from the supposed motions (d) and (e), and they will play no role in our discussion. Even neglecting motions (d) and (e), however, the remaining motions embrace a total of six rheological parameters which, together with the viscosity μ of the substrate, constitute a total of seven independent quantities. The incorporation of all of these into a rigorous theory of interfacial motion is a complicated matter which can be carried through to numerical completion only for special experimental situations. One of these is the case of shallow water waves of plane symmetry moving across an infinite ocean.

3. Wave Damping

A convenient physical picture to carry in mind in considering the effect of oil films upon water waves is that of a drum filled with water. The motion of the drum membrane is inevitably coupled to that of the fluid substrate so that depending upon the rheological properties assigned to the membrane, the degradation of wave energy into heat will proceed by mechanisms of varying importance. Al-

(5) V. V. Shuleykin, *Fizika Morya*, Moscow (1953). Available as Translation No. 797, U. S. Naval Research Laboratory, Washington, D. C.

(6) K. Wieghart, *Physik. Z.*, **44**, 101 (1943).

(7) A. Frumkin and V. Levitch, *Zh. Fiz. Khim.*, **21**, 1183 (1947).

(8) R. Dorrenstein, *Proc. Koninkl. Ned. Akad. Wetenschap.*, **B54**, 260, 350 (1951).

(9) J. G. Oldroyd, *Proc. Roy. Soc.* (London), **A232**, 567 (1955).

(10) L. E. Scriven, *Chem. Eng. Sci.*, **12**, 98 (1960).

(11) I. N. Sneddon and D. S. Berry, "Handbuch der Physik," Vol. 6, Springer-Verlag, Berlin, 1958.

ways present is the viscous dissipation in the substrate due to its own internal viscosity. Even in the absence of any sort of surface viscosity, this dissipation can be increased by the presence of a surface film for, as Lamb[12] pointed out many years ago, a laterally rigid surface film (one with a high Gibbs elasticity, γ_1) inhibits substrate motion parallel to the interface and thus increases the rate of substrate shear. When the film has viscous properties of its own, the relative contributions to energy dissipation of the modes of motion sketched in Fig. 1 have to be computed by complicated mathematical procedures, for none of the various contributions are additive.

The quantities which are measured in a typical wave experiment are the wave length λ and the wave attenuation Δ of the ripple generated by a mechanical oscillator of frequency f thrust into the interface. In the case of plane ripples, Δ is a measure of the rate of dissipation of wave energy whose physical significance may be assessed by a study of Fig. 2. Suppose a wave train generated by a line source to be moving from left to right along the x axis. The amplitudes $\psi_1, \psi_2, \ldots$ of successive crests are measurable quantities which both theoretically and experimentally are found to decrease exponentially with distance x from the source. A plot of $\ln \psi_i$ against x will thus be a straight line whose slope is defined to be $-\Delta$, or in other words, at any fixed time t the amplitude of the wave train is of the form

$$\psi \sim e^{-x\Delta} \cos (2\pi/\lambda)x$$

The dependence of Δ upon the seven rheological parameters discussed in section 2 plus the frequency f of the source is a complicated matter which becomes simple only in the case of a clean interface uncontaminated by oil. In this case, only the viscosity μ and surface tension γ of the water enter into the calculation; and it can be shown that to a good approximation the attenuation of capillary ripples is

$$\Delta = 8\pi\mu f/3\gamma$$

This formula is in good agreement with experiment.[1]

In planning a study of the action of monolayers in damping water waves, it is of interest to eliminate from the experiment as many as possible of the motions listed in section 2 in order to simplify the interpretation of the results. The typical surface viscosity experiment, for example, restricts all motion to lateral shear in the plane of the interface; and, in a similar way, it is convenient in a wave damping experiment to restrict the film motion as much as possible to those vertical to the interface. This means that the experiments simplest to interpret should be those on laterally rigid monolayers whose molecules are so tightly packed that the Gibbs elasticity γ_1 is effectively infinite. For such monolayers, the weak lateral drag exerted on them by the motion of a low viscosity substrate parallel to the interface is insufficient to initiate lateral motion of any sort in the plane of the interface. We consequently do not need to know in this case

(12) H. Lamb, "Hydrodynamics," Dover Press, New York, N. Y., 1945, p. 632.

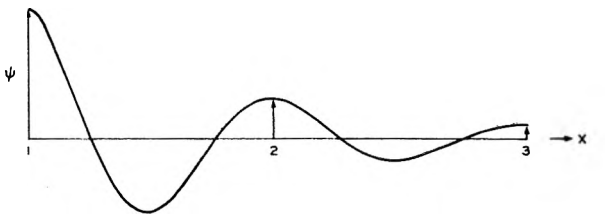

Fig. 2.—Attenuation of the amplitude ψ of a ripple as a function of distance X from the source.

the precise values of the rheological constants associated with motions (b) and (c); and the only relevant parameters entering into the theoretical calculation of Δ are the independently known quantities μ and γ, plus the unknown hypothetical monolayer viscosity coefficient η for vertical shear. It is with such monolayers that the experimental portion of this paper will be concerned.

4. Experimental

The apparatus used in these experiments has been described elsewhere.[1] Briefly, it consisted of a long, narrow, rectangular tank which contained distilled water to a depth of about 4 in. A lucite cover fitting over the tank protected the water surface from wind and dust, and through a small hole in this cover projected the vertical support for the wave source. The surface was observed through a cathetometer which was mounted above the tank parallel to its long axis. The cathetometer scale was used directly to measure wave lengths λ, while depth of focus readings from the cathetometer telescope could be interpreted in terms of wave amplitude. The measured amplitudes were of the order of magnitude of one micron, and from this figure can be estimated the percentage increase in interfacial area upon passage of a ripple as being about 10^{-6} per cent. The water surface was thoroughly cleaned before use by scattering talc powder over it and then sucking off the surface layer through a small capillary until all talc had been removed. During a run, it was illuminated by stroboscopic light of the same frequency as the wave source so that individual crests appeared to stand still. Before each run, the tank was freshly recoated with paraffin.

Initial attempts to spread monolayers from a spreading solvent proved unsuccessful when repeated trials yielded monolayers whose attenuation varied by as much as 100%. Curiously, the surface tension of such monolayers was quite reproducible; but even flushing the atmosphere in the tank with air for as long as a half hour failed to remove or even diminish the irreproducibility in the attenuation. When pure solvent was spread on clean water, however, the evaporation appeared to be complete, for the initial surface tension and wave attenuation could be recovered unaltered. This phenomenon appears to have some bearing on the suggestion of Robbins and La Mer[13] that spreading solvents are irreversibly incorporated into monolayers. The final procedure adopted was to scatter small crystals of the film-forming substance over the surface of the water. This method yielded a closely packed, reproducible monolayer, although for octadecanol and stearic acid, the surface tension did not fall to its equilibrium value until after the passage of several days. The surface tension of the interface was calculated from the Kelvin formula

$$\gamma = \frac{\rho f^2 \lambda^3}{2\pi} - \rho g \left(\frac{\lambda}{2\pi}\right)^2$$

in which ρ is the density of the water and $g = 981$ dynes g.$^{-1}$. Over the range of frequencies studied, this formula was found to be reliable to within ± 1 dyne cm.$^{-1}$. All stocks of surface active chemicals were fractionally distilled from commercial samples and recrystallized to constant melting point.

(13) M. L. Robbins and V. K. La Mer, *J. Colloid Sci.*, **16**, 123 (1960).

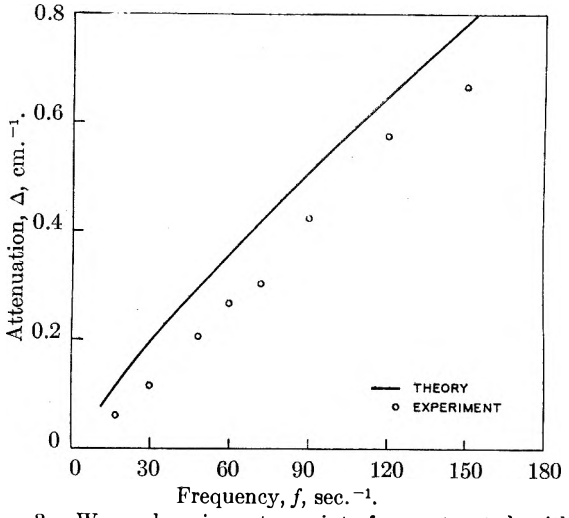

Fig. 3.—Wave damping at an interface saturated with tetradecanol; T = 22–23°.

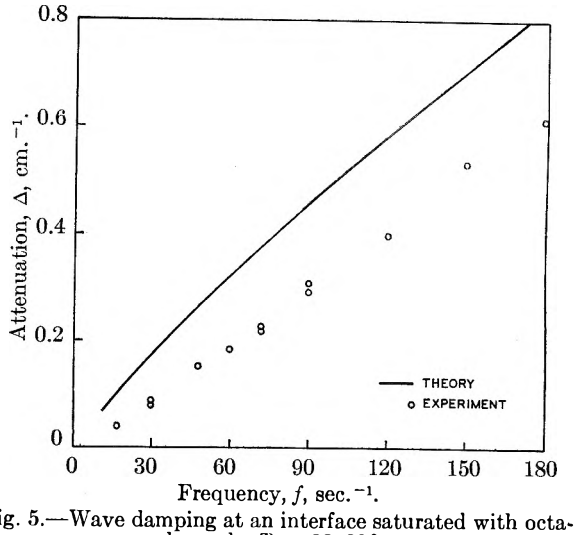

Fig. 5.—Wave damping at an interface saturated with octadecanol; T = 22–23°.

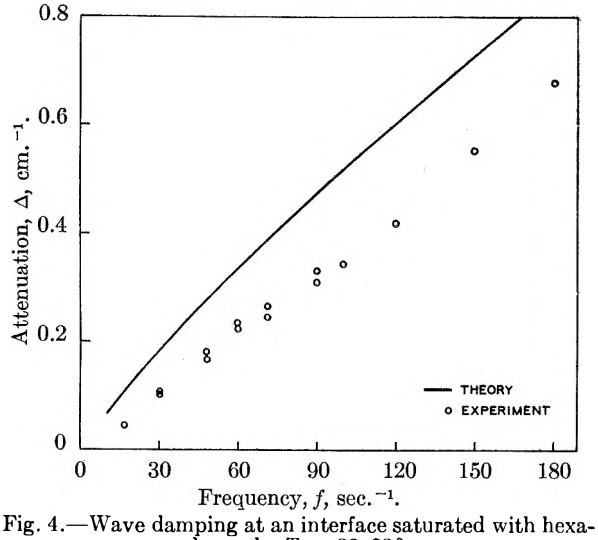

Fig. 4.—Wave damping at an interface saturated with hexadecanol; T = 22–23°.

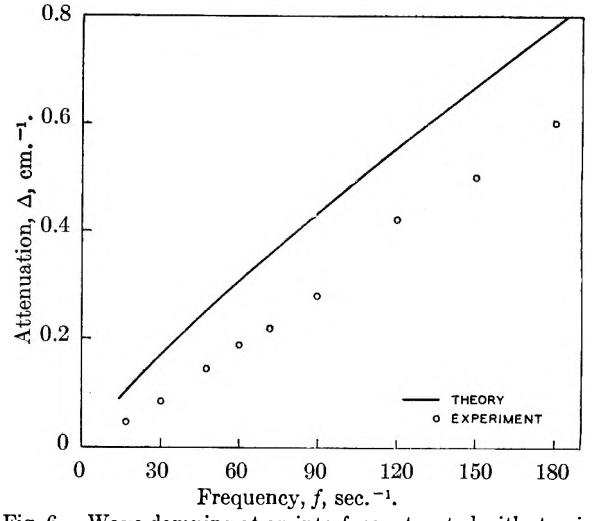

Fig. 6.—Wave damping at an interface saturated with stearic acid; T = 22–23°; substrate = 0.01 N HCl.

5. Results

Plots of wave attenuation Δ as a function of frequency f are given for monolayers of a number of surface active substances in Fig. 3–6. Also plotted are the theoretical curves as calculated using the known viscosity and density of water plus the experimentally measured values of γ and γ_1. The Gibbs elasticity γ_1 was determined independently on a film balance from the force–area curve of the monolayer, but its precise value turns out to be irrelevant to the calculation, for in every case it was so high that the predicted curves differ only negligibly from that calculated from Lamb's hypothesis[12] which is to say that they are the attenuations expected for a laterally rigid monolayer whose viscosity coefficient η for vertical shear is zero. The failure of Lamb's hypothesis is evident, but the unusual feature of these curves is that the failure is in the unexpected direction, for increasing η away from zero exaggerates rather than diminishes the divergence between theory and experiment. In short, there is less experimental attenuation than can be accounted for by the theoretical minimum.

6. Discussion

The result obtained is thus the reverse of that reported by Vines,[14] whose measured attenuations, when they can be compared with the above, are all higher, including that reported for clean water. Vines concluded that his attenuation data for tightly packed monolayers showed positive deviations from Lamb's hypothesis, whereas the author has found negative deviations. Two criticisms can be leveled at his work: his failure to clean the surface adequately and his use of a spreading solvent. Experience in this Laboratory indicates that both effects can lead to serious errors. In any case, the question of whether or not there exists a viscosity coefficient η for vertical shear within the film is unanswered by these experiments. Instead, a new question is raised as to what is the proper boundary condition to be used in our theoretical calculations when we consider the coupling of the motion of the substrate with that of the interfacial film. In all of the calculations reported here, it was assumed that the velocity vector of fluid flow within the sub-

(14) R. G. Vines, *Australian J. Phys.*, **13**, 43 (1960).

strate varied continuously right up to the fluid boundary and that the internal viscosity index μ of the water was constant over the same region. These assumptions are traditional in hydrodynamic calculations, yet one way to account for this experimental result is to abandon them. More specifically if there is a region close to the interface where the viscosity of the water is less than that in the bulk, then the lateral rigidity of the film will no longer be so influential in increasing the rate of shear within the substrate and the attenuation will be less than that expected from the traditional hypothesis. More picturesquely, it may be that a thin layer of low viscosity water effectively lubricates the film from the substrate. Among hydrodynamicists, such a possibility is known as "slip"; but there is abundant experimental evidence in the hydrodynamic literature that slip is non-existent. An incontestably established case of slip would, for example, throw into doubt the whole of experimental viscometry, which is based on the assumption of no slip between the fluid and the walls of Couette or capillary viscometers.

A second alternative would be to incorporate into our theoretical calculations types of motion in the monolayer other than those already considered. Such a generalization would take into full account motions (d) (horizontal shear) and (e) (vertical compression), but the implications of such a modification in the theory have yet to be investigated.

Acknowledgment.—The author is indebted to Professors L. E. Scriven and F. Buff for an illuminating discussion.

DISCUSSION

S. G. MASON (Pulp and Paper Institute of Canada).—With a rigid monolayer, is it assumed that the horizontal velocity component of the interface is exactly zero? In other words, is the locus of a point on the interface a vertical line? If it is elliptical a reduction in rate of dissipation of energy in the substrate may be possible. I would be interested to know if this point has been examined theoretically.

F. C. GOODRICH.—The calculations described here were performed using experimentally measured values of γ_1. It can be demonstrated theoretically that in the limit $\gamma_1 \to \infty$, the horizontal component of the substrate velocity vector is suppressed to zero. For the experiments reported here, γ_1 was already so high that the calculated results differ negligibly from those which would be obtained by deliberately setting the horizontal velocity component equal to zero at the start of the calculation. Thus, to answer your question, the locus of a point in the interface in these experiments is indeed a vertical line; but this result follows automatically from the high, measured value of γ_1. It was not imposed *a priori* on the calculation.

A. S. MICHAELS (Massachusetts Institute of Technology).—Your calculated attenuation constants are based on the premise that the monolayer is *completely* incompressible or inexpansible. Since there must be some variation in surface area due to establishment of the wave, there should be a corresponding change in molecular packing at the interface—hence some compression and expansion of the monolayer must result. Can this perhaps account for the difference between your experimental and predicted attenuation values?

F. C. GOODRICH.—The ratio of maximum wave amplitude to wave length in these experiments was 10^{-4}, and from this figure it is a simple matter to calculate the maximum fractional increase in surface area as of the order of 10^{-8}. This figure is far too small to cause changes in molecular packing of the magnitude required. In order to harmonize theory and experiment, reductions of the compressional modulus γ_1 by factors of $1/2$ to $1/3$ would be required—far greater than are conceivable on the basis of such infinitesimal area changes.

HERMAN E. RIES, JR. (American Oil Company).—Did you determine any complete pressure–area isotherms while the film was subjected (continuously) to vibration? If so, did they agree with those determined without vibration?

F. C. GOODRICH.—Pressure–area isotherms have been determined by this method, and to within experimental error agree with those obtained on the conventional Langmuir balance. Because, however, the surface tension can be measured only to ± 1 dyne cm.$^{-1}$, the technique is not competitive.

A. BAIDINS (du Pont Company).—It may be possible that the deviation from theory is due to the fact that fatty molecules are not rods, but flexible chains, and the damping of wave motion is due to flexing of chains by inertial force. Furthermore, by flexing they could interlock, thus slowing or preventing any shear and breathing motion.

F. C. GOODRICH.—This possibility I have not investigated. It amounts to including in the mathematics the motions (d) and (e) illustrated in Fig. 1.

J. LYKLEMA (University of Southern California).—If the surface potential of the monolayer is sufficiently high the viscosity of the underlying water would increase in the electric field of the double layer. This would certainly affect the damping.

F. C. GOODRICH.—I am aware of the experiments of Andrade and Dodd [*Proc. Roy. Soc.* (London), **A204**, 449 (1951)] in which they report increased viscosity of polar liquids in the presence of an external electric field. Whatever may be the implications of this finding with respect to wave damping by monolayers, the effect is in the wrong direction to account for the experimental results reported here.

R. J. GOOD (General Dynamics).—In view of the Frank–Wen and Frank–Evans theories, as developed by Némethy and Scheraga earlier in this Symposium, I would think that the viscosity of water in the layer immediately beneath the monolayer may well be low. Perhaps for a thickness of a few molecules the viscosity might be that of clusters no larger than two or three molecules—*i.e.*, something of the order of magnitude to be expected for liquid methane or propane at room temperature and the appropriate density. If a "slipping" film were very thin compared to the magnitude of the surface asperities of a solid, then it would be very difficult to detect this slip by hydrodynamic drag studies.

I wish to ask if you have made a calculation, of the type described in your paper, using as adjustable parameters the viscosity of the water in the low-viscosity layer, and/or the thickness of the layer?

Another question not related to the above is the following: What is the explicit form of the relation between Δ, f, μ, γ, and the η for vertical shear?

F. C. GOODRICH.—Calculations of the type you suggest are in progress.

The explicit relationship between Δ and f, γ, μ, η for a laterally rigid monolayer is obtained by calculating a complex root of a certain complicated transcendental equation. The final result could be expressed as an infinite series; but because the results reported here were obtained by iterative calculations on an electronic computer, I have not written down such series explicitly. Partial details will be found in ref. 1.

A. A. BONDI (Shell Development Company).—Don't you consider it possible that the deviation from predicted behavior may be due to the discontinuous character of the film, *i.e.*, the island character of even "densely packed" monolayers observed in Dr. Ries's electron micrographs?

F. C. GOODRICH.—All the calculations reported here are based upon the experimentally determined elasticity coefficients γ, γ_1. Without a hypothesis on how the presence of islands in the film might for some mysterious reason alter these coefficients in a dynamic experiment, I do not see how knowledge of details of the film structure might resolve the difficulty.

K. J. MYSELS (University of Southern California).—I wish to bring up a minor point of history and nomenclature.

Gibbs writes not about surface elasticity but about film elasticity on the page quoted (ref. 2). Furthermore, the films with which Gibbs was concerned were not the Langmuir monolayer films to which Dr. Goodrich refers in connection with his first equation. They were soap films composed of two surfaces plus a thin layer having bulk properties in between. Thus Gibbs's film elasticity is not a simple surface property but one dependent upon the amount of bulk phase present.

Since Gibbs's film elasticity is a well defined operational quantity which can be directly measured [*J. Phys. Chem.*, 65, 1107 (1961)] and thermodynamically calculated for special cases (Gibbs, ref. 2, p. 303), it does not seem advisable to apply the same name or a very similar one to a different concept which Gibbs did not formulate explicitly. As an alternative, I would like to suggest "areal elasticity" since it seems to be the exact two-dimensional analog of what is called volume elasticity for three-dimensional systems. "Areal viscosity" then would be the corresponding viscosity coefficient just as there is a volume viscosity.

IDEAL TWO-DIMENSIONAL SOLUTIONS. III. PENETRATION OF HYDROCARBONS IN MONOLAYERS

BY FREDERICK M. FOWKES*

Shell Development Company, Emeryville, Calif.

Received March 2, 1962

Insoluble monolayers of stearic acid on aqueous substrates are subject to penetration by hydrocarbons or other solvents from the vapor phase. Similarly interfacial monolayers of stearic acid at the oil–water interface are subject to penetration by oil molecules. In both cases, it is shown that the stearic acid and penetrating solvent form ideal two-dimensional solutions. Monolayers of long chain quaternary ammonium salts at the oil–water interface are penetrated by both oil and water simultaneously; this gives rise to the $3kT$ in the gas equation approximation of the equation of state.

Introduction

As surface active molecules (species 1) adsorb or spread as monolayers at liquid surfaces, molecules of the substrate (species 2) originally present in the surface are forced into the adjacent liquid phase. However, in many cases an appreciable mole fraction x_2 of substrate molecules remains in the surface layer. These remaining substrate molecules and the surface-active molecules form a two-dimensional solution in which the film pressure π and partial molecular area of substrate molecules σ_2 determine x_2

$$\pi\sigma_2 = -kT \ln x_2\phi_2 \qquad (1)$$

where ϕ_2 is the activity coefficient of the substrate molecules in the surface solution. Such monolayers with ϕ_2 equal to unity are termed "ideal two-dimensional solutions" and have been found to occur in a great many instances; in fact, ideality of such solutions appears to be the rule with few exceptions. Of course a great many insoluble monolayers and some adsorbed monolayers are essentially free of substrate molecules (ϕ_2 approaches infinity), but when monolayers do include substrate molecules, ϕ_2 is generally very close to unity. Many investigators have found this to be the case for small molecules,[1] and the author has shown this to be the rule for detergents and so-called "gaseous" monolayers.[2] Other two-component monolayers formed by penetration of detergent molecules (species 2) into an insoluble monolayer of species 1 display the same ideality and obey eq. 1 where π is the increase in film pressure as a function of x_2.[3–5]

This paper is concerned with the penetration of hydrocarbon molecules (species 2) into insoluble or adsorbed monolayers of species 1 at surfaces or interfaces; in these systems ϕ of eq. 1 is generally unity or else no penetration occurs.

The Surface Phase.—The surface layer (or layers) of molecules in liquids may well be considered to be a phase separate from the bulk liquids. In this phase the intermolecular distance is considerably greater than in the liquid phase, the surface tension affects the chemical potential of this phase only (except for the pressure effect on the liquid phase in some systems), the composition and chemical potential of species of the surface phase of solutions is quite different from the liquid phase, solutes are far more soluble in the surface phase, and the activity coefficients in surface solutions are far closer to unity than in bulk solutions. Equilibria between the surface phase and liquid phase are established when molecules can be readily exchanged between phases. In the case of insoluble surface films such as stearic acid on water no equilibrium is established with dissolved stearic acid in any of the usual film balance studies. However, in "gaseous" monolayers of stearic acid the surface phase is composed mainly of water and this is in dynamic equilibrium with the water substrate. In the case of detergent monolayers adsorbed on aqueous solutions, both the detergent and water molecules of the surface phase are in equilibrium with the liquid phase. In this paper we consider insoluble surface monolayers of stearic acid (not in equilibrium with any other phase) penetrated by hydrocarbon molecules in equilibrium with hydrocarbon vapor.

At interfaces between dissimilar liquids such as hydrocarbons and water the interfacial region includes two interfacial phases (the adjacent layers of both liquids); these two phases have different tensions, intermolecular distances, and compositions than the liquid phases.[6] Some surface active

* Sprague Electric Co., North Adams, Mass.

(1) *E.g.*, A. Schuchowitzky, *Acta Physicochim. URSS*, **19**, 176, 508 (1944).

(2) F. M. Fowkes, *J. Phys. Chem.*, **66**, 385 (1962).

(3) W. M. Sawyer and F. M. Fowkes, *ibid.*, **62**, 159 (1958).

(4) F. M. Fowkes, *ibid.*, **65**, 355 (1961).

(5) F. M. Fowkes, "Proceedings of the Third International Congress of Surface Activity," Cologne, Vol. II, 1960, p. 161.

(6) F. M. Fowkes, *J. Phys. Chem.*, **66**, 382 (1962).

molecules occupy only one interfacial phase, but others can occupy both at once as will be shown.

Theory.—The same equations will be used as in previous articles of this series.[2,4] The subscript 1 refers to the species forming the monolayer to be penetrated and subscript 2 to the penetrating species. If a second species penetrates the monolayer subscript 3 is used.

Penetration is the equilibration of a species (2) between two phases; at equilibrium its partial molar free energy (G_2) is equal in the two phases. However, when one of the phases has a different pressure, tension, or gravitational constraint the chemical potential μ_2 is different in the two phases. For equilibria between a liquid or vapor phase with the surface phase (at constant pressure and temperature)

$$dG_2(\text{surface}) = d\mu_2(\text{surface}) - N\sigma_2 d\gamma$$
$$dG_2(\text{substrate}) = d\mu_2(\text{substrate})$$
$$dG_2(\text{vapor}) = d\mu_2(\text{vapor})$$
$$dG_2(\text{surface}) = dG_2(\text{substrate}) = dG_2(\text{vapor})$$
$$d\mu_2(\text{surface}) = RT\ d\ln x_2\phi_2$$
$$d\mu_2(\text{substrate}) = RT\ d\ln c_2 f_2$$
$$d\mu_2(\text{vapor}) = RT\ d\ln p_2^*$$

where x_2 and ϕ_2 are the mole fraction and activity coefficient in the surface phase, c_2 and f_2 are the mole fraction and activity coefficient in the substrate, and p_2^* is the fugacity of species 2 in the vapor space.

After equilibration of species 2 between substrate and surface phases

$$kT\ d\ln x_2\phi_2 - \sigma_2 d\gamma - kT\ d\ln c_2 f_2 = 0 \quad (2)$$

and between vapor and surface phases

$$kT\ d\ln x_2\phi_2 - \sigma_2 d\gamma - kT\ d\ln p_2^* = 0 \quad (3)$$

For vapor–surface equilibria in which the vapor acts as an ideal gas, and the changes in surface tension are expressed as film pressure π, eq. 3 becomes

$$kT\ d\ln x_2\phi_2 - kT\ d\ln (p_2/p_2^0) = -\sigma_2 d\pi \quad (4)$$

where p_2/p_2^0 is the relative vapor pressure (p_2^0 is the vapor pressure of pure liquid species 2). In integrated form eq. 4 is

$$kT \ln x_2\phi_2 - kT \ln (p_2/p_2^0) = -\sigma_2 (\pi - \pi_2^0) \quad (5)$$

where π_2^0 is the equilibrium spreading pressure of species 2 on the substrate, and $\bar{\sigma}_2$ is the average partial molecular area of species 2 as defined by

$$\bar{\sigma}_2 = \frac{\int_{\pi_2^0}^{\pi} \sigma_2 d\pi}{\pi - \pi_2^0}$$

To compute x_2 for a mixed monolayer from measured values of A_1 (the area of monolayer per molecule of species 1), it is necessary to know σ_2 and σ_1. The two-thirds power of the molecular volume has been found adequate for predicting σ_2 of small symmetrical molecules such as water and propylene carbonate.[2] For less symmetrical molecules σ_2 may have to be evaluated from π *vs.* p_2 data at constant x_2. Under these conditions we see that eq. 4 leads to

$$\sigma_2 = kT \left(\frac{d\ln p_2}{d\pi}\right)_{x_2} \quad (6)$$

In computing x_2 it is also necessary to know σ_1 and whether or not species 1 is dimerized in the mixed monolayer. These points can be established by use of the relation[2]

$$A_1 = \sigma_1 + \left(\frac{n_2}{n_1 z}\right) z\sigma_2 \quad (7)$$

where z is the dissociation coefficient for molecules of species 1 in the mixed monolayer. If z is unity no association or disassociation occurs; if dimers were formed z would equal 0.5. The value of $n_2/n_1 z$ is calculated from

$$\frac{n_2}{n_1 z} = \frac{x_2}{1 - x_2} = \frac{e^{-\pi\sigma_2/kT}}{1 - e^{-\pi\sigma_2/kT}} \quad (8)$$

Thus for each value of π a corresponding value of $n_2/n_1 z$ is calculated and an A_1 *vs.* $n_2/n_1 z$ plot derived from the normal A_1 *vs.* π relation. The slope gives z, and the intercept σ_1.

Penetration of Surface Monolayers by Solvent Vapors.—The data of Dean and co-workers[7–11] on the effect of hydrocarbon and carbon tetrachloride vapors on the film pressure of stearic acid monolayers may be treated as an ideal two-dimensional solution in which the vapor is in equilibrium with solvent in the monolayer, although a different interpretation was offered originally.

In Fig. 1 and 2 are shown the effects of carbon tetrachloride and dimethylbutane on the film pressure of extremely dilute monolayers of stearic acid.[7] These molecules are nearly spherical in shape so that σ_2 is calculated as the two-thirds power of the molecular volumes (28 and 34 Å.^{2}, respectively). The value of σ_1 is expected to be the maximum molecular area for stearic acid in its most expanded form, 45 Å.^{2}. A check of this value is given in Fig. 1 where the data are plotted according to eq. 7 and the intercepts are 40 and 45 Å.^{2}, respectively.

These mixed monolayers are very simple ones. The stearic acid molecules occupy 45–46 Å.^{2} at pressures less than the "critical demixing pressure" (see Fig. 2), so that the area available to solvent molecules is $A_1 - \sigma_1$. With this area and the known values of σ_2, x_2 values are calculable for each value of A_1. Then from eq. 5 a π–A_1 relation is calculable for any fixed value of p_2. The data of Dean and Li are for $p_2 = p_2^0$, and are shown in Fig. 2 to fit the calculated pressure–area curves very well.

Data obtained later with *n*-hexane also fit the ideal solution equation for monolayers.[5]

Penetration of Oil Molecules into Oil-Soluble Monolayers Adsorbed at the Oil–Water Interface.—Let us consider the monolayer adsorbed between water and a dilute solution of stearic acid (1) in a highly refined naphthenic oil (2).

(7) R. B. Dean and Fa-Si Li, *J. Am. Chem. Soc.*, **72**, 3979 (1950).
(8) R. B. Dean and K. E. Hayes, *ibid.*, **73**, 5583 (1951).
(9) K. E. Hayes and R. B. Dean, *ibid.*, **73**, 5584 (1951).
(10) R. B. Dean and K. E. Hayes, *ibid.*, **74**, 5982 (1952).
(11) K. E. Hayes and R. B. Dean, *J. Phys. Chem.*, **57**, 80 (1953).

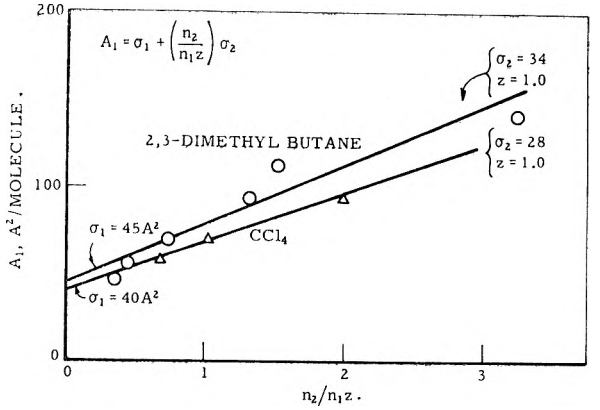

Fig. 1.—Surface solution plot of stearic acid penetrated by CCl_4 (triangles) or dimethylbutane (circles) at 25°. Lines calculated for ideal solutions, points are from data of Dean and Li.

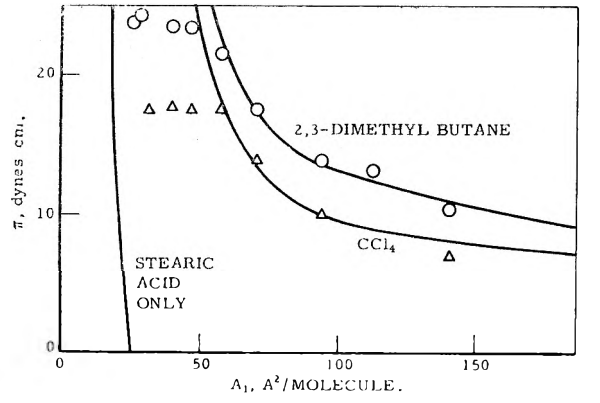

Fig. 2.—Pressure–area isotherms for stearic acid penetrated by CCl_4 or dimethylbutane vapor at 25°. Lines are calculated for ideal surface solutions, points are from Dean and Li.

Water is not soluble in the stearic acid monolayer, nor *vice versa*, so this is essentially a binary system with oil molecules and stearic acid molecules mixed together in the monolayer as an ideal solution. The pressure–area isotherm may be derived from eq. 2 and abbreviated to

$$\pi = \frac{-kT \ln x_2\phi_2}{\bar{\sigma}_2} \qquad (9)$$

using appropriate values of $\bar{\sigma}_2$ and σ_1 (25 Å.^{2} for each), and $\phi_2 = 1$, as is illustrated in Fig. 3. The experimental points are from interfacial tension measurements by Dr. W. M. Sawyer (of these Laboratories) with areas per molecule (A_1) calculated with Gibbs's adsorption equation modified as suggested by Langmuir[12] for adsorption of fatty acids from solutions in which they are predominantly dimeric[13]

$$A_1 = \frac{-kT}{2}\left(\frac{\mathrm{d} \ln c_1}{\mathrm{d}\gamma}\right)_{f_1}$$

One point from the work of Zisman[14] also is shown. The value of σ_2 (25 Å.^{2}) has not been obtained independently, but is an estimated value. Figure 4

(12) I. Langmuir, *J. Franklin Inst.*, **218**, 143 (1934).
(13) D. S. Sarkadi and J. H. deBoer, *Rec. trav. chim.*, **76**, 628 (1957).
(14) W. A. Zisman, *J. Chem. Phys.*, **9**, 534 (1941).

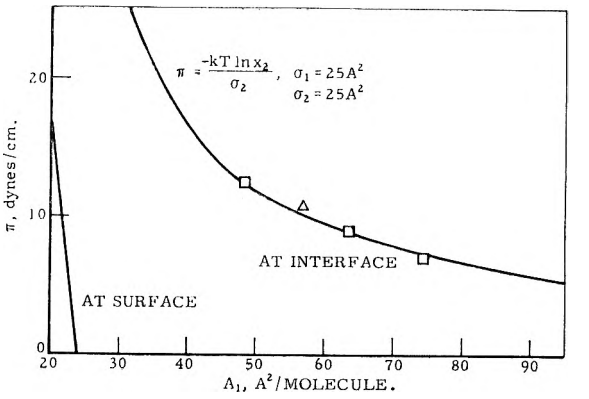

Fig. 3.—Pressure–area isotherm for stearic acid adsorbed at the interface between water and a naphthenic white oil. Line is calculated for ideal two-dimensional solution of stearic acid in oil, and points are experimental. Triangle is from studies of Zisman.[14]

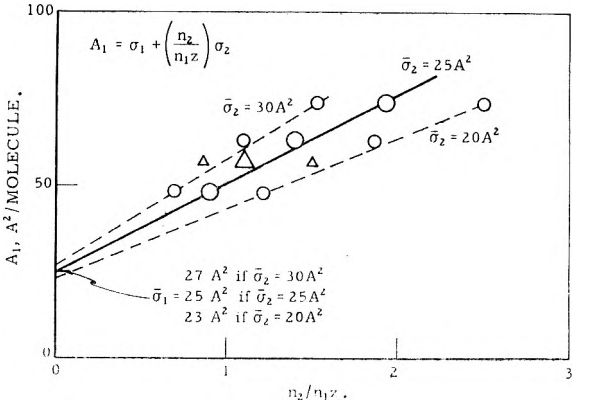

Fig. 4.—Ideal two-dimensional solution plot of stearic acid adsorbed at oil–water interface at 25°. Effect of various values of $\bar{\sigma}_2$.

illustrates the effect of using various values of σ_2. All values (20, 25, or 30 Å.^{2}) fit the data equally well and give identical π–A_1 relations. The difference is only in the predicted value of σ_1, the partial molecular area of stearic acid. An independent measure such as the orientation potential is needed to decide which is correct.

This example shows the frequently observed effect of the expansion of a monolayer at the oil–water interface as compared with its pressure–area relation on the surface of water (Fig. 3). Though the effect usually is explained as resulting from "releasing the forces of cohesion" in the monolayer it is obvious that the expansion is only the area of the oil molecules in an ideal binary solution with the adsorbed molecules and that the exact pressure–area relations of the interfacial film are calculable from known values of σ_1 and $\bar{\sigma}_2$.

Not all surface-active agents form ideal two-dimensional solutions in oil. At least one case of complete insolubility has come to our attention, octadecanol in white oil at 25°.[15] Here there was no swelling of the monolayer in oil.

It is to be expected that at high film pressures a critical pressure may be reached where the activity coefficient ϕ_2 suddenly becomes very large and the

(15) W. M. Sawyer and F. M. Fowkes, *J. Phys. Chem.*, **60**, 1235 (1956).

film changes from a solvated to non-solvated film. This has been shown before[4] and appears again for dimethylbutane in stearic acid at 23 dynes/cm. and for carbon tetrachloride in stearic acid at 17 dynes/cm. (Fig. 2). Some polymeric monolayers swell at the oil–water interface as oil molecules penetrate them, but the equations for ideal solutions do not fit such polymers. A later publication will give the proper equations to use in these cases.

Water-Soluble Monolayers at the Oil–Water Interface.—J. T. Davies has measured the pressure–area relations for long chain quaternary ammonium salts at the oil–water interface, and applied the "gas" equations to the data.[16] While previous investigators had found that ionic films are more expanded than non-ionic, so that the "gas" equations required $2kT$, Davies found that in his system (when the aqueous phase had a low ionic strength) the "gas" equation required a value of $3kT$.

This is now easily explained as due to the quaternary ammonium chloride having a double function in this film. That is, these molecules occupy both adjacent interfacial monolayers, being oil-soluble and yet having ionic groups soluble in water (in contrast to stearic acid). The long hydrocarbon chains formed an ideal solution with the oil at the same time as the quaternary ammonium and the chloride ions formed an ideal solution with the water. If we call the water component 3 and the oil component 2, the film pressure of this system should be

$$\pi = -\frac{kT \ln (1 - zx_1)}{\sigma_3} - \frac{kT \ln (1 - x_1)}{\sigma_2} \qquad (10)$$

If we follow the derivation of the "gas" equations[2] and make the usual linear approximation of $\ln (1 - x_1) = -x_1$, and the usual assumption that $A_1 - (\sigma_1 - \sigma_2)$ or $A_1 - (\sigma_1 - \sigma_3)$ can be approximated by $A_1 - A_0$, eq. 10 becomes

$$\pi(A_1 - A_0) = (z + 1)kT \qquad (11)$$

where z is the number of ions per long chain quaternary ammonium chloride molecule. It is obvious why on very dilute salt solutions where z was nearly 2.0 that $3kT$ was needed in the "gas" equation, but when saturated salt substrates were used (and the long chain amine salt was "salted-out" so that z was less than unity) the "gas" equations required only 1–$2kT$.

(16) J. T. Davies, *Proc. Roy. Soc.* (London), **A208**, 224 (1951).

SURFACE PRESSURE–AREA PROPERTIES OF ORGANIC MONOLAYERS ON MERCURY

BY A. H. ELLISON

Texaco Research Center, Beacon, New York

Received March 2, 1962

A horizontal float type mercury film balance was constructed for this work. The anticipated difficulties of effective sliding barriers and atmospheric contamination were overcome, after the methods of Fahir, by "framing" the mercury surface with thin Mylar film and using supported thin Mylar film strips for sliding barriers and by housing the film balance in a box that was flushed with dry nitrogen. Surface pressure–area curves on mercury were obtained for stearic acid, stearyl alcohol, lauric acid, sebacic acid, *n*-octacosane, benzoic acid, and 1-naphthoic acid. Interpretations of the different types of curves given by these materials indicate that: paraffin chains tend to lie flat on the surface of mercury, but they can be forced into a vertical orientation if a terminal polar group is present; aromatic rings tend to stand on edge on the surface of mercury; and polar groups provide points of strong attachment of molecules to a mercury surface. Equilibrium spreading pressure was measured for each of the materials studied. These measurements provided information on the stability of the films which was an important consideration in interpreting the surface pressure–area curves.

Introduction

Film balance studies of monolayer films of organic materials on water have produced information on film structure which has been basic to an understanding of many other surface phenomena. Such studies are, of course, limited to materials which spread on water and also are insoluble in water. Many materials of interest in the field of boundary lubrication cannot be studied as insoluble monolayers on water because they are either non-spreading on water, *e.g.*, non-polar base oils, or soluble in water, *e.g.*, polar aromatics such as benzoic acid. Mercury should be a near ideal substrate for film balance studies since most organic materials can be expected to spread on mercury[1] and also be insoluble in mercury. Further, for studies of films of interest in the field of boundary lubrication a metal substrate is desirable.

The objects of the work reported here were to develop a film balance suitable for studies of organic monolayers on mercury and to obtain surface pressure–area data for a variety of molecular types in order to obtain preliminary information on the relationships between molecular structure and monolayer structure on mercury.

The only previous mercury film balance work found in the literature was reported by Fahir.[2] His reported work was limited to the high pressure region of the oleic acid curve from which he concluded that there was little difference between the oleic acid monolayers on water and on mercury.

Experimental

Apparatus.—The film balance trough (32 in. × 7 in.) was machined from 1 in. thick Teflon securely bolted to a 0.44 in. thick aluminum base plate. Following the technique used by Fahir,[2] the formation of a meniscus at the junction of a sliding barrier and the trough edge, which would permit a spread film to leak past, was prevented by the use of thin plastic film. A "frame" of 0.001 in. Mylar film was attached to the top of the trough edge and strips of the same film attached to the bottom of conventional barriers were used for sliding barriers. This barrier system is effective because the plastic film adheres strongly to the mercury surface and conforms to it. In order not to restrict this adherence at the junction of the trough edge film and sliding barrier film, the films are mounted so as to extend beyond their supports by about $^3/_{16}$ in.

The horizontal float or Langmuir method of measuring surface pressure was used because it was believed that difficulties would be encountered in the wetting of the plate used in the Wilhelmy method. A leak-proof floating barrier system was made by cutting one large sheet of Mylar film to form the trough edge frame, the floating barrier, and loop-shaped connections between the ends of the floating barrier and the trough edge frame. The loop-shaped connections were not as flexible as the platinum foil connections used on a water film balance, but they were sufficiently flexible near the zero point for accurate surface pressure measurement using a null method. When floating on the mercury surface, to which it adhered strongly, the floating barrier was rigid and did not require support.

The absence of film leakage past these barriers was shown using a film of C^{14}-labeled stearic acid. The film of radioactive acid was spread and compressed to a pressure of 50 dynes/cm. The mercury surface area outside the barriers was monitored for radioactivity for about 15 min. using a G-M tube connected to a rate meter. The area of monitored surface was reduced at intervals to concentrate any escaped film under the window of the G-M tube. No leakage could be detected by this procedure.

The floating barrier was restrained by a typical torsion head assembly. Three "arms" in the form of a "T" were mounted on a torsion strip (5.25 in. long, 0.15 in. wide, 0.005 in. thick phosphor bronze). The vertical arm made a sliding connection with the floating barrier. One horizontal arm was used for calibration; the other was used to apply weight to null the force of surface pressure. A continuous and appropriate range of weights was obtained by means of a chain of the proper weight per unit of length mounted in the same fashion as in a chainomatic balance. The zero position of the floating barrier was determined by an optical method. A plane mirror mounted on top of the "T" shaped torsion assembly reflected the image of a crosshair to a scale with an optical lever arm of about 30 in.

The film balance was enclosed in a housing fitted with controls extending through the housing to manipulate the barriers and the "chainomatic" and with bellows-type neoprene gloves to spread the films. The purpose of the housing was to provide an atmosphere of nitrogen for the mercury film balance. The nitrogen (oil pumped) used for flushing the housing was passed through a column of Drierite, over copper turnings at ~50°, and through a cooling condenser before it passed into the housing.

The mercury was purified by acid washing followed by vacuum distillation. Acid washing was accomplished by passing the mercury dropwise down a two-foot column of 30% nitric acid. Depressions in the column wall caused the mercury drops to follow a zig-zag path down the column and be broken into very tiny droplets. The acid-washed mercury was distilled using a Cenco Improved Vacuum Form still. The delivery tube terminated in a reservoir inside the film balance housing. During distilling operations the reservoir was under vacuum. When the still was shut down the vacuum was relieved by admitting purified nitrogen to the system: thus the mercury in the reservoir was stored under nitrogen. Freshly distilled mercury was used for each day's work. Acid washing of the entire supply of mercury was repeated when necessary. Teflon stopcocks or clamps on short lengths of Tygon tubing were

(1) W. D. Harkins, "The Physical Chemistry of Surface Films," Reinhold Publ. Corp., New York, N. Y., 1952, p. 102.

(2) E. Fahir, *J. chim. phys.*, **27**, 587 (1930).

used where necessary on the distilling apparatus and reservoir to avoid possible contamination of the mercury by the grease used with glass stopcocks.

The mercury in the trough was connected to ground by means of a piece of platinum wire dipping in the mercury.

Under these conditions of nitrogen atmosphere and mercury preparation, one sweeping of the mercury surface with a sliding barrier produced a satisfactory mercury surface. No surface contamination could be detected by moving a sliding barrier toward the floating barrier and surface pressure–area data was satisfactorily reproducible. Over a period of time some contamination is to be expected. However, periodic checks for contamination on the clean surface side of the floating barrier during a run showed that in the time required for a run (approximately 15 min.) this was negligible.

Materials.—Stearic acid, *n*-octacosane, stearyl alcohol, benzoic acid, 1-naphthoic acid, and sebacic acid were Eastman White Label grade; lauric acid was Eastman technical grade. These materials were used without further purification.

C.P. benzene was used as the spreading solvent for all of the films studied with the exceptions of sebacic and 1-naphthoic acids, for which C.P. methanol was used. These solvents were shown to be free of residual film-forming impurities by spreading 0.1 ml. on the mercury surface and observing that no detectable surface pressure developed when the area was reduced by a factor of 40 (approximately 800 to 20 cm.^{2}). The spreading solutions were applied to the surface using a calibrated micropipet delivering 0.0478 ± 0.0002 ml. Concentrations of spreading solutions were adjusted so that 0.0478 ml. contained an amount of material which permitted investigation of the high area/molecule region of the curve with a maximum error of 1% at the low area/molecule region. In some cases the entire curve could not be obtained accurately with one concentration of spreading solution and thus high and low area/molecule regions of the curve were obtained in separate runs. Concentrations from 1×10^{-4} to 5×10^{-4} g./ml. satisfied these requirements.

Procedure.—The Teflon trough was cleaned initially by thorough scrubbing with an aqueous solution of "Tide." After being dried it was wiped with a degreased, lint-free cloth wet with C.P. benzene. Fresh sheets of Mylar film were used for the frame and barriers and, with careful handling during cutting and mounting, did not require further cleaning. The trough was recleaned and the Mylar frame and barriers were replaced when necessary, *i.e.*, when a clean mercury surface could not be maintained for a reasonable time after one or two sweepings of the surface.

With the film balance in place in the housing, the spreading solutions and micropipet were placed on a shelf in the housing and the housing cover was latched tight. The nitrogen flow was started. It was determined in preliminary work that flushing for 2 hr. at a flow rate of 22 ft.^{3}/hr. produced an atmosphere of at least 99.5% N_2 and that this flow rate had to be continued during runs to maintain this atmosphere. After 2 hr. flushing the trough was filled with mercury from the reservoir. The zero position on the scale was located by sweeping both sides of the float and then a film was spread and surface pressure–area data were obtained in the usual manner.

Equilibrium spreading pressure (Π_e) measurements were made by placing a small crystal of the undissolved material on a clean area (250 cm.^{2}) of mercury in the film balance and observing the maximum surface pressure developed by spontaneous spreading. In most cases spreading was quite rapid and the maximum pressure was attained in 2 min. or less. When no pressure developed in 10 min., Π_e was considered to be zero. The maximum deviation in repeated measurements was ±2.0 dynes/cm.

The same mercury could be used for several surface pressure–area runs or Π_e measurements. After a run the film studied may be swept away and confined behind a barrier leaving a satisfactorily clean mercury surface for another run. At the end of a series of runs the "scum" resulting from the sweeping away of several films was compressed to a small area and picked off the surface before the mercury was drained from the trough. This lengthened the time interval between complete washing of the trough and acid washing of the mercury. The trough was drained by means of a tube through the bottom of the trough connected to Tygon tubing which carried the mercury out of the housing to the reservoir of the mercury still.

These experiments were carried out in a controlled temperature room set at 25°. A mercury bulb thermometer in the film balance trough showed the mercury temperature to be 26 ± 1°.

A Fisher–Taylor–Hirschfelder atom model kit was used to construct scale molecular models of the materials studied here. Measurements on these models were made to determine the projected area of the molecule in various orientations with respect to a surface in order to associate the area/molecule observed in surface pressure–area curves with possible molecular orientation in the monolayer. The results of these measurements will be referred to below as the molecular model area in a certain orientation.

Results

General.—Determinations of surface pressure–area data on mercury using the apparatus described above were, for the most part, as straightforward as corresponding determinations on water. For the materials reported here, spreading was always rapid and complete. One difference was observed which was disturbing until it was understood. It was found that the surface pressure–area curves could be reproduced in the low pressure region but could not always be reproduced satisfactorily in the high pressure region. Also, collapse pressures were erratic. The behavior in the high pressure region is that predicted by Cary and Rideal[3] for unstable monolayers, *i.e.*, monolayers of materials that are crystalline solids at the measurement temperature which are compressed to pressures higher than their equilibrium pressure (Π_e) at the measurement temperature. The behavior at low pressures is that predicted for stable monolayers, *i.e.*, monolayers at pressures below Π_e. All of the materials reported here are solids at 26°. Their Π_e values were measured (indicated on the surface–pressure axes of the curves discussed below) and found to be approximately equal to the pressure dividing the reproducible or stable and non-reproducible or unstable regions of the curves. This supports the contention that the non-reproducible behavior results from thermodynamic instability of the monolayers in these surface pressure regions and not from any experimental difficulty. These same materials, *e.g.*, stearic acid, have Π_e values on water at 25° of only a few dynes/cm., yet quite reproducible surface pressure–area data and collapse pressures have been obtained with monolayers of these materials on water up to 30 or 40 dynes/cm. above Π_e. The difference referred to above, therefore, is that monolayer films on mercury compressed to pressures above Π_e collapse or partially collapse, as equilibrium requires, more readily than corresponding films on water.

Collapse of unstable films is explained by Cary and Rideal[3] as being due to the formation of crystalline nuclei in the film which in turn depends upon more or less uncontrollable conditions, such as the presence of dust, vibration, etc. Since in these experiments, dust, vibration, etc., were controlled to the same extent as in conventional film balance studies, no explanation of the difference in collapse behavior can be offered at this time. However, on the basis of the work of Cary and Rideal, erratic

(3) A. Cary and E. K. Rideal, *Proc. Roy. Soc.* (London), **A109**, 301 (1925).

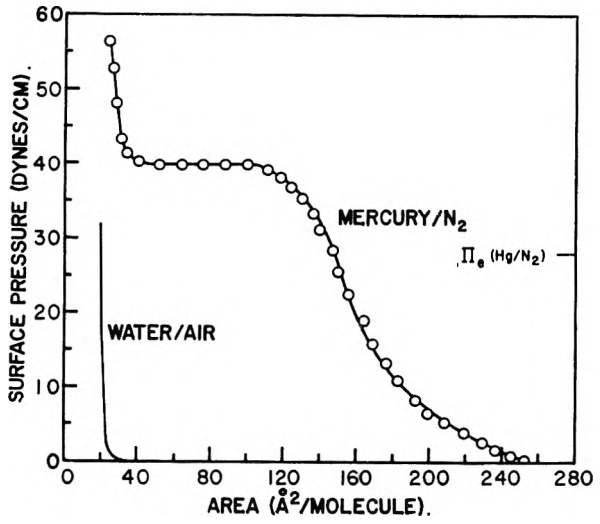

Fig. 1.—Surface pressure–area curves of stearic acid, 26°.

collapse and some degree of non-reproducibility, as found with the films on mercury, is to be expected.

In the surface pressure–area curves shown below, Π_e is indicated on the surface pressure–area axes to show the division between the equilibrium and non-equilibrium portions of the curves. Also, the highest pressure point shown is the collapse pressure for that particular film but, as stated above, a different collapse probably would be observed in a repeat run.

Stearic Acid.—In Fig. 1 the surface pressure–area curve of stearic acid on mercury is shown. For comparison purposes the curve on water also is shown.[4] Since the curve on mercury covers a wide range of area/molecule it was obtained in two separate experiments: one covered the region of the curve above 110 Å.²/molecule and the other covered the region below 110 Å.²/molecule. In repeat runs, the same type of curve was always obtained. There was some variation in the position of the plateau with respect to surface pressure (±5 dynes/cm.) and in the pressure at film collapse. There was little or no variation, however, in the position of the plateau with respect to area/molecule and film collapse never occurred above 30 Å.²/molecule.

It is believed that the curve for the film on mercury reflects the compression of a monolayer which consisted of horizontally oriented molecules at the beginning of the compression (260 Å.²/molecule), of vertically oriented molecules just prior to film collapse (25 Å.²/molecule), and of a mixture of horizontally and vertically oriented molecules at intermediate stages of compression, *i.e.*, from about 140 to 40 Å.²/molecule. (Molecular model areas are 120 Å.² for horizontal and 20 Å.² for vertical orientations.)

The monolayer is unstable in the surface concentration region where some of the molecules must be vertically oriented [(<100 Å.²/molecule)$^{-1}$], since to produce this surface concentration the film must be compressed to pressures higher than Π_e. Equilibrium requires that such a film collapse with some of the film molecules forming a bulk phase until the film pressure has fallen to Π_e. At Π_e the film consists of bulk material in equilibrium with a monolayer at a pressure of Π_e. According to the surface pressure–area curve a pressure equal to Π_e is produced by a surface concentration of (148 Å.²/molecule)$^{-1}$. These considerations are taken to mean that the preferred or equilibrium orientation of the molecules in a stearic acid monolayer at the mercury–N_2 interface at 26° is the horizontal orientation

Stearyl Alcohol, Lauric Acid, and *n*-Octacosane.—A molecule differing only in polar group, such as stearyl alcohol, should produce essentially the same curve as stearic acid. A lower homolog, such as lauric acid, should produce the same type of curve except that the knee of the curve, which corresponds to nearly perfectly packed horizontally oriented molecules, should be displaced toward lower areas/molecule. A non-polar paraffin of longer chain length, such as *n*-octacosane, should produce a curve having a knee at higher areas/molecule, and probably showing film collapse before a surface concentration corresponding to vertical orientation is reached because no polar group is present.

The surface pressure area curves of these materials are shown in Fig. 2. With stearyl alcohol, the high and low area/molecule regions of the curve were obtained in separate runs (division at 100 Å.²/molecule). The observations on reproducibility made with regard to stearic acid apply to stearyl alcohol also. The entire curves of lauric acid and *n*-octacosane were obtained in single runs. The reproducibility of these curves was better than with stearic acid or stearyl alcohol. This is expected since smaller portions of the curves fall in the unstable region.

It can be seen that the curves are essentially in agreement with the predictions even though features are present which partially obscure the predicted features. In the case of stearyl alcohol the slope of the curve above 120 Å.²/molecule is less than that found with stearic acid and the plateau is observed at a lower pressure. Both of these have the effect of reducing the definition of the knee in the curve so that this feature of the prediction cannot be evaluated adequately. The low area/molecule region and the over-all shape of the curve are in agreement with the predicted similarity to the stearic acid curve. The Π_e value for stearyl alcohol (30 dynes/cm.) is close to that observed with stearic acid (28 dynes/cm.).

The predicted features are observed in the lauric acid curve shown in Fig. 2. The knee in the curve is found at smaller area/molecule than with stearic acid and corresponds fairly well with the molecular model area of 90 Å.²/molecule for horizontally oriented lauric acid molecules. The curve approaches the same limiting area/molecule (20 Å.²) at high pressure as stearic acid since, of course, these two molecules which have the same molecular model area in the vertical orientation can be expected to occupy the same area in monolayers of close packed vertically oriented molecules.

The *n*-octacosane curve in Fig. 2 also shows the predicted features. The knee in the curve is ob-

(4) N. K. Adam, "The Physics and Chemistry of Surfaces," Second Ed., Oxford University Press, London, 1938, p. 47.

served at larger area/molecule (180 Å.^{2}) than with stearic acid and, further, it corresponds quite well with the molecular model area of 182 Å.^{2}/molecule for well packed horizontally oriented *n*-octacosane molecules. It can be seen in Fig. 2 that the curve does not show a pressure increase as the area approaches the molecular model area of vertically oriented molecules (20 Å.^{2}/molecule): collapse was always observed at about 60 Å.^{2}/molecule. This is interpreted to mean that the presence of the polar group in the polar materials permits them to be packed in the vertical orientation. The pressure rise between 100 and 90 Å.^{2}/molecule shown in the *n*-octacosane curve in Fig. 2 must be considered significant since the film is stable at the beginning, at least, of this pressure rise. It is possible that this pressure rise reflects the packing of molecules in a coiled or helical structure (with axes parallel to the surface) which could have been produced during compression of the film between 180 and 100 Å.^{2}/molecule. Measurements on a molecular model of *n*-octacosane arranged in various helical structures indicate that this explanation is plausible, but additional evidence is necessary. The equilibrium orientation in the *n*-octacosane film at 26° as indicated by the value of Π_e would be that tentatively attributed to horizontally oriented coiled molecules. It should be pointed out, however, that the precision of the Π_e measurement (± 2 dynes/cm.) is not good enough to rule out extended horizontally oriented molecules.

Sebacic Acid.—The surface pressure–area curve obtained with a sebacic acid monolayer is shown in Fig. 3. This material was studied in order to compare the generally similar surface pressure–area curves obtained with the mono-functional polar paraffins, stearic and lauric acids and stearyl alcohol, with that of an α-ω bifunctional polar paraffin. The curve was readily reproducible, except with respect to collapse pressure, even though the monolayer is unstable at this temperature at any pressure ($\Pi_e = 0$). The sebacic acid curve is believed to reflect the compression of a monolayer of horizontally oriented molecules. The surface pressure rises sharply as the area molecule approaches that in a close packed monolayer of horizontally oriented molecules (molecular model area in the horizontal orientation is 80 Å.^{2}/molecule) and then collapses. The Π_e value of 0 for sebacic acid indicates that at 26° sebacic acid molecules prefer the environment in a bulk crystal to that in a monolayer at the mercury–N_2 interface.

Benzoic and 1-Naphthoic Acids.—The surface pressure–area curves on mercury of benzoic and 1-naphthoic acids are shown in Fig. 4. These materials were studied so as to compare the surface pressure–area properties of the polar paraffin hydrocarbons with the polar aromatic hydrocarbons. The general shapes and positions with respect to the area axes of the curves were readily reproducible, but as usual collapse was erratic. It is believed that both of these curves reflect the compression of monolayers of vertically oriented molecules, *i.e.*, with the planes of the benzene rings of benzoic acid or the fused coplanar benzene rings of 1-naphthoic acid perpendicular or nearly

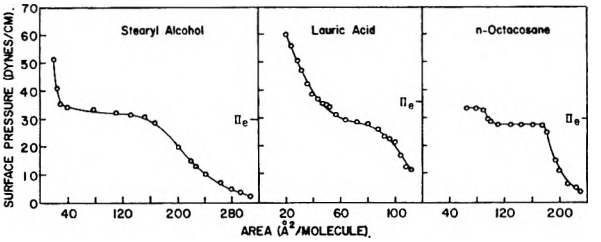

Fig. 2.—Surface pressure–area curves on mercury, 26°.

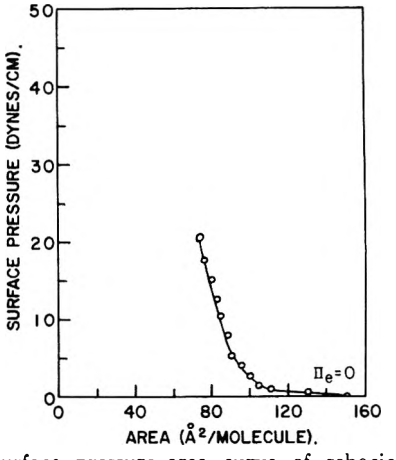

Fig. 3.—Surface pressure–area curve of sebacic acid on mercury, 26°.

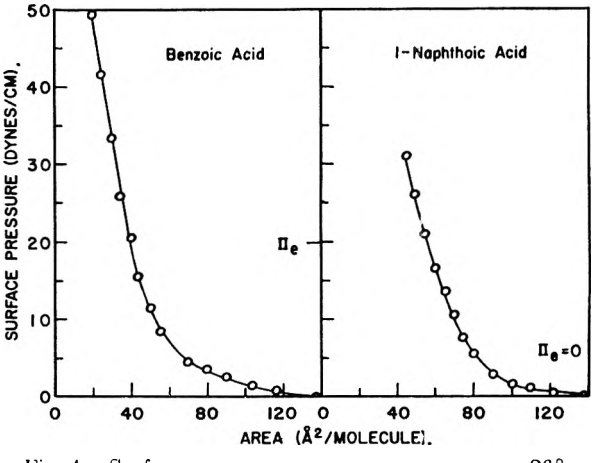

Fig. 4.—Surface pressure–area curves on mercury, 26°.

so to the mercury surface. It is likely that both materials are adsorbed by means of the polar group. Significant surface pressure is not observed at areas large enough to accommodate the molecules lying flat (>70 Å.^{2}/molecule[5] for benzoic acid and >100 Å.^{2}/molecule[5] for 1-naphthoic acid) and the curve rises sharply as the area/molecule approaches that of close packed vertically oriented molecules (about 20 Å.^{2}[5] for benzoic acid and 30 Å.^{2}[5] for 1-naphthoic acid when both are adsorbed by means of the polar group). The Π_e value of 20 dynes/cm. for benzoic acid is given by a monolayer at 26° with a surface concentration of (40 Å.^{2}/molecule)$^{-1}$. The orientation associated with this area/molecule, which we have called the equilibrium orientation, is believed to be with ring

(5) Molecular model areas.

planes perpendicular to the surface. 1-Naphthoic acid, like sebacic acid, is non-spreading on mercury at 26° ($\Pi_e = 0$).

Discussion

On the basis of the materials studied, it appears that at 26° long paraffin chains tend to lie flat on the surface of mercury, that aromatic rings tend to stand on edge on a mercury surface, and that polar groups provide points of strong attachment to a mercury surface. These orientation tendencies were deduced from the surface concentration in a monolayer at Π_e. Since Π_e can be expected to change with temperature and, for a homologous series, with molecular weight,[3] the orientation tendencies cited can also be expected to change with temperature and molecular weight. An example of the latter shown by this work is interesting. This is the tendency to vertical orientation observed with lauric acid in contrast to the horizontal orientation of stearic acid. It was expected that the van der Waals interactions between adjacent paraffin chains would be the dominating force in determining orientation so that the tendency to vertical orientation would be greater for the longer chain acid. For monolayers at Π_e, however, the results indicate that the paraffin chain–mercury substrate interactions are dominating. Further investigation of this point is planned.

Throughout this paper reference is made to a mercury surface; however, no direct evidence is available to indicate the chemical purity of the "mercury" surface used. The mercury surface obtained in this work is characterized by the fact that spreading thereon of the materials studied (in benzene or methanol or with no solvent for those materials having $\Pi_e > 0$) was always rapid and complete. This is in contrast to the mercury surface obtained with less well purified mercury in air which is instantaneously contaminated following sweeping of the surface so that spreading thereon of these materials is impossible.

The possibility that some of the materials studied when spread as a monolayer would react chemically with the mercury surface was considered. For example, the carboxylic acids might be expected to react and form mercury carboxylates. No direct evidence was obtained on this point but the similar behavior of stearic acid and a material believed to be unreactive, such as stearyl alcohol, suggests that carboxylate formation did not occur at least with stearic acid. Further evidence, preferably of a more direct nature, is necessary on the general questions of reaction with the mercury surface.

It is of interest to consider the surface tension or surface free energy of mercury covered with a close-packed monolayer of vertically oriented stearic acid molecules (γ'_{Hg}) in contrast to that of water covered with an identical film (γ'_{H_2O}). (It would be preferable to make this comparison for stable monolayers, but the information is not available for the stable monolayer on water.) The values of these two surface tensions can be calculated from the equation

$$F = \gamma - \gamma' \qquad (1)$$

where F is surface pressure, γ is the surface tension of the clean liquid surface, and γ' is the surface tension of the film covered liquid surface.[6] For the mercury case, F at 20 Å.^{2}/molecule is from Fig. 1 approximately 60 dynes/cm., γ is 475 dynes/cm., so that γ'Hg is 415 dyes/cm. For water F at 20 Å.^{2}/molecule is from Fig. 1 32 dynes/cm., γ is 73 dynes/cm., so that $\gamma'H_2O$ is 41 dynes/cm. It can be seen that these two surfaces which are identical from the standpoint of the nature and packing of the outermost molecular layer have surface tensions or surface free energies which differ by a factor of 10. This shows that the surface tension of a monolayer covered surface is not determined solely by the surface tension of the material comprising the monolayer. The other factor which must be involved is the monolayer–substrate "interfacial" tension as suggested by Bikerman.[7] By substituting in eq. 1 ($\gamma_a + \gamma_{ab}$) for γ' where γ_a is the surface tension of the monolayer material and γ_{ab} is the monolayer–substrate "interfacial" tension, we can estimate the latter for stearic acid–water and stearic acid–mercury. Using the F and γ values from above and an estimated 30 dynes/cm. for γ_a, γ_{ab} is for the water case 11 dynes/cm. and for mercury 385 dynes/cm. Interfacial tensions of organic materials against water and mercury have, of course, been measured[8] and are of the same order of magnitude as those estimated here for monolayer–substrate tensions. Thus while the monolayer–substrate tension may be small in the case of a polar organic monolayer on water, it is substantial for a polar organic monolayer on mercury and the surface tension produced by the latter is correspondingly higher.

In general it is believed that these results show that the use of mercury instead of or in addition to water as the substrate in film balance studies offers many advantages. A greater number of materials can be studied on mercury and if such studies are to be related to phenomena involving monolayers on metal surfaces, the monolayer structure on mercury which is different from that on water is probably a closer approximation.

It is a pleasure to acknowledge the many helpful discussions of this work with Dr. L. C. Roess and the assistance of Mr. D. A. Bauer in the experimental work.

DISCUSSION

HERMAN E. RIES, JR. (American Oil Company).—Did your isotherms indicate that on mercury the *final* collapse pressure for lauric acid is greater than that for stearic acid? If so, what is the explanation?

A. H. ELLISON.—Final collapse pressures were not reproducible. This, as indicated in the paper, is the expected behavior of monolayers compressed to surface pressures higher than Π_e. Thus no attempt was made to obtain a characteristic final collapse pressure for the various materials. Given enough time a monolayer should collapse to a pressure equal to Π_e. Under these conditions lauric acid collapses at a higher pressure than stearic acid.

DEAN W. CRIDDLE.—How reversible is the Π–A isotherm of stearic acid on mercury?

(6) Reference 4, p. 21.

(7) J. J. Bikerman, "The Nature of Surface Pressure," paper presented in the Division of Physical Chemistry at the ACS National Meeting, New York, N. Y., September, 1960.

(8) Reference 1, pp. 25, 29.

A. H. ELLISON.—The Π–A isotherm is reversible up to a pressure of Π_e. Above the pressure of Π_e the film is unstable and shows hysteresis on decompression. If the film is expanded so that the pressure falls to or below Π_e and then recompressed it would be as though a new film had been spread and as stated in the paper not likely to yield a good reproduction of the isotherm above Π_e obtained in the first compression.

J. N. WILSON (Shell Development Company).—The superiority of acid washing over distillation for the purification of mercury suggests that polyatomic clusters exist in mercury vapor, especially at relatively low temperatures. Because of the relatively low specificity of metallic bonding, such clusters may act as carriers to transport metallic impurities through the vapor.

F. M. FOWKES (Shell Development Company).—May I suggest that the pressure–area isotherms of Fig. 1–4 might be easily expressed in terms of the equations developed in paper II of my series on Ideal Two Dimensional Solutions [*J. Phys. Chem.*, **66**, 385 (1962)], treating the monolayers (at least up to $\Pi = \Pi_e$) as surfaces of mercury atoms (component 2) diluted by organic molecules (component 1) which should not be associated on this surface because they are more strongly bound to mercury than to each other [see *J. Phys. Chem.*, **66**, 382 (1962)]. The film pressure Π should be a function of the mole fraction of mercury atoms in the film-covered surface (X_2) and the partial atomic area of mercury (σ_2).

$$\Pi = \frac{-kT \ln X_2}{\sigma_2}$$

THE ADSORPTION OF FLEXIBLE MACROMOLECULES. PART I. THE ISOLATED MACROMOLECULE AT A PLANE INTERFACE[1]

BY A. SILBERBERG[2]

Mellon Institute, Pittsburgh, Penna.

Received March 2, 1962

The adsorption of an isolated, flexible linear polymer molecule of high molecular weight is treated at an infinite plane surface. The question of a possible equilibrium configuration is examined when it is required that some at least of the segments of the polymer molecule are in contact with the surface, and it is assumed that for each segment so placed the internal energy of the system is reduced by an adsorption energy xkT. It is shown that the polymer molecule will split up into sequences of segments; alternate stretches of P_S segments all in the surface and loops of P_B segments all out of the surface, whose size is not a function of molecular weight. The length, P_B, of the loops will decrease and the fraction, p, of segments in the surface will increase as the absorption energy x increases. Several models are considered. For an all adsorbable polymer molecule on an all adsorbing surface, the loops P_B are small and p is large even at small values of x. Such polymer molecules stay close to the surface with practically all their segments, and behave essentially as two-dimensional structures. In cases where not all surface sites are adsorbing, or not all polymer segments are adsorbable, or both, the size of loop is considerably increased and much higher adsorption energies are required. Restrictions limiting the re-entry of an adsorption loop into the surface, as well as any increase in specificity, have a similar effect. It is shown that structural principles affect polymer adsorption in sensitive fashion. The methods described can easily be adapted to discuss a variety of cases and are useful for this reason. It is one of the consequences of this model that the ends of the polymer molecule are on the surface. A discussion of previous theories, which predicted rather different results, is given.

1. Introduction

When a flexible polymer is placed near or onto a plane surface, great distortions of its shape from the average are to be expected which should depend in sensitive fashion on the structural features of the chain and on the chemistry and reactivity of its groups. Adsorption is thus an interesting technique to be employed in polymer studies, but an adequate theoretical apparatus must be developed to make sense of the results obtained.

Most of what has been done to date[3–7] in this direction is based on a set of fundamental papers[3a,3b] by Frisch, Simha, and Eirich in which the problem was first stated and analyzed. Theirs was essentially a two-step approach, involving in the first instance a discussion of the shape of the polymer in the presence of the surface. Then only, with the shape and the degree of intimate contact between polymer and surface characterized and held constant, the thermodynamic equilibrium between surface phase and bulk solution was considered. Unsatisfactory formulations were used, however, for both these aspects in the original papers,[3a,3b] and, although the thermodynamic part has been corrected[6] and the treatment of the isolated molecule improved,[4,7] there remain two serious weaknesses in the treatment: the discussion of the isolated macromolecule should be re-formulated and the shape of the polymer must be introduced as a variable into the full thermodynamic treatment.

In the present series of papers we shall attempt to do both. In Part I we shall discuss the isolated macromolecule at a plane surface. We shall consider first cases where all segments of the polymer can adsorb and where all sites on the surface are adsorbing. We shall consider these cases under a variety of structural restrictions on the chain as it enters or leaves the surface. In addition we shall consider cases where not all surface sites are adsorbing in character and where not all polymer segments can be adsorbed. Emphasis will be put on the method of derivation and it will become clear from the discussion that these methods can easily be extended and applied to a large number of other cases not considered here explicitly. In Part II[8] we

(1) This work was supported by the Air Force Office of Scientific Research under contract No. AF 49(638)541 with Mellon Institute.

(2) On temporary leave of absence from Weizmann Institute of Science, Rehovot, Israel.

(3) (a) H. L. Frisch, R. Simha, and F. R. Eirich, *J. Chem. Phys.*, **21**, 365 (1953); (b) R. Simha, H. L. Frisch, and F. R. Eirich, *J. Phys. Chem.*, **57**, 584 (1953); (c) H. L. Frisch and R. Simha, *ibid.*, **58**, 507 (1954).

(4) H. L. Frisch, *ibid.*, **59**, 633 (1955).

(5) H. L. Frisch and R. Simha, *J. Chem. Phys.*, **24**, 652 (1956).

(6) H. L. Frisch and R. Simha, *ibid.*, **27**, 702 (1957).

(7) W. I. Higuchi, *J. Phys. Chem.*, **65**, 487 (1961).

(8) A. Silberberg, *ibid.*, **66**, 1884 (1962).

shall treat the over-all thermodynamic aspects and derive expressions for the adsorption isotherm, for the surface tension decrement, for surface pressure, and for the parameters characterizing the structure of the monolayer.

2. General Formulation of the Problem.— In all the present considerations we shall regard the polymer molecule as being of high molecular weight.

We place the polymer molecule in the vicinity of a plane surface and ask what configurations it can adopt when at least some of its segments are required to be in contact with the surface. It is clear that the polymer molecule will split up into a series of runs composed of segments which are either all in contact with the surface, or all out of contact with it. In general let there be m_i runs of i segments each all out of the surface and $\bar{m}_j$ runs of j segments each all in the surface. The variables i and j can adopt any value, but if there are P segments all together in the polymer molecule, and we ignore end effects, the values which may be given to m_i and $\bar{m}_j$ are subject to the restrictions

$$\Sigma i m_i + \Sigma j \bar{m}_j = P \qquad (1)$$

and

$$\Sigma m_i = \Sigma \bar{m}_j \qquad (2)$$

We then define functions, $\omega(i)$ and $\bar{\omega}(j)$, representing the thermodynamic probabilities of a run of i segments, in a loop near the surface, and a run of j segments, totally in the surface, respectively. The functions ω and $\bar{\omega}$ are counts of all the distinguishable configurations which can be adopted by a sequence of segments under the restrictions imposed, weighted with any Boltzmann energy factor which might arise. $\omega(i)$ and $\bar{\omega}(j)$ are functions of i and j, respectively, but are independent of $m(i)$ and $\bar{m}(j)$. Their functional structure is fully determined by the restrictions imposed and may be presumed known. What they look like in detail will be discussed in later sections.

If η represents the partition function over all internal degrees of freedom of a polymer segment, we may write the following expression for the partition function Q of the entire system

$$Q = \sum_{m,\bar{m}} \eta^{\Sigma i m_i + \Sigma j \bar{m}_j} \Pi \omega(i)^{m_i} \Pi \bar{\omega}(j)^{\bar{m}_i} \times \binom{\Sigma i m_i}{\Sigma m_i} \binom{\Sigma j \bar{m}_j}{\Sigma \bar{m}_j} \qquad (3)$$

It is our task to determine the equilibrium values of i, j, m, and $\bar{m}$. What we expect to find is a sharp maximum in m and $\bar{m}$ at a certain value of i and j, respectively, with the functions zero practically everywhere else. By way of assumption, therefore, we shall write

$$m(i) = m\delta(i - P_B)$$

$$\bar{m}(j) = m\delta(j - P_S)$$

where δ stands for the δ-function, P_B and P_S are the equilibrium values of i and j, respectively, and m is the total number of runs of each kind. With these assumptions Q reduces to

$$Q = \sum_{P_B,P_S,m} \eta^{(P_B + P_S)m} \omega(P_B)^m \bar{\omega}(P_S)^m \binom{P_B m}{m} \binom{P_S m}{m} \qquad (3a)$$

where the equilibrium values of m, P_B, and P_S are fixed by the requirement that they determine the maximum term of Q. Note that m, P_B, and P_S are not independent of each other but must conform to the accessory conditions (1) and (2). Condition (2) has already been introduced into (3a), and (1) reduces to

$$m(P_B + P_S) = P \qquad (4)$$

under present circumstances. It is appropriate to consider the logarithm of the term in Q and replace the factorials which occur by the Stirling approximation. We thus have

$$\ln Q_{term} = m(P_B + P_S) \ln \eta + m \ln \omega\bar{\omega} + mP_B \ln \frac{P_B}{P_B - 1} + mP_S \ln \frac{P_S}{P_S - 1} + m \ln (P_B - 1)(P_S - 1) \qquad (5)$$

Multiplying (5) by a Lagrangian multiplier λ we define a function

$$\hat{Q} = \ln Q_{term} + \lambda m(P_B + P_S) \qquad (6)$$

and consider the maximum of $\hat{Q}$ with respect to m, P_B, and P_S, now regarded as completely independent. This leads to a set of three equations from which λ may be eliminated to give

$$\frac{\partial \ln \omega}{\partial P_B} - \frac{\partial \ln \bar{\omega}}{\partial P_S} + \ln \frac{P_B}{P_B - 1} \frac{P_S - 1}{P_S} = 0 \qquad (7)$$

$$\ln \omega - P_B \frac{\partial \ln \omega}{\partial P_B} + \ln \bar{\omega} - P_S \frac{\partial \ln \bar{\omega}}{\partial P_S} + \ln (P_B - 1)(P_S - 1) = 0 \qquad (8)$$

as the set of equations to be solved for P_B and P_S simultaneously.

To test whether the solution of (7) and (8) corresponds to a maximum we must look at the second derivatives of $\hat{Q}$. We note that, of these, only $\partial^2\hat{Q}/\partial P_B{}^2$ and $\partial^2\hat{Q}/\partial P_S{}^2$ are non-zero. As necessary conditions for a maximum we thus find

$$\frac{\partial^2 \ln \omega}{\partial P_B{}^2} < \frac{1}{P_B(P_B - 1)} \qquad (9)$$

and

$$\frac{\partial^2 \ln \bar{\omega}}{\partial P_S{}^2} < \frac{1}{P_S(P_S - 1)} \qquad (10)$$

Note that we would still be dealing with an over-all absolute maximum if in one, but not in both, of the equations 9 and 10 the inequality were replaced by an equal sign. If this is the case (and let us assume that P_B reaches such a point) the nature of the solution is altered. P_B must now be regarded as constant and in place of (7) and (8) we find a single equation to be solved for P_S

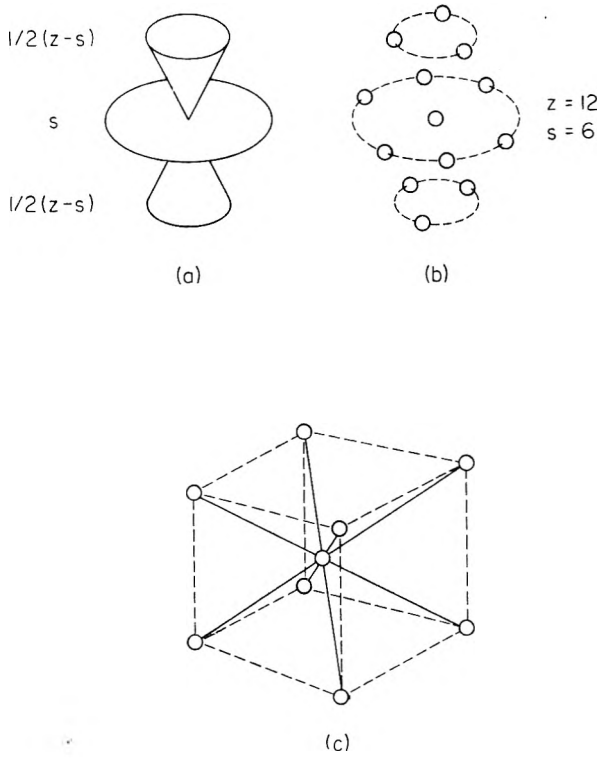

Fig. 1.—Schematic representation of lattice considered: (a, b) hexagonal lattice; (c) cubic lattice.

$$\ln \tilde{\omega} - (P_B^* + P_S)\frac{\partial \ln \tilde{\omega}}{\partial P_S} + P_B^* \ln \frac{P_B^*}{P_B^* - 1} \times \frac{P_S - 1}{P_S} + \ln (P_B^* - 1)(P_S - 1) + \ln \omega(P_B^*) = 0;\ P_B = P_B^* = \text{const.} \quad (11)$$

where P_B^* is the value of P_B corresponding to an equality sign in (9).

A somewhat similar situation would arise if the physical restrictions of the model require one or the other of the variables P_B or P_S to be constant. For example, the structure of the surface could conceivably permit only single point attachment. In this case, $P_S = 1$ and is constant, and we find

$$\ln \omega - (P_B + 1)\frac{\partial \ln \omega}{\partial P_B} + \ln \frac{(P_B - 1)^2}{P_B} + \ln \tilde{\omega}(1) = 0;\ P_S = 1 \quad (12)$$

as the equation for P_B.

Note that knowledge of P_B and P_S gives complete information about the state of the polymer. We shall in particular be discussing P_B and the fraction p

$$p = \frac{P_S}{P_B + P_S} \quad (13)$$

of polymer segments adhering directly to the surface. We want to study these quantities as functions of the model introduced and the parameter values chosen. Explicit forms for ω and $\tilde{\omega}$ must thus be established for each case.

3. Configuration Count on a $Z - S$ Lattice (Hexagonal Lattice).—As first and simplest case we shall consider the type of lattice illustrated in Fig. 1(a) and (b). Each site may be occupied by a chain segment and is surrounded by Z nearest neighbors, *i.e.*, there are assumed to be only Z possibilities of arranging a bond between two adjoining chain segments in the bulk of the system. On the surface, for a chain constrained to stay entirely within it, the coördination number reduces to S. In the vicinity of the surface we may regard the lattice as an array of layers of sites similar to the surface layer with $(Z - S)/2$ ways of stepping from one layer into the next and S possibilities of staying within it.

With these definitions, the problem of counting the number of arrangements on this lattice for a random walk, which sets out from the surface and returns to it after a certain number of steps, without any of the intermediate steps reaching the surface, can be handled in principle. In particular, if the number of steps is small, there is no difficulty about writing down the number of arrangements explicitly. We recall only that an adsorption loop of P_B segments corresponds to a random walk of $P_B + 1$ steps from the surface and back into it, and that we adopt the rule that in the placement of the step from a segment k to segment $(k + 1)$ only the position of segment $(k - 1)$ will exclude a site. In this way, we arrive at the results of column 3, Table I, where cases up to $P_B = 5$ have been treated. The manner of derivation should be obvious.

Let us now consider the expression

$$\omega(P_B) = \left(\frac{Z - S}{2}\right)^2 f^{P_B} (Z - 1)^{P_B - 1} \quad (14)$$

Putting $Z = 12$ and $S = 6$ and equating (14) with the results of column 3, Table I, we can calculate f in each case. The values f found in this way are given in the last column in the table. It is seen therefore that expression 14 with $f = 0.7$ would be a reasonable representation of $\omega(P_B)$ over the range considered. As it will turn out, moreover, that by the use of (14) we arrive at values of P_B which fall within the tested range, we may regard (14) with $f = 0.7$ as adequate to our purpose.

For $\tilde{\omega}$, as is easily seen, we may put

$$\tilde{\omega}(P_S) = S(S - 1)^{P_S - 2} e^{xP_S} \quad (15)$$

where x is the segment adsorption energy, *i.e.*, the reduction in internal energy (in units of kT) per segment occupying a surface layer site.

For P_B and P_S we thus derive the following equations from (7) and (8), respectively

$$\ln \frac{P_S}{P_S - 1} = \ln \frac{P_B}{P_B - 1} + \ln \frac{Z - 1}{S - 1} + \ln f - x \quad (16)$$

$$\ln \frac{1}{(P_S - 1)} = \ln (P_B - 1) + \ln \left[\left\{\frac{1}{2}(Z - S)\right\}^2 S/(Z - 1)(S - 1)^2\right] \quad (17)$$

TABLE I

NUMBER OF CONFIGURATIONS OF AN ADSORPTION LOOP ON A $Z - S$ LATTICE

No. of segments in loop, P_B	Max. no. of layers involved	Total no. of configurations $\omega(P_B)$	f
1	1	$\left(\frac{Z-S}{2}\right)\left(\frac{Z-S}{2}-1\right)$	0.67
2	1	$\left(\frac{Z-S}{2}\right) S \left(\frac{Z-S}{2}\right)$	.66
3	2	$\left(\frac{Z-S}{2}\right)\left(\frac{Z-S}{2}\right)\left(\frac{Z-S}{2}-1\right)\left(\frac{Z-S}{2}\right) + \left(\frac{Z-S}{2}\right) S(S-1) \left(\frac{Z-S}{2}\right)$	.72
4	2	$\left(\frac{Z-S}{2}\right)^2 S \left(\frac{Z-S}{2}\right)^2 + 2\left(\frac{Z-S}{2}\right)^2\left(\frac{Z-S}{2}-1\right) S \left(\frac{Z-S}{2}\right) + \left(\frac{Z-S}{2}\right) S(S-1)^2 \left(\frac{Z-S}{2}\right)$	.72
5	3	$\left(\frac{Z-S}{2}\right)^3\left(\frac{Z-S}{2}-1\right)\left(\frac{Z-S}{2}\right)^2 + \left(\frac{Z-S}{2}\right)^2\left(\frac{Z-S}{2}-1\right)^3\left(\frac{Z-S}{2}\right) + \left(\frac{Z-S}{2}\right)^4(2S^2 + S(S-1)) + \left(\frac{Z-S}{2}\right)^3\left(\frac{Z-S}{2}-1\right)\left(2S(S-1) + S^2\right) + \left(\frac{Z-S}{2}\right)^2 S(S-1)^3$	.70

We note moreover that the conditions (9) and (10) will be satisfied provided P_B and P_S are larger than 1. The results for the numerical case $Z = 12$, $S = 6$, are shown in Fig. 2.

We note in particular that P_B is smaller than 5.5 for positive x and that more than half the segments will be in the surface ($p > 0.5$) when the segment adsorption energy x exceeds $^1/_2(kT)$. The polymer chains are thus flattened into the surface at relatively small segment adsorption energies, and the long loops predicted by the Frisch, Simha, and Eirich model do not occur in this case. Furthermore, the dimensions of the loops are functions only of the lattice parameters Z, S, and f and the adsorption energy x. The total length of the chain P does not influence the character of the solution, provided that it is large enough.

4. Configuration Count on a Cubic Lattice.—(a) The lattice which we have considered in the previous section is the one customarily used in polymer solution theory. For the consideration of a variety of restricted random walks, such as we now propose to do, it is not the most suitable one, however. For this purpose we do better if we consider the cubic lattice illustrated in Fig. 1-(c). For each step on this lattice there are two choices open in each of the principal directions, *i.e.*, with each step we progress either to the left or to the right, up or down, backwards or forwards, by a constant amount. Which choice is taken in each direction is independent of the decisions taken in the other two directions, or, in other words, the random walks along the principal axes of the lattice are independent of each other.

Let us therefore divide up our problem and consider the random walks, along the normal to the surface layer, and parallel to it, separately. We thus look for the number of configurations ω_n and ω_p normal and parallel to the surface, respectively, in the knowledge that

$$\omega(P_B) = \omega_n(P_B)\omega_p(P_B) \qquad (18)$$

for any combination ω_n and ω_p referring to the same number of steps. A similar equation holds for $\bar{\omega}$.

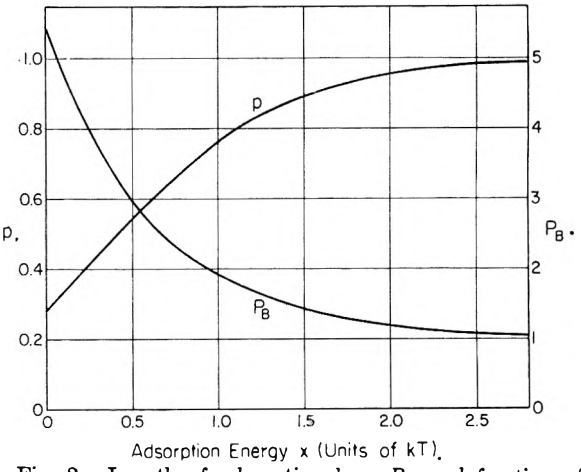

Fig. 2.—Length of adsorption loop P_B and fraction of number of segments p in the surface at various values of the adsorption energy x on a $Z - S$ lattice; $Z = 12$; $S = 6$; $f = 0.7$.

(b) We have shown the progress of a linear random walk in a direction normal to the surface in Fig. 3(a). Along the abscissa we have plotted the position relative to the surface, in units of lattice distances. (One lattice distance corresponds to half the length of side of the cube shown in Fig. 1(c).) Along the ordinate we plot the ordinal number of the segment under consideration. The one dimensional random walk is thus pulled out, concertina fashion, along the ordinate of the figure for our more convenient inspection. The lattice extends from $-\infty$ on the abscissa to position 1 where the outermost layer of lattice sites is assumed to occur. Positions larger than 1 are empty of lattice sites. The lattice sites at position 1, when occupied by a polymer segment, reduce the energy of the system by an amount xkT for each site filled. If a stretch of polymer is totally adsorbed the restrictions of the cubic lattice imply that only every second segment can be at layer line 1. The in-between segments must return to layer line 0 and thus will not contribute an energy change. What we shall call a random walk *in* the surface is in fact a succession of alternations between posi-

tions 0 and 1 in Fig. 3(a). A totally adsorbed stretch has only one configuration along the normal to the surface and if it involves P_S segments will contribute an internal energy change of $(x/2)(P_S + 1)$ units of kT. (Note, that, by definition, an adsorbed stretch starts and ends in layer line 1.) For $\bar{\omega}_n(P_S)$ we thus have

$$\bar{\omega}_n(P_S) = e^{\frac{x}{2}(P_S + 1)} \tag{19}$$

In the case of an adsorption loop of P_B segments we know that it starts in layer line 1 and returns to it in $P_B + 1$ steps. While we must exclude all occupations of layer line 1 by these P_B segments, there is no objection to layer line 0 being occupied. As shown in Fig. 3 the positions of the first step AB and of the last step CD are fixed by these considerations. The $(P_B - 1)$ steps between B and C may be taken anyhow, but are not allowed to reach layer line 1. One of many permissible paths is shown as the dotted line in Fig. 3(a). To count their number we consider all paths between B and C but place an adsorbing wall at layer line 1 to remove, from the total, all paths which touch it. According to Chandresekhar[9] we can find this number if from all paths between B and C we subtract the paths from B to the mirror image point C′ of C, taken with respect to the wall. We thus easily convince ourselves that

$$\omega_n(P_B) = \frac{(P_B - 1)!}{\left(\frac{P_B - 1}{2}\right)!\left(\frac{P_B - 1}{2}\right)!} - \frac{(P_B - 1)!}{\left(\frac{P_B - 1}{2} - 1\right)!\left(\frac{P_B - 1}{2} + 1\right)!} \simeq \frac{2^{P_B + 1}}{(2\pi)^{1/2} P_B (P_B + 1)^{1/2}} \tag{20}$$

where use was made of the Stirling approximation to represent the factorials.

(c) Using the same approach it is also easily shown that the number of paths which go from the surface, but, in l steps, do not necessarily return to it, *i.e.*, may reach any point from the surface without touching or passing through layer line 1 (except perhaps with the last step), is given by

$$\left.\begin{aligned} \omega_{end}(l) &= \frac{(l-1)!}{\left(\frac{l-1}{2}\right)!\left(\frac{l-1}{2}\right)!};\ l \text{ odd} \\ &= 2\,\frac{(l-2)!}{\left(\frac{l-2}{2}\right)!\left(\frac{l-2}{2}\right)!};\ l \text{ even} \end{aligned}\right\} \simeq 2^l \frac{1}{(2\pi l)^{1/2}};\ l \gg 1 \tag{21}$$

(d) We shall in addition be considering cases where not all outer layer line sites are adsorption sites. In such cases it is not necessary to exclude the outer layer to paths between adsorption points as no energy changes are involved. The situation corresponding to this model is illustrated in Fig. 3(b).

The physical reality of this model depends on the assumption that, given a loop of any length between two adsorption sites, no other adsorption point can be reached by the paths between them. We shall later examine how valid this assumption can be made, when this model will be discussed in detail. Now we are concerned only with establishing $\omega_n(P_B)$ for this case. Note that $\bar{\omega}_n(P_S)$ for this model is simply

$$\bar{\omega}_n(P_S) = \bar{\omega}(P_S) = e^x \tag{22}$$

To determine $\omega_n(P_B)$ we proceed as before, for the first and last step, but place the adsorbing wall at position 2 (and the mirror image point C′, consequently, at 4) when considering the configuration of the intervening $(P_B - 1)$ steps. We find

$$\omega_n(P_B) = \frac{2}{(P_B + 3)} \frac{(P_B + 1)!}{\left(\frac{P_B + 1}{2}\right)!\left(\frac{P_B + 1}{2}\right)!} \simeq \frac{2^{P_B + 3}}{(2\pi)^{1/2}(P_B + 3)(P_B + 1)^{1/2}} \tag{23}$$

(e) In assessing the influence of the surface in restricting configurations it should be recalled that the total number of configurations for $P_B + 1$ steps in one dimension is 2^{P_B+1}. The restrictions which apply to equation 20 thus reduce this number by a factor $(2\pi)^{1/2} P_B (P_B + 1)^{1/2}$. In terms of entropy this represents a decrease by an amount $k \ln [(2\pi)^{1/2} P_B (P_B + 1)^{1/2}]$ for each loop of length P_B. Note that this is in fact relatively little. Even if P_B is large, say of order 100, this loss in entropy could be compensated for by a gain, in other ways, of about $8kT$ of energy.

If, moreover, we allow for the additional freedom implied by equation 23, the entropy loss in a loop of about 100 segments would be counterbalanced by an even smaller energy change of about $6.5kT$. It should be clear therefore why long loops do not, as a rule, survive the adsorption process if a small energy gain per segment may be made in the surface.

(f) To round off this discussion we must find out what happens in the directions parallel to the surface and establish ω_p and $\bar{\omega}_p$. As the simplest assumption to make we shall consider first that the random walks in these directions are completely uninterfered with. Under these circumstances

$$\omega_p(P_B) = 2^{2(P_B + 1)} \tag{24}$$

$$\bar{\omega}_p(P_S) = 2^{2(P_S - 1)} \tag{25}$$

(g) To assume such a measure of freedom may, however, be rather naïve. It should be realized that we have put no restriction on the configurations, resulting either from multiple occupancy of the same lattice site or from steric interference. As a small step in this direction, and in order mainly to test out the effect of having some such restric-

(9) S. Chandresekhar, *Rev. Modern Phys.*, **15**, 1 (1943).

tions put in, we shall consider limiting the possibilities of return into the surface. What we have in mind is illustrated in Fig. 4(a). The adsorption loop depicted there is restricted by the assumption that the outer layer surface sites within the shaded area cannot be occupied by the returning loop. The ends of an adsorption loop are thus constrained to be at least d lattice distances apart.

We have already made use of the fact that the number of configurations for a random walk of $(P_B + 1)$ steps, consistent with an end separation of ξ lattice distances, is given by

$$\frac{(P_B + 1)!}{\left(\frac{P_B + 1}{2} + \frac{\xi}{2}\right)!\left(\frac{P_B + 1}{2} - \frac{\xi}{2}\right)!}$$

or, using the Stirling approximation, by

$$\frac{2^{P_B + 1}}{\left(\frac{\pi}{2}(P_B + 1)\right)^{1/2}} e^{-\xi^2/2(P_B + 1)}$$

If there is a separation $\pm\xi_1$ into one direction and $\pm\xi_2$ into another, independent direction, at right angles to it, such that

$$\xi_1^2 + \xi_2^2 = \xi^2$$

the number of configurations consistent with a separation $|\xi|$ thus turns out to be

$$\frac{1}{4}\frac{2^{2(P_B + 1)}}{\frac{\pi}{2}(P_B +} e^{-\xi^2/2(P_B + 1)} \qquad (26)$$

where the factor $^1/_4$ allows for the fact that there are four ways of arriving at $|\xi|$. Expression 26 is thus the density of configurations reaching a point a distance ξ from the origin of the configurations. If we integrate (26) over the whole area we find, as expected, that

$$\frac{1}{4}\frac{2^{2(P_B + 1)}}{\frac{\pi}{2}(P_B + 1)} \int_0^\infty e^{-\xi^2/2(P_B + 1)} 2\pi\xi \, d\xi = 2^{2(P_B + 1)}$$

i.e., the integration gives the total number of configurations (24). Here we wish to assess the number of configurations with end-points falling outside a distance d from the origin. Applying (26), we thus find, after suitable integration, that

$$\omega_p(P_B) = 2^{2(P_B + 1)} e^{-d^2/2(P_B + 1)} \qquad (27)$$

(h) Another powerful restriction of the random walk parallel to the surface would occur if not all outer layer sites were adsorbing. We could visualize, for example, that only layer points D lattice spaces from each other could adsorb with an energy effect (Fig. 4(b)). As can be seen, points A and B of the adsorption loop shown in the figure are in the surface, but they are so without an energy effect. The end-point of a loop of P_B segments will thus be nD lattice distances from the origin where $n = 1, 2, 3, \ldots, (P_B + 1)/D$. The number of configurations leading to a point for which $\xi = nD$ are given

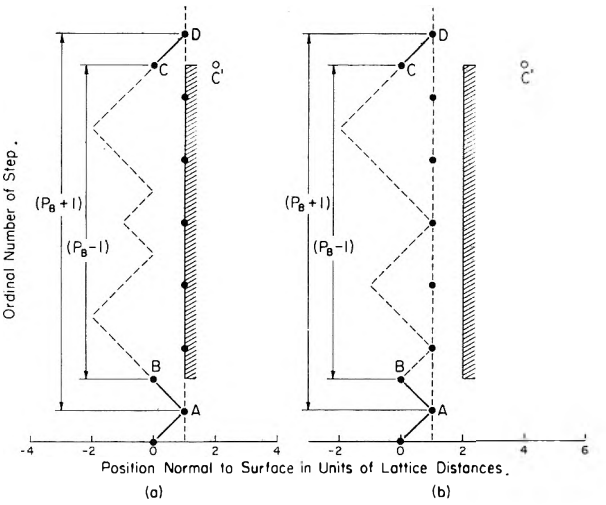

Fig. 3.—Schematic representation of a linear random walk normal to the surface. The random walk is pulled out, concertina fashion, for inspection, with each step findings its appropriate location along the ordinate. The lattice stretches from $-\infty$ to layer line 1 which is thus the physical surface. The steps AB and CD must be taken as shown. The $(P_B - 1)$ intervening steps may be taken in any way which does not take them up to or beyond an absorbing wall (shown shaded) and placed as indicated. A possible permitted path is shown dotted. (a) Occupation of surface layer sites is forbidden; (b) occupation of surface layer sites is permitted.

by (26) and since there are $8n$ points at distance nD we have

$$\omega_p(P_B) = \sum_{n=1}^{\frac{1}{D}(P_B + 1)} \frac{8n}{4}\frac{2^{2(P_B + 1)}}{\frac{\pi}{2}(P_B + 1)} e^{-\frac{(nD)^2}{2(P_B + 1)}} \qquad (28)$$

It is obvious that the above is a very rapidly converging series, provided

$$(P_B + 1) < D^2 \qquad (29)$$

We shall break it off therefore after the second term, and thus find

$$\omega_p(P_B) = \frac{4}{\pi}\frac{2^{2(P_B + 1)}}{(P_B + 1)} e^{-\frac{D^2}{2(P_B + 1)}} \times \left[1 + 2e^{-\frac{3D^2}{2(P_B + 1)}}\right] \qquad (30)$$

We can now proceed to a discussion of explicit cases.

5. Cubic Lattice; All Polymer Segments Adsorbable; All Surface Sites Adsorbing; Return into Surface Restricted.—As all surface sites are adsorbing we cannot permit interior segments of adsorption loops to enter the outer lattice layer. Hence we shall be using (19) and (20) for $\bar{\omega}_n$ and ω_n, respectively. For $\bar{\omega}_p$ and ω_p, in keeping with the restrictions envisaged, we shall put (25) and (27), respectively. We thus have

$$\bar{\omega}(P_S) = 2^{2(P_S - 1)} e^{\frac{x}{2}(P_S + 1)} \qquad (31)$$

and

$$\omega(P_B) = \frac{2^{3(P_B+1)}}{(2\pi)^{1/2}P_B(P_B+1)^{1/2}} e^{-\frac{d^2}{2(P_B+1)}} \quad (32)$$

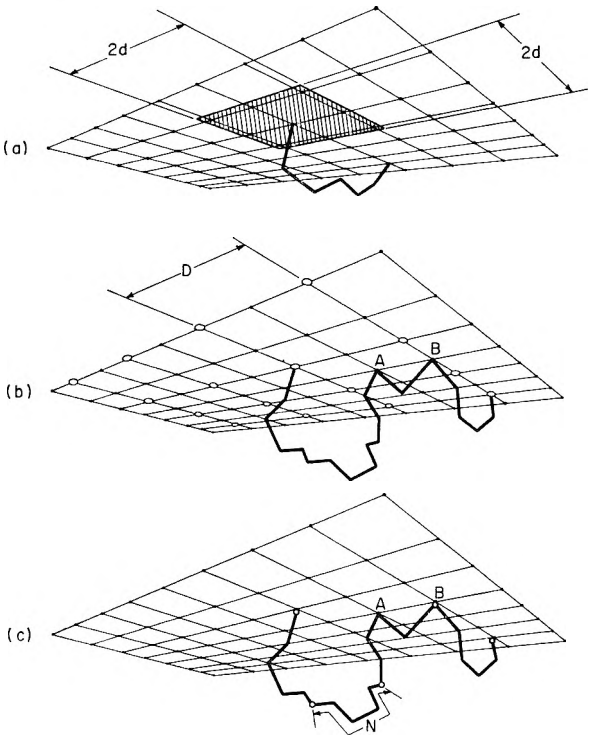

Fig. 4.—Restrictions on adsorption loops in a cubic lattice. The diagrams visualize the outer layer line surface sites (corresponding to position 1 in Fig. 3) seen from below. The lattice site positions occur at the intersections of the lines as shown. Each such square corresponds to the side of the cube in Fig. 1(c) and its edge measures out 2 lattice distances. (a) The ends of the adsorption loop are precluded from being closer than d lattice distances apart. The area shaded is excluded to the returning path. (b) Not all surface layer sites are adsorbing. Those which are, are shown as open circles and are D lattice distances apart. Points A and B may occupy surface sites without energy change. (c) Not all polymer segments are adsorbable. Those which are, are shown as open circles in the chain and are N segments apart. Point A is in the surface without energy change. Point B, however, represents an adsorption.

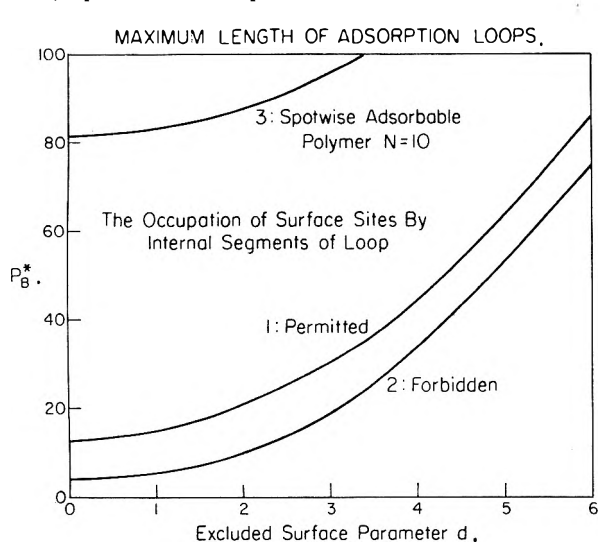

Fig. 5.—Maximum length, P_B^*, of adsorption loops for various values of the excluded surface parameter, d.

for substitution into (7) and (8). These are then solved for P_B and P_S.

Examining the restrictions (9) and (10) we find that the solution is valid for

$$(P_B+1)\left[1 - \frac{2(P_B+1)^2}{P_B^2(P_B-1)}\right] < 2d^2 \quad (33)$$

only, so that, depending on the value of d, the number of segments in an adsorption loop may not exceed a certain value P_B^*. How this number depends on the parameter d is shown in Fig. 5, curve 2. Curve 1 refers to a hypothetical case, analogous to the above, where instead of (20) for ω_n we have used (23). Internal segments of the adsorption loops may enter outer layer sites in this case. As such contacts would be energy contributing, this is not a realistic model and was plotted only for the interest the curve possesses when the definition of the parameters is changed. We shall discuss this presently.

The parameters p and P_B are plotted as functions of x in Fig. 6 and 7 as curves 2 and 3 for the cases $d = 2$ and $d = 4$, respectively. In Fig. 6, in addition, we have considered the case $d = 8$, as curve 4. Points at energy values x above the break refer to P_B values below the critical given by (33). Points below the break are a continuation of the solution by the use of equation 11. They represent a gradual dissolution of the adsorbed stretches into loops of constant length P_B^*.

It should further be noted that we must have $P_B > d - 1$ (see Fig. 4(a)) as otherwise the adsorption loops could not span the excluded area. The curves for $d = 4$ and $d = 8$ in Fig. 6 and 7 thus come to abrupt stops beyond which adsorption is complete on this model.

Note moreover that the abscissas in Fig. 6 and 7 have different meanings, although they refer to the same model. In Fig. 6 we have averaged x over the adsorbed segments, including those at layer line 0 in Fig. 3. For the cubic lattice model, now discussed, *i.e.*, for curves 2, 3, and 4 in Fig. 6, the abscissa is thus $x/2$. In Fig. 7, on the other hand, we were interested in comparing the actual binding strength of the surface interactions. The abscissa is thus x in all cases.

It is interesting to note that increases in d sharpen up the rapidity of the transition in the value of p. As curve 4, Fig. 6, shows, an energy change of $0.5kT$ brings about a change in p from 0.03 to 0.97 when $d = 8$.

Note moreover that curves 1 and 2 in Fig. 6 which refer to entirely different lattices agree with each other approximately, except at high p values where P_B is small and the models may be expected to diverge. As pointed out in section 3, p is large, for positive adsorption energies, and reaches about 0.75, when the energy change per segment is one kT. This is true for both curves 1 and 2 in Fig. 6, which refer to the least specialized conditions.

We have so far assumed that temperature is constant and that the different values of x correspond to different systems. If ΔE_{Ads} is the energy change in the adsorption of a segment, in conventional energy units, we have

$$x = \frac{\Delta E_{Ads}}{kT} \tag{34}$$

and we may regard x as an inverse temperature, if ΔE_{Ads} is constant. The abscissas in Fig. 6 and 7 are thus proportional to $1/T$, and the changes observed may be interpreted as a gradual melting out of adsorbed stretches of segments and their expansion into loops, which increase in size with increase in temperature. The breaks thus mark transitions in the state of the polymer molecule at the surface.

6. Cubic Lattice. All Polymer Segments Adsorbable; Not All Surface Sites Adsorbing; Return into the Surface Unrestricted.—We are discussing the situation depicted in Fig. 4(b). No totally adsorbed stretch larger than one segment can occur. We are thus dealing with the case envisaged in the last part of section 2. $P_S = 1$ and we have equation 12 to solve for P_B.

Remembering that under the conditions proposed we must use (22) for $\bar{\omega}$, and (23) and (30) for ω_n and ω_p, respectively, we have

$$\bar{\omega}(1) = e^x \tag{35}$$

and

$$\omega(P_B) = \frac{2^{3(P_B+1)}\, Y[1 + 2Y^3]}{\left[\frac{\pi(2\pi)^{1/2}}{16}\right](P_B + 3)(P_B + 1)^{3/2}} \tag{36}$$

with

$$Y = \exp\left[-\frac{D^2}{2(P_B + 1)}\right] \tag{37}$$

Substitution of these into (12) then gives the desired solution. The restrictions (9) and (10), moreover, must be satisfied and it turns out that these requirements are stronger than (29) so that the assumptions made in deriving (30) will always be consistent with the above solution.

The values which P_B can assume are bounded. We must have $P_B > D - 1$ (see Fig. 4(b)). On the other hand the restrictions (9) and (10) set on upper bound to P_B, which may be read approximately from curve 1, Fig. 5, if we interpret the abscissa in terms of D, according to

$$d = \frac{\left(1 - \frac{14}{3P_B}\right)}{\sqrt{3}} D$$

For the case $D = 10$ the solution is plotted as curve 5 in Fig. 7. Note the big shift along the energy axis and the large P_B values which are obtained in this case. If $x = 6$, for example, P_B increases from about 1 (on a uniformly adsorbing surface, curves 1 or 2), to about 40, in the case here considered.

Apart from the approximations leading to equation 30 we have one further source of inaccuracy in our derivation. We have permitted internal segments of loops to occupy surface sites, as is logical in this case. This, however, does not preclude the possibility that an adsorption site, *i.e.*, an active surface site, is on occasion occupied by an

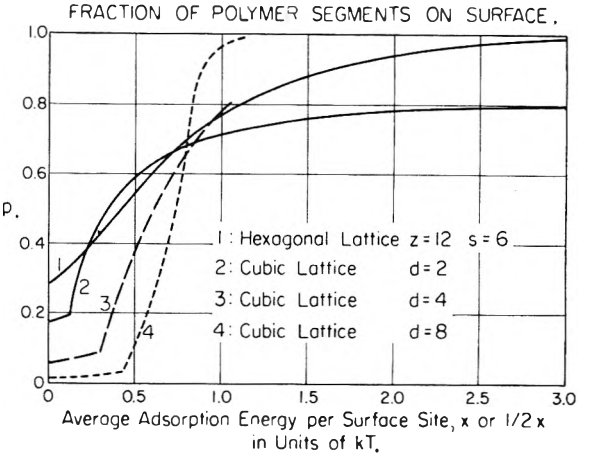

Fig. 6.—Fraction, p, of polymer segments on surface at various adsorption energies. The energy is averaged over the segments in the adsorption stretch. For the cubic lattice the abscissa, consequently, is $^1/_2\, x$.

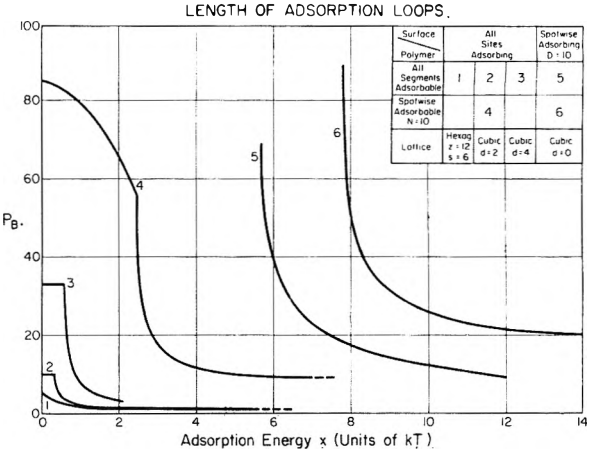

Fig. 7.—Average number of segments, P_B, in an adsorption loop in dependence on the segment adsorption energy, x.

internal loop segment. Such configurations (which we have included in the count) are not permitted. Their number, however, is only a fraction of the order $1/D^2$ of all the configurations and will be negligible if $D \gg 1$, as is here assumed.

7. Cubic Lattice; Not All Polymer Segments Adsorbable; All Surface Sites Adsorbing; Return into the Surface Restricted.—We have so far assumed that the segments into which the polymer is divided are both of the right size to occupy one lattice site and of uniform adsorption properties. We shall now treat a case where the ability of the polymer to adjust to the lattice is unchanged, but only every Nth segment will, when in the surface, make an energy contribution. All other segments may occupy surface sites, but this occupation does not involve an energy change.

Figure 4(c) illustrates what we have in mind. Only the segments indicated by open circles are adsorbing. The section of polymer chain we have shown consists of two loops, as only segment B, but not A, is adsorbable and changes the energy of the system.

From the point of view of the adsorption process, we shall, now, find it convenient to define as an

adsorption segment only the adsorbable segment, ignoring for the moment its $(N - 1)$ immediate non-specific neighbors. In Fig. 4(c) we have shown 5 such adsorption segments. The first one in the surface, then a sequence of two, out of the surface, and then a sequence of two again, in the surface. The treatment of section 2 can thus be applied substituting only adsorption segments for what we have called segments before. We will indicate with primes all symbols, previously used, but which now refer to enumerations in units of adsorption segments.

We thus have the polymer adsorbed in stretches of P_S' adsorption segments, all in the surface, and in loops of P_B' adsorption segments, all out of the surface.

An adsorption stretch is composed of $(P_S' - 1)$ loops of $(N - 1)$ segments each. For each of these loops of $(N - 1)$ segments we use (23) for the configuration count normal to the surface and (27) for the configuration count parallel to it. For all the $(P_S' - 1)$ loops, which are attached at P_S' points, we thus have

$$\bar{\omega}(NP_S') = 2^{3(P_S' - 1)N} \times \left[\frac{4}{(2\pi)^{1/2}} \frac{e^{-d^2/2N}}{N^{1/2}(N+2)}\right]^{(P_S' - 1)} e^{xP_S'} \quad (38)$$

The use of (23), in the above, implies that we have permitted access to surface sites to the $(N - 1)$ non-specific segments between each pair of adsorbed adsorption segments. This is only reasonable. If we wish to do the same for the $[N(P_B' + 1) - 1]$ internal segments of an adsorption loop, however, we do not preclude the possibility that in some configurations one or more of the P_B', supposedly non-adsorbed adsorption segments, will be at the surface. This we do not want, and it is necessary therefore to examine the situation. Let $\bar{\Omega}_i$ be the number of configurations normal to the surface such that no undesired contact is made in an adsorption loop of i adsorption segments. Let Ω_i be the corresponding total number of configurations where no adsorbable segment is excluded from the surface. Obviously for $i = 0$

$$\bar{\Omega}_0 = \Omega_0$$

and is given by (23), if we replace P_B there by $N - 1$. We have

$$\bar{\Omega}_0 = \Omega_0 = 2^N\gamma \quad (39)$$

with

$$\gamma = \frac{4}{(2\pi)^{1/2}N^{1/2}(N+2)} \simeq \frac{4}{(2\pi)^{1/2}N^{3/2}} \quad (40)$$

For loops, involving a finite number of adsorption segments, we have

$$\bar{\Omega}_1 = \Omega_1 - \Omega_0^2$$

$$\bar{\Omega}_2 = \Omega_2 - 2\Omega_1\Omega_0 + \Omega_0^3$$

$$\bar{\Omega}_3 = \Omega_3 - 2\Omega_2\Omega_0 + 3\Omega_1\Omega_0^2 - \Omega_0^4, \text{ etc.}$$

where it is easily seen that the terms in these expressions stand for successive over-corrections introduced in the effort to eliminate unwanted configurations. Only with the last term in each case is the final answer for $\bar{\Omega}_i$ established. If we now make use of the fact that

$$\Omega_i = 2^{(i+1)N} \frac{\gamma}{(i+1)^{3/2}}$$

we can express the above series as expansions in powers of γ.

$$\bar{\Omega}_0 = \Omega_0$$

$$\bar{\Omega}_1 = \Omega_1[1 - 2.83\gamma]$$

$$\bar{\Omega}_2 = \Omega_2[1 - 3.67\gamma + 5.2\gamma^2]$$

$$\bar{\Omega}_3 = \Omega_3[1 - 4.08\gamma + 8.5\gamma^2 - 8\gamma^3], \text{ etc.}$$

It follows from (40), however, that for large N the parameter $\gamma \ll 1$, so that the difference between $\bar{\Omega}_i$ and Ω_i may be neglected. Using (23) and (27) therefore without further modifications, we have, with P_B there replaced by

$$P_B = N(P_B' + 1) - 1 \quad (41)$$

the following expression for ω

$$\omega(P_B'N) = 2^{3(P_B' + 1)N} \frac{4}{(2\pi)^{1/2}} \times \frac{e^{-\frac{d^2}{2N(P_B' + 1)}}}{N^{1/2}(P_B' + 1)^{1/2}[N(P_B' + 1) + 2]} \quad (42)$$

Substituting (38) and (42) into suitably modified equations 7 and 8 we can solve for P_B' and P_S'. An upper limit for P_B' is found by using (42) in a modified equation 9. From (38) and (10) it follows that $P_S' > 1$. Working out the corresponding value of P_B^*, according to equation 41, we have shown, as curve 3 in Fig. 5, what this restriction implies. It is seen that much longer loops are permitted on this model for the same value of d.

Beyond the point where the present solution breaks down, we can perform the same sort of analysis as in section 5 for totally adsorbable polymers, by keeping P_B' constant at $P_B'^*$. We can determine P_S' in this region by the use of an analog of equation 11.

We have plotted the solution in terms of average P_B-values derived according to

$$\overline{P_B} = \frac{(N-1)(P_S' - 1) + N(P_B' + 1) - 1}{1 + [P_S' - 1]} = N\frac{P_B'}{P_S'} + (N - 1) \quad (43)$$

as curve 4 in Fig. 7 for the case $N = 10$, $d = 2$. Much larger values are obtained at the same values of x if we compare with the totally adsorbing chain. It is obvious that $\overline{P_B} = 9$ is an asymptotic limit and represents total adsorption on this model. Note however that the critical value of x, at which rapid desorption begins, has risen from 0.33 (curve 2) to about 2.5 in the present case.

The curvature of the portion of curve 4 below the break is due to the decreasing contribution of the P_S' loops to the average.

8. Cubic Lattice; Not All Polymer Segments Adsorbable; Surface Only Spotwise Adsorbing; Return into the Surface Unrestricted.—The type of situation we have in mind here corresponds to a superposition of the surface in Fig. 4(b) and the polymer of Fig. 4(c). We are thus considering a fairly high degree of specific matching between polymer and surface. Although this seems a much more complicated situation, the concept of an adsorption segment allows us to adapt equation 12 to the present case. For $\tilde{\omega}$ and ω we make the appropriate extension and find, in analogy to (35) and (36)

$$\tilde{\omega}(NP_S') = e^x \tag{44}$$

$$\omega(NP_B') = \frac{2^{3(P_B'+1)N}\, Y'^{[1+2Y']}}{\left[\frac{\pi(2\pi)^{1/2}}{16}\right] N^{5/2}\,[P_B'+1]^{5/2}} \tag{45}$$

where

$$Y' = \exp\left[-\frac{D^2}{2N(P_B'+1)}\right] \tag{46}$$

and where, as before, we have replaced $\bar{\Omega}_i$ by Ω_i on the assumption that $N \gg 1$, and where use was made of (30) instead of (27) for ω_p.

Remembering that $P_S' = 1$ in this case and is constant, we have plotted the results, expressed as $\overline{P_B}$ (equation 43), in the case $D = 10$, $N = 10$, as curve 6, Fig. 7. Considerably larger x values are required for adsorption in this case, showing that high adsorption energies are needed when the adsorption of a flexible polymer molecule is specific.

9. Cubic Lattice; End Effects.—We have in all the preceding discussion assumed that the polymer is so long that end effects can be neglected. In particular, when writing down the accessory condition (4) we have absorbed the number of segments in the ends (assumed to be small) in the constant P. If, however, we consider that there are l segments in each of the two ends we should modify (4) to read

$$m(P_B + P_S) + 2l = P \tag{47}$$

and include a term $\omega_{end}^2(l)$ in Q, equation 3. For $\omega_{end}(l)$ we may use the expression, equation 21, derived before. The equilibrium of the system demands in this case that

$$\frac{\partial^2 \ln \omega(l)}{\partial l^2} < 0$$

From (21), however, we see that

$$\frac{\partial^2 \ln \omega(l)}{\partial l^2} = \frac{1}{2l^2}$$

and that therefore no equilibrium situation exists. This means in practice that the ends of the chain are in the surface.

10. Discussion and Conclusions.—Our results may be summarized as follows: Provided that the macromolecule is large enough, the contact with the surface will tend to split it into units, whose size and structure are determined, only, by the nature and morphology of the surface and of the polymer molecule. The size of these adsorption loops and stretches does not depend on molecular weight.

In cases where all surface sites and polymer segments are adsorbing and the molecule is reasonably flexible, the adsorption loops are short and the polymer molecule stays close to the surface, even if the adsorption energies are low. At about one kT energy change per interaction adsorption is almost complete with more than 70% of the segments in contact with the surface.

As the loops are short and most of the segments are in the surface, the distribution of segments in the vicinity of the surface has a maximum at the surface itself and then falls off rapidly. Beyond $^1/_2P_B$ lattice distances, no polymer segments at all are found, but, already much closer to the surface, the segment concentration is low. The adsorbed polymer molecule is thus an essentially two-dimensional structure and behaves rather like a polymer molecule in a spread film.

When structural restrictions are put in, the quantitative details of this picture are altered. Changes which limit the freedom of adjustment of the polymer molecule to the surface increase the size of the loops, thicken the surface adsorption layer, and increase the energy requirements for adsorption. This is very clearly demonstrated in Fig. 7.

Adsorption will occur even in sterically unfavorable cases, however, at segment adsorption energies which do not have to be exceptionally large. At room temperature the energy scale in Fig. 7 does not exceed 8 kcal. per contact.

The steep portions of the curves in Fig. 7 mark an abrupt change in adsorption characteristics. Remembering that x is a measure of the intensity of interaction, we may interpret x, say, as an inverse temperature. The results of Fig. 7 thus point to the existence of a critical temperature at which desorption takes place. In another way of looking at the results one can conclude that mixtures of rather similar polymer species could be separated, if an adsorbent were used for which the x values of the two species placed one slightly above, the other slightly below, the desorption point. A separation on the basis of composition and structure rather than molecular weight would be achieved.

The analysis of section 2 is generally applicable to all cases for which admissable models for ω and $\tilde{\omega}$ can be devised. While the expressions given here for ω and $\tilde{\omega}$ take account of a number of situations, and can be combined and modified, a variety of further cases will result from the introduction of specific restrictions tailored to the need of the new problem. Interesting behavior patterns can thus be analyzed by following this general line of approach. The application of these concepts to the interactions between polymer molecules and surfaces of enzymes and other catalysts should be obvious. Of interest in this connection is the point made in section 9 that the terminal segments of an adsorbed polymer molecule have the tendency to stay on the surface. If polymerization occurs at an

interface the growing end of the chain will thus always be in contact with the surface.

The over-all picture which emerges from this investigation deviates in all essentials from the conclusions of Frisch, Simha, and Eirich.[3a,3b] Their predictions call for large P_B-values, proportional to the square root of molecular weight, with p extremely small.

To understand the discrepancy we must review their derivation of p. They identify p with the average over the polymer of the probability $p(\tau)$ that a random walk, starting at the surface, will have returned to it in τ steps. To determine $p(\tau)$ they treat a random walk problem of τ steps near a perfectly reflecting wall and find that $p(\tau)$ is a function of the position of τ from the end of the molecule. Generating configurations in this way they arrive at a p-value which depends on the inverse square root of molecular weight. A real surface has the property, however, that the random walk is not reflected, but can continue in it in two out of three dimensions and that a small reduction in energy per segment can compensate largely for the entropy loss in the third. As compared with the number of paths reflected from an ideal wall, the real number of distinguishable paths leading the τth element into the surface is far smaller. It is heavily biased, however, in favor of configurations in which many stretches have been spent in the surface. These configurations are periodic sequences of, on the average, P_S segments in, and P_B segments out of, the surface. The probability $p(\tau)$ does not, therefore, depend on whether τ is at a certain total distance away from the end of the polymer molecule, but whether or not it is one of the P_S segments of the period $(P_B + P_S)$ segments in which τ happens to lie. We are assuming here of course that for most positions τ on the polymer molecule, $\tau \gg (P_B + P_S)$.

Frisch subsequently[4] improved this treatment by considering a diffusion problem near a reflecting wall exerting forces. His continued use of a reflecting wall, however, did not eliminate the overcount of what are in fact indistinguishable configurations. Insufficient allowance was made, moreover, for the energy rich configurations which snake along the surface.

A correction for this latter effect was recently introduced into the Frisch model by Higuchi.[7] A set of difference equations was found which explicitly considers the conditions prevailing at the wall, in the layer adjacent to it, and in layers deeper in the solution. A square well potential is introduced to mark out the first layer. The use of reflecting wall statistics, however, still biases this picture in favor of the loops and the anchor-like drag of the adsorbed stretches on all configurations is thus not brought into sufficient prominence. Although much larger values of p are now predicted, they still depend on molecular weight and the adsorption energies, at which they are presumed to occur, are large enough to require the stipulation of a definite mechanism such as hydrogen bonding.

With p determined as described above, the further treatment of Frisch, Simha, and Eirich involves the solution of a problem analogous to equation 3 but with

$$\omega(P_B) = (1 - p)^{P_B}$$

$$\bar{\omega}(P_S) = p^{P_S}$$

It is thus assumed that the probabilities of being in and out of the surface are constant over the segments and equal to the averages. Working this out one finds $P_B = 1/p$ and $P_S = 1/(1 - p)$ as was to be expected. The large P_B values thus correspond to the small p-values derived.

It is of interest that recent experimental work supports the view that p is large (of the order of 0.5) and that most adsorption properties become molecular weight independent at high enough molecular weight. As concentration and solvent effects are involved, however, discussion and comparison with experiment will be deferred to Part II.

Some of the recent observations of Fontana and Thomas[10] are, however, of particular interest. These authors worked with a number of long chain alkyl esters of polymethacrylic acid. Studying the adsorption on silica they could arrive at p by a spectral method which distinguished between the number of bound and free CO-groups. They find p-values of about 0.4. By studying sedimentation rates of carbon black particles coated with these polymer molecules the surface layer thickness was determined and turned out to be about 25 Å. When a 1:5 copolymer of vinylpyrrolidone and alkyl methacrylate was tested, however, much thicker layers were found, in qualitative agreement with our expectations for a spotwise adsorbable polymer.

Nomenclature

P: no. of segments in the polymer molecule

P_B: no. of segments in a hanging absorption loop

P_S: no. of segments in a stretch of totally adsorbed segments

m: no. of repeating periods into which the polymer molecule is broken up

$$m \cong \frac{P}{P_B + P_S}$$

ΔE_{Ads}: energy change per segment placed at an adsorption site

x: adsorption energy in units of kT

$$x = \frac{\Delta E_{Ads}}{kT}$$

Z: coördination number of bulk lattice

S: coördination of surface lattice

$m(i)$: no. of loops of length i segments, all out of the surface

$\bar{m}(j)$: no. of adsorbed stretches of length j segments all in the surface

$$\Sigma m_i = m$$

$$\Sigma \bar{m}_j = m$$

(10) B. J. Fontana and J. R. Thomas, *J. Phys. Chem.*, **65**, 480 (1961).

$$\Sigma(im_i) + \Sigma(j\bar{m}_j) = P$$

$\omega(i)$: no. of configurations (distinguishable paths), weighted with any Boltzmann factor, which lead away and back to the surface under the restrictions imposed, in $(i + 1)$ steps

$\bar{\omega}(j)$: no. of configurations (distinguishable paths), weighted with any Boltzmann factor, for $(j - 1)$ steps taken totally in the surface

$\omega_n(i)$: no. of distinguishable arrangements, weighted with any Boltzmann factor, of $(i + 1)$ steps taken in a direction normal to the surface, under the restrictions imposed

$\omega_p(i)$: no. of distinguishable arrangements, weighted with any Boltzmann factor, of $(i + 1)$ steps taken parallel to the surface under the restrictions imposed

$$\omega(i) = \omega_n(i)\omega_p(i)$$

D: no. of direct line lattice distances separating adsorption points on a spotwise adsorbing surface

N: no. of segments per adsorbing segment in a spotwise adsorbable polymer molecule

d: minimum no. of lattice distances separating the ends of an adsorption loop

Q: partition function

λ: Lagrangian multiplier

ξ: no. of lattice distances separating the ends of an adsorption loop

l: no. of segments in a terminal adsorption loop

η: partition function over all internal degrees of freedom of each segment

f: factor expressing influence of surface restrictions, per segment, on short loops on a Z, S lattice

p: fraction of total number of segments adsorbed to the surface

Y: see equation 37 for definition

γ: see equation 40 for definition

Ω_i: no. of configurations normal to the surface for a loop of a spotwise adsorbable polymer molecule of i adsorption segments, all internal segments being permitted access to surface sites

$\bar{\Omega}_i$: no. of configurations normal to the surface for a loop of a spotwise adsorbable polymer molecule of i adsorption segments, only non-adsorbable internal segments being permitted access to surface sites

P_B^*: maximum no. of segments in an absorption loop

$\bar{P}_B$: av. no. of segments in polymer molecules where different size loops co-exist

Note: Where any of the above symbols appear with primes they refer to an enumeration in terms of adsorption segments.

THE ADSORPTION OF FLEXIBLE MACROMOLECULES. PART II. THE SHAPE OF THE ADSORBED MOLECULE; THE ADSORPTION ISOTHERM SURFACE TENSION, AND PRESSURE[1]

BY A. SILBERBERG[2]

Mellon Institute, Pittsburgh, Penna.

Received March 16, 1962

The known facts about the adsorption of macromolecules at surfaces, in particular the concentration, temperature, and molecular weight dependence of the adsorption isotherm, and of surface tension and pressure, and the shape of the adsorbed polymer molecule are reviewed. A model is introduced, based on the concepts used in discussing the isolated macromolecule at the surface (Part I), in which the adsorbed polymer molecules are attached to the interface by stretches of segments in the surface alternating with loops pending away from it. These loops are considered to set up a thin surface adjoint bulk phase of rather high polymer concentration. The partition function for the entire system is written down, and equations determining the equilibrium values of all variables derived from it. In the process, a new and rather simple method of determining the entropy of mixing of polymer molecules with low molecular weight solvent is introduced and discussed. The behavior, so predicted, is found to coincide in all essentials with the observed facts. It is found, in particular, that adsorption reaches a plateau value which maintains itself over a wide range in concentration. The plateau value is molecular weight dependent, adsorption increasing with increasing molecular weight, but at a decreasing rate, becoming independent of it, when it is very high. The temperature dependence of adsorption is small and segment adsorption energies can be quite low. Despite this the polymer molecules are practically flattened into the surface. Some half the segments are directly in the surface and the adsorbed layer is very thin. The shape of the adsorbed polymer molecule is largely independent of molecular weight and concentration, but depends strongly on the factors restricting polymer accommodation to the surface. The low rate to equilibrium and the inability to "wash off" adsorbed polymer films is explained. The theoretical isotherm apparently fits a Langmuir plot, but not for the usual reasons. Surface tension decrement and surface pressure are shown to be nearly the same for very dilute polymer solutions. Surface tension and adsorption are related by the Gibbs equation. A surface equation of state is derived. Ideal behavior is predicted in the limit of low surface adsorption. Other limiting cases previously considered in the literature also are covered.

1. Introduction

From the experimental record a fairly clear picture can be drawn today of the behavior of flexible macromolecules at interfaces. The most extensive data cover the adsorption from solution at solid surfaces,[3-20] some information exists about adsorption from aqueous solution at the mercury surface,[21,22] only a little is known about the surface tension of polymer solutions,[23-25] but a great deal more has been learned about spread films.[26-31] Curiously enough essentially the same model can account for the behavior of macromolecules under these seemingly very different conditions.

Let us now review the established facts of polymer adsorption; facts which any theory must be able to predict and explain. First at solid surfaces (or at the mercury interface):

(a) The amount of polymer adsorbed per unit surface increases extremely rapidly with polymer concentration of the equilibrium solution and then reaches a plateau value which does not change appreciably with further increase in bulk concentration.[4-15,17-19,21,22] In some cases, particularly where high molecular weight material is used, the initial rise in adsorption occurs at concentrations too small to be detected and the plateau extends over the entire experimentally accessible range of concentrations.[11,17,19]

(b) The adsorption is molecular weight dependent. The amount adsorbed increases with molecular weight at small molecular weights.[4-8,10,12,14,15,19,21,22] As the molecular weight increases, however, the amount adsorbed tends to a limiting value, *i.e.*, it becomes less and less dependent on the size of the macromolecules and eventually at high enough molecular weights no further dependence can be detected.[6,7,17,21,22] Use can be made of this

(1) This work was supported in part by the Air Force Office of Scientific Research under Contract No. AF 49(638)541 with Mellon Institute.

(2) On temporary leave of absence from Weizmann Institute of Science, Rehovot, Israel.

(3) (a) I. Claesson and S. Claesson, *Phys. Rev.*, **73**, 1221 (1948); (b) S. Claesson, *Discussions Faraday Soc.*, **7**, 321 (1949); (c) L. E. Amborski and G. Goldfinger, *Rubber Chem. Technology*, **23**, 803 (1950).

(4) W. Heller and W. Tanaka, *Phys. Rev.*, **82**, 302 (1951).

(5) E. Jenckel and B. Rumbach, *Z. Elektrochem.*, **55**, 612 (1951).

(6) I. M. Kolthoff, R. G. Gutmacher, and A. Kahn, *J. Phys. Chem.*, **55**, 1240 (1951).

(7) I. M. Kolthoff and R. G. Gutmacher, *ibid.*, **56**, 740 (1952).

(8) E. Treiber, G. Porod, W. Gierlinger, and J. Schurz, *Makromol. Chem.*, **9**, 241 (1953).

(9) J. F. Hobden and H. H. G. Jellinek, *J. Polymer Sci.*, **11**, 365 (1953).

(10) G. Kraus and J. Dugone, *Ind. Eng. Chem.*, **47**, 1809 (1955).

(11) A. Nevo, A. De Vries, and A. Katchalsky, *Biochim. Biophys. Acta*, **17**, 536 (1955).

(12) J. Koral, R. Ullman, and F. R. Eirich, *J. Phys. Chem.*, **62**, 541 (1958).

(13) O. E. Öhrn, *Arkiv. Kemi*, **12**, 397 (1958).

(14) J. S. Binford and A. M. Gessler, *J. Phys. Chem.*, **63**, 1376 (1959).

(15) H. L. Frisch, M. Y. Hellman, and J. L. Lundberg, *J. Polymer Sci.*, **38**, 441 (1959).

(16) M. Gottlieb, *J. Phys. Chem.*, **64**, 427 (1960).

(17) B. J. Fontana and J. R. Thomas, *ibid.*, **65**, 480 (1961).

(18) R. Perkel and R. Ullman, *J. Polymer Sci.*, **54**, 127 (1961).

(19) S. Ellerstein and R. Ullman, *ibid.*, **55**, 123 (1961).

(20) H. L. Steinberg, W. H. Grant, and F. L. McCrackin, Abstracts of Papers, 140th ACS National Meeting, Chicago, September, 1961.

(21) I. R. Miller, *J. Phys. Chem.*, **64**, 1790 (1960).

(22) I. R. Miller, *Trans. Faraday Soc.*, **57**, 301 (1961).

(23) A. Couper and D. D. Eley, *J. Polymer Sci.*, **3**, 345 (1948).

(24) A. Katchalsky and I. R. Miller, *J. Phys. Colloid Chem.*, **55**, 1182 (1951).

(25) H. L. Frisch and S. Al-Madfai, *J. Am. Chem. Soc.*, **80**, 3561, 5613 (1958).

(26) H. B. Bull, *ibid.*, **67**, 4, 8 (1945).

(27) D. J. Crisp, *J. Colloid Sci.*, **1**, 49, 161 (1946).

(28) H. W. Fox, P. W. Taylor, and W. A. Zisman, *Ind. Eng. Chem.*, **39**, 1401 (1947).

(29) H. B. Bull, *J. Biol. Chem.*, **185**, 27 (1950).

(30) H. Hotta, *J. Colloid Sci.*, **9**, 504 (1954).

(31) D. D. Eley and D. G. Hedge, *Discussions Faraday Soc.*, **21**, 226 (1956).

effect to fractionate polymer samples of not too high molecular weight.[4,7]

(c) The polymer molecule is adsorbed with a large number of its segments in direct contact with the surface.[14,16,17,21-23] The fraction, p, which these segments constitute of the polymer molecule is of order 0.5 and depends little on molecular weight[17,21,22] and is practically independent of the concentration in the equilibrium bulk phase and of the fraction θ of the surface covered by the adsorbed polymer segments.[17] It is, moreover, largely independent of the nature of the solvent used[16,17] and even of the adsorption characteristics of the surface.

(d) The polymer molecule is broken up, by contact with the surface, into short sequences of segments; stretches of segments all in contact with the surface alternating with loops of segments all out of contact with it. As the loops pending into the solution are short, the adsorbed polymer layer is often only some 30 to 50 Å. thick.[14,16,17,20]

(e) The temperature dependence of adsorption is small, indicating that moderate adsorption energies only are involved.[5,12,15,18,19] Both positive and negative coefficients have been found, adsorption in some cases increasing and in others decreasing with increase in temperature.

(f) The amount adsorbed from a solution is largest when a poor solvent for the polymer is used and decreases progressively with increase in solvent power.[5-7,9,12,17-19] This again shows that the segment adsorption energies are small, of the order of van der Waal's interactions in most cases.

(g) Equilibrium takes a very long time to establish,[3a,6,7,9,14,15,23-25] particularly with high molecular weight samples. In fact some of the early published data may be in error due to this factor not being properly appreciated. (For a discussion see Frisch, Hellman, and Lundberg.[15])

(h) The adsorbed polymer layer is often impossible to remove by washing with pure solvent.[11,12,14,15,20] Even increasing the temperature of extraction may be only partially successful.[15,19,20] Irreversibility has therefore been suspected. It is to be noted, however, that when the change is made to a better solvent the polymer can be removed.[7,12,19] We shall be able to show that the difficulty is only a practical one and in no sense implies that the phenomena cannot be treated by equilibrium thermodynamics.

(j) The adsorption data can in general be fitted to a Langmuir isotherm,[9,12,14,15,17] the best straight lines being obtained for the highest molecular weights.[4]

The facts which emerge from measurements of surface tensions and surface pressure of spread films (at relatively large areas per molecule) may be summarized as follows:

(k) The surface tension of a polymer solution does not change appreciably with changes in equilibrium bulk concentration.[21-24] Such changes as do occur are most pronounced for the low molecular weight fractions.[23] Taking the surface tension of the pure solvent as reference, the surface tension of a solution of given concentration is most affected by the highest molecular weight solute.[23,25] Both increments and decrements have been observed, but usually the surface tension is lowered.

(l) The surface pressure π of a spread film plotted against the area A per monomer is practically independent of molecular weight.[28,30] When, however, A tends to infinity, the intercept of a πA against $1/A$ plot, theoretically, gives the molecular weight of the polymer.[26] While this method has been applied successfully in many cases[26,29] it is sometimes found to be unreliable.[30]

On the theoretical side adsorption isotherms have been derived for rods by Mackor and van der Waals[32] and for stiff and flexible polymer molecules with all segments in the surface by Sarolea.[33] Flexible macromolecules, of which not all segments are necessarily in the surface, have been treated by Frisch, Simha, and Eirich.[34-38] In their approach they first considered the equilibrium of the isolated macromolecule at the surface and derived parameters characterizing its shape. According to these considerations the molecule is attached to the surface with only a very few of its segments. Most of the other segments are in very large loops whose size increases with the square root of the molecular weight. The parameter p, on this model, is thus very small, and the surface film thickness, large. The thermodynamics of adsorption are then treated, but the shape of the polymer molecule is not allowed to vary in the process. Within the limitations of this restriction an isotherm is arrived at[38] which reduces to the Sarolea isotherm[33] under the appropriate parameter changes. Both the Frisch–Simha isotherm and the Sarolea isotherm explain the plateau behavior (point (a) in the above enumeration) but cannot account for most of the other phenomena observed, particularly the large values of p (point (c) above) and the molecular weight dependence of the plateau (point (b) above).

In view of the generally unsatisfactory nature of these theoretical formulations a valuable qualitative discussion of the molecular weight dependence of the amount adsorbed has recently been given by Perkel and Ullman.[18] Various possible shapes of the adsorbed polymer molecule were considered and the molecular weight dependence to be expected under the circumstances worked out.

Frisch and Simha[37,38] have also derived expressions for surface tension and surface pressure. Their latest surface equation of state, derived from their corrected thermodynamic treatment,[38] reduces to the Singer[39] equation of state for flexible macromolecules with all segments in the surface when the appropriate parameter changes are made. For the more usual case, where some of the segments pend into the solution and the results depend, critically,

(32) E. L. Mackor and J. M. van der Waals, *J. Colloid Sci.*, **7**, 535 (1952).

(33) L. Sarolea, *Acad. Roy. Bely. Classe des Sciences*, [5] **40**, 1131 (1954).

(34) H. L. Frisch, R. Simha, and F. R. Eirich, *J. Chem. Phys.*, **21**, 365 (1953).

(35) R. Simha, H. L. Frisch, and F. R. Eirich, *J. Phys. Chem.*, **57**, 584 (1953).

(36) H. L. Frisch and R. Simha, *ibid.*, **58**, 507 (1954).

(37) H. L. Frisch and R. Simha, *J. Chem. Phys.*, **24**, 652 (1956).

(38) H. L. Frisch and R. Simha, *ibid.*, **27**, 702 (1957).

(39) S. J. Singer, *ibid.*, **16**, 872 (1948).

upon the polymer shape, their model again becomes inadequate.

A new approach has thus been attempted in the present series of papers.

In Part I[40] we have discussed the behavior of the isolated macromolecule at a surface and could show that interaction with the surface will cause the polymer molecule to adopt a shape where there are short stretches of segments all in the surface connected together by short loops pending away from it. The parameter p thus tends to be large. The length of the fully adsorbed stretches and the length of the adsorption loops are independent of molecular weight, in other words, the shape of the polymer molecule at the surface is not influenced by its length. Only the adsorption energy, *i.e.*, the energy change per segment brought into contact with the surface, and various steric factors specific to the type of lattice, or to the structure of the polymer molecule, can affect its shape. Segment adsorption energies of the order of kT are quite sufficient to flatten the polymer molecule almost completely into the surface in most cases.

The picture which emerges for the isolated macromolecule is thus rather different from that predicted by the Frisch, Simha, and Eirich model, and already accounts for a number of the experimental observations, notably, that the parameter p is large, that the adsorbed film is thin, and that the segment adsorption energies are small. Moreover, the molecular weight independence of the plateau adsorption value at high molecular weights is a reasonable and necessary consequence of this type of adsorption behavior, as the Perkel and Ullman[18] discussion shows. Solvent effects have been ignored, however, and the equilibrium with polymer molecules in the bulk solution not taken into account. It is the main purpose of the present paper to introduce these factors into the model.

In section 2 we shall define the parameters characterizing the system and formulate the method of approach. Much will depend on an appropriate configuration count in which due allowance has been made for the mixing of differently sized units on the type of lattice we shall be considering. A useful approach to this problem will be proposed in section 3 and then applied to the surface phase in section 4. In section 5 we shall discuss the energy of mixing and in section 6 write down explicitly the equations governing the equilibrium of the system. From this, using the formulation of section 2, we can derive a revised system of equations (as compared with Part I[40]) for determining the shape of the polymer molecule, and expressing the adsorption isotherm, the surface tension, and surface pressure. In section 7 we shall discuss the nature of the adsorption isotherm determined, and its dependence on the various parameters introduced. In section 8, similarly, we shall discuss surface tension and surface pressure. The mostly excellent agreement of these predictions with experiment will be analyzed in section 9 and the appropriate conclusions will be drawn in section 10.

Note: In order to avoid breaking up the text with long equations we have collected these in an Appendix at the rear and will refer to them by a number, prefixed with the letter "A."

2. **General Formulation of Problem.**—(a) In Part I[40] we have considered the behavior of a flexible macromolecule on a number of differently restricted lattices. One of these lattices was characterized by a coördination number Z in the bulk and a coördination number S on the surface. We saw that in this case a rather simple formula may be derived describing the configuration count of a polymer molecule adsorbed to the surface. For this reason, and as it is also the lattice generally considered for polymer solutions, we shall base our present derivations exclusively on this model.

The following are then the essential characteristics of this lattice: Each lattice point may be occupied either by a polymer segment, or by a solvent molecule. Any segment or solvent molecule so placed is surrounded in the bulk by Z nearest neighbors with whom it stands in interactions and in the surface by S such nearest neighbors. (An illustration is given in Fig. 1(a) and (b) of Part I.[40]) Only the placement of the segment immediately preceding a selected segment in the chain will specifically exclude a site in the placement of the next segment.

We now consider a polymer molecule in contact with the surface. We know that it is split up by this contact into sequences of segments which are, alternately, in and out of the surface. We have illustrated this schematically in Fig. 1. We recognize that if there are m sequences of segments per polymer molecule in contact with the surface there will be, as drawn in Fig. 1, $(m + 1)$ sequences of segments pending into the solution. Let there be P_S segments per sequence in the surface and P_B segments per sequence out of the surface. As our treatment in Part I has shown we can assume that, at equilibrium, the values of m, P_S, and P_B will be uniquely characterized. For us at present it is more convenient to change variables and to recognize that there are four different kinds of segments in the polymer molecule. There are m segments which are adsorbed and stand at the head of sequences. These we have indicated by black squares in Fig. 1. There are t segments which are adsorbed, but do not stand at the head of sequences, shown as black circles. There are $m + 1$ segments at the head of loops, shown by open squares, and u segments not at the head of loops, shown by open circles. If P is the total number of segments per polymer molecule we have

$$P = 2m + 1 + u + t \qquad (1)$$

As P, m, u, and t are very large numbers we could neglect small numbers, *i.e.*, the 1 in equation 1, in comparison with them. For the consideration of certain limiting cases, however, it will be important not to make this approximation too soon. We shall, therefore, retain these small corrections in our formulas and make the simplification only at the end.

With these new definitions (see Fig. 1) we now find

$$P_S = \frac{m + t}{m} \qquad (2)$$

(40) A. Silberberg, *J. Phys. Chem.*, **66**, 1872 (1962).

$$P_B = \frac{m + 1 + u}{m + 1} \tag{3}$$

$$p = \frac{m + t}{P} = \frac{mP_S}{P} \cong \frac{P_S}{P_S + P_B} \tag{4}$$

where p is the fraction of segments in direct contact with the surface as already mentioned.

We have seen[40] that the number of distinguishable configurations of the polymer molecule on the surface under these circumstances is (neglecting energy factors) given by

$$\left[\left(\frac{Z - S}{2}\right)^2 (Z - 1)^{P_B - 1} f^{P_B}\right]^{m-1} \times$$

$$[S(S - 1)^{P_S - 2}]^m \left[\left(\frac{Z - S}{2}\right)(Z - 1)^{P_B} f^{P_B}\right]^2 =$$

$$\left(\frac{Z - S}{2}\right)^{2m+1} (Z - 1)^u f^{m+1+u} \times$$

$$(S)^m (S - 1)^{t-m} \tag{5}$$

where f is a constant, for P_B not too large ($P_B \leqslant 5$), and has the value 0.7 when $Z = 12$ and $S = 6$. It is obvious how the factor $S^m (S - 1)^{t-m}$ for the adsorbed stretches is arrived at. It is also clear that there should be a factor $[(Z - S)/2]^{2m+1}$. The factor $(Z - 1)^u$ would be operative if all arrangements of the u non-head loop segment were equally permitted in the coördination sphere of their predecessors. In a loop, this is not possible, however, and we recognize f, therefore, as the factor which introduces the restrictions imposed by the presence of the surface on the arrangement possibilities of the $(m + 1 + u)$ segments in loops. It is reasonable, moreover, to suspect that special restrictions may occur every time the chain enters or leaves the surface. For this reason we introduce an additional restrictive factor g for each such transition and find in place of (5) the following configuration count

$$\psi_{1,S} = \left(\frac{Z - S}{2}\right)^{2m+1} \times$$

$$g^{2m} (Z - 1)^u f^{m+1+u} S^m (S - 1)^{t-m} \tag{6}$$

to characterize the polymer molecule at the surface. For the polymer molecule in the bulk the corresponding expression is obviously

$$\psi_1^* = Z(Z - 1)^{P-2} = Z(Z - 1)^{2m-1+u+t} \tag{7}$$

(b) Let us now assume that the lattice has N_S surface sites and that there are N_P polymer molecules adsorbed to it. If there are in addition N_P^* unbound polymer molecules and N_{P_T} is the total number of polymer molecules, then obviously

$$N_{P_T} = N_P + N_P^* \tag{8}$$

We will find that, in general, the concentration of polymer segments in the bulk phase is low, much lower in fact than the concentration set up in the vicinity of the surface by the polymer segments deriving from the adsorption loops. It is reasonable, therefore, to treat that portion of the bulk lattice into which the loops are penetrating as a separate solution of much higher concentration. The number of layers of lattice sites near the surface affected in this way is taken to be γP_B (see Fig. 1). It is reasonable to assume that

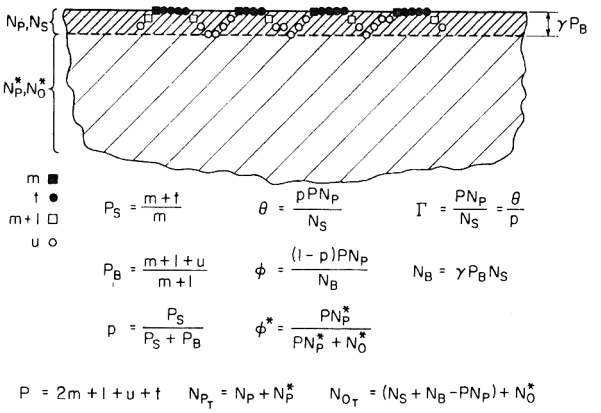

Fig. 1.—Schematic representation of adsorbed polymer and surface phase.

$$\gamma = \frac{1}{2} \tag{9}$$

but we shall leave γ explicit in our formulas. Only when quantitative evaluations are sought will we make use of (9). There are consequently

$$N_B = \gamma P_B N_S \tag{10}$$

lattice sites in the surface adjoint bulk phase and we can define

$$\phi = \frac{(1 - p)PN_P}{N_B} \tag{11}$$

as the volume fraction of polymer segments in this phase.

In deriving ϕ we have ignored the possibility that some of the segments belonging to the N_P^* non-adsorbed polymer molecules may occupy some of the N_B sites. As their concentration is very small, however, we can restrict our treatment to cases where this effect will be neglected. If ϕ^* is the volume fraction of polymer segments in the equilibrium solution we shall thus require

$$\phi^* \ll \phi \tag{12}$$

as a limiting condition upon the model.

If N_0^* is the number of solvent molecules lying below the dotted level indicated in Fig. 1, we have

$$\phi^* = \frac{PN_P^*}{PN_P^* + N_0^*} \tag{13}$$

and

$$N_{0_T} = N_0^* + (N_S + N_B - PN_P) \tag{14}$$

where N_{0_T} is the total number of solvent molecules in the system.

The fraction θ of the N_S surface sites occupied by polymer segments is given by

$$\theta = \frac{pPN_P}{N_S} = \frac{(m + t)N_P}{N_S} = \gamma P_S \phi \quad (15)$$

and should be clearly distinguished from the total number Γ of adsorbed segments per surface site

$$\Gamma = \frac{PN_P}{N_S} = \frac{\theta}{p} \quad (16)$$

We have seemingly introduced a large number of different parameters. They can, however, all be reduced into terms of the seven variables N_S, N_P, $N_P{}^*$, $N_0{}^*$, m, u, and t. For any given system, moreover, P, N_{P_T}, and N_{0_T} will be constant. The equations 1, 8, and 14, therefore, reduce the number of independent variables to four. As, in addition, we shall be holding N_S constant when considering the internal equilibrium of the system, we shall expect the treatment to yield three determining equations. Two of these will be the analogs of the two equations derived in Part I[40] for P_B and P_S; the third will be the adsorption isotherm.

(c) If for the moment we ignore equations 1, 8, and 14 and regard the seven variables describing the system as independent, we can express the partition function Q_T for the total system in the following way

$$Q_T = Q^* Q_S$$

$$Q^* = \Sigma\Sigma Q^*(N_P{}^*, N_0{}^*) \quad (17)$$

$$Q_S = \Sigma\Sigma\Sigma\Sigma\Sigma Q_S(N_P, N_S, m, t, u)$$

where Q^* and Q_S are the partition functions for the bulk phase and surface phase, respectively, and Q^* and Q_S are the general terms in these partition functions. Q^* is a function only of $N_P{}^*$ and $N_0{}^*$. Q^* is a sum over Q^* involving all combinations of values of the variables $N_P{}^*$ and $N_0{}^*$. Q_S, Q_S, and the variables N_P, N_S, m, t, and u are similarly related. The separation of Q_T in this fashion is made possible by the independence of Q^* and Q_S of each others variables implied by the restriction (12).

As is well known the values of the variables which determine the maximum of the logarithm of the general term (under the restrictions imposed) closely correspond to the equilibrium values of the variables and the logarithm of the maximum term, *i.e.*, the logarithm of the general term with the equilibrium values substituted into it is a representation of the logarithm of the partition function and with it of the free energy of the system.

We now define a reference state where at the same temperature and pressure all the solvent and polymer molecules are separated into the unmixed pure species. The pure solvent phase however has a surface of N_S sites. We thus have

$$Q_T{}^{REF} = (Q_0{}^{REF})^{N_{0_T} - N_S} (Q_{0,S}{}^{REF})^{N_S} (Q_P{}^{REF})^{N_{P_T}} \quad (18)$$

as the partition function of the reference state where $Q_0{}^{REF}$ and $Q_{0,S}{}^{REF}$ are the partition functions of a solvent molecule in the bulk and on the surface of pure solvent, respectively, and $Q_P{}^{REF}$ is the partition function of a polymer molecule in the pure polymer phase.

Dividing (17) by (18) we arrive at a reduced partition function $\overline{Q_T}$

$$\overline{Q_T} = \frac{Q_T}{Q_T{}^{REF}} = \overline{Q^*} \cdot \overline{Q_S}$$

$$\overline{Q^*} = \Sigma\Sigma\overline{Q^*}(N_P{}^*, N_0{}^*) \quad (19)$$

$$\overline{Q_S} = \Sigma\Sigma\Sigma\Sigma\Sigma\overline{Q_S}(N_P, N_S, m, t, u)$$

where $\overline{Q^*}$ and $\overline{Q_S}$ are the reduced partition functions, and $\overline{Q^*}$ and $\overline{Q_S}$, the reduced general terms for the bulk and surface phase, respectively.

We can now determine the equilibrium values of the six variables N_P, $N_P{}^*$, $N_0{}^*$, m, t, and u (N_S = const.) by finding which values of these variables makes the reduced general term

$$\overline{Q_T} = \overline{Q^*} \cdot \overline{Q_S}$$

or rather its logarithm, $\ln \overline{Q_T}$, largest under the restrictions imposed by equations 1, 8, and 14. We multiply these accessory conditions by Lagrangian multipliers λ_1, λ_2, and λ_3, respectively, and find the following set of equations

$$D_P + \lambda_2 - P\lambda_3 = 0 \quad (20)$$

$$D_m + 2\lambda_1 - \lambda_3 N_P \left(2 + \frac{1}{\phi}(P_B - 1)\right) = 0 \quad (21)$$

$$D_u + \lambda_1 - \lambda_3 N_P \left(1 - \frac{1}{\phi}\right) = 0 \quad (22)$$

$$D_t + \lambda_1 - \lambda_3 N_P = 0 \quad (23)$$

$$D_0{}^* + \lambda_3 = 0 \quad (24)$$

$$D_P{}^* + \lambda_2 = 0 \quad (25)$$

where

$$D_P = \frac{\partial \ln \bar{Q}_T}{\partial N_P} = \frac{\partial \ln \bar{Q}_S}{\partial N_P} \quad (26)$$

$$D_m = \frac{1}{N_P}\frac{\partial \ln \bar{Q}_T}{\partial m} = \frac{1}{N_P}\frac{\partial \ln \bar{Q}_S}{\partial m} \quad (27)$$

$$D_u = \frac{1}{N_P}\frac{\partial \ln \bar{Q}_T}{\partial u} = \frac{1}{N_P}\frac{\partial \ln \bar{Q}_S}{\partial u} \quad (28)$$

$$D_t = \frac{1}{N_P}\frac{\partial \ln \bar{Q}_T}{\partial t} = \frac{1}{N_P}\frac{\partial \ln \bar{Q}_S}{\partial t} \quad (29)$$

$$D_0{}^* = \frac{\partial \ln \bar{Q}_T}{\partial N_0{}^*} = \frac{\partial \ln \bar{Q}^*}{\partial N_0{}^*} \quad (30)$$

$$D_P{}^* = \frac{\partial \ln \bar{Q}_T}{\partial N_P{}^*} = \frac{\partial \ln \bar{Q}^*}{\partial N_P{}^*} \quad (31)$$

are functions related to chemical potentials.

Eliminating λ_1, λ_2, and λ_3 from among equations 20 to 25 we arrive at

$$D_m - D_u - D_t + \frac{P_B}{\phi} D_0{}^* = 0 \quad (32)$$

$$D_u - D_t - \frac{1}{\phi} D_0^* = 0 \quad (33)$$

$$D_P - D_P^* + PD_0^* = 0 \quad (34)$$

as the three equations characterizing the equilibrium for given N_S. Of these (32) and (33) may be regarded as the analogs of the equations derived in Part I[40] establishing the values of P_B and P_S. Equation 34, as we shall see, is the adsorption isotherm.

We now may consider variations in the value of N_S. This can be done in two ways. First we may do this keeping m, u, t, N_P, N_P^*, and N_0^* constant. This maintains polymer shape and prevents exchange between surface phase and substrate. The monolayer is being compressed like an adsorbed film. If π is the surface spreading pressure, we thus find

$$\frac{\mathcal{A}_0 \pi}{kT} = \frac{\partial \ln \overline{Q_T}}{\partial N_S} = \frac{\partial \ln \overline{Q_S}}{\partial N_S} = D_{N_S} \quad (35)$$

where D_{N_S} is defined by the above, $\mathcal{A}_0$ is the area per surface adsorption site, k is the Boltzmann constant, and T is the absolute temperature.

If, while changing N_S, we allow exchange to take place and equilibrium to establish itself we shall be measuring not surface pressure, but the surface tension increment $\Delta\sigma$ with respect to the pure solvent. We are thus considering the total free energy change and find

$$-\frac{\mathcal{A}_0 \Delta\sigma}{kT} = \frac{\mathrm{d} \ln \overline{Q_T}}{\mathrm{d}N_S} = D_{N_S} - (1 + \gamma P_B) D_0^* \quad (36)$$

Surface pressure and surface tension thus differ from each, apart from sign, only in the appearance of the term $(1 + \gamma P_B)D_0^*$. We shall see, however, that this term is negligible under most conditions.

Our problem is solved, therefore, if we can derive the quantities D_P, D_m, etc., defined in equations 26, 27, 28, 29, 30, 31, and 35. For this purpose we must find $\overline{Q_T}$.

The general term in a partition function can as a rule be split into a configurational factor and a Boltzmann energy factor. An implied assumption in the derivation so far has been that the seven variables introduced are adequate for the characterization of both these factors. That this is the case is not necessarily obvious at this stage, and in fact will require a number of further assumptions.

We shall discuss what these are in deriving $\overline{Q_T}$ in the next three sections.

3. Configuration Count in a Bulk Solution.—Let us ignore energy factors for the moment and consider only counts of distinguishable configurations.

If we are given a lattice of N_T^* identical sites and have to place on it N_T^* units, all of which are distinguishable, we can do this in $(N_T^*)!$ recognizable arrangements. If we agree that N_0^* of the N_T^* units cannot be distinguished among themselves and that the remaining

$$N_T^* - N_0^* = PN_P^*$$

units are also separate and indistinguishable among themselves, the number of recognizable configurations is reduced radically, and is given by

$$\frac{(N_T^*)!}{(N_0^*)!(PN_P^*)!} \quad (37)$$

(Note: the N_P^* polymer molecules are here broken up into (PN_P^*) free and indistinguishable segments.)

If it is believed that the PN_P^* segments are not all alike, but are ordered into N_P^* sequences of P segments each, where only the N_P^*P-sequences are indistinguishable from each other but the individual segments may be recognized by their ordinal position in the sequence, the number of configurations goes up to

$$\psi_2^* = \frac{(N_T^*)!}{(N_0^*)!(N_P^*)!} \quad (38)$$

Although we have been talking of an array of equivalent lattice sites we have not yet required that these sites be coördinated in any particular way. Normally for molecules occupying only one site at a time this does not matter. When dealing with polymer molecules which occupy P sites simultaneously, however, there is an imposed restriction upon the number of permitted configurations which we must now assess.

If Ω_m is the number of ways of putting the N_T^* lattice sites (occupied as they are in one of the permitted arrangements of (38)) together such that each site is surrounded by Z nearest neighbors, but with no regard paid as to which segment or solvent molecule is brought next to which other, and if Ω_P is the number of ways of putting these sites together such that polymer segments following each other in the sequence are made to occupy adjoining sites, the number of permitted arrangements for chemically linked polymer chains can be expressed in terms of (38) and these definitions and is obviously

$$\frac{(N_T^*)!}{(N_0^*)!\,(N_P^*)!} \frac{\Omega_P}{\Omega_m} \quad (39)$$

We are saying, in other words, that (38) is the configuration count when all the $[(Z/2)N_T^*]$ nearest neighbor contacts on the lattice are equivalent and any of the Ω_m random assemblies of the sites into a lattice of coördination number Z is equally permitted. If the number of ways of assembling the sites into a lattice is reduced to Ω_P, the permitted configuration count will be reduced in the ratio Ω_P/Ω_m.

It will be obvious that we are not dealing here with anything new, but with a classical problem in polymer solution theory, and that many other ways of arriving at explicit formulas in place of (39) exist.[41] Frisch and Simha in their treatment,[38] for example, have used the differential equation method of Miller.[41] We have found it more convenient, however, to follow the present approach to the problem.

The assembly of the lattice such that there are

(41) See for example, A. R. Miller, "The Theory of Solutions of High Polymers," Oxford Clarendon Press, 1948.

$(Z/2)N_T^*$ nearest neighbor contacts altogether with each site sharing in Z of them is obviously equivalent to the distribution of $[(Z/2)N_T]^*$ objects, $Z/2$ at a time, among N_T^* recipients, and Ω_m, consequently, is given by

$$\Omega_m = \frac{\left(\frac{Z}{2}N_T^*\right)!}{\left(\frac{Z}{2}!\right)^{N_T^*}} \tag{40}$$

In considering the arrangements Ω_P we have obviously ψ_1^* (see equation 7) ways of arranging each of the N_P^* polymer molecules on the lattice (the presence simultaneously of other polymer molecules on the lattice is assumed not to interfere with these arrangements). In so assembling these polymer chains we have in fact allocated $(P-1)N_P^*$ of the $[(Z/2)N_T^*)]$contacts of the lattice. The remainder are the so-called "external" contacts and it is assumed here, as in all other equivalent derivations, that these can be arranged at random in the further putting together of the lattice. Note, however, that there are now only $(N_0^* + N_P^*)$ recipients which will accommodate the full number, $Z/2$ each, of the external contacts and that the remaining $(P-1)N_P^*$ recipients have room for $((Z/2) - 1)$ contacts only. The number of ways Ω_P of assembling the lattice thus turns out to be

$$\Omega_P = \left(\frac{\psi_1^*}{2}\right)^{N_P^*} \times \frac{\left[\frac{Z}{2}N_T^* - N_P^*(P-1)\right]!}{\left[\frac{Z}{2}!\right]^{N_0^* + N_P^*}\left[\left(\frac{Z}{2}-1\right)!\right]^{N_P^*(P-1)}} \tag{41}$$

where the factor $(1/2)^{N_P^*}$ was introduced to allow for the two ways of choosing which of the terminal segments of the polymer chain is the head segment.

Dividing (41) by (40) then yields

$$\psi_3^* = \frac{\Omega_P}{\Omega_m} = \frac{\left[\frac{Z}{2}N_T^* - (P-1)N_P^*\right]!}{\left[\frac{Z}{2}N_T^*\right]!} \times \left(\frac{Z}{2}\right)^{N_P^*(P-1)}\left(\frac{\psi_1^*}{2}\right)^{N_P^*} \tag{42}$$

for the ratio required in (39). For the configuration count of the N_P^* polymers and N_0^* solvent molecules we thus find in place of (39)

$$\psi_2^* \cdot \psi_3^* \tag{43}$$

where ψ_2^* and ψ_3^* are given by (38) and (42), respectively, and the polymer arrangement factor ψ_1^*, which is contained in ψ_3^*, is given by (7).

From ψ_1^*, ψ_2^*, and ψ_3^* we can derive the corresponding factors in the reference state by putting either N_0^* or N_P^* to zero. We find

$$\psi_{1,P}^{REF} = \psi_1^* \tag{44}$$

$$\psi_{2,P}^{REF} = \frac{(PN_P^*)!}{(N_P^*)!} \tag{45}$$

$$\psi_{3,P}^{REF} = \frac{\left[\frac{Z}{2}PN_P^* - (P-1)N_P^*\right]!}{\left[\frac{Z}{2}PN_P^*\right]!} \times \left(\frac{Z}{2}\right)^{N_P^*(P-1)}\left(\frac{\psi_1^*}{2}\right)^{N_P^*} \tag{46}$$

$$\psi_{1,0}^{REF} = 1 \tag{47}$$

$$\psi_{2,0}^{REF} = 1 \tag{48}$$

$$\psi_{3,0}^{REF} = 1 \tag{49}$$

Using these, the factors in the reduced general term, $\overline{Q^*}$, turn out to be

$$\overline{\psi_1^*} = 1 \tag{50}$$

$$\overline{\psi_2^*} = \frac{(N_T^*)!}{(N_0^*)!(PN_P^*)!} \tag{51}$$

and

$$\overline{\psi_3^*} = \frac{\left[\frac{Z}{2}N_T^* - (P-1)N_P^*\right]!}{\left[\frac{Z}{2}N_T^*\right]!}\frac{\left[\frac{Z}{2}PN_P^*\right]!}{\left[\frac{Z}{2}PN_P^*q\right]!} \tag{52}$$

where

$$q = 1 - \frac{2}{Z}\left(1 - \frac{1}{P}\right) \tag{53}$$

is the polymer internal contact exclusion parameter.

The product

$$\overline{\psi_2^*} \cdot \overline{\psi_3^*} \tag{54}$$

thus determines the configurational factor in $\overline{Q^*}$.

4. Configuration Count for the Surface Phase.—We shall now apply the method developed in section 3 to a discussion of the surface phase.

We shall find it convenient to separate the surface phase still further into two parts, the surface itself of N_S sites and the adjoint bulk phase of N_B sites (see Fig. 1). It becomes necessary first to distribute the polymer molecule between these two phases in the requisite number of runs and the number of ways of doing this is obviously

$$\psi_{4,S} = \overline{\psi_{4,S}} = \binom{m+u}{m}^{N_P} \binom{m+t-1}{m-1}^{N_P} \quad (55)$$

We now have polymer chains of $(m + t)$ segments (divided up into m connected sequences) in the surface layer and polymer chains of $(m + 1 + u)$ segments (divided up into $(m + 1)$ connected sequences) in the adjoint bulk phase. For the moment we shall treat these phases and the polymer structures which they contain as completely independent of each other. In analogy to (38) and (42) we thus derive the following factors for these two phases

$$\psi_{2,S} = \frac{N_S!}{[N_S - (m+t)N_P]!\, N_P!} \quad (56)$$

$$\psi_{2,B} = \frac{N_B!}{[N_B - (m+1+u)N_P]!\, N_P!} \quad (57)$$

$$\psi_{3,S} = \frac{\left[\frac{S}{2}N_S - tN_P\right]!}{\left[\frac{S}{2}N_S\right]!} \left(\frac{S}{2}\right)^{tN_P} \left(\frac{\psi'_{1,S}}{2}\right)^{N_P} \quad (58)$$

$$\psi_{3,B} = \frac{\left[\frac{Z}{2}N_B + \frac{Z-S}{4}N_S - uN_P\right]!}{\left[\frac{Z}{2}N_B + \frac{Z-S}{4}N_S\right]!} \times \left(\frac{Z}{2} + \frac{Z-S}{4}\frac{N_S}{N_B}\right)^{uN_P} \left(\frac{\psi''_{1,S}}{2}\right)^{N_P} \quad (59)$$

where $\psi'_{1,S} \cdot \psi''_{1,S} = \psi_{1,S}$ is given by (6). Although this can easily be done, no explicit formulations for $\psi'_{1,S}$ and $\psi''_{1,S}$ will be given. In all applications only their product, $\psi_{1,S}$, appears. In the derivation of (59) it is assumed that the $(Z/2)N_B + [(Z - S)/4]N_S$ interactions in the adjoint bulk phase are uniformly distributed over the N_B lattice sites, *i.e.*, the coordination number of this phase is not Z but $Z[1 + [(Z - S)/2Z](N_S/N_B)]$ on the average.

What we still lack is the factor which will knit the two parts of the surface phase into one unit by eliminating the overcount so far introduced. Let us, therefore, examine the situation as it exists at present. We have two separate phases each containing N_P polymer molecules, the surface phase involving polymer structures of $(m + t)$ segments and the bulk phase with polymer structures of $(m + 1 + u)$ segments. Not all these segments are, however, required to occupy adjoining lattice sites. If we examine expressions (58) and (59) we will note that the restriction has been applied to only t and u of these internal interactions, respectively. There are $(m - 1)$ gaps left in the "surface" polymer chains and m gaps in the "bulk" polymer chains. Although a definite sequence of segments is required by the use of (56) and (57) no lattice placement correlation has yet been demanded for the segments bordering the gaps. When the two phases are required to be together, however, the site for the head segment of each connected sequence is very clearly designated by the requirement that it has to coincide with the tail of the corresponding sequence in the other phase. There are thus sites in each of these phases whose occupation by polymer segments is laid down, not by random rearrangements within the phase, but by decisions taken outside the system. It implies that we were overcounting when in (56) and (57) we specified $N_S!$ and $N_B!$ as the total number of possible configurations on the lattice. This was based on the assumption that all lattice sites in the phase were available for random occupation. In fact $(m - 1)N_P$ sites in the surface phase and $(m + 1)N_P$ sites in the bulk phase are marked out for occupation by polymer segments and are not available. We can thus achieve the state where the polymer molecules are again properly connected together by introducing a factor

$$\psi_{5,S} = \frac{[N_S - (m-1)N_P]!}{N_S!} \times \frac{[N_B - (m+1)N_P]!}{N_B!} N_P! \quad (60)$$

which will make the appropriate adjustments to (56) and (57) and contains a factor $N_P!$ to allow for the number of ways in which the "separated" polymers can be recombined. [Note that we are following a convention whereby the head segment which carried the identity of the polymer molecule is one of the m head segments in the surface.]

For the reference state of the molecules composing the surface phase we have in analogy to (44) to (49)

$$\psi_{1,P}^{REF} = \psi_1^* \quad (61)$$

$$\psi_{2,P}^{REF} = \frac{(PN_P)!}{N_P!} \quad (62)$$

$$\psi_{3,P}^{REF} = \frac{\left[\frac{Z}{2}PN_Pq\right]!}{\left[\frac{Z}{2}PN_P\right]!} \left(\frac{Z}{2}\right)^{N_P(P-1)} \left(\frac{\psi_1^*}{2}\right)^{N_P} \quad (63)$$

$$\psi_{1,0}^{REF} = \psi_{2,0}^{REF} = \psi_{3,0}^{REF} = 1 \quad (64)$$

If ΔW is the energy change from the reference state to the state characterized by the combination of variables N_P^*, N_0^*, N_P, m, t, and u, we can now write an expression for the general term $\overline{Q_T}$ in the reduced partition function. Multiplying together the expressions (51), (52), (56), (57), (58), (59), (55), and (60) and dividing by (61), (62), (63), and (64) we find

$$\bar{Q}_T = \left[\frac{[N_0^* + PN_P^*]!}{[N_0^*]![PN_P^*]!}\frac{\left[\frac{Z}{2}N_0^* + \frac{Z}{2}qPN_P^*\right]!}{\left[\frac{Z}{2}N_0^* + \frac{Z}{2}PN_P^*\right]!}\frac{\left[\frac{Z}{2}PN_P^*\right]!}{\left[\frac{Z}{2}qPN_P^*\right]!}\right]\times$$
$$\left[\frac{\left(\frac{Z-S}{2}\right)^{2m+1} q^{2m}(Z-1)^u f^{m+1+u} S^m (S-1)^{t-m}}{Z(Z-1)^{P-2}}\right]^{N_P}\times$$
$$\left[\frac{[N_B-(m+1)N_P]!\,[N_S-(m-1)N_P]!}{[N_B-(m+1+u)N_P]!\,[N_S-(m+t)N_P]!N_P!}\right]\times$$
$$\left[\frac{\left[\frac{Z}{2}N_B + \frac{Z-S}{4}N_S - uN_P\right]!\left[\frac{S}{2}N_S - tN_P\right]!\left[\frac{Z}{2}PN_P\right]!}{\left[\frac{Z}{2}N_B + \frac{Z-S}{4}N_S\right]!\left[\frac{S}{2}N_S\right]!\left[\frac{Z}{2}qPN_P\right]!}\right]\times$$
$$\left[\frac{\left(\frac{Z}{2} + \frac{Z-S}{4}\frac{N_S}{N_B}\right)^{uN_P}\left(\frac{S}{2}\right)^{tN_P}}{\left(\frac{Z}{2}\right)^{(2m+u+t)N_P}}\right]\binom{m+u}{m}^{N_P}\binom{m+t-1}{m-1}^{N_P} e^{-\Delta W/kT} \quad (65)$$

In the above the various factors which we have been discussing will easily be recognized. Taking the logarithm of this expression and applying the Stirling approximation for the factorials then leads to

$$\ln \bar{Q}_T = N_P\mathbf{A} + mN_P\mathbf{B} + uN_P\mathbf{C} + + tN_P\mathbf{D} + N_B\mathbf{K} + N_S\mathbf{L} + N_0^*\mathbf{O}^* + N_P^*\mathbf{P}^* + \mathbf{E} \quad (66)$$

where the functions **A**, **B**, **C**, **D**, **K**, **L**, **O***, **P***, and $\mathbf{E} = -\Delta W/kT$ are given by equations A1, A2, A3, A4, A5, A6, A10, A11, and A12, respectively.

We shall now discuss how **E** above was determined.

5. Energy of Mixing.—Implicit in the use of such expressions as (52) is the assumption that arrangements of the external contacts on the lattice are random. There are obviously three types of contacts to be considered, solvent–solvent contacts associated with a potential energy V_{00}, external polymer segment–segment contacts associated with a potential V_{PP}, and polymer segment–solvent contacts associated with a potential V_{0P}. Each of these potentials is taken with reference to a state where the interacting molecules are at infinite separation. Let there be X_{00}, X_{PP}, and $2X_{0P}$ of these contacts, respectively. For any given system the sum $(X_{00} + X_{PP} + 2X_{0P})$ is constant. The configurational energy is then given by

$$W = X_{00}V_{00} + X_{PP}V_{PP} + 2X_{0P}V_{0P} \quad (67)$$

and will depend to a marked extent on the values assumed by the variables X_{00}, X_{PP}, and X_{0P}. If however the values of V_{00}, V_{PP}, and V_{0P} are all approximately alike W will remain indifferent to wide fluctuations in the number X_{00}, X_{PP}, and X_{0P} and a random arrangement of interaction may be assumed. Although this will not be true in general it applies approximately in many cases.

If we assume random mixing we can easily find expressions for X_{00}, X_{PP}, and X_{0P} in terms of the over-all particle numbers already introduced as variables.

Let us see how this works. Treating as an example the equilibrium bulk phase, we have

$$X_{00}^* + X_{0P}^* = \frac{Z}{2}N_0^* \quad (68)$$

$$X_{PP}^* + X_{0P}^* = \frac{Z}{2}qPN_P^* \quad (69)$$

by stoichiometry, and

$$\frac{X_{00}^*}{X_{0P}^*} = \frac{X_{0P}^*}{X_{PP}^*} = \frac{\frac{Z}{2}N_0^*}{\frac{Z}{2}qPN_P^*} \quad (70)$$

as a consequence of random mixing. Solving these equations then gives

$$X_{00}^* = \frac{Z}{2}N_T^*\frac{(1-\phi^*)^2}{(1-\phi^*)+\phi^*q} \quad (71)$$

$$X_{PP}^* = \frac{Z}{2}N_T^*\frac{(\phi^*q)^2}{(1-\phi^*)+\phi^*q} \quad (72)$$

$$X_{0P}^* = \frac{Z}{2}N_T^*\frac{(1-\phi^*)(\phi^*q)}{(1-\phi^*)+\phi^*q} \quad (73)$$

In the reference state for these molecules we have obviously

$$X_{00}^{REF} = \frac{Z}{2}N_0^* = \frac{Z}{2}N_T^*(1-\phi^*) \quad (74)$$

$$X_{PP}^{REF} = \frac{Z}{2}qPN_P^* = \frac{Z}{2}N_T^*q\phi^* \quad (75)$$

$$X_{0P}^{REF} = 0 \quad (76)$$

so that the energy change ΔW^* accompanying their mixing is given by

$$\Delta W^* = N_T^* x_{0P} \frac{(1 - \phi^*)(\phi^* q)}{(1 - \phi^*) + (\phi^* q)} kT \quad (77)$$

where x_{0P} is the energy of mixing parameter defined as

$$x_{0P} = \frac{Z}{2} [2V_{0P} - V_{00} - V_{PP}] \frac{1}{kT} \quad (78)$$

For the surface phase we must consider, separately, the surface layer, the contact area between surface layer and adjoint bulk phase, and the adjoint bulk phase. The procedure is analogous to that outlined above and the results of Table I are arrived at in this fashion.

Note only that in the reference state for the solvent a surface of N_S sites is assumed, *i.e.*, there are N_S solvent molecules in the reference state at a potential other than the rest. If in the bulk the solvent molecule is at a potential $(Z/2)V_{00}$ with respect to a state of infinite separation of all molecules, the solvent molecule in the surface is at a potential

$$-\frac{Z - S}{4} V_{00} - x'kT$$

lower than the solvent molecule in the bulk of the pure solvent. x' in the above is the solvent adsorption energy, *i.e.*, the reduction in energy, in units of kT, per solvent molecule in contact with the surface. As V_{00} is negative, x', which may be taken to be positive, counteracts what would otherwise be a rise in internal energy at the surface.

If each polymer segment at the surface reduces the internal energy of the system by an amount $x''kT$, the bringing of a polymer segment from solution, in the bulk (where it is surrounded by solvent) into the surface (where it displaces a solvent molecule) is associated with an energy change

$$\left(-\frac{Z - S}{4} V_{0P} - x''kT\right) - \left(-\frac{Z - S}{4} V_{00} - x'kT\right) = -\frac{Z - S}{4} (V_{0P} - V_{00}) - xkT$$

where $x = x'' - x'$ is the change in adsorption energy, in units of kT, when a polymer segment becomes attached to a solvated surface.

Summing up the results of Table I we arrive, after some rearrangements, at equation A12 for ΔW. The parameter

$$x_0 = \frac{Z}{2} [V_{0P} - V_{00}] \frac{1}{kT} \quad (79)$$

which appears in (A12), is obviously related to the displacement of adsorbed solvent by polymer segments and is a measure of the change in solvation energy accompanying the adsorption of a polymer

TABLE I
INTERACTION COUNTS FOR RANDOM MIXING

System	Internal contact exclusion parameter	Total no. of external contacts	X_{00}	X_{PP}	$2X_{0P}$	Occupation of surface No. of solvent molecules	Occupation of surface No. of polymer segments
Surface layer	$q_s = 1 - \frac{2}{S}\left(1 - \frac{1}{P_S}\right)$	$\frac{S}{2}N_S[(1 - \theta) + \theta q_s]$	$\frac{S}{2}N_S\frac{(1 - \theta)^2}{(1 - \theta) + \theta q_s}$	$\frac{S}{2}N_S\frac{(\theta q_s)^2}{(1 - \theta) + \theta q_s}$	$\frac{S}{2}N_S\frac{2(1 - \theta)\theta q_s}{(1 - \theta) + \theta q_s}$	$N_S(1 - \theta)$	$N_S\theta$
Contact layer	$q_c = 1 - \frac{8}{Z - S}\frac{1}{P_S}$	$\frac{Z - S}{4}N_S[(1 - \theta) + \theta q_c]$	$\frac{Z - S}{4}N_S(1 - \theta)(1 - \phi)$	$\frac{Z - S}{4}N_S\theta\phi q_c$	$\frac{Z - S}{4}N_S[(1 - \theta)\phi + \theta(1 - \phi)q_c]$	...	..
Adjoint bulk phase	$q_B = 1 - \frac{2}{Z}\left(1 - \frac{1}{P_B}\right)$	$\frac{Z}{2}N_B[(1 - \phi) + \phi q_B]$	$\frac{Z}{2}N_B\frac{(1 - \phi)^2}{(1 - \phi) + \phi q_B}$	$\frac{Z}{2}N_B\frac{(\phi q_B)^2}{(1 - \phi) + \phi q_B}$	$\frac{Z}{2}N_B\frac{2(1 - \phi)\phi q_B}{(1 - \phi) + \phi q_B}$	...	..
Equilibrium bulk phase	$q = 1 - \frac{2}{Z}\left(1 - \frac{1}{P}\right)$	$\frac{Z}{2}N_T^*[(1 - \phi^*) + \phi^* q]$	$\frac{Z}{2}N_T^*\frac{(1 - \phi^*)^2}{(1 - \phi^*) + \phi^* q}$	$\frac{Z}{2}N_T^*\frac{(\phi^* q)^2}{(1 - \phi^*) + \phi^* q}$	$\frac{Z}{2}N_T^*\frac{2(1 - \phi^*)\phi^* q}{(1 - \phi^*) + \phi^* q}$	...	..
Reference state	$q = 1 - \frac{2}{Z}\left(1 - \frac{1}{P}\right)$	...	$\left(\frac{Z}{2} - \frac{Z - S}{4}\right)N_S +$ $\frac{Z}{2}[N_B - PN_P] + \frac{Z}{2}N_0^*$	$\frac{Z}{2}[N_P + N_P^*]Pq$	...	N_S	..
Associated energy level	...	...	V_{00}	V_{PP}	V_{0P}	$-x'$	$-x''$

segment. The energy of mixing parameter x_{0P} has already been defined (see eq. 78) and

$$x = x'' - x' \tag{80}$$

is the segment adsorption energy in units of kT.

6. The Equations Determining the Equilibrium State.—We can now make explicit the formal set of equations 32, 33, and 34 which determine the equilibrium at N_S held constant. From (66) we find the following expressions for the quantities defined in (26) to (31)

$$D_P = \mathbf{A} + m\mathbf{B} + u\mathbf{C} + t\mathbf{D} + \mathbf{E}_P \tag{81}$$

$$D_m = \mathbf{B} + \mathbf{M} - \frac{(P_B - 1)}{\phi}\mathbf{K} + \mathbf{E}_m \tag{82}$$

$$D_u = \mathbf{C} + \mathbf{U} + \frac{1}{\phi}\mathbf{K} + \mathbf{E}_u \tag{83}$$

$$D_t = \mathbf{D} + \mathbf{T} + \mathbf{E}_t \tag{84}$$

$$D_0^* = \mathbf{O}^* + \mathbf{E}_0^* \tag{85}$$

$$D_P^* = \mathbf{P}^* + \mathbf{E}_P^* \tag{86}$$

where all the bold-faced symbols are expressed in the Appendix. Substitution of (82) to (85) into (32) and (33) then yields

$$\frac{P_B}{\phi}(\mathbf{K} - \mathbf{O}^*) + (\mathbf{C} + \mathbf{D} - \mathbf{B}) + (\mathbf{U} + \mathbf{T} - \mathbf{M}) + \mathbf{y}_{(0P)} + 2\ln g = 0 \tag{87}$$

$$\frac{1}{\phi}(\mathbf{K} - \mathbf{O}^*) + (\mathbf{C} - \mathbf{D}) + (\mathbf{U} - \mathbf{T}) - \bar{\mathbf{x}}_{(0P)} = 0 \tag{88}$$

respectively, in which the energy terms which arise have been replaced by $\mathbf{y}_{(0P)}$ and $\bar{\mathbf{x}}_{(0P)}$, respectively (see equations A13 and A14).

From (33), (84), and (85) we now find

$$D_u = D_t + \frac{1}{\phi}D_0^* = \mathbf{D} + \mathbf{T} + \mathbf{E}_t + \frac{1}{\phi}(\mathbf{O}^* + \mathbf{E}_0^*) \tag{89}$$

and from (32), (89), (84), and (85) we obtain

$$D_m = 2D_t - \frac{1}{\phi}(P_B - 1)D_0^* = 2\mathbf{D} + 2\mathbf{T} + 2\mathbf{E}_t - \frac{1}{\phi}(P_B - 1)(\mathbf{O}^* + \mathbf{E}_0^*) \tag{90}$$

Rearranging (82) and (83) leads to

$$\mathbf{B} = D_m - \mathbf{M} + \frac{1}{\phi}(P_B - 1)\mathbf{K} - \mathbf{E}_m \tag{91}$$

$$\mathbf{C} = D_u - \mathbf{U} - \frac{1}{\phi}\mathbf{K} - \mathbf{E}_u \tag{92}$$

respectively, into which (90) and (89) may be substituted, respectively, to give alternate expressions for **B** and **C**. Note that (91) and (92) (so substituted) are reformulations of the shape determining equations 87 and 88. With their aid, however, equation 81 for D_P may be given the following form, more convenient to our purpose

$$D_P = P(\mathbf{D} + \mathbf{T}) + \mathbf{A} - \mathbf{B} + \mathbf{D} - (m+1)\mathbf{M} - u\mathbf{U} - (t-1)\mathbf{T} - (m+1)\mathbf{E}_m - u\mathbf{E}_u + [P - (t-1)]\mathbf{E}_t + \mathbf{E}_P \tag{93}$$

With (93), (85), and (86) the third equilibrium determining equation 34 can be made to read

$$\mathbf{G}^* = P\Delta + \mathbf{H} \tag{94}$$

where $\mathbf{G}^*$, Δ, and $\mathbf{H}$ are given by (A17), (A23), and (A18), respectively.

Equation 94 is the adsorption isotherm and we shall discuss the results predicted by (94), solved in conjunction with (87) and (88), in the next section.

7. Discussion of Solution.—The essential character of the solution is determined by the form of (94).

The expression $\mathbf{G}^*$ on the left-hand side depends on the concentration ϕ^* in the equilibrium bulk phase. It is positive for small ϕ^* and is approximately given by $-\ln \phi^*$. At high concentrations the second term in $\mathbf{G}^*$ (equation A17) takes over, rendering it negative and proportional to P. Let us re-emphasize, however, that in the dilute concentration range (where most results which we wish to discuss are to be found) we may replace $\mathbf{G}^*$ by $-\ln \phi^*$.

On the right-hand side of (94) the term $\mathbf{H}$ contains a term $\ln P$, but is otherwise independent of P. The factor Δ (see A23) is essentially independent of P.

If there is to be equality between the two sides, Δ will have to be small, of order $1/P$, and will, in fact, be effectively zero. Changes in P and, to a large extent in ϕ^*, will thus cause no more than a slight variation of Δ around the zero mark.

As the shape of the polymer molecule and its concentration at the interface determine the value of Δ, we can conclude that these parameters will, on the whole, be as insensitive to changes in molecular weight and to changes in the equilibrium concentration as Δ itself. The very flat plateau, and the astonishing indifference of the adsorbed film to changes in bulk concentration over several decades, thus find their explanation. Indeed, the inability to remove polymer molecules, by washing them off the surface, is only an expression of the fact that the surface is still in equilibrium with the solvent. Note that removing the adsorbent, with the adsorbed layer, from a solution where $\phi^* = 10^{-3}$ to a solution where $\phi^* = 10^{-23}$ involves a change in Δ of only

$$\frac{2.303 \times 20}{10000} = 4.6 \times 10^{-3}$$

if $P = 10^4$.

Although this picture is modified when P is smaller and ϕ^* larger we shall in the first instance analyze the shape of the polymer molecule and its

concentration at the surface in cases where Δ has been put to zero.

(a) **The Dilute Solution, High Molecular Weight Case.** ($\Delta = 0$).—We shall in all cases simplify the formulas given in the Appendix by neglecting terms of order $1/m$ or $1/P$ in comparison with 1. In addition we shall put $x_{0P} = 0$, *i.e.*, we shall treat the athermal mixing case. Considerable simplifications in the expression are thereby achieved. Remembering that we have as a condition

$$\phi^{**} \ll \phi$$

we shall in addition neglect $\mathbf{O}^*$ in comparison with $\mathbf{K}$ in equations 87 and 88, which thus become independent of ϕ^*.

As determining equations for the equilibrium shape of the polymer we thus have

$$\ln \frac{1}{(P_S - 1)} = \ln (P_B - 1) + \ln \left[\left(\frac{Z - S}{2} \right)^2 \frac{S}{(S-1)^2} \frac{1}{Z-1} \right] - \ln \left[\frac{\left(1 - \frac{\phi}{P_B}\right)\left(1 - \frac{\theta}{P_S}\right)}{\left(1 - \frac{2}{Z}\phi \frac{(1 - 1/P_B)}{\left(1 + \frac{Z-S}{2Z\gamma}\frac{1}{P_B}\right)}\right)\left(1 - \frac{2}{S}\theta\left(1 - \frac{1}{P_S}\right)\right)} \right] - \frac{P_B}{\phi} \ln \left[\frac{\left(1 - \frac{\phi}{P_B}\right)\left(1 - \frac{2}{Z}\phi \frac{(1 - 1/P_B)}{\left(1 + \frac{Z-S}{2Z\gamma}\frac{1}{P_B}\right)}\right)^{Z/2}}{(1-\phi)} \right] - \mathbf{y}_{(0P)} + \left[\frac{P_B - 1}{\frac{2Z\gamma}{Z-S} P_B + 1} \right] \quad (95)$$

$$\ln \left(\frac{P_S}{P_S - 1} \right) = \ln \left(\frac{P_B}{P_B - 1} \right) + \ln \left[f \frac{Z-1}{S-1} \right] - \bar{\mathbf{x}}_{(0P)} + \ln \left[\frac{(1-\phi)\left(1 - \frac{2}{S}\theta\left(1 - \frac{1}{P_S}\right)\right)}{\left(1 - \frac{2}{Z}\phi \frac{1 - \frac{1}{P_B}}{1 + \frac{Z-S}{2Z\gamma}\frac{1}{P_B}}\right)(1-\theta)} \right] + \frac{1}{\phi} \ln \left[\frac{\left(1 - \frac{\phi}{P_B}\right)\left(1 - \frac{2}{Z}\phi \frac{(1 - 1/P_B)}{1 + \frac{Z-S}{2Z\gamma}\frac{1}{P_B}}\right)^{Z/2}}{(1-\phi)} \right] - \frac{1}{P_B} \left[\frac{P_B - 1}{\frac{2Z\gamma}{Z-S} P_B + 1} \right] \quad (96)$$

where $\mathbf{y}_{(0P)}$ and $\bar{\mathbf{x}}_{(0P)}$ are given by (A13) and (A14), respectively.

In our calculations we shall assume

$$\begin{aligned} Z &= 12 \\ S &= 6 \\ f &= 0.7 \\ g &= 1 \\ \gamma &= 0.5 \\ x_{0P} &= 0 \end{aligned} \quad (97)$$

We can define a new function Λ (see A19)

$$\Lambda = \ln (P_S - 1)\left(1 - \frac{2}{S}\theta\left(1 - \frac{1}{P_S}\right)\right) \quad (98)$$

and comparing (98) with (95), find that $(\Lambda - \mathbf{y}_{(0P)})$ can be calculated knowing ϕ and P_B only (see (A21); in the one place where θ/P_S still occurs in this equation it can be replaced by $\gamma\phi$ according to (15)).

The other determining equation 88 (or (96) above) can be rearranged to define Δ (compare (A22) and (A24) with (88)). In this way we obtain an expression, (A25), for Δ which again depends on ϕ and P_B only. Δ can thus also be plotted for given ϕ against P_B. It is thus possible to derive the P_B value, for given ϕ, at which $\Delta = 0$. The corresponding value of $(\Lambda - \mathbf{y}_{(0P)})$ is also read off.

On the other hand we can plot Λ, at constant θ, against ϕ (using (A19) and (15) to eliminate P_S).

When $g = 1$ and $x_{0P} = 0$, as we have assumed, $\mathbf{y}_{(0P)}$ is proportional only to x_0 (see (A13)). Different cases will arise therefore depending upon the value assigned to x_0. By matching Λ values at $\Delta = 0$ the corresponding values of P_B, P_S, ϕ, θ, and x at equilibrium are determined from these plots.

We have shown what these solutions look like in terms of θ and ϕ at various adsorption energies x in Fig. 2 and have plotted the shape parameters p and P_B and the amount adsorbed Γ in Fig. 3. Believing that not too much reliance should be put on the form of the solution below $\phi = 0.1$ (because ϕ^* may approach ϕ in order of magnitude) we have shown in Fig. 3 only the part of the curves referring to $\phi > 0.1$. For given x and x_0 the results of Fig. 2 and 3 thus represent the shape and concentration of the surface film over most of the practical concentration range and for molecular weights in excess of P, say, 10^4.

The following points should be noted

(i) The shape and amount adsorbed is independent of the molecular weight.

(ii) The shape and amount adsorbed is independent of the equilibrium concentration ϕ^*. These two points have already been discussed.

(iii) The adsorbed layer is thin (P_B lies between 2 and 3) and the fraction of adsorbed segments is

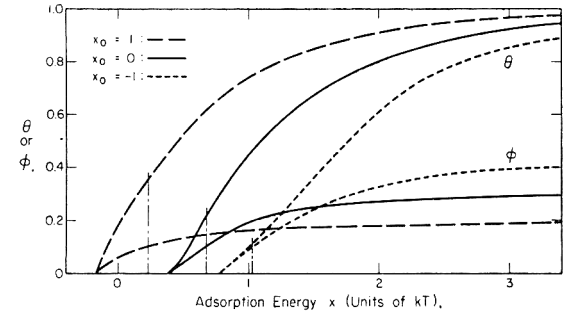

Fig. 2.—Dependence of surface occupation parameter θ and ϕ on adsorption energy x (units of kT) for $\Delta = 0$ and the x_0-values indicated (conditions (97)). Values below $\phi = 0.1$ probably are unreliable.

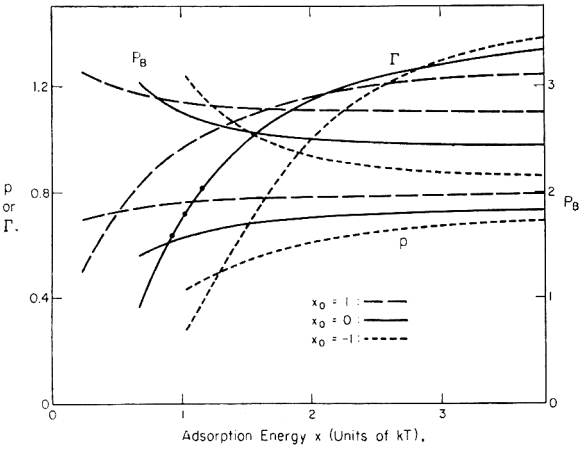

Fig. 3.—Dependence of the parameter characterizing the polymer monolayer, p, P_B, and Γ, on adsorption energy x (units of kT) for $\Delta = 0$ and the x_0-values indicated (conditions (97)): ●, data of Ellerstein and Ullman[19] calculated on the basis of $\mathfrak{a}_0 = 10$ Å.^{2} and a segment adsorption energy of 700 cal.

high (p about 0.7) irrespective of the values of x and x_0. We thus expect almost identical adsorption behavior of similarly structured polymer molecules on good adsorbing surfaces. Note that p is large even at the small adsorption energies here considered. Good adsorption of polymer molecules should thus be the rule on all except the most unfavorable surfaces. The amount adsorbed Γ (in polymer segments per surface site) is of the order 1 over most of the range considered. The surface is highly occupied ($\theta \sim 0.8$) and a concentrated bulk phase ($\phi \sim 0.25$) is adjoint to it.

(iv) Increase of x obviously favors adsorption, but the adsorption energy need only be small. In fact beyond a point where the adsorption energy is $2kT$ (about 1 kcal.) no further strong improvement is to be expected. It should be stressed, however, that x is a displacement energy resulting from the replacement of an adsorbed solvent molecule by a polymer segment (see (80)). For a given system (assuming the adsorption energy to be independent of temperature), x is a measure of inverse absolute temperature. It is possible therefore to assess the temperature dependence in the absence of specific effects. Under the circumstances envisaged the most profound changes in Γ occur in the realm of low adsorption energies ($x \simeq 1$) but even there Γ decreases only by a small amount, *i.e.*, by about 1% of its value for every 3° increase in temperature.

(v) Increase in the parameter x_0 favors adsorption as it favors the replacement of adsorbed solvent by polymer segments. Positive x_0 implies a lower energy level for the solvent when tied to itself as compared with the solvent in interaction with the polymer ($V_{0P} > V_{00}$). As this would be one of the characteristics of a poor solvent, we expect adsorption to be best from poor solvents.

(vi) We can see this also from an analysis of how a non-zero, positive x_{0P} would affect the adsorption. By carefully considering all terms involved, it can be concluded that, for the same x, θ would go up and p go down, *i.e.*, Γ, the amount adsorbed, would be increased as the solvent is made worse.

(vii) A similar analysis shows that restrictions on the polymer molecule in entering or leaving the surface ($g < 1$) would lead to a decrease in the amount adsorbed under otherwise identical conditions.

(b) Adsorption Characteristics at Constant ϕ.—We shall now discuss the isotherm (94) without recourse to its special properties at $\Delta = 0$. For this purpose we solve the equations 87 and 88, under the simplifications already outlined, and for $Z = 12$, $S = 6$, $f = 0.7$, $g = 1$, $\gamma = 0.5$, $x_{0P} = 0$, and $x_0 = 0$, for various values of ϕ.

With ϕ held constant, we derive Λ from (A19) for arbitrary P_S. As $\mathbf{y}_{(0P)} = 0$ in this case, we can read the value of P_B corresponding to Λ, at the constant ϕ-value chosen, from a plot of Λ against P_B. The value of Δ is found similarly, so that $\bar{\mathbf{x}}_{(0P)}$ (which equals x in this case) may be deduced from (A23). We are in particular interested in the variation of the parameters p, P_B, and Δ with x at constant ϕ, and have shown this in Fig. 4(a) and (b).

Note that the heavy lines cutting across the curves at constant ϕ in Fig. 4(a) are the solutions for $\Delta = 0$ already plotted in Fig. 3 (case $x_0 = 0$). The lines at $\phi = 0$ are identical with the solutions published for the isolated coil, for this case, in Part I[40] (Fig. 2 of that paper).

We note, first of all, that p decreases and P_B increases as the surface concentration rises. This is as expected. We also see that Δ undergoes appreciable variations as ϕ increases at constant x, and that it passes from positive to negative values. Reference to equation 94 and to expression (A17) for $\mathbf{G}^*$ shows that ϕ will increase as ϕ^*, the concentration in the bulk phase, is increased. Unless P is not too large, however, ϕ^* will be insignificantly small for most of the range where Δ is positive. The case $\Delta \simeq 0$ has already been discussed. When $\Delta < 0$ the second term in $\mathbf{G}^*$ takes over, and ϕ^* rises rapidly (the approximate ϕ^* levels are indicated in Fig. 4(b)). We thus see that for most of the dilute concentration range of practical interest, the system will stay close to $\Delta = 0$.

There exists a range of x-values, however, (below 0.4 for the case considered here) where $\Delta < 0$ for all values of ϕ. No adsorption will occur in these cases until sufficiently large concentrations exist in the bulk phase to enable equilibrium to be established. No plateau in the sense discussed by us here is to be expected under these circumstances.

Most of the range at negative Δ-values is, however, not well represented by the present model as ϕ^* can no longer be neglected against ϕ there.

We shall now use the data in Fig. 4(a) and (b) to derive theoretical isotherms at a given adsorption energy.

(c) **The Adsorption Isotherm.**—Assuming that x is fixed, say $x = 1$, we can derive from Fig. 4 the values of the parameters p and P_B at given ϕ. From these, θ and P_S can be calculated. Substituting these data into equation A18, **H** in equation 94 can be determined for various values of P. As Δ is known, for given ϕ the right-hand side of (94) is evaluated. Equating $\mathbf{G}^*$ with this value we can solve for ϕ^*. Γ can then be plotted against ϕ^* for various P values. The result is shown in Fig. 5.

In Fig. 5(a) we have plotted Γ over a wide concentration range using a logarithmic scale for ϕ^*. In Fig. 5(b) we have chosen a range of concentrations in which a great many of the experimental investigations have been placed. In addition we have shown in Fig. 5(b), as dotted lines, how some of these data look on a Langmuir type plot. The dotted portion of the curves in Fig. 5(a) refer to a range where the model is unreliable as ϕ^* is no longer small as compared with ϕ. The upward trend of the curves at high ϕ^* is however confirmed by these calculations. Figure 5 illustrates very clearly how plateau behavior becomes the rule at high P, but how with low molecular weight fractions relatively big changes in Γ may be found, not only with changes in P, but also with changes in ϕ^*, provided the concentration range is wide enough.

8. Surface Tension Increment and Surface Pressure.—We have deduced equations 35 and 36 for the surface pressure and tension, respectively, in terms of the quantity D_{Ns} defined by (35). Applying (35) to (66) leads to the following expression for D_{Ns}

$$D_{Ns} = \mathbf{L} + \gamma P_B \mathbf{K} + \mathbf{E}_{Ns} \qquad (99)$$

which, when substituted together with (85) into (36), gives

$$\left[-\frac{\alpha_0 \Delta\sigma}{kT} \right] = (\mathbf{L} + \gamma P_B \mathbf{K} + \mathbf{E}_{Ns}) - (1 + \gamma P_B)(\mathbf{O}^* + \mathbf{E}_0^*) \qquad (100)$$

It will turn out, moreover, that in the range in which our solution applies (*i.e.*, where $\phi^* << \phi$), the second term in (100) may safely be neglected. Comparing (35) and (36), therefore, we find

$$\left[-\frac{\alpha_0 \Delta\sigma}{kT} \right] \cong \mathbf{L} + \gamma P_B \mathbf{K} + \mathbf{E}_N = \left[\frac{\alpha_0 \pi}{kT} \right] \qquad (101)$$

showing that surface pressure and tension are the same in these cases (except for sign) and that a monolayer adsorbed from a dilute polymer solution will act like a spread film.

Given a solution of the problem under a certain set of circumstances, $\Delta\sigma$ may be calculated from (100) in dependence on ϕ, θ, or ϕ^*. We have taken the case $Z = 12$, $S = 6$, $f = 0.7$, $g = 1$, $\gamma = 0.5$, $x_{0P} = 0$, $x_0 = 0$, and $x = 1$, worked out above for the isotherm. Choosing $x = 1$ may not be too meaningful for surface tension as it implies a specific interaction at the air–solution interface. We shall assume, however, that the adsorbed segments can accumulate an energy of this kind at the free interface. The results obtained are shown in Fig. 6(a), (b), and (c).

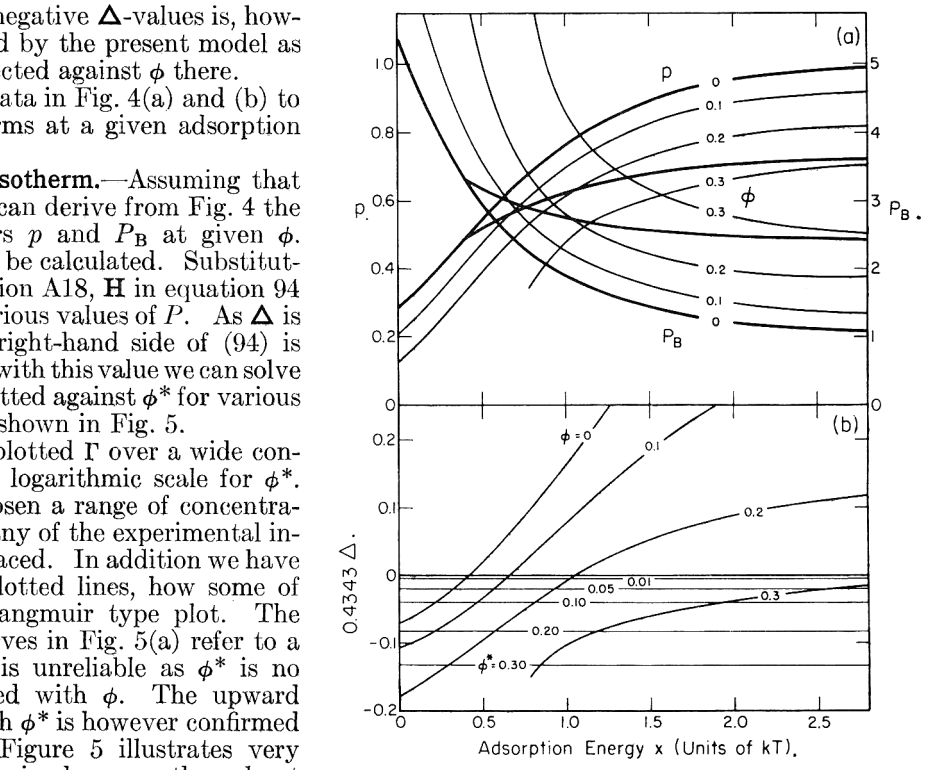

Fig. 4.—Dependence of polymer shape parameters p and P_B (a), and the function Δ (b), on adsorption energy x (units of kT) for various values of ϕ as indicated (conditions (97) and $x_0 = 0$). The heavy lines cutting across the lines at constant ϕ in (a) are the lines at $\Delta = 0$ (for the case $x_0 = 0$) taken from Fig. 3 The values of ϕ^* resulting from (94) for negative Δ-values are indicated in (b).

In Fig. 6(a) we have shown the data for $\Delta\sigma$ plotted against ϕ. The dotted region in the upper reaches of the figure is unreliable, corresponding to a range where ϕ^* is no longer negligible as compared with ϕ. It is also the region where the term $(1 + \gamma P_B)D_0^*$ (which marks the difference between π and $\Delta\sigma$) just ceases to be negligibly small. Except for sign, therefore, the ordinates in Fig. 6 may be interpreted either as surface tension or as surface pressure. In other words, a polymer monolayer adsorbed from solution will behave like a spread film provided the degree of surface coverage θ is not too large (see Fig. 6(b)).

Although the influence of P on the curves in Fig. 6(a) and (b) is small, an intercept is found in the plot of Fig. 6(b), in the limit of θ going to zero, which depends upon molecular weight. We can see this better by studying the limiting behavior of equation 101. We thus find, after expansion of the logarithms and neglect of higher than second order terms in θ

$$\left[-\frac{\alpha_0 \Delta\sigma}{kT} \right] = \left[\frac{\alpha_0 \pi}{kT} \right] = \frac{\Gamma}{P} + \frac{\theta^2}{2}\beta \qquad (102)$$

where β is given by (A27).

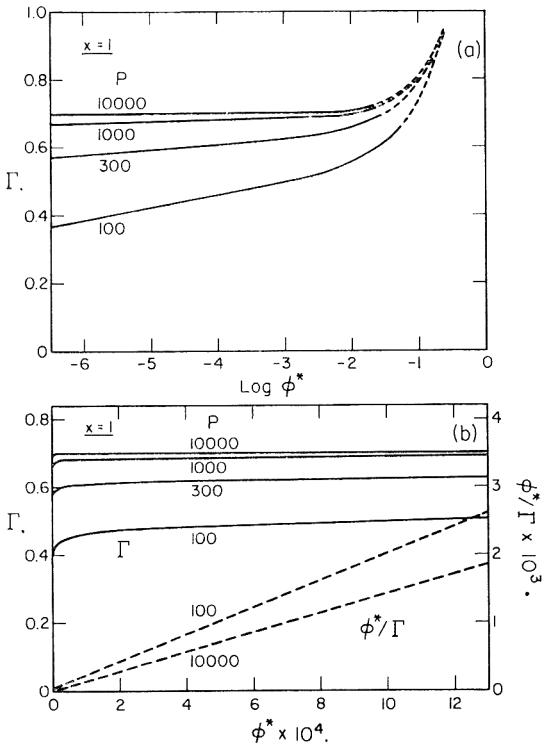

Fig. 5.—Theoretical adsorption isotherm for various degrees of polymerization (a) as a function of log ϕ^*, (b) as a function of ϕ^* ($x = 1$, $x_0 = 0$; conditions (97)). Dotted lines in (b) are Langmuir plots ($\phi^*/\Gamma \sim \phi^*$) of the corresponding curve shown as full line in (b). The dotted portions of the curves in (a) are unreliable as ϕ^* is too large in relation to ϕ.

[*Note:* In deriving (102) it is important that the term $\ln(1 - (\theta/P_S)(1 - 1/m))$ in **L** is not reduced to $\ln(1 - (\theta/P_S))$. It is actually this small difference which contributes the linear term, $\Gamma/P = \theta/pP$, in (102).]

In order to obtain the correct molecular weight from the intercept it is thus most important that $[-\mathcal{A}_0\Delta\sigma/kT]$ reduced by Γ and not by θ be plotted. We have illustrated this in Fig. 6(b). Only the dotted line representing $[-\mathcal{A}_0\Delta\sigma/kT](1/\Gamma)$ gives the correct intercept of 0.01. The other intercept corresponds to $1/pP$. When $p = 1$ it becomes immaterial which concentration units are employed. There may have been cases, however, where θ was determined in the belief that Γ was being measured. This, and the fact that extrapolation from too large Γ values have been used, could account for some statements that limiting ideal behavior does not arise.

It is of interest to express the ordinate scale in Fig. 6(a) in terms of practical units. Assuming that work is being done at room temperature and that $\mathcal{A}_0 = 10$ Å.^{2} we find that $\Delta\sigma \simeq -1$ dyne/cm. when the ordinate scale reads 0.025.

The slope of the curves in Fig. 6(a) and (b) is seen to be only little affected by changes in molecular weight. Its magnitude, however, depends strongly on the interaction parameters and would be much reduced if a poor solvent, for which both x_0 and x_{0P} are positive, were used (see β, equation A27). In fact, the slope could, in some cases, even become slightly negative. Note that β reduces to q_S and is simply related to S (as is often assumed on the basis of the Singer[39] equation) only when $P_S \to \infty$ and $x_{0P} = 0$. When this is not the case misinterpretation of data may result.

Limiting behavior will not in general be attained if $\Delta\sigma$ is plotted against ϕ^*. The arrows in Fig. 6(a) and (b) indicate the region where $\phi^* = 10^{-6}$. The portions of the curves below the arrows thus refer to polymer solutions of concentration much more dilute than can usually be measured, whereas extrapolation from the portion above the arrows is obviously unjustified.

How $\Delta\sigma$ depends on bulk concentration is shown in Fig. 6(c). We see that $\Delta\sigma$ becomes progressively less dependent on ϕ^* and on P as the molecular weight is raised.

This plot is of interest in view of its relation to the Gibbs equation. According to Gibbs the isothermal variation of surface tension is given by

$$-\frac{1}{kT}\,d\sigma = \Gamma_P\, d\ln a_P + \Gamma_0\, d\ln a_0 \quad (103)$$

where Γ_P and Γ_0 are the surface excesses of polymer and solvent, respectively, in number of molecules per unit area; and a_P and a_0 are the activities of polymer molecules and solvent in the solution. Assuming extreme dilution we may put

$$a_P \sim \frac{1}{P}\phi^*$$

$$a_0 \sim (1 - \phi^*)$$

so that

$$-\frac{1}{kT}\,d\sigma = \left[\Gamma_P - \Gamma_0\frac{\phi^*}{1-\phi^*}\right] d\ln\phi^* \simeq \Gamma_P\, d\ln\phi^* \quad (104)$$

By definition

$$\Gamma_P = \frac{\Gamma}{\mathcal{A}_0}\cdot\frac{1}{P} \quad (105)$$

so that

$$\frac{\partial}{\partial\log\phi^*}\left[-\frac{\mathcal{A}_0\Delta\sigma}{kT}\right] = \frac{2.303\,\Gamma}{P} \quad (106)$$

according to Gibbs; in other words the slopes in Fig. 6(c) should be inversely proportional to $1/P$. We have shown in Table II the slopes as read off Fig. 6 and as calculated from equation 106 using the Γ-values obtained from Fig. 5(b). Agreement is satisfactory, remembering that an average value for Γ was used and limiting behavior was attained only approximately. It is thus possible, in principle, to derive Γ from equation 106. In practice, however, this is an unattractive technique, as it involves working over a wide range of low concentrations over which $\Delta\sigma$ changes only slightly.

It is interesting to note that the proportionality of $(\partial/\partial\log\phi^*)\,[-\mathcal{A}_0\Delta\sigma/kT]$ to $1/P$, which is not obvious from equation 101, is a consequence of the form of the isotherm (94). Writing

$$\frac{\partial}{\partial \log \phi^*}\left[-\frac{\mathfrak{A}_0\Delta\sigma}{kT}\right] = \left\{\frac{\partial}{\partial\phi}\left[-\frac{\mathfrak{A}_0\Delta\sigma}{kT}\right]\right\} \times \left\{\frac{\partial\phi}{\partial\Delta}\right\}\left\{\frac{\partial\Delta}{\partial \log \phi^*}\right\} \qquad x = \text{const.}$$

as a product of three factors we see that the first of these is positive and independent of P (Fig. 6(a)), the second is negative and independent of P (Fig. 4(b)), and the third, from (94), is negative and proportional to $1/P$. Together they thus explain the sign and order of magnitude of the slope.

TABLE II

COMPARISON WITH GIBBS EQUATION

P	$\frac{\partial\left[-\frac{\mathfrak{A}_0\Delta\sigma}{kT}\right]}{\partial \log \phi^*}$ (Fig. 8(c))	Γ (Fig. 7(b))	$\frac{2.303\ \Gamma}{P}$ (Eq. (106))
100	10.0×10^{-3}	0.45	10.3×10^{-3}
300	5.0×10^{-3}	.60	4.6×10^{-3}
1000	1.3×10^{-3}	.68	1.6×10^{-3}
10000	0.3×10^{-3}	.70	0.2×10^{-3}

Note, moreover, that the agreement found has nothing to do with the limiting behavior of $\Delta\sigma$ as $\theta \rightarrow 0$ where, as the linear term in (102) shows, it becomes proportional to Γ/P. The $\Delta\sigma$ values which were used for the data in Table II refer to points above $\phi^* = 10^{-6}$, *i.e.*, to the range above the arrows in Fig. 6(a) and (b), a range where even the second-order approximation (102) for $\Delta\sigma$ starts to become inadequate.

The data of Fig. 6 are good only for qualitative comparison with experiments at free surfaces. For more quantitative results the case $x = 0$ and, say, $x_0 = 1$, rather than $x = 1$, $x_0 = 0$ should be discussed.

9. Comparison with Other Theories and with Experiment.—(i) The predictions of the present model are embodied in equations 87, 88, 94, and 100. If the simplifying assumptions, $m >> 1$, $\phi >> \phi^*$, are applied, (87) and (88) reduce to (95) and (96), respectively, and (101) may be used for (100). Of these equations, (94) is the isotherm and (101) is the surface equation of state.

If the appropriate parameter changes are made, (94) reduces to the isotherm of Sarolea[33] and (101) to the surface equation of state of Singer[39] for flexible macromolecules with all segments in the surface. Equations 95 and 96 reduce to the corresponding equations derived in Part I[40] (determining the behavior of the isolated macromolecule) when ϕ is allowed to go to zero.

In form the isotherm (94) agrees with that of Frisch and Simha.[38] Their derivation, however, does not tie the shape of the polymer molecule at equilibrium to its adsorption behavior (and thus contains p as an unknown), while we have been able to recast the isotherm, to our advantage in the discussion, by appropriate use of equations 95 and 96. Previous calculations of p[35,42,43] have not been very satisfactory and refer to the isolated macromolecule. Errors are introduced if these values are used in place of the equilibrium value of p, as Fig. 4(a) shows.

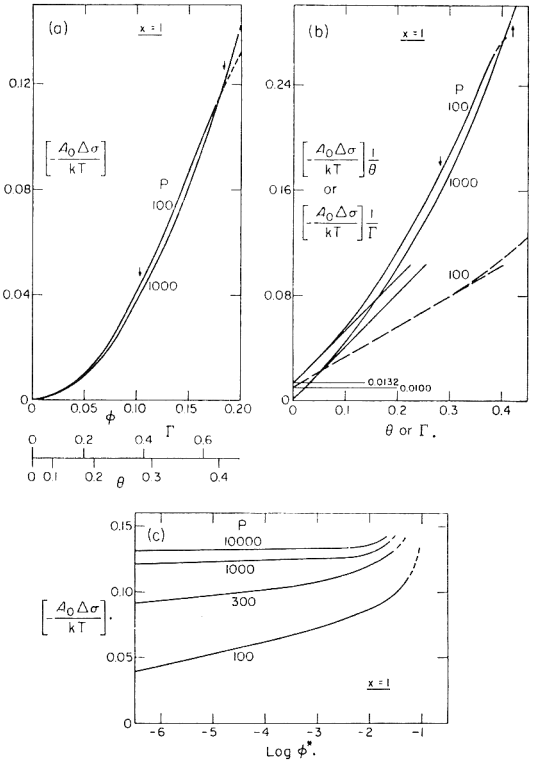

Fig. 6.—Surface tension measurement in dependence on ϕ, θ, Γ, and ϕ^* for various degrees of polymerization ($x = 1$, $x_0 = 0$; conditions (97)). The dotted upper portions of the curves are unreliable as ϕ^* is too large in relation to ϕ. Within the undotted regions of the curves approximation (101) is valid and surface pressure π may be substituted for surface tension decrement ($-\Delta\sigma$). The black arrows indicate the positions on the curves where $\phi^* = 10^{-6}$ in (a) and (b). Points below the arrows refer to even smaller bulk concentration. (a) Scales of θ and Γ are indicated in the diagram. (b) Reduced surface tension decrement or surface pressure is plotted. Note that correct intercept is obtained only when Γ is used as concentration variable (dotted line). The other intercept represents $(1/pP)$. Limiting slopes, calculated from (A27), are shown.

(ii) We already have discussed in section 1 the failure of these earlier theories to account for some of the observed facts. Comparison of present predictions and the data, on the other hand, shows agreement in all essentials. If the review presented in the Introduction was kept in mind, this will probably have become obvious as we proceeded with the analysis of the model. It is unnecessary, therefore, to repeat the entire discussion, and we will only take a closer look at the experimental data in this section and make a more detailed comparison. We shall follow the order of presentation of section 1.

(a) The form of the isotherm (sharp rise and plateau) is almost universally confirmed by the data. In most cases, however, the experiments were performed over a limited concentration range only and rather low molecular weight materials were used. As can be seen from Fig. 5(b) a plateau can form in such cases, but it is not the kind of very flat plateau, the "true" plateau, which sets in with high molecular weight materials, and which

(42) H. L. Frisch, *J. Phys. Chem.*, **59**, 633 (1955).
(43) W. I. Higuchi, *ibid.* **65**, 487 (1961).

maintains itself even over a logarithmic concentration scale (Fig. 5(a)).

It will be noticed that our model predicts Γ values (*i.e.*, number of segments per surface site) of order 1. Many reports are extant in the literature giving Γ values much in excess of this, in some cases by an order of magnitude. If Γ_S is the amount of polymer adsorbed in mg./m.^{2} we have the following equation relating Γ to the practical quantity Γ_S

$$\Gamma = 6.02 \frac{\mathcal{A}_0}{M_g} \Gamma_S$$

where $\mathcal{A}_0$ is the area per surface site in Å.^{2} and M_g is the molecular weight of each segment. Even if Γ_S can be measured accurately there remains room for speculation about Γ due to uncertainties about the value to be assigned to $\mathcal{A}_0$, *i.e.*, the surface area required for each adsorbed segment. $\mathcal{A}_0$ is most frequently determined from models supposedly representing the shape of the adsorbed polymer segment in the surface and values much in excess of 20 Å.^{2} have been used. Work on spread films[27-29] suggests, however, that areas much smaller (even less than 10 Å.^{2} in some cases) should be used. Correspondingly smaller Γ-values would then result. We may look upon the results of Frisch, Hellman, and Lundberg[15] for Γ_S as among the most reliable. Their adsorbent was the only one we saw characterized where a unique surface area was determined by various methods. (In most other cases widely discrepant results, or unsupported results, are reported.) Great care was taken, moreover, in this case to ensure that equilibrium was attained. From their data assuming $\mathcal{A}_0 = 20$ Å.,^{2} Γ turns out to be 0.33. Other results, notably those of Fontana and Thomas,[17] Kraus and Dugone,[10] and Ullman and collaborators[18,19] also yield Γ-values of the order 1. These can be derived without going beyond reasonable assumptions in the models which have to be introduced for $\mathcal{A}_0$, or the limits of uncertainty in Γ_S. Multilayer adsorption could occur, however, and the whole problem of adsorption from concentrated solution merits further theoretical investigation.

Given different lattice parameters, moreover, the present model will be altered. As we will see presently the values of p, predicted, are higher than those observed and p depends in sensitive fashion on surface and lattice parameters.[40] As $\Gamma = \theta/p$ a smaller p would result in larger Γ.

(b) As shown by Fig. 5 the dependence of adsorption on molecular weight is significant below degrees of polymerization of 1000 and becomes limiting above degrees of polymerization in excess of 10,000. This is confirmed consistently by the data. If we try to represent the results in the form

$$\Gamma = \text{const. } P^{\alpha}$$

as Ullman and collaborators[18,19] do, we find values for α ranging from 0.04 to 0.17 (Fig. 5(b)). The values found by Perkel and Ullman,[18] in a corresponding range of concentrations, in the case of polymethylsiloxanes, were about 0.4, and by Ellerstein and Ullman,[19] using polymethyl methacrylate, about 0.04. Reasonable quantitative agreement is thus found.

It will be noted from Fig. 5(a) that the molecular weight dependence is most pronounced at low concentrations, ϕ^*, and decreases progressively as ϕ^* is increased. This effect has been observed by Heller and Tanaka.[4]

(c) The high values of p observed, in cases where such determinations could be made,[16,17,21,22] are explained by this model. Note, moreover, that no specially large adsorption energies have to be postulated. It is curious, however, that p is practically unaffected in value by all the parameter changes we have considered. (This is also observed experimentally. Fontana and Thomas[17] for example, expressed surprise that p was independent of θ to such a large extent.) It seems that p is most affected by the structural restrictions on the polymer molecule in the surface. The fact that p, experimentally,[17,21,22] seems to be closer to 0.4 in value than to 0.7 is thus an indication that we may either have permitted too much flexibility to the chains in the surface or not have made sufficient allowance for steric restriction and entanglements in the concentrated surface phase, or both.

(d) Although adsorbed layers, as thin as we are inclined to suspect on our model, have been demonstrated in recent experimental work,[14,16,17,20] there exists a considerable amount of evidence that much thicker films can arise on occasion.[3c,20,13] Much larger loops would of course be expected[40] when special surface and polymer types are used. Multiple layer adsorption is a possibility, moreover, and some evidence for it exists.[16] It is likely, however, that insufficient time to equilibrium could have been allowed in many cases where thick films have been reported. The careful analysis of Öhrn[13] of the effect of adsorption on the viscosity of very dilute polymer solutions in capillary instruments may perhaps be explained this way. Öhrn reports layer thicknesses of the order of 1000 Å. and more. The times to equilibrium allowed were small, however, and it is not too clear whether the dimensions of the adsorbed layer in the presence of the velocity gradient at the capillary wall can be compared with the static equilibrium theory here presented.

(e) It has been pointed out that the temperature dependence of adsorption is small and that the adsorption energies consequently must be small. Taking the data of Ellerstein and Ullman,[19] for example, with $\mathcal{A}_0 = 10$ Å.^{2}, one can deduce agreement with the predictions of present theory when a segment adsorption energy of 700 cal. (about 1.2 kT) is assumed, as Fig. 3 shows. Note that this is not the total binding energy of the segment to the surface, but the excess over the solvent adsorption energy. It assumes, moreover, that the energies of binding are themselves temperature independent and that the solution of polymethyl methacrylate in toluene, to which the data refer, is athermal.

(f) The improved adsorption of polymer molecules from poor solvents has already been explained. The poor solvent may be regarded as making a contribution to x and thus effectively translating the point of adsorption to higher x-values. It is interesting that the molecular weight dependence of adsorption becomes more pronounced in a poorer solvent.[12] This would be expected on the basis of

Fig. 4(b). We note that the change in ϕ for a given departure of Δ from zero is the larger, the larger x is. The effects of molecular weight are thus enhanced at larger x, *i.e.*, also in a poorer solvent.

(g) The slowness of the adsorbed layer to attain equilibrium is due to the enormous activation energies involved. Assuming polymer molecules of $P = 10{,}000$ segments we have with $p = 0.5$ an energy of 3500 kcal. to overcome when removing the polymer molecule from the surface in a case where, as we have just illustrated, the adsorption energy is 700 cal. This is then the order of magnitude of the energy barrier which separates the state of the polymer molecule on the surface and in solution. A polymer molecule coming from solution into the surface may be expected to "bounce" off the interface quite a number of times before becoming attached. Even when attachment has occurred the adsorption process may proceed *via* a series of transition states.[9] Only adsorption data obtained after extremely long time may thus be compared with the predictions of equilibrium theory. The time to equilibrium, moreover, increases rapidly with molecular weight, indicating the need for particular caution in such cases. In several instances the more rapid rate of adsorption of low molecular weight material may have misled the experimenter into the belief that low molecular weight material is more extensively adsorbed.[3a,9]

(h) We have already pointed out that the adsorbed layer may remain in equilibrium with almost pure solvent with only a minor adjustment of its concentration. This has been confirmed by attempts to dissolve the adsorbed layer by leaving it in contact with solvent for several weeks.[15] Only the switch to a good solvent removes the film.

(j) It has been pointed out that adsorption data can as a rule be fitted to a Langmuir type plot. The fallacy in this has already been discussed by Koral, Ullman, and Eirich.[12] It is obvious of course that in plotting ϕ^*/Γ against ϕ^* one is putting undue importance on those regions where ϕ^* is large. As Γ is constant over that range, the plot is essentially one of ϕ^* against ϕ^*, as is shown by the small (effectively zero) intercept on the ϕ^*/Γ-axis of these plots. It will be clear, moreover, why the highest molecular weight fractions, which give the most constant plateau values, conform best with this type of plot.[4]

(k) The surface tension of polymer solutions has not been investigated much.[23-25] Although surface tension is most affected by the high molecular weight fraction,[23,25] as expected on our model (see Fig. 6), the concentration dependence of surface tension is least pronounced for the highest molecular weights.[23] The most illuminating investigation is the one of Couper and Eley[23] on a series of rather low molecular weight polyoxyethylene glycols. Their investigation covered concentrations from $\phi^* = 10^{-6}$ to 10^{-1} and they could demonstrate a linear relationship between σ and log ϕ^* over this wide concentration range, much as Fig. 6(c) predicts. They were able to show, moreover, that the slopes of their plots are inversely proportional to molecular weight (see equation 106). As they had no independent method of deriving Γ, they arbitrarily put it equal to 1, and thus derived molecular weights somewhat smaller than the true ones. The data of Frisch and Al-Madfai[25] are harder to interpret as they covered only a small and rather high concentration range in their measurements ($\phi^* \simeq 10^{-2}$), in which, moreover, the expected upward curvature becomes pronounced. A lower limit to Γ may, however, be estimated from their data and the true Γ is found to lie above it.

(l) As surface pressure can generally be determined, and plotted against Γ (at ϕ^*-values which are effectively zero), additional information can be derived from these measurements (see Fig. 6(a,b)). Molecular weights can be calculated from the intercept and interaction parameters in the surface deduced from the slope. Great care must be exercised, however, that low surface coverages only are used for extrapolation. Some deviations that have been observed in the molecular weight determined in this way[30] probably are due to errors of this kind. It is interesting to note that the tendency for π to flatten out at higher Γ values in the case of low molecular weight samples (see Fig. 6(a)) has been noted by Fox, Taylor, and Zisman.[28]

10. Conclusions

Summarizing we may conclude as follows:

(a) In the range where the present model is expected to apply ($\phi^* << \phi$) good agreement is found. The features of polymer behavior at surfaces (see Introduction) are explained, the order of magnitude of the effects is correctly reproduced, and the range of molecular weights, concentrations, and energy changes, where the phenomena occur, accurately predicted. This applies both to adsorption behavior and to surface tension and pressure. The predictions are embodied in equations 87 and 88 (or (95) and (96)), the isotherm (94), and the surface equation of state (101). The solution, in a particular case, is given in the figures. Note that specification of P, x, and x_0 in addition to the parameters in (97) fully determines the polymer shape, the isotherm, and the surface equation of state.

(b) It is shown that surface tension and adsorption are connected by the Gibbs equation. Even if this is not a very useful method for determining Γ of high molecular weight materials,[22] it demonstrates the value of the Gibbs model.

(c) Surface tension and pressure are equivalent when the concentration of the polymer in the bulk solution is low.

(d) It is important to reduce surface pressure by the total number $\Gamma = \theta/p$ of polymer segments per surface site (and not by θ) if polymer molecular weights are to be determined from the intercept at $\Gamma = 0$.

(e) Times to equilibrium are of necessity long in these cases.

(f) The fraction of segments in the surface, p, and the length of the loops, P_B, are determined primarily by the structural model introduced and are amazingly insensitive to changes in other parameters (for isolated coil behavior see Part I[40]). In these considerations we have discussed mainly the simplest possible case.

In a final remark let us point out that adsorption possesses some of the characteristics of phase sepa-

ration in bulk solution, with the interaction between polymer molecule and surface taking the place of the interparticle interactions generally responsible for such phenomena.

Nomenclature and Definitions (Symbols occurring only close to their definition in the text are not listed).

P: total no. of segments in each polymer molecule

m: no. of runs of adsorbed stretches in the polymer molecule

$m + 1$: no. of adsorption loops in the polymer molecule

t: total no. of adsorbed segments, per polymer molecule, not at the head of adsorbed stretches

u: total no. of segments out of the surface, per polymer molecule, but not at the head of an adsorption loop

$$P = 2m + 1 + u + t$$

P_S: no. of polymer segments in an adsorbed run at equilibrium (all in the surface)

$$P_S = \frac{m + t}{m}$$

P_B: no. of polymer segments in an adsorption loop at equilibrium (all out of the surface)

$$P_B = \frac{m + 1 + u}{m + 1}$$

p: fraction, of total no. of polymer segments, in the surface

$$p = \frac{m + t}{P} \cong \frac{P_S}{P_B + P_S}$$

γP_B: no. of layer lines of lattice sites in addition to the surface layer in the surface phase

N_S: no. of lattice sites in the surface layer

N_B: no. of lattice sites in the surface adjoint bulk phase

$$N_B = \gamma P_B N_S$$

N_{P_T}: total no. of polymer molecules

N_{0_T}: total no. of solvent molecules

N_P: total no. of polymer molecules attached to the surface

N_P^*: total no. of polymer molecules not attached to the surface

$$N_{P_T} = N_P + N_P^*$$

N_0^*: total number of solvent molecules not in the surface phase

$$N_{0_T} = (N_S + N_B - PN_P) + N_0^*$$

θ: fraction of surface sites on which polymer segments are adsorbed; fraction of surface area covered by polymer molecules

$$\theta = \frac{(m + t)N_P}{N_S} = \frac{pPN_P}{N_S}$$

ϕ: volume fraction of polymer molecules in the adjoint bulk phase of the surface phase

$$\phi = \frac{(m + 1 + u)N_P}{N_B} = \frac{(1 - p)N_P P}{N_B} = \frac{\theta}{\gamma P_S}$$

ϕ^*: volume fraction of polymer molecules in the equilibrium bulk phase

$$\phi^* = \frac{PN_P^*}{PN_P^* + N_0^*}$$

Γ: no. of polymer segments adsorbed per surface site

$$\Gamma = \frac{PN_P}{N_S} = \frac{\theta}{p}$$

Z: coördination no. of the bulk lattice

S: coördination no. of the surface lattice

f: loop restriction parameter per segment of an adsorption loop

g: steric restriction parameter for loop end segments

q: internal contact exclusion parameter for polymer segments in the equilibrium bulk phase

$$q = 1 - \frac{2}{Z}\left(1 - \frac{1}{p}\right)$$

q_B: internal contact exclusion parameter for polymer segments in the adjoint bulk phase

$$q_B = 1 - \frac{2}{Z}\left(1 - \frac{1}{P_B}\right)$$

q_S: internal contact exclusion parameter for polymer segments in the surface

$$q_S = 1 - \frac{2}{S}\left(1 - \frac{1}{P_S}\right)$$

x: drop in internal energy (in units of kT) in the adsorption of a polymer segment at a solvated surface

V_{00}: depth of interaction potential per contact between solvent molecules

V_{PP}: depth of interaction potential per contact between polymer segments

V_{0P}: depth of interaction potential per contact between solvent molecule and polymer segment
k: Boltzmann constant
T: absolute temperature
x_{0P}: heat of mixing parameter

$$x_{0P} = \frac{1}{kT}\left[\frac{Z}{2}\left(2V_{0P} - V_{PP} - V_{00}\right)\right]$$

x_0: heat of solvation parameter

$$x_0 = \frac{1}{kT}\left[\frac{Z}{2}\left(V_{0P} - V_{00}\right)\right]$$

Q_T: over-all partition function; Q_T general term
Q_S: partition function of surface phase; Q_S general term
Q^*: partition function of equilibrium bulk phase; Q^* general term

$$Q_T = Q_S \cdot Q^*$$

Q_T^{REF}: partition function of reference state
Q_0^{REF}: partition function of a solvent molecule in the bulk of pure solvent
$Q_{0,S}^{REF}$: partition function of a solvent molecule in the surface of pure solvent
Q_P^{REF}: partition function of a polymer molecule in pure polymer bulk phase
$\overline{Q_T}$: reduced partition function; Q_T general term

$$\overline{Q_T} = \frac{Q_T}{Q_T^{REF}} = \frac{Q_S \cdot Q^*}{Q_0^{REF} \cdot Q_P^{REF}} = \overline{Q_S} \cdot \overline{Q^*}$$

λ: Lagrangian multipliers
X_{0P}: total no. of external contacts between solvent molecules and polymer segments at equilibrium
X_{00}: total no. of contacts between solvent molecules at equilibrium
X_{PP}: total no. of external contacts between polymer segments at equilibrium
X_{00}^{REF}: total no. of contacts between solvent molecules in the reference phase of pure solvent with surface
X_{PP}^{REF}: total no. of external contacts between polymer segments in the reference phase of pure polymer without surface
ΔW: total internal energy change in mixing the equilibrium system from reference state
D_p, D_m, D_u, etc.: see eq. 26 to 31 and 35, and 81 to 86, and 92 for definitions
ψ_1, ψ_2, etc.: factors in the general term of the partition function
Ω_m, Ω_P: lattice assembly arrangements
$\Delta\sigma$: surface tension increment above pure solvent
π: surface pressure
$\mathcal{A}_0$: area per surface site
For bold face symbols, Λ, and β see Appendix

Appendix

$$\mathbf{A} = \ln\left[\left\{\frac{Z-S}{2}f\right\}\left\{\frac{Z-1}{Zq^{Z/2}}\right\}\frac{1-\frac{1}{m}}{P_S-\frac{1}{m}}\frac{1}{2\pi}\frac{p(1-\phi)\left(1-\frac{\theta}{P_S}\left(1-\frac{1}{m}\right)\right)}{\theta\left(1-\frac{\phi}{P_B}\right)}\right] + \ln\left[\frac{\left(P_B-\frac{1}{m+1}\right)\left(P_S-\frac{1}{m}\right)}{m^2\left(1-\frac{1}{m}\right)(P_B-1)(P_S-1)}\right]^{1/2} \quad \text{(A1)}$$

$$\mathbf{B} = \ln\left[\left\{\left(\frac{Z-S}{2}\right)^2\left(\frac{S}{S-1}\right)fg^2\right\}\left\{\frac{1}{q^{(Z/2-1)}(Z-1)}\right\}^2 \times \frac{\left(P_B-\frac{1}{m+1}\right)\left(P_S-\frac{1}{m}\right)}{\left(1-\frac{1}{m+1}\right)\left(1-\frac{1}{m}\right)}\frac{(1-\phi)}{\left(1-\frac{\phi}{P_B}\right)}\frac{(1-\theta)}{\left(1-\frac{\phi}{P_S}\left(1-\frac{1}{m}\right)\right)}\right] \quad \text{(A2)}$$

$$\mathbf{C} = \ln\left[\{(Z-1)f\}\left\{\frac{1}{q^{(Z/2-1)}(Z-1)}\right\}\frac{P_B - \frac{1}{m+1}}{P_B - 1}\frac{(1-\phi)}{\left(1 - \frac{2}{Z}\phi\frac{(1-1/P_B)}{\left(1 + \frac{Z-S}{2Z}\frac{1}{\gamma P_B}\right)}\right)}\right] \tag{A3}$$

$$\mathbf{D} = \ln\left[\{(S-1)\}\left\{\frac{1}{q^{(Z/2-1)}(Z-1)}\right\}\frac{P_S - \frac{1}{m}}{P_S - 1}\frac{(1-\theta)}{\left(1 - \frac{2}{S}\theta\left(1 - \frac{1}{P_S}\right)\right)}\right] \tag{A4}$$

$$\mathbf{K} = \ln\left[\frac{\left(1 - \frac{\phi}{P_B}\right)\left(1 - \frac{2}{Z}\phi\frac{(1-1/P_B)}{\left(1 + \frac{Z-S}{2Z}\frac{1}{\gamma P_B}\right)}\right)^{Z/2}}{(1-\phi)}\right] \tag{A5}$$

$$\mathbf{L} = \ln\left[\frac{\left(1 - \frac{\theta}{P_S}\left(1 - \frac{1}{m}\right)\right)\left(1 - \frac{2}{S}\theta\left(1 - \frac{1}{P_S}\right)\right)^{S/2}\left(1 - \frac{2}{Z}\phi\frac{(1-1/P_B)}{\left(1 + \frac{Z-S}{\gamma 2Z}\frac{1}{P_B}\right)}\right)^{(Z-S)/4}}{(1-\theta)}\right] \tag{A6}$$

$$\mathbf{M} = \left[\left(1 - \frac{1}{P_B}\right)\frac{(P_B - 1)}{\left(\frac{2Z\gamma}{Z-S}P_B + 1\right)}\right] - \frac{1}{2m}\left[\frac{P_B - 1}{P_B - \frac{1}{m+1}} + \frac{P_S - 1}{\left(P_S - \frac{1}{m}\right)\left(1 - \frac{1}{m}\right)}\right] \tag{A7}$$

$$\mathbf{U} = \left[-\frac{1}{P_B}\cdot\frac{(P_B - 1)}{\left(\frac{2Z\gamma}{Z-S}P_B + 1\right)}\right] - \frac{1}{2(m+1)}\left[\frac{1}{(P_B - 1)\left(P_B - \frac{1}{m+1}\right)\left(1 + \frac{1}{m}\right)}\right] \tag{A8}$$

$$\mathbf{T} = -\frac{1}{2m}\left[\frac{\left(1 - \frac{1}{m}\right)}{(P_S - 1)\left(P_S - \frac{1}{m}\right)}\right] \tag{A9}$$

$$\mathbf{O}^* = \ln\left[\frac{(1 - \phi^*(1-q))^{Z/2}}{(1-\phi^*)}\right] \tag{A10}$$

$$\mathbf{P}^* = \ln\left[\frac{(1 - \phi^*(1-q))}{\phi^*}\right] + P\left(\frac{Z}{2} - 1\right)\ln\left[1 - \phi^*(1-q)\right] - P\frac{Z}{2}q\ln q \tag{A11}$$

$$\mathbf{E} = -\frac{\Delta W}{kT} = -x_{0P}\left[N_B\frac{(1-\phi)(q_B\phi)}{(1-\phi) + (q_B\phi)} + \frac{S}{Z}N_S\frac{(1-\theta)(q_S\theta)}{(1-\theta) + (q_S\theta)} + \frac{Z-S}{2Z}N_S\theta(2-\phi) - \frac{4N_S}{ZP_S}\theta(1-\phi)\right] + x_0\left[\frac{Z-S}{2Z}N_S(3\theta - \phi) - \frac{4N_S}{ZP_S}\theta(1-\phi)\right] + x(m+t)N_P - x_{0P}\left[\frac{(1-\phi^*)(q\phi^*)}{(1-\phi^*) + (q\phi^*)}\right](N_0^* + PN_P^*) \tag{A12}$$

$$\mathbf{y}_{(0P)} + 2\ln g = -\left[\frac{P_B}{\phi}\mathbf{E}_0^* + \mathbf{E}_m - \mathbf{E}_u - \mathbf{E}_t\right] = +x_0\left[\left\{\frac{Z-S}{2\gamma Z} + \frac{4}{Z}\right\}\left\{1 - \phi\frac{8}{(Z-S)/2\gamma + 4}\right\}\right] - \frac{4}{Z}\phi x_{0P}\left[\frac{q_B(1-\phi) + \frac{1}{2}q_B^2\left(\frac{ZP_B}{2} + \phi\right)}{[(1-\phi) + q_B\phi]^2} + \frac{\theta}{\phi}\frac{q_S(1-\theta) + \frac{1}{2}q_S^2\theta}{[(1-\theta) + q_S\theta]^2} - 2 + \frac{Z-S}{4\gamma}\frac{\theta}{\phi} - \frac{Z}{4}\frac{P_B}{\phi^2}\left[\frac{(q\phi^*)^2}{(1-\phi^*) + q\phi^*]^2}\right]\right] \tag{A13}$$

$$\bar{\mathbf{x}}_{(0P)} = -\left[\mathbf{E}_u - \mathbf{E}_t - \mathbf{E}_0^* \frac{1}{\phi}\right] = x + x_0\left[\frac{3}{2}\frac{Z-S}{Z}\right] + \phi.r_{0P}\left[\frac{Z-S}{Z} + \frac{S}{Z}\frac{2(q_S\theta)(1-\theta)}{\phi}\frac{\left(1-\frac{2}{S}\right) + q_S\theta\left(1-\frac{1}{S}\right)}{[(1-\theta)+q_S\theta]^2} - q_B\frac{\left[1-\frac{2}{Z}\left(1+\frac{1}{P_B}\right)\right] - \frac{2}{Z}\phi\,[q_B - 2/P_B]}{[(1-\phi)+q_B\phi]^2} - \frac{1}{\phi^2}\frac{(q\phi^*)^2}{[(1-\phi^*)+q\phi^*]^2}\right] \quad \text{(A14)}$$

$$P[\bar{\mathbf{x}}_{(0P)} + \Delta\mathbf{x}] = \{[(P+1)-t]\mathbf{E}_t - u\mathbf{E}_u - (m+1)\mathbf{E}_m + \mathbf{E}_P + P\mathbf{E}_0^* - \mathbf{E}_P^*\} \quad \text{(A15)}$$

$$\Delta\mathbf{x} = x_{0P}\phi\left[q_B\frac{\left[1-\frac{2}{Z}\left(1+\frac{1}{P_B}\right)\right] - \frac{2}{Z}\phi\,[q_B - 2/P_B]}{[(1-\phi)+q_B\phi]^2} - \frac{Z-S}{Z}p - \frac{2S}{Z}\frac{(\theta q_S)^2}{\phi[(1-\theta)+\theta q_S]^2} + q\frac{(1-\phi^*)^2 + q\left(\frac{\phi^*}{\phi}\right)^2(1-\phi)}{\phi[(1-\phi^*)+q\phi^*]^2}\right] + \frac{1}{P}\left[x_0\frac{4}{Z}(1-2\phi) + x_{0P}\left[\frac{(2/Z)(1-\theta)^2}{[(1-\theta)+q_S\theta]^2} - \frac{4}{Z}(1-2\phi)\right]\right] \quad \text{(A16)}$$

$$\mathbf{G}^* = \ln\left[\frac{(1-\phi^*)+q\phi^*}{\phi^*}\right] + P\ln\left[\frac{(1-\phi^*)}{(1-\phi^*)+q\phi^*}\right] \quad \text{(A17)}$$

$$\mathbf{H} = \mathbf{D} + \mathbf{A} - \mathbf{B} - (m+1)\mathbf{M} - u\mathbf{U} - (t-1)\mathbf{T} + \ln q = \ln\left[\frac{p}{\theta}\cdot\frac{\left[1-\frac{1}{P_S}\left(1-\frac{1}{m}\right)\theta\right]^2}{\left[1-\frac{2}{S}\left(1-\frac{1}{P_S}\right)\theta\right]}\cdot\frac{1}{g^2}\cdot\frac{\left(1-\frac{1}{m+1}\right)\left(1-\frac{1}{m}\right)^{3/2}}{2\pi m(P_S-1)\left[\left(P_B-\frac{1}{m+1}\right)\left(P_S-\frac{1}{m}\right)(P_B-1)(P_S-1)\right]^{1/2}}\times \frac{2(S-1)^2(Z-1)^2}{(Z-S)SZ}\right] + \frac{1}{2}\left[\frac{(P_B-1)\left(1+\frac{1}{m}\right)}{\left(P_B-\frac{1}{m+1}\right)} + \frac{1}{\left(P_B-\frac{1}{m+1}\right)\left(1+\frac{1}{m}\right)} + \frac{(P_S-1)\left(1+\frac{1}{m}\right)}{\left(P_S-\frac{1}{m}\right)\left(1-\frac{1}{m}\right)} + \frac{1-\frac{1}{m}}{\left(P_S-\frac{1}{m}\right)} + \frac{\frac{1}{m}\left(1-\frac{1}{m}\right)}{(P_S-1)\left(P_S-\frac{1}{m}\right)}\right] \quad \text{(A18)}$$

(see definitions (A1), (A2), (A4), (A7), (A8), and (A9))

$$\Lambda = \ln\left[(P_S-1)\left(1-\frac{2}{S}\theta\left(1-\frac{1}{P_S}\right)\right)\right] \quad \text{(A19)}$$

$$\Lambda = \ln\left[\frac{S-1}{Z-1}\left\{\frac{1}{q^{(Z/2-1)}}\right\}\left(P_S-\frac{1}{m}\right)(1-\theta)\right] + \frac{P_B}{\phi}(\mathbf{K}-\mathbf{O}^*) + (\mathbf{C}-\mathbf{B}) + (\mathbf{U}+\mathbf{T}-\mathbf{M}) + \mathbf{y}_{(0P)} + 2\ln g \quad \text{(A20)}$$

(see equation 87 and definition (A4))

$$\Lambda = \frac{P_B}{\phi}(\mathbf{K}-\mathbf{O}^*) + \ln\left[\left(\frac{2}{Z-S}\right)^2\left(\frac{S-1}{S}\right)(Z-1)(S-1)\frac{\left(1-\frac{1}{m+1}\right)\left(1-\frac{1}{m}\right)}{(P_B-1)}\times\right.$$

$$\frac{\left(1-\frac{\phi}{P_B}\right)\left(1-\frac{\theta}{P_S}\left(1-\frac{1}{m}\right)\right)}{\left(1-\frac{2}{Z}\phi\frac{(1-1/P_B)}{\left(1+\frac{Z-S}{2Z}\frac{1}{\gamma P_B}\right)}\right)}\Bigg] - (P_B-1)\left[\frac{1}{\frac{2Z}{Z-S}\gamma P_B+1}\right] + \mathbf{y}_{(0P)} + \frac{1}{2m}\left[2-\frac{1}{(P_B-1)\left(1+\frac{1}{m}\right)}-\frac{1}{(P_S-1)\left(1-\frac{1}{m}\right)}\right] \quad \text{(A21)}$$

(see definitions (A2), (A3), (A7), (A8), and (A9))

$$\boldsymbol{\Delta} = \left[\mathbf{D}+\mathbf{T}-\ln\left\{\frac{1}{q^{(Z/2-1)}}\right\}+\bar{\mathbf{x}}_{(0P)}+\Delta\mathbf{x}\right] \quad \text{(A22)}$$

$$= \ln\left[\frac{S-1}{Z-1}\left(P_S-\frac{1}{m}\right)(1-\theta)\right]+\bar{\mathbf{x}}_{(0P)}+\Delta\mathbf{x}-\Lambda-\left[\frac{\left(1-\frac{1}{m}\right)}{2P}\frac{P_B\left(1+\frac{1}{m}\right)+P_S}{(P_S-1)\left(P_S-\frac{1}{m}\right)}\right] \quad \text{(A23)}$$

(see definitions (A4), (A9), and (A19))

$$= \left[\frac{1}{\phi}(\mathbf{K}-\mathbf{O}^*)+\mathbf{C}+\mathbf{U}+\Delta\mathbf{x}-\ln\left\{\frac{1}{q^{(Z/2-1)}}\right\}\right] \quad \text{(A24)}$$

(see equation 88)

$$\boldsymbol{\Delta} = \frac{1}{\phi}(\mathbf{K}-\mathbf{O}^*)+\ln\left[f\cdot\frac{P_B-\frac{1}{m+1}}{P_B-1}\frac{(1-\phi)}{\left(1-\frac{2}{Z}\phi\frac{(1-1/P_B)}{\left(1+\frac{Z-S}{2Z}\frac{1}{\gamma P_B}\right)}\right)}\right] - \frac{P_B-1}{P_B}\left[\frac{1}{\frac{2Z\gamma}{Z-S}P_B+1}\right]+\Delta\mathbf{x}-\frac{1}{2(m+1)}\left[\frac{1}{(P_B-1)\left(P_B-\frac{1}{m+1}\right)\left(1+\frac{1}{m}\right)}\right] \quad \text{(A25)}$$

(see definitions (A3) and (A8))

$$\mathbf{E}_{N_S}-(1+\gamma P_B)\mathbf{E}_0^* = -x_0\left[\frac{4}{Z}\frac{\phi\theta}{P_S}\right]-x_{0P}\left[\gamma P_B\left\{\frac{(q_B\phi)^2}{[(1-\phi)+q_B\phi]^2}-\frac{(q\phi^*)^2}{[(1-\phi^*)+q\phi^*]^2}\right\}+\left\{\frac{S}{Z}\frac{(q_S\theta)^2}{[(1-\theta)+q_S\theta]^2}-\frac{(q\phi^*)^2}{[(1-\phi^*)+q\phi^*]^2}\right\}+\phi\theta\left\{\frac{Z-S}{2Z}-\frac{4}{ZP_S}\right\}\right] \quad \text{(A26)}$$

$$\beta = \left[\left(1-\frac{1}{P_S}\right)\left(\frac{1}{P_S}+q_s\right)+\frac{P_B-1}{\gamma P_S^2}\left\{\frac{1}{P_B}+q_B+\frac{2}{Z}\left(1-\frac{1}{P_B}\right)\frac{1}{P_B\frac{2Z\gamma}{Z-S}+1}\right\}\right]-x_0\left[\frac{8}{\gamma Z P_S^2}\right]-2x_{0P}\left[\frac{P_B}{\gamma P_S^2}q_B^2-\frac{4}{\gamma Z P_S^2}+\frac{S}{Z}q_S^2+\frac{Z-S}{2Z\gamma}\frac{1}{P_S}\right] \quad \text{(A27)}$$

DISCUSSION

F. M. FOWKES (Shell Development Company).—This contribution to the understanding of how polymers adsorb fits the experimental data far better than any previous explanation. I am particularly pleased with the predictions of very small loops. However, we do often find larger values of Γ than the 0.7 presented today.

A. SILBERBERG.—Values of Γ (ratio of number of segments adsorbed to adsorption sites) can be larger than one (see Fig. 3, Part II; other cases have not yet been calculated but one can envisage large Γ values even with monolayer adsorption).

A. BONDI (Shell Development Company).—Do I understand correctly that, in effect, your theory explains why polymers often seem to be irreversibly adsorbed, simply because they are so very strongly adsorbed even out of extremely dilute solution?

Another question I should like to ask is whether you agree that Dr. Huggins's request for incorporation of flexibility might well be handled by incorporating the external degrees

of freedom of a molecule (including those due to internal rotation) into the original partition function of the polymer molecule? If one does that in the manner of Prigogine ("Molecular Theory of Solution") I suspect one will find that the major change will be the form of x, namely that $x = E/fkT$, where f = number of external degrees of freedom per chain link ($= 3c/r$ in Prigogine's nomenclature).

A. SILBERBERG.—The seeming irreversibility of polymer adsorption can, I believe, be explained in this way.

Your basic suggestion of a method for introducing flexibility has in fact been followed in the present treatment, although in a manner rigidly tied to the lattice coördination arrangement assumed (parameters Z and S). One can vary these parameters or introduce additional ones, such as g (Part II), but my purpose so far has been to keep the number of adjustable parameters down. I hope to discuss these and other structural effects in a paper which I have in preparation.

M. J. VOLD (University of Southern California).—The findings that pendant loops of an adsorbed polymer extend only a very few segment lengths into the solution and that the thickness of adsorbed film is independent of molecular weight has a very devastating effect upon at least two heretofore relatively well accepted explanations of experimental effects. One is the flocculation of suspensions by bridging as discussed by La Mer and the other is the stabilization of traditional colloids against coagulation by electrolytes (for example, the gold sols of Heller and Pugh). Both these effects are sensitive to the molecular weight of the polymer and seem to require long pendant loops. Can you provide us with a way out of this seeming dilemma?

A. SILBERBERG.—Large pendant loops whose size depends on molecular weight can be expected during the period which follows upon the successful attachment of a macromolecule to the surface. Only very gradually will the equilibrium configuration predicted in this treatment be approached. In fact, the transition period may be of considerably larger duration than the relaxation times of the other phenomena studied.

Long loops in equilibrium are, moreover, not excluded by the treatment. Under certain conditions, some covered here (see Part I), others not (polyelectrolyte adsorption, for example), the loops are predicted to be long.

The observations quoted by Dr. Vold thus do not necessarily stand in contradiction to the picture here proposed. It should be noted, moreover, that a molecular weight dependence of the amount adsorbed is one of the conclusions of the present treatment.

M. L. HUGGINS (Stanford Research Institute).—I am not clear as to how your theory can relate the observable properties to two molecular parameters which I have shown to be important in three-dimensional polymer solutions (and which also enter into my treatment of polymeric monolayers, presented at Wiesbaden in 1959). One of these parameters is the difference between the molecular interaction energy per unit molecular surface area between unlike molecules and the average of that between like molecules. The other is the change with concentration of the average flexibility per joint in the polymer chain.

A. SILBERBERG.—Of the two parameters you mention the first is, I believe, considered by the treatment and is most closely related to the parameters x_0 and x_{0P} introduced in Part II. Restrictions on the flexibility of links are changed by changing the lattice coördination numbers Z and S, by varying the parameter g (Part II), and by introducing some of the special effects considered in Part I. A dependence on concentration has, however, not yet been envisaged.

ADSORPTION OF A COPOLYMER POLYELECTROLYTE

BY W. SCHMIDT AND F. R. EIRICH

Institute of Polymer Research, Polytechnic Institute of Brooklyn, Brooklyn, N. Y.

Received March 12, 1962

A series of vinyl acetate–crotonic acid copolymers was synthesized and characterized by light scattering and viscosity measurements. The adsorption behavior of these copolymers on anatase was investigated as a function of polymer charge and charge density at several pH values. The results demonstrate a large increase in adsorption capacity with decreasing crotonic acid content and decreasing pH. Formation of a common function for all copolymers connecting adsorption capacity with their states in solution as a function of ΔpH (pH units above the point of precipitation) was observed. The effect of the function of ΔpH was interpreted as producing equal ratios of adsorbing (VA) and non-adsorbing, or even repelling, (COO^-) groups.

1. Introduction

The adsorption of high polymers on liquid–solid interfaces lately has become the subject of detailed experimental and theoretical studies. Among the pertinent investigations, Claesson,[1] Jenckel and Rumbach,[2] Hobden and Jellinek,[3] Lifland,[4] Kraus and Dugone,[5] Koral, Ullman, and Eirich,[6a] Lopatin and Eirich,[6b] Ullman, *et al.*,[6c] and others have ascertained that polymers are readily adsorbed in quantities which would amount to multilayers if completely flat accommodation at the surface were assumed, but would signify incomplete adsorption if the polymer chains were to pack standing end on. The amounts adsorbed as a function of concentration conformed, surprisingly, to Langmuir type isotherms, and the dependence on molecular weight, temperature, type of adsorbent, and solvent was found to be very complex. On porous surfaces fractionation and time effects were found whenever the molecules were as large or larger than a characteristic diameter of the pores. On nonporous adsorbents, the amounts adsorbed rose slowly with molecular weight, and poorer solvents magnified this trend. This tendency, together with the general observation that poorer solvents lead to increased adsorption, have been explained[6a] in terms of the effect of the solvent on the configuration of the polymer in solution.

The effect of temperature on adsorption is in most cases small and depends on the nature of the system. Besides the more usual decreases of adsorption with temperature, increases often are ob-

(1) I. Claesson and S. Claesson, *Arkiv. Kem., Mineral., Geol.*, **19A**, No. 5 (1945).

(2) E. Jenckel and B. Rumbach, *Z. Elektrochem.*, **55**, 612 (1951).

(3) J. F. Hobden and H. H. G. Jellinek, *J. Polymer. Sci.*, **11**, 365 (1953).

(4) J. Lifland, Master's Thesis, Polytechnic Institute of Brooklyn, 1954.

(5) G. Kraus and J. Dugone, *Ind. Eng. Chem.*, **47**, 1809 (1955).

(6) (a) J. Koral, R. Ullman, and F. R. Eirich, *J. Phys. Chem.*, **62**, 541 (1958); (b) G. Lopatin and F. R. Eirich, *Proc. 3rd Intern. Congr. Surface Activity*, **2**, 97 (1960); (c) R. Perkel and R. Ullman, *J. Polymer Sci.*, **54**, 127 (1961).

served which have been related to entropy effects connected with solvent desorption.[6a]

Jenckel and Rumbach[2] postulated that the polymer chain be anchored onto the solid surface at several sites along the chain with the remainder of the coil extending into the solution in the form of loops. This concept led to a detailed statistical adsorption theory for a random coil polymer put forth by Frisch, Simha, and Eirich[7] and further developed by Frisch and Simha.[8] This theory considers the changes in free energy of all the participants (surface, solute, solvent) including the mixing of the loops of the enforced chain configurations with solvent during the adsorption process. The isotherm predicted by this theory is of the Fowler type but under certain conditions can approach the Langmuir type.

Until recently, very little experimental work had been carried out on the adsorption of polyelectrolytes. Michaels and Morelos,[9] investigating the adsorption of sodium polyacrylate and a partially hydrolyzed polyacrylamide on kaolinite in the pH range 5 to 8, found adsorption to decrease with increasing pH. Lopatin[10] and Lauria,[11] investigating the adsorption of PMAA[11a] and PAA on anatase, also found the isotherms to be strongly pH dependent, with both affinity and capacity passing through maxima, but at different pH values. Both investigators[10,11] have reported a rather small molecular weight dependence of the order of $M^{0.05}$ to $M^{0.2}$. The adsorption of PMAA on lower dielectric materials, PS and PMMA beads, also demonstrated capacity dependence on pH, but the capacities on these adsorbents were appreciably higher than for TiO_2.[11]

A new theoretical derivation by Frisch and Stillinger[12a] which relates the rising slope of the adsorption isotherms, *i.e.*, the "affinity" with the state of charge of polymer and surface, dielectric constant, and ionic strength, has been employed to explain some of the results of Lauria, and an unpublished extension of this theory may be applicable to the adsorption "capacities" of this work.[12b]

The purpose of the present investigation was to continue the study of the adsorption behavior of polyelectrolytes on a non-porous surface (anatase) as a function of polymer charge and charge distribution. The variation of polymer charge at constant pH was to be accomplished by the expedient of copolymerization using a hydrophobic comonomer from which a series of increasingly water soluble polyelectrolytes could be derived. The copolymer chosen was crotonic acid–vinyl acetate and the compositions to be studied were similar to those discussed by Katchalsky and Gillis.[13]

(7) H. L. Frisch, R. Simha, and F. R. Eirich, *J. Phys. Chem.*, **57**, 584 (1953).

(8) H. L. Frisch and R. Simha, *ibid.*, **58**, 507 (1954); *J. Chem. Phys.*, **24**, 651 (1956); **27**, 701 (1957).

(9) A. S. Michaels and O. Morelos, *Ind. Eng. Chem.*, **47**, 1801 (1955).

(10) G. Lopatin, Dissertation, Polytechnic Institute of Brooklyn, 1961.

(11) R. Lauria, Dissertation, Polytechnic Institute of Brooklyn, 1962.

(11a) Poly(methacrylic acid), PMAA; poly(acrylic acid), PAA; polystyrene, PS; poly(methyl methacrylate), PMMA.

(12) (a) H. L. Frisch and F. H. Stillinger, American Chemical Society, 140th National Meeting, Chicago, 1961; (b) private communication.

II. Experimental Procedures

A. Materials. Solvent.—The water used in our studies was obtained by distillation of deionized water. Solutions were adjusted and maintained at the desired pH by addition of 0.05 *N* sodium acetate buffer.

Polymers.—The vinyl acetate–crotonic acid copolymers were prepared by bulk polymerization with benzoyl peroxide as the initiator. The crotonic acid was used as received. The vinyl acetate was distilled prior to use.

The monomer mixtures were reacted in sealed Pyrex tubes at a temperature of 70°, using an initiator concentration of 0.035 mole % with respect to monomer. The monomer concentrations used, polymerization times, and % conversion are shown in Table I.

The copolymers formed were isolated by precipitation in 500 ml. of heptane. After decanting the heptane, the copolymers were dissolved in methyl ethyl ketone (10 parts MEK to 1 part polymer), and precipitated by dropwise addition to hot (60°) heptane, with vigorous stirring. This procedure was repeated several times. Copolymers A and B were further treated by dissolving in benzene and freeze-drying.

The copolymers then were dried in a vacuum oven at 68°. Copolymer composition was determined by titration with 0.1 *N* sodium hydroxide in 95% ethanol to a phenolphthalein end-point. The results are given in Table I.

The molecular weights of the copolymers as determined by light scattering (in MEK) are given in Table II. The refractive index increments, dn/dc, as measured by a Rayleigh interferometer, were found to be 0.110, 0.116, and 0.123 for copolymers B, C, and D, respectively. The intrinsic viscosities in MEK and 0.05 *N* sodium acetate solutions also are shown in Table II.

The poly(4-vinyl N,*n*-butyl pyridinium bromide) used for the copolymer titration was prepared from poly(*n*-vinyl pyridine) following the method of Fuoss and Strauss.[14]

Adsorbent Surface.—A sample of anatase especially prepared by the Titanium Pigment Corp. was used as the adsorbent. The specific surface area as determined by the BET method (nitrogen) on a sample outgassed at 400° was 10.9 m.²/g.

The anatase powder was further treated in our Laboratory before adsorption measurements were carried out, by a slightly modified version of the procedure outlined by Lopatin.[10]

Adsorption–desorption cleaning then was carried out by adsorbing copolymer C at pH 6.0, withdrawing the solution from the adsorbent, and adding to the adsorbent NaOH solution to pH 12. Desorption of the copolymer was found to be 96% complete. The adsorbent then was washed with distilled water until neutral, washed with acid, alkali, and water as before, and freeze-dried. Adsorption of the copolymers was determined on this surface.

B. Adsorption Procedure.—A weighed quantity of anatase was shaken with 10 ml. of polymer solution of known concentration for a minimum of 24 hr., centrifuged, and the supernatant analyzed. The difference in concentration and the amount of adsorbent were used to calculate the adsorption per gram (x/m) at the equilibrium concentration. Glass tubes stoppered with polyethylene caps were used. They were weighed, put on a thermostated rotator (30°) for 24 hr., and reweighed to check for leakage. The pH of the supernatant solutions was determined on a Beckman pH meter after each adsorption run. Adsorption runs were set up at pH 7.6, 6.5, 6.0, and 5.5 in the presence of 0.05 *N* sodium acetate–acetic acid.

C. Analytical Method.—With only slight modification, the method outlined by Lopatin[10] was used to analyze for copolymer concentration before and after each adsorption run.

Solutions of known copolymer concentration (2 to 100 p.p.m.) were titrated with poly(4-vinyl-N,*n*-butyl pyridinium bromide) solutions (3.4 to 6.8 mg./100 ml.). The copolymer solutions were buffered to pH 10 with NaOH. The titrant was added in 0.02-ml. increments and the solution allowed to mix for 15–20 sec. (by evolution of N_2)

(13) A. Katchalsky and J. Gillis, *Rec. Trav. Chim.*, **68**, 879 (1949).

(14) R. Fuoss and R. Strauss, *J. Polymer Sci.*, **3**, 246 (1948).

before recording turbidity on a Brice-Phoenix scattering instrument. The peak of turbidity served as a characteristic end-point. In the low concentration region (0.5 to 2 p.p.m.) results were obtained by a direct comparison with a known copolymer solution (1 p.p.m.) rather than from the calibration curve.

Results and Discussion

The monomer concentrations used in the copolymerizations, as previously mentioned, were calculated to provide copolymers similar to those studied by Katchalsky and Gillis.[13] Our analysis (Table I) shows that, in fact, quite similar compositions were obtained. Katchalsky and Gillis were concerned with the variation of pK of polymeric acids with concentration, degree of ionization, and distance between carboxyl groups. The use of their data for the calculation of the number of charged groups on our copolymers for various adsorption runs will be discussed more fully below.

TABLE I

COPOLYMERIZATION DATA

Co-polymer	Monomer concn. Vinyl acetate, g.	Monomer concn. Crotonic acid, g.	Reaction time, hr.	% Conversion	% Crotonic acid in copolymers
A	48.2	1.8	14	14	5.5
B	46.4	3.6	22	13	12.9
C	42.5	7.5	26	8	26.1
D	28.0	22.0	26	5	42.4

In the present syntheses, attempts were made to prepare compounds of approximately the same molecular weight by using constant catalyst concentration and temperature. While the molecular weights as determined by light scattering differ by a factor of 3, the intrinsic viscosities in water vary much less and, *e.g.*, those of copolymers B and C at pH 7.6 and 6.5 are almost the same (see Table II). This must be interpreted as showing that the two copolymers encompass comparable volumes which ought to be due to the greater relative number of carboxyl groups in copolymer C providing a more expanded configuration.

TABLE II

MOLECULAR WEIGHT AND INTRINSIC VISCOSITY DATA FOR COPOLYMERS B, C, AND D

Copolymer	$[\eta]$ in H_2O pH 7.6	$[\eta]$ in H_2O pH 6.5	$[\eta]$ in MEK	Mol. wt. $\times 10^{-3}$ (L.S. in MEK)
B(12.9% CA)	0.563	0.535	0.32	61
C(26.1% CA)	.577	.550	.20	31
D(42.4% CA)	.40	.365	.10	18

The decision of which pH range would be most profitable for our studies was made with reference to the solubility pattern of the copolymers. It was noted that the latter precipitated from solution as the pH was lowered, independently of which acids were used. The pH values for the precipitation varied from 4.8 to 7.0, depending on the copolymer composition, giving a smooth function as shown in Fig. 1. It was decided that adsorption runs would be attempted at several pH's and at appropriate pH intervals in such fashion that approximately "corresponding states" of solution would be obtained (see also Fig. 1), *i.e.*, at definite

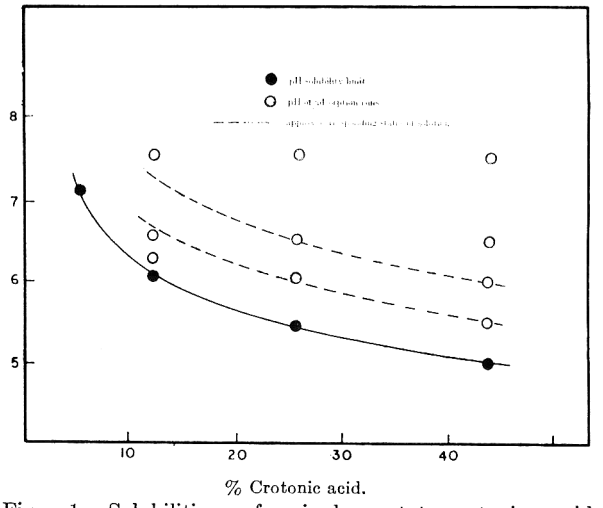

Fig. 1.—Solubilities of vinyl acetate–crotonic acid copolymers.

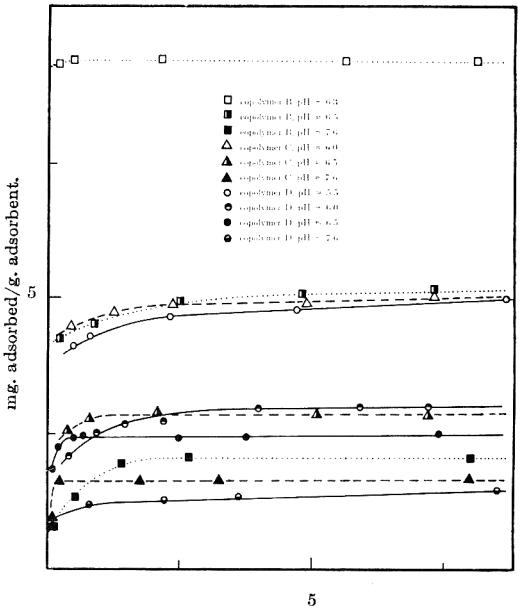

Fig. 2.—Adsorption of copolymers on anatase.

pH increments between a given solution and the limiting pH at which precipitation occurred. Insofar as the solubility range permitted, the adsorption behavior of the copolymer was further compared at constant pH.

The adsorption curves obtained in this way are given in Fig. 2. The results demonstrate a large increase in capacity with decreasing crotonic acid content. The capacity increases markedly in all cases with decreasing pH as found by earlier workers. The adsorption capacities as a function of pH have been summarized in Fig. 3.

Comparing the adsorption of copolymers B, C, and D in the "corresponding states" of solution mentioned, and taking the pH at which the copolymers precipitated as a reference point, the capacities were plotted next *vs.* ΔpH above the point of precipitation. The results, shown in Fig. 4, show formation of a common function for all copolymers. This relationship is indicated similarly

TABLE III

VARIATION OF COPOLYMER DEGREE OF IONIZATION (α) WITH pH

	Copolymer B ($pK \approx 6.5$,[b] $n = 1.3$[a])			Copolymer C ($pK \approx 6.8$,[b] $n = 1.4$[a])			Copolymer D ($pK \approx 7.0$,[b] $n = 1.5$[a])		
pH	α	$\frac{COO^-}{VA}$	$\frac{COO^-}{Molecule}$	α	$\frac{COO^-}{VA}$	$\frac{COO^-}{Molecule}$	α	$\frac{COO^-}{VA}$	$\frac{COO^-}{Molecule}$
7.6	0.88	0.13	80	0.79	0.28	74	0.72	0.53	64
6.5	.50	.074	46	.38	.13	36	.32	.23	28
6.3	.39	.057	35	..	..	..	..	..	..
6.0	.29	.043 (ppt.)	26	.21	.074	20	.18	.13	16
5.5	..	..	..	.105	.037 (ppt.)	10	.09	.067	8
5.0	..	..	..	..	..	..	.045	.033 (ppt.)	4

[a] Taken from Katchalsky and Gillis.[13] [b] Estimated from Oth and Doty.[16]

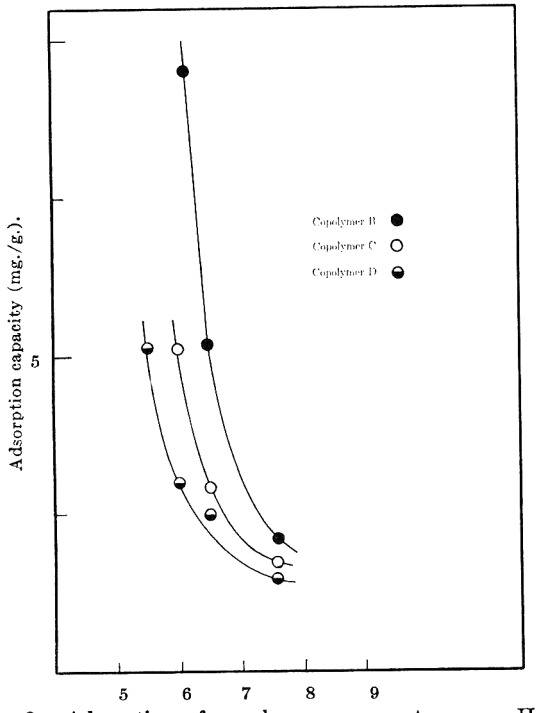

Fig. 3.—Adsorption of copolymers on anatase *vs.* pH of solution.

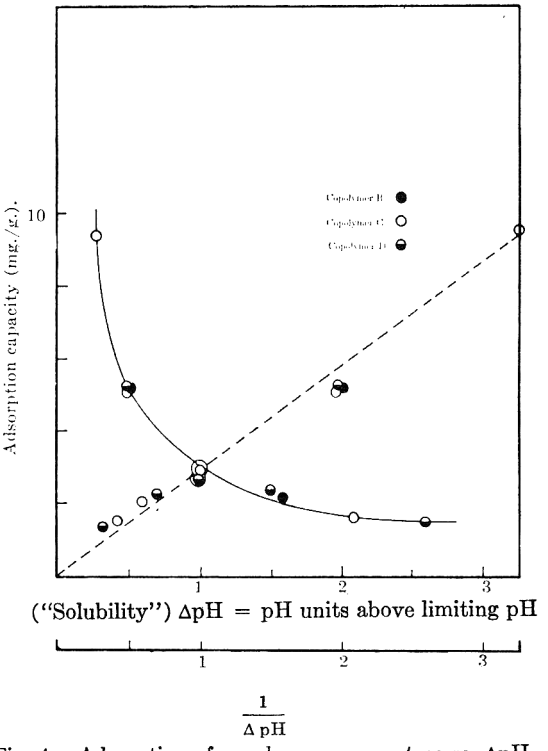

Fig. 4.—Adsorption of copolymers on anatase *vs.* ΔpH.

by Fig. 3, where a constant shift in pH units for the individual copolymer curves will lead to the formation of a single curve like that shown in Fig. 4. This is all the more striking as the copolymers possess rather different molecular weights. Earlier work, however, has shown that the influence of molecular weight on capacities is small, and the mere existence of such a smooth dependence as seen in Fig. 4 points toward the absence of substantial molecular weight effects.

In a first attempt to interpret Fig. 4, one would assume a variation in adsorption capacity due to changes in charge density on the polymer. The degree of ionization (α) may be calculated by means of the equation[15]

$$pH = pK - n \log \frac{1 - \alpha}{\alpha}$$

By assigning pK and n values to copolymers B, C, and D as obtained by extrapolation from the data of Katchalsky and Gillis,[13] the values for α were obtained and used to prepare a plot of the adsorption capacity as a function of charge density. However, the coincidence of the curves in this plot is poor.

The discrepancies are greatly reduced if one assumes higher pK values for the copolymers than those of ref. 13. Based on the work of Oth and Doty[16] regarding variation in pK with concentration, pK values approximately 1.0 unit higher than those given by Katchalsky and Gillis would be quite in order. This increase in pK was estimated by an extrapolation (of our pK according to ref. 13) toward lower concentrations, parallel to the Oth and Doty curve for their change in pK with concentration.

Using these new pK values for calculation of α (see Table III), the adsorption capacities were plotted again as functions of charge density (expressed in $\#COO^-/100$ monomer units) and now approached very closely a unified relationship as is shown in Fig. 4. A slightly modified version was obtained by plotting adsorption capacity as a

(15) A. Katchalsky and P. Spitnik, *J. Polymer Sci.*, **2**, 432 (1947).

(16) A. Oth and P. Doty, *J. Phys. Chem.*, **56**, 43 (1952).

function of the ratio of number of charges per vinyl acetate group, which might characterize the "solubility state" of the copolymers somewhat better than charge density alone. The result is such a close reproduction of Fig. 4 that it supports the interpretation that ΔpH by way of producing equal ratios of non-adsorbing or repelling (COO^-) groups to adsorbing (VA) is the primary variable.

Actually, replacing the abscissa by the ratio VA/COO^- leads inevitably to deviations from the straight line, in that the amounts of x/m become infinite at finite values of VA/COO^-. In order to fit our data, a relationship also going to infinity has to be postulated and this can be done by substituting ΔCOO^-, between a given value of COO^- and that at the limiting pH, into the denominator: $x/m = K (VA/\Delta COO^-)$. Plotting of this curve leads to an interesting intercept b at the ordinate for $VA/\Delta COO^- = 0$. Considering all the facts, it signifies the amount adsorbed at finite charges for vanishing content of vinyl acetate in the copolymers, and thereby probably the adsorption of polycrotonic acid over the pH range considered. Taking cognizance of this intercept, a replot of our data according to $x/m = K VA/\Delta COO^- + b$ reproduces the straight line in Fig. 4, lending a certain amount of interpretation to the primary dependence of our adsorption capacities on $1/\Delta pH$, *i.e.*, is due to the ratio of adsorbing groups over the number of repelling groups beyond those necessary to maintain solubility.

It is interesting that it apparently is not possible to correlate our adsorptive capacities with changes in the number of COOH groups. These vary greatly even at the precipitation point, at which the ratio of COO^-/VA is nearly equal for all three copolymers. One should have expected that in the presence of higher COOH/VA ratios the need for charges to keep the polymer in solution might be reduced, but this is not the case, nor does the lower molecular weight of copolymer D lower the charge requirement. The charge, thus, turns out to be the determining factor, equally much for the solubility limit, as the charge difference beyond it determines the amounts adsorbed. At the same time, the closeness of the linear functionality with $1/\Delta COO^-$ indicates that simultaneous surface and solvent charges must play a very minor part.

MONOLAYER PERMEABILITY AND THE PROPERTIES OF NATURAL MEMBRANES[1]

BY MARTIN BLANK

Department of Physiology, College of Physicians and Surgeons, Columbia University, New York 32, New York

Received March 2, 1962

The results of experiments on monolayer permeability to gases are summarized and the differences between bulk and monolayer processes are discussed in terms of such properties as partition at interfaces and density fluctuations at equilibrium. The rate of monolayer permeation is described in terms of an energy barrier theory where the energy depends on monolayer factors such as the structure (of the polar and lipid parts), the thickness, the compressibility, the surface pressure, as well as on the size of the permeant. The permeation rate of natural membranes is formulated as a monolayer process, since there is strong evidence that lipid monolayers are structural elements of the membrane. The results of this formulation duplicate the main advantages of the older treatment (due to Danielli) but, in addition, it is possible to demonstrate the existence of functional pores, to account for the effects of various chemical agents on membranes, and to offer an explanation for the variability of membrane properties within the same basic model. The conclusions indicate that the current ideas on the structure of natural membranes can account for many of their properties.

I. Introduction

Recent studies on monolayer permeability to gases make it possible to advance some general ideas about the process of monolayer permeation to small uncharged species. At the same time, current investigations on the structure of natural membranes indicate that an understanding of the monolayer state and of monolayer processes may provide the key to understanding the structure and functions of natural membranes. Therefore, it should be possible to link the ideas on monolayer permeation to the present ideas about natural membranes.

The ultra-thin membrane on the surface of cells that is essential for the integrity and many of the properties of the cell is called the plasma membrane. The plasma membrane is believed to be an oriented close packed lipid *bilayer* with polar groups outward. Protein or other non-lipid monolayers are adsorbed tangentially along the polar groups on each side, giving a total membrane thickness of about 75 Å. This model was first suggested in detail by Davson and Danielli[2] in 1934 and belief in it has been considerably strengthened during the last few years. Robertson[3] has reviewed much of the relevant new literature and the various lines of evidence converge on the highly ordered bimolecular leaflet model as the general structure of plasma membranes.

The recent studies on the permeability of layers to gases use monolayers that are about 25 Å. thick and that are composed of molecules with long straight hydrocarbon chains and small polar hydrophilic groups. These are simple molecules which pack efficiently in a monolayer. It is well to keep in mind that the plasma membrane contains bulkier lipids like cholesterol and lecithin as well as

(1) This investigation was supported by a Grant (GM-K3-8158-C1) from the Public Health Service in conjunction with a Research Career Development Award.

(2) H. Davson and J. F. Danielli, "The Permeability of Natural Membranes," Second Edition, Cambridge University Press, Cambridge, 1952.

(3) J. D. Robertson, *Progr. Biophys. and Biophys. Chem.*, **10**, 343 (1960).

protein. Therefore, it must have a different structure and a different permeability. However, one is comparing two systems that are primarily oriented lipid layers and whose thicknesses are of the same magnitude. This reason as well as others to be discussed lead one to believe that the permeation process is similar in the two cases.

The purpose of this paper will be to formulate the process of monolayer permeation. Then, by assuming that the permeability properties of the plasma membrane are due primarily to the bimolecular lipid layer, an attempt will be made to explain many of the observed properties of natural membranes.

II. Permeability Measurements with Monolayers.—Recently, the author reported that close packed monolayers of long chain fatty acids, alcohols, etc., affect the transport of gases (carbon dioxide, nitrous oxide, and oxygen) across a gas–aqueous interface.[4] The gas transport rates with and without a monolayer were measured using a temperature compensated differential manometer, and it was possible to calculate an approximate permeability of the monolayer to the gas. The technique, the validity of the model, and the calculations have been discussed elsewhere[4a] in some detail. Monolayer permeability measurements also have been made by Hawke and Alexander[5] using a technique similar to that used in the study of water transport through monolayers, and the results are in reasonable agreement. The work on water transport, which was aimed at retarding evaporation from reservoirs, has been summarized recently in a research symposium[6] and in a U. S. Government publication.[7]

The results of experiments using several techniques and a number of different monolayers and gases indicate that the permeation process in monolayers differs in essence from the analogous process in bulk phases. This is quite reasonable since the monolayer state is very different from a bulk phase. It is useful to delineate the differences between the macroscopic and the submicroscopic processes in detail, since this suggests a way of formulating the monolayer process. The relevant differences are as follows:

(*1*) *In monolayer permeation the magnitudes of the permeability and of the activation energy are comparable to analogous values for solids.*—The magnitude of the permeability of monolayers to gases lies between the permeability of an oil and that of a wax of the same composition. For an octadecanol monolayer[4a] the value is somewhat closer to that of a wax. This shows that the process probably resembles more closely the permeation of solids as might be expected from the close packed quasi-solid nature of compressed monolayers. This expectation is borne out by the fact that the activation energies for monolayer permeation are on the order of 10 kcal./mole, comparable to the case of the permeation of solids by gases. Liquids, on the other hand, show a very low temperature dependence, on the order of about 3% per degree.

An explanation for the greater permeability of a monolayer than for a solid was offered in terms of the expansion of the monolayer on a water surface. Another important reason for the difference will be given later on in terms of fluctuations in monolayer density.

(*2*) *Unlike the case of bulk permeability (solid or liquid), there are no interfacial partition effects in monolayer permeation.*—The formula used to calculate monolayer permeability, P_f, is

$$P_f = U_f/Apx \qquad (1)$$

where U_f is the gas absorption rate in the presence of a monolayer, A the area, p the pressure, and $x = 1 - U_f/U$ (U being the rate with no monolayer). This was derived by assuming that there is no interaction between the gas and the monolayer and that the monolayer acts as a porous inert barrier (Fig. 1A). If we assume that the monolayer acts as a distinct phase, then one must take into account the various partition coefficients (α's) on the passage of gas between phases. If one works out the effect of partition equilibrium at each interface (Fig. 1B), then the new equation in P_f reads

$$P_f' = U_f/\alpha_{12}Apx \qquad (2)$$

where α_{12} is the gas–monolayer partition coefficient. If this analysis is valid, then P_f' should be the proper way to express monolayer permeability.

Partition coefficients were measured using cetane (hexadecane) as the oil phase since this is similar to the hydrocarbon part of the monolayer. The gas at a given pressure was equilibrated with cetane in a thermostat at 25°. The cetane was then analyzed (using the Van Slyke manometric method) for its gas content which, when converted to N.T.P. conditions, enabled the calculation of α. (Corrections were made for dissolved gas during analysis.) The values of α gas–cetane at 25° are given in Table I (column 2). The third column converts these values into solubilities in order to have a basis for comparing the results of the three gases with those on water vapor. If these values are

TABLE I

PHYSICAL PROPERTIES OF GASES IN PERMEATION EXPERIMENTS

1	2	3	4	5	6
Gas	α(gas/cetane 25°), cm.³ (N.T.P.)/cm.³	Solubility 25°, moles/cm.³ cetane	$10^3 P_f$ (octadecanol), cm./sec.	$10^3 P'_f$, cm./sec.	$\sqrt{\text{Mol. wt.}}$
CO_2	1.04	0.046	4.4	4.2	6.6
O_2	0.19	.0085	3.2	17	5.7
N_2O	1.61	.072	1.0	6.2	6.6
H_2O	..	$<10^{-6}$	300[a]	$>10^7$	4.2

[a] Based on data in ref. 8.

(4) (a) M. Blank and F. J. W. Roughton, *Trans. Faraday Soc.*, **56**, 1832 (1960); (b) M. Blank in "Retardation of Evaporation by Monolayers," V. K. La Mer, ed., Academic Press, New York, N. Y., 1962, pp. 75–95.

(5) J. G. Hawke and A. E. Alexander, ref. 6, pp. 67–75.

(6) American Chemical Society Symposium "Transport Processes Through Monolayers," Sept., 1960, published as "Retardation of Evaporation by Monolayers," V. K. LaMer, ed., Academic Press, New York, N. Y., 1962.

(7) G. B. Magin and L. E. Randall, "Review of Literature on Evaporation Suppression," Geological Survey Professional Paper 272-C, U. S. Govt. Printing Office, Washington, D. C., 1960.

(8) H. L. Rosano and V. K. La Mer, *J. Phys. Chem.*, **60**, 348 (1956).

used for α_{12} the values of P_f (column 4) for the three gases diverge and the new values of P_f' are not in the order of the square root of molecular weights of the gases (last column). This is the expected dependence if the gas dissolves in the monolayer. Furthermore, the measurements of monolayer permeability to water do not fit this pattern at all, since water is virtually insoluble in cetane. One must, therefore, conclude that the monolayer does not act as a phase and does not interact chemically with the penetrating gas. The concept of solubility in a monolayer or partition at a monolayer interface apparently is not meaningful, as would be expected from our knowledge of monolayer structure and dimensions.

(3) *Fick's law is not obeyed in monolayer permeation.*—Since the monolayer does not act as a phase and since the permeating gases are of the same magnitude as the monolayer molecules, the concept of diffusion cannot be valid in the classical sense. Experimentally, the apparent diffusion coefficient varies with the thickness of the monolayer so Fick's law is not obeyed. This has been demonstrated by using monolayers of different chain lengths. Even if one takes into account that more than half of the resistance of a monolayer resides in the polar group and subphase,[9] the addition of a CH_2 group to the monolayer causes the apparent diffusion coefficient to change.

(4) *In monolayer permeation one observes effects that indicate interference between a permeating gas and an inert gaseous component of the system.*—The magnitudes of the permeabilities and of the activation energies for monolayer permeation are considerably lower for gases than for water vapor. Both of these effects are believed to be due to the water that must be present in the monolayer when the subphase is in equilibrium with the gas phase.[10] The water acts as an added resistance by blocking some of the "holes" that normally would be used by the gases that permeate the monolayer, and the amount of water present varies with the temperature. Experiments with subphases in which the vapor pressure was increased by dissolving methanol (as well as some results using ethanol in spreading solutions) also indicate that the vapor acts as a resistance to the passage of another gas.

(5) *The differences between the permeabilities of a monolayer to gases are best explained by the effect of molecular size of the permeating species.*—The most reliable permeability data available are for the cases of monolayer permeability to water vapor and to carbon dioxide. The different values can be explained by considering the work necessary to expand the monolayer to accommodate the different sizes of permeating molecules. The agreement is quite good[10] considering that the molecular size is not known exactly. The less reliable data for nitrous oxide are also in agreement and the data for oxygen, while not in agreement, may be off because of the more frequent collisions with the water vapor molecules that are interfering in these experiments. The actual dependence on molecular size is not linear but exponential.

(9) R. J. Archer and V. K. LaMer, *J. Phys. Chem.*, **59**, 200 (1955).
(10) M. Blank, *ibid.*, **65**, 34 (1961).

A. Physical model. Monolayer is inert porous membrane.

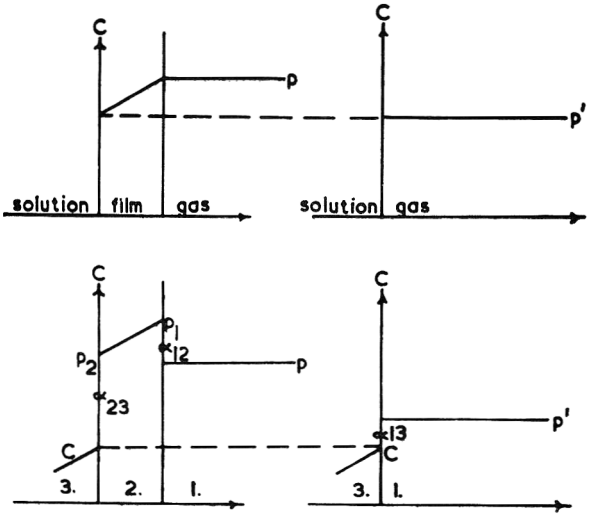

B. Physical chemical model. Monolayer is a distinct phase.

Fig. 1.—Concentration profiles for monolayer permeation.

III. Interpretation of Monolayer Measurements. A. Fluctuations in the Monolayer Density.—The equilibrium surface properties that are commonly measured for monolayers, the pressure, potential, etc., are the average properties of large aggregates of molecules. The aggregates are sufficiently large for the macroscopic averages to have physical meaning. In the case of monolayer permeability, one is dealing with a kinetic property resulting from molecular collisions at many infinitesimal portions of a monolayer. The properties of an infinitesimal portion of a system may be considerably different from the average properties, and for non-equilibrium properties, these are significant.

To get an idea of the variation in monolayer properties, one can follow the general line of reasoning given by Tolman[11] and treat a portion of the monolayer as an open system in equilibrium with the rest of the monolayer which serves as a reservoir. If $\bar{n}$ is the mean number of molecules in the area under consideration, then the actual number, n, at any given time is given by equation 3

$$\frac{\overline{(n-\bar{n})^2}}{(\bar{n})^2} = \frac{RT}{\bar{n}N(\delta\mu/\delta N)} \qquad (3)$$

where R = gas constant, T = absolute temperature, N = number of moles in the area of the system, and μ = chemical potential. It follows from the above that the average fluctuations will depend on the magnitude of N and that the fluctuations will be symmetrical with regard to the equilibrium value, $\bar{n}$. It is possible to evaluate the right-hand side of eq. 3 for the case of a monolayer and

$$\frac{\overline{(n-\bar{n})^2}}{(\bar{n})^2} = \frac{-kT}{A^2\,(\partial\Pi/\partial A)_{T,n}} \qquad (4)$$

where k = Boltzmann constant, A = monolayer area under consideration, and Π = the surface pressure. Since the surface compressibility

(11) R. C. Tolman, "The Principles of Statistical Mechanics," Oxford, 1938, pp. 636–647.

$$C_s = -\frac{1}{A}\left(\frac{\partial A}{\partial \Pi}\right)_T$$

and $\Pi \cong$ const. (n), we can rewrite eq. 4 as

$$\frac{\overline{(\Pi - \bar{\Pi})^2}}{(\bar{\Pi})^2} \cong + \frac{kT}{A} C_s \qquad (5)$$

where Π is now the instantaneous surface pressure and $\bar{\Pi}$ is the mean value. Solving for Π

$$\Pi \cong \bar{\Pi}\left(1 \pm \sqrt{\frac{kT}{A} C_s}\right) \qquad (6)$$

The actual Π in a given area of monolayer depends on the magnitude of the area and on the monolayer compressibility. Monolayers with high values of C_s experience greater fluctuations in surface density than those having lower values of C_s. Fluctuations causing a high Π are not important since they make the monolayer less permeable, but a lower Π is equivalent to the formation of holes in a monolayer. It therefore appears that the compressibility, which is related to fluctuations in monolayer density, is an important property in determining monolayer permeability. This was noted by Rosano and La Mer[8] as the physical property which best correlated with monolayer permeability. The slope of the surface isotherm (related to C_s) is related to another kinetic property, surface flow.[12] It also is related to diffusion rates within a monolayer, since this property arises from the existence of fluctuations in monolayer density.

The fluctuations in monolayer density explain why a monolayer is more permeable than a solid even though the state of aggregation of the molecules is like that of a solid. The permeability is governed not by the average arrangement of molecules but rather by the instantaneous arrangement as determined by the fluctuations. This is important in a monolayer process but not in a macroscopic process where the effects of the fluctuations are lost on passing through many layers.

It should be noted that A in eq. 4, 5, and 6 has not been fixed in this discussion. However, for any monolayer permeation process it would have a value that depends on the frequency and the area of influence of collisions.

B. The Energy Barrier Theory.—The rate of permeation of a monolayer by a gas can be formulated by setting the flux per unit area and time equal to a driving force times a conductance (in this case, the permeability). One can equate the driving force with the number of collisions of the gas per unit area, and unit time. The permeability, however, is not as in macroscopic processes and is best described in terms of an extra energy barrier at the surface. The monolayer prevents the molecules at the lower end of the kinetic energy distribution from passing through, and therefore acts as an energy sieve. This approach parallels the general method of treating diffusion in solids and liquids on the molecular level where the actual events during diffusion are not known but one can conceive of higher energy states through which the permeant must pass.

The original formulation of the monolayer permeation process in terms of an energy barrier is due to Langmuir.[13] A Boltzmann expression (eq. 7) gives the fraction, f, of molecules which have an energy in excess of E, the energy needed to permeate a monolayer.

$$f = \exp(-E/kT) \qquad (7)$$

where k = Boltzmann constant and T = absolute temperature; E is evaluated by assuming that a permeating molecule has to do work against the surface pressure of the monolayer. The work is equal to Πa_0, where a_0 is the cross-sectional area of the permeating molecule. Therefore

$$f = \exp(-\Pi a_0/kT) \qquad (8)$$

Since the rate of permeation should vary directly as the fraction of molecules having the required energy for penetration, f is proportional to the permeability.

As mentioned above, the predicted dependence of the permeability on the molecule size has been demonstrated for the available data. However, the predicted variation of the permeability with Π, although observed in some cases,[8,9,14,15] does not hold generally. Therefore, eq. 8 is not complete. To describe the energy barrier more fully requires a monolayer chain length term which is a function of the surface pressure.[14] This, in addition to the variation of Π with C_s, points up the complexity of the surface pressure as a variable in permeation, and accounts for the inability to find a simple functional dependence of the permeability on Π.

The observed dependence of the energy barrier on the length (number of CH_2 groups) has allowed the extrapolation of the results back to zero CH_2 groups and the determination of the effect of the polar group. In the case of fatty acids,[9] the polar group and associated subphase molecules contribute about 2/3 of the total energy barrier. This means that to characterize completely the permeation process one should include an energy barrier term that is due to the work of permeating the polar group region. The magnitude of this term implies the formation of an ice-like structure in the subphase, but one does not know the number or the orientation of the water molecules involved. Nevertheless, one can say that the energy barrier depends on the surface pressure, at least insofar as it determines the density of polar groups available for bonding with the water.

There are other factors that enter into the energy barrier, the most obvious of which is the shape of the monolayer molecules. For example, cholesterol monolayers at high surface pressures (which are quite incompressible) have no effect on the passage of gases, while saturated straight chain compounds, having approximately the same Π and C_s, have great effects. The difference here appears to be due to the effect of the structure of the polar and hydrocarbon parts of the molecule on the ability to pack in an interface. This factor, which is intrinsic to the

(12) M. Blank and V. K. La Mer, *J. Phys. Chem.*, **61**, 1611 (1957).

(13) I. Langmuir and D. Langmuir, *ibid.*, **31**, 1719 (1927).

(14) M. Blank and V. K. La Mer, ref. 6, pp. 59–66.

(15) G. T. Barnes and V. K. La Mer, ref. 6, pp. 9–33.

monolayer, must also vary with the surface pressure, especially if the molecule can deform or reorient upon compression.

It is possible to summarize our knowledge of the energy barrier by combining the various factors that have been discussed. They are: $K(\mathrm{II})$ the monolayer structure, $l(\mathrm{II})$ the chain length, $E_p(\mathrm{II})$ the polar group contribution to E, $\mathrm{II}(C_s)$, and a_0. The total energy barrier

$$E = E_{CH_2}(K, l, \mathrm{II}, a_0) + E_p(K, \mathrm{II}, a_0) \quad (9)$$

where E_{CH_2} is the contribution of the hydrocarbon chain. Although E has been divided into a number of factors, the surface pressure, chain length, and structure are all related. Therefore, it would be more meaningful to lump $K(\mathrm{II})$, $l(\mathrm{II})$, E_p (II), and $\mathrm{II}(C_s)$ together as a monolayer factor, M, that is distinct from a_0 which depends on the gas that is permeating. Equation 9 then can be abbreviated $E(M, a_0)$. Although the energy term in eq. 8 is much simpler than eq. 9, it contains both monolayer and permeant factors and therefore is a reasonable first approximation to the general dependence of the energy barrier on the variables of the system.

C. Monolayer *vs.* Bulk Processes.—One of the questions in connection with the formulation of monolayer processes is the necessity of eventual overlap with bulk processes. There may be an intermediate range which cannot be treated from either point of view but it seems more likely that there is a gradual change from a monolayer process to a bulk process.

Consider what happens to the permeation rate (or the energy barrier) as one increases the length of the hydrocarbon part of the molecule. The most obvious effect is that E_p of eq. 9 gradually becomes negligible and E_{CH_2}, which varies with the length, plays a much more important role in the total E. It has been shown[10] that $l(\mathrm{II})$ tends to level off as one increases II so there probably is an upper limit even if a quantity analogous to II in bulk phases should increase with the length. Furthermore, if one calculates an apparent diffusion coefficient from the data, this quantity decreases with the length of the chain (in the direction of values for bulk phases). The magnitude of the decrement itself decreases with length, implying a limit. Presumably, this limit would equal the observed diffusion coefficient for bulk phases.

Another aspect of the transition in properties is elucidated from a consideration of the energy barrier. The fact that the addition of a CH_2 group to the chain increases the energy barrier implies that the process of permeation is all-or-none, *i.e.*, a permeant must be able to surmount the entire barrier as one jump or else not get through.[15] In the case of the monolayers studied the greatest number of permeants cross the barrier in one jump but as the barrier is increased fewer molecules will be able to do this. The number of jumps will increase and eventually the energy barrier will no longer increase with the thickness of the layer. This implies agreement with Fick's law. It also implies the necessity for considering solubilities in the kinetics since there would now have to be a certain concentration of permeant in the "extended monolayer" phase.

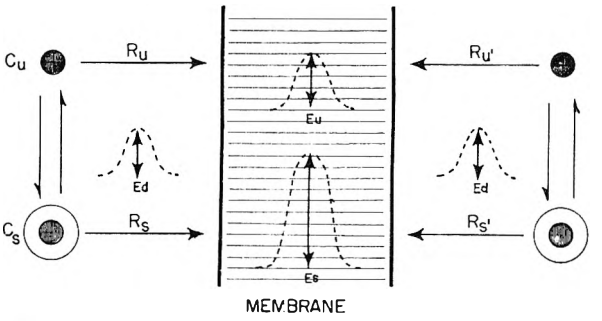

Fig. 2.—Diagram of permeation process (symbols defined in text).

The various factors contained in eq. 9 therefore can be qualitatively extrapolated to the case of bulk phase permeability. The $K(\mathrm{II})$ which causes variations in monolayer properties would probably now be the major determinant of variations in the permeability of bulk phases. It would be related to the size of the holes between adjacent molecules and therefore to the energy necessary to increase the size of the hole to accommodate a permeating molecule.

IV. Applications to Membrane Processes. A. The Permeation Process.—The process of passive membrane permeation to small uncharged molecules can be formulated on the basis of the following assumptions.

(1) The membrane functions as a monolayer and therefore is a homogeneous structure having uniform thickness and no pores.

(2) The permeating molecule exists in solution in different states of hydration. There is an equilibrium concentration of unhydrated molecules given by an expression like eq. 7 where E is the energy of dehydration.

(3) The permeating molecule does not dissolve in the membrane but sees only a structureless energy barrier.

(4) The rate of permeation is determined by the fraction of molecules which has sufficient energy to overcome the energy barrier due to the membrane.

(5) Figure 2 gives a diagram of the process and indicates the directions and energy barriers. The symbols used are: R = permeation rate per unit area, time, gradient; C = concentration; E = energy barrier. The subscripts refer to the unhydrated form (u), the hydrated form (s), and the process of dehydration (d). The primed and unprimed symbols refer to opposite sides of the membrane.

This formulation differs from the Danielli theory[2] in a number of significant respects: (1) In the potential energy diagram the membrane is viewed as a single barrier rather than a series of small barriers. The barriers at the membrane edges are considered to reside in the solution and not in the membrane.

(2) There is no chemical interaction between the membrane and the permeant either on entering or leaving. This eliminates the difficulty of explaining why non-reacting species enter and why reacting species leave.

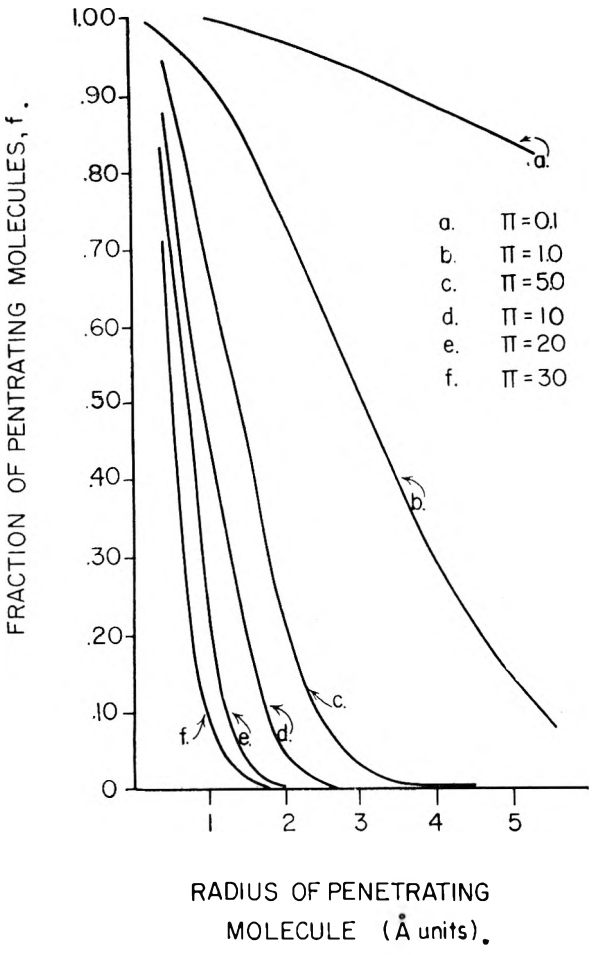

Fig. 3.—Fraction of permeating molecules *vs.* radius of permeating molecule.

(3) There are no pores or fine structure of any kind in the membrane.

(4) The energy barrier depends on a number of the physical properties of the membrane and permeant.

Let us now consider the permeation process. The permeation rate, R, is a product of a concentration difference term, an energy term, and a proportionality constant, K_1 or K_2. The molecule can permeate as a hydrated or as a free species, so

$$\vec{R}_u = R_u - R_u' = K_1(C_u - C_u') \exp(-E_u/kT) \quad (10)$$

and

$$\vec{R}_s = R_s - R_s' = K_2(C_s - C_s') \exp(-E_s/kT) \quad (11)$$

(Obviously the problem is greatly oversimplified since there are bound to be many degrees of hydration in solution.) The total rate is a combination of eq. 10 and 11. If the penetrant is primarily in the C_s form but E_s is high and R_s is very small, a molecule may require less energy to shed its hydration layer and cross the membrane as a free species. The concentration of unhydrated molecules is given by

$$C_u = C_s \exp(-E_d/kT) \quad (12)$$

and the rate of movement of the hydrated molecules *via* dehydration across the membrane is

$$\vec{R}_s = (C_s - C_s')K_2 \exp\left\{\frac{-(E_d + E_u)}{kT}\right\} \quad (13)$$

Equation 12 can be rearranged so that it has the form of an equilibrium constant or a partition coefficient. Therefore, eq. 13 describes a rate that is proportional to a partition coefficient.

Studies on the permeability of natural membranes to a variety of substances have led to a correlation of the permeability with the oil–water partition coefficients. Davies[16] has shown that in the diffusion of ions between water and nitrobenzene, the water to oil rate depends on the partition coefficient while the reverse rate does not. Since the ions are hydrated in the aqueous phase but not in the oil phase, the partition coefficient measures the process of dehydration on going into oil. In the experiments with monolayers, where molecules go from gas to liquid, partition coefficients do not appear, since the diffusing species is not hydrated in the gas phase. Where the molecules pass through the monolayer from the liquid to the gas one expects permeabilities that correlate with partition coefficients and this has been found qualitatively.[10] The explanation for this can be twofold. The hydrated molecule is larger, so it must do more work to permeate, and the rate is slower. Or there is an extra step, dehydration, which decreases the rate. Both explanations are in terms of effects that are measured by partition coefficients even though there is no solubility in the monolayer.

Although there were a number of differences in the assumptions, the results of this formulation of the rate do not differ from those of Danielli in the general form of the equations, in the dependence of the rate on the temperature, and under certain conditions, in the dependence of the rate on a factor that is like a partition coefficient. The major advantages of the Danielli formulation therefore are conserved. The way in which this formulation differs is that the energy barrier can now be considered in terms of its components and this results in the derivation of a number of membrane properties on the basis of the monolayer model.

B. A Model for a Porous Membrane.—Pores are believed to exist in plasma membranes since there are two general factors that govern permeability. For lipid soluble substances the oil–water partition coefficient is important while for non-lipid soluble substances the molecular size is important. This presumes two permeation pathways, one through the membrane which is basically lipid, and another through an aqueous channel. The operational water filled channels in membranes possess "effective pore radii" of about 3.5 Å. for red blood cell[17] and nerve membranes,[18] respectively. The nature of these "pores" is not known but it is believed that they are not distinct structures.

(16) J. T. Davies, *J. Phys. Chem.*, **54**, 185 (1950).
(17) A. K. Solomon, *J. Gen. Physiol.*, **43**, 1 (1960).
(18) L. J. Mullins, *ibid.*, **43**, 105 (1960).

There are several properties of monolayers that support the monolayer membrane analogy. The first point in common with membranes is that there can be two modes of monolayer penetration. One, which is dependent on molecular size, is exhibited by simple gases and has been discussed in detail here. The other mode is exhibited by larger molecules and involves an actual penetration and incorporation into the monolayer. However, the strongest support for the monolayer model is that functional pores will exist in a membrane if we assume that E_s and E_u of Fig. 2 have the same dependence as in the case of monolayers. Let us assume that eq. 8, which is a first approximation to the monolayer energy barrier, is valid in the case of membranes. We can then calculate the value of f as a function of a_0 and II.

Since a_0 can be set equal to $3.14r^2$, f can be expressed as a function of r, the molecular radius. The value of f as a function of r is plotted for various values of II in Fig. 3 (for a temperature of 37°). Since the permeability of the monolayer to the molecules is directly proportional to f, Fig. 3 gives the variation of permeability of a membrane with molecular radius of the permeant.

These curves are similar to curves describing the porous behavior of membranes and a curve at $5 <$ II < 10 dynes/cm. would give f approximately equal to zero at a pore radius of about 3.5 Å. However, the calculations have ignored the more complicated dependence of E on II as given by eq. 9, so it is not possible to make any inferences about the surface pressure corresponding to a pore radius of 3.5 Å. Actually f never equals zero because of the exponential factor, so there is not an absolute cut-off in permeability above a certain radius. This raises the possibility that membranes occasionally can let through larger molecules than pore size would predict.

The assumption that membrane properties can be approximated by monolayer properties has led to a model of a homogeneous membrane having functional pores. This eliminates the need for a complicated "mosaic" membrane (having lipid and pore regions).

C. Interaction of Chemicals with Membranes and Monolayers.—Keeping in mind the limitations imposed by the complex dependence of E on II, let us see the major effects of variations in II assuming eq. 8. Figure 3 shows that it is possible to obtain relatively large changes in permeability by small changes in surface pressure. An increase in II decreases f and *vice versa*. Although this result would be expected intuitively, Fig. 3 offers a framework for considering recent experiments on monolayers as membrane models. For example, Skou[19] has found a correlation between the ability to block nerve conduction and the ability to raise the surface pressure of monolayers of nerve lipid extracts. Shanes[20] has found that certain compounds that increase membrane permeability also dissolve lipid monolayers and reduce the surface pressure. The parallelism of the effects of both activators and

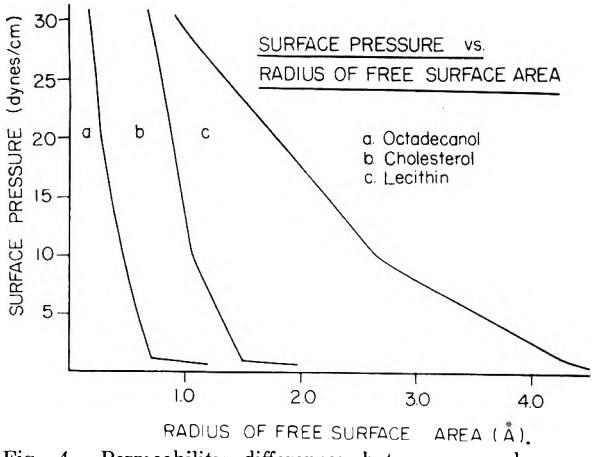

Fig. 4.—Permeability differences between monolayers—surface pressure *vs.* radius of free surface area.

inhibitors on excitable membranes and their effects on monolayer surface pressure give strong support to the proposed monolayer membrane analogy. Further support comes from the extensive investigations of Schulman and co-workers[21] on similar problems and the observed correlation between membrane and monolayer properties.

D. Special Effects in Membrane Permeability.—Narcosis due to chemically inert substances such as nitrogen and the rare gases occurs in living systems. Although the exact cause is not known, it is believed to be due to some change in membrane permeability. Experiments on monolayers have shown that an inert substance such as water can affect monolayer permeability to carbon dioxide and to other gases.[10] The water molecules that pass through the monolayer collide non-selectively with other molecules that are attempting to pass through. The net result is a decrease in the flux of molecules in both directions. This kind of process may be involved in natural membranes when nitrogen or rare gases are present in high concentrations. The inert molecules may interfere with the carbon dioxide and oxygen and prevent them from crossing the membranes at their normal rates. The effect is non-specific but the result is a build-up of carbon dioxide and waste products coupled with a deficiency of oxygen and essential chemicals in the cells.

The monolayer model therefore is capable of explaining this special case of membrane permeability without having to postulate specialized structures or properties. (It should be added that this effect may also be the basis for the action of a wide range of gaseous anesthetic agents.)

E. A Molecular Basis for Variability in Membrane Permeability.—The surface isotherms for two constituents of plasma membranes, cholesterol and a lecithin, show that the cholesterol monolayer is much less compressible. Octadecanol, which was used in the monolayer permeation experiments, is about as compressible as cholesterol but is much less permeable. This is true because octadecanol and cholesterol differ considerably in the free area that is available in the monolayers. To show this we can assume that the area is 'fully" covered at

(19) J. C. Skou, *Biochim. Biophys. Acta*, **30**, 625 (1958).

(20) A. M. Shanes and N. L. Gershfeld, *J. Gen. Physiol.*, **44**, 345 (1960).

(21) J. H. Schulman, *et al.*, *Progr. Biophys. and Biophys. Chem.*, **5**, 41 (1955).

II = 40 dyncs/cm., lower II so that the monolayer expands, and calculate a radius of the free surface area. Figure 4 gives a plot of these data for the three substances. The free areas are in order lecithin > cholesterol > octadecanol and the differences are quite pronounced. This points up the difference in the intrinsic permeabilities of monolayers (the K of eq. 9) of these three compounds when compared at the same II.

The variation in the permeabilities of various membranes of the same basic structure and at the same surface pressure can be ascribed to slight variations in the constituents, *i.e.*, the relative amounts of cholesterol and lecithin. There is an increasing amount of evidence in favor of this idea. In the case of red blood cells, for example, van Deenan[22] has offered an explanation for the variations in red blood cell permeability between species on the basis of the lecithin and fatty acid content of the membrane. His more recent results[23] have extended these ideas to a greater variety of membranes. It therefore seems possible to achieve an almost infinite variety of membrane permeability properties by the variation of the lipid constituents in the monolayer model.

(22) J. de Gier and L. L. M. van Deenan, *Biochim. Biophys. Acta*, **49**, 286 (1961).

(23) J. H. Veerkamp, I. Mulder, and L. L. M. van Deenan, *ibid.*, **57**, 299 (1962).

MOLECULAR WEIGHT, LIMITING AREA, AND FLEXIBILITY OF UNIMOLECULAR LAYERS OF SERUM ALBUMIN AND ITS DERIVATIVES[1]

BY MITSUO MURAMATSU AND HARRY SOBOTKA

Department of Chemistry, Mount Sinai Hospital, New York, N. Y.

Received March 12, 1962

Unimolecular layers of bovine serum albumin and a number of its derivatives have been studied with the use of H. J. Trurnit's spreading technique. The influence of electrolytes upon the limiting area per molecule has been examined. Values for molecular weight and flexibility have been derived from the FA/F curve. The influence of acetylation of epsilon-amino groups and of phenolic hydroxyl groups and the coupling of the protein with diazo compounds modify the physical properties of the unimolecular layers; these changes are ascribed to changes in the steric and electrostatic pattern of the molecule.

The determination of the physical properties of unimolecular layers of proteins had been limited by the empirical character of spreading methods, which left experimentors in a state of uncertainty about the completeness of spreading; with some techniques an unknown part of the applied protein dissolved in the hypophase, with others some of the material remained unspread and required a prolonged induction period for unfolding to constant area. The spreading technique, recently devised by Trurnit,[2] is based on calculable, predictable conditions and on well considered dimensions of the equipment. In the following we report on one of the first examples for the application of this technique.

We had studied the alteration of the properties of bovine serum albumin upon its modification by coupling with diazo compounds[3a-c] and had, in the course of this work, been led to compare azo proteins with other chemically modified proteins. Thus, we had a number of BSA-derivatives of known composition available.

Protein monolayers have been used in the study of the mechanisms of biochemical processes of enzymatic[4] and immunochemical[5] significance, also in the fields of muscle physiology,[6,7] carcinogenesis,[8] and hemolysis.[9] The interpretation of the observations in these subjects has much to gain from advances in the structural knowledge of proteins. As a first step an attempt must be made to correlate the structure of native protein in dissolved and crystalline state. Investigations of the composition and of the primary structure, *i.e.*, the sequence of the amino acids in the protein molecule, have been carried out in the dissolved state; the results have been confirmed and supplemented by X-ray crystallography, which has added valuable information on the three-dimensional configuration and constellation.

The spreading of proteins deprives them of the possibility of expanding in the third dimension; thus, it simplifies the topological situation by excluding certain linkages occurring in native proteins; it reduces structural and configurational questions to such concepts as flexibility and distance between adjacent peptide chains, characteristics which depend on electrostatic and van der Waals forces and which express themselves in the area per molecule. These properties may be influenced by

(1) The experimental work was carried out with the support of Grant RG-4736 of U.S. Public Health Service.

(2) H. J. Trurnit, *J. Colloid Sci.*, **15**, 1 (1960); H. Sobotka and H. J. Trurnit, "Unimolecular Layers in Protein Analysis," in "Laboratory Manual of Analytical Methods of Protein Chemistry," Eds., P. Alexander and R. J. Block, Vol. 3, Pergamon Press, London, 1961, pp. 212, 218.

(3) (a) H. Sobotka and A. V. Luisada-Opper, *Ninth International Colloquium on Protides of the Biological Fluids*, Bruges, 1961, in press; (b) M. Tabachnick and H. Sobotka, *J. Biol. Chem.*, **234**, 1726 (1959), **235**, 1051 (1960); (c) A. V. Luisada-Opper, H. Sobotka, and J. D. Chanley, *ibid.*, **236**, 2250 (1961).

(4) H. J. Trurnit, *Arch. Biochem. Biophys.*, **47**, 251 (1953); D. F. Cheesman and H. Schuller, *J. Colloid Sci.*, **9**, 113 (1954); L. G. Augenstine, *et al.*, *J. Phys. Chem.*, **61**, 1380, 1385 (1957); **62**, 1231 (1958).

(5) S. J. Singer, *J. Biol. Chem.*, **182**, 189 (1950); S. McGavin and K. Iball, *Trans. Faraday Soc.*, **49**, 984 (1953).

(6) A. Lajtha and E. K. Rideal, *Arch. Biochem. Biophys.*, **33**, 252 (1951).

(7) D. F. Cheesman, *J. Physiol.*, **116**, 34P (1952).

(8) D. F. Cheesman, *Biochem. J.*, **56**, xlii (1954).

(9) J. H. Schulman and E. K. Rideal, *Proc. Roy. Soc.* (London), **B122**, 46 (1937); B. A. Pethica and J. H. Schulman, *Biochem. J.*, **53**, 177 (1953).

the presence in the hypophase of electrolytes and other polar substances.

Methods and Materials

Surface Balances.—The surface pressure and surface area in the gaseous region of the films was measured by a float-type torsion balance; we used a Kel-F (polytrifluoroethylene) float of 0.05 mm. (2 mils) thickness and a torsion wire of phosphobronze of 0.1 mm. (4 mils) diameter. The accuracy of this balance was ±0.01 dyne/cm. For the determination of pressure and area in the condensed region, a Wilhelmy type of balance was used which permitted the estimation of pressures up to 40 dynes/cm. with an accuracy of 0.1 dyne/cm. In both balances the readings were magnified by a lamp and scale system. The calibration of the pressure and the evaluation of the film area were carried out by conventional methods.

Protein Preparations.—Crystalline bovine serum albumin (BSA) was obtained from Armour Pharmaceutical Company. For reasons, given in our publications on azoprotein,[3] we blocked the epsilon-amino groups of the lysyl residues by acetylation. This leads to acetyl bovine serum albumin, (N,O)AcBSA, with acetyl groups bound to 96% of the 59 lysyl residues and to 89% of the phenol groups of the 19 tyrosyl residues. By partial hydrolysis at pH 11.5, N-acetyl bovine serum albumin, NAcBSA, was prepared in which only the lysyl residues were acetylated. This compound was coupled with diazotized *p*-aminobenzoic acid under conditions described elsewhere,[3] yielding azo-acetyl BSA, AzAcBSA. The sample used contained 8 monoazotyrosyl and 4 monoazohistidyl residues per molecule.

Spreading.—The water for the hypophase and for the protein solutions was distilled three times over alkaline permanganate in ground glass apparatus. The protein solutions, with or without additives, were dropped from a micropipet onto the hemispherical top of a glass rod, placed in the tray. The rod was 5 mm. in diameter and its top was 100 mm. above the surface of the hypophase. The dropping speed was adjusted so that, according to Trurnit's calculation, less than 0.5% of the protein escaped spreading.

The above method, using native proteins, leads to monolayers which immediately assume a constant area; thus, the incidence of atmospheric contamination and fluctuations of temperature can be avoided, as one does not have to wait up to 24 hr. until the films are stabilized. Regardless of this advantage, the apparatus for the measurement in the gaseous region was placed in a chamber where the temperature was kept constant within ±0.01°, and where dust was excluded.

Results

Measurements in the Condensed Region.—Figure 1 illustrates the experimental results for monolayers of BSA and (N,O)AcBSA, spread from aqueous solution upon a hypophase of water. Numerous experiments were carried out to detect the effects of the time which elapsed between spreading and measurement, and of additives, such as potassium chloride and isoamyl alcohol. In the case of these proteins no change with time nor with the presence of electrolytes was observed in the force/area measurements.

The case of N-acetylated BSA is illustrated in Fig. 2. When this protein is spread from aqueous solution, it exhibits an induction period phenomenon: the film expands in the course of 2 and 4 hr. to reach areas which are up to one-third larger than at time $t = 0$. This induction period remains unaffected by frequent compression and decompression of the film. The effect is eliminated and the larger and constant values for area may be immediately obtained, when the protein has been dissolved in 0.5 N potassium chloride solution. It is immaterial whether the potassium chloride originally is contained in the protein solution or in the hypophase.

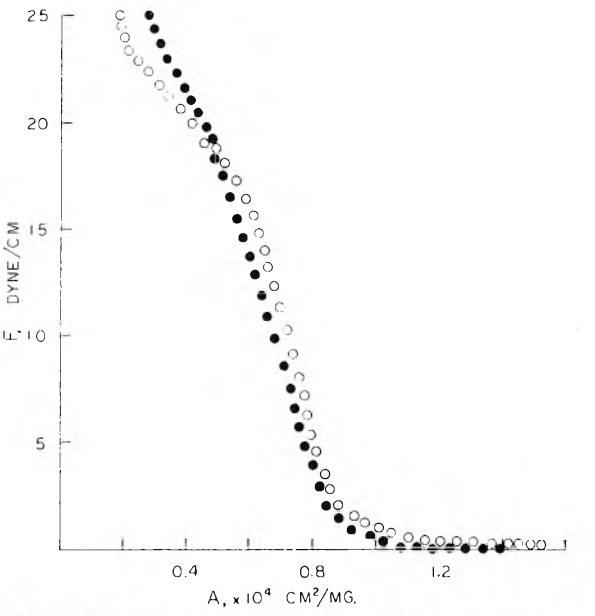

Fig. 1.—F/A curves for BSA, ○, and (N,O)AcBSA, ●, spread from aqueous solution; $t = 0$ hr.

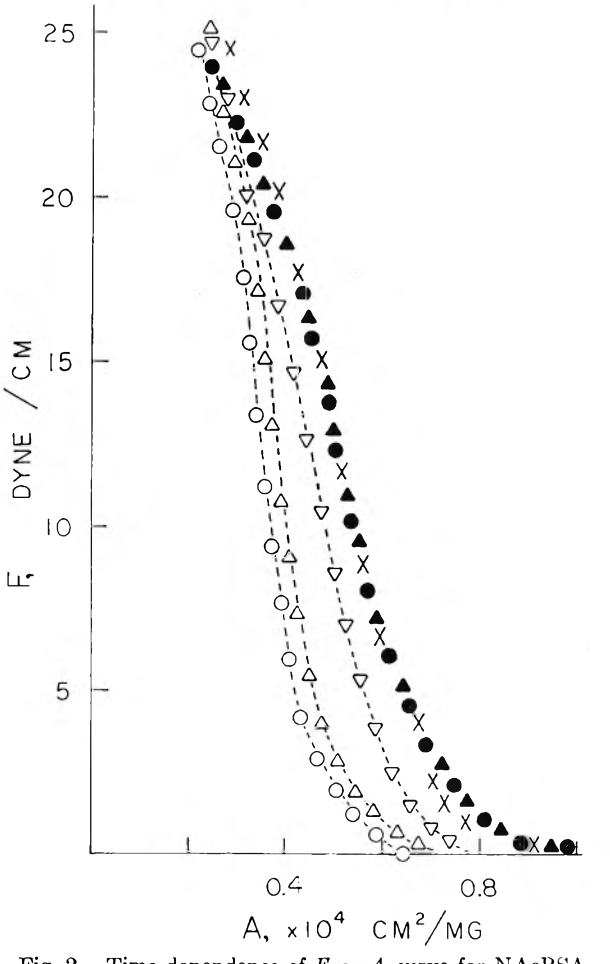

Fig. 2.—Time dependence of $F \sim A$ curve for NAcBSA. Spreading medium water: $t = 0$ hr. ○, $t = 2$ hr. △, $t = 4$ hr. ▽. Spreading medium 0.5 N KCl: $t = 0$ hr. ●, $t = 2$ hr. ▲, $t = 22$ hr. ×.

Induction is even more pronounced in the case of monolayers of AzAcBSA, as shown in Fig. 3.

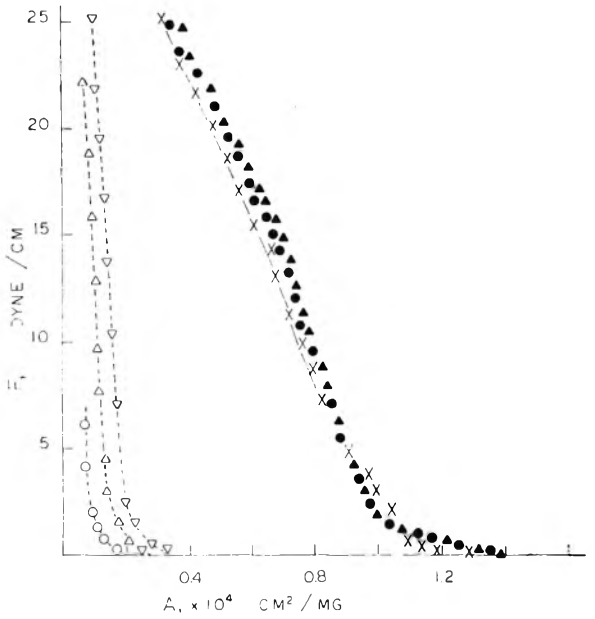

Fig. 3.—Time dependence of $F \sim A$ curve for AzAcBSA. Spreading medium water: $t = 0$ hr. ○, $t = 2$ hr. △, $t = 5$ hr. ▽. Spreading medium 0.5 N KCl: $t = 0$ hr. ●, $t = 2$ hr. ▲, $t = 20$ hr. ▼.

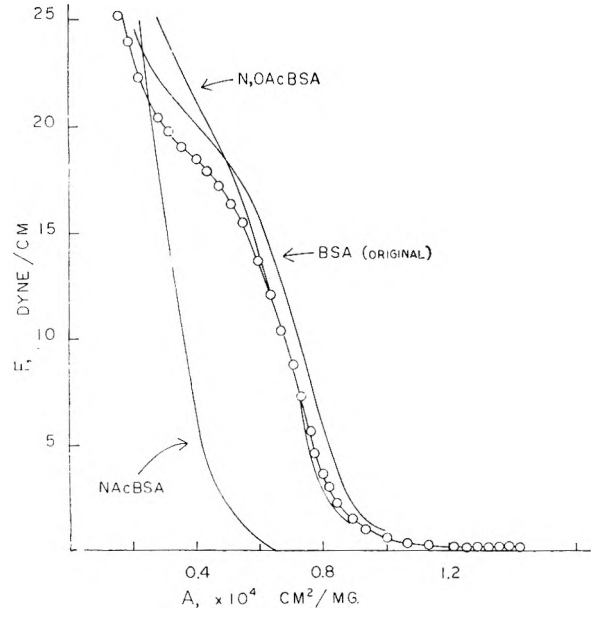

Fig. 4.—$F \sim A$ curve of monolayer of "treated" BSA spread from water; $t = 0$ hr.

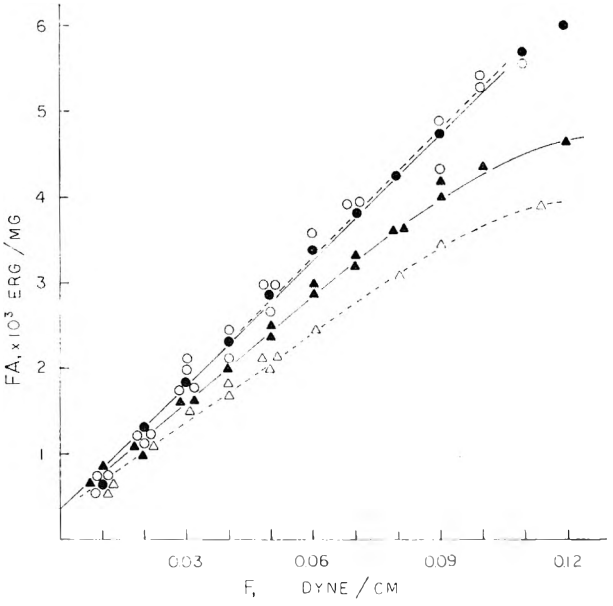

Fig. 5.—"----" FA *vs.* F plot for gaseous monolayers of BSA, ○, and NAcBSA, △, spread from water, and "———" from BSA, ●, and from NAcBSA, ▲, from KCl solution (0.5 N).

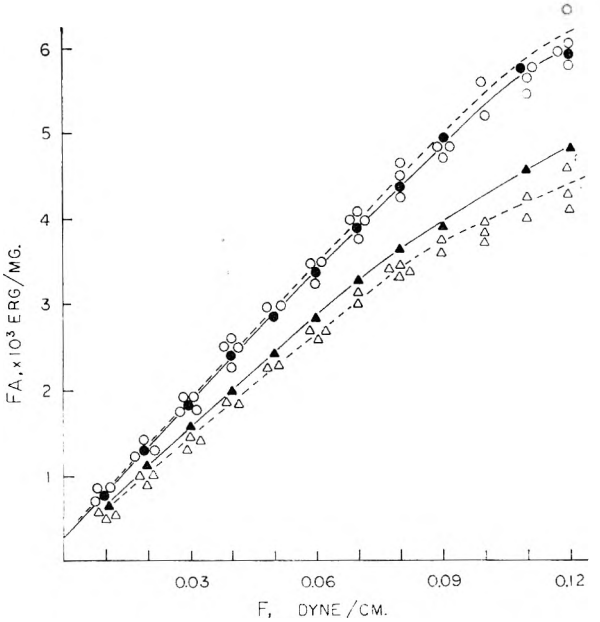

Fig. 6.—FA *vs.* F plot for gaseous monolayers of (N,O)-AcBSA (circles) and AcAzBSA (triangles), spread from water (outlined symbols) and KCl solution (0.5 N) (solid symbols).

Spreading from aqueous solution results in a very tightly condensed monolayer, which slowly expands with elapsing time. Addition of potassium chloride or sodium chloride leads to films with much larger area. In the presence of electrolytes the film area is independent of the elapsed time. Again, the electrolyte may be present originally in the spreading solution or in the hypophase or in both.

In a separate experiment we examined whether the synthetic procedures involved in acetylation and in the subsequent hydrolysis of the O-acetyl linkages were responsible for these changes. Bovine serum albumin was subject to the same conditions as during acetylation, but in the absence of acetic anhydride, and subsequently to alkali treatment at pH 11.5. As shown in Fig. 4, the behavior of BSA monolayers was not affected by this treatment. The difference in the behavior between acetylated and native BSA must be ascribed to the actual presence of the acetyl groups.

Measurement in the Gaseous Region.—In the gaseous region the measurements were carried out with the float-type balance from 0.01 to 0.5 or 0.8 dyne/cm. on freshly prepared monolayers. From the data obtained, one can estimate the molecular

TABLE I

LIMITING AREA, MOLECULAR WEIGHT, AND FLEXIBILITY OF MODIFIED BOVINE SERUM ALBUMIN AND DERIVATIVES

	Spreading medium	Limiting area: m.²/mg.	Limiting area: Å.²/molecule	Film molecular weight	% flexibility
BSA	Water	0.89 ± 0.00	9,600 ± 700	65,000 ± 5,000	1.7
BSA	KCl (0.5 *N*)	0.89 ± 0.01	10,100 ± 1,000	68,000 ± 6,000	1.7
NAcBSA	KCl (0.5 *N*)	0.69 ± 0.00	8,500 ± 500	74,000 ± 4,000	1.9
N,OAcBSA	Water	0.85 ± 0.02	10,400 ± 800	74,000 ± 4,000	2.0
N,OAcBSA	KCl (0.5 *N*)	0.85 ± 0.02	10,400 ± 800	74,000 ± 4,000	1.9
AzAcBSA	KCl (0.5 *N*)	1.05 ± 0.05	12,900 ± 1,800	74,000 ± 7,000	1.3

weight of spreadable large molecules such as proteins according to Bull.[10]

The graph of FA as ordinate *vs.* F as abscissa follows a straight line with a slight break around $F = 0.1$ to 0.15 dyne/cm., depending on film material and spreading method. The two linear parts, divided by this break, have been termed by Bull the A and B phases for the lower and higher pressure regions, respectively. Based on analogy with the three-dimensional gas laws, Bull demonstrated that the intercept of the phase A portion of the curve with the ordinate axis is inversely proportional to the molecular weight and permits its calculation. In practice the intercept of the curve on the y-axis is obtained by the least square method, rather than by geometrical extrapolations; at the same time, the standard deviation is calculated.

Figures 5 and 6 contain the FA/F plots for the protein studied; Table I gives the values calculated for the molecular weights. As in the condensed region, very little difference was noticed in the case of BSA and (N,O)AcBSA between monolayers spread from aqueous solution and from KCl solution. With NAcBSA and AzAcBSA such differences were caused by the nature of the spreading medium as in the condensed region.

Discussion

In experiments with protein monolayers, the most serious and troublesome problem is how to define the equilibrium state, in which protein molecules are considered to be completely unfolded. In the present paper, we take as a criterion for complete unfolding of polypeptide chains the fact that the value F/A is independent of time. Aiming at a spreading method, leading to quick equilibration, we must consider two processes in the formation of monolayers: one is the process of carrying all molecules from bulk to surface, and the other is the unfolding of the individual molecules. The former process precedes the latter, which takes place as a spontaneous reaction at the air–water interface. Thus, satisfaction of the first condition suffices to attain the "real" equilibrium, but the rate at which equilibrium is reached depends on the rate of unfolding.

In the case of BSA and (N,O)AcBSA, the unfolding is instantaneous; thus the experimental condition necessary to get time-independent monolayers is simply the adoption of Trurnit's method. One needs neither to wait for a long time, nor to add salt to the spreading solution nor the hypophase, factors being considered desirable and sometimes necessary to attain equilibrium of BSA monolayers spread by conventional methods.[6,11] Trurnit's method saves waiting time and diminishes tedious procedures to attain equilibrium for monolayers without intercurrent contamination.

On the other hand, the results for NAcBSA and AzAcBSA show that to attain equilibrium, salt solution must be used in these instances as the spreading medium, in addition to adopting Trurnit's method. The addition of isoamyl alcohol to the spreading solution, with or without salt, exerted little or no influence. Addition of salt to the hypophase proved to be necessary if the protein was spread from salt solution.

The role of surface active substances, such as isoamyl alcohol, added to the spreading solution, consists of increasing the spreading coefficient.[6,12] The facilitation of spreading and unfolding of protein molecules by salt solution was accounted for either by the salting-out effect[13] or by the diminution of intramolecular cohesion, because of reduced electrostatic attraction between ionizable groups.[14] Thus, the smaller limiting area of monolayers of NAcBSA and AzAcBSA, spread from aqueous solution, can be ascribed to the strong intramolecular attraction, which is weakened by the addition of electrolytes. The role of salt in the spreading solution must consist of facilitating the uncoiling of the protein molecule by cancellation of ionic charges which cause intramolecular attraction.

This type of attraction, which may cause entanglement of polypeptide chains, may even occur in gaseous films of NAcBSA and AcAzBSA, if they are spread from aqueous medium without salt, as shown in Fig. 5 and 6. This entanglement comes from the essential nature of these proteins, not from too high a surface concentration of the condensed film. The values of limiting area, listed in the third column of Table I, were obtained by extrapolation of the linear part of the curve to the abscissa. They represent the minimum area at the state of closest packing as monomolecular layer and are expressed in m.²/mg.

Let us pay attention to the behavior of gaseous films as shown in Fig. 5 and 6. The linear relationships appearing in these figures can be expressed as

$$FA = A_0F + K \qquad (1)$$

where A_0 and K denote slant and intercept on the

(10) H. B. Bull, *J. Biol. Chem.*, **185**, 27 (1950).

(11) J. S. Mitchell, *Trans. Faraday Soc.*, **33**, 1129 (1937); E. G. Cockbain and J. H. Schulman, *ibid.*, **35**, 1266 (1939).

(12) H. A. Dieu, *Bull. soc. chim. Belges*, **65**, 847 (1956).

(13) A. J. G. Allan and A. E. Alexander, *Trans. Faraday Soc.*, **50**, 863 (1954).

(14) D. F. Cheesman and J. T. Davies, "Advances in Protein Chemistry," Vol. 9, Academic Press, New York, N. Y., 1954, p. 439.

ordinate, respectively. The fifth column of Table I shows the values for molecular weight, obtained by evaluation[10] of K. The increases of molecular weight by chemical modifications are not large in comparison with the limited sensitivity of our surface balance. It should be noted that the values 65,000 ± 5,000, or 68,000 ± 6,000, for film molecular weight of BSA are in agreement with those obtained by osmotic (mol. wt. 69,000),[15] X-ray (65,000),[16] and sedimentation and diffusion studies (65,360).[17] The calculation of limiting area in Å.²/molecule, which appears in the fourth column of Table I, is based on the film molecular weight listed in the fifth column. These values show that the molecule is not broken up by chemical modifications, although synthetic processes include quite rigorous conditions, including hydrolysis of the CH_3CO–tyrosyl linkages at pH 11.5. The present results prove the non-breakage of the polypeptide backbone throughout the reactions BSA → N,-OAcBSA → NAcBSA → AzAcBSA under these synthetic conditions. This also is supported by the result illustrated in Fig. 4, which shows that the protein backbone is not affected under the conditions of the synthetic procedures.

Two FA/F plots may intercept the ordinate at the same point, but show a different gradient. The identity of the intercepts yields identical molecular weights. The different values for the other parameter, the gradient, can be interpreted as indicators for the flexibility of the molecule. The concept of flexibility of unimolecular films of polymers has been developed by Singer[18] and by Davies.[19] Let A_L be the limiting area per molecule, a_L the limiting area per monomer, in our case the average area per amino acid residue, x the number of amino acid residues in the protein, and z the "coördination number" in a two-dimensional quasi-crystalline lattice set; F, A, T, and R have their conventional significance. Then

$$F = \frac{RT}{a_L}\left\{\frac{x-1}{x}\cdot\frac{z}{2}\ln\left(1-\frac{2}{z}\cdot\frac{a_L}{a}\right) - \ln\left(1-\frac{a_L}{a}\right)\right\} \quad (2)$$

according to Singer.[18] By expanding formula 2, neglecting the higher terms, and assuming $A_L = a_L x$, we tranform to

$$FA = RT + \frac{A_L}{A}\cdot xRT\left\{\frac{1}{2} - \frac{x-1}{x}\cdot\frac{1}{z}\right\} \quad (3)$$

an equation essentially the same as that proposed by Hotta.[20]

The subsequent transformation of eq. 3 leads to

$$FA = A_L x\left\{\frac{1}{2} - \frac{x-1}{x}\cdot\frac{1}{z}\right\}F + RT \quad (4)$$

From eq. 4 and 1 one obtains

$$z = \frac{x-1}{x}\cdot\frac{1}{\frac{1}{2} - \frac{1}{x}\cdot\frac{A_0}{A_L}} \quad (5)$$

This is the simplest expression for the calculation of the "coördination number" z, which in turn gives the % flexibility = $100(z-2)/2$ as defined by Davies.[19] The values for flexibility are given in the last column of Table I.

Chemical modifications evidently affect the limiting area and the flexibility of BSA. For example it is probably the attachment of the acetyl radical to the lysyl residues on N-acetyl BSA (perpendicular to the film surface) which produces closer packing of the film and an increase in its flexibility.

Acetylation seems to be responsible for decrease of the ionization of the epsilon-amino groups[21] and resultant increase of the van der Waals attraction of the lysyl side chain; both factors, the decrease of ionization and the increase of cohesive forces, tend to diminish the hydrophilic character of the lysyl side chain. It has been pointed out[22] that the hydrophilic nature of the lysyl chain is overwhelmed at moderate pressure by the van der Waals forces between the lysyl side chains in films at an air–water interface. The decrease in polarity of the epsilon-amino group, due to its acetylation, also weakens the electrostatic interaction with negative residues in the polypeptide chain, leading to increased flexibility. This explanation agrees with the observation[23] that increasing formylation of the lysyl residues parallels increasing reactivity of the protein with metal ions; the elimination of the positive charges of the epsilon-amino groups liberates anionic residues in this loosening-up process.

A larger limiting area and additional increase in flexibility are observed as the results of acetylation of the hydroxyl groups in the tyrosyl residues, as compared to merely N-acetylated BSA. The increment of limiting area due to O-acetylation, which is in the neighborhood of 1800 A.²/molecule, can hardly be ascribed to the additional space occupied by not more than 17 acetyl groups even if they are assumed to be in entirely horizontal position. The increase in area must be due to the disappearance of the OH-groups and the consequent rupture of hydrogen bonds.[24] N,O-acetylated BSA is evidently more loosely folded than N-acetylated BSA with fewer cross linkages by hydrogen bonds. This also increases its flexibility.

The coupling of a substantial portion of the tyrosyl and histidyl residues with diazotized *p*-aminobenzoic acid results in a substantial increase in limiting area, a decrease in flexibility, and increased difficulty of unfolding the chains. The interaction of these new, relatively unwieldy anionic groups with positive residues is responsible for resistance to uncoiling in spreading. The decrease

(15) G. Scatchard, A. C. Batchelder, and A. Brown, *J. Am. Chem. Soc.*, **68**, 2320 (1946).
(16) B. W. Low, *ibid.*, **74**, 4830 (1952).
(17) J. M. Greeth, *Biochem. J.*, **51**, 10 (1952).
(18) S. J. Singer, *J. Chem. Phys.*, **16**, 872 (1948).
(19) J. T. Davies, *Biochim. Biophys. Acta*, **11**, 165 (1953).
(20) H. Hotta, *J. Colloid Sci.*, **9**, 504 (1954).
(21) I. M. Klotz, *Cold Spring Harbor Symp. Quant. Biol.*, **14**, 97 (1950).
(22) J. T. Davies, *Biochem. J.*, **56**, 509 (1954).
(23) M. Muramatsu and T. Sasaki, *Radioisotopes* (Tokyo), **7**, 42 (1958).
(24) T. Isemura and T. Yamashita, *Bull. Chem. Soc. Japan.*, **32**, 1 (1959).

in flexibility may be due to the same cause; besides, the two aromatic groups of each azo structure may encumber the free movement of the polypeptide chain. It is quite likely that the increase of negative charges by coupling at the tyrosyl residues does not affect the flexibility in the same manner as the decrease of positive charges by modification of the lysyl residues. Flexibility will be affected by nature, amount, and position of the local charges rather than by the total number of charges.

DISCUSSION

F. M. FOWKES (Shell Development Company).—The determination of molecular weights from the intercepts of Fig. 5 and 6 is obviously very difficult because small experimental errors at low pressures strongly influence the result. May I suggest you try the method I proposed very recently [*J. Phys. Chem.*, 66, 385 (1962)] by which molecular weights are obtained from the slope of a straight line plot in which all experimental points influence equally the calculated molecular weight.

M. MURAMATSU.—The estimation of the intercept is of course apt to involve an error, if we extrapolate graphically. However, applying the least squares method to the straight part of the curve provides a good estimate of the curve's inclination and permits a more accurate estimation of the intercept by calculation. As I have not yet read your paper, I have no way to apply your equation to our results.

FILM PENETRATION AND ADSORPTION. THE EFFECT OF VERATRINE AND PROCAINE ON THE DESORPTION KINETICS OF MONOLAYERS OF MONOÖCTADECYL PHOSPHATE

BY NORMAN L. GERSHFELD

National Institute of Arthritis and Metabolic Diseases, National Institutes of Health, Public Health Service, U. S. Department of Health, Education, and Welfare, Bethesda 14, Maryland

Received March 2, 1962

At pH 7.2, monoöctadecyl phosphate is slightly soluble in water, and thus its monolayers slowly desorb. The desorption process involves loss of film material and diffusion through an unstirred layer which is directly beneath the film. Subsequent loss to the bulk of the solution proceeds by convection currents. As the surface pressure is raised, the rate of desorption decreases due to enhanced van der Waals interaction between the hydrocarbon chains of the monolayer. Veratrine (2×10^{-6}–2×10^{-5} M) speeds up the loss of film material from the surface by penetrating the hydrocarbon region of the oriented monolayer. Procaine at low concentrations (10^{-4} M) likewise increases the desorption rate by penetrating the ionic region of the monolayer, but at higher concentrations is adsorbed beneath the monolayer which slows down the desorption process. Parallelism of this behavior with pharmacological activity of these drugs is noted, and possible mechanisms for their action at the cellular level are presented.

Introduction

Previously published papers[1–4] have suggested relationships between pharmacological actions of drugs and their interactions with monolayers. The nature of these interactions, however, could not be completely elucidated: it remained undecided whether the drugs penetrate into the monolayer or are adsorbed underneath them. It is the purpose of this paper to describe a system which appears to give a clearer distinction between film penetration and adsorption, and which departs from the conventional equilibrium systems previously used to study monolayer–drug interactions.

The kinetics of desorption of monoöctadecyl phosphate monolayers on water, first in the absence and then in the presence of drugs in the substrate, was investigated with a view toward completing our understanding of the nature of the monolayer–drug interactions. Two drugs, veratrine and procaine, were chosen to demonstrate these interactions because both affect the ionic permeabilities of cells, although in markedly different ways.[5] By understanding the mechanisms whereby each of these drugs interacts with the monolayer it may also be possible to increase our knowledge of the action of these drugs on cellular processes.

Experimental

A. Materials. Monoöctadecyl phosphate was isolated from a mixture of the di- and monoalkyl phosphate by repeated extractions with ether of the more soluble monoalkyl phosphate; the monophosphate was recrystallized from hot cyclohexane; m.p. 85.5–86°.[6]

Benzene and methanol (A. R. grade) were each percolated through a column of Florisil and silica gel to remove surface active contaminants. Solutions of monoöctadecyl phosphate in a mixture of benzene and methanol (20:1) were used to spread monolayers on the buffered substrates.

Buffered solutions were prepared with $NaH_2PO_4 \cdot H_2O$ (Fisher certified reagent) in distilled water, titrating with NaOH to pH 7.2; total phosphate was $2 \times 10^{-3} M$.

Procaine (Gaine and Ingram, U.S.P.) and veratrine (Penick and Co.) were used without further purification. Procaine was dissolved directly in distilled water; veratrine, which is only slightly soluble in water, was first dissolved in a small volume of 0.1 N HCl, neutralized with 0.1 N NaOH, and then added to the buffered distilled water.

B. Method.—Monoöctadecyl phosphate films were spread from the benzene–methanol solution onto the surface of the aqueous phase buffered to pH 7.2, first in the absence of drugs and then with either drug present in the substrate. A commercial Langmuir-type film balance was used to measure surface pressures. The tray was heavily coated with paraffin and the float assembly was modified with polyethylene end-loops and an aluminum float coated with a thin layer of Teflon. The movable barrier was propelled by a screw-drive shaft manipulated from the outside of the Lucite box which covered the film balance. The areas at which the films were spread were always about 20–50% greater than

(1) E. Kimoto, *Kyushu Mem. Med. Sci.*, **4**, 35 (1953); **4**, 165 (1953).

(2) J. C. Skou, *Acta Pharmacol. Toxicol.*, **10**, 317 (1954); **10**, 325 (1954).

(3) N. L. Gershfeld and A. M. Shanes, *Science*, **129**, 1427 (1959).

(4) A. M. Shanes and N. L. Gershfeld, *J. Gen. Physiol.*, **44**, 345 (1960).

(5) A. M. Shanes, *Ann. N. Y. Acad. Sci.*, **55**, 1 (1952).

(6) This sample was provided by Dr. Robert Fox, whose contribution is gratefully acknowledged. The method of separation was suggested by Dr. H. Fales.

the area producing the desired surface pressure. The kinetics of film dissolution was followed at constant surface pressure by decreasing the film area and observing the changes in area as a function of time. Zero time was considered as the time when the first drops of film-forming solution were spread on the substrate. The film was compressed to the area necessary to produce the desired surface pressure (this compression took about 40 sec.); the first area reading was taken at 1 min. Each set of observations was performed with a fresh substrate to eliminate contamination by previously dissolved film material. Duplicate runs gave good agreement (less than 3% variability). All solutions were kept at 25° for 1 hr. before their addition to the film balance. The temperature in all experiments was 25 ± 0.5°.

Results and Discussion

A. Kinetics of Desorption of Monoöctadecyl Phosphate Monolayers.—Octadecyl phosphate monolayers are slightly soluble in water above pH 6 and consequently unstable.[7] If the films on water are kept at constant surface pressure (F), and the logarithm of the area (A) plotted as a function of time, an initial variable rate is observed which, after 15–20 min., becomes constant (Fig. 1A). Ter Minassian-Saraga[8] discussed the desorption process of similar systems and found that the rate could be interpreted by a two-step process; (a) the desorption of the film molecules from the surface into, and (b) diffusion through, the thin unstirred water layer which exists beneath the film; in the bulk of the substrate mixing occurs by convection currents. According to this model, the initial rate of desorption can be represented by the equation

$$\frac{-\mathrm{d} \ln A}{\mathrm{d}\sqrt{t}} = k_\mathrm{i} \qquad (1)$$

where A is the film area, k_i is a constant and a function of D, the diffusion constant, and K_d, the desorption coefficient.[8] A steady-state arises when a constant concentration gradient of desorbed film molecules exists in the unstirred layer, *i.e.*, when the rate at which the film molecules enter the unstirred layer equals their rate of removal by convection currents to the bulk of the substrate. The rate equation may then be represented by

$$\frac{-\mathrm{d} \ln A}{\mathrm{d}t} = k_\mathrm{s} \qquad (2)$$

where k_s is a constant and a function of D, K_d, and ϵ, the thickness of the unstirred layer. From the ratio of the slopes

$$\frac{k_\mathrm{s}}{k_\mathrm{i}} = \frac{\sqrt{\pi D}}{2\epsilon} \qquad (3)$$

the diffusion coefficient of the film material may be estimated. Figure 1 (A and B) demonstrates the validity of eq. 1 and 2 for films of monoöctadecyl phosphate. Values of k_s may be obtained from the slopes of the linear portions of the rate curves for times greater than 15–20 min. Plots of the initial portion of the rate curves as a function of $\sqrt{t}$ (Fig. 1B) give constant slopes from which k_i may be calculated.

(7) H. C. Parreira and B. A. Pethica, "Proc. 2nd Int. Congress of Surface Activity," Academic Press, New York, N. Y., Vol. I, 1957, p. 44.

(8) L. Ter Minassian-Saraga, *J. chim. phys.*, **52**, 181 (1955).

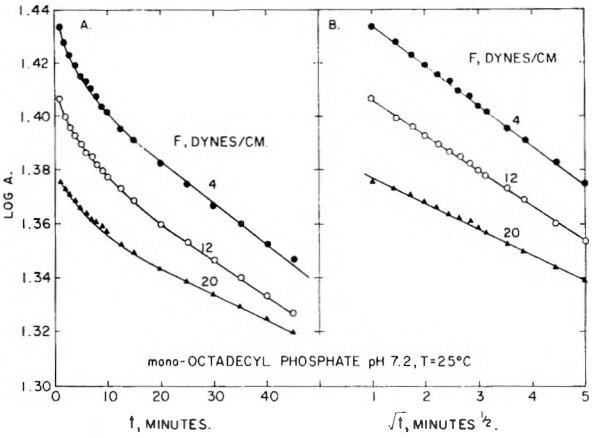

Fig. 1.—Desorption kinetics at constant surface pressure of monoöctadecyl phosphate monolayers on water, pH 7.2: (A) d(log A)/dt plot for the complete curve; (B) d (log A)/d$\sqrt{t}$ plot for the initial variable portion of the rate curve.

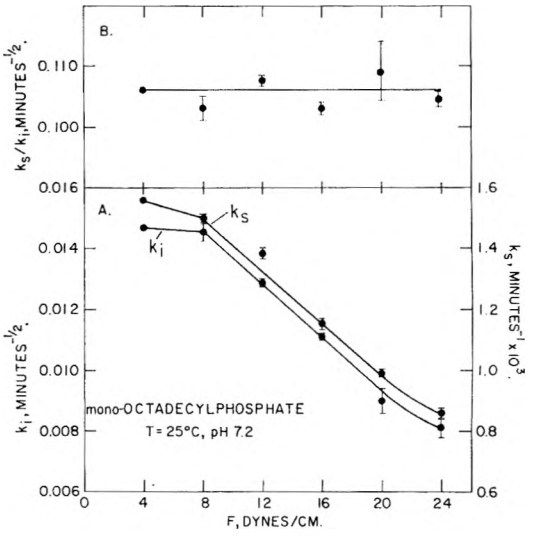

Fig. 2.—Comparison of the initial and steady-state rates of the desorption process of monoöctadecyl phosphate monolayers: A, rate constants k_i and k_s as a function of surface pressure F; B, ratios $k_\mathrm{s}/k_\mathrm{i}$ as a function of F. Length of lines at each point represents limits of values obtained for duplicate runs.

Since k_i reflects the process of loss of film material from the surface, conditions which alter k_i should be indicative of changes in the energy barriers involved in the transfer of molecules from the film to the unstirred layer. That such is the case can be seen in Fig. 2A, where k_i is plotted as a function of the surface pressure. With increasing surface pressure, k_i decreases. Since monolayers of octadecyl phosphate form condensed films[7] at high surface pressures, it is reasonable to attribute the declining rate of desorption to the adlineation of the hydrocarbon chains with a concomitant increase in van der Waals forces. The resulting increase in film stability arises from the mutual interaction between the chains. The values of k_s parallel those of k_i over the range of surface pressures studied; the ratios $k_\mathrm{s}/k_\mathrm{i}$ are essentially independent of the surface pressures (Fig. 2B) as predicted by eq. 3. The value of $k_\mathrm{s}/k_\mathrm{i}$[9] is 0.106 ± 0.002 min.$^{-1/2}$.

B. Procaine and its Effect on the Kinetics of Film Desorption.—Procaine, only slightly surface active at pH 7.2, contains a tertiary aliphatic amino group, $pK_a = 9.05$,[10] which is almost completely ionized at pH 7.2, and an aromatic amino group, $pK_a = 2.2$,[10] which is essentially uncharged at this pH. Because of the presence of these two hydrophilic amino groups at either end of the molecule, procaine is likely to be adsorbed in a horizontal orientation in the air–water interface.[11,12]

When procaine is present in the substrate, the rate curves for monooctadecyl phosphate desorption retain the same time relations that exist in the absence of drug, *i.e.*, an initial variable rate, followed by a linear steady state rate (Fig. 3). As the concentration of procaine in the substrate is decreased, the rate of film desorption is increased (Fig. 3A). Furthermore, in the presence of 10^{-3} *M* procaine, an increase in the surface pressure increases the rate at which the desorption takes place (Fig. 3B), contrary to the behavior of the phosphate films alone. The fact that an interaction between the film and procaine has occurred is shown by a large increase in surface pressures at film areas where neither the monooctadecyl phosphate nor the procaine solution alone appreciably change the surface tension of the substrate. For example, in the absence of drug, no surface pressures were recorded above 40 Å.^{2} for the monolayer and even at a concentration of 5×10^{-3} *M* procaine, the surface tension of water was reduced only about 0.5 dyne/cm.[4] Since there is a large increase in film area with procaine in the substrate some type of film penetration occurs. Whether the penetration is that of the interposition of procaine between the hydrocarbon chains, or only between the phosphate groups, is clarified in Fig. 4. This figure shows plots of the film areas (A) obtained by extrapolating the initial portion of the rate curves to $\sqrt{t} = 0$ (that is, the equilibrium areas the film would occupy in the absence of desorption) as a function of surface pressure (F). Curve 1, Fig. 4 shows the results for the phosphate film in the absence of drug and is typical of the behavior of a condensed film[12]; the limiting area at $F = 0$ is 29 Å.^{2}, in good agreement with previous results.[7] With increasing procaine concentrations, the limiting film areas for the condensed regions of the F–A curves increase from about 30 Å.^{2} for 10^{-4} *M* procaine to 95 and 100 Å.^{2} for 10^{-3} and 5×10^{-3} *M* procaine, respectively. In effect, the limiting area of about 100 Å.^{2} appears to approach the upper limit for the saturation of the phosphate film by procaine; this suggests that the interaction of procaine with the film molecules is governed by stoichiometric considerations. Since the area occupied by a molecule of monooctadecyl phosphate is 29 Å.^{2} (assuming that the alkyl phosphate is essentially in a vertical orientation when $F > 4$ dynes/cm.), the area which remains is occupied by procaine ($100 - 29 = 71$ Å.^{2}) at the saturation limit of the film. This area, 71 Å.^{2}, almost coincides with that occupied by a molecule of procaine oriented horizontally at the air–water interface, *i.e.*, 67 Å.^{2},[4] which leads to the conclusion that at

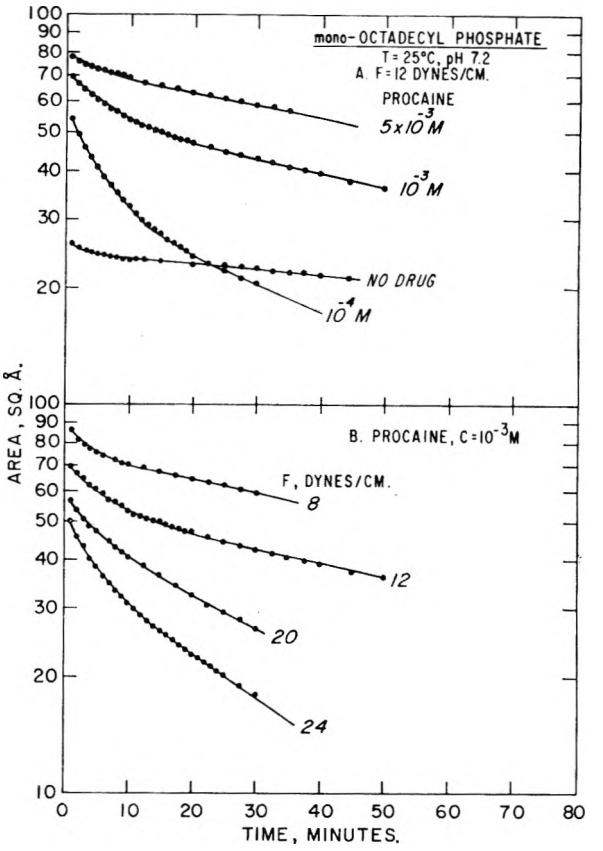

Fig. 3.—The effect of procaine on the desorption kinetics at constant surface pressure of monooctadecyl phosphate monolayers: A, effect of varying procaine concentration, constant surface pressure, $F = 12$ dynes/cm.; B, effect of surface pressure, procaine concentration 10^{-3} *M*. Ordinate is film areas divided by initial number of film molecules.

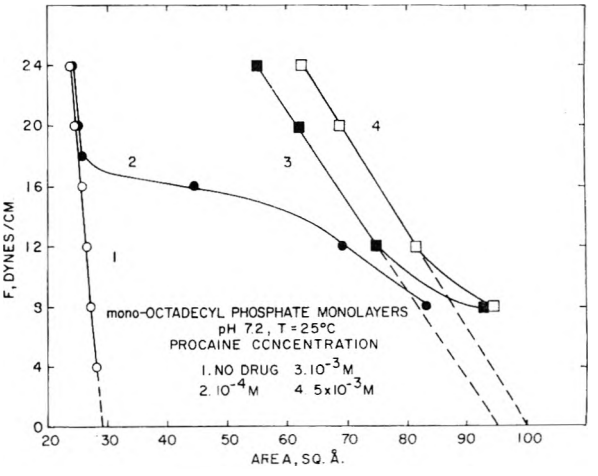

Fig. 4.—The effect of procaine on the F–A curves of monooctadecyl phosphate monolayers in the absence of desorption. Areas obtained by extrapolating d log $A/d\sqrt{t}$ curves to $\sqrt{t} = 0$.

(9) If a thickness of 1 mm. for the unstirred layer is assumed,[8] from eq. 3 $D = 2 \times 10^{-6}$ cm.^{2}/sec.

(10) I. M. Kolthoff, *Biochem. Z.*, **162**, 289 (1925).

(11) This is further confirmed by the fact that F–A curves calculated from γ–C observations of procaine solutions at pH 7.2,[4] indicate that procaine monolayers are gaseous.[12] N. L. Gershfeld, unpublished results.

(12) N. K. Adam, "The Physics and Chemistry of Surfaces," Third Ed., Oxford University Press, London, 1941.

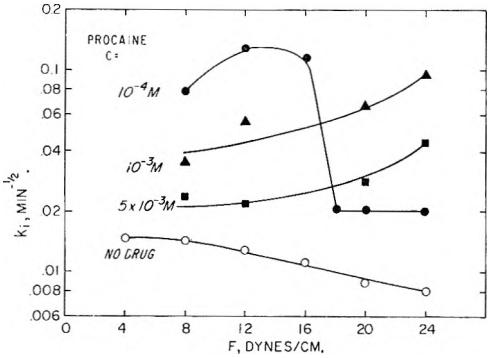

Fig. 5.—The effect of procaine on the rate constant k_i, for the initial step in the desorption of monoöctadecyl phosphate monolayers, as a function of surface pressure, F.

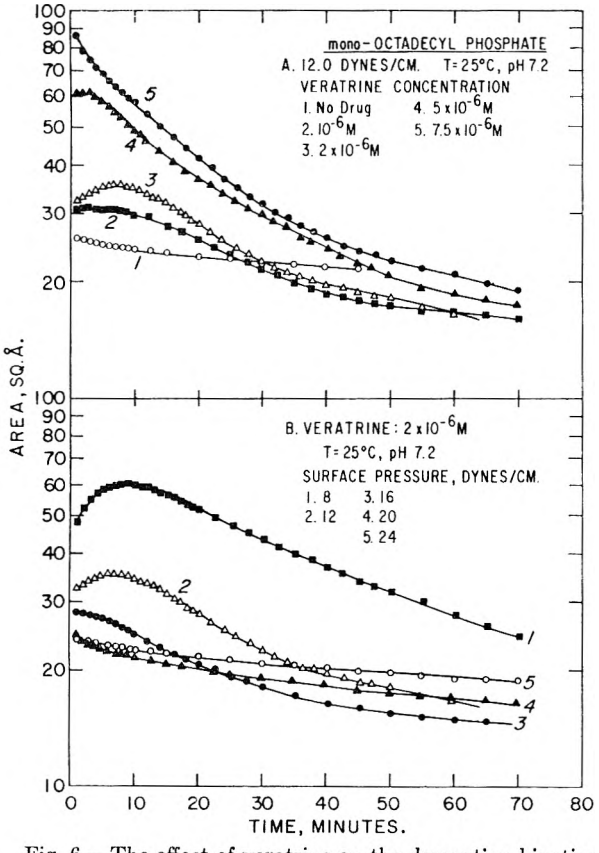

Fig. 6.—The effect of veratrine on the desorption kinetics of monoöctadecyl phosphate monolayers on water, pH 7.2: A, effect of varying veratrine concentration, constant surface pressure, F = 12 dynes/cm.; B, effect of surface pressure, veratrine concentration 2×10^{-6} M. Ordinate is film areas divided by initial number of film molecules.

saturation the alkyl phosphate and procaine form an equimolar mixed film. This strongly suggests that procaine penetrates only into the ionic region of the monolayer. Separation of the phosphate groups in the monolayer prevents the close packing of the hydrocarbon chains in the film and causes a decrease in the energy barrier for film desorption. The resulting structure is a loosely packed monolayer as is also indicated by the flat portion of curve 2, Fig. 4. It has been found that loosely packed films of lauric acid also desorb more rapidly at higher surface pressures than at lower ones.[8]

If film penetration were the only process involved in the procaine–film interaction, then one would expect an increase of the rate of film desorption with increasing drug concentration, rather than the decrease actually observed. To account for these findings it is necessary to propose a secondary, non-specific adsorption by procaine beneath the monolayer. As the concentration of procaine in the substrate increases, the saturation point for procaine in the film is approached and the non-specific process of adsorption at the lower surface of the film becomes more prominent. The latter effect acts to reduce the rate of desorption, perhaps by forming a diffusion barrier beneath the mixed film.[13]

In Fig. 5, the values of k_i for the alkyl phosphate film–procaine system are plotted against the surface pressure; the results summarize the effects of this drug on the desorption process. In addition, we find for a procaine concentration of 10^{-4} M that the initial rate constant at 8 dynes/cm. is increased about fivefold over the value observed for the film in the absence of drug, and the rate of desorption is still higher when the surface pressure is raised to 12 dynes/cm. Above 16 dynes/cm., however, the rate constant decreases sharply to a value much closer to that of the drug-free system. This last effect coincides with the sharp rise in surface pressure observed in curve 2, Fig. 4, at areas below 30 Å.^{2}, which indicates that only a small amount of procaine can penetrate the monolayer. This fact is also shown by the observation in Fig. 5 (see above) that the rate of desorption does not fall to the value expected for the drug-free system even at low drug concentrations (10^{-4} M) and high surface pressures (24 dynes/cm.).

The values of k_s generally parallel the k_i values; the mean ratio for all the observations is 0.116 ± 0.017 min.$^{-1/2}$, indicating that the diffusion coefficient for the alkyl phosphate remains essentially unchanged.

C. The Effect of Veratrine on the Desorption Kinetics.—The alkaloid veratrine is highly surface-active[3,14]; like procaine, it has a tertiary amino group, pK_a = 8.85,[10] which is almost completely ionized at pH 7.2. F–A curves of veratrine monolayers indicate that at surface pressures of about 7 dynes/cm. the major axis of the molecule assumes a vertical orientation at the air–water interface; monolayer collapse occurs at about 10 dynes/cm.[14]

Like procaine, veratrine at very low concentrations (2×10^{-6}–2×10^{-5} M) interacts with the phosphate monolayer and penetrates the film, as indicated by the higher initial areas observed with increasing veratrine concentration (Fig. 6A). At concentrations of drug below 5×10^{-6} M, instead of a continuous decline of the area with time, there appears at first a time-dependent *increase* of the film area, which is especially pronounced at the lower surface pressures (Fig. 6B). This time-dependent increase in area is consistent with the

(13) E. G. Cockbain and J. H. Schulman, *Trans. Faraday Soc.*, **35**, 716 (1939), report that the stability of amine monolayers also is increased when benzoic acid is adsorbed beneath the film as evidenced by an increase in the collapse pressure.

(14) N. L. Gershfeld, *Biochim. Biophys. Acta*, **42**, 282 (1960).

idea that veratrine penetrates into the hydrocarbon portion as well as the ionic region of the monolayer.[15] Film penetration probably also is facilitated by the fact that veratrine can orient itself vertically[14] with its bulky non-ionic moiety in the monolayer. One would expect penetration into the lipid to be diminished as the hydrocarbon chain adlineation increases when the surface pressure increases, and indeed, this actually is observed (Fig. 6B). When the concentration of veratrine is 7.5×10^{-6} M, the maximum in the rate curve disappears (Fig. 6A, curve 5). In this case the rate of penetration is increased, presumably due to the higher concentration gradient of the drug; penetration is essentially completed before the first measurement at one minute is taken.

The penetration into the film obscures the initial portion of the desorption curve; consequently it is necessary to examine the steady-state portion of the curve to see the effect of veratrine on the rate of desorption. Since the values of k_s parallel k_i for both the drug-free system and the procaine system (see Fig. 2 and section B), it is a reasonable assumption that the results found for k_s in the veratrine system will be applicable to the values one would observe of k_i, if the latter were uncomplicated by the penetration effect.

The values of k_s for the phosphate film–veratrine system were obtained from the linear portions of the rate curve, usually 45 min. after the start of the experiment (Fig. 6B). The results are plotted in Fig. 7, which shows that veratrine at a concentration of 2×10^{-6} M raises the rate of alkyl phosphate desorption; as the surface pressure increases, however, the rate constant decreases and approaches the value observed for the drug-free system. If the drug concentration is raised to 2×10^{-5} M, the rate constant for film desorption is increased still further (Fig. 7).

Thus film penetration by veratrine disrupts the lateral cohesive forces which exist between the oriented hydrocarbon chains, thereby increasing the rate of film desorption. As the surface pressure of the film is increased the energy barrier for penetration is elevated, thus reducing the amount of veratrine in the film; consequently the desorption rate of the film is diminished.

It appears that the concentration of veratrine in the film is not limited by stoichiometry as in the case of procaine; the rate of film desorption continues to increase with the concentration of drug. Presumably this phenomenon is related to the much higher surface-activity of veratrine compared to that of procaine.[4,16]

In summary, then, veratrine penetrates into the lipid region of the monolayer "palisade" due (a) to the high surface activity of the drug and (b) to its ability to orient itself vertically in the air–water

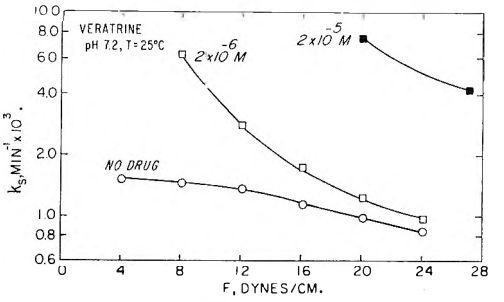

Fig. 7.—The effect of veratrine on the rate constant k_s, for the steady state desorption of monoöctadecyl phosphate monolayers, as a function of surface pressure, F.

interface.[17] Procaine, on the other hand, penetrates only into the ionic region of the monolayer, and as the drug concentration is increased, the ionic sites in the film are saturated. The interaction between the ionic groups in the film and the ionic and polar groups of the drug are the essential factors for determining the properties of this system. For example it has been found that procaine does not penetrate uncharged monolayers of *n*-octadecyl alcohol and methyl stearate.[18] At higher concentrations, procaine is adsorbed beneath the surface film.

The cell membrane, which controls the movement of ions across the cell, has been described as a bimolecular lipid film which is stabilized by a protein network.[19] The use of monoöctadecyl phosphate monolayers is an attempt to simulate the phospholipid components of the membrane, and to demonstrate drug interactions in a simple system which may also have some analogy with the interactions of the drugs with the cell membrane. For example, veratrine[5] and low concentrations of procaine[20,21] both increase the ionic permeability of cell membranes; they also disrupt the alkyl phosphate monolayers by film penetration. Procaine at higher concentrations counteracts stimuli which cause increases in ionic permeability of cell membranes,[21] while in the alkyl phosphate monolayer it counteracts film instability. Thus, these parallels in behavior by the cell membrane and the monolayer with respect to drug action suggest that these drugs, which cause a general increase in ionic permeabilities, exert their effects by penetrating the membrane. In contrast local anesthetics like procaine are active by being adsorbed at the surface of the membrane.[22]

Acknowledgment.—The author wishes to express his appreciation to Dr. W. A. Zisman for permitting him the use of the technical facilities of the Naval Research Laboratories, and for the many helpful suggestions he has made during the course of this project.

(15) J. H. Schulman and E. K. Rideal, *Proc. Roy. Soc.* (London), **B122**, 29 (1937).

(16) The upper limit for the amount of veratrine in the surface film is probably governed by the solubility of the drug in the substrate.

(17) The interaction between the ionic groups of the film and drug is important but not a necessary condition for film penetration, because film penetration by veratrine has also been observed with monolayers of *n*-octadecanol and methyl stearate. (N. L. Gershfeld, unpublished results.)

(18) N. L. Gershfeld, unpublished results.

(19) J. D. Robertson, in "Progress in Biophysics," Vol. 10, J. A. V. Butler and B. Katz (eds.) Pergamon Press Ltd., London, 1960, p. 343.

(20) T. Sollmann, "A Manual of Pharmacology," 8th Edition, W. B. Saunders Co., Philadelphia, Pa., 1957, p. 332.

(21) G. P. Child, *Federation Proc.*, **8**, 281 (1949).

(22) L. Pauling, *Science*, **134**, 15 (1961), has suggested a similar mechanism for the action of physical narcotics which behave like procaine, at the higher concentrations, on nerve cells.

MOLECULAR INTERACTIONS BETWEEN PHOSPHOLIPIDS AND SALTS AT AIR AND LIQUID–LIQUID INTERFACES

BY HENRI L. ROSANO, HASKEL SCHIFF, AND JACK H. SCHULMAN

Stanley-Thompson Laboratories, Henry Krumb School of Mines, Columbia University, New York 27, N. Y.

Received March 12, 1962

The duplex film method has been used in the understanding of the interaction between polyvalent salts and cephalin at the water/oil interface. Contraction, expansion, and surface pressure increases of cephalin monolayers by injection of calcium ions into the subphase and the pH change of cephalin emulsions by addition of neutral salts have been investigated. This interaction appears to be dependent on: (1) the valency of the salts, and (2) the penetration of *n*-hexadecane into the mixed alkyl alcohol/cephalin monolayer.

Introduction

It has been shown[1,2] that the ionic transport across either permeable, impermeable, or diffusion-blocked non-aqueous liquid membranes can be promoted by the addition of suitable phospholipids (cephalin or lecithin at the appropriate pH) in the oil phase. This mechanism was explained as an independent cationic–anionic exchange at the two liquid/liquid interfaces. In order to elucidate the monolayer–salt interaction at the oil/water interface, the duplex film method was applied. The uniqueness of the duplex film method[3] is that it measures directly the force-area per molecule isotherm at the liquid/liquid interface. This permits the direct study of the interaction between the different "oil" molecules and the monlayer. This interaction is the measurement of the penetration of the "oil" molecules into the monolayer even under conditions of negative interfacial tension. This "negative interfacial tension" (γ_i) occurs when the surface pressure of the interfacial film ($\pi_{o/w}$) is greater than the oil/water interfacial tension ($\gamma_{o/w}$); when $\pi_{o/w} > \gamma_{o/w}$

$$\gamma_i = \gamma_{o/w} - \pi_{o/w} \qquad (1)$$

In the case of a duplex film[3]

$$\gamma_i = \gamma_{a/w} - \gamma_{o/a} - \pi_m = \gamma_{o/w} - \pi_{o/w} \qquad (2)$$

where $\gamma_{a/w}$ is the surface tension of the air/water interface, $\gamma_{o/a}$ is the oil/air surface tension, and π_m is the measured spreading pressure of the duplex film. Oil layers from 100 to 350 Å. thick were found convenient; under these conditions *all* the amphipatic molecules are present at the liquid/liquid interface.

The case of an insoluble liquid monolayer of a liquid compound at its collapse pressure (π_c) can be considered as a duplex film one molecule thick. If eq. 2 is applied for different compounds, it is found that π_c is identical to π_m at the collapse pressure. The measured oil/water interfacial tension (γ_i) is equal to $\gamma_{a/w} - \gamma_{o/a} - \pi_c$. All are measurable terms for different compounds and duplex film mixtures. So, it can be concluded that the liquid monolayer at the collapse pressure is equivalent to a duplex film where the "oil phase" corresponds to the hydrocarbon portion of the molecules, with an "independent" oil/air tension, and a water/oil interfacial pressure due to the polar groups of the molecules. This was indicated theoretically long ago by Langmuir. At the collapse pressure, lenses will form if the sum of the interfacial tension and the oil/air surface tension of the liquid compound is equal to or greater than the surface tension of the "oil phase" as described above. By addition of a suitable oil with a lower surface tension than this "oil phase," spreading will proceed. This results in the formation of a duplex film. Experimentally, it has been shown[3] that under these conditions of surface wetting, hydrocarbon molecules will penetrate into the monolayer above its collapse pressure (π_c).

To illustrate the concept of the duplex film method, several examples are given. For the case of an oleic acid monolayer and drop: γ_i = 12 dynes/cm.; $\gamma_{o/w}$ = 42 dynes/cm. (by considering the hydrocarbon portion of the molecule as the oil phase similar to a C_{16} hydrocarbon); $\gamma_{a/w}$ = 72 dynes/cm.; $\gamma_{o/a}$ = 29 dynes/cm. (surface tension of a C_{16} hydrocarbon); $\pi_{o/w}$, interfacial surface pressure; and π_c = 31 dynes/cm. collapse pressure of the oleic acid monolayer (25°).

By substituting π_c for π_m in eq. 2 all the terms balance, 12 = 42 − $\pi_{o/w}$ = 72 − 29 − 31, justifying the assumption that at the collapse pressure the monolayer is a separate two-dimension liquid phase.

For *n*-octyl alcohol: γ_i = 7.7 dynes/cm.; $\gamma_{o/w}$ *n*-octane = 50 dynes/cm.; $\gamma_{a/w}$ = 71.2 dynes/cm.; $\gamma_{o/a}$ = 27.5 dynes/cm.; π_c = 36 dynes/cm. (at 30°). Equation 2 becomes: 7.7 = 50 − $\pi_{o/w}$ = 71.2 − 27.5 − 36, which balances perfectly.

For the case of the cephalin duplex system described in this paper (at 30°: π_c = 42 dynes/cm. (Fig. 2)); $\gamma_i \approx 0$ dyne/cm.; $\gamma_{o/w}$ = 7.0 dynes/cm. (30% pentanol, 70% hexadecane); $\gamma_{a/w}$ = 71.2 dynes/cm.; $\gamma_{o/a}$ = 28.5 dynes/cm. (30% pentanol, 70% hexadecane). By substituting in eq. 2 this balances within experimental error: 0 = 7 − $\pi_{o/w}$ = 71.2 − 28.5 − 42. This case is interesting in that $\pi_{o/w} = \gamma_{o/w}$ = 7 dynes/cm., which is the condition for spontaneous emulsification. The interface holds together owing to the superimposed tension $\gamma_{o/a}$ (28.5 dynes/cm., 30% pentanol, 70% *n*-hexadecane) resulting in an overall positive tension.

Cases for $\pi_{o/w} > \gamma_{o/w}$ have been discussed by

(1) J. H. Schulman and H. L. Rosano, "Retardation of Evaporation by Monolayers," Academic Press Inc., New York, N. Y., 1962; *Third Int. Congr. Surface Activity, Cologne, II*, 112 (1960).

(2) H. L. Rosano, P. Duby, and J. H. Schulman, *J. Phys. Chem.*, **65**, 1704 (1961).

(3) J. H. Schulman and J. B. Montagne, *Ann. N. Y. Acad. Sci.*, **92**, 366 (1961).

Schulman and Montagne.[3] This results in microemulsion formation and is the adopted definition of negative interfacial tension.

The surface tension of a 0.01 *M* cephalin–30% 1-pentanol, 70% *n*-octane solution is 20.3 dynes/cm. (at 30°); the interfacial tension $\gamma_i \simeq 0$ dyne/cm.; so, the sum of these two tensions is smaller than the surface tension of the cephalin hydrocarbon (28.5 dynes/cm.). The direct consequence is surface spreading and the formation of a duplex film. This is in contrast to the case of the oleic acid quoted above. The duplex film method permits quantitative results to be made of the conditions for interaction between calcium and magnesium ions with phospholipid monolayers.

Previous work has never been able to distinguish between the different interfacial structures (monolayer, emulsion, or suspension) of the phospholipid molecules and their reactivities with ions, charged colloids, and biologically active substances. This work possibly explains not only these differences but also: (1) the blockage of the sodium and potassium carrier transport by calcium and biologically active molecules[1,4]; (2) the decrease in pH when a neutral salt is added to phospholipid molecules; and (3) the influence of polar oils and salts on the absorption of water dispersable charged colloids (*e.g.*, dyes) into a non-aqueous medium.

Experimental

Carrier Transport.—Fifty mM./l. of NaCl was opposed to 50 mM./l. of KCl (at 30°) and the oil phase membrane consisted of 1-pentanol with 0.01 *M* cephalin. As previously described,[1] Na^+–K^+ exchange takes place. Increasing amounts of $CaCl_2$ were added to the two aqueous compartments.

Duplex Film Method.—Cephalin (phosphatidyl ethanol amine, Nutritional Biochemicals Corp., Cleveland, Ohio) was dissolved in *n*-hexane (b.p. 65–67°, purified, Fisher Scientific Co.) to which additions of *n*-hexadecane or 30% 1-pentanol and 70% *n*-hexadecane mixture were added. The molecular ratio cephalin, *n*-hexadecane, or the 1-pentanol–*n*-hexadecane mixture was approximately 1 to 35, giving at collapse pressure a duplex film thickness of about 350 Å. The surface pressure (Wilhelmy's method) was measured with a sand blasted platinum plate (5-cm. perimeter) suspended from a Roller Smith torsion balance (500 mg. max.) mounted on an adjustable elevating stand. A fused silica trough immersed in a 30° thermostated water bath was used as a Langmuir trough.

Interfacial Titration.—The study of the effect of various salts on the pH of a cephalin (animal cephalin) 1-pentanol dispersion was made by adding 50 ml. of 0.01 *M* cephalin solution in 1-pentanol to 50 ml. of distilled water and agitating by means of a magnetic stirrer. The solutions (salts or biologically active substances) were added with a buret and the pH was determined by a Beckman pH meter "Zeromatic" model. The pH meter was connected with a Wheelco recorder which permitted expansion of the pH scale.

Results

Duplex Films.—Figure 1 shows that nearly complete inhibition of the ionic exchange taking place between Na^+ and K^+ migrating across 1-pentanol oil layer in the presence of cephalin occurs at 2 mM./l. of $CaCl_2$. It is interesting that this is the concentration of Ca^{+2} in physiological saline. At concentrations of Ca^{+2} of about 1 mM./l. an interfacial "skin," probably of calcium cephalinate, can be observed. The fluctuations in the points

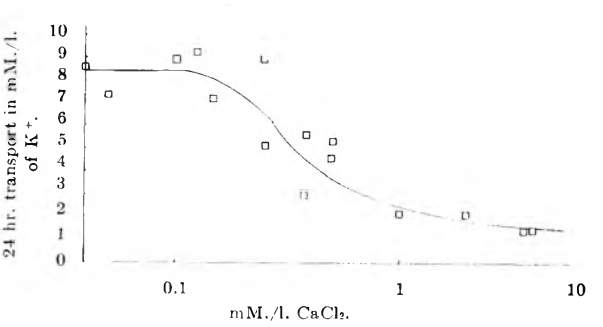

Fig. 1.—Inhibition by addition of calcium of the sodium–potassium carrier transport.

50mM./l. NaCl $CaCl_2$ | Cephalin (0.01 *M*) 1-pentanol | 50 mM./l. KCl $CaCl_2$

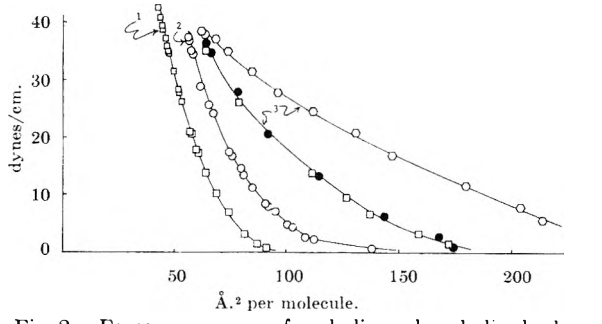

Fig. 2.—Force–area curve of cephalin and cephalin duplex films with and without calcium, magnesium, and sulfate ions in the substrate: (1) cephalin ± *m*-xylene ± Ca^{+2} ± Mg^{+2} ± SO_4^{-2}; (2) cephalin + duplex (30% 1-pentanol, 70% *n*-hexadecane) ± Mg; (3) cephalin + duplex + 20 mM./l. Ca^{+2}.

at lower concentrations probably are due to fracture of the skins by stirring. In order to study the calcium phospholipid interactions at the oil/water interface, the duplex film method was used. The water used was always a 0.002 *M* NaCl solution in bi-distilled water. The presence of NaCl was required for the measurement of surface potentials of the monolayers and the duplex films. These results will be published elsewhere.

Curve 1 of Fig. 2 shows the π–A curve of phosphatidyl ethanolamine dissolved in *n*-hexane with and without the presence of *n*-hexadecane or *m*-xylene as additives. No penetration of the cephalin film occurs (no increase in area) and no duplex is formed. The additives can be seen as minute lenses floating on the monolayer. Addition to the underlying solution of 0.01 *M* $CaCl_2$, $MgCl_2$, or $MgSO_4$ does not affect the monolayer. On the other hand, if 1-pentanol is added to *n*-hexadecane with the cephalin, a duplex film is obtained. No lenses can be seen and curve 2 shows that expansion of the monolayer is realized. Under these conditions film penetration by the hydrocarbon additives occurs. This has been indicated[1] by interfacial tension measurements at the hydrocarbon/water interface with increasing amounts of 1-pentanol giving approximately 0 dyne/cm. at 30% 1-pentanol, 70% petroleum ether/water interface. Addition of 0.01 *M* $MgCl_2$ and 2 mM./l. of $CaCl_2$ under this duplex film shows no effect, but now 20 mM./l. of $CaCl_2$, but not $MgCl_2$, shows a marked expansion (curve 3, Fig. 3). 1-Pentanol being somewhat soluble in the subphase, the expansion depends on the time the duplex film is

(4) H. L. Rosano, J. H. Schulman, and J. B. Weisbuch, *Ann. N. Y. Acad. Sci.*, **92**, 457 (1961).

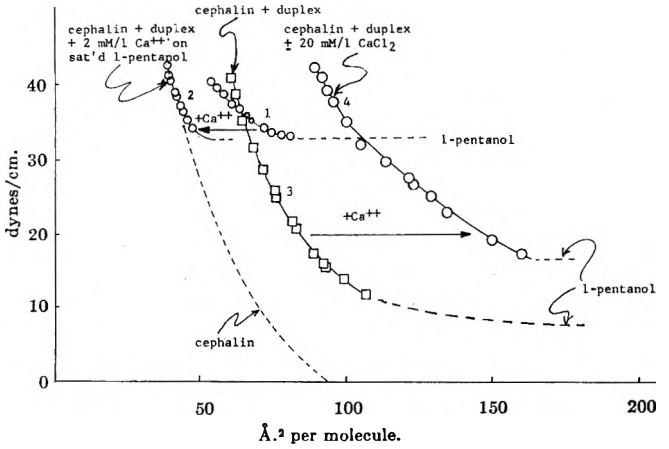

Fig. 3.—Expansion and contraction of cephalin duplex films by addition of calcium in the substrate in the presence of 1-pentanol: duplex = 30% 1-pentanol + 70% *n*-hexadecane; substrate always contains 0.002 *M* NaCl and different concentrations of 1-pentanol; temp. = 30°.

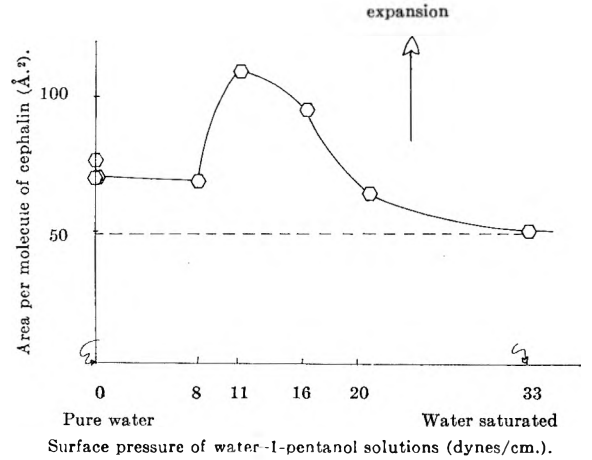

Fig. 4.—Effect of 20 mM./l. of $CaCl_2$ on cephalin + duplex (*n*-hexadecane 70%; 1-pentanol 30%) film at 33 dynes/cm.; 30°.

held on the surface at large areas ($\pi_m = 0$). This expansion does not explain the solid film observed in the carrier experiment (Fig. 1) where 1-pentanol as the oil membrane alone was used. To this effect the substrate was saturated with 1-pentanol. The portion of surface isotherm (curve 1, Fig. 3) above saturation surface pressure of 1-pentanol indicates a marked expansion. The addition of 2 mM./l. of $CaCl_2$, which previously was ineffective, now shows a dramatic contraction of the duplex film. This isotherm superimposes a cephalin surface isotherm at the liquid/air interface indicating that all additives have been expelled from the phospholipid monolayer. By spreading the duplex film on a subphase containing various amounts of 1-pentanol, curves 3 and 4 of Fig. 3, marked expansions were observed. Expansions of cephalin monolayers were also observed by Alexander, Teorell, and Aborg[5] at benzene/water interface only when isopropyl alcohol was added as a solvent for cephalin. The significance of the presence of isopropyl alcohol was not indicated by the authors, but since no expansion takes place with *m*-xylene in our duplex film experiment, it can be concluded that cephalin does not interact with calcium at benzene/water interface alone. A systematic study of expansion and contraction of cephalin duplex film on 20 mM./l. of $CaCl_2$ on substrate containing varying quantities of 1-pentanol was undertaken next.

Figure 4 shows a maximum expansion when the cephalin monolayer is opened out by the additives to an area of 110 Å.² (at 33 dynes/cm.) when the surface pressure of the 1-pentanol solution is 11 dynes/cm. This optimum effect suggests two opposing operating mechanisms. It has been shown above that *n*-hexadecane does not penetrate a cephalin monolayer alone but addition of 1-pentanol enables marked penetration by *n*-hexadecane to take place (Fig. 2 and 3). Calcium injected underneath a cephalin monolayer likewise does not permit the penetration of *n*-hexadecane alone. However, calcium interacts strongly with cephalin in the presence of 1-pentanol giving contraction. The role of 1-pentanol can be understood in two ways: (1) permitting the interaction of calcium with cephalin, and (2) allowing an enhanced penetration of *n*-hexadecane into the calcium cephalinate film, above that which is found for the cephalin 1-pentanol duplex. By injecting calcium chloride under this duplex film with appropriate 1-pentanol–*n*-hexadecane mixture, at constant area, marked surface pressure rises are observed as the *n*-hexadecane penetrates into the calcium cephalin lattice.

By using a 1:1 cephalin–oleyl alcohol + *n*-hexadecane duplex, where *n*-hexadecane molecules penetrate, there is now no measurable effect due to calcium ions. This possibly is due to steric factors holding the cephalin molecules too far apart for the calcium cephalinate to form.

Interfacial Titration.—The pH of a dispersion of cephalin in *n*-hexadecane in water upon addition of salts gave no measurable stable changes. The emulsions of cephalin dissolved in 1-pentanol produce a lowering of the initial pH in the presence of salts. When cephalin in a 70% *n*-hexadecane–30% 1-pentanol mixture is titrated with $CaCl_2$, a similar lowering of pH is observed. This is directly analogous to the interaction between calcium and the duplex film mentioned above. The addition to cephalin–1-pentanol emulsions of monovalent ions such as Na^+, K^+, and substituted monoamines give pH changes which are smaller than the diamine salts or polyvalent ions (Fig. 6). The salts of chelating agents such as copper and uranyl show very strong effects on the cephalin–1-pentanol emulsions.

Previous work on titration of phospholipids by Wadsworth, Maltaner, and Maltaner,[6a] Dervichian,[6b] and Stenhagen[6c] reported that the addition of different salts produces a lowering of the pH. The pH change was attributed to an ionic exchange between the cation and the hydrogen at-

(5) A. E. Alexander, T. Teorell, and G. G. Aborg, *Trans. Faraday Soc.*, **35**, 1200 (1939).

(6) (a) Wadsworth, Maltaner, and Maltaner, *Am. J. Physiol.*, **97**, 74 (1931); (b) D. G. Dervichian, "Proc. 2nd Inter. Conf. (1955)," Butterworths Scientific Publications, 1956, pp. 3–13; (c) E. Stenhagen, *Skand. Arch. Physiol.*, **77**, 77 (1937).

tached to the phosphoric acid group. This process is reversible by addition of HCl. The results appear independent of the carboxyl group in serin cephalin at these acid pH's. Calcium does not interact with fatty acid monolayers at these pH's. The results in Fig. 6 explain the carrier transport inhibition between Na^+ and K^+ across a non-aqueous layer in the presence of cephalin by Ca^{+2}, uranyl^{+2}, and curare^{+2}.

The interesting recent publications of Hirt and Berchtold[7] show that the extraction into a lecithin non-aqueous solution (*e.g.*, CCl_4, $CHCl_3$, alkyl alcohols, and ketones) of a water-soluble anionic dye (*e.g.*, tropalein o) is markedly influenced by the following two factors.

(1) The dielectric constant and interfacial orientatation of the non-aqueous liquid molecules. For example 1-pentanol in the alkyl alcohol series produces an optimum dye absorption in the presence of salts and amines, whereas nitrobenzene, CCl_4, and nonyl alcohol completely inhibit the absorption. This paper suggests that the absence of interaction of calcium ions with lecithin in the presence of these solvents is due to their high surface or interfacial tension, which corresponds to no surface spreading and no lecithin monolayer penetration, and also spacing effects due to the higher alcohols.

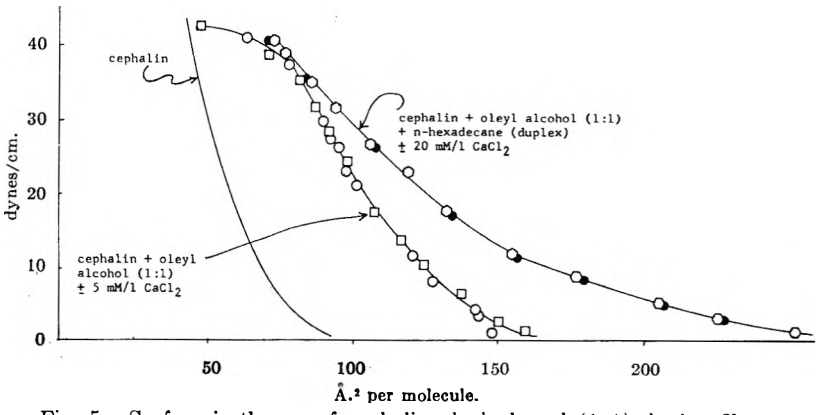

Fig. 5.—Surface isotherms of cephalin oleyl alcoyol (1:1) duplex films.

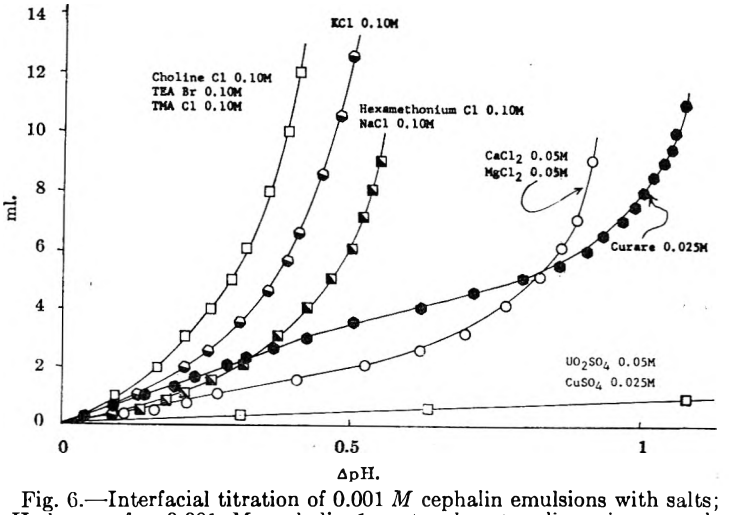

Fig. 6.—Interfacial titration of 0.001 *M* cephalin emulsions with salts; pH change of a 0.001 *M* cephalin–1-pentanol–water dispersion on addition of various salts.

(2) This absorption is markedly dependent on the valency of the cation and on the number of ionized amino groups per reacting molecule. This is directly analogous to the results on Fig. 6 and for the interaction of the salts with the cephalin duplex film.

Discussion

It can be seen from Fig. 2 that *n*-hexadecane, only in the presence of 1-pentanol, can penetrate into the calcium cephalinate film. Calcium cephalinate is more soluble in a 1-pentanol–*n*-hexadecane mixture than in either of the single components, the solubility series being 1-pentanol–*n*-hexadecane > 1-pentanol > *n*-hexadecane. Therefore, the mixed solvent penetrates the cephalin film spread on a calcium substrate. In the case of a duplex film, the calcium cephalinate is held at the interface, as seen from the area per molecule determinations (π–A curves). On Fig. 3, the ratio between the amount of 1-pentanol and *n*-hexadecane was varied by changing the concentration of 1-pentanol in the subphase. The maximum expansion of the surface area can be explained in terms of "surface solubilization" analogous to the bulk solubilization as mentioned above.

It is known that basic metal ions expand out fatty acid and long chain anionic compound monolayers. This expansion is found by force–area curves. No increase in surface pressure at constant area is ever observed when the metal salt is injected into the substrate.[8] By using the duplex film method, Schulman and Montagne[3] found that if 2-amino 2-methyl propanol (AMP) is injected under a stearic acid film at a constant area of 20 Å.^{2}, no penetration or rise in surface pressure takes place unless non-polar oil molecules are added to make a duplex film. AMP behaves similarly to basic metal ions, and produces two-dimensional lattices by H-bonding. Into these, the oil molecules will penetrate and produce increases in surface pressure at constant area.

In an analogous way, calcium injected under cephalin monolayers breaks the phosphoric acid–amine polar group *intra*molecular association, permitting *inter*molecular association between neighboring cephalin molecules. This permits surface lattices to form. This again enables the oil molecules to penetrate and give pressure rises at constant area.

Thus, calcium injected under a cephalin mono-

(7) R. Hirt and R. Berchtold, *Experientia*, **14**, 436 (1958); **15**, 373 (1959); *Med. Exp l.*, **2**, 269 (1960).

(8) (a) G. A. Wolstenholme and J. H. Schulman, *Trans. Faraday Soc.*, **46** 475 (1950); (b) J. G. N. Thomas and J. H. Schulman, *ibid.*, **50**, 1131 (1954).

layer in the presence of oil molecules produces a monolayer penetration and pressure rise at constant area.

As indicated,[3] duplex formation corresponds to the disappearance of minute droplets of the now spreading hydrocarbon. When spreading on the monolayer occurs, penetration of the hydrocarbon molecules into the cephalin monolayer also takes place.

Since the surface tension of the hydrocarbons decreases with diminishing chain length (hexadecane 29 dynes/cm.; octane 20.5 dynes/cm.), enhanced spreading and penetration likewise take place on decreasing the hydrocarbon chain length. A similar phenomenon is observed in the formation of microemulsions where it is necessary for the oil phase molecules to have a smaller chain length than the interphase forming molecules.[9] Likewise, the aromatic hydrocarbons (*m*-xylene) have high surface tensions and will not spread or penetrate into the cephalin or stearic acid monolayers at the air/water and oil/water interfaces. Presumably, the non-interaction of Mg ions with the cephalin duplex films is due to their inability to break the internal salt linkage (phosphoric acid–amine).

Acknowledgments.—This investigation was supported by P. H. S. Research Grant No. B-2067 (C) from the National Institute of Neurological Diseases and Blindness.

(9) J. H. Schulman, W. Stoeckenius, and L. M. Prince, *J. Phys. Chem.*, **63**, 1677 (1959).

CONFORMATION AND FRICTIONAL PROPERTIES OF POLYSTYRENE IN DILUTE SOLUTIONS

By D. McIntyre, A. Wims, L. C. Williams, and L. Mandelkern

Polymer Structure Section, National Bureau of Standards, Washington 25, D. C.

Received March 15, 1962

A high molecular weight fraction of polystyrene was studied by light scattering, sedimentation, and viscosity. Measurements were made in cyclohexane at 35, 45, and 55°, and also in benzene at 40°. It was found that the intrinsic viscosity and frictional coefficient of the polymer were exponential functions of the expansion factor. The equations that fit the data are: $[\eta]/[\eta]_\theta = \alpha^{2.33}$ and $(f/\eta)/(f/\eta)_\theta = \alpha^{0.6}$. The relations are in good agreement with recently published theories of Kurata–Yamakawa and Kurata–Stockmayer–Roig.

The hydrodynamic properties of polymer solutions have been studied intensively in the past fifteen years in order to assess the validity of the many theoretical descriptions of the conformation of the polymer chain, its variation with solvent interaction, and its effect on the molecular frictional coefficient. To examine these effects systematically requires the concurrent measurement of the radius of gyration of a polymer fraction by light scattering, the virial coefficient by light scattering or osmotic pressure, and the frictional coefficient by viscosity, sedimentation, or diffusion. The measurements ought to be made on several fractions of known molecular weight and molecular weight distribution over a large molecular weight range.

There are very few such comprehensive studies reported in the literature. Perhaps the most thorough study is that of Oth and Desreux,[1,2] who examined a series of fractions of polystyrene from 100,000 to 3,000,000 molecular weight by light scattering, viscosity, and sedimentation. Another less extensive study of the polystyrene system was made by Krigbaum and Carpenter[3] and earlier by Outer, Carr, and Zimm.[4] The latter studied several fractions of polystyrene in different solvents by light scattering and viscosity measurements; the former studied a single high molecular weight fraction, molecular weight 3.2×10^6. In one respect these two studies differ from the study of Oth and Desreux. In going from a poor solvent (a theta solvent) to a good solvent the polymer coil in solution expands. Oth and Desreux's work indicates that the expansion remains gaussian whereas the other work indicates that it does not. A very recent study by Kirste and Schulz[5,6] on polymethyl methacrylate fractions also shows a non-gaussian expansion.

Theoretical work has made very rapid progress during this interval of experimental work, and there is a pressing need for more extensive and reliable experimental data. The theoretical as well as experimental situation has been summarized in two recent reviews.[7,8] The hydrodynamic relations proposed by Flory[9,10] have been a springboard for much of the experimental work and are given in eq. 1, 2, and 3. These relations are based upon the assumptions of an asymptotic limit in the Kirkwood–Riseman[11] or Debye–Bueche[12] treatments of the partially draining polymer coil in the region of experimental interest. Also it is assumed that the effective hydrodynamic radius is proportional to the root-mean-square, r.m.s., end-to-end distance of the segments, $(\overline{R^2})^{1/2}$. The equivalent hydro-

(1) J. Oth and V. Desreux, *Bull. soc. chim. Belges*, **63**, 285 (1954).

(2) J. Oth and V. Desreux, *ibid.*, **66**, 303 (1957).

(3) W. R. Krigbaum and D. K. Carpenter, *J. Phys. Chem.*, **59**, 1166 (1955).

(4) P. Outer, C. I. Carr, and B. H. Zimm, *J. Chem. Phys.*, **18**, 830 (1950).

(5) R. Kirste and G. V. Schulz, *Z. physik. Chem.* (Frankfurt), **27**, 20 (1961).

(6) G. V. Schulz, *Makromol. Chem.*, **35A**, 99 (1960).

(7) M. Kurata, H. Yamakawa, and H. Utiyama, *ibid.*, **34**, 139 (1959).

(8) A. Peterlin, *ibid.*, **34**, 89 (1959).

(9) P. J. Flory, *J. Chem. Phys.*, **17**, 303 (1949).

(10) P. J. Flory and T. G Fox, *J. Am. Chem. Soc.*, **73**, 1904 (1951); L. Mandelkern and P. J. Flory, *J. Chem. Phys.*, **20**, 212 (1952).

(11) J. G. Kirkwood and J. Riseman, *ibid.*, **16**, 565 (1948).

(12) P. Debye and A. M. Bueche, *ibid.*, **16**, 573 (1948).

dynamic radius increases in proportion to an expansion factor, α, defined in eq. 1, which changes in a known manner with excluded volume and molecular weight, M. The intrinsic viscosity, $[\eta]$, and the frictional coefficient, f/η_0, then can be related to the above quantities by eq. 1, 2, and 3, where $(\overline{R^2})_0^{1/2}$ is the r.m.s. end-to-end distance under random flight statistics, or experimentally under Flory theta conditions. P and Φ are constants.

$$\alpha = (\overline{R^2})^{1/2}/(\overline{R^2})_0^{1/2} \quad (1)$$

$$[\eta] = \Phi \frac{(\overline{R^2})_0^{3/2}}{M} \alpha^3 \quad (2)$$

$$f/\eta_0 = P(\overline{R^2})_0^{1/2}\alpha \quad (3)$$

More recent considerations of the excluded volume and its effect on the hydrodynamic radius have resulted in eq. 4 and 5 of Kurata.[7,13]

$$[\eta] = \Phi \frac{(\overline{R^2})_0^{3/2}}{M} \alpha^{2.43} \quad (4)$$

$$f/\eta_0 = P(\overline{R^2})_0^{1/2}\alpha^{0.652} \quad (5)$$

These relations are valid only for polymer systems that are reasonably close to theta conditions. However, Kurata, Stockmayer, and Roig[14] have allowed for an ellipsoidal expansion of the polymer molecule. They then use eq. 6 to obtain the molecular weight dependence over the whole solvent range.

$$[\eta]/[\eta]_\theta = \alpha^{2.43} \quad (6)$$

In this work, light scattering, sedimentation, and viscosity measurements were made on a single very high molecular weight fraction of polystyrene in an attempt to measure both the r.m.s. radius of gyration and the frictional properties from theta conditions to those of a very good solvent. These results then are related to the above theories.

Experimental

Materials: Polymer.—Styrene (Eastman) was freed of inhibitor, vacuum distilled, then sealed in a dilatometer under high vacuum where it was thermally polymerized at room temperature for approximately 9 months to 50% conversion (by weight). The reaction mixture then was dissolved in methyl ethyl ketone and precipitated by mixing with methanol. The intrinsic viscosity of the whole polymer was 4.86 dl./g. in benzene. Two portions of the polymer then were dissolved in methyl ethyl ketone in a 0.5% mixture for separation into rough fractions. The high molecular weight rough fractions then were combined and refractionated in two portions starting with a 0.1% solution in methyl ethyl ketone. The high molecular weight fractions of this intermediate fractionation then were combined, and the final fractionation into three fractions was from a 0.05% solution of the intermediate fractions. The center fraction was used in this work and represented 2.5% of the original sample.

Solvents.—The cyclohexane used was Fisher reagent grade. The material was distilled before use and then checked for refractive index by a dipping refractometer. The variation of the refractive index of the different batches of cyclohexane used was ±0.0001 refractive index unit. The cyclohexane was purposely not distilled from sodium. The benzene was ACS reagent grade and was distilled from sodium before use.

Partial Specific Volume.—The partial specific volume was determined with pycnometers having a volume of approximately 40 cc. in a bath controlled to ±0.001°. The densities could be determined within $\pm 1 \times 10^{-5}$ for cyclohexane at 35° and $\pm 2 \times 10^{-5}$ for cyclohexane at the higher temperatures. The polymer used in these experiments was not the above mentioned high molecular weight polymer, but was a low molecular weight polymer of molecular weight 180,000. This polymer had been prepared by McCormick using an anionic polymerization of styrene initiated by sodium-naphthalene.[15]

Viscosity Measurements.—The specific viscosity measurements were made in an Ubbelohde viscometer at all temperatures. All of the runs except those at 55° were run in a dilution viscometer. The runs at 55° were made in a nondilution viscometer whose design minimized any possible evaporation. Kinetic energy corrections were applied. The flow times in cyclohexane and benzene were above 170 sec. at all temperatures. The specific viscosities also were measured in a capillary viscometer with three different bulb heights in order to obtain specific viscosities at three different shear rates. A maximum shear gradient was calculated for the viscometers using an average value for the height of the liquid column. For cyclohexane at 35° the shear rates were calculated to be 1666 for the Ubbelohde viscometer and 960, 430, and 100 sec.$^{-1}$, respectively, for the other viscometer. For cyclohexane and benzene at other temperatures the shear rates were calculated with corresponding densities and viscosities.

Refractive Index Increment.—The Hilger interferometer was used to measure the refractive index of the above mentioned, anionically polymerized polystyrene. Measurements were made at one concentration in benzene at 40°, 0.1690 g./dl. The method is discussed elsewhere.[16]

Sedimentation Velocity Measurements.—The Spinco Model E ultracentrifuge with a temperature controlling unit was used with schleiren optics and a phase plate. All of the cyclohexane and benzene runs were made at a speed of approximately 42,000 r.p.m. The data were analyzed from the peaks in the first few photographs after a distinct boundary had been formed. The distances of sedimentation were small and about the same in all cases in order to minimize the pressure corrections.

Sedimentation Equilibrium.—The LKB model of the Svedberg centrifuge was used at 35° with cyclohexane solutions.[17] The speed was 28 r.p.s., and the experiment ran approximately 14 days before equilibrium in the 7-mm. column was definitely established.

Light Scattering Measurements.—All of the measurements were made on a photometer described previously.[18] The angular measurements were made from 15 to 150°. The light scattering cell assembly consisted of an outer cylinder of glass about 12.7 cm. in diameter which had ground and polished flat surfaces for the entry and exit of the incident beam. Inside the cylinder there was black absorbing glass from 0 to 170° to eliminate the back reflections of the incident and scattered light. The cylinder was filled with xylene, and the scattering cell, a 2.5-cm. diameter cylinder, was positioned in the center of it. The whole cell assembly was thermostated by pumping fluid through coils immersed in the xylene, and through a cored out base and surrounding jacket. The xylene in the outer cylinder was stirred. The light scattering cells had tight fitting Teflon caps. A copper-constantan thermocouple inside the outer cylinder, capable of measuring to ±0.02°, showed no change in the temperature during the course of the measurements after the solution had equilibrated with the thermostating fluid. The solutions were prepared by filtering through ultrafine filters. Two independently prepared solutions, and subsequent dilutions in the cell, were measured at each temperature. Concentrations were

(13) M. Kurata and H. Yamakawa, *J. Chem. Phys.*, **29**, 311 (1958).

(14) M. Kurata, W. H. Stockmayer, and A. Roig, *ibid.*, **33**, 157 (1960).

(15) Courtesy of Dr. H. W. McCormick, Dow Chemical Co., Midland, Michigan; H. W. McCormick, *J. Polymer Sci.*, **36**, 341 (1959).

(16) J. H. O'Mara and D. McIntyre, *J. Phys. Chem.*, **63**, 1435 (1959).

(17) L. Mandelkern, L. C. Williams, and S. G. Weissberg, *ibid.*, **61**, 271 (1957).

(18) D. McIntyre and G. C. Doderer, *J. Res. Natl. Bur. Std.*, **62**, 153 (1959).

determined after the measurements at a given temperature by pipeting a known volume of solution, evaporating the solvent, drying in a high vacuum drying pistol at 100°, and weighing the residual polymer. Concentrations at different temperatures were calculated using the density of the solvent only.

Measurements were made with 546 and 436 mμ vertically polarized light from a medium pressure mercury arc. The scattered beam received by the phototube had an angular acceptance of approximately 1°. Angular corrections for the cell are less than 1.5% even at the very low and high angles. The corrections are based on the symmetrical excess scattering from a solution of very low molecular weight polystyrene in cyclohexane. The cell corrections based on fluorescence measurements are less than 0.5% at all angles. The absolute turbidities are based on the averages of determinations of molecular weights in these Laboratories using this absolute photometer and the equilibrium ultracentrifuge. For relative purposes during this study, the scattering of a polystyrene–toluene solution was measured absolutely at several temperatures, also measured in the above cell, and the solution then was placed in a small cylindrical cell for reference use with the above cell assembly.

Experimental Results

1. Centrifugation. A. Partial Specific Volume $\bar{v}$.—Table I lists the densities (ρ), concentrations (c_2), weight fractions (ω_2), and apparent specific volumes (φ) in units of g. and ml. at different temperatures for different solutions of polystyrene. Where duplicate determinations have been made

Table I

Partial Specific Volume Determination

Temp., °C.	$c_2 \times 10^3$	$\omega_2 \times 10^3$	ρ	φ
		Cyclohexane		
35	0.000	0.000	0.76399	
	1.356	1.772	.76445	0.865
	2.003	2.620	.76456	.940 (±0.003)
	4.153	5.427	.76524	.915
	7.537	9.837	.76617	.930
		$\bar{v} = 0.928$		
45	0.000	0.000	0.75447	
	1.070	1.418	.75484	0.867 (±0.062)
	1.634	2.165	.75496	.932 (± .028)
	2.928	3.876	.75534	.931 (± .008)
	3.787	5.012	.75559	.934 (± .013)
		$\bar{v} = 0.934$		
55	0.000	0.000	0.74466	
	1.253	1.682	.74508	0.892 (±0.005)
	2.029	2.722	.74532	.926 (± .002)
	4.294	5.756	.74596	.934 (± .002)
		$\bar{v} = 0.936$		
		Benzene		
40	0.000	0.000	0.85726	
	1.365	1.592	.85758	0.897 (±0.004)
	2.243	2.615	.85776	.911
	3.953	4.606	.85812	.917 (±0.001)
		$\bar{v} = 0.917$		

they are represented by the average value with the average deviation in parentheses. The value below each set of results is the best value of $\bar{v}$ determined graphically by plotting specific volume against weight fraction according to eq. 7 and giving less significance to the very low concentrations. The apparent specific volume is calculated according to eq. 8.

$$\bar{v}_2 = V_{sp} + (1 - \omega_2)\left(\frac{\partial V_{sp}}{\partial \omega_2}\right) \qquad (7)$$

$$\varphi = \frac{1}{\rho_1}\left[1 + \frac{\rho_1 - \rho_{soln}}{c_2}\right] \qquad (8)$$

B. Equilibrium Centrifugation.—The average value of the weight average molecular weight was 3.6×10^6. However, the more relevant quantity for this study is a measure of polydispersity, namely M_z/M_w. This ratio varied from unity to 1.2.[19] The speed was probably a little too high and the concentration gradient in the cell was not as gradual as one might like. Nevertheless, the fact that the polydispersity ratio is not greater than 1.2 is of some value in interpreting the light scattering radius.

C. Sedimentation Velocity.—Table II lists the sedimentation constant and its reciprocal. These values were obtained by extrapolating the reciprocal sedimentation coefficient linearly to zero concentration according to eq. 9. K_s also is tabulated in Table II and is the slope defined by eq. 9. The concentrations ranged from 0.01 to 0.07%.

$$1/S = 1/S_0(1 + K_s c_1) \qquad (9)$$

Table II

Sedimentation Velocity Data

°C.	$1/S_0$	$S_0 \times 10^{13}$	K_s	$(1 - \bar{v}\rho)/S_0$
		Cyclohexane		
35	3.56	28.1	5.06	1358
45	3.45	29.0	15.7	1568
55	2.94	34.0	35.7	1594
		Benzene		
40	5.08	19.68	100.4	2144

2. Viscosity.—The relative viscosities range from 1.03 to 1.20 at the highest shear rates. The relative viscosities in the work with the variable shear rate viscometer only went as low as 1.09. Table III presents the intrinsic viscosity at the high shear rate, and also lists the intrinsic viscosity extrapolated linearly to zero shear rate, $[\eta]_0$.

Table III

Intrinsic Viscosities

°C.	$[\eta]$, dl./g.	$[\eta]_0$, dl./g.
	Cyclohexane	
35	1.50	1.50
45	2.219	2.22
55	2.62	2.72
	Benzene	
40	6.36	7.04

3. Light Scattering.—Table IV lists the light scattering constants used in this work. (dn/dc) for cyclohexane solutions is taken from reference 16. The refractive index, n, is interpolated from values in Timmermans.[20a] K_v is the constant for

(19) The accuracy of this parameter depends upon the certainty of the concentration gradient at the end of the cell. This instrumental problem has not been satisfactorily solved.

(20) (a) J. Timmermans, "Physicochemical Constants of Pure Organic Compounds," Elsevier, 1950; (b) B. H. Zimm, *J. Chem. Phys.*, **16**, 1093, 1099 (1958).

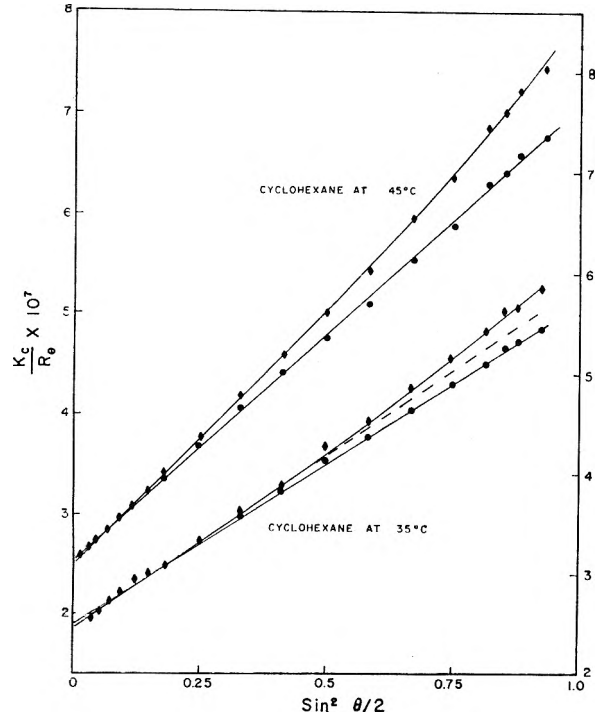

Fig. 1.—Reciprocal scattering curves at zero concentration for polystyrene fraction in cyclohexane at 35 and 45°: diamonds are experimental data, circles are corrected for $h = 4$.

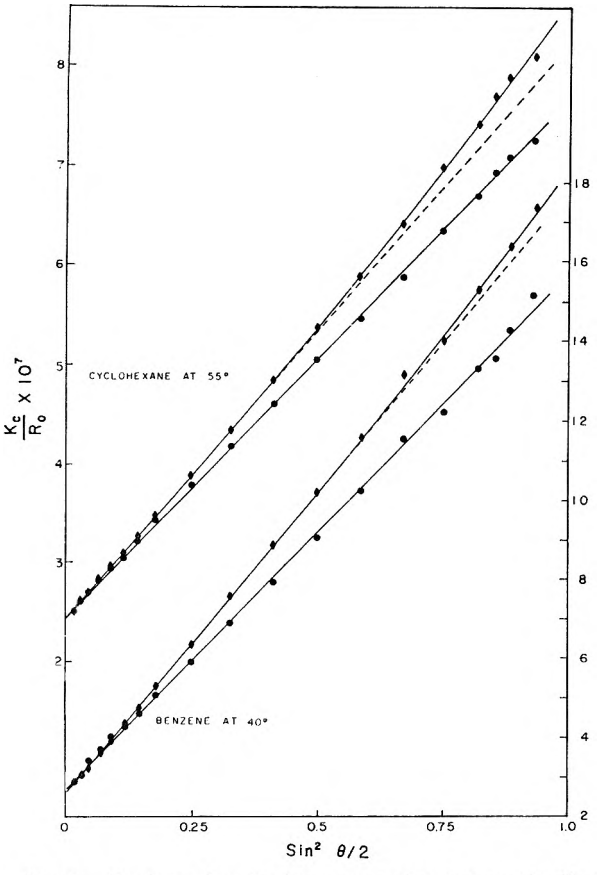

Fig. 2.—Reciprocal scattering curves at zero concentration for polystyrene fraction in cyclohexane at 55° and benzene at 40°: diamonds are experimental points, circles are corrected for $h = 4$.

vertically polarized light that occurs in eq. 10 and 11 for light scattering in polymer solutions.[20b]

$$\frac{Kc}{R_\theta} = \frac{1}{M_w P(\theta)} + 2A_2 c \qquad (10)$$

$$K_{V.P.} = \frac{4\pi n^2 (dn/dc)^2}{\lambda^4 N_0} \qquad (11)$$

R_θ is the Rayleigh's ratio at scattering angle θ, A_2 is the second virial coefficient in c.g.s. units, λ is the wave length, and $P(\theta)$ is the particle scattering function.

TABLE IV

LIGHT SCATTERING CONSTANTS FOR POLYSTYRENE

°C.	n	dn/dc, ml./g.	$Kv \times 10^7$
		436 mμ	
		Cyclohexane	
35	1.428	0.1814	0.1220
45	1.422	.1849	.1256
55	1.418	.1884	.1297
		Benzene	
40	1.510	.1160	.15578
		546 mμ	
		Cyclohexane	
35	1.422	.1705	4.332
45	1.418	.1739	4.482
55	1.415	.1772	4.633
		Benzene	
40	1.491	.1106	2.005

Table V represents the derived data from a plot of Kc/R_θ against $[\sin^2(\theta/2) + kc]$, reference 20b. The limiting slopes of the zero concentration curve and the zero angle curve are reported in terms of their molecular quantities, the radius of gyration (Å.), and the virial coefficient (c.g.s. units). The limiting curves were drawn so as to make their intercepts coincident. This value is given as the molecular weight. The data are listed separately for the 436 and 546 mμ measurements. The agreement of the molecular weights at both wave lengths of light is reassuring. The average values of these molecular constants also are given. Therefore the molecular weight average is given with the benzene results included and excluded.

Figures 1 and 2 represent the data at 546 mμ for (Kc/R_θ) at zero concentration plotted against $\sin^2(\theta/2)$. The r.m.s. z-average radius of gyration is determined from eq. 12, where λ' is the effective wave length in the solution.

$$(\overline{R^2})_z^{1/2} = (3/16)\left(\frac{\lambda'^2}{\pi^2}\right)\left(\frac{\text{slope}}{\text{intercept}}\right) \qquad (12)$$

It is known that the polydispersity of the sample can have a drastic effect on the determination of the limiting slope of these curves. In Fig. 1 and 2 there also are plotted corrections to the experimental scattering curve which allow a better estimation of the limiting slope. These corrections were made using the tabular values listed by Zimm[20b] for a heterogeneity parameter of four,

Table V

Experimental Light Scattering Results

°C.	$M_w \times 10^{-6}$	$(\overline{S^2})_z^{1/2}$	$A_2 \times 10^5$
	546 mμ		
	Cyclohexane		
35	4.03	626	0.0
45	3.96	746	7.5
55	4.10	817	11.6
Average	4.03 ± 0.05		
	Benzene		
40	3.93	1234	34.8
Average	4.00 ± 0.06		
	436 mμ		
	Cyclohexane		
35	3.92	604	0.0
45	3.97	754	5.7
55	4.12	828	9.7
Average	4.00 ± 0.08		
	Benzene		
40	3.95	1218	37.1
Average	3.99 ± 0.06		

Average values

$M_w = (4.00 \pm 0.06) \times 10^6$

°C.	$A_2 \times 10^5$	$(\overline{S^2})_z^{1/2}$, Å.	$(\overline{R^2})_z^{1/2}$, Å.
	Cyclohexane		
35	0.0	615 ± 9	1506
45	6.6 ± 0.9	750 ± 4	1837
55	10.7 ± 0.9	822 ± 5	2013
	Benzene		
40	35.9 ± 1.2	1226 ± 13	2792

corresponding to $M_z/M_w = 1.2$. Zimm made these corrections on the assumption that the distribution of molecular weights in a polymer sample could be described in many cases by eq. 13. The function $\omega(M)\,dM$ is the weight fraction of polymer in the interval M to $M + dM$, and h and λ are parameters that have the relations shown in (13) when the distribution is normalized. M_n, M_w, and M_z are the number, weight, and z-average molecular weights, respectively.

$$\omega(M)dM = \frac{\lambda^{h+1}M^h e^{-\lambda M}}{h!} \qquad (13)$$

$$\lambda = \frac{h}{M_n} = \frac{h+1}{M_w} = \frac{h+2}{M_z} \qquad (14)$$

The values of the radii determined from these corrected plots are given in column 1 of Table VI. The corrected plots do not give as good a linear representation of the experimental points at low angles as the original experimental curve. There is a bias of the low angle points on the line that best fits the high angles. A lower heterogeneity parameter would avoid this problem, but the corrected slopes then would be very close to the experimental slopes anyway. As can be seen in column 2 of Table VI, the changes in radius of gyration are not very large even with a parameter of four.

Table VI

Corrected Light Scattering Results

	—Radius of gyration— (1)	(2)	—Virial coeff. (Fig. 3)— (3)	(4)
°C.	Cor. $(\overline{S^2})_z^{1/2}$, Å.	Ratio (cor./uncor.)	$A_2 \times 10^5$	$M_w \times 10^{-6}$
	Cyclohexane			
35	603	0.979	0.0	4.03
45	716	.955	6.4	3.98
55	775	.942	8.8	4.10
	Benzene			
40	1140	.930	32.0	3.79

Figure 3 is a plot of the extrapolated values of the scattering at zero angle for each concentration. Since the agreement of molecular weights between 436 and 546 mμ in Table V is very good, the average values for both wave lengths are used to plot the scattering at zero angle in Fig. 3. The values of the virial coefficients and molecular weight determined in this manner are listed in columns 3 and 4 of Table VI. No attempt was made to make the molecular weights coincide with the values listed in Table V.

Discussion

Polymer Dimensions.—To compare the experimental data with the theory relating polymer dimensions to frictional properties and excluded volume, it is essential to know the molecular weight distribution of the polymers studied. Neither in this study nor in other previously published studies has the distribution been definitely known. The exponential distribution shown in eq. 13 generally has been assumed although Newman, Krigbaum, Laugier, and Flory[21] corrected their values of Φ by assuming a Lansing–Kraemer distribution.[22]

Since it usually is experimentally difficult to measure angular scattering in the interval between 15 and 0°, it may be necessary when studying very high molecular weight compounds to make assumptions about the distribution before a reliable estimate of the z-average radius of gyration can be obtained. Although the results are not shown in Fig. 1 and 2, the light scattering data also were analyzed by assuming a monodisperse sample and actually comparing the theoretical particle scattering factor for a random coil with the experimental curve. (The approximate size was obtained by a direct extrapolation of the experimental curves.) The monodisperse calculations began to diverge from the experimental curve at $\sin^2(\theta/2) \cong 0.1$ even in cyclohexane at 35°. Two different values of h (4, 19) in the exponential distribution in eq. 13 then were assumed, and the experimental data were corrected using the tabular values in reference 2. Neither set of corrections adequately represents the experimental data at low angles. The line of best fit for the high angles distinctly makes all of the low angles fall below the line, and the effect is worse for the higher h. A more detailed plot shows that this is a very salient fact. There seems little doubt that the two lowest points

(21) S. Newman, W. R. Krigbaum, C. Laugier, and P. J. Flory, *J. Polymer Sci.*, **14**, 451 (1954).

(22) W. D. Lansing and E. O. Kraemer, *J. Am. Chem. Soc.*, **57**, 1369 (1935).

in the scattering curve for cyclohexane at 35° are due to "dirt." The other experimental curves are linear in the low angle region with only small random deviations at even the lowest angles of measurement. If a more polydisperse sample is assumed, the experimental data can be corrected to fit the low angles better. However, considerations of the fractionation and the sedimentation results indicate that the fraction may, if anything, be less polydisperse. Furthermore, the net effect would be to make the uncorrected and corrected values of the radius agree more closely. For further calculations in this paper the z-average values of the radius of gyration from the uncorrected plots are preferentially used. The corrected values listed in Table VI also are discussed at various times.

Molecular Weights and Molecular Weight Distribution.—It was hoped at one time that the equilibrium centrifuge would determine the molecular weight very accurately and thereby eliminate many problems in the extrapolation of angular dependent functions. This molecular weight determination was not a straightforward measurement. The results reported here on the centrifuge were not run at the most favorable speed and concentration, and as a result the concentration gradient rises steeply toward the end of the cell. These experiments will be repeated at a later date with this and other high molecular weight fractions. The region of the cell in which any very large particles that might affect the z-average radius are concentrated was not visible in these runs. However, at least 95% of the cell was visible, and any upsweep in the gradients was accentuated in order to get a maximum value for the polydispersity (M_z/M_w). There is considerable value in knowing that the polydispersity was never higher than 1.2.

There is a distinct tendency for the molecular weights determined in benzene to be lower than those in cyclohexane. If the light scattering constants are known equally well in the two systems, it is possible that the extrapolation is exhibiting the behavior discussed by Loucheux, Weill, and Benoit.[23]

Virial Coefficient.—The virial coefficients listed in Tables V and VI do not differ for the low temperature cyclohexane data. However, the difference for the other two solvent conditions is appreciable, approximately 12% for both. The scatter of the data at zero angle is sufficiently great so that when the zero angle data for the two wave lengths are averaged and plotted without regard to the zero concentration intercept the slope is decreased. The extrapolation in the case of benzene from the last concentration to the intercept is particularly long and hazardous. With such a high virial coefficient these solutions ought to be run at lower concentrations. Further calculations in this paper are based upon the virial coefficients in Table III. It is interesting to note that the precision of the radii determinations in this system is appreciably better than the precision of the virial coefficients.

(23) C. Loucheux, G. Weill, and H. Benoit, *J. chim. phys.*, **55**, 540 (1958).

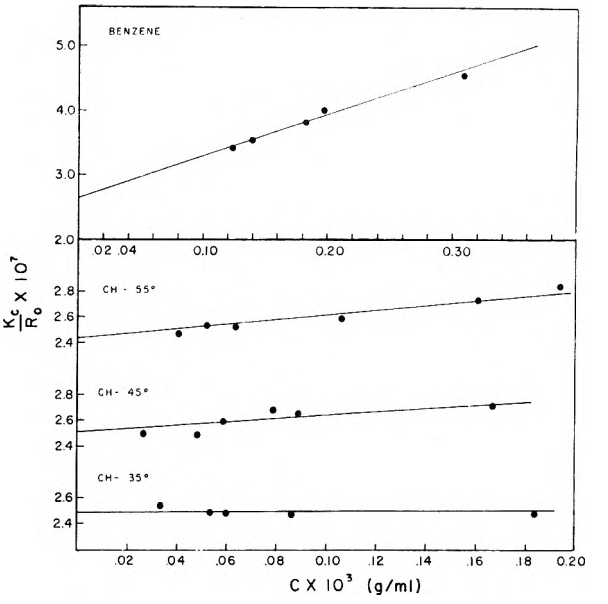

Fig. 3.—Reciprocal scattering curves at zero angle for polystyrene fraction in cyclohexane at 35, 45, and 55°; and benzene at 40°.

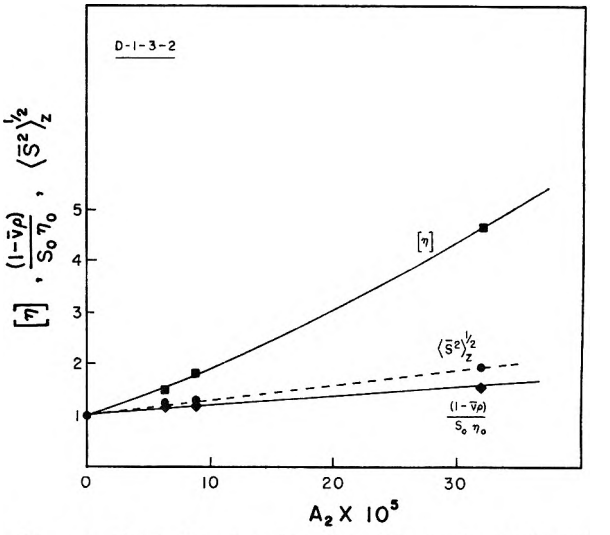

Fig. 4.—Intrinsic viscosity $[\eta]$, frictional coefficient $(1 - \bar{v}\rho)/\eta_0 S_0$, and r.m.s. radius of gyration $(\bar{S}^2)_z^{1/2}$ of polystyrene fraction as a function of virial coefficient A_2. (The ordinates are normalized to unity at $A_2 = 0$.)

$(\overline{R^2})_\theta/M$.—The ratio of the square of the end-to-end distance (under theta conditions) to the molecular weight should give considerable information about the microstructure of the polymer chain. If the polymer were monodisperse, this parameter would be readily available from experiment. In attempting to compare much of the existing data in the literature on polymer dimensions, particularly with high molecular weight material, it must be remembered that the fractions are not monodisperse and often are derived from polymerizations carried out to high conversions of monomer. Often the polymer preparations are not given in any detail.

Table VII lists some of the reported values of this parameter. All of the work was done on frac-

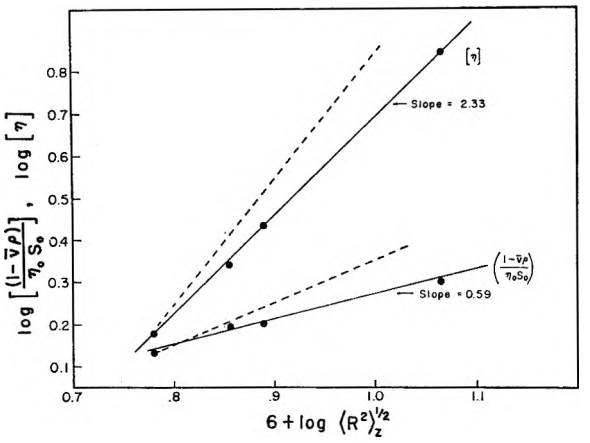

Fig. 5.—Log $[\eta]_0$ and log $(1 - \bar{v}\rho)/\eta_0 S_0$ as a function of log $(\bar{R}^2)_z^{1/2}$ (dotted lines are for slopes of 3 and 1, respectively).

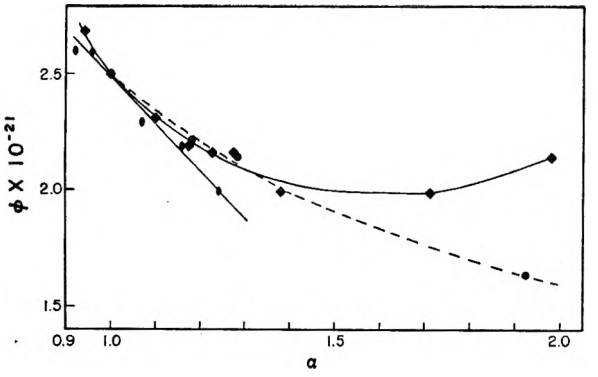

Fig. 6.—Φ plotted as a function of α: circles and ovals are for polystyrene from the present work and reference 3, respectively; diamonds for polymethyl methacrylate from reference 6.

TABLE VII

VALUES OF $(\bar{R}^2)_z/M_w$

Ref.	$\frac{(\bar{R}^2)_z}{M_w} \times 10^{16}$	$M_w \times 10^{-6}$	Preparation of polymer
16	0.57	1.61	Benzoyl peroxide, 70°, 100% conv., bulk
3	.54	3.20	Thermal
1	.62	2.8	High conversion
	.41	1.065	High conversion
	.59	0.372	High conversion
24	.48	1.61 (interpolated)	Benzoyl peroxide, 40–120°, bulk
25	.32	1.46	Commercial sample
	.28	1.00	Commercial sample
	.33	0.74	Commercial sample
26	.47	5	Thermal, 25°, 6 mo.
	.54	2.13	Thermal, 125°
	.77	1.75	Thermal, 125°
	.58	1.00	Commercial sample
	.66	0.675	Thermal, 125°
This work	.57	4.0	Thermal, 25°, 9 mo., bulk

tions of unknown polydispersity, and the comparison must be made on reported values of $(\bar{R}^2)_z/M_w$ even though the reduced number-average ratio would be more significant. There are very few generalizations that can be made, but a guess might be made that the most careful fractionations result in a value between 0.5 and 0.6. The data of reference 6 are very unusual and must be attributed to either large experimental error or branching in the commercial polymer. In view of the different methods of preparation, it is surprising that there are no other significant differences. Four of the references including this study used cyclohexane[1,3,16] and the other three used mixed solvents to achieve theta conditions.

Variation of $(\bar{S}^2)_z^{1/2}$ with A_2.—Zimm, Stockmayer, and Fixman[27] have shown that the mean square end-to-end (or displacement) length of a polymer chain can be expressed by eq. 15, where n is the number of segments in the chain, a is the unperturbed effective length of a link, and β is the volume excluded to the center of one segment by the presence of another. They also found that the radius of gyration of the molecule could be represented by eq. 16.

$$\bar{R}^2 = na^2[1 + 4/3\ z + \ldots],$$

$$\text{where } z = \left(\frac{3}{2\pi na^2}\right)^{3/2} \beta n^2 \quad (15)$$

$$\bar{S}^2 = \frac{na^2}{6}\left[1 + \frac{134}{105} z + \ldots\right] \quad (16)$$

Zimm[28] directly related the excluded volume to the second virial coefficient in the single contact approximation by eq. 17; N_0 is Avogadro's number, and M is the molecular weight.

$$A_2 = \frac{N_0 n^2 \beta}{2M^2} \quad (17)$$

Other terms can be added to this expression but the expression is valid only in the vicinity of theta where z is small. These expressions when combined give the relation in eq. 18 for the radius of gyration and the virial coefficient.

$$\bar{S}^2 = \bar{S}^2_0\left[1 + 0.0572\left(\frac{M}{\bar{S}^2_0}\right)^{3/2}\left(\frac{2}{N_0}\right) M^{1/2} + \ldots\right] \quad (18)$$

When a sample is polydisperse, an equation for the z-average radius of gyration must be determined in order to compare the results directly with experiment. By using the exponential distribution in eq. 13, the above equation can be modified as shown in eq. 19, which is similar to Krigbaum's expression.

(24) N. T. Notley and P. J. W. Debye, *J. Polymer Sci.*, **17**, 99 (1955).

(25) S. N. Chinai, P. C. Scherer, C. W. Bondurant, and D. W. Levi, *ibid.*, **22**, 527 (1956).

(26) F. D. Kunst, *Rec. trav. chim.*, **69**, 125 (1950); Thesis, Univ. of Groningen, 1950.

(27) B. H. Zimm, W. H. Stockmayer, and M. Fixman, *J. Chem. Phys.*, **21**, 1716 (1953); M. Fixman, *ibid.*, **23**, 1656 (1955).

(28) B. H. Zimm, *ibid.*, **14**, 164 (1946).

$$(\overline{S^2})_z = (\overline{S^2_0})_z \left[1 + \frac{(h+2)^{3/2}}{(h+1)^2} \left(\frac{2\Gamma(h+3.5)}{\Gamma(h+3)} - \frac{\Gamma(h+2.5)}{\Gamma(h+2)} \right) \right] \quad (19)$$

Figure 4 shows a plot of $(\overline{S^2})_z^{1/2}$ for the present sample over a very large virial coefficient range. Although it appears on this scale to be almost linear, on a larger scale the benzene value definitely falls below the line that satisfies the cyclohexane data. The experimental value for the slope of the plot of $(\overline{S^2})_z^{1/2}$ against A_2 is 0.366×10^4. If the experimental value for $[(\overline{S^2})/M]^{1/2}$ is put into eq. 18 on the assumption of a monodisperse polymer (or $h = \infty$ in eq. 19), the theoretical value is calculated to be 0.328×10^4. A polydispersity corresponding to $h = 4$ would decrease this slope by less than 5%.

It is interesting to compare the other published data. On replotting the data of $(\overline{S^2})_z^{1/2}$ against A_2 for references 3 and 4 the slopes are calculated to be 0.63×10^4 and 0.255×10^4, respectively. These slopes are based upon points very close to theta and should correspond closely to the theoretical calculations. Since the value of $(R)_z^2/M_w$ in Table VII is the same for this work and that of reference 16, the ratio of the experimental slopes should be proportional to the square root of the molecular weights, or 0.63. The actual ratio of the experimental slopes is 0.76. Since the points of reference 3 are on a gradual curve it is possible to take the portion representing the higher virial coefficients and compute a slope of approximately 0.4×10^4.

The virial coefficients in this work seem high, especially when they are compared to the values of reference 3 for a comparable molecular weight and temperature in cyclohexane. The refractive index increment in reference 3 is considered to be constant, whereas in this work it is not. Correspondingly, the light scattering constant K increases in this work by about 6%. This would make higher virial coefficients if applied to Fig. 3 of reference 3 with a fixed intercept, but it is not known whether this can totally account for the difference.

Intrinsic Viscosity.—Figure 4 shows the variation of the intrinsic viscosity at zero shear rate with the virial coefficient. Figure 5 presents the dependence of the intrinsic viscosity on the experimental radius of gyration. The data also may be expressed in the form shown in eq. 20. If the corrected radii of gyration in Table VI are used instead of the values in Table V, the exponent in the relation can be changed to 2.53. Kurata, Yamakawa, and Utiyama[7] have shown theoretically that the exponent for this equation in the vicinity of theta is 2.43, when the polymer is monodisperse. When the sample is polydisperse, the exponent, n, would be given by eq. 21. (eq. 27 in reference 7) for an exponential distribution.

$$[\eta]/[\eta]_\theta = \alpha^{2.33} \quad (20)$$

$$n = \frac{105}{67} p(x_w) \frac{(h+1)^2(h+2)[\Gamma(h+1)]^2}{\Gamma(h+3/2)\Gamma(h+7/2)} \quad (21)$$

The data in the vicinity of theta from the present work would give an exponent of 2.26. The dotted line in the graph indicates the slope for an exponent of 3.

The relation given by Flory in eq. 2 is based upon the use of a number average radius and molecular weight in a polydisperse system.[21] In order to calculate the parameter Φ it is necessary to correct the measured weight average molecular weight and z-average radius. Krigbaum and Carpenter have given corrections for this quantity.[3] For corrections near the theta temperature for a polydispersity parameter $h = 4$, Φ can be corrected to give a theta value for these data of 2.5×10^{21}, which decreases with A_2. This decrease in Φ was noted earlier by Krigbaum and Carpenter.[3] Recently some additional data on polymethyl methacrylate have been presented by Schulz.[6] Taking the values from their graph and normalizing their theta value of Φ to 2.5×10^{21} the plot in Fig. 6 is obtained. It should be noted that the curve for these polystyrene results shows a monotonically decreasing function for Φ for the entire solvent range.

Sedimentation Frictional Coefficient.—It is well known that the frictional coefficient of a molecule is related to its radius. In the model proposed by Flory eq. 22 was derived. Kurata and Yamakawa,[13] by considering the effect of the non-

$$f/\eta_0 = P(\overline{R^2})^{1/2} = P'(\overline{S^3})_\theta^{1/2}\alpha \quad (22)$$

gaussian expansion of the polymer molecule, arrived at eq. 23.

$$f/\eta_0 = P(\overline{S^2})_\theta^{1/2}\alpha^{0.7652} \quad (23)$$

The frictional coefficient is related to the sedimentation constant, S_0, by eq. 24. Thus it is necessary to know several additional factors besides

$$f/\eta_0 = \frac{M(1 - \bar{v}\rho)}{\eta_0 S_0} \quad (24)$$

the sedimentation constant to calculate the frictional coefficient. Even the sedimentation coefficients determined during a run must in principle be corrected for pressure effects on the viscosity and density. Since the effect of pressure on the partial specific volume is unknown, this factor is considered constant. In these experiments, in which the temperature of the solvent was varied, no pressure corrections were applied to the density and viscosity because accurate corrections are not known. The only data available on the pressure dependence of viscosity in cyclohexane are those of Bridgman.[29] The data are given at 30 and 75°. At 75° both cyclohexane and benzene have about the same pressure dependence. The corrections made for cyclohexane at 35° increase the sedimentation coefficient by 1%. Since the exact corrections at other temperatures are unknown, and the data were obtained under the same conditions, it is felt that all of the data should be left uncorrected.

The partial specific volume was considered to be constant (0.93) over the various temperatures in cyclohexane, and was set equal to 0.92 for benzene at 40°. The results of the partial specific volume

(29) P. W. Bridgman, *Proc. Am. Acad. Arts Sci.*, **61**, 57 (1926).

determination are very interesting in themselves, but the data are not sufficiently accurate to establish any information about the enthalpies of dilution. They strongly suggest that the simple explanation of Streeter and Boyer[30] is not correct. They had found that when there were either very strong solvent–polymer interactions (good solvents) or very strong polymer–polymer interactions the partial specific volume had a maximum value. At the intermediate cases there was a decrease of the partial specific volume. Cyclohexane at 55° is an intermediate case although there is some expansion of the polymer size simply due to an increase of temperature, yet the $\bar{v}$ does not change. The data are in good agreement with the data of Rosen[31] and Griffel, Jessup, Cogliano, and Parks.[32] Whether the change in the apparent specific volume at low concentrations is real can be settled only by more refined work. Rosen found just the opposite trend, and his differential measurements were far more sensitive to the difference of densities needed to calculate the apparent specific volume.

The dependence of the frictional coefficient on the polymer size and on the virial coefficient is shown in Fig. 5 and 4, respectively. It should be noted that the dotted line of Fig. 5 has a slope of unity. The frictional coefficient follows eq. 23, where an exponent of 0.6 is used because the uncertainty in the data does not allow an accuracy better than ± 0.05 to be assigned to the slope. The value of 0.6 for the slope agrees closely with the value given by Kurata.

$$(f/\eta)/(f/\eta)_\theta = \alpha^{0.6} \qquad (25)$$

There are in conclusion several experimental studies including this study of polystyrene that indicate that the intrinsic viscosity and the frictional coefficient increase less than would be predicted on the basis of the original theory of Flory. This study has shown that the intrinsic viscosity and the frictional coefficient are related to the expansion factor, α, by an exponent that agrees well with the theories of Kurata and Yamakawa. Also, the increase of the radius of the polymer molecule with the virial coefficient agrees well with recent theories of the excluded volume. These recent theories are valid at temperatures not far from theta.

(30) D. J. Streeter and R. F. Boyer, *Ind. Eng. Chem.*, **43**, 1790 (1951).

(31) B. Rosen, *ibid.*, **27**, 559 (1955).

(32) M. Griffel, R. S. Jessup, J. C. Cogliano, and R. P. Parks, *J. Res. Natl. Bur. Std.*, **52**, 217 (1954).

It therefore is surprising that the effects seem to be nearly the same in solvents that are far from theta solvents. However, Kurata, Stockmayer, and Roig found that the molecular weight dependence of the intrinsic viscosity was in better agreement with experimental results in good solvents when they used the ratio of intrinsic viscosities under any solvent condition to that at theta as $\alpha^{2.43}$ and considered an ellipsoidal expansion of the molecule far from theta conditions.

DISCUSSION

H. WARD.—This comment concerns the problem of determining number average molecular weights from ultracentrifuge data. In principle it seems feasible to measure number average sedimentation constants quite directly by light absorption *provided* that the sedimenting species all carry the same number of light absorbing groups per molecule. This could be effected, for example, by tagging the ends of a linear polymer with a chromophore.

D. McINTYRE.—The determination of the number-average molecular weight is possible if at any point in the cell either M_n is known or the concentration is zero. As Dr. Ward indicates, the performance of an end group analysis and the simultaneous determination of the total concentration at any point in the cell would allow the number-average molecular weight of the sample to be determined.

S. R. ERLANDER (Northern Regional Research Laboratory).—With regard to Dr. Ward's statement, work has been done on amylose by tagging the end group of each molecule with a radioactive unit. I see no reason why the tagging method cannot be applied to ultracentrifuge work to obtain M_n. In addition, one can for practical purposes assume that the concentration at the meniscus (C_a) is equal to zero if the schlieren pattern coincides with the base line at the meniscus. Under the conditions that $C_a = 0$, the number-average molecular weight at the cell bottom equals the total weight-average molecular weight as given by Yphantis. One can use the previously determined M_w to obtain a more accurate extrapolation of the pattern at the cell bottom. Hence, the number-average molecular weight could be obtained from sedimentation–equilibrium studies by first obtaining M_w and then obtaining a pattern where the value of C_a is essentially zero.

D. McINTYRE.—The earlier experimental work of Williams and Wales used the above method to determine the number-average molecular weight. The problem of establishing a point in the cell where the concentration is definitely known to be zero is, of course, difficult.

H. A. ENDE (Chemstrand Research Center).—You point out the importance of knowing the molecular weight distribution of the polystyrene samples in order to interpret more accurately the results of your measurements and that neither in the present work nor in previously published studies has the distribution been definitely known. Recently J. J. Hermans and I have used the density gradient technique to determine M_n and M_w, or any other molecular weight average. This method utilizes the moments of molecular weights which can easily be related to moments of the concentration distribution in the polymer band formed by density gradient centrifugation.

VELOCITY SEDIMENTATION STUDIES ON PRESSURE AND CONCENTRATION DEPENDENT SYSTEMS

BY IRWIN H. BILLICK

Analytical Research Division, Esso Research and Engineering Company, Linden, New Jersey

Received March 5, 1962

The sedimentation behavior of a system in which pressure and concentration dependence were present has been studied as a function of molecular weight, solvent, and speed of centrifugation. Anionically polymerized polystyrene was investigated in cyclohexane, a poor solvent, at 35°, and in toluene at 25°. Analysis of the data according to the series solution of Fujita's differential equation yielded values for the sedimentation coefficient, at zero concentration and atmospheric pressure, the concentration dependence parameter, and the pressure dependence parameter. It was found that concentration does not contribute greatly to the slope of the sedimentation coefficient *vs.* time curve within experimental precision. The value found for the pressure dependence coefficient agrees with the literature and was not found to be influenced by molecular weight or speed of centrifugation.

Introduction

The simultaneous dependence of the sedimentation coefficient on hydrostatic pressure and solute concentration has been investigated by several workers in the past,[1,2] both experimentally and theoretically. However, the most fundamental approach, from a mathematical point of view, was given by Fujita.[3] A differential equation of flow was proposed for the sedimentation behavior of a monodispersed, non-diffusing solute, explicitly in terms of the sedimentation coefficient, at zero concentration, a pressure dependence parameter, and a concentration dependence parameter.

The equation which was set forth was solved by Wales[4] both analytically and with a digital computer. Evaluation of the sedimentation coefficient at zero concentration and one atmosphere pressure from experimental data is possible using Wales' analytical solution only if the values of the pressure and concentration dependence parameters are known, or by a curve fitting technique.[5] In a previous publication,[6] we have given a solution to Fujita's equation which would permit the direct determination of all the unknown parameters.

The purpose of this article is to show that velocity sedimentation data can be evaluated adequately using these solutions. An investigation has been carried out using near monodispersed polymer under varying conditions of molecular weight, solvent, concentration, and centrifuge velocity.

Experimental

Three anionically polymerized polystyrene samples were used. Two of these, S-5 and S-10, were furnished through the courtesy of Dr. H. W. McCormick of the Dow Chemical Co. The other sample, S-111, was distributed by H. Mark under the auspices of the Commission on Macromolecules of the IUPAC. All the samples used had a very narrrow molecular weight distribution as indicated by the low values of M_w/M_n given in Table I.

Ultracentrifugation was carried out in a Spinco Model E centrifuge equipped with an RTIC temperature control unit. Polymer solutions using cyclohexane at 35°, a poor solvent, and toluene at 25°, a good solvent, were investigated.

During a given run, acceleration was carried out at constant current until the desired speed was reached. The automatic camera was started when the speed had reached $^2/_3$ its final value and the zero time of sedimentation was taken at this point.[9,10]

TABLE I

POLYMER MOLECULAR WEIGHTS

Sample	$M_w \times 10^{-5}$	M_w/M_n
S-5[7]	0.975	..
S-10[7]	2.51	1.04
S-111[8]	2.39	1.08

Sedimentation rates were studied as a function of solute concentration and in the case of one polymer sample, S-111, as a function of angular velocity. In studying the effect of velocity, only the behavior in a poor solvent was investigated. Solutions were prepared and the run at highest speed usually was made first. Upon completing a run, the cell was removed from the rotor and placed on a wrist-action shaker. The cell was shaken very gently under a heat lamp until the polymer was all dispersed and then run at another speed. This procedure was repeated until all the runs at that particular concentration were carried out.

The position of the maximum of the refractive index gradient was measured using a Gaertner toolmaker's microscope. Although some diffusion was apparent during sedimentation, it has been assumed[11] that the maximum may be used in place of the boundary position measured from the second moment.

Calculations and Results

The solutions to Fujita's equation[6] were expressed in the form of a series, in which the independent variable was either time or position of the boundary from the center of rotation. In this article we will deal only with the form given by eq. 1, although the results are the same when the other variable is used.

$$S = \frac{\ln r/r_0}{\omega^2 t} = \frac{S_0^0}{1+\alpha}\left[1 - \frac{m(2\alpha+1)-\alpha}{1+\alpha} \times \frac{S_0^0}{1+\alpha} \times \omega^2 t - \cdots\right] \quad (1)$$

In eq. 1, r is the radial distance of the boundary, r_0 is the radial distance of the meniscus, t is the time, ω is the angular velocity, and S_0^0 is the sedimentation coefficient at one atmosphere pressure and infinite dilution. The definition for α, the concentration dependence parameter, is given by

(1) J. Oth and V. Desreux, *Bull. soc. chim. Belges*, **63**, 133 (1954).
(2) H. G. Elias, *Makromol. Chem.*, **24**, 30 (1959).
(3) H. Fujita, *J. Am. Chem. Soc.*, **78**, 3598 (1956).
(4) M. Wales, *ibid.*, **81**, 4758 (1959).
(5) M. Wales, *J. Polymer Sci.*, in press.
(6) I. H. Billick, *J. Phys. Chem.*, **66**, 565 (1962).
(7) H. W. McCormick, *J. Polymer Sci.*, **36**, 341 (1959).
(8) H. Mark, data accompanying distribution of sample.
(9) E. G. Pickels in "Methods of Medical Research," Vol. 5, A. C. Corcoran, Ed., Year Book Publishers, Chicago, Ill., 1953.
(10) R. Trautman, *J. Phys. Chem.*, **60**, 1211 (1956).
(11) H. Fujita, *J. Chem. Phys.*, **24**, 1084 (1956).

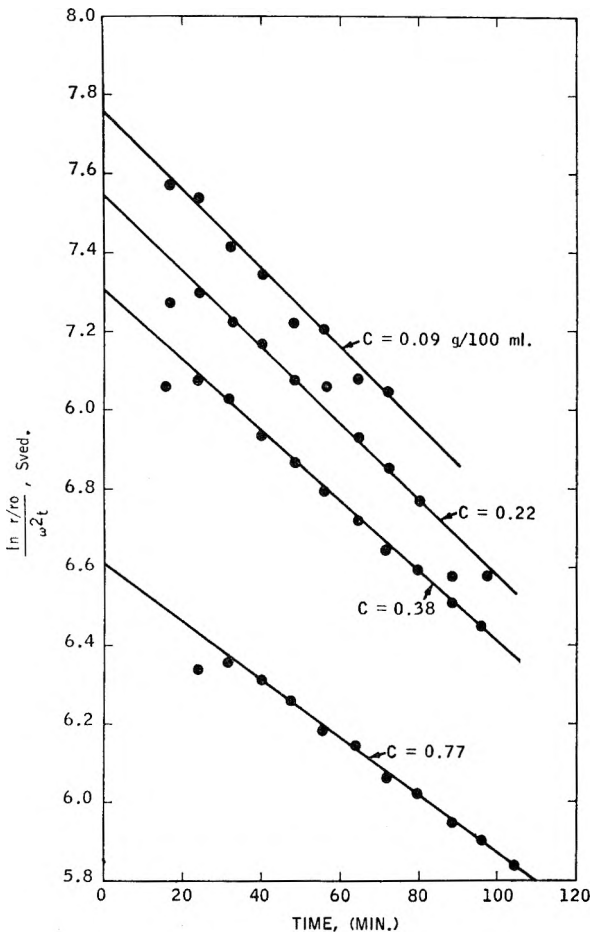

Fig. 1.—Change of apparent sedimentation coefficient with time of centrifugation of polystyrene S-10 in cyclohexane, 35°, at various concentrations; ultracentrifuge speed was 59,780 r.p.m.

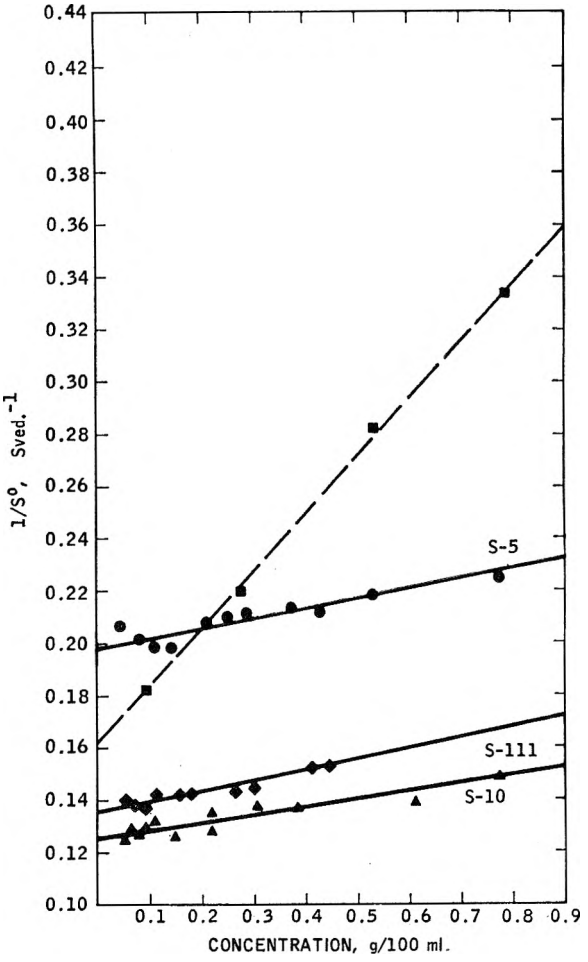

Fig. 2.—Concentration dependence of the pressure corrected sedimentation coefficient: solid lines for polystyrene in cyclohexane at 35°; dotted line for polystyrene S-10 in toluene.

$$S^0 = \frac{S_0^0}{1 + \alpha} = \frac{S_0^0}{1 + kC_0} \qquad (2)$$

where k is a constant and C_0 is the initial concentration. Like the value of α, m, the pressure dependence parameter, varies from experiment to experiment and is defined as

$$m = {}^1/_2\mu\omega^2 r_0^2 \rho_0 \qquad (3)$$

where ρ_0 is the density of the solvent and μ is a constant characteristic of the solute–solvent system.

Values for $S_0^0/(1+\alpha)$ could be obtained by plotting S *vs.* $\omega^2 t$ and extrapolating to zero. However, this method of calculation suffers from a lack of precision for two reasons. First, the experimental setting of zero time suffers from lack of precision. Second, a decrease in precision results from the use of a plot of ln r/r_0 *vs.* $\omega^2 t$ and extrapolating to zero. The difficulty in a procedure of this type has been amply discussed by Baldwin[12] for the case of concentration dependence alone, but the situation in our case is the same. Figure 1 illustrates a plot of S *vs.* $\omega^2 t$, but only serves to illustrate the magnitude of the change in S with time.

(12) R. L. Baldwin, *Biochem. J.*, **65**, 503 (1957).

To increase the precision, we have rewritten eq. 1 in the form

$$\ln r = \ln r_0 + S^0\omega^2 t - B(\omega^2 t)^2 + \cdots \qquad (4)$$

and have calculated the values of S^0 and B by a least squares procedure.

The calculations were carried out, using a program written in Fortran, on an IBM 7090 computer. The values of S^0 and B do not involve the measured value of r_0 and are not influenced by small errors in the absolute value of t. Details of this method of calculation will be presented elsewhere.

Typical results obtained by this procedure are given in Table IIa for cyclohexane solutions and in Table IIb for toluene solutions. As a result of the least squares calculations, we also have obtained values for the standard errors of estimate of S^0 and B. These figures, which give a rough estimate of the precision, also are included in the tables.

If the original assumption regarding the concentration dependence holds, a plot of $1/S^0$ *vs.* C_0 should be linear and independent of velocity. Figure 2 illustrates the concentration dependence and it is apparent that this assumption holds for both solvent systems. Only points obtained at 59,780 and 50,740 r.p.m. are included in Fig. 2;

TABLE IIa

SEDIMENTATION DATA FOR POLYSTYRENE IN CYCLOHEXANE

Sample	Speed, r.p.m.	Concn., g./100 ml.	S^0, sved.	Stand. error	B	Stand. error	$B/(S^0)^2$	m	$\mu \times 10^9$
S-10	59,780	0.78	6.70	0.01	34.6	0.4	0.77	0.80	1.4
		.38	7.27	.01	37.2	.4	.70	.73	1.7
		.15	7.92	.17	51.6	6.2	.82	.83	1.5
		.09	7.66	.10	38.6	4.8	.66	.66	1.2
S-111	59,780	.44	6.51	.01	29.2	0.5	.69	.72	1.3
		.27	7.02	.01	40.1	.4	.81	.83	1.4
		.11	7.05	.02	33.8	.5	.68	.69	1.2
	44,770	.44	6.71	.01	20.6	.5	.46	.51	1.7
		.24	7.06	.01	23.1	.4	.46	.50	1.7
		.11	7.33	.08	27.4	4.0	.51	.52	1.6
	29,500	.44	6.85	.08	10.7	4.7	.23	.30	2.3
		.16	7.30	.21	14.6	1.6	.27	.30	2.3
		.11	7.59	.12	25.8	7.0	.45	.46	3.4

TABLE IIb

SEDIMENTATION DATA FOR POLYSTYRENE IN TOLUENE

Sample	Speed, r.p.m.	Concn., g./100 ml.	S^0, sved.	Stand. error	B	Stand. error	$B/(S^0)^2$	m	$\mu \times 10^9$
S-10	59,780	0.78	3.00	0.02	5.6	0.3	0.63	0.76	1.2
		.53	3.55	.01	7.1	0.1	.56	.69	1.1
		.27	4.55	.05	12.2	1.1	.59	.68	1.1
		.09	5.48	.11	13.4	3.6	.45	.50	0.8

however, values of the sedimentation coefficient of S-111 obtained at lower velocities also fall on the curve shown, within experimental error, but they have been omitted for the sake of clarity.

The values for the sedimentation coefficient at zero concentration and pressure obtained by a least squares analysis of the data given in Fig. 2 are listed in Table III. As has been reported previously,[7,13] the value for k in a poor solvent is much less than that found in a good solvent.

TABLE III

CONCENTRATION DEPENDENCE OF POLYSTYRENE

Solvent	Sample	S_0^0, sved.	k 100 ml./g.
Cyclohexane	S-5	5.01	0.19
	S-111	7.38	.27
	S-10	7.93	.24
Toluene	S-10	6.19	1.37

Once a value of k is known, the slope of eq. 2 can be corrected for radial dilution effects and m or μ can be calculated. The contribution of the concentration dependence to the slope is not large as can be seen from the data given in Tables IIa and IIb. The values for $B/(S^0)^2$ are a function of both pressure and concentration dependence according to eq. 5. These data can be compared with

$$B/(S^0)^2 = \frac{m(2\alpha + 1) - \alpha}{1 + \alpha} \qquad (5)$$

values for m which are characteristic of the pressure dependence alone. Since m varies from experiment to experiment, values of μ calculated according to eq. 3 are also given.

A summary of the values of μ obtained under the varying experimental conditions of molecular weight, solvent, and speed of centrifugation is presented in Table IV. The results for μ were obtained by averaging the data at constant speed, but varying concentrations. The standard deviation, σ, of the data is included in the table to indicate the precision.

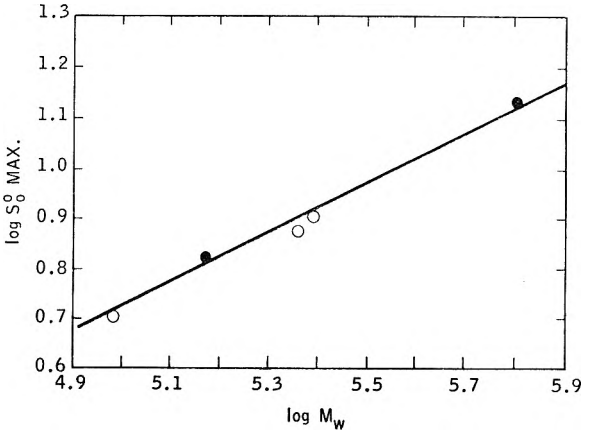

Fig. 3.—Log-log plot of S^0_{0max}, in cyclohexane, *vs.* M_w: filled circles, data of Wales[5]; open circles, this work.

TABLE IV

PRESSURE CORRECTION COEFFICIENT FOR POLYSTYRENE

Solvent	Sample	Speed, r.p.m.	$\mu \times 10^9$	$\sigma \times 10^9$
Toluene	S-10	59,780	1.05	0.13
	S-10	59,780	1.37	.19
	S-5	59,780	1.48	.14
	S-111	59,780	1.33	.09
		50,740	1.54	.14
		44,770	1.60	.14
		39,460	1.68	.14
		35,600	1.78	.32
		29,500	1.78	.86
		24,630	2.25	1.94

(12) H. J. Cantow, *Makromol. Chem.*, **30**, 169 (1959).

Discussion of Results

Using previously derived equations, we have calculated μ, the pressure dependence coefficient, directly from sedimentation measurements. The final values of μ were obtained after correction for concentration dependence, which tends to increase the sedimentation coefficient with time, an effect opposite to that of pressure. The magnitude of the contribution of the concentration dependence to deviation of the sedimentation coefficient at zero time can be seen from a comparison of columns 8 and 9 in Tables IIa and IIb.

In cyclohexane at 35°, a poor solvent, the concentration dependence is small. At a concentration of 0.44 g./100 ml., $B/(S^0)^2$ is only about 4% lower than m, at the highest velocity. The influence of concentration increases, as one would expect, with decreasing speed and with an increase in the value of k. Thus, in cyclohexane at 29,500 r.p.m. and a concentration of 0.44 g./100 ml., m is 13% higher than $B/(S^0)^2$. In toluene, a good solvent, m is greater than $B/(S^0)^2$ by 12% even at top speed.

Although this effect of concentration on the slope is apparent in each individual case, it should be noted that the correction is of the order of the precision of the determination. In fact, at high speed, where the pressure correction is most important, the correction for concentration can be ignored, within experimental error, for the poor solvent system and probably in the good solvent, as well.

If there is any effect of speed of centrifugation, or, to a limited extent, molecular weight on μ, the data presented in Table IV do not show any indication of a trend. It is probably safe to conclude from our results that the values of μ obtained for polystyrene in cyclohexane agree within experimental precision regardless of the conditions of speed or molecular weight.

Although the definition[3] of μ has been given in terms of the variation of the frictional coefficient with pressure, it has been the practice[1] to use the coefficient describing the pressure change of the solvent viscosity in its place. Following this procedure and using the values for this coefficient and the compressibilities of the solvent summarized by Baldwin and van Holde,[14] and a value for the compressibility of polystyrene found by Cheng and Schachman,[15] μ has been calculated.

For the polystyrene–toluene system, a value of $\mu = 1.0 \times 10^{-9}$ was calculated and for polystyrene–cyclohexane, $\mu = 2 \times 10^{-9}$. The value which Wales found[5] by his curve fitting technique for polystyrene–cyclohexane was $\mu = 2.2 \times 10^{-9}$. In light of the precision of our data, the agreement may be considered to be very good.

The compatibility of our approach with that of Wales[5] is shown by plotting log $S_0{}^0{}_{max}$ obtained by both techniques *vs.* the log M_w, as shown in Fig. 3. Even though Wales' results were obtained at 34°, Fig. 3 will serve to illustrate that the two methods appear to be consistent.

Finally, it can be seen from eq. 4 that a knowledge of μ is not needed to obtain the sedimentation coefficient independent of pressure. However, knowledge of μ is necessary to calculate S^0 at some point in the cell, such as in boundary spreading analysis. In such a case, μ can be obtained directly from the ultracentrifuge experiment with sufficient accuracy to correct the data for the effects of pressure.

DISCUSSION

R. TRAUTMAN (Plum Island Animal Disease Laboratory, USDA).—Did the true zero sedimentation time show a systematic deviation from the time at $^2/_3$ operating speed? Would this be less in a non-pressure dependent system?

I. H. BILLICK.—The zero time correction was randomly scattered both positively and negatively about the time at $^2/_3$ operating speed. For the most part the correction was less than 1 min. I doubt that the fact the system is pressure dependent would have any effect.

(14) R. L. Baldwin and K. E. van Holde, *Fortschr. Hochpolymer. Forsch.*, **1**, 451 (1960).

(15) P. Y. Cheng and H. K. Schachman, *J. Am. Chem. Soc.*, **77**, 1498 (1955).

FLOTATION EQUILIBRIUM IN THE ULTRACENTRIFUGE

BY J. A. FAUCHER AND G. KEGELES

Union Carbide Chemicals Co., South Charleston, W. Va. and Clark University, Worcester, Mass.

Received March 5, 1962

For the case of flotation equilibrium in the ultracentrifuge it is shown that the dc/dx curve has a maximum which does not occur in sedimentation equilibrium. The existence of such a maximum allows a new method of calculating the molecular weight. Calculations for a monodisperse system indicate that well defined peaks are best formed at speeds of 10,000 r.p.m. or greater and occur at distances of 0 to 2 cm. from the axis of rotation. For polydisperse systems the peak is related to a molecular weight which lies between the z and $z + 1$ averages when an extrapolation to infinite speed is made. It should be noted that the peaks described here are not observable in conventional ultracentrifuges, which are limited to the range of 5 to 7 cm. from the rotational axis. In order to perform experiments utilizing such peaks, it will be necessary to modify rather radically the existing commercial instruments.

Introduction

The theory and operation of the ultracentrifuge have been so far almost entirely devoted to the case in which the dissolved substance is denser than the solvent and consequently sinks upon application of a strong centrifugal field. Recently, with the advent of interest in such light polymers as polyethylene, it has become virtually necessary to carry out ultracentrifuge experiments in which the solute floats rather than sinks.

At first sight, the analysis of such a situation should involve no new points of view but only minor and obvious changes in the mathematical apparatus which is used to calculate molecular weights. However, in closely examining this case we have found that there is indeed a fundamental difference, one which appears to allow a new method for calculating the molecular weight, both in mono- and polydisperse systems. This difference lies in the character of the dc/dx *vs.* x curves for the two cases.

Theory.—If we consider the process of sedimentation equilibrium, in which the speed is kept low enough so that a separate peak is not formed, the observed schlieren pattern is given by the solid line in Fig. 1. (Actually with schlieren optics one sees dn/dx *vs.* x, but we may assume $dn/dx = k\, dc/dx$.) With a conventional ultracentrifuge we can observe only a limited extent of the x values—generally 5.7 to 7.2 cm.—but it is clear that the over-all dc/dx curve is a monotonically increasing function of x, as shown by the dotted portion of Fig. 1.

In the case of "flotation equilibrium" shown in Fig. 2, the observed dc/dx curve (solid line) is the reverse of that in Fig. 1. (Since c is decreasing with increasing x it is convenient to plot $-dc/dx$ here. Often k is found to be negative for such systems, so that dn/dx remains positive and directly observable with no alteration of the optics.) However, from eq. 1 below it is evident that dc/dx must approach zero at the center of rotation. Thus the complete $(-dc/dx)$ curve must look like the dotted line of Fig. 2. The important point is that in this case there must be a maximum in the $-dc/dx$ function, *i.e.*, a place where d^2c/dx^2 is zero. This fact, which does not appear to have been noted explicitly before, is the basis for the following development.

We start with the well known equation of sedimentation equilibrium for a single solute species in an ideal solution

$$\frac{dc_i}{dx} = \frac{M_i c_i (1 - \bar{V}\rho)\omega^2 x}{RT} \tag{1}$$

where the symbols have their customary meaning. This is applicable to both sedimentation and flotation. Differentiating both sides with respect to x we have

$$\frac{d^2c_i}{dx^2} = \frac{M_i(1 - \bar{V}\rho)\omega^2}{RT}\left[c_i + x\left(\frac{dc_i}{dx}\right)\right] \tag{2}$$

Substitute dc_i/dx from (1) into (2)

$$\frac{d^2c_i}{dx^2} = \frac{M_i c_i(1 - \bar{V}\rho)\omega^2}{RT}\left[1 + M_i\frac{(1 - \bar{V}\rho)\omega^2 x^2}{RT}\right] \tag{3}$$

From the argument above—see Fig. 2—there is a point, x^*, on the dc/dx curve where d^2c/dx^2 is zero. Consequently, we may set eq. 3 equal to zero at that point, obtaining

$$M_i = \frac{-RT}{(1 - \bar{V}\rho)\omega^2(x^*)^2} \tag{4}$$

This is the new method for calculating molecular weight mentioned in the Introduction. We see that in principle only a single measurement of the appropriate x value is necessary to determine the molecular weight of the solute.

In general, peaks in the dc/dx curve are not observable in the conventional ultracentrifuge because they are formed rather close to the center of rotation. However, it is easy to calculate the shape of the schlieren pattern, at least for a monodisperse solute. The equation for the equilibrium concentration at any point is given by the relation (ref. 1, eq. 4)

$$c(x) = \frac{AMc_0(x_b^2 - x_a^2)\exp[-AM(x_b^2 - x^2)]}{1 - \exp[-AM(x_b^2 - x_a^2]} \tag{5}$$

where c_0 is the initial concentration, x_b and x_a are, respectively, the bottom and the meniscus positions, and $A = (1 - \bar{V}\rho)\omega^2/2RT$. The dc/dx function is obtained by differentiation of (5)

$$\frac{dc}{dx} = \frac{2A^2xM^2c_0(x_b^2 - x_a^2)\exp[-AM(x_b^2 - x^2)]}{1 - \exp[-AM(x_b^2 - x_a^2)]} \tag{6}$$

As an example we shall consider a hypothetical polymer whose molecular weight is 10,000, $(1 - \bar{V}\rho) = -0.746$, and $T = 373°K$. These numbers are roughly those for the flotation of polyethylene in bromobenzene. Further, we shall use an imaginary cell whose bottom is at $x_b = 10$ cm. and the meniscus on the center of rotation, $x_a = 0$. Figure 3 shows the form of dc/dx curves for $R/\omega^2 = 200$, 100, and 50, corresponding to about 6200, 8700, and 12,300 r.p.m. It is apparent that the peak becomes larger and sharper as the speed increases. In this process, however, it moves very close to the center of rotation, being at 1.5 cm. for 12,300 r.p.m.

So far we have considered only a monodisperse system. It is of interest to generalize to the polydisperse case by summing eq. 3 over all species.

$$\sum_i \frac{d^2c_i}{dx_i^2} = \frac{d^2c}{dx^2} = \frac{(1 - \bar{V}\rho)\omega^2}{RT} \left\{ \sum_i M_i c_i + \frac{x^2(1 - \bar{V}\rho)\omega^2}{RT} \sum_i M_i^2 c_i \right\} \quad (7)$$

Now, in general, although each species has its own point, x^* where d^2c_i/dx^2 is zero, nevertheless for a reasonably sharp distribution one may expect that the summation of the $(-dc_i/dx)$ curves will show a single peak. At this point d^2c/dx^2 will be zero and the equation holds

$$\frac{\sum_i M_i^2 c_i(x^*)}{\sum_i M_i c_i(x^*)} = \frac{-RT}{(1 - \bar{V}\rho)\omega^2(x^*)^2} = \bar{M}_{zx^*} \quad (8)$$

Thus the position of the peak leads to the so-called z-average of the (redistributed) solute at the particular point x^*. Actually eq. 8 is implicit in the classical paper of Lansing and Kraemer.[1] Their eq. 12 in our symbols reads

$$\bar{M}_{zx} = \frac{d^2c}{dx^2} \left[\frac{RT}{(1 - \bar{V}\rho)\omega^2 x \dfrac{dc}{dx}} \right] - \frac{RT}{(1 - \bar{V}\rho)\omega^2 x^2} \quad (9)$$

At the point x^*, where d^2c/dx^2 is zero, this simplifies at once to give (8).

Although the $\bar{M}_{zx^*}$ given by (8) is not an average of the original sample, nevertheless the existence of a peak permits a very simple determination of $\bar{M}_z$ of the redistributed material. An increase of speed causes the position of the peak to move closer to the center of rotation. In the limit, as x^* approaches zero, $\bar{M}_{zx^*}$ can be related to the original sample in the following way.

We start by assuming a continuous distribution of molecular weights, $f(M)$. For this case it is easily shown[2] that the concentration at any point in the cell is given by

$$c(x) = c_0 A(x_b^2 - x_a^2) \int_0^\infty \frac{M f(M) \exp[-MA(x_b^2 - x^2)]dM}{1 - \exp[-MA(x_b^2 - x_a^2)]} \quad (10)$$

(1) W. D. Lansing and E. O. Kraemer, *J. Am. Chem. Soc.*, **57**, 1369 (1935).

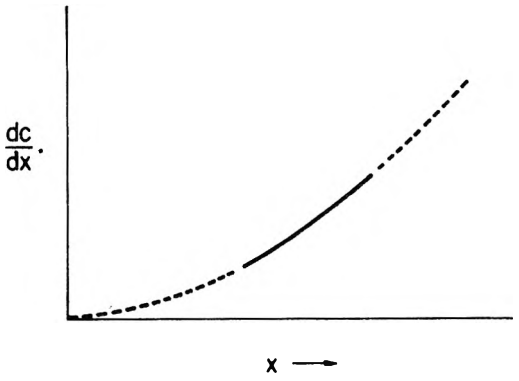

Fig. 1.—Schlieren pattern for sedimentation equilibrium.

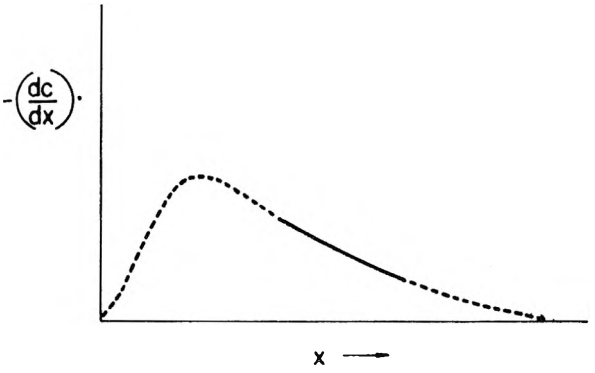

Fig. 2.—Schlieren pattern for flotation equilibrium.

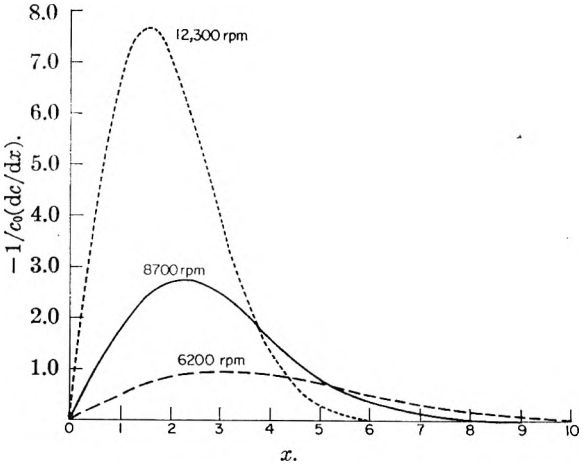

Fig. 3.—Flotation of a species with molecular weight of 10,000 at different speeds.

This, of course, is just the polydisperse analogy of eq. 5. The dc/dx and d^2c/dx^2 functions are obtained by differentiation of eq. 10. When they are substituted into (9) we obtain

$$M_{zx} = \frac{\int_0^\infty \frac{M^3 f(M) \exp[-MA(x_b^2 - x^2)]dM}{1 - \exp[-MA(x_b^2 - x_a^2)]}}{\int_0^\infty \frac{M^2 f(M) \exp[-MA(x_b^2 - x^2)]dM}{1 - \exp[-MA(x_b^2 - x_a^2)]}} \quad (11)$$

This holds for any point in the cell. We now

(2) J. W. Williams, K. E. Van Holde, and R. L. Baldwin, *Chem. Rev.*, **58**, 715 (1958), see eq. 91.

take x_a to be zero, multiply numerator and denominator of each integrand by $\exp(MAx_b^2)$ and consider the point, x^*, where the peak is formed

$$M_{zx^*} = \frac{\int_0^\infty \frac{M^3 f(M)\ \exp[MA(x^*)^2]\ \mathrm{d}M}{\exp(MAx_b^2) - 1}}{\int_0^\infty \frac{M^2 f(M)\ \exp[MA(x^*)^2]\ \mathrm{d}M}{\exp(MAx_b^2) - 1}} = \frac{-1}{2A(x^*)^2} \quad (12)$$

To make further progress we must now consider a specific distribution function for $f(M)$. For this purpose let us take the so-called exponential distribution[3]

$$f(M) = \left(\frac{k}{M_0}\right)^{k+1} \frac{M^k}{k!} \exp(-kM/M_0)$$

which is normalized so that $\int_0^\infty f(M)\mathrm{d}M = 1$. The integrals in (12) now can be done explicitly

$$\bar{M}_{zx^*} = \frac{-1}{2A(x^*)^2} = \frac{(3+k)}{(-Ax_b^2)} \frac{\zeta(r+1, s)}{\zeta(r, s)} \quad (13)$$

where for simplicity we have written $r = 3 + k$ and $s = [-A(x^*)^2 + k/M_0]/-Ax_b^2$ and $\zeta(r, s) = \sum_{m=0}^{\infty} \frac{1}{(m+s)^r}$ is the generalized Riemann zeta function.[4] As the speed of rotation increases indefinitely x^* approaches zero while $-A$ approaches infinity, but the product $-A(x^*)^2$ approaches a limit. We obtain

$$\lim_{x^*\to 0} \bar{M}_{zx^*} = \lim_{x^*\to 0}\left[\frac{-1}{2A(x^*)^2}\right] = \lim_{x^*\to 0} \frac{(3+k)}{-A(x^*)^2 + \frac{k}{M_0}} \quad (14)$$

since as $s \to 0$ $\zeta(r, s) \sim s^{-r}$. Thus it is clear that the product $-A(x^*)^2$ approaches the limit $k/(5 + 2k)M_0$, and hence

$$\lim_{x^*\to 0} \bar{M}_{zx^*} = M_0\left(1 + \frac{5}{2}k\right) \quad (15)$$

With the usual definitions

$$\bar{M}_n = \int_0^\infty f(M)\mathrm{d}M / \int_0^\infty \frac{f(M)}{M}\,\mathrm{d}M$$

$$\bar{M}_w = \int_0^\infty Mf(M)\mathrm{d}M / \int_0^\infty f(M)\ \mathrm{d}M, \text{ etc.},$$

it is easily shown that for an exponential distribution

$$\bar{M}_w = \left(1 + \frac{1}{k}\right) M_0,\ \bar{M}_z = \left(1 + \frac{2}{k}\right) M_0, \text{ and } \bar{M}_{z+1} = \left(1 + \frac{3}{k}\right) M_0$$

Hence we see that eq. 15 describes a sort of $z + {}^1/_2$ average defined by

$$\bar{M}_{zx^*} = \bar{M}_{z+1/2} = \frac{\int_0^\infty M^{3/2} f(M)\ \mathrm{d}M}{\int_0^\infty M^{1/2} f(M)\ \mathrm{d}M}$$

Although the limit of $\bar{M}_{zx}^*$ as $x^* \to 0$ is equal to the $z + {}^1/_2$ average for any exponential distribution, this does not seem to be exact for all other distributions. However, numerous sample calculations have indicated that for other distributions this relation is very nearly true. It thus appears that a determination of the limiting value of $\bar{M}_{zx}^*$ should be a rather sensitive test of polydispersity in a whole polymer or polymer fraction.

In conclusion, we should like to note that although we have reason to be confident of the calculations made here, it must be emphasized that the peaks described have not yet been observed experimentally. The most compelling reason for this is that the usual commercial centrifuges do not permit data to be obtained at x values so near to the center of rotation. This appears to be purely an experimental problem. Machines to observe these peaks undoubtedly can be built if there is enough motivation to do so. We believe that the simplicity of determining $\bar{M}(x^*)$ or $\bar{M}_{zx}^*$ from measurements of the x position alone should provide such motivation. There remains, of course, a further practical problem in that it may take some time for the equilibrium peak to form, particularly in a region where the field is rather weak.[5]

(3) D. S. Villars, *J. Polymer Sci.*, **21**, 265 (1956).

(4) E. T. Whittaker and G. N. Watson, "A Course of Modern Analysis," Cambridge University Press, 1950, Chapter XIII.

(5) For non-ideal systems all these conclusions imply extrapolation to very low concentrations. Experimentally, when the shape of the normalized curve, Fig. 3, becomes independent of concentration at a given speed and temperature, non-ideality has been extrapolated out.

MOLECULAR WEIGHT DETERMINATIONS WITH A MAGNETICALLY SUPPORTED ULTRACENTRIFUGE[1]

BY P. E. HEXNER, R. D. BOYLE, AND J. W. BEAMS

Department of Physics, University of Virginia, Charlottesville, Virginia

Received March 1, 1962

A magnetically suspended ultracentrifuge has been used to determine the molecular weights and related properties of various substances. Techniques are described which make this apparatus particularly suitable for equilibrium studies of macromolecules in the 10^5 to 10^7 molecular weight range.

The equilibrium method is generally considered to be the most reliable of the several centrifuge techniques for molecular weight determinations and related problems because it is based upon rigorous equilibrium thermodynamic theory.[2] In fact, in the case of large macromolecules of unknown shapes, particularly with synthetic polymers, the equilibrium method is probably the only centrifuge technique which yields direct meaningful results. The principal practical disadvantage has been the long centrifuging time required for equilibrium to take place. However, in recent years this problem essentially has been solved through the use of one or a combination of three techniques for effectively reducing the equilibrium time.

The first is the use of short ultracentrifuge cell columns as discussed by Van Holde and Baldwin[3] and illustrated by Yphantis[4] and others. In general the time required to reach equilibrium is proportional to the length of the column squared. Secondly, a considerable decrease in the time required to reach equilibrium is found both experimentally[5,6] and theoretically[7] in the case where the rotor speed is very slowly decreasing. Thirdly, the introduction of a predetermined step function reduction in angular speed was found to reduce greatly the centrifuging time without sacrifice of accuracy.[8]

Experimental

An improved magnetically suspended ultracentrifuge has been described in detail elsewhere,[5,6] so only its essential characteristics need be mentioned here. The rotor is magnetically suspended in a vacuum and "coasts" freely during the sedimentation experiments. It loses less than one part in 10^8 of its speed per second when the pressure surrounding the rotor is between 10^{-6} and 10^{-7} mm. For rotor speeds of 100 r.p.s. as used in some equilibrium centrifugation, this amounts to less than $^1/_{10}$ r.p.s. per day. The rotor may be accelerated or decelerated during an experiment by a detachable high speed electric motor. The rotor is free of all hunting, and its speed is measured routinely to better than one part in 10^5. The rotor temperature is constant and known to at least one part in 10^4. The centrifuge may be used either for sedimentation equilibrium or velocity of sedimentation experiments, although its principal use has been for the former. The maximum speed is set only by the strength of the rotor and the minimum can be made as small as desired, since stability is independent of the speed.

One type of ultracentrifuge cell used is shown in Fig. 1. It contains two sector-shaped compartments, has a depth of 1 cm., and is 2.7 cm. in diameter. Circular shaped cells have also been used in this Laboratory as well as circular and sector-shaped multichannel cells which permit multiple determinations during the course of one experiment. The one-piece cells are made of either anodized duralumin or Kel-F. It is to be noted that pressure is applied to the quartz or glass windows normally by five pressure screws, which eliminates distortion of the windows often found when they are tightened using screw caps. Although it is much easier to construct circular or rectangular rather than sector-shaped compartments and the equilibrium concentration distribution is theoretically independent of the shape of the cell, the sector-shaped compartments have been found to be much preferable. This probably is due to convection currents set up in the non-sector-shaped cells which are easily observed with the associated optical system.

The sedimentation in the cell is measured by a Jamin type interferometer which is used with parallel light as shown in Fig. 2. Two light sources at equal optical distances from the lens L_1 can be alternated during an experiment by placing the mirror M_w into or out of the beam. One is a 1500-watt projection lamp which serves as a white light source and the other a 1200-watt mercury arc lamp which is used with a filter as a monochromatic light source. The lens L_1 focuses the light on the "chopper" slit K′ mounted in the rotor with its length along the radius. The light is then focused by the lens L_2 on a small hole S_1. This provides a small point source. The lens L_3 renders the light parallel which is reflected from M_4, limited by the slit S_2 before incidence upon the first Jamin plate I_1. The Jamin plate splits the light into two parallel displaced beams. Each of the beams passes through a sector compartment of a compensating ultracentrifuge cell K_1, then through a compartment of an identical cell K_2 mounted in the rotor, and impinges on a second Jamin plate I_2 where the two beams are reunited. I_1 and I_2 are matched glass interferometer plates 30% silvered on the front and 100% silvered on the back. The light is then focused by L_4 on spectroscopic plates which are sensitive in the spectral region used. Each of the two identical cells, K_1 and K_2, contains two sector shaped vacuum tight compartments side by side, one of which contains the solvent and the other the solution. The cells are so placed that the light beam which traverses the compartment in K_1 containing the solvent passes through the compartment in K_2 containing the solution and *vice-versa*.

The optical system is adjusted, while the rotor is at rest, using the monochromatic light source. The fringes are accurately aligned parallel to the radius of the cell and made very broad. White light is then substituted for the monochromatic light and the Jamin plates are further adjusted to give a single broad white light fringe which covers the entire field of view on the plate P. This is possible because the optical paths of the two beams between I_1 and I_2 are equal. The centrifuge is then started and the concentration gradient produced in the compartment of K_2 containing the solution will give rise to fringes which lie along lines of constant radial distance if the adjustment of I_1 and I_2 is done properly. These fringes and the cell K_2 are in accurate focus on the photographic plate P; *i.e.*, there is a point to point correspondence between cell and fringes which immediately shows any convection in the cell if it exists. The change in con-

(1) Supported by N. I. H. Grant and Navy Bureau of Weapons Grant.

(2) (a) T. Svedberg and K. O. Pedersen, "The Ultracentrifuge," Oxford University Press, New York, N. Y., 1940; (b) H. K. Schachman, "Ultracentrifugation in Biochemistry," Academic Press, New York, N. Y., 1959.

(3) K. E. Van Holde and R. L. Baldwin, *J. Phys. Chem.*, **62**, 734 (1958).

(4) D. A. Yphantis, *Ann. N. Y. Acad. Sci.*, **88**, 586 (1960).

(5) J. W. Beams, R. D. Boyle, and P. E. Hexner, *J. Polymer Sci.*, **57**, 161 (1962).

(6) J. W. Beams, R. D. Boyle, and P. E. Hexner, *Rev. Sci. Instr.*, **32**, 645 (1961).

(7) W. J. Archbald, private communication.

(8) P. E. Hexner, L. E. Radford, and J. W. Beams, *Proc. Natl. Acad. Sci. U. S.*, **47**, 1848 (1961).

centration Δc in the cell is given by the relation $\Delta c = (\lambda/KL)\Delta n$ where $K = \Delta u/\Delta c$, L is the thickness of the cell, λ is the wave length of the light, Δu the change in refractive index of the solution under test, and Δn is the number of fringes produced on the plate. Also, $\lambda \Delta n = L \Delta u$. K is measured outside the centrifuge by a differential refractometer or a Michelson type interferometer. The position of the fringes on the plate P are measured by a comparator and a special microphotometer. From these measurements of the positions of the fringes produced by monochromatic light, the change in concentration between any two points in the cell is determined. The position of the central white light fringe gives the position in the cell where the concentration is the same as the initial uniform concentration c_0 in the cell before the centrifuging is started. Consequently, with the known value of c_0, the concentration c_r at every point in the cell can be determined. Also, it should be noted that with this optical system little or no extrapolation to the ends of the cell is required.

When equilibrium is obtained in the centrifuge cell K_2, for dilute solutions, the molecular weight M is given by the relation

$$M = \frac{2RT \ln (c_2 f_2/c_1 f_1)}{4\pi^2 N^2 (1 - \bar{v}\rho)(r_2^2 - r_1^2)} \qquad (1)$$

where c_1 and c_2 are the concentrations at the radial distances r_1 and r_2 in the ultracentrifuge cell, T is the absolute temperature, R is the gas constant, f_1 and f_2 are activity coefficients, ρ is the density of the solution, $\bar{v}$ is the partial specific volume, and N is the number of r.p.s. For an ideal monodisperse dilute solution eq. 1 becomes

$$c_r = \frac{c_0 AM(b^2 - a^2) \exp\langle -AM(b^2 - r^2)\rangle}{1 - \exp\langle -AM(b^2 - a^2)\rangle} \qquad (2)$$

where $A = (1 - \bar{V}\rho)\, 4\pi^2 N^2/2RT$, b is the peripheral radius of the cell, and a is the radius of the top or meniscus in the cell. Also

$$\int_a^b c_r r \, dr = c_0 \int_a^b r \, dr$$

Consequently, a plot of ln c *vs.* r^2 gives a straight line for an ideal monodisperse solution at equilibrium. In general, if the curve is concave upward, polydispersity is indicated, and if concave downward, the solution is probably non-ideal. From the slope of this line the value of the molecular weight can be determined. At the radial distance where $c_r = c_0$, eq. 2 may be written

$$1 - \exp\langle -AM(b^2 - a^2)\rangle = AM(b^2 - a^2) \exp\langle -AM(b^2 - r^2)\rangle$$

and the molecular weight is obtained[9] by solving for M. This, of course, does not require waiting for equilibrium to be established and can be carried out in a short centrifuging time. The position of the "hinge point" can be precisely determined from two photographs, one with white light and one with monochromatic light.[5,6] Also, it might be noted that this "hinge point" can be determined by photographs taken with two monochromatic, widely separated wave lengths such as 5460.74 and 4358.35 Å of the mercury arcs, or the ruby Laser light 6943 Å. and either of the mercury lines. Incidentally, the pulsed Laser may be used without the chopper slit.

The above measurements give c_r as a function of r. From these values $\partial c/\partial r$ can be derived. On the other hand, it sometimes is desirable to measure $\partial c/\partial r$ directly. This also can be carried out with the interferometer shown in Fig. 2. It will be observed that the light beam is incident on the first Jamin mirror I_1 at approximately 45°. This is done to get a proper separation of the two beams which pass through the two compartments in K_1 and K_2. On the other hand, if the light is incident normally on I_1 then the beams are not separated. Consequently, the beams may be made to have any separation from zero to at least the distance between the centers of the two cell compartments by varying the angle of incidence on I_1 and I_2 accordingly. If now the distance between the beams is reduced and the plates I_1 and I_2 oriented so that the two beams are separated in a direction parallel to the radius rather than perpendicular to the radius as in Fig. 2, then one sees in the field of view images of the two compartments of K_2. With proper adjustment, fringes will appear in the image of the compartment containing the solution if a concentration gradient exists. The number and position of these fringes make it possible to determine $\partial c/\partial r$ directly. No fringes should appear in the image of the compartment containing the solvent unless distortions in the windows occur so that this image serves as a control.

(9) W. J. Archibald, *J. Phys. Chem.*, **51**, 1602 (1947).

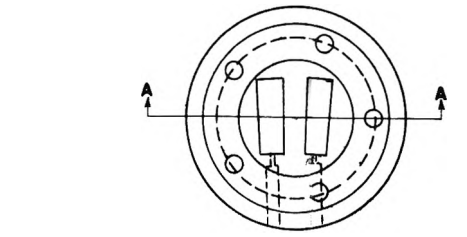

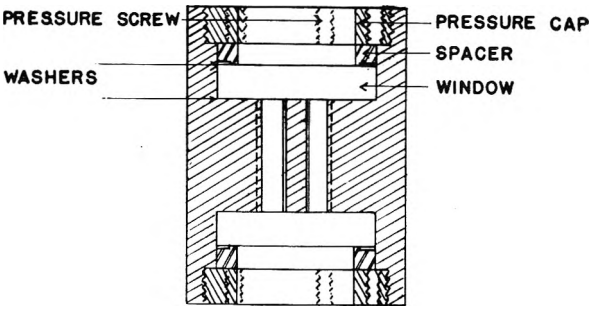

Fig. 1.—Sector-shaped cell.

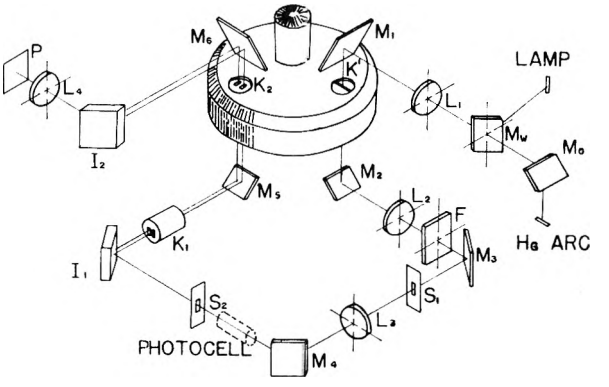

Fig. 2.—Optical method of measuring sedimentation.

Results and Discussion

The method of shortening the time required to attain sedimentation equilibrium by a predetermined reduction in angular speed early in an experiment has proven to be most useful in recent experiments with very large macromolecules. As reported previously,[8] a ribonuclease molecular weight determination can be reduced with no apparent loss of precision from 14 to approximately 2 hr. with a 3 mm. cell The real value of the method becomes more apparent with two specific examples.

An 18S protein, extracted from green leaves of bean plants, having a molecular weight of ap-

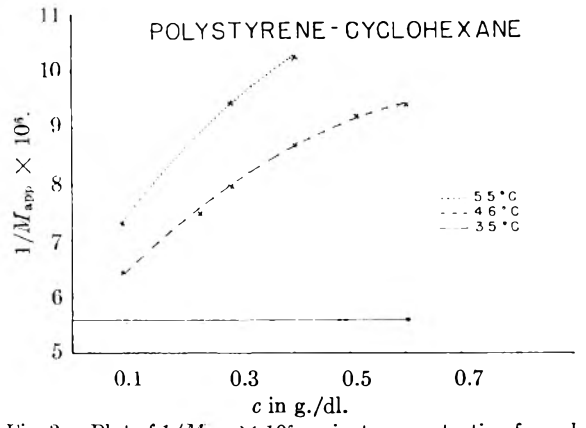

Fig. 3.—Plot of $1/M_{app} \times 10^6$ against concentration for polystyrene (M_w = 180,000) in cyclohexane at 35, 46, and 55°.

proximately 2.75×10^5, requires a sedimentation equilibrium time on the order of 5 days with a 3 mm. cell, at maximum permissible speeds. Even though the magnetically suspended ultracentrifuge is well suited for experiments of this duration, the sample both dissociates and aggregates after prolonged exposure at temperatures of interest. Due to the polydispersity of the sample, the Archibald approach to equilibrium method[9] yields inconclusive results. By reducing the rotor speed from 100 to 80 r.p.s., equilibrium is achieved in 10 hr.

A sample of polystyrene with a weight average molecular weight of 3.5×10^6 in cyclohexane at 35° requires 14 days to reach equilibrium in a 3 mm. cell at the maximum permissible speed of 28 r.p.s. Again, the magnetically suspended ultracentrifuge is quite capable of operating for this duration, but a 14 day experiment is at best inconvenient. Utilizing the "cut back" method from 28 to 20 r.p.s., excellent results were obtained in approximately two days. This sample also illustrates the stability of the rotor suspended in a vacuum of 10^{-6} Torr by the magnetic field. No hunting of the rotor was observed at these speeds and excellent photographs were obtained at 20 r.p.s., a speed at which stable operation of a mechanically linked rotor is very difficult.

A well fractionated, essentially monodisperse sample of polystyrene, kindly furnished by Dr. D. McIntyre of the National Bureau of Standards, has been used extensively with this apparatus to determine the accuracy of the "cut back" method in the 10^5 molecular weight range and to study the behavior of polymers in solutions at temperatures other than theta.[10] Table I shows the results obtained at 35°, the theta temperature in cyclohexane, the first experiment listed being a "true" equilibrium run of 36 hr. duration. The other results were obtained using the "cut back" method in approximately 5 hr. Figure 3 shows results obtained at 46 and 55°.

The purpose of the temperature variation experiments is to determine whether it is possible to find the true molecular weight of a polymer by extrapolation to infinite dilution of data obtained

(10) P. J. Flory, "Principles of Polymer Chemistry," Cornell University Press, Ithaca, N. Y., 1953.

TABLE I

Concn., g./dl.	M_w
0.4805	179,000
.0903	180,500
.2312	180,100
.4935	179,200
.6110	179,500

at temperatures other than theta.[11,12] Figure 3 indicates that the answer to the question depends, at least in the case of a relatively low molecular weight and essentially monodisperse polymer, on the deviation from theta temperature and on the accuracy desired. Data with this sample in benzene at room temperatures confirm the above conclusions. Experiments on a higher molecular weight polymer with a greater M_z/M_w ratio are now being conducted.

Comparative measurements on the above sample have been made,[13] using an L.K.B. Produkter ultracentrifuge with a Lamm scale optical system at the National Bureau of Standards, and a Spinco Model E ultracentrifuge with a Raleigh interferometric system at the Department of Biochemistry of the University of Virginia School of Medicine. The results are very encouraging although the quantitative agreement of the molecular weights is not exact. The dispersion of the numerical results with the magnetically suspended ultracentrifuge is much smaller than with the other instruments. This is probably due to the difficulty of measuring the concentration gradient near the ends of the cell with the Lamm scale optical system in the case of the L.K.B. centrifuge, and to variations in speed and relative instability of the rotor at low speeds with the particular Model E used. Only constant angular speed equilibrium runs were performed with the L.K.B. The "cut back" procedure was attempted with the Model E and, although relatively successful at higher speeds with samples such as ribonuclease, did not significantly reduce the equilibrium time with this sample due to stirring during "cut back" at low speeds.

The precision of the magnetically suspended ultracentrifuge has been coupled with a Burroughs 205 digital computer to gain valuable information on the molecular weight distribution in polydisperse samples. This essentially is a self-consistent guessing procedure made feasible by the rapidity of computer calculations. In a system of n components, the concentration in the cell at some point r from the center of rotation at time t is the sum of the concentrations of the n components. Assuming the same buoyancy and specific refractive increments for all components, this can be written

$$c(r,t) = \sum_{i=1}^{n} c_i(r,t) = \sum_{i=1}^{n} A_i e^{\lambda_i r^2} + \sum_{i=1}^{n} F_i(r,t)$$

where $F_i(r,t) = 0$ at $t = \infty$.

(11) L. Mandelkern, L. C. Williams, and S. G. Weissberg, *J. Phys. Chem.*, **61**, 271 (1957).

(12) H. Fujita, A. M. Linklater, and J. W. Williams, *J. Am. Chem. Soc.*, **82**, 379 (1960).

(13) P. E. Hexner, H. G. Kim, F. N. Weber, D. McIntyre, L. C. Williams, R. F. Bunting, and D. W. Kupke, in press.

Since the only unknowns in the above equations are c_{0i} and M_i, both contained in A_i, λ_i, and F_i, educated guesses for the unknowns are self-consistently programmed into the computer until the results agree with the experimental data. If an adequate supply of sample is available, a series of equilibrium runs is made to ensure uniqueness and to preclude the use of the time dependent term in the above equation. Excellent results have been obtained with this method on known mixtures and with proteins which have a tendency to aggregate.

In the case where n is very large, the above method is not practical and the problem reduces to solving an integral equation. A formal solution has been found, but practicability awaits a sample with a known distribution.

The magnetically suspended ultracentrifuge has yielded excellent results with low molecular weight compounds such as sucrose, raffinose, ribonuclease, insulin, lysozyme, and others.[5,6,14] Its greatest potential, however, seems to be in the field of large macromolecules of unknown shapes due to the extreme stability of the rotor at very low speeds and the inherent advantages of the associated optical system.

(14) R. D. Boyle and P. E. Hexner, *Science*, **134**, 339 (1961).

Acknowledgments.—The authors are greatly indebted to H. G. Kim (American Machine and Foundry Fellow) and F. N. Weber, who participated in most of the experiments, and to R. F. Bunting, D. W. Kupke, and D. McIntyre for valuable advice. F. Linke, P. Sommer, and their co-workers constructed most of the apparatus.

DISCUSSION

L. GROPPER (Beckman Instruments, Inc.)—At low speed when the cell is tilted to offset gravity in the downward direction, are the optics tilted also?

P. E. HEXNER.—The mirrors directly below and above the cell are tilted proportionately to ensure that the light passes through the cell normal to the direction of the resultant forces.

R. TRAUTMAN (Plum Island Animal Disease Laboratory, USDA).—Is it better to tilt the cell or solve the equations for equilibrium in a gravitational and centrifugal field?

P. E. HEXNER.—The purpose of tilting the cell is to prevent convection due to the non-radiality of the resultant forces on the particles. The equations must be solved in two dimensions in this case.

NORMAN G. ANDERSON (Oak Ridge National Laboratory).—You are very close to the point where the centrifuge can be eliminated and gravity itself used to produce the gradient.

P. E. HEXNER.—Since this is a very interesting and stimulating field we certainly hope that the centrifuge will not be eliminated. For large enough particles gravity can, of course, be used to produce a concentration gradient.

A STUDY BY INTERFERENCE OPTICS OF SEDIMENTATION IN SHORT COLUMNS[1]

By F. E. LaBar and R. L. Baldwin

Department of Biochemistry, Stanford University School of Medicine, Palo Alto, California

Received March 10, 1962

The use of interference optics to study equilibrium sedimentation in short columns is reported here. A standard system (sucrose in water) has been used to give a direct estimate of the accuracy of these experiments. In measurements at four different speeds the largest discrepancy found between theory and experiment corresponds to a difference of 0.16 fringe out of a total as large as 50 fringes. Methods of computing the results are discussed and an exact equation for equilibrium sedimentation is given for the case, applicable to sucrose, in which the apparent molecular weight is a linear function of concentration. The method for computing D from the rate of approach to equilibrium, which is based on the Mason–Weaver equation, has been reinvestigated by use of the more exact equation of Nazarian and the correction terms have been shown to be negligible.

Introduction

Sedimentation equilibrium can be achieved rapidly by using short columns of solution.[2,3] The time needed to reach equilibrium can be predicted[2] from an equation based on the theory of Mason and Weaver[4] for sedimentation in a rectangular cell and constant field. This equation has been tested[2] by plotting ln ϵ *vs.* t where ϵ is a parameter, based on the difference in concentration between ends of the column, which measures the deviation from equilibrium. Once ϵ falls below a given value this graph should be a straight line whose slope yields the diffusion coefficient D. Surprisingly, values for D found in this way were comparable in accuracy to the molecular weights found from equilibrium data. The theory of Mason and Weaver applies only approximately to sedimentation in a sector-shaped cell and centrifugal field. Recently Nazarian[5] used a perturbation treatment to obtain a series solution for the centrifuge case which includes the Mason–Weaver equation as zero-order terms. One aim of the present work was to use Nazarian's equation to reinvestigate this method of measuring D.

With the expectation of more accurate experimental results,[6,7] we turned from schlieren to Rayleigh interference optics. A system of known properties (sucrose in water) has been used to study the agreement between theory and experiment, both during the transient period and at equilibrium. A second aim was to find methods of calculation which make full use of the potential accuracy, and to see if the theory need be extended to include effects such as pressure dependence. An equation has been obtained in closed form for the equilibrium sedimentation of a concentration-dependent system when the apparent molecular weight is a linear function of concentration.

Experimental

Materials.—Sucrose was obtained from the National Bureau of Standards (Standard Sample 17, lot #5901) and concentrations of sucrose solutions were computed from the weights of sucrose and water, corrected for air buoyancy. 1,3-Butanediol[7] was purchased from Eastman Organic Chemicals and redistilled before use. The fluorochemical FC 43,[8] obtained from Spinco Division, Beckman Instruments, was used as a liquid base for the column of solution.

Sedimentation Experiments.—A Spinco Model E ultracentrifuge, equipped with temperature control, was used. The double-sector cell had sapphire windows and an epoxy-resin centerpiece. An aperture mask was made by Spinco which fastens onto the holder for the upper collimating lens. Both translational and rotational positions of this mask can be set as desired. In addition to a Wratten 77A filter, we used a Bausch and Lomb second-order interference filter to isolate the Hg line at 546 mμ. Eastman Spectroscopic IIG plates were used to photograph the interference patterns. They were read on a Gaertner two-dimensional microcomparator (M 2001 RS). Figure 1 shows one of the photographs.

The procedure for finding reference baselines was suggested by J. M. Creeth. After the end of an experiment the cell was emptied without taking it apart, the two sides rinsed and refilled with water to the previous level, and the reference baseline recorded at the appropriate speed. In reading the plates from an experiment the position (R) of a given fringe (j') was recorded. A different procedure has to be used for the reference baselines: the height (Z) of a central fringe was read at several values of R and the vertical spacing between fringes (ΔZ = 0.0296 cm.) was used to convert the reference baseline to a plot of j' *vs.* R, where j' here takes on fractional values. These were added algebraically to the integral values of j' from the experiment. An additional correction to j' was made for the sedimentation of 1,3-butanediol added to the solvent side of the cell (see Results).

The two optical constants needed are F, the magnification factor relating cell distance to distance on the plate, and a', the physical distance through the cell along the optic axis. F was found in the usual way, by photographing a ruled disk centered in the rotor. To find a' the distance between outer faces of the cell windows was measured with a specially adapted micrometer caliper, and the thickness of the windows was subtracted to give a'. Before tightening the cell with a torque wrench a' was 1.207_0; after 2.5 turns it decreased to 1.201_7. The thickness of the free centerpiece was found to be 1.206_2.

Focusing the Optics.—The use of Rayleigh optics for the ultracentrifuge has been critically described by Richards and Schachman.[7] We give here a brief description of methods for focusing the optics. To get good interference patterns it is critical to have a narrow source slit, to use an interference filter, to replace the quartz windows by sapphire ones in runs at high speed, and to align the source slit, aperture mask, and cylinder lens correctly. The maximum width of the source slit can be computed by the rule[8] that its value should not exceed $^1/_4$ the spacing between interference fringes formed at the plane of the schlieren diaphragm. The vertical spacing of the fringes on the plate is 0.0296 cm., the magnification factor of the cylinder lens–camera lens pair is 3.65, and so the width of the source slit

(1) This research was supported by grants from the National Science Foundation (Grant No. G8146) and from the National Institutes of Health (PHS Grant No. A 4763).

(2) K. E. Van Holde and R. L. Baldwin, *J. Phys. Chem.*, **62**, 734 (1958).

(3) D. A. Yphantis, *Ann. N. Y. Acad. Sci.*, **88**, 586 (1960).

(4) M. Mason and W. Weaver, *Phys. Rev.*, **23**, 412 (1924).

(5) G. M. Nazarian, *J. Phys. Chem.*, **62**, 1607 (1958).

(6) J. S. Johnson, G. Scatchard, and K. A. Kraus, *ibid.*, **63**, 787 (1959).

(7) E. G. Richards and H. K. Schachman, *ibid.*, **63**, 1578 (1959).

(8) Jenkins and White, "Fundamentals of Optics," McGraw-Hill Book Co., Inc., New York, N. Y., 1957, p. 322.

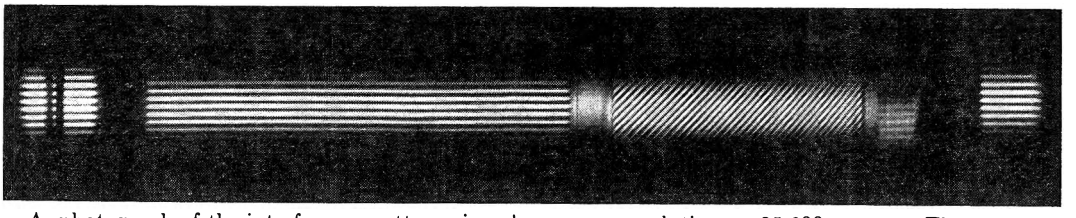

Fig. 1.—A photograph of the interference pattern given by a sucrose solution at 35,600 r.p.m. The concentration is 5.424 g./dl. Sapphire windows were used in the ultracentrifuge cell, and 1,3-butanediol[7] was added to raise the refractive index on the solvent side.

should not exceed 0.02_0 mm. Also, one should look at the source slit in the microcomparator to see if the sides are parallel and straight.

In aligning the optics we have found it convenient to use a plumb line as a primary standard of reference, and also to cut a hole at the back of the camera for direct viewing. If instead the aperture mask is used as the primary reference in focusing, as is often done, then the source slit, cylinder lens, and aperture mask must be re-positioned each time the drive is changed. With the procedure given here, only the translational position of the aperture mask need be changed. First the image of the source slit at the schlieren diaphragm is made vertical when the slit is in the schlieren position. This automatically sets the Rayleigh position of the slit if one uses the new slit assembly from Spinco with a Rayleigh slit at right angles to the schlieren slit. (That the two are at right angles can be checked and adjusted by means of a microcomparator.) Suspend one plumb line (a hair is suitable) just in front of the schlieren diaphragm, a second one through the target opening in front of the camera, and place a ground glass over the hole in the camera for observation. When the slit image falls on the first plumb line a thick shadow appears on the ground glass; this becomes vertical when the slit image is vertical. The adjustment should be sensitive to $\pm 0.05°$. Narrow the source slit to improve definition of this shadow and use the set screw to fix the schlieren position of the source slit. With the rotatable source slit it was difficult to reproduce the schlieren and Rayleigh positions, so that the new assembly seems to be a definite improvement. Next use the same method to make the schlieren diaphragm vertical when the drum reads 0.00°. (This is done so that the 90.00° position of the schlieren diaphragm can be used to align the axis of the cylinder lens.) Replace the first plumb line by the metal line on the phaseplate and open the chamber slightly to improve definition of the shadow on the ground glass. In setting the drum always approach a given angle from the same direction (*e.g.*, from higher to lower angles) because of backlash. The axis of the cylinder lens can now be set by use of the phaseplate. Open the chamber, place a ground glass over the lower collimating lens, set the schlieren diaphragm at 90.00°, and use the adjusting screws on the cylinder lens mount to obtain maximum definition of the image of the metal line. This is a simple test and sensitive to $\pm 0.02°$. One should view the image with a hand lens rather than a ground glass in this step. To find the correct rotational position of the aperture mask, first set the schlieren diaphragm at 90° and fasten a ruled glass at the camera so that the lines are parallel to the image of the metal line. Then take out the cylinder lens and move the camera lens until the aperture mask is in focus, with the chamber open. Rotate the mask until its edges are parallel to the lines on the ruled glass (*cf.* the comments by Trautman in ref. 7). To set the translational position of the aperture mask in the offset arrangement,[7] use the same system but insert the rotor with a thread stretched across the scribe lines of one cell hole. Turn the rotor until a shadow from the thread crosses the upper slit image (the left slit of the aperture mask). For satisfactory definition of this shadow, use a narrow source slit and close the chamber. Move the mask, keeping its same rotational alignment, until the shadow from the thread is parallel to the edges of the mask, with the shadow in the center of the upper slit image.

Theory

Correction Terms Given by Nazarian's Equation.—Nazarian[5] solved the continuity equation for a sector-shaped cell

$$\left(\frac{\partial c}{\partial t}\right)_r = -\left(\frac{1}{r}\right)\left[\frac{\partial (rJ)}{\partial r}\right]_t \qquad (1)$$

using Lamm's flow equation

$$J = cs\omega^2 r - D\left(\frac{\partial c}{\partial r}\right)_t \qquad (2)$$

for the case in which s and D are constants, independent of concentration and pressure. In these equations c is concentration on a weight per volume scale (here g./ml.), t is time, r is distance from the center of rotation, J is flow per unit area, ω is the angular velocity ($\omega^2 r$ is the centrifugal field strength), and s and D are the sedimentation and diffusion coefficients of the solute. His solution takes the form

$$c(y,t) = c_{eq} + \{\exp[(y/2\alpha) + (\lambda/4\alpha)(2y-1)^2]\} \times \sum_{m=1}^{\infty} A_m(\alpha) u_m(y) e^{-E_m t} \qquad (3)$$

$$y = (r-a)/(b-a) \qquad (3a)$$

$$\alpha = D/s\omega^2 \bar{r}(b-a) \qquad (3b)$$

$$\lambda = (b-a)/2\bar{r} \qquad (3c)$$

$$\bar{r} = (b+a)/2 \qquad (3d)$$

where a, b are the upper and lower ends of the column of solution, and the notation has been altered to avoid conflict with other terms used here. Fujita[9] has obtained an approximate solution which is similar in form and which can be used to analyze the very early stages of sedimentation as well as the later stages considered here. Each of the functions A, u, and E in equation 3 is written as a series in ascending powers of λ, the zero-order term being identical with the corresponding quantity in the Mason–Weaver equation.

$$A_m = A_m^{(0)} + \lambda A_m^{(1)} + \ldots \qquad (4a)$$

$$u_m = u_m^{(0)} + \lambda u_m^{(1)} + \ldots \qquad (4b)$$

$$E_m = E_m^{(0)} + \lambda^2 E_m^{(2)} + \ldots \qquad (4c)$$

The departure from equilibrium can be measured by a parameter ϵ, defined in terms of the difference in concentration between ends of the cell.[2]

$$\epsilon = (\Delta c_{eq} - \Delta c_t)/\Delta c_{eq} \qquad (5)$$

$$\Delta c = c_b - c_a \qquad (5a)$$

(9) H. Fujita, to be published.

$$\Delta c_{eq} = c^0/\alpha \qquad (5b)$$

When Nazarian's equation is solved for ϵ, the result is

$$\epsilon = (\alpha/c^0)e^{\lambda/4\alpha} \sum_{m=1}^{\infty} A_m(\alpha)e^{-E_m t}\,[u_m(0) - e^{1/2\alpha}u_m(1)] \qquad (6)$$

where c^0 is the initial, uniform concentration. It is convenient to use this equation to measure D when t is large enough that only the first term ($m = 1$) determines the value of ϵ. Then

$$\ln \epsilon = \ln K' - E_1 t + 0(t^2) \qquad (7)$$

$$K' = (\alpha/c^0)e^{\lambda/4\alpha} A_1[u_1(0) - e^{1/2\alpha}u_1(1)] \qquad (7a)$$

It is easily shown[5] that $E_1^{(2)}/E_1^{(0)} \sim 0.3$ while $\lambda \sim 0.05$. Consequently $\lambda^2 E_1^{(2)}/E_1^{(0)} \sim 1 \times 10^{-3}$ and we need consider only the zero-order term of E_1.

$$\ln \epsilon = \ln K' - E_1^{(0)}t + 0(\lambda^2) + 0(t^2) \qquad (8)$$

$$E_1^{(0)} = \pi^2 U(\alpha)D/(b - a)^2 \qquad (8a)$$

$$U(\alpha) = 1 + (1/4\pi^2\alpha^2) \qquad (8b)$$

Equation 8 is the same as the one used previously[2] to measure D except that K' differs from the earlier K by a term of order λ. When K' (equation 7a) is expanded as a series in $1/\alpha^2$, one has

$$K' = K\,\{1 - (\lambda/\alpha)[9.472 \times 10^{-2} - 1.51 \times 10^{-4}\,(1/\alpha^2) + 0(1/\alpha^2)^2] + 0(\lambda^2)\} \qquad (9)$$

$$K = \frac{4[1 + \cosh(1/2\alpha)]}{\pi^2 U^2(\alpha)} = 0.81057 \times [1 + 1.184 \times 10^{-2}(1/\alpha^2) + 0(1/\alpha^2)^2] \qquad (9a)$$

Consequently when D is found from the *slope* of $\ln \epsilon$ *vs.* t, or by an equivalent procedure, the correction terms introduced by using Nazarian's equation, in place of the Mason–Weaver equation, are negligible.

Range of ϵ Which Can be Used to Find D.—We turn next to the question of when the higher terms ($m = 2,3\ldots$) in equation 6 become negligible. Since this is determined chiefly by the relative magnitudes of the terms $\exp(-E_m t)$ for $m = 1,2,3\ldots$, and since these are nearly the same in the Nazarian and Mason–Weaver equations, we may use the latter to answer this question. Numerical solutions to the Mason–Weaver equation, obtained with an IBM calculator, were kindly made available to us by D. A. Yphantis. Values of ϵ were computed from these and compared to the first term ($m = 1$) of the series. The results are shown in Fig. 2 as $F(\alpha, \epsilon)$ *vs.* ϵ for three values of α: $F(\alpha, \epsilon)$ is $\ln(K/\epsilon)/\ln(K/\epsilon_1)$, where ϵ is the value given by the IBM calculator and ϵ_1 has been computed from the term with $m = 1$. Figure 2 gives a direct measure of the error caused by neglecting terms $m = 2,3\ldots$ in finding D from equation 8. One can see that the error becomes negligible for ϵ between 0 and 0.5 when α is 1.538 or 3.077, but that the useful range of ϵ is

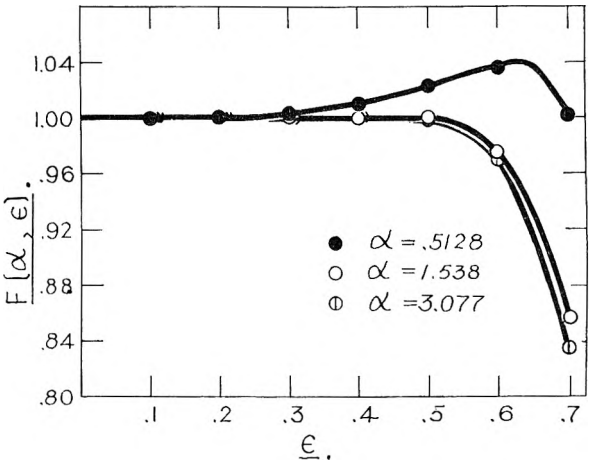

Fig. 2.—The range of ϵ in which D can be measured by equation 8: when $F(\alpha,\epsilon)$ differs from 1, the higher terms omitted from equation 8 contribute significantly to ϵ.

smaller than this for $\alpha = 0.5128$. In a typical sedimentation equilibrium experiment α is 1 or more. The practical reason for this becomes clear when one remembers that $\Delta c_{eq}/c^0 = 1/\alpha$. In the experiments reported here the smallest value of α was 3.4 and values of ϵ less than 0.5 were used to compute D.

An Exact Equation for Concentration Dependence of Equilibrium Data.—To make a quantitative test of the agreement between theory and experiment, it is necessary to have an accurate equation for computing the results. The precision obtainable with interference optics is good enough that errors due to approximation should be less than 0.1%. The equations used in an earlier study[2] contain only the first terms of series expansions: these are satisfactory for use with schlieren optics, whose accuracy is about 1%, but could be unsatisfactory here. Fortunately activity and density data for sucrose in water predict a linear dependence on concentration of the apparent molecular weight: for this case the equation can be integrated in closed form, yielding a simple result.

It is convenient to write the starting equation, which takes into account concentration but not pressure dependence (*cf.* Williams, *et al.*[10]), in terms of the reduced distance ϕ which takes values from 0 to 1.

$$\frac{1}{c}\frac{dc}{d\phi} = A + Bc \qquad (10)$$

$$\phi = (r^2 - a^2)/(b^2 - a^2) \qquad (10a)$$

$$A = M(1 - \bar{v}\rho_0)(b - a)\omega^2\bar{r}/\nu RT \qquad (10b)$$

$$B = (A/c)[(1 - \bar{v}c)/(1 + c\partial \ln y/\partial c) - 1] \qquad (10c)$$

This empirical representation of the concentration dependence is allowable only when B is found to be constant. In these equations M is molecular weight and $\bar{v}$ partial specific volume of the solute, y is its activity coefficient on the c scale (g./ml. solution), ρ_0 is the density of the solvent, and R, T are the

(10) J. W. Williams, K. E. Van Holde, R. L. Baldwin, and H. Fujita, *Chem. Revs.*, **58**, 715 (1958).

gas constant and the absolute temperature. For a salt ν is the number of ions per molecule; for a non-ionizing substance ν is 1. The term $(1 - \bar{v}c)$ expresses the dependence of $(1 - \bar{v}\rho)$ on c. Since the specific refractive increment does not vary in this range of concentration for sucrose,[11] we will give only the calculation of c as a function of ϕ, rather than relating this to the difference in refractive index between solution and solvent.

Integration of equation 10, for constant A and B, yields

$$\ln (c/c_a) = A\phi - \ln \left[\frac{1 + (B/A)c_a}{1 + (B/A)c}\right] \quad (11a)$$

or

$$c = c_a e^{A\phi}/[1 + c_a(B/A)(1 - e^{A\phi})] \quad (11b)$$

One can find c_a in terms of the initial concentration c^0 by means of the condition derived from conservation of mass.

$$\int_0^1 c\,d\phi = c^0 \quad (12)$$

Substitution of (11b) into (12) gives

$$c_a = (1 - e^{-Bc^0})/(B/A)(e^A - 1) \quad (13)$$

An equation for Δc is given by substituting (11b) into

$$\Delta c = \int_0^1 \frac{dc}{d\phi}\,d\phi \quad (14)$$

with the result

$$\Delta c = c_a(e^{A+Bc^0} - 1) \quad (15)$$

It follows from equation 15 that

$$\ln (c_b/c_a) = A + Bc^0 \quad (16)$$

when one remembers that $c_b = c_a + \Delta c$. This can be shown also, with less ease, by setting $\phi = 1$ in equation 11a. For $\phi \to 0$, application of l'Hospital's rule shows that

$$\lim_{\phi \to 0} \frac{\ln (c/c_a)}{\phi} = A + Bc_a \quad (17)$$

Finally, for comparison with "method II" of Van Holde and Baldwin,[2] we note that equation 10 yields directly

$$\frac{\left(\frac{dc}{d\phi}\right)_b - \left(\frac{dc}{d\phi}\right)_a}{\Delta c} = A + B(c_b + c_a) \quad (18)$$

Results

Extrapolation of Fringe Data to Ends of the Column.—The data read from a photographic plate are a set of coördinates (j',R) where j' is the fringe number, read from an arbitrary origin, and R is the position on the plate of this fringe, again read from an arbitrary origin. The distance between two points $(R_2 - R_1)$ is related to the distance $(r_2 - r_1)$ between corresponding points in the cell by the magnification factor F: $(R_2 - R_1) = F(r_2 - r_1)$. Provided the specific refractive increment dn/dc is constant, one can define a fringe number j which is proportional to concentration.

$$j = kc \quad (19)$$

$$k = a' \frac{dn}{dc}/\lambda' \quad (19a)$$

Here λ' is the wave length of light used and a' is distance through the cell along the optic axis. Once the necessary "baseline" corrections have been made to j' and the value of j has been determined at some point in the cell (*e.g.*, $r = a$), then j at any point is found from

$$j_r = j_a + (j_r' - j_a')_{corr} \quad (20)$$

The number of fringes crossed in scanning from the top to the bottom of the column, $\Delta j'$, consists of two parts: an integral part given by $(n - 1)$, the number of fringes contained between the first and n'th fringes crossed, and a fractional part contained between the ends of the column and the first and n'th fringes.

$$\Delta j' = (n - 1) + (j_1' - j_a') + (j_b' - j_n') = (j_b' - j_a') \quad (21)$$

One can find $(n - 1)$ by counting but some method of extrapolation is needed to get $(j_1' - j_a')$ and $(j_b' - j_n')$. A simple method is to plot $-\log \Delta R$ *vs.* $\bar{R}_i - R_a$ at the top, or $R_b - \bar{R}_i$ at the bottom of the column. Here ΔR is the distance between two adjacent fringes and $\bar{R}_i$ is the average of the two fringe positions. Such a plot is shown in Fig. 3. The simplest way of finding $(j_1' - j_a')$ with the use of this plot is to read from the graph the value of $\log \Delta R$ at $(R_1 + R_a)/2$ and then set $(j_1' - j_a')$

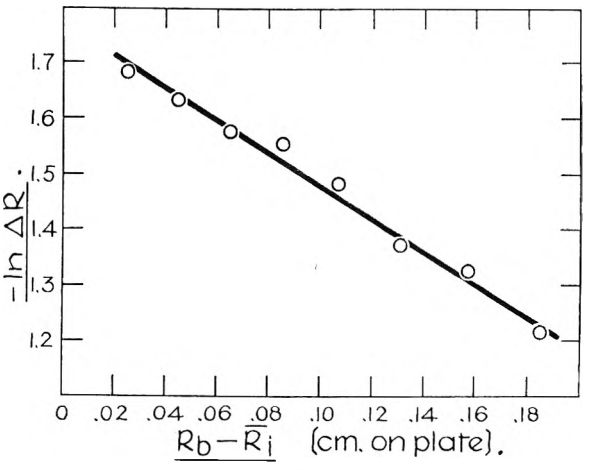

Fig. 3.—The plot used to measure the fractional part of $\Delta j'$: ΔR is the spacing between white fringes, and $-\ln \Delta R$ is plotted against the position $\bar{R}$ of the corresponding black fringes (in this case, against $R_b - \bar{R}$). One can find the number of fringes between the last fringe read (n) and the bottom of the column (b), by measuring $R_b - R_n$ and taking ΔR from this graph at $\bar{R} = (R_b + R_n)/2$, or by use of equation 26 (see Table I).

(11) L. J. Gosting and M. S. Morris, *J. Am. Chem. Soc.*, **71**, 1998 (1949).

$= (R_1 - R_a)/\Delta R$, using this value for ΔR. Another way is discussed below.

One expects the plot in Fig. 3 to be a straight line, over short distances, because of the exponential relation between j and ϕ (equation 11b). Provided the restriction to small distances is kept, one can ignore the effects of concentration dependence or heterogeneity and also replace ϕ by the more convenient experimental quantity $(R - R_a)$ or $(R_b - R)$. Thus if j is related to R by the approximate equation

$$j = (k_1/k_2)e^{k_2(R-R_a)} + \ldots \qquad (22)$$

we see that dj/dR also is exponential in $(R - R_a)$

$$\frac{dj}{dR} = k_1 e^{k_2(R-R_a)} + \ldots \qquad (23)$$

and replacing dj/dR by $\Delta j'/\Delta R$,[12] while noting that $\Delta j' = 1$, we have a linear relation between log ΔR and $(R - R_a)$

$$-\log \Delta R = \log k_1 + \frac{k_2}{2.303}(\bar{R}_i - R_a) + \ldots \qquad (24)$$

After finding k_1 and k_2 from the slope and intercept of this plot, one can compute $(j' - j_a')$ from each fringe position by means of equation 22, and then compare the results for succeeding fringes.

$$j' - j_a' = (k_1/k_2)[e^{k_2(R-R_a)} - 1] + \ldots \qquad (25)$$

The corresponding equations for the bottom of the column are

$$-\log \Delta R = \log k_1 - \frac{k_2}{2.303}(R_b - \bar{R}_i) + \ldots \qquad (26a)$$

$$j_b' - j' = (k_1/k_2)[1 - e^{-k_2(R_b-R)}] + \ldots \qquad (26b)$$

Use of these equations is illustrated in Table I. Values for $(j_b' - j_n')$ agree within ± 0.03 fringe when computed from successive fringe positions.

Table I

Measurement of the Fractional Part of $\Delta j'$[a]

Fringe # (i)	$R_b - R_i$	$(j_b' - j_i')$[b]	$(j_b' - j_n')$
n	0.206	1.16	1.16
$n-1$	.397	2.18	1.18
$n-2$	.599	3.19	1.19
$n-3$	.808	4.17	1.17
$n-4$	1.028	5.15	1.15
$n-5$	1.267	6.14	1.14
$n-6$	1.525	7.14	1.14
$n-7$	1.806	8.13	1.13
		Av.	1.16 ± 0.03

[a] This table shows the calculation, from each of eight fringe positions, of the number of fringes remaining between the last fringe read (n) and the bottom of the cell (b). The data are from a photograph taken during the transient period: $t = 48.4$ minutes at 42,040 r.p.m. ($\epsilon \sim 0.4$). [b] Computed from equation 26b, with k_1 and k_2 taken from the intercept and slope of Fig. 3: $k_1 = 5.80$, $k_2 = 0.293$.

(12) By expansion into a Taylor's series, one can show that $(\Delta j/\Delta R)_{\bar{R}}/(dj/dR)_{\bar{R}} = 1 + (k_2\Delta R)^2/24 + \ldots$.

This method was used to find Δc during the transient period as well as at equilibrium. The plots of $-\log \Delta R$ *vs.* $(\bar{R}_i - R_a)$ or $(R_b - \bar{R}_i)$ were found to be linear during the transient period: in fact Fig. 3 and Table I show data from the transient period. One expects such a linear plot from the boundary condition ($J = 0$ at $r = a,b$) which can be rearranged to read $(\partial \ln c/\partial\phi)_t = A + Bc$ (compare equations 2 and 10). One of the IBM computer solutions to the Mason–Weaver equation was used to check that $\ln (\partial c/\partial r)$ is a linear function of $(r - a)$ or $(b - r)$ during the transient period. At an early time ($s\omega^2 t = 2 \times 10^{-4}$, $\Delta c/c^0 = 0.0662$) in an experiment for which $\alpha = 1.538$, there was a linear relation between $\ln (\partial c/\partial r)$ and y (equation 3a) for $0 \leq y \leq 0.04$ and $0.96 \leq y \leq 1.00$. This linear relation could be used to extrapolate measurements of $\partial c/\partial r$ to a or b in finding molecular weights by the Archibald method. However one should not expect it to hold over a useful range of $(r - a)$ under the conditions of a transport experiment ($\alpha << 1$) when a moving boundary is resolved.

Correction for the Sedimentation of 1,3-Butanediol.—Because of the low molecular weight of sucrose (342.3) it is necessary to use a high concentration in order to have a reasonable value for Δj_{eq} in a short-column experiment. However the quality of the interference fringes becomes poor when there is too large a path length difference between the solution and solvent sides of the cell. Richards and Schachman[7] suggested adding a non-sedimenting substance to raise the refractive index on the solvent side, and they introduced 1,3-butanediol for this purpose. They were unable to observe any sedimentation of the butanediol. If the extent of its sedimentation compared to sucrose were of the order of 1%, it would be very difficult to observe directly and yet would represent a significant correction in our experiments. Consequently, we determined $\bar{v}$ for 1,3-butanediol so that we could compute $M(1 - \bar{v}\rho)$ and estimate from this the amount of sedimentation.

A Linderstrøm-Lang density gradient column was used for this purpose. The two organic liquids used to give the density gradient were *o*-dichlorobenzene and *n*-dodecane (suggested by R. C. Warner); they were saturated with water at 25° before use, and then filtered through wet filter paper to take out the surplus water. Standard solutions of sucrose were used to calibrate the column. Temperature was controlled to $\pm 0.001°$ by means of a Jumo thermoregulator connected to two 125-watt infrared lamps. Eleven measurements on a 1.16 g./100 ml. solution of butanediol in water gave the following values for $\bar{v}$[13] at 25°: 0.980 ml./g. (8 drops), 0.982 ml./g. (2 drops), 0.983 ml./g. (1 drop), or an average value of 0.981 $\pm$ 0.001 ml./g. The ratio of the values of $M(1 - \bar{v}\rho)$ for butanediol over sucrose is 0.013, so that the correction is approximately 1.3%.

An approximate measurement of the diffusion coefficient of butanediol in water also was made,

(13) Computed from $\bar{v} = [1 - (\rho - \rho_0)/c]/\rho_0$, where ρ is the density of the solution, ρ_0 is the density of water, and c is g. butanediol/ml. of solution.

in order to compute the correction to Δc at any time by means of equation 8. A value for D_{25} of $1.0_1 \times 10^{-5}$ cm.^{2} sec.$^{-1}$ was found when a solution containing 1.98 g. butanediol/100 ml. was diffused against water in a boundary-forming cell at 12,590 r.p.m.

The Method of Computing D.—According to the data in Fig. 2, we may use equation 8 to compute D when $\epsilon \leq 0.5$, provided $\alpha > 1$. The method used previously[2] was to plot log ϵ *vs.* t and find D from the slope. This is satisfactory but one would like to know what range of ϵ gives the most accurate estimate of D. As equilibrium is approached and $\epsilon \to 0$ the per cent error in ϵ becomes large, but this is partly compensated by the wider separation of successive values of log ϵ. If each value of ϵ is in error by the same absolute amount (this corresponds roughly to a constant absolute error in Δc), then one can show that the error in D(obsd.) is inversely proportional to ϵ log (ϵ_0/ϵ) when D is computed from

$$D = \frac{(2.303)(b - a)^2 \log (\epsilon_0/\epsilon)}{\pi^2 U(\alpha)(t - t_0)} \qquad (27)$$

where t_0 is the time at which the first useful photograph was taken ($\epsilon_0 \sim 0.5$). With this procedure D is found without any question of how to draw the best straight line, and values computed from successive photographs indicate the precision of the measurement. The results given here were computed in this way; in finding the averages, each value of D was weighted by ϵ log (ϵ_0/ϵ).

According to this analysis, the error would be further reduced by computing D from $(1/t)$ log (K'/ϵ) (equation 8) rather than from $[1/(t - t_0)]$ log (ϵ_0/ϵ), as in equation 27. However this would require knowing within a few seconds the time at which sedimentation started in these short-column experiments. Since a few minutes are needed to bring the ultracentrifuge to its operating speed, this is not practical.

Results for D.—The results from four short-column ($b - a \sim 0.4$ cm.) and one long-column ($b - a \sim 0.8$ cm.) experiments are shown in Table II. Values for D agree with the data of Gosting and Morris[11] within the precision of this experiment, which is about 2%. The data do not show any effect of varying the speed. There is a trend in the values for $(b - a)$ although the first four experiments were done without refilling the cell. After each experiment the cell was taken out, shaken, and run at a new speed. Presumably the changes in $(b - a)$ reflect distortion of the epoxy-resin centerpiece: probably an aluminum double-sector centerpiece would have been better. After trying out various methods for locating R_b and R_a (such as use of the boundary condition) we went back simply to reading them from the plate. Correct location of R_b and R_a plays an important role in finding D since it affects both the values for ϵ and the computation of D from ϵ (equation 27).

Results for M.—The simplest way of finding M with interference optics is to measure $\Delta j/j^0$, which does not require finding j (equation 19) at some point in the cell. Also $\Delta j/j^0$ gives the weight-average molecular weight if all solutes have the same $\bar{v}$ and dn/dc. For a single solute it yields the apparent molecular weight at a concentration $(c_b + c_a)/2$ according to Van Holde and Baldwin,[2] who retained the first terms of a series expansion.

$$\frac{\Delta c_{eq}}{c^0} = \frac{\Delta j_{eq}}{j^0} = A + B(c_b + c_a)/2 + \ldots \qquad (28)$$

(M is found from A by equation 10b.) The equations given here do not yield a simple expression for M^{app} in terms of $\Delta j/j^0$ (see equations 13 and 15). However they can be used to check the accuracy of equation 28. When Δj_{eq} was predicted from known values of A, B,[14] and j^0, the same answer was obtained from equation 28 as from equations 13 and 15, within 0.1%, for each of the experiments given here. Thus equation 28 is a good approximation under the conditions of these experiments where $1 + (B/A)c \sim 0.9$.

TABLE II

MEASUREMENTS OF D

R.p.m.	$(b - a)$(cm.)	D^{obs}/D^a
42,040	0.4583	1.016 ± 0.010
35,600	.4548	1.004 ± .018
29,500	.4538	0.984 ± .022
24,630	.4538	1.037 ± .016
42,040	.8040	0.994 ± .014

[a] Computed from equation 27. The estimate of the precision is based on agreement of values from successive photographs. The known value of D was taken from the work of Gosting and Morris,[11] from which D was reckoned to be 4.84×10^{-6} cm.^{2} sec.$^{-1}$ at 25.3° and a concentration of 5.4 g./dl.

To compare theory with experiment, predicted and experimental values of Δj_{eq} are given in Table III. The agreement is quite good, the difference being 0.10–0.16 fringe out of a total number as large as 50 fringes. The comparison does not show any obvious dependence on speed, as it would if effects of pressure dependence were significant.

TABLE III

COMPARISON OF OBSERVED AND PREDICTED VALUES FOR Δj_{eq}[a]

R.p.m.	$(\Delta j_{eq})_{obs}$[b]	$(\Delta j_{eq})_{pred}$[c]	$\delta(\Delta j)$
42,040	50.40	50.30	0.10
35,600	35.95	35.79	.16
29,500	24.63	24.53	.10
24,630	17.26	17.10	.16

[a] $(\Delta j)_{eq}$ is the number of fringes crossed in scanning the plate from top to bottom of the column of solution, plus a correction for distortion and also for sedimentation of the 1,3-butanediol added to the solvent side of the cell. It is closely proportional to M^{app} at $(c_b + c_a)/2$ (equation 28), and depends also on ω^2 and column height. [b] Computed by means of the extrapolation equations 25 and 26. [c] Computed from known values[11] for the molecular weight, partial specific volume, specific refractive increment, and activity coefficient of sucrose in water, and from the weight concentration, by means of equations 13 and 15.

In order to make direct use of data from the center of the column, another way of computing the results was studied. This is shown in Fig. 4 where $(1/\phi)$ ln (j/j_a) is plotted *vs.* ϕ. Predicted

(14) The activity and density data for sucrose quoted by Gosting and Morris[11] are consistent with a constant value for B/A of -1.647 ml./g. at concentrations up to 0.06 g./ml.

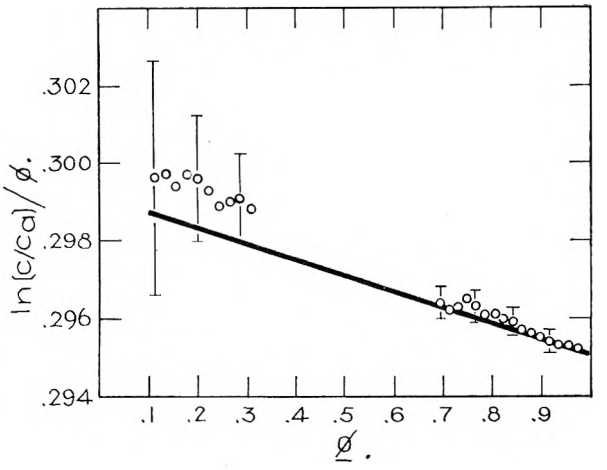

Fig. 4.—A way of plotting the equilibrium results which makes direct use of data from the center of the solution column. The quantity $(1/\phi)$ ln (c/c_a) is proportional to the apparent molecular weight, evaluated at a concentration specified by equation 11b. Dependence of the apparent molecular weight on concentration makes this plot slope downward while heterogeneity would make it slope upward. The slope of the line is theoretical and the points are experimental; a bar through every fourth point shows the effect of changing $j - j_a$ by ± 0.05 fringe.

values of this quantity are given by equation 11a and, at $\phi = 1$ and 0, by equations 16 and 17. The solid line, which is nearly straight, gives the theoretical slope. Every fourth point has a bar showing the effect of an uncertainty of ± 0.05 fringe in $(j - j_a)$. The points at small values of ϕ are much less precise than those near $\phi = 1$. This method of computing the results yielded some improvement in each case in the agreement between theory and experiment, but the effect was not striking. The plot indicates that the precision is slightly better than the accuracy of these experiments: the predicted value of ln (j_b/j_a) in Fig. 4 is 0.2944, which clearly falls below the experimental points near $\phi = 1$. The difference is only 0.2%, however. To use this method of computation it was first necessary to find j_a, which was done by means of equation 13 and the known values of A, B, and j^0. With an unknown system one would have to find j_a by numerical integration (making use of equation 12) or by such means as locating the white-light fringe.

Discussion

Choice of Speed.—With interference optics it is necessary to choose a speed such that the fringes are not packed too closely to be resolved. The concentration gradient increases from the top to the bottom of the column and so the fringes are most tightly packed at the bottom. Consequently we can specify resolution of all the fringes by setting an upper limit on dj/dr at b: 100 fringes per cm. cell distance has proved suitable in our work. Omitting effects of concentration dependence, we may write

$$\Delta j_{eq} = Aj^0 = Akc^0 \qquad (29)$$

where k is given by equation 19, and

$$\left(\frac{dj}{dr}\right)_b = \frac{A j^0 (b/\bar{r})}{(1 - e^{-A})(b - a)} \qquad (30)$$

Combination of these two equations gives

$$\left(\frac{dj}{dr}\right)_b = \frac{\Delta j_{eq}}{(b - a)} \left[\frac{A(b/\bar{r})}{1 - e^{-A}}\right] \qquad (31)$$

We consider two cases. In the first, j^0 is large and the problem is to reduce ω sufficiently that $\Delta j_{eq}/(b - a) < 100$. A will be small and so it follows from equation 31 that dj/dr at $b \sim \Delta j_{eq}/(b - a)$. Setting $\Delta j_{eq}/(b - a) = 100$ in equation 29 gives

$$\omega = \left[\frac{100RT}{j^0(M/\nu)(1 - \bar{v}\rho)b}\right]^{1/2} \text{(case 1)} \qquad (32)$$

In the second case j^0 is small and one wants to raise ω so as to increase Δj_{eq}, while still resolving all the fringes. One can do this as follows. (1) Choose a value for Δj_{eq}. (2) Find A from equation 29 (j^0 is considered fixed). (3) Compute $A/(1 - e^{-A})$ and find $(b - a)$ from equation 31, after setting dj/dr at $b = 100$. (4) Find ω from equation 10b, or

$$\omega = [ART/(M/\nu)(1 - \bar{v}\rho)(b - a)\bar{r}]^{1/2} \qquad \text{(case 2)} \qquad (33)$$

Factors Controlling the Time Needed for Equilibrium.—As emphasized in an earlier study,[2] the time needed to reach equilibrium in this experiment depends chiefly on the diffusion coefficient and on the square of the column depth (see equation 8). The parameter α, which includes $s\omega^2\bar{r}$ (equation 3b) also enters but in such a way that ϵ shows little dependence on ω^2. In the conditions normally used for equilibrium sedimentation, the transient period actually is described fairly well by the form of the Mason–Weaver equation obtained on taking the limit as $\omega^2 \to 0$. Figure 5 illustrates the point that ϵ shows very little dependence on ω^2: $(1 - \epsilon)$ is given as a function of $t/(b - a)^2$ for four experiments in which the speed was varied from 42,040 to 24,630 r.p.m. There is no observable difference between the four graphs, plotted on this scale.

The time needed to reach equilibrium can be shortened considerably by use of a boundary-forming cell[15] or by reducing the speed at a chosen time.[16] These procedures avoid a disadvantage inherent in the use of short columns: the precision increases with Δj and so is greater for long columns. The precision of these short-column experiments is quite good, however. With short columns one can use provisional values for ϵ together with equation 8 to check that equilibrium has been reached, and also one can measure D.

In Fig. 5 we saw that ϵ, and hence $\Delta c_t/\Delta c_{eq}$, is essentially independent of ω^2 although it is a function of $(b - a)^2$. One expects Δc_t to be independent of $(b - a)$ early in the experiment, when there is still a "plateau" region in the center of the cell with $\partial c/\partial r = 0$, because the flow processes at the two ends of the cell are not connected. Figure 6 confirms this expectation. Two experiments, one at $(b - a) = 0.458$ and the other at 0.804 cm.,

(15) R. A. Pasternak, G. M. Nazarian, and J. R. Vinograd, *Nature*, **179**, 92 (1957).

(16) P. E. Hexner, L. E. Radford, and J. W. Beams, *Proc. Natl. Acad. Sci.*, **47**, 1848 (1961).

show the same curve of $\Delta c/c^0$ *vs.* t so long as the "plateau" region lasts in the shorter column.

Measurement of Diffusion Coefficients.—One can use equation 8 to measure D with more confidence, now that the correction terms from Nazarian's equation have been shown to be negligible, and the valid range of ϵ has been clearly defined. Effects of concentration dependence have not yet been studied and the method may prove to be impractical for strongly concentration-dependent systems. The behavior of heterogeneous substances has been discussed previously[2] but not yet studied experimentally. It is possible that a useful method for detecting heterogeneity could be based on the plot of ln ϵ *vs.* t.

The precision of the measurements shown in Table II is not much better than that found with schlieren optics.[2] This is disappointing in view of the significant gain in precision when interference optics are used to obtain the equilibrium data (Table III). The difficulty may be in locating accurately the ends of the column: this affects Δc_t, from which ϵ is computed, and also the calculated value of D varies as $(b - a)$.[2]

Measurement of Molecular Weights.—The data in Table III indicate that with the short-column method one can measure the molecular weight of an unknown substance with an accuracy of 0.5% or better. To do this j^0 and $(1 - \bar{v}\rho)$ must be known with corresponding accuracy, and effects of concentration dependence must be mild enough to allow accurate extrapolation to $c = 0$. For a substance of high molecular weight the range of concentration used for extrapolation usually will be 0.1–1.0 g./100 ml. solution. In many cases the measurement of $\bar{v}$ is now likely to be the limiting source of error.

It often happens with physical measurements that ten times as many factors must be taken into account to get an accuracy of 0.1% as compared to 1%. It would not be surprising if this proves true in changing from schlieren to Rayleigh optics. For example we have found it necessary in this work to correct for sedimentation of the 1,3-butanediol, as well as measuring the distortion of the fringes when both sides of the cell have only water, to consider the accuracy of the equation from which M is computed, and to measure the change in a' on tightening the cell. Since we were studying sucrose, c^0 could be found by weight: in our experience the capillary type of boundary-forming cell has not given j^0 reproducibly with the required accuracy of 0.1%, even when the top of the sucrose solution is well below the capillary. A differential refractometer cell may be the best solution to this problem. It is not unlikely that other factors remain to be taken into account: for example, an explicit correction for pressure dependence may be needed, although the data in Table III do not show this, and the non-radial interference slit above the solvent side of the cell may complicate the interference pattern. Although it is difficult to locate accurately the ends of the column using Rayleigh optics, the uncertainty in $(b - a)$ is partially canceled in finding M from the ratio $\Delta j_{eq}/(b - a)$ since Δj_{eq} is roughly proportional to $(b - a)$ in experiments at low speed.

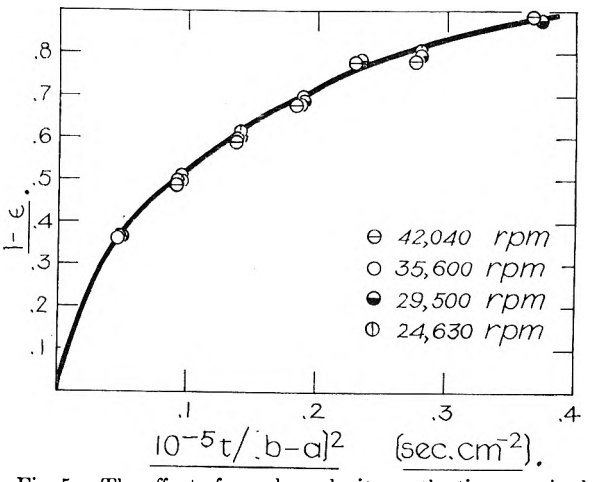

Fig. 5.—The effect of angular velocity on the time required to reach equilibrium. Theory predicts only a small dependence on speed: see equation 8.

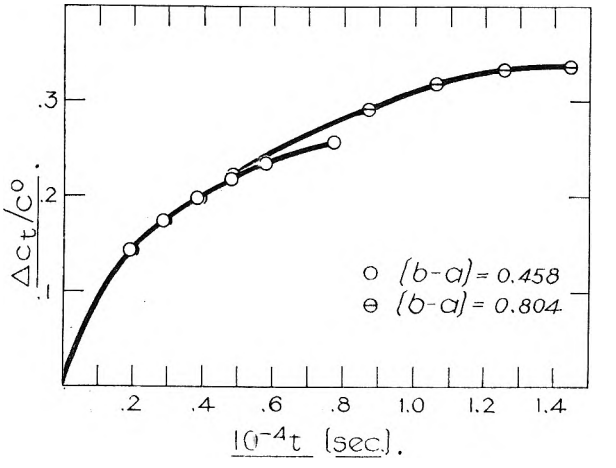

Fig. 6.—The effect of column depth $(b - a)$ on the plot of Δc *vs.* t: Δc is the difference in concentration between ends of the column. As long as the "plateau" region lasts in the shorter column, the two curves coincide. The speed was 42,040 r.p.m. in both experiments.

Acknowledgment.—We are grateful to D. A. Yphantis for the loan of numerical solutions to the Mason–Weaver equation obtained by him with the use of a differential analyzer.

DISCUSSION

R. TRAUTMAN (Plum Island Animal Disease Laboratory, USDA).—In measuring the diffusion coefficient using long columns, is it possible to obtain experimental values for the parameter ϵ and also to carry out the experiment in a reasonable time—the long column requiring considerable time to achieve equilibrium?

F. E. LaBAR.—Yes, this is accomplished by doing two experiments. The apparent molecular weight is determined from a short column equilibrium experiment, and then $\Delta c_{eq}/c^0$ is calculated for the long column by eq. 5b and 3b. In this way experimental values for ϵ are obtained in long column experiments.

INTERFERENCE OPTICAL STUDIES OF RESTRICTED DIFFUSION

BY HYOUNGMAN KIM,[1] BHAILAL S. PATEL,[2] AND GERSON KEGELES

Department of Chemistry of Clark University, Worcester, Mass.

Received March 5, 1962

Measurements of restricted diffusion in the late stages, after the spreading boundary has reflected from the walls of the container, were made by Thovert[3] in the early part of this century with the aid of optical methods. Harned and co-workers[4] have demonstrated the great value of the restricted diffusion method by their conductivity cell measurements for the late stages of diffusion in a series of electrolytes, verifying for the first time the Nernst equation and the Onsager–Fuoss theory[5] for diffusion in very dilute electrolyte solutions. The present study describes the development of optical interferometric equipment and methodology for the application of restricted diffusion studies to solutions whose electrical conductivity might be insufficient to permit the application of conductimetric diffusion observations.

Introduction

In the event that the diffusion coefficient of a system is highly concentration-dependent, it has been pointed out that any method for the determination of this coefficient which relies on Fick's second law of diffusion may be subject to error.[6] Such errors led for a number of years to some of the failures which investigators experienced in their attempts to verify the Onsager–Fuoss theory[5] for the diffusion of strong electrolytes in very dilute solutions. Harned and co-workers,[4] by applying conductimetric methods to electrolyte solutions, and studying the progress of diffusion only in the very late stages,[3] when the concentration and the diffusion coefficient became very nearly independent of position in the column, were able to perform measurements under conditions where Fick's second law of diffusion became applicable.

It was felt that the introduction of modern interferometric optical methods might permit the extension of such techniques[3,4] with reasonable accuracy to systems whose electrical conductivity might be insufficient to permit the application of conductimetric diffusion observations.

General Experimental Requirements.—Harned and coworkers have emphasized the extremely stringent requirements for constancy of temperature, or the damping out of all rapid temperature fluctuations, when the stabilizing density gradient in the diffusing column approaches zero. They employed a plastic cell mounted on a massive iron or brass block inside a vacuum-type desiccator or plastic air-bath, which itself was suspended in a water thermostat. For the present purposes it is also necessary to be concerned about precise positioning of the cell in a high quality optical system, with simultaneous freedom from mechanical vibrations. The restricted diffusion method, to be mathematically simple, also requires a cell of precisely constant cross-section, which can be filled completely with liquid, but in which all communication with filling channels is completely removed in the diffusing position. Moreover, since diffusion proceeds for a very long time, absolute confidence must obtain that the diffusing channel is free from leaks of any kind to or from other parts of the cell. For this reason, optical interference methods based on the requirement for a nearby reference liquid channel built into the cell are effectively ruled out. Thus, various types of shearing interferometers suggest themselves.

Experimental Arrangement.—As a result of these considerations, a single channel, 6-cm. optical path, stainless steel cell of the shearing type was designed and constructed.[7] The general arrangement of the cell follows that of Claesson[8] as modified by Longsworth.[9] It is emphasized, however, that, in contrast to Claesson's procedure,[8] the cell is greased to prevent leaks, and that the empty space surrounding the inner, sliding block is left filled with air rather than solvent, to avoid the possibility of leaks. The inner block is clamped between two optical flats and a spring and roller,[9] and in this position is slid laterally across the lower diffusing channel by means of a screw actuated by a pulley. The latter is operated from outside by means of a string, to avoid heating of the cell after thermal equilibration. In the filling position (C_F, Fig. 1) the cell is first turned upside down, and the less dense liquid is filled into the sliding block through channel 1, with the aid of a long steel needle attached to a hypodermic syringe. After the liquid has reached the port of the filling hole, the cell is rotated so that all air is displaced into channel 2. A plug designed to close the filling port allows intercommunication between these channels, permitting expansion or contraction of the liquid in channel 2 during thermal equilibration. With the cell erect again as shown in Fig. 1, an additional quantity of the less dense liquid is inserted through the top of channel 2 with a syringe. Filling of the denser liquid into the lower portion of the diffusing channel in the main cell frame is performed through channel 3, with the aid of a steel needle attached to a hypodermic syringe. The short channel in the sliding block acts as a liquid reservoir during the thermal equilibration period. Channel 2 then is sealed, and the cell is placed for equilibration on a heavy copper frame which is suspended, nearly completely immersed, in a water-bath thermostat. The cell, after this preliminary thermal equilibration, is removed quickly with gloves and placed in a lucite plastic air bath which is surrounded by the water-bath thermostat. Although the cell position is determined by metal stops, the closed plastic container is everywhere interposed between such metal parts and the thermostat water, to damp out temperature fluctuations. The air bath now is covered with a tight-fitting plastic lid fitted with a communicating air tube, and the water level is brought up over the cover. The closures in the direction of the optical track are made by lenses connected to the water bath through flexible rubber diaphragms, and arranged to pass a parallel beam of light through the space occupied by the cell. After further thermal equilibration, the sliding block of the cell is moved to the diffusing position, C_D, Fig. 1. A mask contains a pair of stationary double slits permitting light to pass through the air space above the sliding block to give reference fringes. These may be compared with similar fringes from the cell, or with Gouy interference fringes, by rotation of a small movable attached mask, operated by a string passing through the air tube of the plastic air bath. The entire air bath and lenses are supported by a metal framework connected to heavy steel ship-channels which form the optical bench. These channels are supported by three massive concrete pillars, each weighing nearly two tons, and the pillars themselves are free of the floor and rest on a bed of sand in a pit below floor level. To reduce the mechanical vibrations usually introduced by a stirring motor, thermostat water

(1) Presented to the faculty of Clark University in partial fulfillment of the requirements for the Ph.D. degree.

(2) Postdoctoral fellow 1957–1959.

(3) J. Thovert, *Compt. rend.*, **133**, 1197 (1901); **141**, 717 (1905).

(4) H. S. Harned and D. M. French, *Ann. N. Y. Acad. Sci.*, **46**, 267 (1945); H. S. Harned, *Chem. Rev.*, **40**, 461 (1947); H. S. Harned and R. L. Nuttall, *J. Am. Chem. Soc.*, **69**, 736 (1947).

(5) L. Onsager and R. M. Fuoss, *J. Phys. Chem.*, **36**, 2689 (1932).

(6) A. R. Gordon, *Ann. N. Y. Acad. Sci.*, **46**, 285 (1945).

(7) We are indebted to Dr. Amilcare Biancheria, formerly of these Laboratories, and to Mr. David W. Mann (deceased) and Mr. Bert Wheeler, of the David Mann Instrument Co., Lincoln, Mass., for the cell design and construction.

(8) S. Claesson, *Nature*, **158**, 834 (1946).

(9) L. G. Longsworth, private communication.

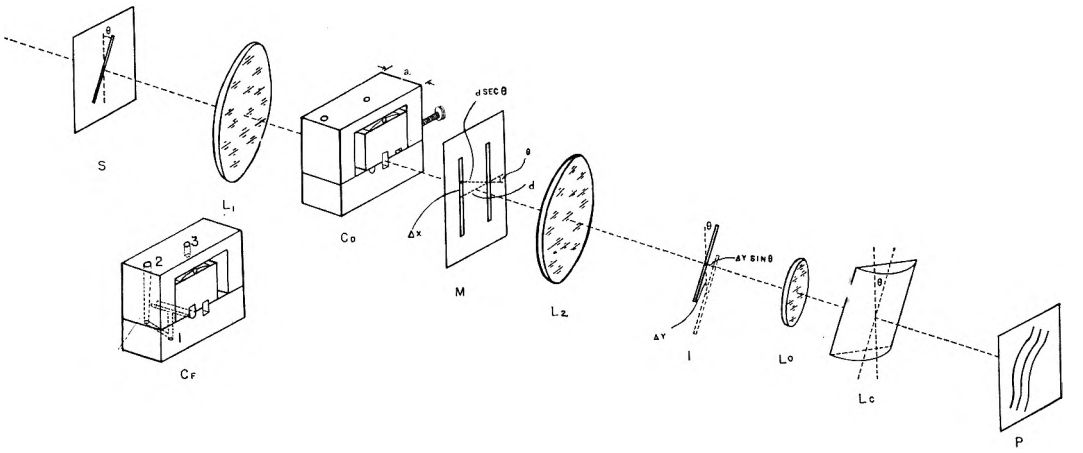

Fig. 1.—Diagrammatic arrangement of optical system: S, source slit; L_1 and L_2, collimating (schlieren) lenses; C_D, cell in the diffusing position; C_F, cell in the filling position; M, double slit mask (exaggerated); I, slit image; L_O, objective lens focussed on the cell C_D; L_C, cyclindrical lens focussed on slit image I; P, photographic plate receiving images from lens L_O and L_C.

circulation is provided by a pump mounted in the sand pit, the outlet at the bottom of the thermostat returning water to the pump. Connections are provided by pipe, interrupted by lengths of rubber hose to reduce transmission of vibration from the pump.

The optical arrangement itself is based on a shearing interferometer principle, in which coherent light passing through adjacent levels in the diffusing column is again reunited, producing an interference phenomenon dependent on the gradient of refractive index in the column. A number of shearing interferometers have been described in the recent literature for similar applications.[10-17] Of these, the arrangement of Wiedemann, with slight modifications, has been tried, since it involves the use of readily available optical elements of high quality usually employed in versatile cylindrical lens schlieren optical systems of the Philpot–Svensson type.[18,19] One advantage of this arrangement is that it also permits observation of the diffusion process with the Gouy interference method.[20-24] This can be done, if desired, by rotation of the cylinder-lens axis to the horizontal, and observation at the usual photogaphic plate position,[9] thus employing the cylinder lens for simple projection of the Gouy interference pattern.

The method of Wiedemann, as employed in the present study, involves the use of a source slit and a cylinder lens with parallel axis, inclined with respect to the vertical position customary when the schlieren system is employed as a cylinder lens Rayleigh interferometer.[25] A simplified diagram is indicated in Fig. 1, to permit a first-order calculation of the optical sensitivity. With this arrangement, the tilt of the source slit and the cylinder lens axis through the angle θ causes light from regions in the cell lying in planes not horizontal, but, instead, perpendicular to the new, tilted cylinder lens axis to superpose at the photographic plate. With the aid of two vertical masking slits at the cell separated by a distance d, Fig. 1, this causes superposition of light from pairs of levels in the cell separated vertically by the shear $\Delta x = d \tan \theta$. If the mean gradient of refractive index in the region x is dn/dx, then the difference in refractive index at the two slits is approximately

$$\Delta n = (dn/dx)\Delta x = (dn/dx)d \tan \theta \qquad (1)$$

In the slit image plane this system gives rise to a system of tilted equally spaced interference fringes in the absence of any gradient of refractive index, whose spacing at right angles to their extension, ΔY, is given by

$$\lambda^0 = d(\sec \theta)\Delta Y/b \qquad (2)$$

Here λ^0 is the wave length of light *in vacuo*, and b is the optical lever from the region of the cell to the slit image plane or, in the present case of parallel light, is equal to the focal length of the collimating lens on the image side of the cell. At the photographic plate the fringe spacing in the same direction is given by $G\Delta Y$, where G is the combined camera and cylinder lens magnification factor in the direction at right angles to the cylinder lens axis. A given value of refractive index increment Δn from eq. 1 then corresponds to a number, j, of fringes displacement at the photographic plate, equal to $a\,\Delta n/\lambda^0 = ad(dn/dx)(\tan \theta)/\lambda^0$, which corresponds to a distance

$$Gj\Delta Y = G\{ad(dn/dx)(\tan \theta)/\lambda^0\}\{b\lambda^0/d \sec \theta\} = (Gab\ dn/dx)\sin \theta \qquad (3)$$

Therefore each fringe, if completely visible, should constitute a plot of $[Gab(dn/dx)]\sin \theta$ against the reduced height coördinate $Fx \cos \theta$, where F is the camera lens magnification factor of the cell in the direction of the cylinder lens axis. It is of interest to see how the central diffraction zone appears in the resulting pattern, as predicted from Fig. 1. The mean vertical deflection $Y = ab(dn/dx)$ in the slit image plane now is magnified by the cylinder lens along the direction perpendicular to the lens axis, where the component of this deflection is $[ab(dn/dx)]\sin \theta$. Thus the displacement of the diffraction zone at the photographic plate is $[Gab(dn/dx)]\sin \theta$, which is identical with the displacement coördinate of the corresponding interference fringe, according to eq. 3.[26] It is therefore apparent that, as long as this first-order theory is reasonably accurate, this method offers the advantage that the interference fringes are continuous, and never disappear out of the central diffraction zone, as is the case with the single-slit source Rayleigh cylinder-lens interferometer.[25,27,28]

(10) H. Svensson, *Acta Chem. Scand.*, **4**, 399, 1329 (1950).
(11) R. T. Holman and L. Hagdahl, *Anal. Chem.*, **23**, 794 (1951).
(12) G. Kegeles and H. A. Sober, *ibid.*, **24**, 654 (1952).
(13) E. Wiedemann, *Helv. Chim. Acta*, **35**, 2314 (1952).
(14) W. Weinstein, *Nature*, **172**, 461 (1953).
(15) O. Bryngdahl, *Acta Chem. Scand.*, **11**, 1017 (1957).
(16) E. Ingelstam, *J. Opt. Soc. Am.*, **47**, 536 (1957).
(17) M. Françon, *ibid.*, **47**, 528 (1957).
(18) J. St. L. Philpot, *Nature*, **141**, 283 (1938).
(19) H. Svensson, *Arkiv Kemi, Mineral., Geol.*, **22A**, No. 10 (1946).
(20) G. L. Gouy, *Compt. rend.*, **90**, 307 (1880).
(21) G. Kegeles and L. J. Gosting, *J. Am. Chem. Soc.*, **69**, 2516 (1947).
(22) L. G. Longsworth, *ibid.*, **69**, 2510 (1947).
(23) C. A. Coulson, J. T. Cox, A. G. Ogston, and J. St. L. Philpot, *Proc. Roy. Soc.* (London), **A192**, 382 (1948).
(24) L. J. Gosting and L. Onsager, *J. Am. Chem. Soc.*, **74**, 6066 (1952).
(25) H. Svensson, *Acta Chem. Scand.*, **3**, 1170 (1949).

(26) This is, incidentally, the correct explanation for the warping of the interference fringe envelope in the neighborhood of the image of a very sharp boundary, as sometimes observed with Rayleigh interferometers when the cylinder lens axis is not quite vertical.
(27) E. Calvet, *Compt. rend.*, **223**, 597 (1945).
(28) J. St. L. Philpot and G. H. Cook, *Research*, **1**, 234 (1948).

This method appears to offer the distinct advantage also characteristic of certain others,[14-17] that the optical sensitivity is not fixed by the apparatus, but may be increased continuously by a rotation of optical elements to increase the shear, in the present instance by rotation of the source slit and the cylinder lens toward the horizontal. Figure 1 illustrates the intuitive conclusion that, with a cell of limited vertical dimensions, it is not possible to increase the shear without limit. However, Wiedemann[13] already has computed the more stringent limitations in his arrangement which exist on the approach of sin θ toward unity. Qualitatively these might be described as the result of too great a shear, which then produces two diffraction envelopes shaped approximately according to eq. 3, but no longer overlapping sufficiently, due to their difference in coördinates $Fx \cos \theta$, to provide interference fringes. However, we have noted with great amusement that if the source slit and the cylinder lens gradually approach the horizontal, a tilted Gouy interference fringe pattern forms, widens, and finally replaces the Wiedemann diagram. Moreover, the maximum displacement in the Gouy pattern is always located at approximately the "peak" of the Wiedemann dn/dx diagram, and it finally is apparent that the maximum displacement corresponds to the limiting approximate geometrical optical eq. 3 when sin $\theta = 1$

$$(G\Delta Y)_{max} \approx Gab(dn/dx)_{max} \qquad (4)$$

Hence the Gouy method develops the ultimate theoretical sensitivity obtainable from the shearing interferometer in the same optical system, using the same optical elements.

It is not possible to apply the Gouy method as developed for freely diffusing boundaries,[20-24] however, directly to the problem of restricted diffusion, as the refractive index function and its gradient have different forms in the two types of experiments.

Theory

It now is necessary, therefore, to reconsider for the application of both the Wiedemann and the Gouy interferometric arrangements, the solution of the differential equations for restricted diffusion.[3,4] In the present case we start with exactly equal volumes of the two liquids, which may be taken to be solution of concentration C_1 above and solution of initial concentration C_2 below the shearing plane. Taking the depth coördinate of the cell, measured downward from the top, as h, and the total depth l, we have the boundary conditions $C(h,0) = C_1$ for $0 \leq h < l/2$, $C(h,0) = C_2$ for $l/2 < h \leq l$, and $\partial C(h,t)/\partial h = 0$ for $h = 0$, l on the differential equation $\partial C(h,t)/\partial t = D[\partial^2 C(h,t)/\partial h^2]$, provided that if D is a function of C, we use the solution only for the time range where C is essentially constant throughout the apparatus. This generates the Fourier series solution

$$C(h,t) = \frac{C_1 + C_2}{2} - \frac{2(C_2 - C_1)}{\pi} \sum_{m=1}^{\infty} \frac{1}{m} \sin \frac{m\pi}{2} \cos \frac{m\pi h}{l} e^{-m^2(\pi/l)^2 Dt} \qquad (5)$$

which can be written out in the form

$$C(h,t) = \frac{C_1 + C_2}{2} - \frac{2(C_2 - C_1)}{\pi}\left[\cos \frac{\pi h}{l} e^{-(\pi/l)^2 Dt} - \frac{1}{3} \cos \frac{3\pi h}{l} e^{-9(\pi/l)^2 Dt} + \frac{1}{5} \cos \frac{5\pi h}{l} e^{-25(\pi/l)^2 Dt} + \ldots\right] \qquad (6)$$

It is now convenient, in order to take advantage of the symmetry of the cell, to measure depth coördinates x taken from the middle of the cell. That is, we define $x = h - l/2$, and re-express eq. 6 in terms of x

$$C(x,t) = \frac{C_1 + C_2}{2} - \frac{2(C_2 - C_1)}{\pi}\left[\cos \frac{\pi(x + l/2)}{l} e^{-(\pi/l)^2 Dt} - \frac{1}{3} \cos \frac{3\pi(x + l/2)}{l} e^{-9(\pi/l)^2 Dt} + \frac{1}{5} \cos \frac{5\pi(x + l/2)}{l} e^{-25(\pi/l)^2 Dt} + \ldots\right],$$

or

$$C(x,t) = \frac{C_1 + C_2}{2} - \frac{2(C_2 - C_1)}{\pi}\left[-\sin \frac{\pi x}{l} e^{-(\pi/l)^2 Dt} - \frac{1}{3} \sin \frac{3\pi x}{l} e^{-9(\pi/l)^2 Dt} - \frac{1}{5} \sin \frac{5\pi x}{l} e^{-25(\pi/l)^2 Dt} - \ldots\right] \qquad (7)$$

Since the shearing interferometric method in use here develops a first difference in the refractive index function at adjacent levels, it is desirable to use eq. 7 to generate a corresponding relationship for the gradient of concentration in the restricted diffusion experiment. This may be done by taking first differences from eq. 7, at two adjacent levels, $x - \delta$ and $x + \delta$

$$C(x - \delta,t) = \frac{C_1 + C_2}{2} - \frac{2(C_2 - C_1)}{\pi}\left[-\sin \frac{\pi(x - \delta)}{l} e^{-(\pi/l)^2 Dt} - \frac{1}{3} \sin \frac{3\pi(x - \delta)}{l} e^{-9(\pi/l)^2 Dt} - \frac{1}{5} \sin \frac{5\pi(x - \delta)}{l} e^{-25(\pi/l)^2 Dt} - \ldots\right] \qquad (8)$$

$$C(x + \delta,t) = \frac{C_1 + C_2}{2} - \frac{2(C_2 - C_1)}{\pi}\left[-\sin \frac{\pi(x + \delta)}{l} e^{-(\pi/l)^2 Dt} - \frac{1}{3} \sin \frac{3\pi(x + \delta)}{l} e^{-9(\pi/l)^2 Dt} - \frac{1}{5} \sin \frac{5\pi(x + \delta)}{l} e^{-25(\pi/l)^2 Dt} - \ldots\right] \qquad (9)$$

$$\frac{C(x+\delta,t)-C(x-\delta,t)}{2\delta}=\frac{2(C_2-C_1)}{\pi}\left[\cos\frac{\pi x}{l}\frac{\sin\pi\delta/l}{\delta}e^{-(\pi/l)^2Dt}+\right.$$
$$\left.\frac{1}{3}\cos\frac{3\pi x}{l}\frac{\sin 3\pi\delta/l}{\delta}e^{-9(\pi/l)^2Dt}+\frac{1}{5}\cos\frac{5\pi x}{l}\frac{\sin 5\pi\delta/l}{\delta}e^{-25(\pi/l)^2Dt}+\ldots\right] \quad (10)$$

$$\lim_{\delta\to 0}\frac{C(x+\delta,t)-C(x-\delta,t)}{2\delta}=\frac{2(C_2-C_1)}{\pi}\left[\frac{\pi}{l}\cos\frac{\pi x}{l}e^{-(\pi/l)^2Dt}+\right.$$
$$\left.\frac{1}{3}\cdot\frac{3\pi}{l}\cdot\cos\frac{3\pi x}{l}e^{-9(\pi/l)^2Dt}+\frac{1}{5}\cdot\frac{5\pi}{l}\cdot\cos\frac{5\pi x}{l}e^{-25(\pi/l)^2Dt}+\ldots\right]$$

which is the result one would obtain by differentiating eq. 7

$$\frac{dC(x,t)}{dx}=\frac{2(C_2-C_1)}{l}\left[\cos\frac{\pi x}{l}e^{-(\pi/l)^2Dt}+\cos\frac{3\pi x}{l}e^{-9(\pi/l)^2Dt}+\cos\frac{5\pi x}{l}e^{-25(\pi/l)^2Dt}+\ldots\right] \quad (11)$$

That this is valid also may be checked by requiring that $dC/dx = 0$ for $x = -l/2$ and $x = +l/2$, and $dC/dx = max$ for $x = 0$. From eq. 11, if it may be assumed that the refractive index of the liquid is a linear function of the solute concentration, it follows that the refractive index gradient is

$$\frac{dn(x,t)}{dx}=\frac{2(n_2-n_1)}{l}\left[\cos\frac{\pi x}{l}e^{-(\pi/l)^2Dt}+\cos\frac{3\pi x}{l}e^{-9(\pi/l)^2Dt}+\cos\frac{5\pi x}{l}e^{-25(\pi/l)^2Dt}+\ldots\right] \quad (12)$$

where n_1 and n_2 are the refractive indices of the original upper and lower solutions, respectively.

Wiedemann Method.—A convenient application of this method to eq. 12 is to measure the maximum height of the gradient curve in the direction perpendicular to the direction of the cylinder lens axis. From eq. 3 and 12 this height is given by the value at $x = 0$

$$H_{max}=Gab(\sin\theta)(dn/dx)_{max}$$
$$=\frac{2Gab(n_2-n_1)}{l}(\sin\theta)$$
$$[e^{-(\pi/l)^2Dt}+e^{-9(\pi/l)^2Dt}+e^{-25(\pi/l)^2Dt}+\ldots] \quad (13)$$

The experimental requirements to make this an absolute method are independent measurements of (1) $n_2 - n_1$, or of the specific refractive index increment and the two concentrations C_1 and C_2, (2) the optical factors Gab, (3) the inclination θ of the cylinder lens axis with the vertical, (4) the depth of the cell, and (5) the time of diffusion. In preliminary experiments, using sucrose and β-alanine solutions at 25°, values of dn/dc were taken from the literature.[29,30] The composite optical factors Gab were determined from the spacing of interference fringes photographed at the plate after being generated by a Rayleigh double slit of measured separation placed in the cell position. The inclination θ was measured from the superposition of straight reference fringes on the shadow of a vertical mask, tested with a plumb line. The cell depth, l, was measured by means of a David Mann comparator to be 1.9878 cm. For ideal diffusion, the time can be taken from the instant of boundary formation, to within a negligible correction here. However, for non-ideal diffusion, only times sufficiently long to give essentially uniform concentration allow the use of Fick's second law of diffusion. At such times only the first term of eq. 10 might be used, according to Thovert's[3] and to Harned's approach.[4] A plot of $\ln H_{max}$ *vs.* t would then give a slope of $-(\pi/l)^2D$, from which the diffusion coefficient is readily determined in principle. In practice, it is difficult to produce a large enough deflection at such late times to supply satisfactory precision of measurement.

Gouy Method.—The basic results from the calculations relating to the use of this method for free diffusion[21,22,24,29] may be used as a starting point for the restricted diffusion application. The path difference $P - P'$ for pairs of rays which superpose by geometric optics is given by

$$a(n-n')-2ax\frac{dn}{dx}=P-P' \quad (14)$$

where n is the refractive index and dn/dx the gradient of refractive index at the level x, n' is the refractive index at the symmetrical level $-x$, and a is the cell thickness. According to wave theory, when the number of interference fringes is not too small, eq. 14 becomes equal to $Z_j\lambda^0$ for interference minima, where Z_j represents a zero in the Airy integral[21,29] and λ^0 is the wave length of the light. If the number of fringes becomes ten or less, it is important to examine the errors in this approximation, and to use a more extended theory.[24] When the conditions for restricted diffusion as given by eq. 7 and 11 are superposed on eq. 14, there results

(29) L. J. Gosting and M. S. Morris, *J. Am. Chem. Soc.*, **71**, 1998 (1949).

(30) H. C. Donoian and G. Kegeles, *ibid.*, **83**, 255 (1961).

$$Z_j/j_m \simeq \frac{4}{\pi}\left[\left\{\sin\frac{\pi x}{l}\,e^{-(\pi/l)^2Dt} + \frac{1}{3}\sin\frac{3\pi x}{l}\,e^{-9(\pi/l)^2Dt} + \frac{1}{5}\sin\frac{5\pi x}{l}\,e^{-25(\pi/l)^2Dt} + \ldots\right\} - \frac{\pi x}{l}\left\{\cos\frac{\pi x}{l}\,e^{-(\pi/l)^2Dt} + \cos\frac{3\pi x}{l}\,e^{-9(\pi/l)^2Dt} + \cos\frac{5\pi x}{l}\,e^{-25(\pi/l)^2Dt} + \ldots\right\}\right] \quad (15)$$

where j_m is the original number of fringes, given by

$$j_m = a(n_2 - n_1)/\lambda^0 \quad (16)$$

The corresponding displacement of the interference fringe minimum, as magnified at the photographic plate with the factor G, from the undeviated slit image is given by

$$Y_j = Gab\frac{dn}{dx} = 2Gb\cdot j_m(\lambda^0/l)\left[\cos\frac{\pi x}{l}\,e^{-(\pi/l)^2Dt} + \cos\frac{3\pi x}{l}\,e^{-9(\pi/l)^2Dt} + \cos\frac{5\pi x}{l}\,e^{-25(\pi/l)^2Dt} + \ldots\right] \quad (17)$$

Two alternative methods of calculation have suggested themselves. In the first, it is assumed that the time t is so long that only the first terms in the Fourier series in eq. 15 and 17 need be retained. Then, from these equations

$$Z_j/Y_j = \frac{2l}{\pi Gb\,\lambda^0}\,[\tan z_j - z_j] \quad (18)$$

where $z_j = \pi x/l$. Equation 17 can now be rewritten in terms of z_j, including only the first Fourier term

$$Y_j = 2Gbj_m(\lambda^0/l)(\cos z_j)e^{-(\pi/l)^2Dt} \quad (19)$$

Knowing the values[29] of Z_j from the fringe minima numbers, j, and the maximum original number of fringes, j_m, and the corresponding experimental values, Y_j, one can evaluate $\tan z_j - z_j$ from eq. 18. This then makes it possible to obtain the corresponding value of $\cos z_j$. For this purpose, an extensive tabulation of values of $\cos z_j$ *vs.* $\tan z_j - z_j$ was made at close intervals of z_j, with the aid of an IBM 709 computer. Once the value of $\cos z_j$ is obtained by reference to this table, it is inserted into eq. 19 and a fringe system constant for a given time is obtained

$$Y_j/\cos z_j = K_t = 2Gbj_m(\lambda^0/l)e^{-(\pi/l)^2Dt} \quad (20)$$

From this, the diffusion coefficient can be evaluated in the case of ideal diffusion as

$$D \propto -\left(\frac{l}{\pi}\right)^2\left(\frac{1}{t}\right)\ln K_t \quad (21)$$

or in the case of non-ideal diffusion at sufficiently long times from

$$d\ln K_t/dt = -\left(\frac{\pi}{l}\right)^2 D \quad (22)$$

There is a potential source of systematic error in this method which increases in importance as the original number of fringes becomes small, and also as the time becomes long, which is largely the result of a superposed diffraction effect. It is of interest that the error in using the Airy integral approximation in the case of free diffusion has been evaluated[24] for Gouy experiments involving small path differences, and that this error becomes minimized as the most deflected Gouy fringes are observed. Consequently, it was felt desirable to arrange a method of computation which might not require extremely long times, but would make use of higher order terms in the Fourier series of eq. 15 and 17, and also would attempt to extrapolate out the errors in the Airy integral approximation. A suggestion was obtained from the extrapolation method used by Akeley and Gosting[31] to obtain solute diffusion coefficients in three-component ideal free diffusion experiments. They found that the apparent fringe system constant computed from $Y_j/e^{-\zeta_j^2}$, where $\zeta_j \equiv x/2\sqrt{Dt}$, is a linear function of $Z_j^{2/3}$, which can be extrapolated to $Z_j = 0$ to give the correct C_t value for the system. We now seek to express eq. 12 and 15 as Taylor's series expansions about $z_j = 0$. There results

$$Z_j/j_m \simeq \frac{4}{3\pi}z_j^3\left\{e^{-(\pi/l)^2Dt} + 9e^{-9(\pi/l)^2Dt} + 25e^{-25(\pi/l)^2Dt} + \ldots\right\} \quad (23)$$

and

$$Y_j \simeq 2Gbj_m(\lambda^0/l)\left[\left\{e^{-(\pi/l)^2Dt} + e^{-9(\pi/l)^2Dt} + e^{-25(\pi/l)^2Dt} + \ldots\right\} - \frac{z_j^2}{2}\left\{e^{-(\pi/l)^2Dt} + 9e^{-9(\pi/l)^2Dt} + 25e^{-25(\pi/l)^2Dt} + \ldots\right\}\right] \quad (24)$$

From these equations, it then is found that

$$Y_j \simeq 2Gbj_m\,(\lambda^0/l)\left[\alpha(t) - \frac{1}{2}\left(\frac{3\pi}{4j_m}\right)^{2/3}\beta(t)^{1/3}\,Z_j^{2/3}\right] \quad (25)$$

where

$$\alpha(t) = e^{-(\pi/l)^2 Dt} + e^{-9(\pi/l)^2 Dt} + e^{-25(\pi/l)^2 Dt} + \ldots \quad (26)$$

and

$$\beta(t) = e^{-(\pi/l)^2 Dt} + 9e^{-9(\pi/l)^2 Dt} + 25e^{-25(\pi/l)^2 Dt} + \ldots \quad (27)$$

According to eq. 25, a plot of Y_j *vs.* $Z_j^{2/3}$ should be linear, and extrapolate at $Z_j = 0$ to give $\alpha(t)$, defined by eq. 26. While the saddle-point integrations of Gosting and Onsager[24] should be repeated for the case of restricted diffusion to obtain a precise evaluation of the errors in using the Airy integral approximation, it seems intuitively correct that, in this case also, the errors will be minimized for systems containing few fringes, if extrapolation is made to $Z_j = 0$.

The diffusion coefficient then is computed directly from eq. 26. First, an approximate value of D is obtained from the first Fourier term. Then, this is inserted into the right-hand side of eq. 26, which is compared with the experimental value of $\alpha(t)$. If $\alpha(t)$ is smaller than the right-hand side, D is incremented by a fixed amount, and the comparison between $\alpha(t)$ and the right-hand side is made again This process is repeated until the right hand side becomes equal to the experimental value of $\alpha(t)$, indicating that convergence has been obtained, and this value of D then is retained. The whole computation was programed for the IBM 709 computer.[32]

Experimental

Fisher reagent grade sucrose, after being kept in a desiccator, was used for the diffusion run without purification. Six Rayleigh pictures were taken immediately after boundary formation with the double slit in front of the diffusing channel. This, together with Gouy pictures taken during the early stages of free diffusion, was used for the calculation of the total number of fringe minima, j_m. Kodak Super Panchro-Press plates were used.

As the boundary is formed the glass surfaces adjacent to the sliding block are covered with thin films of grease. This effect is pronounced only in the neighborhood of the shearing plane, but this makes it difficult to count the integral number portion of the j_m value in very early photographs. Successive trials of integers in the j_m values were used, therefore, for the calculation of C_t[21-22] until reasonably constant C_t values were obtained for a given time. The Gouy pictures in the late stage of restricted diffusion were taken using Kodak Metallographic plates.

The Rayleigh pictures for determination of the undeviated slit image were taken after the sucrose solution in the cell became homogeneous. For this the cell was taken out from the water bath and put upside down overnight. The cell position was changed several times and the cell then was replaced in the water bath, after preliminary temperature equilibration on the copper frame. The cell temperature had to be brought to 25° because the δ-correction was found to be influenced by the temperature. Successive Rayleigh pictures were taken until the δ-correction became constant. The $Gb\lambda^0$ value was found to be 0.01281.

For the evaluation of D values the zero time corrections were not applied because they made an insignificant change in the final results.

Results

Table I shows the diffusion coefficients of sucrose in water at 25 ± 0.02° using the Gouy method. The diffusion coefficients in the second column were obtained by the $Z_j^{2/3}$ extrapolation method (eq. 25). This shows an internal self-consistency of 0.3%. The average value agrees with the values obtained by Gosting and Morris[29] to within the present experimental error.

TABLE I

DIFFUSION COEFFICIENTS OF SUCROSE IN WATER AT 25°

$(C_1 + C_2)/2 = 1.0012$[a]

$C_2 - C_1 = 0.0985$

Time, sec.	$Z_j^{2/3}$ extrapolation method, $D \times 10^5$, cm.²/sec.	Tangent function method, $D \times 10^5$, cm.²/sec.
43,204	5.157	
45,004	5.144	
48,605	5.120	
52,205	5.135	
59,406	5.135	
64,807	5.132	4.909
66,607	5.131	4.891
72,007	5.142	4.937
77,408	5.102	4.886
82,808	5.164	4.972
93,609	5.102	4.967
97,210	5.134	4.984
136,814	5.157	4.952
Mean	5.135	Mean 4.937
Av. dev.	0.014 = 0.27%	Av. dev. 0.032 = 0.65%

[a] C_1 = concentration of upper solution in g. per 100 ml. of solution; C_2 = concentration of lower solution in g. per 100 ml. of solution.

The third column shows the D values obtained by the tangent function method (eq. 18 and 19). The D-values were evaluated from photographs taken only after 17 hr. of diffusion, when the second term of the Fourier series becomes negligible. The discrepancy appears to bear out that diffraction errors are produced in the tangent function method, as predicted in the discussion following eq. 22.

Discussion

In its present stage of development, the method is self-consistent to about 0.3% in the diffusion coefficient, if time is counted from the instant of boundary formation. Since the diffusion coefficient for non-ideal solutions can be determined correctly only by differences between successive times of diffusion at sufficiently long times to provide essentially uniform concentration in the column, a decrease in precision is to be expected. However, this can be compensated by an improvement in the design of the optical system. In order to obtain larger deflections of light, the optical lever, b, can be increased appreciably above its present value of 34.5 inches. The cylindrical lens magnification factor, G, can also be increased very appreciably above its present value of 1.3. An over-all increase of 5–10 times in the deflection of Gouy fringes thus is achievable. It is expected that this can be accomplished with no great sacrifice in the accuracy with which these fringes can be measured with the comparator, at late stages of diffusion. Therefore we look forward to an im-

(31) D. F. Akeley and L. J. Gosting, *J. Am. Chem. Soc.*, **75**, 5685 (1953).

(32) We are indebted to Dr. J. L. Bethune for assistance with the Fortran program.

provement in the equipment which may provide differential diffusion data of accuracy approaching 0.1 to 0.2%, at very low concentrations. For certain poorly conducting systems involving extensive solute–solute interaction, such data would be quite significant if they could be obtained.

Acknowledgments.—This work was initiated with the aid of a grant from Research Corporation. Further support was obtained under U. S. Public Health Service Grant A-3508. IBM Computer calculations were made possible by the availability of the M.I.T. Computation Center at Cambridge, Mass., through the New England Cooperating Colleges arrangement. We wish to thank Dr. J. L. Bethune for help in aligning the optics.

STABILITY OF EMULSIONS TO ULTRACENTRIFUGATION: DISCONTINUITY AT THE CRITICAL MICELLE CONCENTRATION

BY SELWYN J. REHFELD

Shell Development Company, Emeryville, California

Received March 7, 1962

A new and rapid method for quantitatively studying the mechanical stability of emulsions has been developed employing the ultracentrifuge. This experimental method offers the possibility of separating the coagulation of emulsions into distinct steps: aggregation and coalescence. Emulsions of benzene in an equal volume of water, stabilized with various concentrations of sodium dodecyl sulfate, were evaluated for mechanical stability by measuring the volume fraction of emulsion that remains after various times in the ultracentrifuge at 25,980 r.p.m. The mechanical stability decreases with decreasing emulsifier concentration. Plots of volume fraction of emulsion remaining stable *vs.* the logarithm of the concentration of emulsifier show a definite discontinuity. This sharp change in mechanical stability occurred at an emulsifier concentration corresponding closely to the critical micelle concentration (c.m.c.) determined in earlier studies. The results indicate that at emulsifier concentrations below the c.m.c., a non-linear relationship between mechanical stability and time occurs.

Introduction

Coagulation of emulsions is generally considered to take place in two steps; the first of these is aggregation, in which droplets of the dispersed phase form aggregates, while the second step is coalescence of the droplets.

The present work was undertaken to evaluate the mechanical stability of oil–water emulsions as a function of concentration of surface active agent. Ultracentrifugation was found to offer a means for accomplishing the aggregation step very rapidly and thus producing a highly concentrated emulsion before appreciable coalescence can occur. The coalescence process then could be studied independently.

Experimental

Materials.—The emulsifying agent, sodium dodecyl sulfate (NaDS), was synthesized at this Laboratory. An aqueous solution of this material showed no minimum in surface tension–concentration curves. Reagent grade benzene, manufactured by Allied Chemical, was the oil phase in these experiments.

Procedure.—A series of emulsions of benzene in water was prepared with various concentrations of emulsifying agent. A 1:1 phase ratio by volume was used. A Gifford–Wood Eppenbach homo-mixer was used to emulsify these systems at a speed of about 7000 r.p.m. (Variac setting of 110 volts) and for exactly 5 min. Care was taken to reproduce conditions exactly in preparing the emulsions. Immediately after preparation 0.7 ml. of the emulsion was injected into an ultracentrifuge cell (12 mm. light path and a 4 degree sector angle). The cell then was placed in an analytical rotor and subsequently centrifuged in a Beckman Spinco Model E ultracentrifuge at 25,980 r.p.m. (other speeds also can be used) and at 25.0 ± 0.1°. Photographic records were made of the cell at regular time intervals (4 min.) during the experiment. The first picture was taken immediately upon attainment of the pre-set centrifugal speed. The time required to attain this speed was 2 min. and 45 seconds ± 15 seconds. During centrifugation three layers develop in the cell: benzene (coagulated emulsion), the remaining stable emulsion, and the aqueous layer.

As a result of the increasing emulsion concentration due to removal of water (aggregation step) a sizeable reduction in the volume of the emulsion occurs while the rotor is coming up to speed. With unstable emulsions various degrees of coagulation also occur leading to the development of a benzene layer distinct from the concentrated emulsion layer. The volume fraction of the cell[1] occupied by the remaining emulsified layer was designated as ϕ. Plots then were made of ϕ_0 and ϕ_{20} *vs.* the logarithm of the emulsifier concentration. (The subscript on ϕ denotes the time in minutes after the centrifuge reaches constant speed.)

Experimental Results

Boundary Changes during Centrifugation.—The boundary between the uncoalesced emulsion and the aqueous phase forms some time within the first three minutes of centrifugation and remains in a constant position during the entire run even when there is complete coalescence of the emulsion. This fact indicates that almost all of the aqueous phase of the emulsion is separated from the benzene droplets very early in the centrifugation process, leaving a very concentrated emulsion consisting of benzene droplets, adsorbed emulsifier, and a very small amount of water. At this stage the system can be described as an aggregated and compressed emulsion. The droplets must assume some shape other than spherical (polyhedral?) in order to have a dispersed phase constituting so nearly 100% by volume of the concentrated emulsion. Any further decrease in the volume of this aggregated emulsion is the result of coalescence of the benzene droplets and consequent separation into a distinct benzene phase.

Figure 1 shows the results of centrifugation of an emulsion of 50% v. benzene in 50% v. water stabilized with 2.1% w. sodium dodecyl sulfate. The actual volumes found, 48% v. benzene droplets in 52% v. aqueous phase, indicate a loss in volume of benzene by evaporation in the emulsification

(1) T. Svedberg and K. O. Pedersen, "Ultracentrifuge," Oxford Press, New York, N. Y., 1940, p. 7.

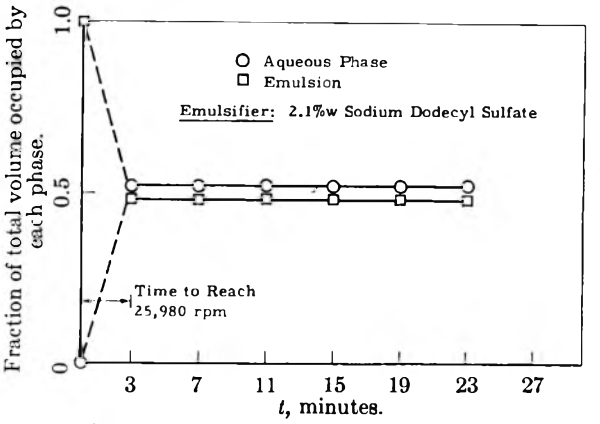

Fig. 1.—Volume changes occurring in a stable emulsion as a function of time.

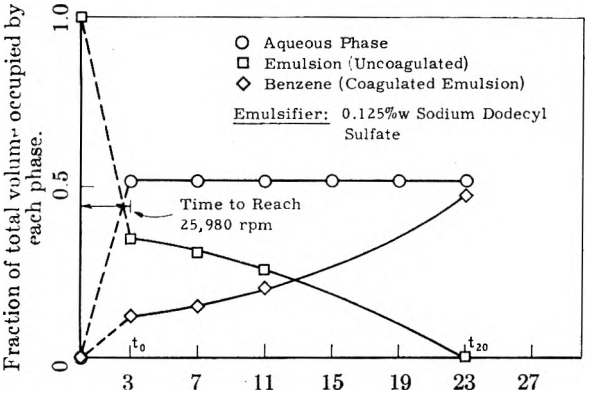

Fig. 2.—Volume changes occurring in an unstable emulsion as a function of time (in min.).

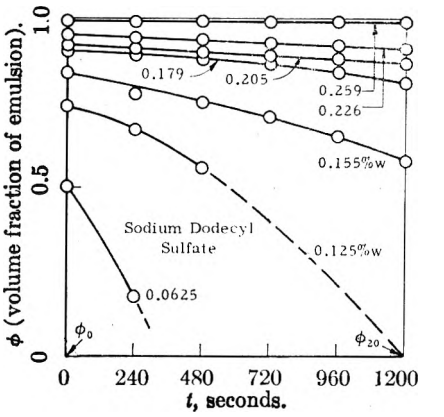

Fig. 3.—Fraction of emulsion remaining after t, seconds of centrifugation.

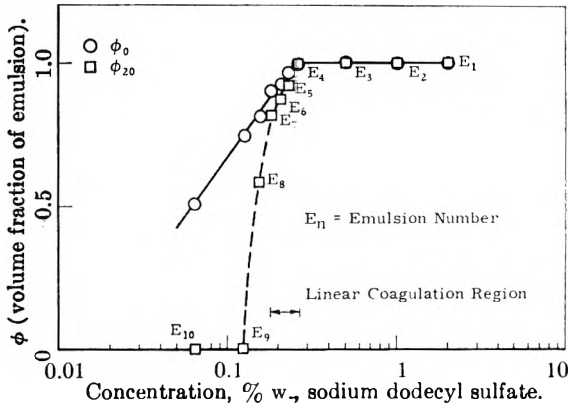

Fig. 4.—Fraction of emulsion at time t_0 and t_{20} as a function of concentration.

step. In this run the emulsion was stable throughout, the only effect being the removal of almost all of the aqueous phase to leave a flocculated but stable benzene emulsion.

Figure 2 shows the result for an unstable emulsion of 50% v. benzene in 50% v. water stabilized with only 0.125% w. of sodium dodecyl sulfate. During the first three minutes the aqueous phase is separated from the benzene droplets and the aggregated emulsion has coalesced to some extent, producing a definite benzene layer in addition to the remaining emulsion layer and aqueous phase.

Plots of the volume fraction of emulsion, ϕ, *vs.* time for a series of emulsions stabilized with NaDS are shown in Fig. 3. (Note that emulsions prepared with concentrations of NaDS below 0.18% w. gave non-linear plots.) The ϕ_0 and ϕ_{20} for each of the emulsions were plotted against the logarithm of NaDS concentration. A discontinuity was found at a concentration of 0.26% w. NaDS (see Fig. 4). It is interesting that this value closely approximates the accepted value of the critical micelle concentration (c.m.c.) of NaDS.

In the literature the values reported for the c.m.c. of NaDS by various methods are in the region of 0.18 to 0.25% w.[2] The spectroscopic method utilizing dyes[3] gives the low value and the pH method[4] the high value.

Values of 0.18% w. (spectroscopic method), 0.22% w. (conductivity method), and 0.22% w. (surface tension method) were found in this Laboratory for the c.m.c. of the NaDS used in these experiments.

Discussions and Conclusions.—In the experiments described here, the oil droplets in oil-in-water emulsions have been forced by centrifugation into very closely packed arrays which can be described as aggregated emulsions. The resistance of the aggregated droplets to coalescence arises from the existence of very thin water films between droplets and from the presence of ionized emulsifier adsorbed on the particle surfaces. The coalescence of emulsion drops has been shown by Gillespie and Rideal[5] to be related to the rate of drainage of the thin films separating them, the probability of film rupture being an inverse function of film thickness. Van den Tempel's[6] studies also indicated that the rate of coalescence of aggregated emulsions is determined by the average lifetime of the films separating the droplets. He derived equations which indicate that coalescence is a first-order process but his experimental data did not conclusively show a first-order process. Our results, obtained by a quite different experimental approach, indicate that the rate of coales-

(2) W. C. Preston, *J. Phys. and Colloid. Chem.*, **52**, 84 (1948).

(3) W. D. Harkins, "Physical Chemistry of Surface Films," Reinhold Publishing Corp., New York, N. Y., 1952.

(4) A. S. C. Lawrence and M. P. McDonald, "Second International Congress of Surface Activity," Vol. I, Academic Press, New York, N. Y., 1957, p. 385.

(5) T. Gillespie and E. K. Rideal, *Trans. Faraday Soc.*, **52**, 173 (1956).

(6) M. Van den Tempel, "Second International Congress of Surface Activity," Academic Press, New York, N. Y., 1957, Vol. I, p. 439.

cence varies as a function of emulsifier concentration. Further studies of the kinetics of coalescence will be reported at a later date.

The sharp change observed in stability of emulsions to centrifugation when the emulsifier concentration passes through the critical micelle concentration is believed to be associated with the density of packing of adsorbed emulsifier on the particle surface. As the emulsifier concentration is raised from very low values, the amount of emulsifier adsorbed on the emulsion particle increases and the area of the particle surface per adsorbed emulsifier molecule decreases. At the critical micelle concentration the density of packing is at its highest value with the area per adsorbed emulsifier molecule approaching the actual molecular cross section. At this point, the mechanical stability of the adsorbed emulsifier layer can reasonably be expected to be greatest in view of the well known force–area curves for adsorbed monolayers. The addition of emulsifier in excess of the critical micelle concentration should only increase the number of micelles in the aqueous phase without appreciable effect on the density of packing of the adsorbed emulsifier.

Acknowledgments.—The writer wishes to thank Drs. F. M. Fowkes and W. M. Sawyer for determining the c.m.c. of the emulsifier used in these experiments.

DISCUSSION

S. J. REHFELD.—I wish to add the following to the experimental details given in this paper: The original particle size of the emulsions was approximately 1 μ; this was determined microscopically. After 3 min. of centrifugation, the time required to bring the rotor to 25,980 r.p.m. and then stopping the run, the particle size had increased approximately tenfold. This increase in particle size also occurred above the critical micelle concentration with no visible coagulation occurring. Therefore, the interfacial area was reduced drastically and the emulsifier concentration in the aqueous phase will be almost equal to but less than the emulsifier concentration originally used to prepare the emulsion.

This increase in droplet size also has been observed using a more viscous oil, *n*-hexadecane.

R. D. VOLD (University of Southern California).—Would you not agree that the separated oil should not be called a coagulated emulsion? The rate of appearance of clear oil may be a measure of a rate of flocculation, a rate of coalescence, a rate of mass transfer of larger oil "drops" through the flocculated compressed emulsion, or a rate of coalescence of discrete drops with the bulk oil. Calling the separated clear oil "coagulated emulsion" is merely likely to confuse the issue.

S. J. REHFELD.—The process of coagulation is considered to take place in two steps, first aggregation, which results in two or more particles coming into close contact with no change in particle diameter (this step is reversible), and secondly, coalescence, the flowing of two or more particles together to form a new droplet of larger diameter. At this point a problem in terminology does exist. When does a droplet cease to be called a droplet but a continuous oil phase? The rate of coagulation is defined as the rate of transition of oil droplets to a clear continuous oil phase; it would be proper, therefore, to refer to the continuous oil phase as coagulated emulsion, which also describes the final product in the coagulation process.

W. C. SIMPSON (Shell Development Company).—Can you comment on the applicability of this technique to emulsions stabilized with surface active agents other than sodium dodecyl sulfate?

S. J. REHFELD.—The ability of Dresinate 214, a commercial emulsifier composed predominantly of the potassium salt of dehydroabietic acid, to stabilize oil–water emulsions to ultracentrifugation was examined using the same technique reported in this paper. A sharp break in the mechanical stability was found to occur between 1.1 and 1.2 weight % Dresinate 214.

The critical micelle concentration of this emulsifier was determined by Dr. W. M. Sawyer using interfacial and surface tension techniques. A sharp break in both surface and interfacial tension *vs.* concentration occurred also between 1.1 and 1.2 wt. % Dresinate 214.

AN ULTRACENTRIFUGAL METHOD FOR THE QUANTITATIVE DETERMINATION OF EMULSION STABILITY[1]

BY ROBERT D. VOLD AND ROBERT C. GROOT

Department of Chemistry, University of Southern California, Los Angeles 7, California

Received March 12, 1962

A method was developed for use of the ultracentrifuge to determine the rate of separation of Nujol from Nujol–water emulsions stabilized with sodium dodecyl sulfate (SDS). This rate remains constant throughout separation of a large proportion of the oil in the emulsion, and can be used as a measure of the stability. The effect of differences in the purity and concentration of the SDS and of changes in the speed of centrifugation on the ultracentrifugal stability was determined. It is desirable to maintain constant drop size distribution despite differing SDS concentration in order to obtain unambiguous results. The ultracentrifugal stability increases with increasing bulk concentration of SDS until the equilibrium concentration in the aqueous phase reaches the critical micelle concentration, and thereafter is independent of concentration. The results are also correlated with the extent of adsorption of SDS at the oil–water interface.

Introduction

The process of demulsification can be separated into two steps: flocculation, which decreases the number of kinetically independent units but causes no change in the total number of primary particles, and coalescence, which results in the ultimate separation of the oil as a bulk phase. In this paper emulsion stability is used exclusively to refer to the rate of coalescence. The chief objective of the present work was development of a satisfactory measure of this rate so as to permit quantitative comparison between experiment and the predictions of different theories as to the rate-determining step in the process. More particularly, it would be valuable to ascertain whether the rate of drainage of water from the thin lamellae separating approaching oil drops, or the rate of rupture of the adsorbed film of stabilizer coating the drops, is the more important factor.

Many attempts have been made to measure the stability of emulsions in terms of changes in size distribution,[2-5] interfacial area,[6-10] or otherwise.[11,12] However, those based on counting techniques are exceedingly tedious while those based on change of interfacial area or drop volume with time may be very insensitive to small but important changes occurring in the emulsion. Moreover, the latter methods may be useful only with quite unstable emulsions since Nujol emulsions stabilized with sodium dodecyl sulfate (SDS) (present work) showed very little change in total interfacial area over a period of three weeks. Likewise, the average drop size in a 20% heat-bodied linseed oil (M 37 oil)–80% water emulsion stabilized with 1% technical SDS did not change significantly over a period of a month.[13]

Earlier attempts[14-16] to use rate of separation of free oil under gravity as a measure of emulsion stability were not regarded as promising because of the long time required for each measurement and the uncertainty as to whether all the demulsified oil had separated sufficiently so as to be visually detectable. Interesting results had been obtained[17] using a bucket type centrifuge, but preliminary experiments showed that Nujol–water emulsions did not separate oil sufficiently rapidly under these conditions. In extensive experiments with a Servall angle centrifuge at 10,000 r.p.m., oil separation was sufficiently rapid but reproducibility was unsatisfactory because of boundary disturbances occurring during deceleration or during the handling of the system necessary to separate and measure the demulsified oil.

Hence a method was developed using a Spinco ultracentrifuge permitting observation of the emulsion while undergoing centrifugation.[18] This method is described in detail and its use illustrated by application to determination of the effect of the concentration of SDS on the stability of Nujol–water emulsions. However, it must be emphasized that results of the ultracentrifugal method will not necessarily correlate with the shelf stability of the same emulsion since they pertain to the highly concentrated cream remaining after rapid separation of most of the water in the ultracentrifugal field.

The adsorption of SDS at the oil–water interface was also determined in these systems so as to permit correlation of the ultracentrifugal stability with the extent of coverage of the oil droplets with adsorbed emulsifier.

Materials and Techniques

Ultracentrifugal Method.—A Beckman Spinco Model E ultracentrifuge was used in this work with a 12 mm. 4°

(1) A partial report of work done under contract with the U. S. Department of Agriculture and authorized by the Research and Marketing Act. The contract was supervised by the Northern Utilization Research and Development Division of the Agricultural Research Service.

(2) S. Berkman, *J. Phys. Chem.*, **39**, 527 (1935).

(3) E. K. Fischer and W. D. Harkins, *ibid.*, **36**, 98 (1932).

(4) H. H. G. Jellinek, *J. Soc. Chem. Ind.*, **69**, 225 (1950).

(5) E. S. Rajagopal, *Kolloid Z.*, **167**, 17 (1960).

(6) A. King and L. N. Mukerjee, *J. Soc. Chem. Ind.*, **57**, 431 (1938).

(7) A. King and L. N. Mukerjee, *ibid.*, **58**, 243 (1939).

(8) L. N. Mukerjee and S. N. Srivastava, *Kolloid Z.*, **147**, 146 (1956).

(9) H. Lotzkar and D. Maclay, *Ind. Eng. Chem.*, **35**, 1294 (1943).

(10) N. E. Lloyd, *J. Colloid Sci.*, **14**, 441 (1959).

(11) M. van den Tempel, *Rec. trav. chim.*, **72**, 433 (1953).

(12) A. S. C. Lawrence and O. Mills, *Discussions Faraday Soc.*, **18**, 98 (1954).

(13) Unpublished data obtained in this Laboratory by B. Levy and R. L. Vold.

(14) E. L. Lederer, *Kolloid Z.*, **71**, 61 (1935).

(15) D. F. Cheesman and A. King, *ibid.*, **83**, 33 (1938).

(16) D. F. Cheesman and A. King, *Trans. Faraday Soc.*, **36**, 241 (1940).

(17) R. C. Merrill, *Ind. Eng. Chem. (Anal. Ed.)*, **15**, 743 (1943).

(18) While this work was in process it came to the authors' attention that Dr. E. R. Garrett was using an ultracentrifuge to study pharmaceutical emulsions. This work has now been published [*J. Pharm. Sci.*, **51**, 35 (1962)], but deals primarily with rate of flocculation and creaming although some measurements of oil separation are also reported.

standard cell having a capacity of about 0.8 ml. The emulsion is introduced through a hypodermic needle. Since small slicks of free oil often were observed in these emulsions after standing overnight they were swirled gently and inverted 20 times or so prior to sampling in order to obtain a uniform sample without changing the drop size distribution. On starting the ultracentrifuge, the current is held at 6 amp. until a speed of 10,000 r.p.m. is reached, and then at 14 amp. until the desired operating speed is attained. The time required for acceleration to a constant speed of 39,460 r.p.m. was 8 min. Zero time in the oil separation experiments was taken as the time at which constant speed was reached. All runs were made at 25°.

Upon centrifugation the emulsion separates into transparent layers of oil and water separated by a layer of opaque, concentrated emulsion. These give sharp boundaries on a photographic plate which change position with time as more oil is separated from the emulsion. Determination of the positions of the boundaries on a series of such plates taken at successive time intervals permits calculation of the rate of separation of oil from the emulsion. Measurements were made with a travelling microscope reading directly to 0.01 mm., determining the distance from the top of the cell to the oil–emulsion and emulsion–water interfaces, and to the bottom of the cell. Each distance was measured eight times and the best average value used.

The volume corresponding to a length, Δ, in the sector-haped cell is given by

$$V = \frac{4}{360}\pi h[(R_a + \Delta)^2 - R_a^2] = \frac{\pi h}{90}[2\Delta R_a + \Delta^2]$$

where R_a is the distance from the center of rotation to the top of the cell, and h is the thickness of the cell. A graph was plotted of the volume as a function of the measured value of Δ from the top of the cell using an optical enlargement of 2.17. This plot then was used to determine the volume from the differences between the measured distances to the different interfaces.

The per cent of the initially emulsified oil which has separated at any given time is determined by dividing the volume of the oil layer by the sum of the volumes of the oil layer and the creamed emulsion. This implies that so little water remains in the creamed emulsion by the time steady speed centrifugal velocity is reached that its amount is immeasurable by the technique used. That this assumption is correct is proved by the fact that the sum of the volumes of clear oil and creamed emulsion remained constant throughout all runs independent of the amount of oil separated, as did that of the water layer. For example, in a typical run lasting 135 min. the length of oil plus emulsion was constant at 1.625 ± 0.0034 cm., while the water layer was 1.413 ± 0.0040 cm.

That the layer of clear oil contains no emulsified water was shown by adding 0.05% of Orange II to one emulsion and finding after centrifugation that the aqueous layer was colored orange while the oil layer was completely colorless. The presence of residual traces of water in the emulsion layer is shown by its opacity and also by the fact that it showed a trace of color when Orange II was present in the system. Moreover, although slightly translucent during and immediately after centrifugation, it gradually became slightly more opaque on standing in contact with the aqueous layer, indicative of slow imbibition of additional water.

The per cent of the initially emulsified oil which has separated then is plotted against the time of centrifugation. The rate of separation at the given speed is determined from the slope of the linear portion of the curve.

Materials.—In the earlier experiments testing reproducibility, for which numerical data are not recorded, Fischer Scientific Co. technical SDS was used without purification. In all other experiments a specially purified sample of SDS was used prepared by H. M. Princen following Dreger's method.[19] The pure SDS, prepared from a mixture of two fractions of lauryl alcohol of setting points 23.40 and 23.71°, was extracted for a few days with ether in a Soxhlet extractor to remove traces of lauryl alcohol, and then stored in a desiccator over calcium chloride until used. There was no minimum in the surface tension–concentration curve, this showing that the sample was nearly free of lauryl alcohol.[20] In one set of experiments this SDS was again extracted with ether for 24 hr. just before use to further reduce the concentration of lauryl alcohol, since even very small quantities can change the adsorbed layer of SDS at a surface from a mobile to a rigid film.[21]

Nujol from Plough, Inc., New York, was used without purification. The manufacturer's values for its constants are: Saybolt viscosity 360 to 390 at 100°F. and specific gravity 0.880 to 0.900 at 60°F.

Bottled distilled water was used without further purification.

Preparation of Emulsions.—In general the requisite volumes of Nujol and an aqueous solution containing the desired concentration of SDS were poured into a cut-off 500-ml. graduated cylinder and stirred 5 min. at 5000 r.p.m. with a Brookfield counter-rotating mixer, a stirrer with two counter-rotating blades which reduces absorption of air and foaming. The resultant emulsion was further dispersed by passing it four times through a Cenco hand homogenizer. All results reported pertain to emulsions about 20 hr. old except for one set dealing specifically with the effect of aging.

In earlier experiments establishing the reproducibility of the method and studying the effect of changes in the speed at which the ultracentrifuge was run, for which numerical data are not reported, the emulsions used were prepared from 50 ml. of Nujol and 50 ml. of 0.2% technical SDS solution. Emulsions used to determine the effect of changing the rate of acceleration of the centrifuge were prepared the same way except that purified SDS was used.

It is necessary that emulsions used to study the effect of SDS concentration on stability all have the same distribution of drop size so that they will have the same interfacial area and calculable degrees of surface coverage. Since preparation by the same procedure but with different initial concentrations of SDS would result in different drop size distributions the following method was employed. A series of emulsions was prepared by adding 150 ml. of Nujol to 120 ml. of 0.2% SDS solution and emulsifying as described above. After standing 20 hr. the emulsion was stirred gently by hand with several slow inversions to reincorporate any separated oil or cream, and divided into 50-ml. portions. From each of these 5 ml. was removed, and then 5-ml. portions of SDS solutions of varying concentrations added with gentle hand stirring to give 50-ml. samples of 50–50 oil–water emulsions of presumably identical drop size distribution but varying concentrations of SDS. Ultracentrifuge runs were generally made on the same day on which the additional SDS solution was added to the 20-hr. old stock emulsion. In Table I all emulsions made from the same stock by this addition process are given the same Roman numeral since they are more likely to be directly comparable than others of the same composition but made from a different stock emulsion.

That this procedure was generally successful is shown by the agreement between results obtained on different emulsions prepared by this technique. The error in the case of occasional discordant runs probably arises either because of irreproducibility in the preparation of the emulsion or from the difficulty of obtaining a completely representative sample in withdrawing the very small volume used in the ultracentrifuge cell.

Determination of Adsorption Isotherms.—These were determined with the same emulsions used for study of the effect of concentration on stability following Cockbain's method,[22] except that the aqueous phase was separated for analysis by centrifugation. Twelve hours after preparation of the final emulsions from the 20-hr. old stock, 25-ml. samples were centrifuged for 30 min. at 5000 r.p.m. in a Servall angle centrifuge subsequent to gentle hand mixing prior to sampling. The separated aqueous layer was removed with a hypodermic needle, and recentrifuged an additional 30 min. to ensure complete removal of any oil or emulsion. Errors may occur due to incomplete separation of the emulsion or to coalescence occurring during centrifugation but the reproducibility and internal consistency of the results suggest that these are generally not serious, although occasionally results on a series of emulsions from a given preparation may vary erratically. The concentra-

(19) E. E. Dreger, *Ind. Eng. Chem.*, **36**, 610 (1944).

(20) G. D. Miles and L. Shedlovsky, *J. Phys. Chem.*, **48**, 57 (1944).

(21) M. B. Epstein, A. Wilson, C. W. Jakob, L. E. Conroy, and J. Ross, *ibid.*, **58**, 860 (1954).

(22) E. G. Cockbain, *Trans. Faraday Soc.*, **50**, 874 (1954).

TABLE I

ULTRACENTRIFUGAL STABILITY AT 39,460 R.P.M. AND INTERFACIAL ADSORPTION OF NUJOL–WATER EMULSIONS STABILIZED WITH SODIUM DODECYL SULFATE

Stock[a] emulsion	Emulsion number	Initial concn. of SDS, % on water phase	Rate of oil sepn., %/min.	Extrapolated % oil separated at zero time	Equilibrium concn. SDS: Moles × 10^3/ liter in aqueous phase	Equilibrium concn. SDS: Moles × 10^5 adsorbed per ml. oil	Fraction of saturation adsorption
I	120A	0.2	0.51	22	2.96	0.398	..
II	125A	.2	.55	25	3.00	.409	0.64
III	131A	.2	.50	21	2.84	.410	.66
IV	160	.2	.49	23	2.78	.416	.65
II	126B	.3	.32	14	5.90	.451	.70
III	132B	.3	.31	10	5.70	.472	.76
IV	161	.3	.30	16	5.38	.504	.78
IV	162	.35	.28	10	6.59	.557	.86
I	123C	.4	.15	1.5	8.11	.577	..
II	127C	.4	(.24)[b]	(4.4)[b]	8.40	.549	.86
III	133C	.4	.17	2.0	7.93	.596	.96
IV	163	.45	.16	3.8	9.66	.597	.93
I	124D	.5	.14	2.6	...	...	..
II	128D	.5	(.20)[b]	(3.3)[b]	11.73	.563	.88
III	134D	.5	.14	0.7	11.78	.558	.89
I	122E	.6	.14	.3	...	...	..
IV		.4	..	...	7.89	.600	.93
IV		.5	..	...	11.68	.568	.88
IV		.6	..	...	14.51	.633	(.98)[b]
IV		.7	..	...	17.68	.662	(1.03)[b]
IV		.9	..	...	25.03	.622	0.96
V[c]	200	.2	.62	25	...	...	..
VI[c]	210	.2	.63	24	3.45	.350	.64
VI		.3	..	...	6.51	.391	.71
V	203	.35	.26	7.1	...	...	..
VI	213	.35	.25	6.5	7.88	.427	.78
V	204	.4	.22	5.7	...	...	..
VI	214	.4	.23	5.4	9.48	.441	.81
V	205	.45	.23	4.7	...	...	..
VI	215	.45	.21	4.1	11.44	.418	(.76)[b]
A	140[d]	.2	.62	26	...	...	..
B	142[d]	.2	.48	26	...	...	..
A	141[e]	.2	.62	26	...	...	..
B	143[e]	.2	.56	25	...	...	..
C	144	.2	.62	24	...	...	..
D	147	.2	.53	25	...	...	..
E[f]	145	.2	.62	19	...	...	..

[a] Stock emulsions I through VI were prepared with 150 ml. of Nujol and 120 ml. of water, and then adjusted to a 50–50 volume ratio before measurement. Emulsions A through E were prepared using 50 ml. of Nujol and 50 ml. of water. [b] Numbers enclosed in parentheses can be assumed to be in error. [c] The SDS used for preparation of emulsions V and VI was extracted with ether for 24 hr. just prior to use. [d] In these cases the ultracentrifuge was accelerated more rapidly than usual, reaching final speed in 5 min. [e] In these cases the ultracentrifuge was accelerated much more slowly than usual. The speed was increased gradually over a 35 min. period to 13,000 r.p.m., and then to the final speed of 39,460 r.p.m. over the next 5 min. [f] Orange II (0.05% on the water phase) was added to this system before emulsification.

tion of SDS in the aqueous phase was determined by titration with cetylpyridinium bromide,[23,24] eliminating the need for a blank by using a constant volume of 15 ml. of chloroform and 85 ml. of water. The cetylpyridinium bromide was standardized on a relative basis[25] against pure SDS.

The data obtained fitted the linear form of the Langmuir equation

$$C/x/m = 1/ab + C/a,$$

over the whole range from 3.0 to 25 × 10^{-3} mole SDS/l. with no detectable change of slope at the critical micelle concentration[26] (0.0081 mole/l.), as was also found to be the case with Cockbain's data.[22] The equilibrium concentrations of SDS in solution and at the interface, together with the fraction of saturation adsorption reached, *i.e.*, $(x/m)/a$, which is related to the fraction of the surface covered with adsorbed SDS, are given in Table I.

To determine the rate of change of interfacial area with time, three emulsions of 150 ml. Nujol–120 ml. 0.2% SDS were prepared as described previously, combined, and stored in a 1-liter graduated cylinder at room temperature. At different time intervals 200-ml. portions were withdrawn and divided into four 45-ml. samples, to each of which was added 5 ml. of more concentrated SDS solution so as to determine four points on the adsorption isotherm of the resultant 50–50 oil–water emulsion as described above. The interfacial area was determined from the Langmuir plots for these

(23) S. R. Epton, *Trans. Faraday Soc.*, **44**, 226 (1948).

(24) A. S. Weatherburn, *J. Am. Oil Chemists Soc.*, **28**, 233 (1951).

(25) R. D. Vold and N. H. Sivaramakrishnan, *J. Phys. Chem.*, **62**, 984 (1958).

(26) R. J. Williams, J. N. Phillips, and K. J. Mysels, *Trans. Faraday Soc.*, **51**, 728 (1955).

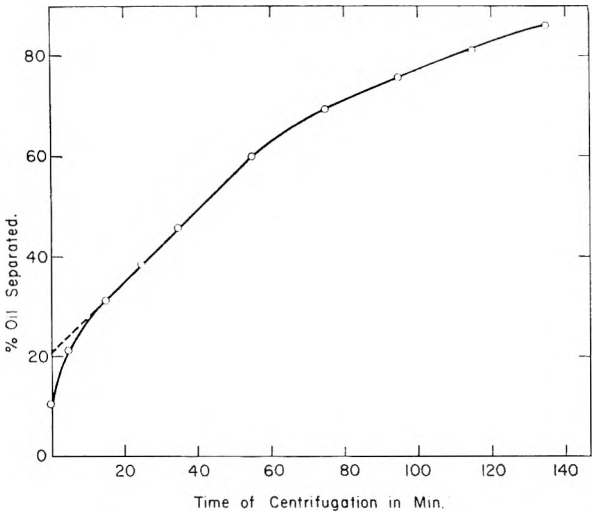

Fig. 1.—Rate of separation of Nujol at 39,460 r.p.m. from a 50 volume % Nujol-in-water emulsion stabilized with 0.2% SDS.

emulsions after 1, 96, and 504 hr. aging, the data being given in Table II.

TABLE II

EFFECT OF AGING ON INTERFACIAL ADSORPTION OF SDS IN NUJOL–WATER EMULSIONS

Initial concn. of SDS, % on water phase	Equilibrium concn. SDS: Moles × 10^3/liter in aqueous phase	Moles × 10^5 adsorbed per ml. oil	Fraction of saturation adsorption
	Emulsion 1 hr. old		
0.2	2.76	0.418	0.61
.3	5.26	.514	.74
.4	8.18	.571	.83
.5	11.39	.597	.87
	Emulsion 96 hr. old		
0.2	2.79	0.416	0.59
.3	5.55	.487	.69
.4	8.22	.566	.80
.5	11.34	.605	.85
	Emulsion 504 hr. old		
0.2	2.75	0.419	0.55
.3	5.56	.485	.63
.4	8.10	.580	.75
.5	11.16	.620	.81

Results

Figure 1 is characteristic of the curves of per cent oil separated *vs.* time of ultracentrifugation when using low concentrations of SDS. Initially oil separates very rapidly but the rate—determined from the slope of the curve—decreases rapidly with time during the first twenty minutes or so, during which period with 0.2% SDS as emulsifier slightly more than 20% of the emulsified Nujol separates as a layer of clear oil. The rate of separation then remains constant for a considerable period until about 60% of all the oil in the system has separated, and thereafter decreases slowly with further separation of oil.

Increasing the concentration of SDS at first decreases the rate of separation of oil from the emulsion and also the amount of oil which is separated rapidly on initial centrifugation before the steady state rate is reached. At higher concentrations the rate becomes independent of the initial concentration of SDS, as is strikingly shown in Fig. 2, all emulsions prepared with SDS concentrations between 0.4 and 0.6% SDS separating oil at the same rate within experimental error.

Quantitative data on the effect of SDS concentration on the rate of separation of oil, the effect of difference in the time of acceleration of the ultracentrifuge to its operating speed on the rate of oil separation, and the extent of adsorption of SDS at the oil–water interface in these emulsions are shown in Table I. Frequently considerable differences were found in the absolute quantity of oil separated by supposedly identical emulsions although the slopes of the linear portions of the curves of oil separated *vs.* time were nearly the same. The linear portions of the curves were therefore extrapolated to zero time, as shown in Fig. 1, and these extrapolated values of per cent oil separated at zero time also listed in Table I.

Generally there was no difficulty in drawing a straight line through the points obtained in the interval between 20 and 60 min. of centrifugation, and extrapolating to zero time so as to obtain the slope and the intercept. In order to avoid arbitrariness, however, the values recorded in Table I, and used in the construction of Fig. 2, were obtained from the best line calculated by the least squares method. Comparison of results obtained by the two methods showed they agreed within 3 to 4% of the value of the slope although occasionally differences as high as 10% were found, the least squares method tending to give lower slopes and higher intercepts.

Figure 2 shows the effect of the concentration of SDS on the rate of separation of oil from the emulsion in the ultracentrifuge. In order to facilitate comparison of runs on different emulsions with the same concentration of SDS the extrapolated per cent oil separated at zero time is subtracted from the actual amounts separated at any given time. Figure 2 also shows the degree to which the loss of oil by the different emulsions conforms to the straight line relationship, and the extent of agreement between runs at the same composition but on different preparations of the emulsion.

With respect to reproducibility, it can be seen from Table I that rates of oil separation generally agreed within 4 to 8% in runs on comparable samples, although occasionally an individual sample differed widely from the average for its composition. Runs at 39,460 r.p.m. on six samples from four separately prepared 50% Nujol–50% water–0.2% tech. SDS emulsions gave an average value for the rate of separation of oil of 0.136 ± 0.004%/min.

The larger irreproducibility in the values for the amount of oil which separates rapidly at the beginning of the run may be due to uncontrolled fluctuations in the degree of dispersion obtained during preparation of the emulsions, or to lack of representative sampling on withdrawing the small samples used in the ultracentrifuge cell. A few large droplets of poorly emulsified oil would have little effect on the measured values of interfacial area but would make a disproportionately large contribution to the volume of oil appearing, and would be likely to separate very rapidly on initial application

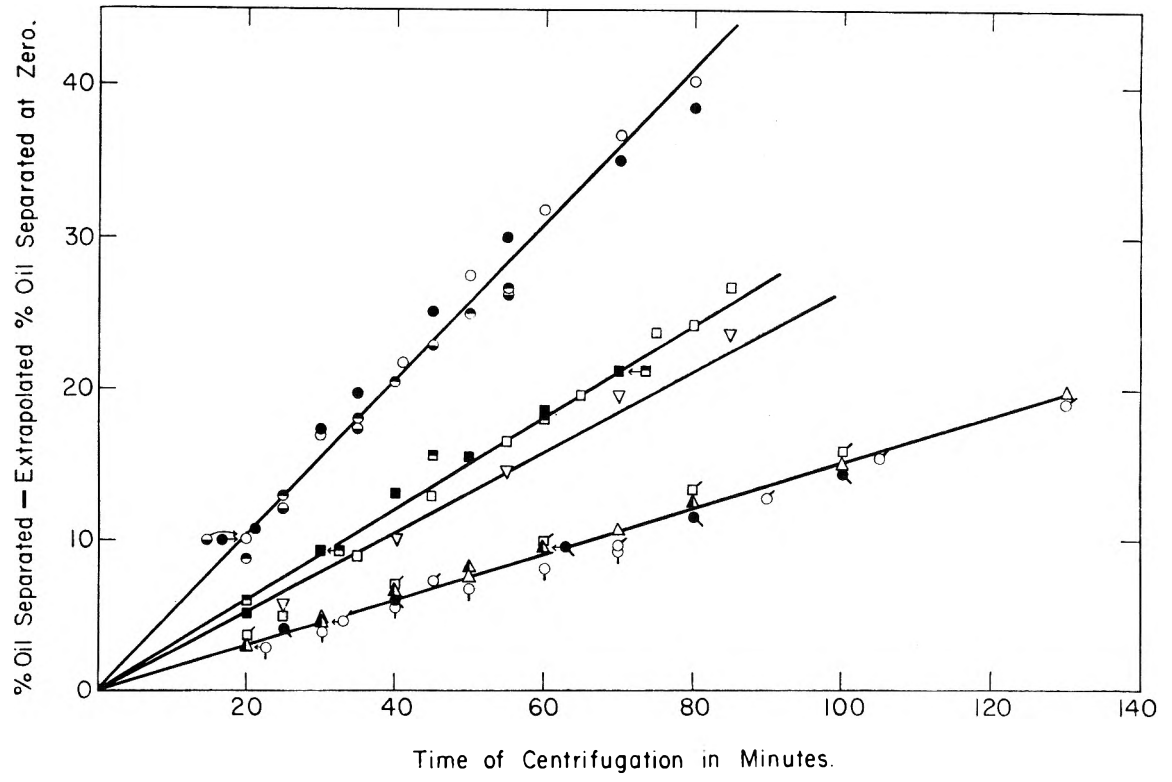

Fig. 2.—Effect of concentration of SDS on the rate of separation of Nujol from Nujol-in-water emulsions centrifuged at 39,460 r.p.m.: ○, ●, ◓, ◒, all 0.2%, from emulsions 120A, 125A, 131A, and 160; □, ◨, ■, all 0.3%, from emulsions 126B, 132B, and 161; ▽, 0.35%, from emulsion 162; △, ◭, both 0.4%, from emulsions 123C, 133C; ◫, 0.45%, from emulsion 163; ♂, ♀, both 0.5%, from emulsions 124D and 134D; ●, 0.6%, from emulsion 122E.

of the ultracentrifugal field. Consequently, two nearly identical emulsions may separate quite different quantities of oil in the initial stage of centrifugation but thereafter behave alike with respect to the rate of further separation of oil.

That the emulsification technique used produced nearly the same initial distribution of droplet sizes in most cases is shown by the relatively constant value found for the oil–water interfacial area of the different stock emulsions. Assuming an area of 50 Å.^{2} per adsorbed SDS molecule,[27-29] the interfacial areas of stock emulsions II, III, and IV of Table I were found to be, respectively, 1.92, 1.85, and 1.93 $\times$ 10^4 cm.^{2}/ml. oil. Adsorption data obtained with emulsion I, however, were so irregular as to prevent determination of its area. Emulsion VI, prepared in the same way as the others but using freshly extracted SDS, had an interfacial area of 1.64 $\times$ 10^4 cm.^{2}/ml. oil.

Effect of Impurities on Ultracentrifugal Stability.—The ultracentrifugal stability decreases the greater the purity of the SDS used as an emulsifying agent. With 50% Nujol–50% water emulsions centrifuged at 39,460 r.p.m. (113,154 *g*) the rate of loss of oil was 0.136%/min. when 0.2% technical SDS was used as emulsifier but rose to 0.51% using pure SDS. Ether extraction of the SDS immediately prior to use further increased the rate to 0.63%/min. Likewise at 0.45% SDS, ether extraction of the SDS just before use increased the rate of separation of oil from 0.16% to 0.22%/min.

Effect of Centrifugal Speed.—Rates of oil separation were determined on duplicate samples of 50 ml. Nujol–50 ml. water emulsions stabilized with 0.2% technical SDS at speeds of 10,589, 25,890, 33,450, 39,460. and 56,100 r.p.m. The rate of oil separation decreased rapidly with decreasing speed of centrifugation, and with the emulsions used was zero for at least 2.5 hr. of centrifugation at 10,589 r.p.m. This suggests the interesting possibility that coalescence may not occur in experiments of this type until the force of the centrifugal field just exceeds the rupture strength of the adsorbed layer of emulsifier, and so may provide a means of measuring the latter.

Effect of Aging on Interfacial Area.—From the Langmuir plots of the adsorption data in Table II it can be calculated that the interfacial area after 1, 96, and 504 hr. is, respectively, 2.07, 2.12, and 2.25 $\times$ 10^4 cm.^{2}/ml. oil if the area per adsorbed SDS molecule is taken to be 50 Å.^{2} It is evident that the rate of change of area with time in this emulsion is too small and too slow to afford a satisfactory criterion of emulsion stability. Moreover, it might have been expected that the area would decrease with time as the drops coarsened, whereas instead it increases somewhat. Consequently the larger drops must disappear from the emulsion more rapidly than the small drops, either by coalescence with each other or by union with the bulk oil phase. A somewhat similar result was also

(27) F. van Voorst Vader, *Trans. Faraday Soc.*, **56**, 1067 (1960).

(28) W. Kling and H. Lange, "Proc. Second Int. Congress Surface Activity," Butterworths Scientific Publications, London, 1957, p. 295.

(29) A. S. C. Lawrence and O. S. Mills, *ibid.*, **1**, 200 (1957).

observed with a heat-bodied linseed oil–water emulsion stabilized with 0.5% technical SDS, where the mean particle diameter determined microscopically was found to be slightly smaller in the redispersed cream after centrifugation at 10^4 g. for 2 hr. than in the original emulsion.[13]

Discussion

Mechanism of the Process.—Considerable interest attaches to just what property of an emulsion is measured by the rate of separation of oil in an ultracentrifuge and to the locus of its separation, whether uniformly throughout the creamed emulsion or predominantly at the oil–emulsion or wall–emulsion interface. That virtually no water is present in the emulsion layer during centrifugation necessarily requires that the oil drops be distorted into a honeycomb-like shape so as to permit packing with very little intervening free space. Under these conditions it is uncertain whether intrinsic differences in rate of coalescence with drop size in the original emulsion would be expected to hold in the centrifuged cream. Moreover, the effect of drop size on stability is not itself very well understood, some investigators predicting and finding that the stability increases with decreasing size,[30] others that it decreases,[7,8,31] while yet others[32] find no obvious relation.

Provided that the rate of coalescence does depend on the size of the drops, it would be expected to change with the extent of coalescence if fractionation of drops according to size had occurred during formation of the creamed emulsion layer in the ultracentrifuge. The rate of separation of oil would still vary with the amount of separated oil if fractionation had occurred, because of the greater contribution to bulk oil resulting from coalescence of larger drops, unless there were an improbable compensation between drop volume and probability of coalescence. That this rate remains constant over the range between 20 and 60% of oil separated suggests that subsequent to the initial rapid elimination of coarsely dispersed material the distribution of drop sizes is probably uniform throughout the residual creamed emulsion. This conclusion is further supported by the fact that the rate of oil separation was not affected by variation in the time used to reach the operating speed of the ultracentrifuge, since variations in the latter would change the extent of fractionation resulting from differential sedimentation of drops of differing size. Possibly, however, the observed constancy of behavior throughout so much of the depth of the creamed emulsion layer is due to the space-filling shape of the distorted oil "drops" therein, since if coalescence is occurring principally at their polyhedral surfaces its rate might be nearly independent of the original size distribution of the drops.

Coalescence at the wall as the rate-determining step is ruled out since the area of the wall–emulsion interface decreases continuously during separation of oil with no change in rate.

(30) E. G. Cockbain and T. S. McRoberts, *J. Colloid Sci.*, **8**, 440 (1953).

(31) T. Gillespie and E. K. Rideal, *Trans. Faraday Soc.*, **52**, 173 (1956).

(32) G. L. Stanko, W. C. Fielder, and G. J. Sperandio, *J. Soc. Cosmetic Chemists*, **5**, 39 (1954).

During the coalescence of drops to form a bulk oil phase, with consequent decrease of interfacial area, the desorbed SDS must either redissolve in the aqueous phase or be accommodated at the residual interface. The adsorption data show that if all the SDS liberated during the 75 min. required for separation of 60% of the oil from a 50% Nujol–50% water–0.2% SDS emulsion dissolved in the water the concentration would increase from 0.08% initially to a final value of 0.15%. Since the rate of separation of oil, which varies with the concentration of SDS in this range, remains constant, it shows that the liberated SDS does not reach the sites where coalescence and further separation of oil are occurring. This also suggests that the emulsion–bulk oil interface is not the chief site of coalescence since if it were it should soon become saturated, resulting in the same rate of oil separation independent of differences in the initial concentration of SDS in the emulsion.

Effect of Initial Concentration of Emulsifier.—As the initial concentration of SDS is increased, the stability of the emulsions first increases and then becomes independent of concentration. However, it is not the initial total concentration of SDS which is significant but the equilibrium concentration in the aqueous phase and the fraction of saturation adsorption reached at the interface.

Stabilization appears to be due principally to adsorption of the simple dodecyl sulfate ion. So long as the equilibrium concentration of SDS in the aqueous phase is below the c.m.c., increasing the total amount of SDS in the system increases the concentration of dodecyl sulfate ion, and therefore the amount of adsorption at the interface, with resultant decrease in the rate of separation of oil. Above the c.m.c. the concentration of the simple ion remains nearly constant despite further increases in SDS concentration, and consequently beyond this point the ultracentrifugal stability should no longer be dependent on the concentration of SDS. In agreement with this view the data in Table I show that the rate of separation of oil becomes constant at initial concentrations of SDS somewhere between 0.35 and 0.4%. At 0.4% the equilibrium concentration of SDS in the aqueous phase is 0.00818 moles/l., slightly higher than the c.m.c.

If it were assumed that the saturation limit of the Langmuir isotherm corresponds to formation of a monolayer of close-packed SDS on the oil drops then the values reported in Table I as fraction of saturation adsorption might be interpreted as being the fraction of the surface covered with adsorbed stabilizing agent. On this basis it is clear that the rate of oil separation decreases rapidly as the extent of coverage increases, but becomes constant as soon as further increase in bulk concentration no longer results in any further increase in adsorption, this occurring at a fractional coverage of about 0.9.

There is considerable doubt, however, whether such an interpretation of the adsorption data is justified since no consideration has been given to the fact that a charged rather than a neutral film is formed.[33] Even more serious is the uncertainty in

the value to be used for the interfacial area in the ultracentrifugal field where the originally spherical droplets are distorted. For the values obtained in the adsorption experiments to apply directly to the ultracentrifugal situation any change of area due to distortion of drop shape must be the same in the angle centrifuge at 5000 r.p.m. as in the ultracentrifuge. If this is actually so, then the fraction of the interface covered with adsorbed SDS in the initial emulsion, where all the oil is present as spherical drops, would be larger than the values shown in Table I.

Acknowledgment.—The authors wish to express their appreciation to J. de Groot for his help in instructing them in the use of the ultracentrifuge.

DISCUSSION

R. D. VOLD.—I wish to direct a question to Dr. Rehfeld. Can you offer any explanation for the fact that in your work, reported in the previous paper in this Symposium, a short period of centrifugation resulted in a large increase in drop size, whereas in our work even after prolonged centrifugation the drop size remained small, as shown by the large difference between initial and equilibrium concentration of surfactant in the aqueous phase, as well as by crude microscopic observation?

S. J. REHFELD (Shell Development Company).—I assume that you mean the difference between the equilibrium concentrations of surface active agent in the aqueous phase as determined using the Servall angle centrifuge and its relation to the amount of oil phase separated in the ultracentrifuge.

The geometry of the Servall centrifuge, the cell shape, and the magnitude of centrifugal force grossly differ from that of the ultracentrifuge. Therefore, the equilibrium concentration of the surface active agent in the aqueous phase after ultracentrifugation must be determined and shown to be approximately equal to the equilibrium concentration found using the Servall angle centrifuge. Until this is done we cannot definitely state that any real difference exists between our observed results on the ultracentrifuge.

S. G. MASON (Pulp and Paper Institute of Canada).—I wish to ask Dr. Vold and Dr. Rehfeld if they consider that there is a 1:1 correspondence between emulsion stability measured with and without a centrifugal field? Also, on stopping the ultracentrifuge does the emulsion layer tend to spring back, *i.e.*, to increase in volume?

S. J. REHFELD and R. D. VOLD.—There is not necessarily a 1:1 correspondence since in the centrifugal field the emulsion already is flocculated whereas in the initial emulsion the oil is present as dispersed drops. On stopping the ultracentrifuge the emulsion layer will spring back only very slightly and increases in volume very slowly. Over a period of hours the compressed emulsion becomes slightly less viscous and more opaque.

EVERETT N. HIESTAND (The Upjohn Company).—Would the authors please comment on the shelf-life stability of flocculated emulsions and on whether they would expect the ultracentrifugal stability to correlate with the shelf-life of these emulsions?

R. D. VOLD.—Shelf-life stability may be defined as the extent to which an emulsion remains unchanged in appearance and macroscopic properties on quiescent standing. If it already is flocculated to begin with, the rate of flocculation is no longer involved, as is the case with normal emulsions, but only the rate of coalescence of drops to form larger drops, and the rate of sedimentation (creaming) of both primary drops and aggregates (assuming a chemically inert system). In the ultracentrifuge, as operated in the present experiments, complete flocculation and gross distortion of drop shape have occurred by the time constant operating speed is reached. Hence the rate of appearance of free oil is governed by the intrinsic rate of coalescence, the rate of transport of oil through the flocculated emulsion, and possibly the rate of coalescence of the creamed oil "drops" with the bulk oil phase. Sedimentation rate through a dilute emulsion of spherical drops would not necessarily be expected to correlate with that through the interlamellar spaces of the distorted, nearly water-free, flocculated emulsion as it exists in the ultracentrifuge. Even if coalescence is the rate-determining step, shelf-life and ultracentrifugal stability may still not correlate if a surface yield value of the adsorbed film is important, since the ultracentrifugal field is so much greater than the gravitational. The question can be unambiguously answered only by additional experimental work.

(33) J. T. Davies and E. K. Rideal, "Interfacial Phenomena," Academic Press, New York, N. Y., 1961, p. 93.

PREPARATIVE ULTRACENTRIFUGATION OF FOOT-AND-MOUTH DISEASE VIRUS THROUGH IMMISCIBLE FLUID INTERFACES INTO A CESIUM CHLORIDE DENSITY GRADIENT[1]

BY RODES TRAUTMAN, SYDNEY S. BREESE, JR., AND HOWARD L. BACHRACH

Plum Island Animal Disease Laboratory, Agricultural Research Service, U. S. Department of Agriculture, Greenport, Long Island, New York

Received March 5, 1962

In order to effect purification in a short time, foot-and-mouth disease virus, type A, strains guinea pig GB and tissue culture 119, was centrifuged in a swinging bucket rotor from aqueous solutions through an immiscible organic layer into a short column of CsCl solution isodense with the virus. The organic layer was made of various combinations of volatile and non-volatile solvents including trichlorotrifluoroethane, chloroform, diethyl phthalate, dibutyl phthalate, diethylhexyl sebacate, octanol, and butanol. Selective penetration occurred when the organic separator was of lower density than the solvated virus particles and the protein contaminants of higher density were not too concentrated at the upper interface. Removal of tissue particles of similar density and size to the virus could be achieved. The solvated density of the virus was increased by addition of CsCl and penetration was demonstrated by sedimentation or flotation for the density range 1.01–1.54 g./ml. Purification factors were computed from analytical ultracentrifuge patterns. Electron micrographs revealed hexagonal close packing of particles in phosphotungstic acid after two cycles of three hr. centrifugation at 37,000 r.p.m. in a 5-ml. SW 39 tube. Sodium ethylenediaminetetraacetate at about 0.03 *M* partially stabilized purified virus and did not interfere with electron microscopy.

Introduction

Organic fluids, both miscible and immiscible with water, have been used in various arrangements in preparative and analytical centrifugation. The miscible systems were selected to change the properties of the solvent, and the centrifugation was of the moving boundary type.[2,3] They will not be considered further; here the interest is with organic fluids that are immiscible with aqueous solutions of salts, proteins, and viruses. Such fluids have been applied for the batchwise purification of biological fluids by the selective denaturation of undesired proteins.

Six other centrifugal uses of immiscible fluids, described in the literature, are shown schematically in Fig. 1 A–F, together with the one of this paper in G. In A, an organic fluid is used to prevent the collapse of the tube.[4] In B, an organic phase below the aqueous solution avoided pelleting solute onto the lusteroid tube, enabling better resuspension.[5] A similar application in the analytical cell (Fig 1C) provided a second meniscus for sedimentation equilibrium measurements such as depicted in the schlieren diagram.[6–8] Figure 1D illustrates the proposal of Stenesh, *et al.*,[9] for density measurements. A compression gradient in the organic phase caused the aqueous drops to move upward to a radius corresponding to their own density.

Of direct relevance to the present work is that of Bendet, *et al.*,[10] (Fig. 1E) where the solute of the upper aqueous phase penetrated the organic fluid. The backward displacement of the aqueous–organic interface was measured to calculate the solute hydrodynamic volume. The shape of the centrifuge cell magnified the displacement. The analytical ultracentrifuge was used and purified preparations were required. For Southern bean mosaic virus and *E. coli*, the density of the organic phase had to be less than the particle hydrodynamic density, corresponding to 0.98 ml./g. and 3.3 ml./g. hydration, respectively.

"Differential flotation" of living cells was proposed by Ballentine and Burford[11] (Fig. 1F). The organic phase density had to be between those of the cells to be separated. Negligible solvent was carried down, permitting the sedimented cells to be freed from original growth medium. Criteria cited by them for the organic phase were: (a) suitable density, (b) negligible solubility in water, (c) physiological inertness, (d) low viscosity, and (e) low volatility. Diffusion pump oils such as phthalic acid esters and di-2-ethylhexyl sebacate were recommended.

The arrangement described in this paper is shown in Fig. 1G,—here the solute (virus) must penetrate the organic phase and emerge into a CsCl solution adjusted to the isodensity of the solute. The organic separator permits the use of a column of CsCl small enough[12] so that sedimentation occurs in a short time. Relatively large volumes of virus can be layered on top of the organic separator. Because the hydrodynamic density of protein contaminants is greater than that of the virus, the process is not principally differential flotation. Rather, organic fluids were chosen to permit differential penetration. For the virus of interest, foot-and-mouth disease virus (FMDV), the batchwise shaking of infectious aqueous fluids showed that chloroform,[13] chloroform and butanol, or

(1) Presented at the 36th National Colloid Symposium, Stanford University, June, 1962.

(2) E. D. Rees and S. J. Singer, *Arch. Biochem. Biophys.*, **63**, 144 (1956).

(3) H. L. Crespi, R. A. Uphaus, and J. J. Katz, *J. Phys. Chem.*, **60**, 1190 (1956).

(4) L. Levintow and J. E. Darnell, Jr., *J. Biol. Chem.*, **235**, 70 (1960).

(5) D. R. Stanworth, K. James, and J. R. Squire, *Anal. Biochem.*, **2**, 324 (1961).

(6) H. K. Schachman, "Ultracentrifugation in Biochemistry," Academic Press, New York, N. Y., 1959, p. 186.

(7) D. A. Yphantis, *Ann. N. Y. Acad. Sci.*, **88**, 586 (1960).

(8) J. E. Hearst, J. B. Ifft, and J. Vinograd, *Proc. Natl. Acad. Sci., U. S.*, **47**, 1015 (1961).

(9) Described by Schachman, ref. 6, p. 178.

(10) I. J. Bendet, C. E. Smith, and M. A. Lauffer, *Arch. Biochem. Biophys.*, **88**, 280 (1960).

(11) R. Ballentine and D. D. Burford, *Anal. Biochem.*, **1**, 263 (1960).

(12) K. E. Van Holde and R. L. Baldwin, *J. Phys. Chem.*, **62**, 734 (1958).

(13) G. Pyl, *Arch. Exptl. Veterinaermed.*, **7**, 238 (1953).

trichlorotrifluoroethane[14] resulted in purification without loss of infectivity, while trichlorotrifluoroethane, with or without heptane, selectively separated virus from unassembled protein subunits.[15,16] Even though these chemicals are volatile, it will be shown that they can be employed.

The development of isodensity centrifugation for the analytical study, as well as purification, of viruses was initiated by Meselson, *et al.*,[17] and has been reviewed, along with moving zone density gradient methods, by Spinco.[18] Studies on FMDV indicated that the CsCl isodensity value was 1.43 ± 0.01 g./ml., which is significantly higher than that of most protein contaminants of density about 1.33 g./ml.[19] The CsCl phase in Fig. 1G thus acts in a differential flotation manner allowing further purification and concentration without pellet formation.

A virus is a useful colloid for studying the processes involved in penetrating interfaces because its infectivity assay permits measurement of concentration changes as great as 10^6-fold, even in the presence of other protein and nucleoprotein contaminants. This paper presents data on such penetration by FMDV to develop preparative procedures for its concentration and purification from crude harvest fluids.

Experimental

Virus Source and Assay.—Laboratory stock FMDV, type A, strain GB, highly adapted to guinea pigs, was inoculated into the hind pads of guinea pigs and both the infectious vesicular fluid (VF) and foot pads (FP) were harvested 24 hr. later. Infectivity titrations were made in suckling mice[20] using decimal dilutions with a litter of 10 mice per dilution and with litter mates randomized as suggested by Subak-Sharpe.[21] Mice were inoculated intraperitoneally with 0.03 ml. of the dilution. End-points, computed by the Spearman-Kärber Method,[22] had a standard deviation of 0.2 log unit. Some of the organic fluids killed suckling mice when injected undiluted, but none did so at 10^{-1} dilution; hence there was no interference with the virus assay. CsCl solutions and normal serum also had no deleterious effect on the mice.

Tissue culture (TC) adapted FMDV, type A, strain 119, was collected from infected bovine kidney epithelial cell cultures, precipitated with methanol, resuspended, and clarified.[14] This concentrated TC virus solution (SP_{ntc}) was titrated by the plaque assay method[23] in 4-oz. prescription bottles, using a 0.1 ml. inoculum. In this series of experiments there was a standard deviation of about 20%. SP_{ntc} or VF purified further by organic solvent extractions are denoted as aqueous phase (AqPh).[14]

Solutions.—Trishydroxymethylaminoethane buffer solutions were used at 0.16 *M*, except for electron microscopy. CsCl and disodium ethylenediaminetetraacetate (EDTA) were used as obtained from Fisher Scientific Co., Fairlawn, N. J. The pH of these solutions was adjusted to 7.4–7.8 before use.

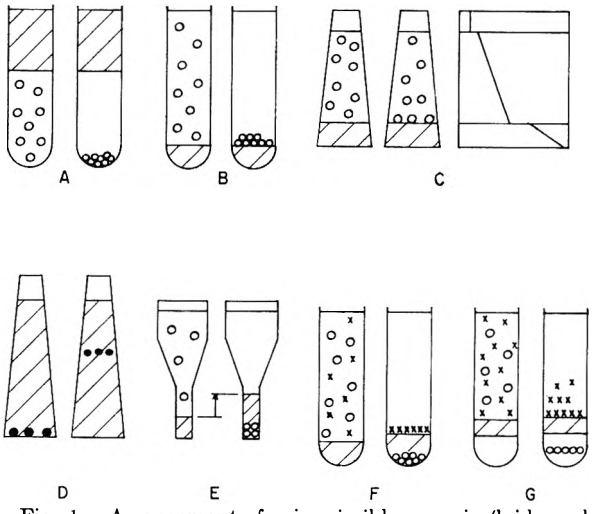

Fig. 1.—Arrangements for immiscible organic fluids and aqueous solutions in ultracentrifugation. In each group, the left hand figure shows the initial loading; the right hand, after centrifugation; the purpose of the organic fluid (cross hatched) is to: A, occupy space[4]; B, provide a liquid bottom[5]; C, provide a second meniscus[6-8] (schlieren diagram at extreme right); D, make a compression gradient[9] for aqueous droplets (solid circles) E, indicate hydrated volume[10]; F, cause differential flotation[11]; and G, separate aqueous columns (this paper). Open circles represent faster component of higher density than crosses of slower s-rate and lower density.

The organic chemicals were used without purification or water saturation. Trichlorotrifluoroethane (F) was obtained from Allied Chemical Corp., Baton Rouge, La., as "Genetron 113"; di-2-ethylhexyl sebacate (S) from Consolidated Vacuum Corp., Rochester, N. Y., as "Octoil-S"; diethyl phthalate (E) and dibutyl phthalate (B) from Eastman Organic Chemicals, Rochester, N. Y.; chloroform (C); *n*-octanol (O), and *n*-butanol (A) from Fisher Scientific Co. The lusteroid tubes were softened by E in 1 day, and by B in 2 weeks. The other chemicals had no effect.

Density Measurements.—Aqueous solutions were measured in bromobenzene–*m*-xylene gradients at 25° in 100-ml. graduated cylinders by the method of Jacobsen and Linderstrøm-Lang,[24] using standards determined by pycnometry. Organic solutions were measured in analogous manner in aqueous salt gradient columns. The "nominal" density at 25° of mixtures was computed by linear interpolation by volume of handbook values for the density of the chemicals used and was found in agreement with the measured value. Because of volatility and partial miscibility, the "nominal" density is used to denote the composition initially mixed.

Preparative Ultracentrifugation.—A Spinco (Beckman Instruments, Inc., Spinco Division, Palo Alto, Calif.) swinging bucket rotor, SW 39, was used in the Model L ultracentrifuge operated at 37,000 r.p.m. at 4–10° without brake. In those cases in which tubes were to be centrifuged further, the rotor was slowly reaccelerated, taking about 6 min. to reach 37,000 r.p.m.

The 5 ml. lusteroid centrifuge tubes were filled as follows (Fig. 1G): first, 0.9 ml. of density 1.42 g./ml. CsCl solution (~ 40% w./w.); next, 0.9 ml of the desired organic fluid mixture was layered; then, 3.3 ml. of the virus solution was slowly discharged onto the center of the organic meniscus.

After centrifugation, the tubes were removed to a 4° room and inspected for light scattering, using a narrow light beam. A tightly-banded light scattering zone (LS) at a density of about 1.43 ± 0.01 was indicative of FMDV.[19] Fractions were removed by pipetting from the top with a Pasteur pipet, from a puncture in the side with 22 gage needle on a 1-ml. syringe, or by drop-out from a puncture in the bottom, depending upon which fractions were desired without contamination by the others. Most fractions were assayed for infectivity in addition to noting the presence of LS and the location of debris and protein gel.

(14) H. L. Bachrach and S. S. Breese, Jr., *Proc. Soc. Exptl. Biol. Med.*, **97**, 659 (1958).

(15) M. Mussgay, *Z. Hyg. Infektionskrankh.*, **146**, 48 (1959).

(16) F. Brown and B. Cartwright, *J. Immunol.*, **85**, 309 (1960).

(17) M. Meselson, F. W. Stahl, and J. Vinograd, *Proc. Natl. Acad. Sci., U. S.*, **43**, 581 (1957).

(18) "Spinco Technical Reviews. An introduction to density gradient centrifugation," Beckman Instruments, Inc., Spinco Division, Palo Alto, Calif., 1960.

(19) R. Trautman and S. S. Breese, Jr., *J. Gen. Microbiol.*, **27**, 237 (1962).

(20) H. H. Skinner, W. M. Henderson, and J. B. Brooksby, *Nature*, **169**, 794 (1952).

(21) H. Subak-Sharpe, *Arch. Ges. Virusforsch.*, **11**, 1 (1961).

(22) See review by D. J. Finney, "Statistical Method in Biological Assay," Hafner Publ. Co., New York, N. Y., 1952.

(23) H. L. Bachrach, J. J. Callis, W. R. Hess, and R. E. Patty, *Virology*, **4**, 224 (1957).

(24) C. F. Jacobsen and K. Linderstrøm-Lang, *Acta Physiol. Scand.*, **1**, 149 (1940).

TABLE I

EFFECT OF 1% (W./V.) EDTA ON STORAGE OF PURIFIED FMDV UNDER VARIOUS CONDITIONS

Entries[a] are drop in titer in log units

FMDV Strain	Conditions	Time of storage[b] 0–1 day None	0–1 day EDTA	0–1 wk. None	0–1 wk. EDTA	1–4 wk. None	1–4 wk. EDTA	4–16 wk. None	4–16 wk. EDTA
A/GB	Dialyzed			0.2(32)	0.3(18)	1.5[c](7)	1.0[c](16)	3.2[c](7)	1.9[c](4)
A/GB	In 3.4 *M* CsCl			0.7(15)	0.1(6)				
A119	Dialyzed	0.5[c](5)	0.3[c](9)	2.2(13)	0.9(14)	1.8[c](4)	1.8[c](11)	4.3[c](1)	2.3[c](9)
A119	In 3.4 *M* CsCl			0.4(1)	0.3(5)				
A119	Dialyzed, stored −60°			1.5(2)	0.4(2)	2.1 (3)	0.2(4)	≥3.7 (1)	0.6 (1)

[a] Number in parentheses is the number of values averaged. [b] Stored at 4° except as noted in last row. [c] No significant difference with or without CsCl, hence all values were averaged.

Tubes with organic fluid densities above 1.2 g./ml. frequently were difficult to remove from the buckets. This was remedied in later experiments by using 0.2 ml. of H_2O in the bucket, but sometimes tube creases resulted.

Isodensity centrifugation without an organic fluid separator, for control or prior purification, was performed using a modification of the transient method of Matthews[25] and of Trautman and Breese.[19] In this, up to 3.8 ml. of the virus solution was layered over 1.5 ml. of a uniform CsCl solution of density 1.42 g./ml. After three hours centrifugation, the FMDV LS zone was below most of the debris, yet not pelleted.

Analytical Ultracentrifugation.—A Spinco Model E ultracentrifuge equipped with phaseplate schlieren optics was used for moving boundary experiments to determine sedimentation rates and relative concentrations. Both 12 and 30 mm. double sector epon centerpieces were used. Photographs were measured on an optical comparator according to methods described elsewhere.[26]

Electron Microscopy.—Virus suspensions, dialyzed against 0.2 *M* NH_4OAc with or without 1% (w./v.) EDTA, were diluted to an appropriate level with 0.2 *M* $(NH_4)_2CO_3$ for spraying or spreading on formvar coated copper mesh screens. Phosphotungstic acid (2%) brought to pH 7.4 with 1 *N* KOH was mixed with an equal volume of the diluted virus before mounting on screens. Electron micrographs were taken at approximately 26,000× in an RCA EMU-3B electron microscope operated at 100 kv.

Results

Controls.—Since FMDV is a ribonucleic acid nucleoprotein, it was considered that Mg^{++} might afford some stabilization in purified preparations, as with ribosomes.[27] Preliminary data indicated that there was no improvement with 0.02 *M* Mg^{++}. Hence, a chelating agent, 1% (w./v.) EDTA, was tried. The cumulative results for both virus strains that had at least one cycle of CsCl isodensity centrifugation are shown in Table I. The virus was dialyzed against a suitable buffer to remove CsCl as indicated. EDTA improved stability at 4° even for those samples remaining in CsCl. The TC A119 strain is seen to be less stable than A/GB, hence the 0–1 day storage values have been listed separately to show that the loss was not too severe for practical use. Over one week storage at 4° gave too great a loss, even though reduced with EDTA. At −60°, purified virus can be stored for long periods if EDTA is present. EDTA is now routinely used in all solutions, including the CsCl during the centrifugation.

Because bottom fractions below an organic chemical were to be assayed for infectivity in this study, it was necessary to determine the contamination that could be expected without centrifuging. In each of two tubes, layered with infectious fluid above a mixture of F and S organic liquids and left standing 66 hr. at 4°, $<10^{-3}$% of the virus above the organic phase was found in the bottom CsCl phase. This is 1/1000 as much as the 1% level adopted here for evidence of penetration under the centrifugal field.

Factors in Efficacy of Virus Penetration of the Interfaces.—Using the arrangement of Fig. 1G, various mixtures of the organic fluids were surveyed for their effectiveness as a barrier for protein contaminants while permitting the penetration of FMDV. The 183 experiments having the upper (starting virus) aqueous solution at 1.01 g./ml. density were grouped in the various categories in Tables II–V and scored as successes or failures. The effect of density and composition of organic fluid, location of debris, and source of virus were analyzed.

A. Effect of Density and Composition of Organic Phase.—Table II gives the results grouped in the density classes indicated at the top, regardless of the chemicals involved or the location of debris. In many experiments, fractions were taken on either side of the light scattering (LS) zone in the bottom CsCl solution. The infectivity measurements confirmed[19] the identification of such LS with banded virus. Hence 17 experiments that had no infectivity assay were included on the basis of presence or absence of LS. For the 166 main experiments, the criterion for penetration was that >1% virus infectivity was recovered in the entire bottom CsCl solution regardless of LS. In Table II it is seen that, proportionately, success declines above 1.10 g./ml. organic phase density and drops sharply above 1.12 g./ml. In Table III, 151 runs between 1.04 and 1.10 g./ml. were classified according to the organic mixture used. There seems to be no combination of chemicals which has a significantly low ratio of success, hence organic fluids may be selected for other properties than merely passing virus.

TABLE II

EFFECT OF DENSITY OF THE ORGANIC FLUID ON PENETRATION BY FMDV FROM AQUEOUS SOLUTION OF DENSITY 1.01 G./ML.

Entries are number of successful[a] runs/total in each group.

Organic fluid density range,[b] g./ml. 1.02–1.04	1.04–1.06	1.06–1.08	1.08–1.10	1.10–1.12	>1.12
8/8	62/64	35/49	33/38	10/18	1/6

[a] >1% recovery of infectivity in CsCl solution below organic fluid or presence of LS zone. [b] Calculated for 25° from composition of mixture used.

(25) R. E. F. Matthews, *Nature*, **184**, 530 (1959).
(26) R. Trautman, *J. Phys. Chem.*, **60**, 1211 (1956).
(27) M. L. Petermann, *J. Biol. Chem.*, **235**, 1998 (1960).

TABLE III

EFFECT OF COMPOSITION OF THE ORGANIC FLUID OF DENSITY 1.04–1.10 G./ML. ON PENETRATION BY FMDV FROM AQUEOUS SOLUTION OF DENSITY 1.01 G./ML.

Entries are number of successful[a] runs/total in each category

	Density diluent				
Dense organic component	B (Dibutyl phthalate, 1.0416[c])	S (Di-2-ethylhexyl sebacate, 0.9095[c])	O (Octanol, 0.8226[c])	A (Butanol, 0.8057[c])	SA[b]
F (trichlorotrifluoroethane, 1.5635[c])	...	32/38	2/2	...	...
C (chloroform, 1.4801[c])	1/2	23/25	30/31	1/3	..
FC[d]	...	20/26	1/1	...	2/3
E (diethyl phthalate, 1.1133[c])	4/4	6/7	2/3	1/1	...
None	5/5	...	...	...	...

[a] >1% recovery of infectivity in CsCl solution below organic fluid or presence of LS zone. [b] Used in variable proportions. [c] d^{25}_4 g./ml. [d] Used in equal proportions by volume.

If the hydration of FMDV is 1 ml./g., similar to that measured by Bendet, *et al.*,[10] for Southern bean mosaic virus, and if the 1.43 g./ml. isodensity in CsCl is assumed to be the dry density, then the hydrated density would be 1.18 g./ml. Hence it is concluded from Tables II and III that, for penetration, the density of the organic fluid should be less than the hydrated density of the virus. This is consistent with the observations of Bendet, *et al.*[10] Ruled out as factors for penetration are dry density and the nature of the organic fluids. Also eliminated are interfacial tension, viscosity, water solubility, and volatility, because of their wide variation in the mixtures of Table III.

B. Location of Debris after Centrifugation.—It is important for purification that any sediment of non-viral contaminants be retained at the upper interface. Table IV presents the results of 120 runs, using F, C, or FC as the dense component and O or S as the diluent where the location of debris was visible. Those having O as the density diluent are listed in the first row, and those with S, in the second. Considering first the O, it is seen that debris appeared at the lower interface for all densities up through 1.11. Since this is the highest density that should be used to pass virus (from Table II), O is not a good diluent for F or C. But mixtures containing S, indicated in the second row, are seen to retain the debris at the upper interface over 60% of the time. The lower portion of the table gives an analysis of the same S runs of the 1.04–1.11 density range in terms of volume, time, and density to determine the reasons for failure to retain debris at the upper interface. It is seen that a higher percentage of successes was obtained the higher the density, the shorter the time, or the smaller the volume, each factor being practically independent of the others.

The mechanism by which the protein gel and debris got to the lower interface will be considered in the section on density measurements after centrifugation.

C. Effect of the Nature of the Contaminants.—When impure preparations were studied, it was found that the minimum time required to detect a light scattering zone was increased over that with purified preparations, and the zone appeared higher in the CsCl solution. This meant that the mere presence of a narrow light scattering zone of virus in the bottom layer after 3 hr. did not necessarily mean that equilibrium had been reached. The virus could still be moving as a zone to its correct position.

TABLE IV

EFFECT OF DILUENT, DENSITY, VOLUME, AND TIME ON THE RETENTION OF DEBRIS AT UPPER INTERFACE

Entries are the number of runs with visible debris or gel at upper interface/total number of runs made

	Organic fluid density range,[b] g./ml.				
Diluent[a]	1.02–1.04	1.04–1.11	>1.11		
O (octanol)	0/4	0/31	5/5		
S (di-2-ethylhexyl sebacate)	1/1	46/74[c]	5/5		
Density range					
1.04–1.07	1.07–1.11	Vol.(ml.)	Time(hr.)		
10/12	8/8	0.9–1.5	2–3.5		
1/1	7/10	0.9–1.5	4–10		
0/1	2/3	2.0–4.0	2–3.5		
1/10	17/29	2.0–4.0	4–10		

[a] F, C, or FC runs as dense component, either O or S as diluent. [b] Calculated for 25° from composition of mixture used. Aqueous starting virus density was 1.01 g./ml. [c] These runs are further analyzed below.

To demonstrate that the nature of the contaminants was involved, the same 151 runs between 1.04 and 1.10 density of Tables II and III were classified as to the magnitude of the recovery of infectivity and as to the source of the infectious fluid. The results are given in Table V. Consider first the left hand part of the table on guinea pig virus, strain A/GB. Of 13 runs in the first column on vesicular fluid that had been previously clarified by shaking with organic fluids (AqPh), 55% had a recovery of <1%. Foot pad material (FP) had fewer failures, but also only one run with >50% recovery. Untreated vesicular fluid (VF) was best of the three crude starting fluids, with 38% of the 106 runs giving >50% recovery. Equal or superior results were obtained with material that had undergone at least one prior cycle of centrifugation (Purified). It appears that crude materials contain debris of higher s-rate than that of the virus which coats the upper interface impeding penetration of the virus, or there may be a variable denaturation of the debris. Since AqPh runs had lower recoveries than those with VF, the material that blocked the interface was not removed by organic extraction, but was increased by the partial denaturation of some of the protein. A check of this hypothesis was made by using fresh unclotted VF. No LS zone was seen after 3 hr. and only a faint one after 6 hr.

TABLE V

EFFECT OF THE SOURCE OF INFECTIOUS FLUID ON THE RECOVERY OF VIRUS INFECTIVITY

Entries[a] are the number of runs made

Recovery range (%)	Guinea pig A/GB				Tissue culture A119		
	AqPh[b]	FP[c]	VF[d]	Purified[e]	SP_{alc}[f]	AqPh[g]	Purified[e]
>50	2 (15%)[g]	1 (9%)	40 (38%)	5 (42%)	0	0	2
1–50	4 (30%)	9 (82%)	55 (52%)	7 (58%)	2	2	1
<1	7 (55%)	1 (9%)	11 (10%)	0	1	1	0

[a] Number in parentheses is percentage of total runs in each column. [b] Aqueous phase (AqPh) from batchwise extraction of vesicular fluid with chloroform, butanol, or trichlorotrifluoroethane. [c] Suspension of homogenized foot pads (FP). [d] Vesicular fluid, frozen once. [e] After one centrifugation into CsCl, either with or without organic interface. [f] Soluble part of the alcohol precipitate (SP_{alc}). [g] Similar to *b*, but from SP_{alc}.

However, with the same VF, after clotting and centrifuging at low speed, an intense LS zone was obtained in 3 hr. The variable results with VF apparently depended upon treatment prior to freezing, such as clotting and preliminary low speed centrifugation.

The tissue culture fluids showed the same trend, even with the small number of runs made, as seen on the right hand side of Table V.

Both tissue culture concentrates and guinea pig foot pad suspensions were found to contain general light scattering material surrounding the viral light scattering zone in CsCl isodensity runs without organic fluid. However, this non-specific tissue debris was reduced by batchwise organic extraction, and also by sedimentation of the virus through the organic phase.

D. Effectiveness of Organic Fluid in Keeping Aqueous Phases Separate.—The immiscible fluid was selected to compartment the CsCl solution so that sedimentation equilibrium would be reached faster than if the entire tube were used, and to keep contaminants out of the region to be occupied by the virus. One measure of the success in keeping the two aqueous solutions separated is the change in density of the bottom solution after centrifugation. If it is diluted by water from its nominal density of 1.42 with 0.25% of its volume, the density will drop 0.001 g./ml., the limit of error in the measurements made. It can be seen (Table VI) that in the majority of runs the density did not change by more than 0.0005, on the average, even in long runs. Runs at the bottom of the table were grouped on the basis of large density changes. Contamination, indicated by a decrease (negative), occurred with large volumes of crude fluid, long centrifugation time, or mechanical difficulties in the layering or fractionation. As a result it is concluded that both the CsCl solution and the organic phase should be at least 0.8 ml. deep; and if the top fraction is removed, it should not be pipetted all the way to the organic phase because the air–H_2O and H_2O–organic fluid interfaces will condense and leakage around the organic liquid can occur.

The mechanism by which protein gel and debris reached the lower interface is suggested by the density measurements. If the gel became too concentrated, a density inversion with the organic separator could occur. Not only did the gel go to the lower interface, but also some aqueous fluid which diluted the lower CsCl solution.

E. Complications.—There are three complications when using organic fluids in centrifugation: volatility, partial miscibility, and compressibility.

TABLE VI

EFFECTIVENESS OF ORGANIC SEPARATOR AS INDICATED BY CHANGE IN DENSITY OF THE BOTTOM CsCl SOLUTION CENTRIFUGED FOR VARIOUS TIMES

Time (hr.)	Debris[a]	Density change (g./ml.)
3	L	0.001
3	N	.002
3½	U	.001
3½	U	.000
4½	L	.000
5⅓	U	− .002
7½	U	.003
7½	U	.000
7½	L	.001
7½	L	− .002
7½	U	.000
8⅓	U	.001
8⅓	U	− .001
8½	U	.002[b]
9	L	− .001
10	U	.003[c]
	Av.	0.0005
3	L	−0.027[d]
4½	L	− .022[e]
7½	L	− .006[f]
8½	L	− .029[b]
10	U	− .010[c]

[a] Debris located at U, L, upper, lower organic–water interface, respectively. N, purified starting material, no debris visible. [b] Tube unintentionally frozen before run. [c] Standing 51 hr., 4° after run before fractionation. [d] Top sample vol. 4.0 ml., 0.6 ml. organic phase. [e] 0.5 ml. CsCl, 0.6 ml. organic phase inclined to tube at end of run. [f] Red dye indicator in top showed leakage around organic phase when top fraction removed.

Consider first volatility. It is imperative that the desired mixture be made immediately before use and not mixed excessively. This reduces the change in density by evaporation. For the "CS" system, it was best to put the required volume of chloroform in each of three glass tubes, then layer the diethylhexyl sebacate on top. This prevented the chloroform from evaporating. Just before layering the infectious fluid in each tube, the organic fluids were mixed and transferred above the CsCl phase.

All of the fluids used are not completely miscible; that is, on standing they will separate into two phases, the lower one richer in the denser component.[28] This separation is not always visible, but is easily detected by taking drops from the top and

(28) S. Glasstone, "Textbook of Physical Chemistry," 2nd ed., D. Van Nostrand Co., Inc., New York, N. Y., 1946, p. 721.

bottom and measuring their densities in a salt gradient column. All the density diluents used in this study with the trichlorotrifluoroethane were only partially miscible, giving an upper phase on standing less dense than water. Chloroform–diethylhexyl sebacate mixtures at a nominal density of 1.082 g./ml. [30% (v./v.) chloroform] were also partially miscible; nevertheless, their upper phase was more dense than water. This partial miscibility provided an incidental density gradient in the organic fluid, not evident with the non-volatile, miscible fluids such as "ES" or "EB."

The virus solution during loading of the centrifuge tube, even when layered carefully, may separate the partially miscible fluids and carry a portion to the top. A sample of such an upper organic fluid, when introduced into the virus solution, was found to float. In this situation, the organic fluid remaining below the virus solution must have been more dense than calculated from the initial volumes mixed. Some of the organic phase can also be trapped on top by surface tension as the virus solution is layered. Initially it may be more dense, as tested in the same manner, but in a few minutes, evaporation of the volatile component makes it lighter.

The third complication is compressibility of the organic fluids under the centrifugal field. Theoretically, this makes the density greater than that calculated from the composition of the organic phase. Both this and partial miscibility imply that the density of 1.12 g./ml. is probably a lower limit for the hydrodynamic density of the virus. An observed effect of the compressibility was to cause a density inversion due to the field, if the organic fluid density was selected too close to that of the underlying CsCl solution.

Effect of Initial Aqueous Density.—An increase of the solution density with CsCl can increase the solvated density of the virus by dissolving salt in the hydration mantle. For aqueous densities greater than 1.43 g./ml., the virus floated and in these experiments the starting solution was placed below the organic phase and the recovery was computed for the top solution. Figure 2 shows the results of 17 runs not previously counted that had starting aqueous densities greater than 1.01 g./ml. and the six runs indicated in Table II (of aqueous density 1.01) but with organic fluid density greater than 1.12 g./ml. The shaded area indicates the density range of organic fluid that roughly encompasses the successful runs. Line C is the density inversion limit, for below that line, in the sedimentation range, the top aqueous solution would be greater than the organic fluid and thus could not be layered initially. The other sedimentation limit, line B, is drawn from 1.43 g./ml., the CsCl isodensity, to the 1.12 value deduced from Fig. 2, and through the plus and minus signs above 1.43 g./ml. The dashed line A shows the theoretical solvated density line if 1 ml./g. is assumed for the hydration. The discrepancy between lines A and B is due in part to the factors mentioned above under "Complications," or an error in the assumed hydration or partial specific volume.

This figure has a practical application in calculating the density of organic fluid to use for successive recycles of the virus fraction in which the density is decreased by dilution rather than by dialysis. Alternatively the density can be increased by addition of a more concentrated CsCl solution and the virus recycled by flotation.

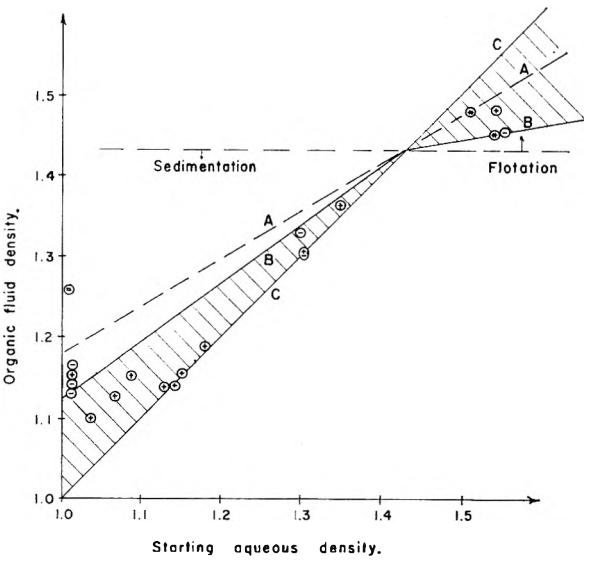

Fig. 2.—Penetration by FMDV of organic separator arranged as in Fig. 1G using aqueous solutions of various initial densities. Circles with plus sign, infectivity recovery >1%; circles with negative sign, recovery <1%; line A, solvated virus density as ordinate as function of aqueous density, assuming isodensity in CsCl at 1.43 g./ml. as dry density and hydration of 1 ml./g.; line B, limit of organic fluid density for recovery >1% drawn from the data shown; line C, density inversion limit for organic density; cross hatched area is the permissible organic fluid density, which above 1.43 g./ml. cannot quite reach line C because of differential compressibilities of organic and aqueous phases.

Purification

A. Analytical Ultracentrifugation.—Calculations from the schlieren patterns revealed that the virus in VF as harvested was 0.1% of the 37 mg./ml. concentration of 4–19 S components (using the specific refractive increment of albumin). After one cycle of 5 hr. centrifugation through the organic separator, the virus was increased to 15% of the total of protein plus virus. This meant that the relative purification factor was 150-fold even though the protein hydrodynamic and dry densities were both greater than that of the organic phase (1.08 g./ml.) and some of the protein appeared in the bottom solution. A second cycle reduced these contaminants below the limit of resolution. If the purification factor were the same as for the first cycle, contaminants would be reduced to 3% of the total unless some were selectively permitted to pass. It is anticipated that purification factors would be even better with lower initial concentration of contaminants.

B. Electron Microscopy.—Figure 3 is a micrograph of FMDV from vesicular fluid prepared by two cycles of centrifugation through the "CS" organic fluid. The initial run was one in the >50% recovery row of Table V. A dilution of the dialyzed virus solution reduced the EDTA to about 0.005 *M* in a mixture of NH_4OAc and $(NH_4)_2CO_3$ chosen to

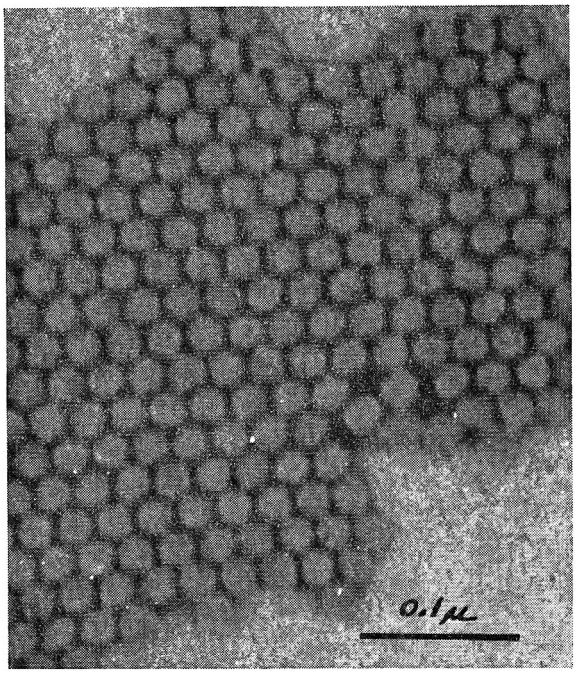

Fig. 3.—Electron micrograph of FMDV A/GB purified by sedimentation through "CS" immiscible fluid twice, dialyzed and dried in phosphotungstic acid; magnification 208,000×.

keep the pH constant on evaporation.[29] It is seen that the purity was sufficient to allow close packing in phosphotungstic acid.

C. Recommended Protocol for FMDV.—Because crude harvest fluids contain debris that alters the interface and because the analytical untracentrifuge patterns showed some contamination by protein, two cycles of centrifugation are now employed. The first is a transient isodensity centrifugation without organic separator (see *Experimental*). This gives a concentration and purification from a relatively large volume in a short (3 hr.) run without pelleting. The virus fraction from the bottom can be either diluted or dialyzed, and for the second cycle is layered over 0.9 ml. of the appropriate organic fluid [30% (v./v.) "C," 70% "S," 1.082 g./ml., for FMDV] which is above 0.9 ml. CsCl solution adjusted to a density slightly below the isodensity value of the virus (use 1.42 g./ml. CsCl for FMDV). Within 4 hr., equilibrium conditions will be closely approached.

Discussion

The mechanism of the stabilization of FMDV by EDTA is not known. Presumably, it is a chelation effect. The fact that EDTA also stabilizes FMDV in strong CsCl solutions suggests that the loss of infectivity in crude CsCl reported elsewhere[19] was due in part to impurities rather than CsCl alone.

The penetration of the organic fluid–water interface may involve solubility or merely a centrifugal forcing-through of the large virus particle. Studies by Rosano, *et al.*,[30] on the passage of salts and water through organic liquid membranes indicated that there must be solubility and that diffusion was the rate limiting step. In the centrifuge, the solute is concentrated at the upper interface and any solute which penetrates is removed by sedimentation or convection. Thus, even if the partition coefficient were minute, material might be expected to be transported into and through the organic phase. Several runs made in density gradients composed solely of organic liquids showed that the virus sedimented as a light scattering zone throughout the cross section of the organic fluid. At the lower interface the virus dissolves CsCl into its hydration mantle, and sediments to its isodensity level. Some of the protein that appeared in the lower solution may also have been transported by this mechanism. The poisoning of the upper interface by contaminants was masked in early runs at low density of organic fluid by the density inversion of the protein gel, which also presumably could carry virus down to the CsCl solution.

Ballentine and Burford's[11] criterion of non-volatility must be relaxed if certain organic liquids are desired for specific effects. Some of the results of density inversion and blocking of the interface by contaminants would also be possible in their system in long runs. It appears that all runs should be short and with as pure starting material as is consistent with the result desired.

No account has been taken in these preparative studies of the effect of overlying liquids in changing the buoyant density of virus, as shown by Hearst, *et al.*[8] This effect, as well as precise correlation of the density for passage with the hydrodynamic density, may perhaps best be studied in the analytical ultracentrifuge. No attempt was made to use pure CsCl solutions with no extraneous ultraviolet absorbing impurities.[31] Pure solutions need only be used in the final cycle where the organic phase separates a small volume of the scarce solution from the contaminated solution above. Also, water saturated organic solutions were not studied. Since water solubility increases considerably with pressure[32] the organic fluid would not remain saturated under the field.

These preparative experiments were not designed to test for attainment of sedimentation equilibrium. Rather, the times were chosen to be at least twice as long as necessary to sediment the virus from the meniscus to the bottom of the upper aqueous solution, and were increased with impure preparations that exhibited blocking of the interface. An estimate of the time for the short column of CsCl to reach equilibrium can be made by an extension of the argument of Van Holde and Baldwin.[12] They showed that the time required to reach within ϵ of sedimentation equilibrium for a dilute, uncharged, ideal solute was directly proportional to the square of the solution depth. Here ϵ is one minus the ratio of the solute concentration difference at the column ends at any time to the difference at equilibrium. Even with the concentrated, charged, and non-ideal CsCl solute it would be expected that their conclusions would still hold, as shown by the following argument.

Van Holde and Baldwin[12] defined a parameter α

(29) D. E. Bradley, *Virology*, **15**, 203 (1961).

(30) H. L. Rosano, P. Duby, and J. H. Schulman, *J. Phys. Chem.*, **65**, 1704 (1961).

(31) J. E. Hearst and J. Vinograd, *Proc. Natl. Acad. Sci., U. S.*, **47**, 1005 (1961).

(32) J. Griswold and J. E. Kasch, *Ind. Eng. Chem.*, **34**, 804 (1942).

that involved the solute molecular weight, partial specific volume, length and density of the solution column, and speed of rotation such that

$$t_\epsilon = F(\alpha)(b - a)^2/D \qquad (1)$$

where t_ϵ is the time to reach within ϵ of equilibrium, a, b are radii of the top and bottom limits of the solution column, D is the diffusion coefficient, and $F(\alpha)$ is a function of ϵ only, if $\alpha > 0.2$. For $\epsilon = 0.01$, $F(\infty) = 0.445$. They showed that α also determined the equilibrium concentrations according to

$$c_b/c_a = e^{1/\alpha} \qquad (2)$$

With 40% (w./w.) CsCl, the equilibrium concentrations can be calculated[33,34] for the case at hand of a 1 cm. column at 37,000 r.p.m. at 9 cm. Using equation 2 in reverse, these give an effective α of 4. Since this is so much larger than the 0.2 mentioned above, it is assumed that equation 1 is also valid for CsCl. Using the value of $D = 2.22 \times 10^{-5}$ cm.^{2}/sec., interpolated from the data of Lyons and Riley,[35] gives $t_{0.01} = 5.6$ hr. Preparative runs need be no longer than this.

Whereas the time to reach equilibrium is independent of the speed, the magnitude of the density gradient is proportional to the square of the speed. A high speed is important in exploratory studies in order to make certain the gradient brackets the density of the virus. Otherwise, the density might be too high for the virus to enter, or if too low, the virus would pellet. At 37,000 r.p.m., a 1 cm. column at the bottom of the SW 39 tube at 25° has a density difference of 0.010 g./ml. in a nominal 1.42 g./ml. CsCl solution.

Acknowledgment.—The technical assistance of Messrs. Charles E. Bennett and Karl H. Axelson is gratefully acknowledged.

DISCUSSION

G. KEGELES (Clark University).—Is there any effect of changing the speed of rotation while keeping all original compositions constant?

R. TRAUTMAN.—The effect of speed has not been studied, but should be an important variable in elucidating the mechanism of penetration.

S. G. MASON (Pulp and Paper Institute of Canada).—This separation may be based largely on the ability of the virus and enveloping water to wet (or coalesce with) the organic phase. If this is true the separation is analogous to the "flotation" process used in ore separation. I wish to suggest that you try the analog of flotation, *i.e.*, allow tiny drops of organic liquid to sediment under gravity through the aqueous layer containing the virus.

R. TRAUTMAN.—The exact analog of the ore "flotation" process has not been tried. However, the virus solution has been shaken with heavier immiscible organic liquids, making an emulsion of oil in water. Upon slight centrifugation to break the emulsion the virus is left in the aqueous phase and not sedimented with the oil droplets. Hence it is concluded that the virus is neither preferentially adsorbed to the interface nor highly soluble in the organic phase.

NORMAN G. ANDERSON (Oak Ridge National Laboratory).—Several years ago Dr. Nichols and I attempted to use a double gradient method to separate proteins. Briefly this method consisted in introducing a pre-formed gradient of Kel-F oil and paraffin oil into an analytical cell, and adding a few drops of a protein solution. At speed, the aqueous material found its own level in the non-aqueous gradient. As centrifugation continued the aqueous layer separated into first two and then many bands as the protein sedimented forming levels having different densities. We hoped to end up with one band containing the aqueous solvent and a second containing a leaflet of protein with only its water of hydration. Instead we always got several bands for reasons we do not understand. The method should be re-explored but may work better with viruses. You may find it possible to eliminate the cesium chloride and use a short non-aqueous gradient instead.

R. TRAUTMAN.—We have some preliminary preparative experiments on organic density gradients in which the virus was seen as a light scattering band. Extending the comment in the Discussion, the water solubility in the organic phase could give several bands depending upon how much water had been removed from the protein solution. Cox and Schumaker [*J. Am. Chem. Soc.*, **83**, 2439 (1961)] report that precipitated protein mixtures give aqueous isodensity bands as separate components, not coprecipitated. It may well be that the analytical centrifuge will be the instrument of choice for elucidating the mechanism of penetration. Your experiment is quite interesting in that respect. We, of course, would like to eliminate the CsCl and hope to pursue the organic gradient work further.

H. K. SCHACHMAN (University of California).—One of the reasons the organic density gradient work referred to in this paper (ref. 9) is unpublished is that separation of the drops occurred. Perhaps the phenomenon Dr. Anderson was looking for occurred.

H. A. ENDE (Chemstrand Research Center).—Since you are separating according to differences in density, would it not be possible to use the normal density gradient technique in separating the FMDV from contaminations? I was thinking of using the density gradient method in connection with fixed partition cells. The conditions for collecting the FMDV in a band could first be established using an analytical ultracentrifuge. Preparative separation then could be achieved by using a cell with two perforated bottoms bordering the region where the band is formed.

R. TRAUTMAN.—Isodensity centrifugation without organic liquid has been used, and in fact has been very helpful as a first step to reduce contaminants before final centrifugation through organic interfaces. One advantage of the organic liquid, not obtained with CsCl alone, is the selective purification from debris of *s*-rate and density similar to the virus. The aim of centrifugation procedures with viruses is to avoid pelleting or even collisions with walls or partitions, since recovery is greatly impaired. The analytical cells are too small for preparative procedures, and the swinging bucket tubes can be fractionated quite well without mechanical compartmentation.

(33) J. B. Ifft, D. H. Voet, and J. Vinograd, *J. Phys. Chem.*, **65**, 1138 (1961).

(34) R. Trautman, *Arch. Biochem. Biophys.*, **87**, 289 (1960).

(35) P. A. Lyons and J. F. Riley, *J. Am. Chem. Soc.*, **76**, 5216 (1954).

THE ZONAL ULTRACENTRIFUGE. A NEW INSTRUMENT FOR FRACTIONATING MIXTURES OF PARTICLES

BY NORMAN G. ANDERSON

Biology Division, Oak Ridge National Laboratory,[1] *Oak Ridge, Tennessee*

Received March 1, 1962

The zonal ultracentrifuge is a new biophysical tool which allows particles to be separated on the basis of sedimentation rate or particle density. The rotor is a hollow cylinder with a total capacity of 1625 ml. divided by vertical septa into sector-shaped compartments. Two fluid-handling lines through the upper shaft connect the edge of the rotor and the central core with a flat rotating seal which presses against an external static seal. All operations, including introduction of the density gradient and the sample layer, and recovery of the gradient with its separated zones of particles, are carried out with the rotor spinning at speeds up to 5000 r.p.m. in a refrigerated evacuated chamber. The gradient is stabilized at all times by the centrifugal field. Particle separation is accomplished at speeds up to 30,000 r.p.m. (51,161 $\times$ g at the maximum radius of 5.08 cm.). Subcellular components, including nuclei, cell membrane fragments, mitochondria, microsomes, ribosomes, and macroglobulin have been isolated using aqueous sucrose gradients. Tobacco mosaic virus and brome mosaic virus have been recovered in a high state of purity from crude extracts in one run. Types I, II, and III polio virus have also been isolated in quantity from tissue culture fluid. A number of alternate rotor configurations now under consideration are presented together with data on the limits of rotor diameter attainable with aluminum and steel rotors.

A preparative ultracentrifuge capable of achieving zonal separations with a resolution approaching that of the analytical ultracentrifuge has been required for the isolation of subcellular particles and viruses, and for the separation of proteins and other macromolecules which differ in sedimentation rate or density. The development of such a zonal ultracentrifuge capable of separating particles down to the $S_{20,w}20$ size range is described in this paper. It appears that zonal separations in centrifuges can only be made in the presence of density gradients. The term zonal ultracentrifuge has therefore been adopted here in preference to the term density gradient ultracentrifuge since the former term implies the presence of a density gradient. A preliminary report of this work has appeared.[2]

Density-gradient centrifugation using swinging-bucket rotors has been extensively reviewed.[3-5] The principles of zonal stability are largely derived from work on density gradient electrophoresis.[6]

Ideally, sedimentation should occur in sector-shaped tubes or compartments to avoid undesirable wall effects. Early low-speed studies in glass centrifuge tubes of modified sector shape[7] demonstrated that excellent separations of liver cell components could be obtained; however, runs as long as 18 hr. were required, and only 2 ml. of sample could be separated per tube. To eliminate the long interval required for filling with the density gradient, a method was devised for loading the tubes while the centrifuge was running, using centrifugal force to prevent mixing.[8] Recovery of the separated zones was still made with the tubes at rest.

Since most of the difficulties encountered centered around the use of tubes, the possibility of eliminating them entirely was next considered. It appeared that a hollow rotor, with the internal volume divided by vertical septa into truly sector-shaped compartments, could be used if (1) the gradient and sample could be introduced, and (2) the separated zones were recovered *while the rotor was spinning.* A low-speed rotor[9] demonstrated the feasibility of this concept, and a medium-speed 625-ml. rotor operating in air showed that gradients could be introduced and recovered with very little change at speeds up to 18,000 r.p.m.

It is essential in rotors of this type to ensure that tangential flow in the rotor is eliminated. Fluid flowing to the rotor edge must be suitably channeled so that it has been accelerated to the tangential velocity obtaining at the edge of the fluid chambers. Similarly, as the gradient is displaced in toward the rotor core during unloading, it is greatly decelerated. In the absence of vertical septa, the energy involved will be dissipated as heat in the process of swirling the rotor fluid. Therefore, compartmentalization of the rotor is essential.

Design Considerations.—The configuration chosen (Fig. 1) for initial high speed studies was dictated largely by the necessity of using existing components as far as possible. A Spinco Model L ultracentrifuge was modified by extending the vacuum chamber 9.9 cm. and adding a rotor temperature sensing and control system. A liquid nitrogen trap was inserted in the vacuum line, and the drain which normally returns oil from the rotor chamber to the vacuum pump was clamped off. The plate containing the overspeed safety pin was also modified to prevent liquids in the chamber from draining down to the drive shaft.

Since the drive and support system was below the rotor, it was necessary to make fluid line connections at the top, and to provide an upper bearing to center the rotor and provide a vacuum seal.

The rotor chamber is 25.72 cm. long, with an inside diameter of 10.16 cm. and a wall thickness of 1.27 cm. The interval volume of 1625 ml. is divided by vertical septa into 36 identical sector-shaped compartments. The upper shaft is hollow with an additional small center tube so that fluid may be pumped into and out of the rotor at the same time.

(1) Operated by Union Carbide Corporation for the United States Atomic Energy Commission.

(2) N. G. Anderson and C. L. Burger, *Science*, in press (1962).

(3) (a) N. G. Anderson in "Physical Techniques in Biological Research," Vol. III, Gerald Oster and Arthur W. Pollister, Editors, Academic Press, Inc., New York, N. Y., 1956, p. 299; (b) Ch. de Duve, J. Berthet, and H. Beaufay, *Progr. Biophys. and Biophys. Chem.*, **9**, 326 (1959).

(4) J. F. Thomson, *Anal. Chem.*, **31**, 836 (1959).

(5) M. K. Brakke, *Advances in Virus Research*, **7**, 193 (1960).

(6) H. Svensson in "A Laboratory Manual of Analytical Methods in Protein Chemistry Including Polypeptides," Vol. I, P. Alexander and R. J. Block, Editors. Pergamon Press Ltd., London, 1960, p. 195.

(7) N. G. Anderson, *Exptl. Cell Res.*, **9**, 446 (1955).

(8) J. F. Albright and N. G. Anderson, *ibid.*, **15**, 271 (1958).

(9) N. G. Anderson, *Bull. Am. Phys. Soc.*, **I**, Series II, 267 (1956).

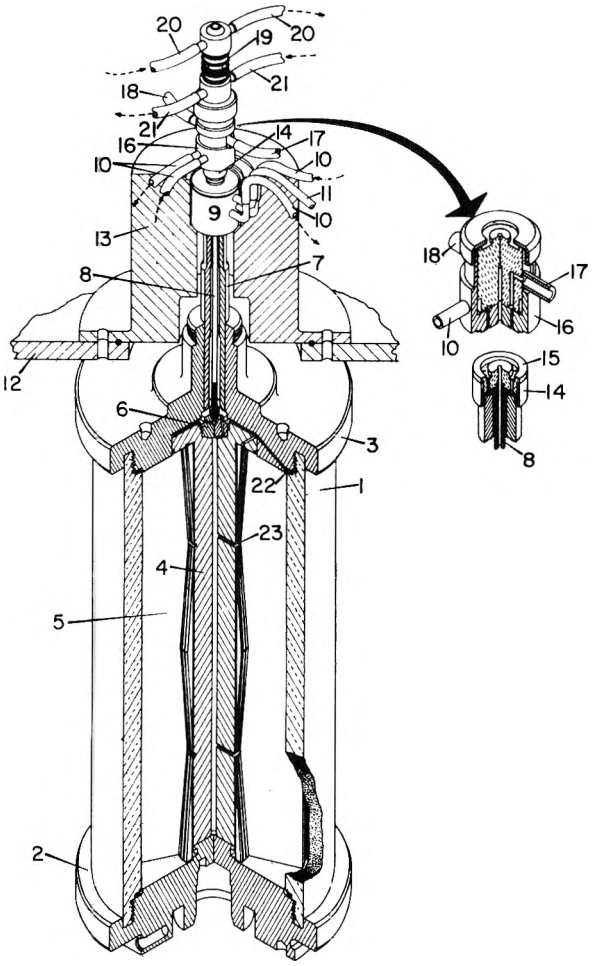

Fig. 1.—Cutaway drawing of zonal ultracentrifuge rotor. Note divisions of internal volume into sector-shaped compartments by vertical septa, central collecting core, and coaxial lines leading to upper seal: 1, tubular rotor wall of 7075-T6 aluminum; 2, lower rotor cap; 3, upper rotor cap; 4, rotor core; 5, septa; 6, fluid line crossover; 7, upper rotor shaft; 8, center upper fluid line; 9, upper bearing; 10, coolant lines; 11, oil line; 12, rotor chamber top; 13, upper bearing housing; 14, rotating seal cup; 15, rotating seal; 16, upper static seal; 17, fluid line leading to rotor center; 18, fluid line leading to rotor edge; 19, seal pressurizing cylinder; 20, fluid line to rotor center running through pressurizing cylinder; 21, fluid line to rotor edge running through pressurizing cylinder; 22, fluid line opening at rotor edge; 23, fluid line opening in central core.

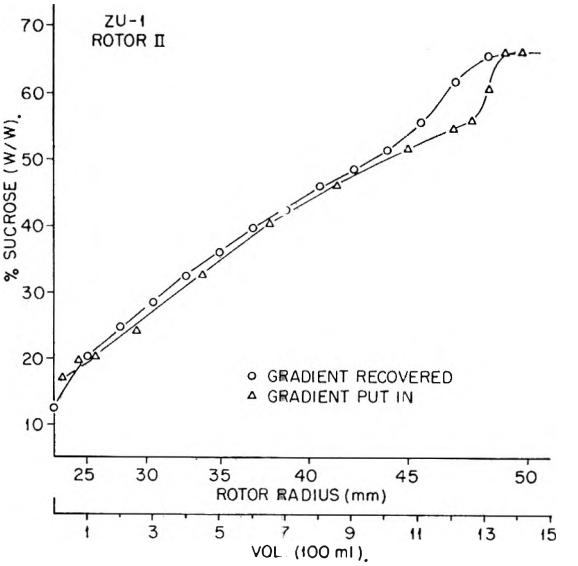

Fig. 2.—Comparison of density gradient produced by gradient engine and gradient recovered after 4 hr. at 20,758 r.p.m.

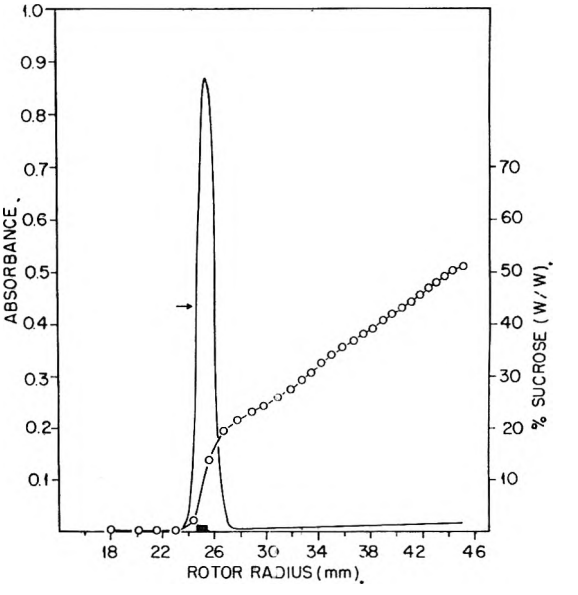

Fig. 3.—Widening of sample zone in zonal ultracentrifuge. Sample introduced as gradient containing 10 ml. of 8% bovine serum albumin and 10 ml. of 17% sucrose (w./w.). Bar indicates width zone would have in the absence of any diffusion or mixing. Sample introduced at 5000 r.p.m., accelerated to 25,000 r.p.m. for 5 min., and unloaded at 5000 r.p.m., 5°.

The center line connects to the rotor wall through four horizontal channels in the rotor cap. The outer line in the upper shaft connects to the central rotor core. The upper shaft ends in a flat Pickels seal made of Teflon filled with a metallic oxide. It presses against a flat static seal of aluminum coated with tungsten carbide. The upper seal and the upper bearings are both cooled with circulating ice water.

Operation.—In operation the empty prechilled rotor is accelerated to 5000 r.p.m. and filled completely at this speed. This is done by pumping a 1200-ml. density gradient to the rotor edge, light end of the gradient first. The gradients most used ranged from 17 to 55% sucrose (w./w.) for tissue fractionation and 12 to 30% sucrose for viral and ribosomal separations. After the gradient was in the rotor a "cushion" of concentrated sucrose (55 or 66%) was pumped into the rotor edge until the light end of the gradient began to flow out the core exit line, indicating that the rotor was completely full.

The sample (contained in a short density gradient) was then pumped into the rotor through the core, forming a sample zone centripetal to the density gradient. This is followed by an "overlay" solution having a density less than that of the sample layer, thus displacing the sample zone away from the core, but leaving the rotor full.

The centrifuge is then accelerated to operating speed (up to 30,000 r.p.m.). After the desired

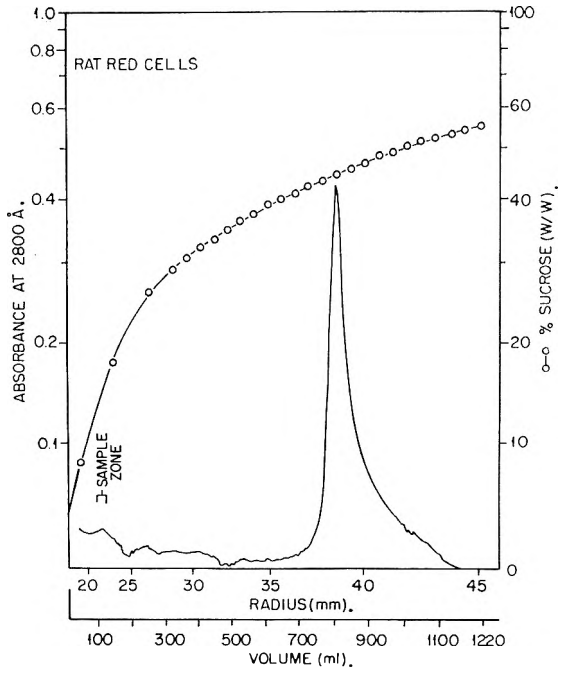

Fig. 4.—Chilled rat red cells centrifuged to equilibrium position 44.7% sucrose (w./w.) in zonal ultracentrifuge. Centrifuged 60 min. at 20,480 r.p.m. Effluent analyzed at 280 mμ using 0.2 cm. cell; 5°.

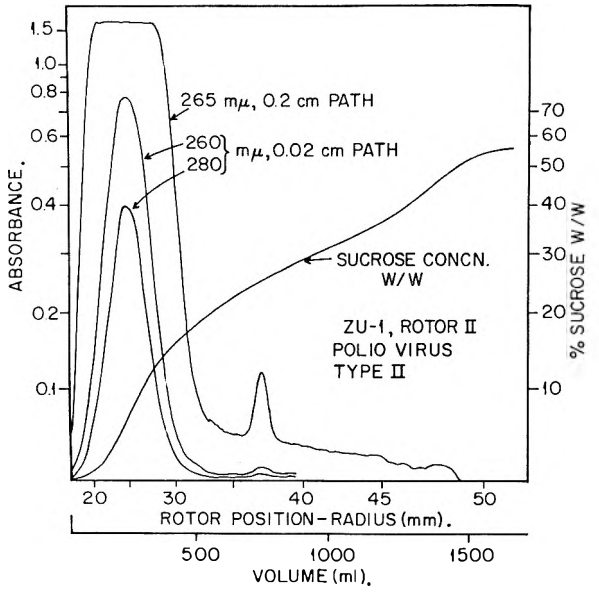

Fig. 5.—Separation of Type II polio virus from soluble proteins and nucleic acid. Centrifuged 180 min. at 27,800 r.p.m.; 5°.

separation has been completed, the centrifuge is decelerated to 5,000 r.p.m., and the gradient displaced out through the central core by pumping a very dense solution to the rotor edge. As the gradient flows out of the rotor it is analyzed continuously for ultraviolet absorbance and, if desired, for protein concentration or enzymatic activity using automated analytical systems to be described elsewhere.

In initial studies carried out at Spinco Division of Beckman Instruments, Inc., considerable instability was observed when a flexible upper shaft was used, or when the septa were omitted. The cause of this instability is not fully understood, but it is largely overcome by using a very stiff upper shaft with a lightly mounted upper bearing.

Performance Studies. Gradient Stability.—The gradient actually introduced into the rotor was analyzed refractometrically before being pumped in, and as recovered from the rotor. The results are shown in Fig. 2. When the short radius of the rotor is considered, the small changes are probably no more than might be expected. To see whether a concentrated sample layer maintains its position in the centrifuge, a sample gradient made from 10 ml. of 8% bovine serum albumin in distilled water and 10 ml. of 17% sucrose was layered over a 1200-ml. gradient varying linearly with rotor radius from 17 to 55% sucrose (w./w.). After the sample was introduced, the rotor was accelerated to 25,000 r.p.m. for 5 min., decelerated to 5,000 r.p.m., and unloaded. The ultraviolet absorbance of the effluent stream (Fig. 3) was recorded and the results were recalculated in terms of the rotor radius. The sample zone at a radius of 25.3 mm. would be 0.65 mm. thick if no mixing or diffusion occurred. The peak recovered had a width of 1.6 mm. at half height, indicating that only a small amount of band-spreading had occurred, due in part to the fact that the core used assumed vertical zones.

Separations may be made in density gradients on the basis of sedimentation rate or, if the equilibrium or isopycnic position is reached, on the basis of density alone. To see whether sharp separations could be obtained with both methods, the following experiments were performed. Chilled rat red cells become paracrystalline and cease to behave osmotically.[10] The equilibrium peak position of these cells is at 44.7% sucrose and shows a very sharp peak (Fig. 4). Whether the tailing of this peak is caused by mixing by laminar flow in the lines or because of inhomogeneities in the density of these cells remains to be determined. It is evident, however, that sharp banding based on approach to equilibrium may be obtained.

For rate studies, polio virus particles were used. These are homogeneous particles with a sedimentation coefficient of approximately 160. A partially purified suspension containing, in addition, soluble proteins and nucleic acid was separated as shown in Fig. 5. The solution represented by the small peak was concentrated and photographed in the analytical ultracentrifuge (Fig. 6) and in the electron microscope. While the preparation appeared to be homogeneous by these two methods of observation, it should be emphasized that the criteria used apply only to the physical properties of the particles and would not distinguish any non-viral particles present having these properties. Thus far, polio virus Types I, II, and III have been isolated in this manner as well as tobacco mosaic virus and brome mosaic virus. It is apparent that the density gradient ultracentrifuge is useful for the isolation of viruses.

More complex mixtures, including homogenates of mammalian tissues, have been successfully re-

(10) E. Ponder, "Hemolysis and Related Phenomena," Grune and Stratton, New York, N. Y., 1948.

solved into their respective components using a gradient in which the larger particles are separated on the basis of their density and the smaller particles on the basis of their sedimentation rate. The six fractions seen (Fig. 7) in liver preparations include nuclei uncontaminated with whole cells, a fraction composed predominantly of "cell wall" material, mitochondria, endoplasmic reticulum with attached granules, ribosomes, and soluble materials. Since these are seen in a single analysis, the method constitutes a new way of visualizing the cell parts. Characteristic differences, including a diminution in the amount of mitochondrial material in tumor tissue, have been seen.

At the speeds presently available, large proteins, such as the macroglobulin of rat serum, which has a sedimentation coefficient of 18 (ref. 11) may be partially separated after prolonged 15-hr. runs. The useful range of the present machine, therefore, is down to approximately $S_{20}20$. We consider it important to develop much higher centrifugal forces in zonal rotors for the following reasons. First, in many colloidal systems, especially synthetic polymer preparations, it is important to be able to fractionate mixtures on the basis of particle size and to obtain sufficient material from several fractions for chemical analysis. Secondly, in the fractionation of protein mixtures, most isolation methods are strongly charge-, or charge-to-mass-ratio dependent. Thus the sequence of serum proteins observed near neutrality in the Tiselius apparatus, the sequence eluted from diethylaminoethylcellulose,[12] and the order in which constituent proteins are precipitated with ammonium sulfate show certain similarities. Not infrequently an isolation procedure yields a mixture of proteins resolvable only in the analytical ultracentrifuge. If a preparative zonal ultracentrifuge of sufficient speed were available, separation on the basis of sedimentation coefficient could be one of the early steps. We have inquired, therefore, into those factors which might limit the speed and resolution obtainable.

Rotor Configurations.—A number of rotor configurations have been considered (Fig. 8). (A) Rotor with vertical axis, supported and driven from below, with coaxial fluid line connections at the top of rotor (at end of upper shaft). (B) Rotor similar to A, but inverted. (C) Vertically mounted rotor, with shafts and bearings at each end, with one fluid line connection at each end. (D) Rotor suspended from above, with removable coaxial filling probe which is inserted for filling at low speed. The probe is removed and the rotor is capped for high speed operation, and then reinserted at low speed for unloading. (E) Internal skimmer rotor. (F) Any of the above systems having two bearings may be mounted, in instances described below, to rotate along a horizontal axis.

Configuration A has been used here to allow use of existing equipment. It is believed, however, that configuration B may prove to be more stable at high speed. It is hoped that a facility for testing

(11) N. G. Anderson, R. E. Canning, M. L. Anderson, and R. H. Shellhamer, *Expll. Cell Res.*, **16**, 292 (1959).

(12) H. A. Sober and E. A. Peterson, *Federation Proc.*, **17**, 1116 (1958).

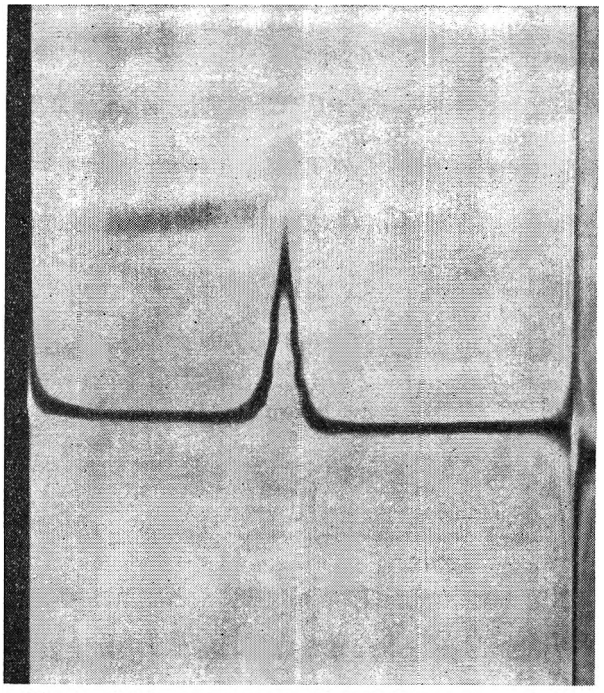

Fig. 6.—Polio virus from small peak in run shown in Fig. 8 observed in the analytical ultracentrifuge. No contamination was detectable; $s_{20} = 148$.

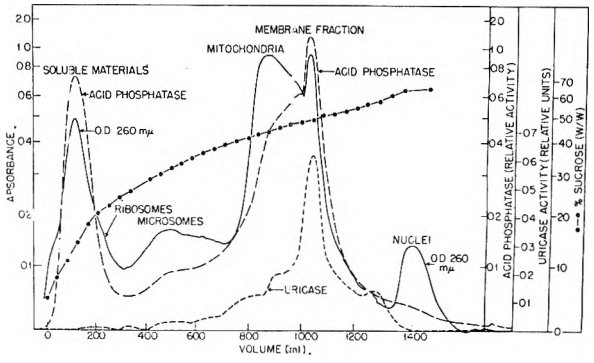

Fig. 7.—Separation of rat liver brei in zonal ultracentrifuge. Centrifuged 240 min. at 20,758 r.p.m. at 5°.

a number of the above rotor systems can be constructed in the near future.

At very high speeds it may be advisable to remove all fluid line connections as suggested in D above and let the rotor hang free, as is done with the Spinco analytical ultracentrifuge. The internal skimming system will probably find its greatest use at speeds below 20,000 r.p.m., where evacuation of the rotor chamber is not essential. The skimmer consists of two stationary disks with an exit port in the center of one. As the fluid reaches the disks it is decelerated, producing a local decrease in the rotational velocity of the liquid and hence in the centrifugal force and pressure in the fluid between the disks. Fluid pressure at the same radius outside the skimmer forces the fluid in the skimmer out the exit port. This principle has been previously used in the gas ultracentrifuge.

One of the greatest difficulties in designing these so-called "hoop-stress" rotors arises from the differential expansion of the rotor cylinder and the cap. In Rotor II used in the present studies the

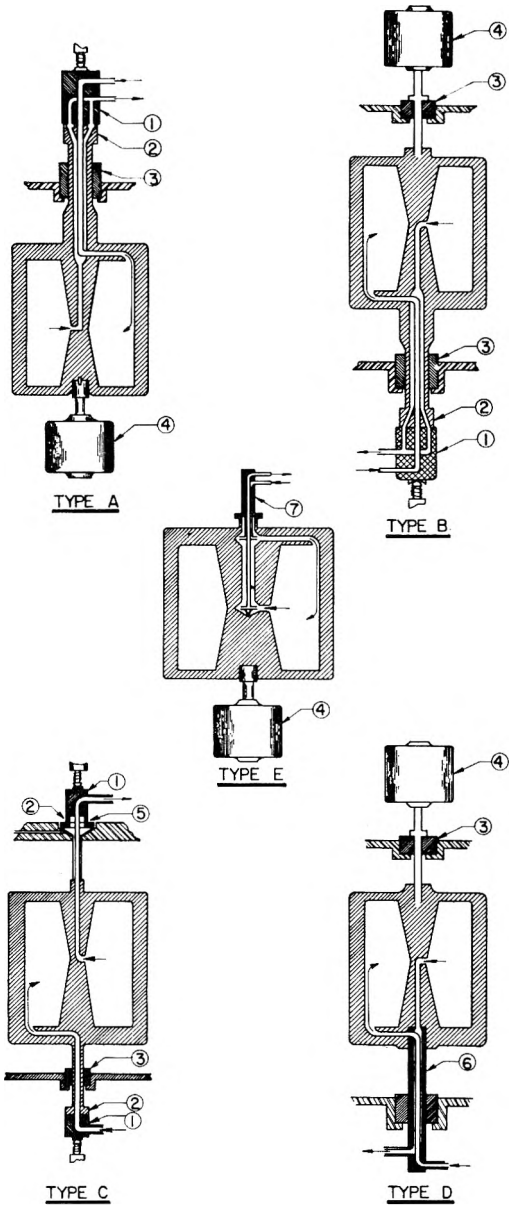

Fig. 8.—Rotor configurations for zonal ultracentrifuges; description included in text: 1, static seal; 2, rotating seal; 3, bearing; 4, drive system; 5, air turbine; 6, removable probe for filling and emptying rotor; 7, stationary skimmer system for making fluid line connections to rotor.

cap is held on by buttress threads on the inside of the cylinder. The cylinder expands during acceleration, and at maximal speed makes contact with an outer rim on the cap. The cap, therefore, is accurately positioned only at rest and at top speed. While there are several ways to predeform the cylinder, or to compensate for expansion by deformation at top speed, these are not satisfactory solutions.

Maximum Speeds.—To obtain information on the speeds obtainable, equations which give the optimum wall thickness and maximal inside diameter at a given rotational speed have been solved on a computer. Some of the results are listed in Table I.

Limitations on Rotor Length.—In cylindrical rotors spinning about a vertical axis, the rotor length is limited only by total rotor weight, rotor stability at high speed, and by the loading and unloading speed, which in turn affects the design of the rotor core.

Future core designs must take into account the fact that no equal-density zone in the ultracentrifuge is ever truly vertical. Rather, each zone will form part of a paraboloid of revolution having the same axis as the rotor according to the equation

$$L = \omega^2 r^2/2 \times 980 \qquad (1)$$

where

L = length of parabola in cm., from vertex to the top of the rotor chamber
r = rotor radius in cm.
ω = angular velocity in radians per second

With the core of rotor II, the maximal diameter is 3.785 cm. A rotor having a core of this upper diameter, according to eq. 1, cannot be longer than 500 cm. if it is to be loaded and unloaded at 5000 r.p.m. The difference in radial position between the top and the bottom of the rotor at the maximal core diameter is approximately 1 mm. For maximal resolution the core should have a large number of collecting bands and should follow eq. 1 in its overall shape.

TABLE I

RADIUS AND WALL THICKNESS OF CYLINDRICAL BOWL ROTORS FOR THE ZONAL ULTRACENTRIFUGE[a]

	Steel (Hytuf alloy)		Aluminum (7075-T6)	
Speed (r.p.m.)	Inside radius (cm.)	Wall thickness (cm.)	Inside radius (cm.)	Wall thickness (cm.)
15,000	15.21	3.51	12.3	4.42
30,000	7.62	1.75	6.12	2.21
45,000	5.08	1.17	4.09	1.48
60,000	3.81	0.879	3.25	1.17
75,000	3.05	.704	2.59	0.935
90,000	2.54	.587	2.16	.780
120,000	1.91	.439	1.63	.587
180,000	1.27	.295	1.07	.384

[a] Kindly computed by Mr. A. A. Brooks, Flow Research Department, Technical Division, Oak Ridge Gaseous Diffusion Plant. Average fluid density assumed to be 1.7. Calculations also assume that the septa are centrally supported.

The optimal gradient to be used in a given instance is, in part, a function of the distribution of particle sizes in the sample. The following considerations favor a convex gradient: (1) the greatest particle capacity ($\sim 1/2$ (dC/dr) $\times$ zone thickness) is needed near the sample zone since the largest concentration of particles will occur in this area; (2) the concentration of particles in a given zone diminishes as it moves centrifugally, according to the familiar equation[13]

$$\frac{C_0}{C_m} = \left(\frac{X_m}{X_0}\right)^2 \qquad (2)$$

and (3) the capacity of the gradient increases rapidly as the difference between particle and solution densities approaches zero.

In practice, linear (with radius) gradients have proved very useful because analysis of sedimenta-

(13) T. Svedberg and K. O. Pederson, "The Ultracentrifuge," Oxford, Clarendon Press, 1940.

tion data is simpler, and because they give good resolution of mixtures containing particles having a very large size range. For example, extremely dense solutions are required to keep cell nuclei from reaching the rotor wall, while very dilute solutions are needed if ribosomes are to be separated in a reasonable time. A linear gradient with a dense "cushion" allows both to be isolated from the same mixture.

The results obtained to date indicate that the zonal ultracentrifuge is a biophysical tool capable of achieving sharp separations of particles on the basis of sedimentation rate or density.

NOTE ADDED IN PROOF.—During 102 runs with this instrument, marked instability above 24,000 r.p.m. has been observed in several instances, resulting in excessive vibration and bearing heating. Self-balancing rotors with no upper bearing are under construction at the present time.

Acknowledgments.—During the development of this centrifuge, discussions with Drs. J. W. Williams, J. W. Beams, M. L. Randolph, E. G. Pickels, and D. G. Sharp have been most helpful. Construction of the rotor, drive system, and upper bearing assembly was carried out under subcontract by the Spinco Division of Beckman Instruments Inc., with additional modifications being made at Oak Ridge. I am indebted to Dr. Jonas Salk for stimulating discussions and for quantities of polio virus, to Dr. Myron Brakke for TMV- and BMV-infected plant tissues and advice on the isolation of viruses from them, and to Dr. C. A. Knight for a large sample of purified TMV. Rotor II and associated equipment were designed by Richard Stallman.

DISCUSSION

W. J. CARTER (MSA Research Corporation).—Have you purified any of the bacteriophages—T-3, in particular?

N. G. ANDERSON.—We have concentrated T-3 by using the zonal rotor as a continuous flow centrifuge, and then purified by zonal sedimentation in a density gradient.

THE BUOYANT BEHAVIOR OF BOVINE SERUM MERCAPTALBUMIN IN SALT SOLUTIONS AT EQUILIBRIUM IN THE ULTRACENTRIFUGE. I. THE PROTEIN CONCENTRATION DISTRIBUTION BY SCHLIEREN OPTICS AND THE NET HYDRATION IN CsCl SOLUTIONS[1a]

BY JAMES B. IFFT[1b] AND JEROME VINOGRAD

Gates and Crellin Laboratories of Chemistry[1c] and Norman W. Church Laboratory of Chemical Biology, California Institute of Technology, Pasadena, California

Received March 15, 1962

Bovine serum mercaptalbumin has been banded in CsCl solutions at sedimentation equilibrium. The schlieren optical system was employed to record the equilibrium distribution of concentration. This distribution appeared to be gaussian, indicating density and molecular weight homogeneity. Methods were developed to obtain the radial distance of the center of the band with a precision of 0.001 cm., the buoyant density to 0.001 g./cm.^{3}, and the standard deviation of the concentration distribution to 2%. The partial specific volume of the protein was measured in buoyant CsCl solution and found to be 0.736 g./cm.^{3}, essentially the same as in water. A net hydration for the salt-free protein of 0.20 g. H_2O/g. was evaluated from the measured buoyant density and the partial specific volume. An apparent molecular weight was calculated from the standard deviation of the band and compared with the molecular weight obtained from two-component sedimentation equilibrium experiments.

Introduction

Sedimentation equilibrium in a density gradient[2] can provide a buoyant density and a molecular weight for the solvated macromolecular species. The method has been used primarily to study the buoyant density of nucleic acids.[3-5] In addition there have been numerous investigations of viruses,[6-8] especially in preparative ultracentrifuges. Some proteins have been examined,[9-11] but there has been no quantitative study of the behavior of a dissolved protein of known molecular weight. This paper presents such a study.

Cox and Schumaker[9] examined bovine serum albumin (BSA) in a CsCl density gradient with absorption optics. They obtained a skewed curve which could not be satisfactorily converted to the protein concentration distribution and concluded that neither the value of the standard deviation nor the value of the buoyant density for soluble BSA could be obtained with sufficient accuracy.

The schlieren optical system was employed in the present work. This system permits the simultaneous recording of the refractive index-gradient curves from the protein solution and reference solution. The baseline must be determined experimentally because the band is so wide, $2\sigma = 0.2$ cm., and the baseline departs sufficiently from linearity over this distance that an interpolation, as is generally used with nucleic acid bands, is unsatisfactory. In order to determine the correct baseline, the two solutions must be spun to equilibrium under identical conditions, *i.e.*, the initial solution densities and column lengths must be identical. Methods are described whereby these conditions can be met.

The expression originally derived[2] for the molecular weight of a banded macromolecule in the absence of interaction between the macromolecule and the solvent is

$$M = \frac{RT\ \rho_0}{\sigma^2(\mathrm{d}\rho/\mathrm{d}r)_0\omega^2 r_0} \qquad (1)$$

The subscript zero denotes quantities evaluated at band center. The quantity r_0 is the radial distance in cm. of the center of the gaussian concentration distribution, which we will refer to as the band, from the center of rotation. The density of the solution at the mode of the band is ρ_0. This density is the physical density of the solution and is a function of both salt composition and pressure. The distance σ is the standard deviation in cm. of the gaussian concentration distribution. The above three quantities are directly measurable.

For approximate calculations, the density gradient generally used in eq. 1 is the composition density gradient,[12] which can be readily evaluated experimentally or by calculation from physical chemical data. Several other types of density gradients, however, have been defined. The effective density gradient,[13] which includes contributions involving the response of the macromolecule to the changing pressure and water activity in the band, must be used to determine the solvated molecular weight. Because neither of these interactions has been evaluated for any protein, the physical density gradient[14] will be employed in this paper, thereby neglecting any protein-solvent interactions. The

(1) (a) This investigation was supported in part by Research Grant H-3394 from the National Institutes of Health, U. S. Public Health Service; (b) Frick Chemical Laboratory, Princeton University, Princeton, New Jersey; U. S. Public Health Service Research Fellow of the National Cancer Institute, 1959-1960; Division of General Medical Sciences, 1960-1961; (c) Contribution No. 2817.

(2) M. Meselson, F. W. Stahl, and J. Vinograd, *Proc. Natl. Acad. Sci. U. S.*, **43**, 581 (1957).

(3) M. Meselson and F. W. Stahl, *ibid.*, **44**, 671 (1958).

(4) R. Rolfe and M. Meselson, *ibid.*, **45**, 1039 (1959).

(5) N. Sueoka, J. Marmur, and P. Doty, *Nature*, **183**, 6 (1959).

(6) L. V. Crawford, *Virology*, **12**, 143 (1960).

(7) J. D. Smith, G. Freeman, M. Vogt, and R. Dulbecco, *ibid.*, **12**, 185 (1960).

(8) J. Weigle, M. Meselson, and K. Paigen, *J. Mol. Biol.*, **1**, 379 (1959).

(9) D. J. Cox and V. N. Schumaker, *J. Am. Chem. Soc.*, **83**, 2439 (1961).

(10) A. Siegel and W. Hudson, *Biochim. Biophys. Acta*, **34**, 254 (1959).

(11) R. M. Bock, private communication.

(12) J. B. Ifft, D. Voet, and J. Vinograd, *J. Phys. Chem.*, **65**, 1138 (1961).

(13) J. E. Hearst and J. Vinograd, *Proc. Natl. Acad. Sci. U. S.*, **47**, 999 (1961).

(14) J. E. Hearst, J. B. Ifft, and J. Vinograd, *ibid.*, **47**, 1015 (1961).

apparent values of the molecular weights thus obtained will be designated M_{app}.

The density gradient method affords a procedure for the evaluation of the net binding of one component of the solvent. The net hydration of the salt-free protein, designated Γ_a', may be calculated from the relation

$$\rho_0 = \frac{1 + \Gamma_a'}{\bar{v}_3 + \Gamma_a' \bar{v}_1} \qquad (2)$$

This expression first was obtained by Williams, *et al.*[15] The partial specific volume of the protein is $\bar{v}_3$ and that of the component selectively adsorbed is $\bar{v}_1$. Because of the precision with which ρ_0 can be measured, this method affords considerable precision in the determination of Γ_a'.

In addition to examining the problems involved in quantitative density gradient experiments with schlieren optics, a further purpose of this work was to determine whether the concentration distribution is gaussian for a homogeneous material of known molecular weight. The system selected for this study was bovine serum mercaptalbumin in aqueous CsCl. BMA prepared by the method of Dintzis[16] has a well characterized molecular weight, is soluble, and is stable in concentrated salt solutions. Of the salts for which composition density gradients have been calculated,[12] CsCl forms the largest density gradient.

Experimental

Materials.—The albumin used in the density gradient experiments was bovine serum mercaptalbumin. The purified protein was kindly supplied by Dr. D. Ridgeway of this Laboratory. The material was prepared from lyophilized Fraction V powder (Armour Lot No. T-94, 101). It was recrystallized three times as the mercury dimer and purified and converted to the monomer on a mixed-bed ion-exchange column according to the method of Dintzis.[16] The colorless, 5% isoionic (pH 4.92) solution was stored at −20° and slowly thawed at 4° as needed. The albumin used in the apparent specific volume measurements was crystallized bovine plasma albumin, Armour Lot No. T-68, 204.

The CsCl and fluorochemical used in the density gradient experiments have been described.[14] The CsCl employed in the apparent specific volume measurements was used as supplied by the Maywood Chemical Co. and was known to be free of rubidium. The acetate buffer solutions were prepared from reagent grade materials.

Examination of Materials.—The BMA described above was examined by two other centrifugal methods to determine its homogeneity and z-average molecular weight. The solutions examined were prepared by mixing the appropriate volumes of the 5% BMA stock solution with 0.2 M NaAc buffer, pH 5.32, and water to yield a 0.1 M acetate buffer solution of the appropriate concentration.

Several sedimentation velocity experiments were conducted at various times during this work. In more sensitive tests for homogeneity, several two-component sedimentation equilibrium runs were performed at several protein concentrations. The short-column technique suggested by Van Holde and Baldwin[17] was employed. Each run with 3 mm. liquid columns was continued for about 5 days at 9,945 r.p.m.

Procedures for Density Gradient Experiments.—The following methods were investigated to determine which was the most satisfactory for providing identical solution column lengths.

A. Selection of Centerpiece and Filling Technique.

Method 1. 4° Centerpiece.—A cell was assembled with a 4°, single-sector, aluminum centerpiece using a molybdenum disulfide grease. The cell was filled with *ca.* 0.7 ml. of CsCl solution of the appropriate density and accurately weighed. After centrifuging to equilibrium, schlieren photographs were taken and the cell was reweighed. Losses of 3–4 mg. generally were observed.

After withdrawal of the cell contents, the cell was refilled (without disassembling) to the same weight with CsCl solution containing BMA. The cell was again centrifuged and equilibrium photographs obtained. Exact superposition of these photographs was then required. The menisci were used for horizontal alignment. A copper wire, 0.003 in. in diameter, was inserted horizontally in front of the schlieren camera to provide a reference line on the plate for accurate vertical alignment. This procedure was found to be the least satisfactory of the three techniques investigated. It is difficult to insert the identical weight of BMA solution. Frequently, in the course of adjusting the weight, some solution was lost between the sheel and the centerpiece and reproducible column lengths were not obtained. Also, inherent in this procedure are the several problems associated with performing duplicate centrifuge runs. The cell windows may distort differently, operating conditions must be held constant, and the time for performing an experiment is more than doubled.

Method 2. Double-Sector Centerpiece.—Another method examined was the use of a double-sector, 2½°, filled-Epon centerpiece. This requires the insertion of identical volumes of baseline and protein solution into each sector. The two sectors must have identical dimensions and must deform identically.

A syringe holder with a micrometer head and Agla brand, all-glass 1-ml. syringes, supplied by Burroughs Wellcome and Co., London, were used. In several of the first experiments, 0.025 ml. of fluorochemical was inserted into each sector in order to locate the cell bottom[18] accurately. In later experiments, fluorocarbon was not added because of occasional filling difficulties and because the position of the cell bottom need be determined with only moderate accuracy. About 0.4 ml. of CsCl solution, which corresponded to an 800 division advance of the micrometer, was inserted into each side of the centerpiece. Number 27 gage needles were used. The ends of the needles had been ground flat, and were bent at right angles near the center of the shaft. They were wiped with a solution of stearic acid in benzene to avoid wetting problems.

This procedure was successful in achieving identical column lengths in only about half of the dozen or so experiments in which it was used. The failures were due to uneven cell distortion, wetting at the filling hole, or problems associated with filling. Numerous attempts were made to perfect the above two methods. Consistent and reproducible results could not be obtained with either technique.

Method 3. Interference Synthetic-Boundary Centerpiece.—The most successful technique involved the use of a double-sector, 2½°, filled-Epon centerpiece with two small grooves, about 0.001 × 0.001 in., connecting the two sectors. One groove is located at the top of the centerpiece to permit equilibration of air pressure. The other groove is near the center of the cell. About 0.40 ml. of baseline solution was placed in one sector and 0.38 ml. of protein solution in the other. At *ca.* 7000 r.p.m., the baseline solution transfers into the BMA solution through the central groove until the column lengths are exactly equalized.

This procedure provides a rapid method of filling the cell and ensures identical column lengths. The disadvantages are minor. One problem is the transfer of protein into the baseline solution. This contamination probably occurs by mass transfer which results from uneven distortion of the sectors at high speed. Diffusion through the groove is considered to be negligible because of the small cross-sectional area of the groove.

The presence of a band of protein at low concentration in the baseline solution introduces some difficulty in drawing the baseline but does not affect the results. Subtraction of such a baseline from the protein distribution curve is equivalent to the subtraction of the gradient of one gaussian distribution from another of the same σ and mode and leads to no change in the distribution.

(15) J. W. Williams, K. E. Van Holde, R. L. Baldwin, and H. Fujita, *Chem. Rev.*, **58**, 715 (1958).

(16) H. M. Dintzis, Ph.D. Thesis, Harvard University, 1952.

(17) K. E. Van Holde and R. L. Baldwin, *J. Phys. Chem.*, **62**, 734 (1958).

(18) R. Trautman, *Biochim. Biophys. Acta*, **28**, 417 (1958).

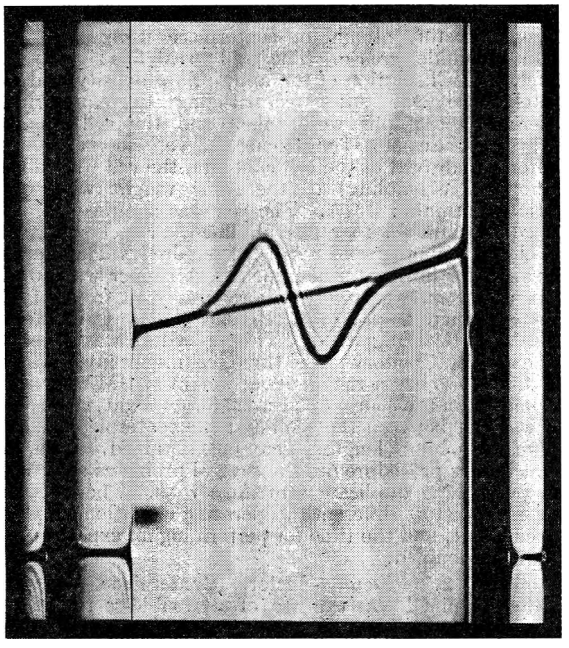

Fig. 1.—Schlieren photograph of 0.1% BMA in 2.59 molal CsCl and of baseline solution at equilibrium; 56,100 r.p.m., 25.0°, pH 5.5.

Another problem occasionally encountered was that the solution in one sector would transfer into the other sector upon deceleration. This is caused by the failure of one of the housing plug gaskets. It does not cause any serious problem except that the solution refractive indices at the conclusion of the run cannot be measured. This was a routine part of each experiment to ensure that no evaporation had occurred. Unless otherwise indicated, all of the experiments described below were performed with a capillary, double-sector centerpiece.

B. General Run Conditions.—All experiments were performed in a standard Spinco Model E analytical ultracentrifuge equipped with an RTIC unit. Measurements were made at an angular velocity of 56,100 r.p.m. and a temperature of 25.0°. The results were recorded on Eastman Kodak metallographic plates with a phase plate in the schlieren optical system. The centerpieces employed were 12 mm. thick. The angular velocity was determined from the time interval between odometer readings made near the beginning and near the end of each run.

The time necessary to attain equilibrium was determined from photographs taken at successive time intervals. The center of the band and the position and height of the maximum and minimum were measured. When no further change was noted after a suitable length of time, the distribution of protein was considered to be at equilibrium. Most experiments were run for 24–30 hr. The minimum time was 22 hr.

C. Preparation of Solutions.—Solutions were prepared by mixing appropriate volumes of concentrated CsCl solutions of density *ca.* 1.8 g./ml., OD^{260} = 0.025, and pH 7.1; 0.1 *M* NaAc buffer, pH 5.5; 5% BMA solution and/or H_2O. Serological and micropipets were used. In order to conserve material and to predetermine accurately the solution densities, dialysis was avoided.

The volumes of water and stock CsCl solution were calculated with a non-additive volume relationship and the relation between density and weight fraction of CsCl.[19] The solution densities then were adjusted, if necessary, by means of a Zeiss refractometer with the relation between refractive index (n) and density[12] such that $n_{\text{BMA Soln}} = n_{\text{baseline}} + 0.0019 \times c$, where c is the protein concentration in g./dl. Adjustments were made until the two refractive indices differed by the maximum permissible amount, ±0.0001, which corresponds to the refractometer reading error. This error limit corresponds to an uncertainty in the density of ±0.001 g./ml. All solutions contained 0.01 *M* acetate buffer and were *ca.* 0.10% BMA unless otherwise noted. The pH of the solutions varied between 5.5 and 5.6.

D. Measurement of Plates.—A typical schlieren photograph of a run of BMA in a CsCl density gradient is shown in Fig. 1. The two narrow, black, vertical lines are the CsCl and fluorocarbon menisci, reading from left to right. The slightly curving, almost horizontal line is the baseline, the refractive index-gradient distribution arising from the effects of composition and pressure on the CsCl solution. The biphasic curve is the refractive index gradient curve of the protein in CsCl.

As pointed out below, an accurate evaluation of σ requires an integration between these two curves. A numerical integration procedure was found to be the simplest and to yield the desired accuracy. Two methods of performing this analysis were investigated.

A Gaertner Comparator, Model M 2001-P, was used for several analyses. The ordinate values of the two curves were read at 0.5-mm. intervals and their difference carried as subtotals on a printing calculator. This method was not found to be satisfactory, largely because of the difficulty in interpolating through the regions in which the interference fringes overlap. The data obtained in the clearly visible regions could be plotted, interpolations made, and the curve remeasured. Because this involves an additional step, the following procedure was employed throughout this work.

An Omega-D II enlarger was used to provide tenfold enlargements of the photographic plate. The enlargements were made on large sheets of vellum by careful placement of a series of dots which locate the center of the bright central fringe. The shading of the first order dark fringes is helpful in placing the dots. This procedure can be performed accurately and rapidly. Smooth curves were drawn through the dots. The positions of the top and bottom reference edges, the menisci, and the cell bottom were similarly located. The area under the biphasic curve was numerically integrated toward the center, using lines drawn parallel to the menisci at 5-mm. intervals and measured with a precision ruler. The mid-point heights of the 5-mm. wide trapezoids were recorded with a printing calculator, as above.

A necessary criterion for a successful experiment is that the areas under the two lobes of the curve be equal. If they are not, either the baseline has been drawn incorrectly, the column lengths are not equal, or the solution densities are not equal. This area requirement is not a sufficient condition for a satisfactory analysis. This was shown for one experiment for which a satisfactory baseline was not available. Several baselines were drawn at different elevations and numerical integrations were performed until the areas differed by less than 1%. The resulting log plots were not linear to 1σ, indicating that the curvature of the baseline selected was incorrect.

The distance between the reference edges of the counterbalance was measured with an optical comparator and found to be 1.595 cm. The top reference edge was assumed to be 5.730 cm. from the axis of rotation at 56,100 r.p.m.

Determination of Apparent Specific Volume of BSA in Water and in Concentrated CsCl Solution.—The apparent specific volumes (φ) of serum albumin in water and in a 2.47 molal CsCl solution, a composition corresponding to the buoyant density, were measured by pycnometric procedures (*cf.*, for instance, "Methods in Enzymology").[20]

The protein solution was prepared by dissolving 4.0 g. of albumin in 80 ml. of twice-distilled water at 5°. Twenty g. of Amberlite MB-3, anion–cation resin, was added and the mixture kept at 5° overnight. The resulting light yellow isoionic solution of pH 5.11 was decanted and used without further purification.

The concentration of this solution was determined by evaporation to dryness. Four weighed aliquots, ranging from 1.0 to 2.5 ml., were evaporated in 30-mm. flat weighing bottles. They were dried at 110° and cooled in a desiccator over P_2O_5. Weighings were made daily until a constant value was obtained after 6 days drying time. A precision of 0.0004 g. protein/g. water was achieved.

(19) J. E. Hearst and J. Vinograd, *Proc. Natl. Acad. Sci., U. S.* **47**, 1005 (1961).

(20) H. K. Schachman, in "Methods in Enzymology," Vol. IV, Edited by S. P. Colowick and N. O. Kaplan, Academic Press, New York, N. Y., 1957, pp. 65–71.

Thirty-five-ml. pycnometers of the flask type with a 1-mm. capillary were used. The volumes were adjusted in a 25 ± 0.02° water bath. Weighings always were made against a tare which was handled in the same manner as the filled pycnometer. All weights were corrected to vacuum.

A. Apparent Specific Volume of BSA in Water.—The weight of the pycnometer filled first with water and then with protein solution was determined. At least two fillings and weighings were carried out for each density determination. A precision of ±0.0003 g. was generally achieved. The apparent specific volume then was calculated from the relation

$$\varphi = \frac{d_0 - d_1}{c' d_0 d_1} + \frac{1}{d_1} \qquad (3)$$

where d_0 is the density of the solvent, d_1 is the density of the solution, and c' is the concentration of the solution in g. protein/g. solvent.

B. Apparent Specific Volume of BSA in 2.47 Molal CsCl Solution.—The determination in CsCl solution is complicated by the two-component solvent. Satisfactory measurements were obtained by mixing exactly equal volumes (22 ml.) of water and a concentrated CsCl solution. The density of the CsCl solution was adjusted refractometrically so that addition of an equal volume of water would yield a composition corresponding to the buoyant density. The masses corresponding to these volumes were accurately weighed in stoppered, 50-ml. flasks, and the solutions were carefully mixed.

The protein solution was similarly prepared. A weighed quantity of BSA solution containing the calculated mass of the water required was again added to a weighed mass of CsCl solution. The masses were adjusted to within about 0.4 mg. in the 35–40 g. weighings. Density measurements of these solutions yielded a value of φ for BSA in a CsCl solution. The measurements in CsCl were conducted in duplicate with different protein solutions in which concentrations were independently determined.

Calculations

The experimental parameters in eq. 1 which must be determined are r_0, ρ_0, $(d\rho/dr)_0$, and σ^2. The center of the gaussian band can be located on the plate to ±0.002 cm. at the intersection of the baseline and the biphasic protein curve. The value of r_0 in cm. is determined by dividing the distance between band center and the top reference edge on the tracing by the magnification factor and adding the result to 5.730. The magnification factor is found by dividing the distance between the reference edges in cm. by 1.595. All other radial distances were obtained similarly.

Hearst, Ifft, and Vinograd[14] have shown that the salt distribution is unaffected by pressure. Thus, the data of Ifft, Voet, and Vinograd[12] can be used to locate r_e, the isoconcentration distance corresponding to ρ_e^0, the initial solution density. The value of r_e was found with an error of about 0.003 cm. The bands were always formed near enough to r_e so that a constant density gradient could be assumed between r_e and r_0. The buoyant density was computed from the approximate relation

$$\rho_0^0 = \rho_e^0 + \frac{\omega^2 r_0}{\beta^0}(r_0 - r_e) \qquad (4)$$

The superscript zero is used throughout to denote quantities evaluated at atmospheric pressure. The values of β^0 which correspond to ρ_e^0 have been tabulated.[12]

The buoyant densities calculated above are a function only of salt composition. The buoyant density corresponding to the physical situation was next calculated as

$$\rho_0 = \rho_0^0(1 + \varkappa P_0) \qquad (5)$$

where $\varkappa$ is the isothermal compressibility of the CsCl solution of this composition and P_0 is the hydrostatic pressure at band center. The value of $\varkappa$ was found from Pohl's data[21] to be 35.2×10^{-6} atm.$^{-1}$. The procedure for the calculation of P_0 has been outlined.[14] The pressured buoyant densities are 0.007 density unit, 0.6% higher than the values determined by means of eq. 4. The physical density gradient at band center was computed from eq. 12 of ref. 14. The compression term is 9.5% of the composition term for this system.

The above treatment neglects any interactions due to the presence of the macromolecule, *e.g.*, the compressibility of the polymer, selective solvation of the polymer, etc. The effects of some of these interactions are considered in a later paper. They can contribute as much as 10–15% to the effective density gradient.

The standard deviation of the gaussian concentration distribution, σ, is the most difficult quantity to obtain with satisfactory precision. A variety of methods are available for the evaluation of σ in the gaussian concentration relation

$$c = c_0 \exp\left[-(r - r_0)^2/2\sigma^2\right] \qquad (6)$$

All of these procedures are based on the supposition that $n - n_0 = Kc$, where n and n_0 are the refractive indices of the protein solution and baseline solution, respectively. The concentration of protein is given by c. The refractive index-increment K, dn/dc, was assumed to be constant over the salt concentration range of interest. The validity of this assumption was investigated. The results, given in Appendix A, indicate that this assumption is valid.

The following procedures were examined:

1. Biphasic Plot.—The simplest procedure for the evaluation of σ, and the only one not requiring a numerical integration, is to replot the two lobes of the protein gradient curve after subtraction of the baseline. The distance from the center of the distribution to each maximum is σ. While this method is rapid, it yields only an approximate value of σ because the maxima are broad. A precision of ±0.005 cm. can be obtained. This corresponds to the precision found by Cox and Schumaker,[9] who used absorption optics.

2. Concentration Plot.—Another procedure, which suffers the disadvantage of being an evaluation made at just one point in the distribution, is to integrate the curve described above to obtain the concentration distribution shown in Fig. 2 and to measure the half-width at an elevation of 0.607 $K'(n - n_0)_{r_0}$. K' is a machine constant.

3. $(dn/dr)/n$ *vs.* $(r - r_0)$ Plot.—A plot of $1/n \cdot dn/dr$ *vs.* $(r - r_0)$ should be linear with slope equal to $-1/\sigma^2$. This procedure is very sensitive to errors at the edges of the protein band. The plots were linear only near the center of the distribution.

(21) F. Pohl, Dissertation, Rheinishe Friedrich-Wilhelms, Universität, Bonn, Germany, 1906.

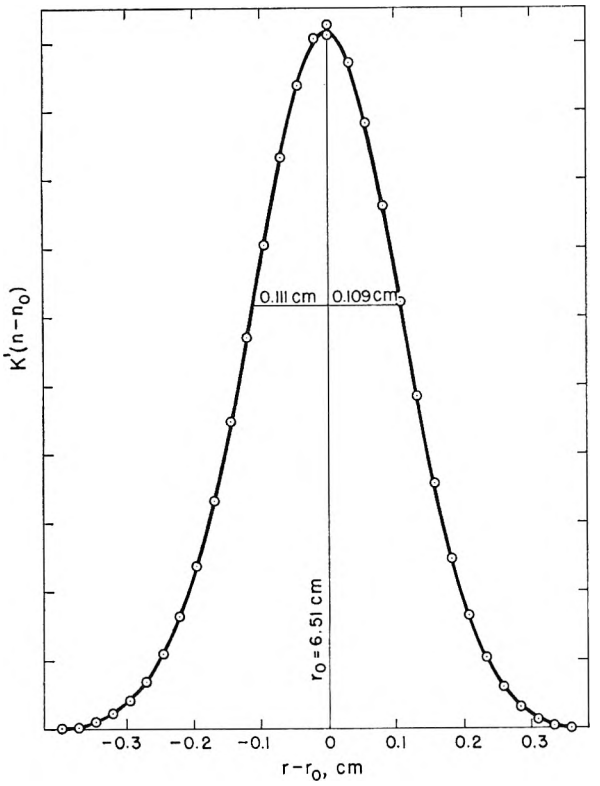

Fig. 2.—Distribution of mercaptalbumin concentration in a CsCl density gradient at sedimentation equilibrium.

4. Logarithmic Plot.—The best procedure and the one used in all of the experiments reported below involved the logarithmic plot. A plot of ln $K'(n - n_0)$ *vs.* $(r - r_0)^2$ is linear for a gaussian concentration distribution with slope inversely proportional to σ^2. The running subtotals of the numerical integrations were plotted as the ordinate values, and the values of $(r - r_0)^2$ in cm. on the tracing as abscissa values on semilog graph paper. The slope of this straight line multiplied by the square of the magnification factor is equal to $-1/2\ \sigma^2$.

The net hydration was calculated from eq. 2. All parameters in the equation must be determined at the same pressure. The partial specific volume of BMA, $\bar{v}_3$, was measured at atmospheric pressure. The partial specific volume of water in the bulk phase can be evaluated by an extrapolation of the $1/\rho$ *vs.* Z_{CsCl} plot[12] at the buoyant composition to pure water. It closely approximates 1.00 ml./g. The buoyant density employed in the equation should be the buoyant density at atmospheric pressure.[14] Pressure dependence information is not available for BMA. Consideration of the data for TMV[14] suggests that the more nearly correct density to use is the compressed density, ρ_0. This will lead to Γ_a' values which are 4–5% lower than the actual values.

Two assumptions made in the original derivation of eq. 1[2] were examined for this system in which wide band widths are encountered. The density gradient was assumed to be constant over the region of a band. The density gradient, however, departs significantly from constancy even over a distance of 2σ in the band, as is shown in Fig. 1 and Fig. 3. The effect of this perturbation was investigated by assuming a linear variation in the density gradient.

If we let $\epsilon = r - r_0$, we may write a three-term Taylor series for $\rho(r)$.

$$\rho(r) = \rho(r_0) + \left(\frac{d\rho}{dr}\right)_{r_0} \epsilon + \left(\frac{d^2\rho}{dr^2}\right) \epsilon^2/2 \quad (7)$$

Substitution of this expression for the density into the ideal equation for two-component sedimentation equilibrium followed by integration between $\epsilon = 0$ and ϵ gives the logarithmic expression

$$\ln \frac{c}{c_0} = - \frac{M \omega^2 \left(\frac{d\rho}{dr}\right)_{r_0}}{2RT\rho(r_0)} \epsilon^2 \left\{1 + \epsilon \left[\frac{(d^2\rho/dr^2)}{3(d\rho/dr)_{r_0}} + \frac{2}{3r_0}\right]\right\} \quad (8)$$

This derivation neglects a term in ϵ^4 which is less than 1% of the correction term. The result of the inclusion of the correction term is a symmetrical upward and downward deviation from linearity in the plot of ln $K'(n - n_0)$ *vs.* ϵ^2. The data from the top half of the distribution should curve upward and that from the bottom half should curve downward from the straight line representing ideal behavior.

The magnitude of the deviation can be readily evaluated for these experiments. The slope of the almost linear $d\rho/dr$ *vs.* r plot in Fig. 3 is 0.060 g./cm.$^{-5}$. Inserting typical values of r_0 and $(d\rho/dr)_{r_0}$ into eq. 8 gives

$$\ln c/c_0 = - \frac{1}{2\sigma^2} \epsilon^2 (1 + 0.25\ \epsilon) \quad (9)$$

At 1σ, the real values of ln c differ by 2.5% from the straight line representing a constant density gradient. Obviously, the error increases as the distance from the center of the band increases.

A second assumption in the original derivation which requires re-evaluation for this system because of the width of the distribution is the neglect of terms of order $(r - r_0)^3$. The expression given in Appendix B reveals that negligible error is introduced by this approximation.

The effect of an error in the numerical integration also was examined. Let us assume that an error δ, either positive or negative, is made at the outer edge of the band. Comparing the log plot of this distribution with that of the correct one, we can express the measured distribution for distances less than 2σ from band center as

$$\ln \frac{c + \delta}{c_0 + \delta} = \ln \frac{c}{c_0}\left(1 - \frac{\delta}{c_0}\right)\left(1 + \frac{\delta}{c}\right) \quad (10)$$

or

$$\ln \frac{c}{c_0} = \ln \frac{c + \delta}{c_0 + \delta} - \frac{\delta}{c_0}\left(\frac{c_0}{c} - 1\right) \quad (11)$$

Depending on the sign of δ, all of the points on the log plot for that lobe of the distribution must be either elevated or depressed.

Results

A. Examination of Materials.—Identical results were obtained from sedimentation velocity experiments performed with 0.9% solutions of the sample of BMA at several stages during this work. The sedimenting peak was symmetrical except for a small amount of a fast component which was estimated to be less than 2% of the sample. A value of $S_{20,w}$ of 4.35 S was obtained from the motion of the maximum of the refractive index-gradient distribution. This value compares favorably with that of 4.27 S obtained from the data of Baldwin[22] for BSA after correcting for concentration and temperature effects.

The results of the two-component sedimentation equilibrium experiments are given in Table I. The time of analysis is given in column 2. Equilibrium was achieved in 24 hr. in each solution although a slow dimerization in the more concentrated solution may be indicated by the high value obtained after 5 days.

Plots of $(dn_c/dr)/r$ *vs.* n_c (where n_c is the refractive index contribution of the protein) were linear over the central 80% of the column length, indicating substantial molecular weight homogeneity. Typically, there is a downward deviation from linearity at the bottom of the cell and a converse deviation at the top. This is the opposite behavior expected if the deviation from linearity is due to the presence of aggregated material. It may be due to window distortion or to a refractive artifact occurring near the menisci as discussed by Trautman.[18]

The slope of the linear portion of this plot was used to calculate the molecular weights given in Table I. The value for $\bar{v}_3$ of 0.734 ml./g. reported by Dayhoff, *et al.*,[23] and confirmed in this study was used in the calculations. Excluding the 72,200 value, the remaining values yield an average of 70,500, in good agreement with other techniques yielding weight average molecular weights.

TABLE I

TWO-COMPONENT SEDIMENTATION EQUILIBRIUM ANALYSES BOVINE SERUM MERCAPTALBUMIN IN 0.1 M NaAc BUFFER, pH 5.5, 9,945 r.p.m., T = 25°

g. BMA/100 ml.	Hours run	Molecular weights
0.84	24	70,300
	86	72,200
0.42	24	70,700
	120	70,400

B. Apparent Specific Volume of BSA.—The values of φ in H_2O and in concentrated CsCl are given in Table II.

TABLE II

APPARENT SPECIFIC VOLUME OF BSA IN WATER AND IN A 2.47 MOLAL CsCl SOLUTION, T = 25.0°

Solvent	c'	d_0	d_1	φ
A. H_2O	0.0467	0.99704	1.00908	0.7347
B. CsCl	.01824	1.28151	1.28277	.7361
	.01877	1.28187	1.28318	.7369
Av. for B				.736

The value of φ for BSA in water agrees favorably with the value 0.7343 reported by Dayhoff, *et al.*[23] Cox and Schumaker[24] recently have reported values of φ in 1.4 molal KCl. Interpolating their data between measurements at 29.9° and 10° gives a value of 0.739 at 25°. Considering the precision of their data and the fact that their measurements were made with a different cation, this number may be regarded as not differing significantly from the value reported here.

C. Density Gradient Experiments.—Repeated numerical integrations have demonstrated that the density gradient given by the baseline and protein solution must not differ by more than 0.2–0.3%. Larger discrepancies lead to poor numerical integrations, which in turn yield non-linear logarithmic plots. In order to achieve this accuracy, the following experimental limits must be met. The densities must be matched to within 0.002 g./ml. This accuracy is required because β, the density gradient parameter, changes rapidly in this density region. Also, the column lengths must be matched to within 0.2 mm.

The following behavior of band formation was observed. An irregularly shaped band is formed after 6–7 hr. A symmetrical band is formed at essentially the correct banding position in about 8–9 hr., depending on how close ρ_e^0, the initial solution density, is to ρ_0^0. The band continues to narrow with a corresponding increase in height at the inflection points until no further change is observed after 15 hr. This was determined by extending several runs for 45 hr. Measurements of photographs obtained at 6–8 hr. intervals indicated no detectable change in band shape or position. This demonstrates not only that equilibrium was established but also that BMA is stable with respect to molecular weight and buoyant density for extended periods of time at room temperature in concentrated CsCl solutions.

The precision of the numerical integrations was determined by duplicate tracings in several experiments. In all cases the area under one lobe was determined with a precision of better than 1.0%. It is significant that in about 4 out of 5 experiments, the area under the top lobe is 1–3% smaller than the area under the bottom lobe.

The concentration distribution evaluated from experiment No. 2 is shown in Fig. 2. The distribution is seen to be slightly skewed toward the top side. Otherwise the data points fall on a reasonably smooth and symmetrical curve out as far as elevations could be measured. The ordinate is in arbitrary units of $K'(n - n_0)$.

The density, density gradient, and refractive index gradient distributions of experiment No. 2 are given in Fig. 3. The density distribution was obtained by a computer method.[12] The composition density gradient then was calculated from this data for $\rho(r)$ using published $\beta(\rho)$ data.[12] The bottom plot is a tracing of the equilibrium photograph similar to that shown in Fig. 1. The ordinate is in arbitrary units and is not superimposable on the middle plot for $d\rho/dr$.

A typical logarithmic plot is presented in Fig. 4.

(22) R. L. Baldwin, *Biochem. J.*, **65**, 503 (1957).

(23) M. O. Dayhoff, G. E. Perlmann, and D. A. MacInnes, *J. Am. Chem. Soc.*, **74**, 2515 (1952).

(24) D. J. Cox and V. N. Schumaker, *ibid.*, **83**, 2433 (1961).

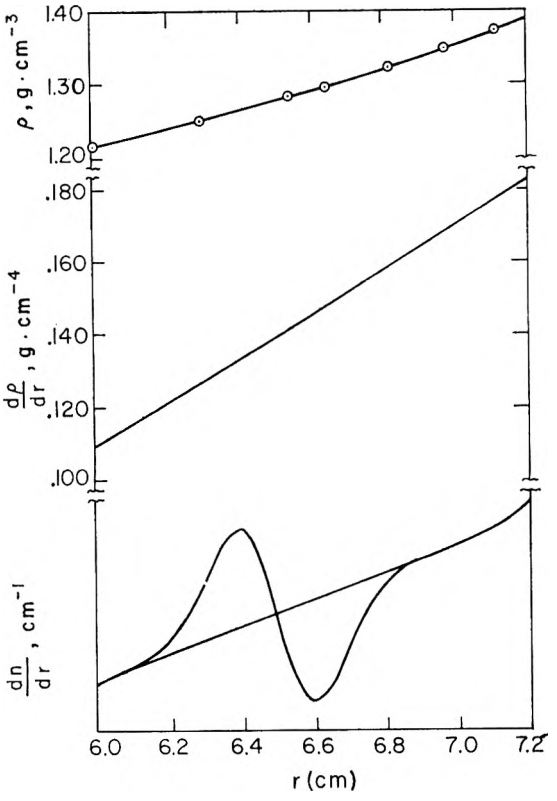

Fig. 3.—Density, density gradient, and refractive index gradient, 0.1% mercaptalbumin in 31.08% CsCl.

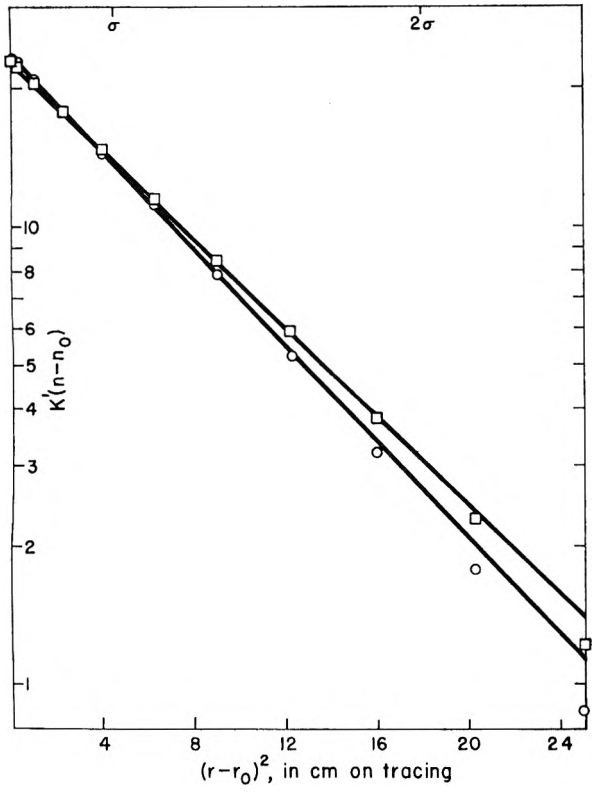

Fig. 4.—Logarithmic plot of experiment No. 6, 0.10% BMA in 2.47 molal CsCl: ○, bottom half of distribution; □, top half.

This is the data obtained from the tracing of a 75° photograph. The behavior noted here is typical of almost all of the experiments performed. The data from the top half are usually linear out to about 2σ and then curve downward. The data from the bottom half, however, are seldom linear beyond 1.5σ and then curve downward. The distances from r_0 in terms of σ are noted along the upper abscissa line.

A set of typical values for σ determined by the various methods described above is given in Table III to demonstrate the precision of the method. The average deviations from the 55 and 85° photographs are 0.002 and 0.001 cm., respectively. It is to be noted that the values of σ determined from the top side of the band generally are higher than those obtained from the bottom side.

TABLE III

STANDARD DEVIATIONS EVALUATED BY VARIOUS METHODS (EXPT. NO. 2; 0.11% BMA in 2.47 MOLAL CsCl SOLUTIONS)

Method	Type	55°[b] (cm.)	85°[b] (cm.)
1. Biphasic plot	Top[a]	0.099	0.107
	Bottom[a]	.106	.104
	Average	.103	.106
2. Concentration plot	Top	.111	.110
	Bottom	.109	.106
	Average	.110	.108
3. $(dn/dr)/n$ *vs.* $(r - r_0)$ plot		.108	.108
4. Logarithmic plot	Top	.113	.109
	Bottom	.109	.107
	Average	.111	.108
Av.		.110	.108

[a] Top is used in this and in all subsequent graphs and tables to indicate that the result was derived from the region of the band closest to the center of rotation. Bottom stands for the other half of the band. [b] Phaseplate angle.

The results of a number of density gradient experiments with BMA in CsCl solutions, conducted and analyzed as described above, are presented in Table IV. Apart from the one high value for ρ_0, it appears that the buoyant density at the pressures in the rotating liquid column can be determined with a precision of ±0.001 g./ml. The buoyant density of BMA in a CsCl gradient is 1.282 g./ml.

TABLE IV

RESULTS OF DENSITY GRADIENT EXPERIMENTS WITH 0.1% BMA IN CsCl SOLUTIONS[a]

	ρ_0	$\left(\frac{d\rho}{dr}\right)_{phys,0}$	σ_{top}	σ_{bot}	M_{app} Top	M_{app} Bottom	Γ'_a
1[b]	1.282	0.153	0.109	0.105	75,500	81,700	0.200
2	1.282	.151	.109	.107	78,800	82,400	.200
3[c]	1.287	.153	.106	.106	81,000	80,700	.184
4	1.282	.153	.105	.104	82,800	83,600	.200
5	1.281	.154	.108	.105	77,400	81,300	.204
6	1.282	.154	.108	.105	76,300	81,100	.200
Av.	1.282				78,600	81,600	0.198

[a] Columns 2, 4, and 5 are physically measured quantities. All other quantities are based on assumptions stated in the text. [b] Non-grooved double-sector centerpiece, 0.15% BMA. [c] As *b*, 0.20% BMA.

Averages should not be taken for the density gradients or the standard deviations because these values relate to experiments performed at slightly different solution densities.

The variation in σ is reflected directly in the two apparent molecular weights. The standard deviations of the M_{Top} and M_{Bot} values are ±2800 and

±1100 respectively, or about 2–3%. The M_{Top} values are about 4% smaller than the M_{Bot} values as a result of the higher values of σ noted previously.

Discussion

Several deviations from ideal gaussian behavior have been noted in the above results. These deviations can be accounted for satisfactorily in terms of the two derivations given in the calculations section above.

The antilog of eq. 9 correctly predicts the observed shape of the concentration distribution given in Fig. 2. The effect of the non-constant gradient is to broaden the band increasingly from the bottom to the top of the distribution.

The data in Fig. 4 from the bottom half of the distribution deviate in the direction and amount predicted by eq. 9. The data from the top half, however, do not curve upward as predicted by eq. 9 but also curve downward. This behavior is attributed to the effect predicted by eq. 11. As noted earlier, the area under the top lobe is generally smaller than the area under the bottom lobe. This may be due to a consistent neglect of a small area of the top lobe near the outer edge of the band. The top lobe is broader than the bottom lobe and greater difficulty is encountered in interpolation. The magnitude of this effect is surprisingly large. Let us assume that $\delta = -0.01$; the measured total area of the top lobe corresponding to c_0 is 1% low. At 2σ, this error amounts to 3% in $\ln c/c_0$. The effect of the non-constant density gradient can be overcome by a very small error in the numerical integration. It is difficult to analyze the situation quantitatively because neither area is known absolutely.

The combination of these two effects predicts that both the concentration plot and the logarithmic plot should yield higher values of σ for the top half of the distribution than for the bottom half. This trend is observed in Tables III and IV.

The procedure followed in this work was to draw straight lines through the linear portion of the logarithmic plot starting at $\epsilon = 0$. We estimate that this method yields values of σ accurate to within 0 to −2%.

Cox and Schumaker[9,24] have reported two studies dealing with the net hydration of BSA. These results may be compared with the values of ρ_0 and Γ_a' in Table IV. They measured the sedimentation velocity of BSA as a function of salt concentration. An extrapolation of a plot of the product of the sedimentation coefficient and the solution viscosity against ρ to zero sedimentation rate presumably yielded values of the buoyant density. From these densities, values of 0.19 and 0.26 g. water/g. BSA for NaCl and KCl solutions, respectively, were obtained. These values compare favorably with the value of 0.20 reported above. There are several serious limitations to the sedimentation velocity method, however. The concentration of salt is varied between a few tenths molar to saturation. Because the chloride binding and the hydration both change significantly with concentration, the sedimenting species is changing as the density of the solution is increased. Furthermore, an extrapolation over a distance equal to the range of $S\eta$ values measured was necessary.

In addition, they studied the behavior of BSA in several density gradient systems. They obtained a buoyant density at atmospheric pressure at 25° in CsCl of 1.295 ± 0.005 g./ml. with absorption optics. The corresponding buoyant density reported in the present paper is 1.275 ± 0.001 g./ml. The discrepancy in these values may be due to the slight difference in the two proteins and to their relatively large experimental error.

The molecular weights given in Table IV are 10,000 units higher than the z-average values given earlier. Several factors point to ambiguities in assigning any real physical meaning to these apparent molecular weights. The net hydration of 0.20 g. H_2O/g. protein indicates that the solvated molecular weight ought to be 84,000. Alternatively a $\Gamma_b' = (M_{app} - M_a)/M_a$ can be calculated. The values of Γ_b' are 25% smaller than the values of Γ_a'. For solvated macromolecules, the effective density gradient,[13] which includes the effect of the change in hydration through the band, must be employed in the calculation of solvated molecular weights. This density gradient is smaller than the physical density gradient. The apparent molecular weight is therefore too small and Γ_b' is less than Γ_a'.

It must be noted that an effective density gradient defined with respect to the protein alone must be employed in the above calculation in order that $\Gamma_a' = \Gamma_b'$. As shown in a subsequent publication[25] such a gradient cannot be obtained for BMA. Only the change in hydration of the BMA-salt complex can be defined. This leads to solvated molecular weights which include the amount of bound salt plus the net hydration of the complex.

Acknowledgment.—The authors wish to thank Dr. John E. Hearst for numerous helpful discussions.

Appendix A

Examination of the Assumption of a Constant Refractive Index Increment.—Let $n_c = n - n_0 = Kc$, and differentiate to obtain the contribution of the protein to the refractive index gradient

$$\frac{dn_c}{dr} = \frac{dc}{dr}(K) + c\frac{d(K)}{dr} \qquad (A1)$$

We assume that (K) varies linearly

$$(K) = (K)_0(1 - k\epsilon) \qquad (A2)$$

where ϵ is the distance from band center and $(K)_0$ is the refractive index increment at $\epsilon = 0$. Combining eq. A1 and A2 gives

$$\frac{dn_c}{dr} = (K)_0\left[\frac{dc}{dr} - k\left(c + \epsilon\frac{dc}{dr}\right)\right] \qquad (A3)$$

Equation A3 can be recast in more readily available terms by substituting the derivative of the gaussian concentration distribution and rearranging,

$$\frac{dn_c}{dr} = -\frac{c}{\sigma^2}(K)_0[\epsilon - k(\epsilon^2 - \sigma^2)] \qquad (A4)$$

Alternatively, we rearrange eq. A4 to examine the behavior of dn_c/dr at positions in the band other than at band center.

(25) J. B. Ifft and J. Vinograd, to be published.

$$\frac{dn_c}{dr} = \frac{-c\epsilon}{\sigma^2}(K)_0\left[1 - k\left(\frac{\epsilon^2 - \sigma^2}{\epsilon}\right)\right] = \left(\frac{dn}{dr}\right)_i\left[1 - k\left(\frac{\epsilon^2 - \sigma^2}{\epsilon}\right)\right] \quad (A5)$$

Equations A4 and A5 show the effect of a non-constant refractive index increment on band shape and position.

A rough estimate of the value of the constant k was obtained by extrapolating the refractive index increment of BSA of 0.001901[26] to 100% protein concentration. Estimation of $(\Delta n/\Delta c)$ at band center and at a distance of about 1σ (0.1 cm.) yielded the approximate value of $k = 0.05$.

At band center, eq. A4 reduces to $dn_c/dr = -kcK_0$. Substitution of typical parameters for a BMA experiment reveals that the downward shift in the refractive index gradient at $\epsilon = 0$ is 0.1% of the maximum gradient in the distribution.

We also may determine the radial shift in the point of intersection of the biphasic curve with the baseline between the actual and the ideal cases. This shift is calculated by setting eq. A4 equal to zero and solving the quadratic in ϵ. The shift of -0.0005 cm. is beyond the accuracy either obtainable or needed in these experiments.

Examination of eq. A5 reveals that there is no correction at $\epsilon = \sigma$. At 2σ, the correction term is *ca.* 0.015. The correction term becomes larger with increasing distance from the center of the band but because there is less than 0.2% of the material beyond 3σ, the contribution to the total area under the curve is negligible.

A plot of the points determined above combined with an examination of the sign of the correction in intermediate regions indicates that the entire distribution is shifted toward the center of rotation while the biphasic shape, to first order, remains unchanged. The magnitude of this effect is so small as not to affect the value of r_0 or σ. The refractive index increment therefore can be considered constant under these experimental conditions.

Appendix B

Examination of the Neglect of Terms of Order $(r - r_0)^3$ in Original Derivation.—The concentration distribution was obtained by assuming a Boltzmann distribution of particles. The energies were calculated as the negative of the distance integral of the force $F = v(\rho_p - \rho_s)\omega^2 r$. The quantity v is the volume of a particle of density ρ_p and ρ_s is the density of the solution at the radial position r. The solution density is assumed to vary linearly with distance. The resulting expression for the mass distribution is

$$c = c_0 \exp\left[-\frac{\epsilon^2}{2\sigma^2}(1 + 0.67\epsilon/r_0)\right] \quad (B1)$$

The cubic term predicts a slight displacement of the concentration distribution toward the center of rotation. At a distance of 1σ from the center of the band in a protein experiment, the measured concentration will differ by about 0.5% from the ideal distribution.

DISCUSSION

H. A. ENDE (Chemstrand Research Center).—You draw attention to some disadvantages involved in using the interference synthetic-boundary centerpiece. An additional problem is probably the fact that the original polymer solution is somewhat diluted by the "baseline solution." When the rotor is decelerated you state that solution in one sector would be transferred to the other sector. These effects introduce an uncertainty in the concentration. We have designed a centerpiece which proved to work satisfactorily and eliminates some of the problems. Each sector is connected to a reservoir by an air channel and a groove. As to aligning we can only say that we did not have any difficulties. It can be shown that a disalignment of 10 min. results in an error of only 0.06 of a fringe as seen by interference optics.

J. B. IFFT.—The dilution problem you mention is of no consequence in the work reported here because the protein concentration need not be known. The transfer of solution on deceleration occurs only occasionally. However, measurement of the solution refractive indices is precluded, as indicated in the paper. For the cell that you have described, the intersections of the groove with each sector must be exactly machined to the same radial position. The interference synthetic-boundary centerpiece utilizes the centrifugal field to provide exactly superimposed menisci without any stringent construction requirements.

R. TRAUTMAN (Plum Island Animal Disease Laboratory, USDA).—Have you detected any increase in the time to reach equilibrium with the other salts, especially KBr, which are bound differently from CsCl?

J. B. IFFT.—No appreciable increase in the time required to reach equilibrium was observed in any of the salt solutions discussed in part II of this work. Experiments generally were extended to at least 36 hr. No detectable change was observed after 24 hr.

H. A. ENDE (Chemstrand Research Center).—Have you measured any concentration dependence of M_{app}? For monodisperse polymers Dayantis and Benoit [*Compt. rend.*, **254**, 2771 (1962)] could show that $1/M_{app}$ is a linear function of the concentration and an extrapolation to zero concentration would yield the true value. I realize that you are working at high ionic strengths due to the presence of CsCl; usually M_{app} in those cases is independent of the polymer concentration. However, in work to be published, J. J. Hermans and I show that for synthetic polymers a clear concentration dependence exists, even if the experiments are performed close to θ-conditions. Is this also the case for proteins under comparable conditions (high ionic strength and nearly isoelectric conditions)?

J. B. IFFT.—As indicated in Table IV of our paper, experiments were conducted at three protein concentrations and no concentration dependence was observed. However, due to the relatively large experimental errors involved, this dependence must be severe in order to be observed.

M. WALES (Shell Development Company).—In regard to data of part II in the expression for ρ_s, are you defining the protein component differently in different salt solutions?

J. B. IFFT.—Yes. The macromolecular species is defined in each salt solution as the BMA molecule plus salt molecules equal in number to the number of anions bound in that particular salt solution.

L. GROPPER (Beckman Instruments, Inc.). I wish to comment on one possible cause of skewing of the gaussian distribution. There is a shift of the top of the peak due to the Weiner skewing. This is caused by the deviation of light through the CsCl gradient and the skewing can be minimized by focusing on the $^2/_3$ level of the cell. The correction is the same as derived from the first order term of a mathematical correction of the gaussian distribution offered by Dr. Vinograd.

J. B. IFFT.—I do not believe that the magnitude of this effect will produce a skewing nearly as large as the effect of the non-constant density gradient which also is present in our system.

(26) G. E. Perlmann and L. G. Longsworth, *J. Am. Chem. Soc.*, **70**, 2719 (1948).

ULTRACENTRIFUGAL AND VISCOMETRIC STUDIES OF THE REVERSIBLE THERMAL DENATURATION OF RIBONUCLEASE[1,2a]

BY D. N. HOLCOMB[2b] AND K. E. VAN HOLDE

Department of Chemistry and Chemical Engineering, University of Illinois, Urbana, Illinois

Received March 7, 1962

Sedimentation velocity and intrinsic viscosity measurements have been used to study the reversible thermal denaturation of ribonuclease-A at pH 2.8. In order to interpret the sedimentation data, the change in apparent specific volume has been measured over the transition temperature range. Sedimentation coefficients were corrected for the effects of the rapid diffusion of ribonuclease and were extrapolated to infinite dilution. The intrinsic viscosities were determined by means of a twin-viscometer technique which allowed direct comparison of solution and solvent flow times at each temperature. If it is assumed that the thermal denaturation can be described as an equilibrium between native ribonuclease and a single denatured form, the equilibrium constant (K) for the reaction can be calculated from either the sedimentation velocity or intrinsic viscosity data. Both methods yield graphs of log K *vs.* $1/T$ which show some curvature at high temperatures; furthermore, the data do not exactly superimpose. These results indicate that the denaturation process is more complex than assumed above. Both methods yield a value of about 65 kcal./mole for ΔH^0, which is somewhat greater than the result which has been reported from optical rotation and spectroscopic methods. The data are definitely not consistent with the hypothesis that the denaturation corresponds to a gradual unfolding with increasing temperature.

Introduction

This paper describes a study of the reversible thermal denaturation of ribonuclease. While this process has been rather extensively investigated by a number of authors, the methods of study reported here have not been used previously. In this work the sedimentation coefficient, the apparent specific volume, and the intrinsic viscosity have been measured as functions of temperature. While numerous methods have been used in studies of the thermal denaturation,[3-7] no previous measurements of the intrinsic (rather than reduced) viscosity or the sedimentation coefficient have been reported throughout the temperature interval of the transition.

It has been found that lowering the pH of the ribonuclease solutions lowers the transition temperature.[5-7] Therefore, in order to make the process more susceptible to study by velocity sedimentation, a relatively low pH (2.8) was chosen for this work.

Experimental

Materials.—The sample of ribonuclease used for most of these experiments was purchased from Pentex, Inc., and was their Lot No. 26Z7, 5× recrystallized. Ribonuclease-A was obtained from this lot by the countercurrent distribution (CCD) procedure of King and Craig.[8,9] The CCD pattern obtained after 200 transfers is shown in Fig. 1. Ribonuclease-A was obtained from the upper and lower phases of tubes 65 and 120, inclusive. The pooled samples were concentrated by removal of solvent in a rotary evaporator and allowed to precipitate overnight in a cold room at 2 to 3°. The precipitated protein then was dialyzed and lyophilized. From 3 g. of Lot No. 26Z7 approximately 1 g. of ribonuclease-A was isolated. Approximately 1 g. of additional material, presumably ribonuclease-B, was obtained from tubes 130 to 199, inclusive. After CCD purification, the ribonuclease-A gave a colorless, but slightly hazy solution. Centrifugation in a bench-top centrifuge yielded clear solutions of ribonuclease-A with a very small amount of solid material collected on the top of the solutions. Before viscosity experiments were performed the solutions were centrifuged and this material was removed. Unless otherwise indicated, all other chemicals used in these experiments were commercial preparations of analytical reagent grade and were used without further purification.

With exceptions as noted, the buffer solutions used in this work were 0.01 M in potassium acid phthalate and 0.15 M in KCl. The pH of the ribonuclease solutions was adjusted to 2.800 with HCl.

Because of the small amount of material available the concentrations of ribonuclease-A solutions were determined from the areas under refractive index gradient curves obtained in synthetic boundary sedimentation experiments. These experiments were carried out at 20° with a rotor speed of about 12,590 r.p.m. The optical system of the ultracentrifuge was calibrated by a synthetic boundary experiment with sucrose for which the specific refractive increment is accurately known.[10] For ribonuclease the specific refractive increment was taken[11] to be 1.9×10^{-3}. The concentrations calculated in this manner should be accurate to ±5%.

Once prepared, all solutions were stored in a cold room at 2 to 3° until used. Measurements generally were made within one week after preparation of the protein solutions and most were made no more than 3 days after preparation. Sedimentation velocity experiments which were made at nearly the same temperatures and with the same solutions, but separated by a period of several days, showed that no change of the sedimentation coefficient, $s_{20,w}$ resulted on storage of the solutions.

Sedimentation Measurements.—The sedimentation measurements were made with a Spinco Model E ultracentrifuge equipped with an RTIC (Rotor Temperature Indicator and Control) unit. The RTIC was calibrated by the test stand method previously described by Baldwin.[12] A check of the calibration at room temperature with the rotor at rest inside the vacuum chamber gave the same RTIC reading as was obtained with the rotor on the test stand outside. The calibration was checked by the test stand method at frequent intervals during the series of experiments. A test of the RTIC calibration also was made by the diphenyl ether method reported by Biancheria and Kegeles.[13] The diphenyl ether used was recrystallized four times and melted at 26.81°, in good agreement with Biancheria and Kegeles' value of 26.83°. With the rotor spinning at 59,360 r.p.m.

(1) Presented at the 36th National Colloid Symposium, Stanford University, Palo Alto, California, June, 1962.

(2) (a) Submitted by D. N. Holcomb to the faculty of the University of Illinois in partial fulfillment of the requirements for the degree of Doctor of Philosophy, April, 1962; (b) Department of Chemistry, University of California, Berkeley, California.

(3) J. G. Foss and J. A. Schellman, *J. Phys. Chem.*, **63**, 2007 (1959).

(4) W. F. Harrington and J. A. Schellman, *Compt. rend. trav. Lab. Carlsberg, ser. Chim.*, **30**, 21 (1956).

(5) C. Tanford and R. E. Weber, private communication; see also R. E. Weber, Ph.D. Thesis, State University of Iowa, 1958.

(6) K. E. Van Holde, unpublished results.

(7) J. Hermans, Jr., and H. A. Scheraga, *J. Am. Chem. Soc.*, **83**, 3283 (1961).

(8) T. P. King and L. C. Craig, *ibid.*, **80**, 3366 (1958).

(9) T. P. King and W. Konigsberg, *Ann. N. Y. Acad. Sci.*, **88**, 571 (1960).

(10) L. J. Gosting and M. S. Morris, *J. Am. Chem. Soc.*, **71**, 1998 (1949).

(11) K. E. Van Holde and R. L. Baldwin, *J. Phys. Chem.*, **62**, 734 (1958).

(12) R. L. Baldwin, *Biochem. J.*, **65**, 503 (1957).

(13) A. Biancheria and G. Kegeles, *J. Am. Chem. Soc.*, **76**, 3737 (1954).

and an RTIC reading corresponding to 31.37 ± 0.03° (using the test stand calibration), the diphenyl ether method gave a temperature of 31.35 ± 0.02°. For high temperature experiments the rotor was placed in an electric oven and preheated to a temperature about 3 to 5 degrees above the temperature at which the sedimentation experiment was to be made. For temperatures above 55°, even with the heater in the chamber operating continually, the rotor temperature generally decreased by about 5° before temperature equilibrium was attained and the run was started. During the course of a sedimentation run the temperature was constant to at least ±0.2° and generally the control was to about ±0.1° or better. All sedimentation velocity measurements were made in cells with Kel-F centerpieces.[14] A wedge and a plain cell were used simultaneously, the wedge cell containing a solution of about 0.4% ribonuclease and the plain cell a solution of about 0.8% ribonuclease. Because of the rapid diffusion of ribonuclease and the consequent rapid flattening of the concentration gradient curve, it was necessary to begin taking photographs as soon as the boundary maximum had separated from the meniscus. Therefore, the earlier photographs were of necessity taken under conditions of non-free diffusion. Usually ten photographs were taken at 8-min. intervals. The photographs were measured on a Bausch and Lomb Bench Comparator, Model 32-12-11-01. The boundary maximum positions could be determined to at least ±0.02 mm. for photographs taken early in the sedimentation experiment and to about ±0.05 mm. for photographs taken near the end of the run when boundary spreading due to diffusion had become prominent.

The molecular weight determination was made by means of the sedimentation equilibrium method described by Van Holde and Baldwin.[11] A solution column height of 3.8 mm. was employed. The measurement was made at a pH of 7.7 in a 0.0078 *M* phosphate–0.15 *M* KCl buffer. Twenty-three hours were allowed for equilibrium to be attained, using a speed of 12,520 r.p.m.

Apparent Specific Volume Measurements.[15]—A pair of dilatometers were constructed by sealing 0.2-ml. measuring pipet capillaries onto bulbs of about 10 ml. volume. In making the measurements, one dilatometer was filled with buffer and the other with protein solution. The dilatometers were weighed to ±0.0001 g. before and after being filled. Once filled, the dilatometers were placed in a large dewar which was equipped with heater, stirrer, and thermometer. The temperature could be estimated to ±0.02° and at any temperature setting could be held constant to at least ±0.05°. The change in the apparent specific volume of ribonuclease then was determined by noting the change in height of the solution column relative to the change in height of the buffer column as a function of temperature. The heights of the columns were measured relative to reference marks on the capillaries with a cathetometer which was accurate to ±0.001 cm. In order to take into account any variations in capillary bore each capillary was calibrated by measuring the length of a mercury thread of known weight at various positions in the capillary. The apparent specific volume measurements presented were made as a function of increasing temperature only. On cooling the dilatometers, complete drainage of solution from the capillary walls was not attained and consequently the data taken on cooling are not reported.

Viscosity Measurements.—The viscosity of the phthalate buffer, relative to water at 25.000 ± 0.005°, was measured with a Cannon-Ubbelhode (D-50/116) viscometer having a flow time of about 200 sec. for water at 25°. A kinetic energy correction was not made for this determination.

(14) In earlier experiments using aluminum centerpieces, erratic results sometimes were observed. The results which were obtained indicated that the inconsistency was due to acid attack on the aluminum. See also V. N. Schumaker and B. Marano, *Arch. Biochem. Biophys.*, **94**, 532 (1961).

(15) This experiment was carried out using a sample of ribonuclease purchased from Sigma Chemical Company (their Lot No. R40B-074, 5× recrystallized, salt and protease free) dissolved in a 0.02 *M* phthalate buffer (no additional KCl). Since the change in apparent specific volume is the quantity of interest, it is felt that the use of a different ribonuclease sample and lower ionic strength buffer should not seriously affect the results. The latter assumption is supported by the data of Cox and Schumaker. See D. J. Cox and V. N. Schumaker, *J. Am. Chem. Soc.*, **83**, 2433 (1961).

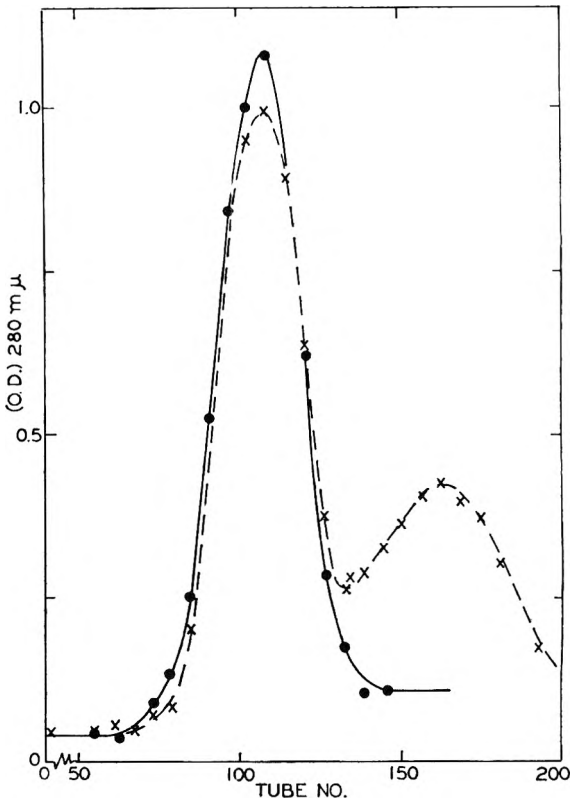

Fig. 1.—Countercurrent distribution pattern obtained with Pentex lot no. 26Z7 ribonuclease. The optical densities at 280 mμ are plotted *vs.* tube number for the lower (filled circles) and upper (crosses) phases. The major peak with a maximum at tube no. 108 is attributed to ribonuclease-A and the smaller leading peak presumably is due to ribonuclease-B. The distribution of ribonuclease between the upper and lower phases at the maximum of the major peak corresponds to a partition ratio (= O.D. (upper)/O.D. lower) of about 0.9, in fair agreement with King and Craig's value of 0.8. The ribonuclease-A used in these experiments was obtained from the upper and lower phases of tubes 65 to 120, inclusive.

A pair of Ostwald–Fenske viscometers, each having a flow time for water at room temperature of about 340 sec., were used for the measurement of the specific viscosity of ribonuclease-A as a function of temperature. Because of the long flow times of these viscometers, no kinetic energy correction was made. The flow times (t) of the viscometers, designated right (r) and left (l), were determined as functions of temperature with conductivity water and a calibration curve of r (= $t_{r,w}/t_{l,w}$) *vs.* T was constructed. The calibration curve for each pair of viscometers was a straight line of very small slope. The viscometer which had the shorter flow time always was filled with protein solution and the other viscometer with solvent. The protein concentrations employed were 0.8, 0.9, and 1.6% (w./v.). The temperature of the water in the dewar flask in which the viscometers were placed was regulated with a Haake thermoregulator and could be maintained to at least ±0.02° at all temperatures employed. The flow times, t_r and t_l, were determined simultaneously for buffer and protein solution with electric timers to about ±0.1 sec. In general, if t_l and t_r both increased or decreased by 0.1 sec. or less in a second measurement from their values for a first measurement the two measurements were taken to be sufficient. If the changes were greater than this, or in opposite directions, further measurements at the particular temperature were made.

Results

Molecular Weights.—Weight- and z-average molecular weights were calculated from the equilibrium ultracentrifugation data by the

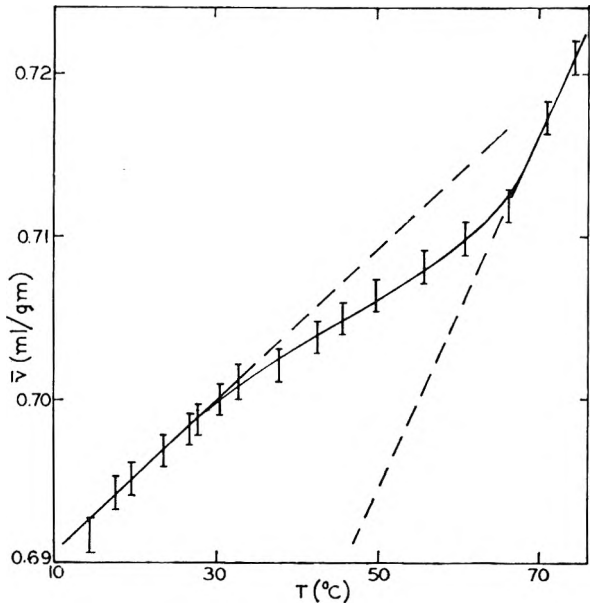

Fig. 2.—The dependence of the partial specific volume upon temperature.

methods discussed by Van Holde and Baldwin.[11] The data led to $M_z = 17{,}700$ and $M_w = 14{,}700$, both values being significantly higher than the formula weight (13,683) of ribonuclease. A sharp increase in the slope of the dn/dr *vs.* r photograph observed near the bottom of the cell indicated that the sample was contaminated by a small amount of a high molecular weight impurity. Assuming a two-component system with one component having the formula weight, the method derived by Sophianopoulos and Van Holde[16] gave the molecular weight and weight fraction of the impurity as 58,000 and 0.02, respectively. The occurrence of some aggregation of the ribonuclease during the evaporation or lyophilization seems quite likely. Further, it has been shown[17] that ribonuclease may aggregate even during cold storage. It is not expected that this small amount of impurity will materially affect the results obtained here.

Temperature Dependence of the Apparent Specific Volume.—Aside from the inherent interest in determining the variation of the partial specific volume, $\bar{v}_2$, of ribonuclease with temperature, it is necessary to know this variation in order to correct the sedimentation velocity data for the variation of "buoyancy" term, $(1 - \bar{v}_2\rho)$, with temperature.[18] The quantity actually measured, the apparent specific volume, may be written as

$$\phi_v(T) = [V(T) - w_1 v_1^0(T)]/w_2 \qquad (1)$$

where $V(T)$ is the total volume of solution at temperature T, w_1 is the weight of solvent, w_2 is the weight of solute, and v_1^0 is the specific volume of pure solvent. For fairly dilute solutions ϕ_v and $\bar{v}_2$ will be nearly equal. With two dilatometers, one containing w_r grams of pure solvent and the other w_1 grams of solvent and w_2 grams of solute, the change in the apparent specific volume between two temperatures ($\Delta\phi_v$) is given as

$$(w_2/A)\Delta\phi_v = (\Delta h - \Delta h_r) - d'\Delta h_r \qquad (2)$$

where Δh and Δh_r are the changes in the meniscus positions in the solution and reference dilatometers, respectively, A and A_r are the cross sectional areas of the capillaries, and $d' = (w_1/w_r)\cdot A_r/A - 1$. Equation 2 gives the temperature dependence of ϕ_v in terms of readily measurable quantities. Using the value 0.695 ml./g. for $\bar{v}$ of ribonuclease at 20° as determined by Harrington and Schellman,[4,11] one may tabulate $\bar{v}$ as a function of temperature. These data are shown in Fig. 2. It is seen that the partial specific volume increases through the thermal transition range from about 0.701 ml./g. at 34° to about 0.712 ml./g. at 66°, corresponding to an increase in $\bar{V}$, the partial molal volume, of about 150 ml./mole. It is evident, however, that there is a decrease in volume in the transition, native⇌denatured protein, at any given temperature. While the magnitude of this volume change depends upon the temperature, the value estimated at the mid-point of the transition (45°) is, by extrapolation of the linear volume *vs.* T curves obtained at high and low temperatures, about 240 ml./mole. From Fig. 2 it can be seen that native ribonuclease shows a temperature dependence of $\bar{v}$ of about 4.5×10^{-4} ml./g./deg., while for denatured ribonuclease the temperature dependence is about 18×10^{-4} ml./g./deg. For native ribonuclease, Cox and Schumaker's data[15] give $(d\bar{v}/dT) \doteq 8 \times 10^{-4}$ ml./g./deg.

Temperature Dependence of the Sedimentation Coefficient.—Sedimentation coefficients of proteins usually are calculated from the slope of the line

$$2.303 \log [(r_*)_t/(r_*)_{t_0}] = s_T\omega^2(t - t_0) \qquad (3)$$

where s_T is the sedimentation coefficient at temperature T and $(r_*)_t$ and $(r_*)_{t_0}$ are the positions of the maximum of the concentration gradient curve at times t and t_0, respectively, t_0 being the time of the first photograph. Alternatively, the values of s_T may be calculated directly from eq. 3 for each photograph after the first one. The derivation of eq. 3 involves the assumption that the diffusion coefficient, D, is zero. For a solute with a non-zero diffusion coefficient it can be shown that instead of the maximum of the refractive index gradient curve, r_*, one should use the second moment of this curve, σ, in eq. 3,[19] and $\sigma^{1/2}$ and r_* will not in general coincide. With the standard cell used in this work the diffusion process in the sedimenting boundary is restricted due to the presence of the meniscus, and with ribonuclease, the maximum of the concentration gradient resolves from the meniscus so slowly that a considerable amount of the time of the sedimentation process is spent under conditions of restricted diffusion. Thus, the discrepancy between $\sigma^{1/2}$ and r_* is outside of experimental error, especially for photographs taken early in the experiments. In most of these ex-

(16) A. J. Sophianopoulos and K. E. Van Holde, *J. Biol. Chem.*, **236**, PC 82 (1961).

(17) D. A. Yphantis, *Ann. N. Y. Acad. Sci.*, **88**, 586 (1960).

(18) See, for example, H. K. Schachman, "Ultracentrifugation in Biochemistry," Academic Press, New York, N. Y., 1959, p. 82.

(19) See, for example, J. W. Williams, K. E. Van Holde, R. L. Baldwin, and H. Fujita, *Chem. Rev.*, **58**, 715 (1958).

periments with ribonuclease, application of eq. 3 yielded considerably higher sedimentation coefficients from the first few photographs than from photographs taken later in the experiments.

The method proposed by Fujita and MacCosham[20] has been used to correct the data for this diffusion effect. The method of calculation has been described elsewhere.[2,21] In a typical sedimentation experiment, eq. 3 led to an average value of the sedimentation coefficient of 1.69 S while a value of 1.63 S was obtained after the data had been corrected for the diffusion effect. The values of s_T have been corrected to conditions of aqueous solvent at 20° by the relation

$$s_{20,w} = s_T\,[\eta_{w,T}/\eta_{20,w}](\eta_B/\eta_w)_{25}\,\frac{(1-\bar{v}\rho)_{20,w}}{(1-\bar{v}\rho)_{T,B}} \quad (4)$$

Use of eq. 4 involves the assumption that the relative viscosity of buffer (η_B/η_w) will be constant over the temperature interval being considered.

The sedimentation coefficient, $s_{20,w}$ at C = 0.8 g./100 ml. for ribonuclease-A in the phthalate–0.15 M KCl buffer is shown in Fig. 3 as a function of temperature. The fact that $s_{20,w}$ remains quite constant over a considerable temperature range below 35° and, over a shorter range above 55° may be taken as evidence that the use of eq. 4 is justified. Plots of $s_{20,w}$ *vs.* temperature were made with data obtained for 0.4% and 0.8% solutions of ribonuclease-A and smooth curves were drawn through each set of data. A curve of $s^0_{20,w}$ then was obtained by a linear extrapolation to infinite dilution of points taken from the two smooth curves. It is in general preferable to use the actual experimental values in making an extrapolation of this type; however, because of frequent cell leaks and two cases of cell distortion, points at both 0.4% and 0.8% concentrations were not available at all temperatures. The dependence of $s_{20,w}$ upon concentration is so small that the results from only two points can be used with confidence. The value of $s^0_{20,w}$ for ribonuclease-A measured here is 1.79 ± 0.02 S at room temperature and in a solution of ionic strength 0.17. Literature values for the sedimentation coefficient[4,22] vary considerably, but the value of 1.90 S reported by Harrington and Schellman[4] is perhaps the most reliable. None of the values previously reported have been corrected for the diffusion effect. Probably of more significance to the difference between the value of $s^0_{20,w}$ obtained in this work and that of Harrington and Schellman (as well as other literature values obtained at pH ≐ 7) is that the solvent conditions are not the same. According to the data of Hermans and Scheraga[7] at pH 2.8 the ribonuclease molecule is in a less compact configuration at room temperature than it is at pH 7. Finally, it is not unreasonable to expect a measurable secondary charge effect at pH 2.8.

(20) H. Fujita and V. J. MacCosham, *J. Chem. Phys.*, **30**, 291 (1959); see also J. M. Peterson and R. M. Mazo, *J. Phys. Chem.*, **65**, 566 (1961).

(21) A. J. Sophianopoulos, C. K. Rhodes, D. N. Holcomb, and K. E. Van Holde, *J. Biol. Chem.*, **237**, 1107 (1962).

(22) H. Neurath and K. Bailey (eds.), "The Proteins," Vol. I, Part B. Academic Press, New York, N. Y., 1953, p. 634.

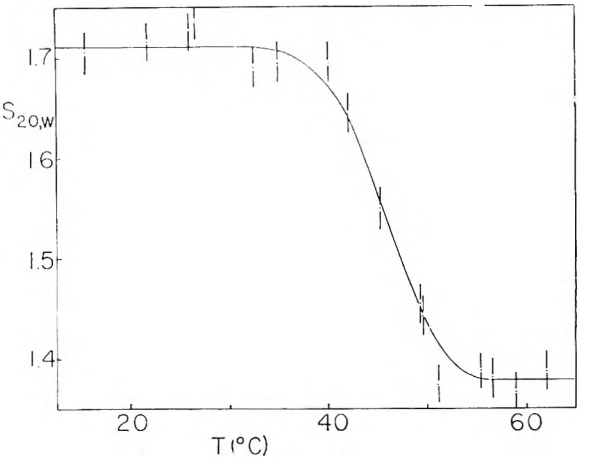

Fig. 3.—A graph of $s_{20,w}$ *vs.* temperature. The solutions contained 0.8% ribonuclease-A in the phthalate–0.15 M KCl buffer at pH 2.8. The units of $s_{20,w}$ are svedbergs (1×10^{-13} sec.). The vertical bars through the points correspond to ±0.02 svedbergs.

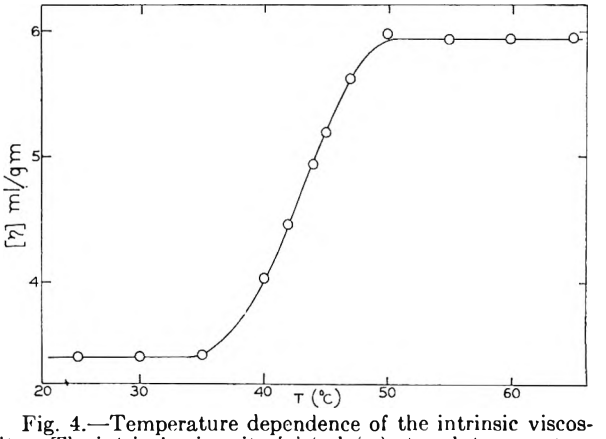

Fig. 4.—Temperature dependence of the intrinsic viscosity. The intrinsic viscosity [η] (ml./g.) at each temperature was obtained by extrapolating to infinite dilution the values of the reduced viscosity, η_{sp}/C, taken from smooth curves drawn through plots of η_{sp}/C for ribonuclease-A in the phthalate–0.15 M KCl buffer at concentrations of 0.8, 0.9, and 1.6%.

Temperature Dependence of the Specific and Intrinsic Viscosities.—The relative viscosities of the protein solutions were calculated from the relationship

$$\eta_r = r\,\frac{t_{l,p}}{t_{r,b}}\,\frac{\rho_p}{\rho_b} \quad (5)$$

where r (= $t_{r,w}/t_{l,w}$) is the previously mentioned viscometer calibration factor, $t_{r,b}$ is the flow time of the right viscometer for buffer, $t_{l,p}$ is the flow time of the left viscometer for protein solution, and ρ_p and ρ_b are the densities of protein and buffer solutions. The densities at a temperature T were calculated as

$$\rho_p(T) = \rho_b(T) + \Delta\rho\ (\text{protein}) \quad (6)$$

and

$$\rho_b(T) = \rho_w(T) + \Delta\rho(KHC_8H_6O_4) + \Delta\rho(KCl) \quad (7)$$

where

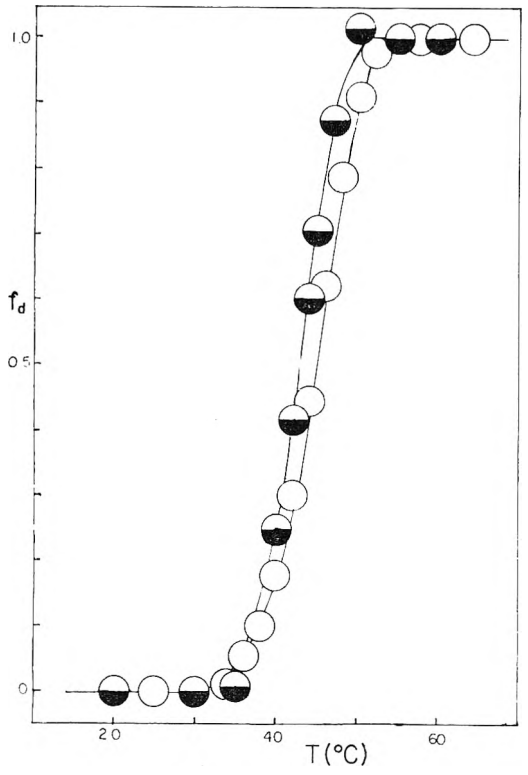

Fig. 5.—Temperature dependence of the fraction of molecules in the denatured configuration. The fraction of molecules in the denatured configuration, f_d, is plotted *vs.* T. The open and filled circles represent data calculated from the temperature dependence of $s_{20,w}$ and of $[\eta]$, respectively. The height of the circles represents the estimated experimental error in f_d; the experimental error in T should be no more than ±0.2°.

$$\Delta\rho(\text{protein}) \doteq (1 - \bar{v}_2\rho_b)c_2/100 \qquad (8)$$

$\Delta\rho$ (X) is the density increment due to component X and c_2 is protein concentration in g./100 ml. Values for $\Delta\rho$ (salt) were obtained from the literature[23]; it was assumed that the density increment due to potassium acid phthalate would be nearly equal to that due to phthalic acid. It also was assumed that any variation of $\Delta\rho$(X) with temperature would have negligible effect on the ρ_p/ρ_b ratio. Figure 4 shows the variation of the intrinsic viscosity ($[\eta]$) of ribonuclease-A with temperature. The points of Fig. 4 are extrapolations to infinite dilution of values taken from smooth curves drawn through plots of η_{sp}/c *vs.* temperature for protein concentrations of 0.8, 0.9, and 1.6%. The intrinsic viscosity of ribonuclease-A measured here is about 3.4 ± 0.2 ml./g. at room temperature. This is in good agreement with the value of 3.3 ml./g. measured by Harrington and Schellman[4] for Armour ribonuclease at pH 7.

Expression of Results as Fraction of Molecules in the Denatured Form.—In the limits of low and high temperatures the specific and intrinsic viscosities and the sedimentation coefficient of ribonuclease approach limiting values. These limiting values are assumed to be characteristic of the native and denatured configurations, respectively. If it is *assumed* that the denaturation reaction is a single step process of the form

$$\text{native protein (n)} \rightleftarrows \text{denatured protein (d)} \qquad (9)$$

then, at any temperature the fraction of molecules in the denatured configuration, f_d, will be given as

$$f_d = 1 - f_n = C_d/(C_n + C_d) = C_d/C \qquad (10)$$

Here C_n and C_d are the concentrations of the protein in the native and denatured states, respectively, and C is the total protein concentration. In the limit of infinite dilution and at a temperature T one may write for the experimentally measured quantities, $\bar{X}_T{}^0$ (which in this work would be either $s^0_{20,w}$ or $[\eta]$)

$$\bar{X}_T{}^0 = (C_nX_n{}^0 + C_dX_d{}^0)/(C_n + C_d) \qquad (11)$$

where the subscripts n and d refer to the native and denatured protein, respectively, and the superscript 0 indicates that the value of X has been extrapolated to zero concentration. Equation 11 also will apply to the values of X measured at finite concentration under certain conditions.[24] From eq. 10 and 11 one may express the fraction of molecules in the denatured state in terms of the measured quantities as

$$f_d = (\bar{X}_T{}^0 - X_n{}^0)/(X_d{}^0 - X_n{}^0) \qquad (12)$$

Using eq. 12 and the experimental data, Fig. 5 showing f_d *vs.* temperature as measured by sedimentation velocity and viscometry has been prepared.

Calculation of Equilibrium Constants.—If the denaturation reaction has the form of eq. 9 then it is possible to write for the equilibrium constant for the transition[25]

$$K = C_d/C_n = f_d/(1 - f_d) \qquad (13)$$

Or, from (12)

$$K = (\bar{X}_T{}^0 - X_n{}^0)/(X_d{}^0 - \bar{X}_T{}^0) \qquad (14)$$

An apparent equilibrium constant, K^*, may be calculated by replacing the values of X^0 in eq. 14 with X, the value of the variable measured at a finite concentration, but K and K^* will be equal only if the equilibrium constant is independent of

(23) International Critical Tables, III, McGraw-Hill, New York, N. Y., 1928.

(24) The effect of concentration dependence of the sedimentation coefficients or reduced viscosities upon the values of apparent thermodynamic parameters (K, ΔH^0) obtained at finite concentration has been investigated. Details are given elsewhere (see ref. 2), but the important facts can be summarized as follows: the difference between the true equilibrium constant and enthalpy values and the apparent quantities depends upon *differences* between the rate of change with concentration of $s_{20,w}$ (or $[\eta]$) for the native and denatured forms. To a good approximation the apparent equilibrium constant will vary with the first power of the concentration and the apparent enthalpy with the second power; in either case this variation should be small.

(25) Since in the determination of equilibrium constants from the sedimentation behavior the pressure at the position of the moving boundary is appreciably greater than atmospheric, the question may arise as to whether the change in equilibrium constant with pressure may be significant. Taking, as a liberal estimate, the average pressure at the boundary as 50 atmospheres and the molar volume change on denaturation as −240 ml./mole suggests that the values of log K may be about 0.2 greater than would be observed at atmospheric pressure. This is about the same as the experimental error.

concentration.[24] Figure 6 is a van't Hoff plot for the data of Fig. 5. The deviation from linearity at high temperature (low $1/T$) has been observed previously by Hermans and Scheraga.[7] They have suggested that this curvature may be due to the existence of more than one reversibly denatured form of ribonuclease.

It can be shown that deviation from linearity in the van't Hoff plot would be obtained if the reaction were not a single step process, but rather one consisting of two (or possibly more) discrete steps

$$\mathrm{N} \underset{K_1}{\rightleftharpoons} \mathrm{B} \underset{K_2}{\rightleftharpoons} \mathrm{D} \qquad (15)$$

Here N, B, and D represent the protein in the native, intermediate, and denatured configurations, respectively, and $K_1 (= C_B/C_N)$ and $K_2 (= C_D/C_B)$ are the equilibrium constants for the first and second steps of the reaction. At a temperature T one may assume

$$\bar{X}_T{}^0 = (C_N X_N{}^0 + C_B X_B{}^0 + C_D X_D{}^0)/(C_N + C_B + C_D) = (X_N{}^0 + K_1 X_B{}^0 + K_1 K_2 X_D{}^0)/(1 + K_1 + K_2 K_2) \qquad (16)$$

Substitution of (16) into (14) gives the measured "equilibrium constant" in terms of the true equilibrium constants as

$$\ln(K) = \ln [(X_N{}^0 - X_B{}^0) + K_2(X_N{}^0 - X_D{}^0)] - \ln [(X_N{}^0 - X_D{}^0) + K_1(X_B{}^0 - X_D{}^0)] + \ln (K_1) \qquad (17)$$

With the assumption that at *low* temperatures $K_1 << 1$ and $K_2 << 1$ and that at *high* temperatures $K_1 >> 1$ and $K_2 >> 1$, it can be shown that the van't Hoff plot would have low and high temperature limiting slopes of d ln (K_1)/d$(1/T)$ and d ln (K_2)/d$(1/T)$, respectively. The two-step mechanism proposed above can, under certain conditions, qualitatively predict the kind of deviation from linearity observed in the van't Hoff plots. Furthermore, according to this mechanism a graph of log K *vs.* $1/T$ will approach a straight line with a slope corresponding to $\Delta H_1{}^0$ at low temperature. The values of K will, however, differ from K_1 by the constant factor $(X_N{}^0 - X_B{}^0)/(X_N{}^0 - X_D{}^0)$, even at low temperature. The value of this factor may differ when different physical methods of measurement are used. Thus, behavior of the kind observed in Fig. 6, where the low-temperature portions of the van't Hoff plots are parallel but displaced from one another, is consistent with such a mechanism.

Another mechanism which has been considered is

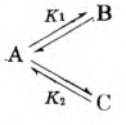

(18)

where A represents native protein and B and C are two denatured forms. Unless $K_1 = K_2$, at all T, either B or C must be the form exclusively present at very high temperature. Taking it to be C,

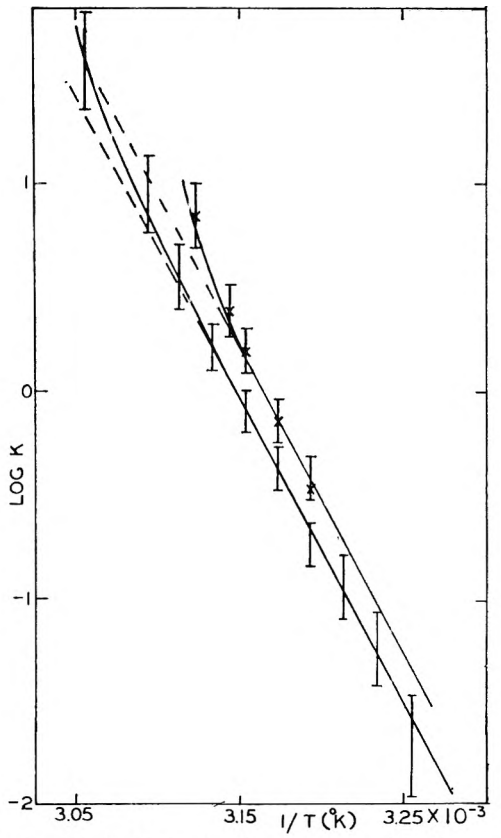

Fig. 6.—Van't Hoff plot for the reversible thermal denaturation. This is a graph of log K *vs.* $1/T$ (°K.) for the data of Fig. 5. The points represent the sedimentation data and the crosses represent the viscosity data. The experimental error is greater at values of $1/T$ corresponding to the upper and lower temperature limits of the transition.

the apparent equilibrium constant obtained turns out to be

$$\ln K = \ln \frac{K_1(X_A{}^0 - X_B{}^0) + K_2(X_A{}^0 - X_C{}^0)}{X_A{}^0 - X_C{}^0 + K_1(X_B{}^0 - X_C{}^0)} \qquad (19)$$

The predictions from this mechanism are qualitatively similar to those given by the former: a straight line for ln K *vs.* $1/T$ at low temperature, with deviation at higher temperature.

A final possible explanation for the curvature of the van't Hoff plots is a difference in heat capacity between native and denatured protein.[26] One would expect the denatured protein to have many additional degrees of freedom and consequently a higher heat capacity than the native protein. Indeed, a value of $\Delta C_p = 9850$ cal./mole deg. has been obtained for the acid denaturation of ferrihemoglobin.[27] Even allowing that ΔC_p for the much smaller ribonuclease molecule should be considerably lower, values of this order would be quite sufficient to produce the degree of curvature observed here. However, a constant difference in heat capacity between product and reactant would lead to a nearly uniform curvature over the entire temperature range. To reproduce accurately

(26) We are indebted to Professor T. E. Phipps for this suggestion.

(27) W. W. Forrest and J. M. Sturtevant, *J. A. Chem. Soc.*, **82**, 585 (1960).

the van't Hoff plots obtained in this work and by Hermans and Scheraga,[7] ΔC_p would have to be much smaller near the low temperature limit of the transition range than at temperatures only 10° higher. This appears to be a somewhat artificial and unjustified assumption.

The data available do not permit a distinction to be made between these possibilities; certainly calorimetric measurements of the process would be of aid at this point.

Thermodynamic Parameters.—Because of the curvature of the van't Hoff plots, the assumption of a single-step reaction such as eq. 9 is of dubious validity. However, the calculation of thermodynamic parameters for such an assumed reaction is useful. The parameters calculated give at least estimates of the enthalpy and entropy changes which occur during the transition and of the free energies of reaction. Further, these values should serve as a basis for comparison of data obtained for different samples and by different methods. Finally, analysis of more complex mechanisms indicates that in some cases the correct ΔH^0 for one step of the reaction can be obtained readily. Accordingly, the linear portions of the van't Hoff plots have been used to calculate the value of ΔH^0 for the denaturation reaction. The temperature at which $K = 1$ is termed the transition temperature, T_{Tr}. The standard state entropy change, ΔS^0, is obtained as

$$\Delta S^0 = \Delta H^0/T_{Tr} \qquad (20)$$

The results are summarized in Table I. Values presented include both "apparent" parameters and those calculated from van't Hoff graphs of data extrapolated to infinite dilution. Only in the case of the viscosity results is a significant concentration dependence of the apparent ΔH^0 seen. When the values of ΔH^0 obtained at various concentrations are plotted *vs.* C^2 and extrapolated[24] to infinite dilution, a straight line is obtained with an intercept of 63 kcal./mole.

The values of the transition temperature measured here are in good agreement with the results of Hermans and Scheraga,[7] but the heat of reaction is significantly higher[28] than their value of 51 kcal./mole. The data of Hermans and Scheraga seem to begin to deviate from linearity at a somewhat lower temperature. The thermodynamic parameters obtained by Tanford and Weber[5] (ΔH^0 = 65 kcal./mole, ΔS^0 = 210 e.u./mole at pH = 2) are in good agreement with the results reported here. In contrast, Kalnitsky and Resnick[29] have obtained a much lower value of ΔH^0 from studies of the variation of enzymatic activity with temperature. Taken together, the results of the various studies suggest that the denaturation process is complex and that different methods of measurement weight differently the stages of the reaction.

Attempt to Represent the Denaturation Process as a Continuous Expansion of the Molecule.—Some protein denaturation reactions seem to involve a continuous change in molecular dimensions as the environment is altered, rather than an equilibrium between a small number of configurational isomers. For example, quite convincing evidence[30] has been presented to indicate that a part of the acid denaturation of bovine serum albumin is of the former type. It would seem worthwhile to consider this possibility for the ribonuclease denaturation, especially since "equilibrium constants" obtained by various physical methods are not identical. The fact that the process has been studied by two methods, sedimentation and viscometry, which depend in *different ways* upon molecular dimensions, allows an investigation of the question.

TABLE I

TRANSITION TEMPERATURES AND THERMODYNAMIC PARAMETERS FOR THE REVERSIBLE DENATURATION OF RIBONUCLEASE AT pH 2.8

Method	Protein concn. (% w./v.)	T_{Tr} (°C.)	ΔH^0	ΔS^0
Sedimentation	0.8	45.2	65	205
Sedimentation	.4	45.0	67	211
Sedimentation	0	44.6[a]	68[a]	214[a]
Viscometry	1.6	45.7	56	176
Viscometry	0.9	44.7	60	189
Viscometry	.8	43.8	61	192
Viscometry	0	42.9[a]	67[a]	212[a]

[a] Calculated from values of $s_{20,w}$ or η_{sp}/C extrapolated to $C = 0$.

If the denaturation process is visualized as a continuous change in an effective hydrodynamic radius of the molecule, R_e, the dependence of $s^0_{20,w}$ and $[\eta]$ upon T may be written as

$$s^0_{20,w} = k/R_e \qquad (21)$$

and

$$[\eta] = k'R_e^3 \qquad (22)$$

The use of constants k and k' is in part justified by the zero slope which is observed in both Fig. 3 and 4 above and below the transition range. If eq. 21 and 22 are valid, then it is possible to calculate the expected variation of the *apparent* fraction of native protein (as measured by one of the above methods) from the observed variation determined by the other method. For example, it can be shown that under these assumptions

$$\frac{f^*_{n,[\eta]}}{f^*_{n,s}} = \frac{R_{e,T}}{R_{e,n}}\left(\frac{R_{e,T}^2 + R_{e,T}R_{e,d} + R_{e,d}^2}{R_{e,n}^2 + R_{e,n}R_{e,d} + R_{e,d}^2}\right) \qquad (23)$$

where $f^*_{n,s}$ represents the apparent fraction of protein in the native state as determined from sedimentation coefficient measurements using eq. 12 and $f^*_{n,[\eta]}$ is the apparent fraction of native protein which should then be observed by intrinsic viscosity measurements. Typical results of these calculations are as follows: at 48°, sedimentation measurements indicate that 21% of the protein is in the native form; eq. 23 then would predict that viscosity measurements should indicate 31% native, if the process is a continuous change, obeying eq.

(28) It should be pointed out that when Hermans and Scheraga's data for pH = 2.89 were plotted in Fig. 6, nearly all of the points fell between the two curves.

(29) G. Kalnitsky and H. Resnick, *J. Biol. Chem.*, **234**, 1714 (1959).

(30) C. Tanford, J. G. Buzzell, D. G. Rands, and S. A. Swanson, *J. Am. Chem. Soc.*, **77**, 6421 (1955).

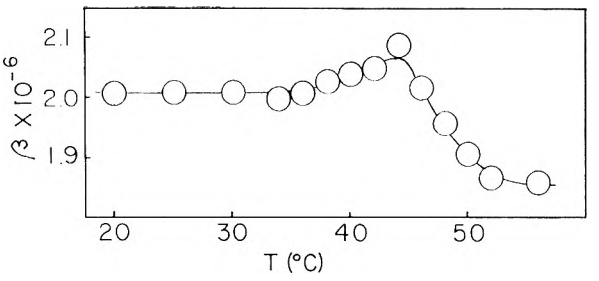

Fig. 7.—Values of the Scheraga–Mandelkern parameter β, calculated from the intrinsic viscosity, sedimentation coefficient at infinite dilution, and partial specific volume, at various temperatures.

21 and 22. The observed value from intrinsic viscosity measurements is about 6%. At 46°, the corresponding values are 38, 50, and 20%. Thus, the observed deviation of $f^*_{n,[\eta]}$ from $f^*_{n,s}$ is opposite to that which would be predicted for a continuous expansion of the molecule.

Calculation of the Scheraga–Mandelkern β.—Scheraga and Mandelkern[31] have treated the hydrodynamic properties of proteins by representing the protein molecule in terms of an effective hydrodynamic ellipsoid of revolution. They have defined a parameter, β, as

$$\beta = \frac{s^0_{20,w}[\eta]^{1/3}\eta_0 N}{M^{2/3}(1 - \bar{V}\rho)_{20,w}} \qquad (24)$$

where $N = 6.023 \times 10^{23}$ is Avogadro's number, η_0 is the solvent viscosity, and the other terms are as previously defined. It has been shown that for prolate and oblate ellipsoids of revolution β should vary from 2.12×10^6 to 3.60×10^6 and from 2.12×10^6 to 2.15×10^6, respectively, as the axial ratio is increased from 1 (corresponding to a sphere) to 300. From the data obtained in this work, β was calculated as a function of temperature using eq. 24. The values so obtained are shown in Fig. 7. It is seen that the results are somewhat anomalous in that at no temperature does β become as large as 2.12×10^6, the minimum value which the Scheraga–Mandelkern theory would predict. From their sedimentation velocity and viscosity studies with native ribonuclease at room temperature and pH = 7, Harrington and Schellman[4] calculate $\beta = 2.09 \times 10^6$. Harrington and Schellman have interpreted this value as suggesting that the axial ratio of ribonuclease in the native configuration may not be very different from unity.

One reason for the low values of β observed here may be the charge effect in the sedimentation measurements. In any event, the change in β is remarkably small over the entire transition. All but two of the values lie within ±5% of the average. Clearly the denatured protein does not even approximate a random coil in its hydrodynamic behavior, for a value of $\beta \doteq 2.79 \times 10^6$ for oxidized ribonuclease has been reported.[4]

Some insight into the behavior of β is afforded by the Debye–Bueche[32] theory. The model chosen by these authors is a uniformly dense spherical aggregate of polymer segments, through which some flow of solvent (as measured by a parameter σ) can occur. In many ways this would seem a more appropriate model for an expanded, but cross-linked, protein molecule than the random coil. The quantity β, as defined in eq. 24, has been calculated for this model. The details of the calculation need not be given here; the result is that for values of σ ranging from infinity (hard sphere) to 5, β varies between 2.12×10^6 and 2.07×10^6. With further decrease in σ, β increases rapidly. Thus the fact that the value of β is nearly the same for the native and reversibly denatured ribonuclease is consistent with the idea that the process involves only a moderate unfolding of the molecule.

Acknowledgments.—The authors wish to express their appreciation for the assistance given by Mr. V. German with the countercurrent distribution work and for the help of Mrs. C. K. Rhodes, who performed some of the ultracentrifuge experiments. This research was supported in part by a Research Grant (A3096) from the Public Health Service.

DISCUSSION

G. KEGELES (Clark University).—Would it be necessary to take account of possible effects on the shape of the sedimentation diagram caused by the existence of the transition reaction during sedimentation?

D. N. HOLCOMB.—The sedimentation diagrams did not appear to be asymmetric. If the transition reaction between the different protein species is sufficiently rapid in both directions of the equilibrium, one would expect a symmetrical peak moving with a weight-average sedimentation rate.

R. TRAUTMAN (Plum Island Animal Disease Laboratory, USDA).—Have you compared the precision or efficiency of the calculation of sedimentation rate using the classical method of integrating over the entire curve (but assuming C_0) with the MacCosham–Fujita method using only the maximum ordinate position (but assuming M)?

D. N. HOLCOMB.—We have not attempted to make such a comparison. It would be interesting to do so. With the exception of only a few experiments, we used two standard cells which contained solution—one with a wedge window and the other with a plain window. Consequently, we do not have solvent base lines on the photographs and this would make the integration somewhat difficult.

S. R. ERLANDER (Northern Regional Research Laboratory, USDA).—With regard to the change in pH in aluminum cells, several years ago Foster and Kromman observed changes in pH in the aluminum cell at pH values of approximately 3 to 4.

D. N. HOLCOMB.—That is correct. We were aware that there might be acid attack on the aluminum alloy at this pH. We hesitated to use Kel-F centerpieces initially, however, because we were not certain as to the stability of these centerpieces at higher temperatures. (This apprehension was later justified in the case of one Kel-F centerpiece which became deformed and unusable after several sedimentation experiments above 60°.)

A. SILBERBERG (Weizmann Institute of Science).—β-values even less than 1.9×10^6 are predicted in the case of short polymer chains if the equations for $[\eta]$ and s proposed by Kuhn and Kuhn [H. Kuhn, W. Kuhn, and A. Silberberg, *J. Polymer. Sci.*, **14**, 193 (1953)] are substituted in the Scheraga–Mandelkern equation. In this theory two parameters are used: the length of the statistical chain element A and the cross-sectional diameter d of the peptide chain. The data available to the authors should enable those to be evaluated.

(31) H. A. Scheraga and L. Mandelkern, *J. Am. Chem. Soc.*, **75**, 179 (1953).

(32) P. Debye and A. M. Bueche, *J. Chem. Phys.*, **16**, 573 (1948).

SUBFRACTIONATION OF THE S_f 20–10^5 LIPOPROTEINS IN A SWINGING BUCKET ROTOR[1]

BY F. T. LINDGREN, A. V. NICHOLS, F. T. UPHAM, AND R. D WILLS

Donner Laboratory, Lawrence Radiation Laboratory, University of California, Berkeley, California

Received March 10, 1962

Human serum lipoproteins of the S_f 20–10^5 class have been subfractionated by accumulative flotation rate techniques employing a NaCl density gradient and a specially designed swinging bucket rotor. A feature of this rotor is that it allows the use of full length 1.27 × 8.89 cm. preparative tubes, providing an increased radial flotation path. Studies of ηS *vs.* ρ allow estimations of hydrated density for lipoproteins within the S_f 20–400 class. Over the S_f 20–10^5 lipoprotein spectra, lipid chemical data on isolated lipoprotein subfractions indicate a progressive increase in glyceride content with increasing S_f rate. Although imperfect fractionation was achieved, this type of subfractionation or modification of it may be useful in exploring accumulative flotation rate separation techniques of particles or macromolecules which differ in size or molecular weight, but which, because they are less dense than water (or the usual solvent), may not be separated on the basis of their hydrated density.

Introduction

Subfractionation of the low-density lipoproteins less dense than serum background (1.006 g./ml.)[2] has consistently presented difficulty. In contrast, the fractionation of lipoproteins of higher density may be achieved by appropriate density adjustments in the background small molecule (salt) solution. Thus, broad lipoprotein classes may be fractionated by differential density ultracentrifugation.[3–5] Further, it is theoretically possible to make very delicate lipoprotein fractionations on a density gradient provided, of course, the solution background in a region of the preparative tube can be properly adjusted to equal the hydrated density of the lipoprotein itself. In practice, this gradient may be a temporary one[6,7] which necessarily will be changing slowly with time or, more ideally, a gradient which corresponds closely to the sedimentation equilibrium gradient[8] characteristic of the particular salt, the salt concentration, and the centrifugal conditions. However, once fractionation has been achieved on the basis of hydrated density, physical homogeneity of the macromolecular preparation is not necessarily assured, since there may exist a considerable degree of particle size inhomogeneity within the same hydrated density class.

On an ultracentrifugal basis the technique of rate separation by sedimentation[9,10] or flotation[11] potentially allows further subfractionation of a given lipoprotein preparation which is either less dense than 1.006 g./ml., or which already has been fractionated on a density gradient. These techniques for separation are also applicable for mixtures of proteins of closely similar hydrated densities which cannot be subfractionated on a density basis, but nonetheless may differ substantially in molecular weight from one another.

In order to achieve optimal conditions for rate separation, it is desirable to use a swinging-bucket type rotor to avoid detrimental convective disturbances inherent in angle preparative ultracentrifugation.[12] Also, if rate fractionation is employed, the resolvability is greater the longer the path length over which the rate separation occurs.

Experimental

Apparatus.—Although swinging-bucket type rotors have been designed[13] or are available commercially, such as the Spinco (SW 39 L., SW 25.., and K6) and Serval (HS) rotors, none provide for use of both full-size 6-ml. and 9-ml., 12.7 mm. diameter preparative tubes. Use of these full-length tubes, particularly the 9-ml. tubes, would present a long radial path (8 cm.) in which to achieve nearly ideal radial sedimentation or flotation. Because of the widespread use of Spinco ultracentrifuges, it seemed desirable to design a swinging-bucket type of rotor that would operate in either the standard Model L or Model E ultracentrifuge. Since these ultracentrifuges utilize a high vacuum for operation, a necessary requirement for the swinging-bucket assembly would be for an effective vacuum seal to prevent possible escape of fluid from the centrifuge preparative tube into the vacuum chamber during operation. Another desirable feature includes the capability for sealing the preparative tubes with standard preparative cap assemblies to achieve an additional safety vacuum seal as well as to provide for ease of insertion and removal of the preparative tube from the centrifuge bucket. These features have been incorporated into a low-speed swinging-bucket rotor described below.

Construction and Testing.—Because of the convenience of either two- or four-bucket operation, it seemed advantageous to design a four-place rotor employing 90° symmetry. The rotor assembly shown in Fig. 1 consists of three parts: a rotor base, a cylindrical rotor, and a locking cylinder which also serves as a suspension coupling for use on a Model E ultracentrifuge. The rotor base, allowing operation in the Spinco Model L ultracentrifuge, was turned down from a retired Spinco preparative rotor. The cylindrical rotor was made from a forged billet of 7075 aluminum. After the cylindrical rotor had been machined slightly oversize, it was subjected to a T-6 heat treatment. This process consisted of maintaining the rotor at 471° for 1 hr., followed by a 52° water quench. The rotor then was reheated to 121° for 24 hr. and air quenched. A final machining of the tempered rotor was made to the specified tolerance (±0.05 mm.) for all dimensions.

(1) Work supported in part by Research Grants H-1882 (C7) and H-2029 (C4) from the National Heart Institute, Public Health Service, Bethesda, Md., and by the U. S. Atomic Energy Commission, Washington, D. C.

(2) Unless otherwise indicated all densities are given at 20°.

(3) R. J. Havel, H. A. Eder, and J. H. Bragdon, *J. Clin. Invest.*, **34**, 1345 (1955).

(4) L. A. Hillyard, C. Entenman, H. Feinberg, and I. L. Chaikoff, *J. Biol. Chem.*, **214**, 79 (1955).

(5) F. T. Lindgren, A. V. Nichols, and N. K. Freeman, *J. Phys. Chem.*, **59**, 930 (1955).

(6) E. M. Russ, J. Raymunt, and D. P. Barr, *J. Clin. Invest.*, **35**, 133 (1956).

(7) J. L. Oncley, K. W. Walton, and D. G. Cornwell, *J. Am. Chem. Soc.*, **79**, 4666 (1957).

(8) F. T. Lindgren, A. V. Nichols, T. L. Hayes, N. K. Freeman, and J. W. Gofman, *Ann. N. Y. Acad. Sci.*, **72**, 826 (1959).

(9) M. K. Brakke, *J. Am. Chem. Soc.*, **73**, 1847 (1951).

(10) N. G. Anderson, *Exptl. Cell Res.*, **9**, 446 (1955).

(11) F. T. Lindgren, H. A. Elliott, and J. W. Gofman, *J. Phys. Chem.*, **55**, 80 (1951).

(12) E. G. Pickels, *J. Gen. Physiol.*, **26**, 341 (1943).

(13) H. Kahler and B. J. Lloyd, Jr., *J. Phys. Chem.*, **55**, 1345 (1951).

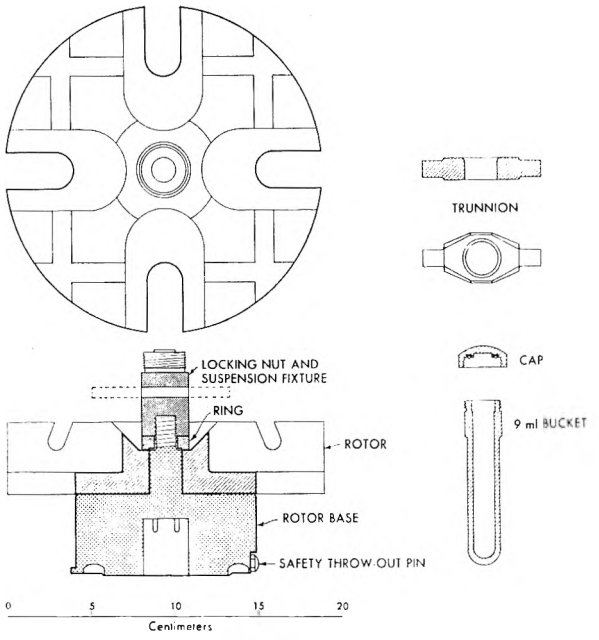

Fig. 1.—Scale drawing of the rotor assembly, a trunnion, and 9-ml. swinging-bucket assembly.

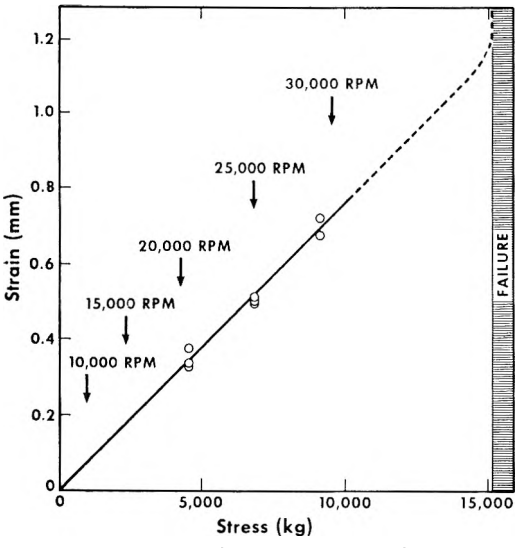

Fig. 2.—Strain–stress relationship obtained from trunnion test, including failure at a 15,060 kg. stress. Comparable operational stress at various rotor speeds is also shown. All tests were made with a Baldwin Southwark 200,000 lb. hydraulic testing machine.

Perhaps the most critical parts of this centrifuge rotor assembly are the trunnions, which should not be excessively massive, yet must support not only their own weight in the centrifugal field, but also that of the preparative tube assemblies. For this reason a special silico-manganese type of steel (Allegheny Ludlam 609) was selected for constructing these trunnions, because of its high elastic limit and its ability to withstand severe stress before bending or breaking. The trunnions shown in Fig. 1 were machined first to 0.25 mm. oversize before the heat treatment. In the heat treatment a hardening temperature of 843 to 899° was maintained for 0.5 hr., followed by an oil quench at room temperature. Thereafter, a drawing temperature of 427° was maintained for 12 to 18 hr. with the trunnions contained within a "neutral pack" to prevent scaling. After this heat treatment the trunnions were machined to full tolerance, which included balancing such that no trunnion differed from another by more than ±0.020 g.

Each trunnion was tested in a special support fixture and a hydraulic press subjected each trunnion to a full 9,070 kg. stress. The stress–strain relationship as determined by the downward deflection of the center of the trunnion is shown in Fig. 2. Also along the stress axis are shown comparable trunnion stresses for operational rotor speeds using fully loaded 9 ml. preparative tube–trunnion assemblies. One trunnion was carried to failure, which occurred at a loading of 15,060 kg. Although a radial cross section through the center of the preparative tube hole was approximately 90% of the combined area of the two support points, failure occurred simultaneously across these two support points. Examination of the trunnion subjected to failure suggested that one pivot failed in shear, whereas the other pivot failed as a result of the severe bending moment developed in the region of failure. Thus, it would appear from this failure (at approximately 10,550 kg./cm.^{2}) that enlarging the radius in the region joining the support pivot and the body of trunnion would potentially increase trunnion strength. The expected ultimate strength of Allegheny Ludlam 609 with our heat treatment is in the neighborhood of 21,000 kg./cm.^{2}.

The 6- and 9-ml. swinging buckets and caps were machined out of ST24 duraluminum and balanced to within ±0.020 g. A thrust shoulder of 2.38 mm. radius was machined on each of the buckets, matching a complementary supporting rim on the trunnions to provide for accurate and reproducible centering of the trunnion assembly during operation. Failure to provide such centering could lead to detrimental rotating couples during operation. Each bucket cap is fitted with an O-ring seal.

Although successfully tested at 20,000 r.p.m., practical operation of this rotor thus far has been confined to rotor speeds of no more than 10,000 r.p.m. (9,800 × g). However, operation at from 15,000 to 20,000 r.p.m. (corresponding to mean forces of 15,000 to 27,000 × g) can be expected with safety factors of approximately 6.4 and 3.5, respectively. Unfortunately, because of the reduced chamber diameter of the Model E ultracentrifuge (relative to the model L), only the 6-ml. swinging buckets can be used in this machine.

Because of the inherent danger of slow leaks and resultant rotor imbalance from an inadequately sealed swinging bucket assembly, simple safety circuits have been incorporated in both our Spinco Model E and Model L ultracentrifuges. These are "vacuum sentinels" which, when in use, instantly shut off the main power to the drive mechanism and simultaneously cut in the full brake should the vacuum fall below a pre-set level, say, 5 × 10^{-3} mm. pressure. Thus, if a leak were suddenly to develop during a run, the rotor could safely and automatically be stopped before serious imbalances might develop. On the Model E ultracentrifuge this sentinel circuit includes an Assembly Products[14] Model 351C meter. For the Model L ultracentrifuge, an Assembly Products 10 mv. (full scale) meter with high-low contacts incorporating a scale calibrated in microns is used. In practice, after operational vacuum has been achieved before a run, the vacuum circuit is transferred by appropriate holding relays to the "sentinel circuit" so that in the event of sudden vacuum loss, even during acceleration, the run should "fail safe."

Accumulative Rate Separation of the S_f 20–10^5 Lipoproteins.—The following fractionation procedure is closely related to gradient differential centrifugation[10] in which a virus solution is layered on top of a density gradient, and following each of several centrifugations in a swinging-bucket rotor, consecutive fractions are collected at the bottom of the preparative tubes. Further, separation of particles on a density gradient by rate zonal centrifugation[9] is also a similar methodology. However, this latter technique is concerned with the separation of discrete molecular entities on the basis of sedimentation rate during a single preparative run. In contrast to both these analogous procedures, the S_f 20–10^5 lipoprotein fractionation described below involves several stages of accumulative rate fractionations by flotation of portions of a lipoprotein distribution.

Although complicated by the presence of a density gradient, the approximate relationships between the conditions of the preparative centrifugation (see Fig. 3) and the anticipated results of fractionation are given below, where:

(14) Assembly Products, Inc., 75 Wilson Mills Rd., Chesterland, Ohio.

r_f = maximum radial depth of top fraction removed
r_b = radial depth at the salt gradient–lipoprotein boundary
r_m = maximum radial depth of preparative tube
F = flotation coefficient at any particular density and temperature[15]
$S_{f(1.063)}$ = flotation coefficient in 1.748 molal NaCl (ρ_{26} = 1.063 g./ml.) at 26°.

Thus, for a swinging bucket preparative run of an equivalent up-to-speed time t, the flotation coefficient (expressed as svedbergs) of particles that are 100% recovered and those particles that are just beginning to arrive at r_f (threshold recovery) may be approximated as follows

$$F(100\%\ \text{recovery}) = \frac{1}{\omega^2 t} \ln \frac{r_m}{r_f} 10^{13}$$

$$F(\text{threshold recovery}) = \frac{1}{\omega^2 t} \ln \frac{r_b}{r_f} 10^{13}$$

Further, a measure of the dispersion in the S_f value[16] of the fractionated lipoproteins may be expressed as

$$\frac{F(100\%\ \text{recovery}) - F(\text{threshold})}{F(100\%\ \text{recovery}} = \frac{\ln r_m - \ln r_b}{\ln r_m - \ln r_f}$$

For maximum resolvability (and for minimum S_f overlapping) the above quantity should be minimized. Thus, efforts to minimize the difference between r_m and r_b (the radial thickness of the lipoprotein layer) should be made, but unfortunately this also reduces the volume and quantity of the lipoproteins to be fractionated. For reasonable quantitative studies this volume need be in the order of 1–2 ml. On the other hand, the difference between r_m and r_f can be maximized within the limitations of rotor design and available radial dimensions of the ultracentrifuge vacuum chamber. It would therefore be desirable to make the effective radial flotation path as long as these considerations permit. Of course, for a given fractionation, a longer flotation path length necessarily requires a correspondingly longer time of centrifugation. For lipoprotein fractionation of the type being considered, our rotor, therefore, allows potentially more favorable centrifugal conditions, particularly in regard to the increased radial flotation path length.

Thus, to achieve the most favorable accumulative rate separation of lipoproteins by flotation, a thin layer of lipoprotein solution should be layered in the bottom of a preparative tube containing an appropriate density gradient. Flotation should proceed until the desired lipoproteins (of a particular S_f class, say, S_f 1590) have all just floated into a *minimum* volume (~0.6 ml.) of solution at the meniscus. This layer is carefully removed with a capillary pipet after the centrifuge is stopped with minimum disturbance. For extensive subfractionation, the process is repeated several times, each time stopping the centrifuge when the desired lipoproteins of the next slower flotation rate have just entered the volume near the meniscus (as the result of the total accumulated ultracentrifugation). In calculating equivalent S_f values for the fractionated lipoproteins, account must be taken of viscosity and solvent density and their changes within the region of the salt gradient over which the flotation occurs. In the present case the lipoprotein hydrated density must be estimated in order to make such calculations. Thus, during the fractionation (at 20°), an S_f 1590 lipoprotein would actually migrate at a mean rate of approximately 1070 svedbergs of flotation over the radial path from r_m to r_{f_1}.

In the present study, we are presenting a somewhat simplified rate separation procedure that achieves fractionation of three subfractions from a S_f 20–10^5 lipoprotein spectrum previously isolated[5] by angle head preparative ultracentrifugation. There are two swinging bucket preparative runs of approximately 2 and 18 hours duration at 9,500 r.p.m. (mean force of 8,860 × g). These runs are directed toward the successive fractionation of approximately the S_f 1360–10^5 and S_f 131–1590 class lipoproteins. After removal of these two fractions, the total bottom fraction (of the last swinging-bucket run) is given a density increment by direct salt (NaCl) addition to achieve a density of 1.065 g./ml. and this total fraction is ultracentrifuged at 40,000 r.p.m. for 8 hr. in a 40.3 angle rotor. This last run yields the total of the remaining smaller particle size S_f 20–157 lipoproteins. Figure 5 illustrates the above indicated amount of overlap that may be anticipated by calculation in each of these fractions. In practice, however, there results a considerably greater overlap in S_f rate of each fraction.

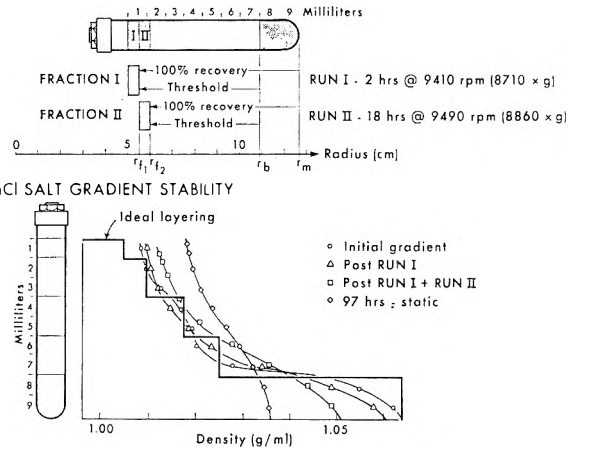

Fig. 3.—NaCl gradient showing position of layered S_f 20–10^5 lipoprotein fraction. Stability of salt gradient is illustrated by the indicated salt reference gradient determined after each run. Above is shown for each run the radial paths over which lipoprotein fractionation occurs. Thus, for fraction I, r_{f_1}, r_b, and r_m determine the radial paths over which 100% recovery of the S_f 1590 lipoproteins and threshold recovery of the S_f 1360 lipoproteins are anticipated. Equivalent up-to-speed time for runs I and II were 2.24 and 18.07 hr., respectively.

The technical details of setting up the NaCl gradient and layering the S_f 20–10^5 lipoprotein fraction (adjusted to a background density of 1.063 g./ml.) into the bottom of the preparative tube are shown in Fig. 3. The gradient is set up by layering into the bottom of a 9 ml. preparative tube successively 1, 2, 2, 2, and 2 ml. aliquots of the indicated solutions of density 1.007, 1.011, 1.019, 1.026 and 1.063 g./ml., respectively, using a blunted spinal needle (no. 23) and a Hamilton 5-ml. capacity gas-tight syringe. The sodium salt of ethylenediaminetetraacetic acid (EDTA) at 50 mg./liter is incorporated into each salt solution to minimize lipoprotein deterioration. Once formed, the NaCl gradient itself is surprisingly stable, although it is changing continuously with time during the run. In order to monitor densities, a NaCl reference gradient is made and centrifuged along with the lipoprotein-containing gradient solutions. Thus, it is possible to maintain control of solution background densities and, following lipoprotein fractionation, to manipulate the densities of the solutions fractionated accurately to the reference density of 1.063 g./ml. All densities were determined to approximately ±0.0003 unit by refractometric measurements using an Abbe Precision refractometer.

It is to be noted in Fig. 3 that the density gradient set up in the preparative tube is not linear, but is deliberately made abrupt in the region of the seventh ml. (in depth). This condition seems desirable since following layering and during the early phase of flotation, there develops a substantial lipoprotein gradient upward from the layered boundary. Since these lipoproteins are of from 0.92–1.00 g./ml. in hydrated density, they can give rise to a negative density gradient, which potentially might disturb the stability of the system. As the lipoproteins first move out from the layered region, this density gradient is steepest and is proportional to the concentration gradient itself. In the later

(15) O. deLalla and J. Gofman, in "Methods of Biochemical Analysis," Vol. I, D. Glick, ed., Interscience Publishers, Inc., New York, N. Y., 1954, p. 459.

(16) Wherever the symbol S_f without a subscript is used in this paper it refers to flotation in a NaCl solution of ρ = 1.063 at 26°.

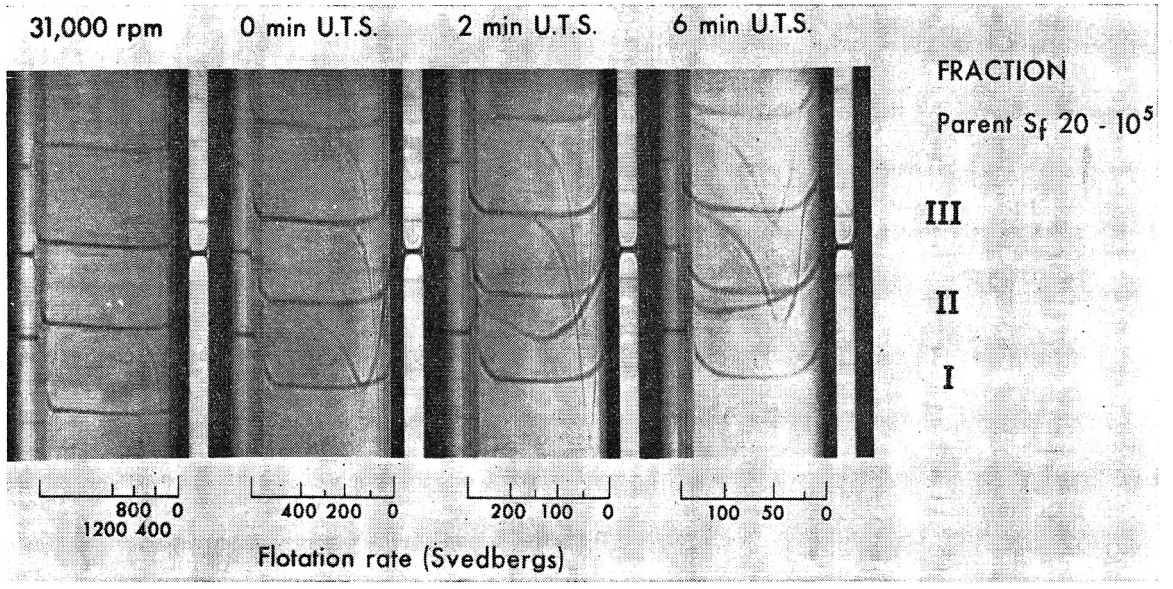

Fig. 4.—Ultracentrifugal schlieren photographs of the parent S_f 20–10^5 lipoprotein fraction (serum sample I) and subfractions I, II, and III. Approximate concentrations for each fraction from top to bottom were approximately 4, 6, 15, and 16 C_0 (C_0 referring to initial serum concentration). Samples were ultracentrifuged in a 4-place analytical rotor at a temperature of 26.0°. An acceleration time of approximately 5.20 min. was required to achieve full speed (52,640 r.p.m.).

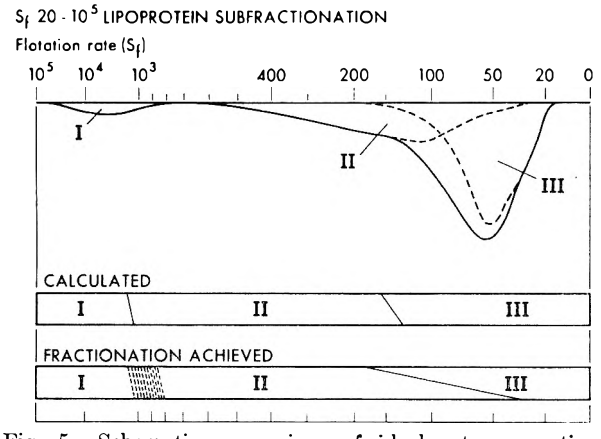

Fig. 5.—Schematic comparison of ideal rate separation anticipated with actual fractionation achieved (Sample I).

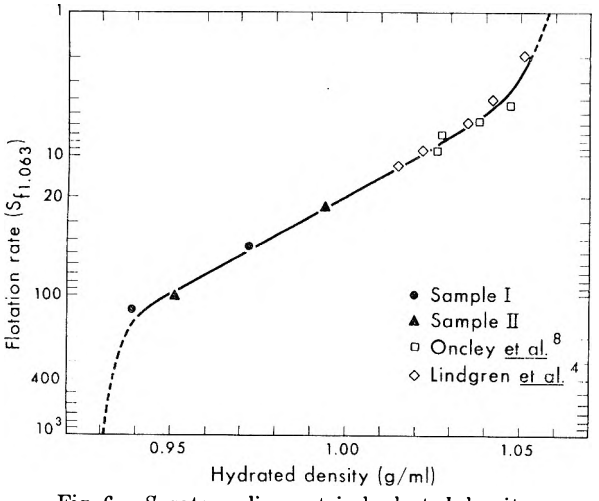

Fig. 6.—S_f rate *vs.* lipoprotein hydrated density.

phases of flotation, as the lipoproteins migrate into the top region of the preparative tube, this lipoprotein concentration gradient is progressively reduced and may ultimately be reversed. Thus, at the end of the first run (2 hr.) the S_f 1590–10^3 lipoproteins have all theoretically migrated to the top of the preparative tube, yet there remains a "negative" lipoprotein density gradient as the result of an increase in lipoprotein concentration with depth. Without the salt gradient to stabilize the system, serious convective disturbances would result. After the second run (18 hr.), the S_f 131–1590 lipoproteins have floated to the top and there remains a relatively subtle S_f 20–157 lipoprotein gradient that may be either slightly negative or positive depending upon the depth in the preparative tube.

Results and Discussion

S_f 20–10^5 lipoproteins (Samples I and II) were fractionated from sera prepared from non-fasting blood of two normal males aged 37 and 46 years, respectively. Ultracentrifugal schlieren photographs for the three subfractions as well as from the parent S_f 20–10^5 lipoprotein fraction (serum sample I) are shown in Fig. 4. It is readily seen that fraction I contains no ultracentrifugally resolvable lipoproteins, indicating the absence of lipoproteins of flotation rate less than approximately S_f 800 (above S_f 800 lipoprotein turbidity effectively prevents visualization on the schleiren photographs). Although differing markedly in lipoprotein distributions, fractions II and III show considerable overlap, particularly in the range of S_f 25 to S_f 150. Notwithstanding this imperfect fractionation, it appears that a practical degree of subfractionation has been achieved. For evaluation, Fig. 5 compares schematically fractionation anticipated (by calculation) under ideal conditions with the fractionation actually achieved. Fractionation was performed on another S_f 20–10^5 lipoprotein preparation (Sample II) with similar results. It would appear that improvement in fractionation might be achieved by slight alteration of the salt gradient shown in Fig. 3. Thus, if in the region of the seventh ml. (in depth) two 0.5 ml. volumes of salt solution of approximate density 1.030 and 1.045 g./ml. were introduced, a more favorable gradient

might be obtained resulting in greater stability, particularly during the early phase of flotation. Ideally, a gradient machine[17] might be usefully employed to optimize the entire gradient.

An ηS *vs.* ρ study was made on subfractions II and III isolated from both parent S_f 20–10^5 lipoprotein samples. Due to the limited amount of lipoprotein, these studies included only two points at densities of approximately 1.063 g./ml. and 1.031 g./ml. The resultant hydrated densities obtained are shown in Fig. 6 which also shows earlier data[7,11] of hydrated densities determined on isolated subfractions of the S_f 0–20 lipoprotein class. Thus, from these combined data, it is now possible to estimate with some accuracy the hydrated density of any low-density serum lipoprotein within the entire S_f 0–400 class.

Another consideration is, of course, the lipid chemical composition of these sub-fractions and a comparison with the composition of the parent S_f 20–10^5 fraction. A preliminary lipid chemical analysis by infrared techniques[18] has been made on the subfractions of Sample I and the data are presented in Table I. It is seen that the glyceride content increases significantly with increasing S_f rate. Other features of composition shift include a sharp drop in cholesterol and phospholipid content with increasing S_f rate. Detailed fatty acid data have been determined and shall be reported elsewhere[19] on all chemical fractions of each lipoprotein subfraction. Preliminary results suggest some differences in the fatty acid distribution obtained from the glyceride, cholesteryl ester, and phospholipid fractions. These glyceride data are consistent with dietary and fat ingestion studies[20,21] which indicate a marked influence of the recently absorbed fat on the composition of the S_f 20–10^5 lipoproteins.

TABLE I

	Parent S_f 20–10^5	Fraction III	Fraction II	Fraction I[a]
Cholesteryl esters	16.6	19.4	9.6	*ca.* 19
Unesterified cholesterol	13.3	11.1	9.2	*ca.* 4
Glycerides	51.1	49.0	64.0	*ca.* 68
Unesterified fatty acids	2.1	2.5	2.8	*ca.* 2
Phospholipids	16.9	18.0	14.3	*ca.* 7

[a] Values uncertain because of the limited amount of total sample size (less than 0.5 mg.).

Acknowledgment.—We thank Mr. Leslie O. Seaborn of the Inorganic Materials Research Laboratories (Lawrence Radiation Laboratory, Berkeley) for carrying out the stress and failure tests on the trunnions, as well as Mr. George E. Jolis and Mr. Jack L. Hill (Lawrence Radiation Laboratory, Livermore) for radiographs and ultrasonic inspection of the rotor assembly. We particularly wish to thank Mr. Pete Dowling and Mr. Jack Kroll (Lawrence Radiation Laboratory, Berkeley) for their helpful suggestions and craftsmanship during the construction of the complete rotor assembly and test fixtures. Also, we appreciate the helpful analysis made by Dr. Karl S. Pister (University of California Engineering Department, Berkeley) of the bending moment developed during stress of the trunnion.

DISCUSSION

R. TRAUTMAN (Plum Island Animal Disease Laboratory, USDA).—Would you, and perhaps Dr. Anderson, care to straighten out the terminology involved in these rate and isodensity procedures?

F. T. LINDGREN.—Yes, I will try. First of all, the subfractionation of the S_f 20–10^5 lipoproteins as presented here is on the basis of differences in flotation rate. The gradient is utilized only for stabilizing the flotation system and to prevent the occurrence of density inversions within regions of the preparative tube during lipoprotein flotation. By collecting *successive* fractions of lipoproteins at the top of the preparative tube, fractionation over essentially the full radial path of the fluid column is utilized. If only a *single* run were made, and the entire contents of the preparative tube were fractionated, greater overlapping of the subfractions would be anticipated. It is with these considerations that the term "accumulative (flotation) rate separation" is employed. In contrast, fractionation by differences in sedimentation rate over a density gradient (rate zonal centrifugation) usually is employed for mixtures of discrete molecular or particulate entities and this is accomplished during a *single*, critical preparative run (ref. 9). The individual molecular species separate on the basis of their different sedimentation rates during such a single run into zones at various depths in the preparative tube. The strictly analogous sedimentation procedure (to our presentation) would be to make *several* preparative runs, and after the conclusion of each one, to collect successive fractions from the bottom of the preparative tube. Although this might be technically difficult, I believe it was suggested as one variation of "gradient differential centrifugation" by Dr. Anderson (ref. 10). Isodensity centrifugal procedures, of course, involve a *single* preparative run in which the density of a region within the preparative tube is appropriately adjusted or becomes equal under the conditions of centrifugation to the density of the molecules or particles being fractionated. Ideally, centrifugation proceeds until only those molecules or particles desired are found within the region of the preparative tube where the densities of the solution and particles are equal.

(17) N. G. Anderson, *Rev. Sci. Instr.*, **26**, 891 (1955).

(18) N. K. Freeman, F. T. Lindgren, Y. O. Ng, and A. V. Nichols, *J. Biol. Chem.*, **227**, 449 (1957).

(19) A. V. Nichols, F. T. Lindgren, and R. D. Wills, in preparation.

(20) J. H. Bragdon and A. Karmen, *J. Lipid Res.*, **1**, 167 (1960).

(21) A. V. Nichols, C. S. Rehnborg, F. T. Lindgren, and R. D. Wills, *ibid.*, **3**, 320 (1962).

STUDIES ON BISMUTH ALLOYS. I. LIQUIDUS CURVES OF THE BISMUTH–COPPER, BISMUTH–SILVER, AND BISMUTH–GOLD SYSTEMS[1]

BY MARCEL W. NATHANS AND MARJORIE LEIDER

Lawrence Radiation Laboratory, University of California, Livermore, California

Received August 10, 1961

The liquidus curves of the Bi–Cu, Bi–Ag, and Bi–Au systems were redetermined by a sampling method. The Bi–Ag curve was somewhat shifted from the previously determined location. The eutectic was found at 262.5 ± 0.2° at 4.95 ± 0.05 atom % silver (2.62 wt. %). The Bi–Cu liquidus agreed fairly well with Kleppa's data over the range investigated by him. The eutectic was determined to be at 270.6 ± 0.1° at 0.46 atom % copper (0.14 wt. %). The Bi–Au liquidus did not agree well with the few experimental data available. Below the peritectic temperature, a completely new liquidus curve was established. The peritectic was found at 371 ± 2° by means of differential thermal analysis, the composition being 23.1 atom % gold (24.1 wt. %). The eutectic is at 13.4 ± 0.2 atom % gold (14.1 wt. %) at 241.5 ± 0.5°. The heats of fusion of the four elements agreed reasonably well with the literature values, except that of bismuth. The results show that the sampling method is, for many cases, well adapted for the determination of liquidus curves.

Introduction

During an investigation of the distribution of small amounts of ternary additions to binary systems involving bismuth, it was found that liquidus data were obtained which differed from those reported in the literature. It was, therefore, considered useful to examine the systems involved in more detail. We are reporting here the results of our liquidus determinations of the binary systems of bismuth with copper, silver, and gold.

These three systems were investigated many years ago by thermal analysis. The results are summarized by Hansen and Anderko.[2]

The Bi–Cu system has been investigated by Jeriomin,[3a] Hiorns,[3b] Portevin,[4] and Heycock and Neville,[5] as well as by Kleppa[6] and others. Although the oldest, Heycock and Neville's work stands among the most precise thermal analyses ever done. Unfortunately, their investigations cover only very dilute solutions, and their materials did not always have the purity available today.

Kleppa used a sampling method which was quite adequate, but he, too, did not cover the complete liquidus range. Among the various determinations by thermal analysis, the work of Jeriomin and that of Heycock and Neville are the most consistent. Kleppa's data do not agree entirely with those of Jeriomin. The sampling data lie above Jeriomin's liquidus.

The eutectic point has been reported at about 0.6° below the melting point of bismuth and at about 0.7 atom % bismuth by Heycock and Neville,[7] and at 0.48 atom % bismuth by Kleppa.[6]

The Bi–Ag liquidus has been investigated by Heycock and Neville[5,7,8] and by Petrenko.[9] Only the latter author covered the entire liquidus range. Recently a portion has been examined by Kleppa.[10] Petrenko reports a eutectic at 262° and 95.3 atom % bismuth.

The Bi–Au system was investigated by Vogel,[11] who reported a eutectic at 240° and 81.1 atom % bismuth. Later, an incongruently melting compound, Au_2Bi, was found by de Haas and Jurriaanse.[12] The peritectic was stated to be at 373°.[13] The fact that Vogel did not observe the peritectic can be explained by the small number of his data and the apparent sluggishness of the formation of Au_2Bi.

The method which we have used consisted of sampling the liquid phase and analyzing the sample. In a few cases sampling yields liquidus curves which coincide with curves obtained from thermal analysis. Generally, however, curves obtained by sampling lie higher than those obtained by thermal analysis. (See, for example, a number of cases cited by Nathans.[14]) The sampling method yields more reliable data because it is a direct measurement under equilibrium conditions, provided that the existence of equilibrium can be ascertained and that a clear separation of the two phases can be effected.

Experimental

Equipment.—The apparatus was a stainless-steel furnace tube with a gas inlet at the bottom, a cooling coil at the top, a flanged head having an opening for a stirrer, a thermocouple well, and a sampling tube. All seals were made by means of O-rings or garlock gaskets. Sampling was done with 2- or 3-mm. i.d. Pyrex or quartz tubes with a piece of porous graphite (National Carbon Co. grade 40) press-fitted into one end to serve as a filter. The sampling tube was inserted into the melt by first passing it through a piece of glass tubing fitted at the top with a rubber cap and at the bottom with a ground glass ball joint. This assembly was attached directly to the furnace sampling tube, which was provided with a ball valve, so that the furnace atmosphere could always be kept isolated. A Norton high-purity alumina crucible contained the melt. The crucible was located inside a graphite secondary with a heavy graphite top as an oxygen getter. The top had suitably located holes for the stirrer, etc. The furnace assembly was inserted in a Kanthal-wound Hevi-Duti clam shell type furnace, 3-in. i.d. and 18-in. long, placed on end. Provisions were made to evacuate or pressurize the furnace or the sampling tube.

Temperatures were measured with a Pt–Pt (10% Rh) thermocouple with its cold junction in an ice bath. The thermocouple was calibrated at the melting points of copper, aluminum, zinc, lead, and tin (NBS certified), and at the

(1) This work was performed under the auspices of the U. S. Atomic Energy Commission.

(2) M. Hansen and K. Anderko, "Constitution of Binary Alloys," 2nd edition, McGraw–Hill Book Co., New York, N. Y., 1958.

(3) (a) K. Jeriomin, *Z. anorg. Chem.*, **55**, 412 (1907); (b) A. H. Hiorns, *Trans. Faraday Soc.*, **1**, 179 (1905).

(4) A. Portevin, *Rev. Met.*, **4**, 1077 (1907).

(5) C. T. Heycock and F. H. Neville, *Phil. Trans. Roy. Soc.* (London), **A189**, 46 (1897).

(6) O. J. Kleppa, *J. Am. Chem. Soc.*, **74**, 6050 (1952).

(7) C. T. Heycock and F. H. Neville, *J. Chem. Soc.*, **61**, 893 (1892).

(8) C. T. Heycock and F. H. Neville, *ibid.*, **65**, 73 (1894).

(9) G. I. Petrenko, *Z. anorg. Chem.*, **50**, 136 (1906).

(10) O. J. Kleppa, *J. Phys. Chem.*, **60**, 446 (1956).

(11) R. Vogel, *Z. anorg. Chem.*, **50**, 145 (1906).

(12) W. J. de Haas and F. Jurriaanse, *Naturwiss.*, **19**, 706 (1931).

(13) F. Jurriaanse, *Z. Krist.*, **90**, 322 (1935).

(14) M. W. Nathans, AEC Rept. No. ANL-5753, July, 1957.

boiling points of *p*-dichlorobenzene and water. The calibration was checked periodically, but no change greater than 0.2 μv. was observed. The temperatures were read to 0.1° with a Rubicon model 2745 potentiometer.

Procedure.—Weighed amounts of each of the two components whose binary liquidus was to be determined were placed in the crucible. The total weight in each case was 400–500 g. In a number of experiments, about 60 to 100 mg. of a ternary addition was present as a radioactive tracer so that data of the type described in a subsequent article[15] could be obtained simultaneously. The effect of this small amount of impurity on the binary liquidus is negligible. About five separate overlapping runs were made to define each curve. This was necessary because sampling became impossible when about a third of the total had precipitated. After loading and emplacement, the furnace was flushed with high-purity nitrogen. Throughout an experiment, the pressure in the furnace was kept about 250 mm. above atmospheric with nitrogen in order to impede the diffusion of small amounts of air through small leaks. The Bi–Cu and Bi–Ag melts were stirred with a tungsten rod flattened at the lower end. Stirring was usually continued during sampling. Bi–Au melts were agitated periodically with the thermocouple well to prevent pick-up of the stirrer metal by the melt. Agitation by gas bubbling through a tube was tried, but later abandoned because the bubbling rate was difficult to control. Although no record was kept of whether the melt was stirred during sampling or not, it was concluded from plots of the data that it did not matter. No particles passed the filter to a detectable degree. This also was checked on several occasions by taking a sample without filter after a suitable settling period.

The charge was generally heated to about 100° above the estimated liquidus temperature and kept there for at least 30 min. One or two samples were taken to check the composition of the melt. Further samples were taken at successively lower temperatures by pressurizing the melt, by suction on the sampling tube, or both. The temperature was held constant for about 15 min. before sampling. Control of the sample size usually was poor. Most sample weights varied between 5 and 15 g. The sample size usually became smaller when a large amount of precipitate had formed. This probably was caused by the increased viscosity of the mass. Following a series of samplings during cooling, a few points were obtained by reheating the melt. In every instance these points fall on the curve obtained from a cooling cycle, showing the existence of true equilibrium. This also was confirmed by a few samples taken after varying periods of constant temperature.

Experiments in the Bi–Cu and Bi–Ag systems above 600° were carried out under a layer of purified flake graphite as additional insurance against oxygen pick-up by the melt. In these experiments, it often was impossible to obtain good samples, probably in part because the filter became clogged when the sampling tube passed through the graphite layer. Sometimes the filter could be reopened, however, by blowing nitrogen through it prior to sampling.

A few points also were obtained by thermal analysis, either before or after a series of samplings. Cooling curves were determined at a cooling rate of about 2–3°/min.

Analytical.—In each case, the entire sample was dissolved in either 8 to 10 *N* HNO_3 or in aqua regia (when gold was present). The samples were analyzed for both components except when a large excess of one interfered with the analysis of the other.

Bismuth was determined by titration with EDTA (about 0.1 *N*). Aliquots containing about 20 mg. of bismuth were added to a solution having a pH less than 2, and containing a few grams of thiourea as indicator and complexing agent. The titrations were carried out at a pH between 2.1 and 2.4. The accuracy was quite sensitive to the pH.

Copper was determined electrolytically after a separation from bismuth. This separation was done by carefully neutralizing the solution with ammonia to a pH of 6 to 7, followed by the addition of ammonium carbonate to prevent the co-precipitation of the copper with the bismuth hydroxide, and filtering. A complete separation from bismuth can be effected by redissolving the precipitate in nitric acid and treatment with ammonium hydroxide and ammonium carbonate, a second and a third time.[6]

In later samples, copper was determined spectrophotometrically with a Cary recording spectrograph. The 807 mμ band was found suitable. Bismuth did not interfere, but the intensity was dependent upon the nitric acid concentration. The acid variation was held small, however, by diluting a suitable aliquot with a 40-fold volume of 2 *N* nitric acid in a volumetric flask. The effect of dust particles in the acid was eliminated by letting the solutions stand overnight and transferring them to the cells with a transfer pipet.

Silver was determined electrolytically in an ammoniacal solution from its EDTA complex. Bismuth did not interfere. Gold was determined coulometrically with a controlled-potential coulometer.[16]

All analyses had a precision of better than ±1%. Material balances were, in all but a few isolated cases, between 99 and 100.5%.

Materials.—**Bismuth:** 99.999% pure droplets from American Smelting and Refining Co., m.p. 271.4°. The major impurity is 0.0001–0.001 % Mg. **Copper:** OFHC copper from stock, m.p. 1083°. The major impurity is 0.0001–0.001 % Ag. **Silver:** 99.99% pure needles from Fairmont Chemical Co., m.p. 961°. The major impurities are 0.001–0.01% Cu and 0.0001–0.001 % Mg. **Gold:** 99.95% pure scrap from stock. The major impurities are 0.003–0.03% Ag, 0.003–0.03% Pd, 0.001–0.01% Pb, and 0.001–0.01% Cu.

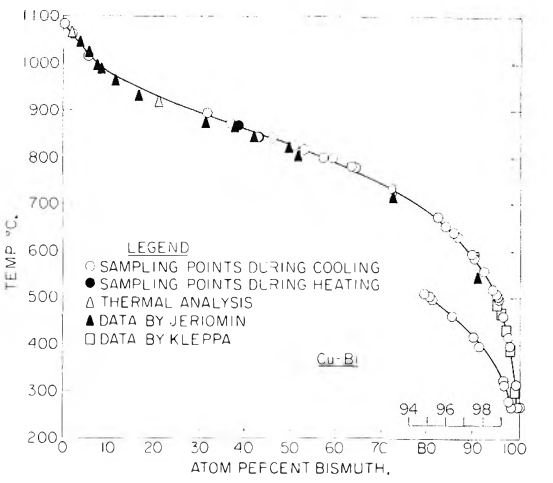

Fig. 1.—Liquidus of the bismuth–copper system.

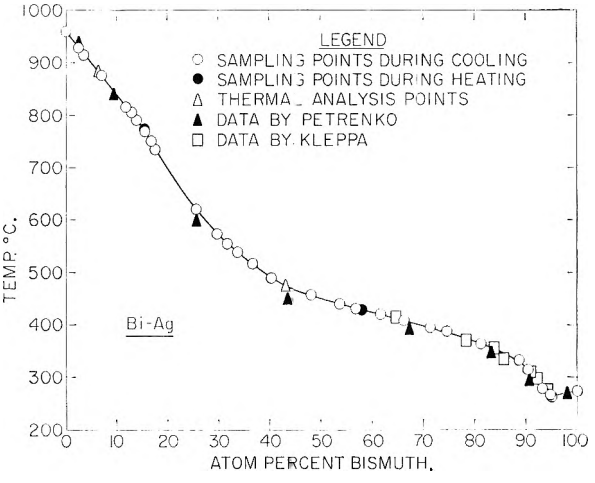

Fig. 2.—Liquidus of the bismuth–silver system.

Results and Discussion

The results are shown in Fig. 1–3, the curves having been drawn from our data alone. Rather than tabulating our actual experimental data,

(15) M. W. Nathans and M. Leider, to be published.

(16) J. E. Harrar and F. B. Stephens, *J. Electroanal. Chem.*, **3**, 112 (1962).

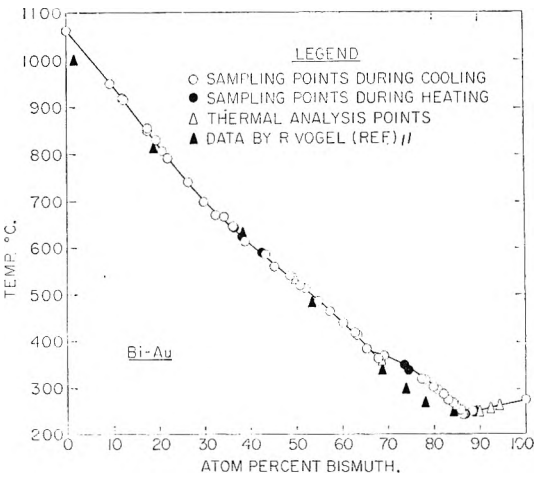

Fig. 3.—Liquidus of the bismuth–gold system.

we show in Tables I through III data as read from the smoothed curves before reproduction. We also have indicated the mean deviation of the experimental data from the curves.

TABLE I

SMOOTHED LIQUIDUS DATA FOR THE Cu–Bi SYSTEM[a]

Temp., °C.	Atom % Cu	Temp., °C.	Atom % Cu
1083	100	650	15.5
1070	98.95	600	11.1
1050	97.35	550	7.3
1025	95.2	525	5.9
1000	92.7	500	4.76
975	89.0	460	3.53
950	83.6	440	2.95
925	77.5	420	2.44
900	70.7	400	2.03
875	63.4	380	1.65
850	56.2	360	1.35
825	49.3	340	1.08
800	43.0	320	0.74
775	36.9	300	0.56
750	31.4	280	0.50
725	26.5	270.6[b]	0.46
700	22.1	271.4	0.00

[a] Standard deviation: 0.2 atom %, 450–700°; 1.4 atom %, 700–1083°. [b] Eutectic, ±0.1°.

TABLE II

SMOOTHED LIQUIDUS DATA FOR THE Ag–Bi SYSTEM[a]

Temp., °C.	Atom % Ag	Temp., °C.	Atom % Ag
961	100	460	53.1
950	99.1	450	50.0
925	94.9	430	42.4
850	90.8	420	38.3
800	86.7	410	34.7
750	83.2	400	31.0
700	80.1	390	27.2
650	76.6	380	23.7
600	72.6	360	17.6
575	70.2	340	13.25
550	67.6	320	10.05
520	63.9	300	7.77
500	61.1	280	6.08
480	57.9	270	5.42
		262.5[b]	4.95

[a] Standard deviation: 0.3 atom %, 260–400°; 0.1 atom %, 400–960°. [b] Eutectic.

TABLE III

SMOOTHED LIQUIDUS DATA FOR THE Au–Bi SYSTEM[a]

Temp., °C.	Atom % Au	Temp., °C.	Atom % Au
1063	100	450	41.2
1050	98.8	400	35.9
1000	94.5	371	33.1[b]
950	90.4	350	27.0
900	86.4	325	23.0
850	82.5	300	19.8
800	78.5	270	16.4
750	74.4	241.1[c]	13.2
700	69.9	250	10.0
650	64.6	260	6.0
600	59.0	270	0.9
550	52.9	271.4	0
500	46.7		

[a] Standard deviation: 0.3 atom %, 240–371°; 0.5 atom %, 371–700°; 0.2 atom %, 700–1065°. [b] Peritectic. [c] Eutectic, ±0.3°.

The few points obtained during reheating agree well with those obtained during cooling. A small number of points obtained by thermal analysis deviate little from the curves.

It appears that at higher copper contents the copper precipitate is rather fine and does not settle rapidly. Samples were taken without a filter from a composition containing about 95% copper. The analyses showed too high a copper content, which indicates poor phase separation, so that the use of a filter is necessary.

In the gold–bismuth system, the sampling data near the peritectic were quite erratic. Our explanation is that the rate of formation of the compound is slow, and that there is still some tendency for pure gold to precipitate as a metastable phase. This could explain why Vogel did not observe the change in slope of the liquidus.[11]

An attempt was made to obtain sampling data on the bismuth-rich side of the silver–bismuth eutectic. We obtained only one point by sampling but were able to get two points by thermal analysis. We feel that this was sufficient to establish this part of the liquidus to about 5% relative to the silver content. The eutectic data are the average of three separate experiments, including a determination from the bismuth-rich side in the case of Bi–Ag.

The Au–Bi peritectic can be established by the intersection of the two parts of the liquidus. It was determined separately, however, with a sample containing about 80 wt. % Au_2Bi and 20% gold. This sample was obtained by treating an ingot originally containing about 50% gold with 8 *N* nitric acid thus removing the excess bismuth. It was subjected to differential thermal analysis with aluminum powder as the inert in a dynamic argon atmosphere and at an upheat rate of 10°/min. Figure 4 shows this record. Concurrently, the temperature of the sample was measured with a potentiometer. The peritectic was established at 371 ± 2°.

The agreement of our liquidus curves with the older data is fair to poor, but is good with Kleppa's data for the Bi–Cu and Bi–Ag systems. The validity of our data was checked by calculating

the heats of fusion from the terminal slope of a log (atom % solute) *vs.* $1/T$ plot. We estimated the distribution coefficient of Bi between solid and liquid Ag as 0.1 from the data given by Hansen and Anderko.[2] Solid solubility was neglected in the remaining cases. Table IV shows a comparison between our calculated values and those chosen by Hultgren from heat content measurements.[17] The data agree well, except for bismuth. This may warrant further investigation.

TABLE IV

HEATS OF FUSION OF Cu, Ag, Au, AND Bi

Element	Cu	Ag	Au	Bi
ΔH_m[a] calcd.	2940	2780	2870	3130[b]
ΔH_m[a] lit.	3120	2855	2955	2600

[a] Calories per gram atom. [b] Average of values 3100, 3300, and 3000 from the Cu–Bi, Ag–Bi, and Au–Bi systems, respectively.

Acknowledgments.—We wish to acknowledge the valuable help and suggestions afforded us by the following members of the analytical laboratory. Dr. R. Bystroff, for his help with the spectrophotometric copper determination, Dr. J. Harrar, for his help with the coulometric gold determination, and Mrs. P. Stephas.

(17) R. Hultgren, Project Supervisor, "Selected Values, Thermodynamic Properties of Metals," Prepared for the USAEC at the Minerals Res. Lab., University of California, 1956.

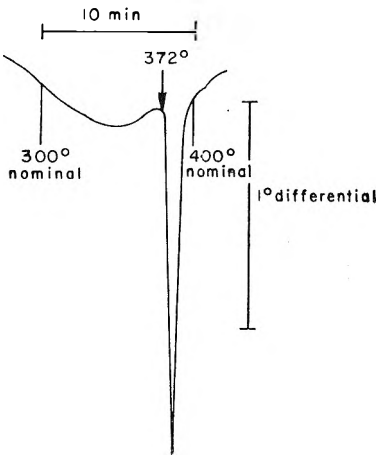

Fig. 4.—Differential thermogram of Au_2Bi.

DIFFUSION IN AN IDEAL MIXTURE OF THREE COMPLETELY MISCIBLE NON-ELECTROLYTIC LIQUIDS—TOLUENE, CHLOROBENZENE, BROMOBENZENE

BY JOHN K. BURCHARD AND H. L. TOOR

Department of Chemical Engineering, Carnegie Institute of Technology, Pittsburgh 13, Pennsylvania

Received October 30, 1961

A modification of the diaphragm cell method has been used to investigate isothermal diffusion in the thermodynamically near ideal liquid system, toluene–chlorobenzene–bromobenzene. Measurements of the binary diffusion coefficients were carried out on the borders of the ternary system. The diffusion coefficients of the systems toluene–chlorobenzene and bromobenzene–chlorobenzene agreed with measurements made elsewhere and the diffusion coefficients of all three binary systems are linear in mole fraction. In the ternary system the difference between the binary diffusion coefficients of any two dilute species in a third species is small. The ternary system was studied at six points covering the whole concentration range. The results are fairly well described by a modification of the diffusion equations for ideal, multicomponent gas mixtures. It is shown from the phenomenological equations that in the absence of cross diffusion coefficients the main coefficients are equal. This is approximately true in the system studied, for the cross diffusion coefficients and the differences between the main diffusion coefficients are an order of magnitude less than the main diffusion coefficients. Consequently, one diffusion coefficient will give an adequate description of this ternary system under most conditions. This diffusion coefficient is found to be simply the molar average of the binary diffusion coefficients at infinite dilution.

Introduction

The relationship between the concentration gradients and diffusion fluxes in systems of more than two components is of considerable practical as well as theoretical interest. Although in sufficiently dilute systems Fick's Law as applied to each species may satisfactorily describe the diffusion process, recent work using the Gouy interferometer has shown that equations which account for interacting flows generally are needed. Such work[1-9] has been concerned with aqueous solutions with one or both solutes electrolytes or sugars, and usually one or both of the solutes has been relatively dilute.

One very interesting class of multicomponent systems which has not been studied is that which is made up of completely miscible non-electrolytic liquids. In these systems the diffusion may be studied over a composition range which includes all ternary and binary combinations of the components, and the object of the present study is to determine the rates of diffusion in a ternary system of this type as functions of the concentrations and concen-

(1) D. M. Clarke and M. Dole, *J. Am. Chem. Soc.*, **76**, 3745 (1954).
(2) R. L. Baldwin, P. J. Dunlop, and L. J. Gosting, *ibid.*, **77**, 5235 (1955).
(3) P. J. Dunlop and L. J. Gosting, *ibid.*, **77**, 5238 (1955).
(4) H. Fujita and L. J. Gosting, *ibid.*, **78**, 1099 (1956).
(5) P. J. Dunlop, *J. Phys. Chem.*, **61**, 994 (1957).
(6) P. J. Dunlop, *ibid.*, **61**, 1619 (1957).
(7) P. J. Dunlop, *ibid.*, **63**, 612 (1959).
(8) I. J. O'Donnell and L. J. Gosting, "The Structure of Electrolytic Solutions," John Wiley and Sons, New York, N. Y., 1957, Chapter 11.
(9) F. E. Weir and M. Dole, *J. Am. Chem. Soc.*, **80**, 302 (1958).

tration gradients over the complete range of compositions.

The phenomenological equations for a ternary system may be written in the form[2]

$$J_i = -\sum_{j=1}^{2} D_{ij} \nabla C_j, \; i = 1,2 \qquad (1)$$

where J_i is the flux with respect to a coördinate moving at the volume average velocity, ∇C_i is the concentration gradient of species i, and the D_{ij} are the multicomponent diffusion coefficients. The flux and gradient of the third species are not independent quantities and are not included in the above equations. In this study, unlike earlier ones,[1-9] there is no distinction between solutes and solvent, so species 3 is arbitrary. The equation for this third species can be derived from eq. 1 and, if there is no volume change on mixing, it may be written in the form

$$J_3 = \left[(D_{11} - D_{22}) \frac{\bar{v}_1}{\bar{v}_3} + \frac{D_{21}\bar{v}_2^2 - D_{12}\bar{v}_1^2}{\bar{v}_2\bar{v}_3} \right] \nabla C_1 - \left[D_{22} + D_{12} \frac{\bar{v}_1}{\bar{v}_2} \right] \nabla C_3 \qquad (2)$$

where the $\bar{v}_i$ are the partial molal volumes.

Although the above equations contain four diffusion coefficients, the Onsager reciprocal relations indicate that only three are independent.[10]

Consider now a ternary system in which the cross diffusion coefficients, D_{ij}, $i \neq j$, of *all* species are assumed to be zero so that

$$J_i = D_{ii} \nabla C_i, \; i = 1,2,3 \qquad (3)$$

Since the first bracket in eq. 2 is a cross diffusion coefficient, and since species 3 is arbitrary, it follows from eq. 1 and 2 that the main diffusion coefficients are all equal

$$D_{11} = D_{22} = D_{33} \equiv D^* \qquad (4)$$

Thus, zero cross coefficients imply equal main coefficients and *vice versa*.[11] It follows from eq. 1 and 2 that the complement of the above statement is also true; non-zero cross coefficients imply unequal main coefficients and *vice versa*.[12]

Although one might expect the above behavior in ideal systems,[13] it is desirable to have some criterion (other than "near" ideality) concerning the conditions under which eq. 3 and 4 might approximate real systems.

To this end, consider a ternary system in which cross diffusion coefficients are not assumed to be zero, but the concentrations of species 1 and 2 are allowed to approach zero together. The equations for these species should then reduce to the binary form since there should be no interactions between two sufficiently dilute species. It follows that D_{12} and D_{21} approach zero and D_{ii} approaches the binary coefficient for dilute i in 3, $\mathfrak{D}_{i3}^0$, $i = 1,2$. Thus, from eq. 1 and 2

$$\lim_{\substack{C_1 \to 0 \\ C_2 \to 0}} J_i = -\mathfrak{D}_{i3}^0 \nabla C_i, \; i = 1,2 \qquad (5)$$

$$\lim_{\substack{C_1 \to 0 \\ C_2 \to 0}} J_3 = (\mathfrak{D}_{13}^0 - \mathfrak{D}_{23}^0) \frac{\bar{v}_1}{\bar{v}_3} \nabla C_1 - \mathfrak{D}_{23}^0 \nabla C_3 \qquad (6)$$

Clearly eq. 3 and 4 are valid at this limit only if $\mathfrak{D}_{13}^0 = \mathfrak{D}_{23}^0$. Since each species in turn can be considered to be species 3, it is concluded that at least at the corners of the concentration field, the necessary and sufficient condition for the absence of cross coefficients and equality of the main coefficients is that[13]

$$\mathfrak{D}_{ij}^0 - \mathfrak{D}_{kj}^0 = 0; \; i, j, k, = 1,2,3 \quad j \neq i,k \qquad (7)$$

Although this condition may be strictly valid only in systems in which all species have identical properties, *i.e.*, in an ideal system, a real system can approximate the simple behavior of eq. 3 and 4 only if the left side of eq. 7 is small compared to the $\mathfrak{D}_{ij}^0$.

The Onsager reciprocal relationships yield an expression relating the D_{ij},[14] and for ideal systems of constant molar density it reduces to the simple form

$$D_{11} + (1 + [x_3/x_2])D_{21} = D_{22} + (1 + [x_3/x_1])D_{12} \qquad (8)$$

where the x_i are mole fractions. This equation also indicates that the main coefficients are equal when the cross coefficients are zero.

Choice of System.—It is logical to choose as the first system for study one which approaches the eq. 7 condition. The system toluene–chlorobenzene–bromobenzene exhibits this behavior. In addition, the binary diffusion coefficients of two of the three binary pairs have been measured accurately over the complete concentration ranges and found to be close to linear with mole fraction.[15]

The materials used were Fisher certified reagents. Analysis by gas chromatography showed negligible impurities.

Experimental

The diaphragm cell method was used in this study. Preliminary studies of the binary systems bromobenzene–chlorobenzene and toluene–chlorobenzene were first carried out in order to compare the diffusion coefficients obtained by this method to those obtained by Caldwell and Babb[15] by a different technique. Following this, the third binary pair, toluene–bromobenzene, was studied in order to complete the mapping of the diffusional behavior on the borders of the ternary field.

The diaphragm cell was patterned after that used by Trevoy and Drickamer.[16] The diaphragm was Pyrex fritted

(10) L. Onsager, *Ann. N. Y. Acad. Sci.*, **46**, 241 (1945).

(11) In a dilute system (dilute 1 and 2 in 3), D_{12} and D_{21} may approach zero although $D_{11} \neq D_{22}$ but, as shown later, species 3 will then have a non-zero cross coefficient.

(12) These results may be generalized to systems of more than three components.

(13) Onsager and Fuoss [L. Onsager and R. M. Fuoss, *J. Phys. Chem.*, **36**, 2689 (1932)] suggested that cross diffusion coefficients would be negligible in ideal systems.

(14) D. G. Miller, *J. Phys. Chem.*, **63**, 570 (1959).

(15) C. S. Caldwell and A. L. Babb, *ibid.*, **60**, 51 (1956).

(16) D. J. Trevoy and H. G. Drickamer, *J. Chem. Phys.*, **17**, 1117 (1949).

glass, porosity M, with Teflon stopcocks in the capillary tubes. The chamber volumes were about 25 ml. and the difference between the volumes of the chambers in a cell was less than 1.5 ml.

The working equation for the diaphragm cell with a binary system is[17]

$$\bar{\bar{\mathcal{D}}}_{12} = \frac{1}{\beta t} \ln \frac{\Delta C_1^0}{\Delta C_1^f} \qquad (9)$$

where

$$\bar{\bar{\mathcal{D}}}_{12} = 1/t \int_0^t \bar{\mathcal{D}}_{12}(t)\, dt \qquad (10)$$

and

$$\bar{\mathcal{D}}_{12}(t) = \frac{1}{C_{1R} - C_{1L}} \int_{C_{1L}}^{C_{1R}} \mathcal{D}_{12}(C_1) dC_1 \qquad (11)$$

The superscripts refer to initial and final concentrations and the subscripts to left and right hand bulbs. For equal bulb volumes and a linear dependence of $\mathcal{D}_{12}$ on concentration, $\bar{\mathcal{D}}_{12}$ is the differential coefficient at the arithmetic average composition. Since this composition does not change with time, $\bar{\bar{\mathcal{D}}}_{12} = \bar{\mathcal{D}}_{12}$.

The cell factor, β, was found by calibrating with 0.5 N HCl diffusing into water at 25°. The value of 3.078×10^{-5} cm.^{2}/sec. from Stokes' data[18] was used for $\bar{\bar{\mathcal{D}}}_{12}$ in eq. 9. The results of several replicas were: β (cell 1) = 0.2038 ± 0.0013 cm.$^{-2}$; β (cell 2) = 0.2079 ± 0.0015 cm.$^{-2}$.

The organic solutions to be used as initial charges to the two chambers were weighed to the desired compositions. The left chamber was completely filled and rinsed with C_L^0 by introducing the solution through one tube and taking the overflow through the second tube. The stopcock on the overflow tube was then closed and a vacuum applied to the other chamber pulling C_L^0 through the diaphragm. Vigorous flushing of the diaphragm to dislodge bubbles in the pores was continued for several minutes.

The cell was inverted, and the right chamber drained. The cell was then righted, and the solution C_R^0 was charged to the right chamber, filling through one tube and rinsing by overflowing through the second tube.

All four stopcocks were then closed and the cell was placed in a water bath maintained at 29.6 ± 0.03° for the preliminary diffusion period of four hours which is required to set up the quasi-steady state concentration profiles in the diaphragm.[18]

At the end of this period, the cell was removed from the bath and each chamber was drained separately, rinsed, and filled by gravity with fresh charges of the original solutions. The cell was then returned to the bath for a diffusion run of approximately one day. Several replicas were made of each run.

It was found that reproducible results could be obtained only with the diaphragm horizontal as indicated by Stokes[19] and with the denser solution on top. Under these conditions the diffusion coefficient was essentially independent of the initial concentration difference.

The final concentrations of the solutions drained from the cells were determined by gas–liquid chromatography, using a Beckman GC-2 instrument with helium as a carrier gas. A 14-ft. stainless steel 1/4 in. diameter column packed with 3% by weight Silicone 550 (Dow Corning Corp.) on firebrick gave good resolution with a short elution time. The recorder was fitted with an integrator so that peak areas as well as heights could conveniently be used in the analyses.

Samples of the original charge solutions as well as a few specially prepared samples were used to calibrate peak height and area ratios as functions of mole fraction.

In analyzing an unknown sample, five determinations of height and area ratios were made and the corresponding mole fraction ratios were read from the calibrations and averaged.

With this method of analysis, the error in a mole fraction determination was usually less than 1/2% of the corresponding mole fraction. Since these mixtures have essentially constant molar densities (partial molal volumes constant and equal) the concentration ratio in eq. 9 is also a mole fraction ratio.

(17) A. R. Gordon, *Ann. N. Y. Acad. Sci.*, **46**, 285 (1945).

(18) R. H. Stokes, *J. Am. Chem. Soc.*, **72**, 2243 (1950).

(19) R. H. Stokes, *ibid.*, **72**, 763 (1950).

Binary Results

The bromobenzene–chlorobenzene and toluene–chlorobenzene systems were each investigated at mean concentrations of 5, 50, and 95 mole %, usually with concentration differences of approximately 10 mole %. Since the results were in agreement[20] with the data obtained by Caldwell and Babb[15] with a different technique, the cells were assumed to be reliable in this type of experiment.

The toluene–bromobenzene system was investigated at mean concentrations of 5, 35, 65, and 95 mole % toluene with initial concentration differences of approximately 10 mole %. Four replicas were run at each point and the results using the more precise peak height measurements are shown in Fig. 1. As in the other binary systems, the diffusion coefficient is linear with mole fraction. The 95% confidence envelope shows the results to be good to about ±2%. The equation of the least squares line through the data is given on the graph.

The six dilute diffusion coefficients are shown in Table I. The predictions of the Wilke and Chang equation[21] are also included for comparison. The values for chlorobenzene–bromobenzene and toluene–chlorobenzene are interpolated from Caldwell and Babb's[15] data and those for the third system are from the present measurements. It is seen that eq. 7 is approximately true. These values of D_{ij}^0 are also shown at the corners of Fig. 2.

Ternary Equations for a Diaphragm Cell.—As in the corresponding binary development,[17] it is assumed that (1) a quasi-steady state is obtained, (2) the diffusion can be treated as if it were unidirectional, (3) the diffusion takes place only in the fluid, (4) the volumetric average velocity within the diaphragm is zero, and (5) the contents of the constant volume bulbs are completely mixed.

With assumptions 1, 2, and 3, eq. 1 reduces to

$$J_i = -\sum_{j=1}^{2} D_{ij} \frac{dC_j}{dz}, \; i = 1,2 \qquad (12)$$

Assumptions 1 and 2 also indicate that the J_i are independent of z, so upon integrating from left to right

$$J_i l_e = \sum_{j=1}^{2} \bar{D}_{ij} \Delta C_j \qquad (13)$$

where $\Delta C_j = C_{jL} - C_{jR}$, l_e is the effective diaphragm length, and

$$\bar{D}_{ij} = \frac{1}{C_{jR} - C_{jL}} \int_{C_{jL}}^{C_{jR}} D_{ij}(C_i, C_j)\, dC_j \qquad (14)$$

From assumption (4) J_i is the flux with respect

(20) The 95% confidence limits on the individual replicas averaged ±3.6% when peak areas were used and ±2.3% when peak heights were used. Since the average difference between the measured diffusion coefficients and values interpolated from Caldwell and Babb's data was 3.1% when peak areas were used and 2.0% when peak heights were used, there is no significant difference between the present measurements and those of Caldwell and Babb.

(21) C. R. Wilke and Pin Chang, *A. I. Ch. E. J.*, **1**, 264 (1955).

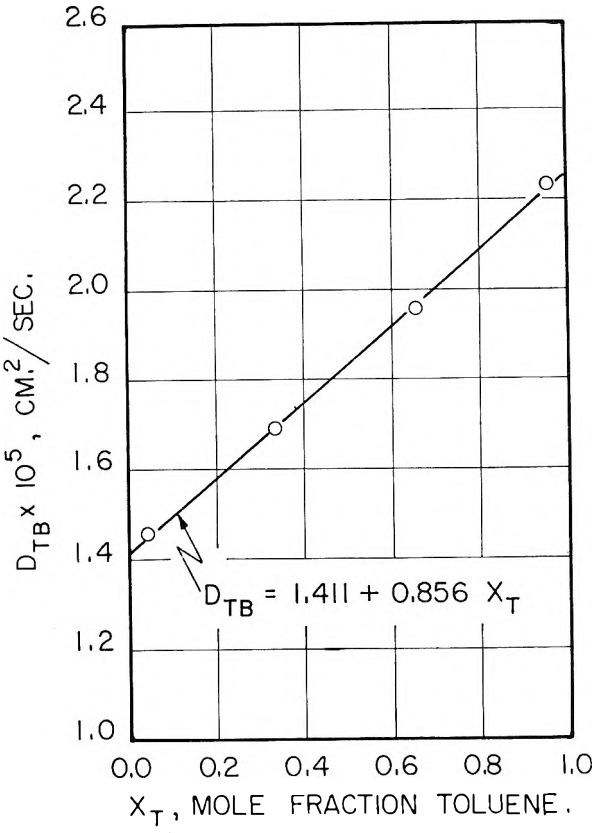

Fig. 1.—Binary diffusion coefficients toluene–bromobenzene.

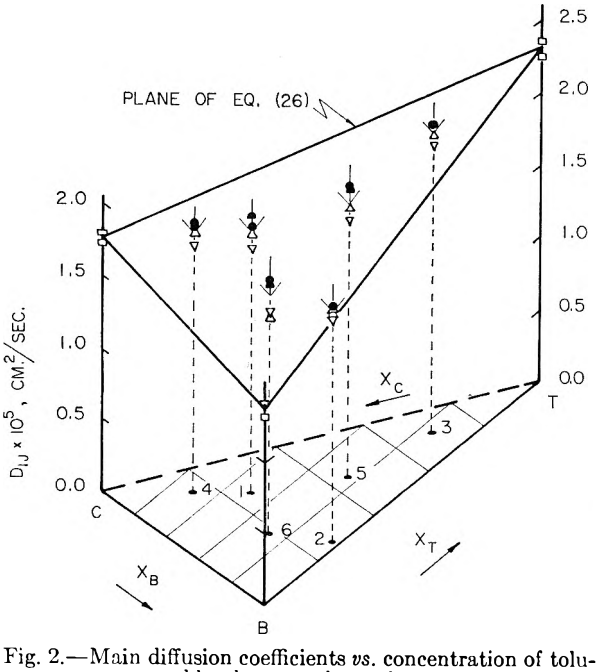

Fig. 2.—Main diffusion coefficients *vs.* concentration of toluene, chlorobenzene, bromobenzene.

to a coördinate fixed in the cell; so using assumption (5)

$$J_i = -\frac{V_L}{A_e}\frac{dC_{iL}}{dt} = \frac{V_R}{A_e}\frac{dC_{iR}}{dt} \qquad (15)$$

where V is the bulb volume and A_e the effective area of the diaphragm. Combining eq. 13 and 15

$$\frac{d(\Delta C_i)}{dt} = -\beta \sum_{j=1}^{2} \bar{D}_{ij}\,\Delta C_j,\ i = 1,2 \qquad (16)$$

where β is the same cell factor as in eq. 9.

All the assumptions except (2) have essentially the same justifications in multicomponent systems as in binary systems. Assumption (1) is valid with a properly designed cell, (3) with large enough pores in the diaphragm, (4) with a horizontal diaphragm and negligible volume changes on mixing, and (5) with mechanical or density stirring.[17] The earlier binary experiments indicate that these assumptions are valid here.[22] Assumption (2) has been shown to be unnecessary in binary systems[23] and in a similar manner this assumption can be shown to be unnecessary in a multicomponent system when the diffusion coefficients are independent of concentration.

Since the $\bar{D}_{ij}$ can be made to remain essentially constant with time, eq. 16 may be treated as a set of two simultaneous linear equations and solved by elementary methods. The solution for ΔC_i at time t is

$$\Delta C_i = H_i e^{\lambda_a t} + K_i e^{\lambda_b t},\ i,j = 1,2 \qquad (17)$$
$$i \neq j$$

where

$$H_i = -\frac{1}{2\sigma}\left[(\lambda_b + \beta\bar{D}_{ii})\Delta C_i^0 + \beta\bar{D}_{ij}\Delta C_j^0\right]$$

$$K_i = \frac{1}{2\sigma}\left[(\lambda_a + \beta\bar{D}_{ii})\Delta C_i^0 + \beta\bar{D}_{ij}\Delta C_j^0\right]$$

$$\lambda_a = -\frac{\beta}{2}(\bar{D}_{11} + \bar{D}_{22}) + \sigma$$

$$\lambda_b = -\frac{\beta}{2}(\bar{D}_{11} + \bar{D}_{22}) - \sigma$$

$$\sigma = \beta\left[\left(\frac{\bar{D}_{22} - \bar{D}_{11}}{2}\right)^2 + \bar{D}_{12}\bar{D}_{21}\right]^{1/2}$$

These equations are transcendental in the diffusion coefficients, but simple approximations which are valid in the present experiments are obtained as follows.

From eq. 16

$$\frac{1}{\beta t}\ln\frac{\Delta C_i^0}{\Delta C_i^f} = \bar{D}_{ii} + \bar{D}_{ij}\frac{1}{t}\int_0^t \frac{\Delta C_j}{\Delta C_i}\,dt,\ i,j = 1,2 \qquad (18)$$
$$j \neq i$$

If σt is small,[24] $\exp(\sigma t) = 1 + \sigma t$. Equation 17 then gives

(22) Experiments with gases [J. B. Duncan and H. L. Toor, *A. I. Ch. E. J.*, **8**, 38 (1962)] indicate that assumption (1) will be valid in a ternary experiment if it is valid in a binary experiment.

(23) H. L. Toor, *J. Phys. Chem.*, **64**, 1580 (1960).

(24) The time scale of an experiment is set by the requirement that $\ln(\Delta C_i^0/\Delta C_i^f)$ in eq. 18 be large enough for accurate measurement. This requires βt to be of the order 10^4 sec./cm.^{2}. Hence for σt to be small, the cross diffusion coefficients and differences between the main diffusion coefficients must be small compared to the main diffusion coefficients.

$$\frac{\Delta C_j}{\Delta C_i} = \frac{\frac{\Delta C_j^0}{\Delta C_i^0}\left[1 + \left(\frac{\bar{D}_{ii} - \bar{D}_{jj}}{2} - \bar{D}_{ji}\frac{\Delta C_i^0}{\Delta C_j^0}\right)\beta t\right]}{1 + \left(\frac{\bar{D}_{ii} - \bar{D}_{jj}}{2} - \bar{D}_{ij}\frac{\Delta C_j^0}{\Delta C_i^0}\right)\beta t}, \quad i = 1,2 \quad i \neq j \tag{19}$$

Now if $\Delta C_j^0/\Delta C_i^0$ is not large the variation of $\Delta C_j/\Delta C_i$ with time as given by eq. 19 is approximately linear, so if ΔC_1^0 is not small compared to ΔC_2^0 eq. 18 and 19 yield

$$\frac{1}{\beta t}\ln\frac{\Delta C_1^0}{\Delta C_1^f} = \bar{D}_{11} + \bar{D}_{12}\left(\frac{\Delta C_2}{\Delta C_1}\right)_a \tag{20a}$$

where subscript a refers to the arithmetic average of the initial and final concentration differences. Similarly, if ΔC_2^0 is not small compared to ΔC_1^0

$$\frac{1}{\beta t}\ln\frac{\Delta C_2^0}{\Delta C_2^f} = \bar{D}_{21}\left(\frac{\Delta C_1}{\Delta C_2}\right)_a + \bar{D}_{22} \tag{20b}$$

When the differences between the main diffusion coefficients and the cross coefficients are small compared to the main coefficients, eq. 20 approximates eq. 17 very closely if all the ΔC_i^0 are of the same magnitude or if ΔC_3^0 is small. Equation 20a is invalid if ΔC_1^0 is very small[25] but since ΔC_3^0 cannot be small when ΔC_1^0 is small, replacing subscript 1 by 3 in eq. 18 and 19 leads to a valid equation which can be reduced to

$$-\frac{1}{\beta t}\ln\frac{\Delta C_3^0}{\Delta C_3^f} = \left(\bar{D}_{11}\frac{\bar{v}_1}{\bar{v}_3} + \bar{D}_{21}\frac{\bar{v}_2}{\bar{v}_3}\right)\left(\frac{\Delta C_1}{\Delta C_3}\right)_a + \left(\bar{D}_{12}\frac{\bar{v}_1}{\bar{v}_3} + \bar{D}_{22}\frac{\bar{v}_2}{\bar{v}_3}\right)\left(\frac{\Delta C_2}{\Delta C_3}\right)_a \tag{20c}$$

If ΔC_2^0 is small, eq. 20b is invalid but replacing subscript 2 by 3 in eq. 18 and 19 also leads to eq. 20c. Consequently, for any arrangement of the initial concentration differences there are two legitimate independent equations which contain the four diffusion coefficients to be determined—any two of eq. 20 if all the initial concentration differences are of the same magnitude, eq. 20b and c if ΔC_1^0 is small, eq. 20a and c if ΔC_2^0 is small and eq. 20a and b if ΔC_3^0 is small.

It is apparent that two experiments with different concentration differences at the same "mean" concentration level will be needed to determine the four integral diffusion coefficients. The extraction of the point coefficients from the integral values may be carried out in general by assuming a particular concentration dependence of the D_{ij} over the range of the experiment and numerically solving eq. 12. However, the proper mean concentrations which must be used in the two experiments will also depend upon the type of concentration dependence chosen. These problems are avoided if the initial concentration differences are made small enough to keep the variation of the D_{ij} across the diffusion path small, for then the integral values may be assumed to be the point values at the arithmetic average composition.[26]

Under these conditions the same "mean" concentration is obtained in two experiments with different concentration differences by making the initial arithmetic averages of the concentrations in the two bulbs the same in both experiments. The arithmetic mean concentrations will not change with time if the bulb volumes are equal and they change only a negligible amount if, as in these experiments, the bulb volumes differ by a small amount.

In the system under study the partial molal volumes are all essentially equal so eq. 20c simplifies to

$$-\frac{1}{\beta t}\ln\frac{\Delta C_3^0}{\Delta C_3^f} = (\bar{D}_{11} + \bar{D}_{21})\left(\frac{\Delta C_1}{\Delta C_3}\right)_a + (\bar{D}_{12} + \bar{D}_{22})\left(\frac{\Delta C_2}{\Delta C_3}\right)_a \tag{20d}$$

and all concentration ratios in eq. 20 may be considered to be mole fraction ratios.

In studying an unknown system the errors caused by approximating eq. 17 by eq. 20 are unknown, so the diffusion coefficients obtained from eq. 20 must be treated as first approximations. With these values the concentration changes predicted by eq. 17 may then be compared with the measured changes or with those predicted by eq. 20. In this manner it was found that in the present study the errors introduced by the use of eq. 20 in place of eq. 17 were negligible.

Ternary Experiments and Results.—The same equipment was used in the ternary and binary experiments except for the replacement of one of the cells. The technique used in the ternary work differed from that used in the binary study only in the analysis of composition. In the ternary work an extra set of calibration curves had to be constructed and instead of calculating separate mole fractions from the measurements of peak height and area ratios, the mole fraction ratios determined by both of these methods were immediately averaged and the average values were then used to calculate mole fractions.

In order to cover the concentration range inside the ternary concentration field, data were taken at six mean concentrations. At each of these mean concentrations two or three experiments were carried out with different initial concentration differences as shown in Table II. Subscript T refers to toluene, C to chlorobenzene, and B to bromobenzene. Each experiment was repeated at least once.

(25) If ΔC_1^0 is identically zero and σt is small, eq. 17 gives approximately

$$\frac{\Delta C_1^f}{\Delta C_3^0} = -\bar{D}_{12}\beta t \exp\left[-\frac{\beta t}{2}(\bar{D}_{21} + \bar{D}_{22})\right]$$

but this equation is not very useful for the determination of diffusion coefficients. If $\bar{D}_{21} = \bar{D}_{11} - \bar{D}_{22} = 0$ the equation is exact, but if eq. 8 is valid, $D_{12} = 0$, and the result is trivial.

(26) If the cross diffusion coefficients are zero and the main coefficients are linear with composition, it can be shown that the measured integral coefficients are still the point values at the arithmetic average composition.

TABLE I

EXPERIMENTAL AND CALCULATED[21] DILUTE BINARY DIFFUSION COEFFICIENTS, CM.²/SEC. × 10⁵

Temperature + 29.6°

System (first component dilute)	$\mathfrak{D}_{ij}^0$ (expt.)	$\mathfrak{D}_{ij}^0$ (calcd.)
Chlorobenzene in bromobenzene	1.36	1.58
Toluene in bromobenzene	1.41	1.58
Bromobenzene in chlorobenzene	1.76	2.09
Toluene in chlorobenzene	1.80	1.89
Chlorobenzene in toluene	2.36	2.60
Bromobenzene in toluene	2.27	2.58

TABLE II

MEAN CONCENTRATIONS AND NOMINAL INITIAL CONCENTRATION DIFFERENCES

Expt.	$\bar{x}_T$	$\bar{x}_C$	$\bar{x}_B$	Δx_T^0	Δx_C^0	Δx_B^0
1-I	0.25	0.50	0.25	0	0.10	−0.10
1-II	.25	.50	.25	−0.10	0	.10
1-III	.25	.50	.25	.06	− .14	.08
2-I	.26	.03	.71	− .08	− .06	.14
2-II	.26	.03	.71	− .14	.06	.08
3-I	.70	.15	.15	.15	− .05	− .10
3-II	.70	.15	.15	.10	.05	− .15
4-I	.15	.70	.15	.15	− .05	− .10
4-II	.15	.70	.15	.10	.05	− .15
5-I	.45	.25	.30	− .05	.15	− .10
5-II	.45	.25	.30	.05	.10	− .15
6-I	.18	.28	.54	− .05	.15	− .10
6-II	.18	.28	.54	.05	.10	− .15

Since the diffusion coefficients are assumed to depend only upon the mean concentration, two of these experiments yield four equations for the four unknown diffusion coefficients at the mean concentration used in the experiments.

The diffusion coefficients obtained at the six points are given in Table IV together with the estimated 95% confidence limits. The main diffusion coefficients are also shown in Fig. 2.

At each of the points 2 to 6 all three values of ΔC_i^0 are the same magnitude so eq. 20a and b are valid.[27] Rewriting eq. 20a in the present nomenclature and summing over repeated experiments

$$\left(\frac{1}{\beta t}\ln\frac{\Delta x_T^0}{\Delta x_T^f}\right)_k = \bar{D}_{TT} - \bar{D}_{TC}\left(\frac{\Delta x_C}{\Delta x_T}\right)_{ak}, \quad k = \text{I,II} \tag{21}$$

where I and II refer to the two sets of experiments with the same mean concentration, but with different concentration differences, and the caps refer to the average values. Substituting the measured values of the capped terms into eq. 21 gives two simultaneous equations from which $\bar{D}_{TT}$ and $\bar{D}_{TC}$ may be calculated. Similarly eq. 20b yields two more independent equations from which $\bar{D}_{CC}$ and $\bar{D}_{CT}$ may be obtained.

The data and calculations at point 4 are shown in Table III. Complete data are given elsewhere.[28] Each of the first two experiments at point 1 were carried out with one of the initial concentration differences close to zero. From the earlier discussion and Table II, it follows that eq. 20b and c apply to the first experiment, and eq. 20a and c to the second. As a test of the over-all procedure the four diffusion coefficients obtained from these equations were then used to predict the final concentration differences in the third experiment at point 1 which was carried out with all the initial concentration differences of the same magnitude. These calculated values are compared to the measured values in Table V. The check is satisfactory.

The uncertainty in a cross diffusion coefficient depends primarily upon the choice of the initial concentration differences and when the uncertainty of one cross coefficient is decreased the other is increased. At points 2 to 4 inclusive $\bar{D}_{CT}$ was determined with minimum uncertainty and at points 5 and 6 $\bar{D}_{CT}$ was determined with minimum uncertainty.

The confidence ranges given for the $\bar{D}_{ij}$ were obtained from an analysis of variances contributed by each experimental value used in the calculations. It can be seen from Table IV that the confidence limits on the main diffusion coefficients run about ±5%, whereas the percentage uncertainty of the cross diffusion coefficients is much greater and more variable.

Discussion

The differences between the main diffusion coefficients average 5% while the cross diffusion coefficients average 2% of the main coefficients so this system approximates the behavior of eq. 3 and 4.

It is not statistically certain that the two main diffusion coefficients at a point actually differ, since the confidence limits overlap in all but one case. However, most of the cross diffusion coefficients which were determined with minimum uncertainty are significantly different from zero, indicating that the main diffusion coefficients probably do differ. As shown in Fig. 2, both of the main diffusion coefficients lie close to the plane whose borders are described by the binary diffusion coefficients.

In Table VI the left and right hand sides of eq. 8 are compared. It is seen that the equation is satisfied at all points within experimental error. However, when the cross diffusion coefficients D_{TC} and D_{CT} are zero the comparison is almost trivial since the equation merely asserts the equality of D_{TT} and D_{CC}, an equality which holds irrespective of the reciprocal relationships. Thus, in the present experiments, the satisfactory check indicates that the magnitude of the difference between the main diffusion coefficients is consistent with the magnitude of the cross diffusion coefficients.

Kinetic Theory of Gases.—The kinetic theory of gases describes the diffusion in a multicomponent system in terms of the binary diffusion coefficients of the system and it is of interest to consider the application of these equations to liquids. The Curtiss–Hirschfelder equations[29] for a mixture of three ideal gases yield[28] eq. 22a–22e.

(27) Subscript 1 is taken as toluene, 2 as chlorobenzene, and 3 as bromobenzene.

(28) J. K. Burchard, Ph.D. Thesis, Carnegie Institute of Technology, Pittsburgh, Pennsylvania, 1961.

(29) C. F. Curtiss and J. O. Hirschfelder, *J. Chem. Phys.*, **17**, 550 (1949).

TABLE III

DATA AND CALCULATIONS—POINT 4

Run	βt[a]	Δx_T^0	Δx_C^0	Δx_T^f	Δx_C^f	$\left(\frac{\Delta x_C}{\Delta x_T}\right)_a$	$\left(\frac{\Delta x_T}{\Delta x_C}\right)_a$	$\frac{1}{\beta t}\ln\frac{\Delta x_T^0}{\Delta x_T^f}$	$\frac{1}{\beta t}\ln\frac{\Delta x_C^0}{\Delta x_C^f}$
4-I (a)	0.14715	0.1503	−0.0502	0.1146	−0.0373	−0.3281	−3.049	1.8368	2.0481
I (b)	.18611	.1503	− .0502	.1069	− .0341				
II (a)	.14543	.1009	.0484	.0769	.0376	.4869	2.054	1.8764	1.7019
II (b)	.18418	.1009	.0484	.0713	.0356				

From eq. 20a: $1.8368 = D_{TT} - 0.3281D_{TC}$; $1.8764 = D_{TT} + 0.4869D_{TC}$

From eq. 20b: $2.0481 = D_{CC} - 3.049D_{CT}$; $1.7019 = D_{CC} + 2.054D_{CT}$

Hence[a] $D_{TT} = 1.853$, $D_{TC} = 0.049$, $D_{CC} = 1.841$, $D_{CT} = -0.068$

[a] Units of $1/\beta t$ and diffusion coefficients are cm.²/sec. $\times 10^{-5}$.

TABLE IV

TERNARY DIFFUSION COEFFICIENTS, CM.²/SEC. $\times 10^5$

Expt.	$\bar{D}_{TT}$	$\bar{D}_{CC}$	$\bar{D}_{TC}$	$\bar{D}_{CT}$
1	1.848 ± 0.066	1.797 ± 0.076	−0.063 ± 0.109	−0.052 ± 0.093
2	1.570 ± .088	1.606 ± .109	− .077 ± .100	− .012 ± .033
3	2.132 ± .098	2.062 ± .108	.051 ± .163	− .071 ± .026
4	1.853 ± .108	1.841 ± .108	.049 ± .162	− .068 ± .026
5	2.006 ± .108	1.890 ± .108	− .020 ± .026	− .198 ± .163
6	1.774 ± .107	1.518 ± .107	− .037 ± .026	.0026 ± .162

TABLE V

COMPARISON OF CALCULATED AND MEASURED CONCENTRATIONS, EXPT. 1-III

	Δx_T^f	Δx_C^f
Expt.	0.0433	−0.1017
Calcd.	0.0420	−0.1017

TABLE VI

COMPARISON OF LEFT AND RIGHT SIDES OF EQ. 8

Expt.	LHS	RHS
1	1.77 ± 0.16	1.67 ± 0.22
2	1.27 ± .82	1.32 ± .39
3	1.99 ± .11	2.12 ± .23
4	1.77 ± .11	1.94 ± .34
5	1.57 ± .38	1.86 ± .12
6	1.78 ± .49	1.37 ± .15

LHS $= \bar{D}_{TT} + (1 + x_B/x_C)\bar{D}_{CT}$

RHS $= \bar{D}_{CC} + (1 + x_B/x_T)\bar{D}_{TC}$

$$D_{11} = \mathfrak{D}_{13}[(1 - x_1)\mathfrak{D}_{12} + x_1\mathfrak{D}_{23}]/\psi \quad (22a)$$

$$D_{12} = x_1\mathfrak{D}_{23}(\mathfrak{D}_{13} - \mathfrak{D}_{12})/\psi \quad (22b)$$

$$D_{22} = \mathfrak{D}_{23}[(1 - x_2)\mathfrak{D}_{21} + x_2\mathfrak{D}_{13}]/\psi \quad (22c)$$

$$D_{21} = x_2\mathfrak{D}_{13}(\mathfrak{D}_{23} - \mathfrak{D}_{21})/\psi \quad (22d)$$

$$\psi = x_1\mathfrak{D}_{23} + x_2\mathfrak{D}_{13} + x_3\mathfrak{D}_{12} \quad (22e)$$

and $\mathfrak{D}_{ij} = \mathfrak{D}_{ji}$

These equations are ambiguous for liquids since, unlike ideal gases, the binary diffusion coefficients are composition dependent. In order to allow for the third component, one might evaluate the $\mathfrak{D}_{ij}$ to be used in eq. 22 at a species i mole fraction in a binary mixture of species i and j of $x_i/(x_i + x_j)$, where x_i and x_j are the mole fractions in the ternary mixture. Since the binary diffusion coefficients are linear in mole fraction in the present study, the $\mathfrak{D}_{ij}$ to be used in eq. 22 are given by

$$\mathfrak{D}_{ij} = \frac{x_j}{x_i + x_j}\mathfrak{D}_{ij}^0 + \frac{x_i}{x_i + x_j}\mathfrak{D}_{ji}^0 \quad (23)$$

The multicomponent diffusion coefficients were calculated from these equations using the values of $\mathfrak{D}_{ij}^0$ from Table I and are compared to the measured diffusion coefficients in Table VII and in Fig. 2.

It can be seen that the experimental main diffusion coefficients are, in most cases, well within experimental error of the predictions of eq. 22 and 23. It is of interest to note that the equations properly predict the largest and smallest D_{ii} except for expt. 2. Usually the experimental values lie between the predicted values.

For the cross terms the experimental values are usually smaller in magnitude than predicted, and where the confidence ranges are relatively small this difference is statistically significant in most cases.

Thus, eq. 22 and 23 predict the ternary diffusion reasonably well from binary diffusion data. The predictions are better for the main terms, but at least the order of magnitude of the cross terms is handled correctly.

Use of a Single Diffusion Coefficient.—Because of the small values of the cross diffusion coefficients, the cross terms in eq. 1 will generally make only a small contribution to the flux. Consequently, a simple, usually adequate approximation to the diffusion in this system is obtained by neglecting the cross terms altogether, for then only one ternary diffusion coefficient, D^*, is needed to describe the diffusion. The D^* can then be calculated by averaging *all* the log terms, for *all* the replicas in a given experiment, *i.e.*, by assuming that differences between the initial conditions I and II give indistinguishable results. However, simply averaging the $\bar{D}_{TT}$ and $\bar{D}_{CC}$ already calculated gives essentially the same results and these values are shown in column 1 of Table VIII.

TABLE VII

COMPARISON OF EXPERIMENTAL DIFFUSION COEFFICIENTS[a] WITH VALUES CALCULATED FROM EQ. 22 AND 23

	D_{TT}		D_{CC}		D_{TC}		D_{CT}	
Expt.	Expt.	Calcd.	Expt.	Calcd.	Expt.	Calcd.	Expt.	Calcd.
1	1.85	1.92	1.80	1.70	−0.06	−0.03	−0.05	−0.18
2	1.57	1.66	1.61	1.54	− .08	− .12	− .01	− .02
3	2.13	2.14	2.06	2.00	+ .05	− .09	− .07	− .13
4	1.85	1.88	1.84	1.72	+ .05	− .01	− .07	− .15
5	2.01	1.99	1.89	1.78	− .02	− .09	− .20	− .16
6	1.77	1.72	1.52	1.57	− .04	− .06	.00	− .13

[a] Units are cm.²/sec. × 10^{-5}.

TABLE VIII

TERNARY DIFFUSION COEFFICIENT, CM.²/SEC. × 10^5

Expt.	D^* (1)	D^* (2)	D^* (3)
1	1.82	1.84	1.81
2	1.59	1.59	1.63
3	2.10	2.12	2.09
4	1.85	1.84	1.80
5	1.95	1.91	1.90
6	1.65	1.64	1.66

From a regression analysis of these D^* at the six concentration points, it is found that they form a plane in D^*–concentration space[30]

$$D^* = 2.36x_T + 1.84x_C + 1.30x_B \quad (24)$$

The multiple correlation coefficient for the equation is 0.995. Values of D^* calculated from this equation are given in column 2 of Table VIII and may be compared with the measured values in column 1. This linear behavior is a natural generalization of the linear behavior of the binary diffusion coefficients.

The binary diffusion coefficients in a system obeying eq. 7 form the borders of the plane given by

$$D^* = \sum_{i=1}^{3} x_i \mathfrak{D}_{ji}^0, \; j \neq i \quad (25)$$

In the system used here $\mathfrak{D}_{ij}^0$ is close to but not identically equal to $\mathfrak{D}_{kj}^0$. If these differences are neglected and the arithmetic averages of the two dilute coefficients at each corner of Fig. 2 (which are given in Table I) are used in eq. 25 one obtains

$$D^* = 2.31x_T + 1.78x_C + 1.38x_B \quad (26)$$

and this is the equation of the plane shown in Fig. 2.

The very close similarity between eq. 24 and 26 is obvious. The values of D^* calculated from eq. 26 are given in column 3, Table VIII. It is apparent that the two planes coincide within experimental error, indicating that the D^* given by the ternary measurements goes to the proper binary limits.

It follows that for many purposes liquid diffusion in the system toluene–chlorobenzene–bromobenzene can be adequately described by eq. 3 and 4 with D^* given by eq. 24 or 26. This is a pleasantly concise result—one diffusion coefficient, easily predicted from dilute binary data, serves for a ternary system.

If this behavior is a general characteristic of multicomponent systems which obey eq. 7, then an approximate description of the diffusion in such systems can be obtained without the necessity of any experimental measurements, for the dilute binary diffusion coefficients can be obtained with at least fair accuracy from available correlations.

Acknowledgment.—The authors are grateful to the National Science Foundation for its financial support of this work.

(30) Since the main diffusion coefficients differ from D^* by only a small amount, the main diffusion coefficients are also essentially linear with mole fraction.

GAS PHASE OXIDATION OF o-XYLENE

BY FRANKLIN J. WRIGHT

Esso Research and Engineering Company, Central Basic Research Laboratory, Linden, New Jersey

Received December 27, 1961

The gas phase oxidation of o-xylene has been investigated in a flow system at atmospheric pressure using a quartz reaction vessel maintained at 650°. The presence of 38 oxidation products has been detected and the variations in the yields of two-thirds of these have been studied as a function of mixture composition and reaction time. Apart from CO, CO_2, CH_4, H_2, and water, 1-methyl-2-vinylbenzene and toluene were the most abundant by-products found. The effect of temperature on the CO/CO_2 ratio has also been observed. The slow combustion of o-xylene has been shown to be a complex process involving many types of reactions such as cracking and alkylation as well as the simultaneous oxidation of the nucleus and of the methyl groups. It has been concluded that ring splitting and the subsequent rapid oxidation of the fission products can occur before the side-chains have been oxidized and takes place *via* the formation of a transient transannular oxide. The experimental facts also suggest that o-tolualdehyde is the principal chain branching intermediate. The mechanism proposed to account for the formation of aromatic hydrocarbons and tarry materials is based on the condensation of free radicals with acetylene.

Introduction

In spite of the increasing importance of aromatics as fuel components for internal combustion engines, knowledge concerning the slow combustion of this class of compounds is relatively scanty. The general kinetics of the three isomers of xylene have been investigated previously.[1] Because the performance of a fuel in an engine is to a considerable extent determined by its slow combustion behavior, it was considered of interest to study in more detail the gas phase oxidation of o-xylene.

The isomers of xylene exhibit striking differences in some of their combustion properties. For instance, the spontaneous ignition temperature of o-xylene is significantly lower (*ca.* 60°) than that of either m- or p-xylene.[2] Similarly, as indicated by the values of 13.6, 15.3, and 15.7 reported[3] for the critical compression ratios of o-, m-, and p-xylene (600 r.p.m., 100°F. inlet temperature), o-xylene is the least resistant to detonation in spark-ignited engines. In keeping with these observations, prior work[1] has indicated that o-xylene is more easily oxidized than either m- or p-xylene. Based on the evidence obtained in that investigation, it was suggested that these differences in the ease of oxidation probably resulted from differences in the rates of the chain branching reactions.

The present investigation therefore was undertaken in the hope that more might be learned about the nature of the branching intermediate.

Based on a kinetic study, Fort and Hinshelwood[4] have concluded that the oxidation of benzene occurs *via* a mechanism involving chains of short lengths. Burgoyne[5] investigated the oxidative behavior of benzene and of a series of substituted benzenes and concluded that the slow oxidation of benzene differs in several respects from that of its alkyl derivatives. Newitt and Burgoyne[6] showed that in the slow oxidation of benzene at pressures of several atmospheres a single series of hydroxy intermediates preceded the breakdown of the ring, whereas in the case of substituted benzenes both side-chain and nuclear oxidation occurred simultaneously.

Norrish and Taylor[7] also concluded that the oxidation of benzene took place *via* a successive hydroxylation of the ring to the dihydroxy stage, before ring splitting and the subsequent rapid oxidation of the fragments occurred. Their study[8] of the cool flames of toluene and ethylbenzene led to a similar conclusion.

The slow combustion of o-xylene has now been investigated in a flow system at atmospheric pressure, using a quartz reaction vessel maintained at 650°. As complete an analysis of the oxidation products as possible has been obtained, and the variation in the yields of many of these has been studied as a function of environment, such as mixture composition and reaction time. This information concerning the stoichiometry of the over-all process has shed considerable light on the mechanism of the reaction. This is particularly so when such evidence is considered in terms of the general kinetics of the reaction and the oxidative behavior of aliphatic compounds.

Experimental

Materials.—Pure Grade (99%) Phillips 66 o-xylene was treated with sodium wire and was further purified by vacuum distillation. No impurities could be detected by gas chromatography. Oxygen was obtained from a cylinder and passed over calcium chloride and phosphorus pentoxide; it was used without further purification. Nitrogen also was obtained from a cylinder and treated in a similar manner.

Apparatus.—The equipment consisted essentially of a quartz reaction vessel placed horizontally in a well regulated electric furnace, and of ancillary equipment for the preparation of the combustible mixtures and the collection of the effluent products.

The reaction vessel was 20 cm. long and 3 cm. in diameter. The well-lagged electric furnace, whose temperature could be controlled accurately to ±1°, had a heavy stainless steel core in order to provide a large thermal inertia and to eliminate temperature gradients along the length of the reaction vessel.

The flow of gases was measured by means of differential flowmeters and the nitrogen stream was saturated with o-xylene by passing it through a thermostated "carburetor." Immediately before entering the reaction vessel, the gases flowed through a mixing vessel maintained at 150°. All connecting leads were electrically heated to avoid condensation. Blank experiments were carried out to ascertain that the nitrogen stream could be saturated under all relevant flow conditions.

The reaction products flowed through a series of three

(1) F. J. Wright, *J. Phys. Chem.*, **64**, 1944 (1960).
(2) J. L. Jackson, *Ind. Eng. Chem.*, **43**, 2869 (1951).
(3) T. A. Boyd, *ibid.*, **26**, 1105 (1934).
(4) R. Fort and C. N. Hinshelwood, *Proc. Roy. Soc.* (London), **A127**, 218 (1930).
(5) J. H. Burgoyne, *ibid.*, **A175**, 539 (1940).
(6) D. M. Newitt and J. H. Burgoyne, *ibid.*, **A153**, 448 (1936).
(7) R. G. W. Norrish and G. W. Taylor, *ibid.*, **A234**, 160 (1956).
(8) R. G. W. Norrish and G. W. Taylor, *ibid.*, **A238**, 143 (1956).

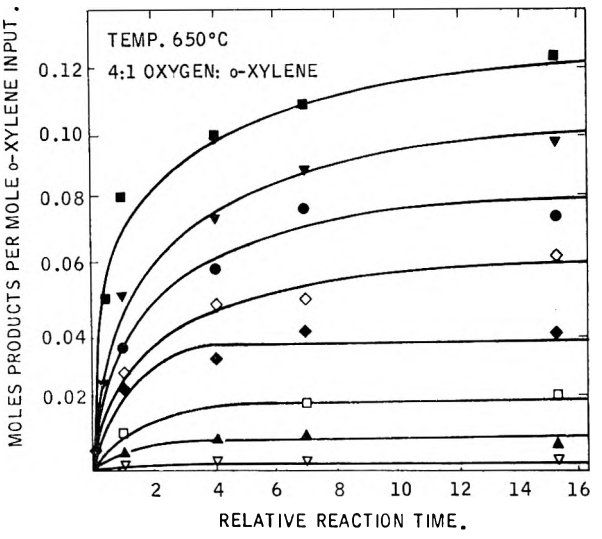

Fig. 1.—■, methylvinylbenzene; ▼, toluene; ●, benzene; ◊, *o*-tolualdehyde; ♦, 1-methyl-2-ethylbenzene; □, phenol; ▲, *p*-xylene; ▽, *m*-xylene.

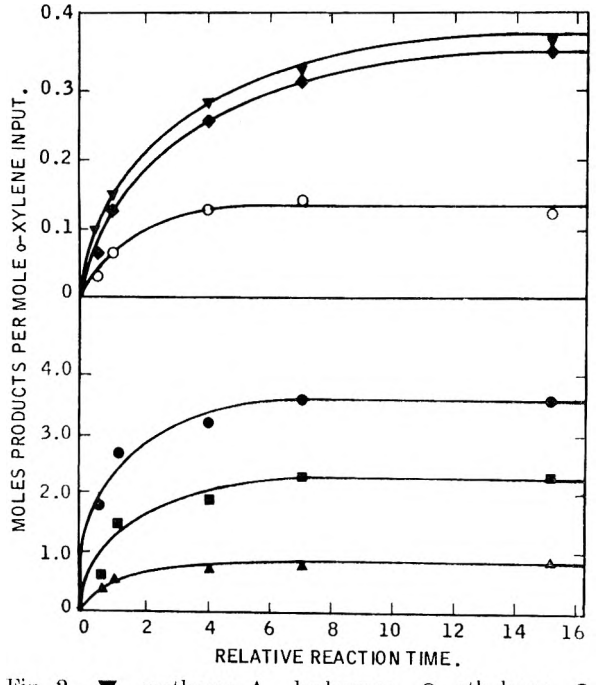

Fig. 2.—▼, methane; ♦, hydrogen; ○, ethylene; ●, oxygen consumed; ■, carbon monoxide; ▲, carbon dioxide.

traps cooled to −80°, the residual gases being collected for analysis. Under all flow conditions, a glass wool plug inserted in the traps efficiently trapped the fine smoke which formed part of the combustion products.

After adjusting the flows, the gases were allowed to pass through the reaction vessel for 30 min. in order to let the reaction come to equilibrium. The products were then directed through the tared traps for a known length of time (15–30 min.). At the completion of a run, both the uncondensed gases and the liquid products were analyzed.

Analysis of Products.—The non-condensable gases were analyzed by means of a Fisher Gas Partitioner. This instrument used two chromatographic columns, one consisting of synthetic zeolite and the other of 30% hexamethylphosphoramide on firebrick. It is capable of separating N_2, O_2, CO, CO_2, and many low molecular weight hydrocarbons. By replacing the helium carrier with argon, it can also be used to detect H_2. Analysis of the effluent gases was also obtained on a mass spectrometer.

The liquid fraction was analyzed by means of a Perkin–Elmer Model 154-C Vapor Fractometer using a 2 m. column of diatomaceous earth supporting diisodecyl phthalate at 150°. At this temperature, this column was found capable of separating many of the products having boiling points below that of naphthalene. In order to get better separation of those products which boil below 80°, the column also was operated at 100°. A number of qualitative analyses were also carried out on a Barber–Coleman gas chromatography unit equipped with a capillary column and an ionization detector. The column was packed with Apiezon "L" and was temperature programmed between 100 and 200°.

Identification of the G. C. peaks was carried out by coupling the chromatography units to a Bendix Type 12–101 Time-of-Flight mass spectrometer and also by subjecting narrow cuts to infrared analysis. Whenever possible, identification of the peaks was confirmed by direct comparison of elution times.

Immediately at the completion of a run, paper chromatography was used to detect the possible presence of peroxides and in particular of hydrogen peroxide. The technique used was that described by Cartlidge and Tipper[9] with ether as the moving phase; ferrous thiocyanate, *p*-phenylenediamine–aldehyde mixtures, and also a 10 vol. % solution of hydrogen iodide in glacial acetic acid were tried as developers. No indications that the oxidation products contained peroxides, however, could be obtained.

Results.—In Table I are given the results of a typical run. Evidence also was obtained for the presence of methylacetylene, vinylacetylene, pentadiene, furan, dihydrofuran, dimethyldiphenylethane, dibenzyl, anthracene, aromatic alcohols, and esters. No quantitative data were, however, obtained for these compounds except for noting that they were present in quite low concentrations. These compounds plus the small amounts of any materials retained in the stopcocks would account for the fact that, in general, material balances somewhat short of 100% were obtained.

A few pyrolysis runs also were carried out for comparison purposes. At 650°, the temperature at which the oxidation was studied, the extent of reaction was small but the presence of toluene, benzene, 1-methyl-2-ethylbenzene, 1-methyl-2-vinylbenzene, *p*-xylene, methane, and hydrogen was detected.

(a) **Variation of Contact Time with a Constant *o*-Xylene–Oxygen Ratio.**—The *o*-xylene to oxygen ratio was kept constant at 1:4, while the relative contact times were varied between 0.25 and 15. In order to avoid having to determine the effective volume of the reactor, the relative contact time is arbitrarily defined as $12.53/V$, where V ml./sec. is the total flow of gases. The variation in yields of some of the products with varying contact times is shown in Fig. 1 and 2. Under no conditions did ignition occur.

(b) **Variation of Oxygen Concentration at a Relative Contact Time of 1.0.**—The rate of flow of nitrogen passing through the carburetor was kept constant at 8.33 ml./sec., corresponding to an *o*-xylene flow of 0.6 ml./sec., and the flow of oxygen was varied between 0.0 and 4.2 ml./sec. Sufficient nitrogen was added to maintain the total flow of gases through the reaction vessel at 12.53 ml./sec. The variation of the yields of some of the products of oxidation with changes in oxygen concentration is given in Fig. 3 and 4.

At an *o*-xylene to oxygen ratio of 1 to 7, ignition occurred in the vessel—the flame flashing back against the direction of flow until it was quenched by the glass wool plug placed in the entry tube. Such a plug was found to be very effective in preventing explosions from occurring in the mixing vessel.

(c) **Variation of Oxygen Concentration at a Relative Contact Time of 0.5.**—The rate of flow of nitrogen through the carburetor was kept constant at 16.66 ml./sec., corresponding to an *o*-xylene flow of 1.2 ml./sec., and the oxygen flow was varied between 0 and 7.2 ml./sec. Sufficient nitrogen was added to maintain the total flow of oxygen and nitrogen at 25.06 ml./sec.

Although the extent of reaction under these conditions was smaller, the variation of the product yields is similar to that observed at relative contact times of 1. Ignition occurred at the same oxygen to *o*-xylene ratio as when the relative contact time was 1.0.

(9) J. Cartlidge and C. F. H. Tipper, *Anal. Chim. Acta*, **22**, 106 (1960).

TABLE I

QUANTITATIVE ANALYSIS OF A TYPICAL RUN

Products	Moles per mole o-xylene input	g.-atoms carbon per 100 g. atoms input	g.-atoms oxygen per 100 g. atoms input	g.-atoms hydrogen per 100 g. atoms input
o-Xylene	0.28	28.0	...	28.0
m-Xylene	.002	0.25	...	0.19
p-Xylene	.005	0.5	...	0.5
Toluene	.075	6.6	...	6.0
Benzene	.045	3.25	...	2.6
1-Methyl-2-ethyl-benzene	.030	3.25	...	3.7
Benzofuran	.035	3.6	0.39	2.1
1-Methyl-2-vinyl-benzene	.095	10.6	...	9.5
Benzaldehyde	.010	1.0	.11	0.75
Phenylacetalde-hyde	.015	1.6	.17	1.5
o-Tolualdehyde	.040	3.9	.44	3.5
Phenol	.009	0.6	.10	0.5
o-Cresol	.006	.5	.07	.5
Naphthalene	.004	.35	...	.3
Formaldehyde	.004	.5	.05	.07
Acetone	.001	.05	.01	.07
Acrolein	.001	.05	.01	.07
Methyl vinyl ketone	.002	.12	.02	.14
Crotonaldehyde	.007	.32	.08	.52
Carbon monoxide	1.45	18.1	16.0	...
Carbon dioxide	0.45	5.6	9.9	...
Methane	.17	2.25	...	7.0
Ethane	.04	0.85	...	2.25
Ethylene	.07	1.75	...	3.0
Hydrogen	.16	...	...	3.25
Oxygen	2.40	...	52.5	...
Water	1.10	...	12.0	22.00
Total		93.49	91.85	98.01

Discussion

As evidenced by Table I, the gas phase oxidation of *o*-xylene is a complex process. The wide variety of products which are formed is a reflection of the large number of reactions which are simultaneously taking place. This multitude of individual steps makes the establishment of a complete mechanism quite difficult. Some general facts do emerge, however, from the analytical curves and the table of products distribution.

1. At both relative contact times studied, none of the curves of product yields against mixture composition shows signs of discontinuity or of marked deformities right to the onset of ignition. This suggests the absence of drastic changes in the mechanism by which *o*-xylene is oxidized or, for that matter, of reactions leading to the end products.

2. Substantial amounts of non-oxygenated compounds are found among the reaction products, particularly 1-methyl-2-vinylbenzene and toluene. From this it must be concluded that cracking and alkylation reactions compete successfully with oxidation in spite of the fact that oxygen is never completely used up. Comparison with pyrolysis experiments clearly indicates that the rate of formation of non-oxygenated compounds is greatly increased by the presence of oxygen.

3. No indications that hydrogen peroxide had been formed could be obtained.

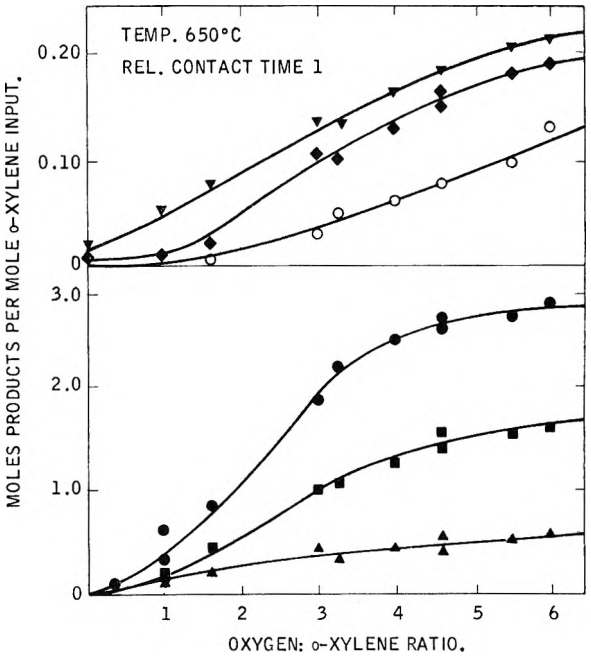

Fig. 3.—▼, methane; ♦, hydrogen; ○, ethylene; ●, oxygen consumed; ■, carbon monoxide; ▲, carbon dioxide.

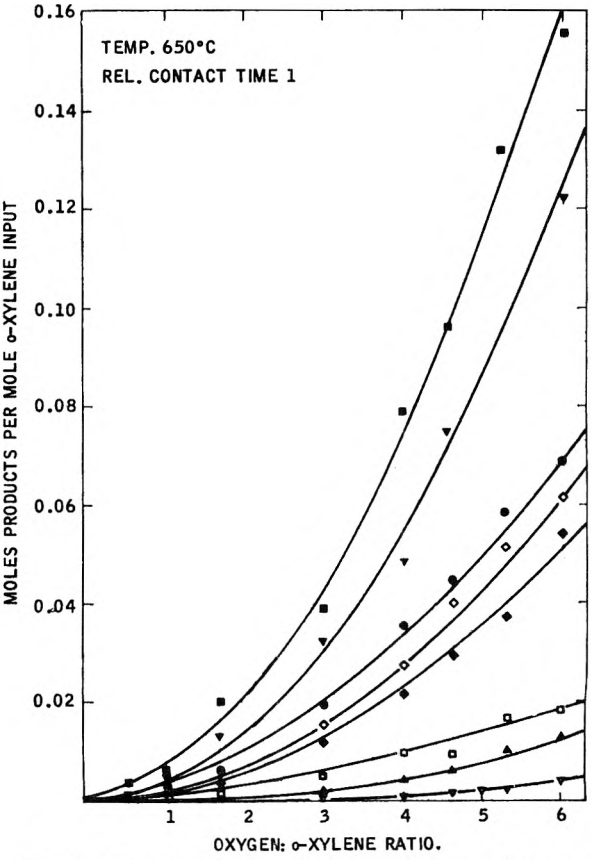

Fig. 4.—■, methylvinylbenzene; ▼, toluene; ●, benzene; ◊, *o*-tolualdehyde; ♦, 1-methyl-2-ethylbenzene; □, phenol; ▲, *p*-xylene; ▽, *m*-xylene.

4. Relatively small amounts of aliphatic compounds were recovered. Under the experimental conditions employed, this was to be expected, since aliphatic compounds are generally much more readily oxidized than aromatic ones.

5. Substantial quantities of various aldehydes as well as phenolic compounds are formed but with the exception of methyl ethyl ketone and acetone, no other ketones could be detected.

6. Approximately half of the *o*-xylene consumed formed aromatic by-products, a clear indication of the stability of the benzene ring toward oxidation.

In attempting to elucidate the main combustion process, it is convenient to consider side-chain and nuclear reactions separately. Once the ring has been cleaved, the resulting straight chain fragments are rapidly oxidized, presumably in a manner analogous to that of aliphatic hydrocarbons. The reactivity of the benzene ring thus ultimately resolves itself into the problem of its cleavage.

Side-Chain Oxidation.—Pyrolysis experiments indicate that some thermal decomposition or cracking of the hydrocarbon does occur at 650°. The radicals formed in this manner could therefore initiate the oxidation process. On thermochemical grounds,[10,11] however, the primary initiation reaction is more likely to be

$$CH_3C_6H_4CH_3 + O_2 \longrightarrow CH_3C_6H_4CH_2\cdot + HO_2\cdot \quad (1)$$
$$\Delta H = 33 \text{ kcal./mole}$$

followed by

$$CH_3C_6H_4CH_3 + HO_2\cdot \longrightarrow CH_3C_6H_4CH_2\cdot + H_2O_2 \quad (2)$$

The failure to detect hydrogen peroxide among the oxidation products would indicate that reaction 2 does not take place to any appreciable extent. However at the temperatures considered here, hydrogen peroxide would decompose rapidly while at the same time it would act as an oxidizing agent.

Reaction of xylyl radical with oxygen results in the rapid formation of a peroxy radical.

$$CH_3C_6H_4CH_2\cdot + O_2 \longrightarrow CH_3C_6H_4CH_2OO\cdot \quad (3)$$

At temperatures above 300°, peroxy radicals have been shown to decompose rather than abstract hydrogen to form hydroperoxides.[12,13] The course of the side-chain oxidation of *o*-xylene will therefore be determined by the thermal decomposition of the benzyl peroxy radical. The observed products thus are thought to arise from this radical by internal rearrangement followed or accompanied by decomposition in a manner analogous to that followed by aliphatic compounds.[14,15] On this basis, the relatively smaller yields of alcohols compared to that of the aldehydes can readily be understood since the reaction leading to alcohols

$$CH_3C_6H_4CH_2OO\cdot \longrightarrow CH_3C_6H_4CH_2OOH \longrightarrow CH_3C_6H_4CH_2OH + OH \quad (4)$$

has to compete with the more probable thermal decomposition of the peroxy radicals to aldehydes

$$CH_3C_6H_4CH_2OO\cdot \longrightarrow CH_3C_6H_4CHO + \cdot OH \quad (5)$$

Branching Intermediate.—Previous kinetic work[1] has indicated that the greater ease of oxidation of *o*-xylene compared to that of *m*- or *p*-xylene results from differences in the rates of the branching reactions. It was shown that the reactivity of the branching intermediate in the oxidation of *o*-xylene was significantly greater than that of the intermediates responsible for the branching reactions in the oxidation of *m*- and *p*-xylene. Moreover, the reactivities of these latter two intermediates were essentially the same.

On the basis of these results and the present observations, *o*-tolualdehyde is now proposed as one of the branching intermediates in the *o*-xylene oxidation. Not only could the oxidation of this aldehyde provide the necessary branching, but its stationary concentration is large enough for it to be effective. Moreover, the differences in the manner in which *o*-, *m*-, and *p*-tolualdehyde oxidize could account for the observed differences in the rates of oxidation of the three isomers. Thus, according to the sequence

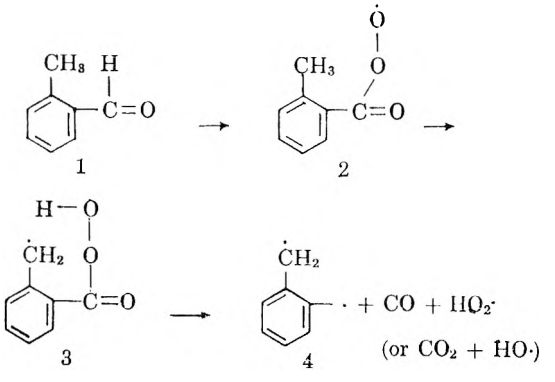

the oxidation of *o*-tolualdehyde would yield a reactive diradical which on further reaction would give two free radicals. On the other hand, in the case of both *m*- or *p*-tolualdehyde, the oxidation would proceed as

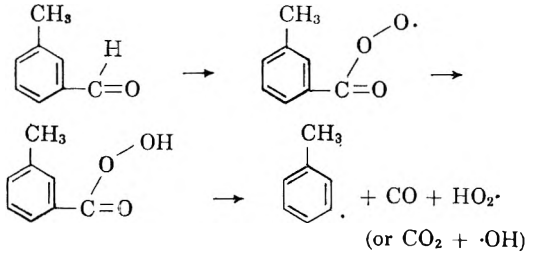

(10) P. Gray, *Trans. Faraday Soc.*, **55**, 408 (1959).
(11) M. Szwarc and D. J. Williams, *J. Chem. Phys.*, **20**, 1171 (1952).
(12) J. W. Falconer and J. H. Knox, *Proc. Roy. Soc.* (London), **A250**, 493 (1959).
(13) C. Satterfield and R. Wilson, *Ind. Eng. Chem.*, **46**, 1001 (1954).
(14) A. D. Walsh, *Trans. Faraday Soc.*, **43**, 297 (1947).
(15) H. C. Bailey and R. G. W. Norrish, *Proc. Roy. Soc.* (London), **A212**, 311 (1952).

There are two essential differences in these sequences of steps. First, because of the proximity of the methyl group, H abstraction will occur unimolecularly in the case of the *o*-isomer, whereas the parallel reaction with the other isomers would of necessity have to be bimolecular. Second, whereas a reactive diradical would be formed with the *ortho*-compound, in the case of *m*- and *p*-xylene a methyl phenyl radical would result. These radicals, as well as having only a single unpaired electron, might also be expected to isomerize rapidly to relatively stable benzyl radicals. They would thus be less efficient chain propagators. It might therefore be expected that *o*-xylene will oxidize more readily.

Nuclear Oxidation.—It has been suggested by Norrish and Taylor[7] that in benzene oxidation, the ring is successively hydroxylated and that dihydroxy compounds are the precursors to ring fission. They also postulated that the ring cleavage occurred *via* the formation of *meso*-oxide type transient intermediates.

The absence of catechol or hydroquinone and the detection of a number of aliphatic fragments, such as methyl vinyl ketone, acrolein, and crotonaldehyde suggest, however, that in the case of *o*-xylene, the formation of phenolic compounds does not necessarily have to precede the splitting of the ring. Rather, attack of the ring by oxygen can occur more or less readily no matter what the substituents on it may be. The basis for this hypothesis is that the transient formation and subsequent rapid decomposition of *meso*-oxides would readily explain the presence of some of the aliphatic fragments found among the oxidation products. The direct formation of

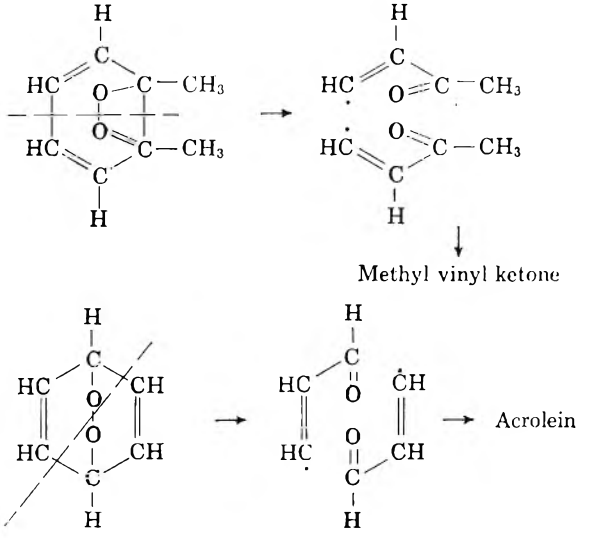

such transannular oxides would violate spin conservation rules and the probability of such a step would thus be expected to be low. This might account for the stability of the benzene ring toward oxidation. The formation of furan and pyran derivatives during the course of oxidation of aliphatic hydrocarbons has been explained by Bailey and Norrish[15] as

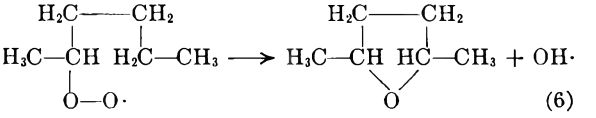

(6)

The formation of benzofuran undoubtedly occurs by a similar, albeit somewhat more complex, mechanism probably involving styrene or a styryl radical which might be expected to be formed thermally from ethylbenzene, one of the oxidation by-products. The presence among the oxidation products of benzofuran as well as *ortho*-substituted phenols also indicates that nuclear attack can occur before a side-chain is completely removed.

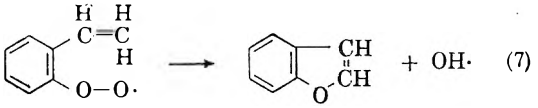

(7)

Cracking and Alkylation.—The by-products of *o*-xylene oxidation contain relatively large amounts of non-oxygenated compounds such as 1-methyl-2-ethylbenzene, 1-methyl-2-vinylbenzene, naphthalene, anthracene, *p*- and *m*-xylene, and various tarry materials of unidentified structure. Also present are hydrocarbons such as benzene and toluene. As indicated by pyrolysis experiments, all of these compounds also are formed in the absence of oxygen but in smaller yields. These increases in the rates of formation in the presence of oxygen reflect the well known catalytic influence of oxygen on thermal cracking reactions.[16]

The various hydrocarbons that have been detected must undoubtedly be formed by the condensation of radicals produced in the course of the reaction. Because of the variety of such radicals, many combinations are possible and only a few of the more likely ones will be considered.

The most abundant of the non-oxygenated hydrocarbons found is 1-methyl-2-vinylbenzene. A likely mode for its formation is through thermal cracking of 1-methyl-2-ethylbenzene, which is also present in substantial amounts. In fact, Szwarc[17]

$$CH_3C_6H_4CH_2CH_3 \longrightarrow CH_3C_6H_4CH{=}CH_2 + H_2 \quad (8)$$

has shown that in the pyrolysis of ethylbenzene, styrene and hydrogen both are formed. He suggested that these products could be accounted for in part by an intramolecular reaction such as (8) and in part by the reaction

$$C_6H_5CH_2CH_2\cdot \longrightarrow C_6H_5CH{=}CH_2 + H\cdot \quad (9)$$

The formation of 1-methyl-2-ethylbenzene could most readily be explained as resulting from the recombination of methyl and *o*-xylyl radicals. Since the yields of 1-methyl-2-vinylbenzene and of its probable precursor 1-methyl-2-ethylbenzene, are relatively large, it must be presumed that such recombination will occur readily in spite of the fact that the radicals involved might be expected to react with oxygen or to abstract hydrogen from

(16) M. Letort and M. Niclause, *Colloq. C.N.R.S. sur la Combustion*, 47 (1948).

(17) M. Szwarc, *J. Chem. Phys.*, **17**, 431 (1949).

the parent hydrocarbon, both present in high concentrations. This difficulty would be resolved if 1-methyl-2-ethylbenzene and 1-methyl-2-vinylbenzene were to be formed by disproportionation of two *o*-xylyl radicals, *e.g.*

$$CH_3C_6H_4CH_2\cdot + \cdot CH_2C_6H_4CH_3 \longrightarrow CH_3C_6H_4CH{=}CH_2 + CH_3C_6H_5 \quad (10)$$

The concentration of *o*-xylyl radicals might be expected to be substantial since they are readily formed from *o*-xylene either by thermal cracking or by hydrogen abstraction according to reaction 1. Some support for this mechanism can be found in the work of Madorsky and Straus,[18] who observed random chain scission of poly-*p*-xylene at 415°. Among the volatile decomposition products identified were benzene, toluene, xylene, *p*-methylstyrene, and *p*-ethyltoluene.

The appearance of small amounts of diphenyl and dimethyldiphenyl among the oxidation products indicates that, even in the presence of molecular oxygen, radical recombination of phenyl and substituted phenyl radicals can occur to some extent. This conclusion is further substantiated by the occurrence of polymeric and tarry materials since these are visualized as resulting from the addition of aromatic free radicals to unsaturates such as ethylene or acetylene, in accordance with the mechanism of carbon formation suggested by Porter.[19-21] Thus, 1-methyl-2-vinylbenzene, 1-methyl-2-ethylbenzene, phenylacetylene, naphthalene, and anthracene can be considered as intermediates in the series of steps which lead to polymer formation. The successive addition of unsaturated hydrocarbons to aromatic free radicals will occur with the concurrent loss of hydrogen and will result in the formation of a larger condensed ring containing an unpaired electron. The subsequent condensation of such ring systems into even larger ones might be expected to occur quite readily since, in view of the mobility of the free electron, the steric factor for such reactions should be about the same as for methyl radical recombination.[22]

(18) S. L. Madorsky and S. Straus, *J. Res. Natl. Bur. Std.*, **55**, 223 (1955).

(19) G. Porter, *J. Imp. Coll. Eng. Soc.*, **8**, 42 (1954).

(20) G. Porter, "Combustion Researches and Reviews," AGARD, London, 1955, p. 108.

(21) G. Porter, "4th Int. Symposum on Combustion," Williams and Wilkins Co., Baltimore, 1953, p. 248.

(22) A. S. Gordon, S. R. Smith, and J. R. McNesby, "7th Int. Symposium on Combustion," Butterworth, London, 1958, p. 317.

Although any unsaturated hydrocarbon might be expected to condense with aromatic free radicals, acetylene addition offers the most likely path since the larger free radicals formed through such a process should be relatively stable to the inverse reaction. Those that result from the addition of ethylene, on the other hand, would be more thermally unstable and might be expected to break down to ethylene and a small free radical. Therefore, more ethylene than acetylene ought to be found in the effluent gases and this is, in fact, what is observed.

CO/CO_2 Ratio.—From a survey of a number of gas phase oxidations of paraffins, olefins, and aldehydes, Skirrow and Tipper[23] concluded that at a fixed temperature the CO/CO_2 ratio decreases as the oxygen/fuel ratio is increased and increases with increasing temperature provided the relative reactant concentrations are fixed.

As illustrated in Table II, these generalizations do not apply to the present case of *o*-xylene oxidation—in fact quite opposite trends are observed. In keeping with these results, similar increases in the CO/CO_2 ratio with increasing oxygen/fuel ratio are also evident from Taylor and Norrish's data[7] on the gas phase oxidation of benzene. It must be concluded consequently that the mechanism by which CO and CO_2 are formed in the oxidation of aliphatics and aromatics is different. In view of the multiplicity of reactions which occur during the oxidation of aromatics, this is not unexpected.

TABLE II

o-Xylene:oxygen ratio	CO/CO_2 650°	600°
1:1	2.1	4.0
1:3	2.5	5.2
1:6	3.4	7.5

Acknowledgment.—We are grateful to the Analytical Research Division for their help in the identification of the chromatographic peaks. In particular, we wish to thank Dr. Brown and Mr. Rearick for their interpretation of the mass spectrographic data, and Messrs. Quiram and Wanless for their infrared work.

We also wish to acknowledge Mr. John Baron, Jr.'s, able assistance with the experimental work.

(23) G. Skirrow and C. F. H. Tipper, "7th Int. Symposium on Combustion," Butterworth, London, 1958, p. 134.

CAGE EFFECTS AND SCAVENGING MECHANISMS IN THE PHOTOCHEMISTRY OF THE IODIDE ION IN AQUEOUS SOLUTIONS

BY JOSHUA JORTNER, MICHAEL OTTOLENGHI, AND GABRIEL STEIN

Department of Physical Chemistry, The Hebrew University, Jerusalem, Israel

Received December 28, 1961

Scavenging mechanisms in the photochemistry of the iodide ion were investigated. The nature of the scavenged species is discussed. An iodine atom–electron pair is formed from the primary excited state. H^+ ions promote specifically the formation of H atoms from these electrons. H^+ ion and aliphatic alcohols were employed as scavengers for the H atoms. At high scavenger concentration a limiting quantum yield of 0.290 ± 0.005 was observed at 25° and 2537 Å. independent of the nature of the scavenger. Application of specific scavengers made discrimination possible between H atoms and their precursors formed from the dissociation of the excited state of the ion. The dependence of the quantum yield on the scavenger concentration was found to be in agreement with general scavenging equations.

Introduction

In previous work[1] the photochemistry of evacuated aqueous KI solutions was investigated. The pH dependence of the initial quantum yield, which was found to be independent of I^- concentration and light intensity, could be interpreted adequately by a diffusion controlled scavenging mechanism.[2] The introduction of H atoms into the bulk was found to be facilitated by H^+ ions, acting as an efficient scavenger. However, we were unable to establish with certainty the nature of the species scavenged by the H^+ ion. It was postulated that in the photochemical cage together with an iodine atom either an electron or an H atom is formed, and undergoes a random diffusion process. It may then be captured by the I atom, leading to a secondary recombination, scavenged by H^+ ion, or diffuse into the bulk.

The purpose of the present work is the investigation of the nature of the fragments formed from the excited state of the ion. We attempt to discriminate between H atoms and their precursors by using specific scavengers. Further theoretical and experimental investigation of diffusion controlled scavenging mechanisms is presented.

Theoretical

Diffusion-Controlled Scavenging.—Radicals produced in pairs in the liquid phase by a thermal, radiation-chemical, or photochemical process may undergo primary recombination which is kinetically equivalent to thermal deactivation of the excited state. Radicals escaping primary recombination may undergo secondary diffusive recombination with their original partners or diffuse into the bulk.

Various semiquantitative treatments were presented for the effects of an efficient scavenger on secondary recombination.[2-9] The experimental results of our work will be treated by applying the general approach of Noyes.[2,3]

The total reaction probability of the two original partners is given by

$$\beta' = \int_0^\infty h(t)\,dt \qquad (1)$$

In the presence of a scavenger capable of reacting with one of the radicals the probability of this radical being scavenged, instead of it recombining with another radical in a secondary geminate recombination, is

$$\int_0^\infty (1 - e^{-k_s[S]t})h(t)\,dt \qquad (2)$$

where [S] is the scavenger concentration and k_s is the long time rate constant for the scavenging reaction. The dependence of the reactivity on the "age" of the radicals produced[2,10] was not considered in the present treatment.

The *residual yield* γ_r is defined as the quantum yield in the presence of the scavenger at concentration which is sufficient to prevent radical recombination in the bulk, but is too low to compete with secondary recombination. We denote by Γ the cross-section for radical production, *i.e.*, the quantum yield of radical pairs escaping primary recombination. Thus we set

$$\gamma_r = \Gamma(1 - \beta') \qquad (3)$$

$$\beta' = 1 - \frac{\gamma_r}{\Gamma} \qquad (3a)$$

The total quantum yield for radical scavenging obtained in the presence of a scavenger S at a concentration at which it prevents radical recombination in the bulk and competes with secondary recombination will be denoted by γ, and given by

$$\gamma = \gamma_r + \Gamma \int_0^\infty h(t)(1 - e^{-k_s[S]t})\,dt \qquad (4)$$

In Noyes' early treatment[2] $h(t)$ was introduced in the form

$$h(t) = 0 \quad 0 < t < 4a^2/\beta'^2 \qquad (5)$$

$$h(t) = at^{-3/2} \quad t > \frac{4a^2}{\beta'^2}$$

(1) J. Jortner, R. D. Levine, M. Ottolenghi, and G. Stein, *J. Phys. Chem.*, **65**, 1232 (1961).
(2) R. M. Noyes, *J. Am. Chem. Soc.*, **77**, 2042 (1955).
(3) R. M. Noyes, *ibid.*, **78**, 5486 (1956).
(4) A. H. Samuel and J. L. Magee, *J. Chem. Phys.*, **21**, 1080 (1953).
(5) J. C. Roy, R. R. Williams, and W. H. Hamill, *J. Am. Chem. Soc.*, **76**, 3274 (1954).
(6) R. A. Wijsman, *Bull. Math. Biophys.*, **14**, 121 (1952).
(7) L. Monchick, *J. Chem. Phys.*, **24**, 381 (1956).
(8) H. A. Schwarz, *J. Am. Chem. Soc.*, **77**, 4960 (1955).
(9) H. Fricke, *Ann. N. Y. Acad. Sci.*, **59**, 567 (1955).
(10) R. M. Noyes, *J. Phys. Chem.*, **65**, 763 (1961).

Substitution of (5) in (4) leads to Noyes' formula[2]

$$\gamma = \gamma_r + 2a\Gamma\sqrt{\pi k_s[S]} - \frac{\Gamma 4a^2 k_s[S]}{\beta'} + \ldots \quad (6)$$

for low [S] values

$$\gamma = \gamma_r + \alpha\Gamma\sqrt{[S]} \quad (6a)$$

where

$$\alpha = 2a\sqrt{\pi k_s}$$

This equation yields the theoretical basis for the linear dependence of the quantum yield on the square root of the scavenger concentration at low [S], and it was previously applied by us.[1] However, at high scavenger concentrations deviations from linearity in the plot γ *vs.* [S] appear.

We attempt to derive a scavenging equation adequate for the whole concentration region. $h(t)$ is described by the continuous function[3]

$$h(t) = at^{-3/2}\, e^{-\pi a^2/\beta'^2 t} \quad (7)$$

Substitution in eq. 4 leads to the result

$$\gamma = \Gamma\left(1 - \int_0^\infty at^{-3/2}\, e^{-\pi a^2/\beta'^2 t}\, e^{-k_s[S]t}\, dt\right) \quad (8)$$

The Laplace transform $f(k_s[S])$ of $h(t)$ is given by

$$f(k_s[S]) = \int_0^\infty e^{-k_s[S]t}\, h(t)dt = \beta' e^{-(2a/\beta')\sqrt{\pi k_s[S]}} \quad (9)$$

Thus the general expression for the quantum yield is obtained

$$\gamma = \Gamma(1 - \beta' e^{-(2a/\beta')\sqrt{\pi k_s[S]}}) \quad (10)$$

Application of eq. 3 leads to the result

$$\ln\left(1 - \frac{\gamma}{\Gamma}\right) = \ln\left(1 - \frac{\gamma_r}{\Gamma}\right) - \frac{2a}{\beta'}\sqrt{\pi k_s[S]} \quad (11)$$

For the limiting cases eq. 10 and 11 reduce to

$$S << \frac{\beta'^2}{4a^2\pi k_s};\ \gamma \longrightarrow \gamma_r$$

$$S \longrightarrow \infty;\ \gamma \longrightarrow \Gamma \quad (12)$$

The general scavenging equation is reduced to Noyes' equation for relatively low scavenger concentration. When

$$\frac{2a}{\beta'}\sqrt{\pi k_s\,[S]} < 1 \quad (13)$$

the exponent in eq. 10 can be expanded leading to

$$\left(1 - \frac{\gamma}{\Gamma}\right) = \beta'\left(1 - \frac{2a}{\beta'}\sqrt{\pi k_s[S]}\right) \quad (14)$$

leading to eq. 6.

Thus the linear dependence of γ on $\sqrt{[S]}$ will hold for $S << \beta'^2/\alpha^2$. For typical values of α = 1 l.$^{1/2}$ mole$^{-1/2}$ obtained in this work Noyes' relation will hold within 5% or better up to scavenger concentrations of 0.1 *M*.

It is interesting to compare the results of Noyes' treatment with the equation of Roy, Hamill, and Williams[5] which is based on similar assumptions. Their equation can be written in the form

$$\ln \gamma = A + B\sqrt{[S]} \quad (15)$$

where A and B represent constants related to microscopic diffusion parameters. For low [S] values (15) is identical with (6) if

$$A = \ln \gamma_r;\ B = \frac{\alpha\Gamma}{\gamma_r} \quad (16)$$

All cage-scavenging models of this type lead to the conclusion that the quantum yield should be independent of light intensity.

The species formed in the scavenging process may be a reactive radical. In the presence of added scavengers consecutive scavenging may occur, in which a species formed by the interaction of one of the scavengers with a radical originally produced reacts with a second scavenger specifically. To treat this mechanism we consider the general reaction scheme

$$(R_1 + R_2)_I \longrightarrow R_1 + R_2 \quad \gamma_r^I \quad (17)$$

$$(R_1 + R_2)_I + S_1 \longrightarrow (R_2 + RS_1)_{II} \quad k_{s_1} \quad (18)$$

$$(R_2 + RS_1)_{II} \longrightarrow R_2 + RS_1 \quad \gamma_r^{II} \quad (19)$$

$$(R_2 + RS_1)_{II} + S_2 \longrightarrow \text{Products} \quad k_{s_2} \quad (20)$$

The radical pair R_1 and R_2 in cage I may undergo diffusion into the bulk with quantum yield γ_r^I, or the radical R_1 may be scavenged by S_1 leading to a new radical pair in cage II. The scavenging of the radical RS_1 by S_2 from cage II should be treated by application of the general eq. 10. Assuming that the scavenger concentrations $[S_1]$ and $[S_2]$ are sufficiently high to prevent any radical recombination in the bulk the general expression for the quantum yield for the products formation is given by

$$\gamma = \gamma_r^I + \Gamma_{II}(1 - \beta_{II}' e^{-(2a_{II}/\beta_{II}')\sqrt{\pi k_{S_2}[S_2]}} \quad (21)$$

where Γ_{II}, the cross-section for radical production, in cage II is related to Γ by

$$\Gamma_{II} = \Gamma(1 - \beta_I' e^{-(2a_I/\beta_I')\sqrt{\pi k_{S_1}[S_1]}} - \gamma_r^I$$

β_I' and β_{II}' present the total reaction probabilities in cages I and II. γ_r^I is the residual yield from cage I presented by eq. 3. The residual yield from cage II is presented in an analogous way

$$\gamma_r^{II} = \Gamma_{II}(1 - \beta_{II}') \quad (22)$$

In this approximation Γ_{II} depends on $[S_1]$, reaching at high S_1 concentration the limiting value $(\Gamma - \gamma_r^I)$. For sufficiently low S_2 concentration and at constant $[S_1]$ the extended form of Noyes' relation is obtained

$$\gamma = \gamma_r^I + \gamma_r^{II} + \Gamma_{II} 2a_{II}\sqrt{\pi k_{s_2}[S_2]} \quad (23)$$

This result indicates that within the framework of the present approximation Noyes' relation holds

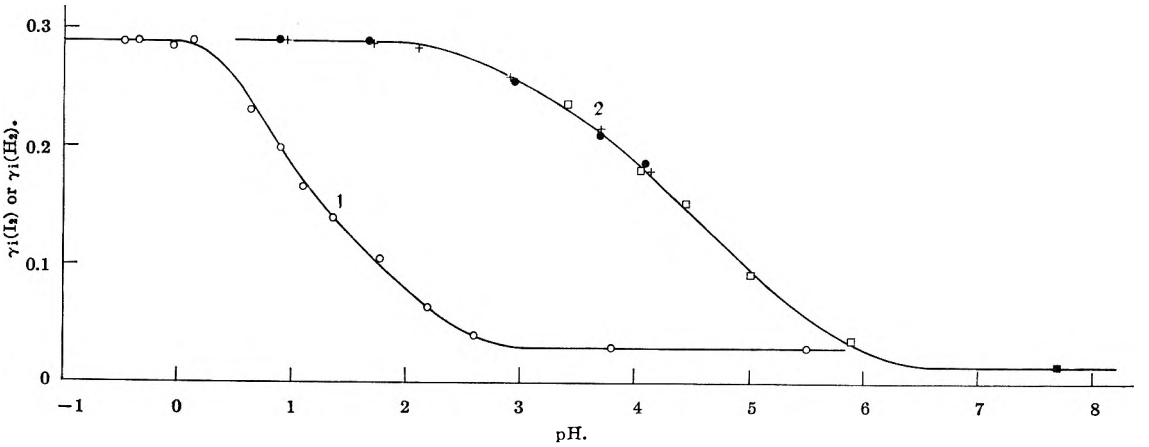

Fig. 1.—The pH dependence of initial quantum yields. (1) Iodine and hydrogen yields in evacuated solutions. The pH values below pH 0 represent $-\log [H^+]$. (2) Hydrogen yield in the presence of alcohols: ●, 1 *M* methanol, H_2SO_4 solutions: +, 1 *M* isopropyl alc., H_2SO_4 solutions; □, 1 *M* isopropyl alc., 5×10^{-3} *M* acetic acid–acetate buffer; ■, 1 *M* isopropyl alc., 5×10^{-3} *M* sodium monophosphate buffer.

for both ordinary and consecutive scavenging mechanisms.

The most serious approximation involved in the present treatment is the assumption that γ_r^I is a constant independent of S_1 concentration. The simple treatment of scavenging from a photochemical cage by S_1 does not discriminate between radicals scavenged in the bulk and in the solvent cage. However when consecutive scavenging is considered the spatial distribution of the radicals formed by interaction with the scavenger S_1 should be taken into account. At extremely high S_1 concentration the cross-section for the formation of cage II may reach the limiting value Γ and then the simple scavenging eq. 10 will be applicable and the residual yield will be due to diffusion from cage II. Because of this difficulty it is not easy to determine quantitatively the source of the residual yield, which may be due to diffusion from both cages I and II. We have used the two limiting approximations (a), γ_r^I is constant independent of S_1 so that $\Gamma_{II} = \Gamma - \gamma_r^I$; (b), $\gamma_r^I = 0$ so that $\Gamma_{II} = \Gamma$. It was found that the parameter $2a_{II}\sqrt{\pi k}$ is not very susceptible to the approximation involved.

Experimental

Photochemical experiments were carried out at 2537 Å., using a low pressure mercury lamp. The experimental technique was substantially that previously used.[1] Experiments were carried out at 25°.

Materials and Solution.—Solutions at high acid concentrations were prepared by evacuation of freshly prepared neutral KI solutions and the acid solutions in two different vessels and mixing in the vacuum system. The initial I_2 concentration did not exceed 2×10^{-7} *M*. The pH below 4.5 was adjusted by H_2SO_4. In the pH region 3.4–5.9, 5×10^{-3} *M* acetic acid–sodium acetate buffer was employed while at pH 7–8, 5×10^{-3} KH_2PO_4–Na_2HPO_4 buffer was used. At certain pH values the acetate and the sulfate systems were used in alternate experiments and identical results obtained. Thus acetate has no specific influence on the results. All chemicals used were of Analar grade. The water used was triply distilled from alkaline potassium permanganate and phosphoric acid. D_2O was prepared by distillation from alkaline permanganate followed by distillation from potassium hydrosulfate (to remove traces of permanganate), and two final distillations.

Analysis.—The analytical procedures for the determination of hydrogen and iodine were described previously.[1] Formaldehyde was identified and determined in irradiated aqueous methanol solutions by chromotropic acid.[11] The deuterium content of the gas evolved from methanol–D_2O solutions was determined by mass-spectrographic analysis.

Results and Discussion

The pH Dependence of γ_i in Evacuated Solutions.—In ref. 1 the pH dependence of the initial quantum yields, γ_i, in evacuated solutions was investigated in the pH region 0.6–7. In the present work the H^+ concentration region was extended and experiments were carried out up to 4 *N* H_2SO_4. Figure 1 curve 1 represents the dependence of γ_i on $[H^+]$ over the whole region in the absence of any other scavenger. The hydrogen yields observed were equal to the I_2 yields. At high acid concentration the quantum yield reaches an upper *limiting yield* $\gamma_{i\,lim} = 0.290 \pm 0.005$ at 25°. Such behavior is theoretically predicted for efficient scavenging competing with secondary recombination. At relatively low pH the analysis of the bulk reactions in this system indicates[1] that every H atom introduced into the bulk oxidizes another I^- ion. Thus the limiting value obtained for the quantum yield of I_2 and H_2 production in this system leads to the value $\Gamma = 0.29$ for the cross-section for photodissociation.

The pH Dependence of γ_i in the Presence of Aliphatic Alcohols.—The photochemistry of the iodide ion in aqueous solutions in the presence of isopropyl alcohol and methanol was investigated. These aliphatic alcohols were chosen, as recent radiation chemical investigations indicate that they act as specific scavengers for hydrogen atoms.[12] The initial quantum yields for H_2 evolution from these solutions were found to depend on pH and alcohol concentration (Fig. 1, 2, 3). Figure 1 curve 2 represents the pH dependence of the initial quantum yields for H_2 evolution investigated over a wide pH region in the presence of aliphatic alcohols. These results were obtained at high alcohol concentration where the quantum yield is independent of this scavenger concentration. Identical results were obtained in 1 *M* methanol and 1 *M* isopropyl

(11) C. E. Bricker and H. R. Johnson, *Ind. Eng. Chem., Anal. Ed.*, **17**, 400 (1945).

(12) J. T. Allan and G. Scholes, *Nature*, **187**, 218 (1960).

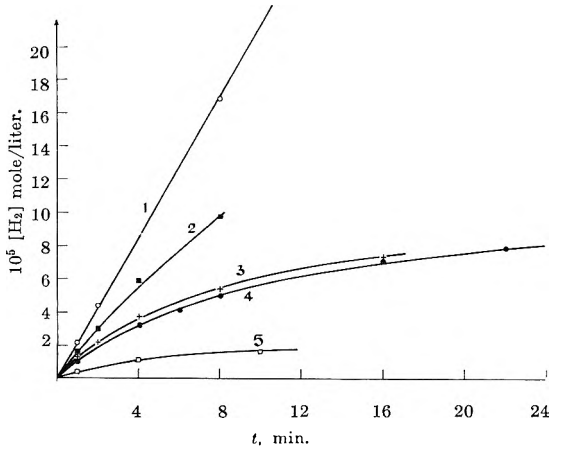

Fig. 2.—Hydrogen yields in isopropyl alc. solutions: (1) 1.01 M isopropyl alc., pH 1.72; (2) 2.1×10^{-3} M isopropyl alc., pH 2.92; (3) 1.01×10^{-2} M isopropyl alc., pH 1.72; (4) 1.45×10^{-3} M isopropyl alc., pH 2.92; (5) 1.4×10^{-4} M isopropyl alc., pH 2.92.

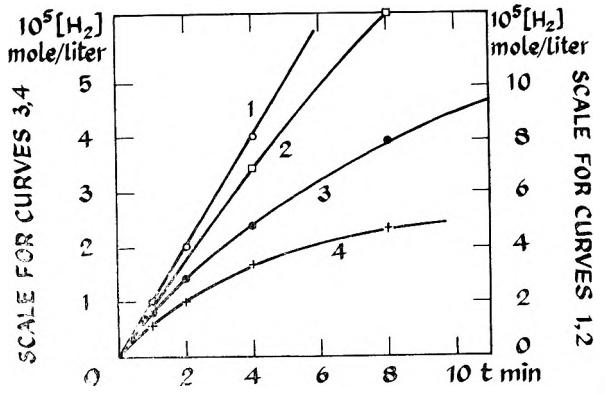

Fig. 3.—Hydrogen yields in methanol solutions: (1) 1 M methanol, pH 2.92; (2) 0.22 M methanol, pH 2.92; (3) 0.022 M methanol, pH 2.92; (4) 0.01 M methanol, pH 2.92.

alcohol solutions. Experiments carried out in H_2SO_4 solutions and in the presence of 5×10^{-3} M acetate buffer did not reveal any specific anion effect on the mechanism of H_2 evolution in the presence of alcohols.

The pH dependence of the initial H_2 yields in this system indicates that these aliphatic alcohols may act as efficient scavengers only at relatively low pH. At pH < 2 the yield is independent of H^+ ion concentration, and total scavenging occurs yielding the limiting value 0.29 ± 0.01 which is identical with the yield in evacuated solutions at high acid concentration.

The pH dependence of $\gamma(H_2)$ in the presence of an efficient scavenger for H atoms cannot be reconciled with any mechanism involving a direct H atom formation from the excited state of the ion.[13,14] These experimental results can be explained only if we assume the presence of two forms of "H atoms" formed in the photochemical system.[1] The acid form present at pH < 2 efficiently dehydrogenates the aliphatic alcohols while the other form does not, and reacts with the iodine atom leading mainly to a back reaction in the solvent cage. Thus with decreasing pH the nature of the species available to the aliphatic alcohol is changed. These conclusions are consistent with the scheme for consecutive scavenging.[1]

$$I^-aq \xrightarrow{h\nu} I^-aq^* \longrightarrow (I + e)_I \xrightarrow{H^+} (I + H)_{II} \quad (24)$$

where ( ) represents the solvent cage where particles may undergo secondary recombination.

In this scheme it is assumed that the atomic hydrogen precursor formed by the dissociation of the excited state of I^- is an electron, which does not lead to dehydrogenation of the aliphatic alcohol. This electron can undergo a secondary recombination process with the iodine atoms in the solvent cage I, or be scavenged by a H^+ ion yielding a hydrogen atom, resulting in the formation of cage II. It will be shown later that the quantum yield for the processes in which H atoms as such are scavenged is also independent of light intensity. This shows that cage type recombination exists between I and H too and that the distribution of H atoms is not homogeneous. The pH dependent yield at high alcohol concentration represents the efficiency of electron scavenging by H^+ from cage I. This pH dependence of γ_i (curve 2, Fig. 1) was analyzed according to the general scavenging mechanism. The experimental results were found to be in agreement with eq. 11. These results presented in Fig. 4 yield a support for the scavenging mechanism. From Fig. 4 we obtain for the scavenging reaction of electrons by H^+ ions

$$\frac{2a}{\beta'}\sqrt{\pi k_{H^+ + e}} = 85 \text{ mole}^{-1/2}\,l.^{1/2},\ \beta' = 0.725 \text{ and}$$

hence $\gamma_r = 0.08 \pm 0.005$ and

$$2a\sqrt{\pi k_{H^+ + e}} = 62 \text{ mole}^{-1/2}\,l.^{1/2}$$

Application of the square root plot according to eq. 6 leads to a lower value of $2a\sqrt{\pi k_{H^+ + e}} = 30 \pm 10$ mole$^{-1/2}$ l.$^{-1/2}$. The difference obtained between these two treatments will be discussed.

Dependence of γ_i on Alcohol Concentration.—Hydrogen atoms formed in cage II can be scavenged by any efficient scavenger for H atoms. To get a further insight into this reaction mechanism the dependence of the quantum yield, $\gamma_i(H_2)$, on the concentration of methanol and isopropyl alcohol was investigated. These results are presented in Fig. 5.

The dependence of the quantum yield on methanol concentration at constant pH indicates that down to 0.2 M methanol the quantum yield is independent of the scavenger concentrations. At lower concentrations the quantum yield decreases, indicating the effect of secondary recombination. The gerneral mechanism for this system is in the form

$$(I + e)_I \longrightarrow I + e \quad (25)$$

$$(I + e)_I + H^+ \longrightarrow (I + H)_{II} \quad (26)$$

$$(I + H)_{II} \longrightarrow I + H \quad (27)$$

(13) T. Rigg and J. Weiss, *J. Chem. Soc.*, 4148 (1952).

(14) J. Franck and F. Haber, *Sitzber. preuss. Akad. Wiss. Physik. Math. Klasse*, 250 (1931).

$$(I + e)_I \longrightarrow I^- \quad (28)$$

$$(I + H)_{II} \longrightarrow I^- + H^+ \quad (29)$$

$$(I + H)_{II} + RH \longrightarrow I + R + H_2 \quad (30)$$

$$(I + H)_{II} + H^+ \longrightarrow I + H^+ + H \quad (31)$$

$$H^+ + e \longrightarrow H \quad (32)$$

$$H + RH \longrightarrow R + H_2 \quad (33)$$

reactions 28 and 29 represent secondary recombinations in the solvent cage. The residual yield is due to reactions 25 and 27. The scavenging reaction 30 leads to the formation of H_2. These results will be treated by application of a general equation for consecutive diffusion controlled scavenging.

Scavenging of H Atoms by Methanol and Isopropyl Alcohol.—The dependence of the quantum yield on methanol concentration is interpreted in terms of H atoms scavenging from cage II. In Fig. 6 the experimental results are plotted according to the scavenging equations. From the extended Noyes relation (23) we obtained $\gamma_r^I + \gamma_r^{II} = 0.08 \pm 0.005$ and $\Gamma_{II} 2a_{II}\sqrt{\pi k_{CH_3OH + H}} = 0.45$ mole$^{-1/2}$ l.$^{1/2}$. At pH 2.9 the yield is 0.260 and by setting $\gamma_r^I = 0.08$ obtained from Fig. 4 we get $\Gamma_{II} = 0.26 - 0.08 = 0.18$. Hence we obtain $2a_{II} \times \sqrt{\pi k_{CH_3OH + H}} = 2.5$ mole$^{-1/2}$ l.$^{-1/2}$.

The general consecutive scavenging equation (21) was applied in the form

$$\ln\left(1 - \frac{\gamma - \gamma_r^I}{\Gamma_{II}}\right) = \ln \beta_{II}' - \frac{2a_{II}\sqrt{\pi k_{CH_3OH + H}[CH_3OH]}}{\beta_{II}'} \quad (34)$$

with $\gamma_r^I = 0.08$ and $\Gamma_{II} = 0.18$. This treatment leads to $\beta_{II}' = 1$ and $2a_{II}\sqrt{\pi k_{H + CH_3OH}} = 3.8$ mole$^{-1/2}$ l.$^{1/2}$. A similar treatment for the scavenging of H atoms by isopropyl alcohol leads to $\beta_{II}' = 1$; $2a_{II}\sqrt{\pi k_{CH_3CHOHCH_3 + H}} = 20$ mole$^{-1/2}$ l.$^{1/2}$. The result $\beta_{II}' = 1$ indicates that the scavenging of the electron by H^+ to give an H atom has not significantly changed the probability of recombination in cage II. However this result does not mean that the residual yield from cage II is zero, since we have set $\Gamma_{II} = \Gamma - \gamma_r^I$ in the present approximation.

Consecutive Scavenging by H^+ Ions.—H^+ ions act in this system as scavengers in two consecutive steps. In the first step hydrogen atoms are formed in cage II through electron capture by H^+ ions (eq. 17). The effect observed in the pH region 2.5–6 in the presence of organic scavengers is due to this (curve 2, Fig. 1). A pH dependence in evacuated solutions in the absence of organic scavengers (curve 1, Fig. 1) is observed in the pH region below pH 2.5. This pH dependence is interpreted in terms of H atom scavenging by hydroxonium ions,[1] given schematically by eq. 31. The scavenging of H atoms by H^+ ions takes place in the pH region where complete scavenging of cage I has occurred already.

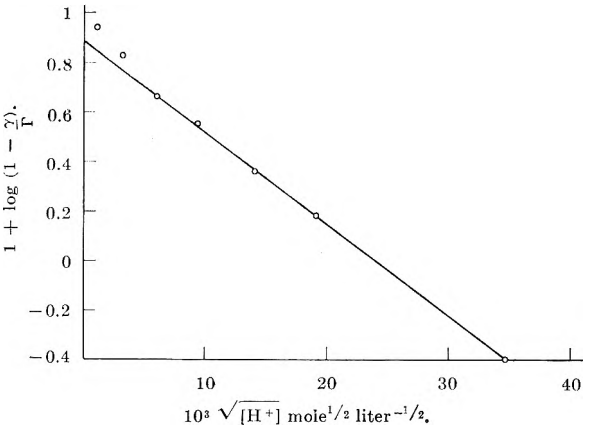

Fig. 4.—The dependence of $\gamma(H_2)$ on $\sqrt{[H^+]}$ according to eq. 11.

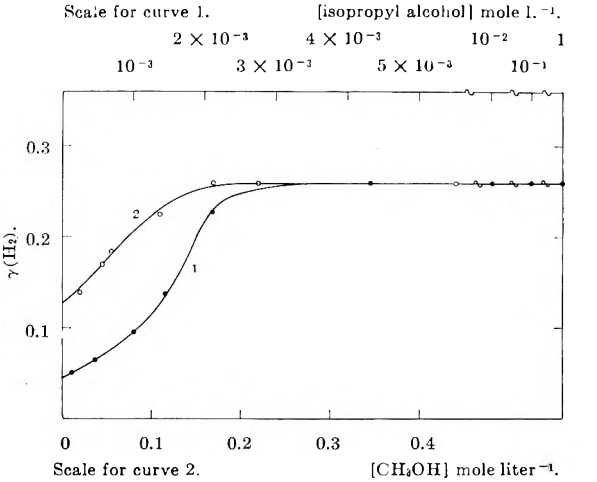

Fig. 5.—Dependence of $\gamma(H_2)$ on alcohol concentration: (1 ●, isopropyl alc. solutions; (2) ○, methanol solutions.

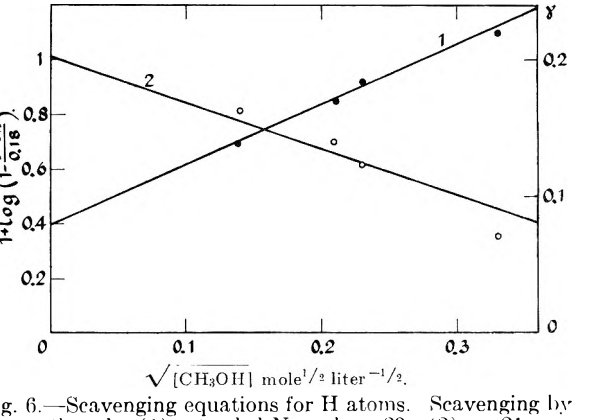

Fig. 6.—Scavenging equations for H atoms. Scavenging by methanol: (1) extended Noyes' eq. 23; (2) eq. 21.

It was shown[1] that the experimental results can be represented adequately by the Noyes relation. The parameters previously obtained[1] have to be interpreted in terms of eq. 23, setting $\Gamma_{II} = \Gamma - \gamma_r^I = 0.21$. Similar results have been obtained by application of the Roy–Hamill–Williams equation (Fig. 7). At high H^+ concentration (pH < 0.7) deviation from Noyes' relation was observed[1] which is due to the inadequacy of eq. 23 at high scavenger concentration. The experimental results over the whole H^+ concentration region were adequately

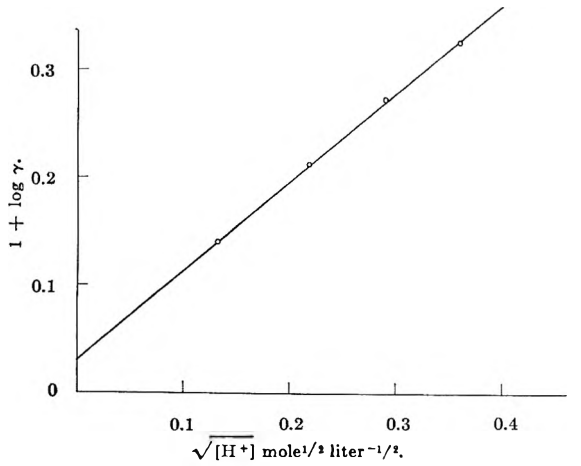

Fig. 7.—Roy-Hamill-Williams plot for scavenging of H atoms by H^+ ions.

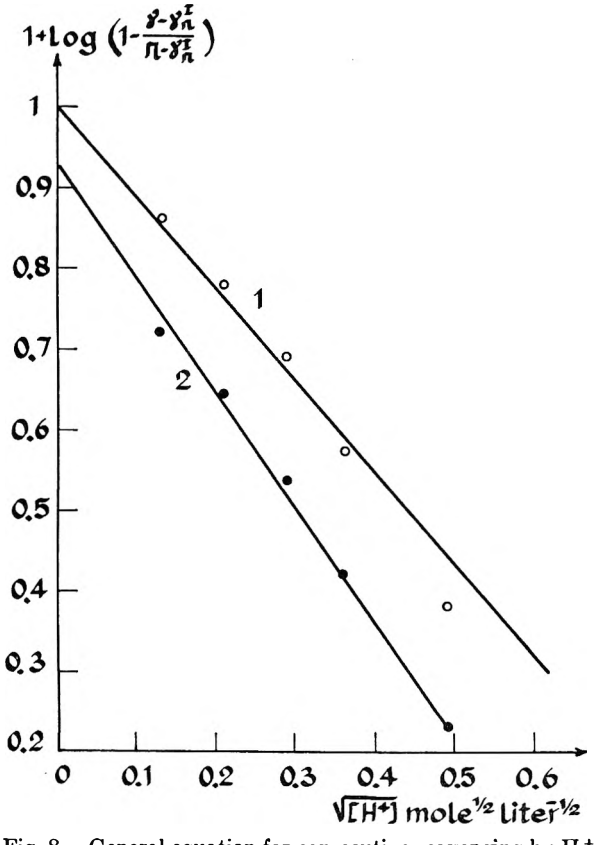

Fig. 8.—General equation for consecutive scavenging by H^+ ions (eq. 35): (1) $\gamma_r{}^I = 0.08$; (2) $\gamma_r{}^I = 0$.

represented by the consecutive scavenging equation

$$\ln\left(1 - \frac{\gamma - \gamma_r{}^I}{\Gamma - \gamma_r{}^I}\right) = \ln \beta_{II}' - \frac{2a_{II}}{\beta_{II}'}\sqrt{\pi k_{H+H^+}[H^+]} \quad (35)$$

Two limiting approximations were applied for the treatment of eq. 35. (a) It was assumed that the residual yield $\gamma_r{}^I$ is given by its maximum value of 0.08. This treatment is analogous to that in the presence of alcohols. (b) As the experiments considered were carried out in the low pH region where, as indicated by Fig. 3, H^+ completely scavenges cage I we set $\gamma_r{}^I = 0$. This is equivalent to the assumption that the cross-section for cage II is Γ, and eq. 35 is reduced to eq. 11.

The results obtained from these treatments (Fig. 8) are presented in Table I. The two limiting approximations of eq. 35 yield identical scavenging constants. However these results do not make possible the identification of the source of the residual yield.

TABLE I

SCAVENGING DATA FOR THE REACTION $H + H^+$

Eq.	$2a\sqrt{\pi k_{H+H^+}}$, mole$^{-1/2}$ l.$^{1/2}$	$\gamma_r{}^I + \gamma_r{}^{II}$	β_{II}'
23	1.57	0.092 ± 0.003	
15	1.2	0.100 ± 0.01	
35	2.6		1
11	2.55		0.8

The inspection of the results obtained for H atom scavenging by H^+ and methanol indicates that the rate constants k_{H+H^+} and k_{H+MeOH} are comparable. Application of the "absolute" rate constant[15] $k_{H+MeOH} = 10^5$ l. mole^{-1} sec.$^{-1}$ obtained from radiation chemical study at low pH leads to the estimation $k_{H+H^+} = 5 \times 10^4$ l. mole^{-1} sec.$^{-1}$, lower than our previous tentative estimation.[1]

The scavenging reaction 31 may proceed by the formation of H_2^+

$$(I + H)_{II} + H^+ \longrightarrow I + H_2^+ \quad (31a)$$

or alternatively by a charge transfer from H to H^+[17]

$$(I + H)_{II} + H^+ \longrightarrow I + H^+ + H \quad (31b)$$

leading to the separation of H and I which is kinetically equivalent to scavenging.

In a previous work[1] we attempted to discard the mechanism involving H_2^+ formation as it was previously shown that this reaction is a relatively slow process.[16] The kinetic treatment presented in that work[16a] involves a homogeneous kinetic treatment[16b] that leads to a lower limit for the rate constant,[16b,c] which may be underestimated by one order of magnitude. Thus the reaction mechanism 31a cannot be definitely excluded.[17]

Scavenging Mechanism by the Aliphatic Alcohols.—Hydrogen atoms will react with aliphatic alcohols by hydrogen atom abstraction. The scavenging mechanisms by the two alcohols will be presented in the form

$$(I + H) + CH_3OH \longrightarrow I + \dot{C}H_2OH + H_2 \quad (36)$$

(15) J. Rabani, *J. Phys. Chem.*, **66**, 361 (1962).

(16) (a) G. Czapski, J. Jortner, and G. Stein, *ibid.*, **63**, 1769 (1959); (b) **65**, 956 (1961); (c) **65**, 960 (1961).

(17) The charge transfer mechanism (31b) requires that in acid solutions, deuterium atoms should exchange with water at a rate which is at least as high as k_{H+H^+} observed in this work. The available experimental data show that this exchange reaction is slow. (T. W. Davis, S. Gordon, and E. J. Hart, *J. Am. Chem. Soc.*, **80**, 4487 (1958); H. L. Friedman and A. H. Zeltman, *J. Chem. Phys.*, **28**, 878 (1958); K. C. Kurien and M. Burton, Summary of Proceedings of the Fourth Informal Conference on the Radiation Chemistry of Water, University of Notre Dame, Indiana, 1961.) The lack of exchange in the case of H_2^+ may be resolved, *e.g.*, by assuming that in the species usually referred to as the solvated hydrogen molecule ion the protons are not equivalent.

TABLE II

INITIAL QUANTUM YIELDS IN EVACUATED KI SOLUTIONS IN THE PRESENCE OF ALCOHOLS. $[I^-] = 0.15\ M$

System	Concn., mole l.$^{-1}$	pH	$\gamma(I_2)$	$\gamma(H_2)$	$\gamma(CH_2O)$
Isopropyl alc.	1	2.05	10^{-3}	0.28 ± 0.01	
Isopropyl alc.	1	3.40	10^{-3}	$.24 \pm .01$	
Isopropyl alc.	4.3×10^{-3}	2.92	6×10^{-3}	$.26 \pm .01$	
Methanol	2.2×10^{-1}	2.92	10^{-2}	$.26 \pm .01$	0.27 ± 0.02

$$(I + H) + CH_3CHOHCH_3 \longrightarrow \cdot CH_3\overset{OH}{\overset{|}{C}}CH_3 + H_2 + I \quad (37)$$

Very low I_2 yields are obtained in the presence of alcohols. These results are summarized in Table II.

The low γ values for I_2 production are due to back reactions.

In methanol solution the radical CH_2OH formed acts as a reducing agent in the reactions leading to the formation of formaldehyde.

$$CH_2OH + I \longrightarrow CH_2O + H^+ + I^- \quad (38)$$

$$CH_2OH + I_2 \longrightarrow CH_2O + H^+ + I + I^- \text{ (or } I_2^-) \quad (39)$$

The presence of formaldehyde in irradiated methanol solution was confirmed by analysis with chromotropic acid. The quantum yield of CH_2O in this system yields

$$\gamma(H_2) = \gamma(I_2) + \gamma(CH_2O)$$

The experimental results lead to a reasonable material balance.

The Effect of Monophosphate Ion in the Presence of Alcohols.—An interesting influence of the $H_2PO_4^-$ ion on the reaction mechanism was observed in neutral solutions. At pH 6.25 we find $\gamma(H_2) = 0.05$ in 1 M isopropyl alcohol solution in the presence of $5 \times 10^{-3}\ M$ KH_2PO_4. This value is higher than $\gamma(H_2) = 0.033$ obtained at this pH in the absence of the monophosphate ion. In the same system at pH 5.92 in the presence of 1 M KH_2PO_4 we obtain $\gamma(H_2) = 0.23$ compared with $\gamma(H_2) = 0.040$ in the absence of monophosphate. These preliminary results indicate a specific effect of the monophosphate ion on the mechanism of the conversion of electrons of H atoms.

The Nature of the Residual Yield in the Presence of Alcohols.—The quantum yield $\gamma(H_2)$ obtained in 1 M alcohol solutions at pH > 6 is much lower than the value 0.08 expected for the residual yield from the semiquantitative treatment of the scavenging mechanism. These results indicate that the species diffusing into the bulk are not efficiently scavenged by alcohols. Thus we conclude that the residual yield in the neutral pH region consists mainly of electrons diffusing into the bulk. The conversion of a small fraction of these electrons to H atoms, scavenged by the alcohols, may occur through the bulk reaction 32 or, alternatively, may involve a dissociative electron capture by H_2O[18] leading to H and OH^-_{aq}. The experimental data available in this pH region are not accurate enough to make a discrimination between these two processes possible. However, the small value of $\gamma(H_2)$ in this region indicates that these reactions are not efficient. In alkaline solutions at pH 14 the quantum yield in the presence of 1 M methanol or isopropyl alcohol was found to be less than 0.005. Similar results on the effect of alkali on the residual yield were obtained by Norrish and Edgecombe.[19]

Photochemistry of I^- in the Presence of Methanol in D_2O.—The decrease of $\gamma(H_2)$ with decreasing methanol concentration at constant pH is attributed to secondary recombination of I and H atoms. A further support to the assumption that this decrease is not due to bulk recombination reactions was obtained from experiments in D_2O. The isotopic composition of the gas produced by irradiation of I^- in 98% D_2O in the presence of CH_3OD is presented in Table III.

TABLE III

PHOTOCHEMISTRY OF 0.15 M KI IN 98% D_2O IN THE PRESENCE OF CH_3OD. $H_2SO_4 = 1.4 \times 10^{-3}\ N$

CH_3OD, M	γ in D_2O	γ in H_2O	HD, %	H_2, %	D_2, %	$(H/D)_g$
0.22	0.33	0.260	89.8	9.6	0.6	1.22
0.055	0.22	0.185	91.7	7.3	1	1.10

These results indicate that the quantum yields for gas evolution in D_2O are higher than in H_2O. The results for ordinary water are presented for comparison in the third column of Table III. These conclusions were confirmed by a detailed investigation of the photochemistry of I^- in D_2O.[20] In D_2O a similar dependence of γ on methanol concentration as in H_2O was observed. The main gaseous product is HD in agreement with the proposed scavenging mechanism by methanol. These results provide a further support for the cage effect in this system, ruling out the possibility that the decrease of γ is due to bulk recombination reactions. The minor content of D_2 rules out any appreciable contribution of D atom recombination in the bulk. The increased H content in the gaseous phase compared to the hydrogen content of the solution is due to the photochemical isotope effect.[21,22] The results presented in Table III yield an isotope separation factor $S = (D/H)_l \times (H/D)_g$ of the order of 5 in qualitative agreement with previous results.

The Applicability of the Scavenging Equations.—The experimental results of the present work can

(18) D. M. Lea, "Action of Radiation on Living Cells," Cambridge University Press, 1947.

(19) R. G. W. Norrish and F. H. C. Edgecombe, *Proc. Roy. Soc.* (London), **A253**, 154 (1959).

(20) J. Jortner, M. Ottolenghi, and G. Stein, to be published.

(21) A. Farkas and L. Farkas, *Trans. Faraday Soc.*, **34**, 1120 (1938).

(22) J. Jortner and G. Stein, *J. Appl. Radiation and Isotopes*, **7**, 198 (1960).

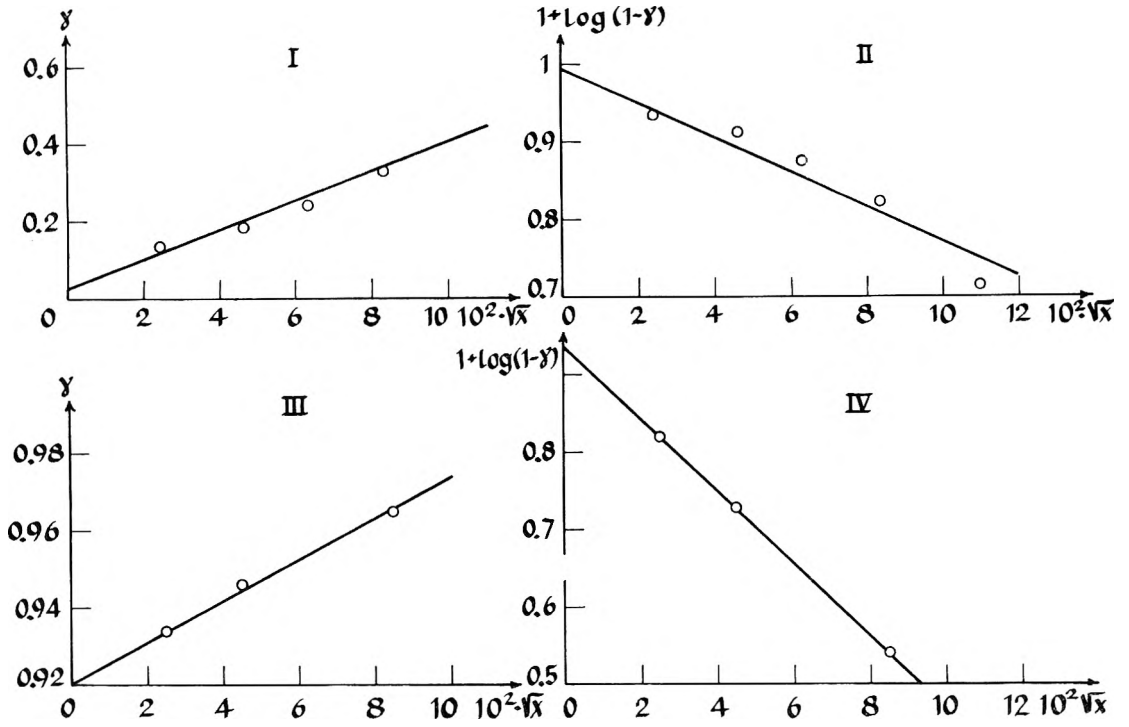

Fig. 9.—General analysis of some thermal and photochemical scavenging reactions: I, II, photolysis of azo-bis-isobutyronitrile[25]; I, eq. 6; II, eq. 11; III, IV, thermal decomposition of acetyl peroxide[23]; III, eq. 6; IV, eq. 11.

be interpreted in terms of scavenging mechanisms of two distinct species: the H atom precursors, (which presumably are electrons) and the genuine H atom. The treatment of the scavenging reaction by application of eq. 6 and 11 leads to somewhat differing results. The application of the Noyes relation (6) leads to results for the parameter $2a\sqrt{\pi k}$ which are 30–50% lower than the results obtained from the more general eq. 11. In order to investigate this point further, the available literature,[23–27] which can be interpreted in terms of radical scavenging competing with secondary recombination of a radical pair, was treated by application of eq. 6 and 11. These results include the photolysis of azo-bis-isobutyronitrile[25] and the thermal decomposition of acetyl peroxide.[23b] The experimental results for the photodissociation of the trihalide ions[23a] were not applied as the value of Γ is not available. These experimental results are reproduced in Fig. 9 and in Table IV.

The scavenging parameters obtained for these two systems show the same trend as indicated by our results. We attribute the discrepancy between the results of eq. 6 and 11 to the approximations involved in our treatment. It was assumed that the reactivity of the radicals with the scavenger is independent of the time since its formation. However the rate constant ${}^0k$ applicable to the initial reactivity and the long-time rate constant k are related by[2,10]

$$k = {}^0k(1 - \beta') \qquad (40)$$

For the scavenging mechanism in the case of the iodide system we find $\beta' = 0.7$. Thus the scavenging rate constant decreases by a factor of 3 until its final long-time value is reached. The Noyes relations 6 and 23 are applicable for low scavenger concentration in the region where the long-time rate constant can be applied. On the other hand the slope of the curve obtained by application of eq. 11 is mainly determined by experimental results at high scavenger concentrations. This procedure leads to higher values of the scavenging rate constant. As this complication was not taken into account in the present work the treatment should be regarded as semiquantitative and the scavenging parameters as approximate.

TABLE IV
APPLICATION OF EQUATIONS 11 AND 6 TO DIFFUSION-CONTROLLED SCAVENGING PROCESSES

System	Scavenger	Γ	β'	γ_r	$2a\sqrt{\pi k_s}$, mole$^{1/2}$ l$^{-1/2}$ Eq. 6	Eq. 11
Photolysis of Azo-bis-isobutyronitrile in benzene soln. (ref. 25)	I_2	1	~1	0.03	1.2	1.8
Thermal decomposition of acetyl peroxide in toluene soln. (ref. 23b)	I_2	1	0.08	0.915	0.17	0.29

The treatment presented in this work did not take into account ionic effects on reaction rates between the scavengers and the species scavenged. As this latter may be the negatively charged electron, the distribution of ionic scavengers and the presence of added ions may be of some influence.

Acknowledgment.—This work was sponsored by the Israel Atomic Energy Commission.

(23) (a) J. C. Roy, W. H. Hamill, and R. R. Williams, *J. Am. Chem. Soc.*, **77**, 2953 (1955); (b) *J. Phys. Chem.*, **60**, 823 (1956).

(24) D. L. Banbury, R. R. Williams, and W. H. Hamill, *J. Am. Chem. Soc.*, **78**, 6228 (1956).

(25) J. C. Roy, J. R. Nash, R. R. Williams, and W. H. Hamill, *ibid.*, **78**, 519 (1956).

(26) J. R. Nash, R. R. Williams, and W. H. Hamill, *ibid.*, **82**, 5974 (1960).

(27) H. A. Gillis, R. R. Williams, and W. H. Hamill, *ibid.*, **83**, 17 (1961).

THE EFFECT OF NITROUS OXIDE AND THE NATURE OF INTERMEDIATES IN THE PHOTOCHEMISTRY OF THE IODIDE ION IN AQUEOUS SOLUTION

BY JOSHUA JORTNER, MICHAEL OTTOLENGHI, AND GABRIEL STEIN

Department of Physical Chemistry, The Hebrew University, Jerusalem, Israel

Received December 28, 1961

The nature of the intermediates formed from the excited state of the I^- ion was considered. The scavenging mechanism by N_2O was investigated. Nitrous oxide was found to act as a specific scavenger for electrons. Semiquantitative treatment of the scavenging mechanisms is carried out. Chemical evidence for the transient formation of electrons in the photochemical system is presented. The mechanism of radical formation by the dissociation of the excited state is discussed.

Introduction

In the preceding paper[1] we investigated the photochemistry of KI solutions over a wide pH region in the presence of specific scavengers. The experimental results could be adequately interpreted in terms of a consecutive scavenging model. H^+ ions act as scavengers for electrons formed from the dissociation of the excited state. They yield H atoms which can be scavenged by H^+ ion or by organic solutes, *e.g.*, aliphatic alcohols.

In the present work we investigated the nature of the intermediates formed from the excited state. Nitrous oxide was used by Dainton, *et al.*,[2,3] in a recent radiation chemical[2] and photochemical investigation[3] in an attempt to discriminate between various forms of H atoms. The experimental results were interpreted by these authors[3] by assuming that nitrous oxide is inert to H_2^+ but reacts rapidly with H atoms. These conclusions are at variance with a recent kinetic analysis of the reactivity of H atoms in aqueous N_2O solutions,[4] which suggests that N_2O actually acts as a specific scavenger for solvated electrons. A further investigation of this problem appeared desirable.

The experimental results presented in the present and the preceding work make possible a further insight into the mechanism of the utilization of the optical excitation energy in a chemical radical formation process.

Experimental

The photochemical experiments at 2537 Å. were performed as described in previous work.[1,5] All experiments were carried out at 25°.

Procedure.—N_2O-containing solutions were prepared by evacuation of the neutral KI solution and the separate container containing sulfuric acid as previously described. The branch containing the reaction vessel and the acid container were isolated from the vacuum system. The N_2O gas used was a Matheson product. The gas was purified from traces of O_2 by freezing several times in a liquid air trap and pumping the uncondensable gases. Finally the liquid air trap was removed and the pressure of the gas was measured by a mercury manometer or a McLeod gage. Then the photochemical branch was connected to the vacuum line containing the purified N_2O.

An equilibration during 2–3 hours was carried out, the solutions in the reaction cell and the acid container being strongly stirred by Teflon coated magnetic stirrers. The partial pressure of the N_2O, P_{N_2O}, was calculated from the volume ratio of the isolated branch and the vacuum line. The acid was added to the reaction cell before irradiation.

The pressure of the gas evolved from irradiated solution was determined by a McLeod gage. The water vapor in the system was condensed in a CO_2–acetone trap and the N_2O in a liquid nitrogen trap. The composition of the gas was determined by simultaneous measurement of the pressure by Pirani and McLeod gages. The composition of the gas was determined by calibrating the Pirani gage with N_2–H_2 mixture. N_2O concentration was calculated from available solubility data.[6]

Results

Photochemistry of Aqueous Neutral KI Solutions in the Presence of N_2O.—In the present work a previous investigation[3] of the photochemistry of the iodide ion in the presence of N_2O was extended, in an attempt to use nitrous oxide for establishing the nature of the species produced, and for a further test of the scavenging mechanism. The dependence of the quantum yield in neutral unbuffered solutions (pH 6) on I^- and N_2O concentration was investigated. The initial yields are presented in Table I and the complete curves in Fig. 1. The gas evolved from the irradiated neutral solutions was found to be pure N_2, at pH 6 and P_{N_2O} = 640 mm., $\gamma(N_2) = 0.29 \pm 0.01$. Thus $\gamma(N_2) = \gamma(I_2)$, confirming previous results.[3]

TABLE I

PHOTOCHEMISTRY OF I^- IN N_2O SOLUTIONS AT pH 6

Temp., 25°; light intensity $I = 1.5 \times 10^{-6}$ eins. $l.^{-1}$ sec.$^{-1}$

P_{N_2O}, mm.	C_{N_2O}, M	I^-, M	γ_i
644	2.0×10^{-2}	0.15	0.295 ± 0.005
500	1.58×10^{-2}	.15	.293 ± .005
491	1.55×10^{-2}	.15	.290 ± .005
427	1.35×10^{-2}	.15	.294 ± .005
250	7.9×10^{-3}	.15	.290 ± .005
147	4.65×10^{-3}	.15	.290 ± .005
92	2.9×10^{-3}	.15	.265 ± .005
45	1.42×10^{-3}	.15	.235 ± .005
23	7.3×10^{-4}	.15	.219 ± .004
4.6	1.45×10^{-4}	.15	.161 ± .003
0.04	1.26×10^{-6}	.15	.092 ± .002
525	1.65×10^{-2}	1×10^{-3}	.28 ± .03[a]
525	1.65×10^{-2}	5×10^{-3}	.286 ± .005
525	1.65×10^{-2}	1.5×10^{-2}	.290 ± .005
525	1.65×10^{-2}	3.7×10^{-2}	.290 ± .005

[a] γ corrected for incomplete light absorption.

However, these results show that the quantum yield is independent of the I^- concentration over a wide region, indicating that the iodide ion does

(1) J. Jortner, M. Ottolenghi, and G. Stein, *J. Phys. Chem.*, **66**, 2029 (1962).

(2) F. S. Dainton and D. B. Peterson, *Nature*, **186**, 878 (1960).

(3) F. S. Dainton and S. A. Sills, *ibid.*, **186**, 879 (1960).

(4) G. Czapski and J. Jortner, *ibid.*, **188**, 50 (1961).

(5) J. Jortner, R. Levine, M. Ottolenghi, and G. Stein, *J. Phys. Chem.*, **65**, 1232 (1961).

(6) A. Seidell, "Solubilities of Inorganic and Organic Compounds," Supplement to the third edition, D. Van Nostrand, New York, N. Y., 1955.

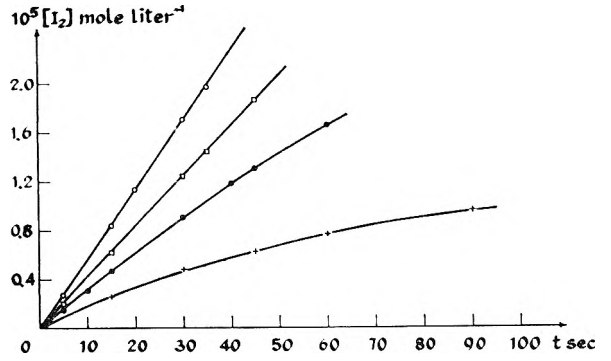

Fig. 1.—The dependence of I_2 production at constant light intensity on N_2O concentration; $J = 1.5 \times 10^{-6}$ einstein $l.^{-1}$ $sec.^{-1}$: ○, $N_2O = 1.6 \times 10^{-2} M$; □, $N_2O = 7.3 \times 10^{-4} M$; ●, $N_2O = 1.45 \times 10^{-4} M$; +, $N_2O = 1.26 \times 10^{-6} M$.

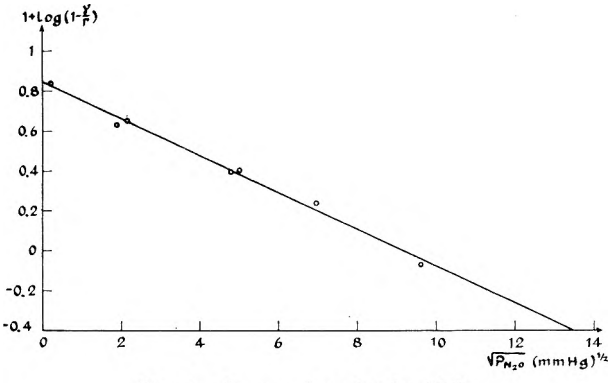

Fig. 2.—Scavenging plot for N_2O.

not take part in the primary radical formation process. This result is in variance with previous suggestions.[3]

At high N_2O concentration a limiting constant quantum yield independent of the scavenger concentration is obtained. This value $\Gamma = 0.293$ at 25° and 2537 Å. is identical with the limiting quantum yield obtained in other scavenger systems.[1,7]

As indicated by our previous results for the scavenging reaction in the presence of alcohols,[1] these specific scavengers for H atoms are not efficient in the neutral pH region (pH > 4). In this pH region H^+ ions are not present in sufficient concentration to serve as efficient scavengers for electrons, and thus H atoms are not produced. We thus conclude that the limiting yield obtained in the presence of N_2O in neutral solutions arises from the scavenging by N_2O of the precursors of H atoms, *i.e.*, electrons, formed from the dissociation of the excited state. The reaction mechanism in neutral N_2O solutions is presented in the form

$$(I + e)_I + N_2O \longrightarrow I + N_2 + O^- \quad (1)$$

For energetic reasons the back reaction between O^- and I is unfavorable in aqueous solution. The sum of the electron affinity of O and hydration energy of O^- (165 kcal.)[8] is higher than the corresponding sum for I (147 kcal).[8]

At pH below 10, O^- is effectively converted into an OH radical by

$$O^- + H_2O \longrightarrow OH + OH^- \quad (2a)$$

or

$$O^- + H^+ \longrightarrow OH \quad (2b)$$

The OH radicals thus formed act as an efficient oxidizing agent for I^- [9] by a diffusion controlled reaction

$$OH + I^- \longrightarrow I + OH^- \quad (3)$$

The equivalence of the quantum yields for nitrogen and iodine production is consistent with this mechanism.

Dependence of $\gamma(I_2)$ on N_2O Concentration at pH 6.—In the concentration region below $C_{N_2O} = 3.14 \times 10^{-3}$ mole $l.^{-1}$ the quantum yield in N_2O solutions at pH 6 is found to be dependent on N_2O concentration (Table I). This effect is attributed to the competition between the scavenging reaction and secondary recombination of the iodine atom and the electron in the solvent cage. The experimental results were analyzed by application of the general scavenging equation[1]

$$\ln\left(1 - \frac{\gamma}{\Gamma}\right) = \ln\left(1 - \frac{\gamma_r}{\Gamma}\right) - \frac{2a_I}{\beta_I'}\sqrt{\pi k_{(N_2O + e)}[N_2O]} \quad (4)$$

Figure 2 shows that the experimental results are consistent with eq. 4 over the whole concentration region. These results for electron scavenging by N_2O are compared in Table II with our previous results[1] for electron scavenging by H^+. The agreement between the values of γ_r^I in both cases shows the consistency of the treatment for two different scavengers. Assuming that the two scavenging processes involve the same radical pair, the results of Table II give the rate constant ratio for scavenging by H^+ and N_2O $k_{H^+ + e}/k_{N_2O + e} = 5$.

TABLE II

KINETIC DATA FOR ELECTRON SCAVENGING

Scavenger system	$\frac{2a_I}{\beta_I'}\sqrt{\pi k_8}$ mole$^{-1/2}$ $l.^{1/2}$	β_I'	γ_r^I
H^+, 1 *M* alcohol soln.	85	0.725	0.08 ± 0.005
N_2O, pH 6	38	0.759	0.07 ± 0.005

Effect of Light Intensity in the Presence of N_2O.—The dependence of $\gamma(I_2)$ on light intensity in neutral solutions containing N_2O is important for establishing the reaction mechanism, making possible the discrimination between ordinary bulk kinetics and diffusion controlled cage scavenging. The results presented in Table III indicate that

(7) The limiting quantum yield in neutral solutions reported in ref. 3 is 0.16. In ref. 3 the wave lengths range was 2000–2600 Å. (light source and the temperature not specified). We have found a quite substantial temperature effect on the limiting quantum yield. At 10° we find $\Gamma = 0.20$.

(8) Heats of solution are taken from Latimer, Pitzer, and Slansky, *J. Chem. Phys.*, **7**, 108 (1939), the heat of solution of O^- taken to be equal to that of OH^-. Electron affinities from H. O. Pritchard, *Chem. Rev.*, **52**, 529 (1953).

(9) C. B. Senvar and E. J. Hart, *Proc. 2nd Int. Conf. Peaceful Uses At. Energy*, **29**, 19 (1958).

$\gamma_i(I_2)$ is independent of light intensity over a rather wide range.

TABLE III

DEPENDENCE OF $\gamma_i(I_2)$ ON LIGHT INTENSITY AT pH 6 $[I^-] = 0.15\ M$

J, einstein l.$^{-1}$ sec.$^{-1}$	$\gamma_i(I_2)$ $[N_2O] = 1.7 \times 10^{-2}$ M	$\gamma_i(I_2)$ $[N_2O] = 1.42 \times 10^{-3}$ M
15.0×10^{-7}	0.292	0.240
12.35×10^{-7}	.298	.235
6.05×10^{-7}	.294	.236
1.78×10^{-7}	.288	.230
Mean value	.293 ± 0.005	.235 ± 0.005

Any bulk mechanism will assign the reduction of the quantum yield below the limiting yield Γ to the competition between the recombination reaction of I atoms and the reducing radical in the bulk and the scavenging of the radical by N_2O. This will lead to the dependence of γ on light intensity in the N_2O concentration region where $\gamma < 0.29$. The experimental results at $N_2O = 1.4 \times 10^{-3}$ mole l.$^{-1}$ are in variance with this conclusion, yielding a strong support to the assumption that the decrease of $\gamma(I_2)$ with decreasing N_2O concentration is due to recombination in the cage.

The pH Dependence in N_2O Solution.—The pH dependence for I_2 formation in N_2O solution at $C_{N_2O} = 0.01\ M$ is presented in Fig. 3. This pH dependence is qualitatively similar to that previously observed.[3] In the present case initial yields are presented. When the pH is decreased below 3 a lowering of the quantum yield is observed, rising again to the limiting yield at high acid concentration. This behavior is in complete agreement with the general mechanism involving H atom formation by electron scavenging by H^+. In the pH region below 3 both H^+ and N_2O act as efficient scavengers for the cage $(I + e)_I$. Thus in the low pH region parallel scavenging occurs by both scavengers.

The general reaction mechanism in N_2O solutions will be presented in the form

$$(I + e)_I + N_2O \longrightarrow I + OH + N_2 \qquad k_{N_2O + e} \quad (1)$$

$$(I + e)_I \longrightarrow I + e \qquad \gamma_r^I \quad (5)$$

$$(I + e)_I + H^+ \longrightarrow (I + H)_{II} \qquad k_{H^+ + e} \quad (6)$$

$$(I + H)_{II} + H^+ \longrightarrow I + H^+ + H \qquad k_{H^+ + H} \quad (7)$$

$$(I + H)_{II} \longrightarrow I + H \qquad \gamma_r^{II} \quad (8)$$

When the pH is decreased below 3 the radical pair $(I + H)_{II}$ is formed, in the solvent cage. In the absence of an efficient scavenger for H atoms they will undergo a secondary recombination lowering γ below the limiting value Γ. It is assumed (and will be further discussed) that N_2O is a poor scavenger for H atoms. An increase of $\gamma(I_2)$ is observed at pH < 2 as the H^+ concentration increases, reaching a value sufficient for efficient scavenging of H atoms by H^+ ions.[1] These results can be quantitatively accounted for by considering a general model for parallel scavenging.

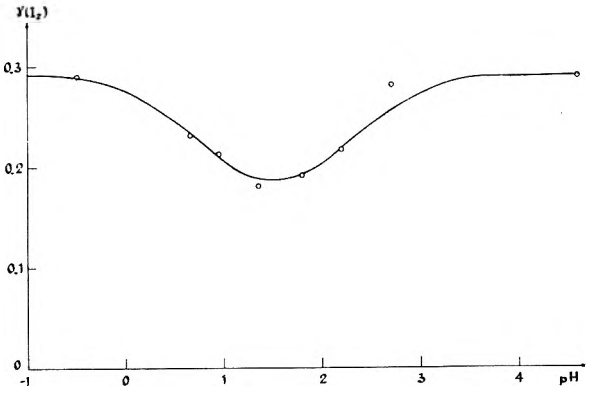

Fig. 3.—The pH dependence of $\gamma(I_2)$ in the presence of $1.6 \times 10^{-2}\ M$ N_2O: open circles, experimental data; solid curve, calculated from eq. 12.

Parallel Scavenging Model.—We consider a system where $i = 1 \ldots n$ efficient scavengers react with a radical undergoing secondary recombination. The parallel scavenging reactions are pseudo first order with rate constants $k_{S_i}[S_i]$. Applying the general considerations presented in previous work[1] the quantum yield for the depletion of the scavenger S_1 will be given by

$$-\frac{1}{J}\frac{d[S_i]}{dt} = \frac{k_{S_i}[S_i]}{\sum_{i=1\ldots m} k_{S_i}[S_i]}\Gamma\left(1 - \beta' e^{-(2a/\beta')\sqrt{\pi \sum_{i=1\ldots m} k_{S_i}[S_i]}}\right) \quad (9)$$

Parallel Scavenging by N_2O and H^+.—The pH dependence of the quantum yield of iodine production at relatively high N_2O concentration was investigated. For $C_{N_2O} > 3 \times 10^{-3}$ mole l.$^{-1}$ the results in neutral solution indicate that $\sqrt{[N_2O]} >> \beta'/2a\sqrt{\pi k_{N_2O + e}}$; thus the exponential term in eq. 9 can be neglected.

The total quantum yield is thus presented in the form

$$\gamma(I_2) = \gamma_r^I + (\Gamma - \gamma_r^I)\,\delta + (\Gamma - \gamma_r^I)(1 - \delta)\left(1 - \beta_{II}'\, e^{-(2a_{II}/\beta_{II}')\sqrt{\pi k_{H^+ + H^+}[H^+]}}\right) \quad (10)$$

where

$$\delta = \frac{k_{(N_2O + e)}[N_2O]}{k_{(N_2O + e)}[N_2O] + k_{(H^+ + e)}[H^+]}$$

In deriving this equation it is assumed that cage I yields a constant residual yield γ_r^I which is totally scavenged in the bulk contributing to the I_2 yield. The rest of the electrons in cage I are subjected to parallel scavenging by H^+ and N_2O. The fraction δ scavenged by N_2O fully contributes to the total yield while $1 - \delta$ is the relative efficiency for H atom production in cage II. Assuming that all the electrons are scavenged from cage I, the cross-section for the formation of cage II is $(\Gamma - \gamma_r^I)(1 - \delta)$. H atoms are then scavenged according to the ordinary eq. 4. Equation 10 can be transformed into the form

$$\gamma = \Gamma - (\Gamma - \gamma_r^I)(1 - \delta)\beta_{II}' e^{-(2a_{II}/\beta_{II}')\sqrt{\pi k_{H^+ + H^+}[H^+]}} \quad (11)$$

Inserting the numerical data previously obtained[1]

$$\beta_{II}' = 1; \quad \frac{2a_{II}}{\beta_{II}'}\sqrt{\pi k_s} = 2.6 \text{ mole}^{-1/2}\,\text{l.}^{1/2}; \quad \Gamma = 0.29_3; \quad \gamma_r^I = 0.08$$

we obtain

$$\gamma = 0.29_3 - \frac{0.21e^{-2.6[H^+]}}{1 + \frac{k_{(N_2O+e)}[N_2O]}{k_{(H^+ + e)}[H^+]}} \quad (12)$$

In Fig. 3 the experimental results are compared with the theoretical curve based on eq. 12. Fair agreement was obtained setting the rate constants ratio $k_{H^+ + e}/k_{N_2O + e} = 1$–5. The best agreement was obtained setting this rate constants ratio to 2, used in Fig. 3. These results are consistent with the comparison of the results for electrons scavenged by H^+ and by N_2O presented in Table II.

In the pH region where competition occurs between scavenging by H^+ and N_2O the quantum yield is expected to depend on N_2O concentration over the whole range employed by us, in contrast to the behavior at neutral pH where at high N_2O concentration the quantum yield is constant. The experimental results entirely confirm this prediction. In Table IV the dependence of $\gamma(I_2)$ on N_2O concentration at pH < 3 is presented.

TABLE IV

THE DEPENDENCE OF $\gamma(I_2)$ ON N_2O CONCENTRATION AT pH < 3

P_{N_2O}, mm.	$10^3 C_{N_2O}$, mole l.$^{-1}$	$\gamma(I_2)$ expt.	pH	$\gamma(I_2)$ calcd. Eq. 13	$\gamma(I_2)$ calcd. Eq. 12
500	16	0.218	2.2	0.195	0.220
293	9.2	.164	2.2	.165	.184
155	4.9	.132	2.2	.133	.172
285	9.0	.105	1.8	.130	.140

The comparison of the experimental results with the prediction of eq. 12 setting $k_{H^+ + e}/k_{H_2O + e} = 2$ is reasonable. However the calculated values are somewhat too high. We attribute this discrepancy to the approximation involved in the derivation of the consecutive scavenging model.[1] Besides, the application of eq. 12 is based on the assumption that every H atom introduced into the bulk by scavenging by H^+ oxidizes another I^- ion. This may not be applicable for pH 2.2 and 1.8. Therefore we have estimated the dependence of $\gamma(I_2)$ on N_2O concentration by applying our previous experimental results for evacuated solutions.[1,5] The quantum yield was represented in the form

$$\gamma(I_2) = \delta\Gamma + (1 - \delta)s\Gamma \quad (13)$$

where s represents the ratio of the quantum yield at the given pH in evacuated solution to the cross-section Γ. Agreement was obtained by applying eq. 13 at relatively low N_2O concentration.

The decrease of the quantum yield and its dependence on N_2O concentration at pH < 3 indicates that H atoms produced at this pH do not act efficiently with N_2O. These results can be interpreted by assuming the conversion of electrons to H atoms. These results cannot be interpreted by the hypothesis of Dainton, *et al.*,[2,3] who assumed conversion of H atoms to H_2^+ molecule ion. If H_2^+ would have been formed in this pH region the quantum yield for I_2 production would remain unchanged, as this species efficiently oxidizes I^- ions.[10]

Discussion

Chemical Evidence for Solvated Electrons in Water.—The photochemical results presented in this work yield chemical evidence for the formation of H atom precursors in water differing in their reactivity from H atoms as such. Recent radiation chemical data point in the same direction.

The fate of electrons, formed in the primary ionization process in the radiolysis of aqueous solutions, has been discussed previously.[11-12] Experimental evidence has recently been accumulating indicating the existence of two different forms of H atoms in irradiated solutions exhibiting different reactivity with specific scavengers. Barr and Allen[13] have shown that H_2O_2 is efficiently decomposed by the reducing species produced by ionizing radiation in neutral solutions, while H_2O_2 is less reactive with the species formed by the reaction

$$H_2 + OH \longrightarrow H + H_2O \quad (14)$$

or by ionizing radiation in acid solution.[13] An investigation of the decomposition of H_2O_2 by atomic hydrogen generated in the gaseous phase[14] indicated the identity of H atoms as such with the "acid form" produced by ionizing radiation and with the species produced by the reaction of OH radical with molecular hydrogen. The results of Allan and Scholes[15] and those obtained by the use of H atoms[14] led to the conclusion that the "neutral form" produced by ionizing radiation is the solvated electron. The result of radiation chemical investigation of aqueous solutions of monochloroacetic acid[16] was similarly interpreted. The relative radiation stability of nitrous oxide in irradiated acid solution[2] was attributed to the acid form of H atoms, which was assumed to be H_2^+.[2] However this conclusion is not consistent with the relative slow rate of formation of H_2^+.[9] The results of Dainton and Peterson[2] can be interpreted[4] in terms of an efficient decomposition of N_2O by solvated electrons and its stability to decomposition by genuine H atoms.

Kinetic evidence in the gas phase indicates that the activation energy for the reaction

(10) G. Czapski, J. Jortner, and G. Stein, *J. Phys. Chem.*, **64**, 1792 (1960).

(11) (a) A. H. Samuel and J. L. Magee, *J. Chem. Phys.*, **21**, 1080 (1953); (b) G. Stein, *Discussions Faraday Soc.*, **12**, 243 (1952).

(12) R. L. Platzman and H. Frohlich, *Phys. Rev.*, **92**, 1152 (1953).

(13) N. F. Barr and A. O. Allen, *J. Phys. Chem.*, **63**, 928 (1959).

(14) G. Czapski, J. Jortner, and G. Stein, *ibid.*, **65**, 964 (1961).

(15) J. T. Allan and G. Scholes, *Nature*, **187**, 218 (1960).

(16) E. Hayon and J. Weiss, *Proc. Int. Conf. Peaceful Uses At. Energy*, **29**, 80 (1958).

$$N_2O + H \longrightarrow N_2 + OH \qquad (15)$$

is 16.6 kcal. mole^{-1},[17] in agreement with an approximate previous estimation.[18] As the frequency factor for this reaction is 4×10^{11} l. mole^{-1} sec.$^{-1}$ [17] this reaction proceeds slowly in the gas phase at room temperature. The analysis[4] of some kinetic data[2] for the reactivity of H atoms in acid solution containing N_2O indicates that reaction 15 in aqueous solution is a relatively slow process, in agreement with the gas phase experiments. Two studies of negative ion formation in N_2O were published recently. The results of electron impact experiments[19] indicate that O^- ions are produced in N_2O with an onset at zero electron energy. The results of a mass spectrometric investigation[20] confirm these conclusions. These results indicate that in the gaseous phase the reaction

$$N_2O + e \longrightarrow N_2 + O^- \qquad (16)$$

proceeds efficiently. In the liquid phase the O^- ion will be stabilized by solvation. This independent evidence yields further support to our conclusions regarding N_2O as specific scavenger for electrons in aqueous solutions. The rate constants ratio $k_{H^+ + e}/k_{N_2O + e} = 2$–5 obtained from our photochemical experiments appears to be consistent with the radiation chemical results of Dainton and Peterson.[2]

In the present photochemical investigation we tried to select various specific scavengers for the discrimination between H atoms as such and their precursors. H^+ ion was found to act as an efficient scavenger for H atom precursors, *i.e.*, solvated electrons. The reaction

$$H^+_{aq} + e_{aq} \longrightarrow H \qquad (17)$$

appears to be efficient, in agreement with recent radiation chemical data.[15,16,21] This may proceed by direct electron capture by the hydroxonium ion, or by a general acid-catalyzed mechanism

$$H_3O^+ + H_2O + e_{aq} \longrightarrow H_2O + H_2O + H \qquad (17')$$

The increase of the quantum yield in the presence of the monophosphate ion at pH 5.9[1] may indicate the operation of such a mechanism. However at present this suggestion should be considered as tentative.

The nature of the solvated electrons formed in the photochemical system should be briefly considered. The most probable model involves an electron bound in the polarization field of the dielectric medium.[22–24] The time required for the solvation process of the electron is of the order of the relaxation time of the solvent molecules. A similar model is applicable for the thermalized electrons produced by ionizing radiation in water.[11b,24] The lifetime of this species is long enough in aqueous solutions to make its detection possible by reaction with specific active scavengers.

Mechanism of Primary Radical Formation.—The photochemical results presented in this work can be unambiguously interpreted by assuming the operation of a cage mechanism, and the decrease of the quantum yield with decreasing scavenger concentration should be assigned to secondary recombinations. The independence of the quantum yield on light intensity definitely rules out any bulk recombination mechanism. In our previous work[5] we have pointed out that the alternative mechanism involving the interaction of H^+ ion with the excited state followed by electron scavenging with direct formation of H atoms is not favored by the experimental data. At high scavenger concentration a limiting quantum yield of 0.290 ± 0.005 at 25° is obtained independent of the nature of the scavenger.

The absolute value of this limiting quantum yield probably is accurate within 10%, as it was determined by chemical actinometry using independently uranyl and ferrous oxalate actinometers. This result indicates that under our experimental conditions the limiting quantum yield of radicals which can be scavenged at 25° is about 33%. Thus the cross-section for primary radical formation is smaller than unity. This result rules out the direct interaction of the scavenger with the spectroscopic excited state of the ion, indicating that the fragments which can be scavenged are formed by a secondary process.

The photochemical results can be correlated with the spectroscopic data for this system. Recent experimental and theoretical investigations[25–27] indicate that the excited state can adequately be described by a spherical symmetrical excited orbital involving a considerable charge expansion. The role of the hydration configuration in formation of this excited state has been repeatedly stressed.[25,27] The upper limit for the lifetime of the first spectroscopic excited state is the relaxation time of the solvent molecules. During the relaxation process the electron is detached from the excited state of the absorption center resulting in the formation of two distinct species: an I atom and a solvated electron.

The detachment of the electron competes with deactivation of the excited state, which probably proceeds by a radiationless transition to the ground state. The cross-section for radical formation should be dependent on temperature and on the solvent. Our results on these problems will be published separately.

The electron thus formed by the dissociation of the excited state can be scavenged by specific scavengers, *e.g.*, H^+, N_2O, and O_2. This mechanism yields the major contribution to radical production. The present picture indicates that the major pathway of H atom production in this photochemical system does *not* involve a dissociative electron capture by a water molecule but electron capture by H^+. The scavenging

(17) C. P. Fenimore and G. W. Jones, *J. Phys. Chem.*, **63**, 1154 (1959).
(18) H. W. Melville, *J. Chem. Soc.*, 1243 (1934).
(19) G. J. Schultz, *J. Chem. Phys.*, **34**, 1778 (1961).
(20) R. K. Curran and R. E. Fox, *ibid.*, **34**, 1590 (1961).
(21) A. R. Anderson and E. J. Hart, *J. Phys. Chem.*, **65**, 805 (1961).
(22) L. Landau, *Phys. Z. Sowjetunion*, **3**, 664 (1933).
(23) J. Jortner, *J. Chem. Phys.*, **30**, 839 (1959).
(24) J. Weiss, *Nature*, **186**, 751 (1960).
(25) J. Franck and R. L. Platzman, *Z. Physik*, **138**, 411 (1954).
(26) M. Smith and M. C. R. Symons, *Trans. Faraday Soc.*, **54**, 338, 346 (1959).
(27) G. Stein and A. Treinin, *ibid.*, **55**, 1086, 1091 (1959).

experiments definitely rule out the mechanism of Franck and Haber[28] for this system.

The results with N_2O prove also that the role of the positive H^+ ion is not unique and that another, neutral electron scavenger can lead to a similar process.

The present picture involves a thermal electron detachment process from the excited state of the solvated negative ion, leading to the formation of a solvated electron in the aqueous solution. The formation of a thermalized electron is plausible in the case of an excited iodide ion, where the electron in the expanded orbital is acted upon only by the polarization field of the medium.

Franck and Scheibe[29] in their original work postulated a photodetachment process as the primary light absorbtion act of negative ions in solution. Our results show that this occurs only as the result of a secondary thermal process.

Acknowledgment.—This research was sponsored by the Israel Atomic Energy Commission.

(28) J. Franck and F. Haber, *Sitzber. preuss. Akad. Wiss. Physik Math. Klasse*, 750 (1931).

(29) J. Franck and G. Scheibe, *Z. physik. Chem.*, **A139**, 22 (1928).

THE EFFECT OF OXYGEN ON THE PHOTOCHEMISTRY OF THE IODIDE ION IN AQUEOUS SOLUTIONS

BY JOSHUA JORTNER, MICHAEL OTTOLENGHI, AND GABRIEL STEIN

Department of Physical Chemistry, The Hebrew University, Jerusalem, Israel

Received December 28, 1961

The effect of O_2 on the photochemistry of aqueous iodide solutions was investigated. O_2 was found to act as a scavenger for both electrons and H atoms. The reaction mechanisms are discussed and kinetic data for the reaction of O_2 with electrons and H atoms are derived. The photochemical results are compared with data from radiation chemistry.

Introduction

Radiation chemical investigations[1] indicate that oxygen dissolved in aqueous solutions acts as an efficient scavenger for both solvated electrons and for H atoms.[1]

Following the preceding work,[2] the effect of O_2 on the photochemistry of the iodide ion was investigated. The investigation of the oxygen effect on this system is of importance for a further insight into the specific scavenging mechanisms of H atoms and their precursors.

Experimental

The experimental technique was similar to that previously employed.[2] Evacuated neutral potassium iodide solutions were equilibrated with air or oxygen for 2–3 hr. The pH was adjusted by acid added just before irradiation, which was carried out as fast as possible to avoid thermal oxidation. The kinetics of the post-irradiation effect in aerated solution were measured by the determination of the time dependence of the I_2 concentration in the reaction vessel after stopping the irradiation. The thermal oxidation was followed by a similar technique.

Results

Some experimental difficulties were encountered in the experimental investigation of this system at low pH. The effect of the thermal oxidation of I^- at pH < 2.5 is appreciable. Short irradiation times (15 sec.) were used, and corrections for thermal oxidation were introduced. The derivation of the experimental results for the initial quantum yields was further complicated by the observation of a post-irradiation effect in aerated solutions. It was assumed that this effect is due to the production of H_2O_2 in irradiated solutions. To confirm this hypothesis a kinetic study of this process was carried out. We measured the dependence of the I_2 concentration (determined as the optical density D_τ) on the time τ after stopping the irradiation. First-order kinetic curves were obtained by plotting ln $(D_\infty - D_\tau)$ as a function of τ (Fig. 1). The experimental values of D_τ were corrected for thermal oxidation. From the first-order rate constants k the second-order rate constants $k/[I^-]$ were obtained, in agreement with the result for thermal oxidation of I^- by H_2O_2.[3] These results indicate that H_2O_2 is produced in the photochemical system.

TABLE I

POST-IRRADIATION EFFECT IN IRRADIATED KI SOLUTIONS

$[I^-] = 0.15\ M$, $J = 15 \times 10^{-7}$ einstein sec.$^{-1}$ l.$^{-1}$

pH	k, min.$^{-1}$	$k/[I^-]$, l. mole^{-1} min.$^{-1}$	D_0	D_∞
1.29	0.048	0.75	0.265 ± 0.02	0.48 ± 0.03
0.83	0.22	3.37	0.26 ± 0.02	0.50 ± 0.03

As the thermal oxidation of I^- by H_2O_2 during the short irradiation period is negligible, the initial $[I_2]_0$ concentration corrected for the post-irradiation effect was obtained from extrapolation of log $(D_\infty - D_\tau)$ to $\tau = 0$. We find (Table I) $2D_0 = D_\infty$, *i.e.*, $2[I_2]_0 = [I_2]_\infty$. Thus the quantum yield for H_2O_2 production is equal to that of I_2 during irradiation. The quantum yield at low pH could be evaluated by measuring $\gamma(I_2) + \gamma(H_2O_2)$. This was done by determination of I_2 yield after the completion of the post-irradiation effect about 60 min. after stopping the irradiation.

Dependence of γ on pH and O_2 Concentration—In Fig. 2 and 3 we represent the dependence of the initial quantum yield for I_2 production on pH and O_2 concentration. These quantum yields were corrected for thermal oxidation and do not include contribution of the oxidation by H_2O_2. γ_i at

(1) N. F. Barr and A. O. Allen, *J. Phys. Chem.*, **63**, 928 (1959).

(2) J. Jortner, M. Ottolenghi, and G. Stein, *ibid.*, **66**, 2037 (1962).

(3) H. A. Liebhafsky and A. Mohamed, *J. Am. Chem. Soc.*, **55**, 3977 (1933).

$[O_2] = 2 \times 10^{-4}$ M in air saturated solution at pH 2.56 and 3.56 was found to be independent of the light intensity J. The pH dependence of $\gamma(I_2)$ in Fig. 2 is represented in the concentration region of O_2 where $\gamma(I_2)$ is independent of O_2 concentration.

At low pH values (below 2) $\gamma_i(I_2)$ is independent of H^+ concentration and attains the limiting value $\gamma_i = 0.29 \pm 0.02$ at 25°, which is again identical with the limiting quantum yield obtained in other scavenger systems.[2]

When the pH is increased $\gamma_i(I_2)$ decreases. The independence of γ on J indicates that this decrease has to be assigned to secondary radical recombination.

At pH 2.56 in air saturated solutions $\gamma(I_2) = 0.26$. This value is identical with the result $\gamma = 0.26$ obtained in the presence of high concentration of alcohols at this pH.[4] Thus it appears that at pH 2.5–3.0 the decrease of the quantum yield is due mainly, as in the case of alcohols, to the formation of the radical pair $(I + H)_{II}$ and the scavenging of the H atom by O_2. However at higher pH values the γ values obtained in the presence of O_2 and alcohols do differ markedly. At pH 3.56 $\gamma(I_2) = 0.16$ in air saturated solutions and $\gamma(I_2) = 0.225$ in the presence of 1 M methanol or isopropyl alcohol.[4] This indicates that in the presence of oxygen an additional mechanism is operating. As radiation chemical studies[1] indicate, O_2 is an efficient scavenger for electrons. Thus at low H^+ concentrations (pH > 3) electron capture by O_2 will occur. This reaction will compete efficiently with electron capture by H^+, leading to the formation of O_2^-. This ion may however reduce an iodine atom to I^- leading to a deactivation back reaction. Alternatively O_2^- can react with H^+ ion yielding HO_2. This scavenging reaction will compete with the back reaction $I + O_2^-$. The hydroperoxy radical yields H_2O_2 by oxidation of another I^- ion.

Reaction Mechanism in the Presence of O_2.— The experimental results for the initial quantum yield in oxygen containing solutions are interpreted in terms of a parallel—consecutive scavenging mechanism

$$(I + e)_I + H^+ \longrightarrow (I + H)_{II} \quad k_{H^+ + e} \quad (1)$$

$$(I + H)_{II} + O_2 \longrightarrow I + HO_2 \quad k_{O_2 + H} \quad (2)$$

$$(I + e)_I + O_2 \longrightarrow (I + O_2^-)_{III} \quad k_{O_2 + e} \quad (3)$$

$$(I + O_2^-)_{III} + H^+ \longrightarrow I + HO_2 \quad k_{H^+ + O_2^-} \quad (4)$$

Followed by

$$I^- + HO_2 \longrightarrow I + HO_2^- \quad (5)$$

$$2I^- + H_2O_2 + 2H^+ \longrightarrow I_2 + 2H_2O \quad (6)$$

The radical pairs I, II, and III may also contribute to the residual yield.

An exact mathematical treatment of this system is complicated. We attempt to present an approximate treatment applying simplifying assumptions as presented before.[2,4]

(4) J. Jortner, M. Ottolenghi, and G. Stein, *J. Phys. Chem.*, **66**, 2029 (1962).

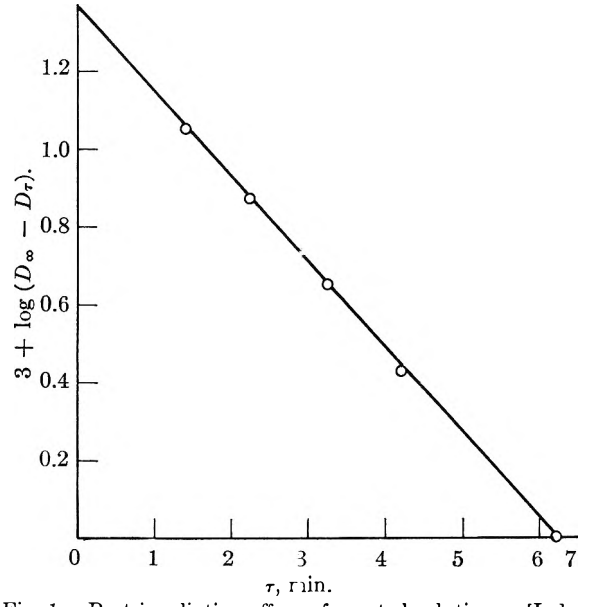

Fig. 1.—Post-irradiation effect of aerated solution: $[I^-] = 0.15$ M, pH 0.83.

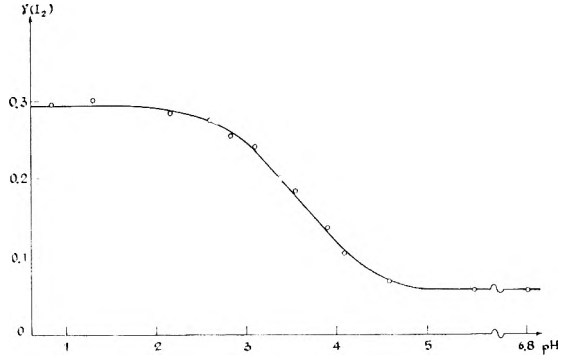

Fig. 2.—The pH dependence of $\gamma(I_2)$ (corrected for the contribution of the post-irradiation effect) in aerated solutions.

The quantum yield in the presence of O_2 is presented in the general form

$$\gamma = \gamma_r^I + A[\, W(1 - \beta_{II}' e^{-(2a_{II}/\beta'_{II})\sqrt{\pi K'_{O_2}}}) + (1 - W)(1 - \beta_{III}' e^{-(2a_{III}/\beta_{III}')\sqrt{\pi K_{H^+}'}})] \quad (7)$$

A represents the total cross-section for electron scavenging from cage I by O_2 and H^+. Assuming that the radical pair I yields the residual yield γ_r^I independent of the two scavenger concentrations we set

$$A = \Gamma[1 - \beta_I' e^{-(2a_I/\beta_I')\sqrt{\pi K_{O_2} + K_{H^+}}})] - \gamma_r^I \quad (8)$$

The constants K in eq. 7 and 8 are defined by

$$K_{O_2} = k_{O_2 + e}[O_2]$$

$$K_{O_2}' = k_{O_2 + H}[O_2]$$

$$K_{H^+} = k_{H^+ + e}[H^+]$$

$$K_{H^+}' = k_{H^+ + O_2^-}[H^+]$$

W represents the fraction of radicals from cage I scavenged by H^+, *i.e.*, $W = K_{H^+}/(K_{H^+} + K_{O_2})$; thus the cross-section for the formation of cage II is WA.

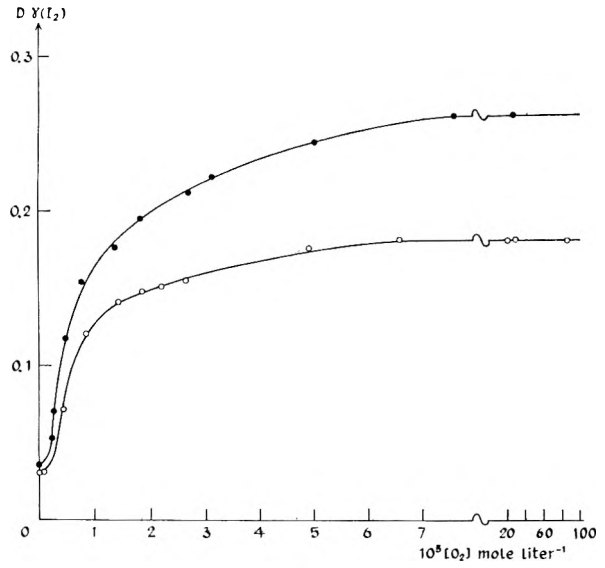

Fig. 3.—Dependence of $\gamma(I_2)$ and O_2 concentration: ● pH 2.56; ○, pH 3.56.

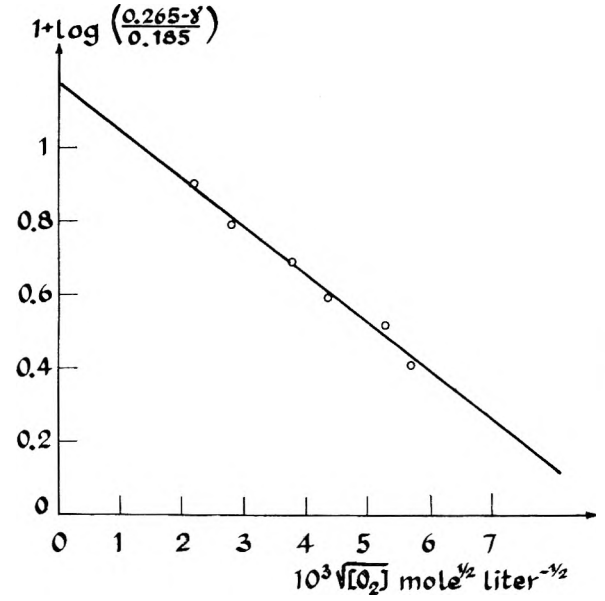

Fig 4.—Scavenging of H atoms by O_2 at pH 2.56.

Equation 7 can be transformed into the form

$$\gamma = \gamma_r^I + A[1 - W\beta_{II}' e^{-(2a_{II}/\beta_{II}')\sqrt{\pi K_{O_2}'}} - (1 - W)\beta_{III}' e^{-(2a_{III}/\beta_{III})'\sqrt{\pi K_{H^+}'}}] \quad (7')$$

Scavenging of H Atoms by O_2.—At sufficiently high H^+ concentrations, at pH < 3, we assumed that the reaction path involves scavenging by H^+ (reaction 1) and the contribution of reaction 3 is negligible. Equation 7′ is reduced to the form

$$\gamma = \gamma_r^I + [\Gamma(1 - \beta_I' e^{-2a_I/\beta_I'\sqrt{\pi K_{H^+}}}) - \gamma_r^I] \times (1 - \beta_{II}' e^{-(2a_{II}/2\beta_{II}')\sqrt{\pi K_{O_2}}}) \quad (9)$$

This equation was applied for the treatment of the dependence of $\gamma(I_2)$ on O_2 concentration at pH 2.56. At limiting high O_2 concentration the quantum yield is (Fig. 3)

$$\Gamma(1 - \beta_I' e^{-(2a_I/\beta_I')\sqrt{\pi K_{H^+}}}) = 0.26$$

The rate constant $k_{O_2 + H}$ was evaluated by plotting $\log [(0.26 - \gamma)/(0.26 - 0.08)]$ as a function of $\sqrt{[O_2]}$. From Fig. 4 we obtain $\beta_{II} \sim 1$ and $2a_{II} \times \sqrt{\pi k_{H + O_2}} = 260$ mole$^{-1/2}$ l.$^{1/2}$.

Scavenging of O_2^- by H^+.—For high pH $K_{O_2} \gg K_{H^+}$ and at high O_2 concentration where $A = \Gamma - \gamma_r^I$ we set $W = 0$ and thus obtain from eq. 7′, for the scavenging reaction of O_2^- by H^+

$$\ln\left(\frac{\Gamma - \gamma}{\Gamma - \gamma_r^I}\right) = \ln \beta_{III}' - \frac{2a_{III}}{\beta_{III}'}\sqrt{\pi k_{H^+ + O_2^-}[H^+]} \quad (10)$$

We have assumed that eq. 10 is applicable for pH > 3.5. From the experimental results in this high pH region we obtained $\beta_{III}' = 1$ and $2a_{III} \times \sqrt{\pi k_{H^+ + O_2^-}} = 60 \pm 20$. This result indicates that the rate constant $k^{H^+ + O_2^-}$ is high, in agreement with kinetic data[5] which indicate that the rates of neutralization of bases in solution are diffusion controlled.

Semiquantitative Treatment of Experimental Results in the Presence of O_2.—The numerical values for β_{II}', β_{III}', $2a_{II}\sqrt{\pi k_{H + O_2}}$, and $2a_{III} \times \sqrt{\pi k_{O_2^- + H^+}}$ obtained from the above approximate treatments may be substituted now in eq. 7′ yielding

$$\gamma = 0.08 + [0.29(1 - 0.725e^{-50\sqrt{[H^+] + \alpha[O_2]}}) - 0.08] \times \left[1 - \left(\frac{e^{-260\sqrt{[O_2]}}}{1 + \alpha([O_2]/[H^+])} - \frac{e^{-60\sqrt{[H^+]}}}{1 + ([H^+]/\alpha[O_2])}\right)\right] \quad (11)$$

where $\alpha = k_{O_2 + e}/k_{H^+ + e}$. For the parameters specifying electron scavenging by H^+, appearing in A, we chose $\beta_I = 0.725$ and $(2a_I/\beta_I')\sqrt{\pi k_{H^+ + e}} = 50$. This value is somewhat lower than that obtained in the presence of alcohols,[4] but is consistent with the results for competitive scavenging of electrons by H^+ and N_2O.[2]

The experimental results do not make possible the exact evaluation of α. However, reasonable agreement of the experimental results with eq. 11 is obtained for $\alpha = 1-5$ showing that the efficiency of O_2 and H^+ as electron scavengers is of the same order of magnitude.

The comparison of the experimental results with those obtained from eq. 11 is presented in Table II.

The good agreement of the calculated and experimental results should be accepted with some reservation. The general treatment presented in this work is too approximate for a quantitative treatment of this complicated system.

Discussion

The Residual Yield in O_2 Solutions.—The quantum yield obtained at pH > 4.5 in air and oxygen saturated solutions is independent of pH. This

(5) M. Eigen and K. Kusten, *J. Am. Chem. Soc.*, **82**, 5952 (1960).

TABLE II

QUANTUM YIELDS IN THE PRESENCE OF OXYGEN. CALCULATED RESULTS FROM EQUATION 11 WITH $\alpha = 3$

pH	$[O_2]$, mole l.$^{-1}$	$\gamma(I_2)$, expt.	$\gamma(I_2)$, calcd.
1.0	2.3×10^{-4}	0.290 ± 0.005	0.290
2.15	2.3×10^{-4}	$.285 \pm .005$	.275
2.6	2.3×10^{-4}	$.260 \pm .005$	.270
2.8	2.3×10^{-4}	$.246 \pm .005$	.250
3.9	2.3×10^{-4}	$.133 \pm .005$	.155
4.1	2.3×10^{-4}	$.110 \pm .005$	.140
2.56	6.6×10^{-5}	$.250 \pm .005$	.240
2.56	3.95×10^{-5}	$.230 \pm .005$	.235
2.56	2.5×10^{-5}	$.207 \pm .005$	.210
2.56	1.32×10^{-5}	$.190 \pm .005$	.175
2.56	0.83×10^{-5}	$.150 \pm .005$	.170
3.56	6.6×10^{-5}	$.180 \pm .005$	.171
3.56	3.95×10^{-5}	$.167 \pm .005$	.168
3.56	2.5×10^{-5}	$.150 \pm .005$	.153
3.56	1.32×10^{-5}	$.137 \pm .005$	.142
3.56	0.83×10^{-5}	$.122 \pm .005$	.133

quantum yield, $\gamma = 0.065 = 0.01$, represents the experimental determination of the residual yield. In the presence of oxygen the residual yield represents the sum of the residual yields γ_r^{I} and γ_r^{III}. As indicated by the experimental results in the presence of alcohols at high pH[2] hydrogen atom scavengers are not efficient for the residual yield in neutral solution. On the other hand, O_2 is an efficient scavenger for electrons. The residual yield in the presence of O_2 is about equal to the extrapolated values of $\gamma_r^{I} = 0.07$ and 0.08 obtained[2,4] from the pH dependence in the presence of alcohols and from scavenging by N_2O. These results indicate that the residual yield from cage I involves solvated electrons and not H atoms diffusing into the bulk.

Relative Rate Constants for the Reactivity of H Atoms.—The experimental results from the scavenging experiments make possible the evaluation of relative rate constants for the reactivity of various scavengers with H atoms and electrons. The relative rate constants for the reactivity of H atoms with various scavengers are shown in Table III and compared with kinetic data obtained from radiation chemical investigations.[6] These radiation chemical investigations were carried out at low pH to assure that H atoms as such are involved in these reactions.[6] The agreement between the photochemical and radiation chemical data is fair and indicates the consistency of the mechanisms derived.

TABLE III

KINETIC DATA FOR THE REACTIVITY OF H ATOMS

Scavenger	$2a_{II}\sqrt{\pi k_r}$, mole$^{-1/2}$ l.$^{1/2}$	$\frac{k_{H+S}}{k_{H+O_2}}$ (photochemical data)	$\frac{k_{H+S}}{k_{H+O_2}}$ (radiation-chemical data)[6]
Methanol	3.88	16×10^{-5}	8.5×10^{-5}
Isopropyl alc.	20	5×10^{-3}	2.6×10^{-3}
H^+	2.6	10^{-4}	...
O_2	260		

The Reactivity of Electrons.—Molecular oxygen in the photochemical system was found to act as an efficient scavenger for electrons. The rate constant for the reaction

$$O_2 + e_{aq} \longrightarrow O_2^-{}_{aq} \qquad (12)$$

is about equal to the rate constant for the reaction

$$H^+{}_{aq} + e_{aq} \longrightarrow H \qquad (13)$$

This result is in complete agreement with a recent radiation chemical investigation of the pH dependence of the decomposition of H_2O_2 in the presence of O_2.[7]

Czapski and Allen[7] concluded that for the reducing radicals produced from the radiolysis of neutral aqueous solutions, the rate constants for reactions 12 and 13 are equal within a few per cent. In a similar way agreement was obtained[2] between photochemical and radiation chemical data for the relative rate constants for scavenging electrons by H^+ and N_2O. These results indicate the identity of H atom precursors formed by thermal electron detachment from the excited state of the iodide ion, with the reducing species formed from the radiolysis of neutral aqueous solutions.

Acknowledgment.—This research was sponsored by the Israel Atomic Energy Commission.

(6) J. Rabani, *J. Phys. Chem.*, **66**, 361 (1962).

(7) G. Czapski and A. O. Allen, BNL. 5576, 1961; *J. Phys. Chem.*, **66**, 262 (1962).

STRAIN BIREFRINGENCE OF A SOLUTION OF ROD-SHAPED MOLECULES[1]

BY S. J. GILL AND F. R. DINTZIS

Department of Chemistry, University of Colorado, Boulder, Colorado

Received April 9, 1962

A theoretical calculation is made for birefringence induced in a system of rod-shaped molecules which have been subjected to a two dimensional strain of constant area. A series expression is developed for the orientation of a system of rods which have the particular optical and geometrical properties of the strained system; then the birefringence of this system is given by an expression developed from assumptions of Peterlin and Stuart. This expression is used in conjunction with birefringence measurements to obtain the optical factor, $g_1 - g_2$, for concentrated solutions of poly-γ-benzyl-l-glutamate in 1,2-dichloroethane. An average optical factor of $(5.4 \pm 1.0) \times 10^{-8}$ was obtained for these solutions; this compares with a value of about $(4.0 \pm 0.1) \times 10^{-8}$ obtained from flow birefringence measurements (by Doty) and electric birefringence (by O'Konski) on dilute solutions.

I. Introduction

An anisotropic state can be induced within an originally isotropic medium by a number of different procedures. The most familiar use electric, magnetic, or shear fields.[2] The anisotropic state can be characterized conveniently by measurements of the induced birefringence. It then often is possible to relate the macroscopic measurement of birefringence of the oriented state with the molecular properties of the system. In this respect the application to macromolecular systems has been particularly rewarding.

One of the first molecular models suggested to interpret induced birefringence effects was that of the rigid rod particle.[3,4] One then could ascribe specific optical and geometrical properties to the particle and consider the resulting effects of orientation in different fields. Peterlin and Stuart considered this problem for the cases of magnetic, electric, and continuous flow fields.[2] The application of flow birefringence has been extensive.[5] Recently, O'Konski[6] and Tinoco[7,8] have employed the method of electric field orientation.

The same general method is applicable to nonfluid systems. In this case, orientation of optically anisotropic particles can be induced by deformation of the material. Kratky,[9] and Kuhn and Grün[10] describe the case of induced birefringence from simple extension of an elastic matrix imbedded with rigid rod macromolecules. Hermans[11] and others[12] have studied the properties of cellulose by extending this reasoning to include effects of jointed rods.

Recently a technique was developed for suddenly straining a viscoelastic fluid.[13] The strain is characterized as two dimensional strain with constant area. A transient birefringence is observed following the application of this strain to concentrated polymer solutions. The method has been used to study relaxation behavior of concentrated solutions.[14] Under favorable conditions where the relaxation is not too rapid, it is possible to estimate the induced birefringence at the moment of straining. For a concentrated solution of coil-like molecules it has been possible to apply the theory of rubber-like elasticity and estimate the number of effective network points.[15]

In the present paper we wish to give a derivation of theoretical expressions which are applicable to a constant area strain for a system of rigid rod macromolecules. These expressions are used to interpret strain birefringence measurements on concentrated solutions of polybenzylglutamate. The results compare reasonably well with dilute solution properties obtained by O'Konski[6] and Doty.[16]

II. Theoretical

The symmetry of simple extension strain allowed Kuhn and Grün[10] to choose the conventional spherical coördinate system to describe the orientation distribution function of rod-like particles as a function of strain. For our case of plane strain a different coördinate description is used in order to separate variables. For comparative purposes the notation of Kuhn and Grün will be used where applicable.

The right-handed coördinate system (Kuhn and Grün) is shown in Fig. 1. The orientation of the rod particle is specified by two angles, α and φ, the first lying in the yz plane and the second in the xy plane. These angles arise from projections of the rod direction upon the appropriate planes.

A plane strain of constant area transforms the original coördinates (x,y,z) to a new set (x',y',z') according to

$$x' = \lambda x,\ y' = y,\ z' = \lambda^{-1}z \qquad (1)$$

where λ represents the stretch or extension ratio in the x direction.

Before deformation, the orientation distribution function, $\Psi(\alpha,\varphi)$, of a system of these rod particles is uniform over the area of a unit radius sphere. The probability of finding a rod oriented from α to $\alpha + d\alpha$ and φ to $\varphi + d\varphi$ is given by

(1) This work was presented in part at the 141st National Meeting of the American Chemical Society, Washington, D. C., March, 1962.
(2) A. Peterlin and H. A. Stuart, *Z. Physik*, **112**, 129 (1939).
(3) Lord Rayleigh, *Phil. Mag.*, **44**, 28 (1897).
(4) P. Boeder, *Z. Physik*, **75**, 258 (1932).
(5) R. Cerf and H. A. Scheraga, *Chem. Rev.*, **51**, 185 (1952).
(6) C. T. O'Konski, K. Yoshioka, and W. H. Orttung, *J. Phys. Chem.*, **63**, 1558 (1959).
(7) I. Tinoco, Jr., *J. Am. Chem. Soc.*, **81**, 1540 (1959).
(8) I. Tinoco, Jr., and W. G. Hammerle, *J. Phys. Chem.*, **60**, 1619 (1956).
(9) O. Kratky, *Kolloid-Z.*, **64**, 213 (1933).
(10) W. Kuhn and F. Grün, *ibid.*, **101**, 248 (1942).
(11) P. H. Hermans, "Contribution to the Physics of Cellulose Fibres," Elsevier Publ. Co., Inc., Amsterdam, 1946.
(12) J. J. Hermans, "Flow Properties of Disperse Systems," Interscience Publishers, Inc., New York, N. Y., 1953.
(13) S. J. Gill, *J. Appl. Polymer Sci.*, **1**, 17 (1959).
(14) R. Toggenburger and S. J. Gill, in preparation.
(15) S. J. Gill and R. Toggenburger, *J. Polymer Sci.*, in press.
(16) P. Doty, cited as a private communication in ref. 5.

$$d\Psi = \frac{\sin \Lambda \sec^2\alpha}{4\pi(1 + \sin^2\varphi \tan^2\alpha)^{3/2}} d\alpha\, d\varphi \quad (2)$$

Following plane deformation, the element of the orientation distribution may be found from the relations

$$\tan \alpha = \lambda \tan \alpha', \sin \varphi = \frac{\lambda \sin \varphi'}{[1 + (\lambda^2 - 1)\sin^2\varphi']^{1/2}}$$

and (3)

$$d\varphi = \frac{\lambda \sec^2\varphi'}{1 + \lambda^2\tan^2\varphi'} d\varphi', d\alpha = \frac{\lambda \sec^2\alpha'}{1 + \lambda^2\tan^2\alpha'} d\alpha'$$

as

$$d\Psi' = \frac{\lambda^3 \sin \varphi' \sec^2\varphi' \sec^2\alpha' [1 + (\lambda^2 - 1) \sin^2\varphi'] d\alpha' d\varphi'}{4\pi[1 + (\lambda^2 - 1)\sin^2\varphi' + \lambda^4\sin^2\varphi'\tan^2\alpha']^{3/2} [1 + \lambda^2\tan^2\varphi']} \quad (4)$$

The distribution function of the strained state $\Psi'(\alpha',\varphi')$ can be found from comparison of eq. 4 with

$$d\Psi' = \Psi'(\alpha',\varphi')\, d\alpha'\, d\varphi' \quad (5)$$

The birefringence $(\Delta n)_y$ or $n_z - n_x$ observed in the direction of the y axis may now be calculated following the assumptions of Peterlin and Stuart.[2] The squared refractive indices in the x and z directions are given by

$$n_x^2 = n_1^2 + 4\pi c \left[g_2 - (g_1 - g_2) \int\int \frac{\Psi'(\alpha',\varphi') \cos^2\varphi'}{1 + \sin^2\varphi'\tan^2\alpha'} d\varphi'\, d\alpha' \right] \quad (6)$$

$$n_z^2 = n_1^2 + 4\pi c \left[g_1 - (g_1 - g_2) \int\int \frac{\Psi'(\alpha',\varphi')}{1 + \sin^2\varphi'\tan^2\alpha'} d\varphi'\, d\alpha' \right]$$

where n_1 is the refractive index of the solvent, the optical anisotropy of the rod is characterized by the factor $g_1 - g_2$, and c is the volume fraction of the rods in solution.

The birefringence can then be expressed as

$$(\Delta n)_y = n_z - n_x = \frac{2\pi c(g_1 - g_2)}{\bar{n}} \left[1 - 2\left\langle \frac{1}{1 + \sin^2\varphi'\tan^2\alpha'} \right\rangle + \left\langle \frac{\sin^2\varphi'}{1 + \sin^2\varphi'\tan^2\alpha'} \right\rangle \right] \quad (7)$$

where $\bar{n}$ is the refractive index of the solution, and the suitable averages are given by eq. 8.

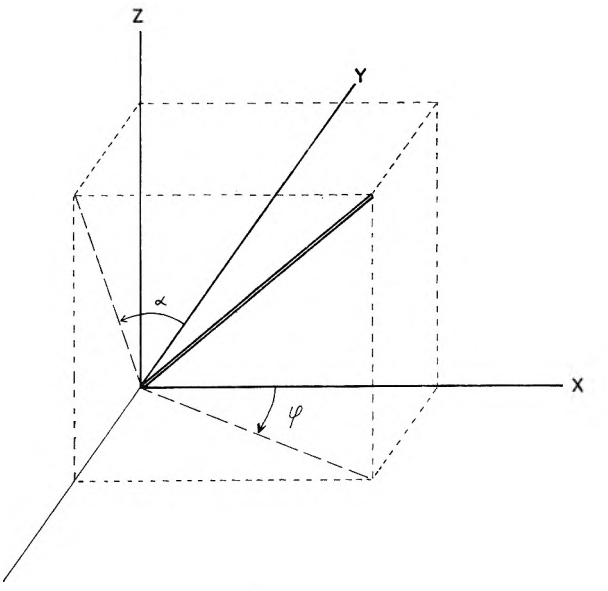

Fig. 1.—Right-handed coördinate system with angles α and φ indicating direction of rod.

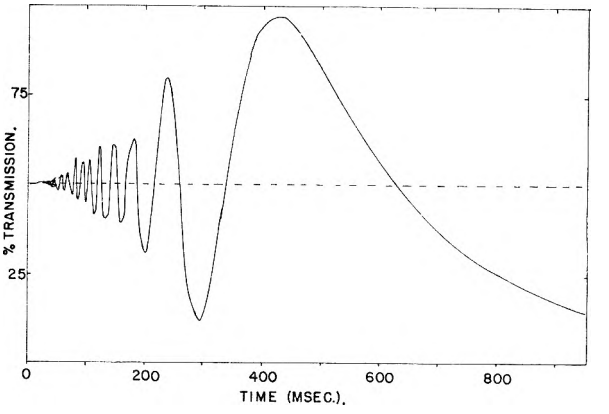

Fig. 2.—Photograph trace of light transmission for a relaxing solution of 8% PBG (450,000) in mixed solvent at 35° between crossed nicol prisms. The dotted line indicates a calibration mark of 45° retardation.

$$\left\langle \frac{1}{1 + \sin^2\varphi'\tan^2\alpha'} \right\rangle = \int\int \frac{\Psi'(\alpha',\varphi')}{1 + \sin^2\varphi'\tan^2\alpha'} d\varphi'\, d\alpha' \quad (8)$$

$$\left\langle \frac{\sin^2\varphi'}{1 + \sin^2\varphi'\tan^2\alpha'} \right\rangle = \int\int \frac{\Psi'(\alpha',\varphi') \sin^2\varphi'}{1 + \sin^2\varphi'\tan^2\alpha'} d\varphi'\, d\alpha'$$

It is convenient to evaluate the indicated averages (8) in terms of a parameter ϵ which is equal to $\lambda^2 - 1$ by a series expansion and term by term integration. Evaluation to the third approximation gives the expression for the birefringence as

$$(\Delta n)_y = \frac{2\pi c(g_1 - g_2)}{5\bar{n}} \left[2\epsilon - \epsilon^2 + \frac{11}{21}\epsilon^3 - \dots \right] \quad (9)$$

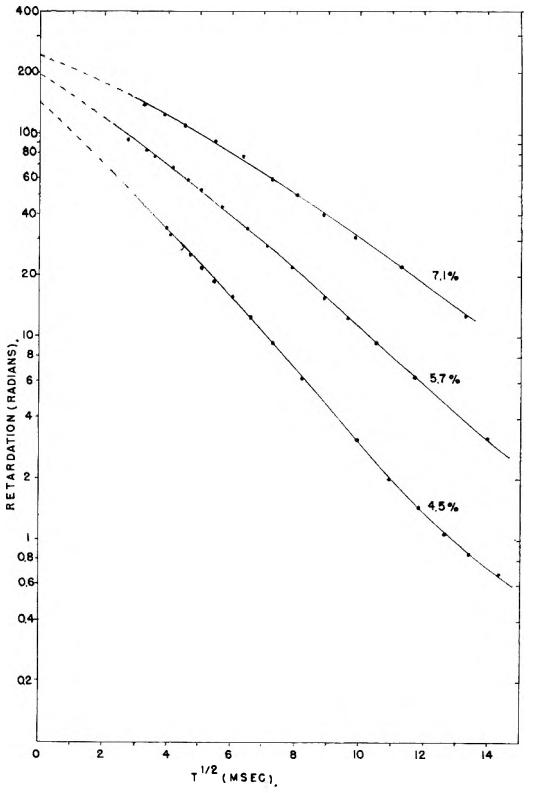

Fig. 3.—Relaxation of optical retardation of solutions of PBG (450,000) in mixed solvent at 35°

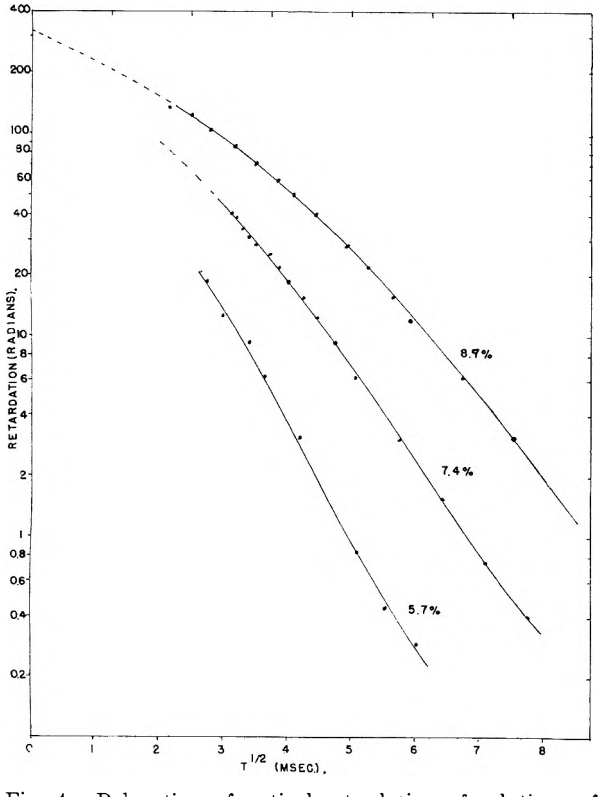

Fig. 4.—Relaxation of optical retardation of solutions of PBG (275,000) in mixed solvent at 35°.

The preceding expressions are strictly valid for dilute solutions. From considerations given by Bragg and Pippard[17] on form birefringence of macromolecular crystals, the effect of optical interaction between rods in concentrated solutions will introduce correction terms of the order of $1 + c$, provided the indices of refraction of rod material and solvent are not too different from each other.

III. Results and Discussion

An experimental situation which approaches the preceding theoretical requirements may be found in concentrated solutions of polybenzylglutamate (PBG) in rod-like configuration. Strain birefringence measurements, using a technique previously described,[13,15] have been made on such solutions in the solvent mixture of 76% by volume of dichloroacetic acid with ethylene dichloride. Above 30° the polypeptide is essentially in the rod form[18]; measurements at 35° were used for calculation purposes. The low viscosity with the mixed solvent system at 15° allows highly concentrated solutions to be handled easily. At 35° these solutions become very viscous and relax relatively slowly. Solutions of PBG in pure ethylene dichloride to not have these practical advantages and consequently were not as satisfactory.

The birefringence that arises upon a known instantaneous strain is the quantity needed. It is necessary to extrapolate readings of birefringence (or retardation) at different times back to the moment of strain. For slowly relaxing materials this can be done with reasonable success. The relaxation of a solution having a high initial value of retardation gives the wave pattern shown in Fig. 2. Several factors limit retardation measurements to a time of about 5 msec. after strain: mechanical vibration, the large retardation itself, the band width of the light filter, and the rapid relaxation at short times. Nevertheless, an extrapolation to zero time can be made reasonably well for the favorable cases. This situation is illustrated in Fig. 3 and 4, where it has been found advantageous to plot the logarithm of the retardation against the square root of the time. It is apparent that the extrapolation becomes more inaccurate as the initial relaxation rate increases.

Our apparatus has an effective optical path of 9.1 cm. with a strain factor of 0.36 ± 0.02. Filtered light of 0.546μ was used for all measurements. The most certain results are shown in Table I.

TABLE I

Mol. wt.	Wt. %	Concn., calcd. vol. fraction c	$(\Delta n)_y$ extrapd. to zero time	Calcd. $g_1 - g_2$
450,000	7.1	7.8×10^{-2}	$(23 \pm 2) \times 10^{-5}$	$(5.5 \pm 1) \times 10^{-4}$
450,000	5.7	6.4×10^{-2}	$(18 \pm 2) \times 10^{-5}$	$(5.5 \pm 1) \times 10^{-4}$
450,000	4.5	5.0×10^{-2}	$(13 \pm 2) \times 10^{-5}$	$(5.1 \pm 1) \times 10^{-4}$
275,000	8.9	9.9×10^{-2}	$(31 \pm 3) \times 10^{-5}$	$(5.6 \pm 1) \times 10^{-4}$

In these calculations a polymer density of 1.32 g. cm.$^{-3}$ and solvent density of 1.48 g. cm.$^{-3}$ have been used.[6] A value of 1.465 was measured for the refractive index of the 7.0% solution. The birefringence $(\Delta n)_y$ is calculated from the retardation δ by $(\Delta n)_y = 95.6 \times 10^{-8}\delta$. Somewhat higher, but more uncertain, values of $g_1 - g_2$ were obtained

(17) W. L. Bragg and A. B. Pippard, *Acta Cryst.*, **6**, 865 (1953).

(18) B. H. Zimm, P. Doty, and K. Iso, *Proc. Natl. Acad. Sci. U. S.* **45**, 1601 (1959).

for lower concentrations in mixed solvent solutions and for solutions of PBG in pure ethylene dichloride.[19] In those cases the initial relaxation was very high.

The results can be compared with two independent measurements. A value of 4.0×10^3 has been obtained by Doty[16] from flow birefringence on a sample of 195,000 molecular weight in ethylene dichloride. A result of 4.1×10^3 also has been calculated by O'Konski[6] on measurements of the Kerr effect for a similar solution. The effect of molecular weight on $g_1 - g_2$ should be insignificant for this large a molecular weight. Solvent refractive index difference is relatively small for the mixed solvent system and pure ethylene dichloride. Thus a comparison of these measurements with ours seems quite valid.

Our measurements have given consistently higher values of the optical factor. This may be due to interferences and differences that are present in concentrated solutions. The essential agreement of the $g_1 - g_2$ value obtained in the strain birefringence case of a concentrated solution with those values from dilute solution measurements suggests that the orientation change of rigid rod-like molecules in a concentrated matrix follows the macroscopic deformation of the material.

Acknowledgment.—This work was supported by the Directorate of Chemical Sciences of the Air Force Office of Scientific Research.

(19) R. Toggenburger, Ph.D. Thesis, University of Colorado, 1961.

THE LOW TEMPERATURE HEAT CAPACITY AND ENTROPY OF MERCUROUS SULFATE TO 300°K.[1]

BY M. N. PAPADOPOULOS AND W. F. GIAUQUE

Low Temperature Laboratory, Departments of Chemistry and Chemical Engineering, University of California, Berkeley, Cal.

Received April 23, 1962

The heat capacity of Hg_2SO_4 has been measured from 15 to 300°K. and these results have been combined with the work of Brackett, Hornung, and Hopkins from 4–20°K. to prepare tables of thermodynamic properties of this substance. The entropy at 298.15°K. was found to be 47.963 gbs. mole^{-1} (gibbs = defined cal./defined deg.).

The heat capacity of Hg_2SO_4 has been measured previously in this Laboratory by the late Professor P. W Schutz, who withheld his data from publication for some unknown reason, but probably some error was suspected. For this reason we have reinvestigated the heat capacity of Hg_2SO_4 which is of particular interest in connection with work on the thermodynamics of the Clark and Weston cells.

The apparatus used for measuring heat capacity was the same as that described[2] previously in connection with the measurements on $CdSO_4$ and its hydrates.

Experimental

Preparation of Hg_2SO_4.—Mercurous sulfate was precipitated by the slow addition of 0.5 *M* H_2SO_4 to a solution which started as 0.05 *M* $Hg_2(NO_3)_2$ + 0.03 *M* HNO_3. The apparatus consisted of a 40-l. Pyrex jar, thermostated at 75°, and painted black for protection against light. An atmosphere of pure nitrogen was used to exclude air. The bottom of the jar was covered with mercury. A Lucite tray was placed above the mercury to collect the portion of the Hg_2SO_4 precipitate to be used and thus avoid the necessity of separating mercury from it. Since Hg^{+2} is present to the extent of 1% as a matter of equilibrium with Hg_2^{+2} and Hg, the sulfuric acid solution was added dropwise over a period of 67 days to minimize any tendency for mercuric impurity to co-precipitate in the mercurous sulfate. The solution was stirred and circulated over the mercury by means of a Lucite stirrer and the Hg_2SO_4 was allowed to remain in contact with the solution for 3 months after precipitation was complete.

The Hg_2SO_4 was transferred to a gas-tight metal–plastic glove box under conditions which excluded direct light and maintained an atmosphere of nitrogen. The salt was washed with successive portions of 0.05 *M* H_2SO_4 and then with absolute ethyl alcohol and anhydrous diethyl ether. Following this it was transferred to a light shielded vacuum desiccator and a high vacuum was maintained for several days. The substance then was transferred to the calorimeter in the dry nitrogen-filled glove box.

The Hg_2SO_4 consisted of white conglomerated small crystals. Crystal faces averaged about 0.1 mm. in size.

Analysis.—Hg_2SO_4 was analyzed for sulfate by precipitation of $BaSO_4$ as follows: the Hg_2SO_4 samples were oxidized to mercuric by means of a few drops of concentrated HNO_3. The clear solution was placed on a steam bath and 1 or 2 drops of $Ba(NO_3)_2$ reagent were added, with stirring, until nuclei of $BaSO_4$ appeared. The remaining reagent then was added dropwise to a slight excess. The precipitate was collected on a Pyrex fritted disk crucible which had been prefired at 500° before weighing. The crucible and precipitate then were placed in an oven which was gradually heated to 500°. Co-precipitation of nitrate was checked as usual by moistening the fired precipitate with H_2SO_4 and reheating. No co-precipitation of nitrate was found. It was necessary to make small corrections for the solubility losses.[3]

Three analyses gave the ratio of SO_4^{-2}/Hg_2SO_4 as 0.19318, 0.19312, and 0.19317, average 0.19316 compared to the theoretical 0.19317; thus it appears that there was no co-precipitation of $HgSO_4$.

Results

Heat Capacity and Thermodynamic Properties of Hg_2SO_4.—The heat capacity observations are given in Table I and the derived thermodynamic quantities are given in Table II. One defined calorie was taken equal to 4.1840 absolute joules and 0°C. = 273.15°K. The unusually high heat capacity of Hg_2SO_4 at 15°K. made extrapolation below this temperature uncertain and it was de-

(1) This work was supported in part by the National Science Foundation.

(2) M. N. Papadopoulos and W. F. Giauque, *J. Am. Chem. Soc.*, **77**, 2740 (1955).

(3) A. Seidell, "Solubilities of Inorganic and Metal Organic Compounds," 3rd Ed., Vol. 1, D. Van Nostrand Co., New York, N. Y., 1940, p. 183.

cided that measurements to the liquid helium region were necessary. These recently have been carried out on the same preparation of Hg_2SO_4 by Brackett, Hornung, and Hopkins,[4] who covered the range 4–20°K. Their results joined smoothly with the present results and give the value of the entropy as 1.311 gbs. mole^{-1} at 15°K.

TABLE I

HEAT CAPACITY OF Hg_2SO_4

Gbs. mole^{-1} (gibbs = defined cal./defined deg.)
M.w. = 497.28. 0°C. = 273.15°K.
1.1677 moles in calorimeter

T, °K.	C_p	T, °K.	C_p	T, °K.	C_p
15.67	3.576	79.27	16.61	182.44	25.20
17.82	4.310	86.21	17.41	189.80	25.65
19.91	5.090	92.90	18.10	197.27	26.18
22.03	5.763	99.19	18.75	204.65	26.58
24.12	6.343	105.35	19.33	212.02	27.16
26.38	6.946	111.42	19.90	219.41	27.46
29.96	7.880	117.28	20.43	227.24	27.88
32.74	8.547	123.23	20.92	235.10	28.32
36.78	9.459	129.35	21.43	242.83	28.56
40.23	10.25	135.70	21.94	250.43	29.13
43.70	10.93	142.35	22.45	257.76	29.47
47.74	11.69	148.83	22.91	265.47	29.93
51.92	12.47	155.05	23.36	272.83	30.33
56.70	13.29	161.58	23.81	280.73	30.65
61.98	14.15	168.36	24.29	289.39	30.95
67.29	14.99	175.33	24.76	298.61	31.56
72.88	15.79				

TABLE II

THERMODYNAMIC PROPERTIES OF Hg_2SO_4

Gbs. mole^{-1} (gibbs = defined cal./defined deg.)
M.w. = 497.28. 0°C. = 273.15°K.

T, °K.	C_p	S	$-\left(\frac{F - H_0^\circ}{T}\right)$	$\left(\frac{H - H_0^\circ}{T}\right)$
5	0.102[a]	0.027[a]	0.006[a]	0.021[a]
10	1.358[a]	0.395[a]	.114[a]	.281[a]
15	3.308[a]	1.311[a]	.349[a]	.962[a]
20	5.072	2.507	.736	1.771
25	6.578	3.812	1.220	2.592
30	7.874	5.129	1.764	3.365
35	9.090	6.436	2.338	4.098
40	10.191	7.719	2.928	4.791
45	11.184	8.974	3.526	5.448
50	12.105	10.199	4.131	6.068
55	12.991	11.395	4.738	6.657
60	13.840	12.562	5.339	7.223
70	15.361	14.811	6.529	8.282
80	16.674	16.945	7.692	9.253
90	17.804	18.971	8.829	10.142
100	18.824	20.898	9.939	10.959
110	19.767	22.736	11.018	11.718
120	20.649	24.495	12.069	12.426
130	21.479	26.182	13.089	13.093
140	22.265	27.804	14.084	13.720
150	23.014	29.365	15.049	14.316
160	23.731	30.872	15.991	14.881
170	24.419	32.330	16.909	15.421
180	25.081	33.743	17.805	15.938
190	25.717	35.115	18.680	16.435
200	26.331	36.449	19.535	16.914
210	26.926	37.749	20.371	17.378
220	27.503	39.016	21.190	17.826
230	28.062	40.252	21.992	18.260
240	28.605	41.458	22.778	18.680
250	29.135	42.635	23.548	19.087
260	29.653	43.785	24.304	19.481
270	30.160	44.911	25.047	19.864
273.15	30.318	45.262	25.278	19.984
280	30.658	46.015	25.777	20.238
290	31.148	47.097	26.492	20.605
298.15	31.542	47.963	27.066	20.897
300	31.632	48.161	27.198	20.963
310	32.112	49.204	27.890	21.314
320	32.588	50.227	28.571	21.656

[a] Values taken from Brackett, Hornung, and Hopkins.[4]

The entropy of Hg_2SO_4 at 298.15°K. was found to be 47.963 gbs. mole^{-1}, in good agreement with the value 48.0, the somewhat uncertain result of Schutz.

Acknowledgment.—We thank W. P. Cox, E. W. Hornung, and R. H. Sherman for assistance with the low temperature measurements.

(4) T. E. Brackett, E. W. Hornung, and T. E. Hopkins, *J. Am. Chem. Soc.*, **82**, 4155 (1960).

THE FREEZING POINT–SOLUBILITY CURVE OF AQUEOUS SODIUM HYDROXIDE IN THE REGION NEAR THE ANHYDROUS–MONOHYDRATE EUTECTIC[1]

BY G. E. BRODALE AND W. F. GIAUQUE

Low Temperature Laboratory, Departments of Chemistry and Chemical Engineering, University of California, Berkeley, Cal.

Received April 27, 1962

The composition and melting point of the NaOH–NaOH·H_2O eutectic have been found to be 73.1 wt. % NaOH and 62.61°, respectively. This melting point is in good agreement with the more accurate value of 62.63° obtained by Murch and Giauque. No evidence of a hydrate intermediate between NaOH and NaOH·H_2O was found. The measurements cover the range 69.8 to 75.4 wt. % and 62.61 to 100.6°.

In connection with a recent investigation of the thermodynamic properties of NaOH and NaOH·H_2O in this Laboratory, it became important to have a more accurate determination of the eutectic composition of these substances.

Experimental

Preparation of Sodium Hydroxide.—Sodium hydroxide was prepared in a nitrogen-filled glove box in a manner similar to that described by Murch and Giauque,[2] except that cold nitrogen from the liquid nitrogen supply was passed over the metallic sodium, and water, which had been boiled to remove CO_2, was dropped slowly onto the metal. The smaller heat of reaction with liquid, as compared with gaseous water, and the cooling effect of the nitrogen moderated the reaction (which still requires a great deal of caution). The maximum concentration of NaOH used, 77%, was obtained by evaporation in the nitrogen-filled glove box by means of a heat lamp. Lower concentrations were then obtained by dilution. It had been shown by the previous work[2] that this method of preparation produces a very small concentration of carbonate (~0.01%).

In the present work 5–10-g. samples were taken with a pipet constructed with a removable tip containing a "coarse" fritted glass filter. A "fine" fritted glass filter was tried but proved to be too slow. The sample weights were corrected for buoyancy. The temperatures were measured with a strain free platinum resistance thermometer (L. and N. no. 718169) calibrated at the National Bureau of Standards. It was checked at the ice point and a correction of −0.05° was applied. The platinum thermometer was encased in a Pyrex glass tube. Since glass can be attacked by sodium hydroxide, the tube was checked for loss in weight and the effect of such impurity was shown to be negligible. The experiment was carried out with samples of about 350 g. in a platinum bottle. The platinum bottle contained a Teflon coated spin bar. It was supported by a 1/8 in. aluminum plate and about 0.5 in. of spun glass insulation between it and the magnetic stirrer drive. It was enclosed in a 10 in. length of 6 in. aluminum pipe. The pipe was wound with an electric heater and wrapped with 0.5 in. of spun glass. The top was similarly enclosed. The pipe temperature was controlled to within 0.5°. The whole assembly was in 1 atm. of nitrogen.

Results

The Freezing Point–Solubility Curve.—Most of the early work on the phase relationships in aqueous sodium hydroxide was done by Pickering.[3] He prepared various concentrations, solidified the material, and then, on melting, noted the temperature at which the last evidence of solid could be detected. He comments on the fact that the monohydrate "crystallizes very easily in large, pointed, and semi-transparent crystals." Apparently, the monohydrate was easily observed and although there is a considerable scatter in his points in the monohydrate melting region, a curve through his observations is in reasonably good agreement with the present results. However, we were very suspicious concerning the accuracy with which one could observe the disappearance of the last crystals of anhydrous NaOH from the very concentrated aqueous solution. The tendency would be to assign too low a temperature to a given concentration. We have found that Pickering's observed temperatures along the NaOH curve are about 20° too low. Pickering did not measure either the composition or temperature of the eutectic between NaOH and NaOH·H_2O and a curve through his observations on the anhydrous phase would give a eutectic mixture too rich in NaOH at too low a temperature.

The results which cover the range from 62.61 to 100.6° and concentrations from 69.8 to 75.4% by weight are given in Table I.

TABLE I

FREEZING POINT–SOLUBILITY CURVE FOR AQUEOUS SODIUM HYDROXIDE

Wt. % NaOH	*T*, °C.	Phase
68.95[a] Monohydrate	65.10[a]	NaOH·H_2O
69.8	65.1	NaOH·H_2O
71.3	64.3	NaOH·H_2O
73.1	62.61	NaOH·H_2O–NaOH
73.2	66.4	NaOH
73.5	72.1	NaOH
74.5	85.2	NaOH
75.4	100.6	NaOH

[a] Taken from Murch and Giauque, ref. 2.

By comparison with the results of Murch and Giauque,[2] we suspect that the measurements at 65.1 and 64.3° are about 0.1° too high. The stability of the eutectic temperature made it possible to observe it with greater accuracy.

The results indicate that no hydrate intermediate between NaOH and NaOH·H_2O, such as has been suggested by de Forcrand[4] and Mauret,[5] appeared during these measurements. This observation is in agreement with the experiments and conclusion of Murch and Giauque.

(1) This work was supported in part by the National Science Foundation.

(2) L. E. Murch and W. F. Giauque, *J. Phys. Chem.*, **66**, 2052 (1962).

(3) S. U. Pickering, *J. Chem. Soc.*, **63**, 890 (1893).

(4) R. de Forcrand, *Compt. rend.*, **133**, 223 (1901).

(5) M. Mauret, *ibid.*, **240**, 2151 (1955).

THE THERMODYNAMIC PROPERTIES OF SODIUM HYDROXIDE AND ITS MONOHYDRATE. HEAT CAPACITIES TO LOW TEMPERATURES. HEATS OF SOLUTION[1]

BY L. E. MURCH AND W. F. GIAUQUE

Low Temperature Laboratory, Departments of Chemistry and Chemical Engineering, University of California, Berkeley, Cal.

Received April 27, 1962

The heat capacities of sodium hydroxide (12–320°K.), and sodium hydroxide monohydrate (14–338.25°K.) have been measured and used to prepare smooth tables of thermodynamic properties. The melting point of the NaOH–NaOH·H_2O eutectic was found to be 335.78°K. (0°C. = 273.15°K.) and the eutectic heat of fusion is 3207 ± 100 cal. mole^{-1}. The heat of fusion of NaOH·H_2O is 3776 ± 30 cal. mole^{-1} at its melting point, 338.25°K. These values of the heats of fusion are based on the eutectic composition of 73.1 wt. % of NaOH. The heats of solution of a series of solids with NaOH·(0 to 1) H_2O gave a straight line relationship and thus no evidence was found for an intermediate hydrate such as NaOH·$^2/_3H_2O$ or NaOH·$^1/_2H_2O$ as has been suggested by others on the basis of similar but less accurate measurements. Also, NaOH·H_2O with a small water deficiency and NaOH with a small amount of water appear to give the same eutectic temperature, indicating no intermediate hydrate. The calorimetric data have been used with the third law of thermodynamics to calculate the dissociation pressure of water over the system NaOH·H_2O–NaOH and the results are in excellent agreement with the dissociation pressure observations of Baxter and Starkweather, who investigated NaOH·("lowest hydrate")–NaOH, which shows that no intermediate hydrate appeared in their experiments. NaOH = NaOH(inf. dilute soln.)$\Delta H_{298.15°K.} = -10{,}653 \pm 10$ cal. mole^{-1}. NaOH·H_2O = NaOH(inf. dilute soln.)$\Delta H_{298.15} = -5134 \pm 10$ cal. mole^{-1}. NaOH, $S_{298.15} = 15.400$ gbs. mole^{-1}. NaOH·H_2O, $S_{298.15} = 23.775$ gbs. mole^{-1}. NaOH·H_2O = NaOH + H_2O(g), $\Delta H_{298.15} = 16{,}039$ cal. mole^{-1}, $\Delta H_0^0 = 14{,}870$ cal. mole^{-1}, $(P_{H_2O})_{298.16} = 0.14$ mm.

Despite the importance of sodium hydroxide, there are few accurate thermodynamic data on this substance and its numerous solid hydrates. Douglas and Dever[2] have made accurate heat content measurements on solid and liquid NaOH over the range from 298 to 1000°K. and its low temperature heat capacity has been measured to 60°K. by Kelley and Snyder.[3] There were no heat capacity data on NaOH below 60°K. and none of the solid hydrates appears to have been investigated.

This paper presents heat capacity data on NaOH from 12 to 320°K. and on NaOH·H_2O from 14°K. through its melting point at 338.25°K. The only previous investigation of the heat of solution of the above solids in water appears to be that of de Forcrand,[4] who dissolved a series of solids containing water over the range 0 to 1 H_2O per mole of NaOH. A plot of the data from this pioneer experiment shows them to be quite inaccurate. However, de Forcrand interpreted the observations as indicating the presence of a hydrate NaOH·2/3H_2O and the existence of an intermediate hydrate generally has been accepted by various authors for the past 60 years.

Recently, Mauret[5] has suggested NaOH·0.5H_2O as the composition of the assumed intermediate hydrate. Actually there are no data of sufficient accuracy ever to have justified the assumption of any intermediate hydrate within the range 0–1.

We have repeated de Forcrand's experiment with presently available accuracy and find that all heats of solution lie on an accurately straight line when plotted against moles H_2O/mole NaOH; thus no intermediate hydrate was indicated.

It has ordinarily been assumed that NaOH and NaOH·H_2O solidify from its concentrated aqueous solutions as pure compounds and we assumed this in beginning the present experiments. Thus, samples of NaOH with a small excess of water and NaOH·H_2O with a small deficiency of water were used to infer the heat capacities of pure substances.

Experimental

Preparation and Analysis of the Samples.—The sodium hydroxide samples were prepared by passing moist nitrogen gas over sodium metal and drying the resulting liquid solution to the desired composition. The sodium used was Baker and Adamson Reagent Grade, which contains less than 0.01 mole % of impurities. The nitrogen gas was produced by boiling liquid nitrogen obtained from the laboratory fractionating unit, which includes very complete removal of CO_2 from air at 270 atm. by adsorption in 40% KOH solution. The distilled water for humidifying the nitrogen was boiled immediately before use to remove any dissolved carbon dioxide.

Sealed cans of sodium and a gold calorimeter were placed in a gas tight metal glove box with a Plexiglas window. This was flushed for several hours with dry nitrogen gas. A can of sodium then was opened and the exterior portions of the metal were removed with a stainless steel knife and discarded. Approximately 0.25 lb. of sodium was placed on a platinum wire mesh which was suspended above a flat platinum dish. The humidified nitrogen gas then was passed through the glove box and a liquid solution of sodium hydroxide dripped down into the platinum dish. The glove box also contained a heat lamp which was used to evaporate the solution to its final composition. To obtain sodium hydroxide with only a small amount of water, it was necessary to heat overnight at about 350°.

Following the heating, the molten sample was poured into the previously weighed gold calorimeter. Both before and after pouring, samples were removed for carbonate analysis. The calorimeter then was capped, removed from the glove box, and weighed. Later the cap was soldered in place.

The carbonate determinations were accomplished by dissolving small portions of the sample in water and transferring the liquid to 100-ml. centrifuge tubes with narrow tapered graduated bottoms. Barium carbonate was precipitated by an excess of barium chloride solution and the tubes were centrifuged. The precipitate was compared visually with various precipitates of known amount. The accuracy of this method was about 5×10^{-6} mole or about 0.005% of the total moles of sodium hydroxide used in the analysis portion.

Following the calorimetric measurements, the sodium hydroxide was removed by washing the calorimeter with water, weighing the washings, and titrating aliquot parts of

(1) This work was supported in part by the National Science Foundation.

(2) T. B. Douglas and J. L. Dever, *J. Res. Natl. Bur. Std.*, **53**, 81 (1954).

(3) J. C. R. Kelley and P. E. Snyder, *J. Am. Chem. Soc.*, **73**, 4114 (1951).

(4) R. de Forcrand, *Compt. rend.*, **133**, 233 (1901).

(5) P. Mauret, *ibid.*, **240**, 2151 (1955).

the total. The standard acid used in the titration was constant boiling sulfuric acid as described by Kunzler.[6] The amount of water in the samples was obtained by difference.

Sodium hydroxide monohydrate was made in the same manner except that less heating was required to produce a sample of approximately the desired composition. A representative sample of the material added to the calorimeter was obtained by taking two portions before pouring and two after pouring.

The sample of $NaOH \cdot 0.04014H_2O$ in the calorimeter weighed 247.543 g. and contained about 0.01 mole % of Na_2CO_3.

The sample of $NaOH \cdot 0.97776H_2O$ investigated weighed 219.456 g. and contained about 0.013 mole % of Na_2CO_3.

The weights were corrected for buoyancy. The density of NaOH was taken as 2.13 g. cm.$^{-3}$, and that of $NaOH \cdot H_2O$[7] as 1.72 g. cm.$^{-1}$. Mol. wt. NaOH = 40.005; mol. wt. $NaOH \cdot H_2O$ = 58.021.

Description of Gold Calorimeter VI.—The general features of the calorimetric apparatus were very similar to those described by Giauque and Egan[8] and need not be mentioned. However, the calorimeter, which will be used in subsequent work under the designation Gold Calorimeter VI, was considerably different and should be described briefly. It is shown in Fig. 1, which is largely self-explanatory. There were eight vanes 0.025 cm. thick in the calorimeter.

Gold wire, 0.0031 in. in diam. and containing about 0.1% silver, was used to wind a resistance thermometer–heater on the 1.0 mm. thick outer cylindrical wall of the calorimeter, but the procedure was different from that described by Giauque and Egan. Two layers of China silk, each 0.003 in. in thickness, were placed on the outer surface with the aid of three coats of Formvar varnish. (Nylon cloth was tried and proved unsatisfactory due to wrinkling.) The varnish was dried for 3 hr. at 125°.

The gold wire and silk thread 0.004 in. in diam. were wound in parallel over the silk cloth. The tension during winding on a lathe is essentially all in the silk thread which was used to crowd the gold wire into a closely wound helix of 467 turns. The ends of the gold wire were soldered to turns of 0.010-in. diam. double silk insulated copper wire; thus, the gold–copper junctions were kept very close to the calorimeter temperature to avoid thermoelectric effect. The gold windings were covered with two layers of the same silk cloth, painted with three more coats of Formvar varnish and dried at 125°. The double silk insulated copper lead wires from the lower end of the calorimeter were placed between the two outer silk layers. The entire assembly was covered with heavy gold leaf to reduce radiation.

A Leeds and Northrup strain-free platinum resistance thermometer, no. 1215333, calibrated by the National Bureau of Standards, was placed in an axially located vertical well that extended from the bottom to above the middle of the calorimeter as shown in Fig. 1. Rose's alloy was used to establish good thermal contact between the standard thermometer and the calorimeter. The two thermometers were compared at the beginning and end of each measurement. The gold thermometer gave a continuous record of the surface temperature.

The introduction of molten NaOH into the calorimeter at about 350° posed an unusual problem, because such a temperature not only would destroy the external thermometer, but also would cause flow of the low melting alloy and undesirable diffusion into the gold well holding the standard thermometer. This problem was solved by introducing the molten NaOH before the gold thermometer and any low melting alloy were added. The later introduction of the low melting $NaOH \cdot H_2O$ caused no difficulty.

One defined calorie was taken as 4.1840 absolute joules and 0°C. as 273.150°K. (triple point of water = 273.16 exactly).

Results

Heat Capacities of NaOH and $NaOH \cdot H_2O$.—As mentioned previously, the low temperature calorimetric measurements were made on samples with the over-all composition $NaOH \cdot 0.04014H_2O$ and $NaOH \cdot 0.97776H_2O$. Although we infer later

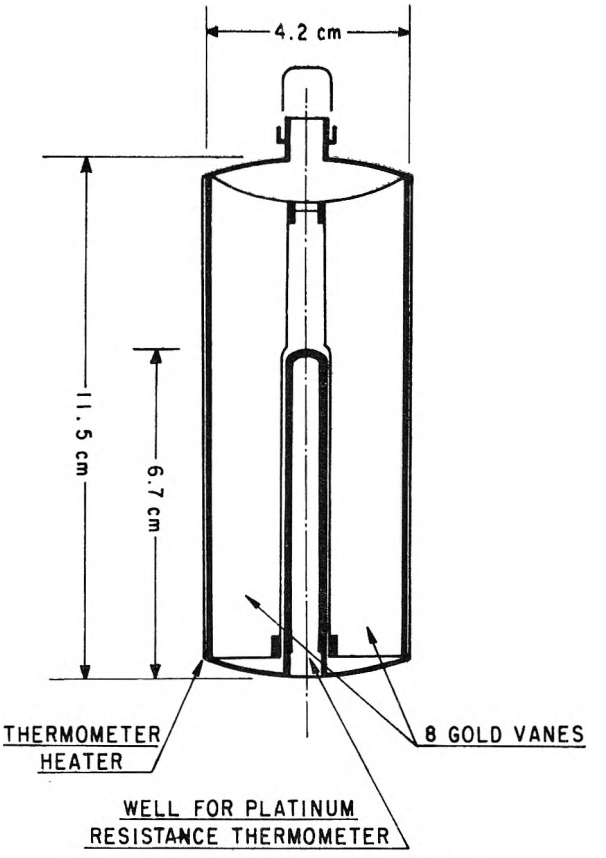

Fig. 1.—Gold calorimeter no. VI.

TABLE I

MOLAL HEAT CAPACITY OF $NaOH \cdot 0.04014H_2O$

1 "mole" = 0.95986 mole of NaOH + 0.04014 mole of $NaOH \cdot H_2O$

0°C. = 273.15°K. Units are gbs. mole^{-1}

T, °K.	C_p	T, °K.	C_p	T, °K.	C_p
Series I		85.144	5.556	243.138	13.332
12.748	0.0463	92.324	6.161	251.057	13.519
14.363	.0786	99.766	6.755	258.958	13.709
15.832	.1086	107.193	7.323	267.063	13.896
17.549	.1443	114.598	7.863	274.857	14.067
19.604	.1991	121.771	8.356	282.256	14.231
22.245	.2825	128.834	8.791	290.534	14.381
24.849	.3773	136.310	9.248	298.800	14.550
28.316	.5403	143.615	9.657	307.266	14.678
30.865	.6782	151.497	10.062	315.571	15.004[b]
32.618	.7912	159.657	10.455	Series II	
35.345	.9696	166.922	10.789	299.577	14.558
38.570	1.1918	174.234	11.097	307.097	14.736[b]
42.135	1.4982	181.839	11.408	314.655	14.927[b]
46.276	1.8531	189.477	11.657	Series III	
50.82	2.24[a]	197.459	11.970	285.744	14.239
55.682	2.693	205.038	12.226	293.601	14.397
60.983	3.211	212.952	12.480	301.237	14.574
66.496	3.750	220.978	12.718	308.931	14.794[b]
72.358	4.310	228.521	12.928	315.868	15.020[b]
78.532	4.904	235.742	13.123		

[a] Lost insulating vacuum. Value given no weight. [b] Premelting of NaOH–$NaOH \cdot H_2O$ eutectic, to be discussed below.

(6) J. E. Kunzler, *Anal. Chem.*, **25**, 93 (1953).
(7) J. A. Wunderlich, *Acta Cryst.*, **10**, 462 (1957).
(8) W. F. Giauque and C. J. Egan, *J. Chem. Phys.*, **5**, 45 (1937).

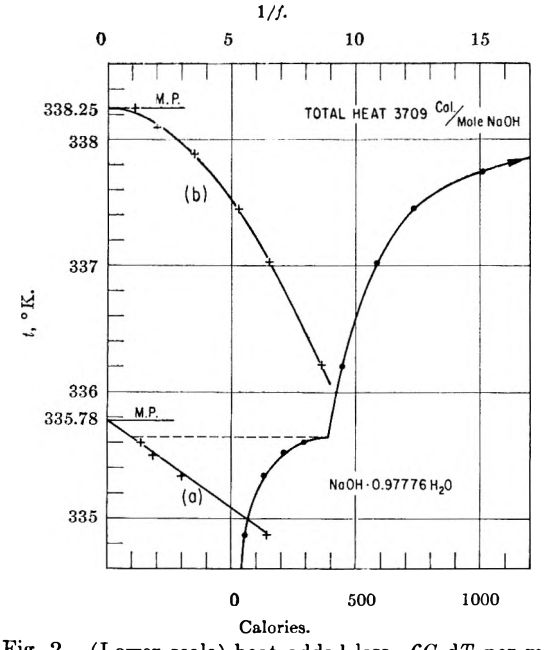

Fig. 2.—(Lower scale) heat added less $\int C_p dT$ per mole NaOH·0.97776H_2O. (Upper scale) Reciprocal of fraction melted (a) eutectic mixture, (b) NaOH·H_2O.

that sodium hydroxide may possibly form a dilute solid solution, NaOH·0.010H_2O, the data were considered to be representative of mixtures of 0.95986 mole of NaOH + 0.04014 mole of NaOH·H_2O, and 0.02224 mole of NaOH + 0.97776 mole of NaOH·H_2O. Even if the solid solution does exist, this should cause little error.

The observed data are given in Tables I and II. Smooth curves through the observations were used in computing the properties of NaOH and NaOH·H_2O at even values of temperature. These values are given later.

The heat capacities are given in gibbs mole^{-1} (gbs. mole^{-1}).[9] This unit also is used later for entropy, free energy/temperature, and heat content/temperature.

The Heats of Fusion and Melting Points of NaOH·H_2O and its Eutectic with NaOH.—The measurement of the heat of fusion of NaOH·H_2O was complicated by the fact it was off the monohydrate composition. Thus the total heat of fusion applies to the melting of some eutectic mixture as well as to the monohydrate.

The procedure adopted was as follows: one run started well below the melting point of the eutectic and continued to a temperature above the melting point of the monohydrate. In order to allocate the proper portion of this total heat to the eutectic and the residual monohydrate, a second series of short runs was made to determine the melting temperature as a function of heat input. The $\int C_p dT$ was subtracted from the heats added to give the net heat used for fusion. These results are shown in Fig. 2 as the curve with two sections convex upward. The uninterrupted run had the highest accuracy and was given 100% weight in evaluating energy. The second series of many short runs gave a total heat of fusion 0.22% lower due to the increased sources of error, but the curve of temperature *vs.* heat added should provide an accurate shape factor. The increments of the interrupted run were all increased by 0.22% to bring them into conformity with the more accurately known total heat although the effect of doing this was trivial in determining the heat used for the eutectic.

The integral heats added, including the 0.22% adjustment, *vs.* temperature during the detailed heat of fusion are given in Table III.

(9) 1 gbs. = 1 defined cal./defined °K. W. F. Giauque, E. W. Hornung, J. E. Kunzler, and T. R. Rubin, *J. Am. Chem. Soc.*, **82**, 62 (1960).

TABLE II

MOLAL HEAT CAPACITY OF NaOH·0.97776H_2O

1 "mole" = 0.02224 mole of NaOH + 0.97599 mole of NaOH·H_2O

0°C. = 273.15°K. Units are gbs. mole^{-1}

T, °K.	C_p	T, °K.	C_p	T, °K.	C_p
Series I		93.237	9.437	258.243	19.684
14.640	0.172	100.640	10.125	266.451	20.041
15.805	.226	108.459	10.838	274.178	20.354
17.270	.304	116.411	11.521	281.991	20.718
19.265	.426	124.296	12.156	290.056	21.056
21.385	.583	132.233	12.754	298.196	21.424
23.770	.785	140.212	13.343	306.534	21.690
26.190	1.011	148.182	13.877	314.703	22.295[a]
28.719	1.298	155.870	14.350	321.495	22.698[a]
31.728	1.663	163.733	14.839	338.25	Melted NaOH·H_2O
35.341	2.115	171.810	15.306	343.751	37.74
38.665	2.553	179.627	15.760	348.539	37.25
41 563	2.954	187.407	16.177	353.697	37.42
45.091	3.443	195.224	16.609	Series II	
49.493	4.083	202.756	16.999	301.862	21.610
54.442	4.728	210.416	17.383	310.080	22.002[a]
59.433	5.409	218.191	17.759	338.25	Melted NaOH·H_2O
64.481	6.087	226.063	18.168	343.751	38.19
69.989	6.779	233.965	18.542	349.527	37.77
76.196	7.522	241.893	18.915	355.027	38.63
82.888	8.322	249.963	19.305		

[a] Premelting of NaOH–NaOH·H_2O eutectic, to be discussed below.

TABLE III

HEAT ADDED MINUS $\int C_p dT$ FOR 1 "MOLE" OF NaOH·0.97776H_2O, CAL. MOLE^{-1}

T, °K.	$E - \int C_p dT$	T, °K.	$E - \int C_p dT$
327.84	4.3	336.202	445.7
330.73	6.4	337.025	585.5
333.319	17.5	337.447	730.6
334.873	58.5	337.869	1107.9
335.339	130.4	338.077	1881.4
335.517	210.3	338.255[a]	3416.0
335.604	292.5	NaOH·H_2O melting complete	
Eut. melting complete		(338.25)	3708.9
(335.64)	(390)	338.25	True m.p.
335.78	True m.p		

[a] Temperature too high. See discussion in text.

Figure 2 shows the break in the curve at 390 cal. mole^{-1} of NaOH present, as the heat required to melt the eutectic. Figure 2 at (a) shows a plot of temperature *vs.* the reciprocal of the fraction of the eutectic melted and this is extrapolated to the eutec-

tic melting point, 335.78°K., at the hypothetical limit of $(1/f) = 0$. It may be noticed that the upper temperature limit of eutectic melting occurs 0.14° lower than the true melting point due to impurity. Impurity such as carbonate would be soluble and relatively concentrated in the small amount of liquid resulting from eutectic melting. This may be shown to correspond to a total impurity of 0.023 mole % in the sample.

A similar treatment of the sample of NaOH·0.04014H_2O gave 120 cal. for the amount of heat associated with 1 mole of NaOH. The melting temperature was found to be 336.1°K., which agrees approximately with the more accurate value 335.78° K.

Three sets of measurements were made on the eutectic melting accompanying the heat capacity measurements of the NaOH·0.04014H_2O. All of the series were broken into partial runs but the third run was specifically designed to give detailed information concerning the shape of the temperature *vs.* fraction melted curve in the upper portions which are useful in the T *vs.* $1/f$ plot. The second run was designed to give the most accurate value of the total energy through the whole region. The first run terminated with a broken vacuum line before melting was complete but was useful in showing energy agreement over the region covered.

The useful information is presented in brief form in Table IV which as in Table III shows the detailed run corrected to exact agreement with the more accurately measured total energy. The data on the eutectic melting during measurements on the NaOH·0.0401H_2O are considerably less accurate than those on the monohydrate, partly because the heat of fusion per mole of NaOH present is only about 1/3 of the former and both values are the excess over $\int C_p dT$. Also, the vacuum was poor and variable during these measurements in the range above 300°K. The later work on NaOH·H_2O had improved conditions. However, all of the three series of excess heat absorption agreed to within 5%.

TABLE IV

HEAT ADDED MINUS $\int C_p dT$ FOR 1 "MOLE" OF NaOH·0.04014 H_2O, cal. mole^{-1}

T, °K.	$E - \int C_p dT$	T, °K.	$E - \int C_p dT$
Series 2		Series 3	
317.86	0.0	332.865	26.0 from Series 2
320.92	3.2	334.97	55.65
323.99	4.9	335.188	69.3
327.01	6.5	335.343	84.1
329.88	8.9	335.457	99.7
332.25	22.2	335.569	114.5
334.58	37.3	336.131	120
335.40	82.5		
336.50	120		

According to phase relationships, such as those indicated on the diagram given by Standiford and Badger[10] showing NaOH·0.5H_2O as an existing phase, an over-all composition of NaOH·0.04014-H_2O should lead to a peritectic at about 370°K. between NaOH and NaOH·0.5H_2O and no eutectic. The fact that heat absorption occurred below 336° K. could mean that a portion of a hydrate such as NaOH·0.5H_2O failed to crystallize in the present experiments on NaOH·0.04014H_2O, although we consider that there never have been experimental data good enough to provide a reasonable basis for assuming the existence of a solid with a composition at or near NaOH·0.5H_2O. The sample was cycled through the region of heat absorption several times without changing the heat requirement appreciably. We concluded that no peritectic reaction such as that indicated by Standiford and Badger occurred during the cycling, especially considering the opportunity for a reaction between the small amount of monohydrate surrounded by such a large excess of anhydrous NaOH.

We hesitate to make an alternative assumption that the temperature 336.1°K. corresponds to the peritectic temperature of NaOH and a compound such as NaOH·0.5H_2O, for which there is no evidence, and it seems necessary to assume that the two heat absorptions apply to the melting of the same eutectic at 335.78°K.

If the compositions of the two primary eutectic phases were known, the two eutectic heats, together with the over-all compositions of the NaOH·0.97776H_2O and NaOH·0.04014H_2O, will give both the molal heat of fusion of the eutectic and its composition. When this calculation was made assuming pure NaOH and NaOH·H_2O as the phases, the eutectic composition derived was 72.3 wt. % NaOH. However, Brodale and Giauque[11] found the eutectic composition to be 73.1%. In order to obtain the correct value of the eutectic composition it would be necessary to increase the 120 cal. "eutectic melting heat" to 157 cal. mole^{-1} of NaOH present.

There are at least two rather obvious ways of explaining this discrepancy.

A. When the molten sample of NaOH·0.04014-H_2O, at 350°, was poured into the gold calorimeter, it was essentially quenched and the dissolved water may well have been dispersed in microscopic phase regions, possibly with a considerable size distribution, ranging to macroscopic. It is difficult to predict the effect of this on the eutectic heat of fusion, melting temperature range, and composition. Assuming NaOH as an essentially pure phase, solidification of the eutectic would mean adding NaOH to the macroscopic enclosing solid, leaving microscopic NaOH·H_2O. We would expect that both the microscopic melt and the microscopic NaOH·H_2O would be subjected to large negative pressures as the bulk material cooled and that the solid monohydrate would have the much larger negative pressure. Thus the free energy of the NaOH·H_2O would be reduced much more than its partial molal free energy in the microscopic melt and the melting point would be raised. Also, some of the microscopic melt inclusions may have failed to crystallize, thus reducing the measured heat of fusion. The plot of T *vs.* $1/f$, which yields T = 336.1°K. by extrapolation rather than 335.78°K., as obtained from the monohydrate, would lose much of

(10) F. C. Standiford and W. L. Badger, *Ind. Eng. Chem.*, **46**, 2400 (1954)

(11) G. E. Brodale and W. F. Giauque, *J. Phys. Chem.*, **66**, 2051 (1962).

its meaning since its slope would be a function of the effect of particle size on melting temperatures over the size distribution. There is at least some reason to suspect the slope of the T *vs.* $1/f$ curve of $NaOH \cdot 0.04014H_2O$ which appears to be about 40% greater than would be expected from the impurity as otherwise estimated. It is difficult to see how the production of microscopic phase deposition could have been avoided. It is somewhat analogous to the well known mechanism used in "precipitation hardening" of alloys. It would explain the observed average melting temperature around 336.1°K. *vs.* the 335.78°K. value from the water-rich sample. Not only do we have confidence in the thermometry, but Brodale and Giauque[11] checked the lower value at 335.76°K. The temperature discrepancy is far beyond the limit of error and leads us to prefer the above explanation rather than the one which follows.

B. It is, however, also possible, as a limiting case, that the solid eutectic phases are a dilute equilibrium solid solution of $NaOH \cdot H_2O$ in NaOH and pure $NaOH \cdot H_2O$.

It is, of course, possible that a combination of (A) and (B) have complicated the measurements. The data have been analyzed on assumption (B) and this is important, because if a solid solution of $NaOH \cdot H_2O$ in NaOH is present in the eutectic of the well behaved low melting $NaOH \cdot 0.97776H_2O$, the effect should be considered. Fortunately, it is possible to show that the molal heats of fusion of the eutectic and $NaOH \cdot H_2O$, as derived from the results on $NaOH \cdot 0.97776H_2O$, are independent of the amount of water which may possibly be present in the NaOH phase as a solid solution.

The analysis is as follows; the two phases are $NaOH \cdot H_2O$ and solid solution $NaOH \cdot AH_2O$. $NaOH \cdot 0.04014H_2O$ will contain $0.95986/(1 - A)$ moles $NaOH \cdot AH_2O$ and $(0.04014 - A)/(1 - A)$ moles $NaOH \cdot H_2O$ and this phase controls the amount of related eutectic. $NaOH \cdot 0.97776H_2O$ will contain $(0.97776 - A)/(1 - A)$ moles $NaOH \cdot H_2O$ and $0.02224/(1 - A)$ moles $NaOH \cdot AH_2O$ and this phase controls the amount of related eutectic.

Considering the over-all eutectic composition, let the molal ratio $H_2O/NaOH = B$. The eutectic wt. % of NaOH = 73.1%.

$$B = 0.817$$

The ratio moles $NaOH \cdot H_2O$/moles $NaOH \cdot AH_2O = (B - A)/(1 - B)$ in the eutectic. Combining the above equations it is found that

$NaOH \cdot 0.04014H_2O$ has

$$\frac{(0.04014 - A)}{(B - A)} \text{ moles eutectic}$$

and

$NaOH \cdot 0.97776H_2O$ has

$$\frac{0.02224}{(1 - B)} = 0.1216 \text{ moles eutectic}$$

It may be noted that the number of moles of eutectic in the water-rich sample is independent of A. The eutectic heat of fusion is $390/0.1216 = 3207 \pm 100$ cal. mole^{-1} and $120/3207 = (0.04014 - A)/(B - A)$ from which A is found to be 0.010 and the solid solution $NaOH \cdot 0.010H_2O$, at the eutectic melting point, 335.78°K.

Using the above compositions it is found that the amount of monohydrate to be melted after the conclusion of the eutectic melting is $1 - 0.1216 = 0.8784$ mole. The melting heat added after the completion of eutectic fusion was 3317 cal. mole^{-1} of NaOH present in the sample, and the heat of fusion of $NaOH \cdot H_2O = 3317/0.8784 = 3776 \pm 30$ cal. mole^{-1}, and this result is independent of A, since the analytical result B contains the information.

The consequences of correcting the heat capacity measurements for $NaOH \cdot H_2O$ in possible microscopic states or in solid solution in NaOH requires comment. In the case of the derived data for pure $NaOH \cdot H_2O$, based on a sample $NaOH \cdot 0.97776H_2O$, the effect should be negligible. There is such a small proportion of the nearly pure NaOH phase present that a considerable error in its heat capacity would be necessary to produce an effect. There is of course no expectation of microscopic phases in the $NaOH \cdot 0.97776H_2O$ sample.

The possibility of error in deriving the heat capacity of pure NaOH is greater but should be quite small, not only because the amount of $NaOH \cdot H_2O$ in the NaOH is small, but because in general the heat capacity of microscopic phases is not greatly different from that of the macroscopic material. The principal interfacial surface tension effect is on the heat content and the increase at the absolute zero is comparable with that at ordinary temperatures, thus requiring only a minor heat capacity effect. It is believed that little error will be made by assuming that all $NaOH \cdot H_2O$ in the $NaOH \cdot 0.04014H_2O$ sample may be considered to have the same heat capacity as pure $NaOH \cdot H_2O$ and this has been done.

A curve of T *vs.* 1/fraction of $NaOH \cdot H_2O$ melted is shown at (b) in Fig. 2. The fraction of monohydrate melted at any point included the portion melted as part of the eutectic. This particular plot is not as appropriate as that for the eutectic melting temperature since the lowering in this case is essentially all due to NaOH, which may be regarded as a dissociation component of the compound. In such a case the melting temperature curve must be flat at the compound composition and linear extrapolation of the T *vs.* $1/f$ curve between 1.0 and 0 is not valid. For this reason the $1/f$ *vs.* T curve was given zero slope as it approached the T axis. The melting point was found to be 338.25 ± 0.05°K.

The melting of an off composition substance such as that considered here presents some difficulty in its final stages as follows: as the melting proceeds, the heavier residual solid will sink to the bottom and final melting will produce a liquid somewhat closer to the composition of pure $NaOH \cdot H_2O$ near the melting surface than that in the upper portion of the calorimeter. A close examination of the temperature data near the final melting temperature indicated that the small amount of

residual solid had brought the calorimeter temperature to the true melting point.

The Heats of Solution of NaOH and NaOH·H_2O.—Since the idea that a solid phase of composition at or near NaOH·0.5H_2O got its start from the early heat of solution work of de Forcrand,[4] it was decided to repeat his experiment.

Five solid samples of various proportions of NaOH and H_2O in the range of 0–1 H_2O/NaOH were investigated. The measurements were carried out in a calorimeter similar to that described by Kunzler and Giauque.[12] The various compositions were prepared in a manner similar to that used for the heat capacity determinations. The samples were sealed in glass cylinders with thin glass cover plates cemented with Apiezon wax on the bottom end and paraffin on the top end. The cover plates were broken under water by lowering a glass plunger to start the solution process. The weights were corrected for buoyancy.

The results are given in Table V. Corrections from the final concentration to infinite dilution were made by means of the data in Circular 500 of the National Bureau of Standards.[13]

TABLE V

HEATS OF SOLUTION OF SOLID SAMPLES OF OVER-ALL COMPOSITION NaOH·$X$$H_2O$ IN THE RANGE 0–1H_2O

Wt. sample	Mole ratio H_2O/NaOH sample	Mole ratio H_2O/NaOH final soln.	$\Delta H_{25}°$, cal. mole^{-1}	Corr. to infinite diln., cal. mole^{-1}	$\Delta H_{25}°$ to infinite diln., cal. mole^{-1}
15.9634	0.97447	181	−5147	−137	−5284
14.6635	.79230	185	−6138	−137	−6275
14.4166	.51715	171	−7552	−137	−7789
11.8207	.26192	191	−9077	−137	−9214
11.4267	.11810	184	−9871	−137	−10,008

The heat of solution data are plotted in Fig. 3, where they are compared with the measurements of de Forcrand.[4] The present results show that the heat of solution is accurately linear when plotted *vs.* moles H_2O/mole NaOH. This gives no support to the suggestion that there is an intermediate compound between NaOH and NaOH·H_2O.

The data of de Forcrand are scattered about the straight line through the present results and we consider that any inference that an intermediate hydrate was present during his experiments, such as NaOH·2/3H_2O which he suggested, is not justified.

It also should be mentioned that Mauret,[5] who suggested NaOH·0.5H_2O, did so on the basis of loss in weight during the evaporation of solutions over the range 100 to 160° until a change in slope in the amount *vs.* time curve appeared. We prefer to interpret his experimental observation of a gradually changing rate as corresponding to the appearance of solid NaOH. At these temperatures the saturated liquid has approximately the composition NaOH·0.5H_2O. We do not see how such an experiment can give information on the composition of a solid phase. His X-ray data are inconclusive.

(12) J. E. Kunzler and W. F. Giauque, *J. Am. Chem. Soc.*, **74**, 3472 (1952).

(13) "Selected Values of Chemical Thermodynamic Properties," Series I, Natl. Bur. Std. (U. S.), Circ. 500, Table 92-3, Feb. 1, 1952.

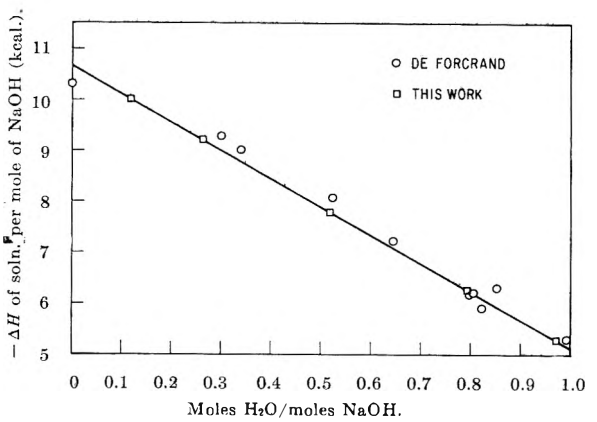

Figure 3.

Extrapolation of the straight line in Fig. 3 gives

NaOH = NaOH(infinite diln.)$\Delta H_{298.15°K}$ = $-10{,}653 \pm 10$ cal. mole^{-1}

NaOH·H_2O = NaOH(infinite diln.)$\Delta H_{298.15°K}$ = -5134 ± 10 cal. mole^{-1}

From the comments made previously concerning the possibility of a dilute solid solution of NaOH·H_2O in NaOH as an equilibrium solid phase, one must consider the possibility that the solids in the heat of solution experiments contained phases such as NaOH·H_2O and a dilute solid solution such as NaOH·0.010H_2O. This would not invalidate the conclusion with respect to the absence of evidence for an intermediate compound such as NaOH·0.5H_2O.

However, with respect to the extrapolated value for the heat of solution of pure NaOH, the existence of a dilute solid solution would mean the assumption of Raoult's law over a range within 1 mole % of the pure substance, which should lead to little error.

The effect of possible microscopic phase regions is more difficult to visualize. The most concentrated sample was NaOH·0.1181H_2O and this seems less likely to have produced microcrystals in a mixture of 0.1181 mole NaOH·H_2O + 0.8819 mole of NaOH. In any case, no deviation from linearity in the heats of solution was observed at this point.

Thermodynamic Properties of NaOH and NaOH·H_2O.—Values of C_p at even values of the temperature were read from smooth curves through the data for NaOH·0.04014H_2O and NaOH·0.97776-H_2O. The values for the pure phases were then obtained by calculation.

Tables of the heat capacity C_p^0, the entropy S^0, $-(F^0 - H_0^0)/T$, and $(H^0 - H_0^0)/T$ were prepared by the usual methods. F and H refer to free energy and heat content, respectively.

The values are given in Tables VI and VII. The table for NaOH was extended to 1000°K. by combination with the data of Douglas and Dever.[2] The low temperature heat capacity data were

joined smoothly with the values derived from the heat content differences of Douglas and Dever at higher temperatures. A recalculation of the heat content differences in terms of the data in Table VI gives values 0.3% high at 100° and 0.1% low at 200°, and these amounts are well within the limit of accuracy at these temperatures.

TABLE VI

THERMODYNAMIC PROPERTIES OF NaOH

Units are gbs. mole^{-1}

T, °K.	C_p^0	S^0	$-(F^0 - H_0^0)/T$	$(H^0 - H_0^0)/T$
15	0.088	0.020	0.007	0.013
20	.198	.059	.015	.044
25	.364	.119	.029	.090
30	.597	.205	.051	.154
35	.895	.319	.081	.238
40	1.263	.462	.119	.343
45	1.671	.634	.166	.467
50	2.098	.832	.223	.609
55	2.545	1.052	.288	.764
60	3.016	1.294	.362	.932
70	3.967	1.830	.532	1.298
80	4.877	2.422	.731	1.691
90	5.832	3.056	.954	2.102
100	6.631	3.712	1.197	2.515
110	7.384	4.380	1.456	2.924
120	8.185	5.053	1.727	3.325
130	8.717	5.726	2.009	3.716
140	9.292	6.393	2.298	4.094
150	9.810	7.052	2.594	4.459
160	10.294	7.701	2.893	4.809
170	10.737	8.339	3.194	5.145
180	11.140	8.964	3.497	5.467
190	11.510	9.577	3.801	5.775
200	11.850	10.176	4 105	6.071
210	12.172	10.762	4.408	6.354
220	12.468	11.335	4.710	6.625
230	12.737	11.895	5.010	6.885
240	12.996	12.443	5.309	7.134
250	13.238	12.979	5.605	7.374
260	13.472	13.503	5.899	7.604
270	13.694	14.016	6.190	7.826
273.15	13.759	14.174	6.281	7.893
280	13.900	14.517	6.478	8.039
290	14.086	15.008	6.764	8.244
298.15	14.228	15.400	6.995	8.405
300	14.260	15.489	7.047	8.442
310	14.413	15.959	7.327	8.632
320	14.561	16.419	7.604	8.815
323.15	14.606	16.562	7.691	8.871
330	14.700	16.869	7.878	8.992
335.78	14.776	17.125	8.035	9.090
338.25	14.807	17.233	8.102	9.131
340	14.830	17.310	8.149	9.161
350	14.945	17.741	8.417	9.324
375	15.220	18.782	9.073	9.709
400	15.520	19.773	9.711	10.062
425	15.936	20.726	10.332	10.394
450	16.481	21.652	10.935	10.717
475	17.178	22.561	11.523	11.038
500	17.963	23.462	12.097	11.365
525	18.806	24.358	12.660	11.698
550	19.711	25.254	13.212	12.042
566.0(α)	20.303	25.827	13.560	12.267
566.0(β)	(20.56)	28.51	13.56	14.951
575.0	(20.56)	28.84	13.80	15.038
592.3(β)	(20.56)	29.45	14.25	15.200
592.3(l)	20.58	32.01	14.25	17.765
600	20.57	32.28	14.48	17.801
650	20.50	33.92	15.91	18.012
700	20.43	35.44	17.25	18.186
750	20.36	36.84	18.51	18.333
800	20.29	38.16	19.70	18.458
850	20.22	39.38	20.82	18.564
900	20.15	40.54	21.89	18.654
950	20.08	41.62	22.89	18.731
1000	20.01	42.65	23.85	18.796

TABLE VII

THERMODYNAMIC PROPERTIES OF NaOH·H_2O

Units are gbs. mole^{-1}

T, °K.	C_p^0	S^0	$-(F^0 - H_0^0)/T$	$(H^0 - H_0^0)/T$
15	0.190	0.057	0.014	0.043
20	.484	.149	.035	.114
25	.909	.301	.072	.229
30	1.468	.514	.127	.387
35	2.098	.787	.201	.586
40	2.771	1.112	.294	.818
45	3.470	1.479	.405	1.074
50	4.166	1.881	.532	1.349
55	4.856	2.310	.674	1.636
60	5.543	2.762	.829	1.933
70	6.846	3.717	1.173	2.544
80	8.060	4.711	1.553	3.158
90	9.170	5.726	1.960	3.766
100	10.157	6.744	2.387	4.357
110	11.054	7.754	2.829	4.925
120	11.898	8.753	3.282	5.471
130	12.377	9.737	3.740	5.997
140	13.403	10.703	4.203	6.500
150	14.078	11.651	4.668	6.983
160	14.708	12.580	5.134	7.446
170	15.306	13.490	5.599	7.891
180	15.884	14.381	6.062	8.319
190	16.438	15.255	6.523	8.732
200	16.968	16.111	6.981	9.130
210	17.479	16.952	7.436	9.516
220	17.982	17.777	7.887	9.890
230	18.477	18.587	8.335	10.252
240	18.958	19.383	8.779	10.604
250	19.440	20.167	9.218	10.949
260	19.898	20.939	9.655	11.284
270	20.341	21.698	10.087	11.611
273.15	20.480	21.934	10.222	11.712
280	20.783	22.446	10.515	11.931
290	21.210	23 183	10.939	12.244
298.15	21.544	23.775	11.281	12.493
300	21.620	23.909	11.359	12.550
310	22.018	24.624	11.775	12.849
320	22.402	25.329	12.188	13.141
323.15	22.521	25.548	12.317	13.231
330	22.775	26.024	12.597	13.427
335.78	22.936	26.421	12.832	13.589
338.25(S)	23.074	26.590	12.931	13.659

The Dissociation Pressure of Water over the System NaOH·H_2O–NaOH from the Third Law of Thermodynamics.—The above data, combined with available data on water, enable the calculation

of the dissociation pressure of sodium hydroxide monohydrate as a function of temperature.[14]

$$H_2O(g),\ S_{298.15°K} = 45.106 \text{ gbs. mole}^{-1}$$

$$\left(\frac{H^0 - H_0^0}{T}\right)_{298.15°K} = 7.941 \text{ gbs. mole}^{-1}$$

$$NaOH\cdot H_2O = NaOH + H_2O(l)$$

$$\Delta H^0_{298.15} = 5519 \text{ cal. mole}^{-1}$$

$$H_2O(l) = H_2O(g) \qquad \Delta H^0_{298.15} = 10{,}520 \text{ cal. mole}^{-1}$$

$$NaOH\cdot H_2O = NaOH + H_2O(g)$$

$$\Delta H^0_{298.15} = 16{,}039 \text{ cal. mole}^{-1}$$

Using data from Tables V and VI

$$\Delta H_0^0 = 14{,}890 \text{ cal. mole}^{-1}$$

$$\Delta S^0_{298.15} = 36.731 \text{ gbs. mole}^{-1}$$

$$\Delta F_{293.15°K} = 5088 \text{ cal. mole}^{-1} = -RT \ln P_{H_2O} \text{ (atm.)}$$

$$P_{H_2O} = 1.86 \times 10^{-4} \text{ atm.} = 0.14 \text{ mm. at } 298.15°K.$$

Baxter and Starkweather[15] made careful determinations of the vapor pressure of water over sodium hydroxide and its "lowest hydrate" at 0, 25, and 50°. Their results are given in Table VIII together with values calculated by means of the present data and the third law of thermodynamics.

TABLE VIII

CALCULATED AND OBSERVED VALUES OF THE DISSOCIATION PRESSURE OF WATER OVER $NaOH\cdot H_2O$–NaOH, MM.

T, °K.	P_{calcd}	P_{obsd}	B. + S.(actual obs)
273.15	0.012	0.04	(0.05, 0.03, 0.03)
298.15	0.14	0.15	(0.16, 0.15, 0.15)
323.15	1.14	1.15	(1.13, 1.15, 1.16)
335.78	1.93	Eutectic	

The excellent agreement, particularly at 323.15°K., where observational accuracy is greatest, indicates that NaOH and $NaOH\cdot H_2O$ approach zero entropy at limiting low temperatures. The lack of agreement at 273.15°K. is not surprising in view of the low pressure and presumably the slower equilibrium rate. We regard fortuitous cancellation of equal amounts of zero point entropy as highly improbable in such a case.

The agreement also indicates that the "lowest" hydrate in the experiment of Baxter and Starkweather was $NaOH\cdot H_2O$. They passed moist air over pea-sized pieces of NaOH in a tube 70 cm. long and 1.5 cm. in diam. and the extensive surface should have provided considerable opportunity for the formation of any stable intermediate hydrate such as $NaOH\cdot 0.5H_2O$.

Acknowledgment.—We thank G. V. Calder for assistance with the experimental measurements and G. E. Brodale for assisting with the calculations.

(14) "Selected Values of Chemical Thermodynamic Properties," Series III; Natl. Bur. Std., March 31, 1947; June 30, 1948.

(15) P. Baxter and H. W. Starkweather, *J. Am. Chem. Soc.*, **38**, 2038 (1916).

EXPERIMENTAL INVESTIGATIONS ON THE LIGHT SCATTERING OF COLLOIDAL SPHERES. IV. SCATTERING RATIO[1]

BY WILFRIED HELLER AND RICHARD TABIBIAN[2]

Chemistry Department, Wayne State University, Detroit, Michigan

Received August 28, 1961

Light scattering of 18 monodisperse polystyrene and polyvinyltoluene latices was investigated at an angle of 90° with respect to an incident linearly polarized beam whose electric vector was, in succession, parallel and perpendicular to the plane of observation. The ratio of the two quantities obtained, designated as "scattering ratio," σ—which is closely related to depolarization and polarization ratio—was found to be a very useful quantity for absolute particle size determinations except for particle diameters $<1/4\ \mu$ (on use of visible light), a particular advantage being the relative insensitivity to changes in the solid angle of the scattered beam. Partial investigation of the spectra of σ eliminated the problem of multivaluedness of results inherent in any measurement of lateral light scattering. The concentration dependence of σ was investigated in detail. The particle diameters obtained from σ, evaluated on the basis of theoretical data derived from the Mie theory, agreed very satisfactorily with electron microscopic results (range covered, 135 to 824 mμ).

I. Introduction

Size determinations on colloidal spheres from the total scattering at 90° with respect to the direction of the primary beam give results which are in satisfactory agreement with electron microscopic data[3] if the Mie theory is used. This method requires an instrument constant in order to translate the experimental data into absolute light scattering data. The principal objective of the present investigation is to outline a new modification of 90° measurements, related to depolarization measurements, which yields an absolute method of particle size determination. It consists of measuring the ratio of the total intensities of light scattered at 90° from an incident monochromatic linearly polarized beam whose electric vector vibrates first

(1) This work was supported by the Office of Naval Research. A preliminary account of this work was given at the 134th National Meeting of the American Chemical Society, Chicago, Illinois, September, 1958.

(2) E. I. du Pont de Nemours & Co., Elastomer Chemicals Department, Wilmington, Delaware.

(3) R. Tabibian and W. Heller, *J. Colloid Sci.*, **13**, 6 (1958).

parallel and, subsequently, perpendicular to the plane of observation. This ratio has been designated as "scattering ratio."[4]

II. Definitions

The light scattered by an isotropic sphere at an angle γ of 90° relative to the reverse direction of an incident *unpolarized* beam is completely linearly polarized if $\alpha \rightarrow 0$ [5] and if the scattering process is not complicated by scattering from neighboring spheres. The plane of polarization of the scattered light is perpendicular ($\perp$) to the plane of observation. This is characteristic for Rayleigh scattering, *i.e.*, pure dipolar scattering. For spheres of larger relative size, α, the light scattered at 90° is found to be only partially polarized, a component vibrating in the plane of observation with an intensity $J_{||}$ being observed in addition to the perpendicular component of intensity $J_\perp$. Here, J is the intensity, at γ, of the scattered beam per unit intensity of the incident beam at unit distance from the sphere. The intensity of both $J_\perp$ and $J_{||}$ depends upon the diameter, D, the relative refractive index of the particles, m, and the vacuum wave length, λ_0, of the incident light. The state of polarization of the scattered light, determined by inserting an analyzing prism in the path of the scattered beam can, therefore, be used as a criterion of their size. It may be expressed in different ways, the various possible definitions being interrelated. The definition of interest here is the depolarization

$$\Delta = (J_{||}/J_\perp)_s \qquad (1)$$

a quantity introduced by Gans.[6] This quantity simply represents the ratio of intensities of the two orthogonal components of light scattered by one sphere from incident unpolarized light.[7] The subscript, s, added to the conventional definition of Δ specifies that the symbols $\parallel$ and $\perp$ pertain to the electric vectors of the scattered components. Since $J_\parallel$ and $J_\perp$ vary with α, Δ-measurements are suitable and have been used for particle size measurements.

Instead of operating with an incident beam of unpolarized light, one may use *linearly polarized* light obtained by inserting a polarizing prism between light source and scattering system. We shall consider two cases: (a) the electric vector of the incident polarized beam is perpendicular to the plane of observation; (b) it is in the plane of observation. In the former case, finite scattering occurs at any α, the scattered beam is linearly polarized, and its electric vector is perpendicular to the plane of observation. In the latter case, scattering of finite intensity occurs only outside of the range of Rayleigh scattering, the scattered beam again being fully polarized with the electric vector vibrating in the plane of observation. The variation in the intensity of the scattered beam with α has been computed for both cases considering a wide range of α-values[4] and several relative refractive indices m. The ratio of the two intensities, defined as "scattering ratio"

$$\sigma = (J_{||}/J_\perp)_i \qquad (2)$$

also varies extensively with α so that it provides an alternate method for determining *absolute particle sizes* (no need for an instrument constant). (The subscript i specifies here that the symbols $||$ and $\perp$ pertain to the electric vector of the incident beam.)

In view of the full polarization of the scattered beam in both case (a) and case (b), it is clear that for spheres

$$\sigma = \Delta \qquad (3)$$

so that the choice between σ and Δ-measurements depends exclusively on methodical considerations.[8] σ-measurements have the following experimental advantages: (1) The minor aberrations in the light path of the primary beam due to rotation of a polarizing prism inserted in the path of the primary beam (σ-measurement) have a smaller effect upon the measurements than the minor aberrations of the scattered beam due to rotation of an analyzing prism inserted in the path of the scattered beam. (2) The absence of the refracting analyzing prism necessary in Δ-measurements simplifies calculation of the solid angle pertinent to the scattered light received by the photocell. (3) The solid angle which can be used for the scattered beam in Δ-measurements is far more restricted because of the transmittance of natural light through an analyzing prism at sufficiently large solid angle.

In actual experiments, one does not determine the intensity of light scattered by one sphere but that scattered by a dispersed system containing N spheres per ml. *viz.*

$$I_\perp = J_\perp N r^2 I_0, \text{ and} \qquad (4)$$

$$I_{||} = J_{||} N r^2 I_0 \text{ ergs cm.}^{-3} \text{ sec.}^{-1} \qquad (4a)$$

Here, r is the photometric distance, I is the intensity scattered per unit solid angle through a differential cone at the angle γ, and I_0 is the intensity of the primary beam. From $I_\perp$ and $I_{||}$ one derives the corresponding pair of specific scattered intensities

$$I_\perp/I_0\varphi = J_\perp r^2/V = 6J_\perp r^2\pi^2/\lambda^3\alpha^3 \text{ and} \qquad (5)$$

$$I_{||}/I_0\varphi = J_{||} r^2/V = 6J_{||} r^2\pi^2/\lambda^3\alpha^3 \qquad (5a)$$

where φ is the volume fraction of the spheres and V the volume of one sphere. On considering, instead, the concentration, c, in g./100 g., one obtains the corresponding pair

$$(I_\perp/I_0 c) = (I_\perp/I_0\varphi)(\rho_{12}/\rho_2) \times 10^{-2} \qquad (6)$$

(4) W. Heller, W. J. Pangonis, and N. Economou, *J. Chem. Phys.*, **34**, 971 (1961).

(5) $\alpha = \pi D/\lambda$, where D is the diameter of the sphere and λ is the wave length in the medium.

(6) R. Gans, *Phys. Z.*, **28**, 661 (1927).

(7) The definition of eq. 1 is limited to 90°, where $J_{||} \rightarrow 0$ as the particle diameter approaches zero. If used at other γ-values, $J_{||}/J_\perp$ therefore no longer represents the degree of depolarization. The term "polarization ratio" used by LaMer and co-workers (M. Kerker and V. K. LaMer, *J. Am. Chem. Soc.*, **72**, 3519 (1950), and later papers by LaMer and associates) is then more suitable. At 90°, of course, the polarization ratio is identical with the depolarization Δ.

(8) A combination of both techniques provides a sensitive means of ascertaining whether or not the scattering particles are spherical, since for non-spherical particles $\sigma \neq \Delta$.

$$(I_{||}/I_0c) = (I_{||}/I_0\varphi)(\rho_{12}/\rho_2) \times 10^{-2} \quad (6a)$$

Here ρ_2 is the density of the spheres and ρ_{12} is that of the entire system.

It is clear that the ratio of each of the three preceding pairs of equations, *viz.*, $I_{||}/I_{\perp}$, is identical with $J_{||}/J_{\perp} = \sigma$ provided that interference between the scattering of the N spheres does not complicate matters. This complication of multiple scattering is easily excluded by extrapolating the experimental $(I_{||}I_{\perp})$-values to zero concentration. It is, therefore, useful to introduce the symbol σ_0 in order to emphasize the fact that the experimental ratio has been extrapolated to zero concentration and is, therefore, directly comparable to the ratio $(J_{||}/J_{\perp})$ derived from theory. In contradistinction, σ shall refer to experimental data obtained at finite concentration. It may be noted that the concentration of the dispersed system does not enter explicitly in the value σ_0 in contradistinction to measurements of the specific-turbidity[9] or of the specific intensity of light scattered at 90° from an unpolarized beam.[3]

III. Experimental Procedure

The model systems used were monodisperse latices of polystyrene and polyvinyltoluene made available through the courtesy of Dr. J. W. Vanderhoff of the Dow Chemical Co. The latex samples as received contained 30–50% solids. The preparation of dilute latex for the light-scattering measurements was carried out in the following manner. A small amount of latex was diluted with freshly prepared double distilled water in a centrifuge bottle of 250-ml. capacity to reduce the concentration to about 0.5–1.0%. The dilute latex was then centrifuged at about 350 *g* for 20 min. to remove any agglomerates that might have been present. One hundred ml. of the supernatant suspension was pipetted into a flask. The polymer concentration was determined by accurately weighing out about 25 g. of this suspension and evaporating it to dryness in a partial vacuum at 80° and then weighing the dried solids. A series of dilutions was made volumetrically from the remainder of the centrifuged latex by adding double distilled water to portions measured with a 10-ml. buret into volumetric flasks. The volume additivity, verified in these systems, allowed the concentration to be expressed in grams per 100 g. for any of the diluted samples obtained. These samples were kept in Pyrex glassware which had been carefully cleansed and subsequently steamed out for several minutes. To safeguard against any changes taking place in the samples upon prolonged standing at room temperature, all measurements were made within 3 days of the time when they were first prepared.

The apparatus used is shown in Fig. 1. For the present work, the interchangeable light source, S, was always a Hg-vapor lamp, type AH4. Its brightness can be kept constant, within ±0.25%, by a Sorensen voltage regulator, Model 500-S. The light beam enters the scattering apparatus at the variable entrance slit A_2, after having passed consecutively through a liquid filter, F, a collimating system, L_1L_2, a single prism monochromator, M, and a compensator, C. The section of the scattering apparatus between the apertures A_2 and A_3 is the same as used for turbidity measurements[9] except for the insertion of a Glan–Thompson prism, N, between R and A_3. The scattering cell SC, whose front window faces A_3, is a Rayleigh horn. The shaded rectangular area in the horn represents a cut through the mid-section of the cylindrical volume (0.043 ml.) from which scattered light reaches the phototube at PT_2. The Rayleigh horn, painted black throughout except for the entrance and observation window, has the well known advantage of completely eliminating back reflection of the primary beam by its absorption in the tail. The scattered light leaving the Rayleigh horn through the lateral observation window is recorded at PT_2 by means of an IP 21 photomultiplier tube which is connected with a Photovolt photometer Model 520

(9) R. Tabibian, W. Heller, and J. N. Epel, *J. Colloid Sci.*, **11**, 195 (1956).

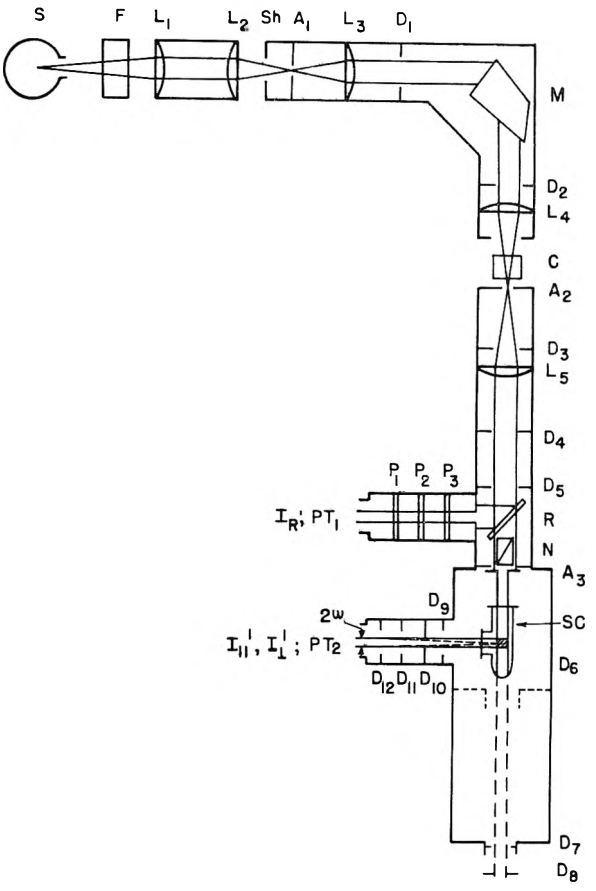

Fig. 1.—Schematic diagram of entire light scattering apparatus: S, light source; F, infrared filter; L, Lenses; Sh, shutter; A, variable apertures; D, fixed diaphragms; M, monochromator; C, compensator for reducing partially polarized light to natural light R, reflecting plane parallel glass plates; N, Glan–Thompson prism; SC, scattering cell assembly; P, rotatable polaroids; PT, photomultiplier positions.

modified so as to give a higher sensitivity than the standard model. A light-tight rectangular box housing the phototube is fastened to a light-tight carriage fitted with guide rails so that the phototube can be switched back and forth between the positions PT_2 and PT_1. At the latter position, the intensity, I_R, of the reference beam is recorded. This beam is split off the main beam by means of the plane parallel glass plate R. The reference beam carries about 11% of the intensity of the beam incident upon R. The intensity of the former can be varied between its original value and zero in 216 approximately equal steps by rotating the three polaroids P_1, P_2, and P_3 between six fixed stops. It is thus always possible to reduce I_R to the order of magnitude of the intensity I' measured at PT_2 I' being between 10^{-8} and 10^{-6} times as large as the intensity I_0 of the primary beam incident upon the scattering system in the Rayleigh horn.

The beam incident upon the Rayleigh horn, in absence of the compensator C, is partially polarized due to the concerted effect of the reflections at the monochromator prism, M, and at the glass plate, R This partial polarization is eliminated by the compensator which consists of two plane parallel glass plates separated by an air space. The angle of incidence of the primary beam upon this double plate is varied by rotating the latter about an axis perpendicular to the primary beam and parallel to the plane of observation. Incorporation of a micrometer screw into the axis of rotation allows one to reproduce with high precision and for any wave length desired that angle of inclination which transforms the primary beam from a partially polarized into a fully polarized beam. The partial polarization of the incident beam, prior to the insertion of C, is taken advantage of for adjusting the Glan–Thompson polarizing prism so that the plane of polarization of the beam inci

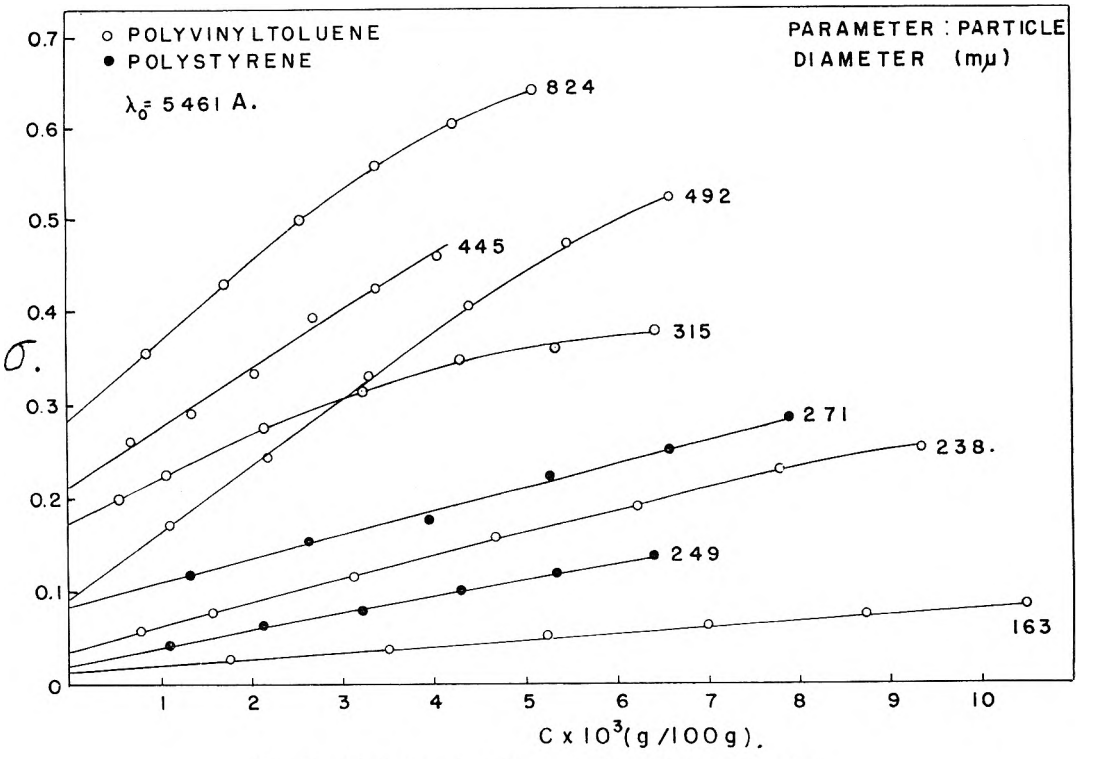

Fig. 2.—Variation of scattering ratio with concentration.

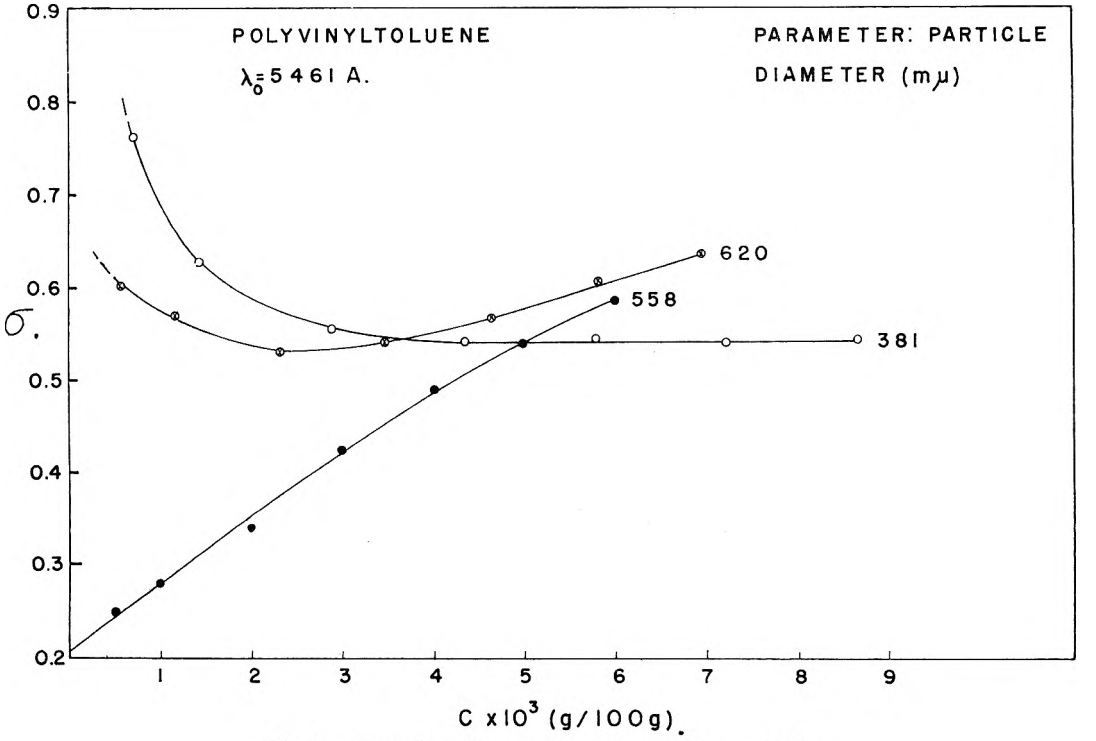

Fig. 3.—Variation of scattering ratio with concentration.

dent upon the scattering system is exactly parallel or perpendicular, respectively, to the plane of observation.[10] After the subsequent insertion of the compensator, the photomultiplier tube is placed so as to face D_8 and the inclination of the compensator is adjusted until no change in galvanometer deflection is noted on rotating the polarizing prism between the two stops, 90° apart. Identity of deflections does not necessarily indicate that the intensities of the two orthogonal components are strictly equal if the photosensitive area is slightly anisotropic. The anisotropy of the photosensitive area of the photomultiplier used was, therefore, checked carefully and, though measurable, was small enough (≤ 0.05) to be neglected in the present work.

The primary beam entering the Rayleigh horn at A_3 is

(10) Since the reflecting faces of the monochromator prism were exactly vertical and the axis of the scattering apparatus exactly horizontal, as checked by a level, the plane of observation was exactly horizontal after adjustment of the prism. This facilitated the other adjustments.

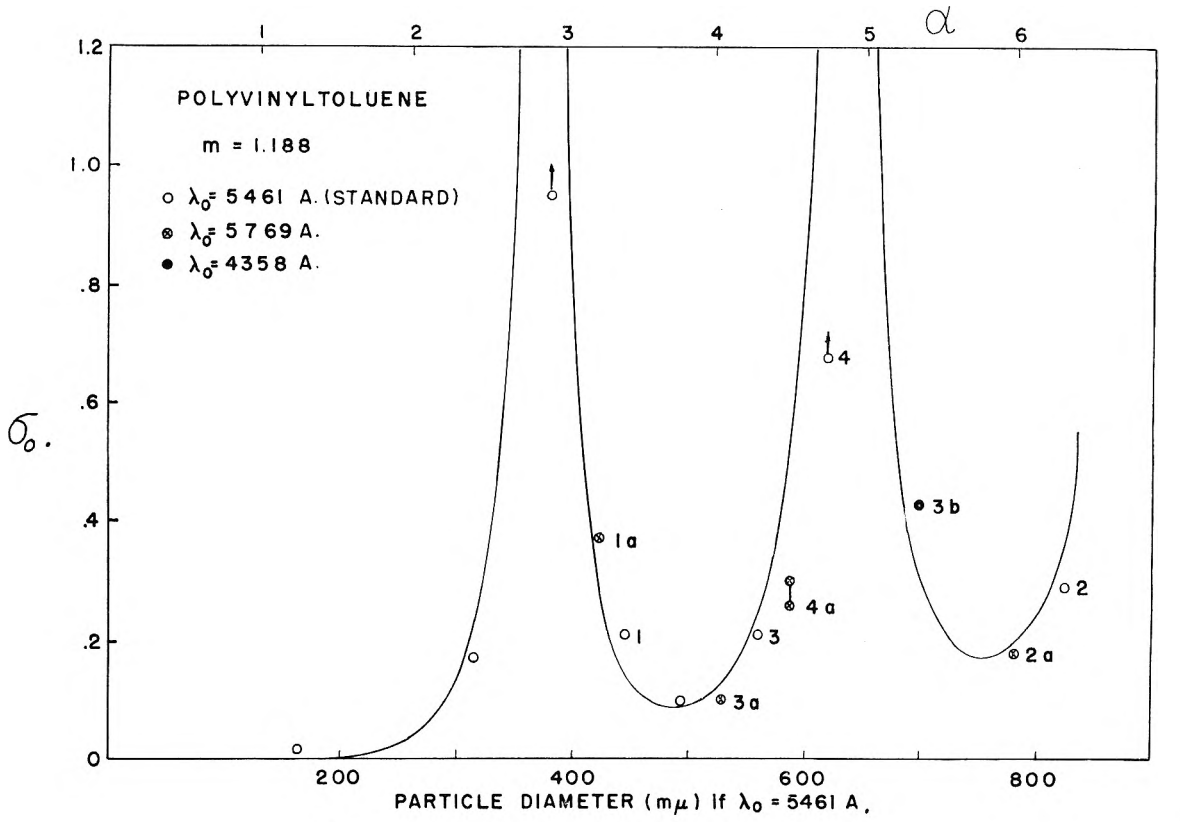

Fig. 4.—Variation of scattering ratio with particle size.

nearly parallel. Its divergence is defined by a solid angle $\omega_0 = 1 \times 10^{-4}$ steradian. The corresponding planar angle, ω, *i.e.*, the half angle at the vertex of a planar projection of the light cone, is 0.33°. The *effective* solid angle of the scattered beam is, after correction for refraction, 4.1×10^{-4} steradian ($\omega = 0.66°$) in presence of D_{12}. This is the arrangement used for most of the work reported elsewhere on 90° scattering from an unpolarized beam.[3] Since the size of the solid angle is far less crucial here (see section IV, C), it was increased in the present work to 1.5×10^{-3} steradian ($\omega = 1.3°$) by removing D_{12}. The resulting increase in the intensity of the scattered beam received by the photocell considerably increased the relative precision of the measurements.

Compilation of the scattering ratio requires two sets of data. First the ratio $I'_{||}/I_R$ is determined, the subscript || meaning, in terms of the experimental procedure, that the plane of polarization of the Glan–Thompson prism is set so as to coincide with the plane of observation. After rotating the prism by 90°, the second set of data, giving $I'_{\perp}/I_R$ is obtained.[11] The ratio of these two quantities gives $I_{||}/I_{\perp}$ since the instrument constant[12] is identical for numerator and denominator.

Most of the measurements of the scattering ratio were made with the Hg green line (vacuum wave length λ_0 = 5461 Å.). Additional data were obtained at other Hg-lines.[13] The limiting quantity

$$\sigma_0 = \lim_{c \to 0} \sigma \qquad (7)$$

was obtained by making measurements at several concentrations and extrapolating to zero concentration. An accurate comparison between the experimental results and the theory is possible only if the relative refractive index, m (relative to that of the dispersing medium), and the density, ρ_2, of the scattering particles are known. The values used here are identical with those previously used[8,9] for polystyrene and polyvinyltoluene, namely 1.199 and 1.188, respectively.

IV. Experimental Results

A. The Variation of σ with Concentration.—The concentration dependence of σ is shown in Fig. 2 and 3 for the standard vacuum wave length of 5461 Å. Nine of the eleven curves shown approximate straight lines very well within the range of low concentrations, so that an extrapolation to σ_0 in most of these cases is quite easy and secure. *This is a considerable advantage* over the (I/I_0c) *vs.* c curves obtained with unpolarized incident light and also over the individual $(I_{||}/I_0c)$ *vs.* c and $(I_{\perp}/I_0c)$ *vs.* c curves which may be constructed from the data collected in connection with σ-measurements. Those curves show, in general, an increase in slope with decreasing concentration. The two samples for which extrapolation of σ is very difficult (Fig. 3) have particle diameters which—at the wave length used and for m = 1.20—lead to a maximal or near maximal value on the σ_0 *vs.* D-curve. This follows from Fig. 4, which will be discussed in more detail below. Additional systems with particle sizes at or near these σ_0-maxima, investigated subsequently by M. Wallach,

(11) Each of these ratios is obtained from individual measurements at PT_2 and PT_1. Several readings were taken in each position and averaged. The individual readings rarely differed by more than ±1% from the average.

(12) The instrument constant allows one to convert the actually measured quantities $I'_{||}$ and $I'_{\perp}$ into the absolute values $I_{||}$ and $I_{\perp}$, respectively. If needed, the constant is obtained by one of the various available calibration procedures (for a brief discussion see ref. 3). It is also possible, in principle, to calculate it. A first attempt in this direction[3] led to an agreement between experimental and theoretical instrument constant to within 15%. The less good agreement reported earlier[3] is due to the fact that the calculated instrument constant was in error by a factor of 2.0.

(13) For these other lines, the compensator setting had to be altered.

confirmed the fact that σ_0-values > 1.0 cannot be derived securely by extrapolation of experimental σ-data. If $m = 1.20$ and if the green Hg-line is used, unfavorable ranges for σ-extrapolations are, according to Fig. 4, particle diameters 350–395, 605–665, and 840–~940 mμ. In these cases, the use of other wave lengths will allow one to circumvent this difficulty of extrapolation (see section V).

At sufficiently high concentrations, σ evidently should approach the value 1.0 corresponding to complete depolarization by multiple scattering. For σ_0 values less than 1.0, the σ *vs.* c curve should therefore have a positive slope. This is found without exception. At σ_0 values greater than 1.0, the $\sigma(c)$ curve should have a negative slope. The initial portion of the two uppermost curves in Fig. 3 agrees with this expectation, but the fact that the negative slope persists even after σ has fallen to values less than 1.0 indicates that an additional factor enters. Special experiments, to be reported in a separate publication, indicated that this complication is due to differences in "apparent" depolarization, due to multiple scattering, of the primary scattered light vibrating in the plane of observation and of that vibrating perpendicular to the plane of observation. These differences are major whenever $J_{||}$ and $J_{\perp}$ differ widely in magnitude. In these cases, σ will reach a minimum value with increasing c, the sooner the larger D is, before rising asymptotically toward the value of 1.0.

One would expect that the limiting (initial) slope of the $\sigma(c)$ curve increases, at least for comparable σ_0 values, with increasing particle size on account of the over-all increase, with it, of scattering and, therefore, of multiple scattering (within the size range considered here). This was found to be true without exception.

B. Variation of σ_0 with Particle Size.—Figure 4 gives the theoretical σ_0 *vs.* D-curve interpolated from the Mie data[4] for $m = 1.188$ (relative refractive index of polyvinyltoluene) and $\lambda_0 = 5460.73$ Å. The data shown by open circles represent the experimental σ_0-values obtained at 5460.73 Å., the others are normalized data pertinent to other wave lengths (see section V). The D-values associated with the experimental σ_0-data were obtained independently from electron microscopy. Two of the data provided with arrows pointed upward represent minimum values, the actual values in each case being likely in excess of 1.0 (these data pertain to the two upper curves of Fig. 3 which cannot be extrapolated safely). With the exception of these two cases for which a definite σ_0-value cannot be given, the experimental σ_0-values associated with a given electron microscopic diameter, D_e, fit satisfactorily the theoretical σ_0 *vs.* D-curve. The same agreement was found for polystyrene ($m = 1.199$).[14]

More important for the practical application of the scattering ratio is a comparison between the electron microscopic diameters, D_e, and the optical diameters, D_0, obtained by associating with the experimental σ_0-values the theoretical diameters derived from the Mie theory. This comparison is carried out in Tables I and II, disregarding, for the moment, the problem of multivaluedness of answers (see section V). The mean deviation between electron microscopic and optical diameters >250 mμ is 2.2% for polyvinyltoluene (Table I). On using instead of $m = 1.188$ rather the value 1.185, the average deviation, which had proved to be less in connection with the $(\tau/c)_0$-values,[9] is essentially the same. In the case of polystyrene (Table II) the mean deviation for diameters >230 mμ is 3.2%. It is interesting to note that the per cent deviation of D_0 is positive throughout for all particles whose diameter is less than approximately 230 mμ. This can readily be explained as an effect of heterodispersion which makes itself felt here in spite of the fact that the spread of the distribution is remarkably narrow.[15] In view of the very strong increase of σ_0 with particle diameter, between $D \sim 200$ and ~350 mμ, particles larger than those corresponding to the mean make a strong contribution while those smaller than the mean make a relatively minor contribution. Thus, both σ_0 and D_0 derived therefrom are bound to be larger than expected for the given mean particle size, $\bar{D}$. Apart from this detail, the agreement between optical and electron microscopic diameters is fairly satisfactory throughout.

TABLE I

COMPARISON OF PARTICLE DIAMETERS FROM SCATTERING RATIO AND ELECTRON MICROSCOPY

(Polyvinyltoluene) ($m = 1.188$)

Sample no.	σ_0	D_0, mμ	D_e, mμ	% Deviation
42	0.014	>163	163	+
23	.17	307	315	−2.5
2012	..[b]	..	381	...
43 B	.37	417	421[a]	−1.0
43 B	.21	431	445	−3.1
44 A	.092	507	492	3.0
43 C	.10	514	528[a]	−2.7
43 C	.21	554	558	−0.7
43 C	.43	685	699[a]	−2.0
44 B	.26–0.30	562–569	587[a]	−3.1–4.3
44 B	..[b]	..	620	...
44 C	.18	772	780[a]	−1.0
44 C	.29	812	824	−1.5

[a] Normalized particle diameters; see text. [b] Extrapolation to σ_0 unsafe; see text.

C. Variation of σ_0 with Solid Angle.—As already stated, all experiments reported pertain to a solid angle ω_0 of 1.5×10^{-3} steradian. This angle, although small, is large compared to that generally used in earlier work[3] which was concerned with the total intensity of the light scattered at $\gamma = 90°$ from an incident unpolarized beam. In those experiments, the numerical results had been found to vary strongly with the solid angle. (See particularly Fig. 9, l.c.) For σ, the situation is much simpler. A few experiments were carried

(14) Part of these latter data was obtained in earlier exploratory work by J. N. Epel and in recent extensions of the present work by T. L. Pugh.

(15) On account of this high sensitivity of σ to heterodispersion, it was selected as a particularly suitable effect for determining size distribution curves, work which shall be reported in a subsequent publication.

TABLE II

COMPARISON OF PARTICLE DIAMETERS FROM SCATTERING RATIO AND ELECTRON MICROSCOPY

(Polystyrene) (m = 1.199)

Sample no.	σ_0	D_0, mμ	D_e, mμ	% Deviation
S 138	0.006	>135	135	+
S 139	.013	>150	150	+
S 151	.025	>219	219	+
S 137	.025	>223	223	+
7065	.036	255	238	+7.1
2023	.022	241	249	−3.2
580 G	.072	>259	259	+
7194	.084	280	271	+3.3
63 A	.24	546	557	−2.0
66 A	.38	809	814	−0.6

out in order to check the expected modest effect of the solid angle. They are reported in Table III. It is apparent that σ hardly varies with ω_0—up to at least 1.5×10^{-3} steradian—at any concentration below 6×10^{-3} g./100 g. This is a *major advantage* of the ratio measurements compared to intensity measurements.

TABLE III

DEPENDENCE OF THE SCATTERING RATIO ON SOLID ANGLE

Sample no.	$C \times 10^3$	σ for ω_{sa} (sterad.) 4.1 $\times 10^{-4}$	8.3 $\times 10^{-4}$	15 $\times 10^{-4}$
7065 (D = 238 mμ)	3.108		0.118	0.115
polystyrene	6.216		.195	.192
	9.324		.265	.255
23 (D = 315 mμ)	1.071		.238	.226
polyvinyltoluene	2.142	0.260	.274	.273
	3.213	0.298	.300	.309

[a] Corrected for refraction (see ref. 3).

V. The Problem of Multivaluedness of σ_0 and its Solution

Measurements of the scattering ratio at a single wave length will give single valued particle sizes only if σ_0 is smaller than at the first maximum of the σ_0 *vs.* D-curve (Fig. 4). At larger σ_0-values, unequivocal answers are possible only on either combining the σ_0-measurement with another light scattering measurement at the same wave length or by studying the variation of σ_0 with wave length. If it is known, *a priori*, that the particle diameter is such, at the standard wave length used, that $\alpha < 4$ (first minimum of the $\sigma_0(\alpha)$-curve in Fig. 4) then it is sufficient to make one additional σ_0-measurement at another wave length in order to remove the multivaluedness. (For other m-values, the respective σ_0-value is different.[4]) For the standard wave length, λ_s, used here (λ_0 = 5461 Å.), the diameter corresponding to the first σ_0-minimum is 500 mμ. For larger particle sizes, the determination of σ_0 at two additional wave lengths or, better still, the compilation of a limited σ_0-spectrum is necessary in order to obtain a single valued answer for D. The analytical principle is the following: since σ_0 depends at constant m only on α, one moves, at constant D, to the left or right in the σ_0 *vs.* α-plot (Fig. 4, considering the upper abscissa) on increasing or reducing, respectively, the wave length used. In a σ_0 *vs.* D-plot compiled for the standard wave length λ_s (Fig. 4, considering the lower abscissa), the determination of σ_0 at another wave length, λ', therefore yields a fictitious diameter which should fit the $\sigma_0(D)$ curve at the D-value

$$D_f = D(\lambda_s/\lambda') \qquad (8)$$

provided of course that m is nearly constant between λ_s and λ'. This analytical principle is illustrated in Fig. 4 and is also taken advantage of in Table I. The point identified in Fig. 4 by the number 1 (actual D_e = 445 mμ) on the first descending branch of the curve refers to measurements at the green Hg line. Investigation of the same system at λ_0 = 5769 Å. yields point 1a. It is, therefore, apparent that point 1 must be associated with a descending branch instead of an ascending branch of the $\sigma_0(\alpha)$ curve. Cases 2 and 2a show that point 2 must be associated with an ascending branch. Cases 4 and 4a are of interest because this example shows that by changing λ_0 one can obtain a σ_0-value by extrapolation if this is impossible at the standard wave length used (see 620 mμ-curve in Fig. 3). The examples of the two wave length analysis show that it reduces the multivaluedness of the result, but it does not eliminate it. The more powerful analytical value of a three wave length analysis follows from point 3. Point 3, obtained at 5461 Å., changes to point 3a on using 5769 Å., and to 3b on using 4358 Å. It is clear that no fit for all three points could be obtained on tentatively assigning to point 3 rather the diameter of 430 mμ or of 315 mμ. The result is, therefore, single valued as to D.

On using this method of partial spectral analysis, it must be borne in mind that m varies with λ. This change is not large enough for the systems investigated here to lead to serious errors. The non-systematical variation of σ_0 on going from 3a to 3 to 3b in Fig. 4 shows that the systematic error due to dispersion is smaller than the over-all experimental error. Nevertheless, as a general rule, it will be advisable to use the additional wave lengths (or spectrum) only for the purpose of defining the pertinent range of the $\sigma(\alpha)$ curves which applies in a given case and to derive the actual particle size only from σ_0 at that wave length for which m is known. If, on the other hand, the dispersion of m is known, averaging of all correspondingly adjusted theoretical σ_0-values will, of course, improve the accuracy of the D-value derived.

NOTES

INFRARED SPECTRUM OF NITRYL PERCHLORATE

By J. R. Soulen and W. F. Schwartz

Research and Development Laboratories, Pennsalt Chemicals Corporation, Wyndmoor, Pa.

Received April 11, 1962

The ionic structure of solid nitryl perchlorate, $NO_2^+ClO_4^-$, has been amply proved by Raman[1,2] and X-ray[3] studies. Its vibrational spectrum thus should consist of the superimposed spectra of the NO_2^+ and ClO_4^- ions. In addition to the Raman work, a limited infrared study also has been made of this compound.[4,5] However, two fundamental vibrational frequencies of the NO_2^+ ion in nitryl perchlorate apparently have not yet been reported. In addition, very little information exists on the lowest fundamental vibrational frequency of NO_2^+ in any of its ionic compounds. We here report the infrared absorption spectrum of NO_2ClO_4 and discuss it in terms of the vibrational frequencies of its constituent ions.

In Fig. 1 the 2–15 μ region was obtained with NaCl optics, and the 15–20 μ region with CsBr optics. No significant absorption occurred from 20–40 μ. Both spectra were obtained in a Nujol mull and polyethylene films were used to protect the windows from attack, as has been found necessary with various nitryl compounds here and elsewhere.[6] The nitryl perchlorate, obtained from Callery Chemical Co., was pumped overnight at 10 μ pressure to remove volatile contaminants which can form by hydrolysis. It was protected rigorously from atmospheric moisture in subsequent handling. Analysis showed 23.95% Cl, 9.72% N (calculated for NO_2ClO_4: 24.37% Cl, 9.63% N), and its X-ray powder diffraction pattern agreed well with that published previously.[7] Because of its extreme deliquescence, the nitryl perchlorate was mulled and the absorption cell components were assembled in a well dried inert atmosphere box, and the spectra were obtained with a Perkin–Elmer 21 or 221 spectrophotometer immediately on removal. The absorptions marked with dots in Fig. 1 also were obtained in blank runs using Nujol alone between polyethylene films, and are thus of no interest.

Significant in the spectrum are the absorptions at 2360, 1100 (middle of very broad band), 937, 625, and 570 cm.$^{-1}$. That at 2360 cm.$^{-1}$ is the ν_3 fundamental of NO_2^+. This has been reported at 2358 in NO_2BF_4 solid,[6] 2360 in NO_2BF_4 solution in HNO_3,[8] 2364 in NO_2PF_6 solid,[6] 2358 in NO_2SbF_6 solid,[6] 2375 in N_2O_5 ($NO_2^+NO_3^-$) solid,[9] and 2360 in anhydrous HNO_3 and HNO_3 solutions in H_2SO_4,[8] indicating the presence of NO_2^+ in these. One other report lists this absorption in NO_2BF_4 solid at 2384–2395 cm.$^{-1}$, but this work[10] has been criticized[6] because of possible reactions with cell windows.

The broad absorption centering around 1100 cm.$^{-1}$ is ν_3 of ClO_4^-, and appears very similar to that found in NH_4ClO_4, $NaClO_4 \cdot H_2O$, $KClO_4$, and $Mg(ClO_4)_2$.[11] A weaker absorption at 937 cm.$^{-1}$ is ν_1 of ClO_4^-. This is a Raman active, infrared inactive fundamental.[4,5] However, some distortion of the tetrahedral ClO_4^- structure allows this absorption in the infrared spectrum of nitryl perchlorate. It also is evident as a weak absorption in NH_4ClO_4, $KClO_4$, and $Mg(ClO_4)_2$.[11] The strong absorption at 625 cm.$^{-1}$ is due to ν_4 of ClO_4^-. This has been reported previously in NO_2ClO_4 at about the same frequency in the infrared[4,5] and at 626 in its Raman spectrum.[2] Infrared or Raman studies of a number of other perchlorates, including those of NH_4^+, Na^+, K^+, Mg^+, and H_3O^+, show this absorption prominently, with its maximum in the range 620–631 cm.$^{-1}$.[2,5,12-14]

Table I

Comparison of Vibrational Frequencies of NO_2^+ and CO_2[a]

Vibrational mode	Activity	Nitryl ion, NO_2^+ in NO_2ClO_4	Nitryl ion, NO_2^+ in NO_2NO_3	CO_2[f]
ν_1 Symmetric stretching	Raman only	1396[b]	1400[d]	(1340)[g]
ν_2 Bending	Infrared only	570[c]	538[e]	667
ν_3 Antisymmetric stretching	Infrared only	2360[c]	2375[e]	2349

[a] All values in cm.$^{-1}$. [b] Ref. 2. [c] This work. [d] Observed originally by J. Chédin (Thesis, Paris, 1937); reported subsequently by him and others. [e] Ref. 9. [f] G. Herzberg, "Infrared and Raman Spectra of Polyatomic Molecules," D. Van Nostrand Co., Inc., New York, N.Y., 1945, pp. 272–273. [g] Under low resolution. Under higher resolution this is two lines, at 1285.5 and 1388.3 cm.$^{-1}$, due to Fermi resonance. This does not occur with NO_2^+ because ν_1 is not approximately $2\nu_2$, as occurs with CO_2.

The final absorption in Fig. 1 at 570 cm.$^{-1}$ must be the low frequency fundamental ν_2 of NO_2^+. In dinitrogen pentoxide, $NO_2^+NO_3^-$, this has been found[9] at 538 cm.$^{-1}$.

NO_2^+ and CO_2 are similar, linear, symmetric species containing 22 electrons. Their vibrational

(1) C. K. Ingold, D. J. Millen, and H. G. Poole, *Nature*, **158**, 480 (1946).
(2) D. J. Millen, *J. Chem. Soc.*, 2606 (1950).
(3) E. G. Cox and G. A. Jeffrey, *Nature*, **162**, 259 (1948).
(4) D. J. Millen, *J. Chem. Soc.*, 2611 (1950).
(5) H. Cohn, *ibid.*, 4282 (1952).
(6) D. Cook, S. J. Kuhn, and G. A. Olah, *J. Chem. Phys.*, **33**, 1669 (1960).
(7) H. G. Norment, P. I. Henderson, and R. L. South, *Anal. Chem.*, **32**, 797 (1960).
(8) R. A. Marcus and J. M. Fresco, *J. Chem. Phys.*, **27**, 564 (1957).
(9) R. Teranishi and J. Decius, *ibid.*, **22**, 897 (1953).
(10) R. W. Sprague, A. B. Garrett, and H. H. Sisler, *J. Am. Chem. Soc.*, **82**, 1062 (1960).
(11) F. A. Miller and C. H. Wilkins, *Anal. Chem.*, **24**, 1283 (1952).
(12) F. A. Miller, G. L. Carlson, F. F. Bentley, and W. H. Jones *Spectrochim. Acta*, **16**, 153, 213 (1960).
(13) O. Redlich, E. K. Holt, and J. Biegeleisen, *J. Am. Chem. Soc.*, **66**, 13 (1944).
(14) D. J. Millen and E. G. Vaal, *J. Chem. Soc.*, 2913 (1956).

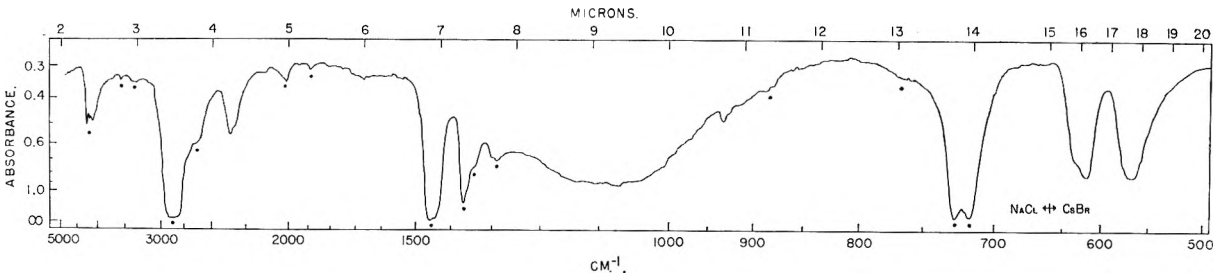

Fig. 1.—Infrared absorption spectrum of nitryl perchlorate.

spectra thus should resemble each other. In Table I their fundamental vibrations are listed. These agree exactly in activity and rather closely in frequency, with the exception of the ν_2 bending mode which occurs at a distinctly lower frequency (15 to 20%) in NO_2^+ than in CO_2. Discussion of the ClO_4^- fundamental frequencies is sufficiently complete[4,5] that it need not be repeated here.

Acknowledgment.—The authors are grateful for the considerable assistance of Miss Ruth Kossatz and her staff of the Infrared Department in carrying out this work. It was supported in part by the U. S. Air Force.

PROTON RESONANCE SPECTRA AND TACTICITY OF POLYSTYRENE AND DEUTERIOPOLYSTYRENES[1,2]

BY S. BROWNSTEIN, S. BYWATER, AND D. J. WORSFOLD

Division of Applied Chemistry, National Research Council, Ottawa, Canada

Received April 14, 1962

Observations of polymer tacticity by proton resonance spectroscopy have now been made on several polymer systems.[3-6] However, only with polymethyl methacrylate and poly-α-methylstyrene have peaks due to isotactic, syndiotactic, and heterotactic environments been clearly resolved. Usually, spin coupling of protons on adjacent carbon atoms produces several lines for each chemically unique species and when their chemical shift is small compared to the spin coupling between them, only a broad envelope of absorption is obtained. One method of removing this obstacle is to substitute deuterium for some of the protons. The smaller spin coupling constants and almost infinite chemical shift combine to simplify the spectrum. This has been done with polypropylene, but the choice of sites for deuterium substitution was such that some chemically non-equivalent protons were spin coupled.[6] As a result, peaks due to all three possible tacticities could not be resolved clearly. A separate peak for the α-proton in isotactic polystyrene has been reported.[7] However, it is barely resolved from the envelope due to the other α- and β-protons. Replacement of the β-hydrogens by deuterium removes all proton–proton spin coupling in the backbone hydrocarbon chain and allows the α-protons in isotactic, syndiotactic, and heterotactic environments to be resolved clearly under appropriate conditions. The proton resonance spectrum of poly-β,β-dideuteriostyrene has been reported previously, but the experimental conditions were not suitable for resolution of the individual peaks.[8]

Experimental

The proton resonance spectra were obtained in a manner described previously.[4] The spectra were obtained on 15 wt. % solutions of polymer in benzene enclosed in a sealed tube at 100°. Peak positions are listed in p.p.m. to high field of benzene as an internal reference. The β,β-dideuteriostyrene was obtained from Merck, Sharp and Dohme of Canada Ltd. and was reputed to be of better than 98% isotopic purity. The polystyrenes were prepared by standard methods using anionic, cationic, and free radical initiators as described before for α-methylstyrene.[4]

Results

It has been shown that there are large solvent effects upon chemical shifts when aromatic molecules are dissolved in aromatic solvents.[9] Advantage was taken of this fact to maximize the chemical shifts of the α-protons by choosing a solvent which shifted them relative to the other protons in the molecule. Benzene was found to have the greatest effect of the many solvents which were tried. The spectrum of isotactic polystyrene in benzene as solvent is shown in Fig. 1. It may be compared with one published previously,[7] to show the improvement in separation of peaks which may be obtained by appropriate choice of solvent. For comparison, the spectrum of a polystyrene polymerized by sodium naphthenide in tetrahydrofuran is included. This polymer is primarily syndiotactic, as will be shown by the measurements on a deuterated sample.

Line widths in proton resonance spectroscopy are a function of the viscosity of the medium.[10] For polymer solutions the macroscopic viscosity is not the significant quantity since the line width of the solvent is generally much narrower than those of the protons in the polymer chain. The degree of segmental motion and internal rotation along the polymer chain appear to be primarily responsible for broadening of the absorption peaks.

(1) Issued as N.R.C. No. 7014.

(2) Presented in part at the symposium on "Spectroscopy of High Polymers," American Chemical Society National Meeting, Atlantic City, 1962.

(3) F. A. Bovey and G. V. D. Tiers, *J. Polymer Sci.*, **44**, 173 (1960).

(4) S. Brownstein, S. Bywater, and D. J. Worsfold, *Makromol. Chem.*, **48**, 127 (1961).

(5) U. Johnsen, *J. Polymer Sci.*, **54**, 56 (1961).

(6) F. Stehling, Paper #45, Division of Polymer Chemistry, American Chemical Society National Meeting, Washington, March, 1962.

(7) R. J. Kern and J. V. Pustinger, *Nature*, **185**, 236 (1960).

(8) F. A. Bovey, G. V. D. Tiers, and G. Filipovich, *J. Polymer Sci.*, **38**, 73 (1959).

(9) A. A. Bothner-By and R. E. Glick, *J. Chem. Phys.*, **26**, 1651 (1957).

(10) J. A. Pople, W. G. Schneider, and H. J. Bernstein, "High Resolution Nuclear Magnetic Resonance," McGraw-Hill Book Co., New York, N. Y., 1959, p. 204.

Fig. 1.—Proton resonance spectra of polystyrenes: (a) isotactic; (b) anionic, primarily syndiotactic.

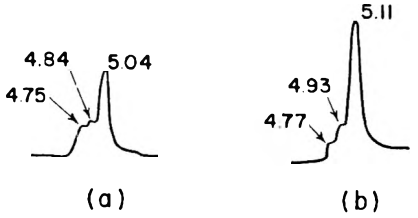

Fig. 2.—Proton resonance spectra of poly-β,β-dideuteriostyrene: (a) polymerized by BF_3 in toluene at $-78°$; (b) polymerized by Na in tetrahydrofuran at 20°.

By determining the spectra at a sufficiently elevated temperature, the rate of segmental motion is sufficient to average the local magnetic environments. The temperature required depends upon the polymeric species, but is largely independent of the average molecular weight of the polymer.[11] For polystyrene in benzene, a temperature of 90° is adequate to remove most of the effects of local magnetic broadening.

The positions of the peaks due to α-hydrogens in isotactic, heterotactic, and syndiotactic environments for a variety of polydeuteriostyrenes are listed in Table I. Some representative spectra are shown in Fig. 2. It can be seen that the line widths are too great, compared with the separation between the lines, to make quantitative estimates of the relative amounts of iso-, hetero-, and syndiotactic species present in the polymer. The increased line widths, compared with the methyl protons of poly-α-methylstyrene, may be due to

TABLE I

POLYMER PEAK POSITIONS

Catalyst	Solvent	Temp., °C.	Isotactic	Heterotactic	Syndiotactic
$SnCl_4$	Toluene	−78	4.75	..	5.07
Na	Tetrahydrofuran	20	4.77	4.93	5.11
AIBN	Benzene	60	4.77	4.88	5.11
BF_3	Nitromethane–ethylene dichloride	−78	4.75	4.88	5.07
BF_3	Toluene	−78	4.75	4.84	5.04
Butyllithium	Toluene	−30	4.81	4.91	5.09
$AlEt_3/TiCl_4$	Benzene	25	4.82		

unresolved proton–deuterium spin coupling or incomplete motional averaging of the local magnetic environment. In all the polymer samples studied, except that prepared by a Ziegler catalyst, the syndiotactic species are predominant. However, there seems to be relatively less of this type in the cationic polymers, compared with the anionic or free radical polymers.

(11) S. Brownstein, S. Bywater, and D. M. Wiles, unpublished results.

Conclusion

The proton resonance spectra of poly-β,β-dideuteriostyrene show separate peaks due to α-protons in iso-, hetero-, and syndiotactic environments. All the usual methods of polymerization, except by Ziegler catalysts, yield polymers which are largely syndiotactic.

THE EFFECT OF PRESSURE ON RADIOLYSIS OF POTASSIUM NITRATE[1]

BY TUNG-HO CHEN AND EVERETT R. JOHNSON

Stevens Institute of Technology, Hoboken, New Jersey

Received April 28, 1962

Potassium nitrate undergoes decomposition by ionizing (gamma) radiation to yield nitrite ion and oxygen,[2-5] *viz.*

$$KNO_3 \xrightarrow{\sim\sim} KNO_2 + {}^1/_2O_2 \qquad (1)$$

A plot of the nitrite yield *vs.* dose shows three distinct regions: an initial curved portion, and two apparent straight line regions where the yield appears to be linear with dose. Neglecting the initial curved portion and concentrating only on the linear regions, it is apparent that there is a "break" in the nitrite yield curve.[2,5,6] It has been found that coincident with this break, the lattice undergoes a 1% density change and just prior to the break, a transition resembling a lambda type transition.[5,6] Also, an isotope effect of 12% has been found prior to the break, but none following the break.[2b] The exact nature of this transition is not known, but was postulated to be initiated by the internal pressure exerted by the trapped oxygen from (1) and possibly the mismatch of nitrite ions. It was believed that the application of external pressure might prevent the transition referred to above from occurring, or delay its appearance. With this idea in mind C.P. KNO_3 was irradiated under about 1900 p.s.i. of He at the center of a cylindrical Co-60 source. The identical geometry was used in obtaining all the values shown in Fig. 1. Dose was determined by Fricke dosimetry with a precision of better than ±1.5%. The minimum over-all precision in these determinations is better than ±2%. The dose rate was 18×10^{18} e.v./g./hr.

Samples of KNO_3 (about 0.6 g.) contained in a 2-mm. i.d. Pyrex tube were placed inside a stainless steel tube. This tube, sealed by a swagelok, was connected directly to a helium cylinder outside the source. The nitrite ion yield was obtained with and without helium pressure. It was calculated that the maximum energy absorbed by the helium was less than 0.3%.

(1) Research supported in part by AEC AT(30-1-)-1824 and in part by NSF grant G-19115.

(2) (a) J. Cunningham and H. G. Heal, *Trans. Faraday Soc.*, **54**, 1355 (1958); (b) J. Cunningham, *J. Phys. Chem.*, **65**, 628 (1961).

(3) G. Hennig, R. Lees, and M. S. Matheson, *J. Chem. Phys.*, **21**, 664 (1953).

(4) C. J. Hochanadel and T. W. Davis, *ibid.*, **27**, 333 (1957).

(5) J. Forten and E. R. Johnson, *Phys. Chem. Solids*, **15**, 218 (1960).

(6) E. R. Johnson and J. Forten, *Discussions Faraday Soc.*, **31**, 238 (1961).

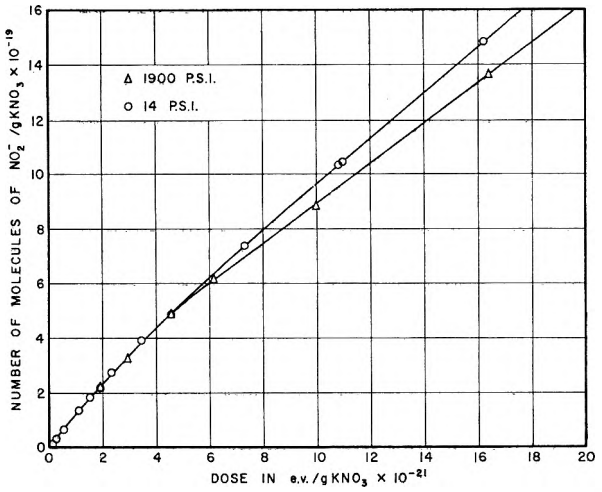

Fig. 1.—Effect of pressure on the decomposition of KNO_3.

Examination of Fig. 1 shows that, contrary to expectations, there is no effect of pressure prior to the break referred to above, nor is there any delay in the appearance of the break. There is, however, an appreciable effect on the yield after the break. Referring to Fig. 1, it is apparent that there is a decrease in the yield beyond an absorbed dose of about 45×10^{20} e.v./g. The difference in nitrite ion yield without pressure is far greater than any possible experimental error and must be considered as real.

This effect of pressure provides further evidence of a particular type of lattice change which occurs in KNO_3 after about 1 mole % decomposition, corresponding to an absorbed dose of about 45×10^{20} e.v./g. A discussion of the kinetics and mechanism for the decomposition of KNO_3 as well as other nitrates is now in preparation.

ASSOCIATION CONSTANTS OF SILVER(I) AND CHLORIDE IONS IN MOLTEN POTASSIUM NITRATE

By D. L. MANNING, J. BRAUNSTEIN,[1a] AND M. BLANDER[1b]

Oak Ridge National Laboratory,[2] Oak Ridge, Tennessee

Received December 23, 1961

In this note the association constants K_1 and K_2 for the formation of the species AgCl and $AgCl_2^-$ in molten KNO_3 at 350 and 436° are presented.

The association constants were evaluated by a method previously described.[3] The activity coefficients of $AgNO_3$ in dilute solutions of Ag^+ and Cl^- in molten KNO_3 were evaluated from e.m.f. measurements.[4] At 350° measurements were made at eight fixed concentrations of $AgNO_3$ ranging from a mole ratio of 4.95×10^{-5} to 1.19×10^{-3}, with each set containing measurements at several concentrations of KCl. At 436° four sets of measurements were made to supplement four sets of measurements[4] previously presented to obtain concentrations of $AgNO_3$ ranging from a mole ratio of 1.14×10^{-4} to 5.35×10^{-3}.[5] The limiting slopes at $R_{KCl} = 0$ of plots of $-\log \gamma_{AgNO_3}$ *vs.* R_{KCl} at each fixed concentration of $AgNO_3$ at 350 and 436° were evaluated graphically[3] and are plotted in Fig. 1a as a function of R_{AgNO_3}. The ends of the plotted lines were dashed when it was not fairly certain that the curve went through the last point. The data of ref. 4 at $R_{AgNO_3} = 3.50$ and 5.35×10^{-3} at 436° are not plotted in Fig. 1. They were not necessary for the evaluation of the association constants and were used as supplementary data only. The limit of this plot of $-(\partial \log \gamma_{AgNO_3})/\partial R_{KCl})_{R_{KCl}=0}$ at $R_{AgNO_3} = 0$ is equal to $(K_1/2.303)$.

A least squares fit of the data for $-\log \gamma_{AgNO_3}$ at each fixed concentration of $AgNO_3$ to the equation

$$-\log \gamma_{AgNO_3} = AR_{KCl} + BR^2_{KCl}$$

led to values of A and B which could be used to evaluate K_1 and K_2. The value of K_1 obtained from the extrapolation of A to $R_{AgNO_3} = 0$, well within the experimental error, agreed with the value of K_1 obtained graphically. The parameter B is plotted in Fig. 1b. The limit of B at $R_{AgNO_3} = 0$, B_0, is equal to $(K_1K_2 - {}^1/_2K_1^2)/2.303$ and was used to evaluate K_2. It should be noted that a relatively large error in B_0 leads to a relatively small error in K_2. An attempt was made to evaluate $K_{1,2}$, the association constant for the formation of Ag_2Cl^+. Because of scatter in the data, all that could be deduced was that $K_{1,2}$ was greater than zero and less than about 40 (in mole fraction units) at 350 and 436°.

The values of K_1 and K_2 at 350 and 436° as well as those at 385°[3] are given in Table I. A comparison of these constants with the theoretical expressions[6,7] for values of $Z = 4$, 5, and 6 led to the values of ΔE_1 and ΔE_2 which also are listed in Table I.

$$K_1 = Z[\exp(-\Delta E_1/RT) - 1] \qquad (1)$$

$$K_1K_2 = \frac{Z(Z-1)}{2}[\exp(-(\Delta E_1 + \Delta E_2)/RT) - 2\exp(-E_1/RT) + 1] \qquad (2)$$

The value of K_1 at 436° (as discussed previously[3]) is about 13% higher than the value computed by Duke and Garfinkel[8] from our data because Duke and Garfinkel neglected to extrapolate to $R_{AgNO_3} =$

(1) (a) On sabbatical leave from the University of Maine, August, 1960–August, 1961; (b) North American Aviation Science Center, P.O. Box 309, Canoga Park, California.

(2) Operated for the United States Atomic Energy Commission by Union Carbide Corporation.

(3) M. Blander, J. Braunstein, and R. M. Lindgren, *J. Am. Chem. Soc.*, **84**, 1529 (1962).

(4) M. Blander, F. F. Blankenship, and R. F. Newton, *J. Phys. Chem.*, **63**, 1259 (1959).

(5) The data have been deposited as Document Number 7127 with the ADI Auxiliary Publications Project, Photoduplication Service, Library of Congress, Washington 25, D.C. A copy may be secured by citing the Document Number and by remitting $1.25 for photoprints, or $1.25 for 35 mm. microfilm. Advance payment is required. Make checks or money orders payable to: Chief, Photoduplication Service, Library of Congress.

(6) D. G. Hill, J. Braunstein, and M. Blander, *J. Phys. Chem.*, **64**, 1038 (1960).

(7) M. Blander, *J. Chem. Phys.* **34**, 432 (1951).

(8) F. R. Duke and H. M. Garfinkel, *J. Phys. Chem.*, **65**, 461 (1961). Note that these authors report K_1 in molality units. Their values of K_1 are to be multiplied by 9.89 to correspond to the mole fraction units used here.

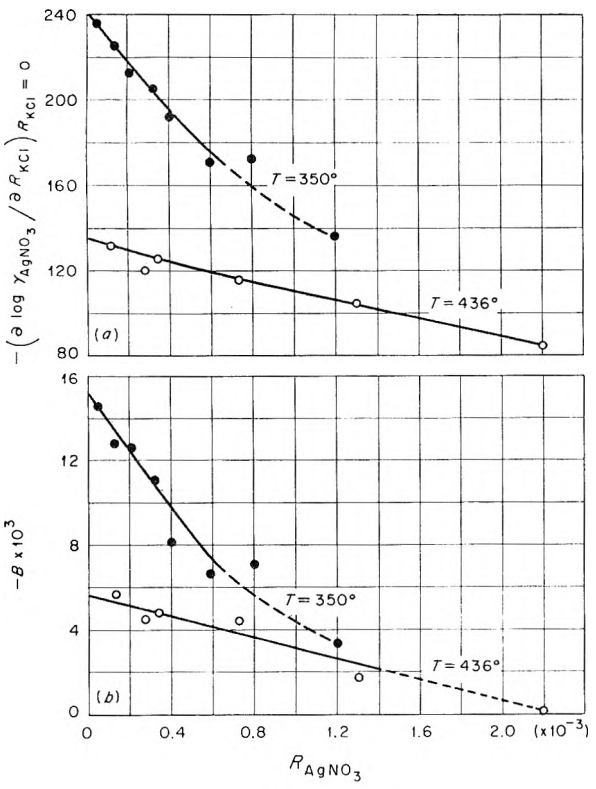

Figure 1.

TABLE I

CALCULATED ASSOCIATION CONSTANTS IN MOLE FRACTION UNITS AND DERIVED PARAMETERS

		T = 350°	T = 385°[8]	T = 436°
K_1 (in mole fraction units)		553 ± 20	460 ± 15	315 ± 12
$-\Delta E_1$ (kcal./mole) for Z =	4	6.12	6.21	6.17
	5	5.85	5.93	5.86
	6	5.62	5.69	5.62
K_2 (in mole fraction units		215 ± 25	169 ± 20	117 ± 12
$-\Delta E_2$ (kcal./mole) for Z =	4	6.15	6.18	6.16
	5	5.81	5.82	5.77
	6	5.52	5.53	5.45

0. The difference makes clear the necessity of a careful analysis of data in order to obtain values of the association constants precise enough for comparison with theory. The calculated values of ΔE_1 and ΔE_2 within the estimated error are constant at all three temperatures and for the three values of Z. It is indicated, therefore, that eq. 1 and 2, with co ıstant values of ΔE_1 and ΔE_2, and for any reasonable choice of Z, can be utilized to predict the temperature coefficients of K_1 and K_2 which are correct within the experimental precision of the measurements.

CATALYTIC ISOMERIZATION OF 2-PENTENE

BY J. C. ROHRER AND J. H. SINFELT

Esso Research and Engineering Co., Linden, New Jersey

Received April 11, 1962

This note presents kinetic data on the skeletal isomerization of 2-pentene over a chlorided alumina catalyst. Included are data on the effect of hydrogen, which are of interest in connection with the observed complex effect of hydrogen on the isomerization of saturated hydrocarbons over a chlorine-containing platinum on alumina catalyst.[1,2] Considerable evidence indicates that the latter reaction involves a step in which olefinic intermediates undergo skeletal rearrangement on acidic alumina sites.[3,4] It was suggested, however, that the effect of hydrogen pressure was not associated with this step.[1,2] The results of the present study serve to check this point.

Experimental

Procedure.—The 2-pentene was contacted with the catalyst in the presence of hydrogen or nitrogen, using a flow reactor technique described previously.[5] A catalyst charge of 4.0 g. was used throughout. The reaction products were analyzed by a chromatographic procedure which also has been described previously.[6]

Materials.—The 2-pentene used in this study was a mixture of 85% *cis*-2-pentene and 15% *trans*-2-pentene, and was obtained from Matheson Coleman and Bell. A chromatographic analysis showed no other components to be present in detectable amounts (about 0.05%). The alumina catalyst used in this work contained 1.2% chlorine. The catalyst was calcined in air for 4 hr. at 593°, and had a surface area of 210 m.²/g. X-Ray diffraction measurements of the alumina prior to calcination showed it to be β-alumina trihydrate, a form of alumina which has been described previously.[7]

Results

When 2-pentene is passed over the promoted alumina catalyst, both double bond migration and skeletal isomerization are observed, the former yielding 1-pentene and the latter a mixture of methylbutenes. Interconversion between *cis*- and *trans*-2-pentene also is observed. Some hydrogenation to pentanes and cracking to C_1–C_4 hydrocarbons also are observed, particularly at the higher temperature (471°). Typical product distribution data are shown in Table I.

Interconversion between *cis*- and *trans*-2-pentene and the formation of 1-pentene occur more readily than skeletal isomerization to the methylbutenes. Thus, at the lowest reactant flow rate used (F/W = 0.18 gram mole 2-pentene charged per hour per gram catalyst), the distribution of *cis*- and *trans*-2-pentene and 1-pentene is roughly in accord with equilibrium data,[8] whereas the ratio of total methyl-

(1) J. H. Sinfelt and J. C. Rohrer, *J. Phys. Chem.*, **65**, 978 (1961).

(2) J. C. Rohrer, H. Hurwitz, and J. H. Sinfelt, *ibid.*, **65**, 1458 (1961).

(3) F. G. Ciapetta, *Ind. Eng. Chem.*, **45**, 162 (1953).

(4) G. A. Mills, H. Heinemann, T. H. Milliken, and A. G. Oblad, *ibid.*, **45**, 134 (1953).

(5) J. H. Sinfelt, H. Hurwitz, and J. C. Rohrer, *J. Phys. Chem.*, **64**, 892 (1960).

(6) J. C. Rohrer and J. H. Sinfelt, *ibid.*, **66**, 950 (1962).

(7) H. S. Stumpf, A. S. Russell, J. W. Newsome, and C. M. Tucker, *Ind. Eng. Chem.*, **42**, 1398 (1950).

TABLE I

TYPICAL PRODUCT DISTRIBUTION DATA FOR 2-PENTENE

Temp., °C.	372	372	372	471	471	471
F/W[a]	0.79	0.18	0.82	0.80	0.18	0.78
Pressure, atm.						
H_2	5.3	5.3	21.3	5.3	5.3	21.3
2-Pentene	0.53	0.53	0.53	0.53	0.53	0.53
Product distribution, mole %						
C_1–C_4[b]				0.9	2.6	..[c]
1-Pentene	7.4	8.7	7.2	8.0	6.1	8.5
trans-2-Pentene	38.5	44.6	32.2	39.1	27.3	34.5
cis-2-Pentene	48.9	24.3	56.3	33.6	19.1	39.7
3-Methyl-1-butene	0.3	0.9		1.0	1.9	0.8
2-Methyl-1-butene	1.3	5.8	1.2	5.0	11.6	4.3
2-Methyl-2-butene	3.7	15.2	3.1	11.4	25.3	8.8
Isopentane		0.2		0.8	4.6	2.6
n-Pentane				0.2	1.5	0.7

[a] Gram moles 2-pentene charged per hr./g. catalyst. [b] Expressed as mole % of 2-pentene converted to C_1–C_4. [c] C_1–C_4 not determined.

TABLE II

RATE DATA FOR SKELETAL ISOMERIZATION OF 2-PENTENE IN PRESENCE OF H_2

Temp., °C.	372	372	372	372	471	471	471	471
Pressure, atm.								
H_2	1.3	5.3	5.3	21.3	1.3	5.3	5.3	21.3
2-Pentene	0.13	0.13	0.53	0.53	0.13	0.13	0.53	0.53
Rate, r[a]	0.026	0.020	0.042	0.035	0.10	0.080	0.15	0.13

[a] Gram moles 2-pentene converted per hr. per g. catalyst to methylbutenes.

butenes to the sum of *cis*- and *trans*-2-pentene and 1-pentene is far from the value at equilibrium, which averages about 3.5 at the temperatures used in this study.[8] However, the distribution of the various methylbutenes formed in the reaction corresponds roughly with that at equilibrium, which is further evidence that double bond migration occurs more readily than skeletal isomerization.

The ratio of isopentane to *n*-pentane in the products at 471° is about 3 or 4 to 1. Increasing hydrogen pressure at a given value of F/W increases the extent of hydrogenation to form both *n*-pentane and isopentane.

Rates of skeletal isomerization of 2-pentene are shown in Table II as a function of temperature and partial pressures of hydrogen and 2-pentene. The reaction rates were determined from data where the levels of conversion to methylbutenes were low (2.6 to 17.4%) and hence represent initial rates. The reaction rates were evaluated using the relation

$$r = \frac{F}{W}\Delta x \qquad (1)$$

where F represents the feed rate of 2-pentene in g. moles/hr., W is the weight of catalyst in grams, and Δx is the fraction of the 2-pentene converted to methylbutenes. The rates shown in Table II actually represent rates of conversion of a mixture of *cis* and *trans*-2-pentenes and 1-pentene to a mixture of methylbutenes. The 2-pentene used as a reactant was a mixture of *cis* and *trans* isomers, and in addition, extensive *cis–trans* interconversion and double bond migration take place before the extent of skeletal isomerization becomes appreciable.

(8) "Selected Values of Physical and Thermodynamic Properties of Hydrocarbons and Related Compounds," API Research Project 44, Carnegie Press, Inc., New York, N. Y., 1953.

The data on the effect of temperature on the rate of skeletal isomerization indicate an apparent activation energy of about 13 kcal./mole. Regarding pressure effects, the rate is roughly 0.5 order with respect to 2-pentene partial pressure and nearly independent of hydrogen partial pressure. Since the experiments in the presence of hydrogen showed little effect of hydrogen pressure, it was decided to determine the effect of eliminating hydrogen completely. In some side experiments on the same alumina, after it had been somewhat deactivated due to prolonged exposure to 2-pentene, it was found that the skeletal isomerization of 2-pentene proceeded satisfactorily when nitrogen was substituted for hydrogen. The rate in the presence of nitrogen relative to that in the presence of hydrogen (r_n/r_h) is

Temp., °C.	416	471
r_n/r_h[a]	1.1	0.85

[a] H_2 or N_2 pressure = 5.3 atm., 2-pentene pressure = 0.53 atm.

Thus, the effect of hydrogen on the rate of skeletal isomerization generally is not very great.

In previous studies on the isomerization of methylcyclopentane[1] and *n*-heptane[2] over a platinum–alumina catalyst containing chlorine, it was found that the presence of hydrogen was necessary for isomerization and that at moderate hydrogen pressures (below 6 atm. at 471°) the rate of isomerization increased markedly with increasing hydrogen pressure. It was suggested that this effect of hydrogen was not associated with the isomerization of olefin intermediates over acidic sites on the alumina, but rather with the reaction on the platinum sites, the role of hydrogen being to keep the platinum free of surface residues. The observation of the present study that the presence of hydrogen is not necessary

for isomerization of olefins over an acidic alumina at similar conditions is in agreement with this conclusion.

THE POLAROGRAPHIC DIFFUSION COEFFICIENT

BY RICHARD J. BEARMAN

Department of Chemistry, University of Kansas, Lawrence, Kansas

Received March 9, 1962

It is well known that the diffusion coefficient is one of the important parameters of the limiting current equations (*e.g.*, the Ilkovic equation) of polarography. Although numerous measurements have been carried out to evaluate polarographic diffusion coefficients, little effort has been expended thus far to compare these with diffusion coefficients determined by other standard techniques. Such comparisons would be valuable in providing further information concerning electrode processes and in checking the fundamental equations of both polarography and diffusion. Professor Adams of this department has undertaken an experimental program of tracer diffusion measurements with these objectives. In this paper, we provide a theoretical framework for the interpretation of his data.

By now, it is commonly realized that in a given system there exist several diffusion coefficients of interest, namely all of the mutual and tracer coefficients. However, the simple derivations of the limiting current equations to be found in standard textbooks[1] do not concern themselves with the distinctions among them. Clearly, for meaningful comparisons between the polarographic diffusion coefficients and the other coefficients, these distinctions must be made. With the purpose of determining the relationship of the polarographic diffusion coefficient to the others, we study in this note the derivation of Fick's law as it applies to common polarography experiments. We find that the polarographic diffusion coefficient is closely related to the tracer diffusion coefficient of the electroactive ion. Strictly speaking, the two coefficients are not equal. Nevertheless, it may be found in practice that they are identical within the limits of validity of the limiting current equations themselves.

The Fundamental Phenomenological Equations.—Fick's law for the diffusion of an ion α along the line of the x direction is often regarded as a consequence of the simple equation[1]

$$u_\alpha = -\frac{U_\alpha}{F}\left(\frac{\mathrm{d}\mu_\alpha}{\mathrm{d}x} + z_\alpha F\frac{\mathrm{d}\varphi}{\mathrm{d}x}\right) \qquad (1)$$

where u_α is the velocity of the ion, U_α is its mobility, $\mathrm{d}\mu_\alpha/\mathrm{d}x$ is the gradient of its chemical potential, z_α is its (signed) charge number, $\mathrm{d}\varphi/\mathrm{d}x$ is the gradient of electric potential, and F is the faraday. For a number of reasons, the most compelling of which is the experimental verification of the Onsager reciprocal relations,[2] it has become increasingly clear that eq. 1 is inadequate even if the mobility is supposed to be a function of composition. The more general equations which are now being used to replace eq. 1 may be written in the following form[3]

$$\frac{\mathrm{d}\mu_\alpha}{\mathrm{d}x} + z_\alpha F\frac{\mathrm{d}\varphi}{\mathrm{d}x} = -\sum_{\beta=1}^{\varkappa} c_\beta\zeta_{\alpha\beta}(u_\alpha - u_\beta)$$

$$\zeta_{\alpha\beta} = \zeta_{\beta\alpha} \qquad (2)$$

where c_β is the concentration of β and $\zeta_{\alpha\beta}$ is the concentration dependent friction coefficient between species α and β. The summation is over all $\varkappa$ species in the system. Equation 2 reduces to eq. 1 when all interactions are negligible except those between the ion α and the solvent.

The Diffusion Coefficients.—We consider a system with only one electroactive species, which we conventionally assume to be a positive ion A. Equation 2 for species A contains $\mathrm{d}\varphi/\mathrm{d}x$ which generally is not accessible by direct measurement.[4] In order to discuss only measurable quantities, it is convenient to eliminate the electric potential from the equation. We may do this by considering any negative ion R in the system and introducing simple positive integers ν_R and ν_A with the property that $\nu_\mathrm{R}/\nu_\mathrm{A} = -z_\mathrm{A}/z_\mathrm{R}$. Multiplying eq. 2 for A by ν_A, eq. 2 for R by ν_R and adding the two equations gives

$$\mathbf{R}T\frac{\mathrm{d}\ \ln c_\mathrm{A}^{\nu_\mathrm{A}}c_\mathrm{R}^{\nu_\mathrm{R}}f_{\mathrm{AR}}^{\nu}}{\mathrm{d}x} =$$

$$-\sum_{\beta=1}^{\varkappa}\nu_\mathrm{A}c_\beta\zeta_{\mathrm{A}\beta}(u_\mathrm{A} - u_\beta) - \sum_{\beta=1}^{\varkappa}\nu_\mathrm{R}c_\beta\zeta_{\mathrm{R}\beta}(u_\mathrm{R} - u_\beta)$$

$$\nu = \nu_\mathrm{A} + \nu_\mathrm{R} \qquad (3)$$

To derive eq. 3, we have written the chemical potential as the sum of a standard potential term and an activity term

$$\mu_\alpha = \mu_\alpha^0(T,P) + \mathbf{R}T\ln c_\alpha f_\alpha \qquad (4)$$

with $\mathbf{R}$ the gas constant, T the absolute temperature, and f_α the single ion activity coefficient. In eq. 3, we have introduced the measurable mean ionic activity coefficient $f_{\mathrm{AR}}^{\nu} = f_\mathrm{A}^{\nu_\mathrm{A}}f_\mathrm{R}^{\nu_\mathrm{R}}$.

The derivation of the limiting current equations requires eq. 3 only in a small region of the diffusion layer near the electrode surface.[5] Because of various surface effects, it is unlikely that eq. 3 or its precursor, eq. 2, applies directly at the surface. Nevertheless, in phenomenological discussions like this one it is ordinarily assumed that the equations do apply for all macroscopic distances from the surface, and that surface effects play a significant role only insofar as they help to determine bound-

(1) G. W. C. Milner, "The Principles and Applications of Polarography and Other Electroanalytical Processes," Green and Co., London, 1957.

(2) P. J. Dunlop and L. J. Gosting, *J. Phys. Chem.*, **63**, 86 (1959).

(3) (a) R. W. Laity, *ibid.*, **63**, 80 (1959); (b) E. Helfand, *J. Chem. Phys.*, **33**, 319 (1960); (c) S. Ljunggren, *Trans. Roy. Inst. Technol. Stockholm*, Sweden, Nr. 172 (1961); (d) R. J. Bearman and J. G. Kirkwood, *J. Chem. Phys.*, **28**, 136 (1958).

(4) E. A. Guggenheim, "Thermodynamics," 3rd Ed., North-Holland Publishing Co., Amsterdam, 1957.

(5) Reference 1, p. 32.

ary conditions. In the present instance, the usual boundary condition is that the velocity of each species other than the electroactive species vanishes at the boundaries. In the small region of the diffusion layer under consideration, this boundary condition is satisfied for practical purposes, and eq. 3 reduces to

$$z_A c_A F\mathbf{R}T \frac{\mathrm{d} \ln c_A^{\nu_A} c_R^{\nu_R} f_{AR}^{\nu}}{\mathrm{d}x} = -\sum_{\substack{\beta=1 \\ \neq A}}^{\kappa} \nu_A c_\beta \zeta_{AR}\, i + c_A \nu_R \zeta_{RA}\, i \quad (5)$$

where $i = z_A c_A F u_A$ is the (signed) current density. We may rewrite the left-hand side of eq. 5 as

$$z_A c_A F\mathbf{R}T \frac{\mathrm{d} \ln c_A^{\nu_A} c_R^{\nu_R} f_{AR}^{\nu}}{\mathrm{d}x} = z_A F\mathbf{R}T \left[c_A \frac{\mathrm{d} \ln c_R^{\nu_R} f_{AR}^{\nu}}{\mathrm{d}x} + \nu_A \frac{\mathrm{d}c_A}{\mathrm{d}x} \right] \quad (6)$$

We now confine ourselves to the case of interest wherein the concentration of A is small and the concentration of R is much greater than that of A—that is, the case where there is a large excess of supporting electrolyte. The first term in the brackets will be negligibly small compared with the second, and Fick's law results from eq. 5 and 6 in a form which leads directly to the limiting current equation[6]

$$i = -z_A F D_A^{\,P} \frac{\mathrm{d}c_A}{\mathrm{d}x}$$

$$D_A^{\,P} = \frac{\mathbf{R}T}{\sum_{\substack{\beta=1 \\ \neq A}}^{\kappa} c_\beta \zeta_{A\beta} - \frac{\nu_R}{\nu_A} c_A \zeta_{RA}} \quad (7)$$

We have denoted the diffusion coefficient of the polarographic experiment by $D_A^{\,P}$. If a second anion R′ is present, we have a second similar equation for i, with a different diffusion coefficient in which $(\nu_R/\nu_A)(c_A\zeta_{RA})$ is replaced by $(\nu_{R'}/\nu_A')(c_A\zeta_{R'A})$. In this event, we must assume that the term involving c_A in each diffusion coefficient is negligible compared with the others. Otherwise, the alternative diffusion coefficients would not be equal and the two versions of eq. 7 would not be consistent with each other. The inconsistency would necessitate the use of the complete eq. 5 which might not lead to the usual limiting current equations. If we had assumed ideality in eq. 2 and had neglected the electric potential gradient term, we could have derived eq. 7 directly without the c_A term. We have preferred, however, to state our approximations in forms which can be verified experimentally. Moreover, our complete expressions may prove useful when the approximations are not valid.

(6) Reference 1, eq. 3.27.

The polarographic diffusion coefficient is related closely to the tracer diffusion (also called the self-diffusion) coefficient D_A of ion A which measures the diffusion of a labeled trace of the ion through a system otherwise in equilibrium. It has been demonstrated elsewhere that[7]

$$D_A = \frac{\mathbf{R}T}{\sum_{\beta=1}^{\kappa} c_\beta \zeta_{A\beta}} \quad (8)$$

In eq. 8, unlike eq. 7, the sum is taken over all species including A. The reason for this is that the tracer species is initially taken to be an extra component, different from A, and is then later set equal to A in all physical characteristics. The tracer diffusion coefficient is composition dependent, and thus, if it is to be compared with the polarographic coefficient, must be measured in a system with the same concentrations as in the polarographic experiment. The tracer diffusion coefficient is not related in general to the conductivity through the Nernst–Einstein equation which is valid at infinite dilution of all species.

Clearly, according to their definitions in eq. 7 and 8, $D_A^{\,P}$ and D_A are not identical. In fact, by comparing denominators, it may be shown readily that $D_A^{\,P} > D_A$ if the friction coefficients are positive. In that case

$$\sum_{\substack{\beta=1 \\ \neq A}}^{\kappa} c_\beta \zeta_{A\beta} - \frac{\nu_R}{\nu_A} c_A \zeta_{RA} = \sum_{\substack{\beta=1 \\ \neq A, \neq R}}^{\kappa} c_\beta \zeta_{A\beta} + \left(c_R - \frac{\nu_R}{\nu_A} c_A \right) \zeta_{RA} < \sum_{\substack{\beta=1 \\ \neq A, \neq R}}^{\kappa} c_\beta \zeta_{A\beta} + c_R \zeta_{RA} + c_A \zeta_{AA} \quad (9)$$

However, in deriving the first of eq. 7, which provides the means of measurement of the polarographic diffusion coefficient, we have supposed that c_A is small. It is therefore likely that consistency requires the neglect of the c_A term in the definition of the coefficient. It is further probable that whenever this c_A term is negligible, the c_A term in the definition of the tracer diffusion coefficient is also negligible. But if both terms can be neglected, $D_A^{\,P}$ and D_A are equal by eq. 7 and 8. It thus appears reasonable that $D_A^{\,P}$ and D_A will be found to be equal within the limits of validity of the limiting current equations. The question as to whether they are identical within experimental uncertainty is, however, more readily settled by experiment than by theoretical analysis.

The author is grateful to Professor Ralph Adams for his friendly encouragement. This research has been supported by a grant from the U. S. Air Force.

(7) (a) R. W. Laity, *J. Chem. Phys.*, **30**, 682 (1959); (b) R. J. Bearman, *J. Phys. Chem.*, **65**, 1961 (1961).

COMMUNICATION TO THE EDITOR

THE IONIZATION POTENTIAL OF (ISO)THIOCYANIC ACID

Sir:

In a mass spectrometric study of ethyl isothiocyanate, we have observed that the ion of m/e = 59 is 93% of the base peak (m/e = 87). The relative abundance of the isotopic mass peak at m/e = 61 indicates that the ion of m/e = 59 may be $HNCS^+$ or $HSCN^+$. The structure of the m/e = 59 ion is discussed further in the concluding paragraph of this communication.

The ionization and dissociation of ethyl isothiocyanate leading to the m/e = 59 ion may be represented by

$$C_2H_5NCS \rightarrow HNCS^+ + C_2H_4 \qquad (1)$$

(the specific structure of the ion is not implied); if this is so, one would expect a fairly low appearance potential for the m/e = 59 ion. Equations similar to eq. 1 have been observed for a number of different systems, such as for 3,4-dithiahexane[1] and triethylphosphite.[2] Using a time-of-flight mass spectrometer,[3] we have determined the appearance potential (by treating our experimental data in the manner described by Warren[4]) for the m/e = 59 ion to be 11.38 ± 0.15 e.v., thus indicating a reasonably simple process, such as that given by eq. 1. The heat of formation of C_2H_5NCS has not been reported in the literature, but $\Delta H_f(CH_3NCS(g))$ = 27.1 kcal./mole.[5] We therefore may estimate $\Delta H_f(C_2H_5NCS(g))$ = 22 kcal./mole using Franklin's group calculations.[6] Since $\Delta H_f(C_2H_4)$ = 12.496 kcal./mole,[7] we calculate $\Delta H_f^+(HNCS)$ = 272 kcal./mole, utilizing our measured appearance potential.

The heat of formation of HNCS has not been reported, but we estimate it to be about 27 kcal./mole by comparison of the heats of formation of a number of HX and CH_3X molecules (X = OH, SH, CN, CHO). Therefore, $I(HNCS) = \Delta H_f^+(HNCS) - \Delta H_f(HNCS)$ = 272 − 27 = 245 kcal./mole, or 10.6 e.v.

It is possible to calculate I(HNCS) based on Franklin's group orbital method.[8] Taking $I(CH_3NCS)$ = 9.25 e.v.,[9] $I(C_2H_5NCS)$ = 9.10 ± 0.15 e.v. determined in the present study in our Laboratory (9.14 e.v. has been reported previously[9]) and the C–C interaction parameter = 1.55, we calculate I(HNCS) = 10.61 e.v., in better-than-expected agreement with the value we derived from the appearance potential of m/e = 59 from C_2H_5NCS. As a by-product of this calculation, the C–NCS interaction parameter was determined to be 2.34. Extending these calculations, we find that $I(CH_3CH_2CH_2NCS)$ = 9.07 e.v., only slightly lower than $I(C_2H_5NCS)$. There is presently no experimental value with which to compare this calculated value.

It is indeed tempting to assume that, in the dissociation leading to the elimination of C_2H_4 (eq. 1), the structure of the ion formed is $HNCS^+$. However, we presently have no experimental evidence that isomerization to $HSCN^+$ has not occurred. The referee of this communication has pointed out that a Franklin group orbital calculation of I(HSCN) from the ionization potentials for methyl and ethyl thiocyanate[9] leads to a value of 10.9 e.v., a value not significantly different from that calculated above for I(HNCS) or indirectly determined by us from the appearance potential of the m/e = 59 ion. Although we estimate that ΔH_f(HNCS) and ΔH_f(HSCN) are very nearly the same, and that ΔH_f^+(HNCS) and ΔH_f^+(HSCN) are also very nearly the same, we are presently studying a series of alkyl thiocyanates in order to attempt to distinguish between the structures of $HSCN^+$ and $HNCS^+$.

The authors wish to thank the referee for his helpful comments.

(1) R. W. Kiser and B. G. Hobrock, *J. Phys. Chem.*, **66**, 1214 (1962).
(2) Y. Wada and R. W. Kiser, personal communication.
(3) E. J. Gallegos and R. W. Kiser, *J. Am. Chem. Soc.*, **83**, 773 (1961).
(4) J. W. Warren, *Nature*, **165**, 811 (1950).
(5) S. Sunner, *Acta Chem. Scand.*, **9**, 837 (1955).
(6) J. L. Franklin, *Ind. Eng. Chem.*, **41**, 1070 (1949).
(7) F. D. Rossini, D. D. Wagman, W. H. Evans, S. Levine, and I. Jaffe, "Selected Values of Chemical Thermodynamic Properties," National Bureau of Standards Circular 500, U. S. Government Printing Office, Washington, D. C., 1952.
(8) J. L. Franklin, *J. Chem. Phys.*, **22**, 1304 (1954).
(9) K. Watanabe, T. Nakayama, and J. Mottl, "Final Report on Ionization Potential of Molecules by a Photoionization Method," December, 1959; Dept. Army 5B99-01-004 ORD- TB-2-0001-00R-1624, Contract No. DA-04-200-ORD 480 and 737.

DEPARTMENT OF CHEMISTRY
KANSAS STATE UNIVERSITY
MANHATTAN, KANSAS
ROGER C. SHENKEL
BRICE G. HOBROCK
ROBERT W. KISER

RECEIVED AUGUST 10, 1962